Characterization of new drug leads and target structures to combat multidrug-resistant tuberculosis

Inaugural dissertation

for the attainment of the title of doctor
in the Faculty of Mathematics and Natural Sciences
at the Heinrich Heine University Düsseldorf

Presented by

Kristin Vill (née Schwechel)
from Wolfhagen

Düsseldorf, September 2024

from the Institute of Pharmaceutical Biology and Biotechnology
at the Heinrich Heine University Düsseldorf

Published by permission of the
Faculty of Mathematics and Natural Sciences at
Heinrich Heine University Düsseldorf

Supervisor: Prof. Dr. Rainer Kalscheuer

Co-Supervisor: Prof. Dr. Marc Jacobsen

The date of oral examination: 23.05.2025

Acknowledgment

First and foremost, I would like to thank my supervisor Prof. Dr. Rainer Kalscheuer for his invaluable advice and support during my PhD study. Thank you for giving me the opportunity and trust to work on many exciting projects, for always being open for new ideas and for sharing broad knowledge. I am very grateful for this experience.

Likewise, I would like to thank Prof. Dr. Marc Jacobsen for being my co-supervisor. Thank you for inspiring meetings, your commitment during the MOI IV graduate school, and for sharing your enthusiasm for *Mycobacterium tuberculosis*.

I am very thankful for the generous funding of the Jürgen Manchot Stiftung and the Graduate School "Molecules of Infection". Thanks for memorable symposia, inspiring scientific environments, and many opportunities offered by the Graduate School. My profound thanks to Prof. Dr. Mary Jackson, Prof. Dr. Anthony Baughn and their research groups for supervising me during but also beyond my lab rotations in Fort Collins and in Minneapolis.

I would like to say a big thanks to all members of our working group, for a lot of fun, advice and understanding whenever it was needed. We really had good times in our lab (especially in the BSL-3 and when the music was turned on). Thanks to Emmanuel Adeniyi, Lasse van Geelen, Di He, Anna-Lene Kiffe-Delf, Violetta Krisilia, Kira Schichel, Steffen Schindler, Viktor Simons, Aron Trucksess, Lin Wang and, Meng Yun Zhang. A big thank you goes to Heike Goldbach-Gecke for her technical support, but also for always having an open ear for me.

Sincere thanks to the pharmaceutical chemistry department, especially to Prof. Dr. Thomas Kurz and Dr. Oliver Michel. Thank you for synthesizing the α-aminooxyacetic acid compounds and for providing chemical advice.

I'd also like to express my gratitude and appreciation for Björn Wefers and Prof. Dr. Heiner Schaal, whose support and help in the BSL-3 facility have been invaluable throughout this study.

From the bottom of my heart, I'd like to thank my family and friends, especially Leo, my parents and my three lovely brothers. Thank you for your encouragement and your unlimited support.

I would like to dedicate this thesis to Leni-Carlotta.

Table of Contents

Abstract

To address the rising problem of multidrug-resistant pathogens, there is an urgent requirement for new medications with inventive approaches and unique modes of action. This work focuses on tuberculosis, a bacterial disease that is responsible for 1.5 million deaths worldwide each year. The tuberculosis epidemic is complicated by its deadly combination with HIV/AIDS, but even more so by the alarming emergence of resistant strains. The first experimental part of this dissertation, described in chapter 3, concentrates on research characterizing the anti-tuberculosis potential of α-aminooxyacetic acid derivatives. The front-runner compounds, KSK-104 and KSK-106, displayed potent activity against *Mycobacterium tuberculosis* H37Rv *in vitro* in a sub-micromolar range, while also demonstrating virtually no cytotoxicity against numerous human cell lines. Furthermore, the two molecules exhibited anti-tuberculosis activity against extensively drug-resistant clinical isolates and internalized bacteria within THP1-derived macrophages. This property is vital for anti-tuberculosis drugs since *M. tuberculosis* is an intracellular pathogen that thrives within macrophages. Analysis of resistant mutants indicated that the compounds function as pro-drugs, undergoing intracellular hydrolysis by two specific amidohydrolases, which were further characterized. Complementation experiments revealed the hypothetical mechanism of action. It is suggested that the active moieties released intracellularly likely act as a "dirty drug", targeting multiple intracellular pathways.

It is evident that new compounds acting differently from the present clinical drugs are necessary to treat patients with drug-resistant tuberculosis. Hence, it is crucial to identify and characterize unknown pathogenicity and virulence factors. The cell wall of *M. tuberculosis* is considered a vulnerable point, making it an appealing target. It has a unique structure with several layers rich in lipids that provide an inherent resistance to most drugs. Despite significant advances in research on cell wall biogenesis, certain key steps are still unclear. In the second part of this dissertation, we identified Rv3277t, an essential protein of *M. tuberculosis*, and MSMEG_1817, its homolog in the surrogate *M. smegmatis*, as GtrA-like transporters that participate in the translocation of glycoconjugates (chapter 4). These conjugates play a significant role in host-pathogen interactions and are produced through a bipartite process in the cytoplasm and periplasm. Although the biosynthesis of glycoconjugates is well understood, the process by which carbohydrates move into the outer leaflet of the cell membrane remains unknown. Using bioinformatics, gene silencing, and phenotypic characterization of mutant strains, we have discovered that the GtrA-like transporters might act as putative floppases. Additionally, we have thoroughly evaluated their contribution to the mannosylation and arabinosylation of

glycoconjugates. We have thus identified a previously unknown component of the biosynthetic pathway for glycoconjugate formation and a potential drug target candidate.

As small molecule inhibitors targeting a single pathogen often prompt the emergence of new resistant strains, innovative strategies will be required to combat infectious diseases in the future. Consequently, the last part of this dissertation introduces a new chemical tool compound to remove bacterial proteins (chapters 5 and 6). The work on bacterial PROTACs is based on the principle of targeted protein degradation, whereby the compounds recruit the mycobacterial degradation pathway. The ClpC1:ClpP1P2 protease represents an alluring target for mycobacteria as both its inhibition and activation prove detrimental to the organism. The Homo-BacPROTACS, which are composed of two cyclomarin A units connected by a linker region, were analysed for the mechanism of their antitubercular activity. Our findings indicate that the dual Clp degraders trigger autodegradation of ClpC1 in conjunction with its ClpC2 caretaker. The new compounds are highly effective against *M. tuberculosis in vitro*, being over 100 times more potent than the parent antibiotic. The study highlights the potential of Homo-BacPROTACs as future antibiotics. Together, our data reveal the importance of developing original drug leads, targets, and strategies contributing to combat the emerging threat of antibiotic-mediated resistance.

Abbreviations

%	percent
°C	degree Celsius
AAA	ATPase associated with diverse cellular activities
ABC	ATP-binding cassette
Ac_1PIM_2	monoacylphosphatidylinositol dimannoside
Ac_1PIM_4	monoacylphosphatidylinositol tetramannoside
Ac_1PIM_5	monoacylphosphatidylinositol pentamannoside
Ac_1PIM_6	monoacylphosphatidylinositol hexamannoside
Ac_2PIM_2	diacylphosphatidylinositol dimannoside
Ac_2PIM_4	diacylphosphatidylinositol tetramannoside
ACP	acyl carrier protein
AcPIM	acylphosphatidylinositol mannoside
Acyl-CoA	cholesterol acyltransferase
ADCL	aminodeoxychorismate lyase
ADP	adenosine di-phosphate
AES	allelic exchange substrate
Aft	arabinofuranosyltransferase
AG	arabinogalactan
AGP	arabinogalactan-peptidoglycan
AIDS	Acquired Immunodeficiency Syndrome
Alr	alanine racemase
AM	arabinomannan
AMR	antimicrobial resistance
anti-TB	anti-tubercular
apra	apramycin
ara	arabinose
aSEC	analytical size exclusion chromatography
ATB	active tuberculosis
ATc	anhydrotetracycline
ATP	adenosine tri-phosphate

AtpE	ATP synthase subunit C
atpE	c-subunit of the F_0ATP synthase
AUTAC	autophagy-targeting chimeras
BacPROTAC	bacterial proteolysis targeting chimeras
BCG	Bacillus Calmette-Guérin
BDQ	bedaquiline
bp	base pair
BSA	bovine serum albumin
CFU	colony forming units
Clp	caseinolytic complex
ClpC	caseinolytic protease proteolytic subunit C
ClpC1:ClpP1:ClpP2	ClpC1P1P2
ClpC2NT	ClpC2 N-terminal remnant (21 residues)
ClpP	caseinolytic protease proteolytic subunit P
CoA	coenzyme A
COVID-19	coronavirus disease
CRD	Clp repeat domain
CuAAC	Cu(I)-catalyzed azide-alkyne cycloaddition
CymA	cyclomarin A
Cyt-bd	cytochrome bd oxidase
d- Ara*f*	d-arabinofuranose
DAAT	D-amino acid transaminase
DC	degradation concentration
DC-SIGN	dendritic cell-specific intercellular adhesion molecule-3-grabbing non-integrin
DCS	D-cycloserine
dCym	desoxycyclomarin C
dCymM	dCym monomer
ddl	d-alanine:d-alanine ligase
DELTA-BLAST	Domain Enhanced Lookup Time Accelerated BLAST
dis	distomer

Dmax	degradation efficacy
DMSO	dimethyl sulfoxide
DNA	deoxyribonucleic acid
dNTP	deoxynucleotide triphosphates
Dol-*P*-Man	dolichylphosphate β-D-mannose
DPA	decaprenyl-monophosphoryl-D-arabinofuranose
DPM	decaprenyl-monophosphoryl-D-mannopyranose
DPMS	dolichyl phosphate mannose synthase
DPR	decaprenyl-monophosphoryl-D-ribofuranose
DprE1	decaprenylphosphoryl-*β*-D-ribose 2′-oxidase
DprE2	decaprenylphosphoryl-D-2-keto erythropentose reductase
DXP	deoxyxylulose 5;-phosphate
e.g.	exempli gratia, for example
Ecu*	ecumicin
EDTA	ethylenediaminetetraacetic acid
EM	electron microscopy
EMB	ethambutol
ER	endoplasmic reticulum
ESI	electrospray ionization
et al.	et alia
ETC	electron transport chain
FA	formic acid
FAD	flavin-dependent monooxygenase
FAS	fatty acid synthase
FDA	Food and Drug Administration
Fig.	figure
Gal	galactose
GC	gas chromatography
GDP	guanosine diphosphate
GFE	Gibbs free energy
GFP	green fluorescent protein

GlcNAc	N-acetylglucosamine
h	hour
H2S	Hydrogen sulfide
HBP	Homo-BacPROTAC
HDAC	histone deacetylase
HIV	Human Immunodeficiency Viruses
HPLC	high performance liquid chromatography
HRP	horseradish peroxidase
HTH	helix-turn-helix
hyg	hygromicin
i.e.	"id est", for example
IFN-γ	interferon-gamma
IGRA	interferon gamma release assay
INH	isoniazid
InhA	enoyl-acyl carrier protein reductase
Ins	insertion
IP	immunoprecipitation
iv	intravenous administration
kan	kanamycin
KasA	β-ketoacyl acyl carrier protein synthase
KatG	catalase-peroxidase
KD	dissociation constants
LAM	lipoarabinomannan
LB	lysogeny broth
LC-MS	liquid chromatography-mass spectrometry
LC-MS/MS	liquid chromatography with tandem mass spectrometry
LFQ	label-free quantitative
LM	lipomannan
Lta	lipotecioic acids
LTBI	latent tuberculosis infection
LYTAC	lysosome-targeting chimera

M. abscessus	*Mycobacterium abscessus*
M. africanum	*Mycobacterium africanum*
M. avium	*Mycobacterium avium*
M. bovis	*Mycobacterium bovis*
M. canetti	*Mycobacterium canetti*
M. caprae	*Mycobacterium caprae*
M. marinum	*Mycobacterium marinum*
M. microti	*Mycobacterium microti*
M. mungi	*Mycobacterium mungi*
M. orygis	*Mycobacterium orygis*
M. pinnipedii	*Mycobacterium pinnipedii*
M. tuberculosis	*Mycobacterium tuberculosis*
M. smegmatis	*Mycobacterium smegmatis*
M. suricattee	*Mycobacterium suricattee*
MADTAC	macroautophagy-targeting chimeras
mAGP	mycolyl-arabinogalactan-peptidoglycan
MALDI-ToF	matrix-assisted laser desorption/ionization-time of flight mass spectrometry
Man	mannose
ManLAM	mannosylated lipoarabinomannan
marR	multiple antibiotic resistance regulator
MBC	minimum bactericidal concentration
MD	coiled-coil domains
MDR-TB	multidrug resistant
MIC	minimum inhibitory concentration
min	minutes
MIT	minimum inhibitory time
MmpL	mycobacterial membrane protein large
MOX	moxifloxacin
Mpt	mannopyranosyltransferase
MRC	membrane-associated oxidoreductase complex

MTBC	*Mycobacterium tuberculosis* complex
MurNAc	N-acetylmuramic acid
NAC	N-acetylcysteine
NaCl	sodium chloride
NAD	nicotinamide adenine dinucleotide
NBD-Cl	4-nitro-7-chloro-benzo-2-oxa-1,3-diazole
NDH	proton-pumping NADH dehydrogenase
nM	nana molar
NMR	nuclear magnetic resonance
NO	nitric oxide
NTD	N-terminal domain
NTM	non-tuberculous mycobacteria
OD	optical density
OM	outer membrane
OxPhos	oxidative phosphorylation
P	phospholipids
P. furiosus	*Pyrococcus furiosus*
PABA	para-aminobenzoic acid
panD	L-aspartate decarboxylase
pArg	phospho-arginine
PAS	para-amino salt of salicylic acid
PBS	phosphate buffered saline
PCR	polymerase chain reaction
PDIM	phthiocerol dimycocerosate
PEP	phosphoenolpyruvate
PG	peptidoglycan
pH	pondus hydrogenium
PI	phosphatidyl-*myo*-inositol
PIM	phosphatidyl-*myo*-inositol mannoside
PIM_2	phosphatidylinositol dimannoside
PIM_4	phosphatidylinositol tetramannoside

PIM_6	phosphatidylinositol hexamannoside
PLP	pyridoxal 5'-phosphate
PMF	proton motive force
PNP/PMP	pyridoxine/pyridoxamine 5'-phosphate
PNPOx	pyridoxine/pyridoxamine 5'-phosphate oxidase
po	oral administration
POA	pyrazinoic acid
POI	protein of interest
PPM	polyprenol-phosphate-mannose
PQC	protein quality control
PRM	parallel reaction monitoring
PROTAC	proteolysis targeting chimeras
PZA	pyrazinamide
R&D	research and development
revTetR	reverse tet repressor
RIF	rifampicin
RNA	ribonucleic acid
RND	resistance-nodulation-cell division
ROS	reactive oxygen species
rpm	revolutions per minute
rpoB	ß-subunit of RNA polymerase
rpsL	small ribosomal subunit protein uS12
RR-TB	rifampicin resistant
rRNA	ribosomal RNA
***Rv3277*t**	annotated Rv3277
S. aureus	*Staphylococcus aureus*
S. flexneri	*Shigella flexneri*
SAR	structure-activity-relationship
SARS-CoV-2	Severe acute respiratory syndrome coronavirus type 2
SD	standard deviation
SDS-PAGE	sodium dodecyl sulfate-polyacrylamide gel electrophoresis

SEC	size-exclusion chromatography
SEM	standard error of mean
SFE	solvation-free energy
SGL	sulfoglycolipids
SNP	single nucleotide polymorphism
SOD-1	superoxide dismutase
SPR	surface plasmon resonance
SRM	spontaneous resistant mutant
STREP	streptomycin
Suppl. Fig.	Supplementary figure
TB	Tuberculosis
tBHP	tert-butyl hydroperoxide
TBS	TRIS-buffered saline
TBST	TRIS-buffered saline with Tween20
TDM	trehalose-6,6-dimycolate
TDR	totally drug resistant
TEMPO	4-hydroxy-2,2,6,6-tetramethyl-1-piperidinyl-oxidanyl
tetO	tet Operator
tetR	tet Repressor
TLC	Thin layer chromatography
TM	transmembrane domain
TMM	trehalose-mono-mycolate
TNF-α	tumor necrosis factor-alpha
TnSeq	transposon-insertion sequencing
TPD	targeted protein degradation
TRIS	tris(hydroxymethyl)aminomethane
UDP	Uracil-di-phosphate
US	United States
v/v	volume per volume
w/v	weight per volume
WGS	whole genome sequencing

WHO	World Health Organization
wt	wild type
XDR	extensively drug resistant
µg	microgram
µL	microliter
µM	micromolar

1. Introduction

1.1 The infectious pathogen *Mycobacterium tuberculosis*

Bacterial human pathogens can cause severe and life-threatening illnesses. The discovery of antibiotics and the advancements in antimicrobial chemotherapy have represented significant improvements in managing bacterial infections. Nonetheless, bacteria have developed resistance mechanisms to a wide range of commonly used drugs. There is an urgent need to develop new drugs and treatment strategies capable of addressing drug-resistant pathogens. Antimicrobial resistance (AMR) has emerged as a global health threat, with estimates suggesting that it could lead to millions of deaths by 2050 if effective treatments are not implemented [1]. The World Health Organization (WHO) has identified a priority list of the most critical drug-resistant bacteria, underscoring the pressing need for new therapeutic options [2].

Here, the ancient killer *Mycobacterium tuberculosis* (*M. tuberculosis*) responsible for the disease tuberculosis is introduced. Tuberculosis (TB) is an airborne infectious disease, typically affecting the lungs, that is a major public health concern and one of the top ten leading causes of death worldwide. Controlling TB represents a distinct global health problem today that is exacerbated by the emerging spread of multidrug and extensively drug-resistant strains of TB. To combat the TB crisis, the WHO has developed “The End TB Strategy”, which aims to eradicate TB in the next years [3].

1.1.1 From ancient times to the discovery of the tubercle bacilli

The history of TB spans thousands of years, making it one of the oldest diseases affecting humanity. Before Koch’s discovery, TB was for a long time a widespread and highly infectious disease with unknown origin. It has been hypothesized that the genus *Mycobacterium* already exists since about 150 million years [4]. Compared to this, *M. tuberculosis* is a young species around three million years old, with a common ancestor of modern strains appearing 15,000 - 20,000 years ago [5-7]. The first indications for TB in humans stem from the presence of bone lesions in a skull dating back 500,000 years in Turkey [8]. However, the first unequivocal confirmation of *M. tuberculosis* occurred through PCR sequencing and identification of

mycobacterial lipids in bone lesions of a 17,000-year-old bison, found in Wyoming, USA [9]. Within the emerging scientific discipline of Palaeomicrobiology, significant efforts were made to study ancient DNA recovered from several burial sites [10].

Throughout the past, TB has been known by different names such as “schachepheth” in the Old Testament [11] or “phthisis” as described in Greek literature [12]. Particularly in the 18th and 19th centuries “consumption” was used as a synonym for TB due to its characteristics of weight loss and the gradual decline of the affected individuals. In 1720, for the first time, Benjamin Marten’s work “A New Theory of Consumption” represented an important understanding and management of TB, offering valuable epidemiological insights [13]. In the 19th and early 20th centuries, TB reached epidemic proportions in Europe and North America, causing significant morbidity and mortality [14]. Especially during the Industrial Revolution, TB had a profound impact on both urban and rural populations. The rapid urbanization, crowded living conditions, and poor sanitation of industrial cities created fertile grounds for the spread of TB. As the first medical TB therapy, sanatoria were established as treatment centers, offering fresh air, rest, and isolation to patients [15].

The discovery of *M. tuberculosis*, the pathogen responsible for the disease TB, marked a significant milestone in medical history. On 24 March 1882, the German physician and microbiologist Dr. Robert Koch communicated to the Berlin Society of Physiology that he had identified the microorganism responsible for the deadly pulmonary tuberculosis and published his groundbreaking work two weeks later [16]. During his presentation, Koch not only presented demonstrations of the tubercle bacillus he had discovered but also introduced his renowned postulates, known as the “Koch-Henle postulates”. Firstly, the bacterial agent must be present in lesions characteristic of the disease, while being absent in other lesions or healthy tissues. Secondly, the microorganism must be isolated and grown in pure culture, requiring that the pathogen be isolated and grown in a laboratory culture, independent from other microorganisms. Third, the cultured microorganism must cause disease when being reintroduced into a previously non-infected animal. These postulates continue to this day to set the rules for the demonstration of an infectious cause of a disease [7]. In summary, with this groundbreaking work, he not only revealed the etiological agent behind the devastating disease TB but also set a benchmark for demonstrating the infectious agent of other diseases.

The identification of *M. tuberculosis* opened the door to further research and a deeper understanding of its prevalence as well as infection patterns. Subsequent investigations into the

pathogenicity and dormancy mechanisms of the bacterium have provided valuable insights into the development of diagnostic tools, treatment regimens, and preventive measures to combat this global health burden.

1.1.2 Pathogenesis and infection of tuberculosis

Understanding the pathogenesis of TB is crucial for developing effective strategies for prevention, diagnosis, and treatment. *M. tuberculosis* is considered a very successful pathogen due to several factors. In the early 1960s, studies on the airborne nature of TB associated with the recognition that some individuals were very efficient and dangerous transmitters of pathogenic bacteria, paving the way for the term “super-spreader” to emerge [17, 18]. Next to the bacilli’s ability to be transmitted via aerosols, it has evolved mechanisms to efficiently infect and invade host cells and causes latent infections that can be reactivated after decades. Although TB is primarily a pulmonary pathogen, it can damage any other tissue of the body.

As TB disease presents a dynamic spectrum, ranging from asymptomatic infection to a potentially life-threatening condition, patients with TB are typically classified into two categories either having latent TB infection (LTBI) [19, 20], characterized by an asymptomatic and non-transmissible state, or active TB (ATB), which is transmissible and can be diagnosed using culture-based or molecular methods [21]. Patients with ATB disease commonly experience symptoms like fever, fatigue, loss of appetite, and weight loss, and those with pulmonary disease can exhibit persistent cough and hemoptysis (coughing up blood) in advanced disease. However, some patients with active, culture-positive disease may not display any symptoms and are best described as having subclinical TB [20].

M. tuberculosis infection occurs when a person inhales a few aerosolized droplets dispersed in the air by a patient with active pulmonary TB (Fig. 1). These droplets can be released into the air by coughing, sneezing, or even talking and are usually trapped by mucus-secreting goblet cells in the respiratory tract, as part of the first-line defense system [22, 23]. However, in certain situations, some droplets can evade this defense and reach the upper areas of the lungs. As soon as the *M. tuberculosis* bacilli enter the alveoli of the host's lungs, they are engulfed by alveolar macrophages due to receptor-mediated phagocytosis [24]. This innate immune response attempts to destroy the infecting bacilli using various proteolytic enzymes and cytokines like tumor necrosis factor-alpha (TNF-α) and interferon-gamma (IFN-γ) [23, 25]. If the bacilli manage to survive this line of defense, they enter a stage of active replication within the macrophages and

diffuse to nearby cells including interstitial macrophages, dendritic cells, and likely epithelial cells [26]. Within a few weeks of exponential growth, the bacterial burden increases dramatically [27]. It was shown in humans and experimental animals that *M. tuberculosis* infection is followed by a delayed adaptive immune response compared to other infections [28]. The increasing bacterial burden induces the release of several cytokines and the production of several small molecules to regulate the infection, known as chemokines [29]. These inflammatory molecules regulate the initiation of the T-cell response and recruitment of other immune cell types including monocytes, neutrophils, and dendritic cells to the primary infection site [30]. The initiated T-cell response may either eliminate the infecting organism or result in granuloma formation.

The granuloma is a crucial feature of pulmonary TB and can be defined as an enormous mass of immune cells [31, 32]. In immunocompetent individuals, although the granuloma is unable to eliminate the pathogen, it restrains the bacilli thereby preventing active disease. However, the bacteria survive within the granuloma, avoiding death by blocking phagolysosome fusion and evading the host's immune response. This allows the bacilli to persist in a dormant or slow-replicating state for decades, representing latent disease [32]. However, if an infected person cannot control the initial lung infection or if a latently infected person's immune system becomes weakened, the granuloma center may undergo a liquefication process by so far unknown process allowing the revived bacteria to multiply uncontrolled. Subsequently, viable bacteria can escape from the granuloma and spread within the lungs (active TB) and even to other tissues through the lymphatic system or the bloodstream [25].

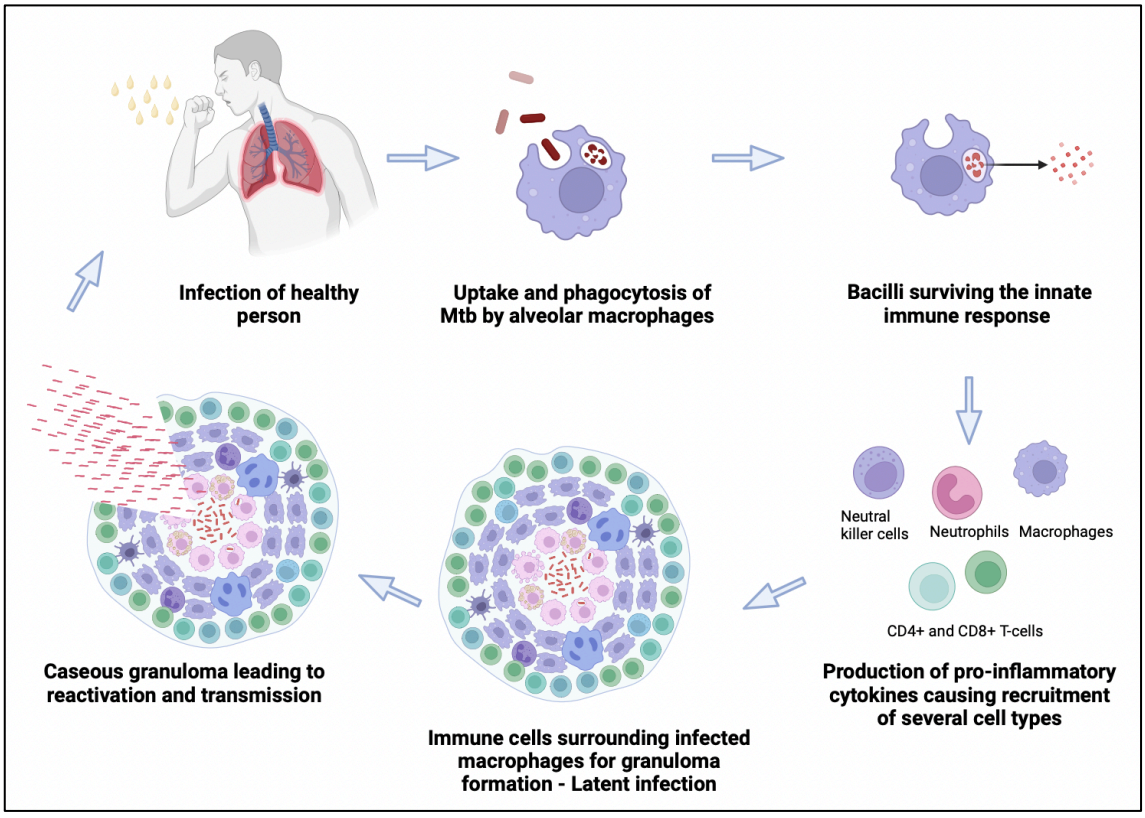

Figure 1: Pathogenic life cycle of *Mycobacterium tuberculosis.* *M. tuberculosis* infection starts when aerosols containing the bacteria from an active disease carrier reach the lungs of a new host. In the lung tissue, bacteria are taken up and phagocytized by alveolar macrophages. Infected macrophages lead to the recruitment of other immune cells, forming the granuloma. Under many circumstances, the infected granuloma can undergo necrosis, forming a necrotic core that supports bacterial growth and transmission to the next host. Figure adapted from Rahlwes, Kathryn et *al.* (2023) and Mukherjee, Srestha et *al.* (2023) using *biorender.com* [30, 33].

The complex and dynamic nature of the infection environment implies that *M. tuberculosis* must endure various stressors and possess the physiological adaptability to adjust to the changing surroundings. TB manifests in the described organized, inflammatory immune structures within the pulmonary lesions (granuloma), comprising a diverse array of cell types surrounding a core of extracellular or intracellular *M. tuberculosis* [21, 34]. Various types of lesions have been characterized, each with characteristic immune cell composition, organization, degrees of necrosis of host cells, and eventually cavitation [35, 36].

The lesion microenvironment, implicated by factors like lipid carbon sources and iron deprivation, or by stressors such as acidic pH and low oxygen levels, can induce a non-replicative or dormant state in *M. tuberculosis*. In a dormant state, *M. tuberculosis* has adapted to these

conditions with alterations in transcriptomic, proteomic, and metabolic activities often leading to high drug tolerance. This phenomenon of tolerance refers to cells that can survive lethal or inhibitory drug concentrations without possessing genetic resistance [37]. It allows a subpopulation of cells ("persisters") to survive extended periods without changing the minimum inhibitory concentration (MIC) for the whole population [37]. Mycobacterial cells are intrinsically heterogeneous in their drug response. Differential drug susceptibility at the single cell level, observed *in vitro* and specific to each drug [38], suggests that there is consistently a subset of *M. tuberculosis* cells that may tolerate a single-drug treatment.This poses a further challenge in clearing the disease as many drugs are designed to target actively replicating cells, limiting their effectiveness against non-replicating cells. However, there are also antibiotics developed that address both, or selectively non-replicating cells giving hope that treatment regimens can be found that kill replicating as well as non-replicating *M. tuberculosis* cells [39]. Targeting tolerant and dormant *M. tuberculosis* cells must be a focus of new TB-drug development.

1.1.3 Mycobacteria and their distinct cell envelope

Mycobacteria are non-sporogenic, rod-shaped bacteria that grow under microaerophilic conditions. The genus *Mycobacterium* comprises over 170 species that can be classified into three main types: (1) the species within the *Mycobacterium tuberculosis* complex (MTBC) – including *M. tuberculosis*, *M. bovis*, *M. africanum*, *M. microti*, *M. canettii*, *M. orygis*, *M. caprae*, *M. pinnipedii*, *M. suricattee*, and *M. mungi* – are responsible for human TB and share a genetic similarity over 99% nucleotide sequence identity [40, 41]; (2) mycobacteria that cause leprosy like *M. leprae*; and (3) non-tuberculous mycobacteria (NTM) such as *M. absecessus*, *M. avium*, *M. marinum*, and *M. smegmatis* that have the potential to cause diseases affecting the lungs, lymph nodes, or skin, particularly in individuals with compromised immune systems [42, 43].

Mycobacteria can survive under harsh environmental conditions over extended periods of time. One major reason for that is its unique, lipid-rich cell wall structure that provides a strong impermeable barrier against noxious compounds and drugs, playing a critical role in the virulence of these Gram-positive bacteria [44, 45]. The cell envelope of *M. tuberculosis* is composed of four main layers: the plasma membrane or inner membrane, the peptidoglycan-arabinogalactan (AGP) complex, an asymmetrical outer membrane, and the external capsule (Fig. 2).

The innermost membrane is the plasma membrane, which shares similarities with other bacterial membranes containing (glyco)lipids, lipoglycans, (lipo)proteins, and phospholipids such as phosphatidylethanolamine, phosphatidyl-*myo*-inositol (PI), cardiolipin, phosphatidylserine, and phosphatidylglycerol [46]. Phospholipids represent the basic structure of bacterial biomembranes, maintaining bilayer fluidity and supporting the stability [47]. It has been reported that certain phospholipids like the non-covalently linked PIs are essential for *M. tuberculosis* survival, and PI-based glycoconjugates can be found in the inner and outer membranes of all *Mycobacterium* species [48]. A prominent group of these molecules comprises the family of phosphatidyl-*myo*-inositol mannosides (PIMs) and their highly glycosylated counterparts, lipomannan (LM) and lipoarabinomannan (LAM) [49]. The innermost membrane is followed by the AGP, building the periplasmic space, which is comprised of peptidoglycan (PG) covalently attached to the heteropolysaccharide arabinogalactan (AG). The AG is, in turn, covalently attached to an asymmetrical outer bilayer membrane, the mycomembrane, via mycolic acids [33, 50]. The AG-bound mycolic acids form the bulk of the inner leaflet of the mycomembrane, while the outer leaflet consists of non-covalently attached (glyco)lipids and lipoglycans, such as PIM, LM, LAM, but also phthiocerol dimycocerosate (PDIM), mannosylated LAM (ManLAM) and trehalose-6,6'-dimycolate (TDM) mediate the adaptability of *M. tuberculosis* [44]. Together, the mycolyl-arabinogalactan-peptidoglycan (mAGP) complex is essential for viability of the bacilli, and enzymes involved in its biosynthesis are targets for several TB drugs [51, 52]. Finally, there is a loosely attached capsular-like structure around the mycomembrane, mainly composed of polysaccharides and proteins, with minor amounts of lipids. The outermost capsule is only weakly connected to the mycomembrane [53].

The organization of the *M. tuberculosis* cell envelope confers high intrinsic resistance to many therapeutic agents and the host's defense mechanisms [45, 51]. The latter is a further important function of the cell envelope due to its interference with the human immune response during infection. PDIMs and LAMs are, among others, responsible for the inactivation of macrophages and phagosomal escape of *M. tuberculosis* during infection [44]. Because of its unusual surface, functions, and the capacity to adapt to various stress conditions, *M. tuberculosis* has become a successful pathogen that quickly spreads through aerosols, infecting human hosts easily and thereby becoming a global epidemic.

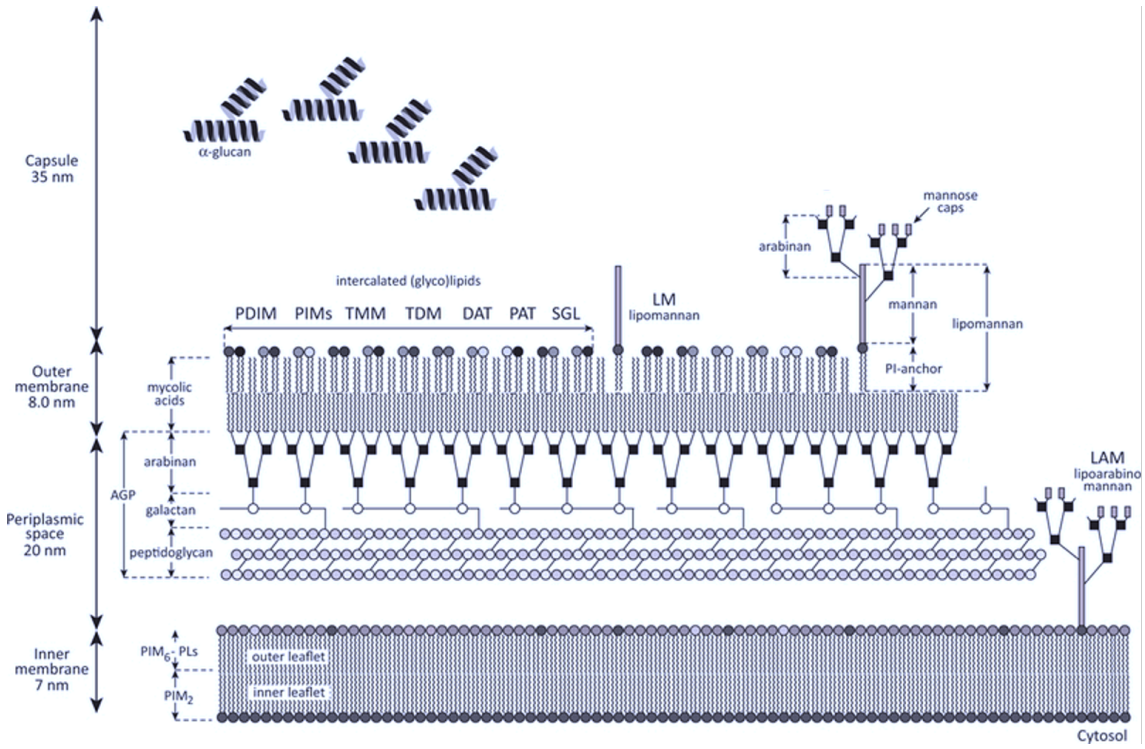

Figure 2: The *M. tuberculosis* cell envelope. The cell envelope of *M. tuberculosis* encompasses four main layers: (1) the plasma membrane (2) the peptidoglycan-arabinogalactan complex (AGP), (3) an assymetrical outer membrane or "mycomembrane", covalently linked to AGP via mycolic acisd, and (4) the external capsule. The inner leaflet of the outer membrane is composed of long chain (C60–C90) fatty acids, with the outer leaflet mostly including a variety of non-covalently attached (glyco)lipids and lipoglycans, including trehalose mono- (TMM) and dimycolates (TDM), sulfoglycolipids (SGL), phosphatidylinositol mannosides (PIMs), lipomannan (LM) and lipoarabinomannan (LAM), and lipoproteins/proteins, with some of them being glycosylated. The capsule mostly consists of neutral polysaccharides such as glycogen-like α-glucan and lower amounts of arabinomannan (AM) and mannan. Figure adapted from Kalscheuer et *al*. (2019) [44].

1.1.4 Prevalence and epidemiology of tuberculosis

Although *M. tuberculosis* is such an old infectious agent, TB continues to pose a significant global health threat in terms of its prevalence and infection rates. According to the WHO, TB is one of the top ten causes of death worldwide, with an estimated number of 10.6 million new cases and 1.4 million deaths (among HIV-negative people) occurring in 2021. Additionally, 187,000 deaths occurred among HIV-positive people [54]. Before the Coronavirus (COVID-19) pandemic, TB was even the leading cause of death worldwide from a single infectious agent, ranking above

HIV/AIDS. Over the past few years, as COVID-19 has dominated the scientific literature and the media, other infectious diseases like TB have been neglected [55]. Moreover, the COVID-19 pandemic has set back years of progress in TB control efforts, disrupting diagnosis, treatment, and prevention programs leading to increased TB cases and deaths. Above that, the health impacts of *M. tuberculosis* and COVID-19 co-infections are not fully understood. Both pathogens master immunomodulation and further research will be needed to clarify their potential interplay, and implications for co-infection in the lungs [56].

While many TB cases and deaths arise from primary TB occurring after initial infection, a quarter of the world's population is estimated to be infected latently. During LTBI, the bacteria can remain quiescent for years after the initial exposure before developing active disease [57, 58]. In fact, 5-10% of people infected with LTBI develop an active disease during their lifetime, and the risk is even higher for people harboring a weakened immune system, for example, due to co-infections. Geographically, TB disproportionately affects low- and middle-income countries (Fig. 3A). In 2021, most people who developed TB were living in South-East Asia (45%), Africa (23%), and the Western Pacific (18%). Factors that increase TB infection rates include undernourishment, HIV infection, alcohol use disorders, smoking, and diabetes [54].

In the last decades, the emergence of drug-resistant TB strains increased, and these resistant strains are now present in most countries. Resistance against rifampicin (RR-TB), being the most effective first-line drug, is of greatest concern. When resistance extends to both rifampicin and isoniazid, the phenomenon is defined as multidrug-resistant TB (MDR-TB), requiring treatment with second-line drugs. Extensively-drug resistant TB is a subgroup of MDR-TB with additional resistance to at least one of the fluoroquinolones and any of the injectable second-line drugs with very limited treatment options [59]. In 2021, there was an estimated number of 450,000 cases of drug-resistant TB, with the highest numbers found in the Russian Federation and several countries of Eastern Europe and Central Asia (Fig. 3B), representing an increase of 3.1% compared to 2020 [54]. Drug resistance occurs when anti-TB medications are compromised due to various factors, including improper prescription by healthcare professionals, usage of subpar medications, and early treatment discontinuation by individuals [60, 61].

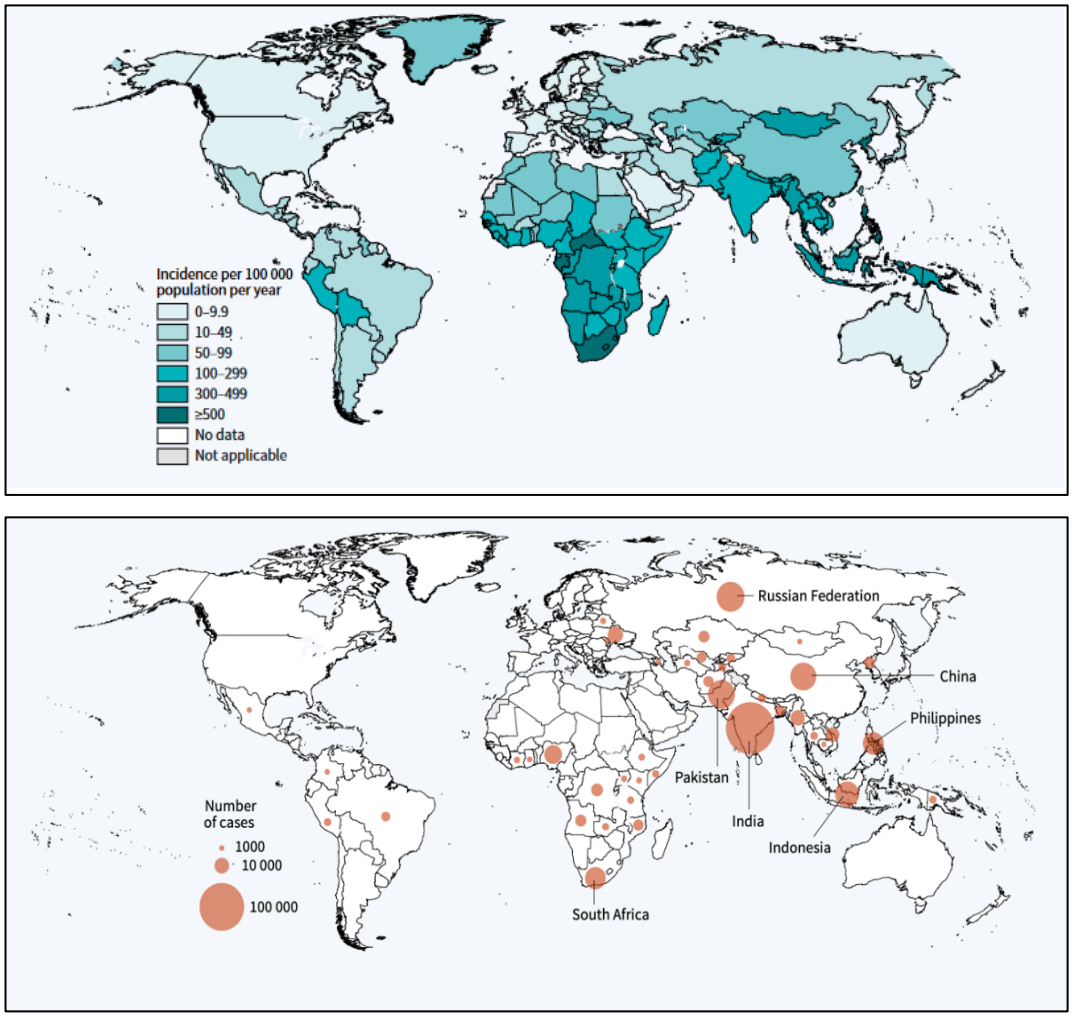

Figure 3: Estimated incidence rates of people infected with TB and rates of MDR-/RR-TB in 2021. A) More than ten million people fell ill with TB in 2021 with the highest number of cases in South East Asia, Africa, and the Western Pacific. **B)** Half a million people have been infected with drug-resistant TB with the highest proportions found in the Russian Federation and several countries of Eastern Europe and Central Asia. Estimated incidence rates are shown for countries with at least 1,000 incident cases, and the seven countries with the highest burden are labeled. Pictures adapted and data from WHO, Global Tuberculosis Report (2022) [54].

In recent years, collaborative efforts among researchers from academia, non-profit virtual R&D organizations, and industry have expanded the TB drug discovery pipeline. However, the cure rates of MDR-TB and XDR-TB remain low due to long-duration regimens, side effects, and poor patient adherence. To address this, there is a pressing need to develop novel TB drugs with new mechanisms of action and new treatment strategies.

1.2 Therapy of Tuberculosis

1.2.1 From palliative care to the golden era of antibiotics

Efforts to fight TB over the centuries have been met with tragedy and frustration [62]. Historically, TB treatment consisted of palliative care like herbal poultices, chemical preparations, dietary interventions, and climatic prescriptions as well as the isolation of infected patients to minimize the spread of the disease [63]. The first early successes in controlling the disease were attributed to the development of a new institution, the sanatoria. The establishment of these structures relied on Roman physicians, summarized in the Italian aphorism 'Lana, letto, latte' (wool, bed, milk) [63]. Despite the modest successes of sanatorium assistance in the early nineteenth century, TB continued to be the plague of society. In addition to deprivation and poor hygienic conditions, global conflicts empowered the spread of the disease dramatically. During the First World War, pulmonary TB decimated European soldiers in trenches, so a large number of veterans were admitted to sanatoria in the post-war period [64].

At the beginning of the 20th century, the first achievements were obtained in the development of antimicrobial agents. The discovery of penicillin in 1929 by Alexander Fleming was described as the first antibiotic successfully hampering bacterial growth [65]. Ernst Chain and Howard Florey designed the first methods for the large-scale extraction and purification of penicillin G, a β-lactam antibiotic, making it widely available by the mid-1940s [66]. This marked the beginning of the golden era of antibiotics between the 1940s and the 1970s accompanied by the discovery of several currently used antibiotic classes, like aminoglycosides, sulfonamides, and quinolones [67].

1.2.2 Antibiotics and Chemotherapy for drug-sensitive Tuberculosis

The discovery of new antibiotics brought hope for the cure of TB. Particularly the discovery of **streptomycin** (STREP) in 1944 represented a milestone for modern TB treatment. Selman Waksman and Albert Schatz demonstrated that STREP was 50 times more active against *M. tuberculosis* than the previous compounds that were isolated from bacteria of the order Actinomycetales [68-70]. A clinical trial conducted in 1948 revealed that STREP monotherapy improved the conditions of 51% of patients. However, the trial also uncovered that 20% of recruited patients developed resistance against streptomycin within the first 6 months [71].

STREP belongs to the aminoglycoside antibiotics which inhibit bacterial protein biosynthesis by binding to the 16S ribosomal RNA (16S rRNA) of the 30S ribosome 30 [72]. Resistance of *M. tuberculosis* against STREP is associated with mutations in the *rpsL* gene, encoding the ribosomal protein S12, or with base substitutions in the 16S rRNA [73].

At the same time, Jörgen Lehmann synthesized the **para-amino salt of salicylic acid** (PAS) with the help of the Swedish pharmaceutical company Ferosan [74, 75]. PAS disrupts folate metabolism by competitive binding to dihydrofolate reductase, thereby inhibiting the growth of bacteria [75]. Since PAS demonstrated its effectiveness against STREP-resistant strains of *M. tuberculosis*, it became evident shortly thereafter that employing a combination of those two agents could diminish the development of drug resistance shaping the future of TB clinical trials [71, 76, 77].

In the early 1950s, the exceptional anti-TB efficacy of **isoniazid** (INH) was demonstrated. This small compound, isonicotinyl hydrazine, which had been initially synthesized by Prague chemists Hans Meyer and Josef Mally in 1912, was simultaneously tested in three different laboratories in the early 1950s (Squibb, Hoffmann La Roche, and Bayer) [78, 79]. A range of clinical trials proved INH to be the most efficacious anti-TB drug yet discovered [63]. However, also a range of drug-resistant strains were occurring after INH monotherapy [80]. This finding quickly led to a three-drug combination therapy STREP+PAS+INH [81]. The combination proved to significantly increase cure rates in 90% of patients with as low as 4% disease relapse [62, 82, 83]. Unfortunately, it required up to 24 months of continuous treatment to achieve this, and INH is only active against replicating cells. INH is a nicotinamide analog that acts as a pro-drug being converted into a biologically active form by the *M. tuberculosis*-specific catalase-peroxidase KatG [84-86]. The active form of the drug, an isonicotinoyl radical reacts with nicotinamide adenine dinucleotide (NAD) coenzymes forming an INH-NAD+ adduct [87]. In addition to this mechanism, KatG triggers the peroxidation of INH to generate intracellular reactive INH-derived damaging species. A range of oxidants facilitates the oxidation of INH by KatG, encompassing superoxide, hydrogen peroxide, and alkyl hydroperoxides [88-90]. The primary mode of action of INH is inhibiting the synthesis of mycolic acids [91-93]. Two enzymes involved in the biosynthesis of mycolic acids have been proposed to be targeted by KatG-activated isoniazid: the NADH-dependent enoyl-acyl carrier protein reductase (InhA) and the β-ketoacyl acyl carrier protein synthase (KasA) [94-96]. Together with this, INH-derived radicals lead to respiratory inhibition by the formation of the antimycobacterial free radical NO·[97]. The inhibition of cell

wall lipids together with respiratory inhibition provides a potent anti-TB cocktail attacking several targets [98].

These improvements in the treatment of TB were significant but required continuous treatment for over 24 months. In the 1960s, PAS was replaced by **ethambutol** (EMB) leading to a shortened treatment duration (18 months) and a better tolerance of the drug regimen [99]. EMB was first discovered at Lederle Laboratories of American Cynamid showing a growth-inhibiting activity with a remarkable specificity against *M. tuberculosis* [99, 100]. Early mode-of-action studies showed that EMB is active only against replicating cells, where it was found to affect glycerol metabolism as well as RNA synthesis [101, 102]. Subsequent biochemical studies demonstrated that EMB induces an almost immediate accumulation of the major intermediate of arabinogalactan biosynthesis, β-d-arabinofuranosyl-1-monophosphodecaprenol. This is followed by the sequential accumulation of trehalose mono- and dimycolates and the inhibition of mycolic acid incorporation into the cell wall, suggesting that the primary inhibition of EMB is found at the polymerization step of the mycobacterial cell wall arabinan [103-107]. These findings were confirmed by genetic studies through generating EMB-resistant mutants harboring mutations in the three arabinosyltransferases EmbA, EmbB, and EmbC associated with AG and LAM-biosynthesis [107-109]. Interestingly, however, mycobacterial resistance to EMB seems to be multifaceted indicating that EMB has more than one *M. tuberculosis*-associated target while the exact mechanism of action is still under discussion [110].

The discovery of **pyrazinamide** (PZA) in 1952 was a further cornerstone antimicrobial drug used exclusively for the treatment of TB [111]. Despite PZA's remarkable *in vivo* activity, it was found to lack activity under typical *in vitro* conditions instead requiring incubation at an acidic pH (e.g. 5.5), similar to that occurring during active inflammation [112, 113]. PZA has a sterilizing effect on both, replicating and non-replicating cells and uniquely reduces the duration of chemotherapy from 9 to 6 months [114-117]. Studies of PZA’s mode of action by isolating PZA-resistant mutants revealed that it is another pro-drug hydrolyzed by an amidase, later found to be encoded by the gene *pncA* [118]. The hydrolyzation leads to the intracellular accumulation of its activated form, pyrazinoic acid (POA). The accumulation of POA was initially thought to be associated with dissipation of the mycobacterial membrane potential [119-121]. Further mechanistic models suggested that POA either inhibits mycobacterial fatty acid synthetase I [122] or that POA selectively inhibits *trans*-translation [123]. Most recently, it was proposed that POA interacts with the Coenzyme A (CoA) biosynthesis. This was demonstrated by sequencing of PZA-resistant mutants with a wildtype *pncA* gene revealing mutations in the *panD* gene (*rv3601c*). *PanD*

encodes L-aspartate decarboxylase, a rate-limiting step in the CoA biosynthetic pathway [124-126]. While comprehensive follow-up data demonstrated an incontrovertible association between POA and CoA metabolism, the clinical relevance of *panD* to PZA resistance demands further analysis [127]. Moreover, several other genes, like *clpC1,* have related to POA-resistance [119, 128]. ClpC1 is part of the *M. tuberculosis* caseinolytic protease complex displaying unfoldase and ATPase activities [129, 130]. However, despite the crucial role of PZA in modern TB therapy, the exact mechanism of action is still under discussion.

Rifampicin (RIF), a semisynthetic derivative of the natural product ansamycin, was discovered for its antimicrobial properties in the conditioned media of the soil bacterium *Nocardia mediterranei*, termed rifamycins. Despite being a minor constituent in the extract, rifamycin B gained potency upon incubation in oxygenated water due to the reversible oxidation of a "quinonoid-like" core and subsequent glycolic acid loss by hydrolyzation. This led to the more active rifamycins S and SV, with the latter being effective against *M. tuberculosis*. This insight into the structure-activity relationship (SAR) prompted efforts to enhance its bioavailability, resulting in the development of RIF in the 1960s. The compound's effectiveness was tied to specific molecular features like chain C21 and C23 hydroxyl groups, as well as C1 and C8 phenols [131]. Until today, resistance to RIF is a key factor for treatment failure and fatal clinical outcomes in TB patients [132]. Beyond its significant early bactericidal effect on metabolically active *M. tuberculosis*, RIF also demonstrates potent sterilizing activity on semi-dormant organisms that undergo brief bursts of metabolic activity. Recognizing this, combined with the enhanced efficacy of PZA, has led to a reduction of routine TB treatment from 1 year to 6 months [133]. Subsequent studies have shown that RIF inhibits mycobacterial transcription by targeting RNA-dependent RNA polymerase [134]. Further investigations verified that resistance to RIF develops due to mutations in a specific, well-defined region of the gene that encodes the ß-subunit of RNA polymerase (*rpoB*) [135]. Remarkably, over 96% of RIF-resistant strains carry mutations in the 81 bp region of *rpoB*, facilitating a rapid detection of rifampicin-resistance and/or multidrug-resistance [136].

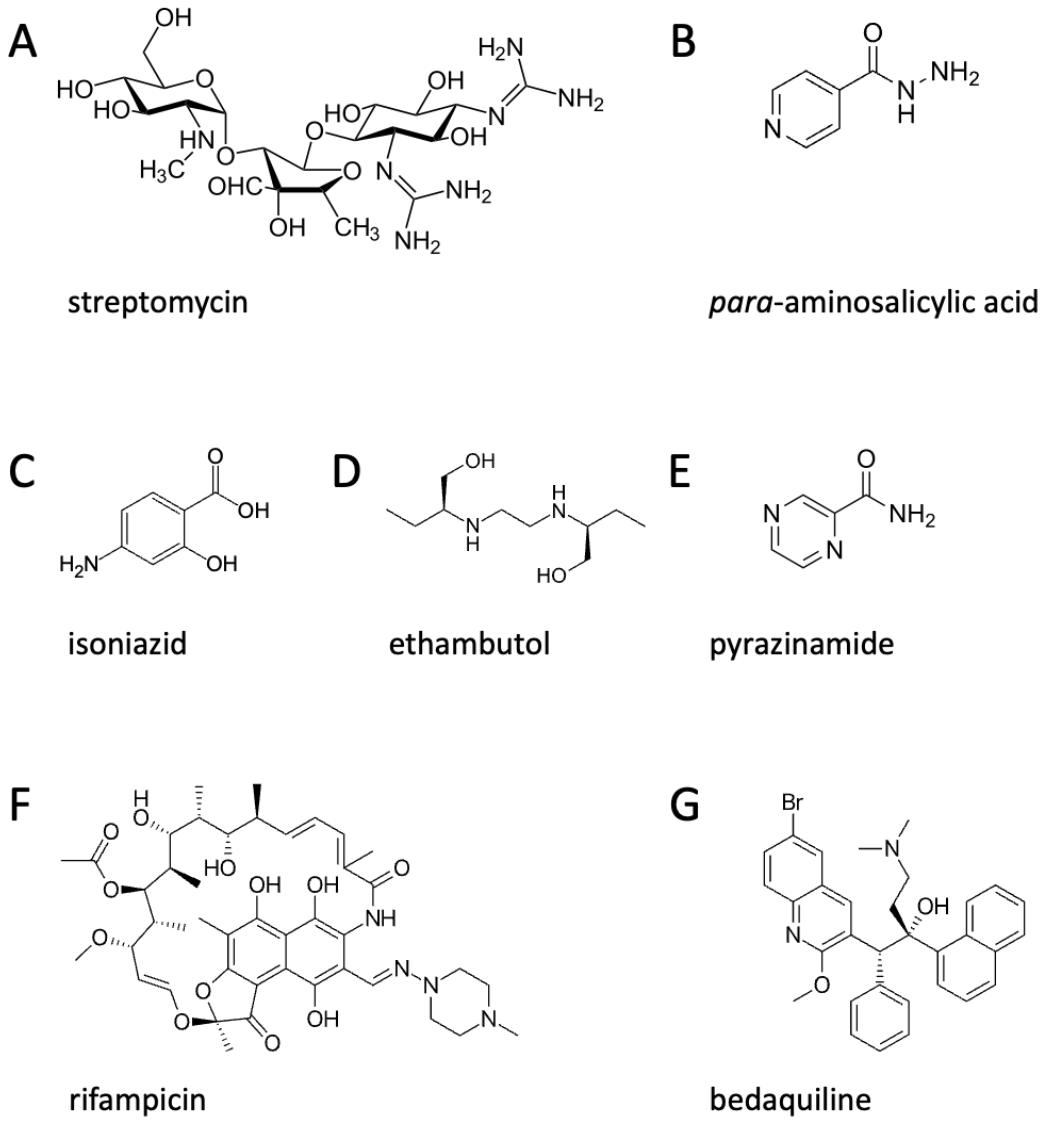

Figure 4: Chemical structures of drugs that were or are used for anti-TB treatment. A-B) Streptomycin and *para*-aminosalicylic acid were the first drugs used for treatment of TB. **C-F)** Isoniazid, ethambutol, pyrazinamide, and rifampicin are the current first-line drugs that are used in a combination therapy for treatment of drug-sensitive TB. **G)** Bedaquiline ist the first new compound since more than 40 years that got approved for TB-treatment and is implemented as a second-line drug for the therapy of drug-resistant TB.

One of the few new clinical drugs being approved for TB treatment in >40 years is **bedaquiline** (BDQ), a diarylquinolone [137]. Its discovery marked a milestone as the first FDA-approved drug emerging from the modern era of molecular sciences. Initially identified through a high-throughput screen against *M. smegmatis*, BDQ displayed effectiveness against *M. bovis* BCG and *M. tuberculosis* [138]. Stereoselective properties were revealed in early structure-activity relationship studies, favoring the (*R, S*) stereoisomer for higher potency against *M. tuberculosis*

[138, 139]. The drug also showcased activity against non-replicating, hypoxic *M. tuberculosis* [140]. In addition, BDQ demonstrated an unusual pattern of action, initially causing bacteriostatic effects before transitioning into a bactericidal phase, with a 4-fold $\log_{10}$ reduction in measurable colony-forming units by day 14 [141]. Insights into the functional target of BDQ revealed the *atpE* gene, which encodes the c-subunit of the F_0ATP synthase [138, 142, 143]. The role of ATP synthase in BDQ's mechanism was further supported by biochemical studies observing reductions in bacterial ATP levels [138-141]. While much evidence suggests that BDQ is targeting the ATP synthase, investigations into resistant mutants of clinical BDQ-resistant isolates revealed that only ~28% harbored mutations in *atpE,* while the rest remained unexplained [144]. A further resolved mechanism is associated with mutations in *Rv0678* that regulate the expression of the MmpS5-MmpL5 efflux pump [145]. A current meta-analysis analyzed all documented BDQ-resistant mutations within the genes *Rv0678*, *atpE*, *mmpL5*, *pepQ*, and *Rv1979* [146], indicating that there are no clear genotypic-phenotypic associations for BDQ which complicates efforts to develop rapid molecular assays for resistant isolates.

1.2.3 Development of drug-resistant TB

As indicated above, TB still requires a lengthy multi-drug combination therapy, given for several months, that has been used for more than 40 years. The current standard of care treatment for drug-sensitive TB involves a 6-months course with two different phases of treatment: During the initial phase of 2 months a combination of INH, RIF, PZA, and ETH is employed followed by a subsequent phase of four months using a two-drug regimen of INH and RIF. The estimated treatment success rate is around 85% [54, 83, 147]. Partially due to the long use of this drug regimen, drug-resistant strains are emerging. As mentioned in chapter 1.1.4, drug resistance in TB is divided into rifampicin-resistant TB (RR-TB), multidrug-resistant TB (MDR-TB), and extensively drug-resistant TB (XDR-TB). While RR-TB strains are monoresistant against RIF, MDR-TB strains are resistant towards RIF and INH. In the case of XDR-TB, resistances to RIF and INH, plus at least resistance to one second-line injectable aminoglycoside (e.g. amikacin and capreomycin) and one fluoroquinolone are present.

Antibiotic resistance has been a "hidden epidemic" still representing a multifaceted public health issue [60, 61, 148]. Recently, the WHO has approved several new drugs for MDR-TB treatment to complement existing tools. Among those is BDQ (described in chapter 1.2.2), which was recommended by the WHO in 2013 as a core drug in the treatment of drug-resistant TB [149] and has recently been identified as the key drug in assembling an all-oral, injectable-free drug regimen

in South Africa [150]. Additionally, two further pro-drugs have reached the market: delamanid which inhibits mycolic acid synthesis as well as pretomanid, which acts through mycolic acid synthesis inhibition and nitric oxide release, respectively [151-154]. Delamanid is a nitro-dihydro-imidazooxazole derivative that was approved for the treatment of MDR-TB by the European Medicines Agency in 2014 but has not yet received FDA approval [59, 155]. Pretomanid is a member of the nitro-imidazooxazines class and was approved by the FDA for the treatment of drug-resistant TB in 2019 [156-158].

To treat MDR-TB, a 4-5 drug regimen is needed with a treatment duration of up to 24 months [148]. In several nations, including India, XDR-TB has emerged as a new challenge to the control of TB [148]. Treatment of drug-resistant TB is even more difficult if co-infections with HIV, hepatitis B, or COVID-19 are present eventually leading to high mortality rates [159, 160]. To achieve high treatment success rates among MDR- and XDR-TB patients, personalized clinical approaches are vital as suggested by the ATS/CDC/ERS/IDSA guidelines, published in 2019 [59]. According to this, the initial phase of treatment should encompass five drugs, while the subsequent phase requires four drugs. The duration of treatment ranges from 15-21 months for MDR-TB and 14-24 months for XDR-TB patients [59]. The guideline outlines several steps for treatment. Prescriptions should involve one later-generation fluoroquinolones (e.g. moxifloxacin, levofloxacin) followed by two high-priority drugs (bedaquiline and linezolid). The next step should include two highly effective drugs such as clofazimine and D-cycloserine (DCS). If the strain's susceptibility pattern requires, injectable drugs (amikacin or STREP) are introduced. Notably, some drugs, like capreomycin and kanamycin, are no longer recommended due to limitations in terms of effectiveness, tolerability, and administration route. Injectable drugs, while effective, are being gradually replaced by more efficient and less toxic oral medications.

Although significant progress has been made in the development of drugs to treat drug-resistant TB infection, further studies and efforts are urgently required to find safe medications to combat this disease and to finally accelerate the goal of TB elimination.

1.3 Novel drug targets and strategies in *Mycobacterium tuberculosis*

With more than 480,000 reported cases of MDR-TB and 9.5% of reported cases of MDR-TB worldwide classified as XDR-TB, active drugs adressing new pharmacological targets and strategies are indeed needed. Currently, a diverse array of strategies is employed to develop new anti-TB therapies encompassing large-scale cell-based screening trials, virtual screenings, structural biology approaches, and the optimization of existent drugs through molecular modifications and genetic approaches for the identification of new molecular targets [161]. Another research focus is put on the development of novel vaccines as well as new therapeutical strategies such as host-directed therapy or the use of mycobacteriophages.

1.3.1 Advances in cell wall synthesis targets

As the cell wall of *M. tuberculosis* is the primary host-pathogen interaction spot, the inhibition of key enzymes that are responsible for the biosynthesis of these substructures are excellent targets for novel drug development due to the absence of homologous characteristics in the host [162]. An essential substructure of the mycobacterial cell wall is peptidoglycan, a heteropolysaccharide consisting of alternating *N*-acetylglucosamine (GlcNAc) and *N*-acetylmuramic acid (MurNAc) units, cross-linked with short peptides. The biosynthesis of peptidoglycan presents an appealing target for TB treatment, exemplified by the action of carbapenems. Carbapenems, which fall within the category of *β*-lactam antibiotics, possess a distinctive feature - they are not cleavable by *β*-lactamase, an enzyme produced by *M. tuberculosis*. With this, carbapenems can impede the biosynthesis of peptidoglycan by inhibiting L,D-transpeptidase and are included in the treatment of MDR-TB [59, 163, 164].

The mycolic acid layer, composed of long-chain α-alkyl β-hydroxy fatty acids (C60-90), provides the mycobacterial outer membrane with hydrophobic, impermeable, and rigid properties [165, 166]. Mycolic acids are synthesized from acetyl-CoA through at least two elongation systems, the type I and type II fatty acid synthases, also known as FAS-I and FAS-II. The FAS-II system can only be found in bacteria, thereby representing a potential selective antibacterial target. The NADH-dependent enzyme InhA, involved in the FAS-II system is inhibited by the first-line drug INH. The mechanism of action of other small molecules like ethionamide is also related to InhA inhibition [167, 168]. Nowadays, ethionamide is a second-line drug used for MDR-TB treatment. Another crucial enzyme, β-ketoacyl synthase KasA plays a key role in subsequent cycles of fatty

acid elongation, condensing FAS-I-derived acyl-CoAs with malonyl-ACP (acyl carrier protein). KasA is a reported and validated treatment target for TB, demonstrated by the development of JSF-3285, which has been optimized from the confirmed KasA inhibitor DG167 harboring increased anti-TB efficacy [169-171]. Mycolic acids are transported to the outer membrane due to the mycobacterial membrane protein large (MmpL) that is part of the resistance, nodulation, and cell division (RND) family. MmpL3, among the 13 encoded MmpL proteins in *M. tuberculosis*, contributes to outer membrane biosynthesis. The ethylenediamine derivative SQ109 is an MmpL3 inhibitor and has completed phase IIb - phase III clinical trials [172, 173].

The branched-chain AG is the major cell wall polysaccharide constituting about 35% of the cell wall dry mass and is comprised of arabinose and galactose residues, both in furanose configuration. This layer is covalently linked to the peptidoglycan and mycolic acid layers, necessitating several enzymes as potential targets for novel inhibitors targeting the AG formation [174-176]. Examples include arabinosyltransferase enzymes (EmbA, EmbB, and EmbC), which are targeted by the drug ETB [107, 109]. Another enzyme, arabinofuranosyltransferase (Aft), is crucial for the polymerization of arabinofuranyl residues from decaprenylphosphoryl-D-arabinose (DPA), the lipid donor of D-arabinofuranosyl residues for AG. The DPA synthetic pathway is a further potential drug target, with essential arabinosyltransferases like AftA, AftB, AftC, and AftD that are essential for *M. tuberculosis* growth [174, 177]. Moreover, the enzymes decaprenylphosphoryl-*β*-D-ribose 2′-oxidase (DprE1) and decaprenylphosphoryl-D-2-keto erythropentose reductase (DprE2) are crucial enzymes involved in the cell wall synthesis. DprE1 and DprE2 are catalyzing the conversion of decaprenyl-phospho-ribose (DPR) into decaprenyl-phospho-arabinose (DPA) [178, 179]. DprE1 was initially discovered as the target of benzothiazinones, however, several other compounds like azaindoles, aminoquinolones, benzothiazoles, dinitrobenzamides, nitrobenzamides, pyrazolopyridines, quinoxalines, triazoles, and thiadiazoles, demonstrated DprE1 inhibition [161, 180]. The benzothiazinone derivatives BTZ-043 and PBTZ169 are currently in phase II clinical trials, demonstrating a high efficacy against *M. tuberculosis*. Additionally, the non-covalent inhibitors, azaindole TBA-7371 and OPC-167832, currently in phase II and phases I/II clinical trials, respectively, have shown promising results [161, 181]. Overall, targeting various enzymes involved in the biosynthesis of *M. tuberculosis*'s cell wall layers offers encouraging potential for novel drug development to combat TB.

1.3.2 Progress in targeting energy metabolism

With the FDA's approval of the ATP synthase inhibitor BDQ, energy metabolism has become another main research focus as a novel pathway to exploit for TB drug development. This increased interest is due to the essential role of oxidative phosphorylation (OxPhos) and the maintenance of the transmembrane electrochemical gradient for the viability of both, replicating and non-replicating *M. tuberculosis* cells [182]. During OxPhos, electrons are transferred from the central metabolic pathways' donors to molecular oxygen via the electron transport chain (ETC), releasing energy. The released energy is conserved by proton-pumping transmembrane proteins, establishing a proton gradient, and thus generating an electrochemical gradient, called proton motive force (PMF). This bioenergetic pathway creates ATP through the phosphorylation of ADP [183, 184].

Recent discoveries have shown that targeting the terminal oxidases within the OxPhos results in effective growth inhibition of *M. tuberculosis*. Of particular importance is the cytochrome bc1-aa3 supercomplex, which has become a key player for promising drug candidates, demonstrated by the compound Telacebec (Q203), an imidazopyridine derivative, which is currently in phase II clinical trial [185]. Another promising candidate, TB47 showed activity against both drug-sensitive and -resistant strains [186]. Lansoprazole, a gastric proton pump inhibitor, emerged as a potent hit compound in the screening of FDA-approved drugs [187].

Along with the F_1F_0 ATP synthase and cytochrome oxidases, further enzymes like NADH dehydrogenases, succinate dehydrogenases, and menaquinone biosynthesis have come into the focus of interest. NADH dehydrogenases play a pivotal role in maintaining mycobacterial respiratory chain energization by using menaquinone as an electron carrier [188]. While type 1 proton-pumping NADH dehydrogenase (NDH-1) is non-essential for mycobacterial growth and persistence, NDH-2, which is widespread in bacteria but absent in mammals, holds promise as an anti-mycobacterial drug target [140, 189]. Due to the essentiality of the related menaquinone biosynthesis pathway, several chemical inhibitors targeting various enzymes, such as MenA, MenB, MenG, MenD, and MenE were reported to exhibit strong efficacy in inhibiting *M. tuberculosis* growth. Derivatives of the novel compound SQ109 are thought to disrupt the biosynthesis of the electron carrier menaquinone and the PMF through uncoupling activity [190]. All in all, the vulnerability of energy metabolism should be investigated further, creating an appealing drug target area.

1.3.3 Current status in vaccine development

Excitingly, cellular immunological mechanisms contribute to the control of TB, and it was demonstrated that TB vaccines are among the most promising candidates for reducing antimicrobial resistance [191]. That is why intensive emphasis of the last couple of decades has been focused on the development of new vaccine candidates based on killed pathogens, live attenuated agents, or subunit recombinant antigens formulated with adjuvants. Mathematical modeling by the WHO has predicted that an effective vaccine deployed for adults with 50% efficacy over 2025-2050 could cumulatively avert 37.2 - 76 million cases and 4.6 - 8.5 million deaths. Also, it would save up to 3 billion United States (US) dollars for treatment costs [192]. Very recently, the possibility of protecting global populations from viral pathogens, such as SARS-CoV-2, was transformed due to massive funding and rapid advances in RNA-based vaccines for immunization. However, similar efforts to combat bacterial pathogens like *M. tuberculosis* have been significantly slower to implement [191, 193].

Over 90 years ago, in 1928, the initial anti-TB vaccine was introduced as an attenuated live strain derived from *M. bovis*, known as BCG-Pasteur. Notably, this vaccine was primarily developed by Albert Calmette and Camille-Guérin at the Pasteur-Institute [194], and > 4 billion doses have been administered in total with ca. 120 million vaccinations per year to prevent severe forms of TB [195]. While the vaccine protects infants and children from severe extrapulmonary TB, its efficacy in preventing the global TB epidemic is limited [196]. It inadequately protects adults from pulmonary TB, as after being administered only once at birth, the protection only lasts up to a decade. Additionally, BCG vaccination is not recommended for HIV-exposed infants, as studies from regions like Argentina and South Africa indicate a heightened risk of BCG-related diseases in children who later develop AIDS [197-199]. So, the question evolves if there are any advances in novel vaccine development for TB.

According to the WHO COVID-19 Vaccine Tracker, within a time of only 3 years, more than 50 vaccines against SARS-CoV-2 have received approval, with an additional 183 candidates undergoing clinical trials [200]. Compared to this, the TB vaccine development pipeline currently only contains a meager number of 16 candidates, and, in the near future, approval of a new vaccine remains uncertain [201]. As pointed out by the Treatment Action Group, the TB vaccine research process remains hampered by insufficient global investment [202] but also due to a lack of complete understanding of the human immune response to this complex pathogen and an absence of validated animal models predictive of human vaccine efficacy.

However, there is also some hope: two positive proof of concept efficacy trials for TB vaccine candidates have been completed recently. In 2019, a promising phase IIb study was published demonstrating the effectiveness of a candidate called M72/AS01$_E$ (GlaxoSmithKline) in preventing pulmonary TB among adults with latent TB infection [203]. The vaccine contains a recombinant fusion protein derived from two *M. tuberculosis* antigens (Mtb32A and Mtb39A), combined with the AS01$_E$ adjuvant system [203]. Vaccine recipients in Kenya, Zambia, and South Africa received two doses of the novel vaccine for one month apart and, over a mean follow-up of 36 months, had 50% fewer cases of bacteriologically confirmed active TB than controls. It was well tolerated and provided critical proof of principle for vaccine-induced immunological control of latent TB infection [204].

The second promising candidate is H4:IC31, a subunit vaccine, consisting of mycobacterial antigens Ag85B and TB10.4, or BCG reactivation [205]. The latter is based on the first indications that BCG reactivation offers moderate protection against infection. This reported randomized, controlled, and partially blinded trial (designated C-040-404; NCT02075203) aimed to assess the efficacy of BCG revaccination and the novel candidate, H4:IC31, in preventing initial or sustained *M. tuberculosis* infection – each of them compared to a placebo. The study included 990 adolescents in the Western Cape of South Africa, equally distributed among the three arms. While neither candidate showed statistically significant protection against the primary endpoint of initial IGRA conversion (defined as conversion from negative to positive of an *M. tuberculosis*-specific Interferon Gamma Release Assay), BCG reactivation demonstrated 45.4% efficacy in preventing sustained conversion (secondary endpoint) reflecting prevention of LTBI. Follow-up studies showed that the protection against sustained *M. tuberculosis* infection conferred by BCG reactivation might rely on multiple immune cell subsets such as CD4 T cells [205]. As BCG is an already licensed intervention, BCG reactivation could represent a useful tool for controlling *M. tuberculosis* infection in populations with a high risk of infection. However, safety and efficacy in HIV-infected, immunocompromised persons need to be further evaluated before implementation.

The success of the first licensed mRNA-based vaccines against COVID-19 has also created a widespread interest in mRNA technology for TB vaccines. Interestingly, the first proof of concepts of an mRNA vaccine against TB was reported already in 2004 [206]. Very recently, almost 20 years later, BioNTech has launched a phase I clinical trial evaluating two investigational RNA-based TB vaccines in BCG-vaccinated volunteers. The global response to

the COVID-19 pandemic highlights how billions of research dollars, innovation, and collaboration resulted in enormous success against the SARS-CoV-2 virus. If the technologies discussed (drug development; drug-targeting strategies; vaccine development) and strategies that were not covered in this article (such as host-directed-therapies [207]; mycobacteriophages [208]) will be applied just as extensively, they could potentially get us closer to our goal of ending TB and, of major importance, to prevent the TB-epidemic from developing into a drug-resistant pandemic.

2. Aim of the thesis

Infectious illnesses claim millions of lives annually. The rise of antibiotic resistance makes a global bacterial pandemic a highly likely future event, urgently calling for research into new antibiotic compounds and approaches. One of the major contributors to the current antimicrobial resistance crisis is *M. tuberculosis*, the causative agent of TB. This study aimed to identify potential new leads and targets for the development and optimization of anti-TB drugs.

Searching after new antibacterial compounds the research of this study described in chapter 3 focused on the functional characterization of α-aminooxyacetic acid derivatives as potential novel antitubercular lead structures. Given that whole genome sequencing of spontaneously resistant mutants indicated that these compounds are likely acting as pro-drugs, this work focused on characterizing the role of the amidohydrolases AmiC and Rv0552 in the mechanism of resistance. This entailed employing genetic modifications, protein isolations, enzymatic activity testing, and structure homology analyses. Furthermore, the mode of action required comprehensive elucidation through proteomic, transcriptomic, and genetic interaction mapping analyses. Bioinformatic pipelines needed to be established and applied.

In chapter 4, the goal was to investigate the function and essentiality of the *M. tuberculosis Rv3277* gene, and its *M. smegmatis* homolog, *MSMEG_1817,* that are involved in the fundamental biosynthesis steps within the complex and unique mycobacterial cell wall. This was done as a means of identifying potential drug targets. The objective was to unravel the role of these floppase-like proteins in cell wall mannosylation and arabinosylation by working with generated conditional *M. tuberculosis* and *M. smegmatis* mutants allowing regulated gene silencing. The generation and analysis of whole-cell lipid and arabinogalactan extracts was required, as was the implementation of follow-up experiments, such as scanning electron microscopy of silenced cells.

The final sections of this research (chapters 5 and 6) endeavored to introduce a novel antibiotic strategy by developing a broadly applicable approach for a new type of antibiotic. The intention was to design bacterial proteolysis targeting chimeras (BacPROTACs) and to further prove their selective degradation of bacterial proteins. Structural and functional elucidations of these compounds aimed to clarify a hitherto unknown mycobacterial defense mechanism, circumventing the resistance mechanism. To this end, gene deletion mutants were generated and whole cell protein lysates were extracted for quantitative proteomics.

3. α-Aminooxyacetic acid derivatives acting as pro-drugs against *Mycobacterium tuberculosis*

Posted preprint on bioRxiv
doi: 10.1101/2024.04.04.587628

Contribution:

- Writing of the manuscript draft
- Cultivation of bacterial strains
- Determination of minimal inhibitory concentrations against *M. tuberculosis* and other *Mycobacteriaceae* via resazurin dye reduction method
- Activity assay against replicating and non-replicating starvation-induced *M. tuberculosis* cells
- Structure-activity relationship analysis of anti-TB drug derivatives
- Isolation of spontaneous KSK-resistant mutants
- Isolation of genomic DNA
- Whole genome sequencing analysis of spontaneous KSK-resistant mutants
- Genetic manipulation of *M. tuberculosis, M. bovis,* and *M. smegmatis* cells to generate various gene deletion mutants, complemented gene deletion mutants, and merodiploid strains
- Structure homology modeling
- Heterologous expression and purification of recombinant proteins in *E. coli* followed by enzymatic activity testing
- Isolation of total genomic RNA followed by quantitative real-time PCR and RNA-seq analysis
- Analysis of RNA-seq by using a high-performance computing system and establishing a pipeline for trimming, mapping, counting of reads and differential expression analysis
- Generation of a transposon mutant library in *M. tuberculosis* H37Ra
- Analysis of transposon insertion sequencing (TnSeq) analysis by using a high-performance computing system and establishing a pipeline for trimming, mapping and counting of reads per TA site followed by the generation of wig-files for the use of the software TRANSIT
- Analysis of synergistic effects by performing checkerboard synergy assays

3.1 Manuscript

α-Aminooxyacetic acid derivatives acting as pro-drugs against *Mycobacterium tuberculosis*

Kristin Vill [1,*], Lasse van Geelen [1,*], Oliver Michel [2,*], Anna-Lene Kiffe-Delf [1], Alexander Berger [2], David Podlesainski [3], Katharina Stenzel [2], Filip Kovacic [4,¶], Beate Lungerich [2], Tanja Gangnus [5], Haidara Majid [5], Bjoern B. Burckhardt [5], Taylor A. Crooks [6], Michael D. Howe [6], Lev Ostrer [6], Ziyi Jia [6], Thomas R. Ioerger [7], Farnusch Kaschani [3], Markus Kaiser [3], Anthony D. Baughn [6], Thomas Kurz [2, §], and Rainer Kalscheuer [1,§]

[1] Heinrich Heine University Düsseldorf, Faculty of Mathematics and Natural Sciences, Institute of Pharmaceutical Biology and Biotechnology, 40225 Düsseldorf, Germany

[2] Heinrich Heine University Düsseldorf, Faculty of Mathematics and Natural Sciences, Institute of Pharmaceutical and Medicinal Chemistry, 40225 Düsseldorf, Germany

[3] Department of Chemical Biology, ZMB, Faculty of Biology, University of Duisburg-Essen, 45177 Essen, Germany

[4] Heinrich Heine University Düsseldorf, Forschungszentrum Jülich, Institute of Molecular Enzyme Technology, 52428 Jülich, Germany

[5] Individualized Pharmacotherapy, Institute of Pharmaceutical and Medicinal Chemistry, University of Münster, 48149 Münster, Germany

[6] Department of Microbiology and Immunology, University of Minnesota Medical School, MN 55455, Minneapolis, USA

[7] Department of Computer Science, Texas A&M University, College Station, Texas 77843, United States

¶ Present address:
Department of Surgery, Massachusetts General Hospital, and Harvard Medical School, Boston, Massachusetts, USA.
Department of Microbiology, Harvard Medical School, Boston, Massachusetts, USA

* These authors contributed equally
§ Authors for correspondence: rainer.kalscheuer@hhu.de, thomas.kurz@hhu.de

ABSTRACT

The emergence of multidrug-resistant strains is exacerbating the treatment of tuberculosis (TB). Therefore, there is an immediate necessity to uncover anti-TB compounds with unprecedented targets. This study introduces antimycobacterial molecules with α-aminooxyacetic acid core structures. The lead compounds KSK-104 and KSK-106 displayed sub-micromolar antibacterial activity against *Mycobacterium tuberculosis* H37Rv and XDR clinical isolates, with no cytotoxicity against human cells. Genetic studies with spontaneously resistant mutants suggested that the compounds are pro-drugs that are intracellularly hydrolyzed by one or both of two specific amidohydrolases, Rv0552 and AmiC. Furthermore, proteomic and transcriptomic analyses and genetic interaction mapping employing transposon insertion sequencing suggest a "dirty drug" mechanism that involves the attack of the various drug cleavage products on multiple intracellular targets. Our results suggest a role of the pyridoxal 5'-phosphate (PLP) synthesis and salvage pathway and/or PLP-dependent enzymes, the oxidative stress network, and of the *Rv3092c-Rv3095* gene cluster in the mode of action.

INTRODUCTION

Tuberculosis (TB) is among the oldest illnesses affecting humanity. Caused by the pathogen *Mycobacterium tuberculosis*, it continues to pose a global health concern, accounting for 1.6 million deaths in 2021.[1] The drugs currently utilized as front-line chemotherapy (isoniazid, rifampicin, pyrazinamide, and ethambutol) were developed over half a century ago with clinical trials determining their optimal combination and duration being mainly conducted in the 1970s.[2] Although the standard treatment is safe and well-tolerated, treatment of drug-sensitive TB requires a combination therapy for six months, which frequently leads to patients' non-adherence and the emergence of drug resistance. The current situation appears grim due to the spread of multidrug (MDR) and extensively drug-resistant (XDR) strains, the fatal combination of TB with HIV/AIDS infection, and the recent setback caused by the coronavirus disease (COVID-19) pandemic, which has led to inadequate TB diagnoses and treatments.[1,3] Recent advances in the development of drugs against drug-resistant TB led to the regulatory approval of bedaquiline, delamanid, and pretomanid, as well as the entry into clinical trials of several new compounds.[4] Furthermore, the development of regimens that shorten treatment is a promising and active research area.[5] While this offers hope for patients, there remains an urgent need to develop novel promising treatments addressing the drug-resistant TB crisis in the future, considering that drug development is a lengthy and risky process. Yet, the development of faster-acting TB drugs with a low risk of resistance remains a challenge, mainly due to the complex biology of the pathogen and the extraordinary pathology of the disease itself. To this end, it is essential to gain a deep understanding of the mode of action of novel compounds and the strategies employed by *M. tuberculosis* to resist their antibacterial effect.

In recent years, high-throughput small molecule library screening campaigns employing *in vitro* cultured *M. tuberculosis* has led to the discovery of several novel growth inhibitors from previously unexplored chemical classes, highlighting the untapped potential of molecules that were previously not envisioned to exhibit activity against the pathogen. Following the same approach by screening of an in-house compound library of the research group Kurz, we identified α-aminooxyacetic acid derivatives as promising novel anti-TB lead compounds. The front-runner compounds, KSK-104 and KSK-106, are *para*-substituted benzoylated derivatives of 2-aminoxy-*N*-(benzyloxy)acetamide. A 1971 patent by Kisfaludy *et al.* first described α-aminooxyhydroxamic acid derivatives as compounds with antimycobacterial activity.[6] However, to the best of our knowledge, no data on their mechanism of action or molecular target have been published, and the development was discontinued for unknown reasons after two follow-up studies in the 1970s. *para*-Substituted benzoylated derivatives of 2-aminoxy-*N*-

(benzyloxy)acetamide such as KSK-104 and KSK-106, which differ from the earlier described compounds, have not been previously reported, nor have their antitubercular activities been evaluated in detail.

Here, we report on the synthesis and anti-tubercular properties of these novel alkoxyamide lead structures. We furthermore provide evidence suggesting that they represent pro-drugs that are activated following intracellular hydrolysis by the putative amidohydrolases AmiC and Rv0552, releasing different active metabolites that act as "dirty drugs" pleiotropically targeting different intracellular pathways, including pyridoxal 5'-phosphate (PLP) synthesis and salvage and/or PLP-dependent pathways, the oxidative stress network as well as the yet uncharacterized *Rv3092c-Rv3095* operon.

RESULTS

Novel α-aminooxyacetic acid molecules as potent anti-TB lead structures.

The potential of α-aminooxyacetic acid molecules to act as antimycobacterials, has been described back in 1971 by Kisfaludy *et al.*.[6] However, although some follow-up studies indicated promising *in vitro* and *in vivo* activity, further reports on the characterization of the molecules for the development of new anti-tuberculosis agents have been missing.[6] It therefore remained unclear how α-aminooxyacetic acid derivatives impact *M. tuberculosis* physiology and growth. During the screening of an in-house α-aminooxyacetic acid compound library, we found two novel compounds, KSK-104 and KSK-106 (subsequently collectively referred to as KSKs) exhibiting potent antibacterial *in-vitro* growth inhibitory activity against cells of the laboratory strain *M. tuberculosis* H37Rv. The structure of both molecules consists of three distinct regions: region B with an aminooxyacetyl backbone, region C with a benzyloxyamine group, and variable region A, occupied by a *para*-phenyl substituted benzoyl group in KSK-104, or a *para*-pentoxy substituted benzoyl group in case of KSK-106 (Figure 1A).

We found that both KSKs show sub-micromolar minimum inhibitory concentrations for inhibiting at least 90% of growth compared to respective solvent controls (MIC_{90}) with KSK-104 having an MIC_{90} of 0.78 µM and KSK-106 of 0.39 µM (Figure 1B). Importantly, extensively drug-resistant (XDR) clinical isolates of *M. tuberculosis* originating from the KwaZulu-Natal region in South Africa were also susceptible to the KSKs with MIC_{90} values ranging from 0.78 to 3.125 µM (Figure 1C). This indicates that the KSKs do not share a similar mechanism of action compared to the clinically used drugs, to which the tested *M. tuberculosis* XDR strains are resistant.

A

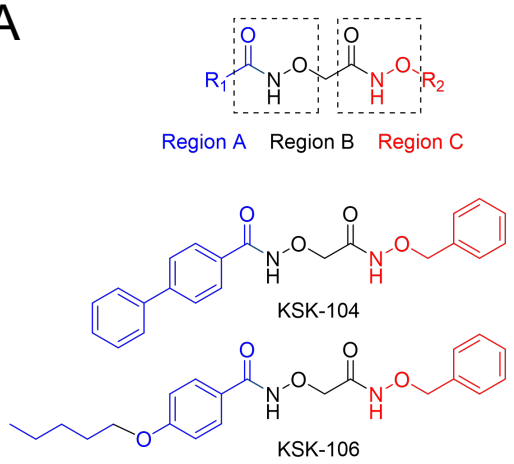

B

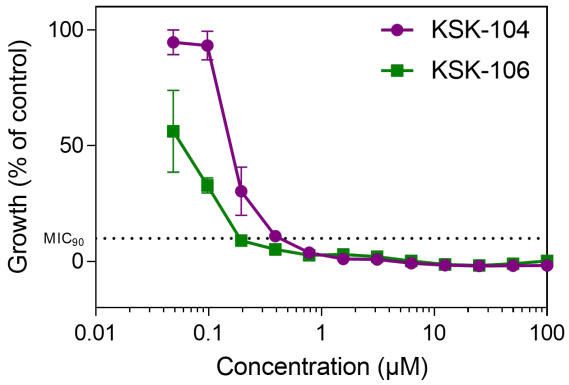

C

Strain	KSK-104	KSK-106	RIF
M. tuberculosis H37Rv	0.78	0.39	0.19
M. tuberculosis mc²6230	0.39	0.78	0.097
M. tuberculosis CDC1551	0.78	0.78	1.56
M. tuberculosis Erdman	0.19	0.19	0.097
M. tuberculosis KZN06	1.56	1.56	>100
M. tuberculosis KZN07	1.56	1.56	>100
M. tuberculosis KZN13	3.125	1.56	>100
M. tuberculosis KZN14	1.56	1.56	>100
M. tuberculosis KZN15	1.56	1.56	>100
M. tuberculosis KZN16	3.125	1.56	>100

Figure 1. Structures of KSK molecules and antibacterial activity against *M. tuberculosis*.
A) Chemical structures of the α-aminooxyacetic derivatives KSK-104 and KSK-106 indicating three regions. The alkoxyamide and benzyloxamide moieties/structures are boxed. **B)** Dose-response curves for KSK-104 and KSK-106 demonstrating a concentration-dependent inhibition of *M. tuberculosis* H37Rv growth. Data are shown as means of triplicates with SD. **C)** MIC_{90} values of rifampicin (RIF), KSK-104 and KSK-106 for various *M. tuberculosis* laboratory strains and for clinical XDR isolates (KZN) originating from the KwaZulu-Natal region, South Africa. Growth was quantified by employing the resazurin reduction assay. Data represent a single experiment with $n = 3$ with no variations in MIC_{90} values observed between individual samples.

Next, we established a flexible straightforward synthesis route for KSK-104 and KSK-106 to obtain sufficient amounts of these novel anti-TB lead structures for pharmacological tests and to enable their optimization through chemical derivatization (Scheme 1).

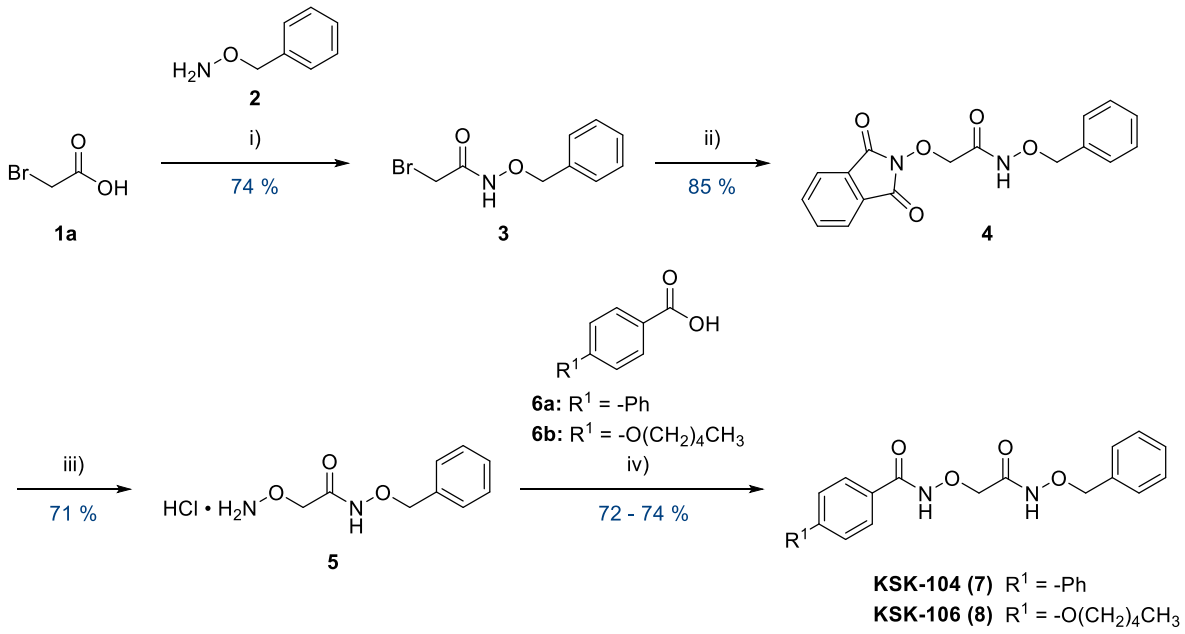

Scheme 1. Synthesis of novel anti-TB lead structures KSK-104 and KSK-106. i) 1.00 eq. IBCF, 1.00 eq. NMM, THF, -20 °C to rt, 16 h; ii) 1.15 eq. NHPI, 1.15 eq. NEt_3, MeCN, reflux, 4 h; iii) 4.00 eq. methylhydrazine, 4.00 eq. HCL in dioxane (4 M), CH_2Cl_2, -10 °C, 16 h; iv) 1.25 eq. EDC·HCl, 0.10 eq. DMAP, 1.20 eq. Et_3N, CH_2Cl_2, rt, 16 h.

The protected intermediate **3** was synthesized via a coupling reaction mediated by isobutylchloroformiate (IBCF) and *N*-methylmorpholine (NMM) between bromoacetic acid (**1a**) and *O*-benzylhydroxylamine (**2**), using a mixed anhydride as the acylating intermediate. The subsequent alkylation of *N*-hydroxyphthalimide (NHPI) with **3** yielded the phthaloyl-protected hydroxylamine **4**. Deprotection of **4** was achieved through methylhydrazinolysis, and the resulting hydroxylamine **5** was isolated as hydrochloride. Finally, EDC-mediated coupling reactions were performed for the acylation of **5**, using either 4-phenylbenzoic acid (**6a**) or 4-pentyloxybenzoic acid (**6b**), to produce KSK-104 (**7**) with a yield of 72% or KSK-106 (**8**) with a yield of 74%, respectively.

The stability of both lead structures, KSK-104 and KSK-106, in aqueous media or human EDTA-plasma was tested at 37 °C to evaluate their suitability for further drug development. In aqueous media, both lead structures exhibited only minor degradation (<4%) over 48 hours both at pH and pH 7.4, respectively (Figure S1, Supporting Information). No degradation of KSK-104 in EDTA-plasma could be detected after 24 h (Figure S2A). KSK-106 showed high stability with

no measurable degradation after 6 hours in human EDTA plasma, and only 20% degradation after 24 hours, giving a calculated half-life of 77.9 hours ex vivo. In whole blood, KSK-106 was less stable, and degraded within 24 hours to 38.4% (ex vivo t1/2 = 18.1 h). The blood-to-plasma ratio was assessed as 0.643±0.046 for KSK-106 in two donors (each n=3), indicating minor distribution into erythrocytes (Figure S2B). Furthermore, good oral bioavailability of more than 60% and 80%, respectively, is suggested for KSK 106, by the P_{app} values of $2.52*10^{-6}$ cm/s for the oily formulation and $1.12 *10^{-5}$ cm/s for the Tween 80/ethanol formulation considering passive membrane transport only (Figure S2C).[7] These results indicate appropriate stability in conditions mimicking physiologically relevant conditions and good permeability.

KSK-104 and KSK-106 are bactericidal and selectively active against tuberculous mycobacteria.

We continued our investigations of the KSKs by characterizing their anti-tubercular and cytotoxicity profiles. We found that KSK-104 and KSK-106 were specifically active against *M. tuberculosis* and *M. bovis* BCG Pasteur, while no growth inhibition of other tested fast-growing mycobacteria such as *Mycobacterium marinum*, *Mycobacterium abscessus* and *Mycobacterium smegmatis* was observed. These results indicate that the compounds are only effective against tuberculous mycobacteria (Figure S3A). Additionally, the compounds have been tested against several nosocomial bacteria and fungi, such as *Staphylococcus aureus* Mu50, *Acinetobacter baumannii* ATCC BAA-1605, *Pseudomonas aeruginosa* ATCC 27853, and *Candida albicans* ATCC 24433 (Figure S3A). Growth of none of these pathogens was affected by the treatment with KSKs suggesting a specific tuberculous mechanism and/or target of the novel compounds. Of note, KSK-104, and KSK-106 showed no cytotoxic effects on various human cell lines originating from different tissues at concentrations up to 100 μM (Figure S3B).

We then monitored the anti-TB effects of both molecules over 35 days performing a time-killing kinetic to investigate how KSK-104 and KSK-106 exert their growth inhibition on *M. tuberculosis*. Both KSK-104 and KSK-106 exhibited a bactericidal effect within the first 9 days of incubation, resulting in a 2 - 3-$\log_{10}$ reduction in viable cell counts as determined by quantifying colony forming units (CFU) (Figure 2A). No further reduction in viability occurred after day 9; in contrast to the tested clinical drugs, however, CFU counts remained constant and no resumption of growth was observed in monotreatment (Figure S4). Since the standard treatment of TB requires a combination therapy employing four different drugs,[8,9] we tested KSK-104 and KSK-106 in combination with the first-line antibiotics isoniazid, rifampicin, and ethambutol as well as with delamanid and bedaquiline (Figure S4). Both KSK compounds showed

an additive effect in combination with isoniazid, rifampicin, ethambutol, and delamanid, indicated by a reduction of viable cell counts to the detection limit of 10^2 CFU/mL. Furthermore, particularly the combination with KSK-106 efficiently suppressed the resurgence of surviving bacteria even after 35 days of incubation. In contrast, bedaquiline substantially dampened the bactericidal effect of KSK compounds, indicating antagonistic drug-drug interference.

M. tuberculosis is an intracellular pathogen, mainly residing and replicating in phagolysosomes of macrophages thereby escaping the immune response mechanisms of the infected host.[10,11] To evaluate whether the KSKs also interfere with intracellular growth, we employed a THP-1 human macrophage infection model that relies on quantifying cell growth of a mCherry-expressing fluorescent *M. tuberculosis* reporter strain. While macrophages treated with the solvent control (DMSO) exhibited a high intracellular bacterial burden, both KSK compounds substantially inhibited intracellular proliferation of *M. tuberculosis* and resulted in a healthy morphology of the treated macrophages (Figure 2B). Remarkably, treatment of infected THP-1 cells with either KSK-104 or KSK-106 at 0.5 μM resulted in bacterial fluorescence lower than the rifampicin (3 μM) and streptomycin (20 μM) controls. These results indicate a stronger potency of both KSKs in killing intracellular *M. tuberculosis* residing in human macrophages (Figure 2B). These results were confirmed by counting CFU after plating bacteria isolated from THP-1 cells infected with the non-fluorescent parental *M. tuberculosis* H37Rv strain (Figure 2C). Conclusively, KSKs can enter relevant human target immune cells and inhibit *M. tuberculosis* growth with higher efficiency than the tested first-line drugs.

The duration of TB therapy is lengthy, in part because current anti-TB drugs are mainly effective against actively growing, replicating mycobacteria, but considerably less active against non-replicating bacteria.[12] Therefore, drugs that inhibit these non-replicating persisting *M. tuberculosis* cells that are known to be highly tolerant against a multitude of clinical drugs are desired.[13] We thus evaluated the activity of the KSKs against both replicating and starvation-induced non-replicating cells of *M. tuberculosis* H37Rv in comparison to the first- and second-line drugs bedaquiline, D-cycloserine, rifampicin, ethambutol, moxifloxacin and delamanid (Figure 2D). While replicating cells were sensitive to all tested compounds including the KSKs, the starvation-induced non-replicating cells were highly tolerant to all tested antimycobacterials, with none of them completely inhibiting growth even at the highest tested concentration. While bedaquiline showed highest potency, KSK-104 and KSK-106 demonstrated at least some activity comparable to that of rifampicin, moxifloxacin, and delamanid. In contrast, D-cycloserine and ethambutol showed no activity against non-replicating cells (Figure 2D).

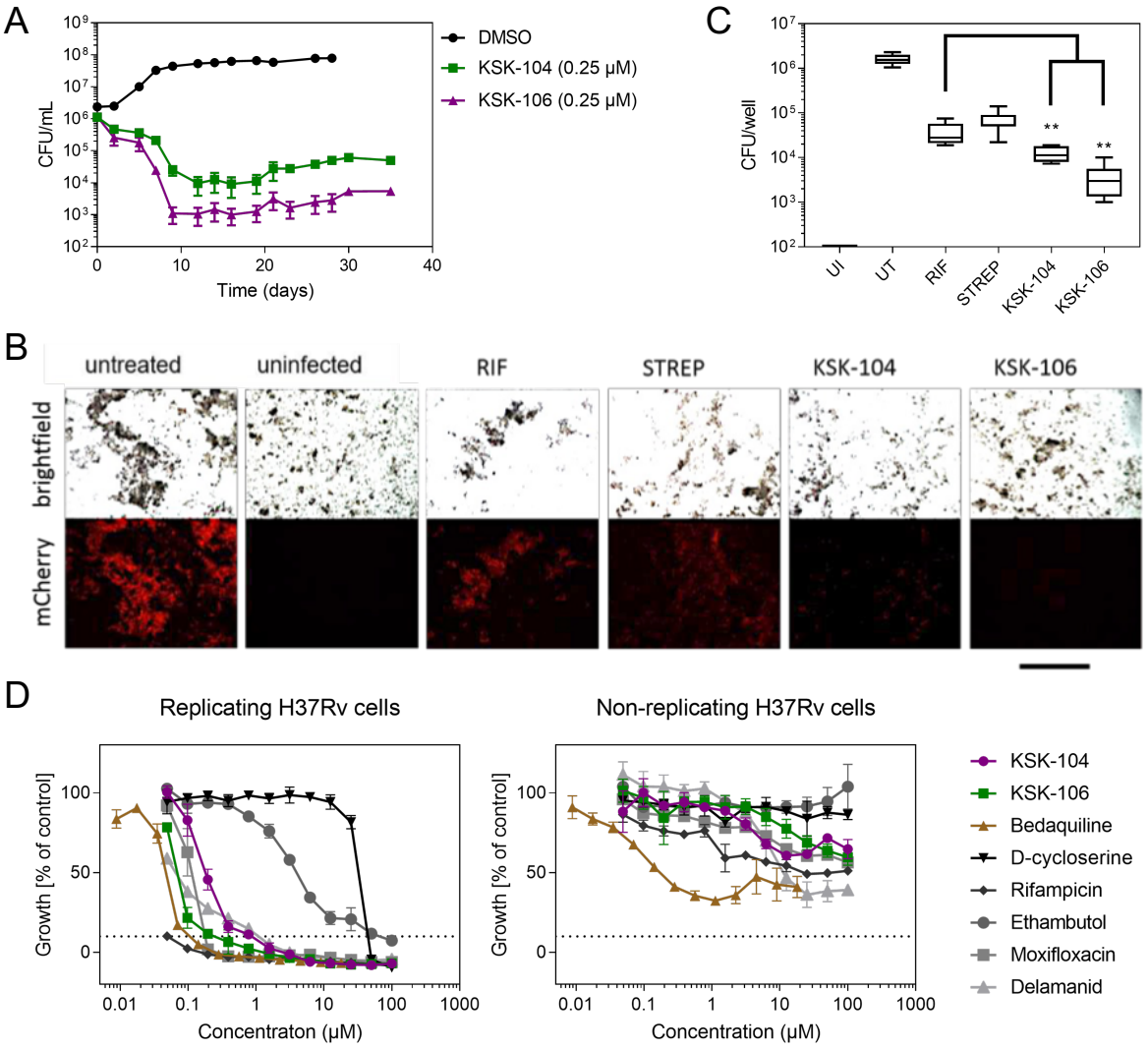

Figure 2. KSKs exhibit a sub-micromolar bactericidal anti-TB activity *in vitro* and in vivo using a THP1 infection model. A) Killing kinetic study by quantifying viable cell count (CFU) following different treatment intervals. *M. tuberculosis* H37Rv cultures treated with KSK-104 or KSK-106. KSK-104 and KSK-106 showed a bactericidal effect. Experiments have been performed in triplicates. Data are shown as mean ± S.D.. **B)** Effects of KSKs on intracellular growth of a constitutively mCherry-expressing *M. tuberculosis* H37Rv reporter strain in a human macrophage THP-1 infection model. THP-1-derived macrophages were treated three hours after infection with either 20 µM DMSO, 0.5 µM KSK-104 or KSK-106, or with the clinical anti-TB drugs rifampicin (RIF, 3 µM) or streptomycin (STREP, 20 µM). After 5 days, fluorescence microscopy was used to visualize internalized bacteria. Representative brightfield pictures of macrophages, and the corresponding fluorescence micrographs are shown. The bar represents 10 µm. **C)** Box-plot of CFU counting after infection of THP-1 macrophages with *M. tuberculosis* H37Rv. Cells were treated with antibiotic and KSK concentrations as described above. UI = uninfected, UT = untreated (DMSO), RIF = rifampicin, STREP = streptomycin. Boxes show

upper and lower quartiles with median. Statistical significance (** $p < 0.01$) was calculated using Kolmogorov-Smirnov-test and student's t-test. All experiments have been performed in triplicates and have been repeated once with similar results. **D)** The activity of KSK-104 and KSK-106 was investigated against replicating and non-replicating *M. tuberculosis* H37Rv cells compared to the several first- and second-line drugs. To generate starvation-induced non-replicating bacilli, cultures of *M. tuberculosis* H37Rv cells were washed, suspended in PBS, and incubated at 37°C for three weeks. Starved cultures were then incubated for 7 days with the drugs. Moderate efficacy against starvation-induced non-replicating cells was observed only for bedaquiline. Growth was quantified by employing the resazurin reduction assay. KSKs exhibited a low activity, comparable to rifampicin, moxifloxacin, and delamanid, while ethambutol and D-cycloserine did not show any activity. Data shown as means of triplicates with SD. The dashed lines indicate 10% residual growth.

The putative amidohydrolases AmiC and Rv0552 mediate resistance and susceptibility towards KSK-104 and KSK-106.

To elucidate the mechanism of action and resistance, we isolated spontaneous single-step resistant mutants of *M. tuberculosis* H37Rv (Figure S5). All resistant mutants isolated against KSK-104 showed high-level resistance as indicated by 32-fold shift in MIC_{90}, and occurred at a frequency of approximately 1×10^{-8}. For KSK-106, all isolated resistant mutants showed a MIC_{90} shift of approximately 1,024-fold and occurred at a rate $< 1 \times 10^{-10}$. Results of whole-genome sequencing of five KSK-104-resistant mutants revealed single nucleotide polymorphisms (SNPs) in the gene *Rv0552,* which encodes a non-essential, conserved hypothetical protein of unknown function (Figure 3A). It is predicted to have amidohydrolase activity and to act on carbon-nitrogen bonds but not on peptide bonds.[14] The mutations included two independent non-synonymous SNPs resulting in amino acid substitutions, H67R and A229D. The KSK-106-resistant mutants all harbored mutations in the *amiC* gene (Rv2888c), which also codes for a non-essential amidohydrolase (Figure 3A). In contrast to the KSK-104 resistant mutants, we found not only SNPs leading to an amino acid exchange (P185T) but also a SNP resulting in a premature stop codon (E129*) as well as insertions causing a frameshift that most likely led to a non-functional protein (insertion +t at position encoding amino acid 100 of 473; insertion +ccgg at position encoding amino acid 347 of 473). The diversity of identified multiple distinct mutations indicated selection and suggested that resistance to KSKs is associated with loss of function of the identified non-essential amidohydrolase genes. In the majority of the analyzed clones, mutations in *Rv0552* and *amiC* were accompanied by additional mutations. These mutations, however, occurred in

diverse genes, which in most cases only had one distinct mutation each. Identical mutations occurring in different mutants strongly suggests that these mutations were copies of a parent clone preexisting in the culture and did not substantially contribute to resistance. In particular, second-site mutations in genes impairing phthiocerol dimycocerosate (PDIM) biosynthesis, such as mutations in *ppsA* and *ppsE*, are known to occur very frequently during *in vitro* culturing of *M. tuberculosis* strains.[15]

To confirm the relevance of *Rv0552* and *amiC* in conferring resistance to KSK-104 and KSK-106, we generated individual site-specific *Rv0552* and *amiC* gene deletion mutants in *M. tuberculosis* H37Rv, using specialized transduction (Figure S6). The resulting independent clones of the *M. tuberculosis* Δ*Rv0552* gene deletion mutant were highly resistant (8-fold increase in MIC_{90}) against KSK-104 with an MIC_{90} of 12.5 µM (Figure 3B). Genetic complementation of the Δ*Rv0552* deletion mutant with the wild-type *Rv0552* gene constitutively expressed from a single copy integrative plasmid (pMV361::*Rv0552*) fully restored the sensitivity to KSK-104. Site-directed mutagenesis was used to generate plasmids containing the specific mutations found in the spontaneously resistant mutants. Complementation with these mutated versions of the *Rv0552* gene by using plasmids pMV361::*Rv0552* H67R or pMV361::*Rv0552* A229D only marginally restored antitubercular activity (Figure 3B). This confirmed that the resistance phenotype depends only on the loss of function of *Rv0552*, ruling out potential polar effects or relevance of secondary mutations. Likewise, loss of the *amiC* gene in the *M. tuberculosis* Δ*amiC* gene deletion mutant conferred high resistance to KSK-106 with a MIC_{90} of 6.25 µM, corresponding to an 8-fold increase in MIC_{90}. The complementation of the Δ*amiC* gene deletion mutant with the wild-type *amiC* gene using plasmid pMV361::*amiC* restored the antitubercular activity of the KSKs, while this effect was not observed when complemented with the mutated versions of the *amiC* gene (Figure 3C). These results demonstrated that the observed resistance to KSK-106 in *M. tuberculosis* is unambiguously linked to loss of function of *amiC*. Interestingly, the Δ*Rv0552* mutant also showed moderate resistance towards KSK-106 with an MIC_{90} of 1.56 µM, while the Δ*amiC* mutant exhibited moderate resistance against KSK-104 with a MIC_{90} of 3.12 µM (each corresponding to a 2-fold increase in MIC_{90}), demonstrating some degree of reciprocal cross-resistances (Figure 3D).

To further analyze the role of the putative amidohydrolases, we generated merodiploid strains of *M. tuberculosis* H37Rv, *M. bovis* BCG Pasteur, and *M. smegmatis* using the same integrative plasmids as above (pMV361::*Rv0552* and pMV361::*amiC*) to overexpress *Rv0552* and *amiC*, respectively. In *M. tuberculosis* H37Rv and *M. bovis* BCG Pasteur, overexpression led to increased susceptibility towards the KSKs compared to the empty vector control (Figures 3E and S7). In contrast, overexpression of the two putative amidohydrolases in the non-tuberculous

species *M. smegmatis* did not result in any activity, indicating that active amidohydrolases are required, but alone not sufficient, for mediating antimycobacterial activity of the KSKs. Of note, while mutations in *amiC* were identified to mediate resistance to KSK-106 in spontaneous resistant mutants, overexpression of *amiC* also increased susceptibility of the recombinant *M. tuberculosis* H37Rv and *M. bovis* BCG Pasteur strains towards KSK-104 (Figure 3E), while overexpression of *Rv0552*, which was identified to mediate resistance to KSK-104 in spontaneous resistant mutants, cross-sensitized recombinant *M. bovis* BCG Pasteur towards KSK-106 (Figure S7).

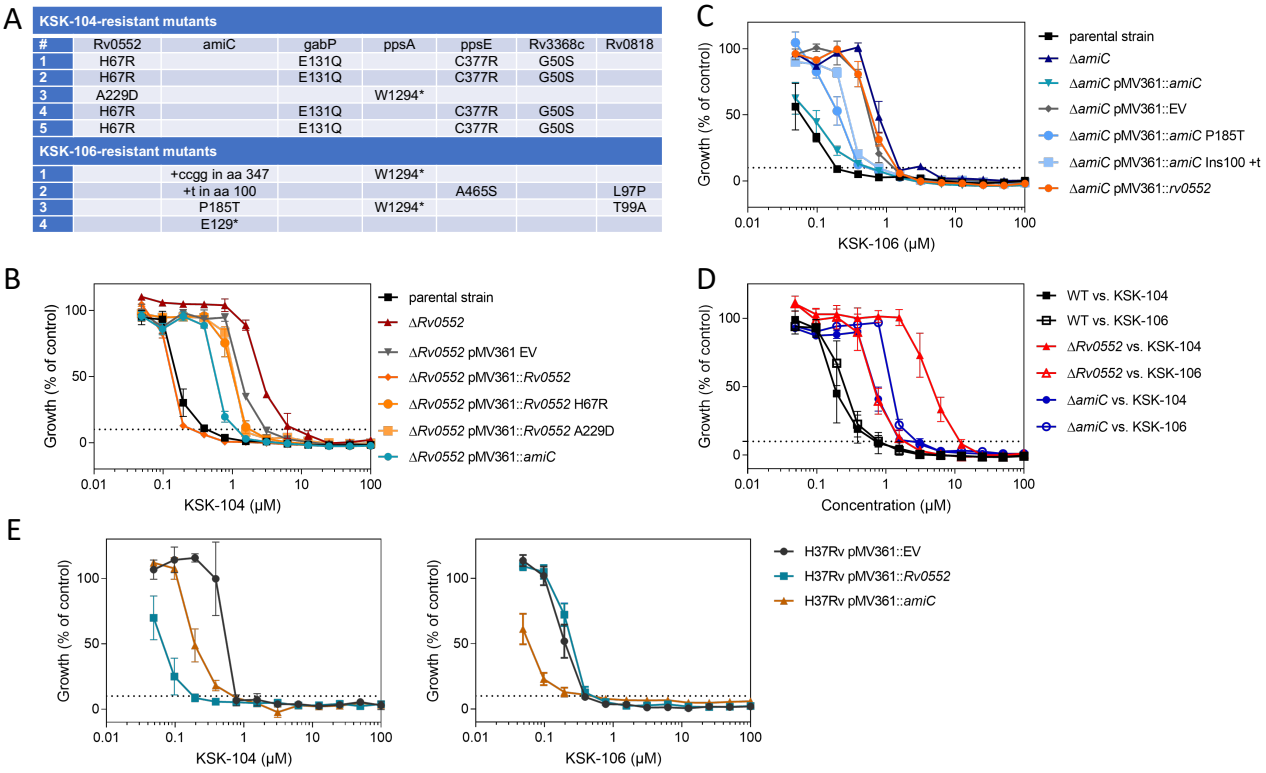

Figure 3. The putative amidohydrolases AmiC and Rv0552 are mediating resistance and sensitivity of *M. tuberculosis* towards KSK-104 and KSK-106. A) Overview of mutations identified by whole-genome sequencing in spontaneous resistant *M. tuberculosis* mutants raised against KSK-104 and KSK-106. Dose-response curve of Δ*Rv0552* **(B)** and Δ*amiC* **(C)** knock-out strains against KSK-104 and KSK-106 compared to the parental strain. Deletion of *Rv0552* and *amiC* conferred resistance towards KSK-104 and KSK-106, respectively. Complementation of the gene deletion mutants with integrating plasmids carrying wild-type genes, pMV361::*Rv0552* and pMV361::*amiC*, restored sensitivity in contrast to the ones carrying mutated genes, pMV361::*Rv0552* H67R, pMV361::*Rv0552* A229D, pMV361::*amiC* P185T, pMV361::*amiC* Ins100 +t. Mutants carrying the empty vector control plasmid pMV361::EV served as negative

controls. **D)** Cross-resistance of Δ*Rv0552* and Δ*amiC* knock-out strains against KSK-104 and KSK-106. Dose-response curves compared to the parental strain show low-level resistance of the Δ*Rv0552* mutant against KSK-106 and of the Δ*amiC* mutant against KSK-104, respectively. **E)** Overexpression of *amiC* or *Rv0552* leads to increased activity of *M. tuberculosis* H37Rv against KSK-104 and KSK-106. Dose-response curves for KSK-104 (top) and KSK-106 (bottom) showing a concentration-dependent growth inhibition of recombinant strains harboring the empty vector control pMV361::EV or the overexpression constructs pMV361::*amiC* or pMV361::*Rv0552*, respectively. Results in **B**, **C** and **E** are mean ± S.D. from three independent biological replicates. Results in **D** are mean ± S.D. from four to six biological replicates, resulting from two independent experiments each measured at least in duplicate. Growth was quantified by employing the resazurin reduction assay. The dashed lines indicate 10% residual growth.

KSKs are pro-drugs that are hydrolyzed intracellularly by the amidohydrolases Rv0552 and AmiC.

The genetic studies demonstrated that loss of function of the non-essential proteins Rv0552 or AmiC mediates resistance towards the antibacterial KSK compounds, while their overexpression causes hypersensitivity. This phenotype has previously been reported to be associated with the activation of pro-drugs.[16,17] In fact, AmiC was previously shown to be involved in activation of amide-containing drugs. Indole-4-carboxamides are hydrolyzed by AmiC to yield 4-aminoindole, which acts as an antimetabolite of tryptophan biosynthesis at the stage of tryptophan synthase (TrpAB).[18] Furthermore, MMV687254, a pyridine carboxamide derivative, also requires AmiC-dependent hydrolysis for antibacterial activity against *M. tuberculosis*, although the antimycobacterial mechanism following hydrolysis remained unknown.[19] Therefore, we hypothesized that the KSKs are pro-drugs that are hydrolyzed by intracellular amidohydrolases, Rv0552 or AmiC, to bioactive metabolites.

To evaluate the predicted role of AmiC and Rv0552 in the activation of, and resistance to, α-aminooxyacetic acid molecules, further biochemical and structural studies were performed. Structure-homology modeling of Rv0552 using Phyre2[20] and PyMOL employing an uncharacterized, metal-dependent hydrolase from *Pyrococcus horikoshii* ot3 (PDB ID 3IGH) as the template provided indications that the H67R mutation observed in resistant mutants might interfere with complexation of a Zn^{2+} ion, thereby potentially impairing hydrolytic activity (Figure S8A). Also, the A229D mutation is predicted to be located in close proximity to the Zn^{2+} ion thereby possibly disturbing hydrolytic activity. Structural modeling of AmiC using a fatty acid amide hydrolase from *Arabidopsis thaliana* as the template (PDB ID 6DII) revealed that

proline 185 is located within the hydrophobic core. Therefore, the P185T mutation could result in protein destabilization and unfolding (Figure S8B). These observations support that antimycobacterial activity of the KSKs probably relies on hydrolytic activity of Rv0552 and AmiC. To further substantiate this, we performed a multiple sequence alignment of AmiC and found that the protein probably belongs to the amidase superfamily (Figure S8C), which comprises a distinctive catalytic Ser-*cis*-Ser-Lys triad conserved among several known hydrolytic enzyme.[21,22] We propose that the triad Ser^{181}-*cis*-Ser^{157}-Lys^{82} represents the catalytic center of AmiC (Figure 4A) as it shares similar positions with that of the 6-aminohexanoate cyclic dimer hydrolase (PDB ID 3A2Q) (Ser^{174}-*cis*-Ser^{150}-Lys^{72}) and the aryl acylamidase (PDB ID 4YJ6) (Ser^{187}-*cis*-Ser^{163}-Lys^{84}).[23,24] In agreement with this, complementation of the *M. tuberculosis* Δ*amiC* gene deletion mutant with a plasmid expressing a mutated AmiC version, with all three catalytically relevant residues being replaced by alanine (pMV361::*amiC* K82A_S157A_S181A), was unable to restore susceptibility of the recombinant strain to both KSKs (Figure 4B).

The hydrolytic activation could affect either the alkoxyamide and/or benzyloxyamide moiety of the lead structures KSK-104 and KSK-106 resulting in different cleavage products (Figure 4C and Figure S9A). To assess whether metabolic cleavage of KSK-104 occurs, the compound was incubated with viable *M. tuberculosis* H37Rv cells. LC-MS analysis of methanol extracts of the cell suspension obtained after 48 h of incubation showed that the parental compound was completely consumed, while two cleavage products accumulated (**6a**, **10**), indicating hydrolysis at both potential cleavage sites (Figure 4D). Incubating KSK-104 in a sterile medium resulted in the formation of small amounts of cleavage product **10**. This suggests that benzyloxyamide hydrolysis of KSK-104 may also occur spontaneously to some extent under the tested conditions, whereas alkoxyamide hydrolysis of KSK-104 is exclusively cell-mediated. KSK-104 hydrolysis to products **6a** and **10** should additionally yield cleavage products **2**, **5** and **9**, which were not detected in the cellular extract. This suggests that further metabolism may occur following the first step of KSK-104 hydrolysis. We confirmed cell-mediated alkoxyamide hydrolysis of KSK-106 by detecting cleavage product **11** (as an analog of **10**) after incubation of *M. tuberculosis* H37Rv cells with KSK-106, while no other predicted cleavage product was detected (Figure S9A+B).

Next, to evaluate whether the antimycobacterial activity of the KSKs arises from a specific hydrolytic product, we tested the susceptibility of *M. tuberculosis* H37Rv cells against all potential KSK-104 (Figure 4E) or KSK-106 (Figure S9C) cleavage products. However, with MIC_{90} values ranging from 25 to >100 μM, the individual compounds were only weakly active or inactive. Furthermore, even different combinations of products that result from alkoxyamide

and/or benzyloxyamide hydrolysis were unable to reproduce the effect of the parental compounds (Figure 4E and Figure S9C). One possible explanation is that the tested metabolites, which bear polar carboxyl and aminoxy groups, are polar and potentially charged under the assay conditions and therefore likely exhibit low permeability through the lipophilic mycobacterial cell wall.[25] From these findings, we conclude that the antibacterial activity of the KSKs relies on efficient diffusion or uptake of the parental compounds by the cells, followed by intracellular hydrolysis by the amidohydrolases AmiC and/or Rv0552. The antibacterial mechanism(s) might then arise from one or more of the emerging intracellular hydrolysis products which are possibly further metabolized.

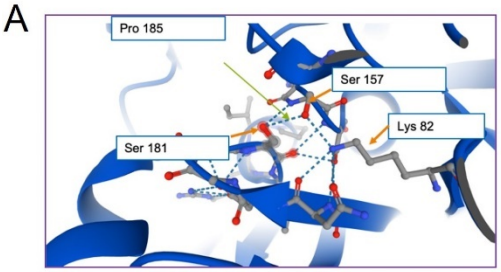

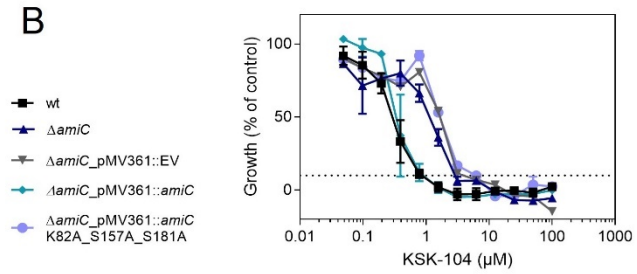

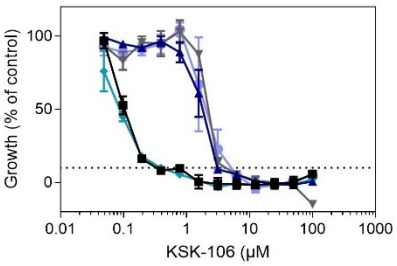

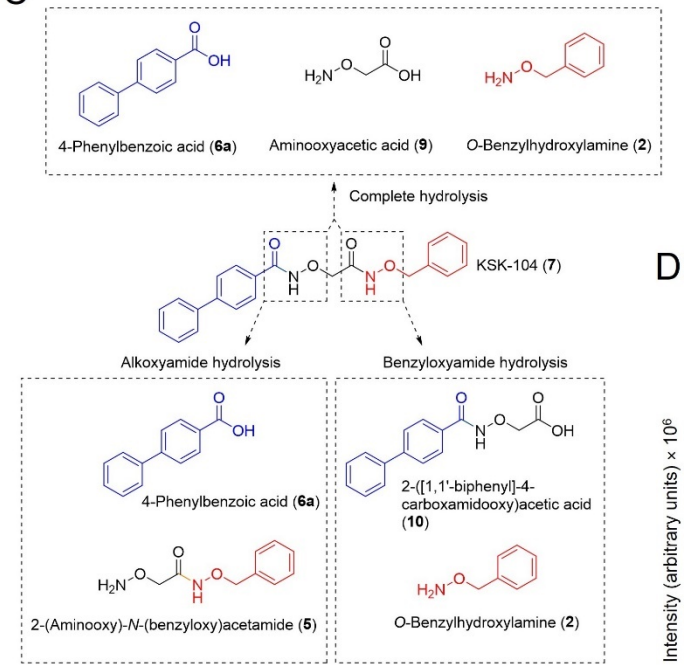

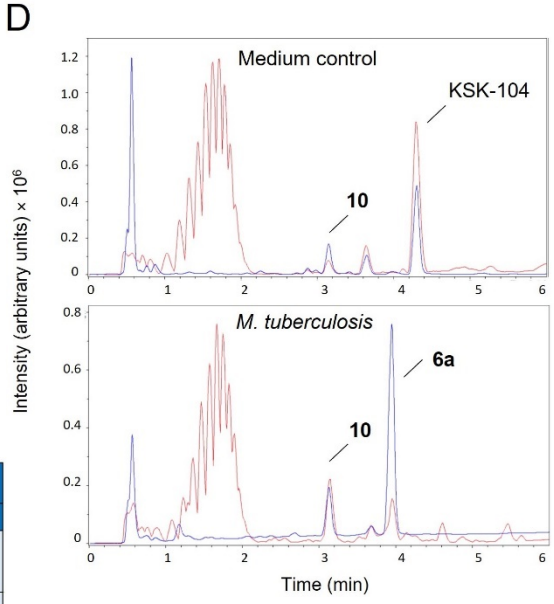

F

Derivative	Structure	MIC90 (μM)		
		WT	ΔamiC	ΔRv0552
15 (OMK61)		0.78	3.125	0.78
16 (OMK241)		3.125	25	1.56
17 (OMK171)		3.125	6.25	25
18 (ABK184)		3.125	3.125	12.5
19 (ABK268)		3.125	6.25	25
20 (ABK203)		0.78	3.125	3.125
21 (ABK275)		12.5	>100	50
22 (ABK311)		1.56	6.25	12.5

E

Compound	MIC_{90} (μM)
KSK-104 (**7**)	0.78
4-Phenylbenzoic acid (**6a**)	>100
6a+9	50
6a+2	>100
9+2	50
6a+9+2	50
6a+5	100
10+2	100

Figure 4. Catalytic activity of Rv0552 and AmiC is required for antimycobacterial effects of KSK-104 and KSK-106. A) AlphaFold prediction of the structure of the active center of AmiC, showing the orientation of the catalytic triad Ser^{181}-*cis*-Ser^{157}-Lys^{82} (https://www.alphafold.ebi.ac.uk/entry/O06418).[26,27] **B)** Dose-response curve for KSK-104 and

KSK-106 of the *M. tuberculosis* Δ*amiC* gene deletion mutant complemented with a plasmid expressing a catalytic site mutant version of AmiC (pMV361::*amiC* K82A_S157A_S181A). The mutant strain containing the empty vector control plasmid pMV361::EV served as the negative control, while the mutant strain expressing wild-type AmiC from plasmid pMV361::*amiC* served as the positive control. Data are means ± SD from three independent biological replicates. Growth was quantified by employing the resazurin reduction assay. The dashed lines indicate 10% residual growth. **C)** Structure of potential hydrolysis products released from KSK-104 by amidohydrolases AmiC and Rv0552. **D)** ESI-LC-MS analysis of methanol extracts obtained after 48 h incubation of 100 µM KSK-104 in sterile 7H9 medium (top) or in 7H9 medium inoculated with *M. tuberculosis* H37Rv cells (bottom). The scan was from 50 to 1500 *m/z* in positive mode. The base peak chromatogram is shown in red, the UV chromatogram at 254 nm is shown in blue. Identified peaks: KSK-104 $[m/z + H]^+ = 377.14$, **6a** $[m/z + H]^+ = 199.07$, **10** $[m/z + H]^+ = 272.09$. **E)** MIC_{90} values of potential KSK-104 hydrolysis products against *M. tuberculosis* H37Rv. Compounds were tested individually and in various combinations. For combination treatments, equimolar mixtures were used containing each compound at the indicated concentration. **F**) Comparison of MIC_{90} values of KSK-104 and KSK-106 derivatives tested against *M. tuberculosis* H37Rv wild type and the Δ*Rv0552* and Δ*amiC* gene deletion mutants.

To further characterize the contribution of the amidohydrolases AmiC and Rv0552 to susceptibility to KSK compounds, we made use of our flexible synthesis capabilities to synthesize various analogs of KSK-104 and KSK-106 using two different routes (Scheme 2). For the synthesis of the *O*-substituted hydroxamic acids (benzyloxyamides) **15** and **17** via route A, hydroxylamine hydrochloride **5** was acylated with carboxylic acids **6c**-**d** in EDC-mediated amide coupling reactions in the presence of trimethylamine and 4-(dimethylamino)pyridine. For Route B, the hydroxamic acids **12a**-**b** were *O*-alkylated with bromoacetic acid (**1a**) or 2-bromopropanoic acid (**1b**) in alkaline medium to furnish the corresponding carboxylic acids **10**, **11** and **13** as intermediates in good yields. The required regioselectivity of these alkylation reactions was investigated by ^{1}H-^{15}N-HSQC-NMR-spectroscopy. Finally, the carboxylic acids **10**, **11** and **13** were reacted with either *O*-benzylhydroxylamine (**2**) or differently *O*-substituted hydroxylamine hydrochlorides **14a**-**e** in EDC-mediated amide coupling reactions to afford the KSK-analogs **16** and **18**-**22**.

The derivatives **15-22** were tested for antibacterial activity against cells of *M. tuberculosis* H37Rv wild type and the Δ*Rv0552* and Δ*amiC* mutants (Figure 4F) (an extensive structure-activity relationship study comprising more than 200 derivatives will be reported elsewhere). We identified that derivatives **15** and **16,** which differ in region C compared to KSK-106, show

reduced relative activity only against the Δ*amiC* gene deletion mutant. In contrast, KSK-104 structural variants **17-19** exhibited substantially lower relative activity only with the Δ*Rv0552* mutant, while compounds **20-22** differing in region C compared to KSK-104 demonstrated a similar shift in MIC_{90} against both deletion mutants (Figure 4F). As indicated by the reduced antimycobacterial activity, the methyl group in region B of **21** strongly impeded the hydrolysis of the benzyloxyamide group not only in the gene deletion mutants but partly already in the wild type of *M. tuberculosis* H37Rv. In agreement with the increased susceptibility to KSK-104 and KSK-106 observed in the overexpression strains (Figure 3E and Figure S7) and the cross-resistance of the Δ*amiC* and Δ*Rv0552* gene deletion mutant against both KSK-104 and KSK-106 (Figures 3D and 4B), these results collectively suggest that both amidohydrolases can principally be partially redundant pro-drug activators of α-aminooxyacetic acid derivatives, with the preference for AmiC or Rv0552 being influenced by the specific substitution pattern of the compounds.

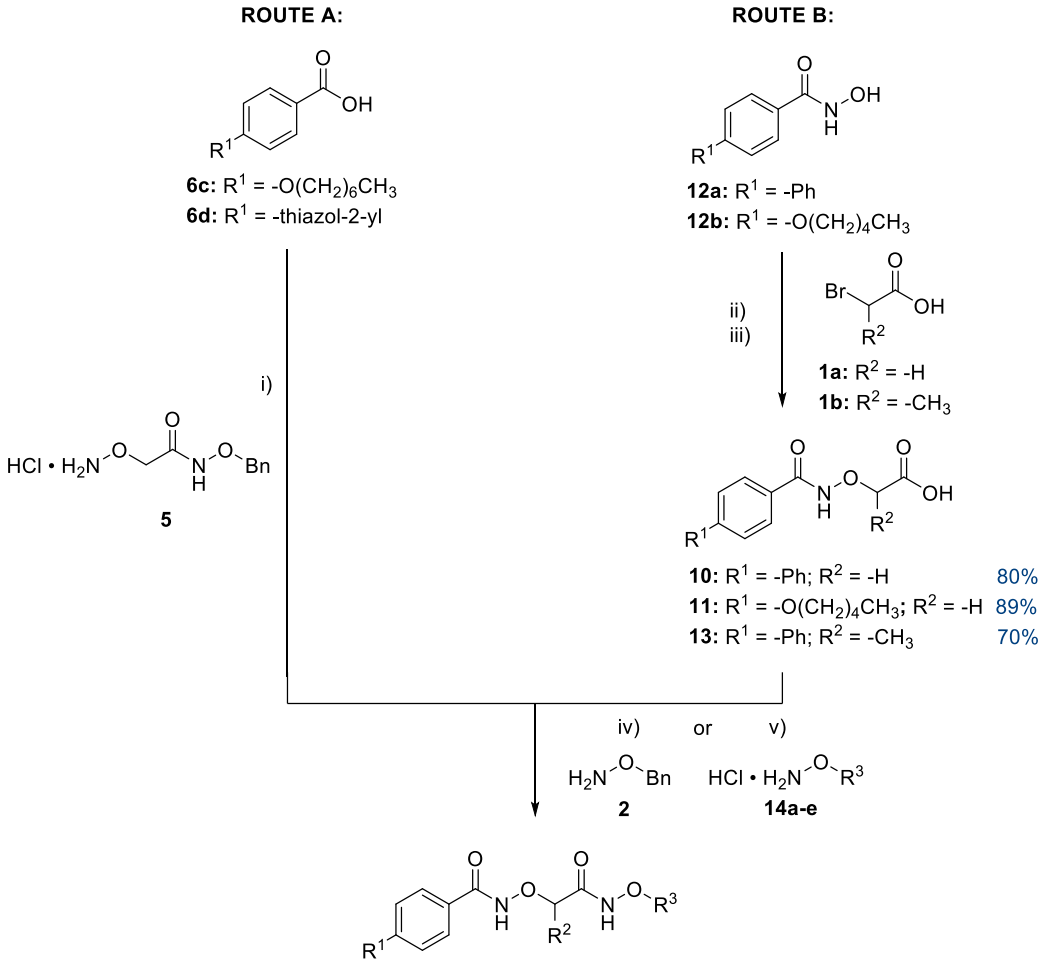

Scheme 2. Synthesis of KSK-analogs 15-22. i) 1.00 eq. of hydroxylamine hydrochloride (**5**), 1.25 eq. EDC•HCl, 0.10 eq. DMAP, 1.20 eq. NEt_3, CH_2Cl_2, rt; ii) 1.00 eq. bromoacetic acid (**1a**), 2.00 eq. NaOH, EtOH, reflux; iii) 1.10 eq. NaH, THF, -10 °C then 1.00 eq. 2-bromopropanoic acid (**1b**), THF, reflux; iv) 1.00 eq. *O*-benzylhydroxylamine (**2**), 1.25 eq. EDC•HCl, 0.10 eq. DMAP, CH_2Cl_2, rt; v) 1.00 eq. H_2NOR^3 hydrochloride (**14a-e**), 1.25 eq. EDC•HCl, 0.10 eq. DMAP, 1.20 eq. NEt_3, CH_2Cl_2, rt.

α-Aminooxyacetic acid derivatives might act as "dirty drugs" affecting multiple intracellular targets.

To reveal molecular insights into pathways that contribute to the antitubercular effects of the studied compounds, we applied complementary approaches including genetic interaction mapping as well as transcriptomic and proteomic stress response profiling.

For an unbiased identification of pathways or targets that are associated with KSK susceptibility or resistance, we performed a genome-wide quantitative analysis of a saturated transposon mutant pool established in *M. tuberculosis* strain H37Ra, employing transposon-insertion sequencing (TnSeq). The mutant pool was subjected to either DMSO solvent control or to a sublethal concentration of 0.18 µM KSK-106 that was found to decrease growth rate by ca. 50% over five generations (Figure S10). A mean saturation of 67.7% (range 65-69%) was observed between samples, where 'saturation' refers to percent of TA dinucleotide sites with one or more insertion. We identified 74 genes with $P_{adj} < 0.05$ resulting in apparent fitness changes of transposon mutants using TRANSIT[28] resampling. Of these genes of interest, 23 met a Log_2-fold change threshold ≤ -0.55 or ≥ 0.55 and seven a Log_2-fold change threshold ≤ -1 or ≥ 1, respectively (Figure 5A). By comparing the composition of the mutant library in the absence and presence of KSK-106, we were able to define 41 genomic regions harboring transposon insertions with a significant increase of mutant abundance during KSK-106 treatment, suggesting that inactivation of the respective genes provides an advantage under the test conditions and contributes to resistance. We also found 33 genomic regions, for which insertions resulted in a significant decrease in mutant abundance over experimental selection, suggesting that these genes are important for fitness under the test conditions as their inactivation led to an increased sensitivity of the cells (Table S1).

Confirming our previous results, mutants harboring inactivating transposon insertions in *amiC* or *Rv0552* led to the strongest enrichment of mutants in the pool upon KSK-106 treatment, consistent with their suggested role in pro-drug activation (Figure 5A-C). These finding are further supported by gain of fitness observed from insertions throughout the open reading frames of these genes (Figure 5B+C). Several genes found to alter mycobacterial fitness in drug-treated cells were already known to affect efficacy against other drugs (Table S2). These are genetic features that likely contribute to general mycobacterial resistance or susceptibility mechanisms that are not specifically linked to the antitubercular effects of KSK-106. These include genes encoding putative drug-efflux pumps (ABC transporter Rv1272c-Rv1273c, the daunorubicin-phthiocerol dimycocerosate-transport ABC transporter DrrA and DrrB, and the resistance-nodulation-cell division (RND) superfamily member MmpL7), [29-32] where transposon insertions led to higher susceptibility to KSK-106 treatment, suggesting that these transporters mediate efflux of the parental compound or bioactive hydrolysis products. Furthermore, insertions in the universal stress protein family gene *Rv3134c*, reported to be part of a complex involved in the bacterial response to a wide range of stresses, [33] resulted in decreased fitness of the corresponding mutants. Additionally, mutants harboring transposon insertions in metabolic genes were also highly overrepresented in the pool following treatment. These included the glycogen metabolism

genes *glgC* and *glgP*, and the glycerol kinase gene *glpK*, where mutations have frequently been reported to produce a general drug-tolerant phenotype. [34-37] In contrast, transposon insertions in genes implicated in the cell wall structure, such as those encoding PE/PPE family members and enzymes involved in the synthesis of the major cell envelope lipid phtiocerol dimycocerosate (*ppsA*, *ppsB*, *ppsC*, *ppsE*), caused a reduced sensitivity towards KSK-106, which might be linked to a reduced cell permeability of the compound (Table S2).

In addition to these general mechanisms, we found several genes that appeared to specifically alter susceptibility to KSK-106 treatment, providing further insights into the KSK-induced mechanism of action (Table S3). Mutants carrying insertions in the *doxX* gene were enriched in the KSK-106 treated group, conferring a fitness advantage (Figure 5D). DoxX, together with the superoxide detoxifying enzyme SodA and the predicted thiol-oxidoreductase SseA, has been described to form a membrane-associated oxidoreductase complex (MRC) that is responsible for coordinating detoxification of reactive oxygen species and thiol homeostasis during *M. tuberculosis* infection. SseA and DoxX are mediating oxidative recycling of thiyl radicals that are generated by the free radical scavenging activity of mycothiol, while oxidized mycothiol is then recycled by mycothione reductase activity. Superoxide anions might be generated during these enzymatic activities, which are detoxified by the superoxide dismutase SodA. It has been reported that loss of DoxX leads to defective recycling of mycothiol and results in higher sensitivity towards oxidative stressors that react with cytosolic thiols such as *tert*-butyl hydroperoxide (tBHP).[38] The increased fitness of *doxX* mutants led us to hypothesize that KSK-106 might affect the oxidative stress network of *M. tuberculosis* in a thiol-specific manner. To test this, we investigated synergism between KSK-106 and the thiol-specific oxidative stressor tBHP. Addition of 0.001 µM tBHP resulted in a significantly higher susceptibility of *M. tuberculosis* H37Rv cells with a more than 16-fold decrease in MIC_{90} against both KSK-104 and KSK-106, while sensitivity to the other tested drugs that do not interfere with the cytosolic thiol pool was not altered (Figure 5E). These results suggest a mechanism by which the treatment with KSK compounds might lead to the production of free radicals that are detoxified in a mycothiol-dependent manner. Inactivation of DoxX by transposon insertions decreases sensitivity towards the compounds by preventing the generation of toxic superoxide anions under these conditions, while the overload of this detoxification system by exogenous tBHP could potentially promote superoxide anion formation.

We also identified a distinct set of genes that are involved in the PLP synthesis and salvage pathway. *De novo* biosynthesis of PLP in *M. tuberculosis* is mediated by PLP synthase, a complex consisting of the PLP biosynthesis protein SnzP, encoded by the gene *Rv2606c*, and the putative glutamine amidotransferase SnoP,[39] while the pyridoxamine 5'-phosphate oxidase PdxH, encoded

by the neighboring gene *Rv2607c*, is involved in PLP salvage.[40] Transposon insertions in *snzP* and *pdxH* caused a loss of fitness and rendered the cells more sensitive toward KSK-106 treatment (Figure 5F), suggesting that KSK-106 treatment might trigger a higher PLP demand within the cell. To test this, we supplemented a PLP-free minimal medium with 100 µg/mL pyridoxine and observed a 4-8-fold increase in MIC_{90} for KSK-104 and KSK-106 treated cells compared to non-supplemented medium, whereas no change was observed for the control antibiotics rifampicin, moxifloxacin, and bedaquiline (Figure 5G).

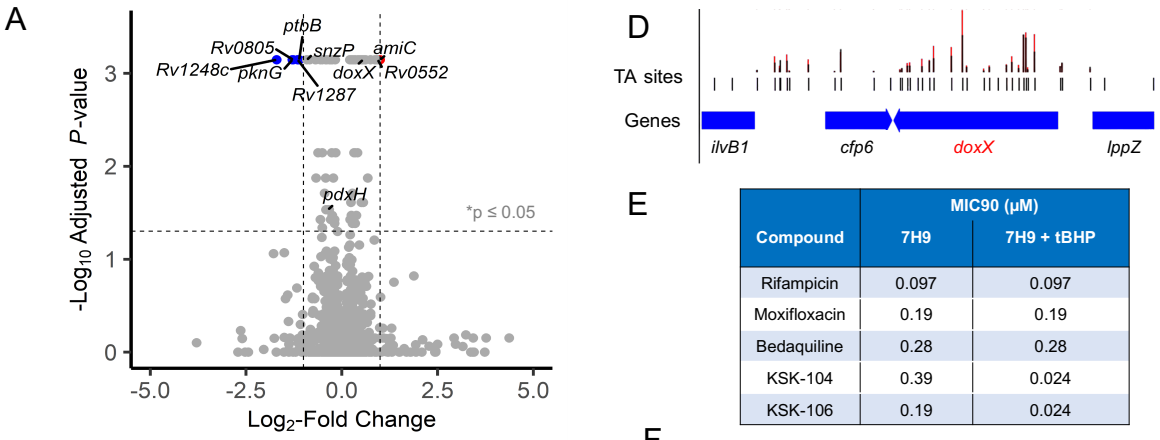

Compound	MIC90 (µM) 7H9	7H9 + tBHP
Rifampicin	0.097	0.097
Moxifloxacin	0.19	0.19
Bedaquiline	0.28	0.28
KSK-104	0.39	0.024
KSK-106	0.19	0.024

Compound	MIC90 (µM) Minimal medium	Minimal medium + pyridoxine
Rifampicin	0.078	0.078
Moxifloxacin	0.39	0.39
Bedaquiline	0.28	0.28
KSK-104	3.125	12.5
KSK-106	1.56	12.5

Figure 5. Genes specifically mediating differential susceptibility towards KSK-104 and KSK-106 treatment in *M. tuberculosis* as revealed by Tn-seq analysis. A) Volcano plot highlighting transposon mutants selected for or against under selective pressure of subinhibitory concentrations of KSK-106. Transposon insertions in genes with gains in fitness denoted in red. Transposon insertions in genes with loss in fitness denoted in blue. Black dotted line denotes threshold for significance of Log2-Fold change of < -1 or > 1 and adjusted p-value of <0.05. **B - D, F)** Abundance of reads at individual TA dinucleotide insertion sites at selected genomic regions in analyzed mutant pools of *M. tuberculosis* strain H37Ra subjected to sublethal treatment with KSK-106 (red bars) or DMSO solvent control (black bars). Relevant genes are highlighted

in red. Enrichment of transposon insertions in the amidohydrolase genes *amiC* (**B)** and *Rv0552* **(C)** in the KSK-106-treated *M. tuberculosis* H37Ra mutant pool, indicating decreased sensitivity of the corresponding transposon mutants. **D)** Enrichment of transposon insertions in the *doxX* gene in the KSK-106-treated *M. tuberculosis* H37Ra mutant pool, indicating decreased sensitivity of the corresponding transposon mutants. **E)** Amending of 7H9 medium with 0.001 µM *tert*-butyl hydroperoxide (tBHP), a thiol-specific oxidative stressor, resulted in a significantly increased sensitivity of cells of *M. tuberculosis* H37Rv towards KSK104 and KSK-106, as indicated by lowered MIC_{90} values. Cells treated with rifampicin, moxifloxacin and bedaquiline served as negative controls to demonstrate specificity. Growth was quantified by employing the resazurin reduction assay. Measurements were done in triplicates revealing identical MIC_{90} values between samples. **F)** Depletion of transposon insertions in genes involved in pyridoxal 5'-phosphate synthesis (*snzP*) and salvage pathway (*pdxH*) in the KSK-106-treated *M. tuberculosis* H37Ra mutant pool, indicating increased sensitivity of the corresponding transposon mutants. Mutants carrying transposon insertions in the pyridoxal 5'-phosphate synthesis gene *snoP* were also depleted, but did not reach the statistical treshhold. **E**) Supplementation of minimal medium with 100 µg/mL pyridoxine led to resistance of cells of *M. tuberculosis* H37Rv towards KSK104 and KSK-106, as indicated by higher MIC_{90} values. Cells treated with rifampicin, moxifloxacin and bedaquiline served as negative controls to demonstrate specificity. Growth was quantified by employing the resazurin reduction assay. Measurements were done in triplicates revealing identical MIC_{90} values between samples.

Next, since interrogation of fitness changes by Tn-Seq is largely limited to non-essential genes, we conducted differential transcriptional and proteomic profiling of KSK-106-treated and untreated cells as alternative approaches to assess which genes or proteins are linked to the mode of action of the α-aminooxyacetic acid derivatives. For transcriptomic analysis of *M. tuberculosis* mc^26030, exponential phase cells were exposed to an inhibitory dose of 1.9 µM KSK-106 (5 × MIC_{90}) for 24 h and compared to DMSO-treated controls. Under this condition, KSK-106 treatment caused a well-defined and very narrow effect on the transcriptome of *M. tuberculosis*. Four genes belonging to the gene cluster *Rv3092c-Rv3095* were highly upregulated in treated cells (Figure 6A). In addition, *Rv3096*, which is adjacent to this gene cluster, was also upregulated more than 2-fold ($p< 0.05$). Although little is known about this gene cluster, two recent studies have explored some of its functions.[41,42] The gene *Rv3095* (*mxyR*) encodes the mycobacterial xylan regulator, which is a member of the family of multiple antibiotic resistance (MarR) transcriptional regulators and may play a role in the metabolic regulation of carbohydrates, including xylan, L-arabinose and galactose.[42] The HTH-type transcriptional regulator gene

Rv3095 is divergently oriented to genes encoding a hydrolase (*Rv3094c*), an oxidoreductase (*Rv3093c*), and an ABC transporter (*Rv3092c*) and convergently oriented to the putative xylanase gene *Rv3096*. It was shown that Rv3094c is likely a flavin-dependent monooxygenase with an FAD-binding site and acyl-CoA dehydrogenase activity that is involved in ethionamide activation by sulfoxidation,[42] while the main route for multistage ethionamide pro-drug activation occurs through conversion to active radicals by the Baeyer-Villiger monooxygenase EthA, followed by further conversion to a toxic adduct with NADH.[43]

To corroborate the transcriptomic results, we investigated the protein stress response of *M. tuberculosis* H37Rv cells following KSK-106 treatment. For this, *M. tuberculosis* H37Rv cells were treated with a sublethal concentration of KSK-106 (0.05 µM, corresponding to 0.125 × MIC_{90}) for 10 days. Proteomic analysis revealed again a very distinct and narrow response profile with a high abundance of the four proteins Rv3092c-Rv3095 in treated cells compared to the DMSO control (Figure 6B), confirming the results of the transcriptome analysis. A similar response was observed for cells of *M. tuberculosis* H37Rv subjected to 0.2 µM KSK-106 treatment (corresponding to 0.5 × MIC_{90}) (Figure S11). Such a distinctive and narrow transcriptomic and proteomic response profile is very unusual and has yet not been reported to occur in response to treatment with other antitubercular antibiotics. To further elucidate the role of the respective gene cluster in resistance and susceptibility towards KSK compounds, we generated a site-specific *M. tuberculosis* Δ*Rv3092c-Rv3095* gene deletion mutant and tested its susceptibility against KSK-104 and KSK-106. Surprisingly, cells lacking the described genes demonstrated marked resistance against KSK-106 with an 8-fold increase in MIC_{90}, and high-level resistance to KSK-104 with a 16-fold increase in MIC_{90} values (Figure 6C). This implies that loss of this gene cluster provides a fitness advantage during treatment with α-aminooxyacetic acid derivatives and suggests that the strong and specific upregulation might represent a misguided stress response that enhances the antitubercular effect of the compounds.

We finally assessed whether identified pathways that influence susceptibility to KSK-104 and KSK-106 cooperate in the antitubercular mechanism of α-aminooxyacetic acid derivatives. For this, we tested the susceptibility of the *M. tuberculosis* Δ*Rv3092c-Rv3095* gene deletion mutant in the presence of pyridoxine and observed enhanced resistance, demonstrating additive effects (Figure 6D).

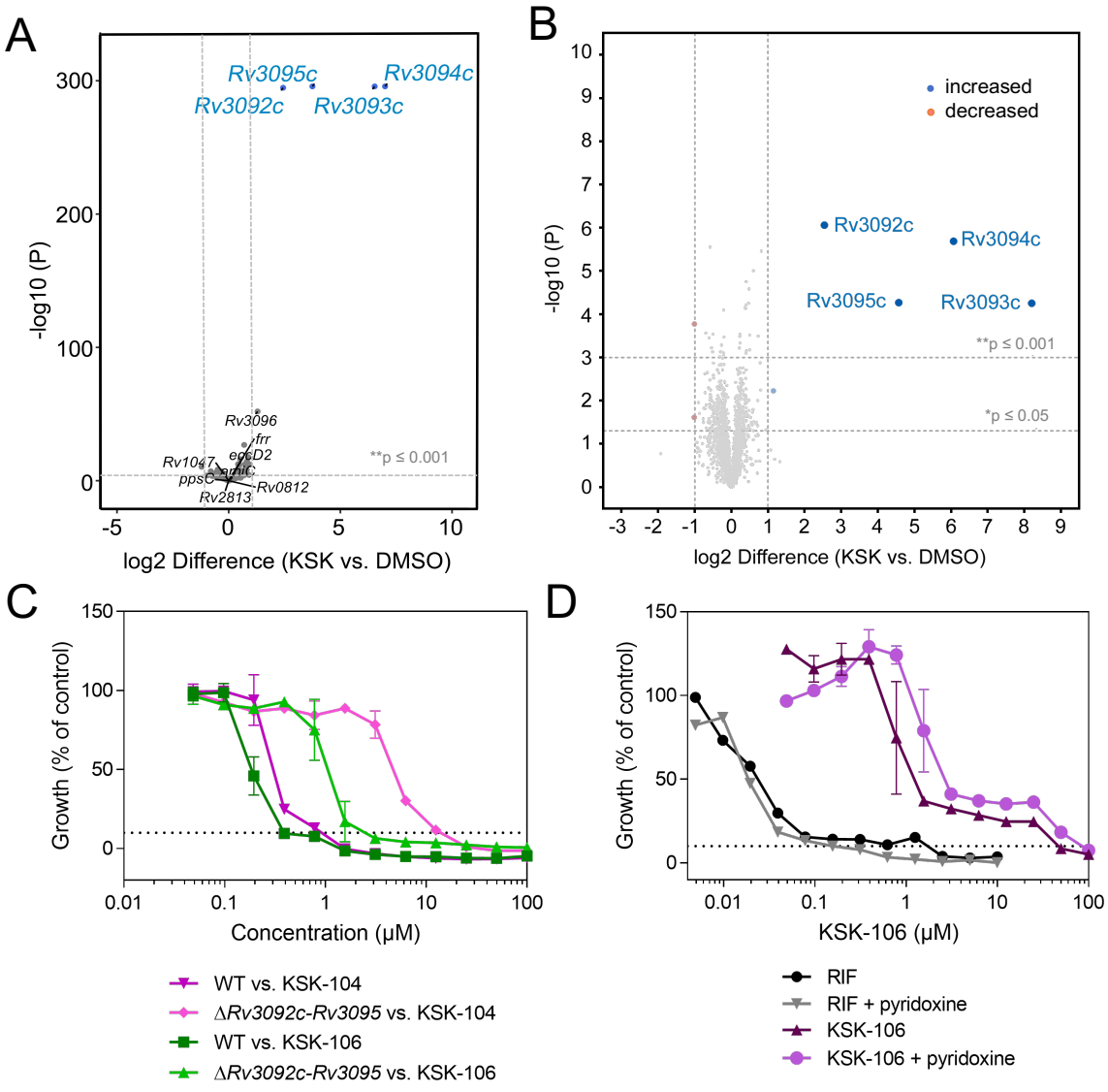

Figure 6. Upregulation of the gene cluster Rv3092c-Rv3095 as a misled stress response in KSK-106 treated *M. tuberculosis* cells. A) Full transcriptome analysis of cells of *M. tuberculosis* strain mc^{2}6230 treated with a lethal concentration of KSK-106 compared to DMSO control. Exponential phase cells were exposed to 1.9 µM KSK-106 (5 × MIC_{90}) for one generation time (24 h) and compared to DMSO treated controls. The plot shows the fold-change (log_2) in gene expression abundance, plotted against p-value ($-log_{10}$). **B)** LC-MS/MS-based whole protein analysis of silenced cells of *M. tuberculosis* H37Rv treated with a sublethal concentration of KSK-106 (0.05 µM, corresponding to 0.125 × MIC_{90}) compared to DMSO control. The volcano plot illustrates the log_2-fold change in abundance in KSK-106 treated vs. non-treated cells (X-axis) and corresponding $-log_{10}$ p values (Y-axis). Proteins complying with the chosen threshold of significance and showing a log_2-fold change ≥ 1 or ≤ -1 are marked in blue or red, respectively. Quantification was done via label free quantification (LFQ) of four to five replicates per sample group. To identify statistically

significant hits from the analysis, $P \leq 0.05$ (Student's T-test; permutation-based FDR with 250 randomizations and FDR = 0.01) was applied. **C)** Dose-response curves of *M. tuberculosis* H37Rv wild type and the Δ*Rv3092c-Rv3095* gene deletion mutant against KSK-104 and KSK-106, demonstrating that the gene deletion leads to resistance against the compounds. **D)** Dose-response curves of the *M. tuberculosis* H37Rv Δ*Rv3092c-Rv3095* gene deletion mutant against KSK-106 during cultivation in minimal medium with or without 100 µg/mL pyridoxine, leading to increased resistance in presence of pyridoxine. Cells treated with rifampicin (RIF) served as negative control to demonstrate specificity. Data in **C**+**D** are shown as means of triplicates ± SD. Growth was quantified employing the resazurin reduction assay. The dashed lines indicate 10% residual growth.

DISCUSSION

In this study, we have elucidated the antitubercular properties of KSK-104 and KSK-106, which belong to the family of α-aminooxyacetic acid derivatives that might pave the way for development of a new class of chemotherapeutics against *M. tuberculosis* infections. These compounds show antibacterial activity against *M. tuberculosis in vitro* and in infected human macrophages in a sub-micromolar range and are active against extensively drug-resistant (XDR-TB) clinical isolates. Furthermore, the KSKs show a large therapeutic window with excellent activity and no cytotoxicity in a broad panel of human cell lines. With a specific effect on tuberculous mycobacteria, the KSKs could facilitate the development of narrow-spectrum bactericidals that offer a reduced risk of resistance development and side effects, while also providing a greater opportunity to maintain a normal commensal microbiota in treated patients.[44,45] Finally, the novel compounds constitute a group of chemical entities that are readily available with a straightforward synthesis route, allowing further derivatization for medicinal chemical optimization.

Similar to other anti-TB medications like isoniazid or ethionamide, the KSKs are pro-drugs. Activation is mediated through hydrolysis by the amidohydrolases AmiC and Rv0552. Genetic studies involving gene deletion mutants and overexpressing recombinant strains revealed that both amidases can simultaneously catalyze pro-drug activation, albeit with various efficacies depending on the substitution pattern of the studied molecules. This partially redundant activation mechanism might partly explain the observed low resistance frequencies. Development of α-aminooxyacetic acid derivatives that represent efficient substrates for both AmiC and Rv0552 might further decrease the likelihood of resistance emergence. AmiC has recently been discovered

to mediate the activation of two other classes of amide-containing pro-drug compounds, indole-4-carboxamides and pyridine carboxamides.[18,19] However, for these compounds, monoactivation only by AmiC occurs, while the studied α-aminooxyacetic acid derivatives differ by involving alternative activation by AmiC and Rv0552. To our knowledge, Rv0552 has not previously been reported to be involved in activation of, or resistance to, antimycobacterial compounds. We acknowledge that redundant amidohydrolase activation of α-aminooxyacetic acid derivatives in the bacilli is attractive, as it will decrease resistance frequency, but substrate promiscuity might also impair *in vivo* efficacy when the compounds are hydrolyzed by host amidohydrolases before they reach the tubercle bacilli. High plasma stability as well as intracellular activity of the studied compounds in infected macrophages indicate that the current candidates are not substantially targeted by host amidohydrolases under the tested conditions, but further in-depth pharmacokinetic studies are required to explore metabolic stability in humans.

Pro-drug activation of α-aminooxyacetic acid derivatives by AmiC and Rv0552 can lead to the formation of various hydrolysis products. Identification of predicted hydrolysis products by LC/MS indicates both alkoxyamide and benzyloxyamide hydrolysis. Since even treatment with the combination of different possible hydrolysis products did not mimic the antibacterial effect of the parental compounds, we conclude that AmiC- and Rv0552-mediated hydrolysis needs to occur intracellularly following the uptake of the parental molecules. At least some of the hydrolysis products are likely subject to further metabolism, as we were unable to detect every corresponding hydrolysis product by LC/MS. Which of the resulting hydrolysis products is responsible for the antitubercular activity of the parental compounds remains to be elucidated, but the observed pleiotropic effects suggest that it is the combination of two or more hydrolysis products or their resulting metabolites that provokes bacterial cell death.

Thus, we propose that the studied α-aminooxyacetic acid derivatives likely act as “dirty drugs” simultaneously attacking different intracellular targets or pathways following intracellular hydrolysis. “Dirty drugs” were previously defined as small (molecular weight ranging from 100-300 g/mol), “fragment-like” antimycobacterials that can hit multiple targets and pathways inside the tubercle bacillus, and were shown to be less prone to the rapid emergence of resistance.[46] Combining complementary untargeted genome-wide genetic, transcriptomic and proteomic analyses, we identified three distinct mechanisms that may be involved in determining susceptibility of *M. tuberculosis* to the studied α-aminooxyacetic acid derivatives.

Genetic interaction mapping connected the activity of the compounds to the oxidative stress network in *M. tuberculosis* cells by demonstrating the specific sensitizing effects of the oxidative stressor tBHP and the membrane protein DoxX. DoxX is an integral membrane protein that facilitates the coordination between cytosolic SseA and secreted SodA.[38] In the cytosol, the

free radical scavenging activity of mycothiol generates mycothiol thiyl radicals. DoxX and SseA enable the conversion of these thiyl radicals into oxidized mycothiol, which is subsequently recycled through the activity of mycothione reductase. As a result of this process, superoxide anions might be produced, that are detoxified by the associated superoxide dismutase SodA.[38] When DoxX is inactivated, fewer superoxide anions may be generated, which might have less severe effects than the accumulation of free radicals. tBHP is known to interact with cytosolic mycothiol,[47,48] which promotes generation of superoxide anions. Our findings are in agreement with mechanisms where the KSK compounds are either inhibiting the activity of SodA to detoxify the generated superoxide anions, directly or indirectly promote the generation of superoxide anions (e.g., by interfering with the respiratory electron transport chain), or lead to the production of free radicals that need to be detoxified in a mycothiol-dependent manner. The exact underlying mechanism needs further investigation. The elevated levels of oxidative stress in human phagocytic cells during infection[49] could enhance the activity of the KSK compounds *in vivo*.

In addition, we found that the PLP synthesis and salvage pathways influence sensitivity towards α-aminooxyacetic acid derivatives. PLP-dependent enzymes are a target for drug therapy in TB, as evidenced by the second-line drug D-cycloserine, underscoring the potential of PLP biosynthesis as a promising drug target.[50,51] The fitness of the cells under KSK-106 treatment is impacted by mutations in the PLP synthesis gene *snzP* and the PLP salvage gene *pdxH*. PdxH enzymatically oxidizes PNP to produce PLP with the aid of flavin mononucleotide (FMN) as a prosthetic group, whereby the C4' alcohol PNP is oxidized to an aldehyde. During catalysis, FMN serves as the immediate electron acceptor, with molecular oxygen acting as the final electron acceptor and generating hydrogen peroxide under aerobic conditions.[52] It has been reported that PLP can function as a potent quencher of reactive oxygen intermediates.[53,54] Our study has demonstrated that exogenous supplementation of pyridoxine in a minimal medium confers resistance of *M. tuberculosis* cells towards KSK-104 and KSK-106. These results suggest that the studied α-aminooxyacetic acid derivatives may inhibit PLP-biosynthesis, otherwise generate an increased demand for PLP, or promote the formation of reactive oxygen species that cannot be quenched in the absence of sufficient PLP supply. Furthermore, complete alkoxyamide and benzyloxyamide hydrolysis of the studied KSKs will generate aminooxyacetic acid (compound **9**), which is a well-known inhibitor of PLP-dependent enzymes.[55] It attacks the Schiff base linkage between PLP and the enzyme, generating PLP oxime *O*-acetic acid.[56] While we found that exogenous aminooxyacetic acid has no direct antibacterial effects on whole cells likely due to poor uptake, the intracellular hydrolytic release of this metabolite might result in inhibition of PLP-dependent enzymes. While bioinformatic prediction of PLP-dependent enzymes is difficult due to low sequence similarities, *M. tuberculosis* is known to harbor at least 30 different PLP-

dependent enzymes,[57] several of which are known to be essential for viability. Pleiotropic attack of these PLP-dependent enzymes by aminooxyacetic acid could contribute to the potent antitubercular effect of the KSKs. Recently, it was shown that *M. tuberculosis* produces hydrogen sulfide (H_2S) in a PLP-dependent manner and that this process can be inhibited by aminooxyacetic acid.[58] In *Escherichia coli*, endogenously produced H_2S protects the cells against oxidative stress.[59] Thus, blocking PLP-dependent H_2S formation by intracellular relase of aminooxyacetic acid might contribute to the increased sensitivity of *M. tuberculosis* cells towards oxidative stress during KSK treatment.

Furthermore, transcriptomic and proteomic analyses of KSK-106 treated cells revealed the role of the gene cluster *Rv3092c-Rv3095* in determining sensitivity towards α-aminooxyacetic acid derivatives. Inactivation of the genes led to notable cross-resistance towards the studied compounds. Little is known about the biological function and specificity of the corresponding proteins. *Rv3092c-Rv3094c* is potentially organized in an operon, whose expression is controlled by Rv3095, which is a transcriptional regulator belonging to the MarR family.[60] While Rv3093c putatively represents a flavin adenine dinucleotide/flavin mononucleotide (FAD/FMN) reductase, Rv3094c was recently shown to be a putative FMN-containing monooxygenase that catalyzes the sulfoxygenation of ethionamide to its S-oxide (ETH-SO) as the first activation step,[41] which then forms a covalent adduct with NAD (ETH-NAD) that targets InhA.[61,62] It is unlikely that the α-aminooxyacetic acid derivatives are directly bioactivated by Rv3094c in a similar manner as they do not contain sulfur. However, it is conceivable that the monooxygenase activity of Rv3094c might generate reactive oxygen species that exacerbate the effect of the KSK compounds. In this regard, we conclude that the strong upregulation of the gene cluster represents a misguided stress response. It was reported that Rv3095 negatively regulates the expression of *Rv3093c* and *Rv3094c*.[41] Counterintuitively, KSKs trigger a stress response that results in the complete deregulation of the gene cluster, where Rv3095 fails to repress the expression of *Rv3093c* and *Rv3094c*. It remains unknown how the KSK compounds elicit this highly specific upregulation.

In conclusion, we here present the synthesis and structural modification of α-aminooxyacetic acid derivatives as a class of bactericidal antitubercular pro-drugs with promising cytotoxicity profile that are active against drug-resistant clinical isolates and exhibit potent intracellular activity in a human macrophage infection model. Partially redundant bioactivation is mediated by the amidohydrolases AmiC and Rv0552 that intracellularly hydrolytically unleash the "dirty drugs" and trigger pleiotropic effects. Future research will aim to elucidate the precise intracellular antibacterial mechanisms and to identify the relevant metabolites. Further structural optimization of the KSK compounds, alongside the performance of *in-vivo* studies, may pave the way for the development of urgently needed *M. tuberculosis*-specific anti-TB drugs.

MATERIAL & METHODS

Generation and cultivation of bacteria

Strains, oligonucleotides and plasmids used in this study are listed in Tables S4-S6. Mycobacterial cultures were grown aerobically at 37 °C shaking at 80 rpm in Middlebrook 7H9 liquid media supplemented with 10% ADS (0.8% NaCl, 5% BSA, 2% dextrose), 0.5% glycerol, 0,025% tyloxapol, and appropriate antibiotics (50 µg/mL hygromycin, 20 µg/mL kanamycin). For growth of *M. tuberculosis* on solidified medium, Middlebrook 7H10 agar supplemented with 10% ADS (5% (w/v) bovine serum albumin; 2% (w/v) glucose; 0.085% (w/v) sodium chloride) and 0.5% (v/v) glycerol was used. For testing growth on media without pyridoxine, *M. tuberculosis* strains were grown in liquid minimal medium [per liter: 0.15 g l-Asparagine × H_2O, 0.5 g $(NaH_4)_2SO_4$, 1 g KH_2PO_4, 2.5 g Na_2HPO_4, 50 mg ferric ammonium citrate, 0.5 g $MgSO_4 \times 7$ H_2O, 0.5 mg $CaCl_2$, 0.1 mg $ZnSO_4$, 0.05% (v/v) tyloxapol, pH 7.0 + 10% ADS and 0.5% glycerol]. *E. coli* cells were grown in lysogeny broth (LB)-medium or LB agar containing the respective antibiotics (150 µg/mL hygromycin, 40 µg/mL kanamycin, 100 µg/mL ampicillin).

Minimum inhibitory concentration assay

The minimum inhibitory concentrations of the tested compounds were quantified by dose-response curves using the resazurin microplate assay. In short, a two-fold serial dilution of tested compounds was prepared in a polystyrene U-bottom 96-well plate (Greiner) to result in dose-response curves ranging from 100 µM to 0.048 µM final concentrations. 50 µl of exponentially growing cells ($OD_{600\ nm} \leq 1$, diluted to 1 x 10^6 CFU/mL) were then added into each well to yield a total volume of 100 µl and cultivated for five days at 37°C (5% CO_2, 80% humidity). Subsequently, 10 µl resazurin solution (100 µg/ml, Sigma Aldrich) was added into each well and incubated overnight. Cells were fixed for 30 min at room temperature after the addition of 10% (v/v) formalin. Growth was quantified based on fluorescence using a microplate reader (TECAN) (excitation: 540 nm, emission: 590 nm). Relative growth was calculated to the DMSO solvent control (= 100% growth) and uninoculated wells (subtraction of background fluorescence = 0% growth). Experiments were performed in triplicates. MIC_{90} values are given as discrete, stepwise values representing the actually tested lowest compound concentration that resulted in 10% residual growth or less.

Cytotoxicity assay

To determine the cytotoxicity of the compounds *in vitro*, human cell lines derived from different tissues were used. THP-1 cells (leukemia monocytic cell line), CLS-54 (adenocarcinoma-derived

lung epithelial cell line), and HUH7 (hepatocyte-derived carcinoma cell line) were grown in RPMI supplemented with 10% fetal bovine serum (FBS). H4 (neuroglioma cell line) and SH-SY5Y (neuroblastoma cell line) cell lines were cultivated in DMEM supplemented with 10% FBS. MRC-5 (normal lung fibroblasts), HEK293 (epithelial-like embryonic kidney cell line), and HEPG2 (hepatocellular carcinoma cell line) cells were grown in EMEM supplemented with 1% non-essential amino acids, 1 mM sodium pyruvate, and 10% FBS. Sterile 96-well flat-bottom polystyrene plates (Greiner) were prepared with a two-fold serial dilution of compounds with 100 µM as the highest concentration. Approx. $5x10^4$ cells were seeded in each well in a total volume of 100 µL per well. The cells were incubated for 48 h at 37°C and 5% CO_2 before viability was quantified using the resazurin reduction assay as described above. All cell lines were obtained from CLS Cell Lines Dienstleistung GmbH.

Killing curve assay

M. tuberculosis H37Rv cells were growing in Middlebrook 7H9 supplemented with 10% ADS, 0.5% glycerol, and 0.05% tyloxapol to the exponential phase. This pre-culture was used to prepare cultures containing 10^6 CFU/mL, which were incubated either with KSK-104 or KSK-106 (0.25 µM) individually or in combination with the anti-tubular drugs isoniazid (10 µM), rifampicin (1 µM), bedaquiline, (0.5 µM), delamanid (0.5 µM) or ethambutol (10 µM). The cultures were incubated shaking at 80 rpm at 37 °C for 35 days. At indicated time points, aliquots were taken, serially diluted, and plated on Middlebrook 7H10 agar plates supplemented with 10% ADS and 0.5% glycerol to quantify colony forming units to determine the effects on the growth of *M. tuberculosis*. After 3 weeks colonies were counted. All experiments were performed as triplicates.

Macrophage Infection Assay

THP-1 cells were grown in RPMI medium supplemented with 10% FBS. Cells were counted using a haemocytometer and 10^5 cells were seeded into each well of a sterile 96-well flat-bottom polystyrene microtiter plate (Greiner) in a total volume of 100 µL. To differentiate the cells to adherent macrophage-like cells, the medium was supplemented with 50 nM phorbol-12-myristate-13-acetate.[63] After differentiation to adherent cells overnight, the macrophage-like cells were washed twice with PBS. An mCherry expressing recombinant *M. tuberculosis* H37Rv reporter strain was used for infection. Cells were grown in Middlebrook 7H9 broth containing 150 µg/mL hygromycin, harvested, washed and resuspended in RPMI supplemented with 10% FBS to a density of $3x10^6$ CFU/mL. 100 µL of this cell suspension was added to each well,

resulting in a multiplicity of infection = 3. After 3 h, cells were washed twice with PBS to remove non-phagocytosed bacteria. PBS was replaced with 100 µL RPMI + 10% FBS containing 0.5 µM KSK-104 or KSK-106 or different antibiotics (3 µM rifampicin, 20 µM streptomycin). After 5 days at 37°C, 5% CO_2 and 85% humidity, the macrophage-like cells were fixed with formalin (5% final concentration), and fluorescence was detected using a Nikon Eclipse TS100 fluorescence microscope. Additionally, viable cell counts were determined by lysing macrophages with ddH_2O for 30 minutes. Dilutions of each well were plated on Middlebrook 7H10 plates and colonies were counted after 3 weeks of incubation at 37°C.

Starvation-induced non-replicating persistence model

To test activity of compounds against non-replicating cells of *M. tuberculosis* H37Rv, cells were grown to stationary phase, harvested, washed thrice with PBS+0.025% tyloxapol, resuspended in PBS + 0.025% tyloxapol in the original culture volume and starved by incubation at 37 C for three weeks. Next, cells were diluted to 1×10^8 CFU/mL with PBS + 0.025% tyloxapol and transferred into 96-well round bottom microtiter plates to a final volume of 100 µl per well, and compounds were added at the indicated final concentrations. After five days of incubation at 37 °C as standing cultures, resazurin solution (10 µl/well from 100 µg/mL stock) was added, and cells were incubated for 48 h at 37 C.

Isolation of spontaneous resistant mutants and whole genome sequencing

Spontaneous resistant mutants were isolated by plating each approximately 6×10^7 – 1x 10^8 cells of *M. tuberculosis* H37Rv or the respective merodiploid or gene deletion strain, on solid media containing either 4, 6, or 10-fold MIC concentrations of the KSK derivatives, respectively. After four to six weeks, colonies were isolated. Genomic DNA from *M. tuberculosis* was isolated using the cetyltrimethylammonium bromide (CTAB)-lysozyme method as described by Larsen et *al.*, [64] quantified using the AccuClear® Ultra High Sensitivity dsDNA Quantitation Kit, and quality was measured by capillary electrophoresis using the Fragment Analyzer and the 'High Sensitivity genomic DNA Assay' (Agilent Technologies, Inc.). Genomes of resistant mutants were sequenced with an Illumina HiSeq 2500 next generation sequencer (at Texas A&M University, College Station, TX , USA) after preparing sequencing libraries using standard paired-end genomic DNA sample prep kit from Illumina. Paired-end sequence data was collected with a read length of 150 bp. Base-calling was performed with Casava software, v1.8. The reads were assembled using a comparative genome assembly method, with *M. tuberculosis* H37RvMA as a

reference sequence (GenBank accession GCA_000751615.1).[65] The mean depth of coverage ranged from 214-282x for KSK-104 mutants, and 12-28x for KSK-106 mutants.

Heterologous gene expression in mycobacteria

The respective gene regions were amplified using the designed oligonucleotides (Table S5) and cloned into the expression vector pMV361, which contains a kanamycin resistance gene and a strong constitutive *hsp60* promoter, using *Hin*dIII and *Pac*I (New England Bioloabs) restriction sites by chemically transformation of *E. coli* NEB-5α cells. Sequenced plasmids containing the respective gene of interest or the pMV361::empty vector (EV) were electroporated into *M. smegmatis* mc^2155, *M. bovis* BCG Pasteur or *M. tuberculosis* H37Rv and plated on 7H10 selective plates as described previously.[64] Single colonies were picked and grown in selective 7H9 media after three weeks of incubation.

Construction of targeted gene deletion mutants

Specialized transduction was employed to achieve gene disruptions in *M. tuberculosis* H37Rv.[66] Briefly, an allelic exchange substrate was designed to replace the gene/s of interest in *M. tuberculosis* with a γδ*res-sacB-hyg*-γδ*res* cassette comprising a *sacB* as well as a hygromycin resistance gene flanked by *res*-sites of the γδ-resolvase. Upstream and downstream flanking regions of the gene/s of interest were amplified by PCR using primers listed in Table S5. Subsequently, the flanking regions were digested with the indicated restriction enzymes and ligated with the *Van91*I-digested p0004S vector. The resulting allelic exchange plasmid was then linearized with *PacI*, cloned, and packaged in the temperature-sensitive phage ΦphAE159, yielding knock-out phages that were propagated in *M. smegmatis* at 30 °C. Allelic exchange in *M. tuberculosis* was performed through specialized transduction at the non-permissive temperature of 37°C, using hygromycin for selection. This led to the resulting gene deletion/s and replacement by the γδ*res-sacB-hyg*-γδ*res* cassette. After isolation of genomic DNA, the obtained hygromycin-resistant transductants were then screened for correct gene disruption by diagnostic PCR analysis (Figure S6).

Site-directed mutagenesis

Suitable primer pairs (Table S5) were designed utilizing the Q5 site-directed mutagenesis kit (New England Biolabs) to generate mutated amidases. The pMV361::*Rv0552* or pMV361::*amiC* constructs were employed as templates and the procedure was conducted as instructed by the

manufacturer. The resultant products were then transformed into competent *E. coli* NEB-5α cells. Plasmids containing the predicted mutations were confirmed through Sanger-sequencing.

Protein homology modelling

The Phyre2 web portal was used for protein modelling, prediction and analysis.[20] Regarding Rv0552, 474 residues (equivalent to 89% of the sequence) were modelled with a 100.0% accuracy rate by the single highest-scoring template. The template for Rv0552 was presented by an uncharacterized, metal-dependent hydrolase from *Pyrococcus horikoshii* ot3 (PDB ID: 3igh). AmiC has also been modelled with a 100.0% confidence rate using the highest-scoring template, resulting in 466 residues being modelled effectively. The structure of *Arabidopsis* fatty acid amide hydrolase was utilized (PDB ID: 6DII) as a template. For further structural analysis, the software tool PyMol was used.[67]

Transposon mutagenesis and sequencing

M. tuberculosis H37Ra cells were mutagenized with the mariner *himar1* transposon via the temperature-sensitive mycobacteriophage phAE180.[68,69] Cultures containing the mutagenized cells, with a starting inoculum of $OD_{600\,nm}$ = 0.01, were grown on Middlebrook 7H9 medium supplemented with 10% OADC, 0.5% glycerol, 0,025% tyloxapol, and 50 µg/ml kanamycin. Cells were incubated at 37°C without or with 0.18 µM KSK-106 for five generation times until the final $OD_{600\,nm}$ = 0.3 was attained. For transposon insertion sequencing, cells were collected, and genomic DNA was extracted as described above. DNA was fragmented and Ilumina P7 adapter with the sequence CAAGCAGAAGACGGCATACGAGAT were ligated using the NeoPrep library prep system (Ilumina). Next, transposon junctions were amplified by using a transposon-specific primer (TCGTCGGCAGCGTCAGATGTGTATAAGAGACAGCCGGGGACTTATCAGCCAACC) and a primer P7 (CAAGCAGAAGACGGCATACGAGAT) using the HotStarTaq master mix kit (Qiagen). The himar1-enriched samples were diluted in a ratio of 1:50. Afterward, amplification was carried out using a p5 indexing primer comprising the sequence AATGATACGGCGACCACCGAGATCTACAC[i5]TCGTCGGCAGCGTC (where [i5] denotes the barcode sequence) and a P7 primer in combination with the HotStarTaq master mix kit from Qiagen. This process added unique barcodes as well as the necessary P5 and P7 flow cell adapter sites required for Illumina sequencing. The PCR protocol employed comprised of an initial denaturation step at 94°C for 3 minutes, followed by a cycle of denaturation at 94°C for 30

seconds, annealing at 55°C for 30 seconds, and extension at 72°C for 30°C. The sequencing was carried out on an Illumina MiSeq system at the University of Minnesota Genomics Center.

After sequencing, transposon and adapter sequences were removed from the 5' end of the sequencing reads using Cutadapt. [70] Furthermore, reads lacking adapter sequences in the 5' trimming process were discarded. After trimming, all sequence reads started with "TA". For analysis, all sequences shorter than 18 base pairs were excluded, and a default error rate of 0.1 was applied during the trimming processes. Next, the trimmed sequence reads were aligned to the *M. tuberculosis* H37Ra reference genome (GenBank no. NC_009525.1) using bowtie2.[71] The alignment permitted a maximum of one base pair mismatch. The genome-mapped sequence reads were printed as a SAM file format, and the count of sequence reads per TA site was determined using the SAMreader_TA script.[72] These SAM files were subsequently converted into WIG files for further analysis in the TRANSIT software using the resampling method for differentially essentiality analysis.[28] In short, this analysis calculates the read counts at each gene for each replicate of each condition. The mean read-out in condition A is subtracted from condition B to calculate the observed difference in means. Following this, the TA sites are permuted for a given number of "samples". or each permutation, we generate a null distribution for the discrepancy in mean read-counts. A p-value was then calculated for the observed discrepancy in mean read-counts P-values were adjusted for multiple testing using the Benjamini-Hochberg procedure.[73]

RNA-isolation and sequencing for transcriptome analysis

At least 20 mL of *M. tuberculosis* mc^{2}6030 cultures were cultivated to the mid-logarithmic phase ($OD_{600\,nm}$= 0.5) in 7H9 broth. Triplicate cultures were treated with a lethal concentration (1.9 µM) of KSK-106, whereas control cells were treated with a n equivalent amount of DMSO. After incubation for one generation time, total RNA was isolated. Cells were pelleted by centrifugation and resuspended in 500 µL of Tri Reagent (Invitrogen) plus 1% polyacryl carrier (Molecular Research Center). The samples were transferred to tubes containing 250 µL of 0.1 mm zirconia beads (BioSpec). The samples were bead-beated twice, each time for one minute with a two-minute break on ice between runs. Samples were centrifuged to pellet the beads and the supernatant solution was transferred to fresh tubes. Next, 50 µL of 5-bromo-3-chloro-propane was added to each sample, which were then vortexed and incubated at room temperature for 10 minutes. Following this, samples were centrifuged for 10 minutes at 10,000 rpm at 4°C before the upper aqueous phase was transferred into a fresh tube. Subsequently, 250 µL of isopropanol was added to each sample, they were inverted and incubated at room temperature for 10 min again. The RNA pellets were then formed by centrifuging the samples at 10,000 rpm for an

additional 15 minutes at 4°C. The supernatant was removed, and 300 µL of 75% ethanol was added. DNase I Turbo (Invitrogen by Thermo Fisher Scientific) was utilized to remove DNA contaminations following the manufacturer's protocol. The supernatant was removed after the re-pelleting of RNA, and the RNA was air-dried for 5 to 10 minutes. Thereafter, the RNA was eluted in 50 µL of RNase-free dH_2O and stored at -80°C for long-term use.

For RNA-seqencing, the Illumina® Stranded Total RNA Prep and Ribo-Zero Plus Ligation kits were employed to convert total RNA into dual-indexed libraries. Briefly, abundant transcripts from total RNA were deleted and bound by specific depletion reagents before the remaining RNA was converted into cDNA throught reverse transcription. Subsequent ligation and amplification steps added adapters for clustering and sequencing on an Illumina system. The libraries were pooled and sequenced on a NovaSeq SP 2x50-bp run. The run generated more than 375 milion pass filter reads with all anticipated barcodes detected and well represented. The mean quality score was ≥Q30f for all libraries. Gel-sizing was done for the libraries, selecting inserts of approximately 200 bps. Raw sequencing reads were quality trimmed (3' adapter CTGTCTCTTATACACATCT) by using the tool CutAdapt and short reads were eliminated. The trimmed reads were aligned with bowtie2 to the *M. tuberculosis* reference genome NC_000962.3. Normalized read counts were counted using FeatureCounts and log2 transformed with DEseq2 for further analysis, wherein differential gene expression was statistically determined. Subsequently, further analysis was carried out using Rstudio. RNA-sequencing was performed at the University of Minnesota Genomics Center.

Proteomic profiling employing LC-MS/MS

Cells of *M. tuberculosis* H37Rv were sublethally treated with either 0.05 or 0.2 µM KSK-106, respectively, in 20 mL Middlebrook 7H9 medium supplemented with 0.5% glycerol, 0.2% glucose, 0.085% NaCl and 0.05% tyloxapol and incubated for 10 days. Cells cultivated in Middlebrook 7H9 medium containing an equivalent amount of DMSO were used a solvent control. Cells were centrifuged at 4 °C and washed thrice with PBS (137 mM NaCl; 2.7 mM KCl; 10 mM Na_2HPO_4; 1.8 mM KH_2PO_4; pH 7.4). Cells were finally resuspended in 2 mL PBS and lysed by bead beating using 100 µm silica-zirconium beads at 50 Hz for 3x3 minutes. Afterwards, 200 µL of a 10% SDS solution was added to each sample, vortexed carefully and incubated for 30 minutes at 4 °C. After centrifugation, the clear supernatant was collected and filter-sterilized thrice through a bacteria-tight 0.2 µM cellulose acetate filter. Protein concentration was measured with BCA assay (Merck Millipore).

For each sample, a volume equivalent to 30 µg of protein was transferred to fresh centrifuge tubes and PBS was added to give a final volume of 115 µL. To eliminate metabolites and non-protein impurities, a methanol-chloroform precipitation was performed. For this purpose, a fourfold excess of methanol was added, followed by 100 µL of chloroform and 300 µL of H_2O, with thorough mixing in between. To facilitate phase separation, the samples were centrifuged at 9,000 g for 5 min, and the upper aqueous layer was then discarded. The precipitated proteins were washed three times with 300 µL of methanol (sedimentation for 2 min at 9,000 g), and the supernatant was discarded. Subsequently, the dried protein pellet was dissolved in 50 µL of 8 M urea (Cytiva, 17131901) in 100 mM NH_4HCO_3 (ABC; Sigma-Aldrich, 11213) and 5 mM dithiothreitol (DTT; Sigma-Aldrich, 11213) was added. After incubating for 40 min with shaking at 1,000 rpm, iodoacetamide (IAA; Sigma-Aldrich, A3221) was added to a final concentration of 20 mM. The mixture was then incubated for an additional 30 min at 37 °C with shaking at 1,000 rpm in the dark and unreacted IAA was afterwards inactivated by addition of DTT to a final concentration of 25 mM. To perform proteolytic digestion, 1 µg of Lys-C (FUJIFILM, 125-05061) was added to each sample, followed by incubation for 3 h at 37 °C with shaking at 1,000 rpm. Subsequently, the urea concentration was reduced to 2 M by the addition of 100 mM ABC. Trypsin (1 µg per sample; Thermo Fisher Scientific, 90057) was added and the digest was continued overnight at 37 °C with shaking at 1,000 rpm. The digest was stopped by addition of formic acid (FA; Fisher Chemical, A11705AMP) to a final concentration of 5% and samples were desalted on self-made C18 StageTips (two discs per tip; 3M, 66883-U) as described before.[74] For LC-MS/MS analysis, the dry peptides were dissolved in 20 µL 0.1% FA (15 min, 1,500 rpm) and a volume of 5 µL was loaded on a self-packed fused silica capillary tube with integrated pico frit emitter (75 µm ID x 37 cm, 15 µm orifice; New Objectives, PF360-75-15-N-5) filled with ReproSil-Pur 120 C18-AQ (particle size 1.9 µm, Pore Size 120 Å; Dr. Maisch, r119.aq.) material. Peptides were separated using a 140 min gradient generated by an EASY-nLC 1000 liquid chromatography (Thermo Fisher Scientific) with the column heated to 50 °C by a PRSO-V1 column oven (Sonation). For gradient mixture, a rising proportion of acetonitrile (ACN; Honeywell, 14261) with 0.1% FA (solvent B) in H_2O (Honeywell, 14263) with 0.1% FA (solvent A) was used (7-35% B in A within the first 120 min, 35-80% in the next 10 min, hold for 10 min) at a flow rate of 300 nL/min. Peptides were ionized using a Nanospray Flex ion source (Thermo Fisher Scientific) with 1,800 V spray voltage and MS acquisition was performed in an Orbitrap Elite spectrometer (Thermo Fisher Scientific). MS1 data acquisition was done in a *m/z* range of 300 to 1,800 at a 60,000 orbitrap resolution with a maximal injection time of 50 ns. For data-dependent MS2 acquisition, the 15 most intense MS1 scans were selected with a dynamic exclusion duration of 120 seconds. For precursor isolation, a 2.0 *m/z* quadrupole isolation width

was used with subsequent CID fragmentation with a normalized collision energy of 35% and data acquisition at rapid ion trap scan rate with 300% of normalized AGC target. For data processing, MaxQuant 2.3.1.0[75] was used with the Uniprot proteome UP000001584 as the protein database. [76] MaxQuant standard settings were applied with LFQ algorithm and retention time alignment turned on.[77] For subsequent statistical analysis Perseus 2.0.7.0. was used.[78] The LFQ data was transformed to the log_2 scale and missing data points were imputed with values from the lower range of the normal distribution. A Student's T-test with permutation-based false discovery rate (FDR) with 250 randomizations and an FDR threshold of 0.01 was performed to identify significantly changed protein groups.

Analysis of KSK cleavage products using LC-MS

Cells of an exponentially growing *M. tuberculosis* H37Rv culture were harvested, washed twice with Middlebrook 7H9 medium containing 0.5% (v/v) glycerol, 0.2% (w/v) glucose and 0.085% (w/v) sodium chloride and resuspended in the same medium to result in an $OD_{600\ nm}$ of 1. A final concentration of 100 µM of KSK-104 or KSK-106 or the corresponding volume of DMSO was added to the cells. After 48 h of incubation, a 2.5 mL aliquot was removed from each culture and lysed by bead beating at 50 Hz for 5x3 minutes using 100 µm silica-zirconium beads. The samples were mixed with equal amounts of methanol and incubated for at least one hour at room temperature, before they were centrifugated for 10 minutes at 14,000 rpm. The supernatants were evaporated by freeze-drying in a Savant SpeedVac (Thermo Scientific), and the dried concentrate was solved in 250 µL methanol. The concentrated methanol extracts were measured using an UHR-QTOF maXis 4G (Bruker Daltonics) coupled to an Ultimate 3000 RS UHPLC (Dionex) at the following parameters: Ascentis Express C18 column, 5 cm x 2.1 mm, 2 µm; injection volume 2 µl; solvents: CH_3CN + 0.1 % FA, H_2O + 0.1 % FA; flow: 300 µl/min; gradient: 10 % CH_3CN to 100 % CH_3CN in 8 min, keep constant for 3 min. ESI-MS was done in positive ion mode with a scan from 50 m/z to 1500 m/z. Measurement was performed at the Center of Molecular and Structural Analytics@Heinrich Heine University (CeMSA@HHU).

Pharmacokinetic investigations using LC-MS/MS

A liquid chromatography coupled to mass spectrometry (LC-MS/MS) method was developed to determine KSK 104, KSK 106 and their main metabolites. Chromatographic separation was conducted using a Waters Acquity UPLC (Waters, Milford, USA) consisting of a binary pump, the column oven and an autosampler. An Aqua 3u C18 125A (100x2.0mm 3 µm, Phenomenex, Torrance, USA) column was utilized, applying 0.1% formic acid in water and methanol as mobile phase A and B. The flow rate was set to 0.5 mL/min and the following gradient was used: 0-1.5

min: 20% B, 1.4-4.0 min 20-50%, 4-4.5 min 50% B, 4.5-5 min: 50-70% B, 5-5.5 min 70-100% B, 5.5-7 min: 100% B, 7-7.5 min: 100-20% B with a re-equilibration time of 2 min. The column oven was set to 50 °C. Mass spectrometric detection was performed with a Waters Quattro Premier XE in electrospray ionization positive multiple reaction monitoring mode. The capillary voltage was set to 3.5 kV, the source temperature to 135 °C, desolvation temperature to 500 °C, the cone gas flow to 50 L/h, and the desolvation gas flow to 900 L/h. The analyte-specific settings were as follows: KSK-104 376.8 → 180.9 m/z (cone voltage (CV): 18 V, collision energy (CE): 20 V) and KSK-106 386.7 → 190.9 m/z (CV 20 V, CE 20 V). Carvedilol was used as the internal standard with the transition measured 406.8 → 100.0 m/z (CV: 36, CE: 29 V).

Plasma and whole blood stability: In vitro plasma/whole blood stability was studied in fresh human ethylenediaminetetraacetic acid (EDTA) plasma and whole blood at 37 °C. Fresh whole blood/plasma was prewarmed to 37 °C and reactions were started by spiking KSK 104 and KSK 106 to a final concentration of 50 ng/mL. Sample aliquots of 100 µL were taken at 0, 2, 4, 6 and 24 hours. Each aliquot was mixed with 300 µL ice-cold acetonitrile containing the internal standard, and directly vortexed followed by 30 min shaking at 800 rpm at room temperature. Then, samples were centrifuged for 10 min at 13.200 xg. 300 µL of the supernatant was evaporated to dryness under a gentle nitrogen stream and shaking at 450 rpm at 60 °C. Samples were reconstituted in 100 µL 50/50 methanol/water (v/v). The assay was conducted in triplicate. *In vitro* plasma half-life ($t_{1/2}$) was calculated by $t_{1/2}=\ln 2/k_e$, where k_e is the slope in the linear fit of the natural logarithm of the fraction remaining of the parent compound vs. incubation time.

Blood-to-plasma ratio: The blood-to-plasma ratio ($K_{B/P}$) was determined to investigate the drug binding of KSK-106 to erythrocytes. Therefore, freshly drawn whole blood was spiked to a final concentration of 50 ng/mL, cautiously shaken to avoid lysis, and incubated at 37 °C for 30 min. Spiked whole blood was centrifuged at room temperature for 10 min at 2,000 x g and the obtained plasma and red blood cell (RBC) fraction was used for analysis. Additionally, plasma and RBC were directly spiked to a final concentration of 50 ng/mL and also incubated for 30 min at 37 °C (reference plasma/RBC; not considering distribution into the red blood fraction). 100 µL of reference plasma/RBC and of plasma/RBC separated from spiked whole blood were precipitated with 300 µL of ice-cold acetonitrile containing 10 ng/mL of the internal standard. Following immediate vortexing, samples were shaken for 30 minutes at 800 rpm at room temperature. Subsequently, samples were centrifuged for 10 min at 13,200 x g and 300 µL of the supernatant was evaporated to dryness under a heated nitrogen stream at 60 °C. The residue was reconstituted in 100 µL 50/50 methanol/water (v/v). Whole blood and plasma of two donors (male and female) in three independent replicates were used for the analysis. The hematocrit was determined volumetrically. The blood-to-plasma ratio was calculated according to Equation 1.

$$K_P^B = \frac{area\ ratio\ RBC\ fraction}{area\ ratio\ reference\ RBC} / \frac{area\ ratio\ plasma\ fraction}{area\ ratio\ reference\ plasma} * H + (1 - H)$$

Equation 1. Calculation of the blood-to-plasma ratio $K_{B/P}$. H: hematocrit, RBC: red blood cell

Permeation: The permeation of KSK 106 was assessed using an automated setup of the Kerski diffusion cell coupled to Hanson Research AutoPlus™ (Teledyne Hanson, Los Angeles, USA).[79] PermeaPad (PHABIOC, Karlsruhe, Germany) was used as a biomimetic barrier to simulate the passive mass transport of the gastrointestinal tract. The formulations to be tested, an oily formulation consisting of Miglyol 812/Transcutol HP 80/20 (v/v) with a concentration of 100 µg/mL as well as a formulation of 10 µg/mL in Tween 80/ethanol/phosphate buffered saline (PBS) pH 7.4 7/3/90 (v/v), were placed onto the barrier. PBS pH 7.4 was used as acceptor medium. Constant environmental conditions of 37 °C and 20% relative humidity (KBF 115 Constant Climate Chamber, Binder GmbH, Tuttlingen, Germany), as well as continuous stirring at 750 rpm (2mag Mixcontrol20, Munich, Germany), were maintained throughout the study period. Fully automated sampling was conducted at 30, 60, 120, 180 and 240 min. For the analysis of the permeability, the cumulative amount of permeated drug (Qt), steady-state flux (Jss), and apparent permeability coefficient (Papp) were calculated using **Equation *2***2, 3 and 4.

$$Q_t = \frac{c_n * V_a + (\sum_{n=1}^{n} c_{n-1}) * V_R}{A}\ [\mu g/cm^2]$$

Equation 2. Calculation of cumulative amount of permeated drug Q_t. c_n: drug concentration at time point n, c_{n-1}: drug concentration at previous time point, V_A: volume of acceptor chamber, V_R: removed volume: A: permeation area

$$J_{SS} = \frac{\Delta Q_t}{(\Delta t * A)}\ [\mu g/cm^2/h]$$

Equation 3. Calculation of the steady state flux J_{SS}. ΔQ_t: difference of Q_t between time points, Δt: time difference, A permeation area

$$P_{app} = \frac{J_{SS}}{CD}\ [cm * s - 1]$$

Equation 4. Calculation of the apparent permeability coefficient (P_{app}). J_{SS}: steady-state-flux, CD: initial drug concentration

Synthesis of lead structures 7, 8 and analogs 15 – 22

General procedure 1 (GP 1): EDC-mediated coupling reactions

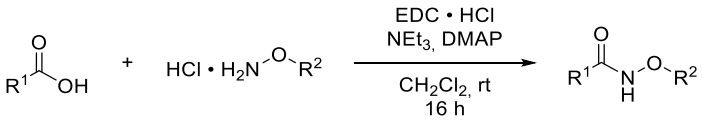

Method A: Under nitrogen atmosphere the appropriate *O*-substituted hydroxylamine hydrochloride (1.00 eq.), triethylamine (1.20 eq.) and *N,N*-dimethylpyridin-4-amine (0.10 eq.) were dissolved in dry dichloromethane (20.0 mL/mmol based on hydroxylamine hydrochloride). After stirring for 10 min at room temperature, the corresponding carboxylic acid (1.00 eq.) and 1-ethyl-3-(3-dimethylaminopropyl)carbodiimide hydrochloride (1.25 eq.) were added. The reaction mixture was stirred for 16 h at room temperature.

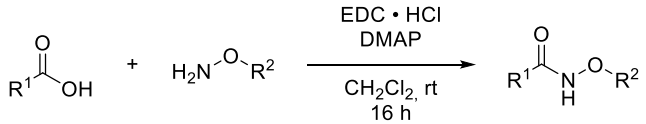

Method B: Under nitrogen atmosphere the appropriate *O*-substituted hydroxylamine (1.00 eq.) and *N,N*-dimethylpyridin-4-amine (0.10 eq.) were dissolved in dry dichloromethane (20.0 mL/mmol based on hydroxylamine). After stirring for 10 min at room temperature, the corresponding carboxylic acid (1.00 eq.) and 1-ethyl-3-(3-dimethylaminopropyl)carbodiimide hydrochloride (1.25 eq.) were added. The reaction mixture was stirred for 16 h at room temperature.

Work-up A: The reaction mixture was washed three times with saturated sodium bicarbonate solution (20.0 mL/mmol based on hydroxylamine hydrochloride), once with 10 % citric acid solution (20.0 mL/mmol based on hydroxylamine hydrochloride) and once with saturated sodium chloride solution (20.0 mL/mmol based on hydroxylamine hydrochloride). The organic layer was dried over anhydrous sodium sulfate, filtered and the solvent was removed under reduced pressure. The crude product was purified by flash chromatography on silica gel (*n*-hexane/ethyl acetate) and subsequently recrystallized from ethyl acetate.

Work-up B: The reaction mixture was washed three times with saturated sodium bicarbonate solution (20.0 mL/mmol based on hydroxylamine) and once with saturated sodium chloride

solution (20.0 mL/mmol based on hydroxylamine). The organic layer was dried over anhydrous sodium sulfate, filtered and the solvent was removed under reduced pressure. The crude product was purified by flash chromatography on silica gel (*n*-hexane/ethyl acetate) and subsequently recrystallized from ethyl acetate.

***N*-(2-((Benzyloxy)amino)-2-oxoethoxy)-[1,1'-biphenyl]-4-carboxamide: KSK-104 (7)**

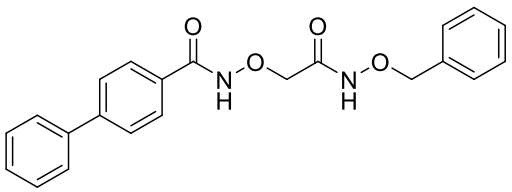

Synthesis according to **GP 1** (method A, work-up A), KSK-104 (**7**) was synthesized from **6a** and **5** and obtained as a colorless solid (72 % yield).

^{1}H-NMR (600 MHz, DMSO-d_6) δ 12.16 (s, 1H), 11.50 (s, 1H), 7.90 – 7.83 (m, 2H), 7.79 (d, J = 8.1 Hz, 2H), 7.76 – 7.70 (m, 2H), 7.50 (t, J = 7.7 Hz, 2H), 7.44 – 7.38 (m, 3H), 7.39 – 7.27 (m, 3H), 4.86 (s, 2H), 4.39 (s, 2H).

^{13}C-NMR (151 MHz, DMSO-d_6) δ 164.91, 164.66, 143.48, 138.95, 135.74, 130.25, 129.06, 128.84, 128.31, 128.21, 127.93, 126.89, 126.69, 77.04, 73.19

HPLC t_R = 13.06 min, purity = 96.2 %

Mp. T_M = 151.2 °C

***N*-(2-((Benzyloxy)amino)-2-oxoethoxy)-4-(pentyloxy)benzamide: KSK-106 (8)**

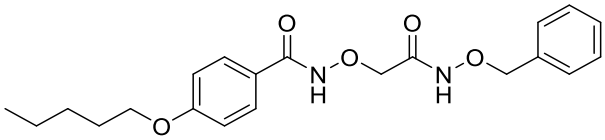

Synthesis according to **GP 1** (method A, work-up A), KSK-106 (**8**) was synthesized from **6b** and **5** and obtained as a colorless solid (74 % yield).

^{1}H-NMR (600 MHz, DMSO-d_6) δ 11.93 (s, 1H), 11.52 (s, 1H), 7.76 – 7.70 (m, 2H), 7.36 (m, 5H), 6.98 – 7.02 (m, 2H), 4.85 (s, 2H), 4.36 (s, 2H), 4.01 (t, J = 6.54 Hz, 2H), 1.71 (m, 2H), 1.32 – 1.40 (m, 4H), 0.89 (t, J = 7.10 Hz, 3H)

^{13}C-NMR (151 MHz, DMSO-d_6) δ 165.14, 164.87, 161.62, 135.74, 129.13, 128.84, 128.31, 123.23, 114.2, 77.03, 73.34, 67.72, 28.23, 27.64, 21.87, 13.9

HPLC t_R = 14.60 min, purity = 99.9 %

Mp. T_M = 134.0 °C

***N*-(2-((Benzyloxy)amino)-2-oxoethoxy)-4-(heptyloxy)benzamide (15)**

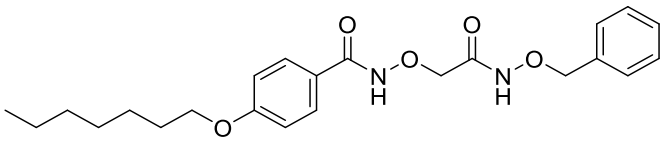

Synthesis according to **GP 1** (method A, work-up A), KSK-Analog **15** was synthesized from **6c** and **5** and obtained as a colorless solid (49 % yield).

^{1}H-NMR (300 MHz, chloroform-*d*) δ 11.42 (s, 1H), 9.43 (s, 1H), 7.70 – 7.62 (m, 2H), 7.35 (ddd, *J* = 2.0, 5.9, 33.2 Hz, 5H), 6.93 – 6.86 (m, 2H), 4.95 (s, 2H), 4.48 (s, 2H), 3.98 (t, *J* = 6.6 Hz, 2H), 1.78 (dt, *J* = 6.5, 8.0 Hz, 2H), 1.51 – 1.24 (m, 8H), 0.95 – 0.84 (m, 3H)

^{13}C-NMR (75 MHz, chloroform-*d*) δ 168.23, 166.34, 163.06, 135.12, 129.43, 129.21, 128.75, 128.57, 121.90, 114.64, 78.38, 75.62, 68.43, 31.88, 29.20, 29.15, 26.05, 22.72, 14.21

HPLC t_R = 17.29 min, purity = 97.9 %

Mp. T_M = 134.3 °C

***N*-(2-(*tert*-Butoxyamino)-2-oxoethoxy)-4-(pentyloxy)benzamide (16)**

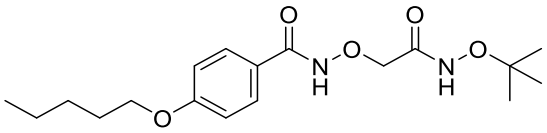

Synthesis according to **GP 1** (method A, work-up A), KSK-Analog **16** was synthesized from **11** and **14a** and obtained as a yellow oil (55 % yield).

^{1}H-NMR (600 MHz, DMSO-d_6) δ 11.98 (s, 1H), 10.91 (s, 1H), 7.77 – 7.69 (m, 2H), 7.03 – 6.97 (m, 2H), 4.39 (s, 2H), 4.02 (t, *J* = 6.5 Hz, 2H), 1.76 – 1.68 (m, 2H), 1.43 – 1.30 (m, 4H), 1.17 (s, 9H), 0.89 (t, *J* = 7.2 Hz, 3H)

^{13}C-NMR (126 MHz, DMSO-d_6) δ 165.60, 165.45, 161.57, 128.99, 123.11, 114.15, 80.76, 73.72, 67.66, 28.09, 27.50, 26.14, 21.69, 13.71

HPLC t_R = 13.95 min, purity = 99.9 %

***N*-(2-((Benzyloxy)amino)-2-oxoethoxy)-4-(thiazol-2-yl)benzamide (17)**

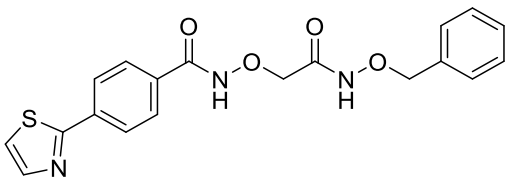

Synthesis according to **GP 1** (method A, work-up B), KSK-Analog **17** was synthesized from **6d** and **5** and obtained as a colorless solid (18 % yield).

^{1}H-NMR (300 MHz, chloroform-*d*) δ 11.26 (s, 1H), 10.16 (s, 1H), 8.05 – 7.96 (m, 2H), 7.92 (d, *J* = 3.3 Hz, 1H), 7.86 – 7.73 (m, 2H), 7.44 (d, *J* = 3.3 Hz, 1H), 7.43 – 7.27 (m, 5H), 4.96 (s, 2H), 4.52 (s, 2H)

^{13}C-NMR (75 MHz, chloroform-*d*) δ 167.10, 166.02, 157.60, 143.49, 136.52, 135.14, 131.72, 129.24, 128.83, 128.64, 128.29, 127.06, 120.54, 78.45, 77.36

HPLC t_R = 10.50 min, purity = 99.9 %

Mp. T_M = 138.1 °C

***N*-(2-Oxo-2-((pyridin-2-ylmethoxy)amino)ethoxy)-[1,1'-biphenyl]-4-carboxamide (18)**

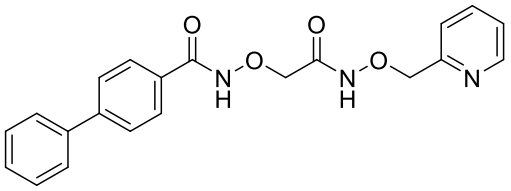

Synthesis according to **GP 1** (method A, work-up B), KSK-Analog **18** was synthesized from **10** and **14e** and obtained as a colorless solid (63 % yield).

^{1}H-NMR (300 MHz, DMSO-d$_6$) δ 4.40 (s, 2H), 4.96 (s, 2H), 7.34 (ddd, J = 7.6, 4.8, 1.2 Hz, 1H), 7.38 – 7.46 (m, 1H), 7.46 – 7.59 (m, 3H), 7.70 – 7.76 (m, 2H), 7.76 – 7.88 (m, 5H), 8.54 (ddd, J = 5.0, 1.8, 0.9 Hz, 1H), 11.64 (s, 1H), 12.06 (s, 1H)

^{13}C-NMR (151 MHz, DMSO) δ 73.6, 78.3, 123.0, 123.7, 127.1, 127.3, 128.3, 128.7, 129.5, 130.7, 137.2, 139.4, 143.8, 149.5, 156.1, 165.3, 165.5

HPLC t_R = 8.77 min, purity = 99.0 %

Mp. T_M = 152.8 °C

***N*-(2-Oxo-2-(phenoxyamino)ethoxy)-[1,1'-biphenyl]-4-carboxamide (19)**

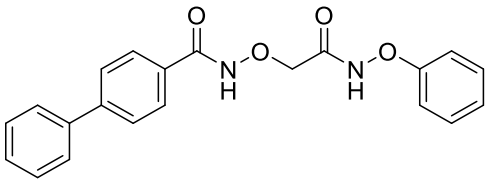

Synthesis according to **GP 1** (method A, work-up A), KSK-Analog **19** was synthesized from **10** and **14c** and obtained as a colorless solid (20 % yield).

^{1}H-NMR (600 MHz, DMSO-d$_6$) δ 4.59 (s, 2H), 7.01 – 7.10 (m, 3H), 7.28 – 7.36 (m, 2H), 7.39 – 7.45 (m, 1H), 7.50 (t, *J* = 7.7 Hz, 2H), 7.74 (d, 2H), 7.81 (d, *J* = 8.0 Hz, 2H), 7.90 (d, *J* = 7.9 Hz, 2H), 12.25 (s, 2H)

^{13}C-NMR (151 MHz, DMSO) δ 73.4, 113.4, 123.0, 127.2, 127.4, 128.4, 128.7, 129.5, 129.9, 130.7, 139.4, 144.0, 159.7, 165.9, 168.4

HPLC t_R = 13.33 min, purity = 96.0 %

Mp. T_M = 135.4 °C

***N*-(2-((Hexyloxy)amino)-2-oxoethoxy)-[1,1'-biphenyl]-4-carboxamide (20)**

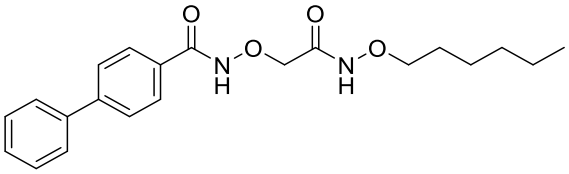

Synthesis according to **GP 1** (method A, work-up A), KSK-Analog **20** was synthesized from **10** and **14b** and obtained as a colorless solid (74 % yield).

^{1}H-NMR (300 MHz, chloroform-d) δ 0.80 – 0.91 (m, 3H), 1.20 – 1.46 (m, 6H), 1.61 – 1.74 (m, 2H), 3.95 (t, *J* = 6.8 Hz, 2H), 4.57 (s, 2H), 7.33 – 7.52 (m, 3H), 7.55 – 7.64 (m, 2H), 7.63 – 7.70 (m, 2H), 7.82 – 7.92 (m, 2H), 9.88 (br s, 1H), 11.43 (br s, 1H)

^{13}C-NMR (126 MHz, chloroform-d) δ 14.1, 22.7, 25.5, 28.1, 31.7, 75.8, 77.1, 127.4, 127.6, 128.0, 128.5, 129.0, 129.1, 139.8, 145.8, 166.2, 167.9

HPLC t_R = 14.93 min, purity = 97.3 %

Mp. T_M = 102.5 °C

***N*-((1-((Benzyloxy)amino)-1-oxopropan-2-yl)oxy)-[1,1'-biphenyl]-4-carboxamide (21)**

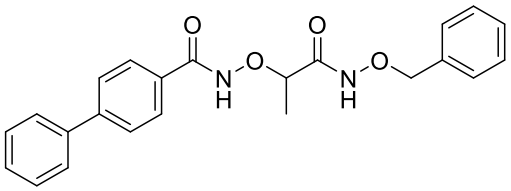

Synthesis according to **GP 1** (method B, work-up A), KSK-Analog **21** was synthesized from **13** and **2** and obtained as a colorless solid (70 % yield).

^{1}H-NMR (600 MHz, DMSO-d$_6$) δ 1.35 (d, J = 6.7 Hz, 3H), 4.40 (q, J = 6.6 Hz, 1H), 4.84 (q, J = 11.0 Hz, 2H), 7.29 – 7.34 (m, 3H), 7.36 – 7.40 (m, 2H), 7.40 – 7.44 (m, 1H), 7.50 (dd, J = 8.4, 7.0 Hz, 2H), 7.73 (dt, J = 6.3, 1.3 Hz, 2H), 7.79 (d, J = 8.0 Hz, 2H), 7.86 (d, J = 8.2 Hz, 2H), 11.45 (s, 1H), 12.02 (s, 1H)

^{13}C-NMR (151 MHz, DMSO) δ 17.2, 77.4, 79.2, 127.1, 127.3, 128.4, 128.6, 128.7, 128.8, 129.4, 129.5, 130.9, 136.2, 139.5, 143.9, 165.4, 168.1

HPLC t_R = 13.33 min, purity = 97.9 %

Mp. T_M = 177.8 °C

***N*-(2-((Cyclohexylmethoxy)amino)-2-oxoethoxy)-[1,1'-biphenyl]-4-carboxamide (22)**

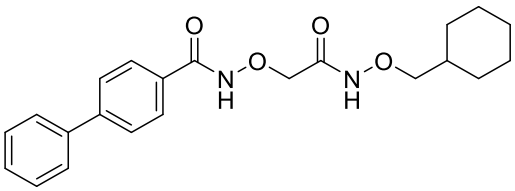

Synthesis according to **GP 1** (method A, work-up A), KSK-Analog **22** was synthesized from **10** and **14d** and obtained as a colorless solid (94 % yield).

^{1}H-NMR (600 MHz, DMSO-d$_6$) δ 0.88 – 0.99 (m, 2H), 1.06 – 1.25 (m, 3H), 1.56 – 1.69 (m, 4H), 1.69 – 1.77 (m, 2H), 3.62 (d, *J* = 6.7 Hz, 2H), 4.39 (s, 2H), 7.39 – 7.46 (m, 1H), 7.50 (t, *J* = 7.7 Hz, 2H), 7.70 – 7.75 (m, 2H), 7.79 (d, *J* = 8.1 Hz, 2H), 7.87 (d, 2H), 11.37 (s, 1H), 12.14 (s, 1H)

^{13}C-NMR (151 MHz, DMSO) δ 25.6, 26.5, 29.6, 36.4, 73.7, 81.1, 127.2, 127.3, 128.3, 128.7, 129.5, 130.7, 139.4, 143.9, 164.8, br s 165.3

HPLC t_R = 14.93 min, purity = 99.0 %

Mp. T_M = 115.6 °C

ACKNOWLEDGEMENT

Financial support for this study was provided to R.K. by the German Research Foundation (Deutsche Forschungsgemeinschaft, DFG, project number KA 2259/4-1) and by the Jürgen Manchot Stiftung (graduate school MOI IV). T.K. acknowledges support from the DFG (project number KU 1577/3-1). Thanks to the CeMSA@HHU (Center for Molecular and Structural Analytics @ Heinrich Heine University) for recording some of the mass-spectrometric data.

Author contributions

Conceptualization, funding acquisition, and supervision, T.K., R.K; microbiological investigation, K.V., L.v.G., A-L.K-D.; chemical synthesis, O.M., A.B., K.S., B.L.; proteome analysis, D.P., F.Ka.; Tn-seq analysis, T.A.C., M.D.H., L.O., Z.J.; pharmacokinetic investigations, T.G., H.M., B.B.B.; data analysis, F.Ko., T.R.I., M.K., A.D.B.; writing – original draft, K.V., L.v.G., O.M., T.K., R.K..

Ethics declarations

Competing interests

All authors declare no competing interests.

REFERENCES

1. World Health, O. (2022). Global tuberculosis report 2022. . licence: cc bY-Nc-sa 3.0 iGo.
2. Mitchison, D.A. (2005). The diagnosis and therapy of tuberculosis during the past 100 years. Am J Respir Crit Care Med *171*, 699-706. 10.1164/rccm.200411-1603OE.
3. World Health, O. (2018). Rapid communication: key changes to treatment of multidrug- and rifampicin-resistant tuberculosis (MDR/RR-TB). World Health Organization.
4. MD, J.L., Boshoff, H.I., and Barry, C.E., 3rd (2018). The present state of the tuberculosis drug development pipeline. Curr Opin Pharmacol *42*, 81-94. 10.1016/j.coph.2018.08.001.
5. Lee, A., Xie, Y.L., Barry, C.E., and Chen, R.Y. (2020). Current and future treatments for tuberculosis. Bmj *368*, m216. 10.1136/bmj.m216.
6. Kisfaludy, L., Dancsi, L., Patthy, Á., Fekete, G., and Szabó, I. (1971). α-aminooxy-acid derivatives with potent antituberculotic effect. Experientia *27*, 1055-1056. 10.1007/BF02138876.
7. Pham-The, H., Garrigues, T., Bermejo, M., Gonzalez-Alvarez, I., Monteagudo, M.C., and Cabrera-Perez, M.A. (2013). Provisional classification and in silico study of biopharmaceutical system based on caco-2 cell permeability and dose number. Mol Pharm *10*, 2445-2461. 10.1021/mp4000585.
8. Dartois, V.A., and Rubin, E.J. (2022). Anti-tuberculosis treatment strategies and drug development: challenges and priorities. Nat Rev Microbiol *20*, 685-701. 10.1038/s41579-022-00731-y.
9. Zumla, A., Nahid, P., and Cole, S.T. (2013). Advances in the development of new tuberculosis drugs and treatment regimens. Nat Rev Drug Discov *12*, 388-404. 10.1038/nrd4001.
10. Cadena, A.M., Fortune, S.M., and Flynn, J.L. (2017). Heterogeneity in tuberculosis. Nat Rev Immunol *17*, 691-702. 10.1038/nri.2017.69.
11. Chandra, P., Grigsby, S.J., and Philips, J.A. (2022). Immune evasion and provocation by Mycobacterium tuberculosis. Nature Reviews Microbiology *20*, 750-766. 10.1038/s41579-022-00763-4.
12. Gengenbacher, M., Rao, S.P.S., Pethe, K., and Dick, T. (2010). Nutrient-starved, non-replicating Mycobacterium tuberculosis requires respiration, ATP synthase and isocitrate lyase for maintenance of ATP homeostasis and viability. Microbiology (Reading) *156*, 81-87. 10.1099/mic.0.033084-0.

13. Mandal, S., Njikan, S., Kumar, A., Early, J.V., and Parish, T. (2019). The relevance of persisters in tuberculosis drug discovery. Microbiology (Reading) *165*, 492-499. 10.1099/mic.0.000760.

14. Consortium, T.U. (2022). UniProt: the Universal Protein Knowledgebase in 2023. Nucleic Acids Research *51*, D523-D531. 10.1093/nar/gkac1052.

15. Domenech, P., and Reed, M.B. (2009). Rapid and spontaneous loss of phthiocerol dimycocerosate (PDIM) from Mycobacterium tuberculosis grown in vitro: implications for virulence studies. Microbiology (Reading) *155*, 3532-3543. 10.1099/mic.0.029199-0.

16. Fraaije, M.W., Kamerbeek, N.M., Heidekamp, A.J., Fortin, R., and Janssen, D.B. (2004). The prodrug activator EtaA from Mycobacterium tuberculosis is a Baeyer-Villiger monooxygenase. J Biol Chem *279*, 3354-3360. 10.1074/jbc.M307770200.

17. Albesa-Jové, D., Chiarelli, L.R., Makarov, V., Pasca, M.R., Urresti, S., Mori, G., Salina, E., Vocat, A., Comino, N., Mohorko, E., et al. (2014). Rv2466c mediates the activation of TP053 to kill replicating and non-replicating Mycobacterium tuberculosis. ACS Chem Biol *9*, 1567-1575. 10.1021/cb500149m.

18. Libardo, M.D.J., Duncombe, C.J., Green, S.R., Wyatt, P.G., Thompson, S., Ray, P.C., Ioerger, T.R., Oh, S., Goodwin, M.B., Boshoff, H.I.M., and Barry, C.E., 3rd (2021). Resistance of Mycobacterium tuberculosis to indole 4-carboxamides occurs through alterations in drug metabolism and tryptophan biosynthesis. Cell Chem Biol *28*, 1180-1191.e1120. 10.1016/j.chembiol.2021.02.023.

19. Singh, P., Kumar, A., Sharma, P., Chugh, S., Kumar, A., Sharma, N., Gupta, S., Singh, M., Kidwai, S., Sankar, J., et al. (2024). Identification and optimization of pyridine carboxamide-based scaffold as a drug lead for Mycobacterium tuberculosis. Antimicrob Agents Chemother, e0076623. 10.1128/aac.00766-23.

20. Kelley, L.A., Mezulis, S., Yates, C.M., Wass, M.N., and Sternberg, M.J. (2015). The Phyre2 web portal for protein modeling, prediction and analysis. Nat Protoc *10*, 845-858. 10.1038/nprot.2015.053.

21. Shin, S., Lee, T.H., Ha, N.C., Koo, H.M., Kim, S.Y., Lee, H.S., Kim, Y.S., and Oh, B.H. (2002). Structure of malonamidase E2 reveals a novel Ser-cisSer-Lys catalytic triad in a new serine hydrolase fold that is prevalent in nature. Embo j *21*, 2509-2516. 10.1093/emboj/21.11.2509.

22. Cilia, E., Fabbri, A., Uriani, M., Scialdone, G.G., and Ammendola, S. (2005). The signature amidase from Sulfolobus solfataricus belongs to the CX3C subgroup of enzymes cleaving both amides and nitriles. Ser195 and Cys145 are predicted to be the active site nucleophiles. Febs j *272*, 4716-4724. 10.1111/j.1742-4658.2005.04887.x.

23. Yasuhira, K., Shibata, N., Mongami, G., Uedo, Y., Atsumi, Y., Kawashima, Y., Hibino, A., Tanaka, Y., Lee, Y.H., Kato, D., et al. (2010). X-ray crystallographic analysis of the 6-aminohexanoate cyclic dimer hydrolase: catalytic mechanism and evolution of an enzyme responsible for nylon-6 byproduct degradation. J Biol Chem *285*, 1239-1248. 10.1074/jbc.M109.041285.

24. Lee, S., Park, E.H., Ko, H.J., Bang, W.G., Kim, H.Y., Kim, K.H., and Choi, I.G. (2015). Crystal structure analysis of a bacterial aryl acylamidase belonging to the amidase signature enzyme family. Biochem Biophys Res Commun *467*, 268-274. 10.1016/j.bbrc.2015.09.177.

25. Kalscheuer, R., Palacios, A., Anso, I., Cifuente, J., Anguita, J., Jacobs, W.R., Guerin, M.E., and Prados-Rosales, R. (2019). The Mycobacterium tuberculosis capsule: A cell structure with key implications in pathogenesis. Biochemical Journal *476*, 1995-2016. 10.1042/BCJ20190324.

26. Jumper, J., Evans, R., Pritzel, A., Green, T., Figurnov, M., Ronneberger, O., Tunyasuvunakool, K., Bates, R., Zidek, A., Potapenko, A., et al. (2021). Highly accurate protein structure prediction with AlphaFold. Nature *596*, 583-589. 10.1038/s41586-021-03819-2.

27. Varadi, M., Anyango, S., Deshpande, M., Nair, S., Natassia, C., Yordanova, G., Yuan, D., Stroe, O., Wood, G., Laydon, A., et al. (2022). AlphaFold Protein Structure Database: massively expanding the structural coverage of protein-sequence space with high-accuracy models. Nucleic Acids Res *50*, D439-D444. 10.1093/nar/gkab1061.

28. DeJesus, M.A., Ambadipudi, C., Baker, R., Sassetti, C., and Ioerger, T.R. (2015). TRANSIT--A Software Tool for Himar1 TnSeq Analysis. PLoS Comput Biol *11*, e1004401. 10.1371/journal.pcbi.1004401.

29. Black, P.A., Warren, R.M., Louw, G.E., van Helden, P.D., Victor, T.C., and Kana, B.D. (2014). Energy metabolism and drug efflux in Mycobacterium tuberculosis. Antimicrob Agents Chemother *58*, 2491-2503. 10.1128/aac.02293-13.

30. Xu, W., DeJesus, M.A., Rücker, N., Engelhart, C.A., Wright, M.G., Healy, C., Lin, K., Wang, R., Park, S.W., Ioerger, T.R., et al. (2017). Chemical Genetic Interaction Profiling Reveals Determinants of Intrinsic Antibiotic Resistance in Mycobacterium tuberculosis. Antimicrob Agents Chemother *61*. 10.1128/aac.01334-17.

31. Pasca, M.R., Guglierame, P., De Rossi, E., Zara, F., and Riccardi, G. (2005). mmpL7 gene of Mycobacterium tuberculosis is responsible for isoniazid efflux in Mycobacterium smegmatis. Antimicrob Agents Chemother *49*, 4775-4777. 10.1128/aac.49.11.4775-4777.2005.

32. Li, X.-Z., and Nikaido, H. (2004). Efflux-Mediated Drug Resistance in Bacteria. Drugs *64*, 159-204. 10.2165/00003495-200464020-00004.

33. Rodriguez, J.G., Burbano, C.S., Nuñez, C., González, C.E., Zambrano, M.M., García, M.J., and Del Portillo, P. (2008). Rv3134c/devR/devS operon of Mycobacterium bovis BCG is differentially transcribed under "in vitro" stress conditions. Tuberculosis (Edinb) *88*, 273-282. 10.1016/j.tube.2007.11.011.

34. Baek, S.H., Li, A.H., and Sassetti, C.M. (2011). Metabolic regulation of mycobacterial growth and antibiotic sensitivity. PLoS Biol *9*, e1001065. 10.1371/journal.pbio.1001065.

35. Pethe, K., Sequeira, P.C., Agarwalla, S., Rhee, K., Kuhen, K., Phong, W.Y., Patel, V., Beer, D., Walker, J.R., Duraiswamy, J., et al. (2010). A chemical genetic screen in Mycobacterium tuberculosis identifies carbon-source-dependent growth inhibitors devoid of in vivo efficacy. Nat Commun *1*, 57. 10.1038/ncomms1060.

36. Gopal, P., Yee, M., Sarathy, J., Low, J.L., Sarathy, J.P., Kaya, F., Dartois, V., Gengenbacher, M., and Dick, T. (2016). Pyrazinamide Resistance Is Caused by Two Distinct Mechanisms: Prevention of Coenzyme A Depletion and Loss of Virulence Factor Synthesis. ACS Infectious Diseases *2*, 616-626. 10.1021/acsinfecdis.6b00070.

37. Minato, Y., Gohl, D.M., Thiede, J.M., Chacón, J.M., Harcombe, W.R., Maruyama, F., and Baughn, A.D. (2019). Genomewide Assessment of Mycobacterium tuberculosis Conditionally Essential Metabolic Pathways. mSystems *4*, 10.1128/msystems.00070-00019. doi:10.1128/msystems.00070-19.

38. Nambi, S., Long, J.E., Mishra, B.B., Baker, R., Murphy, K.C., Olive, A.J., Nguyen, H.P., Shaffer, S.A., and Sassetti, C.M. (2015). The Oxidative Stress Network of Mycobacterium tuberculosis Reveals Coordination between Radical Detoxification Systems. Cell Host Microbe *17*, 829-837. 10.1016/j.chom.2015.05.008.

39. Dick, T., Manjunatha, U., Kappes, B., and Gengenbacher, M. (2010). Vitamin B6 biosynthesis is essential for survival and virulence of Mycobacterium tuberculosis. Mol Microbiol *78*, 980-988. 10.1111/j.1365-2958.2010.07381.x.

40. Mashalidis, E.H., Mukherjee, T., Sledź, P., Matak-Vinković, D., Boshoff, H., Abell, C., and Barry, C.E., 3rd (2011). Rv2607 from Mycobacterium tuberculosis is a pyridoxine 5'-phosphate oxidase with unusual substrate specificity. PLoS One *6*, e27643. 10.1371/journal.pone.0027643.

41. Wan, L., Hu, P., Zhang, L., Wang, Z.-X., Fleming, J., Ni, B., Luo, J., Guan, C.-X., Bai, L., Tan, Y., et al. (2023). Omics analysis of Mycobacterium tuberculosis isolates uncovers Rv3094c, an ethionamide metabolism-associated gene. Communications Biology *6*, 156. 10.1038/s42003-023-04433-w.

42. Mauran, S., Perera, N.T., and Perera, I.C. (2022). MxyR of Mycobacterium tuberculosis Responds to Xylan; an Unusual Ligand for a MarR Family Transcriptional Regulatore. Mol Biol (Mosk) *56*, 103-117. 10.31857/s0026898422010074.

43. DeBarber, A.E., Mdluli, K., Bosman, M., Bekker, L.G., and Barry, C.E., 3rd (2000). Ethionamide activation and sensitivity in multidrug-resistant Mycobacterium tuberculosis. Proc Natl Acad Sci U S A *97*, 9677-9682. 10.1073/pnas.97.17.9677.

44. Alm, R.A., and Lahiri, S.D. (2020). Narrow-Spectrum Antibacterial Agents-Benefits and Challenges. Antibiotics (Basel) *9*. 10.3390/antibiotics9070418.

45. Melander, R.J., Zurawski, D.V., and Melander, C. (2018). Narrow-Spectrum Antibacterial Agents. Medchemcomm *9*, 12-21. 10.1039/c7md00528h.

46. Gopal, P., and Dick, T. (2014). Reactive dirty fragments: implications for tuberculosis drug discovery. Curr Opin Microbiol *21*, 7-12. 10.1016/j.mib.2014.06.015.

47. Fernandes, A.S., Gaspar, J., Cabral, M.F., Rueff, J., Castro, M., Batinic-Haberle, I., Costa, J., and Oliveira, N.G. (2010). Protective role of ortho-substituted Mn(III) N-alkylpyridylporphyrins against the oxidative injury induced by tert-butylhydroperoxide. Free Radical Research *44*, 430-440. 10.3109/10715760903555844.

48. Kučera, O., Endlicher, R., Roušar, T., Lotková, H., Garnol, T., Drahota, Z., and Cervinková, Z. (2014). The effect of tert-butyl hydroperoxide-induced oxidative stress on lean and steatotic rat hepatocytes in vitro. Oxid Med Cell Longev *2014*, 752506. 10.1155/2014/752506.

49. Shastri, M.D., Shukla, S.D., Chong, W.C., Dua, K., Peterson, G.M., Patel, R.P., Hansbro, P.M., Eri, R., and O'Toole, R.F. (2018). Role of Oxidative Stress in the Pathology and Management of Human Tuberculosis. Oxid Med Cell Longev *2018*, 7695364. 10.1155/2018/7695364.

50. Prosser, G.A., and de Carvalho, L.P. (2013). Kinetic mechanism and inhibition of Mycobacterium tuberculosis D-alanine:D-alanine ligase by the antibiotic D-cycloserine. Febs j *280*, 1150-1166. 10.1111/febs.12108.

51. Sievers, M.L., Herrier, R.N., Chin, L., and Picchioni, A.L. (1982). Treatment of isoniazid overdose. Jama *247*, 583-584.

52. di Salvo, M.L., Contestabile, R., and Safo, M.K. (2011). Vitamin B(6) salvage enzymes: mechanism, structure and regulation. Biochim Biophys Acta *1814*, 1597-1608. 10.1016/j.bbapap.2010.12.006.

53. Ehrenshaft, M., Bilski, P., Li, M.Y., Chignell, C.F., and Daub, M.E. (1999). A highly conserved sequence is a novel gene involved in de novo vitamin B6 biosynthesis. Proc Natl Acad Sci U S A *96*, 9374-9378. 10.1073/pnas.96.16.9374.

54. Jain, S.K., and Lim, G. (2001). Pyridoxine and pyridoxamine inhibits superoxide radicals and prevents lipid peroxidation, protein glycosylation, and (Na+ + K+)-ATPase activity reduction in high glucose-treated human erythrocytes. Free Radic Biol Med *30*, 232-237. 10.1016/s0891-5849(00)00462-7.

55. John, R.A., and Charteris, A. (1978). The reaction of amino-oxyacetate with pyridoxal phosphate-dependent enzymes. Biochem J *171*, 771-779. 10.1042/bj1710771.

56. Beeler, T., and Churchich, J.E. (1976). Reactivity of the phosphopyridoxal groups of cystathionase. J Biol Chem *251*, 5267-5271.

57. Percudani, R., and Peracchi, A. (2009). The B6 database: a tool for the description and classification of vitamin B6-dependent enzymatic activities and of the corresponding protein families. BMC Bioinformatics *10*, 273. 10.1186/1471-2105-10-273.

58. Kunota, T.T.R., Rahman, M.A., Truebody, B.E., Mackenzie, J.S., Saini, V., Lamprecht, D.A., Adamson, J.H., Sevalkar, R.R., Lancaster, J.R., Jr., Berney, M., et al. (2021). Mycobacterium tuberculosis H(2)S Functions as a Sink to Modulate Central Metabolism, Bioenergetics, and Drug Susceptibility. Antioxidants (Basel) *10*. 10.3390/antiox10081285.

59. Mironov, A., Seregina, T., Nagornykh, M., Luhachack, L.G., Korolkova, N., Lopes, L.E., Kotova, V., Zavilgelsky, G., Shakulov, R., Shatalin, K., and Nudler, E. (2017). Mechanism of H(2)S-mediated protection against oxidative stress in Escherichia coli. Proc Natl Acad Sci U S A *114*, 6022-6027. 10.1073/pnas.1703576114.

60. Beggs, G.A., Brennan, R.G., and Arshad, M. (2020). MarR family proteins are important regulators of clinically relevant antibiotic resistance. Protein Sci *29*, 647-653. 10.1002/pro.3769.

61. Zhang, H.N., Xu, Z.W., Jiang, H.W., Wu, F.L., He, X., Liu, Y., Guo, S.J., Li, Y., Bi, L.J., Deng, J.Y., et al. (2017). Cyclic di-GMP regulates Mycobacterium tuberculosis resistance to ethionamide. Sci Rep *7*, 5860. 10.1038/s41598-017-06289-7.

62. Vannelli, T.A., Dykman, A., and Ortiz de Montellano, P.R. (2002). The antituberculosis drug ethionamide is activated by a flavoprotein monooxygenase. J Biol Chem *277*, 12824-12829. 10.1074/jbc.M110751200.

63. Altschul, S.F., Gish, W., Miller, W., Myers, E.W., and Lipman, D.J. (1990). Basic local alignment search tool. J Mol Biol *215*, 403-410. 10.1016/s0022-2836(05)80360-2.

64. Larsen, M.H., Biermann, K., Tandberg, S., Hsu, T., and Jacobs, W.R. (2007). Genetic Manipulation of Mycobacterium tuberculosis. Current Protocols in Microbiology *6*, 1-21. 10.1002/9780471729259.mc10a02s6.

65. Ioerger, T.R., Feng, Y., Ganesula, K., Chen, X., Dobos, K.M., Fortune, S., Jacobs, W.R., Jr., Mizrahi, V., Parish, T., Rubin, E., et al. (2010). Variation among genome sequences of H37Rv strains of Mycobacterium tuberculosis from multiple laboratories. J Bacteriol *192*, 3645-3653. 10.1128/JB.00166-10.

66. Jain, P., Hsu, T., Arai, M., Biermann, K., Thaler, D.S., Nguyen, A., González, P.A., Tufariello, J.M., Kriakov, J., Chen, B., et al. (2014). Specialized transduction designed for precise high-throughput unmarked deletions in Mycobacterium tuberculosis. mBio *5*, e01245-01214. 10.1128/mBio.01245-14.

67. DeLano, W.L. (2002). The PyMOL Molecular Graphics System. DeLano Scientific. DeLano Scientific.

68. Rubin, E.J., Akerley, B.J., Novik, V.N., Lampe, D.J., Husson, R.N., and Mekalanos, J.J. (1999). In vivo transposition of mariner-based elements in enteric bacteria and mycobacteria. Proceedings of the National Academy of Sciences *96*, 1645-1650. doi:10.1073/pnas.96.4.1645.

69. Lee, S., Kriakov, J., Vilcheze, C., Dai, Z., Hatfull, G.F., and Jacobs, W.R., Jr. (2004). Bxz1, a new generalized transducing phage for mycobacteria. FEMS Microbiology Letters *241*, 271-276. 10.1016/j.femsle.2004.10.032.

70. Martin, M. (2011). Cutadapt removes adapter sequences from high-throughput sequencing reads. EMBnet.journal *17*. 10.14806/ej.17.1.200.

71. Langmead, B., Trapnell, C., Pop, M., and Salzberg, S.L. (2009). Ultrafast and memory-efficient alignment of short DNA sequences to the human genome. Genome Biol *10*, R25. 10.1186/gb-2009-10-3-r25.

72. Pritchard, J.R., Chao, M.C., Abel, S., Davis, B.M., Baranowski, C., Zhang, Y.J., Rubin, E.J., and Waldor, M.K. (2014). ARTIST: high-resolution genome-wide assessment of fitness using transposon-insertion sequencing. PLoS Genet *10*, e1004782. 10.1371/journal.pgen.1004782.

73. Benjamini, Y., and Yekutieli, D. (2005). False discovery rate-adjusted multiple confidence intervals for selected parameters. J Am Stat Assoc *100*, 71-81. 10.1198/016214504000001907.

74. Rappsilber, J., Mann, M., and Ishihama, Y. (2007). Protocol for micro-purification, enrichment, pre-fractionation and storage of peptides for proteomics using StageTips. Nat Protoc *2*, 1896-1906. 10.1038/nprot.2007.261.

75. Cox, J., and Mann, M. (2008). MaxQuant enables high peptide identification rates, individualized p.p.b.-range mass accuracies and proteome-wide protein quantification. Nat Biotechnol *26*, 1367-1372. 10.1038/nbt.1511.

76. UniProt Consortium, T. (2018). UniProt: the universal protein knowledgebase. Nucleic Acids Res *46*, 2699. 10.1093/nar/gky092.

77. Cox, J., Hein, M.Y., Luber, C.A., Paron, I., Nagaraj, N., and Mann, M. (2014). Accurate proteome-wide label-free quantification by delayed normalization and maximal peptide ratio extraction, termed MaxLFQ. Mol Cell Proteomics *13*, 2513-2526. 10.1074/mcp.M113.031591.

78. Tyanova, S., Temu, T., Sinitcyn, P., Carlson, A., Hein, M.Y., Geiger, T., Mann, M., and Cox, J. (2016). The Perseus computational platform for comprehensive analysis of (prote)omics data. Nat Methods *13*, 731-740. 10.1038/nmeth.3901.

79. Majid, H., Bartel, A., and Burckhardt, B.B. (2021). Development, validation and standardization of oromucosal ex-vivo permeation studies for implementation in quality-controlled environments. J Pharm Biomed Anal *194*, 113769. 10.1016/j.jpba.2020.113769.

3.2 Supporting Information

α-Aminooxyacetic acid derivatives acting as pro-drugs against *Mycobacterium tuberculosis*

Kristin Vill [1,*], Lasse van Geelen [1,*], Oliver Michel [2,*], Anna-Lene Kiffe-Delf [1], Alexander Berger [2], David Podlesainski [3], Katharina Stenzel [2], Filip Kovacic [4,¶], Beate Lungerich [2], Tanja Gangnus [5], Haidara Majid [5], Bjoern B. Burckhardt [5], Taylor A. Crooks [6], Michael D. Howe [6], Lev Ostrer [6], Ziyi Jia [6], Thomas R. Ioerger [7], Farnusch Kaschani [3], Markus Kaiser [3], Anthony D. Baughn [6], Thomas Kurz [2, §], and Rainer Kalscheuer [1,§]

[1] Heinrich Heine University Düsseldorf, Faculty of Mathematics and Natural Sciences, Institute of Pharmaceutical Biology and Biotechnology, 40225 Düsseldorf, Germany

[2] Heinrich Heine University Düsseldorf, Faculty of Mathematics and Natural Sciences, Institute of Pharmaceutical and Medicinal Chemistry, 40225 Düsseldorf, Germany

[3] Department of Chemical Biology, ZMB, Faculty of Biology, University of Duisburg-Essen, 45177 Essen, Germany

[4] Heinrich Heine University Düsseldorf, Forschungszentrum Jülich, Institute of Molecular Enzyme Technology, 52428 Jülich, Germany

[5] Individualized Pharmacotherapy, Institute of Pharmaceutical and Medicinal Chemistry, University of Münster, 48149 Münster, Germany

[6] Department of Microbiology and Immunology, University of Minnesota Medical School, MN 55455, Minneapolis, USA

[7] Department of Computer Science, Texas A&M University, College Station, Texas 77843, United States

¶ Present address:
Department of Surgery, Massachusetts General Hospital, and Harvard Medical School, Boston, Massachusetts, USA.
Department of Microbiology, Harvard Medical School, Boston, Massachusetts, USA

* These authors contributed equally

§ Authors for correspondence: rainer.kalscheuer@hhu.de, thomas.kurz@hhu.de

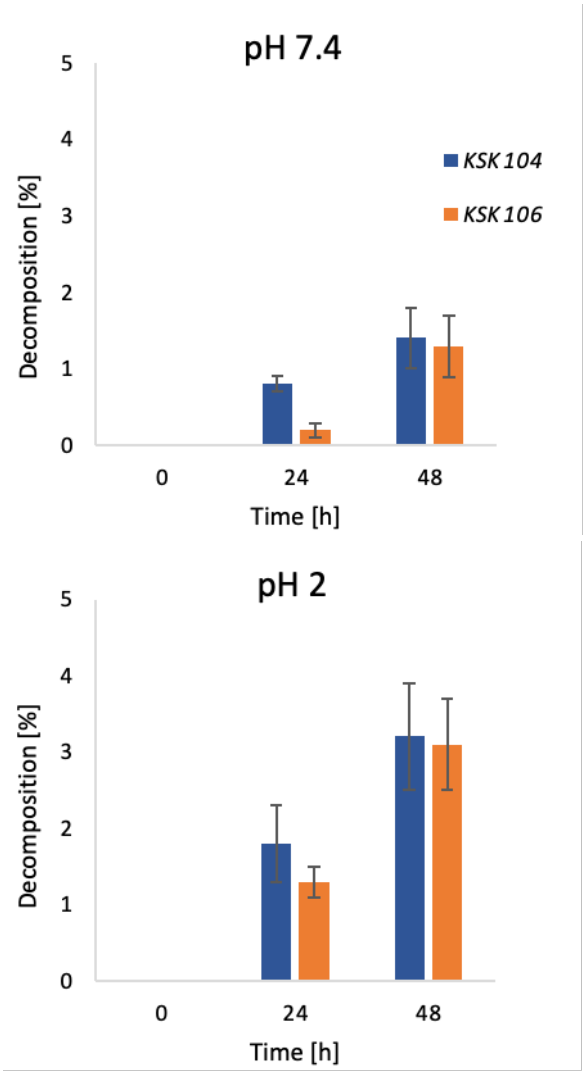

Figure S1. Stability testing of KSK-104 and KSK-106 in aqueous media. Both compounds were dissolved (0.5 mg/mL) in a vehicle of 90% PBS (pH 2 and pH 7.4), 7% Tween® 80 and 3% ethanol (v/v). These solutions were shaken at 37 °C for 48 h, and the compound decomposition was evaluated by HPLC analysis. Values represent means of duplicate measurements (n = 2) ± standard deviation.

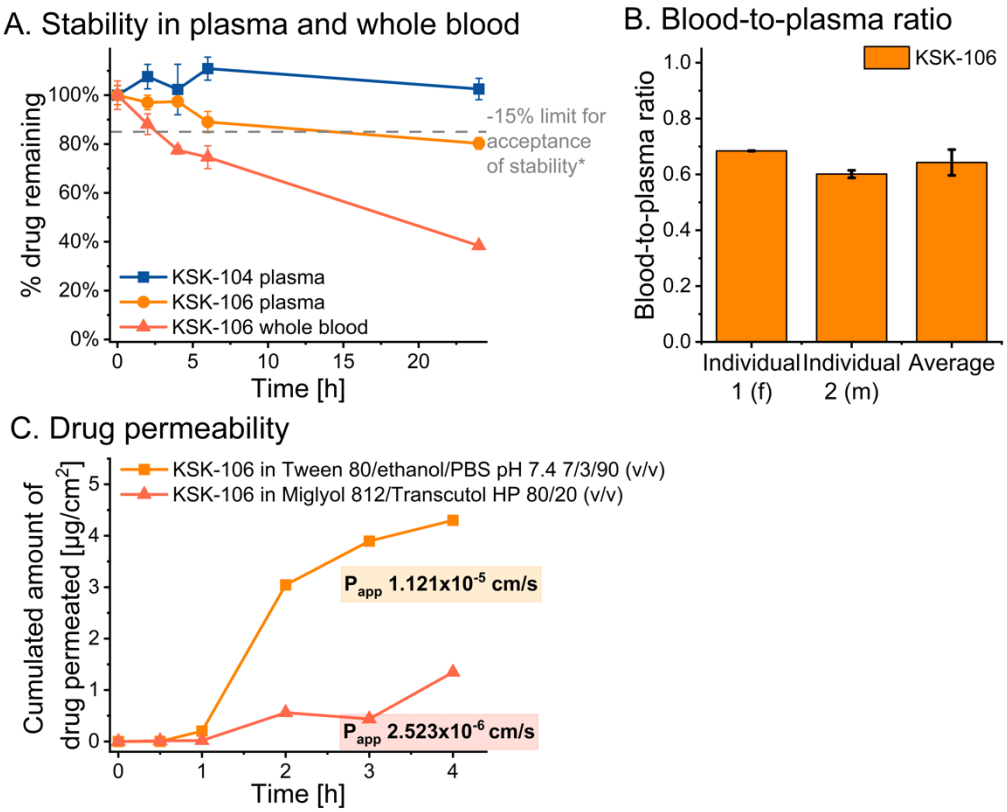

Figure S2. *In vitro* pharmacokinetic testing of KSK-104 and KSK-106. Both compounds were dissolved in human EDTA-plasma (50 ng/mL) and constantly incubated at 37 °C for 24 h (A). KSK-106 was additionally investigated in human EDTA-whole blood. Detection was performed via LC-MS/MS analysis. Values represent means of triplicates (n = 3) ± standard deviation (SD). * indicates the limit of -15%, which was set as acceptance limit for stability according to bioanalytical guidelines of the US Food and Drug Administration. The blood-to-plasma ratio (B) was assessed in human blood donated by one male (m) and one female (f) volunteer in three independent replicates (mean ± SD) for KSK-106 showing only minor sequestration into erythrocytes. Drug permeability of KSK-106 by passive transport (C) was evaluated for two different formulations, quantified by LC-MS, and indicates good permeability. EDTA: ethylenediaminetetraacetic acid, Papp: apparent permeability, PBS: phosphate buffered saline pH 7.4

A

Strain	KSK-104	KSK-106
M. bovis BCG Pasteur	0.78	0.39
M. smegmatis mc^2155	>100	>100
M. abscessus (CF001s)	>100	>100
M. marinum DSM 44344	>100	>100
Staphylococcus aureus Mu50	>100	>100
Acinetobacter baumannii ATCC BAA-1605	>100	>100
Pseudomonas aeruginosa ATCC 27853	>100	>100

B

Cell line	Tissue	IC_{50} [µM]
MRC-5	Lung fibroblasts	> 100
THP-1	Monocytes	> 100
HEPG2	Liver	> 100
HUH7	Liver	> 100
CLS-54	Lung	> 100
HEK293	Kidney	> 100
H4	Brain	> 100
SH-SY5Y	Neuroblasts	> 100

Figure S3. Antibacterial activity and cytotoxicity profile of KSK molecules. A) KSK-104 and KSK-106 have been tested in microbroth dilution assays against various mycobacteria and nosocomial bacteria. Concentrations of MIC_{90} values are given in µM. **B)** Cytotoxicity of KSK-106 against various human cell lines *in vitro*. IC_{50} values are given in µM. Growth in **A** and **B** was quantified employing the resazurin reduction assay. Measurements were performed in triplicates revealing no deviations in the reported MIC_{90} and IC_{50} values.

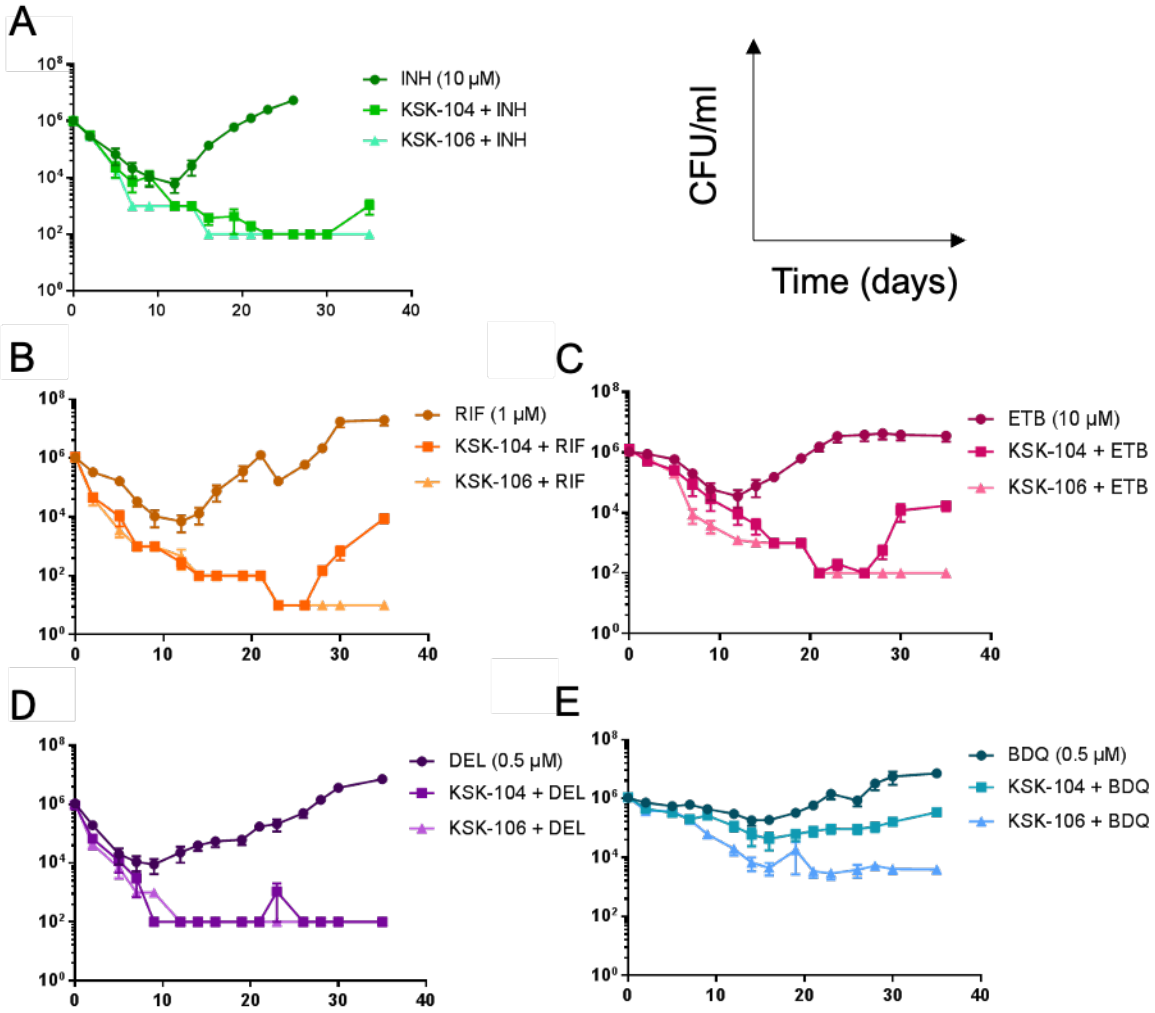

Figure S4. ***In vitro*** **activity of KSK-104 and KSK-106 in combination with different first- and second-line antibiotics.** *M. tuberculosis* H37Rv was treated with the indicated concentrations of clinically used drugs in monotherapy and in combination with 0.25 µM KSK-104 or KSK-106, respectively. Combination with isoniazid (INH, **A**), rifampicin (RIF, **B**), ethambutol (ETB, **C**) and delamanid (**D**) led to additive effects concerning the killing efficacy and delayed resurgence of bacteria surviving the initial treatments. In contrast, combination with bedaquiline (BDQ, **E**) resulted in antagonistic effects. Experiments have been performed in triplicates. The limit of detection was 10 CFU/mL in **B** and 100 CFU/mL in **A** and **C**-**E**. CFU, colony forming units.

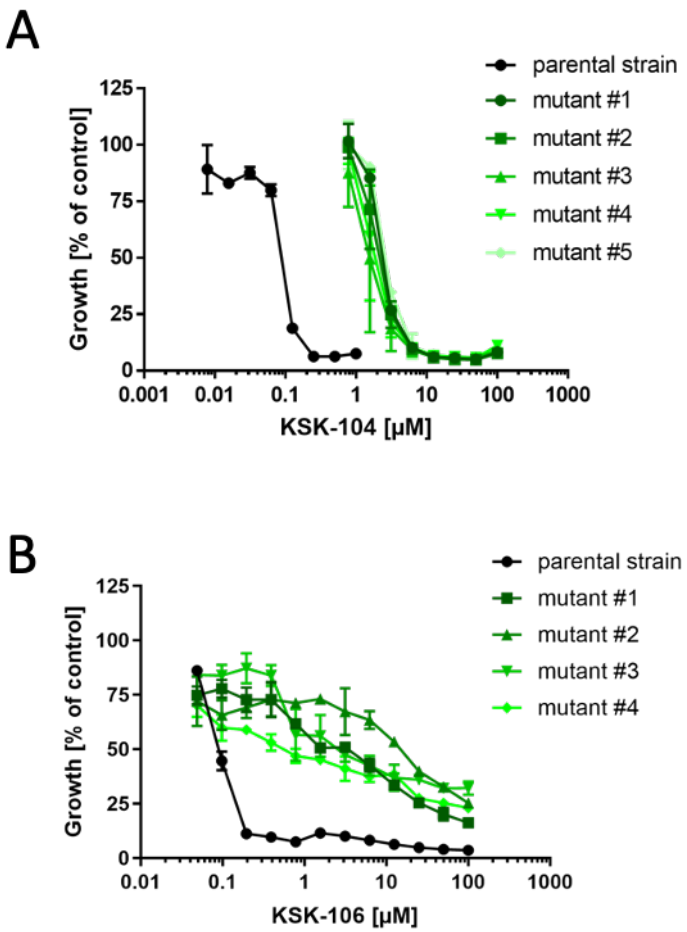

Figure S5. Spontaneous single-step resistant mutants isolated against KSK-104 and KSK-106. SRMs were generated against KSK-104 (**A**) and KSK-106 (**B**). MICs were tested in microbroth dilution assays. Growth in **A** and **B** was quantified employing the resazurin reduction assay. Data shown as means of triplicates with SD. The mutations that were found during the whole-genome-sequencing in the respective mutants are listed in the tables.

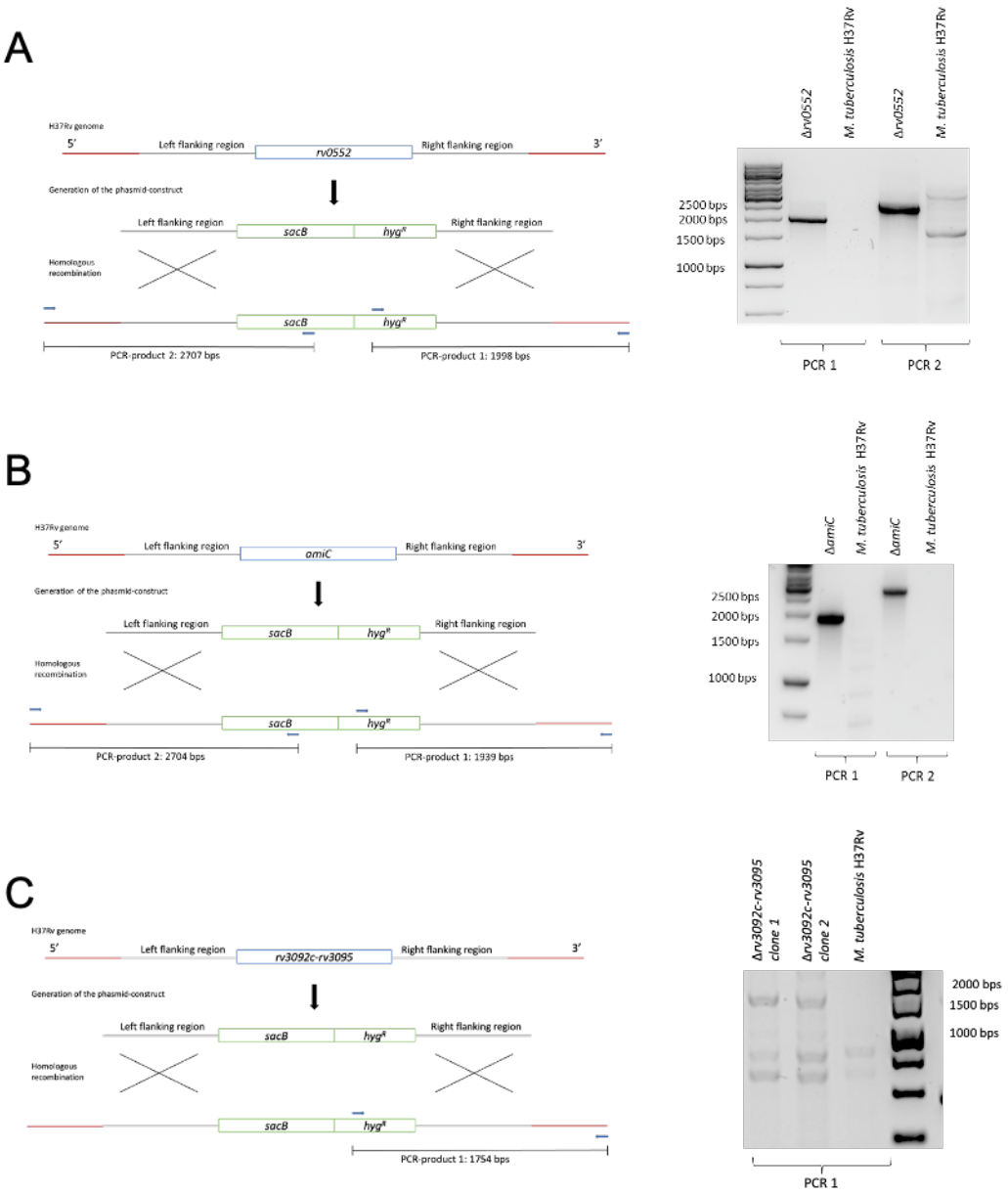

Figure S6. Generation of site-specific gene deletion mutants using specialized transduction. Organization of the respective loci in *M. tuberculosis* H37Rv wild type and **A)** the *Rv0552*, **B)** *amiC* and **C)** *Rv3092c-Rv3095* gene deletion mutants (left panels). The location of flanking regions used to construct the allelic exchange substrate as well as of primers used in diagnostic PCR are indicated. The sizes of the relevant diagnostic PCR products for verification of gene disruption are shown. Diagnostic PCR to verify gene deletion mutants was performed (right panels). **A)** PCR product 1 (2,707 bp) was produced using forward primer binding 1,000 bps upstream of *Rv0552* and reverse primer binding in the *sacB* gene as indicated. PCR product 2 (1,998 bp) was produced using forward primer binding in the hygromycin resistance (hyg^R) gene and reverse primer binding 1,000 bps downstream of *Rv0552*. B) PCR product 1 (2,704 bp) was produced using forward primer binding 1,000 bps upstream of *amiC* and reverse primer binding in the *sacB* gene as indicated. PCR product 2 (1,939 bp) was produced using forward primer

binding in the hygromycin resistance (*hyg*^{R}) gene and reverse primer binding 1,000 bps downstream of *amiC*. **C)** PCR product (1,754 bp) was produced using forward primer binding in the hygromycin resistance (*hyg*^{R}) gene and reverse primer binding 1,000 bps downstream of *rv3095*.

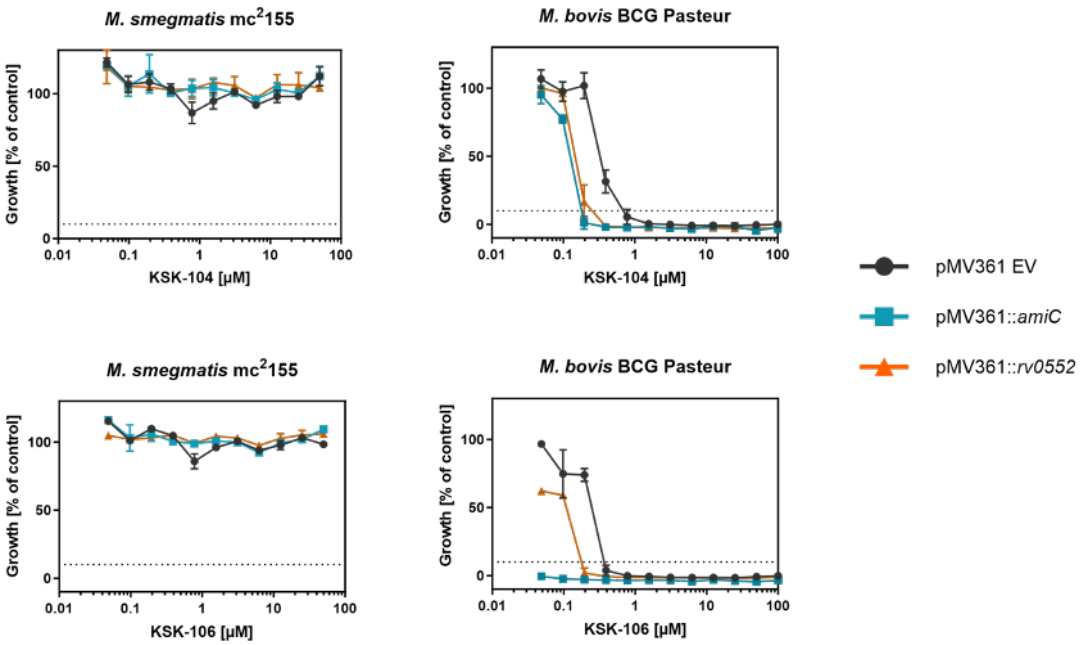

Figure S7. Overexpression of *amiC* or *Rv0552* leads to increased sensitivity of *M. bovis*, but not *M. smegmatis*, towards KSK-104 and KSK-106. Dose-response curves for KSK-104 (top) and KSK-106 (bottom) showing a concentration-dependent growth inhibition of recombinant strains of *M. bovis* BCG Pasteur harboring the empty vector control pMV361::EV or the overexpression constructs pMV361::*amiC* or pMV361::*Rv0552,* respectively, leading to an increased susceptibility of the cells towards the KSKs. In contrast, there was no sensitivity of *M. smegmatis* mc^{2}155 cells towards the KSKs even during overexpression of *Rv0552* or *amiC*. Data shown as means of duplicates ± SD. Growth was quantified employing the resazurin reduction assay. The dashed lines indicate 10% residual growth.

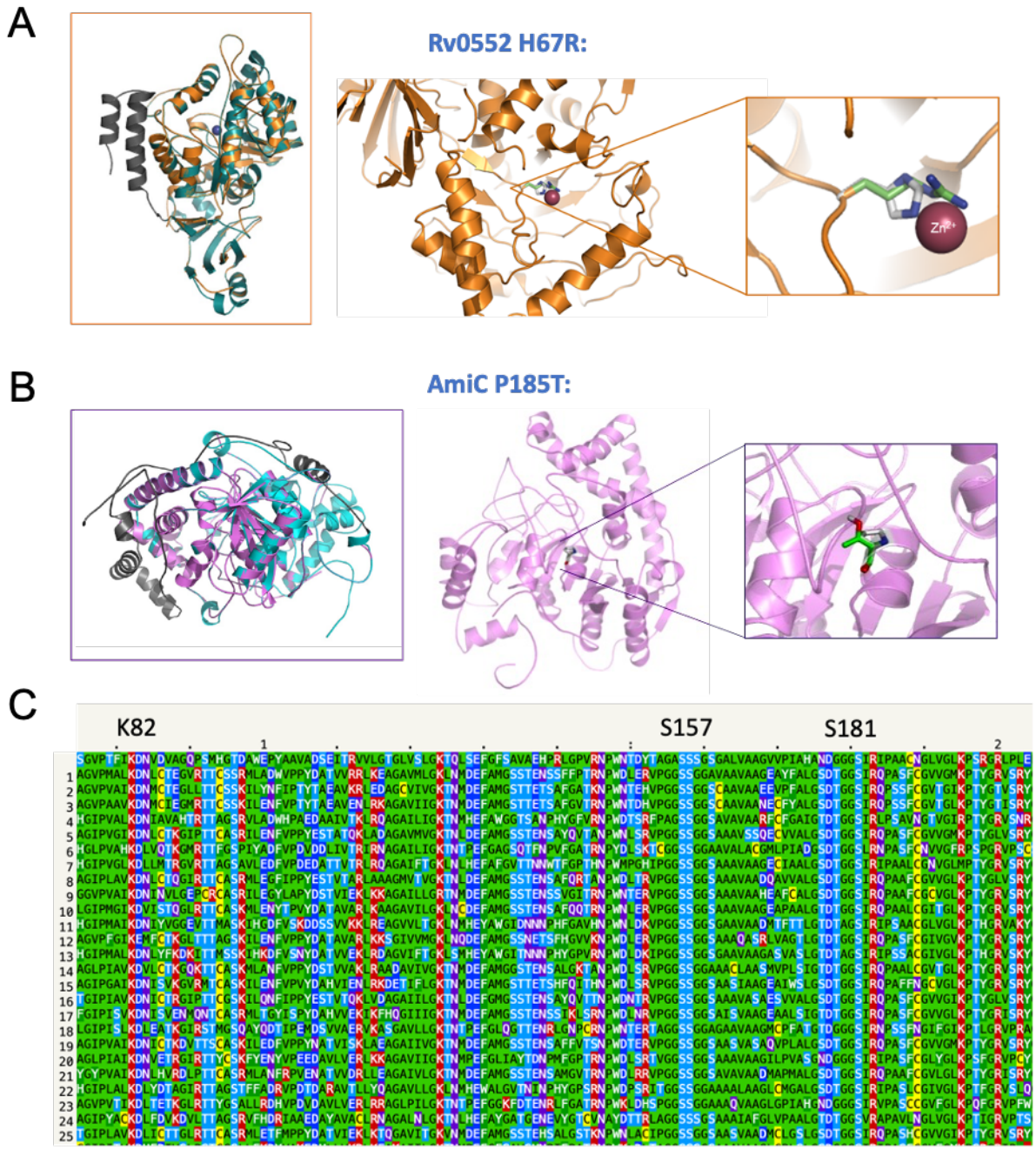

Figure S8. Structural features of the putative amidohydrolases Rv0552 and AmiC. A) Structural homology modeling using Phyre2 revealed that mutations in the gene Rv0552 observed in the spontaneously KSK-104-resistant mutants are likely causing an altered interaction with Zn^{2+} atoms resulting in destabilized and inactive proteins. **B)** Structural homology modeling of AmiC indicating that the observed mutation P195T leads to a loss of rigidity inside the hydrophobic core resulting in a non-accessibility of the active center. **C)** *PSI-Blast Pseudo*-Multiple sequence alignment proposes that AmiC belongs to the amidase signature superfamily. Within this family, Ser-*cis*-Ser-Lys triads have been proposed to form the catalytic center with the specific residues for AmiC expected to be Ser^{181}-*cis*-Ser^{157}-Lys^{82}. Identities of the labeled

sequences: 1) UniRef50_Q2RGY4, 2) UniRef50_C4ZHB9, 3) UniRef50_UPI0001C3563A, 4) UniRef50_B1G4X5, 5) UniRef50_B2IYD7, 6) UniRef50_A5USQ6, 7) UniRef50_D1CAY8, 8) UniRef50_Q2JL51, 9) UniRef50_B3DWT4, 10) UniRef50_A7NKM0, 11) UniRef50_D2KYA7, 12) UniRef50_Q6MRL7, 13) UniRef50_B1HYA7, 14) UniRef50_D2R415, 15) UniRef50_D2RM15, 16) UniRef50_Q113L8, 17) UniRef50_B9DWL8, 18) UniRef50_B3T355, 19) UniRef50_B2A5W7, 20) UniRef50_O28325, 21) UniRef50_A3EU19, 22) UniRef50_A5UXU3, 23) UniRef50_D0MDU0, 24) UniRef50_B9QYT0, 25) UniRef50_A8ZSP8. Residues are coloured by properties: bright-green = hydrophobic, bright-blue = negative charge, dark-green = large hydrophobic, yellow = cysteine, bright-red = positive charge, purple = polar, dull-blue = small alcohol.

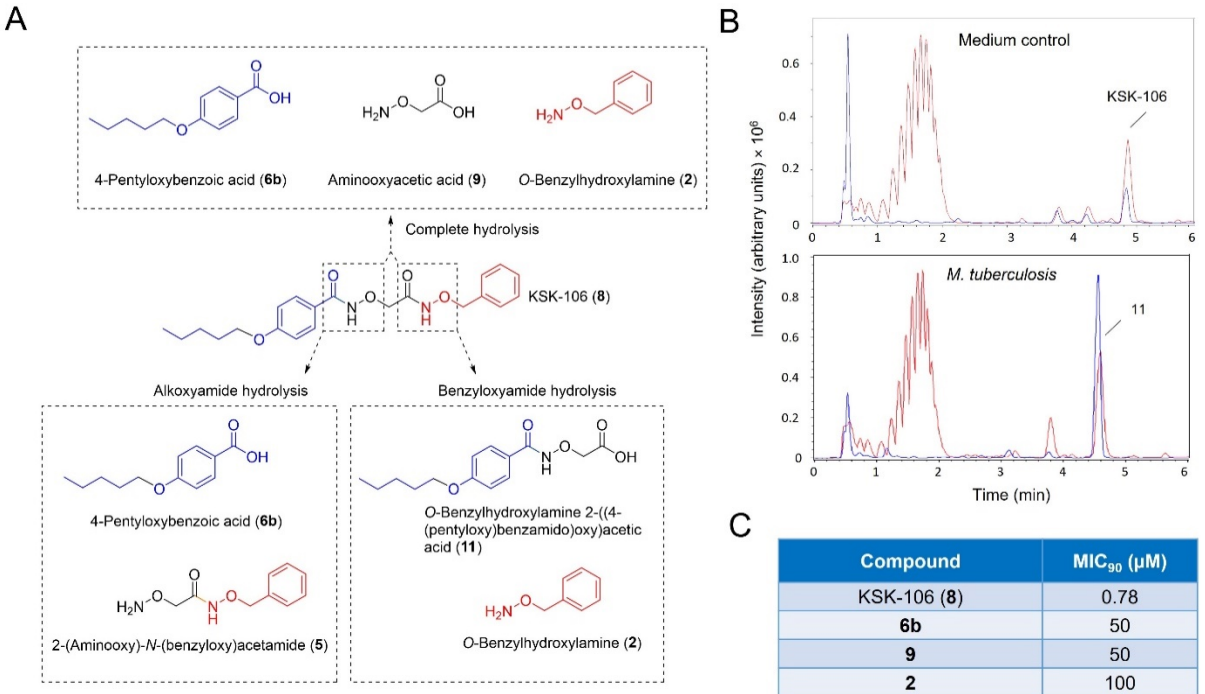

Compound	MIC_{90} (μM)
KSK-106 (**8**)	0.78
6b	50
9	50
2	100
5	50
11	25
6b + 9 + 2	50
6b + 5	100
11 + 2	50

Figure S9. Hydrolytic pro-drug activation of KSK-106 by Rv0552 and AmiC. A) Structure of potential hydrolysis products released from KSK-106 by amidohydrolases AmiC and Rv0552.

B) Qualitative ESI-LC-MS analysis of methanol extracts obtained after 48 h incubation of 100 µM KSK-106 in sterile 7H9 medium (top) or in 7H9 medium inoculated with *M. tuberculosis* H37Rv cells (bottom). Scan was from 50 to 1500 m/z in positive mode. Base peak chromatogram (+all MS) is shown in red, UV chromatogram at 254 nm is shown in blue. Identified peaks: KSK-106 $[m/z + H]^+$ = 387.19, **11** $[m/z + H]^+$ = 209.12. **C)** MIC_{90} values of potential KSK-106 hydrolysis products against *M. tuberculosis* H37Rv. Compounds were tested individually and in various combinations. For combination treatments, equimolar mixtures were used containing each compound at the indicated concentration.

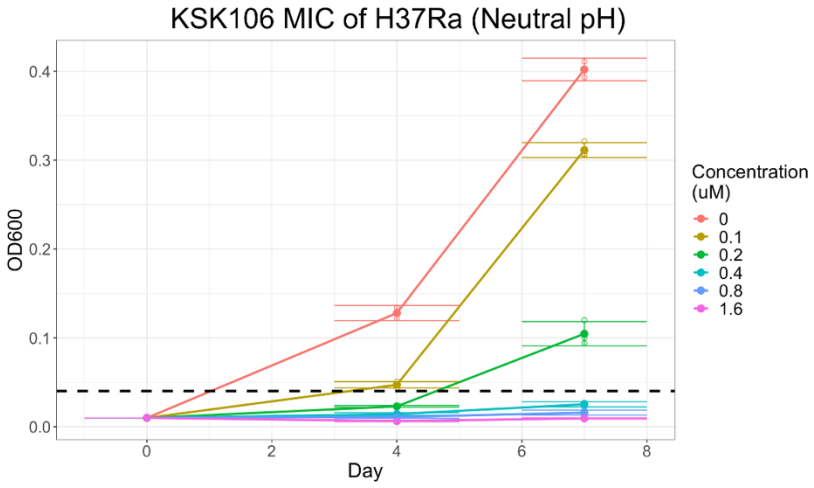

Figure S10. Growth of *M. tuberculosis* H37Ra treated with different KSK-106 concentrations. *M. tuberculosis* H37Ra cells were inoculated with a starting OD_{600nm} of 0.01 from a growing culture in the exponential phase. Cells were treated in triplicates with different concentrations of KSK-106 as indicated in the legend. $OD_{600\ nm}$ was measured after 4 and 7 days. Data shown as means of triplicates with SD. From these data, a concentration of 0.18 µM was estimated to result in ca. 50% growth inhibition after 5 generations.

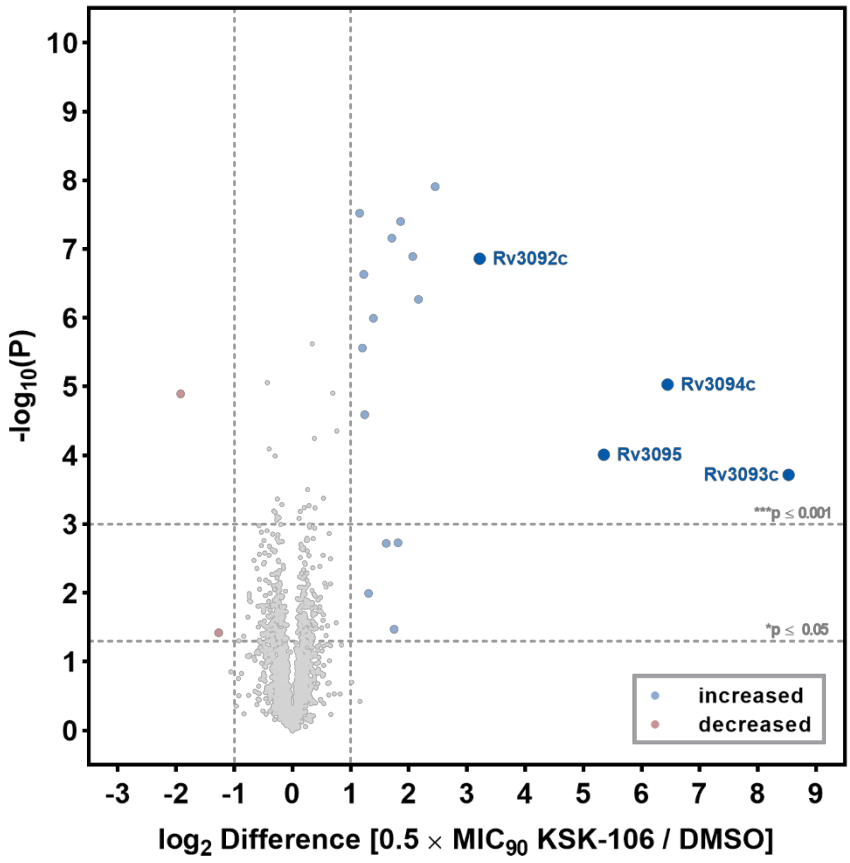

Figure S11. LC-MS/MS-based whole protein analysis of silenced cells of *M. tuberculosis* H37Rv treated with a sublethal concentration of KSK-106 (0.2 µM, corresponding to 0.5 × MIC_{90}) compared to DMSO control. The volcano plot illustrates the log_2-fold change in abundance in KSK-106 treated vs. non-treated cells (X-axis) and corresponding $-log_{10}$ p values (Y-axis). Proteins complying with the chosen threshold of significance and showing a log_2-fold change ≥ 1 or ≤ -1 are marked in blue or red, respectively. Quantification was done via label free quantification (LFQ) of four to five replicates per sample group. To identify statistically significant hits from the analysis, P ≤ 0.05 (Student's T-test; permutation-based FDR with 250 randomizations and FDR = 0.01) was applied.

Table S1. Transposon insertions in genes resulting in apparent fitness changes of transposon mutants of *M. tuberculosis* H37Ra cells during KSK-106 treatment. Genes complying with the chosen threshold of significance $P_{adj}<0.05$ are listed. P_{adj} values were rounded to 3 decimal points. Negative log_2FC values indicate underrepresentation, positive values overrepresentation of the mutants in the pool, demonstrating aggravating or alleviating effects of insertions, respectively.

#Orf	Name	Description	log_2FC	Adj. p-value
Rv2888c	amiC	Probable amidase AmiC (aminohydrolase)	1	0.000
Rv0552	Rv0552	Conserved protein/putative amidohydrolase	0.94	0.000
Rv3696c	glpK	Probable glycerol kinase GlpK (ATP:glycerol 3-phosphotransferase) (glycerokinase) (GK)	0.91	0.000
Rv0544c	Rv0544c	Possible conserved transmembrane protein	0.88	0.000
Rv0545c	pitA	Probable low-affinity inorganic phosphate transporter integral membrane protein PitA	0.87	0.000
Rv0111	Rv0111	Possible transmembrane acyltransferase	0.86	0.000
Rv2241	aceE	Pyruvate dehydrogenase E1 component AceE (pyruvate decarboxylase) (pyruvate dehydrogenase)	0.75	0.000
Rv0546c	Rv0546c	Conserved protein/putative carbon-sulfur lyase	0.62	0.000
Rv2932	ppsB	Phenolpthiocerol synthesis type-I polyketide synthase PpsB	0.59	0.000
Rv2935	ppsE	Phenolpthiocerol synthesis type-I polyketide synthase PpsE	0.57	0.000
Rv2930	fadD26	Fatty-acid-AMP ligase FadD26 (fatty-acid-AMP synthetase) (fatty-acid-AMP synthase)	0.55	0.000
Rv3005c	doxX	Probable membrane oxidoreductase component (MRC) DoxX	0.55	0.000
Rv3484	cpsA	Possible conserved protein CpsA	0.54	0.000
Rv2941	fadD28	Fatty-acid-AMP ligase FadD28 (fatty-acid-AMP synthetase) (fatty-acid-AMP synthase)	0.52	0.000
Rv2933	ppsC	Phenolpthiocerol synthesis type-I polyketide synthase PpsC	0.51	0.007
Rv2931	ppsA	Phenolpthiocerol synthesis type-I polyketide synthase PpsA	0.46	0.000
Rv0806c	cpsY	Possible UDP-glucose-4-epimerase CpsY (galactowaldenase) (UDP-galactose-4-epimerase) (uridine diphosphate galactose-4-epimerase)	0.45	0.000
Rv3066	Rv3066	Probable transcriptional regulatory protein (probably DeoR-family)	0.43	0.007
Rv0678	mmpR5	MarR-like transcriptional regulator	0.42	0.007
Rv1328	glgP	Probable glycogen phosphorylase GlgP	0.41	0.000
Rv2940c	mas	Probable multifunctional mycocerosic acid synthase membrane-associated Mas	0.36	0.007

Table S1 continued

#Orf	Name	Description	log_2FC	Adj. p-value
Rv3717	Rv3717	N-acetylmuramyl-L-alanine amidase	0.36	0.000
Rv1213	glgC	Glucose-1-phosphate adenylyltransferase GlgC (ADP-glucose synthase) (ADP-glucose pyrophosphorylase)	0.35	0.000
Rv2458	mmuM	Probable homocysteine S-methyltransferase MmuM (S-methylmethionine:homocysteine methyltransferase) (cysteine methyltransferase)	0.34	0.007
Rv0172	mce1D	Mce-family protein Mce1D	0.33	0.000
Rv0470c	pcaA	Mycolic acid synthase PcaA (cyclopropane synthase)	0.33	0.007
Rv2721c	Rv2721c	Antigen	0.33	0.000
Rv0554	bpoC	Possible peroxidase BpoC (non-haem peroxidase)	0.31	0.000
Rv2115c	mpa	Mycobacterial proteasome ATPase Mpa	0.31	0.000
Rv0503c	cmaA2	Cyclopropane-fatty-acyl-phospholipid synthase 2 CmaA2 (cyclopropane fatty acid synthase) (CFA synthase) (cyclopropane mycolic acid synthase 2) (mycolic acid trans-cyclopropane synthetase)	0.3	0.000
Rv2914c	pknI	Probable transmembrane serine/threonine-protein kinase I PknI (protein kinase I) (STPK I) (phosphorylase B kinase kinase) (hydroxyalkyl-protein kinase)	0.3	0.000
Rv0169	mce1A	Mce-family protein Mce1A	0.29	0.000
Rv0465c	lrpI	Transcriptional regulatory protein%2C local regulatory protein of icl1	0.29	0.007
Rv3045	adhC	Probable NADP-dependent alcohol dehydrogenase AdhC	0.25	0.035
Rv0019c	fipA	FtsZ-interacting protein A%2C FipA	0.24	0.014
Rv1195	PE13	PE family protein PE13	0.24	0.025
Rv1809	PPE33	PPE family protein PPE33	0.24	0.020
Rv2585c	Rv2585c	Possible conserved lipoprotein/putative ATP-binding cassette (ABC) transport protein (oligopeptide transport)	0.23	0.000
Rv1220c	Rv1220c	Probable methyltransferase	0.22	0.025
Rv1196	PPE18	Surfaced-exposed antigen	0.21	0.014
Rv1808	PPE32	PPE family protein PPE32	0.21	0.000
Rv0483	lprQ	Probable conserved lipoprotein LprQ	-0.17	0.000
Rv2048c	pks12	Polyketide synthase Pks12	-0.17	0.007
Rv1364c	Rv1364c	Possible sigma factor regulatory protein	-0.19	0.025
Rv3720	Rv3720	Possible fatty acid synthase	-0.21	0.031
Rv2203	Rv2203	Possible conserved membrane protein	-0.24	0.007
Rv2936	drrA	Daunorubicin-dim-transport ATP-binding protein ABC transporter DrrA	-0.25	0.000

Table S1 continued

#Orf	Name	Description	log_2FC	Adj. p-value
Rv3010c	pfkA	Probable 6-phosphofructokinase PfkA (phosphohexokinase) (phosphofructokinase)	-0.28	0.014
Rv3719	Rv3719	Conserved protein/putative amide-bond oxidoreductase	-0.28	0.000
Rv2937	drrB	Daunorubicin-dim-transport integral membrane protein ABC transporter DrrB	-0.31	0.007
Rv3057c	Rv3057c	Probable short chain alcohol dehydrogenase/reductase	-0.32	0.000
Rv1813c	Rv1813c	Conserved hypothetical protein	-0.33	0.035
Rv2607	pdxH	Probable pyridoxamine 5'-phosphate oxidase PdxH (PNP/PMP oxidase) (pyridoxinephosphate oxidase) (PNPOX) (pyridoxine 5'-phosphate oxidase)	-0.36	0.040
Rv2942	mmpL7	Conserved transmembrane transport protein MmpL7	-0.39	0.000
Rv3200c	Rv3200c	Possible transmembrane cation transporter	-0.39	0.000
Rv1040c	PE8	PE family protein PE8	-0.41	0.035
Rv1580c	Rv1580c	Probable PhiRv1 phage protein	-0.42	0.007
Rv3134c	Rv3134c	Universal stress protein family protein	-0.42	0.000
Rv3644c	Rv3644c	Possible DNA polymerase	-0.42	0.000
Rv0989c	grcC2	Probable polyprenyl-diphosphate synthase GrcC2 (polyprenyl pyrophosphate synthetase)	-0.44	0.025
Rv3726	Rv3726	Possible dehydrogenase	-0.51	0.007
L_03517	L_03517	hypothetical protein	-0.52	0.035
Rv0146	Rv0146	Possible S-adenosylmethionine-dependent methyltransferase	-0.52	0.000
Rv1273c	Rv1273c	Probable drugs-transport transmembrane ATP-binding protein ABC transporter	-0.55	0.000
Rv2851c	Rv2851c	GCN5-related N-acetyltransferase	-0.63	0.007
Rv0400c	fadE7	Acyl-CoA dehydrogenase FadE7	-0.67	0.020
Rv1421	Rv1421	conserved protein	-0.68	0.000
Rv1272c	Rv1272c	Probable drugs-transport transmembrane ATP-binding protein ABC transporter	-0.76	0.000
Rv2606c	snzP	Possible pyridoxine biosynthesis protein SnzP	-0.91	0.000
Rv0153c	ptbB	Phosphotyrosine protein phosphatase PTPB (protein-tyrosine-phosphatase) (PTPase)	-1.1	0.000
Rv1287	Rv1287	Conserved hypothetical protein	-1.15	0.000
Rv0805	Rv0805	Class III cyclic nucleotide phosphodiesterase (cNMP PDE)	-1.16	0.000
Rv0410c	pknG	Serine/threonine-protein kinase PknG (protein kinase G) (STPK G)	-1.29	0.000
Rv1248c	Rv1248c	Multifunctional alpha-ketoglutarate metabolic enzyme	-1.73	0.000

Table S2. Transposon insertions in genes possibly generally altering mycobacterial fitness of *M. tuberculosis* H37Ra cells during KSK-106 treatment. Negative log_2FC values indicate underrepresentation, positive values overrepresentation of the mutants in the pool, demonstrating aggravating or alleviating effects of insertions, respectively.

#Orf	Name	Description	log_2FC	Adj. p-value
Genes involved in drug efflux				
Rv1272c	*Rv1272c*	Probable drugs-transport transmembrane ATP-binding protein ABC transporter	-0.76	0.000
Rv1273c	*Rv1273c*	Probable drugs-transport transmembrane ATP-binding protein ABC transporter	-0.55	0.000
Rv2936	*drrA*	Daunorubicin-dim-transport ATP-binding protein ABC transporter DrrA	-0.25	0.000
Rv2937	*drrB*	Daunorubicin-dim-transport integral membrane protein ABC transporter DrrB	-0.31	0.007
Rv2942	*mmpL7*	Conserved transmembrane transport protein MmpL7	-0.39	0.000
Genes involved in cell wall assembly and integrity				
Rv1195	*PE13*	PE family protein PE13	0.24	0.025
Rv1808	*PPE32*	PPE family protein PPE32	0.21	0.000
Rv1809	*PPE33*	PPE family protein PPE33	0.24	0.020
Rv1040c	*PE8*	PE family protein PE8	-0.41	0.035
Rv2931	*ppsA*	Phenolpthiocerol synthesis type-I polyketide synthase PpsA	0.46	0.000
Rv2932	*ppsB*	Phenolpthiocerol synthesis type-I polyketide synthase PpsB	0.59	0.000
Rv2933	*ppsC*	Phenolpthiocerol synthesis type-I polyketide synthase PpsC	0.51	0.007
Rv2935	*ppsE*	Phenolpthiocerol synthesis type-I polyketide synthase PpsE	0.57	0.000
Genes associated with universal stress protein family				
Rv3134c	*Rv3134c*	Universal stress protein family protein	-0.42	0.000
Metabolic genes				
Rv3696c	glpK	Probable glycerol kinase GlpK (ATP:glycerol 3-phosphotransferase) (glycerokinase) (GK)	0.91	0.000
Rv1328	glgP	Probable glycogen phosphorylase GlgP	0.41	0.000
Rv1213	glgC	Glucose-1-phosphate adenylyltransferase GlgC (ADP-glucose synthase) (ADP-glucose pyrophosphorylase)	0.35	0.000

Table S3. Transposon insertions in genes altering mycobacterial fitness of *M. tuberculosis* H37Ra cells specific in response to KSK-106 treatment. Negative log_2FC values indicate underrepresentation, positive values overrepresentation of the mutants in the pool, demonstrating aggravating or alleviating effects of insertions, respectively.

#Orf	Name	Description	log_2FC	Adj. p-value
Genes involved in KSK-resistance and activation				
Rv2888c	*amiC*	Probable amidase AmiC (aminohydrolase)	1	0.000
Rv0552	*Rv0552*	Conserved protein/putative endodeoxyribonuclease	0.94	0.000
Gene involved in the oxidative stress network				
Rv3005c	*doxX*	Probable membrane oxidoreductase component (MRC) DoxX	0.55	0.000
Genes involved in pyridoxal-5'-phosphate pathway				
Rv2606c	*snzP*	Possible pyridoxine biosynthesis protein SnzP	-0.91	0.000
Rv2607	*pdxH*	Probable pyridoxamine 5'-phosphate oxidase PdxH (PNP/PMP oxidase) (pyridoxinephosphate oxidase) (PNPOX) (pyridoxine 5'-phosphate oxidase)	-0.36	0.040

Table S4. Strains used in this study.

Strain	Relevant properties	Origin
Mycobacterium tuberculosis H37Rv wild type	Wild type	William R. Jacobs Jr., PhD, Albert Einstein College of Medicine, Bronx, USA
H37Rv pBEN::mCherry (Hsp60)/GFP (Atc)	hyg^R, constitutive expression of mCherry	Reference [1]
H37Rv pMV361::*amiC*	Merodiploid *amiC* strain for overexpression and complementation, kan^R	This study
H37Rv pMV361::*Rv0552*	Merodiploid R*v0552* strain, for overexpression and complementation kan^R	This study
H37Rv pMV361::EV	Empty vector control strain, kan^R	This study
H37Rv Δ*amiC*	Gene deletion mutant of *amiC*, hyg^R	This study
H37Rv Δ*amiC* pMV361::*amiC*	Gene deletion mutant of *amiC*, complemented with a wild type copy of *amiC*, constitutively expressed from a single-copy integrative plasmid, hyg^R, kan^R	This study
H37Rv Δ*amiC* pMV361::EV	Gene deletion mutant of amiC, complemented with a empty vector control plasmid, hyg^R, kan^R	This study
H37Rv Δ*amiC* pMV361::*amiC* P185T	Gene deletion mutant of *amiC*, complemented with a mutated copy of *amiC*, constitutively expressed from a single-copy integrative plasmid, hyg^R, kan^R	This study
H37Rv Δ*amiC* pMV361::*amiC* Ins 100 +t	Gene deletion mutant of amiC, complemented with a mutated copy of amiC, constitutively expressed from a single-copy integrative plasmid, hyg^R, kan^R	This study

Table S4 continued

Strain	Relevant properties	Origin
H37Rv Δ*amiC* pMV361::R*v0552*	Gene deletion mutant of amiC, complemented with a wild type copy of *Rv0552*, constitutively expressed from a single-copy integrative plasmid, hyg^R, kan^R	This study
H37Rv Δ*amiC* pMV361::*amiC* K82A_S157A_S181A	Gene deletion mutant of amiC, complemented with a mutated copy of amiC, constitutively expressed from a single-copy integrative plasmid, hyg^R, kan^R	This study
H37Rv Δ*Rv0552*	Gene deletion mutant of Rv0552, hyg^R	This study
H37Rv *ΔRv0552* pMV361::*Rv0552*	Gene deletion mutant of *Rv0552*, complemented with a wild type copy of *Rv0552*, constitutively expressed from a single-copy integrative plasmid, hyg^R, kan^R	This study
H37Rv Δ*Rv0552* pMV361::EV	Gene deletion mutant of Rv0552, complemented with a empty vector control plasmid, hyg^R, kan^R	This study
H37Rv *ΔRv0552* pMV361::*Rv0552* H67R	Gene deletion mutant of Rv0552, complemented with a mutated copy of Rv0552, constitutively expressed from a single-copy integrative plasmid, hyg^R, kan^R	This study
H37Rv *ΔRv0552* pMV361::*Rv0552* A229D	Gene deletion mutant of *Rv0552*, complemented with a mutated copy of *Rv0552*, constitutively expressed from a single-copy integrative plasmid, hyg^R, kan^R	This study

Table S4 continued

Strain	Relevant properties	Origin
H37Rv *ΔRv0552* pMV361::*amiC*	Gene deletion mutant of *Rv0552*, complemented with a wild type copy of *amiC*, constitutively expressed from a single-copy integrative plasmid, hyg^R, kan^R	This study
H37Rv Δ*Rv3092c-Rv3095*	Deletion mutant of gene cluster *Rv3092c-Rv3095*, hyg^R	This study
M. tuberculosis strain $mc^2$6030	Auxotrophic mutant strain generated from H37Rv lacking RD1 region and *panCD* genes	obtained from William, R. Jacobs Jr., PhD, Albert Einstein College of Medicine, Bronx, USA; reference [2]
M. tuberculosis strain H37Ra	Avirulent strain	obtained from William, R. Jacobs Jr., PhD, Albert Einstein College of Medicine, Bronx, USA;
M. tuberculosis CDC1551	Virulent lab strain	obtained from William, R. Jacobs Jr., PhD, Albert Einstein College of Medicine, Bronx, USA
M. tuberculosis Erdman	Virulent lab strain	obtained from William, R. Jacobs Jr., PhD, Albert Einstein College of Medicine, Bronx, USA
M. tuberculosis KZN06 *M. tuberculosis* KZN07 *M. tuberculosis* KZN13 *M. tuberculosis* KZN14 *M. tuberculosis* KZN15 *M. tuberculosis* KZN16	clinical isolates from KZN, South Africa	obtained from William R. Jacobs Jr., PhD, Albert Einstein College of Medicine, Bronx, USA
M. smegmatis $mc^2$155	Wild type	obtained from William R. Jacobs Jr., PhD, Albert Einstein College of Medicine, Bronx, USA
M. smegmatis pMV361::*amiC*	Merodiploid strain for overexpression of *amiC*, kan^R	This study

Table S4 continued

Strain	Relevant properties	Origin
M. smegmatis pMV361::*Rv0552*	Merodiploid strain, for overexpression of *Rv0552*, kan^R	This study
M. smegmatis pMV361::EV	Empty vector control strain, *kan*^{R}	This study
M. bovis BCG pasteur	Wild type	obtained from William R. Jacobs Jr., PhD, Albert Einstein College of Medicine, Bronx, USA
M. bovis pMV361::*amiC*	Merodiploid strain for overexpression of *amiC*, kan^R	This study
M. bovis pMV361::*Rv0552*	Merodiploid strain, for overexpression of *Rv0552*, kan^R	This study
M. bovis pMV361::EV	Empty vector control strain, *kan*^{R}	This study
M. marinum ATCC 927	Wild type	DSMZ-German Collection of Microorganisms and Cell Cultures GmbH
M. abscessus (CF001s)		Clinical isolate; reference [3]
E. coli NEB 5-alpha	Cloning strain for plasmids	New England Biolabs (Cat.-No. C2987I)
E. coli HB101	Cloning strain for phasmids	Promega (Cat.-No. L2015)

Table S5. Oligonucleotides used in this study.

Oligonucleotide	Sequence [5‘ – 3‘]
HindIII *amiC*	GTCGGAAGCTTCTACTCGGCGATATTTGGGG
PacI *amic*	GGAGGATTAATTAAATZTCGCGCGTACAGCTTC
HindIII *rv0552*	GGGAAGCTTTCACCGCCGATAAACCTGGC
PacI *rv0552*	GGAGGTTAATTAAATGGCCGATGCAGACCTCGTC
5‘ *Rv0552* H67R	GCGGATGGCCGCGTGCCTCAACA
3‘ *Rv0552* H67R	TACTGGAGGCGGTCGTGC
5‘ *Rv0552* A229D	CTGGGTCAAAGTCCATCTCCGAGCATGTG
3‘ *Rv0552* A229D	GGTATCGGCCGATGGTCG
5‘ *amiC* Ins 100/473	ATTCCCACGCGTCGGTGCC
3‘ *amiC* 100/473	CCATACGCGGCCGTCGCC
5‘ *amiC* P185T	TGCAGGCGGCtgtAATACGGATCG
3‘ *amiC* P185T	ACGGGTTGGTCGGGCTCA
5' *amiC* K82A	GACCTTCATCGCAGACAACGTCGACG
3' *amiC* K82A	GGCACTCCACTGAAGAAC
5' *amiC* S157A	AGCGGGTGCCGCATCATCGGGAT
3' *amiC* S157A	GTGTAGTCGGTATTCCACGGATTAC
5' *amiC* S181A	CGGCGGCGGCGCAATCCGTATTC
3' *amiC* S181A	TCGTTGGCGTGCGCGATC
amic LL	TTTCTTTTCACAAAGTGGGACTGGGGCGCGCCGACGG
amiC LR	TTTTGTCTCACTTCGTGCATACCCGGCTAAGCCTGGC
amiC RL	TTGTCTTTGCATAGATTGCTAGCCCGCGTCCGGATCTAG
amiC RR	TCCGTGGTGCATCTTTTGCCGACTTCAGTAACGACCTTG
Rv0552 LL	TTTTCCATAAATTGGGCGCCGTAGTAGACGGTTTC
Rv0552 LR	AAAAAAACCATTTCTTGGCATGGGCTCCAAGCGTAGTG
Rv0552 RR	TTTTTTTTCCATCTTTTGGCCAGGTTGATCACCCGAAAG
Rv0552 RL	GGGTTTTTCCATAGATTGGGTGATACCCGTGCTGCCCCC
5′ *amiC* confirmation	ATCTAAGCGCCGTGACGGTCCAG
3' *amiC* confirmation	TGAAAGAGACCGTCGCTCAC
5' *rv0552* confirmation	ATTCTGAGCAACCGCCGGATG
3' *rv0552* confirmation	AGCAATCTAGCTGACAGCGCAGTCCG
Hyg confirmation	GCACGGGACCAACATCTTCG
sacB confirmation	TTTGTAATGGCCAGCTGTCC
3' *Rv3096* confirmation	TGTCTCGCATTCGGCGAGC
5' *Rv3091* confirmation	TATGGGCGCGGGCTTCGTCTACA
Operon-*Rv3095* LL	TTGCGTTCTCAGAAACTGGACCAGTTCGCCCATACCCTG
Operon-*Rv3095* LR	TTGGCTTTCAGTTCCTGCCGTCGCTAGGTCAGGTGGC
Operon-*Rv3095* RL	TGCGCTCTCAGAGACTGCGATTCCCAACCTCAAATTG
Operon-*Rv3095* RR	TCTTGTTTCAGCTTCTGTTGGGACCGCGCCAGGTAC

Table S5 continued

Oligonucleotide	Sequence [5‘ – 3‘]
5' *amiC* (PCR)	GGCTCGTGTGGCGATTTTCGAC
3' *amiC* (PCR)	TTAATGACGCCCCGCTGGGCTATC
5' *Rv0552* (PCR)	ATAGCACCGTTGGCGTCCACCCGCACCAT
3' *Rv0552* (PCR)	GGCGCATCAAAACTTCAGGACGGTTGAG
5' *amiC* (seq)	AATTATGTCGAGGCCGCCATCGCCCG
3' *amiC* (seq)	GAGAGCATCATGCCCACGG
5' *Rv0552* (seq)	TTATCGTCAGGCGCTCCTCCGGTG
3' *Rv0552* (seq)	TTATTGGAGGCGGTCGTGCTGTCGG
PacI *frr*	GCGTTAATTAAAGCGATGAGGAGGAGCGGCGCAG
HindIII *_frr*	GCGAAGCTTTGTCACGGATTTTGTTGCTGAGCG
PacI *Rv0812*	CGCGGTTAATTAAGGGACATGTTGAGGCAGACG
HindIII *Rv0812*	GAGAAGCTTGCGCTGACCACAACAGAGG
5' NdeI *amiC*- 6xHis-Tag	GGGATGCATATGCACCACCATCACCATCACATGTCGCGCGTACACG C
3' DraIII *amiC*	GGGCACTACGTGCTACTCGGCGATATTTGGG

Table S6. Plasmids and phasmids used in this study.

Plasmid (p) or Phasmid (ph)	Relevant properties
p0004S	*sacB*-hyg^R cassette, oriE-*cos* site cassette; reference [4]
phAE159	Temperature sensitive shuttle phasmid, derivative of mycobacteriophage TM4, amp^R; reference [4]
pMV361(kan)::EV	Integrative *E. coli*-mycobacteria shuttle palsmid, kan^R; reference [5]
pMV361(kan)::*Rv0552*	complementation and overexpression plasmid, kan^R
pMV361(kan)::*amiC*	complementation and overexpression plasmid, kan^R
p0004s-*amiC*-k.o.	Knock-out cassette, hyg^R, sacB, flanking regions of *amiC,* hyg^R
p0004s-R*v0552*-k.o.	Knock-out cassette, hyg^R, sacB, flanking regions of *Rv0552,* hyg^R
p0004s - operon rv3095- k.o.	Knock-out cassette, hyg^R, sacB, flanking regions of *Rv3092c-Rv3095,* hyg^R
phAE159::*amiC*-k.o	Knock-out cassette, hyg^R, sacB, flanking regions of *amiC,* hyg^R
phAE159::*Rv0552*-k.o.	Knock-out cassette, hyg^R, sacB, flanking regions of *Rv0552,* hyg^R
phAE159::operon-*Rv3095*-k.o.	Knock-out cassette, hyg^R, sacB, flanking regions of *Rv3092c-Rv3095,* hyg^R
pMV361::*amiC* P185T	complementation plasmid, kan^R
pMV361::*amiC* Ins100/473+t	complementation plasmid, kan^R
pMV361::*Rv0552* H67R	complementation plasmid, kan^R
pMV361::*Rv0552* A229D	complementation plasmid, kan^R
pMV361::*amiC*_K82A_S157A_S181A	complementation plasmid, kan^R

Synthesis of starting materials and intermediates

4-(Heptyloxy)benzoic acid (6c)

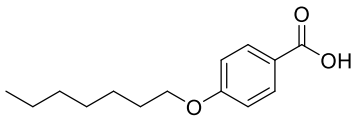

The preparation of **6c** was carried out according to a procedure of CHENG *et al.*[6] 4-(Heptyloxy)benzoic acid (**6c**) was obtained as a colorless solid (62 %, 2 steps). The spectroscopic data correspond to those reported in the literature.

^{1}H-NMR (300 MHz, DMSO-*d*$_6$) δ 7.93 – 7.80 (m, 2H), 7.05 – 6.93 (m, 2H), 4.02 (t, *J* = 6.5 Hz, 2H), 1.79 – 1.64 (m, 2H), 1.48 – 1.19 (m, 8H), 0.94 – 0.79 (m, 3H)

HPLC t_R = 16.32 min, purity = 99.9 %

4-(Thiazol-2-yl)benzoic acid (6d)

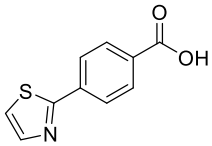

The preparation of **6d** was carried out according to a procedure of TANI *et al.*[7] 4-(Thiazol-2-yl)benzoic acid (**6d**) was obtained as a colorless solid (42 %, 3 steps). The spectroscopic data correspond to those reported in the literature.

^{1}H-NMR (300 MHz, DMSO-*d*$_6$) δ 13.15 (s, 1H), 8.12 – 8.02 (m, 4H), 8.01 (d, *J* = 3.2 Hz, 1H), 7.90 (d, *J* = 3.2 Hz, 1H)

HPLC t_R = 9.05 min, purity = 99.9 %

***N*-Hydroxy-[1,1'-biphenyl]-4-carboxamide (12a)**

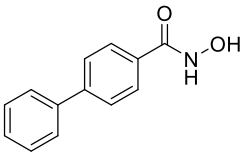

Oxalyl chloride (113 mmol, 2.26 eq.) was slowly added to a solution of biphenyl-4-carboxylic acid (**6a**) (50.0 mmol, 1.00 eq.) and *N,N*-dimethylformamide (50.0 mmol, 1.00 eq.) in 150 mL anhydrous dichloromethane under ice cooling. The reaction mixture was stirred for 1 h at 0 °C and then slowly added to a solution of hydroxylamine hydrochloride (200 mmol, 4.00 eq.) and triethylamine (300 mmol, 6.00 eq.) in 90.0 mL tetrahydrofuran/water (5:1). The suspension was stirred for 16 h at room temperature, the pH was adjusted to 6 with 2 M hydrochloric acid solution and the mixture was extracted four times with 200 mL dichloromethane. The combined organic phases were dried over anhydrous sodium sulfate, filtered and the solvent was removed under reduced pressure. The crude product was recrystallized from water / ethanol and *N*-hydroxy-[1,1'-biphenyl]-4-carboxamide (**12a**) was obtained as white needles (87 % yield). The spectroscopic data agree with those reported in the literature.[8]

^{1}H-NMR (300 MHz, DMSO-d$_6$) δ 7.36 – 7.44 (m, 1H), 7.45 – 7.54 (m, 2H), 7.68 – 7.79 (m, 4H), 7.82 – 7.89 (m, 2H), 9.06 (s, 1H), 11.28 (s, 1H)

^{13}C-NMR (75 MHz, DMSO) δ 126.6, 126.8, 127.5, 128.0, 129.0, 131.5, 139.1, 142.7, 163.8

HPLC t_R = 9.08 min, purity = 99.9 %

Mp. T_M = 197.6 °C

***N*-Hydroxy-4-(pentyloxy)benzamide (12b)**

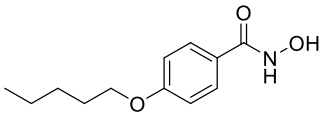

Oxalyl chloride (113 mmol, 2.26 eq.) was slowly added to a solution of biphenyl-4-carboxylic acid (**6b**) (50.0 mmol, 1.00 eq.) and *N,N*-dimethylformamide (50.0 mmol, 1.00 eq.) in 150 mL anhydrous dichloromethane under ice cooling. The reaction mixture was stirred for 1 h at 0 °C and then slowly added to a solution of hydroxylamine hydrochloride (200 mmol, 4.00 eq.) and triethylamine (300 mmol, 6.00 eq.) in 90.0 mL tetrahydrofuran / water (5:1). The suspension was stirred for 16 h at room temperature, the pH adjusted to 6 with 2 M hydrochloric acid solution and the mixture extracted four times with 200 mL dichloromethane. The combined organic phases were dried over anhydrous sodium sulfate, filtered and the solvent was removed under reduced pressure. The crude product was recrystallized from water / ethanol and *N*-hydroxy-4-(pentyloxy)benzamide and (**12b**) was obtained as white needles (73 % yield). The spectroscopic data agree with those reported in the literature.[8]

^{1}H-NMR (300 MHz, DMSO-*d*$_6$) δ 11.04 (s, 1H), 8.88 (s, 1H), 7.88 – 7.57 (m, 2H), 7.09 – 6.81 (m, 2H), 4.00 (t, *J* = 6.5 Hz, 2H), 1.83 – 1.62 (m, 2H), 1.49 – 1.23 (m, 4H), 0.99 – 0.79 (m, 3H)

^{13}C-NMR (75 MHz, DMSO-*d*$_6$) δ 164.02, 160.92, 128.61, 124.74, 114.02, 67.61, 28.26, 27.66, 21.87, 13.91

HPLC t_R = 10.81 min, purity = 98.8 %

Mp. T_M = 150 °C

2-([1,1'-Biphenyl]-4-carboxamidooxy)acetic acid (10)[9]

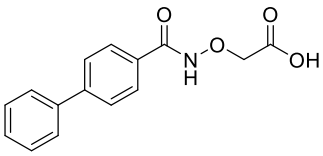

A solution of *N*-hydroxy-[1,1'-biphenyl]-4-carboxamide (**12a**, 34.6 mmol, 1.00 eq.), bromoacetic acid (**1a**, 34.6 mmol, 1.00 eq.) and sodium hydroxide (69.2 mmol, 2.00 eq.) in 200 mL ethanol was refluxed for 8 h. After cooling to room temperature, the solvent was removed under reduced pressure, the residue dissolved in 200 mL distilled water and the pH adjusted with 2 M hydrochloric acid solution to pH 4. The aqueous suspension was extracted four times with 200 mL dichloromethane, the combined organic phases were dried over anhydrous sodium sulfate, filtered and the solvent was removed under reduced pressure. The crude product was recrystallized from ethyl acetate and 2-([1,1'-biphenyl]-4-carboxamidooxy)acetic acid (**10**) was obtained as white needles (80 % yield).

^{1}H-NMR (300 MHz, DMSO-d$_6$) δ 4.53 (s, 2H), 7.37 – 7.45 (m, 1H), 7.45 – 7.55 (m, 2H), 7.68 – 7.74 (m, 2H), 7.74 – 7.81 (m, 2H), 7.82 – 7.92 (m, 2H), 12.07 (s, 1H), 12.99 (s, 1H)

^{13}C-NMR (75 MHz, DMSO) δ 71.8, 126.6, 126.8, 127.9, 128.1, 129.0, 130.5, 139.0, 143.2, 164.6, 170.0

HPLC t_R = 10.23 min, purity = 98.0 %

Mp. T_M = 191.8 °C

2-((4-(Pentyloxy)benzamido)oxy)acetic acid (11)

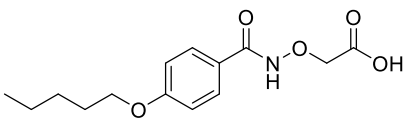

A solution of *N*-hydroxy-4-(pentyloxy)benzamide (**12b**, 10.0 mmol, 1.00 eq.), bromoacetic acid (**1a**, 10.0 mmol, 1.00 eq.), and sodium hydroxide (20.0 mmol, 2.00 eq.) in 40.0 mL ethanol was heated to reflux for 8 hours. After cooling to room temperature, the solvent was evaporated under reduced pressure. The residue was then dissolved in 50.0 mL distilled water, and the pH adjusted to pH 4 using a 2 M hydrochloric acid solution . The aqueous suspension was extracted four times with 40.0 mL dichloromethane, the combined organic phases were dried over anhydrous sodium sulfate, filtered and the solvent removed under reduced pressure. The crude product was recrystallized from ethyl acetate and 2-((4-(pentyloxy)benzamido)oxy)acetic acid (**11**) was obtained as white needles (51 % yield).

^{1}H-NMR (300 MHz, DMSO-*d$_6$*) δ 13.00 (s, 1H), 11.84 (s, 1H), 7.85 – 7.62 (m, 2H), 7.06 – 6.86 (m, 2H), 4.48 (s, 2H), 4.01 (t, *J* = 6.5 Hz, 2H), 1.81 – 1.62 (m, 2H), 1.36 (tdt, *J* = 8.0, 3.6, 2.2 Hz, 4H), 0.97 – 0.81 (m, 3H)

^{13}C-NMR (75 MHz, DMSO-*d$_6$*) δ 170.12, 164.85, 161.49, 129.12, 123.53, 114.12, 71.97, 67.68, 28.23, 27.63, 21.86, 13.90

HPLC t_R = 11.91 min, purity = 99.3 %

Mp. T_M = 162.6 °C

2-([1,1'-Biphenyl]-4-carboxamidooxy)propanoic acid (**13**)

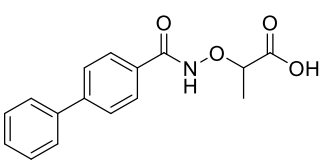

Under a nitrogen atmosphere at -10 °C, a solution of *N*-hydroxy-[1,1'-biphenyl]-4-carboxamide (**12a**, 4.69 mmol, 1.00 eq.) in 20.0 mL of anhydrous tetrahydrofuran was treated with sodium hydride (60% dispersion in mineral oil, 5.16 mmol, 1.10 eq.) and stirred for 10 min. 2-Bromopropanoic acid (**1b**, 4.69 mmol, 1.00 eq.) dissolved in 5.00 mL of absolute tetrahydrofuran was then added dropwise. The reaction mixture was heated to reflux for 24 h. After cooling down to room temperature, the solvent was removed under reduced pressure and the residue was dissolved in 50.0 mL distilled water and the pH was adjusted with a 2 M

hydrochloric acid solution to 1. The aqueous phase was extracted three times with 50.0 mL ethyl acetate, the combined organic phases were dried over anhydrous sodium sulfate, filtered and the solvent was removed under reduced pressure. The crude product was purified by flash chromatography on silica gel using *n*-hexane/ethyl acetate as eluent. 2-([1,1'-Biphenyl]-4-carboxamidooxy)propanoic acid (**13**) was obtained as a light yellow solid (70 % yield).

^{1}H-NMR (600 MHz, DMSO-d$_6$) δ 1.41 (d, J = 7.0 Hz, 3H), 4.54 (q, J = 6.9 Hz, 1H), 7.38 – 7.45 (m, 1H), 7.49 (dd, J = 8.4, 7.0 Hz, 2H), 7.69 – 7.75 (m, 2H), 7.74 – 7.80 (m, 2H), 7.83 – 7.89 (m, 2H), 11.94 (br s, 1H), 12.95 (br s, 1H)

^{13}C-NMR (151 MHz, DMSO) δ 16.9, 79.1, 127.1, 127.3, 128.4, 128.6, 129.5, 131.0, 139.5, 143.7, 165.3, 173.3

HPLC t_R = 12.22 min, purity = 96.8 %

Mp. T_M = 173.8 °C

General procedure 2 (GP 2): Synthesis of hydroxylamines[10]

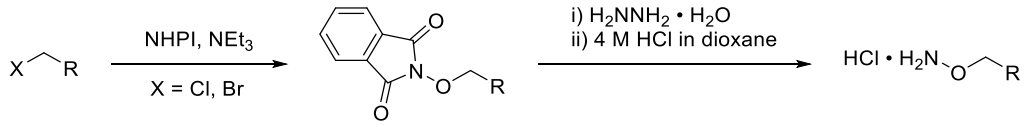

The respective alkyl halide (1.00 eq.), *N*-hydroxyphthalimide (NHPI, 1.20 eq.) and triethylamine (2.00 eq.) were heated to reflux in acetonitrile or *N,N*-dimethylformamide (10.0 mL/mmol of alkyl halide) until complete conversion of the alkyl halide. After cooling down to room temperature, the solvent was removed under reduced pressure, the residue dissolved in ethyl acetate (10.0 mL/mmol based on alkyl halide) and washed four times with saturated sodium hydrogen carbonate solution (10.0 mL/mmol based on alkyl halide). The organic phase was dried over anhydrous sodium sulfate, filtered and the solvent was removed under reduced pressure. The phthaloyl-protected hydroxylamines were used for deprotection (method A or B) without further purification.

Deprotection method A:

The appropriate phthaloyl-protected hydroxylamine (1.00 eq.) was dissolved in ethanol (15.0 mL/mmol based on protected hydroxylamine) and hydrazine monohydrate (2.00 eq.) was added. The reaction mixture was heated to reflux for 2 h and after cooling down to room temperature it was stored for 1 h at 0 °C. The precipitate was isolated by filtration and washed twice with ice-cold ethanol (10.0 mL/mmol based on protected hydroxylamine). The filtrate was cooled to 0 °C and the pH was adjusted to 2 - 3 with 4 M hydrochloric acid in 1,4-dioxane while

stirring continuously. The precipitated hydroxylamine hydrochloride was isolated by filtration and washed with ice-cold 1,4-dioxane (10.0 mL/mmol based on protected hydroxylamine).

Deprotection method B:

The appropriate corresponding phthaloyl-protected hydroxylamine (1.00 eq.) was dissolved in dichloromethane or tetrahydrofuran (15.0 mL/mmol based on protected hydroxylamine) and hydrazine monohydrate (2.00 eq.) was added. The reaction mixture was stirred for 4 h at room temperature, then stored overnight at 7 °C and the precipitate was removed by filtration. The filtrate was washed three times with saturated sodium hydrogen carbonate solution (5.00 mL/mmol based on protected hydroxylamine) and once with saturated sodium chloride solution (5.00 mL/mmol based on protected hydroxylamine). The organic phase was dried over anhydrous sodium sulfate, filtered and the solvent removed under reduced pressure. The residue was dissolved in absolute diethyl ether (5.00 mL/mmol based on protected hydroxylamine) and the pH was adjusted to 1 with 4 M hydrochloric acid in 1,4-dioxane under ice cooling. The suspension was allowed to stand overnight at -20 °C, the precipitated hydroxylamine hydrochloride was isolated by filtration and washed with ice-cold dry diethyl ether (5.00 mL/mmol based on protected hydroxylamine).

***O*-Benzylhydroxylamine hydrochloride (2)**

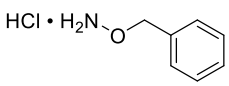

2 was used for **GP 1** without further purification.

***O*-(*tert*-Butyl)hydroxylamine hydrochloride (14a)**

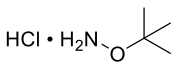

14a was used for **GP 1** without further purification.

***O*-Hexylhydroxylamine hydrochloride (14b)[11]**

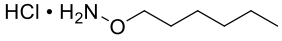

The synthesis was carried out according to **GP 2** (method A). *O*-Hexylhydroxylamine hydrochloride (**14b**) was obtained as a colorless solid (55 %).

^{1}H-NMR (300 MHz, DMSO-d$_6$) δ 0.79 – 0.94 (m, 3H), 1.13 – 1.38 (m, 6H), 1.57 (tt, *J* = 7.4, 6.1 Hz, 2H), 3.99 (t, *J* = 6.5 Hz, 2H), 10.99 (br s, 3H).

Mp.: 151.3 °C

_O_-Phenylhydroxylamine hydrochloride (14c)[12]

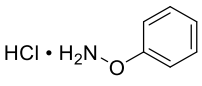

The synthesis was carried out according to **GP 2** (method B). *O*-Phenylhydroxylamine hydrochloride (**14c**) was obtained as a colorless solid (80 %).

^{1}H-NMR (600 MHz, DMSO-d$_6$) δ = 7.06 – 7.11 (m, 1H), 7.15 – 7.21 (m, 2H), 7.35 – 7.40 (m, 2H).

Mp.: 129.5 °C

_O_-(Cyclohexylmethyl)hydroxylamine hydrochloride (14d)[13]

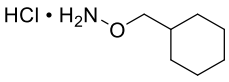

The synthesis was carried out according to **GP 2** (method B). *O*-(Cyclohexylmethyl)hydroxylamine hydrochloride (**14d**) was obtained as a colorless solid (48 %).

^{1}H-NMR (300 MHz, DMSO-d$_6$) δ 0.83 – 1.04 (m, 2H), 1.19 (h, *J* = 12.1 Hz, 3H), 1.55 – 1.73 (m, 6H), 3.81 (d, *J* = 6.1 Hz, 2H), 10.92 (br s, 3H).

Mp.: 178.6 °C

_O_-(pyridin-2-ylmethyl)hydroxylamine dihydrochloride (14e)[14]

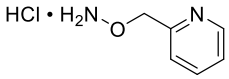

The synthesis was carried out according to **GP 2** (method B). *O*-(Pyridin-2-ylmethyl)hydroxylamine dihydrochloride (**14e**) was obtained as a colorless solid (52 %).

^{1}H-NMR (300 MHz, DMSO-d$_6$) δ = 5.29 (s, 2H), 7.97 (ddd, *J* = 7.9, 5.5, 0.8 Hz, 1H), 8.48 (dt, *J* = 8.0, 1.8 Hz, 1H), 8.88 (dd, *J* = 5.6, 1.5 Hz, 1H), 8.94 (d, *J* = 2.0 Hz, 1H).

Mp.: 188.3 °C

References Supporting Information

1. Martin, C.J., Booty, M.G., Rosebrock, T.R., Nunes-Alves, C., Desjardins, D.M., Keren, I., Fortune, S.M., Remold, H.G., and Behar, S.M. (2012). Efferocytosis Is an Innate Antibacterial Mechanism. Cell Host & Microbe *12*, 289-300. 10.1016/j.chom.2012.06.010.
2. Sambandamurthy, V.K., Derrick, S.C., Hsu, T., Chen, B., Larsen, M.H., Jalapathy, K.V., Chen, M., Kim, J., Porcelli, S.A., Chan, J., et al. (2006). Mycobacterium tuberculosis DeltaRD1 DeltapanCD: a safe and limited replicating mutant strain that protects immunocompetent and immunocompromised mice against experimental tuberculosis. Vaccine *24*, 6309-6320. 10.1016/j.vaccine.2006.05.097.
3. Steindor, M., Nkwouano, V., Stefanski, A., Stuehler, K., Ioerger, T.R., Bogumil, D., Jacobsen, M., Mackenzie, C.R., and Kalscheuer, R. (2019). A proteomics approach for the identification of species-specific immunogenic proteins in the Mycobacterium abscessus complex. Microbes Infect *21*, 154-162. 10.1016/j.micinf.2018.10.006.
4. Jain, P., Hsu, T., Arai, M., Biermann, K., Thaler, D.S., Nguyen, A., Gonzalez, P.A., Tufariello, J.M., Kriakov, J., Chen, B., et al. (2014). Specialized transduction designed for precise high-throughput unmarked deletions in Mycobacterium tuberculosis. mBio *5*, e01245-01214. 10.1128/mBio.01245-14.
5. Jacobs, W.R., Tuckman, M., and Bloom, B.R. (1987). Introduction of Foreign DNA into Mycobacteria Using a Shuttle Phasmid. Nature *327*, 532-535. DOI 10.1038/327532a0.
6. Cheng, X.H., Bai, X.Q., Jing, S., Ebert, H., Prehm, M., and Tschierske, C. (2010). Self-Assembly of Imidazolium-Based Rodlike Ionic Liquid Crystals: Transition from Lamellar to Micellar Organization. Chem-Eur J *16*, 4588-4601. 10.1002/chem.200903210.
7. Tani, S., Uehara, T.N., Yamaguchi, J., and Itami, K. (2014). Programmed synthesis of arylthiazoles through sequential C-H couplings. Chem Sci *5*, 123-135. 10.1039/c3sc52199k.
8. Feng, C., and Loh, T.P. (2014). Rhodium-Catalyzed C-H Alkynylation of Arenes at Room Temperature. Angew Chem Int Edit *53*, 2722-2726. 10.1002/anie.201309198.
9. Mchale, D., Green, J., and Mamalis, P. (1960). Amino-Oxy-Derivatives .1. Some Alpha-Amino-Oxy-Acids and Alpha-Amino-Oxy-Hydrazides. J Chem Soc, 225-229. DOI 10.1039/jr9600000225.
10. Pflieger, M., Hamacher, A., Öz, T., Horstick-Muche, N., Boesen, B., Schrenk, C., Kassack, M.U., and Kurz, T. (2019). Novel α,β-unsaturated hydroxamic acid derivatives

overcome cisplatin resistance. Bioorgan Med Chem *27*, 115036. 10.1016/j.bmc.2019.07.052.

11. High, A., Prior, T., Bell, R.A., and Rangachari, P.K. (1999). Probing the "active site" of diamine oxidase:: Structure-activity relations for histamine potentiation by O-alkylhydroxylamines on colonic epithelium. J Pharmacol Exp Ther *288*, 490-501.
12. Wang, M.Z., Xu, H., Liu, T.W., Feng, Q., Yu, S.J., Wang, S.H., and Li, Z.M. (2011). Design, synthesis and antifungal activities of novel pyrrole alkaloid analogs. Eur J Med Chem *46*, 1463-1472. 10.1016/j.ejmech.2011.01.031.
13. Laruelle, C., Lepant, M., and Raynier, B. (1989) Symmetrical O-substituted dioximes of benzo-fused β-diketocyclo-alkylenes, the processes for their preparation and their application as drugs. United States patent US4804684A.
14. Faolli, A.A., Bleyman, O.I., Kao, W., and Abou-Gharbia, M.A. (1996) Carbamates of rapamycin. United States patent US5550133

4. GtrA-like protein Rv3277 is essential for cell-surface mannosylation of *Mycobacterium tuberculosis*

Unpublished

Contribution:

- Writing of the manuscript draft
- Cultivation of ATc-dependent conditional *M. tuberculosis* and *M. smegmatis* mutants
- Growth kinetics in liquid shaking cultures and CFU-plating under silenced and induced gene expression conditions
- Resazurin microplate assays of conditional *M. tuberculosis* mutants under induced and partially silenced gene expression conditions
- Validation of ATc-dependency of the conditional mutants on solid and liquid media
- Genetic manipulation of the *M. tuberculosis* conditional mutant
- Intracellular growth capacity assay via macrophage infection assay
- Sample preparation for scanning electron microscopy experiments
- Generation of whole-cell protein lysates of *M. tuberculosis* cells followed by Western Blot analysis
- Preparation of lipid extracts from *M. tuberculosis* cells for MALDI-ToF analysis
- Whole-lipid extraction of *M. tuberculosis* cells followed by purification of PIMs/LM/LAM
- Thin layer chromatography
- Extraction of the mAGP layer of *M. tuberculosis* cells followed by generation of alditol acetate derivatives for GC-MS analysis

4.1 Manuscript

GtrA-like lipid floppase Rv3277 is essential for cell surface mannosylation in *Mycobacterium tuberculosis*

Kristin Vill[*], Steffen Schindler[1,*], Lasse van Geelen[1], David Podlesainski[2], Sudagar S. Gurcha[3], Milena Hänisch[1], Kathrin Lindner[1], Martine Gilleron[4], Christoph Gertzen[5], Violetta Krisilia[1], Ben J. Appelmelk[6], Holger Gohlke[5], Jérôme Nigou[4], Gurdyal S. Besra[3], Markus Kaiser[2], and Rainer Kalscheuer[1,§]

[1] Heinrich Heine University Düsseldorf, Faculty of Mathematics and Natural Sciences, Institute of Pharmaceutical Biology and Biotechnology, 40225 Düsseldorf, Germany

[2] Department of Chemical Biology, ZMB, Faculty of Biology, University of Duisburg-Essen, 45177 Essen, Germany

[3] School of Biosciences, University of Birmingham, Edgbaston, Birmingham, B15 2TT, United Kingdom

[4] Institute of Pharmacology and Structural Biology (IPBS), University of Toulouse, CNRS, University of Toulouse III-Paul Sabatier, Toulouse, France

[5] Institute of Pharmaceutical and Medicinal Chemistry, Heinrich Heine University Düsseldorf, 40225 Düsseldorf, Germany

[6] Molecular Microbiology/Medical Microbiology and Infection Control, Amsterdam University Medical Centers, Amsterdam, Netherlands.

* These authors contributed equally

§ Author for correspondence: rainer.kalscheuer@hhu.de

Abstract

Tuberculosis continues to be a threat to health around the globe. The causative agent, *Mycobacterium tuberculosis*, possesses not only the ability to evade the immune system but also a complex cell wall that confers intrinsic resistance to antibiotics and is crucial for pathogenicity. Although research has made great progress on cell wall issues, some key steps in biogenesis of the unique structure remain obscure. Glycoconjugates, which have a vital function in host-pathogen interactions, are synthesized in a bipartite process in the cyto- and periplasm. Although the biosynthesis is well known, the mechanism by which the carbohydrates enter the outer leaflet of the cell membrane remains unknown. Using bioinformatics, gene inactivation and phenotypic characterization of mutant strains, we have identified Rv3277 as a GtrA-like transporter and revealed its role in the translocation of glycoconjugate building blocks. Thus, we have uncovered a missing part in the biosynthetic pathway of glycoconjugate formation and identified a potential new drug target candidate.

Keywords

Tuberculosis, mycobacteria, cell wall, glycoconjugates, floppases

Introduction

Only surpassed by Covid-19 in the last years, tuberculosis (TB) remains one of the most serious infectious diseases with approx. 10.6 million new cases and 1.6 million deaths in 2021 [1]. The increasing emergence of multidrug-resistant strains of the causative pathogen *Mycobacterium tuberculosis* underlines the urgent need for new antibiotics. Much of its pathogenicity is attributed to the unusual, complex cell wall structure (reviewed in [2]). Compared to other Gram-positive bacteria, and in addition to the characteristic mycolic acids, mycobacteria do possess various additional unique cell wall molecules that confer exceptional physicochemical resistance to various stresses, mediate high intrinsic antibiotic resistance by reducing permeability, and/or play important roles in interaction with the host´s immune system [2]. Some of the most abundant cell wall molecules are rich in mannose, arabinose, or both. These glycoconjugates comprise molecules such as phosphatidylinositol mannosides (PIMs), lipomannan (LM), arabinogalactan (AG) and lipoarabinomannan (LAM), some of which have been shown to play important roles in virulence by interaction with various host cell receptors such as the mannose receptor, complement receptors, or the dendritic cell-specific intercellular adhesion molecule-3-grabbing non-integrin (DC-SIGN) [3-8]. Since biosynthesis of these glycoconjugates is essential for viability of *M. tuberculosis*, they offer several validated or potential target structures for chemotherapy of TB, as exemplified by the first-line antibiotic ethambutol that interferes with AG biosynthesis [9, 10].

Giving their outstanding importance for viability and pathogenesis of *M. tuberculosis*, the biosynthesis of arabinosylated and mannosylated mycobacterial cell wall constituents has been extensively investigated over the last decades. However, while large aspects of the biosynthetic pathways and enzymes have been discovered, several essential steps are still unknown. Biosynthesis of the arabinosylated and mannosylated mycobacterial cell wall glycoconjugates are membrane-associated bipartite processes that are initiated at the cytoplasmic side of the plasma membrane. Subsequently, intermediates are translocated ("flopped") to the periplasmic leaflet of the membrane, where they are extended by various arabinosyl- and/or mannosyltransferases. In the biosynthesis of AG, after synthesis at the cytosolic face of the membrane by galactofuranosyltransferases using UDP-galactofuranose as donor substrate, the galactan core C50-P-P-GlcNAc-Rha-Galf_{30} is flipped across the plasma membrane through a Wzm-Wzt-type ABC transporter comprising the proteins Rv3781 and Rv3783 [11]. The subsequent steps in AG assembly take place at the periplasmic side of the plasma membrane by arabinofuranosyltransferases that transfer arabinofuranose residues onto C50-P-P-GlcNAc-Rha-

Galf_{30} utilizing decaprenyl-monophosphoryl-D-arabinofuranose (DPA) as a donor substrate [12]. Similarly, the early steps in biosynthesis of the mannosylated glycoconjugates PIM, LM, and LAM occur at the cytoplasmic side of the plasma membrane. The α-mannopyranosyltransferases PimA (Rv2610c), PimB (Rv2188c) and PimC or a yet-unidentified mannosyltransferase mediate the stepwise mannosylation of the *myo*-inositol moiety of the phospholipid phosphatidyl-*myo*-inositol, employing GDP-mannopyranose as the donor substrate, yielding phosphatidylinositol tetramannoside (PIM_4). Following mono- and diacylation by the acyltransferase Rv2611c and a yet-unknown enzyme, the resulting Ac_1/Ac_2PIM_4 is flopped by an unknown mechanism from the cytoplasmic to the periplasmic side of the plasma membrane [13]. Here, Ac_1/Ac_2PIM_4 serves as a branch point, which can either be extended by the mannopyranosyltransferase PimE (Rv1159) to form higher-order PIMs (Ac_1/Ac_2PIM_6), or by the mannopyranosyltransferase MptA (Rv2174), MptB (Rv1459c) and MptC (Rv2181) to synthesize LM. The mentioned mannopyranosyltransferases represent GT-C type glycosyltransferases that utilize decaprenyl-monophosphoryl-D-mannopyranose (DPM) as the donor substrate [14]. For LAM biosynthesis, a yet-unidentified arabinofuranosyltransferase first primes the mannan core of LM with a few arabinofuranose residues, after which EmbC (Rv3793) extends the primed LM with the addition of 12–16 arabinofuranose residues. Subsequently, the branching enzyme AftC and the arabinofuranosyltransferase AftB, which is also involved in AG biosynthesis, complete the nonreducing arabinan domain of LAM. EmbC, AftC, and AftB all employ DPA as the donor substrate to result in addition of altogether 55–70 arabinofuranose residues to LM. Finally, the arabinan domain of LAM is modified with mannose residues by the mannopyranosyltransferases CapA (Rv1635c) and MptC (Rv2181), both employing DPM as the donor substrate, resulting in ManLAM [13, 15] (for a schematic overview see Supplementary Fig. 1).

The biosyntheses of DPA and DPM, which are required for extension of the arabinosylated and mannosylated glycoconjugates at the periplasmic face of the cytoplasm membrane, are themselves bipartite processes that are initiated at the cytoplasmic side of the plasma membrane and require subsequent translocation to the periplasmic leaflet of the membrane. DPM is synthesized at the cytoplasmic side of the membrane by transfer of mannose from the nucleotide-activated donor substrate GDP-mannopyranose to the membrane lipid carrier C50-P mediated by Ppm1 (Rv2051c), and subsequently needs to be flopped to the periplasmic side of the cytoplasm membrane (Fig. 1). In contrast, DPA requires an activated phosphosugar, phosphoribosylpyrophosphate, which is produced by phosphorylation of ribose-1-phosphate catalyzed by phosphoribosyl-1-pyrophosphate synthetase PrsA (Rv1017). Next, decaprenylphosphoryl-5-phosphoribose synthase UbiA (Rv3806c) transfers

phosphoribosylpyrophosphate to C50-P, yielding decaprenyl-monophosphoryl-D-ribofuranosephosphate, which is subsequently dephosphorylated by Rv3807 to produce decaprenyl-monophosphoryl-D-ribofuranose (DPR). Decaprenylphosphoribose 2′ epimerase composed of DprE1 (Rv3790) and DprE2 (Rv3791) subunits then catalyzes the epimerization of the ribosyl unit of DPR, resulting in DPA (for a schematic overview see Supplementary Fig. 2). Recently, epimerization mediated by DprE1-DprE2 was reported to occur extracellularly at the periplasmic face of the membrane [16]. Thus, this suggests that flopping might occur at the stage of the DPR intermediate. In summary, the biosynthesis of arabinosylated and mannosylated glycoconjugates requires several floppase reactions at the level of DPM, DPR, Ac_1/Ac_2PIM_4 and C50-P-P-GlcNAc-Rha-Galf_{30}, of which only flopping of the galactan core C50-P-P-GlcNAc-Rha-Galf_{30} by the Wzm–Wzt-type ABC transporter Rv3781-Rv3783 has been clearly established [11].

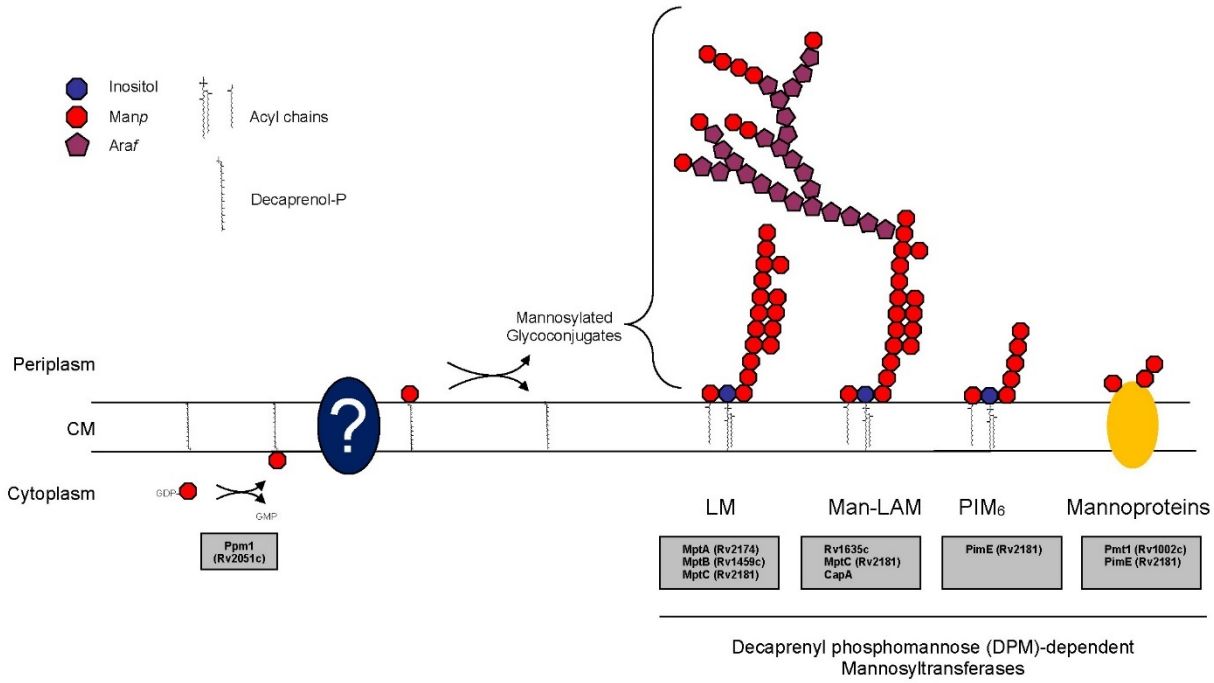

Fig. 1: Schematic representation of the bipartite biosynthesis of decaprenyl monophosphoryl-D-mannopyranose (DPM) in *M. tuberculosis*. DPM synthesis is initiated at the cytoplasmic side of the membrane by transfer of mannose from the nucleotide-activated donor substrate GDP-mannopyranose to the membrane lipid carrier C50-P mediated by Ppm1 (Rv2051c), and subsequently needs to be flopped to the periplasmic side of the cytoplasm membrane by a yet-unknown lipid translocase. At the periplasmic face of the membrane, DPM serves as the donor substrate for various mannopyranosyltransferases for the synthesis of different

mannosylated cell surface glycoconjugates. LM, lipomannan; Man-LAM, mannose-capped lipoarabinomannan; PIM_6, phosphatidyl inositol hexamannoside.

In other prokaryotes, translocases that have similarities to small multidrug resistance transporters can perform lipid floppase function [17]. A well-known class of these floppases is the GtrA-like floppases. They are small, very hydrophobic enzymes of ~120 amino acids. The best-known example is from *Shigella flexneri*, where the gene cluster *gtrA*, *gtrB*, and *gtrX* mediates the conversion of O antigen, the distal portion of LPS, by transferring a glycosyl residue [18]. GtrB catalyzes the transfer of glucose from a nucleotide-activated precursor to a lipid carrier molecule. GtrA then translocates the lipid-linked glucose across the cytoplasmic membrane, where GtrX finally mediates the actual glycosyl transfer [18-20]. In *M. tuberculosis*, Rv3789 codes for a putative GtrA-type multidrug resistance-like transporter located directly upstream of *dprE1*. It was demonstrated that the deletion of the homolog of Rv3789 in *Mycobacterium smegmatis*, Msmeg_6372, resulted in a reduction in the arabinose content of both AG (approximately -15%) and LAM (approximately -35%) and simultaneous accumulation of DPA [21], which is compatible with Rv3789 acting as a DPA floppase. However, deletion of Rv3789 in *M. tuberculosis* resulted in no discernable effects, suggesting the existence of proteins with redundant function and/or complementing mechanisms in this organism. In contrast, studies on Rv3789 by a different research group revealed a *M. tuberculosis* gene deletion mutant that exhibited a phenotype resembling that of the *M. smegmatis* Msmeg_6372 gene deletion mutant, characterized by decreased incorporation of arabinan into AG accompanied by accumulation of the precursor DPA [22]. However, it was later suggested that synthesis of DPA might take place in the periplasm via epimerization of DPR, which implies flopping occurs at the level of DPR and not DPA [16], and it was demonstrated that Rv3789 interacts with the priming arabinosyltransferase AtfA [22]. Thus, it was suggested that Rv3789 might not act as a DPA floppase but rather plays an important, albeit not strictly essential, role by recruiting AftA for AG biosynthesis. On the other hand, heterologous expression of the bona-fide *Escherichia coli* undecaprenylphosphate-4-amino-4-deoxy-L-arabinose floppase, ArnE/ArnF, functionally complemented the lack of Rv3789 and restored LAM formation, favoring the predicted function as a floppase [21]. Regardless of whether Rv3789 is a DPA floppase or just indirectly involved in AG biosynthesis by functioning as a membrane anchor for DPA-dependent arabinosyltransferases, dispensability of the encoding gene proves that one or more other yet-unknown floppases must exist in *M. tuberculosis*.

In this study, we used a bioinformatics approach to identify a second protein in *M. tuberculosis* exhibiting homology to the flippase GtrA of *S. flexneri* [18]. Considering the predicted essentiality of *Rv3277*, we investigated its potential role in the cell wall assembly and evaluated its role for the viability of *M. tuberculosis*.

Results

Identification of the essential gene *Rv3277t* with an alternative translational start site

To identify genes encoding potential GtrA-like proteins, we performed a Domain Enhanced Lookup Time Accelerated BLAST (DELTA-BLAST) search of the *M. tuberculosis* H37Rv genome using the prototypic *S. flexneri* GtrA protein sequence (UniProt accession number Q9T1D7). In addition to Rv3789, this identified a second protein, Rv3277, exhibiting low identity (14.39% in a 139 amino acid overlap) (Fig. 2a). Rv3277 is annotated as a probable essential conserved transmembrane protein comprising 272 amino acids. It is a mycobacterial core protein conserved in many different strains [23] and contains four transmembrane helices according to Alphafold prediction [24], similar to prototypic GtrA.

To examine the predicted essential function of Rv3277, we employed a conditional silencing-approach, which enabled us to fine-tune the expression of the corresponding gene *Rv3277* in *M. tuberculosis*. For this, we inserted four *tet* operator sites upstream of the annotated start codon, allowing concentration-dependent binding of a plasmid-borne reverse tet repressor (revTetR) in presence of anhydrotetracycline (ATc). Unexpectedly however, contrasting its predicted essential function based on genome-wide analyses of transposon mutant pools [25, 26], the c-*Rv3277*_tet-OFF mutant did not show any obvious phenotype in presence of ATc to silence gene expression (Suppl. Fig 3a). When comparing Rv3277 to orthologues in other mycobacteria, we noticed that many of the encoded proteins are much shorter, revealing a substantial 49 amino acid N-terminal extension in the annotated Rv3277 protein (Suppl. Fig. 3b). We thus inspected the nucleotide sequence and identified an alternative open reading frame with a GTG translation start site 147 bp downstream of the annotated ATG translation start site, encoding a truncated version of the annotated *Rv3277* gene, which we refer to as *Rv3277t* (Suppl. Fig. 3c). We therefore presumed false annotation of Rv3277 and hypothesized that the gene is expressed recognizing the alternative GTG start codon, resulting in a protein comprising just 223 amino acids. Insertion of the controllable promoter cassette described above upstream of the alternative GTG start codon led to the generation of the conditional *M. tuberculosis* c-*Rv3277t*_tetOFF mutant

(Suppl. Fig. 3d). Silencing of the target gene in this conditional mutant in the presence of ATc demonstrated the expected phenotype with lack of growth both on Middlebrook 7H10 agar and in Middlebrook 7H9 liquid medium, respectively (Fig. 2b + c). Viability dropped dose-dependently when fully induced cells were plated on ATc-containing solid medium, indicating that loss of Rv3277t function is bactericidal (Fig. 2d). The 147-bp region upstream of the GTG start codon likely includes the native promoter, explaining why our initial silencing approach with the controllable promoter cassette inserted upstream of the annotated ATG start codon was unsuccessful since the gene was still expressed from its endogenous promoter. In addition to our gene silencing experiments, next-generation sequence analysis of a saturated Himar1 transposon library in *M. tuberculosis* supported the assumption that the annotated N-terminal extension of Rv3277 is incorrect as the absence of transposon insertions showed gene essentiality only for potential TA dinucleotide insertion downstream of the mentioned GTG codon [26]. The use of GTG as a translation start site is common in *M. tuberculosis* as it is used in approx. 35% of tubercular genes [27].

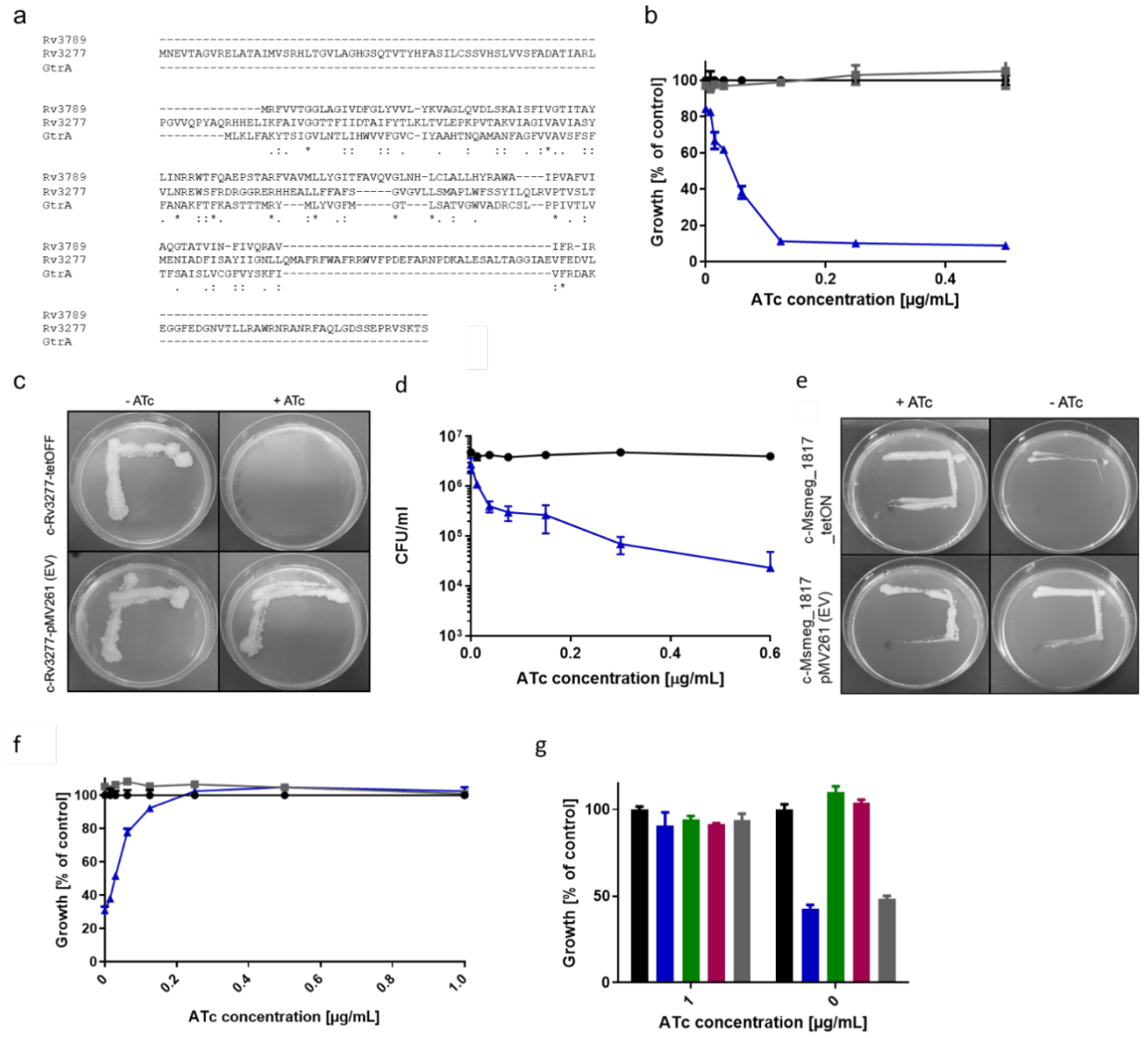

Fig. 2: Demonstration of essentiality of the gene *Rv3277t* in *M. tuberculosis* and its orthologue *MSMEG_1817* in *M. smegmatis*. a, Multiple sequence alignment of *Rv3789* (*M. tuberculosis*), *Rv3277* (*M. tuberculosis*), and *gtrA* (*S. flexneri*) using CLUSTAL by Muscle (3.8). Asterisks show positions that are highly identical, whereas colon and period show positions with lower similar residues. The N-terminus of Rv3277 is not available in the compared proteins. **b – c,** ATc-dependent growth inhibition of the conditional *M. tuberculosis* c-*Rv3277t*_tetOFF mutant (blue), the empty vector control strain (c-*Rv3277t* pMV261, grey) and the *M. tuberculosis* H37Rv wild type (black) in Middlebrook 7H9 liquid medium (**b**) and on Middlebrook 7H10 agar (**c**). Growth in **c** was documented after 14 days of incubation. **d,** Dose-response curves of c-*Rv3277t*_tetOFF (blue) and *M. tuberculosis* wild type H37Rv (black) against increasing concentrations of ATc on 7H10 Middlebrook agar. A fully induced liquid culture was grown to $OD_{600\ nm}$ = 0.3, washed, and serial dilutions were plated on a solid medium containing the indicated ATc concentrations. Colony-forming units were counted after 14 days. A decrease in

viable cell counts indicates a bactericidal effect of loss of Rv3277t functionality. **e - f,** ATc-dependent growth of the conditional *M. smegmatis* c-*Msmeg_1817*_tetON mutant (blue) and of the empty vector control strain (c-*Msmeg_1817* pMV261, grey) on Middlebrook 7H10 agar (**e**) and in Middlebrook 7H9 liquid medium (**f**). Growth in **e** was documented after 3 days of incubation. **g,** Complementation of the conditional *M. smegmatis* c-*Msmeg_1817*_tetON mutant (blue) *via* constitutive expression of a plasmid-borne copy of *Msmeg_1817* (green) or *Rv3277t* (pink). The empty vector control (c-*Msmeg_1817*_tetON pMV361, grey) and the wild type *M. smegmatis* mc^2155 (black) are shown as a reference. Constitutive recombinant expression of both *Msmeg_1817* and *Rv3277t* rescues growth inhibition during silencing of the endogenous *Msmeg_1817* gene in the absence of ATc in Middlebrook 7H9 liquid medium. Data in **b**, **d, f** and **g** are shown as mean values (in = 3) ± SEM.

Rv3277t from *M. tuberculosis* and its orthologue MSMEG_1817 from *M. smegmatis* are functionally homologous proteins

Next, to study the effect of gene silencing in non-tuberculous mycobacteria, we analyzed the orthologue of *Rv3277t* in *M. smegmatis*, which is a fast-growing, non-pathogenic bacterium commonly used as a surrogate to study aspects of biochemistry and physiology of *M. tuberculosis*. The annotated protein MSMEG_1817 exhibits 80% identity on a 223 amino acid overlap to Rv3277t. To fine-tune gene expression in *M. smegmatis*, we generated the c-*Msmeg_1817*_tetON mutant analogous to the c-*Rv3277t*_tetOFF mutant by inserting a promoter cassette comprising four *tet* operator sites upstream of the annotated start codon (Suppl. Fig. 4) and expressing a plasmid-borne tet repressor (TetR) that binds to the operator site in absence of the inducer ATc. The conditional *M. smegmatis* c-*Msmeg_1817*_tetON mutant showed strict ATc-dependent growth, indicating that the studied gene is also essential for *in vitro* growth of *M. smegmatis* (Fig. 2e + f). In order to unambiguously attribute the observed phenotype to the regulation of the target gene and to rule out possible polar effects that might result from integration of a synthetic promotor cassette, the c-*Msmeg_1817*_tetON mutant was genetically complemented. ATc-dependency of growth of the c-*Msmeg_1817*_tetON mutant was rescued by constitutive expression of both *MSMEG_1817* and *Rv3277t* (Fig. 2g). This demonstrated the absence of any polar effects relevant to the observed silencing phenotype and the functional homology between MSMEG_1817 and Rv3277t, allowing inferences to *M. tuberculosis* from studying the protein in *M. smegmatis* [27].

Silencing of *Rv3277t* in *M. tuberculosis* results in altered cell morphology

In order to functionally characterize Rv3277t, we established conditions establishing partial silencing of *Rv3277t* in *M. tuberculosis* H37Rv during growth in liquid culture to allow comparative phenotypic characterization of wild type-like fully induced and of stressed cells (Fig. 3a). Scanning electron microscopy revealed a slightly altered morphology in partially silenced cells with rougher and more irregular surfaces and less rounded, flattened poles (Fig. 3b). Occasionally, one to two blebs were observed emanating from the cell surface in partially silenced cells (Fig 3c), which is somewhat reminiscent to morphological alterations occurring in mycobacterial cells treated with isoniazid [28]. Although the observed alterations in partially silenced cells were rather subtle and no substantial cell lysis was observed, these findings support a potential role for Rv3277t in mycobacterial cell wall biogenesis.

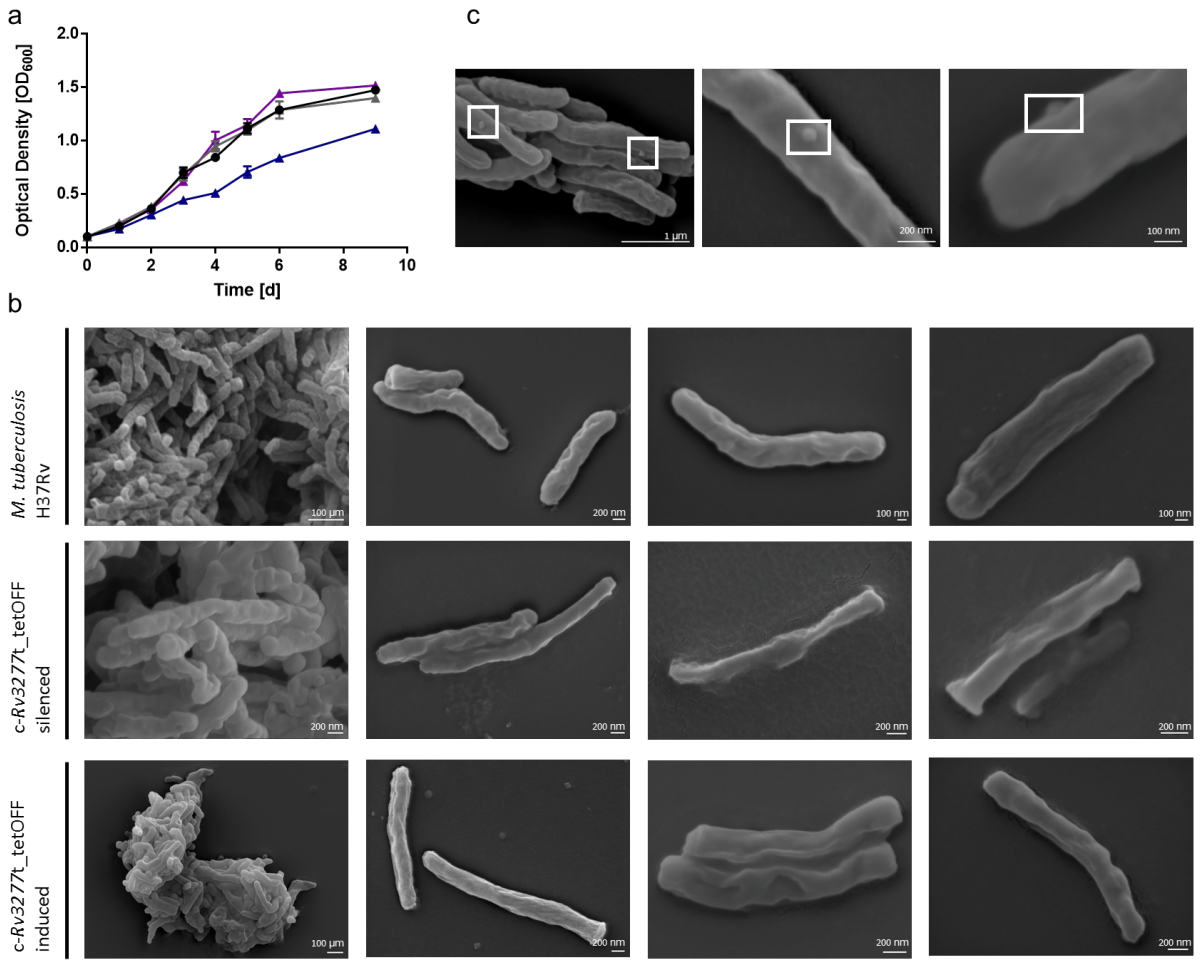

Fig. 3: Partial silencing of *Rv3277t* in *M. tuberculosis* results in altered cellular morphology. **a**, Growth curves in Middlebrook 7H9 medium of partially silenced (blue) and induced (purple) cells of the *M. tuberculosis* c-*Rv3277t*_tetOFF mutant (pink) compared to the empty vector

control strain (c-*Rv3277t* pMV261, grey) and to the *M. tuberculosis* H37Rv wild type (black) strain. For full induction of the target gene, cells of the *M. tuberculosis* c-*Rv3277t*_tetOFF mutant were grown in medium without ATc, whereas 0.3 µg/mL ATc was added for partial silencing. Data represent mean values (n = 3) ± SEM. **b,** Scanning electron microscopy images of partially silenced and induced cells of the *M. tuberculosis* c-*Rv3277t*_tetOFF mutant cultivated in liquid culture compared to wild type. Wild type cells and fully induced cells of the conditional mutant were cultivated for 14 d in medium without ATc, whereas 0.3 µg/mL ATc was added for partial silencing of the conditional mutant. Size of scale bars as indicated. **c,** Scanning electron microscopy images showing occasional blebs forming at the surface of partially silenced cells of the *M. tuberculosis* c-*Rv3277t*_tetOFF mutant**.** Size of scale bars as indicated.

Silencing of *Rv3277t* in *M. tuberculosis* and *MSMEG_1817* in *M. smegmatis* leads to global decrease in mannosylated cell-surface glycoconjugates

Based on the demonstrated impact on mycobacterial cell morphology and its conserved essential function in diverse mycobacteria, we hypothesized that Rv3277t is involved in biosynthesis of one or more core mycobacterial cell wall components that are crucial for viability *in vitro*. Previous studies implicated a role of the related GtrA-like protein Rv3789 in arabinogalactan formation and suggested it might work as a non-essential, redundant floppase involved in translocation of DPA or DPR [16]. Thus, we speculated that Rv3277t could potentially function as a floppase for DPR/DPA or for other decaprenol phosphate-linked carbohydrates as a precursor for glycoconjugate formation. In addition to arabinosylated cell wall polymers, the mycobacterial cell wall is characterized by high abundance of various mannosylated glycoconjugates such as PIM, LM, and LAM, the biosynthesis of which involves mannosyltransferases that require DPM as an activated donor substrate. Since several genes involved in biosynthesis of PIM, LM, and LAM are essential [25, 26], we concluded that the unknown translocase mediating flopping of DPM needs to be likewise crucial for the viability of mycobacteria, and we hypothesized that Rv3277t could have this essential flopping activity.

To study the potential role in mannosylated glycoconjugate biosynthesis, we first analyzed lysates generated from partially silenced cells of the *M. smegmatis* c-*Msmeg_1817*_tetON mutant. Glycoconjugates were separated by SDS-PAGE and probed employing the monoclonal antibodies F30-5, which is specific for the Ara_6 terminal motif of LAM [29, 30], and F183-24, which recognizes alpha-1,2-linked mannosyl residues as present in the mannose cap on higher-order PIMs (Ac_1/Ac_2PIM_6) [30, 31]. Immunoblots employing the anti-LAM and anti-PIM_6

antibodies revealed that cellular levels of both LAM (Fig. 4a, top panel) and PIM_6 (Fig. 4a, bottom panel) were drastically reduced in partially silenced cells of the *M. smegmatis* c-*Msmeg_1817*_tetON mutant compared to fully induced cells, which exhibited wild type levels of these glycoconjugates. Genetic complementation of the c-*Msmeg_1817*_tetON mutant by constitutive expression of either *MSMEG_1817* or *Rv3277t* completely reversed the ATc-dependent silencing effect, unambiguously confirming that the observed phenotype was only attributed to the regulation of the target gene and ruling out relevant polar effects (Fig. 4c). Next, we confirmed the observed phenotypes using complementary methods. Separation by SDS-PAGE of polar lipids extracted from ^{14}C-glucose labeled partially silenced and fully induced cells of the c-*Msmeg*_1817_tetON mutant followed by autoradiographic analysis not only confirmed strongly downregulated levels of LAM in partially silenced cells but also demonstrated a concomitant dramatic decrease of the precursor LM (Fig. 4b). Furthermore, 2D-TLC analysis of the polar lipids fraction extracted from ^{14}C-glucose labeled partially silenced and fully induced cells of the c-*Msmeg*_1817_tetON mutant followed by autoradiographic analysis corroborated the depletion of higher-order PIMs (Ac_1/Ac_2PIM_6), while levels of lower-order PIMs (Ac_1/Ac_2PIM_2) as well as of the precursor phosphatidyl-*myo*-inositol remained unaltered (Fig. 4d).

To corroborate congruent phenotypes in slow-growing mycobacteria, we assessed levels of LAM and PIM_6 in fully induced and partially silenced cells of the *M. tuberculosis* c-*Rv3277t*_tetOFF mutant by immunoblotting. Similar to *M. smegmatis*, we found strongly reduced levels of both mannosylated glycoconjugates in partially silenced cells. (Fig. 4e). To confirm these findings, we performed MALDI-MS analyses of polar lipid fractions isolated from fully induced and partially silenced cells of the *M. tuberculosis* c-*Rv3277t*_tetOFF mutant. In agreement with our observations in *M. smegmatis*, silencing of *Rv3277t* resulted in substantial reduction of mono- and diacylated PIM_6, while levels of lower-order PIM_2 species (PIM_2, Ac_1PIM_2, Ac_2PIM_2) as well as PI remained unaltered (Fig. 4e). Accumulation of the precursors for all higher forms of mannosylated cell wall glycoconjugates, Ac_1PIM_4 and Ac_2PIM_4, was not detectable. However, we observed some accumulation of Ac_1PIM_5 in partially silenced cells, which was not present in fully induced cells (Fig. 4f).

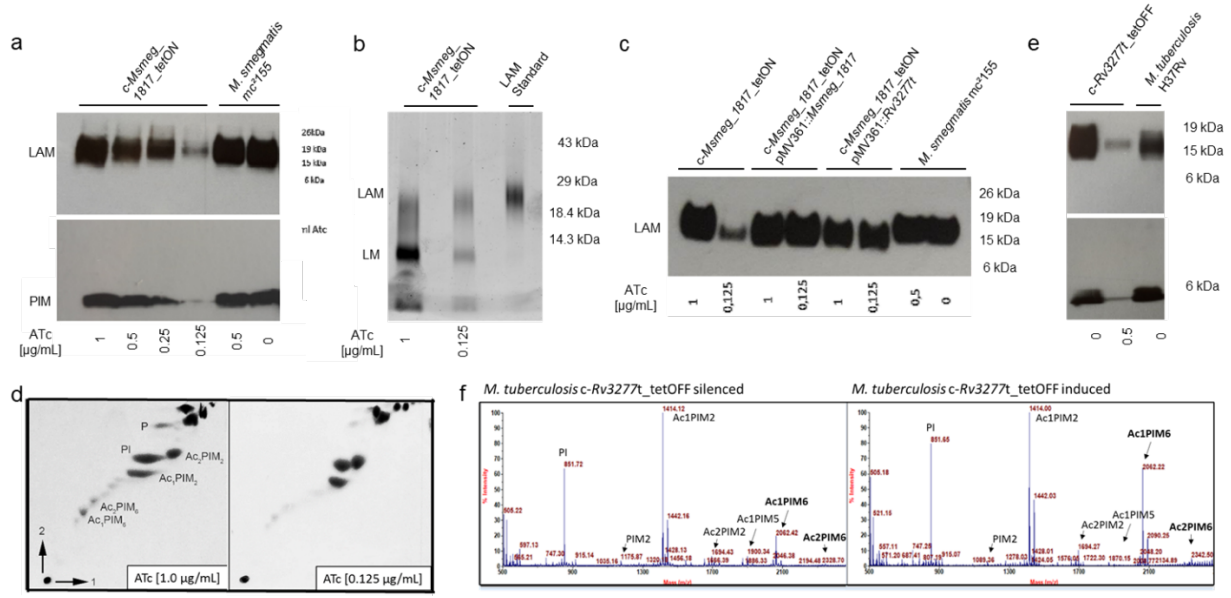

Fig. 4: Silencing of *Rv3277t* in *M. tuberculosis* and of *MSMEG_1817* in *M. smegmatis* blocks biosynthesis of the higher order mannosylated cell wall glycoconjugates PIM_6, LM and LAM. a, SDS-PAGE immunoblot analyses of lysates of fully induced (at 1 µg/mL ATc) and partially silenced (at 0.5, 0.25 and 0.125 µg/mL ATc) cells of the c-*Msmeg_1817*_tetON mutant compared to wild type *M. smegmatis* mc^2155 (left panel), and fully induced (at 0 µg/mL ATc) and partially silenced (at 0.5 µg/mL ATc) cells of the *M. tuberculosis* c-*Rv3277t*_tetOFF mutant compared to wild type *M. tuberculosis* H37Rv (right panel*)*, employing the LAM-specific monoclonal antibody F30-5 (upper panel) and the PIM_6-specific antibody F183-24 (lower panel). Experiments were repeated once with similar results (Suppl. Fig. 5a-c). **b**, SDS-PAGE autoradiographic analysis of the LM/LAM fraction prepared from ^{14}C-glucose labeled fully induced (at 1 µg/mL ATc) and partially silenced (at 0.125 µg/mL ATc) cells of the *M. smegmatis* c-*Msmeg_1817*_tetON mutant. A full, uncut blot photo can be found in Suppl. Fig. 5d. **c,** Genetic complementation of the *M. smegmatis* c-*Msmeg_1817*_tetON mutant by constitutive expression of a plasmid-borne copy of *Msmeg_1817* or *Rv3277t* restores LAM biosynthesis. SDS-PAGE immunoblot analyses of lysates of fully induced (at 1 µg/mL ATc) and partially silenced (at 0.125 µg/mL ATc) cells of the c-*Msmeg_1817*_tetON mutant compared to wild type *M. smegmatis* mc^2155, employing the LAM-specific monoclonal antibody F30-5. **d,** 2D-TLC autoradiographic analysis of polar lipid fractions isolated from ^{14}C-glucose labeled fully induced (at 1 µg/mL ATc) and partially silenced (at 0.125 µg/mL ATc) cells of the *M. smegmatis* c-*Msmeg_1817*_tetON mutant. **e,** SDS-PAGE immunoblot analyses of lysates of fully induced (at 0 µg/mL ATc) and partially silenced (at 0.5 µg/mL ATc) cells of the *M. tuberculosis* c-*Rv3277t*_tetOFF mutant compared to wild type *M. tuberculosis* H37Rv employing the LAM-specific monoclonal antibody

F30-5 (upper panel) and the PIM_6-specific antibody F183-24 (lower panel). **f,** MALDI-ToF MS analysis of lipids extracted from fully induced (at 0 µg/mL ATc) and partially silenced (at 0.5 µg/mL ATc) cells of the *M. tuberculosis* c-*Rv3277t*_tetOFF mutant. The experiment was repeated once with similar results (Suppl. Fig. 5e). P, phospholipids; PI, phosphatidyl-*myo*-inositol; PIM_2, phosphatidylinositol dimannoside; Ac_1PIM_2, monoacylphosphatidylinositol dimannoside; Ac_2PIM_2, diacylphosphatidylinositol dimannoside; Ac_1PIM_6, monoacylphosphatidylinositol hexamannoside; Ac_2PIM_6, diacylphosphatidylinositol hexamannoside.

Impact of MSMEG_1817 on the arabinogalactan composition in *M. smegmatis*

The phenotypes described above resulting from silencing of *Rv3277t* and *Msmeg_1817* in *M. tuberculosis* and *M. smegmatis*, respectively (i.e., global downregulation of all higher forms of mannosylated cell wall glycoconjugates (PIM_6, LM and LAM), which all arise from Ac_1PIM_4 or Ac_2PIM_4,), are compatible with two alternative scenarios. Since all these glycoconjugates are formed via extension of the precursors Ac_1PIM_4 or Ac_2PIM_4 by various mannosyltransferases at the periplasmic site of the cytoplasm membrane using DPM as a substrate, the GtrA-like proteins could either mediate flopping of DPM from the cytoplasmic to the periplasmic face of the membrane or might be somehow required for formation of DPM at the cytoplasmic leaflet. Alternatively, the GtrA-like proteins might rather be required for flopping of the precursors Ac_1PIM_4 / Ac_2PIM_4 from the cytoplasmic to the periplasmic face of the membrane or might be involved in their synthesis from Ac_1PIM_2, / Ac_2PIM_2, at the cytoplasmic leaflet.

To gain hints regarding the specificity of the GtrA-like proteins Rv3277t and MSMEG_1817 in cell wall glycoconjugate formation, the LM/LAM as well as the arabinogalactan fractions were purified from fully induced and partially silenced cells of the *M. smegmatis* c-*Msmeg_1817*_tetON mutant and analyzed for their sugar monomer composition by GC. Consisting with its role in mannosylation, silencing of *MSMEG_1817* led to a gradual increase in the arabinose-to-mannose ratio of LM/LAM (Fig. 5). Surprisingly, however, silencing of *Msmeg_1817* concomitantly also led to a gradual decrease in the arabinose-to-galactose ratio of arabinogalactan (Fig. 5). Collectively, while predominantly controlling mannose incorporation, these findings show that the GtrA-like proteins *Rv3277t* and *MSMEG_1817* also contribute to the incorporation of arabinose into arabinogalactan. The most plausible explanation for the observed phenotypes is the function of Rv3277t and MSMEG_1817 as a floppase that preferentially translocates DPM but to some extent can also translocate DPR or DPA.

	ATc [µg/mL]	Ara : Man ratio of LM/LAM fraction	Ara : Gal ratio of AG fraction
M. smegmatis c-*Msmeg_1817*_tetON	1	2.5 : 1	2.2 : 1
	0.5	3.0 : 1	1.75 : 1
	0.125	3.4 : 1	1.5 : 1

Fig. 5: Impact of MSMEG_1817 on glycoconjugate monomer composition in *M. smegmatis*. Relative composition of LM/LAM and arabinogalactan purified from fully induced and partially silenced cells of the *M. smegmatis* c-*Msmeg_1817*_tetON mutant. Sugar composition was analyzed by GC and ratios were normalized to mannose or galactose content, respectively. Data represent single measurements. Ara, arabinose; Man, mannose; Gal, galactose; LM, lipomannan; LAM, lipoarabinomannan; AG, arabinogalactose.

Characterization of the floppase properties of Rv3277t

To gain insights into the possible flopping activity of Rv3277t, we performed 3D modeling employing the TopModel suite, revealing secondary structures that allow for transmembrane localization [32]. The secondary structure of Rv3277t was modeled based on homology with the template protein dolichyl phosphate mannose synthase (DPMS) of *Pyrococcus furiosus*, which is involved in N-glycosylation of proteins in this archaeon [33]. The cellular location was predicted by the PPM server [34]. Rv3277t is divided into an N-terminal transmembrane domain (TM) consisting of four α-helices and an unfolded C-terminus with periplasmic orientation (Fig. 6a). The TM domain resembles the C-terminal TM domain of the template DPMS in that the four α-helices are arranged as two dimers [33]. It is worth noting that we detected a change from hydrophobic to hydrophilic amino acids (shown as orange sticks) between the two dimeric structures, indicating altered physicochemical properties of the channel-like structure in Rv3277t (Fig. 6b, c). By transferring the co-crystallized detergent lauryl dimethylamine-N-oxide of the DPMS of *P. furiosus* to our model, we demonstrated a potential interaction between the hydrophilic lipid heads and the hydroxyl group of threonine, a hydrophilic amino acid not found in the TM of DPMS (Fig. 6c). In contrast to similar TM domains, the alignment of Rv3277t and the X-ray crystal structure of the DPMS template showed a significant difference between the proteins, as Rv3277t has a shorter N-terminus (Fig. 6d).

To assess whether the identified distinct hydrophilic amino acids in the channel-like structure (T35, K59, N141; Fig. 6c) are critical for the function of Rv3277t, a variant of the

Rv3277t protein, where all three positions were mutated to alanine, was constitutively expressed from an integrative plasmid in the *M. tuberculosis* c-*Rv3277t*_tetOFF mutant. Functionality was then evaluated by the capability to suppress growth inhibition of the *M. tuberculosis* c-*Rv3277t*_tetOFF mutant during ATc-induced silencing of the endogenous *Rv3277t* gene. While ectopic constitutive expression of wild type *Rv3277t* fully suppressed the growth defect during ATc-induced silencing of the endogenous gene, expression of the *Rv3277t*-T35A-K59A-N141A variant resulted in only partial suppression (Fig. 6e), suggesting that hydrophilic amino acids in the channel promote translocation of the probable substrates DPM and DPR/DPA likely by facilitating interaction with the polar head groups.

In order to further characterize the suggested floppase activity of Rv3277t, we sought to test whether heterologous expression of *bona-fide* lipid flippases can phenotypically complement the *M. tuberculosis* c-*Rv3277t*_tetOFF mutant under conditions when *Rv3277t* is silenced. Several studies demonstrated that flippases can exhibit relaxed substrate specificity, so that upon heterologous expression they can restore activity in absence of certain target flippases despite low sequence similarity between these translocases [21, 35-38]. Previously, it was shown that loss of Rv3789 function could be compensated for by heterologous expression of ArnE/F [21], which encode a flippase translocating undecaprenol phosphate-linked 4-amino-4-deoxy-L-arabinose involved in lipid A modification in *E. coli [39]*. Integrative plasmids for constitutive expression of the following genes were generated and electroporated into the *M. tuberculosis* c-*Rv3277t*_tetOFF mutant: the *arnE/F* genes; the *wzxE* gene from *E. coli* encoding an undecaprenol phosphate-linked oligosaccharide translocase involved in O-antigen assembly [40], and *ltaA* from *Staphylococcus aureus*, which represents a member of the major facilitator superfamily (MFS) and is a proton-coupled antiporter flippase for the anchor lipid-linked-disaccharide gentiobiosyl-diacylglycerol [41, 42]. Additionally, the *M. tuberculosis* gene *Rv3789*, encoding a putative GtrA-type multidrug resistance-like transporter, presumably acting as DPA-floppase was used for constitutive expression [21]. Phenotypic functional complementation was evaluated by the capability to suppress growth inhibition of the *M. tuberculosis* c-*Rv3277t*_tetOFF mutant during ATc-induced silencing of *Rv3277t* (Fig. 6f). While constitutive expression of the wild type *Rv3277t* completely suppressed the growth defect of the *M. tuberculosis* c-*Rv3277t*_tetOFF mutant, neither the expression of *Rv3789* nor of the other tested flippases significantly affected the ATc-dependent growth behavior of the mutant cells, resulting in phenotypes comparable to cells containing the empty vector. This strongly suggests that Rv3277c exhibits a narrow substrate specificity that does not overlap with the tested lipid translocases.

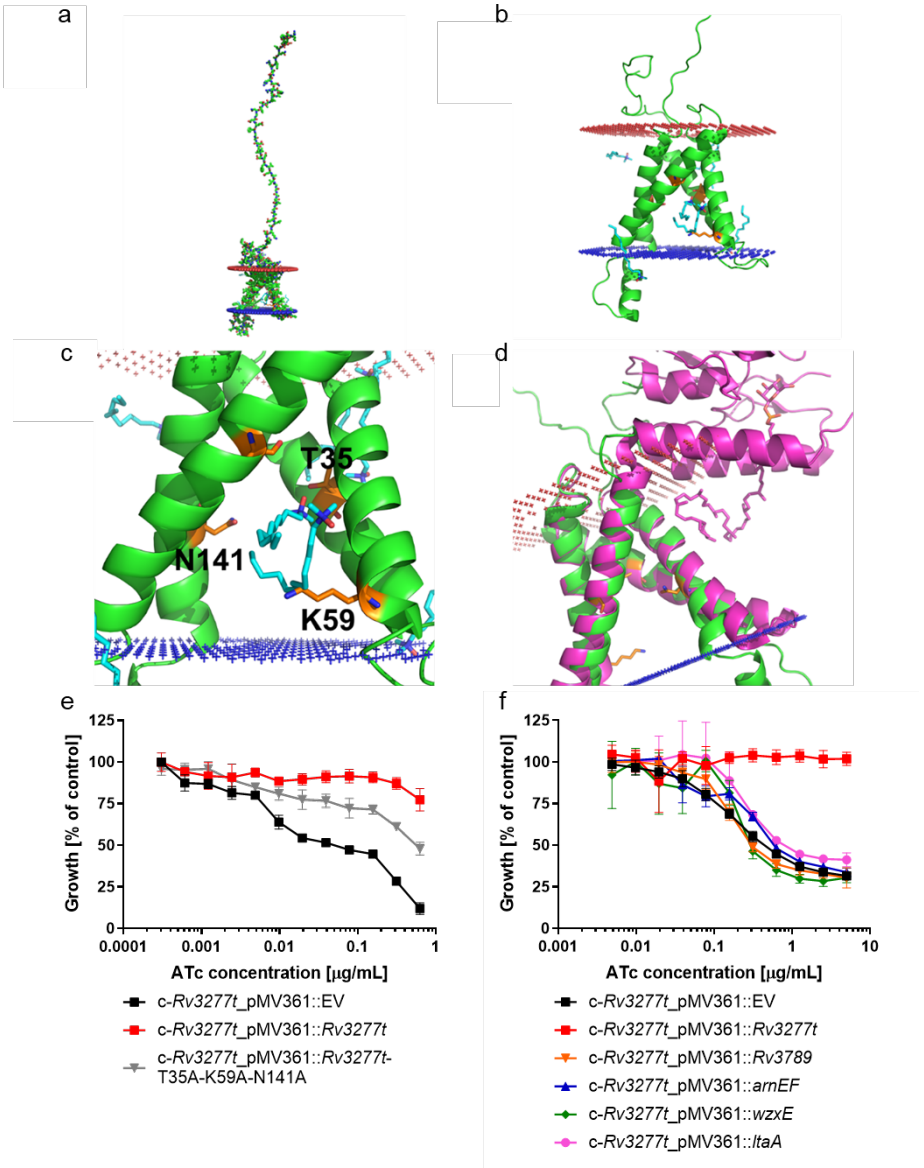

Fig. 6: Homology modeling of Rv3277t exhibits significant similarities to the DPMS of *P. furiosus*. Homology model of Rv3277t (green) made with the TopModel suite [32]. The red and blue dots represent the outer and inner membrane boundaries as predicted by the PPM server, respectively. The orange residues shown as sticks are residues that have undergone a change from hydrophobic to hydrophilic compared to the dolichyl phosphate mannose synthase (DPMS) template (PDB-ID: 5MLZ) **a**, Overview of the Rv3277t homology model. The C-terminus, pointing away from the membrane, is unfolded. **b**, The transmembrane part of the Rv3277t homology model. The co-crystallized detergent lauryl dimethylamine-*N*-oxide of the template DPMS (PDB-ID: 5MLZ) was transferred to the homology model and is shown as blue sticks. **c**, Interactions of the template lipids with the residues changed from hydrophobic to hydrophilic in Rv3277t. Here, the hydroxyl-group of T35 interacts directly with the hydrophilic lipid head. **d**, Alignment of the Rv3277t homology model with the X-ray crystal structure of the template

DPMS (PDB-ID: 5MM1, magenta) with co-crystallized dolichyl phosphate mannose as shown in sticks interacting with the transmembrane region. The synthase part is not present in Rv3277t as it possesses a short N-terminus. **e**, ATc-dependent growth inhibition of the *M. tuberculosis* c-*Rv3277t*_tetOFF mutant complemented with integrative plasmids constitutively expressing either the wild type version (pMV361::*Rv3277t*) or the mutated version of *Rv3277t* (pMV361::*Rv3277t*_T35A_K59A_N141A) compared to the empty vector control (pMV361::EV). Data are shown as mean values (in = 3) ± SEM. **f**, ATc-dependent growth inhibition of the *M. tuberculosis* c-*Rv3277t*_tetOFF mutant complemented with integrative plasmids constitutively expressing the *bona-fide* lipid flippases *wzxE* from *E. coli*, *arnE/F* from *E. coli, ltaA* from *Staphylococcus aureus* and the putative floppase *Rv3789* (from *M. tuberculosis*. Growth dependency was compared to the empty vector control (pMV361::EV) and the *M. tuberculosis* c-*Rv3277t*_tetOFF mutant complemented with the wild type version of *Rv3277t* (pMV361::*Rv3277t*). The average of two independent clones is shown ± SEM, with each measuring point of the two clones determined in triplicates.

Proteome stress response of *M. tuberculosis* during silencing of *Rv3277t*

To understand the importance of Rv3277t for viability of *M. tuberculosis* and to obtain insights into the cellular processes that are affected by silencing of *Rv3277t*, whole protein cell lysates were prepared from fully induced and partially silenced cells of the *M. tuberculosis* c-*Rv3277t*_tetOFF mutant to perform global proteome analysis and comparison of the elicited stress responses. Compared to fully induced conditions, partially silenced cells exhibited a significant change in the abundance of 242 proteins (Fig. 4a). As expected by the role of Rv3277t in cell wall glycoconjugate biosynthesis, gene ontology analysis using Fisher´s exact test revealed that mainly proteins related to lipid metabolism, plasma membrane and cell wall formation were affected in partially silenced cells (Fig. 4b). Within the overall global differential proteome profile, several overlapping, coordinated distinct stress responses could be identified (Supplementary Table 1). Strikingly, we found increased abundance of proteins involved in glycoconjugate mannosylation: the polyprenol-monophosphomannose synthase Ppm1 (Rv2051c) that transfers mannose from GDP-mannose to polyprenol phosphates at the cytosolic face of the membrane to yield the precursor DPM; the mannosyltransferase PimB (Rv2188c) that transfers mannose from GDP-mannose to PIM_1 to yield PIM_2; and the alpha-1-,6-mannopyranosyltransferase MptA (Rv2174) that mediates elongation of mono- and diacylated PIM_4 involved in biosynthesis of the alpha-1-,6-mannan core of LM biosynthesis employing DPM as donor substrate [20,21,36]. This upregulation of enzymes

mediating early steps in mannosylation pathways might represent a directed compensatory stress response to counteract the observed global decrease in mannosylated cell surface glycoconjugates when Rv3277t is silenced. In agreement with adaptations aiming at compensating disturbed cell wall architecture, we also recognized increased protein abundances related to biosynthesis and assembly of other cell wall constituents, such as phthioceroldimycocerosates (PDIM) and related glycolipids (PpsA – PpsD, FadD26, Mas, Pks15, Rv2958c), peptidoglycan (Rv3717, MurG, MurC, RipA) and mycolates (FbpC). Further, upregulation of cardiolipin synthase PgsA2 suggested stimulated phospholipid production. Another distinct response was differential abundance of a large group of proteins belonging to a regulon that is controlled by the copper-sensing transcriptional repressor CsoR and that responds to stress conferred by elevated copper concentrations: CadI (Rv2641), CsoR (Rv0967), CtpV (Rv0969), CysK2 (Rv0848), Rv0430, Rv0500A, Rv0849, Rv0968, Rv2963, RicR (Rv0190) [43]. Downregulation of Rv0500A and strong upregulation of all other mentioned proteins is congruent with cells experiencing copper stress. Additionally, we also found upregulation of proteins that do not belong to the copper stress regulon but are involved in copper homeostasis: MymT (Rv0186A), which is a copper-binding metallothionein, as well as the multicopper oxidase MmcO (Rv0846c) and the outer membrane copper transporter MctB (Rv1698) that are both required for copper resistance [44]. Thus, intriguingly, despite growing bacteria in regular culture medium, cells appear to experience copper stress when Rv3277t is silenced. It is not known whether there is indeed an increased intracellular concentration of copper in silenced cells, and if so, how the impaired cell surface mannosylation is mechanistically connected to this effect. It cannot be ruled out that the copper stress regulon is just misleadingly triggered at normal copper concentration, for example by an aberrant activation of the copper-sensing transcriptional repressor CsoR.

Among the strongest upregulated proteins were 2-methylcitrate synthase PrpC, 2-methylcitrate dehydratase PrpD and the cognate transcriptional regulator PrpR. Accumulation of methylcitrate cycle intermediates has recently been linked to drug tolerance [45]. Therefore, potential stimulation of the methylcitrate cycle by upregulation of PrpC and PrpD might represent an unspecific general stress adaptation.

Regarding processes that are negatively affected by silencing of Rv3277t, we observed lower abundance of several ribosomal proteins (RplQ, RpmC, RpsO, RplU, RpmA, RpmD, RpmF), suggesting global downregulation of protein biosynthesis. Likewise, downregulation of numerous transcriptional regulatory proteins and putative DNA-binding proteins suggests massive perturbation of transcriptional control (CspA, Rv3295, Rv0232, Rv3716c, Rv0081, DosR, CarD, Rv0500A, Rv3788, ArgR, Rv0386, Rv1404). A related coordinated stress response

that could additionally affect the transcriptome is the down-regulation of several antitoxins (VapB29, MazE3, VapB38, VapB33, VapB47) that likely release their corresponding toxins, which putatively exhibit ribonuclease activity. The reduced level of the RNA polymerase-binding transcription factor CarD is particularly noteworthy since this protein is necessary for survival during exposure to several stressors such as oxidative stress, DNA damage, and nutrient limitation [46]. In the same direction, downregulation of several universal stress proteins (Rv1996, Rv2005c, Rv2623, Rv2624c and Rv3134c) and of the chaperone HspX might indicate an impaired ability to adequately respond to various endogenous and exogenous noxes. Therefore, curtailing of different stress adaptation mechanisms may partly explain the lethal effect of Rv3277t silencing. Downregulation of the ribonucleoside-diphosphate reductase subunits NrdF2 and NrdB implies that DNA replication was dampened, while concurrently cell division appeared to be stimulated as presumed by upregulation of FtsK, SepF and FtsQ, which should actually increase the demand of deoxynucleotide triphosphates. Finally, among the strongest downregulated proteins were components of the electron transport chain or factors required for their assembly (NADH-quinone oxidoreductase subunit NuoE, integral membrane cytochrome D ubiquinol oxidase CydA, nitrate reductase-like protein NarX, and cytochrome assembly ABC transporter CydC-CydD), pointing toward impaired aerobic respiration and a curtailed capacity to generate ATP in silenced cells.

a

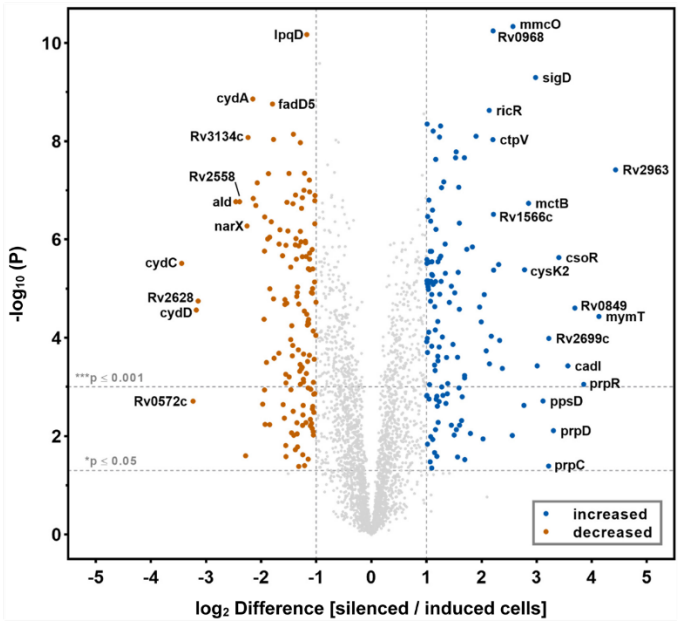

b

Type	Category	Size	Intersec.	Enrichment factor	FDR	p-value
Pathway	Lipid metabolism	61	48	1.668	1.67E-04	2.78E-07
GO	Peptidoglycan-based cell wall [GO:0009274]	354	209	1.251	6.94E-04	5.00E-07
GO	Cytosol [0005829]	343	192	1.186	5.48E-03	1.09E-04
GO	Plasma membrane [0005886]	821	453	1.169	3.17E-05	1.14E-08

c

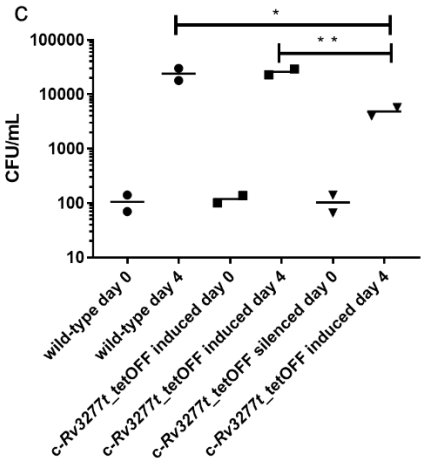

Fig. 7: Silencing *Rv3277t* leads to a drastic change in the proteome composition and impairs intracellular growth in *M. tuberculosis*. a, LC-MS/MS-based whole protein analysis of silenced cells of the *M. tuberculosis* H37Rv c-*Rv3277t*_tetOFF mutant compared to the corresponding fully induced cells. The volcano plot illustrates the $\log_2$-fold change in abundance in silenced vs. induced cells (X-axis) and corresponding -log10 *p* values (Y-axis). Proteins complying with the chosen threshold of significance and showing a $\log_2$-fold change ≥ 1 or ≤ -1 are marked in blue or orange, respectively. For silencing conditions, cells of the *M. tuberculosis* H37Rv c-*Rv3277t*_tetOFF mutant were cultivated in presence of 0.3 µg/mL ATc until they reached the mid-logarithmic phase ($OD_{600\ nm}$ of 0.6 - 0.8). Quantification was done via label free quantification (LFQ) of five replicates per sample group. To identify statistically significant hits from the analysis, P ≤ 0.05 (Student's T-test; permutation-based FDR with 250 randomizations and FDR = 0.01) was applied. See Supplementary Fig. 6 for LC-MS/MS-based control proteomic profiles. **b**, Gene ontology analysis reveals an enrichment of proteins related to plasma membrane and cell envelope formation in silenced cells of the *M. tuberculosis* H37Rv c-*Rv3277t*_tetOFF mutant. Fischer Exact Test was performed with significant protein groups from silenced vs induced cells t-test as input (Benjamini-Hochberg FDR, Threshold value 0.05). **c**, THP-1 derived macrophages were infected with *M. tuberculosis* H37Rv wild type and fully induced (at 0 µg/mL

ATc) cells of the *M. tuberculosis* c-*Rv3277t*_tetOFF mutant at a multiplicity of infection = 3. After washing to remove non-internalized cells, mutant cells were incubated either in the presence of 0.3 µg/mL ATc (silenced) or in absence of ATc (induced). Macrophages were lysed after 4 days of incubation, and lysates were subjected to CFU plating to count viable cells. CFU/mL were calculated after 2 weeks of incubation (n=2). *, $p < 0.05$; **, $p < 0.01$.

Silencing of *Rv3277t* strongly impairs intracellular growth in macrophages

The data so far have demonstrated the essentiality of *Rv3277t* for *in vitro* growth of *M. tuberculosis* in axenic culture. During infection, however, *M. tuberculosis* largely resides and replicates inside macrophages. Thus, we were interested in studying the effect of silencing on intracellular growth capacity in a human macrophage infection model. For this, the *Rv3277t* gene was silenced by addition of ATc after infection of differentiated human THP-1 cells with the *M. tuberculosis* c-*Rv3277t*_tetOFF mutant. Compared to wild type and fully induced cells of the *M. tuberculosis* c-*Rv3277t*_tetOFF mutant, silenced cells showed a significantly reduced intracellular growth (Fig. 7c), demonstrating that Rv3277t is essential in this infection model.

Discussion

For decades, the cell wall has been a useful target for antitubercular therapy. Remarkably, the biosynthetic pathways responsible for the assembly of various cell wall constituents have not been completely deciphered, leaving several potential drug targets undiscovered. In particular, it remained unknown until now how the undecaprenyl phosphate-linked molecules DPM and DPA are translocated from the cytosolic to the periplasmic face of the membrane to serve as activated substrates for membrane-bound mannosyl- and arabinosyltransferases. This study provides evidence for the role of Rv3277t in the translocation of DPM, a crucial step in the biosynthesis of cell wall-associated mannosylated glycoconjugates. Although direct proof of the enzymatic activity of Rv3277t is pending, several lines of evidence strongly support the conclusion that Rv3277t is a DPM floppase and might also contribute to flopping of DPA or DPR. The global impact on cell surface mannosylation affecting glycoconjugates all relying on DPM as the substrate is in agreement with Rv3277t representing a DPM floppase. In contrast, the DPM-independent formation of lower-order PIM species continued normally during silencing of

Rv3277t. The inability of *bona fide* lipid translocases exhibiting relaxed substrate specificity to compensate for the loss of Rv3277t suggests a distinct substrate specificity.

In eukaryotes, a similar bipartite mechanism is known in the context of N-glycosylation of proteins, which occurs in the endoplasmic reticulum (ER) [47]. Here, the dolichylphosphate β-D-mannose synthase (DPMS) utilizes GDP-Man to transfer α-D-mannose to dolichylphosphate, resulting in dolichylphosphate β-D-mannose (Dol-*P*-Man), the eukaryotic pendant to DPM located in the cytoplasm [48]. After translocation of Dol-*P*-Man from the cytosol to the lumen of the ER, the glycosylation of proteins can occur [49]. Interestingly, the state of knowledge is also incomplete in eukaryotes because it is unknown which proteins conduct the translocation. However, it has been shown that *in vitro* DPMS is required for the transfer through membranes [50]. Intriguingly, our molecular modeling revealed a high similarity between Rv3277t and the transmembrane domain of DPMS from *P. furiosus*. Since Rv3277t lacks the cytosolic N-terminal synthase part of the DPMS, we assumed that Rv3277t is not involved in the synthesis of DPM (which is known to be mediated by Ppm1 in *M. tuberculosis*) but rather allows translocation due to the hydrophilic amino acids within the TM domain. This hypothesis is supported by Reichenbach, who suggested that the transmembrane domain of *P. furiosus* DPMS may have a function independent of the N-terminal catalytic domain, since a truncated version lacking the transmembrane domain was reported enzymatically functional [33]. We revealed potential interactions of co-crystallized template lipids with certain hydrophilic amino acids that resemble a “polar pocket” between α-helices in the transmembrane domain of Rv3277t, indicating a binding site for the mannosyl head group [51]. Mutating this polar pocket to a hydrophobic character resulted in strong impairment of Rv3277t function, implying this feature is important in facilitating reorientation of the polar mannosyl head group across the membrane.

Based on findings with other floppases [52-54], inhibition of Rv3277t activity was expected to result in some accumulation of DPM accumulation at the cytosolic face of the membrane. However, none was detectable in partially silenced cells of the *M. tuberculosis* c-*Rv3277t*_tetOFF mutant or the *M. smegmatis* c-*Msmeg_1817*_tetON mutant. We recognized upregulation of the DPM-producing enzyme Ppm1 and of the mannosyltransferases PimB and MptA as part of the stress response in partially silenced cells of the *M. tuberculosis* c-*Rv3277t*_tetOFF mutant, implying potential regulatory feedback mechanisms controlling flux of shared intermediates through the mannosylated glycoconjugate biosynthetic pathways. It can be speculated that DPM sequestration is prevented by hydrolysis to make the lipid anchor undecaprenyl phosphate available for other pathways. Accumulation of Ac_1/Ac_2PIM_4 has been reported in *M. tuberculosis* to result from inactivation of mannosyltransferase PimE [31]. We did

not observe Ac_1/Ac_2PIM_4 accumulation in partially silenced cells of the *M. tuberculosis* c-*Rv3277t*_tetOFF mutant. Instead, we detected some accumulation of Ac_1PIM_5. Ac_1PIM_5 is an intermediate of the extension of Ac_1PIM_4 to Ac_1PIM_6 by the mannopyranosyltransferase PimE (Rv1159) at the periplasmic side of the membrane employing DPM as the donor substrate and does not accumulate in wild type cells due to its rapid further extension [55]. Possibly, when DPM-flopping is blocked by silencing of Rv3277t, there is a build-up of the precursor Ac_1PIM_4, which might be further extended by an unknown mannosyltransferase that uses GDP-mannose as the donor substrate at the cytosolic side of the membrane, resulting in Ac_1PIM_5 as a shunt product.

Our data support a floppase activity of Rv3277t not only with respect to DPM. The specific reduction in the arabinose content of mycobacterial AG in partially silenced conditional mutants provides evidence for an additional role in DPA reorientation. There are conflicting reports concerning the possible function of the GtrA-like protein Rv3789 in AG biosynthesis, either as a translocase mediating flopping of DPA or rather indirectly as a membrane anchor for recruitment of DPA-dependent arabinosyltransferases [22]. Further, it has not been clearly established yet whether precursor translocation occurs at the level of DPA or DPR [16]. The presence of Rv3277t as a floppase contributing to reorientation of DPR or DPA could explain why Rv3789 is important but not strictly required for AG production. However, overall similarity between Rv3789 and Rv3277t is low, and while both proteins harbor a GtrA-typic transmembrane domain comprising four helices, Rv3277t is substantially larger than Rv3789 (223 vs. 121 amino acids) and contains a short N-terminal as well as a larger C-terminal extension. This implies that Rv3277t is not simply redundant to Rv3789 but has additional essential functions.

Consistent with its central role in mannosylated cell wall glycoconjugate biosynthesis, partial silencing of Rv3277t resulted in a compensatory upregulation of Ppm1 that produces the central precursor DPM and of enzymes mediating early steps in PIM and LM synthesis. In addition, upregulation of pathways for the unrelated cell wall components PDIM, mycolates and peptidoglycan potentially also aim at compensating disturbed cell wall architecture. In addition, unexpected pleiotropic effects were observed, including inhibition of protein biosynthesis and massive disturbance of transcriptional control. Some of the responses appear to represent misguided mechanisms that likely potentiate stress to the cells, such as downregulation of different general stress adaptation mechanisms and downregulation of dNTP biosynthesis while concomitantly forcing cell division. One of the most surprising stress responses was induction of the copper responsive regulon and further proteins involved in copper homeostasis. It can be speculated that the impaired cell wall structure might promote uptake of copper from the medium

leading to toxic concentrations. Downregulation of central components of the electron transport chain might promote this process. At least, a curtailed capacity to generate ATP via aerobic respiration likely contributes to an inability to properly cope with the multitude of stressors emerging in silenced cells. The parallel corruption of several elementary cellular processes plausibly explains the bactericidal effect of Rv3277t silencing. In addition to their crucial role for viability of mycobacteria, however, the mannosylated glycoconjugates that are produced in a Rv3277t-dependent manner are also involved in *M. tuberculosis* pathogenicity by interaction with various host cell receptors or by controlling cellular innate immune responses. Thus, the observed intracellular growth defect in infected human macrophages is likely driven both by reduced viability and reduced ability to manipulate the host cell. Further work is necessary to dissect to which extent each aspect contributes to the in vivo phenotype. Regardless, its dual influence on bacterial viability and on pathogen-host interaction suggests that Rv3277t is a particularly interesting target for the development of novel antitubercular chemotherapeutics.

Methods

Bacterial strains and growth conditions

Strains used in this study are listed in Supplementary Table 2. Mycobacterial cultures were grown aerobically at 37 °C shaking in Middlebrook 7H9 broth or statically on Middlebrook 7H10 agar each supplemented with 10% ADS (0.8% NaCl, 5% BSA, 2% dextrose), 0.5% glycerol, 0.05% tyloxapol, and appropriate antibiotics (50 µg/mL hygromycin, 20 µg/mL kanamycin, 10 µg/mL apramycin). *E. coli* was grown in lysogeny broth (LB)-medium or LB agar containing appropriate antibiotics (150 µg/mL hygromycin, 40 µg/mL kanamycin, 100 µg/mL ampicillin 20 µg/mL apramycin).

Generation of conditional mutants

The generation of conditional mycobacterial mutants was conducted employing a modified specialized transduction protocol [56, 57]. The flanking regions of the gene of interest were amplified *via* PCR employing oligonucleotide primers listed in Supplementary Table 3. Subsequently, the flanking regions were treated with *Van91*I and ligated with *Van91*I-digested pcRv1327c-4XtetO vector arms, resulting in integration of a synthetic gene cassette (hyg-Pmyc1-4XtetO) comprising a hygromycin resistance gene and the strong P*myc1* promoter from *M. smegmatis* engineered to contain four *tetO* operator sites immediately upstream of the start codon

of the target gene. This yielded the allelic exchange knock-in plasmids listed in Supplementary Table 4. The resulting knock-in plasmids were linearized with *Pac*I and cloned into the temperature-sensitive TM4-derived phasmid phAE159, yielding the corresponding knock-in phasmids (Supplementary Table 3). Knock-in phages were produced by electroporating the phasmids into *M. smegmatis* at the permissive temperature of 30°C which was propagated in *M. smegmatis*. Targeted gene knock-in in *M. tuberculosis* and *M. smegmatis* was achieved by specialized transduction employing high-titer lysates of the temperature-sensitive mycobacteriophages at the non-permissive temperature of 37°C. Regulated gene expression was established by heterologous expression in the generated knock-in mutants of a plasmid-borne repressor (revTetR or TetR) that binds to the tetO sites either in presence (tetOFF) or absence (tetON) of anhydrotetracyclin (ATc), respectively.

Genetic complementation of conditional mycobacteria mutants

For complementation of the conditional *M. tuberculosis* c-*Rv3277t*_tetOFF mutant and the *M. smegmatis* c-*Msmeg_1817*_tetON mutant, various genes were amplified by PCR using oligonucleotide primers listed in Supplementary Table 3. PCR products were cloned using the restriction enzymes *Pac*I and *Hin*dIII into the single-copy integrative plasmid pMV361(Apra)-PacI, which is a derivative of pMV361(Kan) engineered to contain a unique *Pac*I restriction site and an apramycin resistance gene [57]. The resulting plasmids providing constitutive gene expression from the HSP60 promoter were transformed by electroporation into the conditional mutants and selected on solid medium containing 10 µg/mL apramycin.

Growth determination

To evaluate growth of conditional mutants in liquid medium in dependence of ATc, mycobacteria were grown to $OD_{600\ nm}$ of approx. 0.6 - 0.8 and diluted to 10^6 CFU/mL in Middlebrook 7H9 medium. Subsequently, 50 µL of this suspension was added to each well of a 96-well round-bottom microtiter plate containing a twofold serial dilution of ATc in 50 µl Middlebrook 7H9 medium per well. The microtiter plate was incubated statically at 37 °C for 5 days. Growth was determined via resazurin reduction assay. For this, 10 µl of a 100 µg/mL resazurin solution was added to each well of the microtiter plate and incubated at RT for 24 h. After fixation of cells by adding 100 µL of a 10% formalin solution and incubation at RT for 30 min, the reduction of resazurin was detected by measuring fluorescence (535 nm excitation, 590 nm emission) employing a Tecan Infinite F200 Pro (TECAN, Männedorf, Switzerland). In another experiment, growth in liquid medium was measured in a kinetic manner by growing cultures until reaching

mid-logarithmic phase ($OD_{600\ nm}$ of 0.6 – 0.8), after which they were diluted to an $OD_{600\ nm}$ of 0.01 using Middlebrook 7H9 medium. To induce sub-lethal silencing of the cells of the *M. tuberculosis* c-*Rv3277t*_tetOFF mutant, 0.3 µg/mL ATc was added to the culture media. Subsequently, the $OD_{600\ nm}$ of cultures were recorded daily over several days to obtain growth curves.

For quantification of ATc-dependent growth on solid medium, a culture of mycobacteria was grown to $OD_{600\ nm}$ of approx. 0.6 - 0.8 before 10 µl of serially diluted aliquots of the cell suspension was plated out on Middlebrook 7H10 agar supplemented with increasing concentrations of ATc. Colony forming units were counted after 3 or 14 days for *M. smegmatis* and *M. tuberculosis*, respectively.

Scanning electron microscopy

Liquid cultures of *M. tuberculosis* H37Rv wild type and of the c-*Rv3277t*_tetOFF mutant were grown to an $OD_{600\ nm}$ of 0.5. The conditional c-*Rv3277t*_tetOFF mutant was silenced by addition of 0.3 µg/mL ATc, whereas the induced cells were grown without the addition of ATc. After 14 days of incubation, the cells were centrifuged at 4,000 rpm for 5 minutes and fixed at a final concentration of 2% paraformaldehyde and 2.5% glutaraldehyde for 1 hour. The fixed cells were then washed twice with PBS followed by washing with PBS containing 0.025% tyloxapol. Cells were dehydrated stepwise with a range of ethanol concentrations (50%, 70%, 80%, 90%, 96%, and 100%) for 5 minutes each. Images were captured using a scanning electron microscope ZEISS Supra 55VP.

Preparation of protein lysates

Mycobacteria were grown in 20 mL Middlebrook 7H9 medium supplemented with the indicated concentrations of ATc. After reaching an $OD_{600\ nm}$ of approx. 0.6 - 0.8, the cultures were washed three times with ice-cold PBS and resuspended in 2 mL PBS. Subsequently, the cells were transferred to screw-cap tubes containing silica-zirconium beads and lysed by bead beating at 50 Hz for 3 x 3 min. Next, 200 µl of 10% SDS were added followed by 30 min incubation at 4 °C. Finally, the samples were centrifuged and the supernatant was sterile filtered three times employing 0.2 µm polyethersulfone filters (Sarstedt AG & Co.KG, Nümbrecht, Germany).

Global proteome profiling by LC-MS/MS analysis

Following in-solution digestion (ISD) of protein lysates, peptides were subjected to desalting using homemade C18 StageTips [58]. In brief, the peptide solution was passed through a StageTip

that was pre-conditioned with methanol (MeOH) and equilibrated with 0.5% formic acid (FA). The immobilized peptides were subsequently washed twice with 0.5% (v/v) FA and then eluted from the StageTip using a solution containing 80% (v/v) acetonitrile (ACN) and 0.5% (v/v) FA. The eluted peptides were dried using a vacuum concentrator (Eppendorf) before being resuspended in 10 µl of 0.1% (v/v) FA in preparation for LC-MS/MS analysis.

LC–MS/MS experiments were conducted on an Orbitrap Elite instrument from Fischer Scientific, coupled with an EASY-nLC 1000 liquid chromatography system also from Fischer Scientific, operating in one-column mode [59]. The analytical column was a fused silica capillary with an integrated PicoFrit emitter, packed in-house with Reprosil-Pur 120 C18-AQ 1.9 µm resin from Dr. Maisch. The analytical column was enclosed by a Sonation column oven and connected to a nanospray flex ion source from Thermo. During data acquisition, the column oven temperature was set at 45 °C. The LC was equipped with two mobile phases: solvent A (0.1% formic acid in water) and solvent B (0.1% formic acid in acetonitrile). Both solvents were of UPLC grade from Sigma. Peptides were loaded directly onto the analytical column at a maximum flow rate that did not exceed the set pressure limit of 980 bar, usually around 0.5–0.6 µl/min. Peptides were separated on the analytical column using a 140 min gradient of solvent A and solvent B at a flow rate of 300 nL/min, with a gradient starting at 7% B, followed by 7 to 35% B for 120 min, 35 to 100% B for 10 min, and 100% B for 10 min. The mass spectrometer was operated using Xcalibur software, version 2.2 SP1.48 from Thermo Fischer Scientific in positive ion mode. Precursor ion scanning was performed in the Orbitrap analyzer in the scan range of m/z 300–1,800, with a resolution of 60,000 and the internal lock mass option turned on. The lock mass used was 445.120025 m/z, polysiloxane [60]. Product ion spectra were recorded in a data-dependent fashion in the ion trap in a variable scan range and rapid scan rate. The spray voltage was set at 1.8 kV. Peptides were analyzed using a repeating cycle consisting of a full precursor ion scan followed by 15 product ion scans, where peptides are isolated based on their intensity in the full survey scan for tandem mass spectrum generation that permits peptide sequencing and identification. Collision-induced dissociation energy was set at 35% for MS2 spectra generation. During MS2 data acquisition, dynamic ion exclusion was set to 120 s, with a maximum list of excluded ions consisting of 500 members and a repeat count of one. Ion injection time prediction, preview mode for the orbitrap, monoisotopic precursor selection, and charge state screening were enabled, with only charge states higher than 1 considered for fragmentation.

Immunoblot analysis of glycoconjugates

For the specific detection of the cell wall components, protein lysates were separated by sodium dodecyl sulfate-polyacrylamide gel electrophoresis (SDS-PAGE) and transferred to a PVDF membrane by Western blot transfer according to standard protocols [61, 62]. The membrane was blocked with 10% skim milk for 30 min, washed once with TBS (50 mM Tris, 150 mM NaCl, pH 7.6) containing 0,05% Tween 80 (TBST), and then incubated with the murine monoclonal antibodies F30-5 or 183-24 in 2% skim milk at 4°C overnight as primary antibodies for detection of LAM and PIM_6, respectively [30]. Following washing of the membrane three times with TBST, an anti-mouse antibody conjugated to horseradish peroxidase (HRP) in 2% skim milk was used as secondary antibody. After 1 h incubation at room temperature, the membrane was washed three times with TBST, three times with TBS and once with H_2O. By adding the substrate solution (Lumiglo®Reagent, Cell signaling Technology, Denver, USA), the antibody-linked HRP allowed detection *via* the generation of luminescence. The luminescence was visualized on Amersham Hyperfilm™ MP using the Cawomat 2000 IR developer.

SDS-PAGE analysis of lipoglycans

Lipoglycans were extracted from 10 mL of cultures of fully induced or partially silenced cells of the *M. smegmatis* c-*Msmeg_1817*_tetON mutant grown with 10 µCi/mL of radiolabeled ^{14}C-D-glucose. The bacteria were harvested, dried and resuspended in water. Five consecutive extractions were performed with an equal volume of 50% (v/v) ethanol in water at 85°C for 6 hours. The supernatants were pooled, dried, and subjected to a phenol-H_2O treatment at 65°C. The aqueous phase containing the crude lipoglycans was dialyzed against water, dried, and the incorporation of ^{14}C-glucose was quantified by liquid scintillation. Equal amounts (50,000 cpm) were then loaded onto a 15% SDS-PAGE gel and separated electrophoretically. The visualization was performed autoradiographically by 48 h exposure of X-ray films.

Two-dimensional thin-layer chromatography

Cells of the *M. smegmatis* c-*Msmeg_1817*_tetON mutant were grown to an $OD_{600\ nm}$ of 0.8, and radiolabeled with 10 µCi/mL of ^{14}C-D-glucose during incubation for 4 hours at 37°C. For extraction of polar lipids, 10 mL of culture was harvested, washed twice with PBS and then extracted with 2 mL CH_3OH : 0.3% NaCl [63] (100:10, v/v) and 2 mL petroleum ether for 30 min. After centrifugation, the pellet was resuspended in 2.3 mL $CHCl_3$: CH_3OH : 0.3% NaCl [63] (90:100:30, v/v/v), stirred for one hour and centrifuged again. The pellet was mixed with 750 µl $CHCl_3$: CH_3OH : 0.3% NaCl [63] (50:100:40, v/v/v) for 30 min, centrifuged, and the supernatant

was combined with the previous fraction. After repeating the last step, the combined supernatants were mixed with 1.3 mL of $CHCl_3$ and 1.3 mL of 0.3% NaCl [63], centrifuged, and the lower organic phase was isolated and dried. The dried extract of polar lipids was then resuspended in $CHCl_3$: CH_3OH (2:1, v/v), and the incorporation of ^{14}C-glucose was quantified by liquid scintillation using a 5% aliquot of the lipid extract in 5 mL EcoScint A (National Diagnostics). Equal amounts of the polar lipid extracts (50,000 cpm) were applied to Silica Gel 60 F254 (Merck) aluminum-backed TLC plates and run in the solvent system E for polar lipids: $CHCl_3$: CH_3OH : H_2O (60:30:6, v/v/v) in the first dimension and $CHCl_3$: CH_3CO_2H : CH_3OH : H_2O (40:25:3:6, v/v/v/v) in the second dimension. The visualization was performed autoradiographically by 48 h exposure of X-ray films.

MALDI-ToF mass spectroscopy

Cells of the conditional *M. tuberculosis* c-*Rv3277t*_tetOFF mutant were grown in 100 mL 7H9 medium in duplicates. Cultures were grown first under fully induced conditions to ca. late log phase to obtain biomass before splitting and continue culturing for further 4 days either with or without addition of 1 µg/mL ATc to silence gene expression. Next, the $OD_{600\,nm}$ was measured to allow normalization of the amount of lipid extract used for subsequent analyses. The cells were then harvested and washed twice with water, resuspended in 1 mL water and heat-inactivated in glass tubes by boiling for 30 min.

MALDI-ToF analyses were performed on an AB Sciex TOF/TOF 5800 mass spectrometer using the reflectron mode, as described elsewhere [64, 65]. Briefly, ionisation was accomplished through irradiation using an Nd:YAG laser (349 nm) operating with a pulse rate of 400 Hz. The laser intensity was set at 3500 with continuous stage motion utilised at a velocity of 600 µm/s. The matrix used was 2,5-dihydroxybenzoic acid (Sigma) at a concentration of 10 mg/mL in chloroform/methanol 9:1 or 1:1.

Extraction of AG and lipoglycan fractions and monomeric compositional analysis *via* GC/MS

Cells of the *M. smegmatis* c-*Msmeg_1817*_tetON mutant were grown at the indicated ATc concentrations, harvested, and frozen at -20°C. The thawed cells were then resuspended in PBS containing 2% Triton X-100 (pH 7.2), sonicated, and pelleted at 27,000 *g*. The cell wall was extracted three times with PBS containing 2% SDS at 95°C for one hour, then washed with water, 80% (v/v) acetone in water, and finally with acetone before lyophilization. Cells were hydrolyzed with 2 M trifluoroacetate, reduced with NaB_2H_4, and the alditols resulting from this treatment

were per-*O*-acetylated. The per-*O*-acetylation was performed after mixing the lipoglycans with 0.5 mL DMSO containing 4.8 M dimethylsulfinyl carbanion. The mixture was stirred three times for one hour, mixed with 50 µL of iodomethane and stirred again for one hour. The mixture was diluted with one volume of water, dialyzed against water, and analyzed by GC/MS for alditol acetate sugar composition.

Molecular modeling

The protein sequence of Rv3277t was modeled using TopModel [32] and TopScore [66]. Using default program parameters, the comparative modeling includes template identification, sequence alignment, modeling, refinement, and scoring. This resulted in a homology model with a good TopScore of 0.307, where the unstructured C-terminus has a low confidence and the transmembrane region a high confidence.

Subsequently the orientation in the membrane and the membrane boundaries were predicted using the PPM server [34]. This resulted in a predicted membrane thickness of 29.4 ± 1.3 Å with a transfer free energy ΔG = -45.2 kcal mol^{-1} and a tilt angle of 2° ± 1°.

Macrophage infection assay

THP-1 cells were cultured in RPMI medium supplemented with 10% FBS in a humidified atmosphere with 5% CO_2 at 37 °C. Cell counting was performed using a haemocytometer, and 10^5 cells were added into each well of a 96-well flat-bottom polystyrene microtiter plate (Greiner) in a total volume of 100 µL. To differentiate THP-1 into adherent cells with macrophage-like characteristics, the medium was supplemented with 50 nM phorbol-12-myristate-13-acetate (PMA). Following overnight differentiation, the THP-1 derived macrophages were washed twice with PBS. For infection, cells of the conditional *M. tuberculosis* c-*Rv3277t*_tetOFF mutant grown under fully induced conditions were harvested, washed, and resuspended in RPMI supplemented with 10% FBS to a density of $3x10^6$ CFU/mL. 100 µL of this cell suspension was added to each well containing the differentiated THP-1 cells, resulting in a multiplicity of infection = 3. After 3 hours, the cells were washed twice with PBS to remove non-phagocytized bacteria, and 100 µL RPMI containing 10% FBS was added. To silence target gene expression, the medium contained 0.3 µg/mL ATc. The THP-1 derived macrophages were incubated at 37 °C, 5% CO_2, and 85% humidity for 4 days. After incubation, cells were fixed with formalin (final concentration of 5%) and lyzed with deionized H_2O for 30 minutes. Dilutions of the suspensions from each well were plated onto Middlebrook 7H10 plates. Colonies were counted after 3 weeks of incubation at 37 °C.

References

1. World Health, O., *Global tuberculosis report 2022. .* licence: cc bY-Nc-sa 3.0 iGo, 2022.
2. Batt, S.M., D.E. Minnikin, and G.S. Besra, *The thick waxy coat of mycobacteria, a protective layer against antibiotics and the host's immune system.* Biochem J, 2020. **477**(10): p. 1983-2006.
3. Torrelles, J.B., A.K. Azad, and L.S. Schlesinger, *Fine Discrimination in the Recognition of Individual Species of Phosphatidyl- myo -Inositol Mannosides from Mycobacterium tuberculosis by C-Type Lectin Pattern Recognition Receptors.* The Journal of Immunology, 2006. **177**(3): p. 1805-1816.
4. Kang, P.B., et al., *The human macrophage mannose receptor directs Mycobacterium tuberculosis lipoarabinomannan-mediated phagosome biogenesis.* Journal of Experimental Medicine, 2005. **202**(7): p. 987-999.
5. Schlesinger, L.S., *Macrophage phagocytosis of virulent but not attenuated strains of Mycobacterium tuberculosis is mediated by mannose receptors in addition to complement receptors.* Journal of immunology (Baltimore, Md. : 1950), 1993. **150**(7): p. 2920-30.
6. Villeneuve, C., et al., *Mycobacteria use their surface-exposed glycolipids to infect human macrophages through a receptor-dependent process.* Journal of Lipid Research, 2005. **46**(3): p. 475-483.
7. Tallieux, L., et al., *DC-SIGN is the major Mycobacterium tuberculosis receptor on human dendritic cells.* Journal of Experimental Medicine, 2003. **197**(1): p. 121-127.
8. Armstrong, J.A. and D.a. Hart, *Response of cultured macrophages to Mycobacterium Tuberculosis, with observations on fusion of lysosomes with phagosomes.* Journal of Experimental Medicine, 1971. **134**(3): p. 713-740.
9. Zhang, Y., et al., *Mode of action of pyrazinamide: Disruption of Mycobacterium tuberculosis membrane transport and energetics by pyrazinoic acid.* Journal of Antimicrobial Chemotherapy, 2003. **52**(5): p. 790-795.
10. Mikusová, K., et al., *Biogenesis of the mycobacterial cell wall and the site of action of ethambutol.* Antimicrob Agents Chemother, 1995. **39**(11): p. 2484-9.
11. Savková, K., et al., *An ABC transporter Wzm-Wzt catalyzes translocation of lipid-linked galactan across the plasma membrane in mycobacteria.* Proc Natl Acad Sci U S A, 2021. **118**(17).

12. Wolucka, B.A., et al., *Recognition of the lipid intermediate for arabinogalactan/arabinomannan biosynthesis and its relation to the mode of action of ethambutol on mycobacteria.* J Biol Chem, 1994. **269**(37): p. 23328-35.
13. Jankute, M., et al., *Assembly of the Mycobacterial Cell Wall.* Annu Rev Microbiol, 2015. **69**: p. 405-23.
14. Mishra, A.K., et al., *Lipoarabinomannan and related glycoconjugates: structure, biogenesis and role in Mycobacterium tuberculosis physiology and host–pathogen interaction.* FEMS Microbiology Reviews, 2011. **35**(6): p. 1126-1157.
15. Mishra, A.K., et al., *Lipoarabinomannan and related glycoconjugates: Structure, biogenesis and role in Mycobacterium tuberculosis physiology and host-pathogen interaction.* FEMS Microbiology Reviews, 2011. **35**(6): p. 1126-1157.
16. Brecik, M., et al., *DprE1 Is a Vulnerable Tuberculosis Drug Target Due to Its Cell Wall Localization.* ACS Chemical Biology, 2015. **10**(7): p. 1631-1636.
17. Higgins, C.F. and M.M. Gottesman, *Is the multidrug transporter a flippase?* Trends Biochem Sci, 1992. **17**(1): p. 18-21.
18. Guan, S. and N.K. Verma, *Functional analysis of the O antigen glucosylation gene cluster of Shigella flexneri.* Microbiology, 1999. **145**(5).
19. Allison, G.E. and N.K. Verma, *Serotype-converting bacteriophages and O-antigen modification in Shigella flexneri.* Trends Microbiol, 2000. **8**(1): p. 17-23.
20. Korres, H., et al., *Topological analysis of GtrA and GtrB proteins encoded by the serotype-converting cassette of Shigella flexneri.* Biochem Biophys Res Commun, 2005. **328**(4): p. 1252-60.
21. Larrouy-Maumus, G., et al., *A small multidrug resistance-like transporter involved in the arabinosylation of arabinogalactan and lipoarabinomannan in mycobacteria.* Journal of Biological Chemistry, 2012. **287**(47): p. 39933-39941.
22. Kolly, G.S., et al., *GtrA protein Rv3789 is required for arabinosylation of arabinogalactan in Mycobacterium tuberculosis.* Journal of Bacteriology, 2015. **197**(23): p. 3686-3697.
23. Marmiesse, M., et al., *Macro-array and bioinformatic analyses reveal mycobacterial 'core' genes, variation in the ESAT-6 gene family and new phylogenetic markers for the Mycobacterium tuberculosis complex.* Microbiology (Reading), 2004. **150**(Pt 2): p. 483-496.
24. Jumper, J., et al., *Highly accurate protein structure prediction with AlphaFold.* Nature, 2021. **596**(7873): p. 583-589.

25. Griffin, J.E., et al., *High-resolution phenotypic profiling defines genes essential for mycobacterial growth and cholesterol catabolism.* PLoS Pathog, 2011. **7**(9): p. e1002251.
26. Dejesus, M.A., et al., *Comprehensive essentiality analysis of the Mycobacterium tuberculosis genome via saturating transposon mutagenesis.* mBio, 2017. **8**(1): p. 1-17.
27. Cole, S.T., et al., *Deciphering the biology of Mycobacterium tuberculosis from the complete genome sequence.* Nature, 1998. **393**(6685): p. 537-544.
28. Vilchèze, C., et al., *Inactivation of the inhA-encoded fatty acid synthase II (FASII) enoyl-acyl carrier protein reductase induces accumulation of the FASI end products and cell lysis of Mycobacterium smegmatis.* J Bacteriol, 2000. **182**(14): p. 4059-67.
29. Appelmelk, B.J., et al., *The mannose cap of mycobacterial lipoarabinomannan does not dominate the Mycobacterium-host interaction.* Cell Microbiol, 2008. **10**(4): p. 930-44.
30. Kolk, A.H.J., et al., *Production and characterization of monoclonal antibodies to Mycobacterium tuberculosis, M. bovis (BCG) and M. leprae.* Clinical and Experimental Immunology, 1984. **58**(3): p. 511-521.
31. Driessen, N.N., et al., *Role of phosphatidylinositol mannosides in the interaction between mycobacteria and DC-SIGN.* Infect Immun, 2009. **77**(10): p. 4538-47.
32. Mulnaes, D., et al., *TopModel: Template-Based Protein Structure Prediction at Low Sequence Identity Using Top-Down Consensus and Deep Neural Networks.* Journal of Chemical Theory and Computation, 2020. **16**(3): p. 1953-1967.
33. Gandini, R., et al., *Structural basis for dolichylphosphate mannose biosynthesis.* Nat Commun, 2017. **8**(1): p. 120.
34. Lomize, M.A., et al., *OPM database and PPM web server: Resources for positioning of proteins in membranes.* Nucleic Acids Research, 2012. **40**(D1): p. 370-376.
35. Feldman, M.F., et al., *The activity of a putative polyisoprenol-linked sugar translocase (Wzx) involved in Escherichia coli O antigen assembly is independent of the chemical structure of the O repeat.* J Biol Chem, 1999. **274**(49): p. 35129-38.
36. Marolda, C.L., J. Vicarioli, and M.A. Valvano, *Wzx proteins involved in biosynthesis of O antigen function in association with the first sugar of the O-specific lipopolysaccharide subunit.* Microbiology (Reading), 2004. **150**(Pt 12): p. 4095-105.
37. Alaimo, C., et al., *Two distinct but interchangeable mechanisms for flipping of lipid-linked oligosaccharides.* Embo j, 2006. **25**(5): p. 967-76.
38. Chin, C.Y., et al., *Francisella FlmX broadly affects lipopolysaccharide modification and virulence.* Cell Rep, 2021. **35**(11): p. 109247.

39. Yan, A., Z. Guan, and C.R. Raetz, *An undecaprenyl phosphate-aminoarabinose flippase required for polymyxin resistance in Escherichia coli.* J Biol Chem, 2007. **282**(49): p. 36077-89.

40. Hong, Y., M.A. Liu, and P.R. Reeves, *Progress in Our Understanding of Wzx Flippase for Translocation of Bacterial Membrane Lipid-Linked Oligosaccharide.* J Bacteriol, 2018. **200**(1).

41. Lambert, E., et al., *Evidence for a trap-and-flip mechanism in a proton-dependent lipid transporter.* Nat Commun, 2022. **13**(1): p. 1022.

42. Zhang, B., et al., *Structure of a proton-dependent lipid transporter involved in lipoteichoic acids biosynthesis.* Nat Struct Mol Biol, 2020. **27**(6): p. 561-569.

43. Ward, S.K., E.A. Hoye, and A.M. Talaat, *The global responses of Mycobacterium tuberculosis to physiological levels of copper.* J Bacteriol, 2008. **190**(8): p. 2939-46.

44. Rowland, J.L. and M. Niederweis, *A multicopper oxidase is required for copper resistance in Mycobacterium tuberculosis.* J Bacteriol, 2013. **195**(16): p. 3724-33.

45. Quinonez, C.G., et al., *The Role of Fatty Acid Metabolism in Drug Tolerance of Mycobacterium tuberculosis.* mBio, 2022. **13**(1): p. e0355921.

46. Stallings, C.L., et al., *CarD is an essential regulator of rRNA transcription required for Mycobacterium tuberculosis persistence.* Cell, 2009. **138**(1): p. 146-59.

47. Snider, M.D., *Topography Of Glycosylation In The Rouch Endoplasmatic Reticulum And Golgy Apparatus.* 1987.

48. Orlean, P., C. Albright, and P.W. Robbins, *Cloning and sequencing of the yeast gene for dolichol phosphate mannose synthase, an essential protein.* The Journal of biological chemistry, 1988. **263**(33): p. 17499-17507.

49. Sanyal, S. and A.K. Menon, *Stereoselective transbilayer translocation of mannosyl phosphoryl dolichol by an endoplasmic reticulum flippase.* Proceedings of the National Academy of Sciences of the United States of America, 2010. **107**(25): p. 11289-11294.

50. Haselbeck, A. and W. Tanner, *Dolichyl phosphate-mediated mannosyl transfer through liposomal membranes.* Proceedings of the National Academy of Sciences of the United States of America, 1982. **79**(5): p. 1520-1524.

51. Reichenbach, T., *Structural and biochemical insights into biosynthesis and degradation of N -glycans Structural and biochemical insights into biosynthesis and degradation of N -glycans*. 2020.

52. Zhou, Z., et al., *Function of Escherichia coli MsbA, an essential ABC family transporter, in lipid A and phospholipid biosynthesis.* J Biol Chem, 1998. **273**(20): p. 12466-75.

53. Margolles, A., et al., *The Purified and Functionally Reconstituted Multidrug Transporter LmrA of Lactococcus lactis Mediates the Transbilayer Movement of Specific Fluorescent Phospholipids.* Biochemistry, 1999. **38**(49): p. 16298-16306.

54. Sanyal, S. and A.K. Menon, *Flipping lipids: why an' what's the reason for?* ACS Chem Biol, 2009. **4**(11): p. 895-909.

55. Morita, Y.S., et al., *PimE is a polyprenol-phosphate-mannose-dependent mannosyltransferase that transfers the fifth mannose of phosphatidylinositol mannoside in mycobacteria.* Journal of Biological Chemistry, 2006. **281**(35): p. 25143-25155.

56. Jain, P., et al., *Specialized transduction designed for precise high-throughput unmarked deletions in Mycobacterium tuberculosis.* mBio, 2014. **5**(3): p. e01245-14.

57. Korte, J., et al., *Trehalose-6-Phosphate-Mediated Toxicity Determines Essentiality of OtsB2 in Mycobacterium tuberculosis In Vitro and in Mice.* PLoS pathogens, 2016. **12**(12): p. e1006043-e1006043.

58. Rappsilber, J., M. Mann, and Y. Ishihama, *Protocol for micro-purification, enrichment, pre-fractionation and storage of peptides for proteomics using StageTips.* Nature Protocols, 2007. **2**(8): p. 1896-1906.

59. Michalski, A., et al., *Ultra high resolution linear ion trap orbitrap mass spectrometer (orbitrap elite) facilitates top down LC MS/MS and versatile peptide fragmentation modes.* Molecular and Cellular Proteomics, 2012. **11**(3): p. 1-11.

60. Olsen, J.V., et al., *Parts per million mass accuracy on an orbitrap mass spectrometer via lock mass injection into a C-trap.* Molecular and Cellular Proteomics, 2005. **4**(12): p. 2010-2021.

61. Laemmli, U.K., *Cleavage of Structural Proteins during the Assembly of the Head of Bacteriophage T4.* Nature, 1970. **227**: p. 680-685.

62. Mahmood, T. and P.C. Yang, *Western blot: technique, theory, and trouble shooting.* N Am J Med Sci, 2012. **4**(9): p. 429-34.

63. Trias, J. and R. Benz, *Permeability of the cell wall of Mycobacterium smegmatis.* Molecular Microbiology, 1994. **14**(2): p. 283-290.

64. Gilleron, M., V.F. Quesniaux, and G. Puzo, *Acylation state of the phosphatidylinositol hexamannosides from Mycobacterium bovis bacillus Calmette Guerin and mycobacterium tuberculosis H37Rv and its implication in Toll-like receptor response.* J Biol Chem, 2003. **278**(32): p. 29880-9.

65. Mosquera-Restrepo, S.F., et al., *A Mycobacterium tuberculosis fingerprint in human breath allows tuberculosis detection.* Nat Commun, 2022. **13**(1): p. 7751.

66. Mulnaes, D. and H. Gohlke, *TopScore: Using Deep Neural Networks and Large Diverse Data Sets for Accurate Protein Model Quality Assessment.* J Chem Theory Comput, 2018. **14**(11): p. 6117-6126.

Acknowledgement

Financial support for this study was provided to R.K. by the Jürgen Manchot Stiftung (graduate schools MOI III and IV) and the German Research Foundation (Deutsche Forschungsgemeinschaft, DFG) by project number 270650915 / GRK 2158 and by award number KA 2259/2-1.

Author contribution

Conceptualization, funding acquisition, and supervision, R.K; microbiological investigation, K.V., S.S., L.v.G., M.H., K.L., V.K.; lipid analyses, S.S.G., M.G.; molecular modelling, C.G.; proteome analysis, D.P., data analysis, H.G., J.N., G.B., M.K.; providing reagents, B.J.A.; writing – original draft, K.V., S.S:, R.K..

Ethics declarations

Competing interests

All authors declare no competing interests.

4.2 Supporting information

GtrA-like lipid floppase Rv3277 is essential for cell surface mannosylation in *Mycobacterium tuberculosis*

Kristin Vill[,*], Steffen Schindler[1,*], Lasse van Geelen[1], David Podlesainski[2], Sudagar S. Gurcha[3], Milena Hänisch[1], Kathrin Lindner[1], Martine Gilleron[4], Christoph Gertzen[5], Violetta Krisilia[1], Ben J. Appelmelk[6], Holger Gohlke[5], Jérôme Nigou[4], Gurdyal S. Besra[3], Markus Kaiser[2], and Rainer Kalscheuer[1,§]

[1] Heinrich Heine University Düsseldorf, Faculty of Mathematics and Natural Sciences, Institute of Pharmaceutical Biology and Biotechnology, 40225 Düsseldorf, Germany

[2] Department of Chemical Biology, ZMB, Faculty of Biology, University of Duisburg-Essen, 45177 Essen, Germany

[3] School of Biosciences, University of Birmingham, Edgbaston, Birmingham, B15 2TT, United Kingdom

[4] Institute of Pharmacology and Structural Biology (IPBS), University of Toulouse, CNRS, University of Toulouse III-Paul Sabatier, Toulouse, France

[5] Institute of Pharmaceutical and Medicinal Chemistry, Heinrich Heine University Düsseldorf, 40225 Düsseldorf, Germany

[6] Molecular Microbiology/Medical Microbiology and Infection Control, Amsterdam University Medical Centers, Amsterdam, Netherlands.

* These authors contributed equally

§ Author for correspondence: rainer.kalscheuer@hhu.de

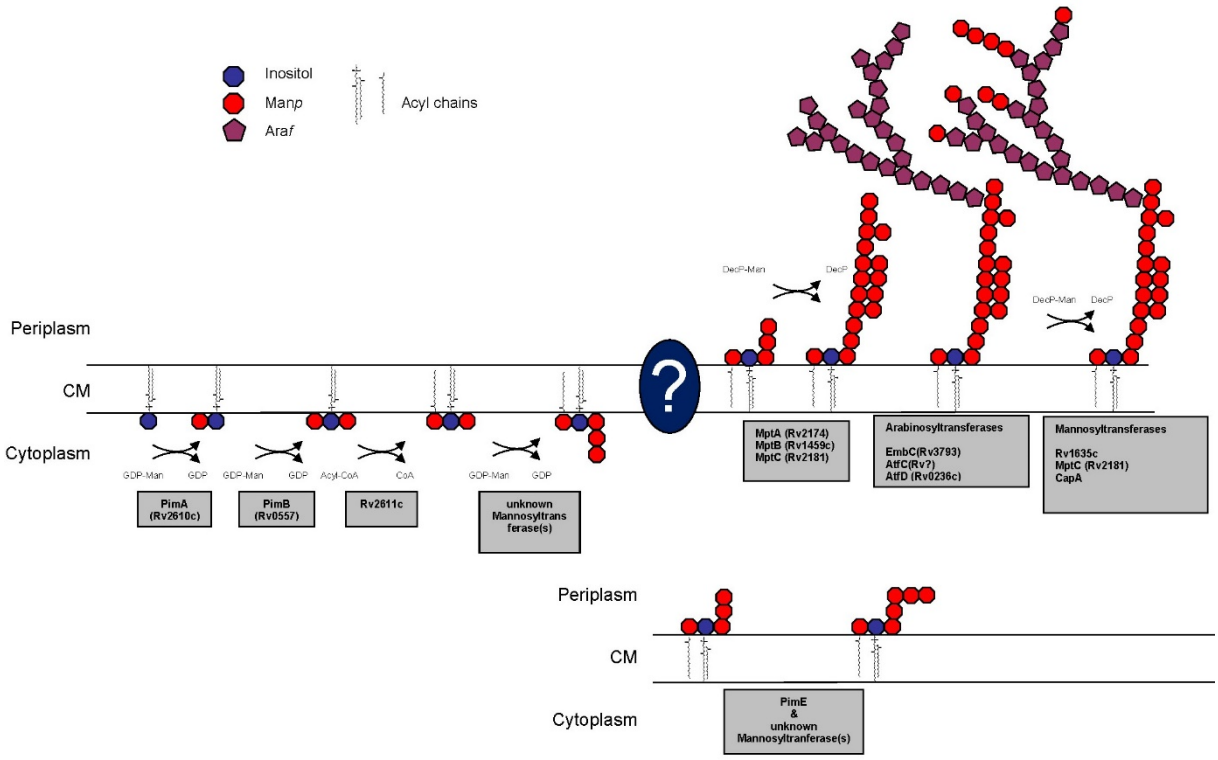

Supplementary Fig. 1: Scheme of the bipartite biosynthesis of phosphatidyl inositol-based mannosylated cell surface glycoconjugates in *M. tuberculosis*. The α-mannopyranosyltransferases PimA (Rv2610c), PimB′ (Rv2188c) and PimC or a yet-unidentified mannosyltransferase mediate the stepwise mannosylation of the *myo*-inositol moiety of the phospholipid phosphatidyl-*myo*-inositol, employing GDP-mannopyranose as the donor substrate, yielding phosphatidylinositol tetramannoside (PIM_4). Following mono- and diacylation by the acyltransferase Rv2611c and a yet-unknown enzyme, the resulting Ac_1/Ac_2PIM_4 is flopped by an unknown mechanism from the cytoplasmic to the periplasmic side of the plasma membrane. Ac_1/Ac_2PIM_4 serves as a branch point, which can either be extended by the mannopyranosyltransferase PimE (Rv1159) to form higher-order PIMs (Ac_1/Ac_2PIM_6), or by the mannopyranosyltransferase MptA (Rv2174), MptB (Rv1459c) and MptC (Rv2181) to synthesize LM. The involved mannopyranosyltransferases represent GT-C type glycosyltransferases that utilize decaprenyl-monophosphoryl-D-mannopyranose (DPM) as the donor substrate. A yet-unidentified arabinofuranosyltransferase first primes the mannan core of LM with a few arabinofuranose residues, after which EmbC (Rv3793) extends the primed LM with the addition of 12–16 arabinofuranose residues. Subsequently, the branching enzyme AftC and the arabinofuranosyltransferase AftB complete the nonreducing arabinan domain of LAM. EmbC, AftC and AftB all employ DPA as the donor substrate to result in addition of altogether 55–70 arabinofuranose residues to LM. Finally, the arabinan domain of LAM is modified with mannose

residues by the DPM-dependent mannopyranosyltransferases CapA (Rv1635c) and MptC (Rv2181), resulting in ManLAM.

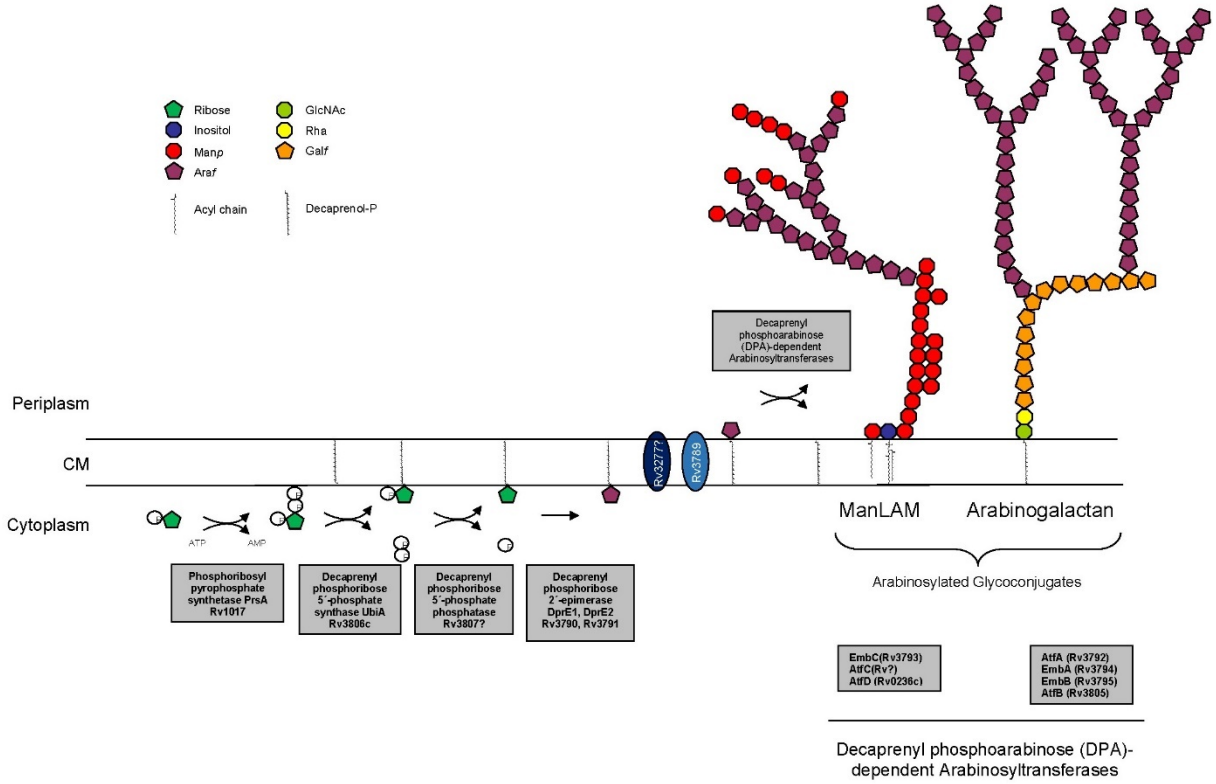

Supplementary Fig. 2: Scheme of the bipartite biosynthesis of decaprenyl monophosporyl-D-arabinofuranose (DPA). Phosphoribosyl pyrophosphate is produced by phosphorylation of ribose-1-phosphate catalyzed by phosphoribosyl-1-pyrophosphate synthetase PrsA (Rv1017). Next, decaprenylphosphoryl-5-phosphoribose synthase UbiA (Rv3806c) transfers phosphoribosyl pyrophosphate to C50-P, yielding decaprenyl-monophosphoryl-D-ribofuranosephosphate, which is subsequently dephosphorylated by Rv3807 to produce decaprenyl-monophosphoryl-D-ribofuranose (DPR). Decaprenylphosphoribose 2′ epimerase composed of DprE1 (Rv3790) and DprE2 (Rv3791) subunits then catalyzes the epimerization of the ribosyl unit of DPR, resulting in DPA. DPA is then translocated from the cytosolic to the periplasmic face of the membrane by the GtrA-like floppase Rv3789 and/or other yet-unknown lipid floppases potentially including Rv3277t. At the periplasmic face of the membrane, DPA serves as the substrate for various arabinofuranosyltransferases involved in arabinosylation of lipomannan or the galactan core C50-P-P-GlcNAc-Rha-Galf_{30}, resulting in formation of lipoarabinomannan (LAM) and arabinogalactan, respectively. LAM is subsequently subject to terminal mannosylation steps, yielding mannose-capped LAM (ManLAM).

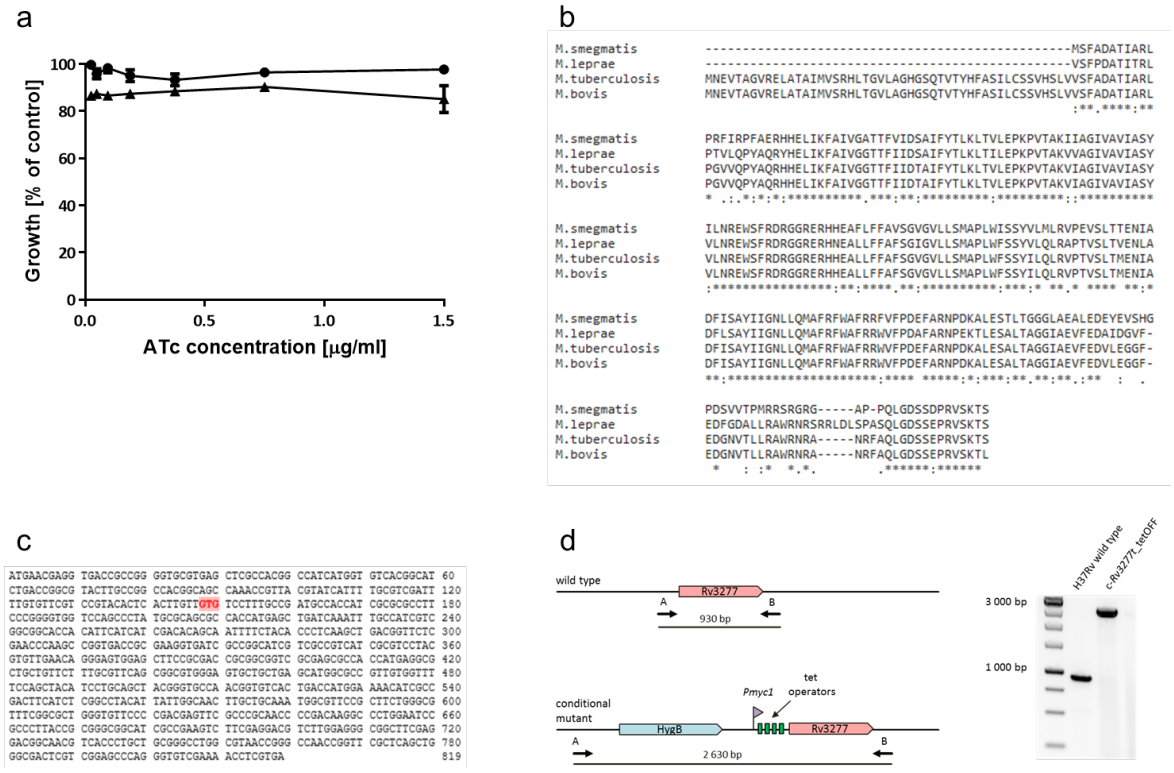

Supplementary Fig. 3: Reannotation of the essential gene *Rv3277* with an alternative starting codon. a, ATc-dependent growth of the conditional *M. tuberculosis* c-*Rv3277*_tetOFF mutant (triangle) and of the *M. tuberculosis* H37Rv wild type strain (circle) indicating no essentiality of the annotated full-length *Rv3277* gene. **b,** Multiple sequence alignment of the *M. tuberculosis* Rv3277 orthologues in *M. smegmatis*, *M. leprae*, and *M. bovis* using CLUSTAL by Muscle (3.8). Asterisks show positions that are highly identical, whereas colon and period show positions with lower similar residues. **c,** Sequence of *Rv3277* as annotated in Mycobrowser. The 5' ATG codon is annotated as the start codon, although the highlighted GTG codon 147 bp downstream was experimentally shown to be the probable start site for translation. **d,** Generation of the *M. tuberculosis Rv3277t* conditional mutant. Organization of the *Rv3277* locus in *M. tuberculosis* H37Rv wild type and the c-*Rv3277t*_tetOFF conditional mutant with the four *tet* operator sites upstream of the annotated start codon (left panel). The relevant primers A and B are indicated. The sizes of the relevant diagnostic PCR products for verification are shown. Diagnostic PCR to verify the generation of the conditional c-*Rv3277t*_tetOFF mutant (right panel). The observed PCR products contained 930 bp for the *M. tuberculosis* H37Rv wild type strain and 2630 bp for the *M. tuberculosis* c-*Rv3277*t_tetOFF mutant strain. Diagnostic PCRs were carried out on genomic DNA of the respective strains.

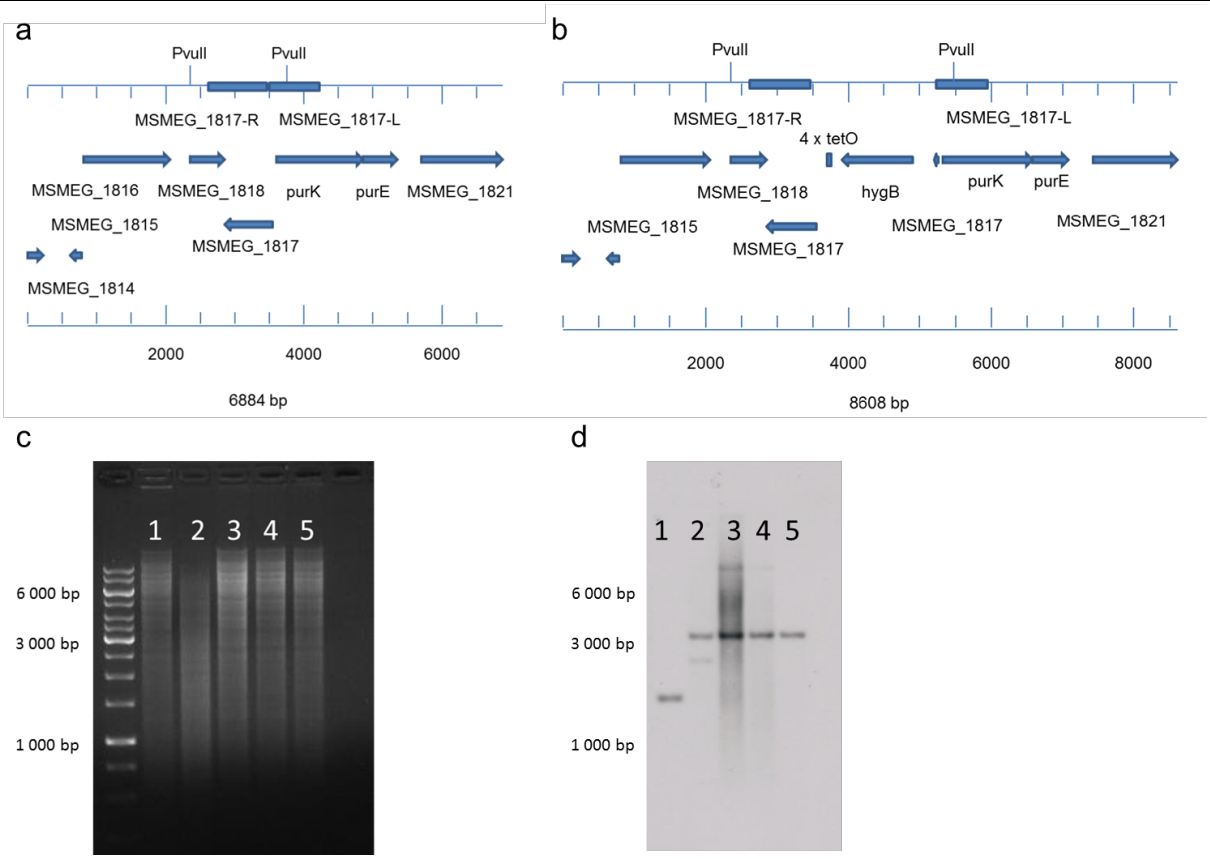

Supplementary Fig. 4: Generation of the c-*Msmeg_1817*_tetON mutant analogous to the c-*Rv3277t*_tetOFF mutant. a + b, *MSMEG_1817* loci with the restriction sites for the Southern blot. Both Sequences were cut with *Pvu*II. The restriction sites are indicated in each map (*Pvu*II). The sequences were hybridized with *MSMEG_1817* -R as probe. *MSMEG_1817* -R and *MSMEG_1817* -L are indicating the flanking arms. **a,** The wild type *MSMEG_1817* locus is shown as a structure with an expected signal of 1321 bp. **b,** The locus of the knock-in mutant *MSMEG_1817* with the additional hygromycin resistance (*hygB*) and the promoter including four operator sites is shown with an expected signal at 3045 bp. **c,** Gel electrophoresis of RNase treated and *Pvu*II digested DNA of *M. smegmatis* mc^2155 (1), and 4 putative mutants (2-5). **d,** Verification of mutants by Southern blot. RNase treated and *Pvu*II digested DNA of *M. smegmatis* mc^2155 (1), and 4 putative mutants (2-5) were electrophoretically separated, transferred to a nylon membrane, and finally hybridized with a probe. Binding was visualized by chemiluminescence using luminol.

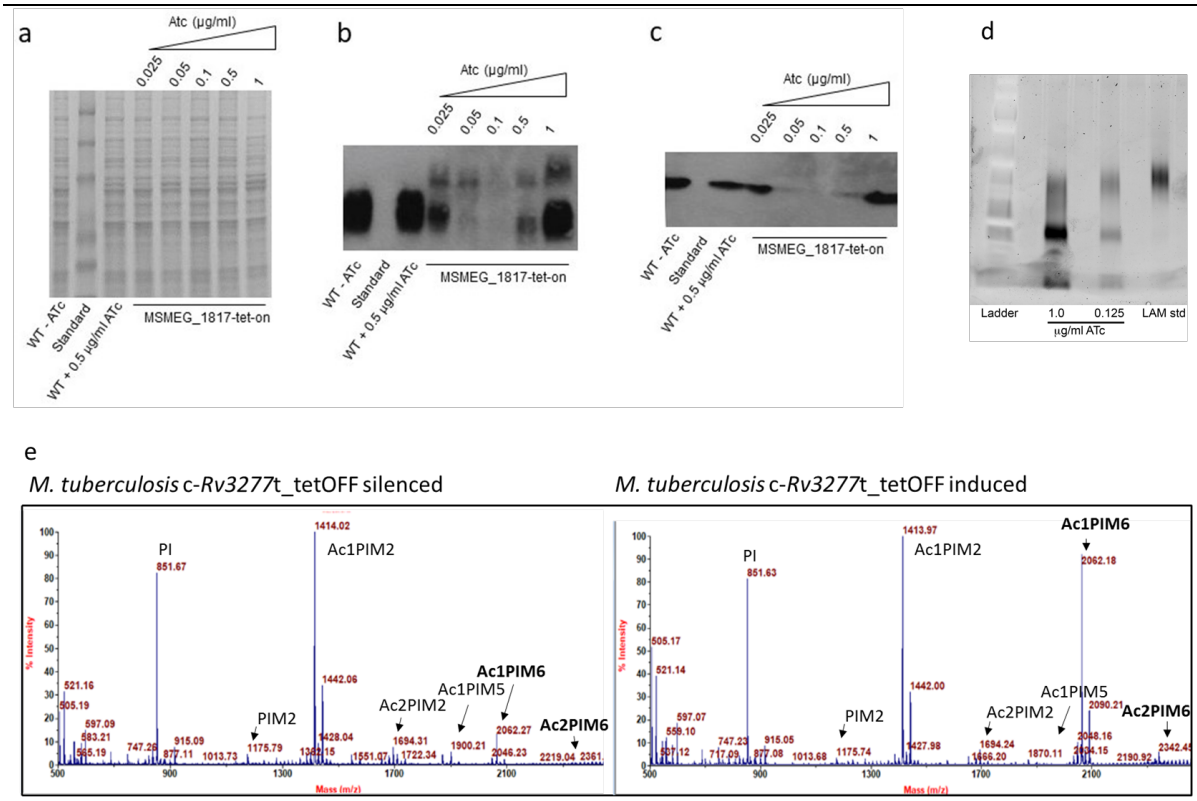

Supplementary Fig. 5: Silencing of *MSMEG_1817* blocks biosynthesis of the higher order mannosylated glycoconjugates LM, LAM and PIM. a, Coomassie-stained SDS-PAGE showing loading controls. **b - c,** SDS-PAGE immunoblots employing the LAM-specific monoclonal antibody F30-5 (b) and the PIM6-specific monoclonal antibody F183-24 (c). The rebounding levels of LAM and PIM6 at the lowest ATc concentration of 0.025 µg/ml probably results from the enrichment of non-regulated suppressor mutants that constitutively express *MSMEG_1817*, explainable by the strong selective pressure that occurs when silencing this essential gene. **d,** SDS-PAGE autoradiographic analysis of the LM/LAM fraction prepared from ^{14}C-glucose labeled fully induced (at 1 µg/ml ATc) and partially silenced (at 0.125 µg/ml ATc) cells of the *M. smegmatis* c-*Msmeg_1817*_tetON mutant. e) MALDI-ToF MS analysis of lipids extracted from fully induced (at 0 µg/ml ATc) and partially silenced (at 0.5 µg/ml ATc) cells of the *M. tuberculosis* c-*Rv3277t*_tetOFF mutant. PI, phosphatidylinositol; PIM_2, phosphatidylinositol dimannoside; Ac_1PIM_2, monoacylphosphatidylinositol dimannoside; Ac_2PIM_2, diacylphosphatidylinositol dimannoside; Ac_1PIM_6, monoacylphosphatidylinositol hexamannoside; Ac_2PIM_6, diacylphosphatidylinositol hexamannoside.

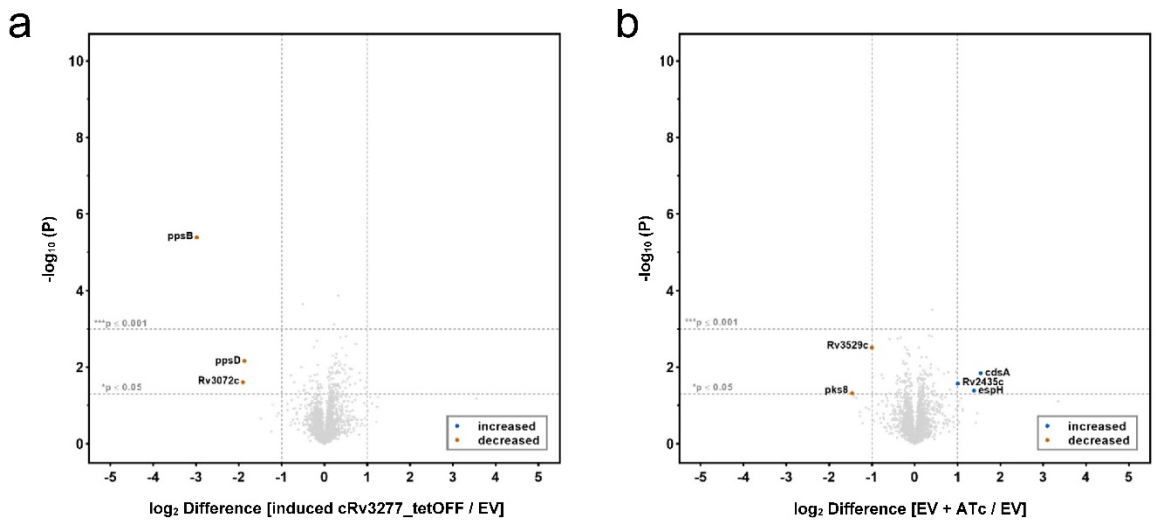

Supplementary Fig. 6: Comparative control LC-MS/MS-based proteomic profilings, related to Fig. 7. **a**, LC-MS/MS-based whole protein analysis of fully induced cells of the *M. tuberculosis* H37Rv c-*Rv3277t*_tetOFF mutant compared to isogenic cells carrying an empty vector control (EV), illustrating largely unchanged protein abundances. **b**, LC-MS/MS-based whole protein analysis of cells of the *M. tuberculosis* H37Rv c-*Rv3277t* knock-in mutant carrying an empty vector control (EV) incubated in presence or absence of ATc, demonstrating minimal effect of ATc on protein abundances. The volcano plots illustrate the $\log_2$- fold change in abundance (X-axis) and corresponding -log10 *p* values (Y-axis). Proteins complying with the chosen threshold of significance and showing a $\log_2$-fold change ≥ 1 or ≤ -1 are marked in blue or orange, respectively. Quantification was done via label free quantification (LFQ) of five replicates per sample group. To identify statistically significant hits from the analysis, $P \leq 0.05$ (Student's T-test; permutation-based FDR with 250 randomizations and FDR = 0.01) was applied.

Supplementary Table 1: Identified response clusters in the proteomic stress profile of silenced vs. induced cells of the *M. tuberculosis* H37Rv c-*Rv3277t*_tetOFF mutant. Chosen threshold: log2 Difference ≤ -1 and ≥ 1; P ≤ 0.05.

Pathway	-Log$_{10}$ (P-value)	Log$_2$ Difference	Gene names	Protein names
Copper stress response	6.396	4.529	Rv2963	Putative permease Rv2963
	6.854	4.105	cysK2 (Rv0848)	O-phospho-L-serine-dependent S-sulfocysteine synthase
	4.600	3.123	csoR (Rv0967)	Copper-sensing transcriptional repressor CsoR
	3.069	2.997	Rv0849	Uncharacterized MFS-type transporter Rv0849
	6.474	2.924	mctB (Rv1698)	Copper transporter MctB
	9.024	2.665	mmcO (Rv0846c)	Multicopper oxidase MmcO
	1.405	2.280	mymT (Rv0186A)	Copper-binding metallothionein
	7.754	2.245	Rv0968	Uncharacterized protein Rv0968
	8.739	2.236	ricR (Rv0190)	Copper-sensing transcriptional repressor RicR
	9.344	2.226	ctpV (Rv0969)	Probable copper-exporting P-type ATPase V
	3.089	2.180	cadI (Rv2641)	Cadmium-induced protein CadI
	1.937	1.723	Rv0430	Uncharacterized protein
	6.608	-1.788	Rv0500A	Putative DNA-binding protein Rv0500A
Electron transport chain	6.203	-1.295	nuoE (Rv3149)	NADH-quinone oxidoreductase subunit E
	8.873	-2.036	cydA (Rv1623c)	Probable integral membrane cytochrome D ubiquinol oxidase (Subunit I)
	6.374	-2.241	narX (Rv1736c)	Nitrate reductase-like protein NarX
	5.751	-2.514	cydC (Rv1620c)	Probable 'component linked with the assembly of cytochrome' transport transmembrane ATP-binding protein ABC transporter CydC
	5.906	-2.684	cydD (Rv1621c)	Probable 'component linked with the assembly of cytochrome' transport transmembrane ATP-binding protein ABC transporter CydD
Cell devision	5.167	1.577	ftsK (Rv2748c)	DNA translocase FtsK
	2.864	1.329	sepF (Rv2147c)	Cell division protein SepF
	6.014	1.166	ftsQ (Rv2151c)	Cell division protein FtsQ
Cell wall	6.268	2.430	pgsA2 (Rv1822)	Putative cardiolipin synthase
	3.264	2.160	ppsB (Rv2932)	Phenolphthiocerol/phthiocerol polyketide synthase subunit B
	3.127	2.156	ppsD (Rv2934)	Phenolphthiocerol/phthiocerol polyketide synthase subunit D
	2.637	2.048	ppsC (Rv2933)	Phenolphthiocerol/phthiocerol polyketide synthase subunit C
	5.663	1.812	Rv3717	N-acetylmuramoyl-L-alanine amidase
	5.261	1.630	fadD26 (Rv2930)	Long-chain-fatty-acid--AMP ligase FadD26

Supplementary Table 1 (continued)

Pathway	-Log10 (P-value)	Log2 Difference	Gene names	Protein names
Cell wall	7.592	1.576	murG (Rv2153c)	Undecaprenyl-PP-MurNAc-pentapeptide-UDPGlcNAc GlcNAc transferase
	5.297	1.416	ppsA (Rv2931)	Phenolphthiocerol/phthiocerol polyketide synthase subunit A
	1.539	1.288	ripA (Rv1477)	Peptidoglycan endopeptidase RipA
	3.161	1.282	pks15 (Rv2947c)	Putative inactive phenolphthiocerol synthesis polyketide synthase type I Pks15
	5.465	1.180	fbpC (Rv0129c)	Diacylglycerol acyltransferase/mycolyltransferase Ag85C (Fibronectin-binding protein C)
	5.525	1.146	murC (Rv2152c)	UDP-N-acetylmuramate--L-alanine ligase
	5.031	1.084	mas (Rv2940c)	Probable multifunctional mycocerosic acid synthase Mas
	5.566	1.047	mmpL10 (Rv1183)	Acyltrehalose exporter MmpL10
Ribosomal proteins	3,637	-1,000	rplQ (Rv3456c)	50S ribosomal protein L17
	4,125	-1,076	rpmC (Rv0709)	50S ribosomal protein L29
	4,276	-1,077	rpsO (Rv2785c)	30S ribosomal protein S15
	4,644	-1,240	rplU (Rv2442c)	50S ribosomal protein L21
	2,801	-1,365	rpmA (Rv2441c)	50S ribosomal protein L27
	3,210	-1,432	rpmD (Rv0722)	50S ribosomal protein L30
	1,534	-1,490	rpmF (Rv0979A)	50S ribosomal protein L32
Stress proteins	6,962	-1,177	Rv2624c	Universal stress protein Rv2624c
	6,039	-1,199	Rv2623	Universal stress protein Rv2623
	3,942	-1,343	Rv2005c	Universal stress protein Rv2005c
	5,242	-1,416	Rv1996	Universal stress protein Rv1996
	6,031	-1,622	hspX (Rv2031c)	Alpha-crystallin (Acr) (16 kDa antigen)
	7,934	-2,141	Rv3134c	Universal stress protein Rv3134c
Antitoxins	1,983	-1,083	vapB29 (Rv0616A)	Putative antitoxin VapB29
	5,637	-1,351	mazE3 (Rv1103c)	Antitoxin MazE3
	7,263	-1,551	vapB38 (Rv2493)	Putative antitoxin VapB38
	1,345	-1,572	vapB33 (Rv1241)	Antitoxin VapB33

Supplementary Table 1 (continued)

Pathway	$-Log_{10}$ (P-value)	Log_2 Difference	Gene names	Protein names
Transcription factors / DNA binding proteins	2,748	-1,050	cspA (Rv3648c)	Probable cold shock protein A
	6,257	-1,054	Rv1404	Probable transcriptional regulatory protein
	5,851	-1,126	Rv3295	Probable transcriptional regulatory protein (Probably TetR-family)
	3,007	-1,148	Rv0232	Probable transcriptional regulatory protein (Probably TetR/AcrR-family)
	4,906	-1,163	Rv3716c	Nucleoid-associated protein Rv3716c
	5,072	-1,262	Rv0081	Uncharacterized HTH-type transcriptional regulator Rv0081
	7,298	-1,427	dosR (Rv3133c)	DNA-binding transcriptional activator DevR/DosR
	6,525	-1,496	carD (Rv3583c)	RNA polymerase-binding transcription factor CarD
	4,449	-1,545	argR (Rv1657)	Arginine repressor
	7,259	-1,628	Rv0386	Probable transcriptional regulatory protein (Probably LuxR/UhpA-family)
	6,608	-1,788	Rv0500A	Putative DNA-binding protein Rv0500A
	6,272	-1,800	Rv3788	Uncharacterized protein Rv3788
dNDP synthesis	4,791	-1,151	nrdF2 (Rv3048c)	Ribonucleoside-diphosphate reductase subunit beta NrdF2
	2,307	-1,326	nrdB (Rv0233)	Ribonucleotide reductase R2-like ligand binding oxidase

Supplementary Table 2: Strains used in this study.

Strain	Relevant properties	Origin
Mycobacterium tuberculosis H37Rv wild type	Wild type	
M. tuberculosis c-*Rv3277*_tetOFF	*Rv3277* silenced, annotated start codon ATG, kan^R, hyg^R	This study
M. tuberculosis c-*Rv3277t*_tetOFF	*Rv3277t* silenced, reannotated start codon GTG, 147 bp downstream, kan^R, hyg^R	This study
M. tuberculosis c-*Rv3277t*_tetOFF pMV361::EV	*Rv3277t* silenced, complemented with an empty vector	This study
M. tuberculosis c-*Rv3277t*_tetOFF pMV361::*Rv3277t*	*Rv3277t* silenced, complemented with a wild type copy of *Rv3277t* constitutively expressed from a single-copy integrative plasmid	This study
M. tuberculosis c-*Rv3277t*_tetOFF pMV361::*Rv3277t* T35A_K59A_N141A	*Rv3277t* silenced, complemented with a mutated copy of *Rv3277t*, harboring the mutations T35A, K59A, and N141A constitutively expressed from a single-copy integrative plasmid	This study

Supplementary Table 2 (continued)

Strain	Relevant properties	Origin
M. tuberculosis c-*Rv3277t*_tetOFF pMV361::*Rv3789*	*Rv3277t* silenced, complemented with a wild type copy of *Rv3789,* constitutively expressed from a single-copy integrative plasmid	This study
M. tuberculosis c-*Rv3277t*_tetOFF pMV361::*arnEF*	*Rv3277t* silenced, complemented with a wild type copy of *arnEF*, isolated from *E. coli,* constitutively expressed from a single-copy integrative plasmid	This study
M. tuberculosis c-*Rv3277t*_tetOFF pMV361::*wzxE*	*Rv3277t* silenced, complemented with a wild type copy of *wzxE*, isolated from *E. coli,* constitutively expressed from a single-copy integrative plasmid	This study
M. tuberculosis c-*Rv3277t*_tetOFF pMV361::*ltaA*	*Rv3277t* silenced, complemented with a wild type copy of *ltaA,* isolated from *S. aureus*, constitutively expressed from a single-copy integrative plasmid	This study
Mycobacterium smegmatis mc^2155 wild type	Wild type	
M. smegmatis c-*Msmeg_1817*_tetON	*MSMEG_1817* silenced, annotated start codon ATG, kan^R, hyg^R	This study
Escherichia coli NEB5α	Cloning strain for plasmids	New England Biolabs (Cat.-No. C2987I)
E. coli HB101	Cloning strain for phasmids	

Supplementary Table 3: Oligonucleotides used in this study. Restriction sites used for cloning purposes are underlined.

Oligonucleotide	Sequence [5‘ – 3‘]
c-*Rv3277*-RR-*Van*91I	TTTTTCCATCTTTTGGGGTGCATGCGTTGCCATC
c-*Rv3277*-RL-*Van*91I	TTTTTCCATAGATTGGATGAACGAGGTGTCAGTG
c-*Rv3277*-LR-*Van*91I	TTTTTCCATTTCTTGGGGCTGGACCACCAGAGG
c-*Rv3277*-LL-*Van*91I	TTTTTTCCATAAATTGGGGAATTATGTGGCCGGAG
c-*Rv3277t*-RR-*Van*91I	TTTTTCCATAGATTGGATGTCCTTTGCCGATGCCACCATC
c-*Rv3277t*-RL-*Van*91I	TTTTTCCATCTTTTGGCCGCTCGAGTTCTACAACATTCC
c-*Msmeg_1817*-RR-Van91I	TTTTTCCATCTTTTGGGGCCAGGATCAACAGTGTGGA
c-*Msmeg_1817*-RL-Van91I	TTTTTCCATAGATTGGATGTCCTTCGCTGATGCAACG
c-*Msmeg_1817*-LR-Van91I	TTTTTCCATTTCTTGGAGCTCATGGTGCCGTTCGGCG
c-*Msmeg_1817*-LL-Van91I	TTTTTCCATAAATTGGTCAGATACTTCGCGGCCACCT
Msmeg_1817-3-HindIII	TTTTTAAGCTTCACGAAGTCTTCGACACCCTGG
Msmeg_1817-5-PacI	TTTTTAATTAATGTCCTTCGCTGATGCAACGATC
c-Rv3277-3-HindIII	TTTTTAAGCTTCACGAGCTTTTCGACACCCTGG
c-Rv3277-5-PacI	TTTTTAATTAATGAACGAGGTGACCGCCGGGGTG
c-*Rv3277t*-PacI	TTTTTAATTAATGTCCTTTGCCGATGCCACCATC
3' *Rv3789* HindIII	AAGCTTGCCCGATTCGACCCTGACC
5' *Rv3789* PacI	GGGCGTTAATTAATGCACCTGTCGGCACAGGTA
5' PacI *arnEF*	GCGTTAATTAATCTGGTGCTGATTCAGTATCGTCC
3' HindIII *arnEF*	GCGAAGCTTGTGTAAAGTGGCAGGGAAAAC
5 PacI *wzxE*	CCGGCGTTAATTAAGCGACTTTGTTGAACTACTTTTCCTGAT
3 wzxE *HindIII*	CGCGGAAGCTTCGATCCCAGTACGTGAATCAGTACAG
5' PacI *ltaA*	GCGGTTAATTAATTTATGGAAAGGTTCCTTTATAT
3' *ltaA* HindIII	GCGGAAGCTTTCTTTATTTTAAAATACGTTTTAACC

Supplementary Table 4: Plasmids and Phasmids used in this study.

Plasmid (p) or Phasmid (ph)	Relevant properties
p0004S	hyg^R
phAE159	Temperature sensitive shuttle phasmid, derivative of mycobacteriophage TM4, amp^R
pc*Rv3277*	Knock-in cassette, hyg^R, sacB, flanking regions of *Rv3277*
phc*Rv3277*	Knock-in cassette, hyg^R, sacB, flanking regions of *Rv3277*
pc*Rv3277t*	Knock-in cassette, hyg^R, sacB, flanking regions of *Rv3277t*
phc*Rv3277t*	Knock-in cassette, hyg^R, sacB, flanking regions of *Rv3277t*
pc*Msmeg_1817*	Knock-in cassette, hyg^R, sacB, flanking regions of *Msmeg_1817*
phc*Msmeg_1817*	Knock-in cassette, hyg^R, sacB, flanking regions of *Msmeg_1817*
pMV261	kan^R
pMV261_revtetR_RBS-Mut.E	kan^R
pMV361	$apra^R$
pMV361_*Msmeg1817*	$apra^R$, complementation plasmid
pMV361_*Rv3277t*	$apra^R$, complementation plasmid
pMV361::*Rv3277t*-T35A-K59A-N141A	$apra^R$, complementation plasmid
pMV361::*Rv3789*	$apra^R$, complementation plasmid
pMV361::*arnE/F*	$apra^R$, complementation plasmid
pMV361::*wzxE*	$apra^R$, complementation plasmid
pMV361::*ltaA*	$apra^R$, complementation plasmid

5. Clp-targeting BacPROTACs impair mycobacterial proteostasis and survival

Published in: Cell
Impact factor: 45.5 (2023)
doi: 10.1016/j.cell.2023.04.009

Contribution:

- Contributed to manuscript drafting
- Determination of minimal inhibitory concentrations against *M. tuberculosis* and other *Mycobacteriaceae* via resazurin dye reduction method
- Generation of targeted gene deletion mutant in *M. tuberculosis* using specialized phage transduction
- Isolation of whole cell protein lysates of *M. tuberculosis* cells after treatment followed by LC-MS/MS analysis
- Isolation of spontaneous homo-BacPROTAC resistant mutants
- Isolation of genomic DNA
- Whole genome sequencing analysis of spontaneous resistant mutants

5.1 Manuscript

Cell

Article

Clp-targeting BacPROTACs impair mycobacterial proteostasis and survival

Graphical abstract

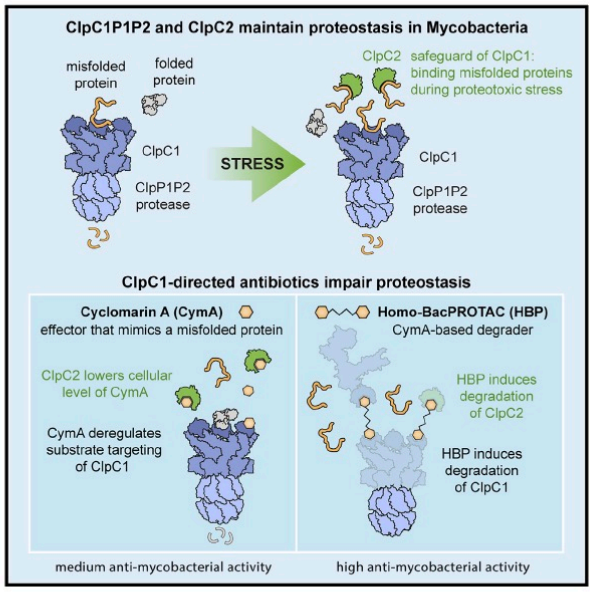

Highlights

- Cyclomarin A and ecumicin hijack ClpC1P1P2 proteases by mimicking damaged proteins
- ClpC2 and ClpC3 function as isolated receptor proteins safeguarding the Clp protease
- Homo-BacPROTACs induce degradation of the essential ClpC1 and its ClpC2 security
- BacPROTACs present potent antibiotics that efficiently kill *M. tuberculosis*

Authors

David M. Hoi, Sabryna Junker, Lukas Junk, ..., Uli Kazmaier, Rainer Kalscheuer, Tim Clausen

Correspondence

lukas.junk@helmholtz-hips.de (L.J.), tim.clausen@imp.ac.at (T.C.)

In brief

Homo-dimeric BacPROTACs induce the self-degradation of essential Clp components of the mycobacterial proteostasis system, introducing a potent antibiotic strategy against *M. tuberculosis*.

Hoi et al., 2023, Cell *186*, 2176–2192
May 11, 2023 © 2023 The Author(s). Published by Elsevier Inc.
https://doi.org/10.1016/j.cell.2023.04.009

CellPress

CellPress
OPEN ACCESS

Cell

Article

Clp-targeting BacPROTACs impair mycobacterial proteostasis and survival

David M. Hoi,[1,9,11,12,13] Sabryna Junker,[1,13] Lukas Junk,[2,3,*] Kristin Schwechel,[4] Katharina Fischel,[5] David Podlesainski,[6] Paige M.E. Hawkins,[7,8] Lasse van Geelen,[4] Farnusch Kaschani,[6] Julia Leodolter,[1] Francesca Ester Morreale,[1] Stefan Kleine,[6] Somraj Guha,[2] Klaus Rumpel,[5] Volker M. Schmiedel,[5] Harald Weinstabl,[5] Anton Meinhart,[1] Richard J. Payne,[7,8] Markus Kaiser,[6] Markus Hartl,[9,12] Guido Boehmelt,[5] Uli Kazmaier,[2,3] Rainer Kalscheuer,[4] and Tim Clausen[1,10,14,*]

[1]Research Institute of Molecular Pathology, Vienna BioCenter, 1030 Vienna, Austria
[2]Saarland University, Organic Chemistry I, 66123 Saarbrücken, Germany
[3]Helmholtz Institute for Pharmaceutical Research Saarland (HIPS), Helmholtz Centre for Infection Research (HZI), 66123 Saarbrücken, Germany
[4]Institute of Pharmaceutical Biology and Biotechnology, Heinrich Heine University, 40225 Düsseldorf, Germany
[5]Boehringer Ingelheim RCV GmbH & Co KG, 1120 Vienna, Austria
[6]University of Duisburg-Essen, Center of Medical Biotechnology, Faculty of Biology, 45141 Essen, Germany
[7]School of Chemistry, University of Sydney, Sydney, NSW 2006, Australia
[8]Australian Research Council Centre of Excellence for Innovations in Peptide and Protein Science, The University of Sydney, NSW 2006, Australia
[9]Max Perutz Labs, Vienna BioCenter, 1030 Vienna, Austria
[10]Medical University of Vienna, 1030 Vienna, Austria
[11]Vienna BioCenter PhD Program, Doctoral School of the University of Vienna and Medical University of Vienna, 1030 Vienna, Austria
[12]University of Vienna, Center for Molecular Biology, Department for Biochemistry and Cell Biology, 1030 Vienna, Austria
[13]These authors contributed equally
[14]Lead contact
*Correspondence: lukas.junk@helmholtz-hips.de (L.J.), tim.clausen@imp.ac.at (T.C.)
https://doi.org/10.1016/j.cell.2023.04.009

SUMMARY

The ClpC1:ClpP1P2 protease is a core component of the proteostasis system in mycobacteria. To improve the efficacy of antitubercular agents targeting the Clp protease, we characterized the mechanism of the antibiotics cyclomarin A and ecumicin. Quantitative proteomics revealed that the antibiotics cause massive proteome imbalances, including upregulation of two unannotated yet conserved stress response factors, ClpC2 and ClpC3. These proteins likely protect the Clp protease from excessive amounts of misfolded proteins or from cyclomarin A, which we show to mimic damaged proteins. To overcome the Clp security system, we developed a BacPROTAC that induces degradation of ClpC1 together with its ClpC2 caretaker. The dual Clp degrader, built from linked cyclomarin A heads, was highly efficient in killing pathogenic *Mycobacterium tuberculosis*, with >100-fold increased potency over the parent antibiotic. Together, our data reveal Clp scavenger proteins as important proteostasis safeguards and highlight the potential of BacPROTACs as future antibiotics.

INTRODUCTION

The overuse of common antibiotics that target protein and nucleic acid synthesis and cell wall assembly has led to the development of pathogenic bacteria harboring multidrug resistance.[1,2] Among these, the extensively drug resistant (XDR) and totally drug resistant (TDR) strains of *Mycobacterium tuberculosis* (*Mtb*) are considered to be highly threatening microbial pathogens,[3,4] which contribute to tuberculosis (TB) constituting the leading global cause of death by bacterial infection. Given the rise of TB infections as a growing and underrecognized threat during the COVID-19 pandemic, the development of further novel antitubercular strategies is urgently needed.[5–7]

One of the most promising *Mtb* drug targets is the ClpC1:ClpP1:ClpP2 (ClpC1P1P2) protease, the mycobacterial equivalent of the eukaryotic proteasome. The Clp proteolytic complex is composed of the AAA (ATPase associated with diverse cellular activities) unfoldase ClpC1 that associates with the ClpP1P2 protease to form a caged degradation chamber. Similar to other Clp proteases, ClpC1 recognizes specific peptide stretches, or degrons, using loops at the entrance of its AAA hexameric ring, whereas the N-terminal domain ($ClpC1_{NTD}$) located on top of the protease functions as a receptor for a separate class of client proteins[8–10] (Figure 1A). Substrates captured by ClpC1 are threaded by ATP-driven power strokes through the pore of the AAA hexamer and translocated into the ClpP1P2 protease chamber for degradation.[11,12]

The ClpC1P1P2 protease is an attractive target for antimicrobial agents due to its essential role in maintaining protein homeostasis and counteracting host-induced stresses, thus making it

Cell
Article

CellPress
OPEN ACCESS

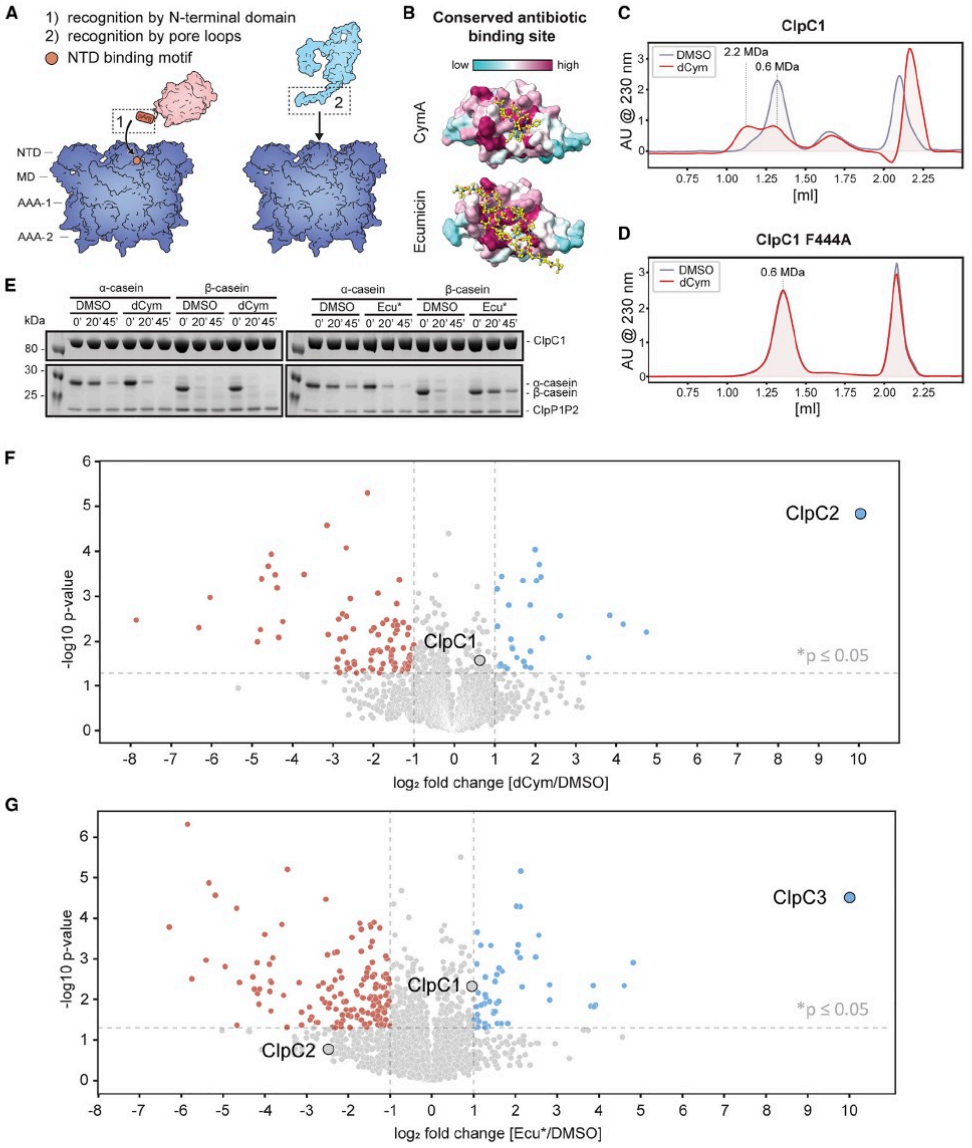

Figure 1. Antitubercular compounds deregulate ClpC1

(A) Substrate recognition by mycobacterial ClpC1 proceeds via specific degrons recognized by the $ClpC1_{NTD}$ or via unfolded protein segments bound by pore loops in the channel formed by the AAA+ ATPase.

(B) $ClpC1_{NTD}$ hydrophobic pocket targeted by antibacterial compounds (upper panel: complex with cyclomarin A, PDB 3WDC; lower panel: complex with ecumicin, PDB 6PBS) is highly conserved, as indicated by the mapped conservation score.

(legend continued on next page)

essential for the full pathogenic potential of mycobacteria.[11,13] Indeed, the Clp protease was identified as a promising mycobacterial target in screening campaigns for lead compounds against alternative drug targets.[14–18] Several antimicrobial agents that target ClpP1P2 or ClpC1 showed antitubercular effects, including efficacy against *Mtb* in human macrophages.[14,18,19] Among the Clp protease targeting antibiotics, acyldepsipeptides are best characterized and interfere with ClpP1P2 by preventing binding of regulatory Clp components.[20–22] Effectors targeting ClpC1 include various natural products such as cyclomarin A, ecumicin, lassomycin and rufomycin.[14,15,18,19,23–25] These cyclic peptides bind to overlapping sites on $ClpC1_{NTD}$ but intriguingly impair ClpC1 activity by seemingly diverse mechanisms. Cyclomarin derived compounds were also recently used to develop small-molecule degraders, called BacPROTACs, that enable ClpC1P1P2-mediated elimination of specific target proteins in mycobacteria.[26]

The antibiotic-binding site on the $ClpC1_{NTD}$ is strongly conserved (Figure 1B), pointing to an important, yet unknown biological function. Given that they bind to the substrate receptor of the Clp protease, we hypothesized that ClpC1-directed antibiotics may induce gross alterations in the Clp degradome of mycobacteria. We thus explored the effect of cyclomarin A and ecumicin on the mycobacterial proteome using quantitative proteomics. In addition to global dysregulation of the proteome at bactericidal concentrations, these data identified two small proteins, which we refer to as ClpC2 and ClpC3, as regulatory components of the mycobacterial Clp degradation system. Using the same ligand-binding sites as those present in ClpC1, the identified Clp proteins compete for substrate binding. Moreover, the two regulatory proteins can sequester ClpC1-directed antibiotics, thus reducing their cytotoxicity. In an effort to overcome ClpC2/ClpC3-mediated protection and efficiently target the Clp degradation machinery as an antibacterial strategy, we synthesized cyclomarin A dimers. These Homo-BacPROTACs (HBPs) were able to direct ClpC1 against itself, inducing its elimination by the ClpC1P1P2 protease, as well as promoting degradation of ClpC2. The HBP degraders exhibited potent killing activity toward *Mtb* in cell culture. Aside from identifying two safeguarding components in the mycobacterial protein quality control (PQC) system, our data highlight the potential of BacPROTACs as antibiotics, allowing us to simultaneously target multiple components of an essential stress response system.

RESULTS

ClpC1-targeting antibiotics imbalance the mycobacterial proteome and induce the expression of small Clp proteins

The most studied natural antibiotics directed against ClpC1 are cyclomarin A and ecumicin[14,18,19] (Figures S1A and S1B). While these two cyclic peptides bind to overlapping $ClpC1_{NTD}$ receptor sites and stimulate ClpC1 ATPase activity to similar degrees, their mode of action differs.[14,18,27] Whereas ClpC1P1P2-mediated degradation has been shown to be enhanced by cyclomarin A, ecumicin instead has been proposed to uncouple the activities of ClpC1 and ClpP1P2, thus reducing protease efficiency. However, the molecular basis underlying their distinct activities is unclear. Likewise, it is not yet known whether and how the deregulation of ClpC1P1P2 may imbalance the mycobacterial proteome. To address these points, we used a recently described ecumicin derivative (Ecu*) (Figure S1B) that exhibits superior antibiotic potency against *Mtb* compared with the parent natural product.[19] As a mimic of the natural cyclomarin A, we used the slightly simplified cyclic peptide desoxycyclomarin C (dCym), which can be produced by chemical total synthesis (Figure S1A).[28,29]

To analyze the molecular basis of ClpC1 deregulation, we reconstituted the interaction of the unfoldase with dCym and Ecu* *in vitro*. As revealed by size-exclusion chromatography (SEC), addition of the antibiotics induced conversion of the ClpC1 hexamer into higher-order oligomers spanning a broad mass range of 0.6–2.2 MDa, as estimated by SEC (Figure 1C). Analysis of the induced peak fraction by negative-stained EM revealed the formation of irregular ClpC1 clusters when incubated with dCym, consisting of 2–4 hexameric particles (Figure S1C). These data are consistent with a recent report showing that cyclomarin A treatment stabilizes higher-order ClpC1 oligomers that have an elevated unfoldase activity.[30] Similar to dCym, we observed that addition of Ecu* resulted in clustering of ClpC1 hexamers (Figure S1D). Together, these data mirror findings in *Bacillus subtilis*, in which ClpC also assembles tetramers of hexamers upon ligand binding to the $ClpC_{NTD}$[26,27] pointing to a broadly conserved mechanism of ClpC regulation. The higher-order complexes are stabilized by contacts between coiled-coil domains (MD) protruding from adjacent hexamers. Aside from promoting oligomer conversion, rearrangement of MD domains destabilizes the auto-inhibited state and induces ATPase activity, thus stimulating unfoldase function.[19,26,27,30] To test whether this activation mechanism is hijacked by dCym, we introduced a site-specific mutation, F444A, a residue at the tip of the ClpC1 MD that is predicted to engage in MD:MD* contacts. Negative-stained EM and SEC analysis confirmed that the F444A mutation abolishes dCym-induced oligomer conversion (Figures 1D and S1E). These data show that dCym binding to ClpC1 induces reorientation of MD coiled-coils thereby transforming the latent hexamer into active higher-order complexes.

To test the effect of ClpC1 deregulation in the context of the full ClpC1P1P2 protease, we analyzed the degradation of model proteins upon incubation with dCym and Ecu*. For the model substrates α-casein and β-casein—which differ in their degree of compactness, secondary structure, and

(C and D) SEC elution profile of ClpC1 and ClpC1 F444A mutant. Size markers are indicated on top. Addition of dCym induces higher-order oligomers for ClpC1, whereas abolishing MD-MD contacts (F444A mutation) prevents oligomerization. All SEC runs were carried out in the presence of ATP, using the double Walker B (DWB) mutation that stabilizes the hexamer.
(E) Substrate degradation of two model substrates, β-casein and α-casein, by ClpC1P1P2 with or without dCym or Ecu*.
(F and G) Quantitative proteomics of *Msm* treated with 10 μM dCym/Ecu*. Data are normalized to the DMSO control. n = 3. See also Figure S1 and Table S1.

Cell
Article

CellPress
OPEN ACCESS

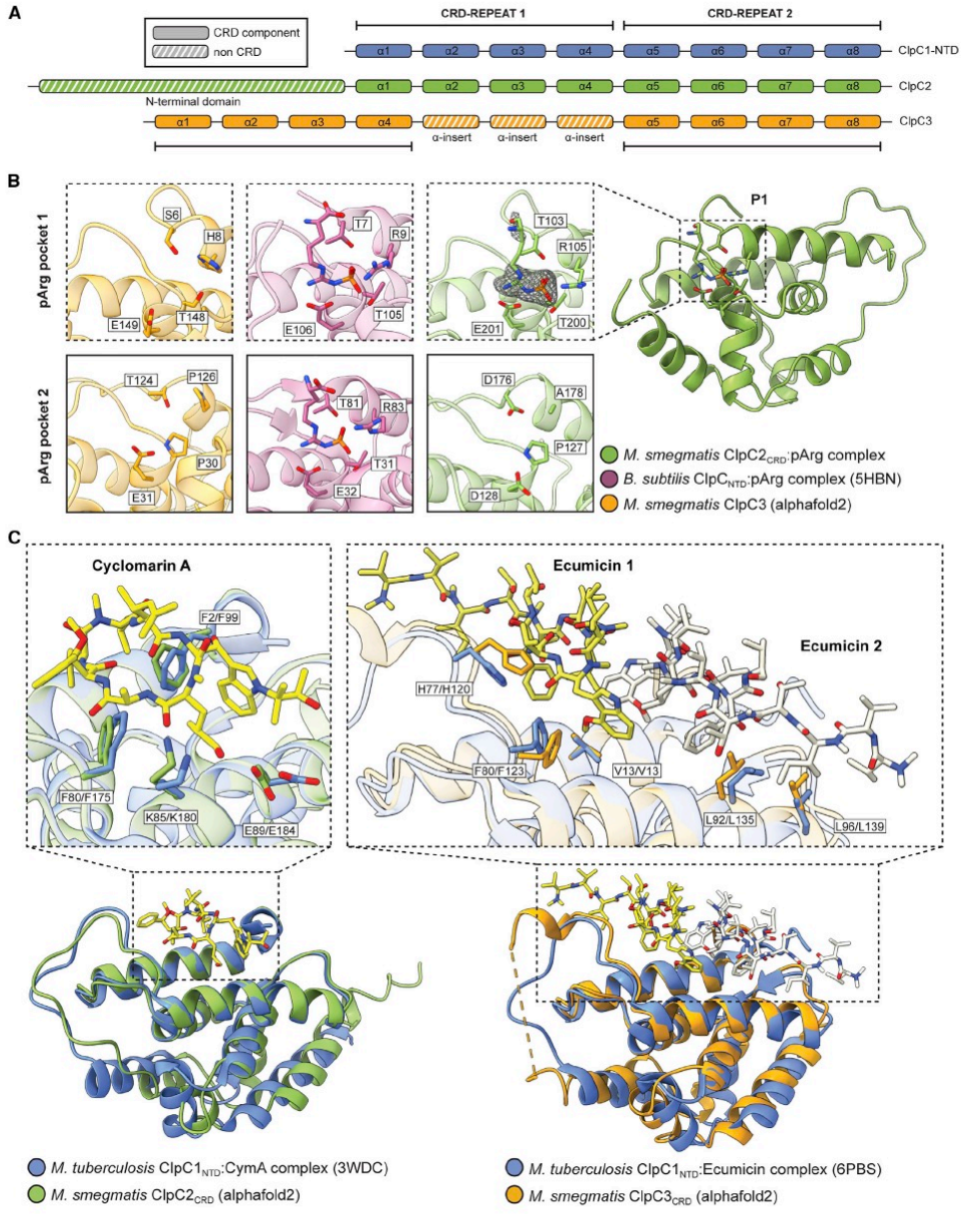

(legend on next page)

hydrophobicity—we observed notable differences. While dCym only accelerated degradation of α-casein, Ecu* exhibited dual effects. It inhibited the degradation of β-casein by ClpC1P1P2 but increased α-casein turnover (Figures 1E and S1F). These data immediately indicated a substrate-dependent mechanism of action for $ClpC1_{NTD}$-directed compounds. Given the disparate effects on the tested substrates *in vitro*, we performed quantitative MS to assess how Ecu* and dCym remodel the complete mycobacterial proteome. We incubated *Mycolicibacterium smegmatis* (*Msm*) cells with both compounds and performed label-free quantitative (LFQ) proteomics. Considering the cytotoxic effect of both antibiotics, we first screened for optimal conditions to characterize changes in proteome composition (Figures S1G and S1H). Under non-bactericidal conditions, neither Ecu* nor dCym treatment resulted in a significant deregulation of the mycobacterial proteome (Figures 1F and 1G). We did observe minor abundance changes, with several potential ClpC1P1P2 target proteins equally affected by Ecu* and dCym incubation (Table S1). However, we noted a remarkable exception to these subtle effects. Each antibiotic resulted in the selective and significant upregulation of one specific, unannotated target protein—one protein responding to each compound. Strikingly, the two proteins show clear homology to the $ClpC1_{NTD}$ domain, the receptor site targeted by the antibiotics. dCym treatment induced a strong increase of MSMEG_2792 (which we will refer to as ClpC2), while Ecu* incubation led to increased levels of MSMEG_3761 (which we will refer to as ClpC3).

In a second proteomics experiment, we used a longer incubation time and a higher, bactericidal dCym concentration. Prolonged incubation with dCym led to the depletion of a large fraction of mycobacterial proteins (Figure S1I). About 30% of the native proteome could no longer be identified by MS and was seemingly absent in bacteria treated for 6 h. Again, the most notable exception to the overall decrease in protein levels was ClpC2, which increased 600-fold in the presence of dCym. Indeed, ClpC2 was among the top 10 most abundant proteins in the dCym-treated mycobacterial cell, with absolute levels almost as high as those of ClpC1 (Figure S1J). In conclusion, our proteomics data show that dCym and Ecu* deregulate ClpC1P1P2, increasing overall protease activity and causing drastic proteome imbalances. Interestingly, this is accompanied by the selective and drastic enrichment of an uncharacterized pair of small Clp proteins, which both contain a $ClpC1_{NTD}$-like domain.

ClpC1, ClpC2, and ClpC3 share a common receptor domain

Phylogenetic analysis indicated that ClpC2 and ClpC3 are restricted to actinobacteria, whereas ClpC1 is much more widely distributed throughout actino- and Gram-positive bacteria. These data also show that ClpC1 and ClpC2 are present in the vast majority of actinobacteria, whereas ClpC3 is only present in a few genera without an obvious evolutionary pattern (Figures S2A and S2B). For example, *Msm* encodes a ClpC3 protein, but the closely related species *Mtb* does not. Sequence alignment of ClpC2, ClpC3, and $ClpC1_{NTD}$ revealed strong conservation of the annotated Clp repeat domain (CRD; sequence identify of 42% with ClpC2 and 39% with ClpC3, Figure S2A). This double 4-helix bundle is present as an N-terminal domain in most HSP100 chaperones, offering an extended surface for substrate binding.[31] ClpC2 contains an additional domain at its N-terminus, while ClpC3 instead has an extended insertion bridging the CRD-repeats between helices 4 and 5 (Figure 2A).

Sequence alignment also indicated that the receptor site for phospho-arginine (pArg), a ClpCP protease degradation signal,[10] is conserved in ClpC1 and ClpC2 but not in ClpC3 (Figure S2A). Though mycobacteria lack an ortholog of the protein arginine kinase McsB present in Gram-positive bacteria,[32,33] a recent proteomics study reported a multitude of pArg sites in *Msm* proteins.[34] These data suggest that the ClpC1P1P2 protease may utilize pArg as a degradation tag to recognize substrate proteins. Consistent with this idea, surface plasmon resonance (SPR) measurements showed that pArg binds strongly to $ClpC1_{NTD}$ and ClpC2 but not to ClpC3 (Table S2; Data S1A). To visualize the binding mode of pArg to ClpC2, we co-crystallized its CRD in complex with pArg and determined the crystal structure at 2.1 Å resolution (Figure 2B; Table S3). Superposition with the pArg complexes of *B. subtilis* ClpC (PDB 5hbn) confirmed the structural conservation of the receptor site, with all residues engaged in pArg binding found to be in a virtually identical position. The binding pocket, which exhibits characteristic electrostatic properties combining positively and negatively charged halves, is formed by the conserved residues Thr103, Arg105, Thr200, Glu201, which together accommodate the phospho-guanidinium group. Accordingly, ClpC2 could compete with ClpC1 for pArg-tagged client proteins. We thus hypothesize that the free substrate receptor modulates substrate binding to the mycobacterial ClpC1P1P2 protease.

To model the putative binding sites for dCym and Ecu*, we compared the structure of ClpC2 and the AlphaFold2 model of ClpC3 with co-crystal structures of ClpC1 ligand complexes (Figure 2C).[35] The dCym binding sites of ClpC2 and ClpC1 are almost identical, as are the binding sites for Ecu* in ClpC1 and ClpC3. Consistently, SPR binding studies revealed a strong binding of dCym to all three Clp proteins, with affinities in the low nM range. Ecu* also bound to the three proteins, albeit with slightly lower affinity (Table S2; Data S1A). Together, these data show that ClpC2 and ClpC3 share substrate-binding sites with ClpC1 and should thus have overlapping substrate selectivity. Modifications in these sites allow for specific differences in substrate selection as reflected by the interactions with the small-molecule ligands pArg, dCym and Ecu*.

Figure 2. CRD receptor domains of ClpC1, ClpC2, and ClpC3

(A) Structural organization of $ClpC1_{NTD}$, ClpC2, and ClpC3 highlighting the Clp repeat domain (CRD).

(B) Molecular model depicting the *Msm* $ClpC2_{CRD}$:pArg crystal structure. The two pArg binding pockets are shown next to it, together with the respective sites of $ClpC_{NTD}$:pArg and the modeled $ClpC3_{CRD}$.

(C) Superposition of *Mtb* $ClpC1_{NTD}$:CymA structure (PDB 3WDC) and $ClpC1_{NTD}$:ecumicin (PDB 6PBS) with ClpC2 and ClpC3, respectively. Conserved residues involved in antibiotic binding are indicated (first number, ClpC1). See also Figure S2, Tables S2 and S3, and Data S1A.

The CRD antibiotic-binding pocket is a receptor site for misfolded proteins

To explore the functional role of the CRD pocket targeted by cyclomarin A and ecumicin, we synthesized a linear ecumicin fragment (Ecu**) containing half of the ecumicin macrocycle, mimicking a natural peptide ligand. Upon confirming the binding of the short Ecu** peptide mimic (*N*-methylated LVAWG, Figure 3A) to $ClpC1_{NTD}$, (K_D = 50 μM, Table S2), we co-crystallized the protein: peptide complex and determined its crystal structure. Notably, peptide binding resulted in dimerization of $ClpC1_{NTD}$, with Ecu** wedged between the two antibiotic-binding sites (Figure 3B). Whereas side chains of *N*-Me-Leu1, *N*-Me-Ala3, and Gly5 were accommodated in the binding site of one protomer, residues Val2 and *N*-Me-Trp4 protruded into the partner $ClpC1_{NTD}$. Though we could not recapitulate binding with a canonical, non-N-methylated LVAWG peptide, the observed binding mode of the linear Ecu** peptide fragment pointed to a putative ClpC1P1P2 degron recognized by the CRD. Dimerization of $ClpC1_{NTD}$ modules could be instrumental in enlarging the binding pocket and achieving high affinity and specificity for cognate substrates. Consistent with our hypothesis, yeast Hsp104, containing a homologous N-terminal domain, utilizes a hydrophobic pocket equivalent to the antibiotic-binding site of ClpC1 to target client proteins[36] (Figure 3C). In fact, ClpC1 and ClpC2 contain functionally conserved Leu, Ile, and Val residues at the bottom of the same pocket, providing a potential interaction site for misfolded proteins. Superposition of the NTDs of ClpC1, ClpC2, and Hsp104 shows that dCym binding renders the hydrophobic pocket of ClpC1 and ClpC2 inaccessible to substrates (Figure S3A). To test the predicted Clp protein substrate recognition site *in vitro*, we performed competition experiments with ClpC1 antibiotics and model substrates (Figure S3B). In pull-down assays, we observed that ClpC2-CRD efficiently interacts with β-casein; however, addition of dCym markedly reduced the amount of bound substrate (Figure 3D). These data suggest that dCym and β-casein directly compete for the same binding site. In contrast, incubation of Ecu or dCym with the full-length ClpC1 unfoldase had mixed effects on the β-casein substrate (Figure 1E), likely due to the presence of receptor sites outside the CRD and the stimulatory effect of the two antibiotics on general ATPase activity (Figure S3C). Finally, we monitored β-casein degradation by ClpC1P1P2 over time, in the presence and absence of ClpC2-CRD (Figure 3E). These data revealed that ClpC2 interferes with ClpC1 substrate degradation, likely by competitive binding of the misfolded protein via the shared dCym binding site.

Taken together, our data suggest that ClpC1-directed antibiotics mimic the hydrophobic core of misfolded proteins that bind to the shared CRD in ClpC1, ClpC2 and ClpC3. To confirm this model, we performed a pull-down of tagged ClpC2 in a *Msm ΔclpC2* strain. As dCym binding was predicted to block interactions between ClpC2 and putative protein substrates, we compared the ClpC2 interactome of mycobacteria with and without dCym treatment (Figure S3D). Remarkably, treatment with dCym led to depletion of the most abundant interaction partners of ClpC2 (Figure 3F; Table S4). Among those interactors, nine proteins have been reported to be partially unfolded proteins preferentially targeted by ClpC1P1P2 and thus enriched in a ClpC1 depleted *Mtb* strain (Figure S3E).[37] We thus propose that ClpC2 competes with ClpC1 for the binding of unfolded proteins.

Together, our findings provide a mechanistic understanding of how dCym and other ClpC1-directed antibiotics interfere with the ClpC1P1P2 protease. The cyclic peptides function as small-molecule mimics of a misfolded protein, allowing them to hijack the bacterial PQC system. By binding to a conserved hydrophobic site in the CRD, used to bind aberrant proteins and activate unfoldase activity, the antibiotics exhibit a dual effect: they stimulate the Clp protease by inducing activated higher-order complexes and in parallel block access to misfolded proteins. Consequently, ClpC1-directed antibiotics cause drastic proteome imbalances leading to the downregulation but also upregulation of cellular targets.

ClpC2 functions as safeguard of the ClpC1P1P2 protease

To test the regulatory role of ClpC2 on the ClpC1P1P2 protease *in vitro*, we synthesized chemical adapters that contained either the pArg or dCym group as degron mimics. As a substrate anchor, we used JQ1, a chemical entity known to tightly bind to the bromodomain1 of BRDT ($BRDT_{BD1}$), our model substrate. Incubation of $BRDT_{BD1}$ with the bi-functional compounds thus yielded pArg and dCym-labeled protein (Figures 4A and S4A). Upon addition of a dCym-JQ1 degrader, we observed efficient degradation of the $BRDT_{BD1}$ substrate. However, substrate degradation by ClpC1P1P2 was strongly inhibited upon addition of equimolar amounts of ClpC2 (Figure 4A). Likewise, when we assayed $BRDT_{BD1}$ degradation in the presence of pArg-JQ1, we observed that ClpC2 was able to inhibit the Clp protease, buffering the introduced degradation tag (Figure 4B). These data suggest that ClpC2 functions as a competitive inhibitor for specific degrons recognized by ClpC1, sequestering potential substrates and preventing their degradation.

To investigate the biological consequences of ClpC2 and ClpC3 as competitive binders of ClpC1 in mycobacteria, we first tested the effect of the small Clp proteins on mycobacterial sensitivity to dCym and Ecu* antibiotics. We performed minimum inhibitory concentration (MIC) assays, using wild type (WT) and knockout *Msm* strains (*Δstrai*, *ΔclpC3*, and *ΔclpC2 ΔclpC3*). In MIC assays, growth of the WT strain was inhibited at concentrations of 2.5 μM dCym or 6 μM Ecu*. Consistent with our *in vitro* data, genomic knockout of *clpC2* or *clpC3* each led to an increased sensitivity of mycobacterial cells against one of the antibiotics (Figures 4C and 4D). The *ΔclpC2* strain showed a 2-fold increase in sensitivity to dCym, while the *ΔclpC3* strain showed a 4-fold increased susceptibility to Ecu* treatment, with each antibiotic specificity corresponding to our earlier proteomics data (Figures 1F and 1G). Combined deletion of *clpC2* and *clpC3* did not further enhance sensitivity against either compound (Figures 4C and 4D). Moreover, we observed that overexpression of ClpC2 or ClpC3 strongly reduced dCym and Ecu* toxicity, respectively, allowing *Msm* growth at antibiotic concentrations 4-fold higher than those tolerated by WT cells. Elevating ClpC2 was more efficient in protecting cells from dCym, whereas ClpC3 upregulation led to higher resistance against Ecu*. Together our findings show that ClpC2 and ClpC3 can reduce the effective intracellular concentration of antibiotics that target the ClpC1 unfoldase. The small Clp proteins thus seem to

CellPress
OPEN ACCESS

Cell
Article

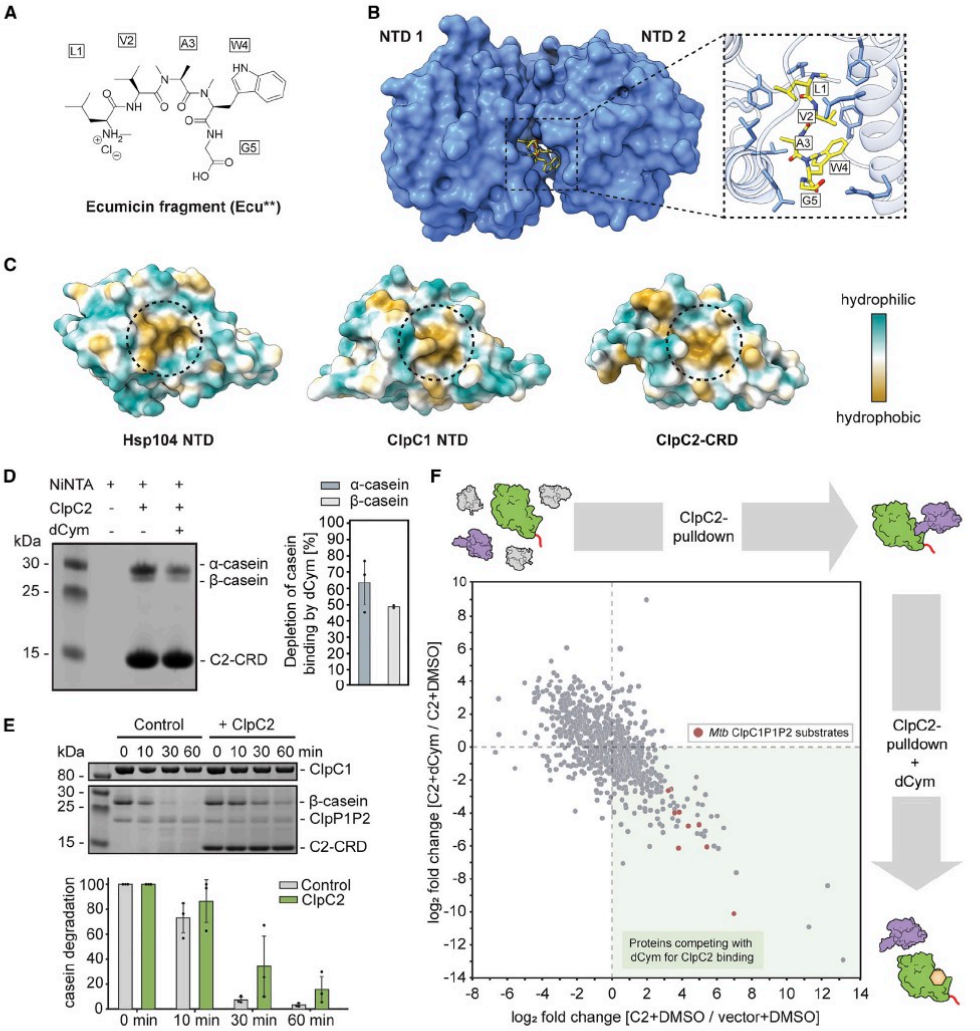

Figure 3. ClpC1-directed antibiotics bind to a hydrophobic pocket in $ClpC1_{NTD}$ used for substrate targeting

(A) Structure of the linear ecumicin fragment Ecu**.

(B) Co-crystal structure of the $ClpC1_{NTD}$:Ecu** complex. Ecu** is bound at the interface of two subunits, with its side chains protruding into the canonic antibiotic-binding sites.

(C) CRD comparison of ClpC1, ClpC2, and Hsp104 (PDB 5U2U), highlighting a common hydrophobic pocket.

(D) Pull-down assay using α- and β-casein as model substrates. Binding to ClpC2 is reduced upon dCym treatment (all proteins at 15 μM, dCym at 25 μM). Quantification represents mean ± SD, n = 3.

(E) *In vitro* degradation assay of β-casein by ClpC1P1P2 in presence of ClpC2. Quantification shows mean ± SD, n = 3.

(F) IP-MS analysis of ClpC2 pull-downs in *Msm*, in the absence (x axis) and presence of dCym (y axis). The most prominent interaction partners, enriched in the ClpC2 pull-down, were not bound to ClpC2 in the presence of dCym. These potential ClpC1 and ClpC2 substrates are seen in the lower right quadrant. Proteins identified in a previous *Mtb* ClpC1P1P2 substrate screen are highlighted in red. See also Figure S3 and Table S4.

Cell
Article

CellPress
OPEN ACCESS

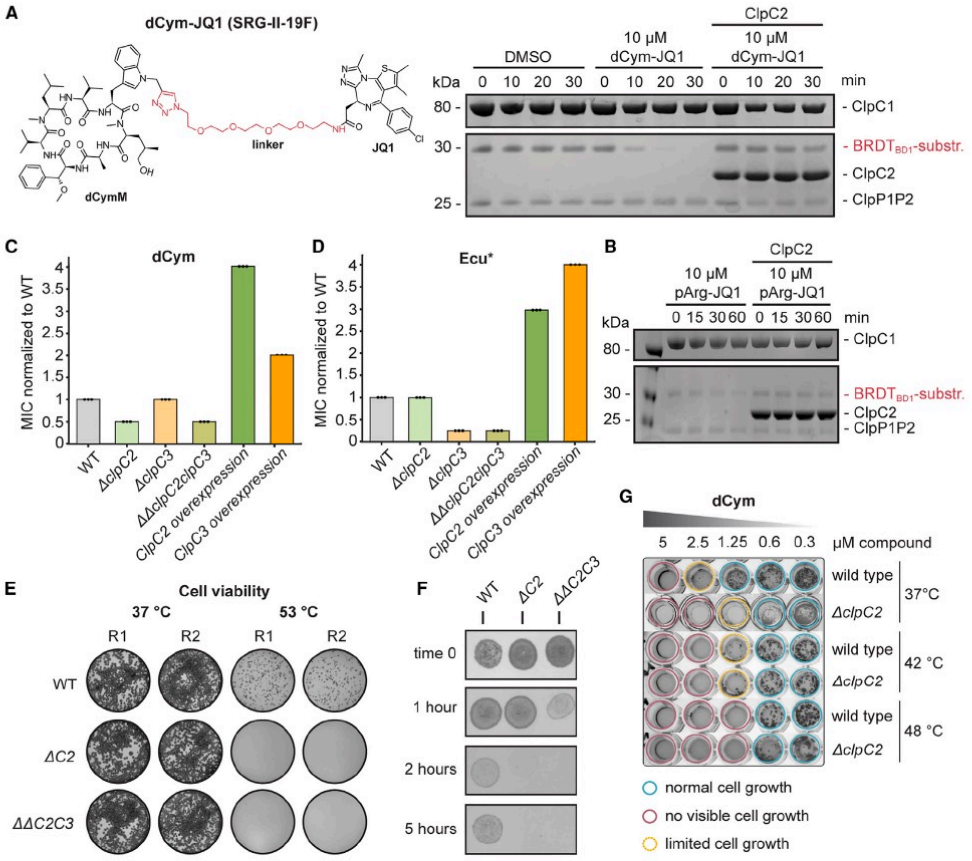

Figure 4. ClpC2 and ClpC3 protect ClpC1 from antibiotics and an overload with protein substrates in *Msm*

(A and B) (A) Degradation assay showing competition of ClpC2 and ClpC1 for the BRDT$_{BD1}$ model substrate labeled with the indicated dCym-JQ1 or (B) with pArg-dCym.

(C and D) MIC assay for dCym or Ecu* treated *Msm* WT and mutant strains. The MIC was visually determined, and bars indicate the first well in which inhibited cell growth was observed, normalized to WT. Uncropped plates are shown in Data S1B.

(E) Cell viability assay showing survival of *Msm* WT and mutants after heat shock (53°C for 4 h, replicates R1 and R2 from four independent biological replicates).

(F) MIT assay upon heat shock treatment. Survival was tested for *Msm* WT and mutants before (t0) as well as 1, 2, and 5 h after heat shock (53°C). n = 3.

(G) Checkerboard assay combining dCym treatment with heat shock conditions for *Msm* wild type and *ΔclpC2* mutant. 96-well plates were prepared with increasing temperature in the first dimension and reducing dCym concentrations in the second dimension (see also Data S1B for uncropped plates, n = 3). See also Figure S4.

represent specialized components of the PQC system that can be induced to counteract antibiotic activity in a specific manner. However, the molecular basis underlying their specific effects on dCym and Ecu* susceptibility in mycobacteria remained unclear. Given the ubiquitous distribution of ClpC2 in actinobacteria and the lack of ClpC3 in the major pathogen *Mtb H37Rv*, we therefore focused our subsequent analysis on the safeguarding role of the ClpC2 scavenger.

To further characterize the effect of ClpC2 on dCym, we performed an antibiotic kill curve assay, in which we followed the toxicity of dCym over time, as measured by colony-forming units (CFUs). While deletion of ClpC2 induced a cell growth inhibitory phenotype, treatment with dCym strongly exacerbated this effect. Upon incubation with dCym, viable *ΔclpC2* cells were reduced to ~30% control cells, as opposed to WT bacteria that were unaffected under these conditions (Figure S4B). These

CellPress
OPEN ACCESS

Cell
Article

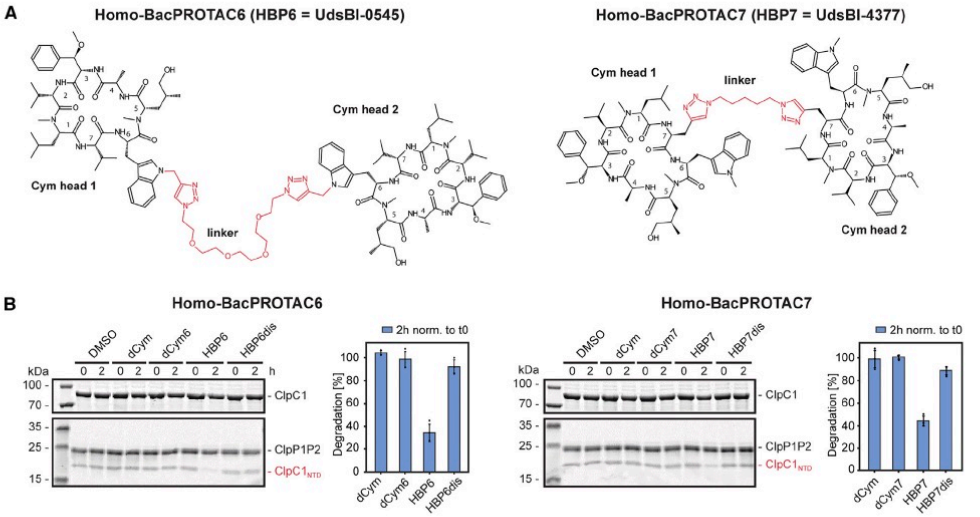

Figure 5. Induced degradation of the ClpC1$_{NTD}$ CRD by HBPs

(A) Chemical structure of HBP6 and HBP7, that differ in their linker attachment points and linker length. See Figure S6B for structures of dCym6 and dCym7.

(B) Degradation assay showing degradation of ClpC1$_{NTD}$, the CRD model substrate, by HBPs (100 μM). Quantification shows mean ± SD, n = 3. See also Figure S5.

data confirm that ClpC2 contributes to the mycobacterial defense against cyclomarin antibiotics. To test if ClpC2 exhibits a more general protective function within the mycobacterial PQC system, we performed kill curve assays for WT and mutants under heat shock conditions (53°C). Both *clpC2* and *clpC2/clpC3* knockouts showed complete lethality after a 4-h heat shock despite partial viability of the WT (Figure 4E). To verify the essentiality of ClpC2 for the stress response, we performed a minimum inhibitory time (MIT) assay monitoring the survival of bacteria over a 5-h heat shock time course. As expected, the *clpC2* mutants were impaired in growth as early as 1-h into heat shock, and both single and double mutants were substantially more sensitive to heat stress (Figure 4F). Finally, we analyzed the combined effect of heat stress and antibiotic treatment in a checkerboard assay. At 37°C, sensitivity to dCym was significantly higher in *clpC2* mutants than in WT. However, elevated temperatures also led to an increased antibiotic sensitivity in the WT strain (Figure 4G). Antibiotic sensitivity at 42°C was comparable to that of the *ΔclpC2* strain, implying that ClpC2 scavengers are fully occupied by heat-shocked proteins, leaving ClpC1 unprotected against dCym. Together, these data highlight the protective role of ClpC2 as a molecular chaperone, buffering stress-induced misfolded proteins as well as antibiotics mimicking the damaged substrates.

Dimeric Homo-BacPROTACs can target the Clp CRD motif *in vitro*

The protective function of ClpC2 relies on its ability to reduce the effective concentration of dCym and related compounds in the cell. In the presence of the scavenger protein, antibiotics must thus be applied in higher amounts to bind ClpC1 and deregulate its housekeeping function. We aimed to overcome the traditional occupancy-based mode of action of cyclomarin by developing event-driven antibiotics that inactivate ClpC1 in a catalytic manner. The recently developed BacPROTAC technology, which allows for the selective elimination rather than inhibition of target proteins, provided an attractive platform for this purpose. The technology relies on bi-functional chemical adapters that bind to a protein of interest (POI) and to the ClpC1$_{NTD}$ substrate receptor, thereby targeting POIs to the Clp protease and inducing their degradation. Importantly, the bi-functional adapters employ dCym derivatives (Figure S1A) that bind to the ClpC1$_{NTD}$. We thus hypothesized that a dimeric degrader containing two dCym heads, which we call HBP in analogy to Homo-PROTACs developed against the E3 component VHL,[38] could induce the degradation of ClpC1. In addition, the compound should be capable of targeting ClpC2 via its dCym binding site. Such dual action was hypothesized to be highly advantageous for the antibiotic activity potential of the HBP degrader, due to simultaneous elimination of the essential Clp protease and its security guard.

Guided by previously developed dCym degraders (Figure S1A),[26] we used either the tryptophan derivative at position 6 or the valine at position 7 as linker attachment points to generate the dimeric HBP6 and HBP7, respectively (Figure 5A; chemical synthesis described in Junk et al.[29]). As a control for selective targeting of the Clp CRD, we fused two distomeric variants of the cyclic peptides, in which all stereocenters are inverted

(Figures S5A and S5C). SPR measurements confirmed that the functional HBP variants bind to $ClpC1_{NTD}$ and ClpC2 with high affinity ($K_D \sim 0.5–2.5$ nM), whereas their distomeric counterparts did not interact with the Clp proteins (Table S2; Data S1A). To estimate the activity of HBPs *in vitro*, we followed ClpC1P1P2 mediated degradation of $ClpC1_{NTD}$. Incubation with HBPs induced elimination of about 80% of the $ClpC1_{NTD}$ substrate (Figure 5B). In contrast, the distomeric controls could not redirect the ClpC1P1P2 protease, excluding indirect effects on substrate depletion. These *in vitro* degradation experiments indicate that HBPs can mark CRD-containing proteins for degradation.

Homo-BacPROTACs reduce the levels of ClpC1 and ClpC2 in *M. smegmatis*

To study whether HBPs could target CRD-containing Clp proteins in mycobacteria, we used *Msm* as a model system. Active HBP compounds had a similar MIC as the parent monomers, indicating that despite their large size, the applied compounds are taken up by mycobacteria (Figures S5B and S6A; for detailed characterization of HBP structure-activity relationships see Junk et al.[29]). To study their *in situ* activity, we carried out an LFQ MS experiment, monitoring changes in the *Msm* proteome upon HBP treatment. As control, we used the inactive HBP distomers, which did not exhibit a bacteriotoxic effect, as well as dCym monomers bearing alkyne groups at the points of linker attachment. Overall, the MS data indicated that monomeric and dimeric dCym variants led to gross perturbation in the proteome. Treatment with both the HBPs and their monomeric heads led to a strong increase of ClpC2 levels, while addition of distomeric controls did not raise ClpC2 abundance (Figures 6A, 6B, and S6B). Importantly, however, only in the case of active HBP dimers did we observe a significant decrease in ClpC1 levels. Moreover, when we compared the ClpC2 levels upon treatment with monomeric dCym and dimeric HBP, we observed that the relative levels of ClpC2 are markedly reduced in the presence of the degrader, evidencing simultaneous targeting of ClpC1 and ClpC2 (Figure 6A). To confirm the proteomics data, we employed a parallel reaction monitoring (PRM) protocol to follow ClpC1 and ClpC2 over time. The quantitative MS data confirmed that both ClpC1 and ClpC2 levels are diminished upon incubation with the dimeric BacPROTACs as compared with the monomeric compounds (Figure 6B). After 24 h, levels of ClpC1 were reduced to ~40%, whereas ClpC2 levels decreased by 45%–60%, as compared with cells treated with monomeric dCym. Together these data highlight the potential of HBP degraders to target the essential ClpC1 unfoldase together with the ClpC2 security guard. However, in *Msm*, this activity seems to be masked by the strong upregulation of ClpC2 upon antibiotic treatment, sequestering the degrader. To confirm its protective role, we studied the effect of HBPs in the *ΔclpC2 Msm* knockout strain. As reflected by MIC_{50} values, the active synthetic degraders had a 7-fold higher potency in the *ΔclpC2* strain than in the WT (Figures 6C and S6C). Compared with the milder effect for the monomeric antibiotic (only 2-fold higher sensitivity in *ΔclpC2*, Figure 4C), these data point to a distinct mode of action of the HBP degrader and highlight its improved efficacy in targeting ClpC1. To further confirm the role of ClpC2 in buffering misfolded proteins and protecting against antibiotics targeting ClpC1, we followed the potency of HBPs under heat shock conditions. Stress-induced protein damage should enhance the load on the PQC system and limit the ability of ClpC2 to protect ClpC1. Consistently, we see that the efficacy of HBPs is drastically improved during heat shock, more than that of the isolated dCym compound (Figure 6D). This disparity further highlights the distinct mode of action of the monomeric and dimeric antibiotics: the bivalent HBP exhibits a dual activity, deregulating and degrading the PQC components ClpC1 and ClpC2.

Homo-BacPROTACs are potent antibiotics killing pathogenic *M. tuberculosis*

Having shown the BacPROTAC induced degradation of ClpC1 and ClpC2 in *Msm*, we tested their potency against the virulent *Mtb* strain H37Rv, a model strain used to explore the effect of antitubercular compounds on pathogenicity. *Mtb* encodes a ClpC2 ortholog that is closely related to the *Msm* ClpC2 (62% sequence identity, 82% homology) but no ClpC3 and expresses a ClpC1 unfoldase containing an N-terminal CRD identical to its *Msm* counterpart. To profile cellular targets of cyclomarin A, we performed pull-down assays with *Mtb* lysates using a biotin probe connected to a simplified cyclomarin derivative.[26] Upon elution with the cyclic peptide, we identified ClpC1 and ClpC2 as main interactors of the cyclomarin derivative (Figure S7A). As expected, *Mtb* ClpC2 also uses its conserved receptor site to bind ClpC1-directed antibiotics. To investigate the antitubercular activity of HBP degraders, we performed dose response curves in *Mtb* WT and *ΔclpC2* deletion strains. Dimeric HBP6 and HBP7 strikingly outperformed the monomer (dCymM) in terms of antibiotic activity, with 115- and 150-fold higher potency, respectively (Figures 7A and S7B). Indeed, the antibacterial effect of dCym monomers was comparable between *Mtb* and *Msm* (MIC_{50} about 10–40 μM), while the pathogenic *Mtb* was much more sensitive to HBP degraders, with low MIC_{50} values ranging from 0.26 to 0.34 μM.

To demonstrate that the antibiotic effect of HBPs is due to ClpC1 degradation, we performed quantitative proteomics comparing active and inactive BacPROTACs. In line with the pronounced toxicity of HBPs toward *Mtb*, we observed a higher ClpC1 degradation efficiency of HBPs in *Mtb* compared with *Msm*, with a 5-fold reduction in ClpC1 levels (Figures 7B and 7C). To estimate the effect of the degrader on ClpC2 levels, we employed a *ΔclpC2* strain, in which the bulk of the Clp protein is absent and thus not responsive to antibiotic-mediated degradation, while a short N-terminal remnant (21 residues; $ClpC2_{NT}$) is still expressed from the endogenous promotor. Proteomics analysis revealed that HBP treatment triggered a 20-fold increase in $ClpC2_{NT}$ levels in the *Mtb ΔclpC2* mutant, presumably resulting from transcriptional upregulation, similar to what we observed in *Msm*. In contrast, treatment of WT cells with HBPs led to a much smaller increase in ClpC2 levels. Compared with $ClpC2_{NT}$ (*ΔclpC2* strain), the amounts of ClpC2 were 5-fold less elevated in WT, suggesting that the dimeric BacPROTAC can target ClpC2 via its CRD and induce its degradation in *Mtb* (Figures 7C, S7C, and S7D). Thus, our data demonstrate that HBPs are potent antitubercular compounds, exhibiting a 115-fold higher potency than parent cyclomarin A compounds. The strongly increased efficacy relies on their distinct mode of

CellPress
OPEN ACCESS

Cell
Article

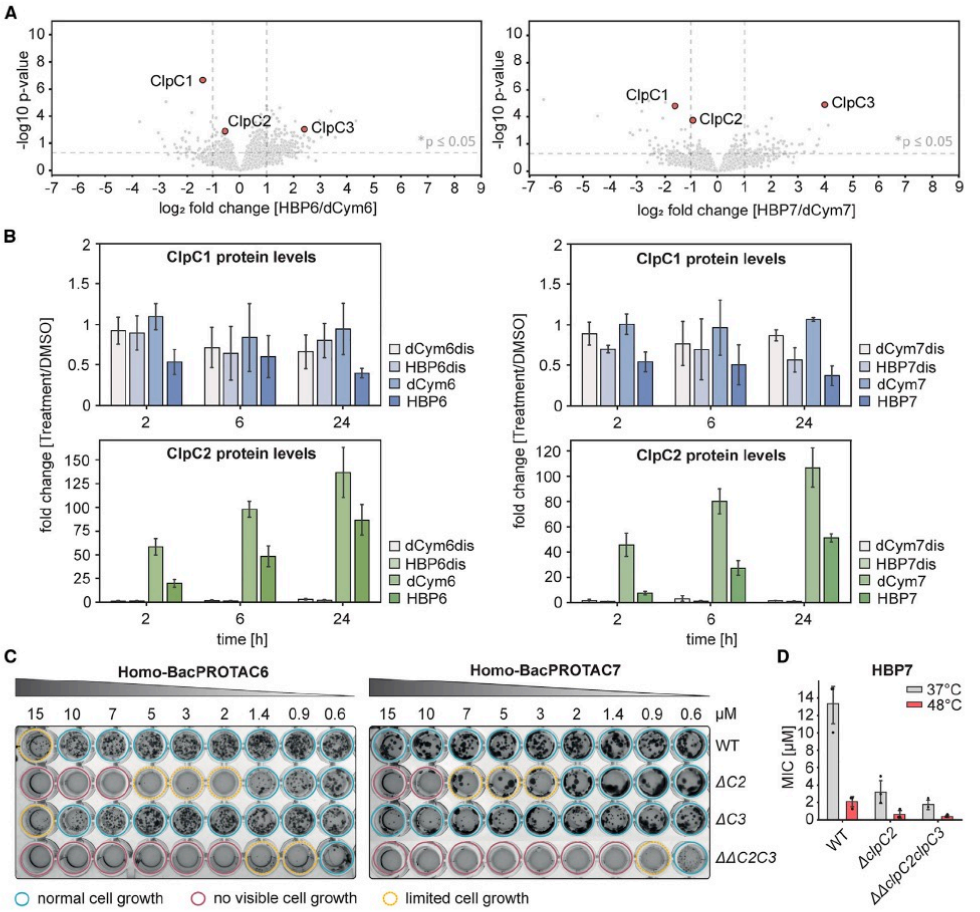

Figure 6. Degradation of ClpC1 and ClpC2 by HBPs in *Msm*

(A) Quantitative proteomics of *Msm* cells treated with HBP6 and HBP7 (12.5 μM, 24 h) normalized to incubation with their monomeric head groups (dCym6 and dCym7). ClpC1 levels decreased to 38% and 34%, whereas ClpC2 levels decreased to 68% and 51%, respectively, upon HBP treatment, in comparison with monomer treatment. n = 3.

(B) PRM analysis of Msm treated with 12.5-μM HBP6 or HBP7. ClpC1 and ClpC2 levels were analyzed over time, confirming ClpC1 and ClpC2 reduction upon incubation with HBP degraders, compared with monomeric and inactive controls. Results are mean ± SD, n = 3.

(C) MIC assays for HBP6 and HBP7, comparing *Msm* mutants with WT. n ≥ 5.

(D) Checkerboard assay combining HBP treatment with heat shock conditions for *Msm* WT and mutants. Plates were prepared with reducing HBP concentrations and placed overnight at 48°C. Afterward, the plates were transferred to 37°C until colonies appeared. Displayed are the mean ± SD, n = 3. See also Data S1B for uncropped plates, and Figure S6.

action, inducing degradation of the housekeeping proteins ClpC1 and ClpC2 rather than inhibiting them.

Given the importance of antibiotic resistance to *Mtb* pathogenesis, we next aimed to assess resistance development against these BacPROTAC degraders. We treated *Mtb* H37Rv with either HBP6 or HBP7 on solid media (at concentrations of ≥ 6 × MIC). In total, we obtained four spontaneous resistant clones, all showing reproducible growth in presence of the two BacPROTACs and exhibiting cross-resistance against HBP6 and HBP7 (Figures 7D and S7E). Whole-genome sequencing revealed that the three HBP6 mutant clones had the same mutation in *clpC1*, resulting in an F80V substitution in the $ClpC1_{NTD}$

Cell
Article

CellPress
OPEN ACCESS

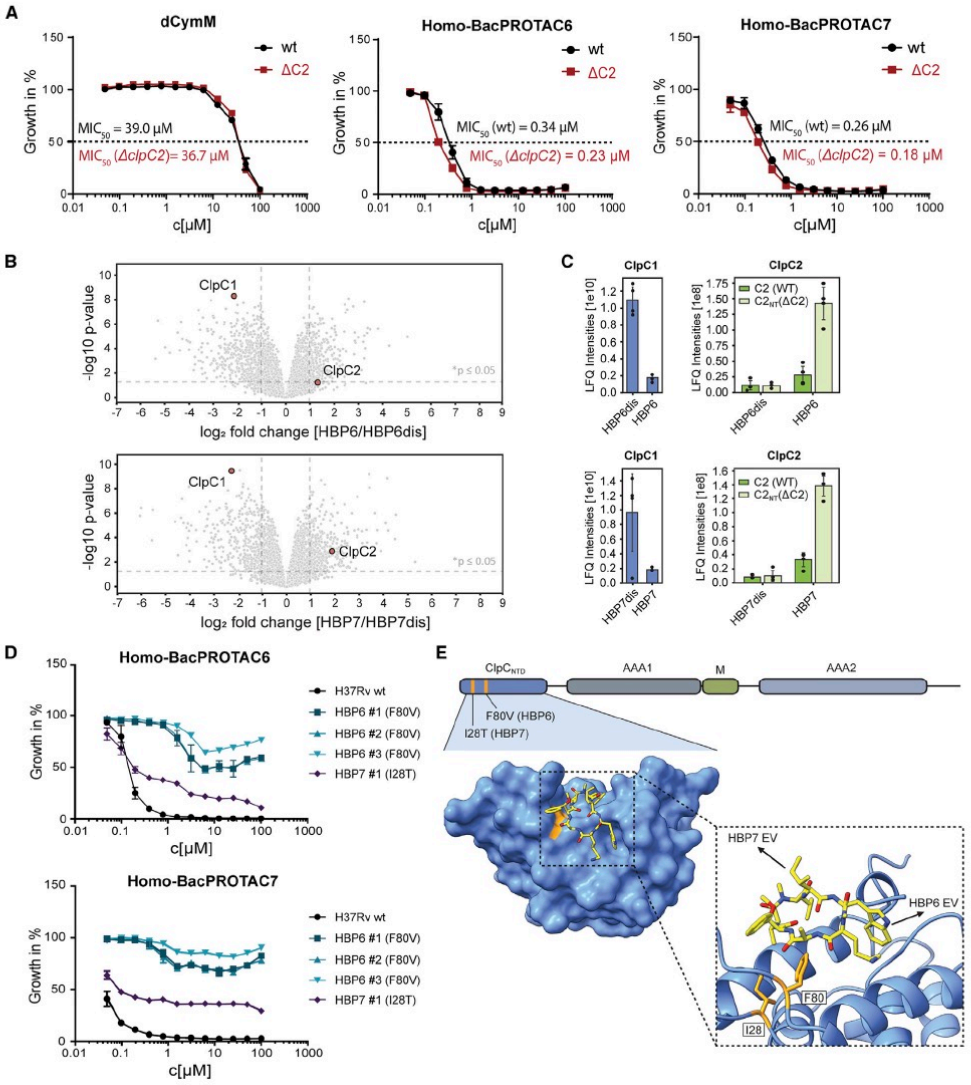

Figure 7. Homo-BacPROTAC treatment impairs growth of *M. tuberculosis*

(A) Dose response curves comparing dCymM monomer and HBP degraders on *Mtb* growth and comparing WT *Mtb* with the *ΔclpC2* mutant. Cells show a 115-fold (WT) and 160-fold (*ΔclpC2*) higher sensitivity to HBP6 compared with dCymM. The mutant is slightly more sensitive than the WT, consistent with the lack of ClpC2's protective function. Results are mean ± SD, n = 3.

(B) Quantitative proteomics of *Mtb* cells treated with HBP6 and HBP7, normalized to treatment with inactive distomers (HBP6-dis, HBP7-dis). Quantification shows mean ± SD, n = 3.

(C) LFQ intensities comparing ClpC1 (left) and ClpC2 (right) degradation induced by HBPs and their corresponding distomers. For quantitative proteomics of *Mtb* WT and *ΔclpC2* cells, the latter was expressing a truncated 21-aa ClpC2 peptide ($ClpC2_{NT}$). While ClpC1 is reduced to similar levels in treated WT and *ΔclpC2*

(legend continued on next page)

(Figure 7E). Phe80 is located at the bottom of the hydrophobic pocket targeted by the cyclic peptide antibiotics, and the critical role of Phe80 in binding cyclomarin A has been previously shown in targeted *in vitro* and *in vivo* interaction studies, where the F80A mutation abolished antibiotic binding.[24] Accordingly, the F80V mutation is expected to markedly reduce HBP affinity for ClpC1, explaining the evolved antibiotic tolerance. The sequenced HBP7 clone, which exhibited weaker resistance against the two HBPs, revealed another mutation, I28T, in the $ClpC1_{NTD}$ (Figures 7D and 7E). The mutated Ile28 is located in close proximity to Phe80, such that the introduced threonine may induce slight rearrangements in the cyclomarin binding pocket corresponding to moderate resistance.

Non-replicating bacteria pose a further challenge to the activity of BacPROTACs, as these persisters are well-known for escaping antibiotic treatment. To investigate HBP potency in dormant cells, we tested pathogenic *Mtb* in a checkerboard assay, in which HBPs were combined pairwise with bedaquiline. By inhibiting the ATP synthase subunit C (AtpE), bedaquiline induces lower intracellular ATP levels, resembling a dormant state in *Mtb*.[40–42] However, treatment of *Mtb* H37Rv cells with bedaquiline had no effect on HBP7 BacPROTAC activity, demonstrating that HBPs work equally well—or even better—as the reference drug rifampicin against persistent cells (Figure S7F).

Together these data reveal ClpC1 as an attractive antibiotic target and confirm the role of the $ClpC1_{NTD}$ in binding BacPROTACs. Considering the threat of persistent bacteria in clinics, our findings further suggest BacPROTACs as promising therapeutic agents that could retain activity against dormant *Mtb* latent in host cells.

DISCUSSION

Perhaps the most threatening bacterial pathogen with regard to antibiotic resistance and infection severity is *Mtb*, the cause of TB. In addition to the long and complex treatment routines required for established antibiotics, second-line TB drugs, including cycloserine, capreomycin, and quinolones exhibit serious side effects that limit their utility. Therefore, novel antitubercular compounds with distinct modes of action able to evade drug resistance are urgently needed.[43] In this study, we pioneered a BacPROTAC antibiotic that overcomes a bacterial PQC security system, is also active in bacteria with a dormant-like phenotype and targets multiple components of the mycobacterial stress response concurrently.

As a critical first step, we revealed the mode of action of ClpC1-directed antibiotics. Our data delineate the dual mechanism employed by cyclomarin A and related antibiotics (ecumicin, rufomycin, and lassomycin), all of which bind to a conserved site at the $ClpC1_{NTD}$ substrate receptor. We show that peptide antibiotics mimic exposed hydrophobic residues of unfolded proteins and bind to a common pocket in HSP100 chaperones. Using substrate mimicry, the antibiotics can hijack the ClpC1P1P2 protease, which performs an essential housekeeping role in mycobacteria.[37] The antibiotics act as competitive inhibitors for misfolded proteins and in parallel, remodel ClpC1 into its active higher-order oligomer state, yielding a permanently activated protease that degrades cellular proteins in an unselective manner. Due to this bimodal activity, dCym treatment leads to massive perturbations in the proteome, as reflected by the up- and downregulation of key cellular factors. Importantly, proteomic analysis identified two small Clp proteins, ClpC2 and ClpC3, that were specifically upregulated upon either cyclomarin A or ecumicin treatment. Characterization of these factors uncovered a bacterial security system that protects the essential ClpC1P1P2 protease. We show that the well-conserved ClpC2 is a specialized Clp regulator. It functions as a scavenger protein shielding the ClpC1P1P2 protease from a surplus of binding partners by using equivalent receptor sites. Deletion of ClpC2 induces a severe thermosensitive phenotype and is lethal under extreme heat shock, suggesting that ClpC2 sequesters misfolded proteins and prevents an overload of the housekeeping protease during proteotoxic stress. Moreover, ClpC2 can sequester antibiotics like CymA that act as small-molecule mimics of a misfolded protein. Binding to ClpC2 lowers the intracellular concentration of the antibiotic and thus ameliorates its impact on ClpC1 and the protease. Due to its protective function, ClpC2 must be considered when developing antibiotics targeting the mycobacterial stress response machinery.

To efficiently shut down the PQC system, we developed bivalent HBP degraders targeting the common Clp receptor domain, CRD. In pathogenic *Mtb*, this pan-degrader exhibited strong antibacterial potency, inhibiting bacterial growth >100-fold more efficiently than the natural monomeric cyclic peptide. By fusing two dCym heads, the bivalent compound redirects the ClpC1P1P2 protease against itself, inducing degradation of ClpC1. Thus, antibiotic activity relies on the auto-knockdown of an essential proteolytic machine. Moreover, HBP degraders reduced not only the level of ClpC1 but also that of its safeguarding protein ClpC2. The simultaneous targeting of the Clp protease and its security system underlies the extraordinary power of the HBP as an antibiotic. We hypothesize that the more pronounced antibiotic effect of HBPs toward *Mtb* compared with *Msm* is due to different cellular levels of ClpC2, leading to more efficient degradation of the ClpC1 unfoldase and a concomitant reduction of the MIC from ~15 μM in *Msm*

bacteria, levels of ClpC2 (WT) and $ClpC2_{NT}$ (*ΔclpC2*) are strikingly different. This difference likely reflects induced degradation of ClpC2 in WT cells, whereas the $ClpC2_{NT}$ peptide is inaccessible to HBP-mediated degradation. Quantification shows mean ± SD, n = 3.

(D) Dose response curves comparing compound susceptibility of four *Mtb* spontaneous resistant mutants against HBPs, carrying different single nucleotide polymorphisms (SNPs, T>G at nucleotide 238 causing F80V: HBP6 #1-#3; T>C at nucleotide 83 causing I28T: HBP7 #1). Mutation of F80 leads to strong growth rescue against treatment with either of the BacPROTACs, which is less pronounced for the I18T mutant. Results are mean ± SD, n = 3. Notably, the sequencing also revealed a second-site deletion in the mycocerosic acid synthase (*mas*) gene, which is involved in biosynthesis of the cell wall lipid phthiocerol dimycocerosate (PDIM), causing a frameshift in all three HBP6 resistant clones. However, since mutations causing PDIM loss are known to occur frequently during *in vitro* culturing of *Mtb* strains,[39] since the mutants show unaltered susceptibility profiles toward other antibiotics, and since the HBP7 resistant clone harbored no mutations in the PDIM biosynthetic gene cluster, the *mas* mutation likely had no effect on the resistance mechanism (Figure S7E).

(E) Resistance mutations against HBP6 (F80V) and HBP7 (I28T) mapped to the crystal structure of $ClpC1_{NTD}$:CymA analog (PDB 7AA4). Mutated residues are highlighted in orange. Arrows indicate the exit vector (EV) positions of HBP6 and HBP7. See also Figure S7.

to ~0.2 μM in *Mtb*. It should also be noted that, in addition to its degrader function, the potency of HBP is enhanced by the inherent cytotoxicity of the incorporated cyclomarin derivatives, which interfere with ClpC1-mediated protein degradation. Thus, the degrader benefits from a dual activity, simultaneously deregulating and destroying a central component of the mycobacterial PQC system. In related medicinal chemistry studies,[29] we found that even intracellular *Mtb* propagating in infected THP-1 cells showed a concentration-dependent reduction in CFU after incubation with HBPs. Moreover, the degrader molecules exhibited promising pharmacokinetic properties and minimal cytotoxicity in a macrophage infection model, as compounds were well-tolerated at the highest concentration tested (50 μM[29]). We conclude that the BacPROTAC approach presents an effective strategy to develop anti-mycobacterial agents, enabling the degradation of essential Clp proteins. Considering the >100-fold increased efficacy of bivalent HBPs over the parent CymA compound, the mechanistic advantages of small-molecule degraders over classic drugs seems to be conserved in BacPROTACs, providing an attractive technology platform to develop next generation antibiotics.

Limitations of the study

Although our study identifies ClpC2 and ClpC3 as specific scavenger proteins against the antitubercular compounds cyclomarin A (dCym) and ecumicin (Ecu*), respectively, their exact molecular mechanism was not fully resolved. For example, the molecular mechanism leading to upregulation of ClpC2 and ClpC3 by dCym and Ecu* has remained elusive. While our data point to transcriptional regulation, the exact nature of these regulatory factors, the identity of the respective stress operon, and their interaction with the small Clp proteins requires further study. Moreover, our *in vitro* studies show that dCym and Ecu* have similar affinities for ClpC2 and ClpC3. Therefore, it is unclear why treatment with these antibiotics leads to the selective upregulation of one of two distinct proteins, which seem to counteract antibiotic activity in a specific manner in the mycobacterial cell. Though our study highlights the underestimated complexity of the mycobacterial stress response system, better understanding of this system and the involved factors will be critical to unleash the full potential of ClpC1-directed antibiotics and small-molecule degraders.

With regard to the degrader mechanism, it should be noted that the binding of HBPs to adjacent CRDs, like those present in the ClpC1 hexamer or ClpC2 dimer, may limit their availability for targeting ClpC1 and ClpC2 subunits in *trans* and directing them for degradation. The intra-molecular ClpC1-ClpC1 and ClpC2-ClpC2 associations may explain the discrepancy between HBP-binding affinity *in vitro* and lower efficacy in cells. Although we consider linker design as a promising strategy to prevent intra-molecular HBP recruitment and enhance degradation activity, addressing this point experimentally is challenging due to the dynamic nature of ClpC1 and ClpC2 oligomers.

STAR★METHODS

Detailed methods are provided in the online version of this paper and include the following:

- KEY RESOURCES TABLE
- RESOURCE AVAILABILITY
  - Lead contact
  - Materials availability
  - Data and code availability
- EXPERIMENTAL MODEL AND SUBJECT DETAILS
- METHOD DETAILS
  - Isolation of chromosomal DNA
  - Construction of mycobacterial mutants
  - Cloning of overexpression constructs
  - Protein expression and purification
  - Surface plasmon resonance (SPR)
  - Analytical size exclusion chromatography (aSEC)
  - Negative staining EM
  - *In vitro* substrate degradation assay
  - *In vitro* ClpC2 pulldown
  - Co-crystallization and structure determination
  - *M. smegmatis* sample preparation for MS analysis
  - Whole cell proteomics & PRM sample preparation
  - Immunoprecipitation (IP) sample preparation
  - Sample quality control for MS analysis
  - Label free quantification mass spectrometry
  - LFQ-MS and IP-MS data analysis
  - Parallel reaction monitoring (PRM) analysis
  - PRM data analysis
  - *M. tuberculosis* samples for MS analysis
  - Pull-down assays in *M. tuberculosis*
  - Whole cell MS from *M. tuberculosis*
  - Minimum inhibitory concentration (MIC) assay
  - Dose response curves in *M. tuberculosis*
  - Checkerboard assay
  - Kill curve assay
  - Minimum inhibitory time (MIT) assays
  - Resistance screens and WGS in *M. tuberculosis*
  - Chemical Synthesis of Ecu**
  - Chemical Synthesis of dCym-JQ1 (SRG-II-19F)
  - 2-((*S*)-4-(4-Chlorophenyl)-2,3,9-trimethyl-6*H*-thieno[3,2-f][1,2,4]triazolo[4,3-a][1,4]diazepin-6-yl)-N-(14-(4-((3-(((2*S*,5*S*,8*S*,11*S*,14*S*,17*S*,20*S*)-5-((*R*)-3-hydroxy-2-methylpropyl)-17-isobutyl-14,20-diisopropyl-11-((*R*)-methoxy(phenyl)methyl)-4,8,16-trimethyl-3,6,9,12,15,18,21-heptaoxo-1,4,7,10,13,16,19-heptaazacyclohenicosan-2-yl)methyl)-1*H*-indol-1-yl)methyl)-1*H*-1,2,3-triazol-1-yl)-3,6,9,12-tetraoxatetradecyl)acetamide (dCym-JQ1 / SRG-II-19F)
  - Synthesis of pArg-JQ1 (BI01826025)
- QUANTIFICATION AND STATISTICAL ANALYSIS

SUPPLEMENTAL INFORMATION

Supplemental information can be found online at https://doi.org/10.1016/j.cell.2023.04.009.

ACKNOWLEDGMENTS

We thank all members of the Clausen group for remarks on the manuscript and Alexander Schleiffer for help with sequence analyses. We thank Juliane Kley for help with crystallization. We acknowledge DESY (Hamburg, Germany) for the provision of experimental facilities at beamline P11 and we would like to thank Johanna Hakanpää for assistance. We thank Stacie Dodgson from

Life Science Editors for editorial assistance. M.K. and D.P. acknowledge funding from the Deutsche Forschungsgemeinschaft (CRC1430), R.K. from the Deutsche Forschungsgemeinschaft (grant number KA 2259/5-1) and the Jürgen Manchot Stiftung (graduate school MOI IV), and M.K. acknowledges funding by INST FUGG for purchasing Lumos MS. This work was further supported by the European Research Council (AdG 694978, T.C.), an FFG Headquarter Grant (no 852936, to T.C.), the Vienna Science and Technology Fund (WWTF 10.47379/LS21029, to T.C., M.H., and M.K), Boehringer Ingelheim (to J.L. and S.J.), and the National Health and Medical Research Council (Investigator grant APP1174941 to R.J.P). F.E.M., J.L., and S.J. are members of the Boehringer Ingelheim Discovery Research global post-doc program. The IMP is supported by Boehringer Ingelheim.

AUTHOR CONTRIBUTIONS

D.M.H., S.J., L.J., A.M., R.K., R.J.P., G.B., U.K., and T.C. designed experiments; L.J., P.M.E.H., S.K., M.K., S.G., and V.M.S. performed the chemical synthesis of the cyclomarin A, ecumicin, and BacPROTAC variants; D.M.H., K.F., J.L., F.E.M., and K.R. performed biochemical assays and binding measurements; K.F. and K.R. contributed to biophysical profiling of BacPROTACs; D.M.H. performed the EM analysis, A.M. the crystallographic analysis; S.J., J.L., K.F., K.S., and L.v.G. prepared bacterial strains and carried out the analyses in bacteria; D.M.H., S.J., D.P., F.K., and M.H. performed the mass spectrometry analysis; T.C., G.B., U.K., and H.W. co-coordinated the research collaborations between Boehringer Ingelheim, IMP, and Saarland University; T.C. coordinated the research project and prepared the manuscript together with D.M.H. and S.J., with input from all authors.

DECLARATION OF INTERESTS

K.F., V.M.S., K.R., H.W., and G.B. were employees of Boehringer Ingelheim at the time of this work.

Received: October 11, 2022
Revised: February 24, 2023
Accepted: April 5, 2023
Published: May 2, 2023

REFERENCES

1. Hutchings, M.I., Truman, A.W., and Wilkinson, B. (2019). Antibiotics: past, present and future. Curr. Opin. Microbiol. *51*, 72–80. https://doi.org/10.1016/j.mib.2019.10.008.
2. Lewis, K. (2020). The science of antibiotic discovery. Cell *181*, 29–45. https://doi.org/10.1016/j.cell.2020.02.056.
3. Allué-Guardia, A., García, J.I., and Torrelles, J.B. (2021). Evolution of drug-resistant Mycobacterium tuberculosis Strains and Their adaptation to the human lung environment. Front. Microbiol. *12*, 612675. https://doi.org/10.3389/fmicb.2021.612675.
4. Cheesman, M.J., Ilanko, A., Blonk, B., and Cock, I.E. (2017). Developing new antimicrobial therapies: are synergistic combinations of plant extracts/compounds with conventional antibiotics the solution? Pharmacogn. Rev. *11*, 57–72. https://doi.org/10.4103/phrev.phrev_21_17.
5. Igarashi, M., Ishizaki, Y., and Takahashi, Y. (2017). New antituberculous drugs derived from natural products: current perspectives and issues in antituberculous drug development. J. Antibiot. (Tokyo) *71*, 15–25. https://doi.org/10.1038/ja.2017.126.
6. Miethke, M., Pieroni, M., Weber, T., Brönstrup, M., Hammann, P., Halby, L., Arimondo, P.B., Glaser, P., Aigle, B., Bode, H.B., et al. (2021). Towards the sustainable discovery and development of new antibiotics. Nat. Rev. Chem. *5*, 726–749. https://doi.org/10.1038/s41570-021-00313-1.
7. Song, W.M., Zhao, J.Y., Zhang, Q.Y., Liu, S.Q., Zhu, X.H., An, Q.Q., Xu, T.T., Li, S.J., Liu, J.Y., Tao, N.N., et al. (2021). COVID-19 and tuberculosis coinfection: an overview of case reports/case series and meta-analysis. Front. Med. (Lausanne) *8*, 657006. https://doi.org/10.3389/fmed.2021.657006.
8. Leodolter, J., Warweg, J., and Weber-Ban, E. (2015). The Mycobacterium tuberculosis ClpP1P2 protease interacts asymmetrically with its ATPase partners ClpX and ClpC1. PLoS One *10*, e0125345. https://doi.org/10.1371/journal.pone.0125345.
9. Schmitz, K.R., and Sauer, R.T. (2014). Substrate delivery by the AAA+ ClpX and ClpC1 unfoldases activates the mycobacterial ClpP1P2 peptidase. Mol. Microbiol. *93*, 617–628. https://doi.org/10.1111/mmi.12694.
10. Trentini, D.B., Suskiewicz, M.J., Heuck, A., Kurzbauer, R., Deszcz, L., Mechtler, K., and Clausen, T. (2016). Arginine phosphorylation marks proteins for degradation by a Clp protease. Nature *539*, 48–53. https://doi.org/10.1038/nature20122.
11. Alhuwaider, A.A.H., and Dougan, D.A. (2017). AAA+ machines of protein destruction in mycobacteria. Front. Mol. Biosci. *4*, 49. https://doi.org/10.3389/fmolb.2017.00049.
12. Sauer, R.T., and Baker, T.A. (2011). AAA+ proteases: ATP-fueled machines of protein destruction. Annu. Rev. Biochem. *80*, 587–612. https://doi.org/10.1146/annurev-biochem-060408-172623.
13. Raju, R.M., Goldberg, A.L., and Rubin, E.J. (2012). Bacterial proteolytic complexes as therapeutic targets. Nat. Rev. Drug Discov. *11*, 777–789. https://doi.org/10.1038/nrd3846.
14. Gao, W., Kim, J.Y., Anderson, J.R., Akopian, T., Hong, S., Jin, Y.Y., Kandror, O., Kim, J.W., Lee, I.A., Lee, S.Y., et al. (2015). The cyclic peptide ecumicin targeting CLpC1 is active against Mycobacterium tuberculosis in vivo. Antimicrob. Agents Chemother. *59*, 880–889. https://doi.org/10.1128/AAC.04054-14.
15. Gavrish, E., Sit, C.S., Cao, S., Kandror, O., Spoering, A., Peoples, A., Ling, L., Fetterman, A., Hughes, D., Bissell, A., et al. (2014). Lassomycin, a ribosomally synthesized cyclic peptide, kills mycobacterium tuberculosis by targeting the ATP-dependent protease ClpC1P1P2. Chem. Biol. *21*, 509–518. https://doi.org/10.1016/j.chembiol.2014.01.014.
16. Zhang, S., Chen, J., Shi, W., Cui, P., Zhang, J., Cho, S., Zhang, W., and Zhang, Y. (2017). Mutation in clpC1 encoding an ATP-dependent ATPase involved in protein degradation is associated with pyrazinamide resistance in Mycobacterium tuberculosis. Emerg. Microbes Infect. *6*, e8. https://doi.org/10.1038/emi.2017.1.
17. Lupoli, T.J., Vaubourgeix, J., Burns-Huang, K., and Gold, B. (2018). Targeting the proteostasis network for mycobacterial drug discovery. ACS Infect. Dis. *4*, 478–498. https://doi.org/10.1021/acsinfecdis.7b00231.
18. Schmitt, E.K., Riwanto, M., Sambandamurthy, V., Roggo, S., Miault, C., Zwingelstein, C., Krastel, P., Noble, C., Beer, D., Rao, S.P., et al. (2011). The natural product cyclomarin kills Mycobacterium tuberculosis by targeting the ClpC1 subunit of the caseinolytic protease. Angew. Chem. Int. Ed. Engl. *50*, 5889–5891. https://doi.org/10.1002/anie.201101740.
19. Hawkins, P.M.E., Hoi, D.M., Cheung, C.Y., Wang, T., Quan, D., Sasi, V.M., Liu, D.Y., Linington, R.G., Jackson, C.J., Oehlers, S.H., et al. (2022). Potent bactericidal antimycobacterials targeting the chaperone ClpC1 based on the depsipeptide natural products ecumicin and Ohmyungsamycin A. J. Med. Chem. *65*, 4893–4908. https://doi.org/10.1021/acs.jmedchem.1c02122.
20. Brötz-Oesterhelt, H., Beyer, D., Kroll, H.P., Endermann, R., Ladel, C., Schroeder, W., Hinzen, B., Raddatz, S., Paulsen, H., Henninger, K., et al. (2005). Dysregulation of bacterial proteolytic machinery by a new class of antibiotics. Nat. Med. *11*, 1082–1087. https://doi.org/10.1038/nm1306.
21. Lee, B.G., Park, E.Y., Lee, K.E., Jeon, H., Sung, K.H., Paulsen, H., Rübsamen-Schaeff, H., Brötz-Oesterhelt, H., and Song, H.K. (2010). Structures of ClpP in complex with acyldepsipeptide antibiotics reveal its activation mechanism. Nat. Struct. Mol. Biol. *17*, 471–478. https://doi.org/10.1038/nsmb.1787.
22. Cobongela, S.Z.Z., Makatini, M.M., Mdluli, P.S., and Sibuyi, N.R.S. (2022). Acyldepsipeptide analogues: a future generation antibiotics for

tuberculosis treatment. Pharmaceutics *14*. https://doi.org/10.3390/pharmaceutics14091956.

23. Kazmaier, U., and Junk, L. (2021). Recent developments on the synthesis and bioactivity of ilamycins/rufomycins and cyclomarins, marine cyclopeptides that demonstrate anti-malaria and anti-tuberculosis activity. Mar. Drugs *19*. https://doi.org/10.3390/md19080446.
24. Vasudevan, D., Rao, S.P., and Noble, C.G. (2013). Structural basis of mycobacterial inhibition by cyclomarin A. J. Biol. Chem. *288*, 30883–30891. https://doi.org/10.1074/jbc.M113.493767.
25. Wolf, N.M., Lee, H., Zagal, D., Nam, J.W., Oh, D.C., Lee, H., Suh, J.W., Pauli, G.F., Cho, S., and Abad-Zapatero, C. (2020). Structure of the N-terminal domain of ClpC1 in complex with the antituberculosis natural product ecumicin reveals unique binding interactions. Acta Crystallogr. D Struct. Biol. *76*, 458–471. https://doi.org/10.1107/S2059798320004027.
26. Morreale, F.E., Kleine, S., Leodolter, J., Junker, S., Hoi, D.M., Ovchinnikov, S., Okun, A., Kley, J., Kurzbauer, R., Junk, L., et al. (2022). BacPROTACs mediate targeted protein degradation in bacteria. Cell *185*, 2338–2353. e18. https://doi.org/10.1016/j.cell.2022.05.009.
27. Maurer, M., Linder, D., Franke, K.B., Jäger, J., Taylor, G., Gloge, F., Gremer, S., Le Breton, L., Mayer, M.P., Weber-Ban, E., et al. (2019). Toxic activation of an AAA+ protease by the antibacterial drug cyclomarin A. Cell Chem. Biol. *26*, 1169–1179.e4. https://doi.org/10.1016/j.chembiol.2019.05.008.
28. Barbie, P., and Kazmaier, U. (2016). Total synthesis of cyclomarin A, a marine cycloheptapeptide with anti-tuberculosis and anti-malaria activity. Org. Lett. *18*, 204–207. https://doi.org/10.1021/acs.orglett.5b03292.
29. Junk, L., Schmiedel, V.M., Guha, S., Greb, P., Fischel, K., Rumpel, K., Kaur, P., Krishnamurthy, R.V., Narayanan, S., Kofink, C., et al. (2022). BacPROTAC-induced degradation of ClpC1 presents a novel anti-mycobacterial concept https://doi.org/10.26434/chemrxiv-2022-8hnrh.
30. Taylor, G., Frommherz, Y., Katikaridis, P., Layer, D., Sinning, I., Carroni, M., Weber-Ban, E., and Mogk, A. (2022). Antibacterial peptide CyclomarinA creates toxicity by deregulating the Mycobacterium tuberculosis ClpC1–ClpP1P2 protease. J. Biol. Chem. *298*, 102202. https://doi.org/10.1016/j.jbc.2022.102202.
31. Lo, J.H., Baker, T.A., and Sauer, R.T. (2001). Characterization of the N-terminal repeat domain of Escherichia coli ClpA—a class I Clp/HSP100 ATPase. Protein Sci. *10*, 551–559. https://doi.org/10.1110/ps.41401.
32. Hajdusits, B., Suskiewicz, M.J., Hundt, N., Meinhart, A., Kurzbauer, R., Leodolter, J., Kukura, P., and Clausen, T. (2021). Mcsb forms a gated kinase chamber to mark aberrant bacterial proteins for degradation. eLife *10*, 1–24. https://doi.org/10.7554/eLife.63505.
33. Suskiewicz, M.J., Hajdusits, B., Beveridge, R., Heuck, A., Vu, L.D., Kurzbauer, R., Hauer, K., Thoeny, V., Rumpel, K., Mechtler, K., et al. (2019). Structure of McsB, a protein kinase for regulated arginine phosphorylation. Nat. Chem. Biol. *15*, 510–518. https://doi.org/10.1038/s41589-019-0265-y.
34. Ogbonna, E.C., and Schmitz, K.R. (2021). Identification of diverse targets of arginine phosphorylation in Mycolicibacterium smegmatis by shotgun proteomics https://doi.org/10.1101/2021.04.05.438432.
35. Jumper, J., Evans, R., Pritzel, A., Green, T., Figurnov, M., Ronneberger, O., Tunyasuvunakool, K., Bates, R., Žídek, A., Potapenko, A., et al. (2021). Highly accurate protein structure prediction with AlphaFold. Nature *596*, 583–589. https://doi.org/10.1038/s41586-021-03819-2.
36. Harari, A., Zoltsman, G., Levin, T., and Rosenzweig, R. (2022). Hsp104 N-terminal domain interaction with substrates plays a regulatory role in protein disaggregation. FEBS Journal *289*, 5359–5377. https://doi.org/10.1111/febs.16441.
37. Lunge, A., Gupta, R., Choudhary, E., and Agarwal, N. (2020). The unfoldase ClpC1 of Mycobacterium tuberculosis regulates the expression of a distinct subset of proteins having intrinsically disordered termini. J. Biol. Chem. *295*, 9455–9473. https://doi.org/10.1074/jbc.RA120.013456.
38. Maniaci, C., Hughes, S.J., Testa, A., Chen, W., Lamont, D.J., Rocha, S., Alessi, D.R., Romeo, R., and Ciulli, A. (2017). Homo-PROTACs: bivalent small-molecule dimerizers of the VHL E3 ubiquitin ligase to induce self-degradation. Nat. Commun. *8*, 830. https://doi.org/10.1038/s41467-017-00954-1.
39. Domenech, P., and Reed, M.B. (2009). Rapid and spontaneous loss of phthiocerol dimycocerosate (PDIM) from Mycobacterium tuberculosis grown in vitro: implications for virulence studies. Microbiology (Reading) *155*, 3532–3543. https://doi.org/10.1099/mic.0.029199-0.
40. Andries, K., Verhasselt, P., Guillemont, J., Göhlmann, H.W., Neefs, J.M., Winkler, H., Van Gestel, J., Timmerman, P., Zhu, M., Lee, E., et al. (2005). A diarylquinoline drug active on the ATP synthase of Mycobacterium tuberculosis. Science *307*, 223–227. https://doi.org/10.1126/science.1106753.
41. Gengenbacher, M., Rao, S.P.S., Pethe, K., and Dick, T. (2010). Nutrient-starved, non-replicating Mycobacterium tuberculosis requires respiration, ATP synthase and isocitrate lyase for maintenance of ATP homeostasis and viability. Microbiology (Reading) *156*, 81–87. https://doi.org/10.1099/mic.0.033084-0.
42. Nguyen, T.V.A., Anthony, R.M., Bañuls, A.L., Nguyen, T.V.A., Vu, D.H., and Alffenaar, J.-W.C. (2018). Bedaquiline resistance: its emergence, mechanism, and prevention. Clin. Infect. Dis. *66*, 1625–1630. https://doi.org/10.1093/cid/cix992.
43. Mabhula, A., and Singh, V. (2019). Drug-resistance in Mycobacterium tuberculosis: where we Stand. MedChemComm *10*, 1342–1360. https://doi.org/10.1039/c9md00057g.
44. Ioerger, T.R., Feng, Y., Ganesula, K., Chen, X., Dobos, K.M., Fortune, S., Jacobs, W.R., Mizrahi, V., Parish, T., Rubin, E., et al. (2010). Variation among genome sequences of H37Rv strains of Mycobacterium tuberculosis from multiple laboratories. J. Bacteriol. *192*, 3645–3653. https://doi.org/10.1128/JB.00166-10.
45. Jain, P., Hsu, T., Arai, M., Biermann, K., Thaler, D.S., Nguyen, A., González, P.A., Tufariello, J.M., Kriakov, J., Chen, B., et al. (2014). Specialized transduction designed for precise high-throughput unmarked deletions in Mycobacterium tuberculosis. mBio *5*. e01245-14. https://doi.org/10.1128/mBio.01245-14.
46. Kiefer, A., Bader, C.D., Held, J., Esser, A., Rybniker, J., Empting, M., Müller, R., and Kazmaier, U. (2019). Synthesis of new cyclomarin derivatives and their biological evaluation towards Mycobacterium tuberculosis and Plasmodium falciparum. Chemistry *25*, 8894–8902. https://doi.org/10.1002/chem.201901640.
47. Beckham, K.S.H., Staack, S., Wilmanns, M., and Parret, A.H.A. (2020). The pMy vector series: a versatile cloning platform for the recombinant production of mycobacterial proteins in Mycobacterium smegmatis. Protein Sci. *29*, 2528–2537. https://doi.org/10.1002/pro.3962.
48. Parish, T., and Stoker, N.G. (2000). Use of a flexible cassette method to generate a double unmarked Mycobacterium tuberculosis tlyA plcABC mutant by gene replacement. Microbiology (Reading) *146*, 1969–1975. https://doi.org/10.1099/00221287-146-8-1969.
49. Neuhold, J., Radakovics, K., Lehner, A., Weissmann, F., Garcia, M.Q., Romero, M.C., Berrow, N.S., and Stolt-Bergner, P. (2020). GoldenBac: a simple, highly efficient, and widely applicable system for construction of multi-gene expression vectors for use with the baculovirus expression vector system. BMC Biotechnol. *20*, 26. https://doi.org/10.1186/s12896-020-00616-z.
50. Varadi, M., Anyango, S., Deshpande, M., Nair, S., Natassia, C., Yordanova, G., Yuan, D., Stroe, O., Wood, G., Laydon, A., et al. (2021). AlphaFold Protein Structure Database: massively expanding the structural coverage of protein-sequence space with high-accuracy models. Nucleic Acids Research *50*, D439–D444. https://doi.org/10.1093/nar/gkab1061.
51. Goddard, T.D., Huang, C.C., Meng, E.C., Pettersen, E.F., Couch, G.S., and Morris, J.H. (2018). UCSF ChimeraX: Meeting modern challenges in visualization and analysis. Protein Sci *27*, 14–25. https://doi.org/10.1002/pro.3235.

52. Emsley, P., Lohkamp, B., Scott, W.G., and Cowtan, K. (2010). Features and development of coot. Acta Crystallogr. D Biol. Crystallogr. *66*, 486–501. https://doi.org/10.1107/S0907444910007493.

53. Cox, J., Neuhauser, N., Michalski, A., Scheltema, R.A., and Olsen, J.V. (2011). Andromeda: a peptide search engine integrated into the MaxQuant environment. J Proteome Res *10*, 1794–1805. https://doi.org/10.1021/pr101065j.

54. Tyanova, S., Temu, T., Sinitcyn, P., Carlson, A., Hein, M.Y., Geiger, T., Mann, M., and Cox, J. (2016). The Perseus computational platform for comprehensive analysis of (prote)omics data. Nat. Methods *13*, 731–740. https://doi.org/10.1038/nmeth.3901.

55. Dorfer, V., Pichler, P., Stranzl, T., Stadlmann, J., Taus, T., Winkler, S., and Mechtler, K. (2014). MS Amanda, a universal identification algorithm optimized for high accuracy tandem mass spectra. J. Proteome Res. *13*, 3679–3684. https://doi.org/10.1021/pr500202e.

56. Käll, L., Canterbury, J.D., Weston, J., and Noble, W.S. (2007). Semi-supervised learning for peptide identification from shotgun proteomics datasets. Nat Methods *4*, 923–925. https://doi.org/10.1038/nmeth1113.

57. Afonine, P.V., Poon, B.K., Read, R.J., Sobolev, O.V., Terwilliger, T.C., and Urzhumtsev, A. (2018). Real-space refinement in PHENIX for cryo-EM and crystallography. Acta Crystallogr D Struct Biol *74*, 531–544. https://doi.org/10.1107/s2059798318006551.

58. Liebschner, D., Afonine, P.V., Baker, M.L., Bunkóczi, G., Chen, V.B., Croll, T.I., Hintze, B., Hung, L.W., Jain, S., McCoy, A.J., et al. (2019). Macromolecular structure determination using X-rays, neutrons and electrons: recent developments in Phenix. Acta Crystallogr. D Struct. Biol. *75*, 861–877. https://doi.org/10.1107/S2059798319011471.

59. Williams, C.J., Headd, J.J., Moriarty, N.W., Prisant, M.G., Videau, L.L., Deis, L.N., Verma, V., Keedy, D.A., Hintze, B.J., Chen, V.B., et al. (2018). MolProbity: more and better reference data for improved all-atom structure validation. Protein Sci. *27*, 293–315. https://doi.org/10.1002/pro.3330.

60. Kendall, S.L., and Frita, R. (2009). Construction of targeted mycobacterial mutants by homologous recombination. Methods Mol. Biol. *465*, 297–310. https://doi.org/10.1007/978-1-59745-207-6_20.

61. Belisle, J.T., Mahaffey, S.B., and Hill, P.J. (2009). Isolation of mycobacterium species genomic DNA. Methods Mol. Biol. *465*, 1–12. https://doi.org/10.1007/978-1-59745-207-6_1.

62. Goude, R., and Parish, T. (2008). Electroporation of mycobacteria. J. Vis. Exp., 761.

63. Schrodinger, LLC (2015). PhysiologyMOL molecular graphics system, version 1.8.

64. Hughes, C.S., Moggridge, S., Müller, T., Sorensen, P.H., Morin, G.B., and Krijgsveld, J. (2019). Single-pot, solid-phase-enhanced sample preparation for proteomics experiments. Nat. Protoc. *14*, 68–85. https://doi.org/10.1038/s41596-018-0082-x.

65. The, M., MacCoss, M.J., Noble, W.S., and Käll, L. (2016). Fast and accurate protein false discovery rates on large-scale proteomics data sets with Percolator 3.0. J. Am. Soc. Mass Spectrom. *27*, 1719–1727. https://doi.org/10.1007/s13361-016-1460-7.

66. Perez-Riverol, Y., Csordas, A., Bai, J., Bernal-Llinares, M., Hewapathirana, S., Kundu, D.J., Inuganti, A., Griss, J., Mayer, G., Eisenacher, M., et al. (2019). The PRIDE database and related tools and resources in 2019: improving support for quantification data. Nucleic Acids Res. *47*, D442–D450. https://doi.org/10.1093/nar/gky1106.

67. Sharma, V., Eckels, J., Schilling, B., Ludwig, C., Jaffe, J.D., MacCoss, M.J., and MacLean, B. (2018). Panorama public: a public repository for quantitative data sets processed in Skyline. Mol. Cell. Proteomics *17*, 1239–1244. https://doi.org/10.1074/mcp.RA117.000543.

68. Zweerink, S., Kallnik, V., Ninck, S., Nickel, S., Verheyen, J., Blum, M., Wagner, A., Feldmann, I., Sickmann, A., Albers, S.V., et al. (2017). Activity-based protein profiling as a robust method for enzyme identification and screening in extremophilic Archaea. Nat. Commun. *8*, 15352. https://doi.org/10.1038/ncomms15352.

69. Rehberg, N., Akone, H.S., Ioerger, T.R., Erlenkamp, G., Daletos, G., Gohlke, H., Proksch, P., and Kalscheuer, R. (2018). Chlorflavonin targets acetohydroxyacid synthase catalytic subunit IlvB1 for synergistic killing of Mycobacterium tuberculosis. ACS Infect. Dis. *4*, 123–134. https://doi.org/10.1021/acsinfecdis.7b00055.

5.2 Supporting Information

Cell
Article

CellPress
OPEN ACCESS

STAR★METHODS

KEY RESOURCES TABLE

REAGENT or RESOURCE	SOURCE	IDENTIFIER
Bacterial and virus strains		
M. smegmatis mc^2-155	ATCC	ATCC 700084
M. smegmatis mc^2 155 ΔclpC2::gmR	This paper	N/A
M. smegmatis mc^2 155 ΔclpC3::gmR	This paper	N/A
M. smegmatis mc^2 155 ΔΔclpC2clpC3::gmR	This paper	N/A
M. smegmatis 607	DSMZ	ATCC 607, DSM 43465
M. tuberculosis H37Rv	William R. Jacobs Jr., Albert Einstein College of Medicine	H37RvMa (Ioerger et al.[44])
M. tuberculosis H37Rv ΔclpC2::hygR	This paper	N/A
ΦphAE159	Jain et al.[45]	N/A
Chemicals, peptides, and recombinant proteins		
M. smegmatis ClpC1	Morreale et al.[26]	N/A
M. smegmatis $ClpC1^{DWB}$	This paper	N/A
M. smegmatis $ClpC1^{DWB\text{-}F444A}$	This paper	N/A
M. smegmatis ClpC1 NTD (1–148)	Morreale et al.[26]	N/A
M. smegmatis ClpP1 with his-tag	Morreale et al.[26]	N/A
M. smegmatis ClpP2 with his-tag	Morreale et al.[26]	N/A
M. smegmatis ClpC2 with his-tag	This paper	N/A
M. smegmatis $ClpC2^{CRD}$ with his-tag	This paper	N/A
M. smegmatis ClpC3 with his-tag	This paper	N/A
$BRDT_{BD1}$-NrdI	Morreale et al.[26]	N/A
α-casein	Sigma-Aldrich	Cat#C6780-5G
β-casein	Sigma-Aldrich	Cat#C6905-1G
Pyruvate kinase	Sigma-Aldrich	Cat#9136-5KU
Lactic dehydrogenase	Sigma-Aldrich	Cat#1254-5KU
NADH	Roche	10128023001
Phosphoenolpyruvate	Sigma-Aldrich	Cat#860077-1G
pArg-JQ1	This paper	N/A
dCym-JQ1	This paper	N/A
Homo-BacPROTAC6	Junk et al.[29]	N/A
Homo-BacPROTAC6dis	Junk et al.[29]	N/A
dCym6	Junk et al.[29]	N/A
dCym6dis	Junk et al.[29]	N/A
Homo-BacPROTAC7	Junk et al.[29]	N/A
Homo-BacPROTAC7dis	Junk et al. [29]	N/A
dCym7	Junk et al.[29]	N/A
dCym7dis	Junk et al.[29]	N/A
dCym	Barbie and Kazmaier[28]	N/A
dCymM	Kiefer et al.[46]	N/A
Ecu* (analogue 6)	Hawkins et al.[19]	N/A
Ecu**	This paper	N/A
LVAWG peptide	This paper	N/A
TCEP	Sigma-Aldrich	Cat#C4706-10G
Tween80	Sigma-Aldrich	Cat# P1754-500ML
Tween20	Sigma-Aldrich	Cat#P9416-100ML

(Continued on next page)

Continued

REAGENT or RESOURCE	SOURCE	IDENTIFIER
Streptavidin	Prospec	
cOmplete, EDTA-free Protease inhibitor cocktail	Roche	05056489001
Trypsin	Promega	V5280
BXT buffer	Iba lifescience	Cat#2-1042-025
Trifluoroacetic Acid	Fisher Scientific	Cat#11378277
Acetonitrile	Merck	Cat#113212
Formic acid	Sigma-Aldrich	27001-1L-M
Iodacetamide	Sigma-Aldrich	Cat#L6125-25G
Bedaquiline	MedChemExpress	HY-14881
Ethambutol	Sigma-Aldrich	E4630
SDC	Sigma-Aldrich	Cat#30970-100G
Middlebrook 7H9 Broth Base	Sigma-Aldrich	M0178-500G
BD Difco Middlebrook 7H10 Agar	Fisher Scientific	DF0627-17-4
HBS-P+ buffer 10x	Cytiva	Cat#BR100671
Critical commercial assays		
High Sensitivity DNA Kit	Agilent Technologies, Inc.	Cat#5067-4626
TruePrep DNA Library Prep Kit V2 for Illumina	Vazyme Biotech Co.	Cat#TD501
EZ-Link™ NHS-PEG4 Biotinylation Kit	Thermo Fisher Scientific	Cat#21455
Amine-coupling kit	Cytiva	Cat#BR100050
Deposited data		
Msm $ClpC2_{CRD}$:pArg Crystal Structure	This paper and Protein Data Bank (PDB)	8B9O
Mtb $ClpC1_{NTD}$:Ecu** Crystal Structure	This paper and Protein Data Bank (PDB)	8B9U
Msm IP-MS proteomics Data of ClpC2 interactome	This paper and PRoteomics IDentification Database	PXD037231
Msm LFQ proteomics Data of dCym/Ecu* treatment (10 μM)	This paper and PRoteomics IDentification Database	PXD037232
Msm LFQ proteomics Data of dCym treatment (150 μM)	This paper and PRoteomics IDentification Database	PXD037234
Msm LFQ proteomics Data of BacPROTAC treatment	This paper and PRoteomics IDentification Database	PXD037235
Msm MS-PRM Data	This paper, PanoramaWeb and PRoteomics IDentification Database	PXD037198
Mtb IP-MS proteomics Data of dCym derivative targets	This paper and PRoteomics IDentification Database	PXD037712
Mtb LFQ proteomics Data of BacPROTAC treatment	This paper and PRoteomics IDentification Database	PXD037730
Oligonucleotides		
Primers for generation of *M. smegmatis* genomic mutants, see Table S5	This paper	N/A
Primers for generation of *M. tuberculosis ΔclpC2*, see Table S5	This paper	N/A
Primers for construction of plasmids for inducible expression in mycobacteria, see Table S5	This paper	N/A
Recombinant DNA		
pET-21a (+) plasmid	Addgene	https://www.addgene.org/
pMyC plasmid	Beckham et al.[47]	RRID:Addgene_42192
p2NIL plasmid	Parish and Stoker[48]	RRID:Addgene_20188

(*Continued on next page*)

Continued

REAGENT or RESOURCE	SOURCE	IDENTIFIER
pGOAL19 plasmid	Parish and Stoker[48]	RRID:Addgene_20190
p0004S	Jain et al.[45]	N/A
pGB-Dest	Neuhold et al.[49]	N/A
Software and algorithms		
AlphaFold	Jumper et al.[35], Varadi et al., 2022[50]	N/A
UCSF Chimera-X	Goddard et al., 2018[51]	https://www.cgl.ucsf.edu/chimerax/
PyMol	The PyMOL Molecular Graphics System, Version 2.0 Schrödinger, LLC	https://pymol.org/2/ (Continued)
Coot	Emsley et al.[52]	https://www2.mrc-lmb.cam.ac.uk/personal/pemsley/coot/
Python 3	Python	https://www.python.org/
RStudio	RStudio	https://www.rstudio.com/
Proteome Discoverer 2.5	Thermo Fisher Scientific	N/A
MaxQuant 2.1	Cox et al., 2011[53]	https://www.maxquant.org/maxquant/
Perseus 1.6	Tyanova et al.[54]	https://www.maxquant.org/perseus/
Cassiopeia	N/A	https://github.com/moritzmadern/Cassiopeia_LFQ
MS Amanda	Dorfer et al.[55]	https://ms.imp.ac.at/
Percolator	Kall et al., 2007[56]	N/A
Biacore Insight Evaluation	N/A	N/A
Geneious	N/A	https://www.geneious.com/
Phenix	Afonine et al., 2018[57], Liebschner et al.[58]	https://phenix-online.org/
MolProbity	Williams et al.[59]	http://molprobity.biochem.duke.edu/ N/A
Prism	GraphPad	https://www.graphpad.com/scientific-software/prism
Other		
Cu/Pd Hexagonal 400 mesh grids	Agar	Cat#AGG2440PD
Nunc™ MicroWell™ 96-Well, Nunclon Delta- Treated, Flat-Bottom Microplate	Fisher Scientific	Cat#167008
U-shaped 96-well glass-coated microplates	Fisher Scientific	Cat#60180-P300
flat 96-well plates Thermo Nunc Microwell	Sigma-Aldrich Fisher	Cat#P8366-50EA
U-shaped 96-well glass-coated microplates Sera-Mag	Fisher Scientific	Cat#60180-P306
Sera-Mag SpeedBeads, variant 1	Cytvia	Cat#45152105050250
Sera-Mag SpeedBeads, variant 2	Cytvia	Cat#65152105050250
PepSwift Monolithic RSLC column	Thermo Fisher Scientific	Cat#164542
XBridge Peptide BEH C18 Column Acclaim	Waters	Cat#186003613
Acclaim PepMap C-18 precolumn	Thermo Fisher Scientific	Cat#160454
Acclaim PepMap C-18 column	Thermo Fisher Scientific	Cat#164942
Eclipse XDB-C18 (5 mm)	Agilent	Cat#990967-902
Pierce™ Avidin Agarose beads	Thermo Fisher Scientific	Cat#20219
Glass microfiber tips	GE Healthcare	Cat#1822-024
Strep-Tactin® Sepharose® resin	Iba lifescience	Cat#2-1201-025
Series S Sensor chip CM5	Cytiva	Cat#29149603
Series S Sensor chip NTA	Cytiva	Cat#BR100532
Zeba™ Spin Desalting Columns, Plates, and Cartridges, 7K MWCO, 0.5–100 mL	Thermo Fisher Scientific	Cat#89882

CellPress
OPEN ACCESS

Cell
Article

RESOURCE AVAILABILITY

Lead contact

Further information and requests for resources and reagents should be directed to and will be fulfilled by the lead contact, Tim Clausen (tim.clausen@imp.ac.at).

Materials availability

All unique materials and reagents generated in this study are available from the lead contact with a completed material transfer agreement. There are restrictions to the availability of the generated BacPROTAC probes and simplified cyclomarin analogues generated in this study due to a limited stock. Reasonable aliquots of the compounds are available until stocks run out from the lead contact with a completed material transfer agreement.

Data and code availability

Coordinates of the $ClpC2_{CRD}$:pArg and the $ClpC1_{NTD}$:Ecu^{**} crystal structures have been deposited at the Protein Data Bank (PDBe) under the accession codes 8B9O and 8B9U. The mass spectrometry proteomics data have been deposited to the ProteomeXchange Consortium via the PRIDE partner repository with the dataset identifier PXD037231, PXD037232, PXD037234, PXD037235, PXD037712 and PXD037730. PRM data has been submitted to PRIDE as well as to PanoramaWeb (PXD037198). The paper does not report original code. Any additional information required to reanalyze the data reported in this paper is available from the lead contact upon request.

EXPERIMENTAL MODEL AND SUBJECT DETAILS

M. smegmatis mc^2-155 (ATCC 7000084) was directly purchased from ATCC and freshly inoculated from glycerol stock. *M. smegmatis* strain ATCC 607 was purchased from DSMZ (DSM 43465) and freshly inoculated from a plate. *M. tuberculosis* H37Rv was obtained from William R. Jacobs Jr. (Albert Einstein College of Medicine) and freshly inoculated from glycerol stock. The genomic knockout strains of *M. smegmatis* mc^2 155 *ΔclpC2::gmR*, *ΔclpC3::gmR*, and *ΔΔclpC2clpC3::gmR* were obtained after homologous recombination using the p2NIL/pGOAL[48] (Addgene plasmid #20188; https://www.addgene.org/20188/; RRID:Addgene_20188 and Addgene plasmid #20190; https://www.addgene.org/20190/; RRID:Addgene_20190) system adapted from Kendall et al[60] as described below and apart from the site of recombination can be considered isogenic to the parental strain. *M. tuberculosis ΔclpC2::hygR* was obtained via specialized phage transduction and apart from the site of integration can be considered isogenic to the parental strain.

Liquid cultures of all strains of *M. smegmatis* mc^2 155 were inoculated with 5 μl of a glycerol stock (OD_{600} 0.5) into in Middlebrook 7H9 medium (Sigma) supplemented with 0.2% (v/v) glycerol and 0.025% (v/v) Tween80 (Sigma) and respective antibiotics if applicable. That is, *M. smegmatis* transformed with the respective pMyC vectors were additionally supplemented with 50 μg/ml Hygromycin and 1 μg/ml Gentamicin was added for the knockout mutants. Constant agitation at 37 °C was applied and main cultures were inoculated out of exponential growing overnight cultures. If applicable, ectopic expression was induced with 0.1% (w/v) acetamide. Cells were harvested by centrifugation (3,000 x g, 5 min, 25 °C) and processed according to the respective experiment. *M. smegmatis* strain ATCC 607 was cultivated as described above except that the medium was supplemented with 0.1% (v/v) glycerol. Solidified medium was prepared using Middlebrook 7H10 agar (Difco) supplemented with 0.5% (v/v) glycerol. MIC assay plates for overexpression strains were supplemented with 0.1% (w/v) acetamide and 50 μg/ml Hygromycin. All plates were incubated for 2.5-5 days at 37 °C. *M. tuberculosis* was grown aerobically at 37 °C in Middlebrook 7H9 liquid media supplemented with 10% DS (2% (w/v) glucose; 0.085% (w/v) sodium chloride), 0.5% (v/v) glycerol and 0.025% (v/v) Tween 80. Solidified medium for *Mtb* was supplemented with 10% ADS (5% (w/v) bovine serum albumin; 2% (w/v) glucose; 0.085% (w/v) sodium chloride) and 0.5% (v/v) glycerol. For the *ΔclpC2* gene deletion mutant, hygromycin was added to a final concentration of 50 μg/ml.

METHOD DETAILS

Isolation of chromosomal DNA

Mycobacterial chromosomal DNA was isolated using an adapted protocol derived from Belisle et al.[61] In short, exponentially growing cells of *M. smegmatis* mc^2 155 were harvested at OD 1.5 by centrifugation for 15 min, 3000 x g, 4 °C. Cells were subsequently washed with TE (10 mM Tris/HCl, pH 8.0, 1 mM EDTA) and the final cell pellet was weighed resulting in 600 mg wet weight. To initiate the isolation, cells were frozen overnight at -80 °C. Subsequently, the thawed pellet was dissolved in 500 μl TE and incubated for 60 minutes with equal volumes of Chloroform:methanol (2:1) (20 °C, 600 rpm shaking with Thermo rocker). Aqueous and organic phase were separated at 2,500 x g for 20 minutes and both phases were carefully removed by pipetting before the tube was dried at 55 °C for 15 min. 375 μl TE were added and the suspension was rigorously dissolved by vortexing. pH was increased to 9.0 and lysis was initiated by adding 0.01 x vol lysozyme (sigma) and incubation at 37 °C for 12 hours. Interfering proteins were handled by adding 0.2 x vol 10% SDS, 0.02 x vol Proteinase K (VWR) and incubation for six hours at 55 °C. Extraction of DNA was performed at room temperature and started by adding an equal volume of phenol/chloroform/isoamylalcohol (25:24:1) for 30 minutes. The

aqueous layer was transferred into a new tube and phenol was washed out by adding an equal volume of chloroform:isoamyl alcohol (24:1) for ten minutes and subsequent centrifugation for 30 min, 12000 x g. To remove waxy polar lipids and to precipitate the DNA, 0.1 x vol 3 M sodium acetate pH 5.2 and 1 x vol isopropanol were added to the clean aqueous phase. The suspension was incubated for 60 minutes at 4 °C before the DNA was fished and winded up with a pipet tip to transfer it into a new tube. Subsequently, the DNA was washed with ice cold (-20 °C) ethanol, centrifuged and ethanol was left to evaporate. Finally, the DNA was dissolved in 100 µl nuclease free water and concentration was measured with DeNovix DS-11 FX+ Spectrophotometer, at the same time checking sufficient purity of the DNA with 260/280 and 260/230 ratio. This procedure resulted in 1.2 µg/µl DNA which was used as template for PCR.

Construction of mycobacterial mutants

The genomic knockout strains of *M. smegmatis* mc^2 155 *ΔclpC2::gmR*, *ΔclpC3::gmR*, and *ΔΔclpC2clpC3::gmR* were constructed via homologous recombination using the p2NIL/pGOAL system adapted from.[60] Briefly, a fusion product, which consists of (i) upstream *clpC2* or *clpC3* homologous region, amplified from freshly isolated mycobacterial chromosomal DNA (mycobacterial DNA was isolated from a late-exponential growth phase culture with an in-house protocol adapted from,[61] see supplemental information, (ii) Kanamycin promotor amplified from p2NIL, (iii) Gentamicin resistance cassette amplified from pGB-Dest,[49] (iv) Kanamycin terminator amplified from p2NIL, and (v) downstream *clpC2* or *clpC3* homologous region amplified from mycobacterial chromosomal DNA was ligated via Gibson assembly into the p2NIL plasmid, and transformed into *E. coli* XL10 Gold. The plasmid *p2NIL-clpC2/3HRup-Kanprom-gmR-Kanterm-clpC2/3HRdown* was ligated with antibiotic cassette 19 from pGOAL19, again transforming into *E. coli* XL10 Gold. The final plasmid was verified by sequencing and transformed into *M. smegmatis* mc^2 155 via electroporation. Preparation of competent cells and electroporation was performed according to.[62] Successful double crossover mutants were verified by sequencing and PRM. All primer sequences are listed in Table S5. To generate *M. smegmatis* mc^2 155 *ΔΔclpC2clpC3::gmR*, electrocompetent cells of *M. smegmatis* mc^2 155 *ΔclpC3::gmR* were transformed with *p2NIL-cas19-clpC2HRup-Kanprom-gmR-Kanterm-clpC2HRdown* to initiate the crossover events.

Rv2667 (=*clpC2*) gene disruption in *Mtb* strain H37Rv was achieved employing specialized transduction.[45] Briefly, an allelic exchange substrate was designed to replace *clpC2* in *Mtb* with a γδ*res-sacB-hyg*-γδ*res* cassette comprising a *sacB* as well as a hygromycin resistance gene flanked by *res*-sites of the γδ-resolvase. Upstream and downstream flanking regions of the *clpC2* gene were amplified by PCR using primers listed in Table S5. Subsequently, the flanking regions were digested with the indicated restriction enzymes and ligated with the *Van91*I-digested p0004S vector.[45] The resulting allelic exchange plasmid was then linearized with *PacI*, cloned, and packaged into the temperature-sensitive phage ΦphAE159,[45] yielding knock-out phages that were propagated in *Msm* at 30 °C. Allelic exchange in *Mtb* was achieved by specialized transduction at the non-permissive temperature of 37 °C, using hygromycin for selection, resulting in gene deletion and replacement by γδ*res-sacB-hyg*-γδ*res* cassette. Obtained hygromycin-resistant transductants were screened for correct gene disruption by diagnostic PCR analysis.

Cloning of overexpression constructs

For overexpression of *clpC2* and *clpC3*, the respective construct was inserted into pMyC[47] (pMyC was a gift from Annabel Parret & Matthias Wilmanns (Addgene plasmid #42192; http://n2t.net/addgene:42192; RRID:Addgene_42192)) via Gibson assembly, using isolated chromosomal DNA as template for insert PCR. ClpC2 was cloned either with a C-terminal 8xHis tag (for MIC assays) or a C-terminal twinstrep tag (for IP) and ClpC3 was cloned with a C-terminal 6xHis tag. All primer sequences are listed in Table S5. The Gibson assembly products were transformed into *E. coli* XL10 Gold and verified by sequencing. For ectopic overexpression, the respective construct was transformed in *M. smegmatis* mc^2 155 as described.[62]

Protein expression and purification

Plasmids for expression in *E. coli* were transformed in BL21 (DE3) cells (ClpC2 His6, ClpC2-CTD His6 and ClpC3 His6 on pET21a vector) or Rosetta (DE3) cells (ClpC1, ClpC1^{DWB}, ClpP1 His4, ClpP2 His4) and grown in LB medium containing the respective antibiotics at 37 °C. Protein expression was induced upon addition of 0.5 mM isopropyl-1-thio-β-D-galactopyranoside (IPTG) at an OD_{600} of 0.8. Subsequently, the temperature was reduced to 21 °C and cell growth resumed overnight. Cells were harvested by centrifugation and lysed by sonication in purification buffer A (50 mM HEPES-NaOH pH 7.5, 75 mM KCl, 2 mM ETDA and 10% (v/v) glycerol) supplemented with protease inhibitor and benzonase. The lysate was cleared by centrifugation followed by filtration of the supernatant (0.2 µm).

For purification of ClpC1 (and ClpC1^{DWB}), the cell pellet was suspended in buffer A. ClpC1 was precipitated from cleared supernatant at 40% (w/v) ammonium sulfate at 4 °C overnight and collected by centrifugation. ClpC1 was resuspended in buffer A and loaded on an anion exchange column (HiLoad 26/10 Q Sepharose column, GE Healthcare) equilibrated by buffer A. The column was washed to baseline absorbance and ClpC1 was eluted in a gradient to 1 M KCl. Pure fractions were pooled, concentrated, and loaded on a size exclusion chromatography (SEC) column (HiLoad, Superdex 200 16/60, GE Healthcare), equilibrated with buffer C, containing 50 mM HEPES-NaOH pH 7.5, 150 mM KCl and 10% (v/v) glycerol. Purification was monitored for homogeneity by Coomassie stained SDS-PAGE. Fractions containing ClpC1 were pooled and concentrated before flash freezing in liquid nitrogen and stored at -80 °C.

For purification of ClpP1 or ClpP2, cells were suspended in buffer B, containing 50 mM HEPES-NaOH pH 7.5, 500 mM KCl and 1 mM TCEP. Cleared lysates were applied to a 5 ml agarose HisTrap column (GE Healthcare) equilibrated with buffer B, the column was washed with additional 50 mM and later 75 mM imidazole. Bound proteins were eluted in a gradient to 250 mM imidazole. Pure fractions were pooled and concentrated for application to SEC (Superdex 200 16/60, GE Healthcare) equilibrated with buffer C containing 50 mM HEPES-NaOH pH=7.5, 150 mM KCl with additional 1 mM TCEP. Purification of ClpC2, ClpC2-CTD or ClpC3 followed the identical protocol, except that buffer B contained 50 mM HEPES-NaOH pH=7.5, 150 mM NaCl, and buffer B contained 50 mM HEPES-NaOH pH=7.5, 150 mM NaCl. Pure fractions were pooled after SEC, concentrated and aliquots were flash frozen in liquid nitrogen, before storage at -80 °C. Processing of full-length ClpP1 and ClpP2 to the mature ClpP1P2 complex was performed as previously described.[8]

Surface plasmon resonance (SPR)

For potent binders (KD < 1 μM), the ClpC1-NTD from *M. tuberculosis* and ClpC2 from *M. smegmatis* were chemically biotinylated using the EZ-Link NHS-PEG4-Biotin kit (Thermo Scientific) according to the manufacturer's instructions. The following modifications were made: The reaction was incubated for three hours, agitating at RT with a molar ratio of 1:5 between biotin reagent and protein in 10 mM HEPES, pH 7.4, 0.05% (v/v) Tween20, 150 mM NaCl (HBS-P+, Cytiva). Zeba Spin desalting columns (Thermo Scientific) were subsequently used to get rid of non-reacted NHS-PEG4-Biotin. Streptavidin (Prospec) was immobilized to a density of 2000-3000 RUs onto all flow cells of a CM5 chip (Cytiva) at 25 °C, in 10 mM sodium acetate pH 5.0 using the amine-coupling kit (Cytiva). Biotinylated ClpC1-NTD and ClpC2 were captured to flow cells 2 and 3. ClpC3 from *M. smegmatis* was captured and coupled via its His6-tag onto flow cell 4 of a NTA chip (Cytiva), which was preloaded (Ni^{2+}) and activated with EDC/NHS according to the manufacturer's instructions. For all three, capture-coupling was performed in HPS-P+ at 25 °C up to a density of 100-500 RUs. Similarly, for weak binders (KD > 1 μM), ClpC1-NTD, ClpC2 and ClpC3 were capture coupled onto flow cells 2, 3 and 4 of a NTA chip, respectively, to a density of 1200 – 2000 RUs. The binding of the compounds was subsequently measured on a Biacore T200 instrument (Cytiva) at 25 °C in 25 mM Tris(hydroxymethyl)aminomethane, pH 7.5, 150 mM NaCl, 1% (v/v) DMSO, 0.01% (v/v) Tween20, in two different protocols depending on the binding potency of the compounds measured. At least three independent measurements were performed for each compound with mean values reported. For potent binders, sensorgrams were recorded at five different compound concentrations in single-cycle mode, at a flow rate of 100 μl/min, 20 s contact time and 600 s dissociation time. dCym served as positive control. Weak binders were measured in multi-cycle mode, at nine concentrations and a flow rate of 30 μl/min, 60 s contact time and 600 s dissociation time. As a positive control, phosphoarginine was used. Sensorgrams were double referenced prior to data analysis using Biacore Insight Evaluation Software. Data were fitted using the 1:1 interaction model with a term for mass-transport included. Single-cycle data were fitted kinetically. For multi-cycle data, steady state affinity fits were used. K_D values are reported in Table S2. Representative sensorgrams and fits are shown in Data S1A.

Analytical size exclusion chromatography (aSEC)

For size exclusion runs, 25 μM $ClpC1^{DWB}$ (inactive ATPase mutant, capable of binding, but not hydrolyzing ATP and stabilized in its hexameric state) or $ClpC1^{DWB\text{-}F444A}$ was premixed together with equimolar levels of dCym or DMSO (%) in running buffer (50 mM Tris pH 7.5, 100 mM NaCl, 5 mM $MgCl_2$ and 0.5 mM ATP). Samples were loaded using a 30 μL loop on a Superose 6 3.2/300 increase column (GE healthcare), previously equilibrated in running buffer. Runs were performed at room temperature at a 0.05 mL/minute flow rate. 100 μL fractions were collected for grid preparation for further electron microscopy analysis.

Negative staining EM

In the presence of dCym, $ClpC1^{DWB}$ elutes at higher molecular weights in a second peak earlier than the ClpC1 hexameric peak. Fractions covering this elution volume were selected for $ClpC1^{DWB}$ and $ClpC1^{DWB\text{-}F444A}$ previously incubated with dCym or DMSO. Grids were prepared with glow-discharged carbon-coated Cu/Pd Hexagonal 400 mesh grids (Agar Scientific) using 5 μl protein sample and stained with a solution of 2% uranyl acetate. The grids were screened and then imaged on a Morgagni microscope equipped with a Morada camera (Olympus-SIS) using a pixel size of 4.7 Å/px.

In vitro substrate degradation assay

The effect of dCym and Ecu* on α-casein and β-casein degradation by mycobacterial ClpC1P1P2 was tested using *in vitro* degradation assays. Hexameric *M. smegmatis* ClpC1 (0.5 μM) together with mature (14-mer complex after pro-peptide cleavage) *M. smegmatis* ClpP1P2 (0.3 μM) was incubated shortly with either 100 μM Ecu* (in DMSO), dCym (in DMSO) or DMSO as control. A final DMSO concentration of 1% was used for all conditions. The assay was set up using 15 μM substrate (α-casein or β-casein), 20 mM phosphoenolpyruvate (PEP) and 10 U/ml pyruvate kinase (Sigma Aldrich) in a buffer containing 50 mM HEPES pH 7.5, 100 mM KCl, 10 mM $MgCl_2$ and 10% (v/v) glycerol. To start the reaction, ATP was added to a final concentration of 5 mM and the reaction was incubated at 37 °C. Timepoints of 5 μl were taken before reaction start and then after 10, 20 and 45 minutes. To stop the reaction, SDS sample buffer was added prior to an SDS-PAGE and Coomassie staining. To test competition for β-casein binding of ClpC2 and ClpC1, ClpC2-CTD equimolar to ClpC1 was added to the degradation assay, without using compound or DMSO.

In addition, to test *in vitro* competition for substrate binding of ClpC2 and ClpC1, the pArg-JQ1 and dCym-JQ1 treatment was carried out using ClpC2 at levels equimolar and in 4x excess to ClpC1. Here, ClpC1, ClpP1P2 and ClpC2 were incubated together with

100 μM compound with $BRDT_{BD1}$-NrdI as substrate (the attached NrdI represents a physiological *B. subtilis* ClpC substrate), while the assay was otherwise carried out as described above.

To account for solubility issues of HBPs, the final reactions contained 1.5 μM substrate protein *M. tuberculosis* ClpC1-NTD, 15 mM PEP and 40 mM $MgCl_2$ in the assay buffer. All other conditions were kept as described above.

In vitro ClpC2 pulldown

Substrate binding to ClpC2 and occupation of the conserved hydrophobic pocket was tested by performing a pulldown of 15 μM ClpC2-His using Ni-NTA agarose beads (Qiagen), together with equal concentrations of the substrates α-casein and β-casein in a buffer containing 50 mM HEPES pH 7.5 and 100 mM KCl. As control, empty beads were incubated with substrate alone. The sample was washed three times with the same buffer containing 25 μM imidazole. To test competition of substrate and antibiotics for the same binding site, after incubation of ClpC2 with substrate, 25 μM dCym was added. His-tagged ClpC2 (and controls) was eluted from the beads by addition of 250 μM imidazole and the samples were subsequently evaluated via SDS-PAGE.

Co-crystallization and structure determination

Purified ClpC2-CTD at a concentration of 15 mg/mL and supplemented with 100 mM pArg was crystallized using a reservoir solution containing 12.5% (w/v) PEG 1000, 12.5% (w/v) PEG 3350, 12.5% (v/v) MPD, 0.02 M of each amino acid and 0.1 M MES/imidazole pH 6.5. Crystals were grown at room temperature, directly harvested and flash-cooled in liquid nitrogen. Diffraction data at a resolution of 2.0 Å were collected at the beamline P11 at DESY (Hamburg, Germany). ClpC1-NTD was purified as previously described.[26] Purified ClpC1-NTD at a concentration of 15 mg/mL and supplemented with 1 mM of Ecu** was crystallized using a reservoir solution containing 10 mM Tris-HCl pH 7.5 and 3.1 M sodium formate. Crystals were grown at room temperature transferred into the reservoir solution supplemented with additional 20 % (v/v) glycerol and flash-cooled in liquid nitrogen. Diffraction data at a resolution of 2.25 Å were collected at an in-house X-ray source. Initial phases were obtained by Molecular Replacement using PHASER and the structure of $ClpC1_{NTD}$ (PDB: 3WDB)[24] as starting model. The model was improved in iterative cycles of manual building using Coot[52] and refinement with Phenix,[58] omitting 5% of randomly selected reflections for calculation of Rfree. Model quality was monitored using MolProbity[59] and the final model exhibited good stereochemistry (Table S3). Structural illustrations were made using PYMOL.[63]

M. smegmatis sample preparation for MS analysis

Exponentially growing cells as described in the experimental models section were harvested by centrifugation at and concentrated to an OD_{600} of 5 in fresh 7H9 medium. 750 μL aliquots were transferred into each well of a 24-well glass-coated microplate (WebSeal Plate+, Thermo Scientific) and treated with either 15 μl DMSO or 15 μl of a 1 mM dCym or Ecu* stock (to achieve a final concentration of 10 μM compound and 1% DMSO per well). Subsequently, another 750 μl cell culture was added to ensure proper mixing of the compound. Each treatment was performed in triplicates. Before treatment, after 30 minutes incubation and after 120 minutes incubation, 250 μL of cell suspension was harvested from each well, and the resulting pellets were flash-frozen in liquid nitrogen. Prior to cell lysis, pellets were thawed, resuspended in 100 μL lysis buffer (50 mM HEPES pH 7.2, 150 mM KCl) and lysed for 10 minutes using a Bioruptor (Diagenode, 10 cycles, 30 seconds on - 30 seconds off) after adding a small amount of glass beads. The lysates were clarified by centrifugation (10 minutes, 4 °C, 20,000 x g), flash-frozen and stored at -80 °C.

For the treatment of *M. smegmatis* mc^2 155 WT and *ΔclpC2::gmR* with higher compound concentration, a culture volume of 600 μl at OD_{600} of ~5 (300 μl + 300 μl) was incubated with a final concentration of 150 μM dCym or DMSO (final concentration = 1%). 250 μl were collected before treatment, after two hours and six hours and processed as described above.

For intracellular degradation proteomics, *M. smegmatis* strain ATCC™ 607™ was used. A final concentration of 12.5 μM Homo-BacPROTAC was applied for treatment. For the intracellular degradation assay, 100 μl concentrated cell suspension (concentrated by factor 5) were incubated for 24 hours. To harvest the cells, 90 μl cell suspension from each well was centrifuged at 4,000 x g and 23 °C for 3 min, resuspended in 100 μl cold lysis buffer (50 mM HEPES pH 7.5, 150 mM KCl, 10% glycerol (v/v)) containing complete protease inhibitor cocktail (EDTA-free, Roche) and stored on ice until lysis. Cells were lysed in a Bioruptor Pico and centrifuged at 21,000 x g and 4 °C for 30 min. The supernatant was flash frozen in liquid nitrogen and stored at -80 °C.

Whole cell proteomics & PRM sample preparation

Cleared lysates were processed according to the single-pot SP3 protocol[64] for low input proteomics sample preparation. Each lysate of 100 μl was reduced with 10 mM dithiothreitol (DTT, Sigma Aldrich) for 45 minutes at 37 °C and subsequently alkylated with 20 mM iodoacetamide (IAA, Sigma Aldrich) at room temperature for 60 minutes. In parallel, a 1:1 mixture of 50 mg/mL Sera-Mag SpeedBeads (GE Healthcare, cat. no. 45152105050250) and 50 mg/mL Sera-Mag SpeedBeads (GE Healthcare, cat. no. 65152105050250), exhibiting different surface hydrophilicity, was washed, and prepared in water. To each lysate, 15 μL of the prepared SP3 bead stock was added and binding was induced by the addition of 100 μL ethanol. To ensure proper binding, samples were incubated on a shaker for five minutes at 24 °C and 1000 rpm. After protein binding, beads were washed three times with 200 μL rinsing solution (80% ethanol in water) while being kept on a magnetic rack. Protein elution from the beads was enforced by addition of 100 mM ammonium bicarbonate buffer (pH = 8.5, Sigma Aldrich). To disaggregate the beads, the tubes were shortly sonicated in a

water bath. For protein digestion, 1:25 wt/wt ratio of trypsin to protein was added and the samples were incubated overnight at 37 °C in a thermo-shaker at 1000 rpm. Finally, 5% TFA was used to adjust the pH to 3, prior to MS analysis.

Immunoprecipitation (IP) sample preparation

Cultures of *M. smegmatis* mc^2-155 cell lines *ΔclpC2:ev* and *ΔclpC2*:ClpC2^{twinstrep} as described in the cloning and cultivation section were harvested by centrifugation, the pellet was taken up in 500 µl buffer (50 mM HEPES pH 7.2, 100 mM KCl) and subsequently lysed for 10 minutes using a Bioruptor (Diagenode, 10 cycles, 30 seconds on - 30 seconds off) after adding a small amounts of glass beads to the suspension. The lysates were clarified by centrifugation, the protein concentration was determined, and the volume was adapted accordingly. For the IP, 20 µl of Twin-strep bead resin (Iba lifescience) was added and the samples were incubated at 4 °C for 20 minutes on a shaker. The supernatant was removed in spin columns and the beads were washed five times with buffer. After elution of proteins from the beads in 100 µl buffer BXT (Iba lifescience), samples were denatured and reduced with SDC (10 µl, 20%) and 10 mM DTT at 60 °C for 10 minutes and subsequently alkylated with 20 mM IAA at room temperature for 30 minutes. The samples were digested with trypsin (1:50 ratio to protein) at 37 °C overnight. To remove SDC, TFA (10%) was added to a final concentration of 1%. Samples were cleared and the supernatants were desalted using spin columns (Pierce).

Sample quality control for MS analysis

Sample amount and quality was determined by HPLC-UV using a Dionex UltiMate 3000 HPLC RSLC nanosystem with a PepSwift Monolithic RSLC column (0.2 x 5 mm, Thermo Fisher Scientific) at 60 °C. Peptides were separated using a 20 minutes 2-90% elution gradient of buffer B (80% ACN, 20% H_2O, 0.1% TFA).

Label free quantification mass spectrometry

LC-MS/MS analysis was performed on a Dionex UltiMate 3000 HPLC RSLC nanosystem using an Acclaim PepMap C-18 precolumn (0.3 x 5 mm, Thermo Fisher Scientific) and an Acclaim PepMap C-18 column (50 cm x 75 µm, Thermo Fisher Scientific) coupled to a Q Exactive HF-X hybrid quadrupole-Orbitrap mass spectrometer (Thermo Fisher Scientific) or a Orbitrap Exploris 480 (Thermo Fisher Scientific). Measurements using FAIMS on the Orbitrap Exploris 480 were performed at CV -45 V and CV -60 V. Peptides were separated using a 180 min linear gradient of 2-35% buffer B (80% ACN, 20% H_2O, 0.1% FA) at a flow rate of 230 nL/min. MS1 spectra were generated in a 380-1,650 *m/z* mass range at a 120,000 orbitrap resolution, AGC target of 3 x 10^6, with a maximum injection time of 50 ms. The top 10 precursors were selected for MS2 analysis using a 0.7 *m/z* quadrupole precursor isolation window, allowing charge states 2-4 and a dynamic precursor exclusion of 30 s. The orbitrap was operated at 45,000 resolution with an AGC of 1 x 10^5 and a NCE of 35% at a maximum injection time of 250 ms.

LFQ-MS and IP-MS data analysis

MS raw data were analyzed using MaxQuant (1.6.17.0) and Proteome Discoverer 2.3 (PD 2.3.0.523, Thermo) and the search was performed against a database of the *M. smegmatis* 2019 Uniprot Reference Proteome with contaminants added. The database search allowed tryptic peptides (≥ seven amino acids) with two missed cleavages at a precursor mass tolerance of 5 ppm and 0.02 Da MS2 tolerance. Static alkylation of cysteine and variable oxidation of methionine was considered. Match between runs and LFQ was enabled (MQ only) and a 1% false discovery rate cutoff was applied at PSM and protein level. In Proteome Discoverer the search engine MS Amanda[55] was used, the Percolator[65] was used for peptide scoring and filtering and protein quantification was performed using the in-house tool IMP-apQuant (https://ms.imp.ac.at/index.php?action=apQuant).

Statistical analysis of PD results as well as data normalization were performed in Perseus 1.6.[54] The samples were first filtered on high confidence FDR level and then normalized by their mean sum. Additionally, contaminants were removed, rows are filtered based on minimal values of 70% and missing values were replaced based on normal distribution.

Statistical analysis of MQ results as well as data normalization was performed in R using the in-house built LaTeX script Cassiopeia (https://github.com/moritzmadern/Cassiopeia_LFQ). Data were filtered for contaminants, for protein groups with less than two razor and unique peptides and for missing valid values in raw intensities with a cutoff of less than three valid values in at least one group. The remaining missing values were imputed from normal distribution. All mass spectrometry proteomics data in this manuscript have been deposited to the ProteomeXchange Consortium (http://proteomecentral.proteomexchange.org) via the PRIDE partner repository[66] with the dataset identifiers PXD037231, PXD037232, PXD037234 and PXD037235.

Parallel reaction monitoring (PRM) analysis

LC-MS/MS analysis was performed on a Dionex UltiMate 3000 HPLC RSLC nanosystem using an Acclaim PepMap C-18 precolumn (0.3 x 5 mm, Thermo Fisher Scientific) and an Acclaim PepMap C-18 column (50 cm x 75 µm, Thermo Fisher Scientific) coupled to a Q Exactive HF-X hybrid quadrupole-Orbitrap mass spectrometer (Thermo Fisher Scientific). Peptides were separated using a 180 min linear gradient of 2-35% buffer B (80% ACN, 20% H_2O, 0.1% FA) at a flow rate of 230 nL/min. MS1 spectra were recorded before every target cycle in a 375-1,500 *m/z* mass range at a 30,000 orbitrap resolution, AGC target of 3 x 10^6, with a maximum injection time of 60 ms. MS2 spectra were generated for targets from the isolation list using a loop count of 10. A 0.7 *m/z* quadrupole precursor isolation window was used, at 30,000 orbitrap resolution with an AGC of 2 x 10^5 and a NCE of 35% at a maximum injection time of 200 ms. For absolute quantification, heavy peptides (JPT) were included in the isolation list.

PRM data analysis

A peptide search was performed in Skyline against a database containing ClpC1, ClpC2 and ClpC3 together with three housekeeping proteins. Tryptic peptides (≥ seven amino acids) were considered, with one missed cleavage and a precursor and MS2 mass tolerance of 10 ppm using the PRM acquisition method. Static alkylation of cysteine and variable oxidation of methionine was considered. For absolute quantification, a C-terminal $^{13}C(6)^{15}N(4)$ label was included. For the analysis, the top three MS2 ions were selected for all proteins and the "total area fragment" was normalized to the "average sum total area fragment" of the housekeeping proteins. For interpretation of absolute quantification, a ratio between light and heavy peptides was calculated. PRM data has been uploaded to the PanoramaWeb[67] repository (https://panoramaweb.org /iBzWpn.url; PXD037198).

M. tuberculosis samples for MS analysis

Cells of *Mtb* H37Rv WT and Δ*clpC2* mutant were grown in 20 ml supplemented Middlebrook 7H9 medium to a final $OD_{600\ nm}$ of 1. Cells were then treated with 7.8 μM HBPs or an equal volume of DMSO as solvent control and incubated for 48 h at 37 °C. Subsequently, cells were centrifuged at 4 °C and washed twice with PBS (137 mM NaCl; 2.7 mM KCl; 10 mM Na_2HPO_4; 1.8 mM KH_2PO_4; pH 7.4). Cells were resuspended in 750 μL of PBS and lysed by bead-beating in a TissueLyser LT (Qiagen) using 100-μm silica zirconium beads (50 Hz; 15 min). Afterwards, an appropriate volume of 4x lysis buffer (4% (w/v) SDS, 40 mM TCEP, 160 mM CAM, 200 mM HEPES) was added to the cells and incubated for 10 min at 95 °C. After centrifugation, the cleared supernatant was collected and used as protein lysate. To remove viable bacteria and ensure safety, the protein lysates were sterile filtered twice through a bacteria-tight 0.2 μM cellulose acetate filter.

Pull-down assays in *M. tuberculosis*

Freshly prepared *M. tuberculosis* H37Rv lysate as described above was divided into samples containing a total amount of 400 μg protein in 499 μL PBS. To each sample, 1 μL of either DMSO or the respective probes (1 mM) were added and the samples were incubated for one hour while shaking (1250 rpm, 30 min at 4 °C, followed by 30 min at room temperature). Pierce™ Avidin Agarose beads (Thermo Fisher Scientific) were equilibrated in PBS and 100 μL of a slurry suspension was added to each sample (approx. 50 μL bead volume). For proper binding of the biotin probes, the samples were incubated for one hour while shaking (1250 rpm) at room temperature. Subsequently, the beads were washed three times with PBS or in case of the competition control group with 20 μM CycloA_D9-containing PBS. An additional washing step was performed with PBS to eliminate most of the competitor. The beads were taken up in 100 μL 6 M urea in 50 mM NH_4HCO_3 (ABC) buffer, containing 20 mM DTT. After one hour of incubation, 40 mM IAA was added for alkylation of proteins and the samples were incubated for one further hour. To inactivate unreacted IAA, an equivalent amount of DTT was added and the urea concentration was reduced to 1 M by diluting the samples with 50 mM ABC buffer. For digestion, 1 μg of Trypsin (Promega) was added to each sample followed by incubation for 13 hours shaking at 37 °C. The peptide solution was acidified to 1% formic acid (FA; Fisher Chemical) and separated from the beads. The beads were washed with 1% FA in 50 mM ABC buffer and the peptide solutions were combined for further processing. To eliminate any residual beads, samples were passed through equilibrated glass microfiber tips (pore size: 1.2 μm, thickness: 0.26 mm, two disks per tip; GE Healthcare, 1822-024). Peptides were desalted on home-made C_{18} StageTips as described before.[68] For analysis, the samples were dissolved in 10 μL of 0.1% FA in water and 4 μL peptide solution was loaded on a fused silica capillary column with integrated 10 μm PicoFrit emitter with a length of 460 mm and an inner diameter of 75 μm (New Objectives PF360-75-10-N-5), self-packed with Reprosil-Pur 120 C18-AQ material (1.9 μm particles with 100 Å pore size, Dr. Maisch). The gradient was generated by an EASYnLC 1200 liquid chromatography (Thermo Fisher Scientific), using 0.1% FA in water (solvent A) and 0.1% FA with 20% water in ACN (solvent B). Peptides were separated using a 105 min gradient at a flow rate of 300 nL/mL at 50 °C. Peptides were ionized using a Nanospray Flex ion source (Thermo Fisher scientific) and MS acquisition was performed in an Orbitrap Fusion Lumos mass spectrometer (Thermo Fisher Scientific). MS1 spectra were recorded in a 375-1,800 *m/z* mass range at a 120,000 Orbitrap resolution, with standard AGC target settings at 50 ms maximum injection time. Data dependent MS2 spectra were generated using a loop cycle of three seconds with a dynamic exclusion duration of 30 seconds. A 1.2 *m/z* quadrupole precursor isolation window was used, at rapid ion trap scan rate with 300% of normalized AGC target and stepped HCD fragmentation (20, 30, 45%) with automated maximum injection time settings.

Whole cell MS from *M. tuberculosis*

Whole proteome samples were prepared following a modified SP3 protocol.[64] To this end, 15 to 20 μg of protein extract prepared as described above were treated with benzonase (40 mU/μL, EMD Millipore, 71206) for 30 min at 37 °C, followed by protein alkylation with 10 mM IAA for another 30 min at room temperature. An equal mixture of hydrophilic (Cytiva) and hydrophobic Sera-Mag SpeedBeads (Cytiva) was equilibrated to water and the beads were added to the samples to a concentration of 1 μg of particles per microliter of sample. Protein binding was induced by adding a similar volume of ethanol to the suspension followed by subsequent incubation for 30 min while shaking (1500 rpm) at room temperature. The beads were collected on a magnetic stand and washed three times with 180 μL of 80% ethanol to eliminate detergents and salts. Digestion was started by adding 100 μL of 25 mM ABC buffer containing 0.6 μg trypsin and 0.6 μg LysC. Disaggregation of the particles was promoted by sonicating the samples in a heated water bath (35-37 °C) in the first 5 min of the digestion reaction. After incubation for another 16 hours at 37 °C while shaking (1500 rpm), the beads were collected on a magnetic stand and the supernatant containing the tryptic peptides was separated from the beads. The particles were then washed with 25 mM ABC buffer and the combined peptide solutions were acidified

to a final concentration of 2% TFA. To eliminate any residual particles, samples were centrifuged at 21,000 g for 2 min and desalted on homemade C_{18} StageTips as described before.[68] Dry peptides were dissolved in 15 μL of 0.1% FA in water and peptide concentration was adjusted to 200 ng/μL. For analysis, 500 ng of peptides were loaded on a fused silica capillary column with integrated 5 μm PicoFrit emitter with a length of 410 mm and inner diameter of 75 μm (ESI Source Solutions PTC3-75-50-SP), self-packed with Kinetex XB-C18 material (1.7 μm core shell with 100 Å pore size, Phenomenex). The gradient was generated by an EASYnLC 1200 liquid chromatography (Thermo Fisher Scientific), using 0.1% FA in water (solvent A) and 0.1% FA with 20% water in ACN (solvent B). Peptides were separated using a 105 min gradient at a flow rate of 350 nL/mL at 50 °C. Peptides were ionized using a Nanospray Flex ion source (Thermo Fisher scientific) and MS acquisition was performed in an Orbitrap Fusion Lumos mass spectrometer (Thermo Fisher Scientific). MS1 spectra were recorded in a 375-1,800 *m/z* mass range at a 240,000 Orbitrap resolution, with standard AGC target settings and an automatic maximum injection time. Data dependent MS2 spectra were generated using a loop cycle of three seconds with a dynamic exclusion duration of 20 seconds. A 1.2 *m/z* quadrupole precursor isolation window was used, at rapid ion trap scan rate with 300% of normalized AGC target and stepped HCD fragmentation (20, 30, 45%) with automated maximum injection time settings. *M. tuberculosis* mass spectrometry proteomics data has been deposited to the ProteomeXchange Consortium via the PRIDE partner repository with the dataset identifiers PXD037712 and PXD037730.

Minimum inhibitory concentration (MIC) assay

Minimum inhibitory concentration testing in *M. smegmatis* was performed using the same agar-based assay as performed in Morreale et al.[26] In brief, a dilution series of each compound is prepared in 96-well plates, followed by adding agar (+ additives if applicable) to each well. Subsequent spotting of equal amounts of exponentially growing cells in each well foregoes the incubation of the plates at 37 °C. The optical readout after a few days allows for semiquantitative analysis of the minimum inhibitory concentration which prevents cell growth. For experiments with overexpression strains, the agar is supplemented with 0.1% Acetamide and 100 μg/ml Hygromycin to continue the expression of the respective gene during plate incubation. In this case, the overexpression is already induced during liquid cultivation.

Dose response curves in *M. tuberculosis*

Minimum inhibitory concentration of compounds in *Mtb* was quantified by dose response curves using the resazurin microplate assay as described previously.[69] In short, a two-fold serial dilution of tested compounds has been prepared in a polystyrene U-bottom 96-well plate (Greiner) to reflect a dose-response curve ranging from 100 μM to 0.048 μM final concentrations. Equal amounts of exponentially growing cells ($OD_{600\ nm} \leq 1$, diluted to 1×10^6 CFU/ml) were then added into each well to a total volume of 100 μl and cultivated for five days at 37 °C (5% CO_2, 80% humidity). Subsequently, 10 μl resazurin solution (100 μg/ml, Sigma Aldrich) was added into each well and incubated overnight. Cells were fixed at room temperature for 30 min after the addition of 10% (v/v) formalin, and growth was quantified based on fluorescence using a microplate reader (TECAN) (excitation: 540 nm, emission: 590 nm). Relative growth was calculated with respect to the DMSO solvent control (= 100%) and uninoculated wells (= 0%). Experiments were performed in triplicates. MIC_{50} values were calculated using GraphPad Prism 7 software.

Checkerboard assay

The Checkerboard analysis was used to evaluate compound susceptibility in presence of additional stressors. The experimental procedure was performed in a MIC or dose response curve assay as described above. For combinations with heat stress in *M. smegmatis*, a simultaneous increase in temperature in the first dimension was combined with reducing compound concentrations in the second dimension in a way that the final plates, already containing compound dilution series as well as cells, were incubated for the respective time at elevated temperatures and subsequently transferred to 37 °C until colonies were grown. Kanamycin was used as control. For dose response curves to simulate low ATP levels, *Mtb* H37Rv was exposed to increasing bedaquiline concentrations and HBPs or Rifampicin.

Kill curve assay

To enable monitoring of cell viability upon stress or compound incubation, exponentially growing liquid cell cultures were incubated with the respective compound in 1% DMSO or exposed to the physical stress over a time of 72 h, respectively. Every few hours, equal amounts of cells (10^3 and 10^4 CFU/ml) were plated in quadruplicates onto 7H10 agar. After incubation at 37 °C for two days, colonies were counted and CFU/ml were calculated and plotted as mean ± SD, normalized to the respective control cultures if applicable.

Minimum inhibitory time (MIT) assays

Minimum inhibitory time testing combines kill curve assays with an optically easier readout. Exponentially growing liquid cultures were exposed to the respective stressor and incubated over time. In our case, flasks were transferred to 53 °C for five hours. Starting with a control before flasks were transferred (t0) as well as after each timepoint (t1 = 1 h, t2 = 2 h, t5 = 5 h), equal amounts of cells were plated onto 7H10 agar. Precisely, a dilution series starting with 5 μl of 1×10^6 cells, followed by three serial 1:10 dilutions, thereby encompassing 5 μl of 1×10^5, 1×10^4, and 1×10^3 cells, respectively, was spotted onto the plate. The plates were then incubated at 37 °C for two days and growth performance is optically compared between the spots.

Resistance screens and WGS in *M. tuberculosis*

Spontaneous single-step resistant mutants were isolated by plating each approximately 6×10^7cells of *Mtb* H37Rv on solid media containing either 12.5 μM HBP6 or 9.4 μM HBP7, respectively. After six weeks, four colonies were isolated and subjected to MIC assays with 1:2 serial dilutions of both compounds. Rifampicin and Ethambutol were used as reference antibiotics in equally generated dose response curves of all clones. For whole genome sequencing (WGS), genomic DNA samples isolated from the mutants were quantified by photometric measurement using a NanoDrop One device (Thermo Fisher Scientific Inc.) and quality measured by capillary electrophoresis using the Fragment Analyzer and the 'High Sensitivity genomic DNA Assay' (Agilent Technologies, Inc.). Library preparation was performed according to manufacturer's protocol using TruePrep DNA Library Prep Kit V2 for Illumina (1ng) (Vazyme Biotech Co.; Ltd). Libraries were normalized to 4 nM and pooled and subsequently sequenced on a MiSeq system (Illumina Inc) with a read setup of 2x250 bp. The reads were assembled and mapped to the reference genome using the CLC Genomics Workbench (Qiagen), using *Mtb* H37RvMA as a reference (GenBank accession GCA_000751615.1).[44] Mean depth of coverage ranged from 73x – 121x. Genetic alterations observed during whole-genome resequencing analyses of spontaneous HBP6- or HBP7-resistant *Mycobacterium tuberculosis* H37Rv mutants were named as followed: HBP6 #1, #2, #3: SNP t→g at nucleotide 238 out of 2547 bp, causing amino acid substitution F80V in *clpC1* and frame shift, deletion -g at nucleotide 60 out of 6336 bp in *mas*; HBP7 #1: SNP t→c at nucleotide 83 out of 2547 bp, causing amino acid substitution I28T in *clpC1*.

Chemical Synthesis of Ecu**

2-CTC resin (1.33 mmol/g) was swelled in 5 vol% iPr$_2$NEt/CH_2Cl_2 (0.015 M) and shaken for 20 min. The solvent was discharged and the resin washed with CH_2Cl_2 (x 5). The resin was treated with the Fmoc-Gly-OH (4 eq. in regards to predicted resin loading) and iPr$_2$NEt (8 eq.) in CH_2Cl_2 (0.05 M) and shaken at room temperature for 16 h. The coupling solution was discharged and washed with CH_2Cl_2 (x 5), DMF (x 5) and CH_2Cl_2 (x 5). The resin was treated with a capping solution of 17:2:1 (v/v/v) CH_2Cl_2/iPr$_2$NEt/MeOH and shaken at room temperature for 30 min. The capping solution was discharged and the resin washed with CH_2Cl_2 (x 5) and DMF (x 5). The resin-bound peptide was treated with a solution of 10 vol% piperidine/DMF (2 x 3 min). The deprotection solution was discharged and collected and the resin washed with DMF (x 5), CH_2Cl_2 (x 5) and DMF (x 5). The combined deprotection solutions were made up to 25 mL using 10 vol% piperidine/DMF and diluted 1:100 with 10 vol% piperidine/DMF. The amount of peptide loaded to resin was determined by measurement of the UV absorbance at λ = 301 nm of the diluted deprotection solution. The resin-bound peptide was treated with a solution of a Fmoc-L-Trp(Boc)-OH acid (4 eq.) and subjected to HATU coupling conditions: HATU (4 eq.), iPr$_2$NEt (8 eq.) in DMF (0.1 M in regards to loaded peptide) and shaken for 2 h at room temperature. The coupling solution was discharged and the resin washed with DMF (x 5), CH_2Cl_2 (x 5) and DMF (x 5). The resin-bound peptide was next Fmoc-deprotected: the resin was treated with a solution of 10 vol% piperidine/DMF (2 x 3 min). The deprotection solution was discharged and the resin washed with DMF (x 5), CH_2Cl_2 (x 5) and DMF (x 5). The resin-bound peptide was treated with a solution of 2-nitrobenzenesulfonyl chloride (4 eq.) and 2,4,6-trimethylpyridine (10 eq.) in NMP (0.1 M in regards to loaded peptide) and shaken at room temperature for 20 min. The protection solution was discharged and the resin washed with DMF (x 5), CH_2Cl_2 (x 5) and THF (x 10). The resin-bound peptide was treated with a solution of PPh_3 (5 eq.) and anhydrous MeOH (10 eq.) in anhydrous THF (0.2 M in regards to loaded peptide). The resin was shaken at room temperature for 1 min at which point an additional solution of DIAD (5 eq.) in THF (0.2 M in regards to loaded peptide) was sucked into the fritted syringe. The resin was shaken for 15 min, the solution was discharged and the resin washed with DMF (x 5), CH_2Cl_2 (x 5) and DMF (x 5). The resin-bound peptide was treated with a solution of DBU (5 eq.) and 2-mercaptoethanol (10 eq.) in NMP (0.1 M in regards to loaded peptide) (2 x 5 min). The deprotection solution was discharged and the resin washed with DMF (x 5), CH_2Cl_2 (x 5) and DMF (x 5). The resin-bound peptide was treated with a solution of a Fmoc-*N*-Me-L-Ala-OH (2 eq.) and subjected to HATU/HOAt coupling conditions: HATU (2 eq.), HOAt (4eq.) and iPr$_2$NEt (4 eq.) in DMF (0.1 M in regards to resin loading) and shaken for 8 h at room temperature. The coupling solution was discharged and the resin washed with DMF (x 5), CH_2Cl_2 (x 5) and DMF (x 5). The resin was then Fmoc-deprotected (using the aforementioned protocol). The resin-bound peptide was treated with a solution of Fmoc-L-Val-OH (4 eq.) according to the HATU/HOAt coupling conditions used previously. Fmoc-L-Val-OH was coupled three times to ensure complete coupling. Coupling progress was monitored *via* UPLC-MS. The resin-bound peptide was then Fmoc-deprotected and treated with a solution of Fmoc-*N*-Me-L-Leu-OH according to the HATU coupling conditions mentioned previously. The resin bound peptide was then Fmoc-deprotected. The resin-bound peptide was washed with CH_2Cl_2 (x 10) and then treated with a solution of 30 vol% HFIP/ CH_2Cl_2 (3 x 20 min). The cleavage solution was discharged, collected and concentrated under a stream of N_2 and dried *in vacuo*. The crude protected linear peptide was purified by preparative RP-HPLC using a Sunfire OBD 5 μm 19 x 150 mm (C18) column using a gradient of 30 – 45% ACN in H_2O (0.1% TFA) over 30 min at a flow rate of 25 mL/min. The peptide was lyophilized to yield the protected linear peptide as a trifluoroacetate salt (86 mg, 82% over 12 steps from resin loading, average of 98% per step). The peptide (1.09 mg, 1.36 μmol) was deprotected with iPr$_3$SiH:TFA:CH_2Cl_2 (2:49:49, v/v/v, 1 mL) and stirred at room temperature for 1 h, then concentrated under a stream of N_2. The peptide was redissolved in ACN:H_2O (1:1, v/v, 1 mL) with 1 drop of AcOH and stirred at room temperature overnight. The peptide was then lyophilized to give the pure deprotected linear peptide (1.0 mg, 82% over 13 steps from resin loading). The peptide was re-lyophilized five times with 0.25 M HCl to convert the trifluoroacetate salt to the hydrochloride salt. NMR data are provided in Data S1**C**.

Chemical Synthesis of dCym-JQ1 (SRG-II-19F)

Reactions were monitored by LC/MS (*Shimadzu Prominence-i LC-2030*, column: *Phenomenex Onyx C18*, 50 x 4.6 mm, *Shimadzu LCMS-2020*, (ESI)). Flash chromatography (reversed phase) was conducted with a *Büchi Reveleris PREP* on *Büchi Flashpure Select C18* cartridges, H_2O/ACN gradient). The compounds were dried by lyophilization from ACN/H_2O overnight. ^1H and ^{13}C spectra were recorded with Bruker AV 500 [500 MHz (^1H), 126 MHz (^{13}C)] spectrometers in $CDCl_3$ at 298 K. Chemical shifts are reported in ppm relative to $Si(CH_3)_4$. The signals of residual $CHCl_3$ in $CDCl_3$ ($\delta(^1H, CHCl_3) = 7.26$ ppm, $\delta(^{13}C, CDCl_3) = 77.16$ ppm) were used as the internal standard. Multiplicities are reported as (singlet), d (doublet), t (triplet), q (quartet) and m (multiplet). High resolution mass spectra were recorded on a *Bruker MAXIS 4G* UHR-TOF (ESI). **[6-propargyl]-dCym** and **JQ1-PEG$_4$-N$_3$** were prepared as described.[26,29]

2-((*S*)-4-(4-Chlorophenyl)-2,3,9-trimethyl-6*H*-thieno[3,2-f][1,2,4]triazolo[4,3-a][1,4]diazepin-6-yl)-N-(14-(4-(((3-(((2*S*,5*S*,8*S*,11*S*,14*S*,17*S*,20*S*)-5-((*R*)-3-hydroxy-2-methylpropyl)-17-isobutyl-14,20-diisopropyl-11-((*R*)-methoxy(phenyl)methyl)-4,8,16-trimethyl-3,6,9,12,15,18,21-heptaoxo-1,4,7,10,13,16,19-heptaazacyclohenicosan-2-yl)methyl)-1*H*-indol-1-yl)methyl)-1*H*-1,2,3-triazol-1-yl)-3,6,9,12-tetraoxatetradecyl)acetamide (dCym-JQ1 / SRG-II-19F)

In a 1.5 mL vial, **[6-propargyl]-dCym** (18.0 mg, 19.0 μmol] and **JQ1-PEG$_4$-N$_3$** (14.8 mg, 23.0 μmol) were dissolved in a mixture of t-BuOH (190 μL) and H_2O (190 μL). 1 M $CuSO_4$ (9.56 μL, 9.56 μmol) and freshly prepared 1 M sodium ascorbate (11.0 μL, 11.0 μmol) solutions were added, the vial was flushed with Argon and stirred at RT for 12 h. Then, the reaction mixture was concentrated *in vacuo* and the residue was purified by flash chromatography (H2O/ACN 70:30 – 5:95). After lyophilization, dCym-JQ1 (28.0 mg, 180 μmol, 84%, purity >95%) was obtained as a white amorphous solid. See Data S1**C** for synthesis scheme, NMR and HPLC data.

Synthesis of pArg-JQ1 (BI01826025)

The synthesis of the pArg-JQ1 basically followed previously published synthesis protocols.[26] In brief, commercially available (+)-JQ1 (150 mg, 0.33 mmol) was dissolved in 4 M HCl in dioxane (5 mL) and stirred for 1 h at RT. The solvent was removed under reduced pressure and the residue was redissolved in DCM (10 mL). Mono-Boc-protected diaminoethyl ether (102 mg, 1.5 eq., 0.50 mmol), HOBt monohydrate (77 mg, 1.5 eq., 0.50 mmol), DIC (77 μL,1.5 eq., 0.50 mmol) and triethyl amine (218 μL, 4.7 eq., 1.57 mmol) were added and the resulting mixture was stirred for 16 h at rt. 5% aq. $NaHCO_3$ solution (10 mL) was added, the organic phase was separated, dried over $MgSO_4$ and evaporated to dryness, resulting in 174 mg (0.30 mmol, 90%) of a white solid that was used in the next step without further purification. The residue was redissolved in 4 M HCl in dioxane (5 mL) and stirred for 4 h at RT. The solvent was removed under reduced pressure and the residue was redissolved in DCM (5 mL). Fmoc-pArg(Tce)$_2$-OH (325 mg, 1.5 eq., 0.44 mmol), HOBt monohydrate (97 mg, 2.1 eq., 0.63 mmol), DIC (196 μL, 4 eq., 1.26 mmol) and triethyl amine (217 μL, 5.2 eq., 1.56 mmol) were dissolved in DCM (20 mL) and added to the first mixture. The resulting solution was stirred for 16 h at RT. 5% aq. $NaHCO_3$ solution (10 mL) was added, the organic phase was separated, dried over $MgSO_4$ and evaporated to dryness. The resulting crude product was dissolved in DCM (6 mL) and diethyl amine (4 mL) were added. This mixture was stirred for 4 h at RT. 5% aq. $NaHCO_3$ solution (10 mL) was added, the organic phase was separated, dried over $MgSO_4$ and evaporated to dryness. The resulting residue was redissolved in DCM (5 mL) and acetic anhydride (54 μL, 1.9 eq., 0.57 mmol) and triethylamine (158 μL, 3.8 eq., 1.14 mmol) was added. The resulting reaction mixture was stirred for 1 h at RT. The mixture was evaporated to dryness and the resulting residue was purified by column chromatography (stationary phase: C18-RP, eluent gradient (acetonitrile: water, 0.1% formic acid): 50:50 → 60:40 → 70:30→ 100:0). Product containing fractions were pooled and evaporated to dryness, resulting in 76 mg (0.074 mmol,23%) of the desired Tce-protected intermediate (TLC (DCM/MeOH 9:1 + 0.5 % formic acid): R_f 0.4). The Tce-protected intermediate (128 mg, 0.11 mmol) was then dissolved in a mixture of NH_4HCO_3 buffer (100 mM, pH 9, 5 mL) and ethanol (5 mL). 10% Pd on carbon (55 mg) was added as a hydrogenation catalyst and the mixture was flushed with argon, then with H_2 for 5 h at RT. The mixture was again flushed with argon, the catalyst was filtered off and the solution was reduced to dryness. The remaining residue was purified by HPLC (C18-RP, gradient: 10% → 60% acetonitrile in water containing 0.1% ammonia). Product containing fractions were pooled and lyophilized, thereby yielding 11 mg (0.0144 mmol, 13%) of the desired pArg-JQ1. See Data S1C for synthesis scheme, NMR and HPLC data.

QUANTIFICATION AND STATISTICAL ANALYSIS

Reported SPR K_D values represent the average ± SD of the indicated number of independent measurements. Volcano plots for proteomics (whole proteome and IP-MS) analysis show the fold-change (log_2) in protein abundance in comparison to control treatment, plotted against *P* value ($-log_{10}$) (two-tailed Student's T-test; triplicate analysis). All MIC data are represented as mean ± SD of the indicated replicate experiments. All degradation assay data are represented as mean ± SD of the indicated replicate experiments. Indicated replicates always refer to independent biological replicates and datasets.

Cell
Article

CellPress
OPEN ACCESS

Supplemental figures

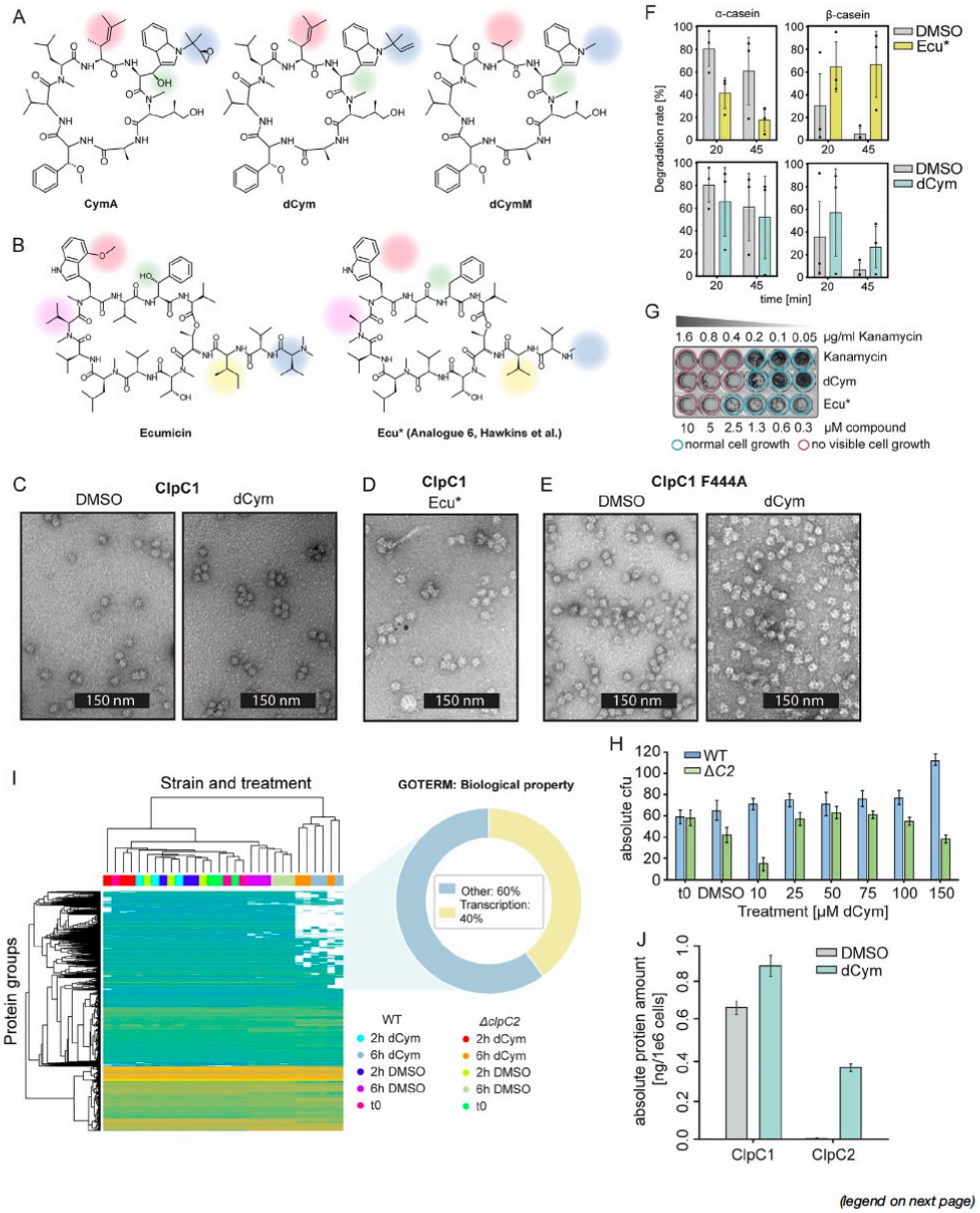

(legend on next page)

CellPress
OPEN ACCESS

Cell
Article

Figure S1. Cyclomarin A and ecumicin derivatives are effective in *M. smegmatis*, related to Figure 1

(A) Structures of natural cyclomarin A (CymA) and derived compounds used in this study. The colors represent the residue positions where the natural compound has been changed.[19,26,46]

(B) Structure of ecumicin and its derivatives used in this study. The colors represent the residue positions where the natural compound has been changed.

(C–E) Negative-stained EM images of ClpC1 and ClpC1^{F444A} mutants with and without bound antibiotics.

(F) Substrate degradation of two model substrates, β-casein and α-casein, by ClpC1P1P2 with or without dCym or Ecu* (Quantification represents mean ± SD, n = 3).

(G) Minimum inhibitory concentration (MIC) assay testing appropriate concentrations of dCym and Ecu* for treatment of wild-type cells. n ≥ 10 independent biological replicates.

(H) Kill curve assay comparing wild type and *ΔclpC2* after treatment with increasing dCym concentrations. 2-h incubation allowed the use of 150-μM dCym without significant growth effects. Reduced viability of *ΔclpC2* with 10 μM dCym likely presents an experimental outlier, due to occasional stronger biofilm formation of stressed *ΔclpC2* cells. The presented dataset shows mean ± SD of three technical replicates.

(I) Quantitative proteomics of *Msm* treated with 150 μM dCym for 2 or 6 h, respectively. The heatmap plots identified protein groups across the different samples. Color coding for different strains and conditions according to the legend. The zoomed in data in circle shows the distribution of the GO terms no longer quantifiable in mutant samples. n = 3 independent biological replicates.

(J) Absolute quantification of ClpC1 and ClpC2 levels. ClpC2 significantly increases upon dCym treatment. Results are mean ± SD from three independent biological replicates. CFU, colony-forming unit.

Cell
Article

CellPress
OPEN ACCESS

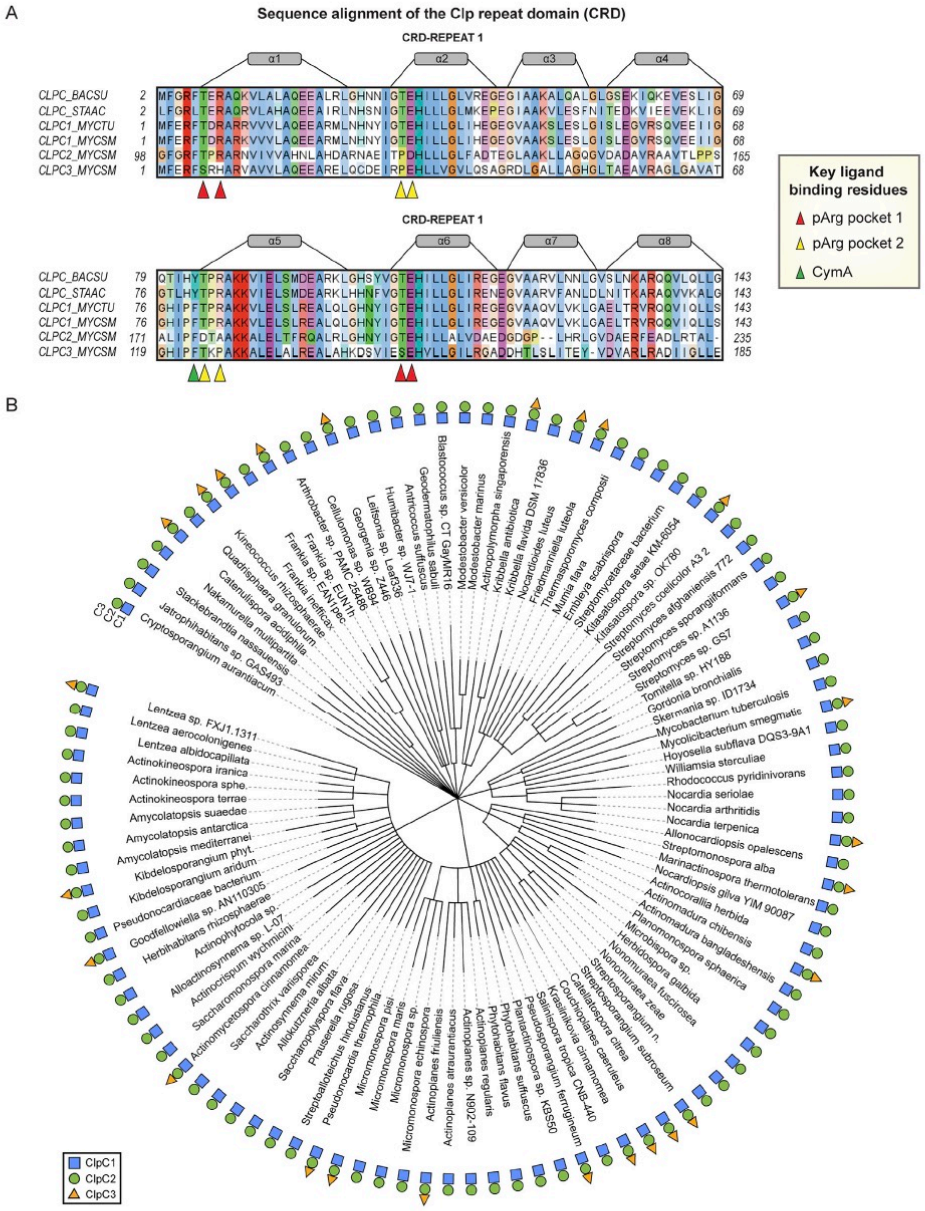

(legend on next page)

CellPress
OPEN ACCESS

Cell
Article

Figure S2. Conservation of Clp proteins, related to Figure 2

(A) Sequence alignment showing the conservation of key binding residues within the CRD of Clp proteins.

(B) Taxonomic tree showing conservation of ClpC1, ClpC2, and ClpC3 in representatives of actinobacterial species. BACSU, *Bacillus subtilis*; STAAC, *Staphylococcus aureus* COL; MYCSM, *Mycolicibacterium smegmatis* mc^2 155; MYCTU, *Mycobacterium tuberculosis* H37Rv.

Cell
Article

CellPress
OPEN ACCESS

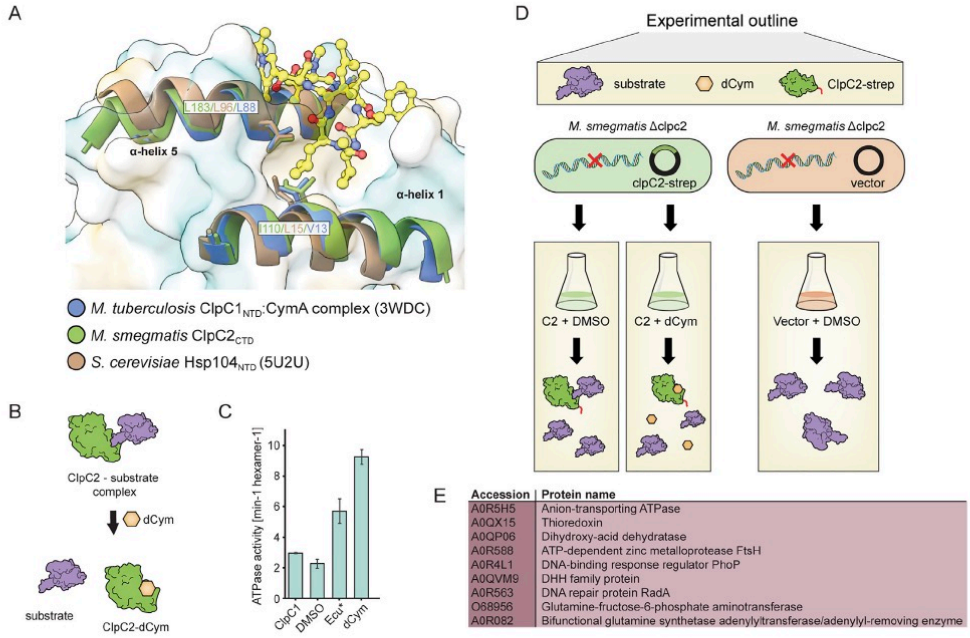

Figure S3. Interactions between dCym and ClpC2, related to Figure 3

(A) Conserved hydrophobic residues implicated in substrate binding to Hsp104 (PDB 5U2U) are blocked by CymA in the $ClpC1_{NTD}$.

(B) Schematic model illustrating competition between dCym and substrate for the same binding site.

(C) ATPase activity assay shows increasing ATPase activity upon compound treatment. Results are mean ± SD from three independent biological replicates.

(D) Experimental outline describing pull-down experiments with ClpC2. *Msm ΔclpC2* overexpresses plasmidic $ClpC2^{twinstrep}$. Interaction partners of ClpC2 are analyzed by IP-MS (left, green). After dCym incubation, interaction partners of ClpC2 compete with dCym for the binding (middle, green). Empty vector was used as control (right, orange).

(E) Among the most abundant hits in ClpC2 pull-down, nine proteins are homologs to proteins previously identified in ClpC1 degradome analysis in *Mtb*.

CellPress
OPEN ACCESS

Cell
Article

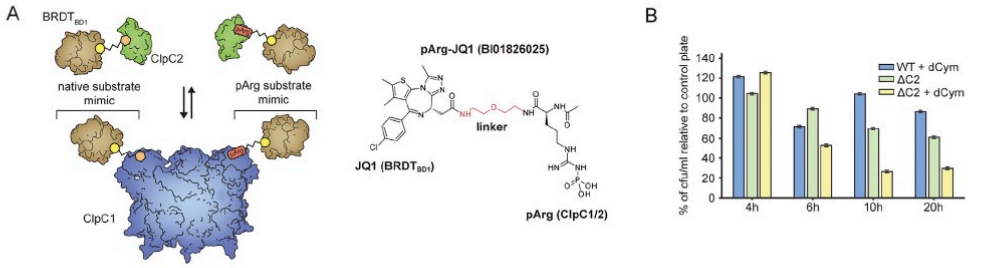

Figure S4. Role of ClpC2 during induced degradation and cell survival, related to Figure 4

(A) ClpC2 (green) competes for binding BRDT$_{BD1}$ model substrates (brown) by either pArg-JQ1 or dCym-JQ1, representing two distinct degradation signals (on the right: structure of the pArg-JQ1).

(B) Kill curve assay, monitoring survival of *Msm* wild type and *ΔclpC2* mutant over time upon dCym treatment. After incubation with 150 μM dCym, equal amounts of cells were plated onto 7H10 agar and CFU/mL were counted to compare cell viability. Deletion of *clpC2* significantly decreases survival. Results are mean ± SD from three independent biological replicates. CFU, colony-forming unit.

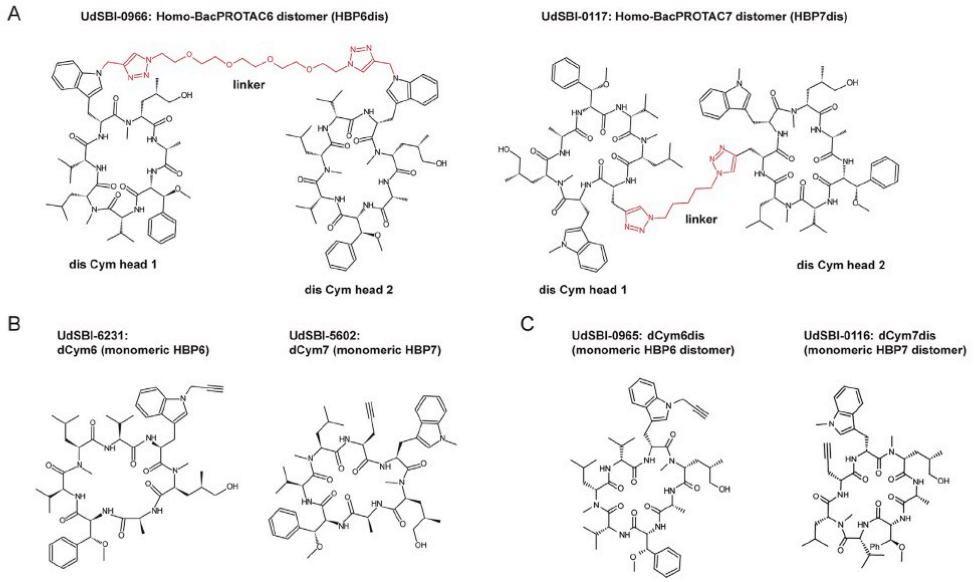

Figure S5. Homo-BacPROTAC distomers and monomers, related to Figure 5
Compound structures for inactive Homo-BacPROTAC6 distomer (A) and Homo-BacPROTAC7 distomer (B) active monomers of Homo-BacPROTAC6 and Homo-BacPROTAC7 (C) inactive monomers of the distomers of Homo-BacPROTAC6 and Homo-BacPROTAC7.

CellPress
OPEN ACCESS

Cell
Article

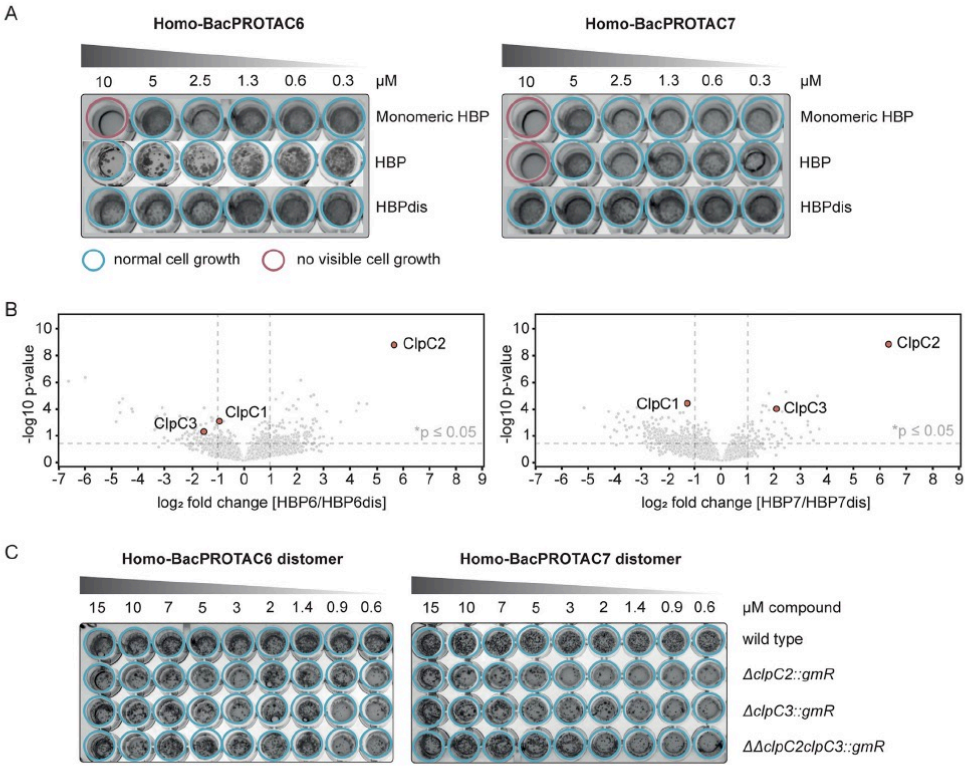

Figure S6. Controls for incubation with Homo-BacPROTACs in *Msm*, related to Figure 6

(A) MIC assays exposing wild-type cells to either active compounds, inactive distomer or the corresponding monomers (+ linker attached). 1:2 dilution series. Activity of both monomeric and dimeric compound is comparable and low for both Homo-BacPROTACs. No MIC has been observed for distomers. n ≥ 6 independent biological replicates.

(B) Quantitative proteomics of Homo-BacPROTACs HBP6 and HBP7 treated *Msm* cells after 24 h, normalized to incubation with inactive distomers (HBP6dis, HBP7dis). n = 3 independent biological replicates.

(C) MIC assays comparing wild type and mutants incubated with corresponding distomers of Homo-BacPROTACs (1:3 dilution series). No MIC can be observed for either distomer in any of the strains. n = 6 independent biological replicates. gmR, gentamicin resistance cassette introduced instead of *clpC2/clpC3*.

Cell, Volume *186*

Supplemental information

Clp-targeting BacPROTACs impair mycobacterial proteostasis and survival

David M. Hoi, Sabryna Junker, Lukas Junk, Kristin Schwechel, Katharina Fischel, David Podlesainski, Paige M.E. Hawkins, Lasse van Geelen, Farnusch Kaschani, Julia Leodolter, Francesca Ester Morreale, Stefan Kleine, Somraj Guha, Klaus Rumpel, Volker M. Schmiedel, Harald Weinstabl, Anton Meinhart, Richard J. Payne, Markus Kaiser, Markus Hartl, Guido Boehmelt, Uli Kazmaier, Rainer Kalscheuer, and Tim Clausen

SUPPLEMENTAL REFERENCES

S1. Lunge, A., Gupta, R., Choudhary, E. and Agarwal, N. (2020). The unfoldase ClpC1 of Mycobacterium tuberculosis regulates the expression of a distinct subset of proteins having intrinsically disordered termini. J Biol Chem 295, 9455-9473. 10.1074/jbc.RA120.013456

SUPPLEMENTAL TABLES

Table S1. *Msm* proteins equally affected by dCym and Ecu* treatment (related to **Fig. 1F-G**).

Decreased protein abundance	
Accession	**Protein name**
A0QUM5	Uncharacterized protein
A0QUM7	Hydrogenase-2, large subunit
A0QS88	Enoyl-CoA hydratase
A0QUM6	Hydrogenase-2, small subunit
A0QXM6	Metal-dependent phosphohydrolase, HD subdomain
A0R087	3-methyl-2-oxobutanoate hydroxymethyltransferase
A0R0H6	Monooxygenase, NtaA/SnaA/SoxA family protein
A0R590	Limonene 1,2-monooxygenase
A0QV53	HAD-superfamily protein hydrolase, subfamily protein IIA
A0QQ30	Glyoxalase family protein
A0QQN1	Membrane protein
A0R6E0	Trehalose synthase/amylase TreS
A0QVJ4	Gamma-glutamylisopropylamide synthetase
A0QXK5	Hydrolase
A0R0H7	Acyl-CoA dehydrogenase-family protein
A0QUY0	Uncharacterized protein
A0R7H3	Uncharacterized protein
A0QT20	Flavin-containing monooxygenase FMO
A0QNJ4	Ppe family protein
A0R1P4	Putative acyl-CoA dehydrogenase
A0R4Z1	Coenzyme A transferase, subunit B
A0QUN9	Hydrogenase expression/formation protein HypD
A0QVQ0	Alkanesulfonate monooxygenase family protein

A0QZC4	N-methylhydantoinase
A0QP15	O-acetylhomoserine/O-acetylserine sulfhydrylase
A0R248	Carbonic anhydrase
A0QUH4	Acyl-CoA dehydrogenase
A0R4Y7	Short chain dehydrogenase
Increased protein abundance	
Accession	**Protein name**
A0R2L4	Base excision DNA repair protein, HhH-GPD family protein
A0R1A4	Uncharacterized protein
A0R470	PLP-dependent aminotransferases
A0QTP7	Transcriptional regulator WhiB
A0R5D5	DNA polymerase III subunit delta
A0QYW5	Hydrolase
A0QX45	Phenolpthiocerol synthesis type-i polyketide synthase ppse
A0R4E0	Amidophosphoribosyltransferase
A0QQT2	DNA or RNA helicase of superfamily protein II
A0QTT5	Uncharacterized protein
A0QSN4	ATP-dependent RNA helicase

Table S2. Surface plasmon resonance spectroscopy data of ligand binding to $ClpC1_{NTD}$, ClpC2 and ClpC3 (related to **Data S1A** and **STAR Methods**).

	$ClpC1_{NTD}$[a] (*M. tuberculosis*)	**ClpC2 (*M. smegmatis*)**	**ClpC3 (*M. smegmatis*)**
Trivial name	**K_D [M]**	**K_D [M]**	**K_D [M]**
dCym7	3.96E-09	2.37E-09	6.72E-09
HBP7	4.91E-10	5.80E-10	1.98E-09
dCym7-dis	> 1.00E-04	> 1.00E-04	> 1.00E-04
HBP7-dis	> 1.00E-04	> 1.00E-04	> 1.00E-04
dCym6	3.04E-09	1.24E-09	7.48E-09
HBP6	1.19E-09	2.38E-09	2.88E-09
dCym6-dis	> 1.00E-04	> 1.00E-04	> 1.00E-04
HBP6-dis	> 1.00E-04	> 1.00E-04	> 1.00E-04
dCym	1.39E-09	7.73E-10	3.27E-09
Ecu*	8.58E-06	5.81E-06	1.15E-05
Ecu**	5.04E-05	n.d.	n.d.
pArg	4.93E-06	9.39E-06	> 1.00E-04

[a]100% sequence identity of the *M. smegmatis* and *M. tuberculosis* ClpC1-NTD

dCym: desoxycyclomarin C, HBP: Homo-BacPROTAC, Ecu*: Ecumicin derivative, Ecu**: linear ecumicin fragment

Table S3. Crystallographic analysis: Data collection and refinement statistics (related to **Fig. 2B**).

	ClpC1$_{NTD}$:Ecu complex**	**ClpC2$_{CTD}$:pArgcomplex**
PDB ID	*8B9U*	*8B9O*
Space group	P3221	C2
Cell dimensions		
a, b, c (Å)	54.77, 54.77, 174.49	51.08, 40.63, 64.43
α, β, γ (°)	90, 90, 120	90, 91.75, 90
Resolution (Å)a	50 – 2.25 (2.30 – 2.25)	50 – 2.00 (2.06 – 2.00)
Rmeas(I)	8.9 (65.3)	5.5 (98.1)
I/σ (I)	19.7 (4.5)	14.9 (1.9)
CC1/2	99.9 (93.3)	99.8 (66.9)
Completeness (%)	98.9 (88.2)	98.9 (89.7)
Redundancy	11.6 (10.5)	4.3 (3.9)
Refinement		
Resolution (Å)	47.84 – 2.25	30.2- 2.0
No. reflections	16,451	8936
Rwork / Rfree	21.2 / 24.9	20.5 / 22.8
No. atoms		
protein	2249	1087
ligand	21	15
water	110	6
B factors		
protein	46.10	67.1
ligand	44.45	64.5
water	44.57	54.0
R.m.s. deviations		
Bond lengths (Å)	0.002	0.006
Bond angles (°)	0.44	0.62

Ramachandran		
favored	99.30	98.54
allowed	0.70	1.46

[a]Values in parentheses are for highest-resolution shell.

Ecu**: linear ecumicin fragment

Table S4. ClpC2 interactors depleted by dCym binding, from weakest to strongest (related to **Fig. 3F**).

Protein IDs	Protein names	Gene names
A0QS51	Hydrolase, alpha/beta fold family protein	MSMEG_1352
A0QUX6	Acetolactate synthase	ilvB
A0QT07	Succinate dehydrogenase, iron-sulfur protein	sdhB
A0QSD8	50S ribosomal protein L16	rplP
A0R573	Uncharacterized protein	MSMEG_6090
A0R6L7	ATP-binding protein	MSMEG_6593
A0QSP8	50S ribosomal protein L13	rplM
A0R4C0	Phosphate import ATP-binding protein PstB	pstB
A0R4B3	Fatty acid desaturase	MSMEG_5773
A0QNP9	Rhamnolipids biosynthesis 3-oxoacyl-[acyl-carrier-protein] reductase	MSMEG_0121
A0R4M3	Short chain dehydrogenase	MSMEG_5885
A0QSL0	Thioredoxin reductase	MSMEG_1516
A0R2Y1	Beta-ketoadipyl CoA thiolase	MSMEG_5273
A0QWZ8	DNA-binding protein	MSMEG_3121
A0R2L2	Uncharacterized protein	MSMEG_5154
A0QZM6	Monoxygenase	MSMEG_4082
A0QNJ7	CbiA domain-containing protein	MSMEG_0067
A0R0D8	Putative oxidoreductase YjgI	MSMEG_4351
*A0R5H5	Anion-transporting ATPase	MSMEG_6193
*A0QX15	Thioredoxin	trx
A0R7K1	Chromosomal replication initiator protein DnaA	dnaA
A0QY24	Hydrolase, alpha/beta hydrolase fold family protein	MSMEG_3508
A0QW25	Uncharacterized protein MSMEG_2782/MSMEI_2713	MSMEG_2782
A0R2C4	Uncharacterized protein	MSMEG_5062
A0QUX8	Ketol-acid reductoisomerase (NADP(+))	ilvC
*A0QP06	Dihydroxy-acid dehydratase	ilvD
A0QTG4	Uncharacterized protein	MSMEG_1832
A0QU61	Cell division ATP-binding protein FtsE	ftsE
A0QUN9	Hydrogenase expression/formation protein HypD	hypD
*A0R588	ATP-dependent zinc metalloprotease FtsH	ftsH
*A0R4L1	DNA-binding response regulator PhoP	phoP

A0R5M2	ATPase associated with various cellular activities, AAA-5	MSMEG_6241
Q59560	Protein RecA	recA
*A0QVM9	DHH family protein	MSMEG_2630
A0R079	Glutamine synthetase	glnA
A0QS64	ABC transporter, ATP-binding protein	MSMEG_1366
A0QNY0	IS1096, tnpR protein; IS1096, tnpR protein	MSMEG_0203;
A0R5H6	Ion-transporting ATPase	MSMEG_6195
A0QPJ7	Transferase	MSMEG_0422
*A0R563	DNA repair protein RadA	radA
A0R345	Nitrile hydratase regulator1	MSMEG_5339
A0R5M3	Alcohol dehydrogenase, iron-containing	MSMEG_6242
A0R753	Integral membrane protein	MSMEG_6783
A0R3L0	von Willebrand factor, type A	MSMEG_5511
A0QR50	RemM protein	MSMEG_0986
*O68956	Glutamine--fructose-6-phosphate aminotransferase [isomerizing]	glmS
A0QRP7	TROVE domain protein	MSMEG_1193
A0QWQ1	AAA ATPase, central region	MSMEG_3021
A0QV45	Uncharacterized protein	MSMEG_2443
A0QYH0	ABC transporter, permease/ATP-binding protein	MSMEG_3655
A0QZ33	Nitrilase/cyanide hydratase and apolipoprotein N-acyltransferase	MSMEG_3880
A0R373	Ectoine/hydroxyectoine ABC transporter solute-binding protein	ehuB
*A0R082	Bifunctional glutamine synthetase adenylyltransferase/adenylyl-removing enzyme	glnE
A0R2V9	Pantothenate kinase	coaA
A0R638	Serine--tRNA ligase	serS
A0QRJ6	Glycerol-3-phosphate dehydrogenase [NAD(P)+]	gpsA

* Proteins identified as potential ClpC1 substrates in previous proteomic analyses [S1].

Table S6. Abbreviations used (related to **Fig. 1-7**, **Fig. S1-S7**, **STAR Methods**).

Abbreviation	Explanation
AAA	ATPase Associated with diverse cellular Activities
ABC	NH_4HCO_3
ACN	acetonitrile
AcOH	acetic acid
AGC	Automatic gain control
aSEC	Analytical size exclusion chromatography
ATR	attenuated total reflection
CFU	colony-forming units
$ClpC1_{NTD}$	N-terminal domain
$ClpC2_{NT}$	truncated 21-aa ClpC2 peptide
CRD	Clp repeat domain
CTC	2-chlorotrityl chloride
CymA	Cyclomarin A
DBU	1,8-Diazabicyclo [5.4.0]undec-7-ene
dCym	desoxycyclomarin C
DIAD	Diisopropyl azodicarboxylate
dis	distomer
DMF	Dimethylformamid
DS	2% (w/v) glucose; 0.085% (w/v) sodium chloride
DWB	double Walker B
Ecu*	Ecumicin derivative
Ecu**	linear ecumicin fragment
FA	formic acid
FFG	Österreichische Forschungsförderungsgesellschaft
gmR	gentamicin resistance
HATU	Hexafluorophosphate Azabenzotriazole Tetramethyl Uronium, 1-[Bis(dimethylamino)methylene]-1H-1,2,3-triazolo[4,5-b]pyridinium 3-oxide hexafluorophosphate
HBP	Homo-BacPROTAC
HBS-P+	10 mM HEPES, pH 7.4, 0.05% (v/v) Tween20
HFIP	Hexafluoroisopropanol
HOAt	1-Hydroxy-7-azabenzotriazole

HR	homologous region
HygR	hygromycin resistance
IR	infrared radiation
MeOD	methanol-d4 (deuterated methanol)
MeOH	Methanol
MIC	minimum inhibitory concentration
MIT	minimum inhibitory time
NMP	N-Methyl-2-pyrrolidone
PDIM	phthiocerol dimycocerosate
PEP	phosphoenolpyruvate
POI	protein of interest
PPh3	triphenylphospan
PRM	Parallel reaction monitoring
SNP	Single nucleotid polymorphism
SRM	Spontaneous single-step resistant mutant
TDR	totally drug resistant
THF	tetrahydrofuran
UTR	untranslated region
WGS	Whole genome sequencing
XDR	extensively drug resistant

Table S5. Oligonucleotides for genomic mutations and overexpression constructs (related to **STAR methods**).

Sequence	Function	Direction	Project
GTCAGAACGAGGCGTCGTCGCC	start of HR upstream to extract from chromosomal DNA	fw	*Msm clpC2* deletion
CGTCAACGTTAGGTTGACGATGATTCGGC	end of HR upstream to extract from chromosomal DNA	rev	*Msm clpC2* deletion
AACGCGGGAATGTACGCGGCCG	start of HR downstream to extract from chromosomal DNA	fw	*Msm clpC2* deletion
AGCCGTGCTTGGAGTAGAACCGC	end of HR downstream to extract from chromosomal DNA	rev	*Msm clpC2* deletion
TATAGAATACATAGGATCCGTCAGAACGAGGCGTCGTC	start of HR upstream + Gibson overhangs into p2NIL	fw	*Msm clpC2* deletion
GATTTTGAGACACAACGTGCTAGCGCCGTCAACGTTAGGTTGACG	end of HR upstream + Gibson overhangs to Kanamycin promotor	rev	*Msm clpC2* deletion
CCTAACGTTGACGGCGCTAGCACGTTGTGTCTCAAAATCTCTGATG	start of Kanamycin promotor + Gibson overhangs into HR upstream	fw	*Msm clpC2* deletion
GCTGCTGCGTAACATAACACCCCTTGTATTACTGTTTATGTAAG	end of Kanamycin promotor + Gibson overhangs into Gentamicin resistance cassette	rev	*Msm clpC2* deletion
ATGTTACGCAGCAGCAACGATG	start of Gentamicin resistance cassette to extract from resource plasmid	fw	*Msm clpC2* deletion
TTAGGTGGCGGTACTTGGG	end of Gentamicin resistance cassette to extract from resource plasmid	rev	*Msm clpC2* deletion
AATACAAGGGGTGTTATGTTACGCAGCAGCAACGATG	start of Gentamicin resistance cassette + Gibson overhangs into Kanamycin promotor	fw	*Msm clpC2* deletion
ATTAACCAATTCTGATTAGGTGGCGGTACTTGGGTC	end of Gentamicin resistance cassette + Gibson overhangs into Kanamycin terminator	rev	*Msm clpC2* deletion
AGTACCGCCACCTAATCAGAATTGGTTAATTGGTTGTAACAC	start of Kanamycin terminator + Gibson overhangs into Gentamicin resistance cassette	fw	*Msm clpC2* deletion
GTACATTCCCGCGTTCCATGGGAATCGCCCCATCATCCAG	end of Kanaymycin terminator + Gibson overhangs into HR downstream	rev	*Msm clpC2* deletion
ATGATGGGGCGATTCCCATGGAACGCGGGAATGTACGCGG	start of HR downstream + Gibson overhangs into Kanamycin promotor	fw	*Msm clpC2* deletion
TAAACTACCGCATTAAAGCTTAGCCGTGCTTGGAGTAGAACC	end of HR downstream + Gibson overhangs into p2NIL	rev	*Msm clpC2* deletion
ACGCCTCGTTCTGACGGATCCTATGTATTCTATAGTGTCACC	vector PCR into p2NIL	rev	*Msm clpC2* deletion
ACTCCAAGCACGGCTAAGCTTTAATGCGGTAGTTTATCACAG	vector PCR into p2NIL	fw	*Msm clpC2* deletion
AACCGTGCCGTTGGTGCAGTTCGACGTAG	start of HR upstream to extract from chromosomal DNA	fw	*Msm clpC3* deletion
CGTCAACTCCTCCGGTTGTACTTCTGGTGG	end of HR upstream to extract from chromosomal DNA	rev	*Msm clpC3* deletion
GCCAGGCGTCGCCGACGCCG	start of HR downstream to extract from chromosomal DNA	fw	*Msm clpC3* deletion
TGCGCCGACCTCCTGCAGTGCCTC	end of HR downstream to extract from chromosomal DNA	rev	*clpC3* deletion
TATAGAATACATAGGATCCAACCGTGCCGTTGGTGCAG	start of HR upstream + Gibson overhangs into p2NIL	fw	*Msm clpC3* deletion
GATTTTGAGACACAACGTGCTAGCCGTCAACTCCTCCGGTTGTAC	end of HR upstream + Gibson overhangs to Kanamycin promotor	rev	*Msm clpC3* deletion
GCTAGCACGTTGTGTCTCAAAATC	start of Kanamycin promotor to amplify gmR cassette as such	fw	*Msm clpC3* deletion
CCATGGGAATCGCCCCATCATC	end of Kanamycin terminator to amplify gmR cassette as such	rev	*Msm clpC3* deletion
CCGGAGGAGTTGACGGCTAGCACGTTGTGTCTCAAAATCTCTGATG	start of Kanamycin promotor + Gibson overhangs into HR upstream	fw	*clpC3* deletion
TCGGCGACGCCTGGCCCATGGGAATCGCCCCATCATCCAG	end of Kanaymycin terminator + Gibson overhangs into HR downstream	rev	*Msm clpC3* deletion
CGATTCCCATGGGCCAGGCGTCGCCGAC	start of HR downstream + Gibson overhangs into Kanamycin promotor	fw	*Msm clpC3* deletion
TAAACTACCGCATTAAAGCTTTGCGCCGACCTCCTGCAG	end of HR downstream + Gibson overhangs into p2NIL	rev	*Msm clpC3* deletion
ACCAACGGCACGGTTGGATCCTATGTATTCTATAGTGTCACC	vector PCR into p2NIL	rev	*Msm clpC3* deletion
CAGGAGGTCGGCGCAAAGCTTTAATGCGGTAGTTTATCACAG	vector PCR into p2NIL	fw	*Msm clpC3* deletion
GGCGTGTTCGACCATGGTGGACTCCCTTTCTCTTATCG	vector PCR into pMyC	rev	*Msm* ClpC2 overexpression
TAAAAGCTTCAGCTTATCGATGTCG	vector PCR into pMyC	fw	*Msm* ClpC2 overexpression
TAAGAGAAAGGGAGTCCACCATGGTCGAACACGCCAAGATC	insert PCR	fw	*Msm* ClpC2 overexpression
CATCGATAAGCTGAAGCTTTTATCAATGGTGATGGTGATGATGGTGATGCTCCAGCTCCGCCGGTTTGGT	insert PCR	rev	*Msm* ClpC2 overexpression
GGTGGACTCCCTTTCTCTTATCG	vector PCR into pMyC	rev	*Msm* ClpC3 overexpression
CCGCCGCCCATCACCATCACCATCACTGATAAAAGCTTCAGCTT	vector PCR into pMyC	fw	*Msm* ClpC3 overexpression
GAAAGGGAGTCCACCATGTTCGAGCGGTTCAGCCG	insert PCR	fw	*Msm* ClpC3 overexpression
AAGCTGAAGCTTTTATCAGTGATGGTGATGGTGATGGGCGGCGGACTCCAGCAGGCC	insert PCR	rev	*Msm* ClpC3 overexpression
CCAAACCGGCGGAGTGGAGCCACCCGCAGTTTGAAAAAG	vector PCR into pMyC	fw	*Msm* ClpC2 pulldown
TCAAACTGCGGGTGGCTCCACTCCGCCGGTTTGGTCATG	insert PCR	rev	*Msm* ClpC2 pulldown
TTTTTC*CATTTCTTGG*-CCCGTTTGATGGCGTTGATGAGC	Upstream flanking region	5' primer	*Mtb* H37Rv *ΔclpC2*
TTTTTC*CATAAATTGG*G-CAGCGATGAGCGGTCCAATCAG	Upstream flanking region	3' primer	*Mtb* H37Rv *ΔclpC2*
TTTTTC*CATCTTTTGG*-CGCGAATGAGCATGGCGTAACCG	Downstream flanking regions	5' primer	*Mtb* H37Rv *ΔclpC2*
TTTTTC*CATAGATTGG*-ATCACCACGCTCGCATCGCTCAC	Downstream flanking regions	3' primer	*Mtb* H37Rv *ΔclpC2*

fw: forward, rev: reverse, *Msm*: *Mycolicibacterium smegmatis* , *Mtb*: *Mycobacterium tuberculosis*
italic: restriction site Van91I

SUPPLEMENTAL RAW DATA

Data S1 | Unprocessed raw data used in the manuscript (related to **Table S2**, **Fig. 4C-D**, **Fig. 4G**, **Fig. 6D**, **STAR methods**).

A) SPR sensorgrams (fitting curve, orange) of the binding of ClpC1, ClpC2 and ClpC3 to indicated ligands. Binding affinities are shown in **Table S2**.

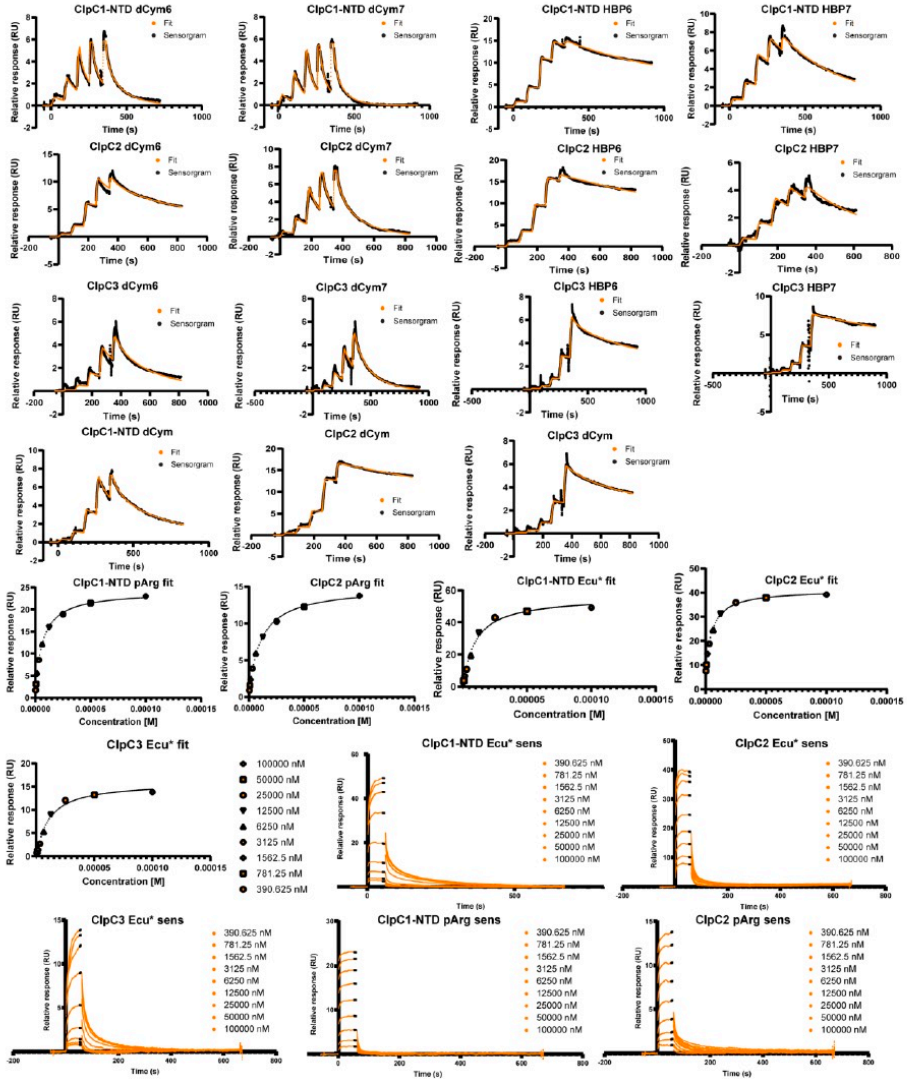

B) Uncropped images of cell culture plate used for MIC measurements **(A) Fig. 4C-D. (B) Fig. 4G. (C) Fig. 6D.**

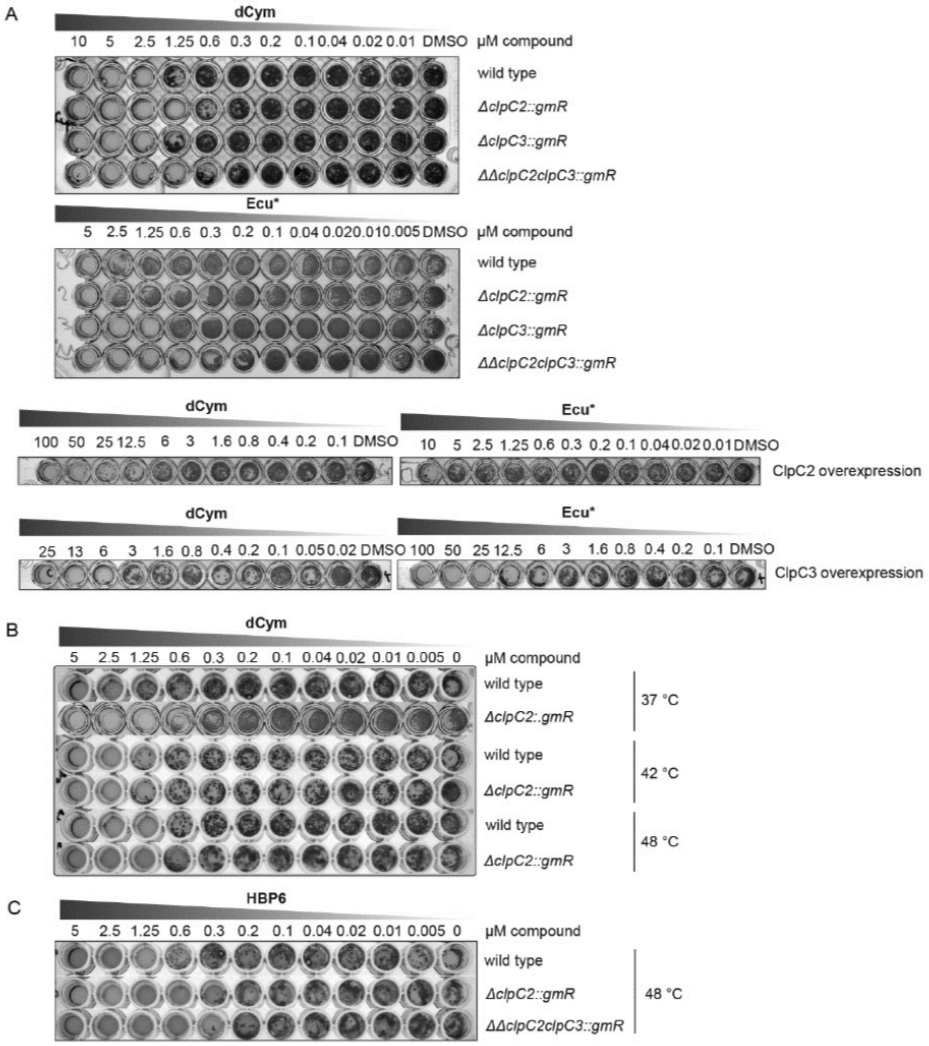

C) Synthesis, NMR data and HPLC traces of used compounds (related to **STAR methods**).

dCym-JQ1 (SRG-II-19F)

Synthesis

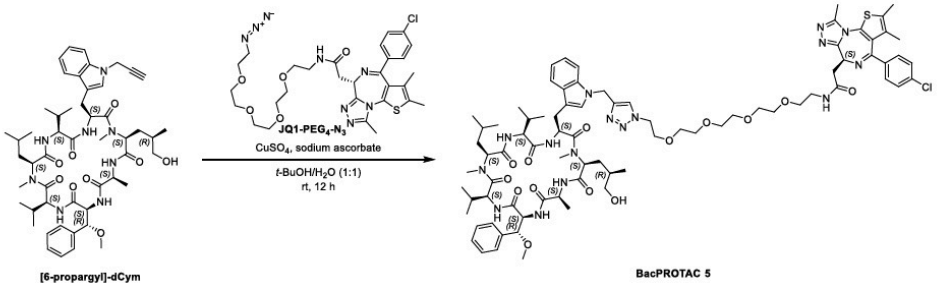

NMR and HPLC data of dCym-JQ1: **HRMS** (ESI): calcd for $C_{80}H_{110}ClN_{16}O_{14}S^+$ $(M+H)^+$: 1585.7791; found: 1585.7724.

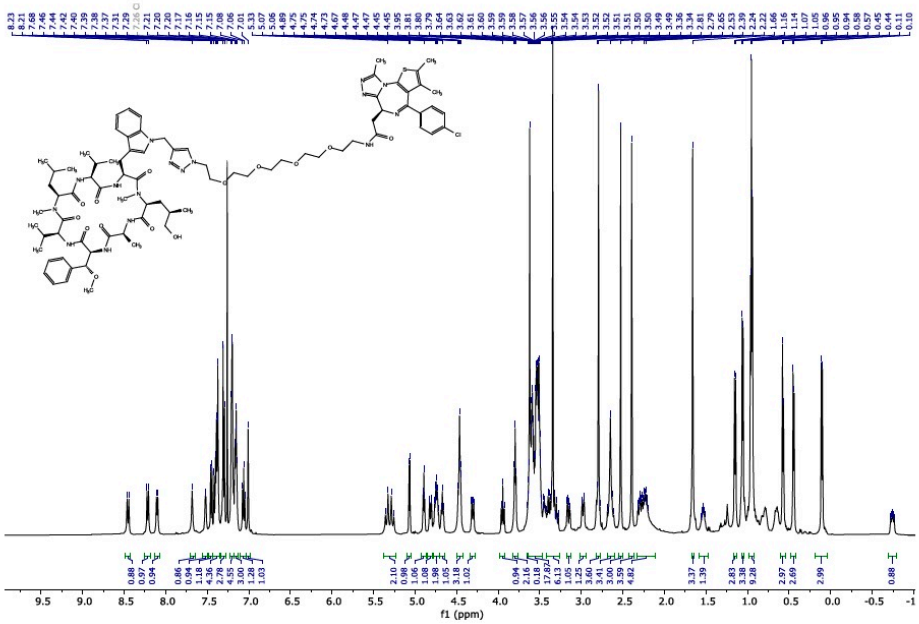

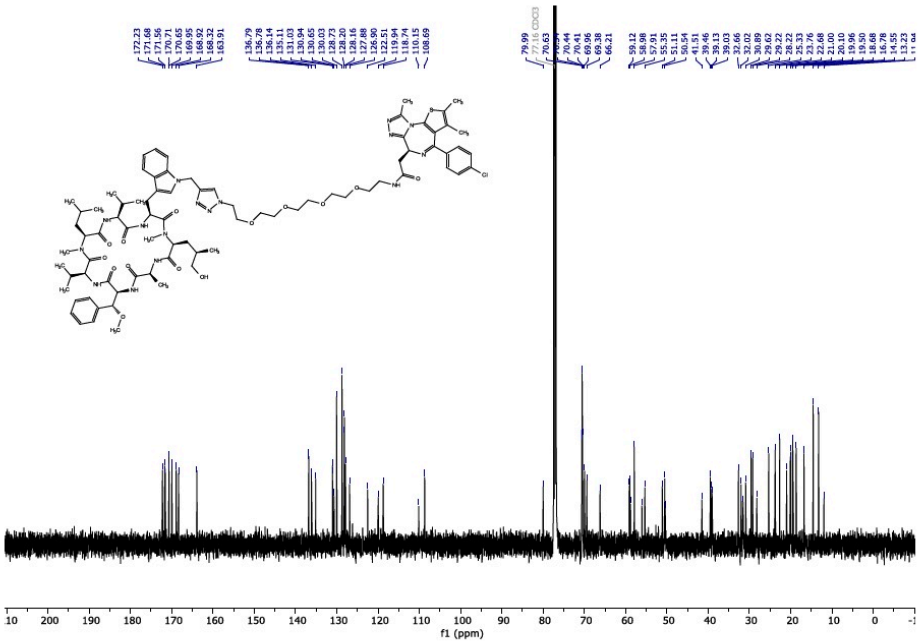

^{1}H NMR (500 MHz, $CDCl_3$) δ -0.86 – -0.61 (m, 1H), 0.11(d, *J* = 6.7 Hz, 3H), 0.45 (d, *J* = 6.4 Hz, 3H), 0.57 (d, *J* = 6.5 Hz, 3H), 0.93 – 0.97 (m, 9H), 1.06 (d, *J* = 6.6 Hz, 3H), 1.15 (d, *J* = 7.2 Hz, 3H), 1.45 – 1.60 (m, 1H), 1.66 (s, 3H), 2.19 – 2.33 (m, 5H), 2.39 (s, 3H), 2.53 (s, 3H), 2.59 – 2.70 (m, 3H), 2.79 (s, 3H), 2.94 – 3.00 (m, 1H), 3.12 – 3.20 (m, 1H), 3.26 – 3.42 (m, 6H), 3.43 – 3.66 (m, 18H), 3.76 – 3.84 (m, 2H), 3.95 (t, *J* = 9.4 Hz, 1H), 4.28 – 4.34 (m, 1H), 4.43 – 4.50 (m, 3H), 4.67 (t, *J* = 6.9 Hz, 1H), 4.71 – 4.78 (m, 2H), 4.79 – 4.85 (m, 1H), 4.89 (t, *J* = 5.1 Hz, 1H), 5.07 (d, *J* = 5.5 Hz, 1H), 5.24 – 5.38 (m, 2H), 7.01 (s, 1H), 7.06 (t, *J* = 7.5 Hz, 1H), 7.13 – 7.18 (m, 3H), 7.18 – 7.22 (m, 4H), 7.28 – 7.34 (m, 3H), 7.35 – 7.43 (m, 4H), 7.45 (d, *J* = 8.0 Hz, 1H), 7.50 – 7.54 (m, 1H), 7.68 (s, 1H), 8.10 (d, *J* = 7.9 Hz, 1H), 8.12 (d, *J* = 9.5 Hz, 1H), 8.45 (d, *J* = 10.4 Hz, 1H). **^{13}C NMR (126 MHz, $CDCl_3$)** δ 11.9, 13.2, 14.5, 16.8, 18.7, 19.5, 20.1, 20.1, 21.0, 22.7, 23.8, 25.3, 28.2, 29.2, 29.6, 30.9, 31.5, 32.0, 32.7, 39.0, 39.1, 39.5, 41.5, 50.4, 50.5, 51.1, 55.3, 56.0, 57.9, 58.8, 59.0, 59.1, 66.2, 69.4, 70.0, 70.4, 70.4, 70.5, 70.6, 80.0, 108.7, 110.1, 118.7, 119.9, 122.5, 126.9, 127.9, 128.2, 128.2, 128.7, 130.0, 130.6, 130.9, 131.0, 135.1, 136.1, 136.8, 136.8, 163.9, 168.3, 168.9, 169.9, 170.6, 170.7, 171.6, 171.7, 172.2

pArg-JQ1 (BI01826025)

Synthesis

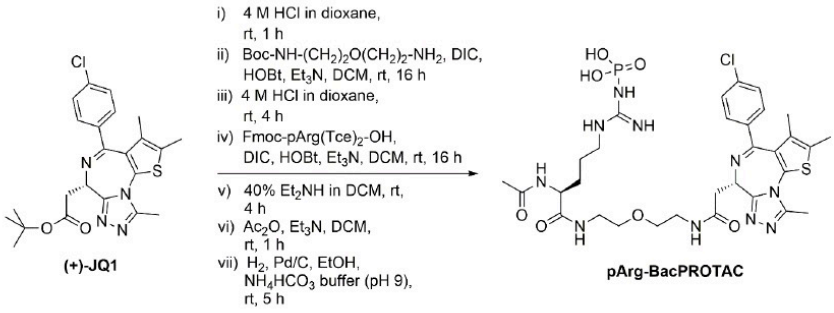

NMR and HPLC data of pArg-JQ1: LC-MS (ESI): R_t = 6.30 min, *m/z* 765.2 calcd for $C_{31}H_{43}ClN_{10}O_7PS^+$, found: 765.2 $[M+H]^+$.

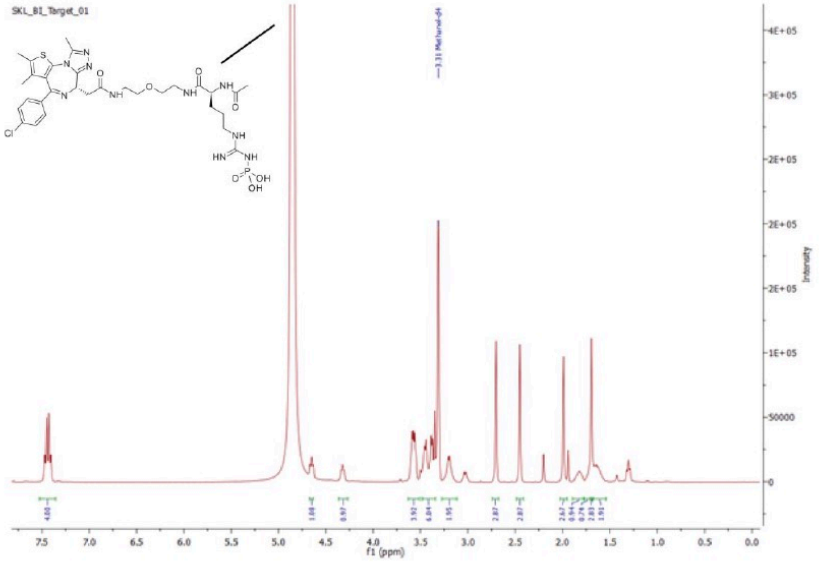

^{1}H-NMR (400 MHz, MeOD): δ 7.44 (dd, J = 17.6, 8.0 Hz, 4H), 4.69 – 4.62 (m, 1H), 4.36 – 4.28 (m, 1H), 3.63 – 3.53 (m, 4H), 3.52 – 3.33 (m, 6H), 3.25 – 3.15 (m, 2H), 2.70 (s, 3H), 2.45 (s, 3H), 1.99 (s, 3H), 1.88 – 1.76 (m, 1H), 1.76 – 1.71 (m, 1H), 1.70 (s, 3H), 1.67 – 1.54 (m, 2H).

Ecu**

NMR Data

HR-MS: (+ESI) Calc. for $C_{30}H_{46}N_6O_6$: 609.3371 $[M+Na]^+$, Found: 609.3376 $[M+Na]^+$; **^{1}H NMR** (MeOD, 500 MHz, major rotamer) δ (ppm); 7.59 (m, 1H), 7.36 (m, 1H), 7.00-7.13 (m, 3H), 5.76 (dd, *J* = 5.0, 12.2 Hz, 1H), 5.36 (q, *J* = 6.5 Hz, 1H), 4.37 (d, *J* = 6.5 Hz, 1H), 3.89 (s, 2H), 3.83 (dd, 5.4, 8.6 Hz, 1H), 3.43 (dd, *J* = 5.0, 15.3 Hz, 1H), 3.29 (dd, *J* = 12.2, 15.3 Hz, 1H), 2.83 (s, 3H), 2.60 (s, 3H), 1.95 (s, 3H), 1.44-1.75 (m, 4H), 1.03 (d, *J* = 6.9 Hz, 3H), 0.92 (d, *J* = 6.4 Hz, 3H), 0.88 (d, *J* = 6.4, 3H), 0.77 (d, *J* = 6.9 Hz, 3H); 0.75 (d, *J* = 6.8 Hz, 3H); **^{13}C NMR** (MeOD, 125 MHz, major rotamer) δ (ppm); 173.2, 173.2, 172.1, 171.9, 169.1, 138.0, 128.6, 124.0, 122.5, 119.9, 119.0, 112.3, 111.3, 61.4, 58.2, 55.8, 51.6, 42.0, 40.7, 32.2, 31.3, 31.3, 25.2, 24.6, 23.1, 22.2, 20.1, 17.4, 13.7; **IR (ATR)**: ν_{max} = 3292, 3077, 2970, 2940, 2879, 1669, 1632, 1561 cm^{-1}; **$[\alpha]_D^{20}$** = -82° (c = 0.19 in MeOH).

6. Homo-BacPROTAC-induced degradation of ClpC1 as a strategy against drug-resistant mycobacteria

Published in: Nature communications
Impact factor: 14.7 (2023)
doi: 10.1038/s41467-024-46218-7

Contribution:

- Contributed to manuscript drafting
- Establishing a starvation-induced non-replicating persistence model
- Activity assay against replicating and non-replicating starvation-induced *M. tuberculosis* cells
- Determination of minimal inhibitory concentrations against *M. tuberculosis* cells via resazurin dye reduction method
- Isolation of whole cell protein lysates of *M. tuberculosis* cells after treatment with Homo-BacPROTACs and monomeric compounds
- Western Blot analysis of ClpC1 degradation

6.1 Manuscript

nature communications

Article

https://doi.org/10.1038/s41467-024-46218-7

Homo-BacPROTAC-induced degradation of ClpC1 as a strategy against drug-resistant mycobacteria

Received: 28 October 2022

Accepted: 12 February 2024

Published online: 05 March 2024

Check for updates

Lukas Junk[1,6] ✉, Volker M. Schmiedel[2,6], Somraj Guha[1], Katharina Fischel[2], Peter Greb[2], Kristin Vill[3], Violetta Krisilia[3], Lasse van Geelen[3], Klaus Rumpel[2], Parvinder Kaur[4], Ramya V. Krishnamurthy[4], Shridhar Narayanan[4], Radha Krishan Shandil[4], Mayas Singh[4], Christiane Kofink[2], Andreas Mantoulidis[2], Philipp Biber[2], Gerhard Gmaschitz[2], Uli Kazmaier[1], Anton Meinhart[5], Julia Leodolter[5], David Hoi[5], Sabryna Junker[5], Francesca Ester Morreale[5], Tim Clausen[5], Rainer Kalscheuer[3], Harald Weinstabl[2] ✉ & Guido Boehmelt[2] ✉

Antimicrobial resistance is a global health threat that requires the development of new treatment concepts. These should not only overcome existing resistance but be designed to slow down the emergence of new resistance mechanisms. Targeted protein degradation, whereby a drug redirects cellular proteolytic machinery towards degrading a specific target, is an emerging concept in drug discovery. We are extending this concept by developing proteolysis targeting chimeras active in bacteria (BacPROTACs) that bind to ClpC1, a component of the mycobacterial protein degradation machinery. The anti-*Mycobacterium tuberculosis* (*Mtb*) BacPROTACs are derived from cyclomarins which, when dimerized, generate compounds that recruit and degrade ClpC1. The resulting Homo-BacPROTACs reduce levels of endogenous ClpC1 in *Mycobacterium smegmatis* and display minimum inhibitory concentrations in the low micro- to nanomolar range in mycobacterial strains, including multiple drug-resistant *Mtb* isolates. The compounds also kill *Mtb* residing in macrophages. Thus, Homo-BacPROTACs that degrade ClpC1 represent a different strategy for targeting *Mtb* and overcoming drug resistance.

Based on the most recent analysis, bacterial antimicrobial resistance (AMR) is associated with 4.95 million deaths globally, with 1.97 million of those directly attributable to resistance[1]. Furthermore, AMR has been associated with prolonged hospital stays, increased healthcare costs, long-term disability, and loss of productivity[2,3]. Therefore, these data highlight that AMR is not only a global public health emergency, but a growing economic and societal burden. One of the reasons for the current AMR crisis is the dramatic slow-down in the development and approval of new antibiotics. The number of new approvals plunged from 63 new antibiotics approved between 1980 and 2000, to only 15 new ones approved between 2000 and 2018[4]. Additionally, the discovery of the last original class of antibiotics dates back to the late

[1]Organic Chemistry I, Saarland University, Campus Building C4.2, 66123 Saarbrücken, Germany. [2]Boehringer Ingelheim RCV GmbH & Co. KG, Dr. Boehringer-Gasse 5-11, 1121 Vienna, Austria. [3]Heinrich Heine University Düsseldorf, Faculty of Mathematics and Natural Sciences, Institute of Pharmaceutical Biology and Biotechnology, 40225 Düsseldorf, Germany. [4]Foundation for Neglected Disease Research, Plot No. 20A, KIADB Industrial Area, Veerapura Village, Doddaballapur, Bengaluru 561203 Karnataka, India. [5]Research Institute of Molecular Pathology, Vienna BioCenter, Vienna, Austria. [6]These authors contributed equally: Lukas Junk, Volker M. Schmiedel. ✉e-mail: lukasjunk0101@gmail.com; harald.weinstabl@boehringer-ingelheim.com; guido.boehmelt@boehringer-ingelheim.com

1980s[5]. Moreover, the concurrent rise of AMR has further diminished the effectiveness of the existing antibacterial drugs, highlighting the need to develop antibacterial agents that act via fundamentally new mechanisms.

In general, mechanisms that govern AMR are similar to those that diminish the effectiveness of anti-cancer treatments[6,7]. Therefore, some of the strategies used to combat drug resistance in cancer may also be implementable in the context of AMR. One such strategy is targeted protein degradation (TPD), which has recently emerged as a promising modality for targeted anticancer therapeutics[8]. Unlike traditional targeted therapeutics that usually exert their effects by inhibiting the target of interest, TPD agents redirect the activity of the cellular protein degradation machinery to degrade the target. A class of TPD agents that have been of growing interest are proteolysis targeting chimeras (PROTACs), small molecules that incorporate two ligands, one for the target of interest, and the other for an E3 ubiquitin ligase; the two ligands are connected via a linker of variable chemical composition and length to complete the PROTAC molecule[9]. All three components of the PROTAC molecule, the two ligands and the linker, play important functional roles to ensure that the target of interest is recruited to the E3 ubiquitin ligase machinery in a way that results in target poly-ubiquitination and subsequent degradation by the proteasome[10]. The approach allows various modifications of the general theme, like the reported proteasomal "self-degradation" of the E3 ligase adaptors von Hippel-Lindau (VHL) and cereblon by dimerized binders[11,12], or lysosome-mediated targeted degradation of extracellular proteins and membrane-associated proteins by LYTACs[13,14], as well as the selective removal of non-protein biomolecules or whole organelles by macroautophagy-targeting chimeras, MADTACs (including AUTACs and ATTECs)[15]. Given the degradation-based mechanism of PROTACs, they exhibit unique pharmacological properties, such as substoichiometric (catalytic) activity that improves efficacy and prolongs response[16], improved selectivity that minimizes off-target toxicity[17], activity against drug-resistant targets, and decreased likelihood of drug resistance[18]. The last two points suggest that a PROTAC-based antibacterial agent may overcome AMR.

However, bacteria don't have a ubiquitin-proteasome system. Instead, Gram-positive bacteria have evolved a recently discovered ClpC:ClpP:McsB system, whereby McsB acts as a "tagging kinase" that phosphorylates arginine residues in substrate proteins, which targets them to ClpC, an ATP-dependent unfoldase that recognizes and unfolds phospho-arginine (pArg) marked proteins and translocates them into the associated protease cage formed by ClpP units[19]. Thus, McsB could be considered as the prokaryotic counterpart to the eukaryotic ubiquitin E3 ligases, whereas pArg represents a small moiety equivalent of the poly-ubiquitin degradation tag. A recent proof-of-concept study validated that PROTAC-like molecules (BacPROTACs) redirect ClpC activity towards non-endogenous model protein substrates, resulting in their degradation via the ClpC:ClpP:McsB system[20]. In order to address whether BacPROTACs represent a viable strategy for antimicrobial drug development, we designed and tested a series of BacPROTACs directly aiming at the ClpCP machinery of *Mycobacterium tuberculosis* (*Mtb*), for two reasons:

First, *Mtb*, the causative agent of tuberculosis (TB), remains one of the deadliest human pathogens, leading to about 1.5 million TB deaths each year. Approximately 3% of new TB and 18% of previously treated TB cases are multidrug- or rifampicin-resistant (MDR/RR)[21]. Moreover, the COVID-19 pandemic has disproportionally affected TB services with the consequence that for the first time in a decade TB mortality has increased in 2021[22,23]. Therefore, developing new treatments for TB remains critically important[23]. Second, approaching the ClpCP system of mycobacteria is also guided by the fact that potent (nM active) binders, so-called cyclomarins, of ClpC1, the mycobacterium ClpC homolog, are described which should accelerate the first proof of concept experiments[24–28].

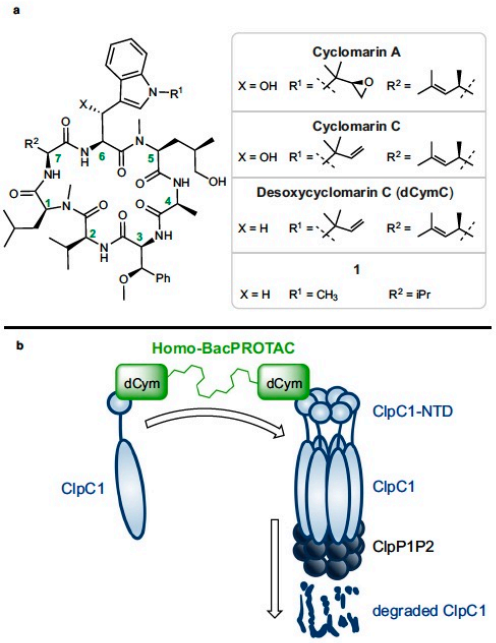

Fig. 1 | Elements and mode of action of Homo-BacPROTACs. a Naturally occurring cyclomarins and simplified synthetic dCym derivatives. The numbering system for amino acid positions used in this work is based on their introduction in the chemical synthesis and is indicated in the structure. **b** Concept for the Homo-BacPROTAC-induced degradation of ClpC1.

Here, we show the feasibility of developing BacPROTACs with anti-*Mtb* activity. Although *Mtb* does not have a homolog of McsB, it does have ClpC1, a homolog of ClpC, also functioning as a core element in the degradation machinery. We use cyclomarins as a chemical starting point for designing "Homo-BacPROTACs" that link two cyclomarin ligands together into a ClpC1-hijacking and targeting degrader molecule. We show that these molecules bind and degrade ClpC1 in vitro and remove a large portion of the intracellular pool of endogenous ClpC1 in a model mycobacterium, *M. smegmatis* (*Msm*). Importantly, these Homo-BacPROTACs exert potent bactericidal activity against both wildtype and multiple drug-resistant *Mtb* isolates, and also kill *Mtb* H37Rv residing in THP-1 macrophages. Taken together, our results suggest that Homo-BacPROTACs targeting *Mtb* ClpC1 for degradation provide a promising starting point for developing TPD-based strategies to thwart AMR.

Results & Discussion

Chemical synthesis of Homo-BacPROTACs

Using simplified desoxycyclomarin derivative **1** (Fig. 1a) as a backbone, we aimed to develop Homo-BacPROTAC molecules that simultaneously bind to two molecules of ClpC1. We hypothesized that the crosslinking of ClpC1 units would induce "self-degradation" of this essential unfoldase (Fig. 1b), leading to more efficient killing of mycobacteria as compared to the parental, non-degrading cyclomarins. Based on previous structure-activity relationship (SAR) studies[29], as well as the high-resolution X-ray crystal structure of ClpC1 N-terminal domain (NTD) bound to cyclomarin A (CymA)[24], we selected amino acids in positions 3, 6, and 7 as suitable exit vectors. The

Article https://doi.org/10.1038/s41467-024-46218-7

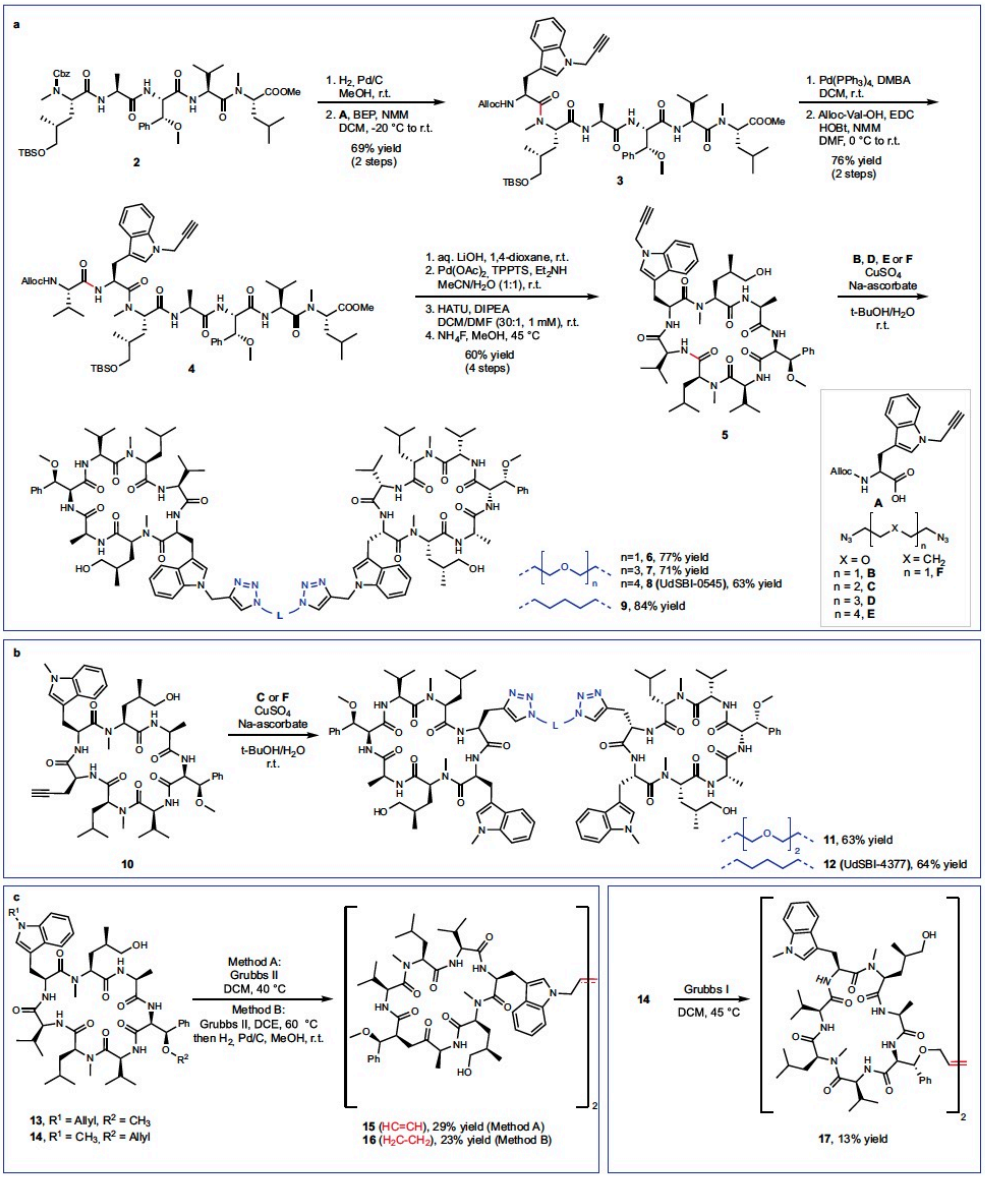

Fig. 2 | Chemical synthesis of Homo-BacPROTACs. a Chemical synthesis of exit vector 6 Homo-BacPROTACs via CuAAC. **b** Synthesis of exit vector 7 Homo-BacPROTACs via CuAAC. **c** Synthesis of exit vector 6 and 3 Homo-BacPROTACs via olefin metathesis. BEP: 2-Bromo-1-ethylpyridinium tetrafluoroborate; DMBA: *N,N'*-Dimethylbarbituric acid; EDC: 1-Ethyl-3-(3-dimethylaminopropyl)carbodiimide hydrochloride; HOBt: 1-Hydroxybenzotriazole; NMM: *N*-methylmorpholine; TPPTS: 3,3',3''-Phosphanetriyltris(benzenesulfonic acid) trisodium salt; HATU: 1-[Bis(dimethylamino)methylene]-1H-1,2,3-triazolo[4,5-b]pyridinium 3-oxide hexafluorophosphate.

dimerization of the cyclic peptides was accomplished using either Cu(I)-catalyzed azide-alkyne cycloaddition (CuAAC) or olefin metathesis. The synthesis of exit vector 6 Homo-BacPROTACs started with literature-known pentapeptide **2** (Fig. 2). A sequence of two *N*-deprotections and peptide couplings with *N*1-propargylated tryptophan **A**[30] and allyloxycarbonyl-protected valine provided linear heptapeptide **4**, which was further converted to cyclomarin derivative **5** in a 4-step sequence. Using CuAAC reactions with different PEG- or alkyl

diazides, the corresponding dimers **6, 7, 8** (UdSBI-0545) and **9** were obtained (Fig. 2a). Two Homo-BacPROTACs bearing the exit-vector at amino acid 7 were synthesized from cyclic peptide **10** which was prepared analogously. The dimeric structures **11** and **12** (UdSBI-4377) were obtained by CuAAC reactions with 1,5-diazidopentane or 1,2-bis(2-azidoethoxy)ethane, respectively (Fig. 2b). By employing the enantiomeric starting materials, we additionally prepared enantiomeric Homo-BacPROTACs **8a** (UdSBI-0966) and **12a** (UdSBI-0117), to serve as distomeric negative controls in the degradation assays. The synthesis of two exit vector 3 Homo-BacPROTACs **SI-39** and **SI-40** was accomplished following the same synthetic route (see Supplementary Information). A propargyl ether attached to the *para*-position of β-methoxy-phenylalanine was used as the exit vector in this case. To obtain Homo-BacPROTACs with a more rigid linker which would also omit the polar triazole groups, we prepared cyclic heptapeptides **13** and **14** bearing either *O*- or *N*-allylated amino acids in positions 3 and 6. These compounds were then dimerized by olefin metathesis yielding Homo-BacPROTACs **15** and **17** (Fig. 2c). For **17**, however, we observed compound decomposition upon storage, which could also serve as an explanation for the low yield obtained in the synthesis of this dimer. Compound **16**, bearing a fully saturated linker was readily obtained by hydrogenation of the double bond in **15**.

In general, cyclic peptides are highly polar, which decreases their cellular permeability. We tested the cellular permeability of Cym derivatives as well as the Homo-BacPROTACs in Caco-2 cell monolayers and observed low permeability for all dimers tested (Supplementary Table 1). Therefore, we introduced peptide backbone modifications at solvent-exposed NH groups to increase the eukaryotic cell permeability. We identified the NH groups of valine and tryptophan as solvent-exposed, using nuclear magnetic resonance (NMR) methods[31,32] (Supplementary Tables 12, 13 and Supplementary Figs. 4–6). Since the NH of valine is involved in an H-bond network with ClpC1-NTD, we assumed that methylation of this amide would be detrimental to the binding affinity, and did not modify this position. Therefore, we focused on methylating the Trp-N^{α}-H (pos. 6), which was solvent-exposed and not involved in protein binding. The synthesis of the Trp-N^{α}-methylated derivatives was accomplished similarly to the other cyclomarin derivatives (Fig. 3). For the challenging couplings of *N*-methylated peptides, we in most cases used a slightly modified protocol introduced by Fuse et al.[33], employing catalytic amounts of *N*-methylimidazole and HCl. We observed lower yields in the cyclization reactions of heptapeptides such as **19** than in the case of non-methylated peptides, which we attribute to a less favorable conformation in Trp-N^{α}-methylated peptides. When conducted at higher temperatures in 1,2-dichloroethane, the cyclizations however yielded the *N*-methylated compounds in synthetically useful yields. The homodimerizations of these derivatives were accomplished using the same conditions as described above.

Structure-Activity Relationship (SAR) study of ClpC1-NTD targeting Homo-BacPROTACs

To characterize Homo-BacPROTACs and compare them to the monomeric derivatives, we used surface plasmon resonance (SPR) to measure the dissociation constants (K_D) towards ClpC1-NTD. We observed that Homo-BacPROTACs displayed an improved binding affinity for the NTD of ClpC1, roughly by a factor of 10 when compared to monomeric compounds (Table 1, Supplementary Table 1). To investigate whether Homo-BacPROTACs bind monovalently to the ClpC1-NTD surface, we performed a stacking experiment (Supplementary Fig. 210). When injecting ClpC1-NTD over a surface of biotinylated ClpC1-NTD saturated with dimeric Homo-BacPROTAC, we observed very limited binding (10% of the expected response), suggesting that only a fraction of the presumably free Cym moieties of the Homo-BacPROTAC were available for binding to the injected protein. The simplest explanation for this result is that the Homo-BacPROTAC is bound bivalently to different ClpC1-NTD molecules on the chip surface.

Along those lines, weaker binding was observed for some Homo-BacPROTACs with rigid linkers, whereas the influence of linker length upon binding was neglectable. The introduction of the methyl group at amino acid 6 led to weaker binding, which remained in the single-digit nanomolar range (Table 1). Exceptions to the latter observation were the two matched pairs **8**/**27** (entry 6) and **15**/**28** (entry 9), in which the matched pairs bind to ClpC1-NTD with nearly equal strength. The intended improved permeability into Caco-2 cells for Trp-N^{α}-methylated derivatives could clearly be observed for monomeric compounds (Table 1, full details in Supplementary Table 1). The alkyne-containing dimerization precursors **20** and **26** showed efflux ratios of 11.8 and 2.2, thereby being more permeable by roughly one order of magnitude compared to their matched pairs lacking the alkylation (entries 2 and 5). The effect was slightly diminished when comparing dCymC to its alkylated counterpart **23** (entry 1) and model compounds **24**/**25**, bearing n-pentyl-triazolyl motifs at the linker attachment points (entry 3). In these cases, N-methylation led to a 1.5 times increase in permeability, respectively. Unfortunately, permeability of Homo-BacPROTACs proved difficult to measure in our hands using a variety of assay conditions. Aqueous solubility remained low throughout the compounds synthesized in this study and could only be improved upon the introduction of more polar side chains. These side chains interfered with compound binding to ClpC1-NTD and were therefore discarded in further designs.

We also measured metabolic stability and saw improvements over the monomeric compounds (full details in Supplementary Table 2), which might be due to oxidative liability of unsaturated side chains in these compounds that are absent from our Homo-BacPROTACs. This improvement in in vitro metabolic stability was reflected in an in vivo PK study of three Homo-BacPROTACs and one monomer (BALB/cAnNCrl mice, 1 mg kg^{-1} bolus IV administration): **5, 6, 8** and **12**. The Homo-BacPROTACs **6** and **8**, which use position 6 (Trp) as exit vector, showed higher c_{max} and AUC, but lower clearance than monomer **5** (Supplementary Table 3). The monomer **5** was metabolized and excreted quickly and was unable to build up meaningful levels in blood. A corresponding oral PK study of these compounds did not result in an interpretable plasma exposure, due to very slow adsorption in the gut caused by the low solubility of the compounds (Supplementary Tables 14–17). Taken together, Homo-BacPROTACs outperformed the parental cyclic peptides in terms of binding affinity and metabolic stability, although additional optimization of these compounds is needed to obtain cellular permeability and oral bioavailability.

Homo-BacPROTACs are potent degraders of ClpC1-NTD

Since the affinity towards ClpC1-NTD of various Homo-BacPROTACs described above is in the sub-nM range, we assessed whether such molecules could induce degradation of their cognate target ClpC1 in a cell-free degradation assay. To this end, a minimal recombinant degradation machinery consisting of full-length *Msm* ClpC1, processed *Msm* ClpP1 and ClpP2, combined with an ATP-regenerating system[20], was adapted to allow quantifiable capillary Western (WES) readout (Supplementary Table 8 and Supplementary Fig. 3). We first used His_6-tagged ClpC1-NTD as substrate and analyzed various Homo-BacPROTACs with respective controls. As shown in Fig. 4, Homo-BacPROTAC **8** (UdSBI-0545) induces efficient removal of ClpC1-NTD substrate with a half-maximal degradation concentration (DC_{50}) of 8.0 μM and a maximum degradation efficacy (D_{Max}) of 83%. Similarly, Homo-BacPROTAC **12** (UdSBI-4377) induces degradation with a DC_{50} of 8.4 μM and a D_{Max} of 81% (Fig. 4a, b and Supplementary Table 8). In contrast, vehicle, dCymC, the matching monomers **5** (UdSBI-6231) and **10** (UdSBI-5602), or Homo-BacPROTAC enantiomers **8a** (UdSBI-0966) and **12a** (UdSBI-0117), did not cause any degradation of the His_6-tagged ClpC1-NTD substrate (Fig. 4a–d and Supplementary Table 8).

Article https://doi.org/10.1038/s41467-024-46218-7

Table 1 | Structure-activity relationships of monomeric dCym derivatives and Homo-BacPROTACs

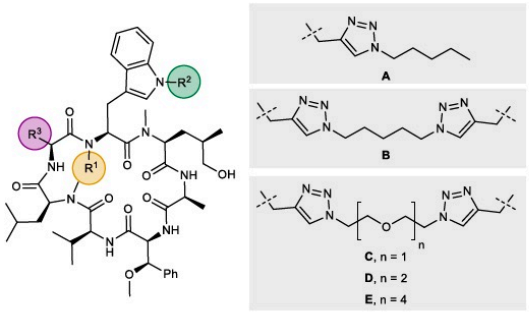

Entry	Compound		R1	R2	R3	ClpC1-NTD KD[a] [nM] Mean ± SD	MIC Mtb H37Rv[b] [μM] Mean ± SD	Influence of N-methylation on permeability[c]
1	dCymC	Monomer	H			1.1 ± 0.4	0.4 ± 0.1	
	23		Me			12.1 ± 0.3	n.d.	1.6
2	**10**	Monomer	H	Me		4.0 ± 0.7	3.1 ± 0.0	>11.8
	20		Me			13.9 ± 0.3	50.0 ± 0.0	
3	**24**	Monomer	H	Me	A	4.6 ± 0.2	n.d.	>1.5
	25		Me			26.1 ± 0.1	6.3	
4	**12** (UdSBI-4377)	Dimer	H	Me	B	0.28 ± 0.08	0.1 ± 0.0	n.d.
	22		Me			0.9 ± 0.3	3.1 ± 0.0	
5	**5**	Monomer	H		*i*Pr	3.5 ± 0.1	1.6	9.3
	26		Me			15 ± 3	6.3	
6	**8** (UdSBI-0545)	Dimer	H	E	*i*Pr	0.4 ± 0.1	0.4 ± 0.4	n.d.
	27		Me			0.4 ± 0.2	<0.1	
7	**6**	Dimer	H	C	*i*Pr	0.9 ± 0.4	0.4 ± 0.3	–
8	**11**	Dimer	H	Me	D	0.4 ± 0.2	0.1 ± 0.0	–
9	**15**	Dimer	H		iPr	1.2 ± 0.8	0.2 ± 0.1	n.d.
	28		Me			1.8 ± 0.1	n.d.	

K_D and MIC values are reported as mean ± SD. The number of measurements performed for each compound are indicated by footnotes in Supplementary Tables 1 and Table 2.
[a]Dissociation constant K_D towards ClpC1-NTD measured by surface plasmon resonance.
[b]Minimum inhibitory concentrations against *M. tuberculosis* H37Rv strain.
[c]Determined by comparison of efflux ratios across Caco-2 monolayers for matched pairs: R_{eff} (N-H)/R_{eff} (N-Me). n.d.: not determined. Bold numbers refer to compounds described in the text.

We also tested whether the Homo-BacPROTACs would be comparably active in a reconstituted degradation assay in which the three *Msm* proteins were replaced by their corresponding *Mtb* homologues. To this end, various Homo-BacPROTACs, their distomers, and matching monomeric compounds were tested in the *Mtb* cell-free degradation assay and we observed Homo-BacPROTAC-mediated degradation of the ClpC1-NTD (Supplementary Table 8), with comparable DC_{50} values and slightly reduced D_{Max} values as seen for *Msm* ClpC1P1P2. As expected, the control compounds did not cause degradation.

We also analyzed whether full-length ClpC1 would be degraded in this assay, by analyzing the stability of the full-length form monitored by a ClpC1-N-terminal antibody in the WES assays, or directly by SYPRO™ Ruby stained SDS-PAGE gels in the presence or absence of ClpC1-NTD as additional substrate. The Homo-BacPROTACs tested induced no or only minor degradation of the full-length ClpC1 under these in vitro conditions (Fig. 4e). Whether this is due to hexamer formation stabilizing ClpC1 protomers or missing cofactor(s) of the protease complex, is currently unclear. Likewise, the exact sequential and structural features of native substrates targeted by ClpC1 are not known, except that partially disordered peptide segments can promote degradation[20].

Homo-BacPROTACs induce degradation of endogenous ClpC1 in *Msm*

Irrespective of the behavior of Homo-BacPROTACs in cell-free assay systems, we wanted to assess their potential to degrade endogenous ClpC1 in *Msm*. Using a capillary Western-based cellular degradation assay, we could show that Homo-BacPROTAC **8** (UdSBI-0545) induced degradation with an average DC_{50} of 0.57 ± 0.40 μM and an average D_{max} of 48 ± 13% after 24 h of incubation in a concentration-dependent manner (Fig. 5a), while the enantiomeric control **8a** (UdSBI-0966) did not lead to intracellular degradation of ClpC1 (Fig. 5b). Homo-BacPROTAC **12** (UdSBI-4377) also induced full-length ClpC1 degradation (average DC_{50} 0.17 ± 0.10 μM; average D_{max} 43 ± 8%), while its enantiomer **12a** (UdSBI-0117) was inactive (Fig. 5b). In addition, the matching monomers **5, 10** and dCymC did not induce degradation of ClpC1 (Fig. 5c). Consistent with our findings, recent proteomics analyses highlighted that although monomeric cyclomarin derivatives and Homo-BacPROTACs both bind to ClpC1 causing strong perturbations in the mycobacterial proteome, only Homo-BacPROTACs induce efficient degradation of ClpC1 in *Mtb* at concentrations and time points consistent with their activity in MIC assays[34]. Together, these two

Article https://doi.org/10.1038/s41467-024-46218-7

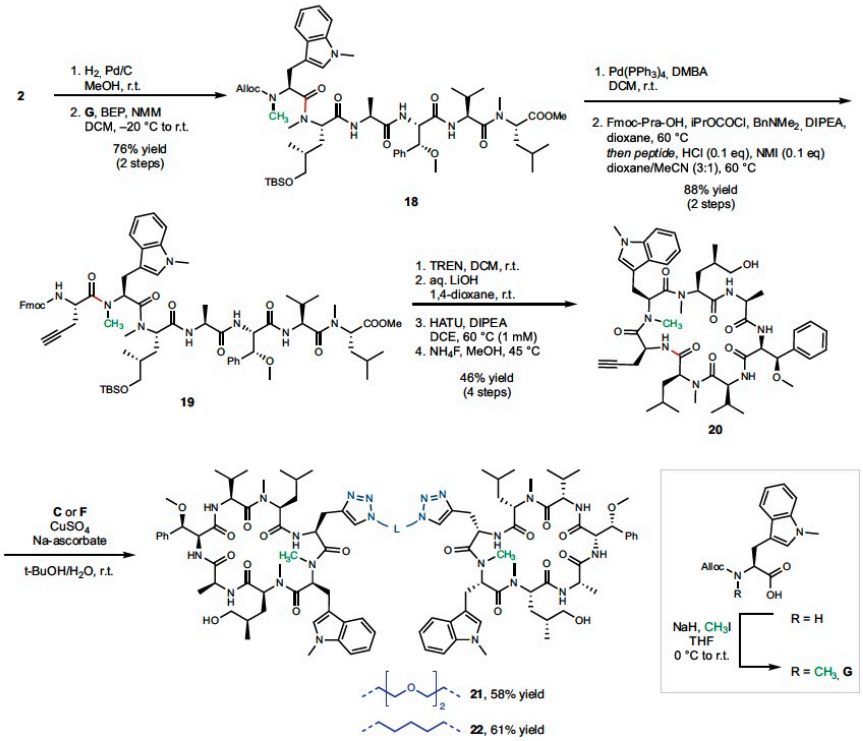

Fig. 3 | Further modifications of exit vector 7 Homo-BacPROTACs. Chemical synthesis of exit vector 7 Homo-BacPROTACs bearing an additional methyl group (shown in green) attached to tryptophan-N$^{\alpha}$. Pra Propargylglycine. NMI *N*-methylimidazole. TREN Tris(2-aminoethyl)amine.

studies thus present the first example of Homo-BacPROTAC-mediated targeted degradation of an endogenous protein in mycobacteria. Several reasons could compromise the cellular activity of Homo-BacPROTACs, preventing complete degradation of their target in *Msm*. Such parameters could include the potentially smaller permeability of these dimeric molecules through bacterial membranes, putative resistance mechanisms, and altered half-life or re-synthesis rate of ClpC1. In fact, further analysis of the moderate degradative efficacy of the Homo-BacPROTACs in *Msm* led to the discovery of an antibiotic scavenger system protecting ClpC1 and the ClpC1P1P2 protease[34].

Biological activity of Homo-BacPROTACs

We further investigated, whether Homo-BacPROTACs would be active in inhibiting the proliferation of pathogenic mycobacteria, and how their cellular activity compares to their matched monomeric compounds or the parental dCymC. We, therefore, assessed the minimum inhibitory concentrations (MICs) against *Mtb* H37Rv in liquid culture resazurin assays. While dCymC inhibits the growth of *Mtb* H37Rv at 0.4 ± 0.1 μM, the alkyne-bearing monomeric derivative **10** does so at 3.1 ± 0.0 μM. Interestingly, the corresponding Homo-BacPROTAC **12** (UdSBI-4377) inhibits the growth of this *Mtb* strain at 0.1 ± 0.0 μM. In this series, the SPR K_D to ClpC1-NTD improves by a factor of 10 from monomeric **10** to dimeric **12**, whereas the MICs for these compounds against *Mtb* improve by a factor of 30. This can be seen as an indication of the catalytic mode of action of Homo-BacPROTACs, since similar improvements in MIC potency on *Mtb* H37Rv by Homo-BacPROTACs as compared to their matching monomeric counterparts were also observed for other series (Supplementary Table 2).

We also tested various Homo-BacPROTACs and control compounds for their MIC on *Msm #607*. Interestingly, the MIC values were higher than those observed for *Mtb* H37Rv and, in addition, very comparable between Homo-BacPROTACs and matching monomers (Supplementary Table 2). This indicates that these two strains of mycobacteria respond differently to Homo-BacPROTACs. Consistently, quantitative proteomics demonstrated the higher efficacy of Homo-BacPROTACs in inducing ClpC1 degradation in the *Mtb* H37Rv strain as compared to *Msm*[34].

To further confirm the qualitative difference in responsiveness between *Msm* and *Mtb*, we assessed whether Homo-BacPROTACs are bactericidal or bacteriostatic. To this end we performed MBC (minimum bactericidal concentration) assays, where, following a MIC assay, compound-treated cultures were replated on 7H9 complete agar in the absence of compound. While growth of colonies could be observed across all tested concentrations (up to 50 μM) of **8** (UdSBI-0545) or **12** (UdSBI-4377) in the case of *Msm #607*, *Mtb* cultures treated with these Homo-BacPROTACs did not form any colonies at concentrations at or above the MIC value. These results are consistent with the notion that Homo-BacPROTACs are bacteriostatic on *Msm #607*, but bactericidal on *Mtb* H37Rv (Supplementary Table 11).

Next, we analyzed whether Homo-BacPROTACs would be selective for mycobacteria, as one would anticipate based on the limited homology within ClpC family members across prokaryotes.

Article https://doi.org/10.1038/s41467-024-46218-7

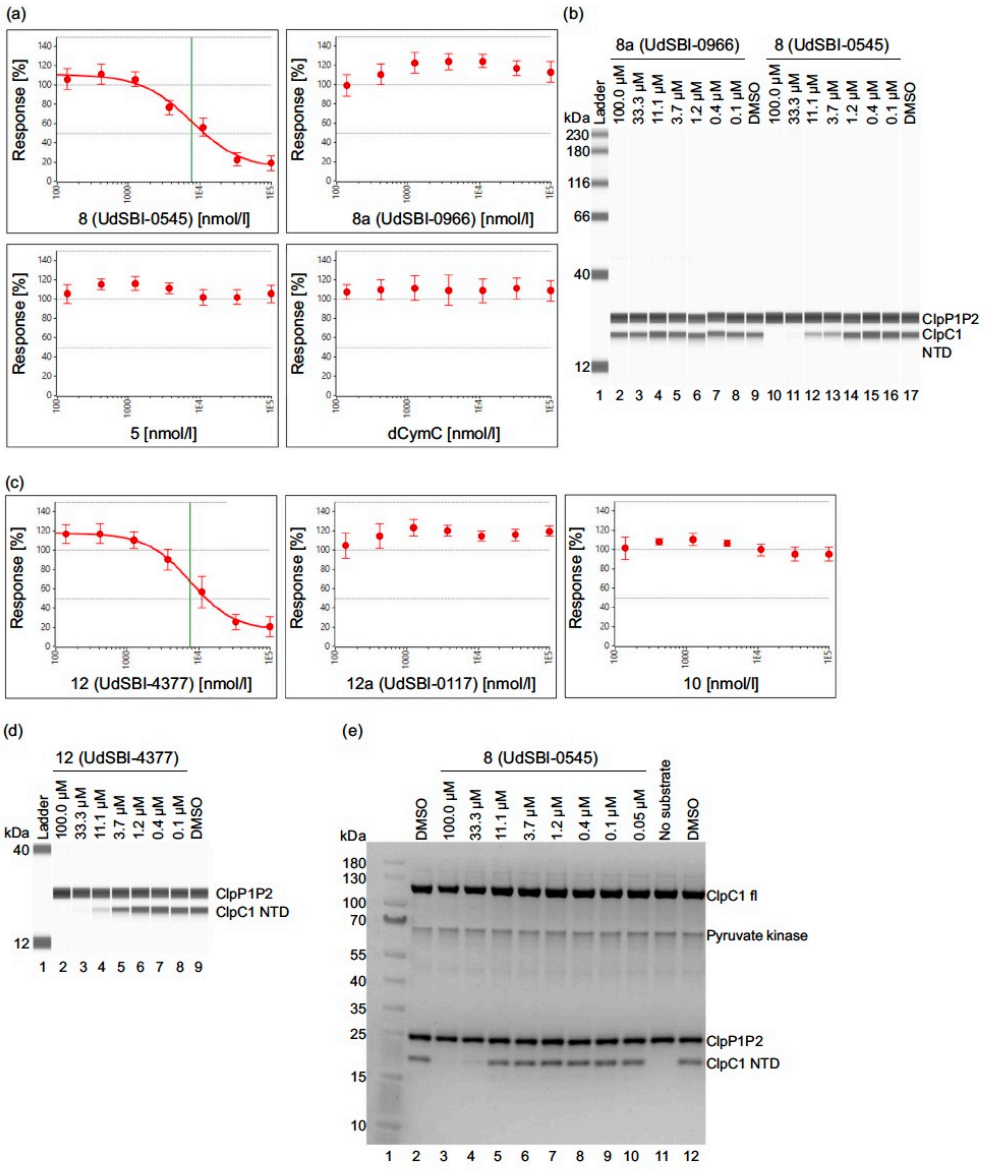

Fig. 4 | Activity of Homo-BacPROTACs in cell-free degradation assays. **a** Degradation curves of ClpC1-NTD in the cell-free degradation assay (quantified by capillary Western (WES)) induced by Homo-BacPROTAC **8** (UdSBI-0545) compared to its enantiomer **8a** (UdSBI-0966), matching monomer **5** and dCymC (3 independent experiments done in triplicates). **b** WES visualization of ClpC1-NTD degradation after titration of Homo-BacPROTACs, developed with anti-His antibody recognizing His6-tagged ClpC1-NTD and processed, His4-tagged ClpP1P2. Concentration-dependent degradation of ClpC1-NTD can be observed for **8** (UdSBI-0545) (lanes 10–13) but not for **8a** (UdSBI-0966) (lanes 2–8). **c** Analogous to **a**, except that exit vector 7-based Homo-BacPROTAC **12** (UdSBI-4377), enantiomer **12a** (UdSBI-0117) and monomer **10** were used. **d** WES-derived gel picture visualizing ClpC1-NTD degradation (lane 2–5) from representative experiment summarized in **c**. **e** SYPRO™ Ruby-stained SDS-PAGE gel from exemplary cell-free degradation assay depicting efficient degradation (lane 3,4) of ClpC1-NTD by Homo-BacPROTAC **8** (UdSBI-0545), while full length ClpC1 is not significantly degraded. Green vertical lines indicate the DC_{50} (for **8**, **12**). Error bars represent mean ± SD of $n = 3$ independent experiments in triplicates. The actual mean DC_{50} values for all cell-free degradation experiments conducted for this study are summarized in Supplementary Table 8. Source data are provided as a Source Data file.

Article https://doi.org/10.1038/s41467-024-46218-7

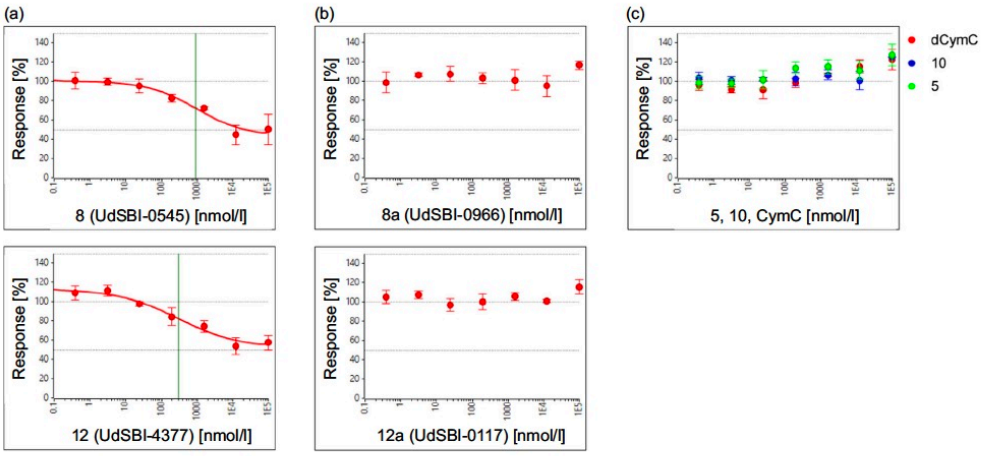

Fig. 5 | Homo-BacPROTACs degrade intracellular ClpC1. a Intracellular degradation of ClpC1 in *Msm #607* cells following a 24 h incubation with Homo-BacPROTACs **8** (UdSBI-0545), or **12** (UdSBI-4377). Green vertical lines indicate the DC_{50} values obtained in that particular experiment. **b** ClpC1 levels in *Msm #607* following a 24 h incubation with distomers **8a** (UdSBI-0966), or **12a** (UdSBI-0117). **c** ClpC1 levels in *Msm #607* following a 24 h incubation with monomers **5** (green), **10** (blue), or dCymC (red). The curves show representative experiments performed in well triplicates. Experiments for each compound were performed independently $n = 3$ (compounds **8, 8a, 12a, dCymC, 5, 10**) or $n = 4$ (compound **12**) times with similar results. Error bars indicate mean ± SD of $n = 3$ well replicates for that given experiment. The actual mean DC_{50} values reported in the text for compound **8** or **12** are calculated from the respective individual DC_{50} values obtained for the independent cellular degradation experiments conducted in this study and are summarized in the Source Data file for Fig. 5a. Source data are provided as a Source Data file.

To this end, various Gram positive and Gram negative bacteria were tested in MIC assays using Homo-BacPROTACs **8** (UdSBI-0545), **12** (UdSBI-4377), and their matching monomers **5** and **10**, respectively. As expected, no inhibition of growth was observed (Supplementary Table 9). To obtain further resolution of potency within the family of mycobacteria, various disease-associated representatives like *M. avium*, *M. abscessus*, *M. fortuitum*, and *M. intracellulare* were assessed. Interestingly, at the tested concentrations, no growth inhibition could be observed for the two Homo-BacPROTACs for these NTM (nontuberculous mycobacteria) strains, while the matching monomeric compounds were active in the single-digit μM range (Supplementary Table 10).

Due to the potent bactericidal activity of these Homo-BacPROTACs towards the well studied *Mtb* H37Rv strain, and the assumption that Homo-BacPROTACs would also be active against drug resistant strains, we investigated whether various *Mtb* isolates, including isolates being resistant to known TB drugs, respond to incubation with Homo-BacPROTACs **8** (UdSBI-0545), or **12** (UdSBI-4377). This includes *Mtb* isolates like the RpoB S450L mutant conferring rifampicin resistance, the *katG* deletion strain, conferring isoniazid resistance, a clincial isolate (FNDR-M1) resistant to moxifloxacin, or the Beijing strain HN878. As can be seen in Table 2, Table 3 and Supplementary Fig. 1, the Homo-BacPROTACs were highly potent on such isolates and outperformed the matching monomers.

Next, we asked to what extent non-growing *Mtb* H37Rv cells would be susceptible to Homo-BacPROTACs, matching monomers or standard-of-care drugs like bedaquiline, D-cycloserine, rifampicin, ethambutol and moxifloxacin. Starvation for three weeks was chosen as a mechanism to induce the non-growing state of the *Mtb* H37Rv cells prior to addition of compounds. Homo-BacPROTACs **8** (UdSBI-0545), or **12** (UdSBI-4377) lost their inhibitory activity similar to several of the TB drugs, while bedaquiline, rifampicin and the matching monomers retained a partial inhibitory activity (Supplementary Fig. 2).

Along those lines, and to assess other dormancy mimicking states, Homo-BacPROTACs were recently tested on Mtb H37Rv cells in combination with bedaquiline[34]. By inhibiting the ATP synthase subunit C (AtpE), bedaquiline induces lower intracellular ATP levels, resembling a dormant state in *Mtb*. The presence of bedaquiline had no effect on the activity of **12** (UdSBI-4377) against *Mtb* H37Rv[34]. Homo-BacPROTAC activity may thus depend under some circumstances on the environmental conditions presented to the *Mtb* cells.

Lastly, pathogenic *Mtb* strains reside in eukaryotic cells including macrophages, which is part of their immune system-evading strategy leading to an indefinite persistence in infected individuals. This may eventually lead to reactivation and thereby the emergence of new tuberculosis cases[36,37]. We, therefore, asked whether the Homo-BacPROTACs can impair the survival of *Mtb* H37Rv in macrophages differentiated from the monocytic leukemia cell line THP-1. We compared the effects of Homo-BacPROTACs to those of their corresponding monomers and the reference antibiotics rifampicin and moxifloxacin, which are known to inhibit the intracellular propagation of *Mtb*. Maximal concentrations of compounds employed in these studies were pretested not to affect uninfected, differentiated THP-1 cells. Exit vector 6 Homo-BacPROTACs clearly showed a concentration-dependent reduction of colony-forming units (cfu) over time with an E_{max} of 1.22–1.27 at 50 μM (Fig. 6a), while exit vector 7 Homo-BacPROTACs were less efficient with an E_{max} ranging from 0.28–0.51 at the same concentration (Fig. 6b). Homo-BacPROTACs performed more efficiently over time than their matched monomeric counterparts (Fig. 6a), or reduced intracellular *Mtb* at lower concentrations (Fig. 6b). These results demonstrate that Homo-BacPROTACs can enter eukaryotic host cells and kill intracellularly residing pathogenic mycobacteria.

In conclusion, we herein describe the synthesis and characterization of Homo-BacPROTACs. These compounds are composed of two cyclic heptapeptides derived from the natural product class of cyclomarins and induce degradation of mycobacterial ClpC1, a

Table 2 | MICs of Homo-BacPROTACs and monomers against clinical isolates resistant to single *Mtb* drugs

Compound	*Mtb* H37Rv	*Mtb* (moxR) FNDR-M1	*Mtb* (RpoB S450L) ATCC 35838	*Mtb* (*katG* del) ATCC 35822
	MIC (μM)			
12 (UdSBI-4377)	0.1 ± 0.0	0.2 ± 0.0	0.2 ± 0.0	0.1 ± 0.0
8 (UdSBI-0545)	0.2 ± 0.1	0.2 ± 0.0	0.2 ± 0.0	0.2 ± 0.0
10	3.1 ± 0.0	1.6 ± 0.0	1.6 ± 0.0	1.6 ± 0.0
5	2.6 ± 0.9	0.7 ± 0.2	0.4 ± 0.0	0.8 ± 0.0
Rifampicin	0.01 ± 0.0	0.01 ± 0.0	**>38.9**	0.01 ± 0.0
Moxifloxacin	0.2 ± 0.0	**19.9 ± 0.0**	0.3 ± 0.0	0.3 ± 0.0
Isoniazid	0.2 ± 0.0	0.1 ± 0.0	0.5 ± 0.0	**>232.2**

Bold numbers refer to compounds described in the text. MIC values reflecting resistance are indicated in bold.
Values represent means and standard deviations from $n = 3$ well replicates.

Table 3 | Homo-BacPROTACs are potent on multiple drug-resistant *Mtb* strains

Compound	MIC *Mtb* # 11291		MIC *Mtb* # 8673		MIC *Mtb* ATCC 35825	
	μM	μg/ml	μM	μg/ml	μM	μg/ml
10	0.4	0.4	0.4	0.4	0.4	0.4
12 (UdSBI-4377)	<0.1	<0.2	<0.1	<0.2	<0.1	<0.2
5	0.2	0.2	0.2	0.2	0.2	0.2
8 (UdSBI-0545)	<0.1	<0.2	<0.1	<0.2	<0.1	<0.2
Moxifloxacin	0.2	0.1	0.1	0.1	0.1	0.1
Streptomycin	0.4	0.3	6.9	4.0	**27.5**	**16.0**
Isoniazid	3.6	0.5	**466.7**	**64.0**	**29.2**	**4.0**
Rifampicin	0.005	0.004	**38.9**	**32.0**	0.005	0.004
Amikacin	3.4	2.0	**>218.6**	**>128.0**	0.1	0.03
Thiacetazone	4.2	1.0	**>541.7**	**>128.0**	4.2	1.0
p-Aminosalicylic acid	6.5	1.0	6.5	1.0	**104.5**	**16.0**

Bold numbers refer to compounds described in the text. MIC values reflecting resistance are indicated in bold.
Values represent means from $n = 2$ well replicates.

component of the bacterial proteolytic machinery. The dimeric compounds are able to redirect the Clp protease against its own ClpC1 subunit, ultimately leading to the "self-destruction" of the essential unfoldase in mycobacteria. We show that Homo-BacPROTACs cause the degradation of ClpC1-NTD in vitro and the degradation of endogenous full-length ClpC1 in Msm cells. Moreover, compared to monomeric counterparts, improved activity against Mtb wild-type cultures, Mtb residing within macrophages and drug-resistant strains is observed.

However, the reported Homo-BacPROTACs have several limitations, primarily with respect to their physicochemical properties, such as solubility and total polar surface area. This limits their bioavailability and pharmacodynamic profiling in vivo and will require further optimization. Our preliminary SAR studies describe potential strategies going forward and opportunities for synthesis of the next generation of Homo-BacPROTACs. In addition, some nontuberculous mycobacteria do not respond to the Homo-BacPROTACs which currently prevents their use in other disease types. A possible explanation could be especially high or upregulated levels of the counteracting ClpC2 and/or ClpC3 proteins, which were shown to dampen the efficacy of Homo-BacPROTACs in *Msm* as compared to *Mtb* cells[35]. Multiple compound-specific parameters such as metabolic stability, bacterial uptake and efflux behavior could also contribute to different responses in NTM strains.

In summary, our study provides the first example of BacPROTACs that induce degradation of an endogenous bacterial protein, which could serve as a blueprint for the development of anti-mycobacterial agents that may eventually overcome antimicrobial resistance.

Methods

Protein Expression and Purification

Full-length *M. smegmatis* ClpC1 (untagged), ClpP1 (C-terminal His_4-tag) and ClpP2 (C-terminal His_4-tag) proteins were cloned, expressed and purified as described[20].

Full-length *M. tuberculosis* ClpC1 (untagged), ClpP1 (C-terminal His_4-tag) and ClpP2 (C-terminal His_4-tag) proteins were cloned, expressed and purified as described[37].

N-terminal propeptides of ClpP1 and ClpP2 were processed with the activator peptide Z-Leu-Leu-H (Benzyloxycarbonyl-L-Leucyl-L-Leucinal) as described[37].

Cloning, expression and purification of *M. tuberculosis* ClpC1 NTD (AA 1-148, UniProt P9WPC9) with a C-terminal non-cleavable hexahistidine tag was based on the protocol described for its homolog ClpC from *B. subtilis*[19], with the following modifications:

Cells were lysed by sonication in 50 mM Tris, pH 8.0, 150 mM NaCl. The cleared lysate was applied to XK16 Ni-NTA beads (Cytiva) and eluted with lysis buffer containing 250 mM imidazole. The protein was further purified by size exclusion chromatography in 50 mM Tris, pH 8.0, 150 mM NaCl on a HiLoad 16/600 Superdex 200 pg column (Cytiva) and ClpC1 NTD containing fractions were pooled. Sequence of the expressed protein:

MFERFTDRARRVVVLAQEEARMLNHNYIGTEHILLGLIHEGEGVAAK SLESLGISLEGVRSQVEEIIGQGQQAPSGHIPFTPRAKKVLELSLREALQLGH NYIGTEHILLGLIREGEGVAAQVLVKLGAELTRVRQQVIQLLSGYQGKLEHH HHHH

All proteins were aliquoted and stored at −80 °C until further use.

SPR binding studies

SPR experiments were performed on T200 and 8k instruments (Cytiva).

ClpC1 NTD protein (*M. tuberculosis*) was chemically biotinylated using an EZ-Link NHS-PEG4-biotin kit (Thermo Scientific). The labelling procedure was performed according to the manufacturer's instructions with the following modifications: A 1:5 molar ratio of biotin reagent to protein was used and the reaction was incubated for 3 h at room temperature under agitation in 10 mM HEPES, pH 7.4, 150 mM NaCl, 0.05 % Tween20 (HBS-P+). Non-reacted NHS-PEG4-Biotin was subsequently removed using a Zeba Spin desalting column (Thermo Scientific).

Streptavidin (Prospec) was immobilized in 10 mM Na acetate, pH 5.0 at a density of 2000 – 3000 RUs onto flow cells 1 and 2 of a CM5 chip (Cytiva) at 25 °C using an amine-coupling kit (Cytiva) under standard conditions. Biotinylated ClpC1 was then captured to flow cell 2 at a density of 100–200 RUs in HBS-P + .

Compound binding was subsequently analyzed at 25 °C in 25 mM Tris(hydroxymethyl)aminomethane, pH 7.5, 150 mM NaCl, 0.01% Tween20, 1% dimethyl sulfoxide.

Sensorgrams were recorded at different compound concentrations in single-cycle mode and double-referenced prior to data analysis using Biacore Insight software. Data were fitted using the 1:1 interaction model with a term for mass-transport included. A few compounds showed deviation from a mono-exponential decay in the form of a slow-off / irreversible component in the later parts of the dissociation phase. It turned out that for these compounds the U-value (uniqueness-value), a statistical fit quality parameter calculated by the Insight software, was unacceptably high. In these cases, the latter part of the dissociation curve was not included in the fit. This resulted in a

Article https://doi.org/10.1038/s41467-024-46218-7

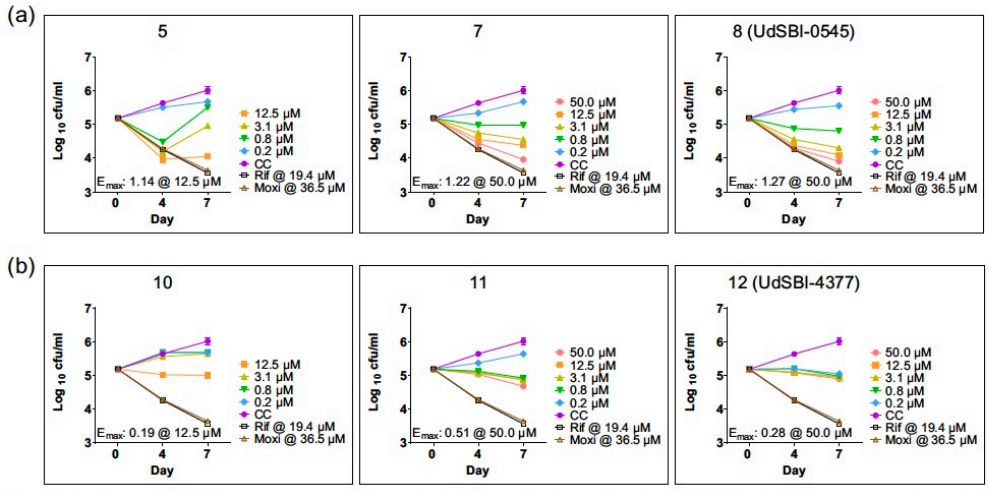

Fig. 6 | Intracellular MIC assay in THP-1 macrophages. a, b Exit vector 6-based Homo-BacPROTACs **7** and **8** (UdSBI-0545), as well as exit vector 7-based Homo-BacPROTACs **11** and **12** (UdSBI-4377) were assessed in a 4- and 7-day incubation on THP-1 macrophages following infection with *Mtb* H37Rv. The Homo-BacPROTACs were compared to their corresponding monomers (**5** for exit vector 6 and **10** for exit vector 7) and the reference antibiotics rifampicin and moxifloxacin, which are known to inhibit the intracellular propagation of *Mtb* H37Rv. Exit vector 6 Homo-BacPROTACs showed a more efficient concentration-dependent reduction of cfu/ml over time with an E_{max} of 1.22 – 1.27 at 50 µM, as compared to exit vector 7 based Homo-BacPROTACs or matched monomers. The various compound concentrations are indicated in different colours, matching across the panels. CC means *Mtb* culture control, where no drug treatment was given. For further details see text. Error bars indicate mean ± SD of $n = 2$ well replicates. The CC, rifampicin and moxifloxacin values were taken as common reference points in the various graphs. Source data are provided as a Source Data file.

significantly improved fit quality as judged by the U-value and visual comparison of sensorgram and fit.

At least two independent measurements were performed for each compound with mean values and standard deviations of these independent measurements reported. The same molar concentrations were used for the evaluation of all SPR experiments. This also applies to monomeric compounds as well as Homo-BacPROTACs, which contain two binding moieties per molecule.

For the stacking experiment, 468 RU of ClpC1-NTD were immobilized on a CM5 chip as described above. The experiment was performed in dual injection mode on an 8k instrument. In short, in the first injection, Homo-BacPROTAC was injected at a fixed concentration of 200 nM. Subsequently, two different concentrations of ClpC1-NTD were injected.

Cell-free degradation assay

The assay was adapted from Morreale et al.[20], with the following modifications:

The assay was performed with degradation machineries from *M. smegmatis* and *M. tuberculosis*.

The final assay mixture contained 0.5 µM *M. smegmatis* or *M. tuberculosis* ClpC1 (hexameric), 0.25 µM *M. smegmatis* or *M. tuberculosis* ClpP1P2 (tetradecameric), 1.5 µM substrate protein *M. tuberculosis* ClpC1NTD, 15 mM phosphoenolpyruvate (PEP, Sigma Aldrich #10108294001), 10 U/ml pyruvate kinase (Sigma Aldrich, #P7768 or P9136). It was performed in a buffer containing 50 mM HEPES pH 7.0, 100 mM KCl, 40 mM $MgCl_2$, 10% (v/v) glycerol.

Compounds were dissolved in 100% (v/v) DMSO, pre-diluted 1:10 with buffer to 10x assay concentration. The final concentration of DMSO in the assay was 1% (v/v). In control experiments, DMSO was added to the same concentration. Reactions were performed in 96-well plates (Eppendorf #951020303, final reaction volume 8 µl). Only the inner 60 wells of each plate were used and wells adjacent to the reaction wells were filled with a matching volume of water. All components except for the compounds and ATP were combined in a master mix. After addition of the compounds to the pre-mix, degradation was started by addition of ATP to a final concentration of 5 mM. The reaction plate was sealed and incubated at 37 °C in an Eppendorf Thermomixer C with heated lid (400 rpm, 90 min) During incubation, a second plate was prepared containing 1.5 µl 5x Fluorescent Master Mix (ProteinSimple) per well, spun down and stored at room temperature. At the end of the incubation, the assay plate was transferred to ice for 30 s and then centrifuged for 5 min at 2200 × g. Reactions were subsequently diluted by adding 2 µl of 0.1 × sample buffer (ProteinSimple) to each well. Next, 6 µl of each reaction were added to the Fluorescent Master Mix, the plate was sealed and incubated at 95 °C for 5 min (non-heated lid). The plates were then allowed to cool down to room temperature and finally centrifuged for 5 min at 2200 x g before analysis.

The WES capillary-based immunoassay platform (ProteinSimple) was used for measurement of the samples according to the manufacturer's instructions. Anti-His tag (0.5 µg/ml, R&D Systems MAB050, for ClpC1 NTD detection) and 6x His tag (Abcam, ab252883, 0.02 µg/ml and 0.1 µg/ml, or ab206500, 0.05 µg/ml and 0.1 µg/ml, for *M. smegmatis* and *M. tuberculosis* ClpP1P2 detection, respectively) were used as primary antibodies, incubated for 60 min and detected using the anti-mouse detection module (ProteinSimple DM-002).

Data analysis was performed using Compass for SW Software (ProteinSimple). Signals were quantified and peaks named (ClpC1 NTD 20–21 kDa, ClpP1P2 26–27 kDa) and the following peak fitting settings were used: Peak Find Threshold 100.0 and Area Calculation by Dropped Lines. All other settings used were the default values.

Resulting ClpC1 NTD areas were divided by ClpP1P2 areas and normalized to the negative control (DMSO/no compound).

DC_{50} values were calculated from these values with Boehringer Ingelheim's MEGALAB DC_{50} application using a 4 parametric logistic

model. The value of the lower asymptote was constrained to >0 % for the calculation of the DC_{50} value. The upper asymptote was constrained to <130%. At least three independent measurements with the *M. smegmatis* machinery and at least two with the *M. tuberculosis* machinery were performed for each compound with mean values and standard deviations reported. All experiments were performed in triplicates. These well replicates were prepared by treating three reactions from the same master mix in the same plate with the same compound dilution.

For SDS-PAGE experiments, reaction samples were treated with 2.7 µl 4x Roti Load 1 (Roth #K929.1), instead of adding sample buffer and fluorescent mastermix, and incubated at 95 °C for 5 min. Samples were then loaded on a 4–12% Bis-Tris Criterion XT Precast gel (BIO-RAD #3450125). The PageRuler Prestained Protein Ladder (Thermo Scientific #26616) was used as a marker. Gels were run in BIO-RAD Criterion cells with a PowerPac Basic (BIO-RAD) and stained using SYPRO™ Ruby Protein Gel Stain (Invitrogen S12000) following the protocol provided by the manufacturer with a few modifications: Gels were incubated in 2 × 100 ml fix solution (50% (v/v) methanol, 7% (v/v) acetic acid) for 30 min, then 100 ml SYPRO™ Ruby protein gel stain overnight and finally in 200 ml wash solution (10% (v/v) methanol, 7% (v/v) acetic acid) for 60 min. After washing the gel in water for 3 × 5 min, it was imaged in an Amersham Imager 680 (Cytiva) on a white trans tray, using a Cy3 detection filter (Epi-RGB = Filter Green 520 nm) and an exposure time of 2 s.

To monitor degradation over time, individual reactions á 8 µl per timepoint and replicate were incubated in 1.5 ml Eppendorf tubes at 37 °C and 400 rpm (Eppendorf Thermomixer compact/comfort). Reactions were stopped after 0, 45, 90, 150, 240 and 360 min. To stop the reactions, tubes were transferred to ice for 10 s and spun down briefly, followed by the addition of 2 µl 0.1x sample buffer to each tube and subsequent treatment with 5x Fluorescent Master Mix as described above. Samples were measured using the WES platform as described. Degradation experiments over time were performed in duplicates, which were prepared by treating two reactions from the same master mix with the same compound dilution. DMSO served as a negative control. Compound 8 was tested at 8 µM and 33 µM.

Experiments were analyzed in Compass for SW software as described above. For further analysis, peak areas were exported to MS Excel. ClpC1 NTD peak areas were divided by ClpP1P2 peak areas and treated samples were normalized against the according DMSO controls for each timepoint. Data were visualized using GraphPad Prism 9.5.0.

Intracellular degradation assay

The intracellular ClpC1 degradation assay was adapted from Morreale et al.[20] as follows:

Compounds dissolved in DMSO were serially diluted by 8-fold to 100x final assay concentration, covering a range of 0.0004–100 µM, and 1 µl compound solution per well was added to a glass-coated 96-well plate (Thermo Scientific #60180-P330). For the negative control, only DMSO was added. Each experiment was performed in triplicates. These well replicates were prepared by adding the same compound dilution to three different wells, each of which would later be filled with the same cell suspension.

M. smegmatis (ATCC™ 607™) cultures were grown in Middlebrook 7H9 liquid culture medium (Sigma #M0178, 0.025% (v/v) Tween80, 0.1% (v/v) glycerol) at 37 °C and 180 rpm. An overnight culture grown to an OD_{600} = 0.2–0.3 was centrifuged at 2264 × *g*, 23 °C, 5 min and concentrated by factor 5. Per well, 100 µl concentrated cell suspension were added, mixed, and sealed. The plate was incubated for 24 h at room temperature without agitation.

To harvest the cells, 90 µl cell suspension from each well were centrifuged at 4000 × *g* and 23 °C for 3 min. The cell pellet was resuspended in 100 µl cold lysis buffer (50 mM HEPES pH 7.5, 150 mM KCl, 10% (v/v) glycerol) containing complete protease inhibitor cocktail (EDTA-free, Roche) and stored on ice until lysis.

Cells were lysed in a Bioruptor Pico in 10 cycles, 30 s on, 30 s off, at 4 °C and then centrifuged at 21000 × g and 4 °C for 30 min. The supernatant was flash-frozen in liquid nitrogen and stored at −80 °C.

Lysates were analyzed by JESS Total Protein Normalization (TPN, ProteinSimple) using the Replex Module (ProteinSimple #RP-001) and the Total Protein Detection Module (ProteinSimple #DM-TP01). Samples were treated and plates prepared according to the manufacturer's instructions. For the detection of ClpC1, anti-ClpC1 C-terminus antibody from sheep at a concentration of 0.005 mg/ml and anti-sheep secondary HRP-conjugated antibody 1:50 (R&D anti-sheep IgG #HAF016) were used. Antibodies used for detection of ClpC1 from *M. smegmatis* and *M. tuberculosis* were generated at MRCPPU Reagents and Services, University of Dundee, UK, by immunizing sheep with the following peptides: MFERFTDRARRVVVLAQEEAR (derived from the N-terminus of ClpC1, corresponding to amino acids 1–21, 100% conserved between *M. smegmatis* and *M. tuberculosis*) and RRTIQREIEDQLSEKILFEEV (derived from the C-terminus of ClpC1, corresponding to amino acids 774–794, 100% conserved between *M. smegmatis* and *M. tuberculosis*). All in vivo work was performed in the United Kingdom under ethical approval and UK Government Home Office licence authority. The standard JESS TPN protocol was used with 60 min primary antibody incubation.

Jess TPN data were analyzed with Compass for SW Software: The ClpC1 peak was fitted with Peak Find Threshold set to 100.0. Resulting ClpC1 peak areas were divided by total protein areas and normalized to the negative control (DMSO/no compound).

From these values, DC_{50} values were calculated with Boehringer Ingelheim's MEGALAB DC_{50} application using a four-parametric logistic model. For the calculation of the DC_{50} value, the values of the lower and upper asymptote were constrained to >0 % and <130 %, respectively. Three or four independent measurements were performed for each compound with mean values reported.

Chemicals and media used for microbiology

The reference drugs or antibiotics viz. Isoniazid (INH), Rifampicin (RIF) and Moxifloxacin (MOX) were procured from Merck USA (erstwhile Sigma-Aldrich). Stock solutions of different drugs were prepared in the respective recommended solvents (e.g. dimethyl sulfoxide (DMSO) for RIF and MOX, or in Milli-Q water for INH). The working solutions were prepared fresh every time at the beginning of the experiment. The various media used for growing different strains at FNDR were: 1) mycobacteria were grown in Middlebrook 7H9 broth supplemented with 10% (v/v) Middlebrook ADC, 0.05% (v/v) Tween-80 and 0.25% (v/v) glycerol), whereas the Gram-positive and Gram-negative strains from ESKAPES panel were grown in Mueller Hinton media (BD/Difco). All the bacteria used at FNDR were grown to a cell number of 10^9 colony-forming units (CFU)/mL and were preserved as glycerol-stocks at −80 °C in 0.5 ml aliquots. A single vial was thawed and used every time for each experiment.

The *Mtb* Beijing lineage HN878 was obtained from the laboratory of Dr. William R. Jacobs Jr., Albert Einstein College of Medicine, Bronx, NY and was grown at the Institute for Pharmaceutical Biology and Biotechnology, Heinrich-Heine-University Düsseldorf, Germany at 37 °C and 80 rpm in liquid Middlebrook 7H9 medium supplemented with 0.2% glucose, 0.085% sodium chloride, 0.5% glycerol and 0.05% tyloxapol.

MIC resazurin microtiter assay for *Mycobacterium tuberculosis* and Nontuberculous Mycobacteria (NTM)

Except where stated otherwise, minimum inhibitory concentrations (MICs) were determined at the Foundation for Neglected Disease Research (FNDR) against the mycobacterial strains by the standard broth dilution method according to Clinical Laboratory Standards

Institute[38,39] guidelines M24. The different mycobacterial strains used were *M. smegmatis* (*Msm*), *M. abscessus* (*Mabs*), *M. fortuitum* (*Mfo*), *M. avium* (*Mav*), *M. intracellulare* (*Mint*), and different *M. tuberculosis* (*Mtb*) strains. The different *Mtb* strains used were drug-sensitive strains (H37Rv ATCC 27294 and 11291), mono drug resistant strains Isoniazid resistant H37Rv ($katG^{del}$) ATCC 35822[40], Rifampicin resistant H37Rv ($rpoB^{S450L}$) ATCC 35838[41], moxifloxacin resistant H37Rv clinical isolate FNDR-M1 as well as multidrug resistant strains (ATCC 35825 and 8673) with drug-resistance against 1st and 2nd-line anti-TB drugs. Briefly, the test compounds were dissolved in DMSO, serially diluted by 2-fold in a 10-concentration dose response (10c-DR) ranging from 128 to 0.25 μg ml^{-1} in 96-well plates. Middlebrook 7H9 broth (containing 10% albumin dextrose catalase supplement, ADC) complete media was used for the assay. Each mycobacterial culture was added as 200 μl in each well to all columns except the media control column (200 μl of media was added) to give a final inoculum of 3–7 × 10^5 cfu/ml.

The quality control (QC) included: media controls, growth controls (including DMSO controls), and the assay specific appropriate reference compounds Rifampicin, Isoniazid, Moxifloxacin, as well as the MDR-*Mtb* specific reference drug controls: Amikacin, Thiacetazone and p-Aminosalicylic acid. The assay plates were incubated at 37 °C, resazurin dye was added on the 3rd day for *Msm, Mabs, Mfo*; and on the 6th day for *Mav*, *Mint*, as well as for the sensitive or MDR *Mtb* strains.

The results were noted on the 4th day for *Msm*, *Mabs*, *Mfo* and on the 7th day for *Mtb*, *Mav*, *Mint* using colorimetric readout. The MIC of the compounds and the reference drugs were recorded. The blue wells indicated inhibition of growth, while the pink wells indicated uninhibited growth. MIC assays were carried out in duplicates or triplicates. MIC is defined as the minimum concentration of any compound that inhibits mycobacterial growth or prevents the colour change from blue to pink at the end of the respective assay period.

For antibacterial activity testing against replicating cells of *Mtb* Beijing lineage HN878, cultures obtained from exponentially growing bacteria were adjusted and seeded at 1 × 10^5 CFU/well in 96-well round bottom microplates, in a total volume of 100 μl containing two-fold serially diluted test compounds with a starting concentration of 100 μM. The plates were incubated as standing cultures at 37 °C for 5 days. 10 μl of a 100 μg ml^{-1} resazurin solution was subsequently added to each well and further incubated for 16 h. To fix the cells, 100 μl of 10% formalin was added to each well (5% final concentration) and incubated for at least 30 min. Subsequently, fluorescence was quantified using a microplate reader (Tecan) (excitation: 540 nm; emission: 590 nm). Percentage of growth was calculated relative to sterile medium (0% growth) and solvent control (100% growth).

Starvation-induced non-replicating persistence model

These assays were performed at the Institute for Pharmaceutical Biology and Biotechnology, Heinrich-Heine-University Düsseldorf, Germany. To test the activity of compounds against non-replicating cells of *Mtb* H37Rv, cells were grown to stationary phase, harvested, washed thrice with PBS-0.025% tyloxapol, resuspended in PBS-0.025% tyloxapol in the original culture volume and starved by incubation at 37 °C for three weeks. Next, cells were diluted to 1 × 10^8 CFU ml^{-1} with PBS-0.025% tyloxapol and transferred into 96-well round bottom microtiter plates to a final volume of 100 μl per well, and compounds were added at the indicated final concentrations. After five days of incubation at 37 °C as standing cultures, resazurin solution (10 μl/well from 100 μg ml^{-1} stock) was added, and cells were incubated for 48 h at 37 °C. Subsequently, cells were fixed and fluorescence was measured as described above.

Determination of Minimum Bactericidal Concentration (MBC)

The minimum bactericidal concentration (MBC) of the respective compounds against *Mycobacterium tuberculosis* (Mtb) or *Mycobacterium smegmatis* (Msm) were evaluated at the FNDR by processing the culture aliquots from the parallel MIC assay plates. Culture aliquots of 100 μl volume from all wells showing growth inhibition were sub-cultured by spread plating onto compound-free Middlebrook 7H9 agar plates supplemented with 10% ADC. These plates were incubated at 37 °C with 5% CO_2 for 4 days for *Msm* and 4 weeks for *Mtb*. The colony forming units per ml (CFU/ml) were enumerated and recorded. MBC was defined as the lowest concentration of the compound that killed or reduced the initial mycobacterial load by >100 fold.

Minimum Inhibitory Concentration (MIC) assay against ESKAPES panel

Minimum inhibitory concentration (MIC) against ESKAPES panel of Gram positive and Gram negative pathogens (*Enterococcus faecium, Staphylococcus aureus, Klebsiella pneumoniae, Acinetobacter baumannii, Pseudomonas aeruginosa, Enterobacter cloacae* and *Salmonella typhimurium* [ESKAPES panel]) were determined at the FNDR by the standard broth dilution method [CLSI, M100]. Briefly, the test compounds were dissolved in DMSO, serially double-diluted in a 10-concentration dose response ranging from 64–0.125 μg/ml in 96-well plates. Mueller Hinton broth (MHB) medium was used to grow ESKAPES panel strains. The individual cultures were added as 200 μL (inoculum of 3–7 × 10^5 cfu/ml) to the respective assay plates in each well to all columns, except the media control (200 μL of medium). Quality controls included: media controls, growth controls, and reference drug inhibitors (Moxifloxacin or any other assay-specific reference drug/s). The assay plates were incubated at 37 °C, and the results were noted on the 2nd day as turbidometric readout. The clear wells indicated inhibition of growth, while the turbid wells indicated uninhibited growth.

Intracellular MIC assay in THP-1 macrophages

These experiments were conducted at the FNDR. To test drug efficacy against *M. tuberculosis* H37Rv in the intracellular compartment, the monocytic macrophage cell line THP-1 (ATCC TIB-202) was used. The THP-1 cells were grown in RPMI medium (Gibco-BRL Life Technologies, Gaithersburg, Md.) in 75 cm^2 flasks at 37 °C in a 5% CO_2 atmosphere. RPMI media was supplemented with 100 mM sodium pyruvate, 200 mM L-glutamine, 3.7 g of sodium bicarbonate per liter and 10% fetal calf serum without any antibiotics. After counting the THP-1 cells in a hemocytometer, viability was determined by trypan blue exclusion, and the cells were seeded in 96-well plates in duplicates with complete RPMI containing 10% fetal calf serum at a density of 1 × 10^5 cells/well (5 × 10^5 cells/ml) and were incubated overnight.

Differentiation of THP-1 cells was induced by incubation of THP-1 cells with 50 nM phorbol 12-myristate 13-acetate (PMA) for 72 h. After this induction, the THP-1 macrophages were infected with *M. tuberculosis* H37Rv strain (ATCC-27294) at a multiplicity of infection (MOI) of 1:10 in the fresh media. The macrophage infection was allowed to take place for 2 h at 37 °C with 5% CO_2. The media containing *M. tuberculosis* was discarded, macrophage monolayers were washed twice with phosphate-buffered saline (with Ca^{2+} and Mg^{2+}) to remove the free bacteria and replenished with the fresh complete RPMI.

For the day-0 infection control, sets of duplicate wells were lysed (0.05% SDS) and enumerated to assess the numbers of intracellular *M. tuberculosis* 2 h post-infection at the beginning of treatment.

For the remaining wells, at 2 h post-infection, the treatment was initiated (test and reference compounds in DMSO) in comparison with the respective no-treatment control (DMSO only). The test and the reference (moxifloxacin and rifampicin) compounds were added to the sets of duplicate wells at indicated concentrations. The final concentration of DMSO in the medium was maintained at 1% for all conditions including the no-drug infection control. Sets of replicates from the infection control, test and reference wells with each drug concentrations were sampled on different time points (days 4 and 7). The wells at the respective time points were washed to remove the

extracellular bacteria. The monolayers lysed with 0.05% SDS were serially diluted and plated onto Middlebrook 7H11 agar plates to enumerate the number of intracellular viable mycobacteria as colony-forming units (CFU/ml). The intracellular mycobacterial killing rates for each concentration of test and reference compounds were generated by plotting the $\log_{10}$ cfu/ml against 0, 4, and 7 days. Maximal antimicrobial effect (Emax) was determined by the formula: Start Log_{10} cfu/ml (D-0)−Residual Log_{10} cfu/ml (D-4 or D-7).

Microsomal stability assays

The kinetics of compound degradation in liver microsomes is assessed in an assay with 1 µmol/l of compound and 0.5 mg/ml liver microsomes in a medium of 100 mM Tris-HCl pH 7.5, 6.5 mM $MgCl_2$ and 1 mM NADPH at 37 °C. The reaction is stopped at multiple time points by adding acetonitrile. After centrifugation, the compound concentration is measured in the supernatants by high-performance liquid chromatography (HPLC) tandem mass spectrometry (MS/MS). The results are fitted to a first-order decay and the half-lives are converted to clearance (stated as % of the liver blood flow (%Qh)) using the well-stirred liver model.

Hepatocyte stability assays

Cryopreserved hepatocytes are incubated in an appropriate buffer system containing 50% species serum. Following an acclimation period (15–30 min) in an incubator (37 °C, 5–10% CO_2, 85–95% humidity) the test compound is added to the hepatocyte suspension (pH 7.4, typical cell density of about 1 million cells/mL; final concentration of test compound is 1 µM, final DMSO concentration <0.05% v/v). The cells are incubated for up to 6 h and samples are taken at 6 different time points. Samples are then quenched with acetonitrile and pelleted by centrifugation. The remaining amount of parent compound in the supernatants is then analysed by HPLC-MS/MS. Clearance is calculated from compound half-lives using the well-stirred liver model and is converted to clearance stated as % of the liver blood flow (% Qh).

PK following iv bolus and po administration to BALB/cAnNCrl mice

Health status and animal husbandry. The in-life experimental procedures were conducted in strict compliance with German and European animal welfare legislation in an AAALAC-accredited facility. Male BALB/cAnNCrl mice (Charles River Laboratories Research Models and Services, 97633 Sulzfeld, Germany) were used. Animals were 9 weeks old at dosing with a body weight of 21.6–24.3 g. Animals were delivered free of pathogens according to FELASA recommendations with a health certificate provided by the breeder. Upon receipt, the state of health and sex was checked. Animals acclimatized for at least 5 days before the commencement of the in-life phase. During acclimation, animals were group-housed in individually ventilated cages, on birch wood granulate bedding with species-specific enrichment (nesting material, mouse igloo, gnawing wood). During experimental conduct, animals were housed in conventional cages with elevated grid floors. Grid floor was used to avoid contamination with test item material excreted via urine and feces and subsequent reuptake during fur grooming. No bedding and enrichment were provided except a cage divider, which can be used as a shelter. Animals always had unlimited access to food and water and received a pelleted, total pathogen-free maintenance diet and tap drinking water, sterilized by filter.

Formulation (iv). On dosing day, test item(s) was dissolved in DMSO (2.86 mg/ml), 13.3 vol. of PEG200 (40% in water for injection) added, and sonicated at 60 °C for 10 min. In case of incomplete dissolution, the formulation was filtered at 40 °C (non-pyrogenic sterile-R filter, 0.2 µm). All formulations were stirred warm until administration. Actual test item content was determined bioanalytically.

Formulation (po). On the day before dosing, test item(s) were suspended in kleptose (20% in WFI) under continuous stirring (3.0 mg/ml). Following 2 min vortexing and 1 h stirring, the formulation was sonicated at 60 °C for 30 min and stirred at ambient temperature overnight. Before dosing, the formulation was vortexed for 2 min followed by ultraturrax treatment for 2 min.

In life phase. Male BALB/cAnNCrl mice (n = 3 per test item and administration route) received a bolus dose of the formulated test item(s) (1 mg/kg iv, 30 mg/kg po) at t = 0 h, and whole blood samples were collected subsequently (35 µl at 0.1 (iv) / 0.25 (po), 0.5, 1, 2, 4, 6 h; 600 µl at sacrifice after 24 h). Animals were euthanized by exsanguination in deep isoflurane anesthesia. Whole blood samples were immediately stored on ice at about 4 °C. Plasma was separated by centrifugation at approximately 10,000 × g for 5 m at +4 °C. Centrifugation of each blood sample was started within 10 m after collection. A single aliquot of at least 15 µL of plasma was prepared and immediately stored at −20 ± 5 °C.

Bioanalytics. Sample proteins were precipitated with ACN (1 + 12, v/v) containing internal standard, and supernatants analyzed by quantitative UPLC-MS/MS: Phenomenex Luna Omega C18, 2.1 × 50 mm, 1.6 µm, 40 °C, gradient between 10% - 90% ACN with 0.1% formic acid. LogD determination: Lipophilicity of the test items, expressed as $\text{chromLogD}_{7.5}$, was assessed by measuring their chromatographic retention times on C18-material. The chromatographic retention versus $\text{logD}_{7.5}$ values of a series of thirteen n-alkan-2-ones (2-butanone – 2-hexadecanone) served as lipophilicity calibration. Chromatographic conditions were as follows: HPLC-UV Agilent 1260/1290 system, UV-detection: 270 nm, C_{18}-column, flowrate: 1.3 ml/min, run time: 6 min, injection volume: 2.0 µl, eluents: A: NH_4OAc-buffer pH 7.5 and B: ACN, Gradient: 0 min: 90% A – 2.60 min: 5% A – 3.55 min: 90% A.

Chemical synthesis

Full details of synthetic procedures and NMR spectra of all compounds (Supplementary Figs. 8–209) are provided in the supplementary information.

All further methods and all data supporting the findings of this study are available within the Supplementary Information.

Reporting summary

Further information on research design is available in the Nature Portfolio Reporting Summary linked to this article.

Data availability

The authors declare that the data supporting the findings of this study are available within the paper, the Source Data file and the Supplementary Information. The SPR data generated in this study are provided in the Source Data file as a separate ZIP folder. The NMR data generated in this study are provided in the Supplementary Information. Should any raw data files be needed in another format they are available from the corresponding authors upon request. Source data are provided in this paper.

References

1. Murray, C. J. et al. Global burden of bacterial antimicrobial resistance in 2019: a systematic analysis. *Lancet* **399**, 629–655 (2022).
2. Roope, L. S. J. et al. The challenge of antimicrobial resistance: What economics can contribute. *Science* **364**, eaau4679 (2019).
3. Jit, M. et al. Quantifying the economic cost of antibiotic resistance and the impact of related interventions: Rapid methodological review, conceptual framework and recommendations for future studies. *BMC Med.* **18**, 1–14 (2020).

4. Cook, M. A. & Wright, G. D. The past, present, and future of antibiotics. *Sci. Transl. Med.* **14**, eabo7793 (2022).
5. Plackett, B. No money for new drugs. *Nat. Outlook* **586**, 50–52 (2020).
6. Kurt Yilmaz, N. & Schiffer, C. A. Introduction: Drug resistance. *Chem. Rev.* **121**, 3235–3237 (2021).
7. Chifiriuc, M. C. et al. Common themes in antimicrobial and anticancer drug resistance. *Front Microbiol.* **13**, 1–12 (2022).
8. Békés, M., Langley, D. R. & Crews, C. M. PROTAC targeted protein degraders: the past is prologue. *Nat. Rev. Drug Discov.* **21**, 181–200 (2022).
9. Ciulli, A. & Trainor, N. A beginner's guide to PROTACs and targeted protein degradation. *Biochemist* **43**, 74–79 (2021).
10. Paiva, S. L. & Crews, C. M. Targeted protein degradation: elements of PROTAC design. *Curr. Opin. Chem. Biol.* **50**, 111–119 (2019).
11. Maniaci, C. et al. Homo-PROTACs: Bivalent small-molecule dimerizers of the VHL E3 ubiquitin ligase to induce self-degradation. *Nat. Commun.* **8**, 830 (2017).
12. Steinebach, C. et al. Homo-PROTACs for the chemical knockdown of cereblon. *ACS Chem. Biol.* **13**, 2771–2782 (2018).
13. Banik, S. M. et al. Lysosome-targeting chimaeras for degradation of extracellular proteins. *Nature* **584**, 291–297 (2020).
14. Ahn, G. et al. LYTACs that engage the asialoglycoprotein receptor for targeted protein degradation. *Nat. Chem. Biol.* **17**, 937–946 (2021).
15. Alabi, S. B. & Crews, C. M. Major advances in targeted protein degradation: PROTACs, LYTACs, and MADTACs. *J. Biol. Chem.* **296**, 100647 (2021).
16. Mares, A. et al. Extended pharmacodynamic responses observed upon PROTAC-mediated degradation of RIPK2. *Commun. Biol.* **3**, 1–13 (2020).
17. Guenette, R. G., Yang, S. W., Min, J., Pei, B. & Potts, P. R. Target and tissue selectivity of PROTAC degraders. *Chem. Soc. Rev.* **51**, 5740–5756 (2022).
18. Burke, M. R., Smith, A. R. & Zheng, G. Overcoming cancer drug resistance utilizing PROTAC technology. *Front Cell Dev. Biol.* **10**, 1–22 (2022).
19. Trentini, D. B. et al. Arginine phosphorylation marks proteins for degradation by a Clp protease. *Nature* **539**, 48–53 (2016).
20. Morreale, F. E. et al. BacPROTACs mediate targeted protein degradation in bacteria. *Cell* **185**, 2338–2353 (2022).
21. *Global Tuberculosis Report*. (World Health Organization, 2020).
22. Pai, M., Kasaeva, T. & Swaminathan, S. Covid-19's devastating effect on tuberculosis Care - A path to recovery. *N. Engl. J. Med.* **386**, 1490–1493 (2022).
23. *Global Tuberculosis Report*. (World Health Organization, 2021).
24. Vasudevan, D., Rao, S. P. S. & Noble, C. G. Structural basis of mycobacterial inhibition by Cyclomarin A. *J. Biol. Chem.* **288**, 30883–30891 (2013).
25. Wolf, N. M. et al. High-resolution structure of ClpC1-Rufomycin and ligand binding studies provide a framework to design and optimize anti-tuberculosis leads. *ACS Infect. Dis.* **5**, 829–840 (2019).
26. Gavrish, E. et al. Lassomycin, a ribosomally synthesized cyclic peptide, kills mycobacterium tuberculosis by targeting the ATP-dependent protease ClpC1P1P2. *Chem. Biol.* **21**, 509–518 (2014).
27. Gao, W. et al. The cyclic peptide ecumicin targeting CLpC1 is active against Mycobacterium tuberculosis in vivo. *Antimicrob. Agents Chemother.* **59**, 880–889 (2015).
28. Wolf, N. M. et al. Structure of the N-terminal domain of ClpC1 in complex with the antituberculosis natural product ecumicin reveals unique binding interactions. *Acta Crystallogr. D. Struct. Biol.* **76**, 458–471 (2020).
29. Kiefer, A. et al. Synthesis of New Cyclomarin derivatives and their biological evaluation towards mycobacterium tuberculosis and Plasmodium Falciparum. *Chem. - Eur. J.* **1**, 8894–8902 (2019).
30. Junk, L., Papadopoulos, E., Kazmaier, U. & Tryptophan, N. 1-Alkylation: Quick and simple access to diversely substituted tryptophans. *Synthesis* **53**, 2503–2511 (2021).
31. Abraham, M. H. et al. An NMR method for the quantitative assessment of intramolecular hydrogen bonding; Application to physicochemical, environmental, and biochemical properties. *J. Org. Chem.* **79**, 11075–11083 (2014).
32. Cierpicki, T. & Otlewski, J. Amide proton temperature coefficients as hydrogen bond indicators in proteins. *J. Biomol. NMR* **21**, 249–261 (2001).
33. Otake, Y. et al. N-methylated peptide synthesis via generation of an Acyl N-methylimidazolium cation accelerated by a Brønsted acid. *Angew. Chem.* **132**, 13025–13030 (2020).
34. Hoi, D. M. et al. Development of a dual Clp-targeting BacPROTAC that impairs mycobacterial proteostasis and survival. *Cell* **186**, 2176–2192 (2023).
35. Meena, L. S. & Rajni, T. Survival mechanisms of pathogenic Mycobacterium tuberculosis H 37Rv. *FEBS J.* **277**, 2416–2427 (2010).
36. Peddireddy, V., Doddam, S. N. & Ahmed, N. Mycobacterial dormancy systems and host responses in tuberculosis. *Front. Immunol.* **8**, 84 (2017).
37. Leodolter, J., Warweg, J. & Weber-Ban, E. The Mycobacterium tuberculosis ClpP1P2 protease interacts asymmetrically with its ATPase partners ClpX and ClpC1. *PLoS One* **10**, 1–21 (2015).
38. Kaur, P. et al. A high-throughput cidality screen for Mycobacterium tuberculosis. *PLoS One* **10**, 1–13 (2015).
39. Shirude, P. S. et al. Azaindoles: Noncovalent DprE1 inhibitors from scaffold morphing efforts, kill Mycobacterium tuberculosis and are efficacious in vivo. *J. Med. Chem.* **56**, 9701–9708 (2013).
40. Rouse, D. A. & Morris, S. L. Molecular mechanisms of isoniazid resistance in Mycobacterium tuberculosis and Mycobacterium bovis. *Infect. Immun.* **63**, 1427–1433 (1995).
41. Garcia, L., Alonso-Sanz, M., Rebollo, M. J., Tercero, J. C. & Chaves, F. Mutations in the rpoB gene of rifampin-resistant Mycobacterium tuberculosis isolates in Spain and their rapid detection by PCR-enzyme-linked immunosorbent assay. *J. Clin. Microbiol.* **39**, 1813–1818 (2001).

Acknowledgements

We are grateful to Dieter Gallemann for providing advice on DMPK profiling and coordinating the work packages at Nuvisan GmbH. We thank James Hastie and the team at MRCPPU Reagents and Services, University of Dundee, United Kingdom for the generation of ClpC1-specific antibodies. Maximilian Scharnweber is acknowledged for valuable input in discussions of biophysical data. Editing support was provided by Life Science Editors. This work was supported by the European Research Council (AdG 694978, T.C.), an FFG Headquarter Grant (no. 852936, T.C.), the Vienna Science and Technology Fund (WWTF LS17-029, T.C.) and Boehringer Ingelheim (L. J., S. G., J. L). Financial support from Saarland University and the DFG (grant 447298507) is gratefully acknowledged. R.K. acknowledges support from the DFG (project number 270650915/GRK 2158) and the Jürgen Manchot Stiftung (graduate school MOI IV). J. L., F. E. M and S. J. are members of the Boehringer Ingelheim Discovery Research global post-doc program. The IMP is supported by Boehringer Ingelheim.

Author contributions

L. J., V. M. S., K. R., P. K., S. N., R.K.S., A. Meinhart, T. C., R.K. and G. B. designed experiments. L. J., S. G., P. B., and G. G. performed the chemical synthesis and analysis of the compounds. P.K., R. V. K., J. L., S. J., K. V., V.K. and L.v.G. performed mycobacterial assays including those under BSL3 level. K. F., J. L., D. H., S. J. and F. E. M. performed microbiological and biochemical assays, as well as binding measurements including analyses. K. R. designed and supervised SPR experiments. P. G. coordinated the synthesis and supply of compound building blocks.

L. J., V. M. S., P. K., U. K., T. C., M.S., H. W. and G. B. coordinated the research collaborations between Boehringer Ingelheim, Saarland University, IMP and FNDR. L. J., V. M. S., C. K., A. Mantoulidis and H. W. contributed to the design of reported compounds. L. J., V. M. S., H. W. and G.B. prepared the manuscript together with input from all authors.

Competing interests

V. M. S., C. K., A. Mantoulidis, P. G., H. W., K. R., K. F., P. B., G. G. and G. B. were employees of Boehringer Ingelheim at the time of this work. The remaining authors declare no competing interests.

Ethical compliance

The authors confirm that the research in this study complies with all relevant ethical regulations. All animal studies were approved by the District Government of Upper Bavaria (Regierung von Oberbayern, Az.: 55.2-2532.Vet_03-17-101). All in-life experimental procedures were conducted in strict accordance with the protocol and in compliance with German and European animal welfare legislation.

Additional information

Supplementary information The online version contains supplementary material available at https://doi.org/10.1038/s41467-024-46218-7.

Correspondence and requests for materials should be addressed to Lukas Junk, Harald Weinstabl or Guido Boehmelt.

Peer review information *Nature Communications* thanks Sudeshna Roy, Richard Lee and the other, anonymous, reviewer(s) for their contribution to the peer review of this work. A peer review file is available.

6.2 Supporting Information

Supplementary Information

Homo-BacPROTAC-induced degradation of ClpC1 as a strategy against drug-resistant mycobacteria

Lukas Junk*$[1],Volker M. Schmiedel$[2], Somraj Guha[1], Katharina Fischel[2], Peter Greb[2], Kristin Vill[3], Violetta Krisilia[3], Lasse van Geelen[3], Klaus Rumpel[2], Parvinder Kaur[4], Ramya V. Krishnamurthy[4], Shridhar Narayanan[4], Radha Krishan Shandil[4], Mayas Singh[4], Christiane Kofink[2], Andreas Mantoulidis[2], Philipp Biber[2], Gerhard Gmaschitz[2], Uli Kazmaier[1], Anton Meinhart[5], Julia Leodolter[5], David Hoi[5], Sabryna Junker[5], Francesca Ester Morreale[5], Tim Clausen[5], Rainer Kalscheuer[3], Harald Weinstabl*[2], Guido Boehmelt*[2]

[1] Organic Chemistry I, Saarland University, Campus Building C4.2, 66123 Saarbrücken, Germany

[2] Boehringer Ingelheim RCV GmbH & Co. KG, Dr. Boehringer-Gasse 5-11, 1121 Vienna, Austria

[3] Heinrich Heine University Düsseldorf, Faculty of Mathematics and Natural Sciences, Institute of Pharmaceutical Biology and Biotechnology, 40225 Düsseldorf, Germany

[4] Foundation for Neglected Disease Research, Plot No. 20A, KIADB Industrial Area, Veerapura Village, Doddaballapur, Bengaluru 561203, Karnataka, India

[5] Research Institute of Molecular Pathology, Vienna BioCenter, Vienna, Austria

Contents

Supplementary Tables 1-11

Supplementary Table 1. Structure-Activity Relationships part 1 (SPR, Caco-2)

compound[1]	Compound descriptor	K_D ClpC1-NTD[2] [nM] Mean ± SD	K_D correlation[3]	k_{off} ClpC1-NTD[4] [s^{-1}] Mean ± SD	Caco-2 permeability[5] P (A-B)	P (B-A)	Efflux ratio	Int. Perm	Permeability Correlation[6] P (A-B)	Ratio
SI-38	[3-OPra]	5.6 ± 0.6$_a$	2	(5 ± 1)E-2	<0.2	18	-	9.1	**>75**	**>31**
SI-64	[6-Me][3-OPra]	11 ± 1$_a$		(2 ± 1)E-1	15	43	2.9	29.0		
SI-40	**[3,3-Tri][5]**	0.66 ± 0.04$_a$	11	9E-4 ± 8E-5	<2.5	<0.7	-	1.60	-	-
SI-66	**[6-Me][3,3-Tri][5]**	7 ± 2$_a$		1E-2 ± 6E-3	<4.8	<2.5	-	3.7		
SI-39	**[3,3-Tri][14-O3,6,9,12]**	0.45 ± 0.04$_a$	4.5	(9 ± 3)E-4	<4.1	<1.7	-	2.9	-	-
SI-65	**[6-Me][3,3-Tri][14-O3,6,9,12]**	1.8 ± 0.7$_a$		1E-2 ± 6E-3	<8.6	<5.1	-	6.9		
14	[3-Allyl]	10 ± 1$_a$		(6 ± 6)E-2	3.3	40	12.1	21.7		
17	**[3,3][4-E2]**	23 ± 5$_a$		4E-3 ± 7E-4	<2.5	0.9	-	1.7		
10	[7-Pra]	4.0 ± 0.7$_b$	3.5	(4 ± 3)E-2	<0.1	14	-	7.1	**>28**	
20	[6-Me][7-Pra]	13.9 ± 0.3$_a$		(3 ± 3)E-1	2.8	28.5	11.8	15.7		
24	[7-Tri][5]	4.6 ± 0.2$_a$	5.7	(4 ± 3)E-2	<0.3	11	-	5.6	**>3**	**>1.5**
25	[6-Me][7-Tri][5]	26.1 ± 0.1$_a$		1E-1 ± 2E-2	0.9	22	25.1	11.4		
SI-74	[7-NMe2Glu]	4 ± 2$_a$	5.9	(6 ± 6)E-2	<0.5	3	>6	1.7	-	-
SI-76	[6-Me][7-NMe2Glu]	26 ± 6$_a$		6E-2 ± 5E-3	<0.1	8.4	>84	4.3		
12	**[7,7-Tri][5]**	0.28 ± 0.08$_c$	3	(7 ± 2)E-4	0.7	0.2	0.3	0.5	0.7	1
22	**[6-Me][7,7-Tri][5]**	0.9 ± 0.3$_a$		1E-2 ± 5E-3	0.5	0.2	0.3	0.3		
11	**[7,7-Tri][8-O3,6]**	0.4 ± 0.2$_d$	9	(7 ± 2)E-4	1.6	4.2	2.6	2.9	0.3	**4.33**
21	**[6-Me][7,7-Tri][8-O3,6]**	3.6 ± 0.9$_a$		(8 ± 4)E-3	<0.5	<0.3	-	0.4		
SI-72	[3-Phe][6-propargyl]	14 ± 6$_a$		(6 ± 1)E-2	0.2	12.5	61.4	6.4		
5	[6-propargyl]	3.5 ± 0.1$_a$	4	(3 ± 2)E-2	1.1	23	20.4	12.1	**13.6**	**9.3**
26	[6-Me][6-propargyl]	15 ± 3$_a$		4E-2 ± 4E-3	15	33	2.2	24.0		
13	[6-allyl]	3.6 ± 0.2$_a$	2.2	(9 ± 2)E-2	2.4	19	7.9	10.7	**14.6**	**3.2**
SI-60	[6-Me][6-allyl]	8 ± 3$_a$		(3 ± 1)E-2	35	88	2.5	61.5		
15	**[6,6][4-E2]**	1.2 ± 0.8$_a$	1.5	(8 ± 5)E-4	2.2	1.8	0.8	2.0	0.4	
28	**[6-Me][6,6][4-E2]**	1.8 ± 0.1$_a$		1E-3 ± 6E-5	0.9	<0.4	-	0.66		
16	**[6,6][4]**	0.5 ± 0.2$_a$	**1**	(4 ± 2)E-4	<1.4	<1.1	-	1.3	-	-
SI-61	**[6-Me][6,6][4]**	0.54 ± 0.06$_a$		(6 ± 2)E-4	<4.2	<1.3	-	2.75		
9	**[6,6-Tri][5]**	0.6 ± 0.2$_e$	2.7	5E-4 ± 8E-5	<0.2	0	-	0.1	-	-
SI-57	**[6-Me][6,6-Tri][5]**	1.6 ± 0.8$_a$		1E-3 ± 7E-4	<2.2	<0.7	-	1.5		
6	**[6,6-Tri][5-O3]**	0.9 ± 0.4$_b$		1E-3 ± 4E-4	<1.7	2.4	-	2.1		
7	**[6,6-Tri][11-O3,6,9]**	0.46 ± 0.05$_b$		1E-3 ± 3E-4	not determined					
8	**[6,6-Tri][14-O3,6,9,12]**	0.4 ± 0.1$_b$	**1**	1E-3 ± 4E-4	<0.6	<0.3	-	0.4	-	-
27	**[6-Me][6,6-Tri][14-O3,6,9,12]**	0.4 ± 0.2$_a$		2E-3 ± 5E-4	<6.4	<1.7	-	4.1		
dCymC	dCymC	1.1 ± 0.4$_f$	10	(1 ± 3)E-2	1.3	3.1	3	2.2	**3**	**1.57**
23	[6-Me]-dCymC	12.1 ± 0.3$_a$		(7 ± 8)E-2	3.9	7.3	1.9	5.6		

[1] bold compounds/descriptors: Homo-BacPROTACs; [2] Dissociation constant K_D of compound binding to ClpC1-NTD determined by SPR. Mean values ± standard deviation. Footnotes indicate the number of measurements performed for the respective compound: a) n = 2, b) n = 4 c), n = 10, d) n = 7, e) n = 3, f) n = 145. For the calculation of all reported SPR values, molar compound concentrations were used throughout, regardless of the number of binding moieties of the molecule. [3] Ratio of K_D values (ClpC1-NTD) of Trp-N^{in}-methylated and non-Trp-N^{in}-methylated compounds. Bold: no measurable influence; [4] Dissociation rate constant k_{off} of compound binding to ClpC1-NTD determined by SPR. Mean values ± standard deviation. The association rate constant k_{on} can be calculated using the formula $k_{on} = k_{off}/K_D$ [5] Permeability across Caco-2 monolayers in *P(A–B)*: apical to basolateral and *P(B–A)*: basolateral to apical direction (values reported in 10^{-6} cm s^{-1}); efflux ratio = P(B–A)/P(A–B); Int. perm: mean value of P(A–B) and P(B–A). [6] Influence of Trp-N^{in} methylation on P(A-B) and efflux ratio. Bold: positive influence.

Supplementary Table 2. Structure-Activity Relationships part 2 (MetStab, MIC). For MIC values, mean ± SD are given with footnotes indicating the number of measurements performed: a) n = 1, b) n = 3, c) n = 5, d) n = 2, e) n = 4, f) n = 6, g) n = 7, h) n = 9

Compound[1]	Compound descriptor	Microsomal Stability [%Qh][2]			Hepatocyte [%Qh][3]			MIC [µM][4]		
		Mice	Rat	Human	Mice	Rat	Human	*Mtb*	*Msm* 607	*Msm* 700084
SI-38	[3-OPra]	73	59	84	15	37	19	1.6$_a$	25.0$_a$	12.5$_a$
SI-64	[6-Me][3-Opra]		n.d.		34	50	22		n.d.	
SI-40	**[3,3-Tri][5]**		n.d.		15	12	n.d.	0.2$_a$	>50$_a$	>50$_a$
SI-66	**[6-Me][3,3-Tri][5]**		n.d.		15	10	12		n.d.	
SI-39	**[3,3-Tri][14-O3,6,9,12]**		n.d.		15	6	12	0.2$_a$	12.5$_a$	12.5$_a$
SI-65	**[6-Me][3,3-Tri][14-O3,6,9,12]**		n.d.			n.d.			n.d.	
14	[3-Allyl]	>88	84	>88	29	57	41	3.1$_a$	1.6$_a$	12.5$_a$
17	[3,3][4-E2]	<24	<23	<24	21	12	n.d.		n.d.	
10	[7-Pra]	>88	85	>88	64	70	12	3.1 ± 0.0$_b$	3.1 ± 0.0$_b$	25.0 ± 0.0$_c$
20	[6-Me][7-Pra]	>88	>88	>88	59	63	34	50.0 ± 0.0$_d$	25.0 ± 0.0$_d$	>50$_d$
24	[7-Tri][5]		n.d.		35	33	n.d.		n.d.	
25	[6-Me][7-Tri][5]	82	62	>88	21	16	30	6.3$_a$	12.5$_a$	12.5$_a$
SI-74	[7-Nme2Glu]	84	85	61	38	49	12	3.1 ± 0.0$_d$	0.8 ± 0.0$_d$	9.4 ± 4.4$_d$
SI-76	[6-Me][7-Nme2Glu]	>88	78	>88	23	52	n.d.	6.3$_a$	12.5$_a$	25.0$_a$
12	**[7,7-Tri][5]**	<24	<23	<24	15	6	12	0.1 ± 0.0$_d$	0.9 ± 0.3$_c$	>50$_c$
22	**[6-Me][7,7-Tri][5]**		n.d.		15	10	12	3.1 ± 0.0$_d$	2.3 ± 1.1$_d$	>50$_d$
11	**[7,7-Tri][8-O3,6]**	<24	<23	<24	15	6	12	0.1 ± 0.0$_d$	1.6 ± 0.0$_d$	1.6 ± 0.0$_e$
21	**[6-Me][7,7-Tri][8-O3,6]**		n.d.		15	6	n.d.		n.d.	
SI-72	[3-Phe][6-propargyl]	>88	87	>88	71	82	12		n.d.	
5	[6-Pra]	>88	>88	>88	58	51	12	1.6$_a$	25.0$_a$	6.3$_a$
26	[6-Me][6-Pra]	>88	>88	>88	67	68	n.d.	6.3$_a$	6.3$_a$	12.5$_a$
13	[6-allyl]	>88	>88	>88	59	65	19		n.d.	
SI-60	[6-Me][6-allyl]		>88	>88	61	57	50		n.d.	
15	**[6,6][4-E2]**	<24	<23	<24	15	6	12	0.2 ± 0.1$_e$	2.3 ± 0.9$_e$	50.0 ± 0.0$_e$
28	**[6-Me][6,6][4-E2]**		n.d.		15	6	n.d.		n.d.	
16	**[6,6][4]**		n.d.			n.d.			n.d.	
SI-61	**[6-Me][6,6][4]**		n.d.		15	6	n.d.		n.d.	
9	**[6,6-Tri][5]**	25	<23	43	15	6	12	0.3 ± 0.1$_d$	0.8 ± 0.0$_d$	>50$_e$
SI-57	**[6-Me][6,6-Tri][5]**		n.d.		15	8	12	n.d.	n.d.	n.d.
6	**[6,6-Tri][5-O3]**	43	<23	70	15	6	12	0.4 ± 0.3$_a$	2.3 ± 0.9$_e$	20.8 ± 15.1$_f$
7	**[6,6-Tri][11-O3,6,9]**	53	40	88	n.d.	n.d.	n.d.	0.1 ± 0.0$_e$	1.4 ± 0.2$_e$	n.d.
8	**[6,6-Tri][14-O3,6,9,12]**	72	40	>88	32	6	12	0.4 ± 0.4$_e$	1.9 ± 0.9$_g$	8.3 ± 5.1$_h$
27	**[6-Me][6,6-Tri][14-O3,6,9,12]**	77	41	>88	15	6	12	<0.1$_a$	1.6$_a$	0.8$_a$
dCymC		56	38	66	46	55	36	0.4 ± 0.1$_e$	2.8 ± 0.4$_e$	n.d.
23	[6-Me] dCymC		n.d.		15	57	13		n.d.	

[1] bold compounds/descriptors: Homo-BacPROTACs; [2] Clearance in microsomes [3] Clearance in hepatocytes; [4] Minimum inhibitory concentrations against *Mtb* H37Rv, *Msm* 607 and *Msm* 700084 determined as described above; [%Qh] = clearance stated as percent related to hepatic blood flow.

Supplementary Table 3. Summary of IV PK studies in BALB/cAnNCrl mice with 1 mg kg^{-1} bolus administration

Compound	C_{Max}[1]	AUC[2]	$T_{1/2}$[3]	VSS[4]	Cl[5]
5	415	164	1.03	4.54	98.8
6	1820	4490	3.33	0.95	3.73
8 (UdsBI-0545)	6710	8580	6.74	0.48	1.90
12 (UdSBI-4377)	3270	3870	1.37	0.42	4.14

[1]dose-normalized maximum plasma concentration (nM/(nmol kg^{-1})); [2] Dose-normalized area under plasma concentration curve (h nM/(nmol kg^{-1})); [3] Half-life in plasma (h); [4] Intravenous volume of distribution at steady state (l kg^{-1}); [5] Plasma clearance (ml min^{-1} kg^{-1})).

5

Supplementary Table 4. Individual and mean plasma concentrations (nmol l^{-1}) and pharmacokinetic parameters of compound **5** after single i.v. (bolus) administration to mice.

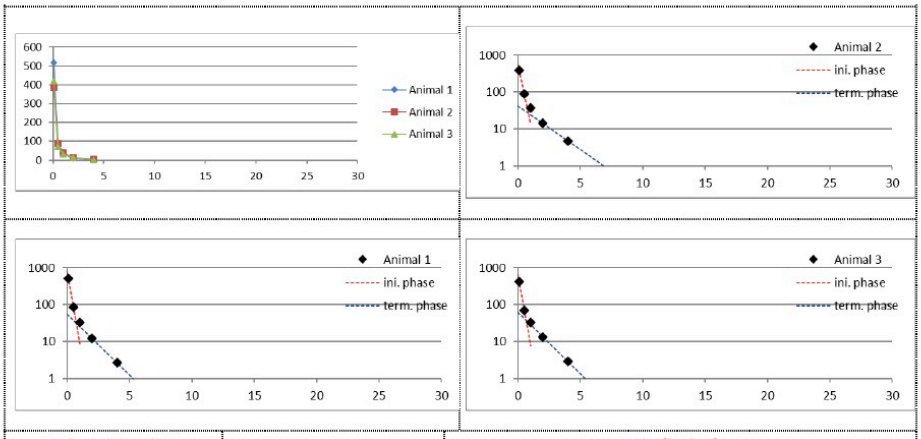

Administration		**iv (bolus)**				
Nominal Dose	µmol kg^{-1}	1.062				
Matrix		Plasma				
Time/Parameter	**Unit**	**Concentration (nmol l^{-1})**				
		Animal 1	**Animal 2**	**Animal 3**	**Mean**	**SD**
0.1	h	518	384	421	441	69
0.5	h	85.1	88.1	71.5	81.6	8.9
1	h	33.6	37.9	32.6	34.7	2.8
2	h	12.3	14.2	13.4	13.3	1.0
4	h	2.7	4.8	2.9	3.5	1.2
6	h	BLOQ	BLOQ	BLOQ	BLOQ	NC
24	h	BLOQ	BLOQ	BLOQ	BLOQ	NC
C_{max}/Dose	nM/(nmol kg^{-1})	488	361	396	415	65
AUC_{0-t}/Dose	h nM/(nmol kg^{-1})	177	161	154	164	12
AUC_{0-inf}/Dose	h nM/(nmol kg^{-1})	180	169	158	169	11
$t_{1/2}$	h	0.9	1.3	0.9	1.0	0.2
MRT	h	0.6	0.9	0.7	0.8	0.2
V_{ss}	l kg^{-1}	3.5	5.6	4.6	4.5	1.0
CL	ml min^{-1} kg^{-1}	92.3	98.5	106.	98.8	6.7
CL PL QH	%	103.0	109.0	117.0	110.0	7.4

Supplementary Table 5. Individual and mean plasma concentrations (nmol l^{-1}) and pharmacokinetic parameters of compound **6** after single i.v. (bolus) administration to mice.

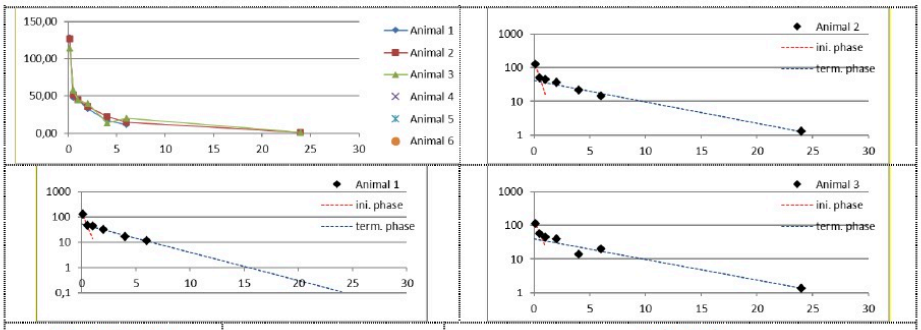

Administration		**iv (bolus)**				
Actual Dose	µmol kg^{-1}	0.0677				
Matrix		Plasma				
Time/Parameter	**Unit**	**Concentration (nmol l^{-1})**				
		Animal 1	**Animal 2**	**Animal 3**	**Mean**	**SD**
0.1	h	128	127	114	123	8
0.5	h	47.9	51.6	58	52.5	5.1
1	h	44.8	45.0	44.5	44.8	0.3
2	h	32.5	36.4	39.6	36.2	3.6
4	h	17.3	22.2	13.8	17.8	4.2
6	h	11.6	14.7	20.6	15.6	4.6
24	h	BLOQ	1.3	1.4	1.3	NC
t_{max}	h	0.1	0.1	0.1	0.1	0
C_{max}	nmol l^{-1}	128	127	114	123	8
AUC_{0-t}/Dose	h nM/(nmol kg^{-1})	2600	5020	5730	4450	1640
AUC_{0-inf}/Dose	h nM/(nmol kg^{-1})	3260	5150	5870	4760	1350
$t_{1/2}$	h	2.7	4.8	4.9	4.1	1.3
MRT	h	3.6	5.1	5.3	4.7	0.9
V_{ss}	l kg^{-1}	1.1	1.0	0.9	1.0	0.1
CL	ml min^{-1} kg^{-1}	5.1	3.2	2.8	3.7	1.2
CL PL QH	%	5.7	3.6	3.2	4.1	1.4

7

Supplementary Table 6. Individual and mean plasma concentrations (nmol l^{-1}) and pharmacokinetic parameters of compound **8** (UdSBI-0545) after single i.v. (bolus) administration to mice.

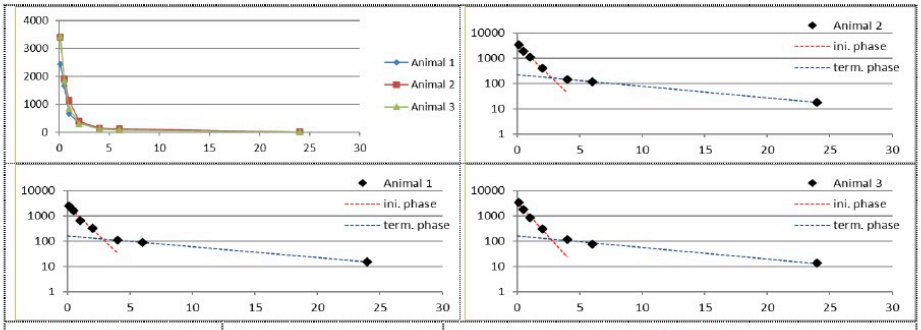

Administration		iv (bolus)				
Nominal dose	µmol kg^{-1}	0.461				
Matrix		Plasma				
Time/Parameter	**Unit**	**Concentration (nmol l^{-1})**				
		Animal 1	**Animal 2**	**Animal 3**	**Mean**	**SD**
0.1	h	2440	3410	3420	3090	563
0.5	h	1650	1900	1850	1800	132
1	h	655	1140	855	883	244
2	h	328	402	307	346	50
4	h	110	144	117	124	18
6	h	90.8	118	77.8	95.5	20.5
24	h	14.8	18.2	13.3	15.4	2.5
C_{max}/Dose	nM/(nmol kg^{-1})	5300	7400	7420	6710	1220
AUC_{0-t}/Dose	h nM/(nmol kg^{-1})	7540	10000	8140	8580	1310
AUC_{0-inf}/Dose	h nM/(nmol kg^{-1})	7860	10400	8420	8900	1350
$t_{1/2}$	h	6.9	6.7	6.6	6.7	0.1
MRT	h	4.5	4.3	3.8	4.2	0.4
V_{ss}	l kg^{-1}	0.6	0.4	0.5	0.5	0.1
CL	ml min^{-1} kg^{-1}	2.1	1.6	2.0	1.9	0.3
CL PL QH	%	2.4	1.8	2.2	2.1	0.3

Supplementary Table 7. Individual and mean plasma concentrations (nmol l^{-1}) and pharmacokinetic parameters of compound **12** (UdSBI-4377) after single i.v. (bolus) administration to mice.

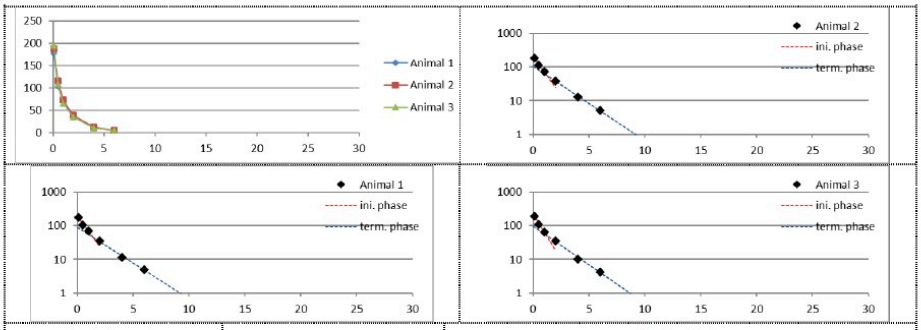

Administration		**iv (bolus)**				
Actual Dose	µmol kg^{-1}	0.0571				
Matrix		Plasma				
Time/Parameter	**Unit**	**Concentration (nmol l^{-1})**				
		Animal 1	**Animal 2**	**Animal 3**	**Mean**	**SD%**
0.1	h	177	187	196	187	9
0.5	h	104	115	109	109	6
1	h	70.4	72.8	64.7	69.3	4.1
2	h	35.2	38.5	35.3	36.3	1.9
4	h	11.4	12.9	10.3	11.5	1.3
6	h	5.0	5.1	4.3	4.8	0.4
24	h	BLOQ	BLOQ	BLOQ	BLOQ	NC
C_{max}/Dose	nM/(nmol kg^{-1})	3100	3280	3440	3270	167
AUC_{0-t}/Dose	h nM/(nmol kg^{-1})	3780	4070	3760	3870	175
AUC_{0-inf}/Dose	h nM/(nmol kg^{-1})	3960	4250	3900	4040	185
$t_{1/2}$	h	1.4	1.4	1.3	1.4	0.1
MRT	h	1.7	1.7	1.6	1.7	0.1
V_{ss}	l kg^{-1}	0.4	0.4	0.4	0.4	0.1
CL	ml min^{-1} kg^{-1}	4.2	3.9	4.3	4.1	0.2
CL PL QH	%	4.7	4.4	4.8	4.6	0.2

Note: Mean PK parameters were calculated by mean plasma concentrations.

BLOQ: Below lower limit of quantification (<1.00 nmol/l).

NC: Not calculated.

9

Supplementary Table 8. *M. smegmatis* and *M. tuberculosis* ClpC1P1P2 in cell-free degradation assays. Footnotes indicate the number of independent experiments performed for the respective compound: a) n = 4, b) n = 5, c) n = 3, d) n = 6, e) n = 2

Compound	Value	***M.smegmatis* ClpC1P1P2**		***M.tuberculosis* ClpC1P1P2**	
		Mean	*SD*	*Mean*	*SD*
dCymC	DC_{50} [µM]	> 100.0_a		> 100.0_e	
5	DC_{50} [µM]	> 100.0_a		> 100.0_e	
6	DC_{50} [µM]	7.5_a	4.6	5.8_a	2.9
	D_{Max}	78%	9%	54%	10%
8 (UdSBI-0545)	DC_{50} [µM]	8.0_b	1.2	8.3_c	3.9
	D_{Max}	83%	6%	54%	4%
8a (UdSBI-0966)	DC_{50} [µM]	> 100.0_a		> 100.0_e	
9	DC_{50} [µM]	8.0_c	1.2	6.8_c	2.2
	D_{Max}	54%	2%	26%	5%
10	DC_{50} [µM]	> 100.0_b		> 100.0_e	
11	DC_{50} [µM]	5.6_a	1.5	5.1_e	0.5
	D_{Max}	87%	3%	74%	6%
12 (UdSBI-4377)	DC_{50} [µM]	8.4_d	1.8	7.1_c	2.6
	D_{Max}	81%	7%	52%	5%
12a (UdsBI-0117)	DC_{50} [µM]	> 100.0_b		> 100.0_e	
16	DC_{50} [µM]	7.0_a	0.9	10.7_c	4.6
	D_{Max}	57%	5%	47%	10%
17	DC_{50} [µM]	> 100.0_a		> 100.0_e	
21	DC_{50} [µM]	5.5_a	1.1	8.6_c	1.2
	D_{Max}	92%	4%	84%	6%
27	DC_{50} [µM]	12.5_c	5.0	24.7_a	14.6
	D_{Max}	91%	2%	74%	4%
SI-39	DC_{50} [µM]	5.8_c	0.6	7.7_c	1.6
	D_{Max}	88%	8%	73%	7%
SI-57	DC_{50} [µM]	23.0_a	9.7	23.7_c	6.8
	D_{Max}	67%	7%	55%	12%
SI-61	DC_{50} [µM]	5.3_a	0.5	7.2_e	0.2
	D_{Max}	42%	3%	42%	7%
SI-65	DC_{50} [µM]	5.2_c	0.8	8.0_e	1.4
	D_{Max}	92%	5%	84%	1%

Supplementary Table 9. MICs of Homo-BacPROTACs and monomers against Gram positive and Gram negative bacteria (ESKAPES panel)

Compound	Gram positive		Gram negative				
	Enterococcus faecium	*Staphylococcus aureus*	*Klebsiella pneumoniae*	*Acinetobacter baumanii*	*Pseudomonas aeruginosa*	*Enterobacter cloacae*	*Salmonella typhimurium*
	µM	µM	µM	µM	µM	µM	µM
5	>50.0	>50.0	>50.0	>50.0	>50.0	>50.0	>50.0
8 (UdSBI-0545)	>50.0	>50.0	>50.0	>50.0	>50.0	>50.0	>50.0
10	>50.0	>50.0	>50.0	>50.0	>50.0	>50.0	>50.0
12 (UdSBI-4377)	>50.0	>50.0	>50.0	>50.0	>50.0	>50.0	>50.0
Moxifloxacin	79.7 ± 0.0	0.3 ± 0.0	1.3 ± 0.0	0.3 ± 0.0	2.5 ± 0.0	0.3 ± 0.0	0.6 ± 0.0

Values represent means and standard deviations of n = 3 well replicates.

Supplementary Table 10. MICs of Homo-BacPROTACs and monomers against non-tuberculous Mycobacteria.

Means and standard deviations of n = 2 independent experiments (one in triplicate, one as unicate) are shown. Values marked with * represent means and standard deviations of n = 3 well replicates from a single experiment.

Compound	***Mycobacterium avium***	***Mycobacterium abscessus***	***Mycobacterium fortuitum***	***Mycobacterium intracellulare***
	µM	µM	µM	µM
10	12.5 ± 0.0	12.5 ± 0.0	12.5 ± 0.0	12.5 ± 0.0
12 (UdSBI-4377)	>50.0	>50.0	>50.0	>50.0
5	6.3 ± 0.0	5.5 ± 1.6	6.3 ± 0.0	6.3 ± 0.0
8 (UdSBI-0545)	>50.0	>50.0	>50.0	>50.0
Moxifloxacin	2.5 ± 0.0	2.5 ± 0.0	0.1 ± 0.0	1.2 ± 0.0
Rifampicin	0.3 ± 0.0*	9.7 ± 0.0*	1.2 ± 0.0*	0.2 ± 0.0*
Amikacin	1.7 ± 0.0*	3.4 ± 0.0*	0.4 ± 0.0*	0.9 ± 0.0*
Clarithromycin	0.3 ± 0.0*	0.7 ± 0.0*	0.7 ± 0.0*	0.2 ± 0.0*

Supplementary Table 11: Homo-BacPROTACs are bactericidal on Mtb, but not Msm cells.

Homo-BacPROTACs **8** (UdSBI-0545) and **12** (UdSBI-4377) display bactericidal activity in *Mtb* H37Rv, but not in *Msm* #607, as demonstrated by replating all respective cultures from one of the triplicate set of wells showing growth inhibition in the MIC assay plate. MBC plating was conducted onto compound-free plates to monitor any colony formation indicative of survivors. An individual example is shown. See Source Data file for details.

	***Msm* #607**				***Mtb* H37Rv**			
Compound	**MIC*** ***Msm* #607**		**MBC**** ***Msm* #607**		**MIC*** ***Mtb* H37Rv**		**MBC**** ***Mtb* H37Rv**	
	µM	**µg/ml**	**µM**	**µg/ml**	**µM**	**µg/ml**	**µM**	**µg/ml**
10	6.3	5.7	>50.0	>45.7	3.1	2.9	12.5	11.4
12 (UdSBI-4377)	0.8	1.5	>50.0	>99.0	0.05	0.1	0.1	0.2
5	25.0	23.5	>50.0	>47.1	1.6	1.5	6.3	5.9
8 (UdSBI-0545)	1.6	3.4	>50.0	>108.5	0.1	0.2	0.1	0.2
Rifampicin	9.7	8.0	ND		0.01	0.01	ND	
Moxifloxacin	0.1	0.1	0.3	0.1	0.1	0.03	0.3	0.1

MIC*: Minimum Inhibitory Concentration

MBC**: Minimum Bactericidal Concentration

Supplementary Fig. 1. MIC on Mtb Beijing strain HN878.

The MIC for the hypervirulent *Mtb* Beijing strain HN878 was determined using the Resazurin assay described above. Homo-BacPROTACs **12** (UdSBI-4377) and **8** (UdSBI-0545) show more efficient inhibition of bacterial growth as compared to the matching monomers **10** and **5** , respectively. Error bars indicate mean ± SD of n = 3 well replicates.

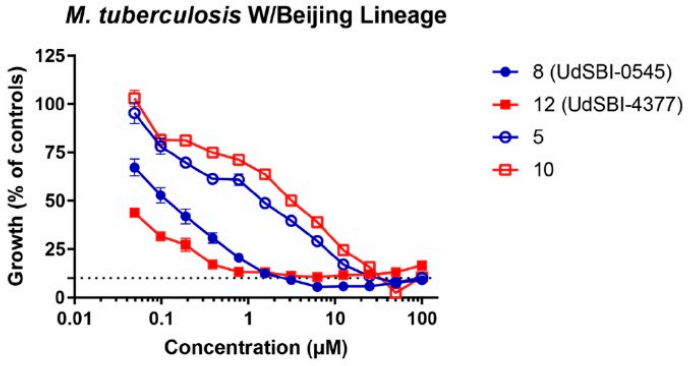

12

Supplementary Fig. 2. MIC on replicating versus starvation-induced, dormant *Mtb* H37Rv cells.

Starvation-induced non-replicating cells of *Mtb* are known to become highly tolerant to a multitude of clinical drugs including the TB antibiotics isoniazid, rifampicin, streptomycin and moxifloxacin[1]. In the used model, we observed strongly reduced susceptibility of all compounds tested, with bedaquiline showing at least partial remaining activity. Error bars indicate mean ± SD of n = 3 well replicates.

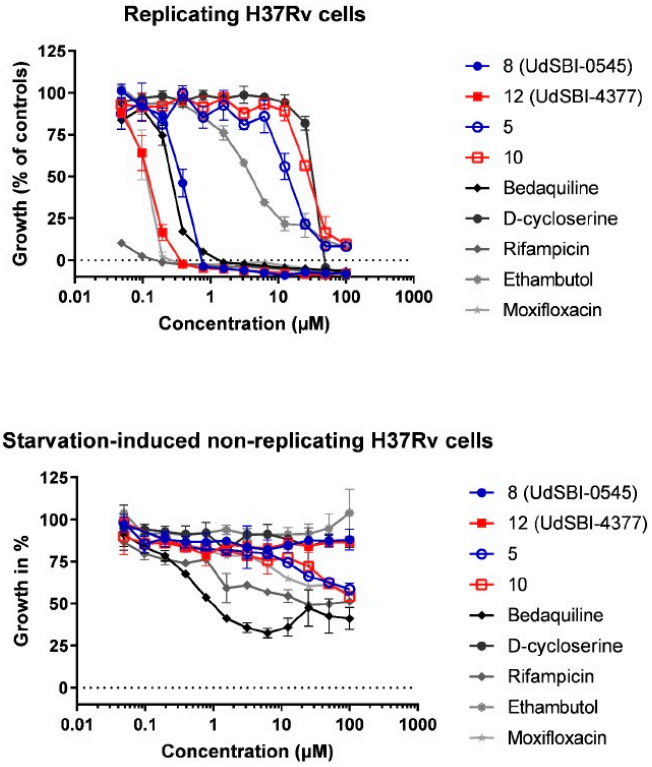

13

Supplementary Fig. 3. BacPROTAC mediated degradation of ClpC1-NTD over time.

Homo-BacPROTAC-mediated cell-free degradation of ClpC1 NTD by the *M. smegmatis* ClpC1P1P2 complex monitored over different incubation times (quantified by WES capillary Western platform). Degradation induced by compound **8** was monitored over six hours at two concentrations (8 µM, 33 µM) at experimental conditions otherwise kept constant and described in the Methods section "Cell-free degradation assay". Means ± SDs of n = 2 well replicates are shown for one representative experiment. The experiment was independently performed twice with similar results. For comparative profiling of compounds in this assay, a 90 min incubation time was chosen.

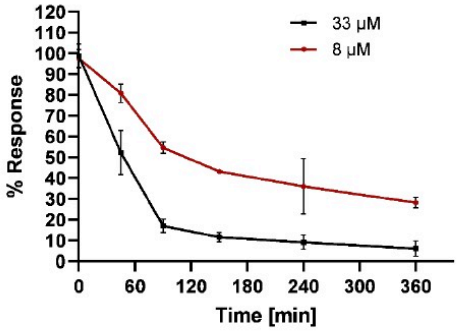

14

Investigation of Intramolecular Hydrogen Bonds (IMHB)

The NMR assignment of N-H protons in **10** was accomplished using ^{1}H-^{1}H-COSY, ^{1}H-^{13}C HSQC and HMBC experiments (for copies of NMR spectra, see below).

N-H acidity coefficient

The difference in ^{1}H NMR chemical shifts in $CDCl_3$ and DMSO-d_6 can be used to approximate the acidity of N-bonded protons.[2] The acidity A_{NMR} can be calculated by the following equation:

$A_{NMR} = 0.0065 + 0.133\ \Delta\delta;\ \Delta\delta = \delta(\text{DMSO-d}_6) - \delta(CDCl_3)$

For $A_{NMR} > 0.15$, no IMHB is present, for $A_{NMR} < 0.05$, a strong IMHB can be assumed.

Supplementary Table 12. Chemical shifts and acidity coefficients for N-H protons in **10**

	position	δ(DMSO-d_6) (ppm)	δ($CDCl_3$) (ppm)	Δδ (ppm)	A_{NMR}	IMHB
Val-NH	**2**	9.13	8.08	1.05	0.146	none
β-OMe-Phe-NH	**3**	7.50	7.27	0.23	0.037	strong
Ala-NH	**4**	8.27	8.46	-0.19	-0.019	strong
Trp-NH	**6**	9.37	7.8	1.57	0.215	none
Pra-NH	**7**	8.13	8.23	-0.1	-0.007	strong

It can be assumed that Val-NH and Trp-NH are not involved in IMHB ($A_{NMR} \geq 0.15$). β-OMe-Phe-NH, Ala-NH and Pra-NH all show values <0.05, indicating that these groups are involved in a strong IMBH network.

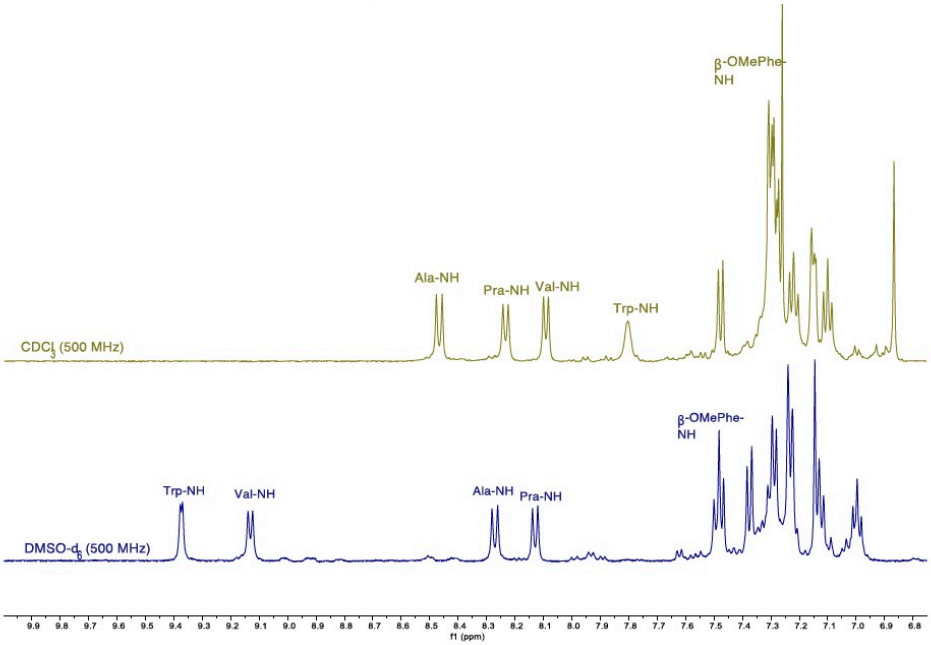

Supplementary Fig. 4. Excerpt from the ^{1}H spectra of **10** in $CDCl_3$ (top, yellow) and DMSO-d_6 (bottom, blue).

NMR Temperature Coefficients

In VT-NMR experiments in DMSO-d_6, the chemical shifts of the N-H protons were determined at different temperatures from 298 K to 338 K in 10 K steps. Linear regression affords the slope of the chemical shifts (Δδ (ppb K^{-1})). These slopes indicate wether the proton is solvent-exposed or part of the IMHB network. Empirically, coefficients < –4.6 ppb K^{-1} indicate a solvent exposed NH, whereas values ≥ –4.6 ppb K^{-1} indicate IMHB interactions.[3] In **10**, the coefficients can be classified in two groups (Table S7; Fig. S2). One group of protons show Δδ values between -2.31 and -1.01 ppb K^{-1} and the other group between -6.76 and -4.59 ppb K^{-1}. It is therefore likely that the first group (β-OMe-Phe, Ala, Pra) is involved in IMHB, whereas the latter group (Val, Trp) is not. This is in accordance with the IMHB network observed by A_{NMR} coefficients as well as the IMHB network in the crystal structure of ClpC1-NTD in complex with Cym A (Fig. S3).

Supplementary Table 13. ^{1}H NMR Chemical shifts (in ppm) of N-H protons in **10** at different temperatures.

AA	position	298 K	308 K	318 K	328 K	338 K	Δδ (ppb K^{-1})	IMHB?
Val-NH	AA2	9.13	9.053	8.99	8.925	8.856	-6.76	solvent exposed
β-OMe-Phe-NH	AA3	7.483	7.464	7.438	7.415	7.392	-2.31	IMHB
Ala-NH	AA4	8.263	8.245	8.225	8.204	8.182	-2.03	IMHB
Trp-NH	AA6	9.359	9.321	9.276	9.228	9.176	-4.59	solvent exposed
Pra-NH	AA7	8.125	8.117	8.107	8.096	8.085	-1.01	IMHB

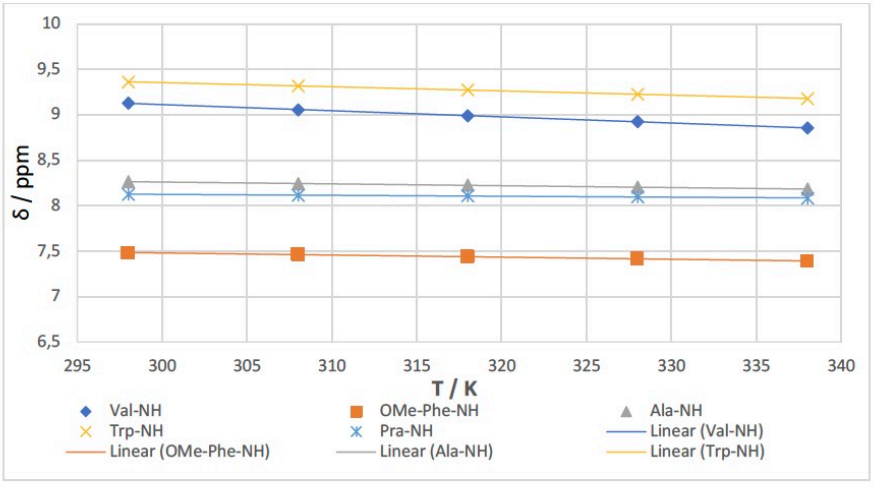

Supplementary Fig. 5. Linear regression of δ(NH)/ppm vs. T/K; *Val-NH*: y = -0.00676x + 11.14; R^2 = 0.9989; *β-OMe-Phe-NH*: y = -0.00231x + 8.173; R^2 = 0.9983; *Ala-NH*: y = -0.00203x + 8.8693; R^2 = 0.9986; *Trp-NH*: y = -0.00459x + 10.732; R^2 = 0.9967; *Pra-NH*: y = -0.00101x + 8.4272; R^2 = 0.9962.

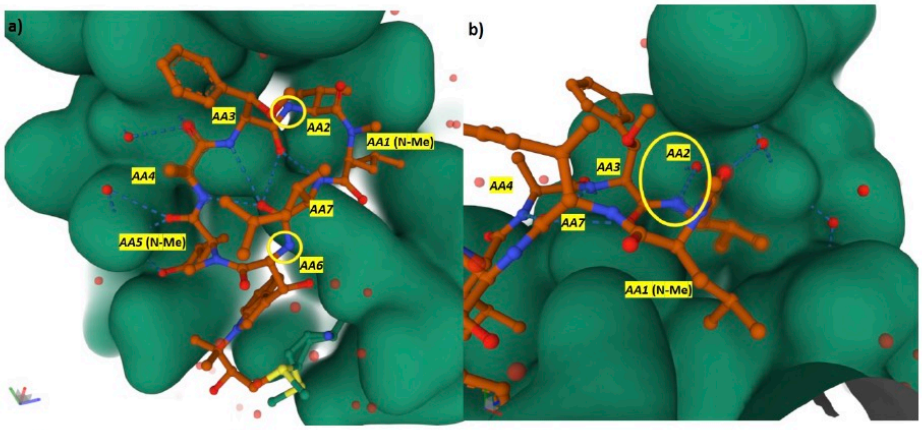

Supplementary Fig. 6. a) IMHB interactions in the crystal structure of CymA bound to ClpC1 NTD (https://www.rcsb.org/structure/3WDC). Yellow circles indicate the two N-H atoms which were determined to be solvent exposed. **b)** The yellow circle indicates a hydrogen bonding network between Val(*AA2*)-N-H, an H_2O-molecule and Gln17/Ile18.

Supplementary Tables 14-17. Pharmacokinetic data after oral administration

Supplementary Table 14. Individual and mean plasma concentrations (nmol l^{-1}) and pharmacokinetic parameters of compound **8** (UdSBI-0545) after single oral gavage administration to mice.

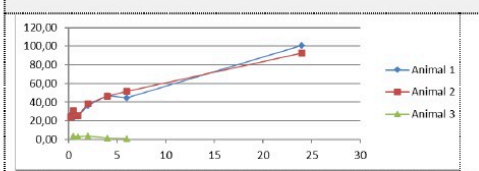

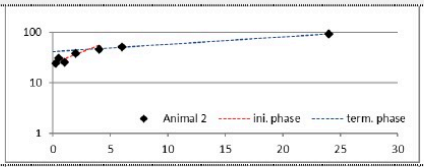

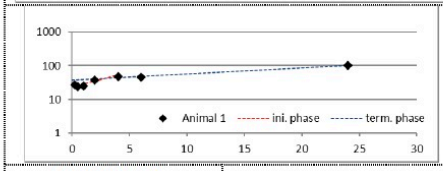

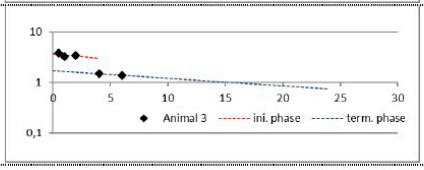

Administration		**oral (gavage)**				
Dose	µmol/kg	9.30				
Matrix		Plasma				
Time/Parameter	**Unit**	**Concentration (nmol/L)**				
		Animal 1	**Animal 2**	**Animal 3**	**Mean**	**SD**
0.25	h	27.2	24.1	BLOQ	25.7	2.19
0.5	h	23.4	31.1	3.80	19.4	14.1
1	h	25.2	25.8	3.24	18.1	12.9
2	h	36.5	38.2	3.41	26.0	19.6
4	h	47.4	46.6	1.48	31.8	26.3
6	h	44.5	51.7	1.38	32.5	27.2
24	h	101	92.4	NR	96.7	6.08
t_{max}	h	24.0	24.0	0.500 [1)]	24.0	0.00
C_{max}/Dose	nM/nmol/kg	10.9	9.95	0.409 [1)]	10.4	0.655
AUC_{0-t}/Dose	h*nM/nmol/kg	165	165	1.38 [1)]	165	0.114
AUC_{0-inf}/Dose	h*nM/nmol/kg	NC	NC	NC	NC	NC
$t_{1/2}$	h	NC	NC	NC	NC	NC
MRT	h	NC	NC	NC	NC	NC
BA	%				NC	

BLOQ: Below lower limit of quantification (<1.00 nmol/L).

NC: Not calculated.

NR: No results, due to missing sample.

1) Value excluded from mean and SD

Supplementary Table 15. Individual and mean plasma concentrations (nmol l^{-1}) and pharmacokinetic parameters of compound **12** (UdSBI-4377) after single oral gavage administration to mice.

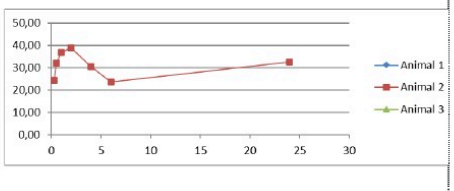

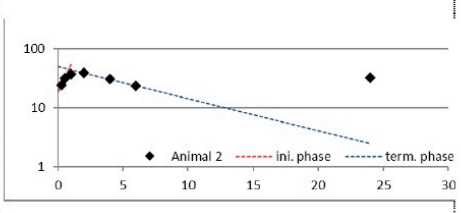

Administration		oral (gavage)				
Dose	µmol/kg	15.1				
Matrix		Plasma				
Time/Parameter	**Unit**	**Concentration (nmol/L)**				
		Animal 1	**Animal 2**	**Animal 3**	**Mean**	**SD**
0.25	h	BLOQ	24.5	BLOQ	NC	NC
0.5	h	BLOQ	32.0	BLOQ	NC	NC
1	h	BLOQ	36.8	BLOQ	NC	NC
2	h	BLOQ	38.8	BLOQ	NC	NC
4	h	BLOQ	30.5	BLOQ	NC	NC
6	h	BLOQ	23.5	BLOQ	NC	NC
24	h	BLOQ	32.5	BLOQ	NC	NC
t_{max}	h	NC	2.00	NC	NC	NC
C_{max}/Dose	nM/nmol/kg	NC	2.56	NC	NC	NC
AUC_{0-t}/Dose	h*nM/nmol/kg	NC	45.5	NC	NC	NC
AUC_{0-inf}/Dose	h*nM/nmol/kg	NC	62.6	NC	NC	NC
$t_{1/2}$	h	NC	5.53	NC	NC	NC
MRT	h	NC	18.0	NC	NC	NC
BA	%		0.7			

BLOQ: Below lower limit of quantification (<1.00 nmol/L).

NC: Not calculated.

Supplementary Table 16. Individual and mean plasma concentrations (nmol l^{-1}) and pharmacokinetic parameters of compound **5** after single oral gavage administration to mice.

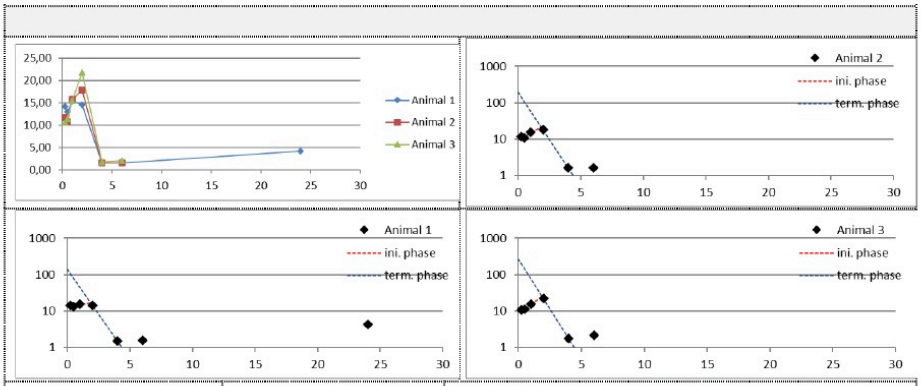

Administration		oral (gavage)				
Dose	µmol/kg	31.9				
Matrix		Plasma				
Time/Parameter	**Unit**	**Concentration (nmol/L)**				
		Animal 1	**Animal 2**	**Animal 3**	**Mean**	**SD**
0.25	h	14.2	11.7	10.6	12.2	1.85
0.5	h	13.0	10.7	11.4	11.7	1.18
1	h	15.3	15.7	15.5	15.5	0.200
2	h	14.5	17.8	21.8	18.0	3.66
4	h	1.49	1.61	1.76	1.62	0.135
6	h	1.54	1.59	2.14	1.76	0.333
24	h	4.22	BLOQ	BLOQ	4.22	
t_{max}	h	1.00	2.00	2.00	1.67	0.577
C_{max}/Dose	nM/nmol/kg	0.480	0.558	0.684	0.574	0.103
AUC_{0-t}/Dose	h*nM/nmol/kg	3.02	1.53	1.74	2.10	0.805
AUC_{0-inf}/Dose	h*nM/nmol/kg	3.14	1.57	1.80	2.17	0.845
$t_{1/2}$	h	0.609	0.577	0.551	0.579	0.0293
MRT	h	11.7	1.98	2.06	5.23	5.57
BA	%				1.2	

BLOQ: Below lower limit of quantification (<1.00 nmol/L).

NC: Not calculated.

Supplementary Table 17. Individual and mean plasma concentrations (nmol l^{-1}) and pharmacokinetic parameters of compound **6** after single oral gavage administration to mice were not available due to bad solubility of the compound (see data below).

Concentration time plots N/A						
Administration		**oral (gavage)**				
Dose	µmol/kg	14.7				
Matrix		Plasma				
Time/Parameter	**Unit**	**Concentration (nmol/L)**				
		Animal 1	**Animal 2**	**Animal 3**	**Mean**	**SD**
0.25	h	BLOQ	BLOQ	BLOQ	BLOQ	NC
0.5	h	BLOQ	BLOQ	BLOQ	BLOQ	NC
1	h	BLOQ	BLOQ	BLOQ	BLOQ	NC
2	h	BLOQ	BLOQ	BLOQ	BLOQ	NC
4	h	BLOQ	BLOQ	BLOQ	BLOQ	NC
6	h	BLOQ	BLOQ	BLOQ	BLOQ	NC
24	h	BLOQ	BLOQ	BLOQ	BLOQ	NC
t_{max}	h	NC	NC	NC	NC	NC
C_{max}/Dose	nM/nmol/kg	NC	NC	NC	NC	NC
AUC_{0-t}/Dose	h*nM/nmol/kg	NC	NC	NC	<1.61[1)]	NC
AUC_{0-inf}/Dose	h*nM/nmol/kg	NC	NC	NC	NC	NC
$t_{1/2}$	h	NC	NC	NC	NC	NC
MRT	h	NC	NC	NC	NC	NC
BA	%				<0.04[1)]	

BLOQ: Below lower limit of quantification (<1.00 nmol/L).

NC: Not calculated.

1) Maximum potential value calculated considering 1 nM concentration (BLOQ) for each time point.

General Information (Chemistry)

Compounds **SI-1–SI-15**, **2a**, **SI-21–SI-34**, **SI-44–SI-49**, **SI-67** and **SI-68** were synthesized by Aragen Life Sciences.

All other compounds were synthesized at Saarland University by the authors. For these, the following applies:

All experiments were carried out in oven-dried glassware (round-bottom flasks or glass vials) under air if not stated otherwise. Anhydrous Dichloromethane (DCM), *N,N*-dimethylformamide (DMF), 1,4-dioxane and acetonitrile (MeCN) were purchased from Acros Organics and used without further purification. Cyclohexane (p.a. grade), Acetonitrile (HPLC grade) were purchased from Fisher Scientific. EtOAc and petroleum ether (PE) were distilled prior to use. Reactions were monitored by LC/MS (Shimadzu Prominence-*i* LC-2030, column: Phenomenex Onyx C18, 50 x 4.6 mm, Shimadzu LCMS-2020, ESI ionization) or by analytical TLC (Polygram SIL G/UV_{254} plates by Macherey-Nagel, visualization with UV-light (254 nm), $KMnO_4$, ninhydrin or cerium molybdate stains). Rotary evaporation was conducted at 40 to 50 °C.

The compounds were purified by automated flash chromatography (normal phase: Grace Reveleris, Teledyne Isco RediSep R_f cartridges, CyH/EtOAc gradient; reversed phase (RP): Büchi Reveleris PREP, Büchi Flashpure Select C18 cartridges, H_2O/MeCN gradient). Final compounds were additionally purified by preparative HPLC (Büchi Releveris PREP, column: Phenonemenex Luna C18, 5 µm, 21.2 x 250 mm, H_2O/MeCN gradient). The compounds were dried by lyophilization from MeCN/H_2O overnight.

NMR spectra were recorded in $CDCl_3$ (δH 7.26 ppm; δC 77.16 ppm) or DMSO-d_6 (δH 2.50 ppm; δC 39.52 ppm) on a Bruker Avance II 400 MHz spectrometer (5 mm BBO Probe, ^{1}H 400 MHz, ^{13}C 101 MHz, 298 K, standard pulse programs from TOPSPIN 3.2 software), a Bruker Avance I 500 MHz spectrometer (5 mm TCI Probe, ^{1}H 500 MHz, ^{13}C 126 MHz, 295 K, standard pulse programs from TOPSPIN 2.4 software), or a Bruker Avance Neo 500 MHz spectrometer (5 mm TCI Prodigy CryoProbe, ^{1}H 500 MHz, ^{13}C 126 MHz, 298 K, standard pulse programs from TOPSPIN 4 software). Chemical shifts (δ) are reported in parts per million (ppm) relative to $Si(CH_3)_4$. Multiplicities are reported as bs (broad signal), s (singlet), d (doublet), t (triplet), q (quartet) and m (multiplet). For mixtures of rotamers in which the signals could not be attributed to either rotamer, the observed integrations for each signal are reported.

High resolution mass spectra were recorded on a *Bruker MAXIS 4G* UHR-TOF (ESI) or a *Finnigan MAT 95* (CI).

Specific optical rotation was measured on a Jasco P-2000 polarimeter in a thermostated (20 °C ± 1 °C) cuvette (path length: 50 mm, λ = 589 nm). The concentrations are given in g/100 ml.

The purity of final compounds was determined via analytical HPLC (column: Luna 3 µm C18(2), 50x4.6 mm; flow: 1 ml min^{-1}; MeCN/H_2O gradient).

Starting materials prepared according to literature procedures:

2 (Cbz-protected pentapeptide);[4]
N^{α}-((allyloxy)carbonyl)-1-(prop-2-yn-1-yl)-L-tryptophan;[5]
methyl N-(((2S,3R)-2-((S)-2-((2S,4R)-2-((S)-2-(((allyloxy)carbonyl)amino)-N-methyl-3-(1-methyl-1H-indol-3-yl)propanamido)-5-((tert-butyldimethylsilyl)oxy)-4-methylpentanamido)propanamido)-3-methoxy-3-phenylpropanoyl)-L-valyl)-N-methyl-L-leucinate (Alloc-protected hexapeptide);[6]
*N*α-((allyloxy)carbonyl)-1-methyl-L-tryptophan;[5]
Allyloxycarbonyl-D-valine;[7]
(2S,4R)-2-(((benzyloxy)carbonyl)(methyl)amino)-5-((tert-butyldimethylsilyl)oxy)-4-methylpentanoic acid;[4]
N^2-(((9*H*-fluoren-9-yl)methoxy)carbonyl)-N^5,N^5-dimethyl-L-glutamine;[8]
*N*α-((allyloxy)carbonyl)-1-(2-methylbut-3-en-2-yl)-L-tryptophan;[4]
(2*S*,3*R*)-2-(((allyloxy)carbonyl)amino)-3,5-dimethylhex-4-enoic acid.[4]

General Synthetic Procedures

The exact reagent amounts and reaction times used are provided in the following chapter.

***GP 1**: N-Cbz-deprotection*

To a solution of the Cbz-protected peptide (1.0 equiv) in MeOH (0.1 M) was added 10 wt% Pd/C (8 mol%). The flask was evacuated (water aspirator) and refilled with H_2 (from a balloon) five times. The reaction mixture was then stirred under H_2 (balloon pressure) until TLC indicated complete conversion (typically 1–2 h). Subsequently, the mixture was filtered over Celite, the filtrate was evaporated *in vacuo* and dried in high vacuum.

***GP 2**: N-Alloc-deprotection*

To a solution of the Alloc-protected peptide (1.0 equiv) in DCM (0.1 M) was added *N*,*N*-dimethylbarbituric acid (DMBA, 3.0 equiv) followed by $Pd(PPh_3)_4$ (0.03 equiv) (under N_2) and stirred until TLC indicated full conversion (typically after 1 h). The reaction mixture was then diluted with EtOAc and washed with sat. $NaHCO_3$ soln. (3x). The combined aqueous phases were back-extractred with EtOAc (1x), the combined organic phases were dried (Na_2SO_4) and evaporated *in vacuo*.

***GP 3:** Peptide coupling with BEP*

The *N*-deprotected peptide was dissolved in DCM (0.1 M) and the acid component (1.2 equiv) and 2-bromo-1-ethylpyridinium tetrafluoroborate (BEP) (1.2 equiv) were added. The mixture was cooled to −20 °C (ice/NaCl) and 4-methylmorpholine (NMM) (2.5 equiv) was added dropwise at this temperature. The reaction mixture was slowly warmed to room temperature overnight and then quenched by the addition of 1 M $KHSO_4$. The mixture was diluted with EtOAc (ca. 20 ml per mmol substrate), transferred to a separatory funnel and shaken vigorously. The phases were separated and the organic phase was subsequently washed with H_2O, sat. $NaHCO_3$ soln. and brine. The organic phase was dried (Na_2SO_4) and evaporated. The residue was purified by flash chromatography.

***GP 4:** Peptide coupling with HOBt/EDC*

The *N*-deprotected peptide was dissolved in DCM (0.1 M) and the acid component (typically 1.1 to 1.3 equiv) was added. The mixture was cooled to 0 °C and 4-methyl morpholine (NMM) (2.0 equiv), $HOBt{\cdot}H_2O$ (1.1 equiv) and EDC (1.1 equiv) were added. The mixture was slowly warmed to room temperature and then diluted with EtOAc and washed with 1 M $KHSO_4$ soln., H_2O, sat. $NaHCO_3$ soln. and brine. The organic phase was dried (Na_2SO_4) and evaporated *in vacuo*. The residue was purified by flash chromatography.

***GP 5**: Peptide coupling with NMI/HCl*[9]

The acid component (1.3 equiv) was dissolved in anhydrous 1,4-dioxane (0.3 M) under N_2-atmosphere. DIPEA (1.3 equiv) and $BnNMe_2$ (0.1 equiv) were added at rt. The mixture was heated to 60 °C and 1 M isopropyl chloroformate solution (1 M in toluene) (1.3 equiv) was added dropwise. After 5 min at 60 °C, a solution of the *N*-deprotected peptide (1.0 equiv), HCl (4 M in 1,4-dioxane) (0.2 equiv) and *N*-methylimidazole (0.1 equiv) in 1,4-dioxane/MeCN 1:1 (0.12 M) was added. The flask was rinsed with additional 1,4-dioxane (final reaction concentration 0.06 M). The reaction mixture was stirred at 60 °C for the specified time. The solvent was then evaporated *in vacuo*, the residue was taken up in EtOAc and washed with 1 M $KHSO_4$ soln., H_2O, sat. $NaHCO_3$ soln. and brine. The organic phase was dried (Na_2SO_4) and evaporated *in vacuo*. The residue was purified by flash chromatography.

***GP 6a:** Global deprotection and cyclization of Alloc-protected heptapeptides*

C-deprotection: The protected heptapeptide (1.0 equiv) was dissolved in 1,4-dioxane (0.1 M) and 1 M aq. LiOH solution (typically 1.2 to 1.8 equiv) was added at rt. The mixture was stirred until full conversion was indicated by LC/MS or TLC. The mixture was then evaporated *in vacuo* and used without purification in the next step.

N-deprotection: The crude *C*-deprotected peptide was dissolved in $MeCN/H_2O$ (1:1, 0.05 M), Et_2NH (5 equiv), triphenylphosphine-3,3',3''-trisulfonic acid trisodium salt (TPPTS) (typically 0.1 equiv) and $Pd(OAc)_2$ (typically 0.05 equiv) were added at rt. The mixture was stirred until LC/MS indicated full conversion and was subsequently evaporated in vacuo. The residue was azeotroped with DCM two times to remove residual H_2O.

Cyclization: The crude *N*- and *C*-deprotected peptide was dissolved in DMF (0.1 M) and the resulting solution was added dropwise to a solution of HATU (typically 3.5 equiv) and DIPEA (typically 5.0 equiv) in DCM (1 mM) over the course of 2–6 hours at 2rt. The mixture was stirred until LC/MS indicated full conversion (typically 16 to 24 h). The solvent was then removed *in vacuo* and the residue was redissolved in EtOAc, washed with 1 M $KHSO_4$, 1 M LiCl, sat. $NaHCO_3$ and sat. NaCl solutions, dried (Na_2SO_4) and evaporated.

TBDMS cleavage: The crude cyclic peptide was dissolved in MeOH (0.1 M), NH_4F (typically 10–20 equiv) was added and the mixture was heated to 45 °C until LC/MS indicated full conversion (typically 18 – 24 h). The reaction mixture was then diluted with EtOAc and washed with $NaHCO_3$ soln. (3x). The combined aqueous phases were back-extracted with EtOAc once. The combined organic phases were dried (Na_2SO_4) and evaporated *in vacuo*. The residue was purified by RP flash chromatography.

***GP6b**: Global deprotection and cyclization of Fmoc-protected heptapeptides*

N-deprotection: The protected heptapeptide (1.0 equiv) was dissolved in DCM (0.1 M) and tris(2-aminoethyl)amine (tris(2-aminoethyl)amine) (10 equiv) was added at rt. The mixture was stirred until full conversion was indicated by LCMS or TLC (typically 30 min) and was then diluted with EtOAc. It was then washed with H_2O (2x) and phosphate buffer (pH = 5.5, 66.7 mM) (2x). The aqueous phases were back-extracted with EtOAc (1x), the combined organic phases were dried (Na_2SO_4) and evaporated *in vacuo*.

C-deprotection: The crude deprotected heptapeptide was dissolved in 1,4-dioxane (0.1 M) and 1 M aq. LiOH solution (typically 2.2 equiv) was added at rt. The mixture was stirred at this temperature until full conversion was indicated by LC/MS and then evaporated *in vacuo*.

Cyclization and *TBDMS cleavage* were perfromed as described in *GP6a*

***GP6c:** Global deprotection and cyclization of 6-N-methylated heptapeptides*

Depending on the N-protecting group, *N-deprotection* and *C-deprotection* were perfomed as described in *GP6a* or *GP6b*.

Cyclization: The crude *N*- and *C*-deprotected peptide was dissolved in DCE (0.1 M) and the resulting solution was added dropwise to a solution of HATU (typically 3.5 equiv) and DIPEA (typically 5.0 equiv) in DCE (1 mM) over the course of 2 – 4 hours at 60 °C. The mixture was then stirred for 16 – 24 h or until LC/MS indicated full conversion. The solvent was then removed *in vacuo*, the residue was redissolved in EtOAc, washed with 1 M $KHSO_4$, 1 M LiCl, sat. $NaHCO_3$ and sat. NaCl solutions, dried (Na_2SO_4) and evaporated.

TBDMS cleavage was performed as described in *GP6a*.

***GP7**: Dimerization of cyclic peptides by CuAAC*

A vial was charged with the alkyne-bearing cyclic peptide (2.0 equiv). A solution of the diazide in *t*-BuOH (typically ca. 20 mg ml^{-1}; 1.0 equiv) was added to the peptide followed by additional *t*-BuOH and H_2O to reach a final concentration of 0.025 M and a ratio *t*-BuOH to H_2O of 1:1. 1 M $CuSO_4$ (aq.) (typically 0.8 equiv) and 1 M sodium ascorbate (aq.) (typically 1.3 equiv) were added, which resulted in a brown coloration of the solution that dissipated after a few seconds. The vial was immediately flushed with Argon and sealed. After full conversion was reached (indicated by LC/MS), the mixture was evaporated *in vacuo* and the residue was purified by RP flash chromatography (followed by prep HPLC in most cases).

Synthesis of the compounds

Synthesis of exit vector 6 Homo-BacPROTACs (6 – 9)

methyl *N*-(((2*S*,3*R*)-2-((*S*)-2-((2*S*,4*R*)-2-((*S*)-2-(((allyloxy)carbonyl)amino)-*N*-methyl-3-(1-(prop-2-yn-1-yl)-1*H*-indol-3-yl)propanamido)-5-((*tert*-butyldimethylsilyl)oxy)-4-methylpentanamido)propanamido)-3-methoxy-3-phenylpropanoyl)-L-valyl)-*N*-methyl-L-leucinate (3)

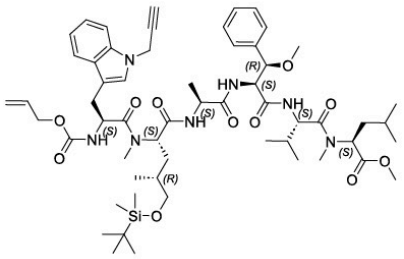

Prepared according to *GP1* and *GP3*: Pentapeptide **2**[4] (803 mg, 894 µmol), Pd/C (80.3 mg) (2 h); Alloc-Trp(propargyl)-OH[5] (344 mg, 1.05 mmol), BEP (289 mg, 1.05 mmol), NMM (0.246 ml, 2.24 mmol) (16 h). Flash chromatography (DCM/EtOAc 100:0 – 60:40) followed by lyophilization afforded **3** (82.0 mg, 76.5 µmol, 69%) as a white amorphous solid. R_f = 0.37 (DCM/EtOAc 1:1).

$[\alpha]_{20}^{D}$ = −58.2 (c 0.5, $CHCl_3$).

^{1}H NMR (500 MHz, $CDCl_3$) *(mixture of rotamers, ratio 3:2)* δ -0.27 – -0.19 (m, 0.3H), -0.05 (s, 0.8H), -0.03 (s, 0.8H), 0.01 – 0.03 (m, 2.5H), 0.03 (s, 2.2H), 0.40 (d, *J* = 6.6 Hz, 0.8H), 0.83 (s, 2.4H), 0.88 (s, 7H), 0.89 – 0.98 (m, 12.9H), 0.99 (d, *J* = 6.9 Hz, 2.4H), 1.19 (d, *J* = 7.0 Hz, 2.3H), 1.22 – 1.28 (m, 1.4H), 1.44 – 1.54 (m, 2.4H), 1.66 – 1.80 (m, 3.1H), 1.86 – 1.92 (m, 0.6H), 1.94 – 2.04 (m, 1.0H), 2.07 – 2.21 (m, 1.2H), 2.36 – 2.43 (m, 1.0H), 2.73 (s, 2.0H), 2.75 (s, 0.9H), 2.97 (s, 1.0H), 3.01 (s, 2.1H), 3.06 (dd, *J* = 9.6, 5.3 Hz, 0.4H), 3.09 – 3.17 (m, 1.1H), 3.21 (dd, *J* = 14.5, 8.1 Hz, 0.9H), 3.28 (s, 1.3H), 3.33 (s, 2.4H), 3.40 (dd, *J* = 9.8, 5.4 Hz, 0.7H), 3.45 (dd, *J* = 9.8, 4.7 Hz, 0.8H), 3.67 – 3.71 (m, 3.0H), 4.17 – 4.23 (m, 0.6H), 4.24 – 4.31 (m, 0.4H), 4.46 – 4.59 (m, 2.2H), 4.63 (dd, *J* = 7.6, 3.4 Hz, 0.6H), 4.70 (dd, *J* = 7.7, 3.6 Hz, 0.9H), 4.75 – 4.91 (m, 5.3H), 4.94 – 5.02 (m, 0.9H), 5.15 – 5.32 (m, 2.3H), 5.35 (dd, *J* = 10.6, 5.3 Hz, 1.0H), 5.59 (d, *J* = 7.6 Hz, 0.3H), 5.80 – 5.92 (m, 1.5H), 6.36 (d, *J* = 6.7 Hz, 0.6H), 6.75 (d, *J* = 7.5 Hz, 0.4H), 6.78 (d, *J* = 7.6 Hz, 0.6H), 7.04 (s, 1.0H), 7.11 – 7.25 (m, 5.5H), 7.27 – 7.32 (m, 2.0H), 7.33 – 7.38 (m, 1.5H), 7.43 (d, *J* = 8.7 Hz, 0.5H), 7.59 (d, *J* = 7.9 Hz, 0.3H), 7.67 (d, *J* = 7.9 Hz, 0.6H), 7.83 (d, *J* = 6.7 Hz, 0.3H).

^{13}C-NMR (126 MHz, $CDCl_3$) *(mixture of rotamers)* δ -5.3, -5.25, -5.21, 15.7, 16.3, 17.4, 17.5, 17.55, 17.59, 17.9, 18.4, 18.5, 19.6, 19.7, 21.53, 21.54, 23.42, 23.44, 24.9, 25.0, 26.07, 26.10, 28.5, 29.0, 29.3, 31.28, 31.35, 31.4, 31.5, 31.7, 32.0, 32.2, 35.75, 35.81, 35.9, 37.1, 49.8, 49.9, 50.9, 51.6, 52.26, 52.28, 54.2, 54.4, 54.60, 54.7, 56.3, 57.6, 57.7, 57.9, 58.0, 65.9, 66.4, 67.4, 68.5, 73.8, 73.8, 77.7, 78.0, 81.3, 81.5, 109.57, 109.65, 109.8, 109.9, 117.8, 118.4, 118.97, 119.04, 120.1, 120.2, 122.4, 122.7, 126.3, 126.4, 127.02, 127.04, 128.18, 128.24, 128.3, 128.4, 128.51, 128.54, 132.2, 132.9, 136.0, 136.2, 137.0, 137.1, 156.0, 156.8, 168.6, 168.7, 168.9, 170.5, 171.68, 171.72, 172.1, 172.2, 172.3, 172.5, 173.4.

Selected diagnostic peaks:

Major rotamer: **^{1}H NMR** (500 MHz, $CDCl_3$) δ 0.02 (s, 3H), 0.03 (s, 3H), 0.88 (s, 9H), 2.39 (t, *J* = 2.5 Hz, 1H), 2.73 (s, 3H), 3.01 (s, 3H), 3.14 (dd, *J* = 13.5, 5.6 Hz, 1H), 3.33 (s, 3H), 3.40 (dd, *J* = 9.8, 5.4 Hz, 1H), 3.45 (dd, *J* = 9.8, 4.7 Hz, 1H), 3.69 (s, 3H), 4.20 (t, *J* = 6.9 Hz, 1H), 4.70 (dd, *J* = 7.7, 3.6 Hz, 1H), 5.35 (dd, *J* = 10.6, 5.3 Hz, 1H), 6.36 (d, *J* = 6.7 Hz, 1H), 6.78 (d, *J* = 7.6 Hz, 1H), 7.04 (s, 1H), 7.67 (d, *J* = 7.9 Hz, 1H). **^{13}C-NMR** (126 MHz, $CDCl_3$) δ 26.10, 32.2, 52.28, 54.7, 57.7, 67.4, 73.78, 156.0.

Minor rotamer: **^{1}H NMR** (500 MHz, $CDCl_3$) δ -0.27 – -0.19 (m, 1H), -0.05 (s, 3H), -0.03 (s, 3H), 0.40 (d, *J* = 6.6 Hz, 3H), 0.83 (s, 9H), 2.39 (t, *J* = 2.6 Hz, 1H), 2.75 (s, 3H), 2.97 (s, 3H), 3.28 (s, 3H), 3.69 (s, 3H), 4.28 (t, *J* = 6.9 Hz, 1H), 5.59 (d, *J* = 7.6 Hz, 1H), 6.75 (d, *J* = 7.5 Hz, 1H), 7.59 (d, *J* = 7.9 Hz, 1H), 7.83 (d, *J* = 6.7 Hz, 1H). δ 26.07, 52.26, 57.6, 73.82. **^{13}C-NMR** (126 MHz, $CDCl_3$) δ 26.07, 52.26, 54.60, 57.6, 68.5, 73.8, 156.8.

HRMS (ESI): calcd for $C_{57}H_{86}N_7O_{11}Si^+$ $(M+H)^+$: 1072.6149; found: 1072.6121.

25

methyl *N*-(((2*S*,3*R*)-2-((*S*)-2-((2*S*,4*R*)-2-((*S*)-2-((*S*)-2-(((allyloxy)carbonyl)amino)-3-methylbutanamido)-*N*-methyl-3-(1-(prop-2-yn-1-yl)-1*H*-indol-3-yl)propanamido)-5-((*tert*-butyldimethylsilyl)oxy)-4-methylpentanamido)propanamido)-3-methoxy-3-phenylpropanoyl)-L-valyl)-*N*-methyl-L-leucinate (4)

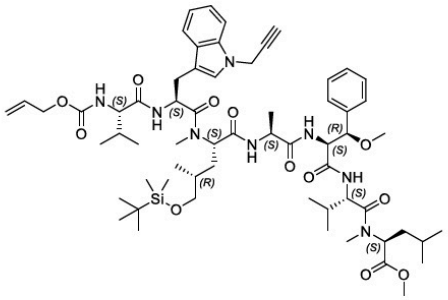

Prepared according to *GP2* and *GP4*: **3** (635 mg, 592 µmol), DMBA (277 mg, 1.78 mmol), $Pd(PPh_3)_4$ (20.5 mg, 17.8 µmol) (1 h); Alloc-L-Val-OH (131 mg, 651 µmol), HOBt (109 mg, 710 µmol), EDC (136 mg, 710 µmol), NMM (0.130 ml, 1.18 mmol) in DMF (6 ml) (18 h). Column chromatography (DCM/EtOAc 100:0 – 60:40) followed by lyohpilization afforded **4** (525 mg, 0.448 mmol, 76% yield) as a white amorphous solid. R_f = 0.30 (DCM/EtOAc 1:1).

$[\alpha]_{20}^{D}$ = –64.2 (c 0.5, $CHCl_3$)

^{1}H-NMR (500 MHz, $CDCl_3$) *(mixture of rotamers, ratio ~2:1)* δ -0.26 – -0.17 (m, 0.3H), -0.05 (s, 1.0H), -0.03 (s, 1.1H), 0.02 (s, 2.0H), 0.03 (s, 2.2H), 0.42 (d, *J* = 6.6 Hz, 0.8H), 0.83 (s, 4.4H), 0.88 (s, 6.0H), 0.88 – 0.91 (m, 19.1H), 0.99 (d, *J* = 6.8 Hz, 2.7H), 1.18 – 1.24 (m, 2.9H), 1.40 – 1.53 (m, 2.8H), 1.66 – 1.80 (m, 5.2H), 1.93 – 2.03 (m, 1.4H), 2.04 – 2.17 (m, 2.1H), 2.36 – 2.43 (m, 1.0H), 2.71 (s, 1.0H), 2.75 (m, 1.8H), 2.95 – 3.00 (m, 3.3H), 3.07 – 3.18 (m, 1.5H), 3.23 (dd, *J* = 14.5, 8.0 Hz, 0.9H), 3.29 (s, 1.1H), 3.33 (s, 2.4H), 3.40 – 3.44 (m, 1.4H), 3.69 (s, 3.2H), 3.98 – 4.08 (m, 0.9H), 4.22 – 4.30 (m, 0.7H), 4.31 – 4.38 (m, 0.4H), 4.51 – 4.68 (m, 2.3H), 4.66 – 4.73 (m, 1.5H), 4.75 – 4.86 (m, 4.6H), 4.89 – 5.02 (m, 1.2H), 5.16 – 5.41 (m, 5.0H), 5.65 (d, *J* = 9.5 Hz, 0.3H), 5.86 – 6.00 (m, 1.0H), 6.34 (d, *J* = 6.9 Hz, 0.6H), 6.74 – 6.83 (m, 1.7H), 7.04 (s, 1.0H), 7.11 – 7.18 (m, 2.0H), 7.19 – 7.24 (m, 4.0H), 7.27 – 7.40 (m, 4.7H), 7.56 – 7.58 (m, 0.4H), 7.67 – 7.69 (m, 0.5H), 8.10 (d, *J* = 7.0 Hz, 0.3H).

^{13}C-NMR (126 MHz, $CDCl_3$) *(mixture of rotamers)* δ -5.3, -5.25, -5.22, 15.9, 17.3, 17.4, 17.5, 17.7, 18.0, 18.4, 18.5, 19.2, 19.3, 19.6, 19.7, 21.5, 21.6, 23.4, 23.5, 24.95, 24.97, 26.07, 26.10, 28.2, 28.8, 29.3, 31.1, 31.3, 31.4, 31.50, 31.55, 31.8, 32.3, 35.76, 35.80, 37.1, 49.4, 49.9, 50.0, 52.3, 54.2, 54.6, 54.7, 56.0, 57.6, 57.66, 57.71, 58.1, 58.2, 60.1, 60.2, 66.0, 66.2, 67.1, 68.6, 73.8, 73.9, 77.7, 78.1, 81.2, 81.4, 109.5, 109.7, 109.75, 109.80, 117.9, 118.1, 118.96, 119.05, 120.1, 120.3, 122.4, 122.7, 126.3, 127.09, 127.14, 128.3, 128.36, 128.41, 128.5, 128.6, 128.7, 132.06, 132.08, 132.2, 132.3, 132.8, 136.1, 136.2, 136.9, 156.2, 156.4, 168.5, 168.7, 170.3, 170.9, 171.6, 171.8, 172.08, 172.11, 172.20, 172.24, 172.5, 172.8.

Selected diagnostic peaks:

Major rotamer: **^{1}H NMR** (500 MHz, $CDCl_3$) δ 0.02 (s, 3H), 0.03 (s, 3H), 0.88 (s, 9H), 2.39 (t, *J* = 2.3 Hz, 1H), 2.75 (s, 3H), 2.98 (s, 3H), 3.23 (dd, *J* = 14.5, 8.0 Hz, 1H), 3.33 (s, 3H), 3.69 (s, 3H), 3.99 – 4.08 (m, 1H), 4.22 – 4.31 (m, 1H), 5.87 – 5.97 (m, 1H), 6.34 (d, *J* = 6.9 Hz, 1H), 7.04 (s, 1H). **^{13}C-NMR** (126 MHz, $CDCl_3$) δ 26.10, 28.8, 31.5, 49.4, 117.9, 156.2.

Minor rotamer: **^{1}H NMR** (500 MHz, $CDCl_3$) δ -0.26 – -0.17 (m, 1H), -0.05 (s, 3H), -0.03 (s, 3H), 0.42 (d, *J* = 6.6 Hz, 3H), 0.83 (s, 9H), 3.29 (s, 3H), 4.32 – 4.37 (m, 1H), 5.65 (d, *J* = 9.1 Hz, 1H), 8.10 (d, *J* = 7.2 Hz, 1H). δ **^{13}C-NMR** (126 MHz, $CDCl_3$) 28.2, 49.9, 118.1, 156.4.

HRMS (ESI): calcd for $C_{62}H_{95}N_8O_{12}Si^+$ $(M+H)^+$: 1171.6833; found: 1171.6830.

(3*S*,6*S*,9*S*,12*S*,15*S*,18*S*,21*S*)-21-((*R*)-3-hydroxy-2-methylpropyl)-9-isobutyl-6,12-diisopropyl-15-((*R*)-methoxy(phenyl)methyl)-1,10,18-trimethyl-3-((1-(prop-2-yn-1-yl)-1*H*-indol-3-yl)methyl)-1,4,7,10,13,16,19-heptaazacyclohenicosane-2,5,8,11,14,17,20-heptaone (5)

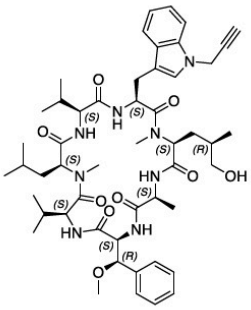

Prepared according to *GP6a*: **4** (509 mg, 434 µmol), 1 M LiOH (521 µl, 0.521 µmol) (3.5 h); $Pd(OAc)_2$ (2.9 mg, 13.0 µmol), TPPTS (14.8 mg, 26.0 µmol), Et_2NH (0.22 ml, 2.17 mmol) (1 h); HATU (576 mg, 1.52 mmol), DIPEA (0.303 ml, 1.74 mmol) (addition over 1.5 h, additional 16 h); NH_4F (322 mg, 8.68 mmol) (17 h). RP flash chromatography (H_2O/MeCN 90:10 - 5:95) followed by lyophilizaiton afforded **5** (247 mg, 262 µmol, 60%) as an off-white, amorphous solid.

$[\alpha]_{20}^{D}$ = -118.5 (c 0.5, $CHCl_3$).

^{1}H-NMR (500 MHz, $CDCl_3$): δ -0.62 – -0.52 (m, 1H), 0.23 (d, *J* = 6.8 Hz, 3H), 0.60 (d, *J* = 6.3 Hz, 3H), 0.64 (d, *J* = 6.6 Hz, 3H), 0.70 – 0.79 (m, 2H), 0.96 (d, *J* = 6.9 Hz, 3H), 0.97 – 1.01 (m, 6H), 1.08 (d, *J* = 6.6 Hz, 3H), 1.10 – 1.16 (m, 1H), 1.17 (d, *J* = 7.3 Hz, 3H), 1.52 – 1.63 (m, 1H), 1.80 – 1.90 (m, 1H), 2.19 – 2.29 (m, 1H), 2.33 (ddd, *J* = 13.4, 10.4, 4.5 Hz, 1H), 2.41 (t, *J* = 2.6 Hz, 1H), 2.51 (bs, 1H), 2.59 (s, 3H), 2.84 (s, 3H), 2.89 – 2.97 (m, 1H), 2.98 – 3.04 (m, 1H), 3.12 (dd, *J* = 13.4, 4.7 Hz, 1H), 3.32 (dd, *J* = 13.7, 10.9 Hz, 1H), 3.36 (s, 3H), 4.05 (t, *J* = 9.5 Hz, 1H), 4.32 (dd, *J* = 11.0, 2.7 Hz, 1H), 4.48 (t, *J* = 8.6 Hz, 1H), 4.73 – 4.78 (m, 2H), 4.80 (dd, *J* = 10.2, 2.5 Hz, 2H), 4.83 – 4.88 (m, 1H), 4.91 (t, *J* = 5.1 Hz, 1H), 5.07 (d, *J* = 5.5 Hz, 1H), 6.92 (d, *J* = 5.4 Hz, 1H), 7.00 (s, 1H), 7.09 – 7.15 (m, 1H), 7.16 – 7.22 (m, 3H), 7.22 – 7.26 (m, 4H), 7.35 (d, *J* = 8.4 Hz, 1H), 7.48 (d, *J* = 8.0 Hz, 1H), 8.12 (d, *J* = 8.0 Hz, 1H), 8.23 (d, *J* = 9.5 Hz, 1H), 8.48 (d, *J* = 10.4 Hz, 1H).

^{13}C-NMR (126 MHz, $CDCl_3$): δ 17.3, 18.7, 19.5, 20.1, 20.2, 21.0, 22.7, 23.7, 25.4, 28.4, 29.3, 29.7, 30.9, 31.7, 31.9, 33.2, 35.8, 39.1, 50.5, 51.2, 55.4, 56.1, 57.9, 59.1, 59.3, 66.0, 74.1, 77.6, 80.0, 108.8, 109.9, 118.9, 120.4, 122.9, 126.4, 128.0, 128.2, 128.3, 128.8, 135.1, 136.0, 168.8, 169.2, 170.1, 170.7, 171.3, 171.6, 172.2.

HRMS (ESI): calcd for $C_{51}H_{73}N_8O_9^+$ $(M+H)^+$: 941.5495; found: 941.5483.

(3*S*,3'*S*,6*S*,6'*S*,9*S*,9'*S*,12*S*,12'*S*,15*S*,15'*S*,18*S*,18'*S*,21*S*,21'*S*)-15,15'-(((((oxybis(ethane-2,1-diyl))bis(1*H*-1,2,3-triazole-1,4-diyl))bis(methylene))bis(1*H*-indole-1,3-diyl))bis(methylene))bis(12-((*R*)-3-hydroxy-2-methylpropyl)-21-isobutyl-3,18-diisopropyl-6-((*R*)-methoxy(phenyl)methyl)-1,9,13-trimethyl-1,4,7,10,13,16,19-heptaazacyclohenicosane-2,5,8,11,14,17,20-heptaone) (6)

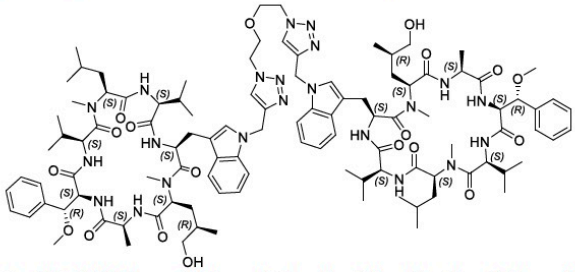

Prepared according to *GP7*: **5** (40.7 mg, 43.2 µmol), 1-azido-2-(2-azidoethoxy)ethane (3.39 mg, 21.6 µmol), 1 M $CuSO_4$ (17.3 µl, 17.3 µmol), 1 M sodium ascorbate (30.3 µl, 30.3 µmol) (5 h). RP flash chromatography (H_2O/MeCN 70:30 – 5:95) followed by lyophilization afforded **6** (34.1 mg, 16.7 µmol, 77%) as a white, amorphous solid.

$[\alpha]_{20}^{D}$ = –102.5 (c 0.5, $CHCl_3$)

^{1}H-NMR (500 MHz, $CDCl_3$): δ -0.60 (t, *J* = 9.1 Hz, 2H), 0.20 (d, *J* = 6.8 Hz, 6H), 0.62 (d, *J* = 6.6 Hz, 6H), 0.65 (d, *J* = 6.8 Hz, 6H), 0.86 (q, *J* = 7.0 Hz, 2H), 0.96 – 1.04 (m, 18H), 1.02 – 1.09 (m, 2H), 1.13 (d, *J* = 6.6 Hz, 6H), 1.18 (d, *J* = 7.1 Hz, 6H), 1.60 (ddd, *J* = 13.4, 11.2, 5.4 Hz, 2H), 1.76 (ddd, *J* = 13.2, 11.0, 5.8 Hz, 2H), 2.23 – 2.36 (m, 4H), 2.55 (s, 6H), 2.86 (s, 10H), 3.06 (d, *J* = 4.3 Hz, 2H), 3.14 (dd, *J* = 13.6, 5.1 Hz, 2H), 3.29 – 3.38 (m, 2H), 3.40 (s, 6H), 3.71 – 3.79 (m, 4H), 4.15 (t, *J* = 9.5 Hz, 2H), 4.35 – 4.45 (m, 6H), 4.50 (t, *J* = 8.4 Hz, 2H), 4.70 – 4.81 (m, 4H), 4.89 (dd, *J* = 10.1, 3.9 Hz, 2H), 4.93 (t, *J* = 5.1 Hz, 2H), 5.11 (d, *J* = 5.5 Hz, 2H), 5.28 (d, *J* = 15.6 Hz, 2H), 5.38 (d, *J* = 15.6 Hz, 2H), 7.01 (s, 2H), 7.11 (t, *J* = 7.3 Hz, 2H), 7.17 (d, *J* = 4.9 Hz, 2H), 7.19 – 7.29 (m, 14H), 7.36 (s, 2H), 7.43 (d, *J* = 8.2 Hz, 4H), 7.50 (d, *J* = 8.0 Hz, 2H), 8.11 (d, *J* = 7.9 Hz, 2H), 8.25 (d, *J* = 9.5 Hz, 2H), 8.39 (d, *J* = 10.4 Hz, 2H).

^{13}C-NMR (126 MHz, $CDCl_3$): δ 16.4, 18.7, 19.4, 20.06, 20.14, 21.0, 22.7, 23.7, 25.3, 28.1, 29.2, 29.7, 30.9, 31.6, 31.9, 32.4, 39.0, 41.3, 50.0, 50.4, 51.1, 55.3, 56.0, 57.9, 58.7, 58.8, 59.0, 66.6, 69.1, 80.0, 108.8, 110.0, 118.8, 120.0, 122.6, 123.4, 126.8, 127.8, 128.18, 128.23, 128.8, 135.1, 136.0, 143.7, 168.6, 168.7, 170.0, 170.7, 171.56, 171.60, 172.2.

HRMS (ESI): calcd for $C_{106}H_{153}N_{22}O_{19}^+$ $(M+H)^+$: 2038.1677; found: 2038.1714.

(3*S*,3'*S*,6*S*,6'*S*,9*S*,9'*S*,12*S*,12'*S*,15*S*,15'*S*,18*S*,18'*S*,21*S*,21'*S*)-15,15'-(((((((oxybis(ethane-2,1-diyl))bis(oxy))bis(ethane-2,1-diyl))bis(1*H*-1,2,3-triazole-1,4-diyl))bis(methylene))bis(1*H*-indole-1,3-diyl))bis(methylene))bis(12-((*R*)-3-hydroxy-2-methylpropyl)-21-isobutyl-3,18-diisopropyl-6-((*R*)-methoxy(phenyl)methyl)-1,9,13-trimethyl-1,4,7,10,13,16,19-heptaazacyclohenicosane-2,5,8,11,14,17,20-heptaone) (7)

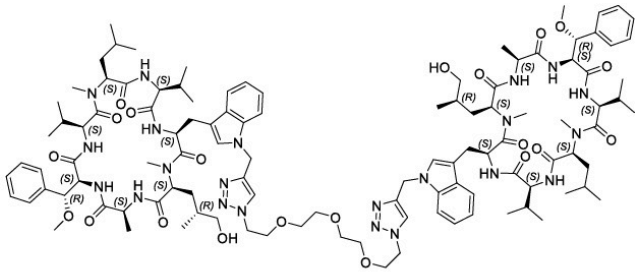

Prepared according to *GP7*: **5** (17.0 mg, 18.1 µmol), 1-azido-2-(2-(2-azidoethoxy)ethoxy)ethoxy)ethane (2.21 mg, 9.03 µmol), 1 M $CuSO_4$ (9.03 µl, 9.03 µmol), 1 M sodium ascorbate (9.03 µl, 9.03 µmol) (4.5 h). RP flash chromatography (H_2O/MeCN 90:10 – 95:5) followed by prep HPLC (H_2O/MeCN 90:10 – 95:5) and lyophilization afforded **7** (14.0 mg, 6.48 µmol, 71%) as a white, amorphous solid.

$[\alpha]_{20}^{D}$ = −114.8 (c 0.5, $CHCl_3$).

^{1}H-NMR (500 MHz, $CDCl_3$): δ -0.80 (dd, *J* = 10.8, 7.5 Hz, 2H), 0.10 (d, *J* = 6.8 Hz, 6H), 0.57 (d, *J* = 6.4 Hz, 6H), 0.61 (d, *J* = 6.6 Hz, 6H), 0.72 (d, *J* = 9.3 Hz, 2H), 0.84 (q, *J* = 6.1 Hz, 2H), 0.93 – 1.00 (m, 18H), 1.08 (d, *J* = 6.6 Hz, 6H), 1.10 – 1.19 (m, 8H), 1.52 – 1.61 (m, 2H), 1.62 – 1.72 (m, 2H), 2.18 – 2.27 (m, 2H), 2.29 (ddd, *J* = 14.7, 10.0, 4.7 Hz, 2H), 2.52 (s, 6H), 2.75 – 2.83 (m, 2H), 2.82 (s, 6H), 2.93 – 3.02 (m, 4H), 3.06 (dd, *J* = 13.5, 4.7 Hz, 2H), 3.21 – 3.30 (m, 2H), 3.30 – 3.36 (m, 4H), 3.35 (s, 6H), 3.40 – 3.46 (m, 4H), 3.75 (t, *J* = 5.2 Hz, 4H), 4.13 (t, *J* = 9.5 Hz, 2H), 4.32 (dd, *J* = 11.2, 2.8 Hz, 2H), 4.42 (td, *J* = 5.0, 2.8 Hz, 4H), 4.48 (t, *J* = 8.5 Hz, 2H), 4.67 – 4.78 (m, 4H), 4.85 (dd, *J* = 10.1, 3.9 Hz, 2H), 4.89 (t, *J* = 5.1 Hz, 2H), 5.07 (d, *J* = 5.5 Hz, 2H), 5.24 (d, *J* = 15.7 Hz, 2H), 5.34 (d, *J* = 15.6 Hz, 2H), 6.98 (s, 2H), 7.08 (t, *J* = 7.4 Hz, 2H), 7.15 – 7.19 (m, 8H), 7.21 – 7.24 (m, 6H), 7.40 (d, *J* = 8.2 Hz, 2H), 7.45 (d, *J* = 7.9 Hz, 2H), 7.52 (s, 2H), 7.63 (d, *J* = 4.9 Hz, 2H), 8.11 (d, *J* = 7.9 Hz, 2H), 8.28 (d, *J* = 9.5 Hz, 2H), 8.45 (d, *J* = 10.3 Hz, 2H).

^{13}C-NMR (126 MHz, $CDCl_3$): δ 16.7, 18.7, 19.4, 20.1, 20.2, 21.0, 22.8, 23.7, 25.3, 28.2, 29.3, 29.7, 30.9, 31.6, 32.0, 32.6, 39.0, 41.4, 50.37, 50.45, 51.1, 55.3, 56.0, 57.9, 58.8, 59.0, 59.1, 66.4, 69.3, 70.3, 70.5, 80.0, 108.7, 110.1, 118.7, 120.0, 122.6, 123.4, 126.8, 127.9, 128.2, 128.3, 128.8, 135.1, 136.1, 143.7, 168.7, 168.9, 170.0, 170.7, 171.57, 171.63, 172.3.

HRMS (ESI): calcd for $C_{110}H_{161}N_{22}O_{21}^+$ $(M+H)^+$: 2126.2201; found: 2126.2183.

(3*S*,3'*S*,6*S*,6'*S*,9*S*,9'*S*,12*S*,12'*S*,15*S*,15'*S*,18*S*,18'*S*,21*S*,21'*S*)-15,15'-(((((3,6,9,12-tetraoxatetradecane-1,14-diyl)bis(1*H*-1,2,3-triazole-1,4-diyl))bis(methylene))bis(1*H*-indole-1,3-diyl))bis(methylene))bis(12-((*R*)-3-

hydroxy-2-methylpropyl)-21-isobutyl-3,18-diisopropyl-6-((*R*)-methoxy(phenyl)methyl)-1,9,13-trimethyl-1,4,7,10,13,16,19-heptaazacyclohenicosane-2,5,8,11,14,17,20-heptaone) (8) (UdSBI-0545)

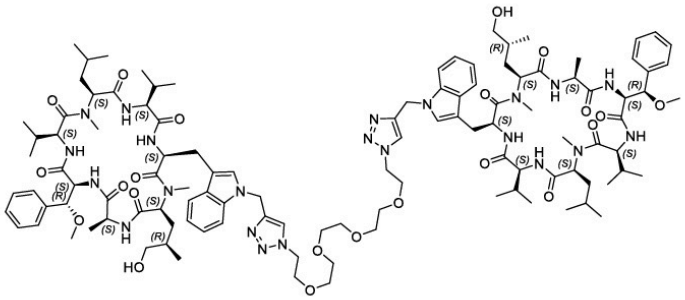

Prepared according to *GP7*: **5** (17.0 mg, 18.1 µmol), 1,14-diazido-3,6,9,12-tetraoxatetradecane (2.60 mg, 9.03 µmol), 1 M $CuSO_4$ (9.03 µl, 9.03 µmol), 1 M sodium ascorbate (9.03 µl, 9.03 µmol) (18 h). RP flash chromatography (H_2O/MeCN 90:10 – 95:5) followed by prep HPLC (H_2O/MeCN 90:10 – 95:5) and lyophilization afforded **8** (12.3 mg, 5.67 µmol, 63%) as a white, amorphous solid.

$[\alpha]_{20}^{D}$ = –98.3 (c 0.5, $CHCl_3$).

^{1}H-NMR (500 MHz, $CDCl_3$): δ -0.81 – -0.74 (m, 2H), 0.09 (d, *J* = 6.8 Hz, 6H), 0.56 (d, *J* = 6.5 Hz, 6H), 0.62 (d, *J* = 6.6 Hz, 6H), 0.67 – 0.78 (m, 2H), 0.93 – 1.01 (m, 20H), 1.09 (d, *J* = 6.8 Hz, 6H), 1.12 – 1.19 (m, 8H), 1.53 – 1.62 (m, 2H), 1.70 (s, 2H), 2.20 – 2.28 (m, 2H), 2.30 (ddd, *J* = 14.2, 10.1, 4.8 Hz, 2H), 2.57 (s, 6H), 2.83 (s, 10H), 3.00 (d, *J* = 10.6 Hz, 2H), 3.06 (dd, *J* = 13.3, 4.7 Hz, 2H), 3.14 (d, *J* = 6.9 Hz, 2H), 3.21 – 3.30 (m, 4H), 3.28 – 3.35 (m, 2H), 3.36 (s, 6H), 3.41 – 3.49 (m, 4H), 3.73 – 3.79 (m, 4H), 4.14 (t, *J* = 9.3 Hz, 2H), 4.31 (dd, *J* = 11.1, 2.9 Hz, 2H), 4.35 – 4.44 (m, 2H), 4.43 – 4.54 (m, 4H), 4.77 (dd, *J* = 10.6, 7.2 Hz, 4H), 4.85 (dd, *J* = 10.1, 3.9 Hz, 2H), 4.91 (t, *J* = 5.1 Hz, 2H), 5.08 (d, *J* = 5.5 Hz, 2H), 5.27 (d, *J* = 15.6 Hz, 2H), 5.45 (d, *J* = 15.6 Hz, 2H), 7.07 (s, 2H), 7.10 (d, *J* = 7.6 Hz, 2H), 7.15 – 7.22 (m, 6H), 7.20 – 7.26 (m, 6H), 7.43 (d, *J* = 8.4 Hz, 2H), 7.46 (d, *J* = 7.6 Hz, 2H), 7.58 (s, 2H), 7.79 (bs, 2H), 8.14 (d, *J* = 7.7 Hz, 2H), 8.31 (d, *J* = 9.5 Hz, 2H), 8.45 (d, *J* = 10.1 Hz, 2H).

^{13}C-NMR (126 MHz, $CDCl_3$): δ 16.9, 18.9, 19.4, 20.1, 20.2, 21.1, 22.8, 23.7, 25.2, 28.2, 29.3, 29.7, 30.9, 31.6, 32.1, 32.7, 39.1, 41.4, 50.4, 50.5, 51.2, 55.3, 56.1, 57.9, 58.8, 59.0, 59.2, 66.1, 69.4, 70.3, 70.4, 70.7, 80.0, 108.7, 110.2, 118.7, 120.1, 122.6, 123.5, 127.0, 128.0, 128.2, 128.3, 128.8, 135.1, 136.1, 143.7, 168.6, 169.0, 170.0, 170.7, 171.5, 171.6, 172.4.

HRMS (ESI): calcd for $C_{112}H_{165}N_{22}O_{22}^+$ $(M+H)^+$: 2170.2463; found: 2170.2490.

(3*S*,3'*S*,6*S*,6'*S*,9*S*,9'*S*,12*S*,12'*S*,15*S*,15'*S*,18*S*,18'*S*,21*S*,21'*S*)-15,15'-((((pentane-1,5-diylbis(1*H*-1,2,3-triazole-1,4-diyl))bis(methylene))bis(1H-indole-1,3-diyl))bis(methylene))bis(12-((*R*)-3-hydroxy-2-methylpropyl)-21-isobutyl-3,18-diisopropyl-6-((*R*)-methoxy(phenyl)methyl)-1,9,13-trimethyl-1,4,7,10,13,16,19-heptaazacyclohenicosane-2,5,8,11,14,17,20-heptaone) (9)

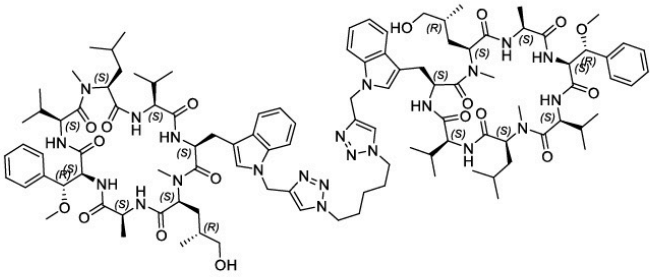

Prepared according to *GP7*: **5** (20.5 mg, 21.8 µmol), 1,5-diazidopentane (1.68 mg, 10.9 µmol), 1 M $CuSO_4$ (8.71 µl, 8.71 µmol), 1 M sodium ascorbate (14.2 µl, 14.2 µmol) (17 h). RP flash chromatography (H_2O/MeCN 70:30 – 5:95) followed by lyophilization afforded **9** (18.7 mg, 9.18 µmol, 84%) as a white amorphous solid.

$[\alpha]_{20}^{D}$ = –107.3 (c 0.5, $CHCl_3$)

^{1}H NMR (500 MHz, $CDCl_3$): δ -0.88 – -0.73 (m, 2H), 0.08 (d, *J* = 6.9 Hz, 6H), 0.57 (d, *J* = 6.4 Hz, 6H), 0.60 (d, *J* = 6.7 Hz, 6H), 0.69 – 0.76 (m, 2H), 0.85 – 0.93 (m, 2H), 0.93 – 1.00 (m, 18H), 1.08 (d, *J* = 6.6 Hz, 6H), 1.12 (d, *J* = 7.2 Hz, 6H), 1.15 (d, *J* = 4.6 Hz, 2H), 1.20 – 1.28 (m, 2H), 1.56 (q, *J* = 6.6 Hz, 2H), 1.61 – 1.70 (m, 2H), 1.80 – 1.90 (m, 6H), 2.19 – 2.26 (m, 2H), 2.26 – 2.33 (m, 2H), 2.48 (s, 6H), 2.71 – 2.78 (m, 2H), 2.82 (s, 6H), 3.00 (dd, *J* = 11.4, 4.5 Hz, 2H), 3.10 (dd, *J* = 13.5, 4.8 Hz, 2H), 3.24 – 3.32 (m, 2H), 3.35 (s, 6H), 4.12 (t, *J* = 9.5 Hz, 2H), 4.20 – 4.29 (m, 4H), 4.30 – 4.35 (m, 2H), 4.47 (t, *J* = 8.5 Hz, 2H), 4.67 – 4.76 (m, 4H), 4.84 (fdd, *J* = 10.1, 4.0 Hz, 2H), 4.89 (t, *J* = 5.1 Hz, 2H), 5.06 (d, *J* = 5.5 Hz, 2H), 5.24 (d, *J* = 15.6 Hz, 2H), 5.37 (d, *J* = 15.6 Hz, 2H), 6.92 (s, 2H), 7.09 (t, *J* = 7.5 Hz, 2H), 7.14 – 7.25 (m, 14H), 7.38 – 7.49 (m, 8H), 8.11 (d, *J* = 7.9 Hz, 2H), 8.27 (d, *J* = 9.6 Hz, 2H), 8.42 (d, *J* = 10.4 Hz, 2H).

^{13}C NMR (126 MHz, $CDCl_3$): δ 16.5, 18.7, 19.4, 20.1, 20.2, 20.9, 22.7, 23.4, 23.7, 25.3, 28.1, 29.2, 29.4, 29.7, 30.9, 31.7, 31.9, 32.5, 38.7, 39.0, 41.3, 50.0, 50.4, 51.1, 55.3, 56.0, 57.9, 58.8, 59.0, 59.1, 66.5, 80.1, 108.7, 110.0, 118.7, 120.1, 122.4, 122.7, 126.7, 127.8, 128.2, 128.3, 128.8, 135.1, 136.2, 143.8, 168.7, 168.8, 170.0, 170.8, 171.5, 171.6, 172.3.

HRMS (ESI): calcd for $C_{107}H_{155}N_{22}O_{18}^+$ $(M+H)^+$: 2036.1884; found: 2036.1908.

Synthesis of enantiomeric exit vector 6 Homo-BacPROTAC (8a)

***tert*-butyl *N*-[(1*S*,2*S*)-1,3-dihydroxy-1-(4-nitrophenyl)propan-2-yl]carbamate (SI-1)**

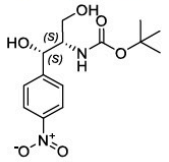

To a stirred solution of (1*S*,2*S*)-2-Amino-1-(4-nitro-phenyl)-propane-1,3-diol (45.0 g, 212 mmol) in MeOH (500 ml, 0.42 M) was added Boc-anhydride (50.9 g, 233 mmol) slowly at 0°C. The mixture was allowed to reach rt. After 12 h, TLC indicated complete conversion. The reaction was quenched with water, extracted with EtOAc, dried (Na_2SO_4) and concentrated in vacuo. The residue was triturated with petroleum ether and diethyl ether to yield crude **SI-1** (60.0 g, 192 mmol, 91%) which was used in the next step without further purification.

^{1}H NMR (400 MHz, DMSO-d_6) δ 1.05 (br s, 1.35H, rotamer), 1.21 (s, 7.65H, rotamer), 3.32 – 3.26 (m, 1H), 3.53 (dt, *J* = 10.5, 6.7 Hz, 1H), 3.73 – 3.61 (m, 1H), 4.76 (t, *J* = 5.2 Hz, 1H), 4.94 (br s, 1H), 5.58 (br s, 1H), 5.76 (d, *J* = 9.4 Hz, 0.15H, rotamer), 6.15 (d, *J* = 9.4 Hz, 0.85H, rotamer), 7.56 (d, J = 8.6 Hz, 2H), 8.17 (d, *J* = 8.6 Hz, 2H).

^{13}C NMR (101 MHz, DMSO-d_6) δ 27.6, 28.0, 57.5, 58.8, 60.7, 61.0, 69.9, 77.6, 122.8, 127.4, 146.3, 152.0, 152.4, 155.1.

MS calcd for $C_{10}H_{13}N_2O_6^+$ $(M - C_4H_9 + 2H)^+$: 257.08; found: 257.09.

The spectroscopic data are in agreement with previously published results.[10]

***tert*-butyl *N*-[(1*S*,2*S*)-3-[(*tert*-butyldimethylsilyl)oxy]-1-hydroxy-1-(4-nitrophenyl)propan-2-yl]carbamate (SI-2)**

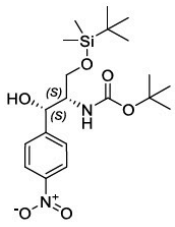

To a stirred solution of crude **SI-1** (60.0 g, 192 mmol) in DMF (300 ml, 0.64 M) were added imidazole (32.7 g, 480 mmol) and TBDMS-Cl (63.4 g, 423 mmol) at 0°C. The mixture was stirred at rt. After 6 h, TLC indicated

complete conversion. The mixture was quenched with cold water and extracted with EtOAc (2x). The combined organic layers were washed with cold brine, dried (Na_2SO_4) and concentrated in vacuo. Silica gel column chromatography (10% EtOAc in petroleum ether) yielded **SI-2** (65.0 g, 152 mmol, 79%).

^{1}H NMR (400 MHz, DMSO-d_6) δ 0.05 (s, 6H), 0.87 (s, 9H), 1.05 (br s, 1.8H, rotamer), 1.22 (s, 7.2H, rotamer), 3.57 – 3.40 (m, 1H), 3.81 – 3.59 (m, 2H), 4.90 (dd, *J* = 5.2, 2.2 Hz, 1H), 5.63 (d, *J* = 5.3 Hz, 1H), 5.88 (br d, *J* = 9.4 Hz, 0.2H, rotamer), 6.23 (br d, *J* = 8.9 Hz, 0.8H, rotamer), 7.56 (br d, *J* = 8.6 Hz, 2H), 8.18 (d, *J* = 8.6 Hz, 2H).

^{13}C NMR (101 MHz, DMSO-d_6) δ -5.4, 17.9, 25.8, 27.6, 28.0, 57.5, 58.9, 62.3, 62.9, 69.9, 77.6, 122.8, 127.4, 146.4, 151.7, 155.1.

MS calcd for $C_{20}H_{35}N_2O_6Si^+$ $(M+H)^+$: 427.23; found 427.24.

The spectroscopic data are in agreement with previously published results.[11]

***tert*-butyl *N*-[(1*S*,2*S*)-3-[(*tert*-butyldimethylsilyl)oxy]-1-methoxy-1-(4-nitrophenyl)propan-2-yl]carbamate (SI-3)**

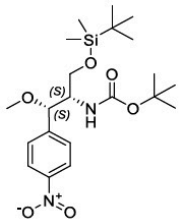

To a stirred solution of **SI-2** (55.0 g, 129 mmol) in DMF (300 ml, 0.43 M) was added LiHMDS (1 M in THF) (129 ml, 129 mmol) at -15°C. After 10 minutes, iodomethane (27.5 g, 193 mmol) was added. The mixture was stirred at –15°C. After 3 h, TLC indicated complete conversion. The reaction was quenched with cold water and extracted with EtOAc (2x). The combined organic layers were washed with brine, dried (Na_2SO_4) and concentrated in vacuo. Silica gel column chromatography (10% EtOAc in petroleum ether) yielded **SI-3** (52.0 g, 118 mmol, 91%).

^{1}H NMR (400 MHz, DMSO-d_6) δ 0.03 (s, 6H), 0.87 (s, 9H), 1.03 (br s, 1.8H, rotamer), 1.23 (s, 7.2H, rotamer), 3.17 (s, 3H), 3.54 – 3.36 (m, 1H), 3.77 – 3.56 (m, 2H), 4.51 (d, *J* = 3.3 Hz, 1H), 6.24 (br d, *J* = 7.9 Hz, 0.2H, rotamer), 6.60 (br d, *J* = 8.4 Hz, 0.8H, rotamer), 7.53 (d, J = 8.4 Hz, 2H), 8.21 (d, *J* = 8.6 Hz, 2H).

^{13}C NMR (101 MHz, DMSO-d_6) δ -5.5, -5.4, 17.9, 25.7, 27.6, 28.0, 57.0, 61.9, 77.6, 80.5, 123.2, 128.3, 146.9, 147.6, 155.1.

MS calcd for $C_{17}H_{29}N_2O_6Si^+$ $(M - C_4H_9 + 2H)^+$: 385.18; found: 385.36.

The spectroscopic data are in agreement with previously published results.[12]

***tert*-butyl *N*-[(1*S*,2*S*)-1-(4-aminophenyl)-3-[(*tert*-butyldimethylsilyl)oxy]-1-methoxypropan-2-yl]carbamate (SI-4)**

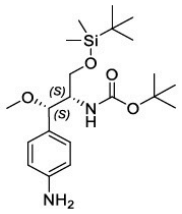

To a solution of **SI-3** (30.0 g, 68.1 mmol) in THF (300 ml, 0.23 M) was added 10 wt% Pd/C (36.4 g, 34.0 mmol). The mixture was stirred at rt under H_2 (50 psi). After 5 h, TLC indicated complete conversion. Subsequently, the mixture was filtered over Celite, rinsed with EtOAc and the filtrate was evaporated in vacuo. Silica gel column chromatography (20% EtOAc in petroleum ether) yielded **SI-4** (22.0 g, 53.6 mmol, 79%).

^{1}H NMR (400 MHz, $CDCl_3$) δ 0.03 (s, 3H), 0.05 (s, 3H), 0.91 (s, 9H), 1.38 (s, 9H), 3.20 (s, 3H), 3.42 (dd, *J* = 9.4, 3.8 Hz, 1H), 3.55 – 3.73 (m, 3H), 4.30 (d, *J* = 4.6 Hz, 1H), 4.89 (d, *J* = 8.8 Hz, 1H), 6.65 (d, *J* = 8.4 Hz, 2H), 7.07 (d, *J* = 8.4 Hz, 2H).

MS calcd for $C_{16}H_{27}N_2O_3Si^+$ $(M - C_4H_9 - OCH_3 + H)^+$: 323.18; found: 323.23.

The spectroscopic data are in agreement with previously published results.[12]

tert-butyl _N_-[(1_S_,2_S_)-3-[(_tert_-butyldimethylsilyl)oxy]-1-methoxy-1-phenylpropan-2-yl]carbamate (SI-5)

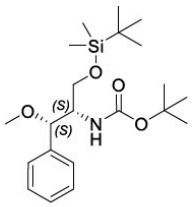

To a stirred solution of **SI-4** (20.0 g, 48.7 mmol) in $CHCl_3$ (200 ml) and water (200 ml) (0.12 M) was added acetic acid (58.4 g, 974 mmol) and sodium nitrite (16.8 g, 244 mmol). The mixture was stirred at rt. After 16 h, TLC indicated complete conversion. The reaction was diluted with water and extracted with DCM (2x). The combined organic layers were dried (Na_2SO_4) and concentrated in vacuo. Silica gel column chromatography (7% EtOAc in petroleum ether) yielded **SI-5** (10.4 g, 26.3 mmol, 54%).

^{1}H NMR (400 MHz, $CDCl_3$) δ 0.06 (s, 3H), 0.07 (s, 3H), 0.92 (s, 9H), 1.35 (s, 9H), 3.25 (s, 3H), 3.47 (dd, *J* = 9.7, 4.2 Hz, 1H), 3.65 (dd, *J* = 9.7, 7.4 Hz, 1H), 3.71 – 3.79 (m, 1H), 4.46 (d, *J* = 4.2 Hz, 1H), 4.88 (d, *J* = 9.1 Hz, 1H), 7.24 – 7.38 (m, 5H).

MS calcd for $C_{21}H_{38}NO_4Si^+$ $(M+H)^+$: 396.26; found: 396.34.

The spectroscopic data are in agreement with previously published results.[4]

tert-butyl _N_-[(1S,2S)-3-hydroxy-1-methoxy-1-phenylpropan-2-yl]carbamate (SI-6)

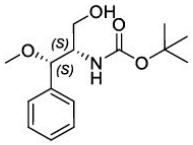

To a stirred solution of **SI-5** (16.0 g, 40.4 mmol) in THF (160 ml, 0.25 M) was added TBAF (1M in THF) (44.5 ml, 44.5 mmol) at 0°C. The mixture was stirred at rt. After 3 h, TLC indicated complete conversion. The reaction was quenched with cold water and extracted with EtOAc (2x). The combined organic layers were washed with brine, dried (Na_2SO_4) and concentrated in vacuo. Silica gel column chromatography (7% EtOAc in petroleum ether) yielded **SI-6** (11.0 g, 39.1 mmol, 97%).

^{1}H NMR (400 MHz, $CDCl_3$) δ 1.34 (s, 9H), 2.66 – 2.83 (m, 1H), 3.26 (s, 3H), 3.62 – 3.73 (m, 2H), 3.77 (dt, *J* = 9.0, 4.7 Hz, 1H), 4.42 (d, *J* = 4.2 Hz, 1H), 5.10 (bs, 1H), 7.25 – 7.40 (m, 5H).

MS calcd for $C_{15}H_{24}NO_4^+$ $(M+H)^+$: 282.17; found: 282.15.

The spectroscopic data are in agreement with previously published results.[12]

(2_R_,3_S_)-2-{[(_tert_-butoxy)carbonyl]amino}-3-methoxy-3-phenylpropanoic acid (SI-7)

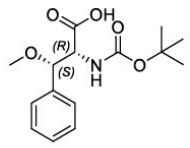

A stirred solution of **SI-6** (11.0 g, 39.1 mmol) in MeCN (88.0 ml) and water (88.0 ml) (0.22 M) was cooled to 0°C and NaH_2PO_4 (1.22 g, 7.82 mmol), (diacetoxyiodo)benzene (1.26 g, 3.91 mmol), TEMPO (1.22 g, 7.82 mmol) and $NaClO_2$ (12.3 g, 137 mmol) were added. The mixture was stirred at rt. After 2 h, TLC indicated complete conversion. The reaction was quenched with 2 M aq. Na_2CO_3 and washed with diethyl ether. The aqueous layer was acidified with 1 N aq. HCl and extracted with EtOAc (3x). The combined EtOAc layers were dried (Na_2SO_4) and concentrated in vacuo to yield crude **SI-7** (9.70 g, 31.4 mmol, 80%) which was used in the next step without further purification.

Major rotamer: **^{1}H NMR** (500 MHz, $CDCl_3$) δ 1.33 (s, 9H), 3.32 (s, 3H), 4.56 (dd, *J* = 9.4, 2.9 Hz, 1H), 4.88 (d, *J* = 2.8 Hz, 1H), 5.33 (d, *J* = 9.4 Hz, 1H), 7.29 – 7.42 (m, 5H), 9.67 (bs, 1H).

^{13}C NMR (126 MHz, CDCl3) δ 28.3, 57.7, 59.1, 80.2, 82.4, 127.0, 128.4, 128.6, 136.9, 155.7, 175.4.

Minor rotamer (selected signals, ratio ~5:1): **^{1}H NMR** (500 MHz, $CDCl_3$) δ 1.15 (s, 9H), 3.29 (s, 3H), 4.40 (dd, *J* = 9.3, 2.9 Hz, 1H), 4.78 – 4.83 (m, 1Hf), 5.88 (d, *J* = 9.3 Hz, 1H).

^{13}C NMR (126 MHz, CDCl3) δ 27.9, 57.6, 60.6, 81.0, 82.8, 127.2, 155.5.

MS calcd for $C_{11}H_{13}NO_5^+$ $(M - C_4H_9 + 2H)^+$: 239.08; found: 239.87.

The spectroscopic data are in agreement with previously published results.[4]

methyl *N*-(((benzyloxy)carbonyl)-D-valyl)-*N*-methyl-D-leucinate (SI-8)

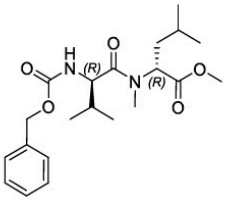

To a solution of methyl N-(*tert*-butoxycarbonyl)-N-methyl-D-leucinate (50.0 g, 193 mmol) in DCM (250 ml, 0.77 M) was added HCl (4 M in dioxane) (240.0 ml) dropwise at 0°C, the mixture was allowed to reach rt and stirred for 3 h. The solvents were evaporated in vacuo and the crude amine was used in the peptide coupling without further purification.

To a solution of Cbz-D-Valine (20.3 g, 80.7 mmol) in DMF (180 ml, 0.45 M) was added DIPEA (56.4 ml, 323 mmol) dropwise at 0 °C followed by portionwise addition of HATU (46.1 g, 121 mmol). After 10 minutes, the deprotected amino acid prepared as described above (15.8 g, 80.7 mmol) was added. The mixture was allowed to reach rt and stirred for 16 . The reaction was quenched with water and extracted with EtOAc. The organic layer was washed with brine, dried (Na_2SO_4) and concentrated in vacuo. Silica gel column chromatography (50% EtOAc in petroleum ether) yielded **SI-8** (25.5 g, 65.0 mmol, 81%).

Major rotamer: **^{1}H NMR** (500 MHz, $CDCl_3$) δ 0.88 (d, *J* = 6.5 Hz, 3H), 0.92 (dd, *J* = 6.7, 2.4 Hz, 6H), 1.02 (d, *J* = 6.8 Hz, 3H), 1.40 – 1.52 (m, 1H), 1.64 – 1.79 (m, 2H), 2.01 – 2.10 (m, 1H), 3.00 (s, 3H), 3.68 (s, 3H), 4.54 (dd, *J* = 9.2, 6.0 Hz, 1H), 5.09 (s, 2H), 5.33 (dd, *J* = 10.6, 5.2 Hz, 1H), 5.52 (d, *J* = 9.2 Hz, 1H), 7.28 – 7.39 (m, 5H).

^{13}C NMR (126 MHz, $CDCl_3$) δ 172.8, 172.0, 156.4, 136.3, 128.5, 128.0, 127.9, 77.3, 77.0, 76.7, 66.8, 55.8, 54.4, 52.1, 36.8, 31.2, 31.1, 24.7, 23.2, 21.3, 19.4, 17.1.

Minor rotamer (selected signals, ratio ca. 16:1): **^{1}H NMR** (500 MHz, $CDCl_3$) δ 2.83 (s, 3H), 3.61 (s, 3H), 5.42 (d, *J* = 9.5 Hz, 1H).

HRMS (ESI) calcd for $C_{21}H_{33}N_2O_5^+$ $(M+H)^+$: 393.2384; found: 393.2400.

The spectroscopic data are in agreement with previously published results.[4]

methyl *N*-(((2*R*,3*S*)-2-((*tert*-butoxycarbonyl)amino)-3-methoxy-3-phenylpropanoyl)-D-valyl)-*N*-methyl-D-leucinate (SI-9)

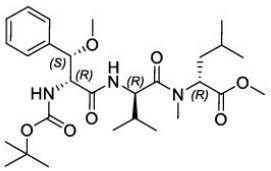

To a solution of methyl **SI-8** (17.0 g, 43.3 mmol) in DCM (85.0 ml, 0.51 M) was added HBr (33% in AcOH) (14.6 g, 91.0 mmol) slowly at 0°C. The mixture was allowed to reach rt and stirred for 2 h. It was degassed with nitrogen to remove excess HBr. The solvents were evaporated in vacuo and the residue was triturated with diethyl ether. The crude amine was used in the peptide coupling without further purification.

To a solution of **SI-7** (17.1 g, 58.1 mmol) in DMF (120 ml, 0.48 M) was added DIPEA (32.8 ml, 194 mmol) dropwise at 0 °C followed by portionwise addition of HATU (22.1 g, 58.1 mmol). After 10 minutes, the deprotected dipeptide prepared as described above (10.0 g, 38.7 mmol) was added. The mixture was allowed to reach rt and stirred for 16. TLC indicated complete conversion. The reaction was quenched with cold water and extracted with EtOAc. The organic layer was washed with brine, dried (Na_2SO_4) and concentrated in vacuo. Silica gel column chromatography (20% EtOAc in petroleum ether) yielded **SI-9** (12.0 g, 22.4 mmol, 58%) as a white solid.

^{1}H NMR (500 MHz, $CDCl_3$) δ 0.91 (d, *J* = 6.5 Hz, 3H), 0.92 – 0.97 (m, 6H), 1.01 (d, *J* = 6.8 Hz, 3H), 1.32 (s, 9H), 1.42 – 1.52 (m, 1H), 1.66 – 1.80 (m, 2H), 2.05 – 2.18 (m, 1H), 3.02 (s, 3H), 3.31 (s, 3H), 3.70 (s, 3H), 4.41 (dd, *J* = 8.5, 3.0 Hz, 1H), 4.87 (dd, *J* = 9.0, 6.2 Hz, 1H), 4.91 (d, *J* = 3.0 Hz, 1H), 5.26 (d, *J* = 8.4 Hz, 1H), 5.33 (dd, *J* = 10.5, 5.2 Hz, 1H), 7.26 – 7.36 (m, 6H).

^{13}C NMR (126 MHz, $CDCl_3$) δ 172.3, 172.2, 169.5, 155.5, 137.4, 128.5, 128.1, 126.8, 81.9, 80.2, 60.0, 57.6, 54.6, 54.1, 52.3, 37.1, 31.7, 31.5, 28.3, 24.9, 23.4, 21.5, 19.6, 17.3.

Minor rotamer (selected signals, ratio ~11:1) **^{1}H NMR** (500 MHz, $CDCl_3$) δ 1.29 (s, 9H), 2.81 (s, 3H), 3.62 (s, 3H), 4.32 – 4.35 (m, 1H), 4.72 (t, *J* = 7.1 Hz, 1H), 5.20 (d, *J* = 9.3 Hz, 1H).

HRMS (ESI) calcd for $C_{28}H_{46}N_3O_7^+$ $(M+H)^+$: 536.3330; found: 536.3347.

The spectroscopic data are in agreement with previously published results.[4]

Methyl *N*-(((2*R*,3*S*)-2-((*R*)-2-((*tert*-butoxycarbonyl)amino)propanamido)-3-methoxy-3-phenylpropanoyl)-D-valyl)-*N*-methyl-D-leucinate (SI-10)

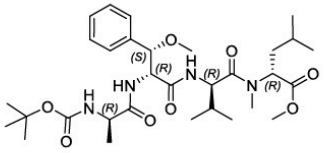

To a solution of **SI-9** (3.00 g, 5.60 mmol) in DCM (15.0 ml, 0.37 M) was added HCl (4 M in dioxane) (5.60 ml, 22.4 mmol) slowly at 0 °C and the mixture was allowed to reach rt and stirred for 4 h. The solvents were evaporated in vacuo and the crude amine was used in the peptide coupling without further purification.

To a solution of Boc-D-Ala-OH (868 mg, 4.59 mmol) in DMF (10.0 ml, 0.46 M) was added DIPEA (3.99 ml, 23.0 mmol) at 0 °C followed by addition of HATU (2.62 g, 6.89 mmol). After 10 minutes, the deprotected tripeptide prepared as described above (2.00 g, 4.59 mmol) was added. The mixture was allowed to reach rt and stirred for 16 . TLC indicated complete conversion. The reaction was quenched with cold water and extracted with EtOAc. The organic layer was washed with brine, dried (Na_2SO_4) and concentrated in vacuo. Silica gel column chromatography (20% EtOAc in petroleum ether) yielded **SI-10** (1.80 g, 2.97 mmol, 60%).

Major rotamer: **^{1}H NMR** (500 MHz, $CDCl_3$) δ 0.91 – 0.94 (m, 6H), 0.96 (d, *J* = 6.7 Hz, 3H), 0.99 (d, *J* = 6.8 Hz, 3H), 1.29 (d, *J* = 7.1 Hz, 3H), 1.45 (s, 9H), 1.70 – 1.77 (m, 3H), 2.09 – 2.18 (m, 1H), 2.99 (s, 3H), 3.33 (s, 3H), 3.69 (s, 3H), 4.08 – 4.18 (m, 1H), 4.68 (dd, *J* = 7.5, 3.6 Hz, 1H), 4.82 (dd, *J* = 8.8, 6.0 Hz, 1H), 4.85 (d, *J* = 3.5 Hz, 1H), 4.88 – 4.95 (m, 1H), 5.36 (dd, *J* = 10.5, 5.3 Hz, 1H), 6.78 (d, *J* = 7.4 Hz, 1H), 7.18 – 7.24 (m, 2H), 7.25 – 7.31 (m, 3H), 7.36 (d, *J*

= 8.8 Hz, 1H). **^{13}C NMR** (126 MHz, $CDCl_3$) δ 17.3, 18.5, 19.7, 21.5, 23.4, 24.9, 28.4, 31.3, 31.5, 37.0, 50.4, 52.3, 54.2, 54.6, 57.6, 57.8, 80.3, 81.3, 127.0, 128.3, 128.4, 136.9, 155.5, 168.5, 172.0, 172.2, 172.5.

Minor rotamer (selected signals, ratio ~15:1): **^{1}H NMR** (500 MHz, $CDCl_3$) δ 1.23 – 1.26 (m, 3H), 1.49 (s, 9H), 2.83 (s, 3H), 3.63 (s, 3H), 4.58 – 4.63 (m, 1H), 6.85 (d, *J* = 8.0 Hz, 1H).

HRMS (ESI) calcd for $C_{31}H_{51}N_4O_8^+$ $(M+H)^+$: 607.3701; found: 607.3726.

The spectroscopic data are in agreement with previously published results.[4]

Methyl (2*R*)-3-[(*tert*-butyldimethylsilyl)oxy]-2-methylpropanoate (SI-11)

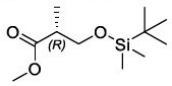

To a stirred solution of (*R*)-3-hydroxy-2-methyl-propionic acid methyl ester (10.0 g, 84.7 mmol) in DCM (100 ml, 0.85 M) were added imidazole (7.48 g, 110 mmol) and TBDMS-Cl (14.1 g, 93.1 mmol) at 0°C. The mixture was stirred at rt. After 3 h, TLC indicated complete conversion. The reaction was quenched with water and extracted with DCM (2x). The combined organic layers were washed with brine, dried (Na_2SO_4) and concentrated in vacuo. Silica gel column chromatography (10% EtOAc in petroleum ether) yielded **SI-11** (19.0 g, 81.8 mmol, 97%).

^{1}H NMR (400 MHz, $CDCl_3$) δ 0.03 (s, 3H), 0.03 (s, 3H), 0.87 (s, 9H), 1.13 (d, *J* = 7.0 Hz, 3H), 2.59-2.70 (m, 1H), 3.62-3.67 (m, 1H), 3.67 (s, 3H), 3.77 (dd, *J* = 9.7, 6.9 Hz, 1H).

For this compound, no mass spectrometric data could be obtained.

The spectroscopic data are in agreement with previously published results.[13]

(2*R*)-3-[(*tert*-butyldimethylsilyl)oxy]-*N*-methoxy-*N*,2-dimethylpropanamide (SI-12)

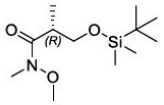

To a stirred solution of **SI-11** (18.0 g, 77.5 mmol) in THF (180 ml, 0.43 M) was added *N,O*-dimethylhydroxylamine hydrochloride (12.1 g, 124 mmol) and it was stirred for 10 minutes at rt, before the mixture was cooled to −30 °C. Then, iPrMgCl (2 M in THF) (116 ml, 232 mmol) was added. The mixture was stirred at −30 °C. After 1 h, TLC indicated complete conversion. The reaction was quenched with aq. NH_4Cl and extracted with EtOAc (2x). The combined organic layers were washed with brine, dried (Na_2SO_4) and concentrated in vacuo. Silica gel column chromatography (5-10% EtOAc in petroleum ether) yielded **SI-12** (20.0 g, 76.5 mmol, 99%) as a colorless liquid.

^{1}H NMR (400 MHz, $CDCl_3$) δ 0.04 (s, 3H), 0.05 (s, 3H), 0.87 (s, 9H), 1.07 (d, *J* = 7.0 Hz, 3H), 3.11-3.19 (m, 1H), 3.19 (s, 3H), 3.53 (dd, *J* = 9.5, 6.1 Hz, 1H), 3.71 (s, 3H), 3.84 (dd, *J* = 9.4, 8.3 Hz, 1H).

MS calcd for $C_{12}H_{28}NO_3Si^+$ $(M+H)^+$: 262.18; found: 262.38.

The spectroscopic data are in agreement with previously published results.[14]

methyl (*S*)-2-(((benzyloxy)carbonyl)amino)-5-((*tert*-butyldimethylsilyl)oxy)-4-methylpent-2-enoate (SI-13)

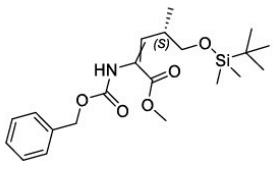

To a stirred solution of **SI-12** (15.0 g, 57.4 mmol) in THF (150 ml, 0.38 M) at 78 °C was added DIBALH (1 M in hexane) (115 ml, 115 mmol) and the mixture was stirred at -78 °C. After 1 h, TLC indicated complete conversion. The reaction was quenched with sat. aq. K-Na-tartrate solution at 0°C and stirred for 2 h at rt. It was extracted with EtOAc (2x). The combined organic layers were washed with brine, dried (Na_2SO_4) and concentrated in vacuo. The crude aldehyde was directly used in the next step without further purification.

To a stirred solution of the crude aldehyde (12 g, 59.3 mmol) in THF (450 ml, 0.13 M) at −78 °C was added 1,1,3,3-tetramethyl guanidine (7.16 g, 62.3 mmol) and stirred for 5 minutes. Then a solution of *N*-Cbz-α-phosphonoglycine trimethyl ester (21.6 g, 65.2 mmol) in THF (450 ml) was added dropwise. The mixture was allowed to reach rt and stirred for 16 h, until TLC indicated complete conversion. It was quenched with water and extracted with EtOAc (2x). The combined organic layers were washed with brine, dried (Na_2SO_4) and concentrated in vacuo. Silica gel column chromatography (10% EtOAc in petroleum ether) yielded **SI-13** (12.0 g, 29.4 mmol, 50%).

^{1}H NMR (400 MHz, $CDCl_3$) δ 0.03 (s, 3H), 0.05 (s, 3H), 0.88 (s, 9H), 1.01 (d, *J* = 6.8 Hz, 3H), 2.73-2.88 (m, 1H), 3.41 (t, *J* = 9.2 Hz, 1H), 3.64 (dd, *J* = 9.6, 4.8 Hz, 1H), 3.67-3.85 (m, 3H), 5.08-5.20 (m, 2H), 6.20 (d, *J* = 9.4 Hz, 1H), 6.97-7.08 (m, 1H), 7.29-7.38 (m, 5H).

MS calcd for $C_{21}H_{34}NO_5Si^+$ $(M+H)^+$: 408.22; found: 408.35.

The spectroscopic data are in agreement with previously published results.[4]

methyl (2*R*,4*S*)-2-{[(benzyloxy)carbonyl]amino}-5-[(*tert*-butyldimethylsilyl)oxy]-4-methylpentanoate (SI-14)

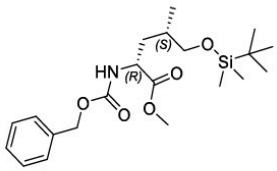

To a stirred solution of **SI-13** (10.0 g, 24.5 mmol) in DCM (350 ml, 0.07 M) under Argon atmosphere was added (*S*)-MonoPhos (705 mg, 1.96 mmol) and $[Rh(cod)_2BF_4]$ (398 mg, 981 µmol). The resulting mixture was stirred under H_2 (350 psi) in a steel reactor. After 48 h, TLC indicated complete conversion. The mixture was filtered over Celite and the filtrate was concentrated in vacuo. Silica gel column chromatography (7% EtOAc in petroleum ether) yielded **SI-14** (6.40 g, 15.6 mmol, 64%) as a brownish liquid.

^{1}H NMR (400 MHz, $CDCl_3$) δ 0.00 (s, 3H), 0.01 (s, 3H), 0.85 (s, 9H), 0.88 (d, *J* = 6.9 Hz, 3H), 1.49-1.58 (m, 1H), 1.62-1.76 (m, 1H), 1.82-1.95 (m, 1H), 3.35 (dd, *J* = 10.0, 6.1 Hz, 1H), 3.51 (dd, *J* = 9.9, 4.9 Hz, 1H), 4.30-4.45 (m, 1H), 3.70 (s, 3H), 4.98-5.13 (m, 2H), 5.59 (d, *J* = 7.8 Hz, 1H), 7.24-7.36 (m, 5H).

MS found for $C_{21}H_{36}NO_5Si^+$ $(M+H)^+$: 410.24; found: 410.22.

The spectroscopic data are in agreement with previously published results.[4]

(2*R*,4*S*)-2-(((benzyloxy)carbonyl)(methyl)amino)-5-((*tert*-butyldimethylsilyl)oxy)-4-methylpentanoic acid (SI-15)

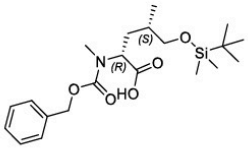

To a stirred solution of **SI-14** (5.00 g, 12.2 mmol) in MeOH (25.0 ml, 0.49 M) was added 1 M aq. NaOH (13.4 ml, 13.4 mmol) at 0°C. The resulting mixture was stirred at rt. After 16 h, TLC and LCMS indicated complete conversion. The mixture was diluted with water and acidified to pH 2-3 with aq. $KHSO_4$ solution. It was extracted with EtOAc (2x). The combined organic layers were washed with brine, dried (Na_2SO_4) and

concentrated in vacuo. The obtained crude Cbz-amino acid was used in the next step without further purification.

To a stirred solution of crude Cbz-amino acid (2.30 g, 5.81 mmol) in THF (50.0 ml, 0.12 M) at −4 °C was added Iodomethane (5.78 g, 40.7 mmol). Then sodium hydride (60%) (558 mg, 14.0 mmol) was added in portions over 10 minutes at -4 °C. The mixture was stirred at the same temperature. After 76 h, TLC and LCMS indicated complete conversion. The reaction was quenched with water and acidified to pH 2-3 with diluted $KHSO_4$ solution. It was extracted with EtOAc (2x), washed with brine, dried (Na_2SO_4) and concentrated in vacuo. Silica gel column chromatography (8% EtOAc in petroleum ether) yielded **SI-15** (1.29 g, 3.15 mmol, 54%).

Major rotamer: **^{1}H NMR** (500 MHz, $CDCl_3$) δ 0.04 (s, 3H), 0.05 (s, 3H), 0.87 – 0.93 (m, 11H), 1.48 – 1.72 (m, 2H), 2.01 – 2.16 (m, 1H), 2.90 (s, 3H), 3.40 (dd, *J* = 10.0, 4.6 Hz, 1H), 3.45 (dd, *J* = 10.1, 5.0 Hz, 1H), 3.50 (d, *J* = 4.9 Hz, 2H), 4.92 (dd, *J* = 10.5, 5.1 Hz, 1H), 5.11 – 5.22 (m, 2H), 7.34 (dd, *J* = 20.9, 3.7 Hz, 5H). **^{13}C NMR** (126 MHz, CDCl3) δ -5.4, -5.3, 17.7, 18.4, 26.0, 30.7, 32.0, 32.5, 56.9, 66.5, 67.7, 127.9, 128.0, 128.6, 136.6, 157.2, 177.7.

Minor rotamer (selected signals, ratio ~3:2): **^{1}H NMR** (500 MHz, $CDCl_3$) δ -0.03 (s, 3H), -0.01 (s, 3H), 0.86 (s, 9H), 0.96 (d, *J* = 6.7 Hz, 3H), 2.92 (s, 3H), 4.78 (dd, *J* = 10.4, 5.0 Hz, 1H). **^{13}C NMR** (126 MHz, $CDCl_3$) δ -5.4, 17.8, 18.4, 26.0, 31.1, 32.2, 32.4, 66.4, 67.8, 128.0, 128.2, 136.4, 156.5.

MS found for $C_{21}H_{36}NO_5Si^+$ $(M+H)^+$: 410.24; found: 410.32

The spectroscopic data are in agreement with previously published results.[4]

Methyl *N*-(((2*R*,3*S*)-2-((*R*)-2-((2*R*,4*S*)-2-(((benzyloxy)carbonyl)(methyl)amino)-5-((*tert*-butyldimethylsilyl)oxy)-4-methylpentanamido)propanamido)-3-methoxy-3-phenylpropanoyl)-D-valyl)-*N*-methyl-D-leucinate (2a)

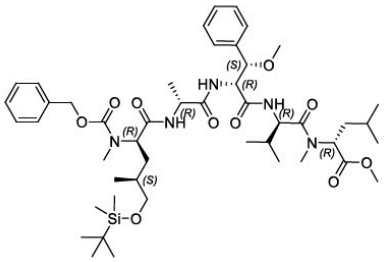

To a solution of **SI-10** (2.00 g, 3.30 mmol) in DCM (10.0 ml, 0.33 M) was added HCl (4 M in dioxane) (4.12 ml, 16.5 mmol) at 0 °C and the mixture was allowed to reach rt and stirred for 3 h. The solvents were evaporated in vacuo, the residue was triturated with petroleum ether and the crude amine was used in the peptide coupling without further purification.

To a solution of deprotected tetrapeptide as described above (1.50 g, 2.96 mmol) in DMF (15.0 ml, 0.20 M) were added DIPEA (2.57 ml, 14.8 mmol), HATU (1.69 g, 4.44 mmol) and **SI-15** (1.21 g, 2.96 mmol). The mixture was stirred for 16 . TLC and LCMS indicated complete conversion. The reaction was quenched with cold water and extracted with EtOAc. The organic layer was washed with brine, dried (Na_2SO_4) and concentrated in vacuo. Silica gel column chromatography (10-100% EtOAc in petroleum ether) yielded **2a** (2.00 g, 2.23 mmol, 75%) as a light brownish solid.

$[\alpha]_{20}^{D}$ = +58.0 (c 1.0, $CHCl_3$).

Major rotamer: **^{1}H NMR** (500 MHz, $CDCl_3$) δ -0.02 – 0.08 (m, 6H), 0.88 (s, 9H), 0.90 – 0.97 (m, 12H), 1.00 (d, *J* = 6.8 Hz, 3H), 1.23 (d, *J* = 7.0 Hz, 3H), 1.46 – 1.52 (m, 1H), 1.53 – 1.63 (m, 2H), 1.66 – 1.79 (m, 2H), 1.92 – 2.02 (m, 1H), 2.08 – 2.16 (m, 1H), 2.84 (s, 3H), 2.98 (s, 3H), 3.32 (s, 3H), 3.39 – 3.45 (m, 1H), 3.49 – 3.55 (m, 1H), 3.69 (s, 3H), 4.30 – 4.38 (m, 1H), 4.67 (dd, *J* = 7.5, 3.6 Hz, 1H), 4.69 – 4.75 (m, 1H), 4.78 – 4.84 (m, 2H), 5.11 – 5.21 (m, 2H), 5.35 (dd, *J* = 10.6, 5.1 Hz, 1H), 6.43 – 6.51 (m, 1H), 6.66 (d, *J* = 7.2 Hz, 1H), 7.11 – 7.21 (m, 2H), 7.29 – 7.38 (m, 9H). **^{13}C NMR** (126 MHz, $CDCl_3$) δ -5.3, 17.3, 17.6, 18.1, 18.5, 19.7, 21.5, 23.4, 24.9, 26.1, 30.0, 31.2, 31.4, 31.6,

32.3, 37.0, 49.3, 52.3, 54.2, 54.6, 56.9, 57.7, 57.9, 67.2, 67.8, 81.3, 126.9, 127.9, 128.3, 128.4, 128.5, 128.7, 136.6, 136.8, 157.4, 168.4, 170.9, 171.6, 172.1, 172.2.

Minor rotamer (ratio ~2:1, selected signals) **^{1}H NMR** (500 MHz, $CDCl_3$) δ 4.59 (s, 1H), 6.16 – 6.21 (m, 1H), 6.55 – 6.61 (m, 1H).

HRMS (ESI): calcd for $C_{47}H_{76}N_5O_{10}Si^+$ $(M+H)^+$: 898.5356; found: 898.5321.

((Allyloxy)carbonyl)-D-tryptophan (SI-16)

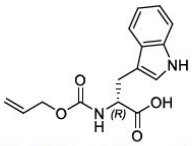

D-Tryptophan (10.0 g, 49.1 mmol) and Na_2CO_3 (10.3 g, 123 mmol) were dissolve in a mixture of THF (100 ml) and water (123 ml). The mixture was cooled to 0 °C and a solution of allyl chloroformate (5.23 ml, 49.1 mmol) in THF (22 ml) was added dropwise. The resulting solution was slowly warmed to rt over the course of 18 h. The solvent was concentrated in vacuo, the residue was dissolved in EtOAc and washed with 1 M HCl. The aqueous phase was extracted with EtOAc (3x). The combined organic phases were washed with brine, dried (Na_2SO_4) and evaporated. Recrystallization from pentane/Et_2O yielded **SI-16** (11.5 g, 39.7 mmol, 81%) as a white solid.
$[\alpha]_{20}^{D}$ = –40.6 (c 0.5, $CHCl_3$).

Melting point: 122 – 124 °C

^{1}H NMR (400 MHz, DMSO) δ 2.98 (dd, *J* = 14.6, 9.7 Hz, 1H), 3.17 (dd, *J* = 14.6, 4.6 Hz, 1H), 4.20 (ddd, *J* = 9.7, 8.1, 4.6 Hz, 1H), 4.34 – 4.48 (m, 2H), 5.14 (dd, *J* = 10.5, 1.6 Hz, 1H), 5.24 (dd, *J* = 17.2, 1.8 Hz, 1H), 5.85 (ddt, *J* = 17.3, 10.5, 5.3 Hz, 1H), 6.95 – 7.01 (m, 1H), 7.04 – 7.09 (m, 1H), 7.15 (d, *J* = 2.3 Hz, 1H), 7.34 (d, *J* = 8.0 Hz, 1H), 7.50 (d, *J* = 8.2 Hz, 1H), 7.53 (d, *J* = 7.9 Hz, 1H), 10.83 (s, 1H), 12.65 (bs, 1H).

^{13}C NMR (101 MHz, DMSO) δ 26.9, 54.9, 64.4, 110.1, 111.4, 117.0, 118.1, 118.4, 120.9, 123.7, 127.1, 133.5, 136.1, 155.8, 173.7.

HRMS (CI): calcd for $C_{15}H_{17}N_2O_4^+$ $(M+H)^+$: 289.1183; found: 289.1196.

N^{α}-((allyloxy)carbonyl)-1-(prop-2-yn-1-yl)-D-tryptophan (SI-17)

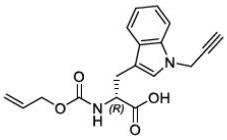

SI-16 (1.44 g, 5.00 mmol) was dissolved in DMF (10.0 ml) under N_2. KO*t*-Bu (1.18 g, 10.5 mmol) was added at rt and the mixture was stirred until all solids were dissolved, resulting ina a pale yellow color. After cooling to 0 °C, propargyl bromide (0.754 ml, 7.00 mmol) was added in one portion. TLC control indicated full conversion after 15 min. The reaction mixture was quenched after 23 min by addition of 1 M HCl and then extracted with EtOAc. The organic phase was subsequently washed with 1 M HCl (2x), H_2O (2x) and brine (1x), dried (Na_2SO_4) and evaporated. The residue was purified by flash chromatography (CyH/[EtOAc+2%HOAc] 100:0 - 6:4), which yielded **SI-17** (1.15 g, 3.53 mmol, 71%) as an orange-red resin. R_f = 0.28 (PE/EtOAc/HOAc 70:30:1).

$[\alpha]_{20}^{D}$ = -38.1 (c 1.0, $CHCl_3$).

^{1}H NMR (400 MHz, DMSO) δ 3.00 (dd, *J* = 14.7, 9.7 Hz, 1H), 3.18 (dd, *J* = 14.7, 4.6 Hz, 1H), 3.37 (t, *J* = 2.5 Hz, 1H), 4.22 (ddd, *J* = 9.7, 8.1, 4.5 Hz, 1H), 4.36 – 4.50 (m, 2H), 5.03 (d, *J* = 2.5 Hz, 2H), 5.15 (dd, *J* = 10.5, 1.6 Hz, 1H), 5.25 (dd, *J* = 17.2, 1.7 Hz, 1H), 5.86 (ddt, *J* = 17.3, 10.5, 5.3 Hz, 1H), 7.07 (t, *J* = 6.9 Hz, 1H), 7.13 – 7.22 (m, 1H), 7.23 (s, 1H), 7.47 (d, *J* = 8.2 Hz, 1H), 7.54 – 7.62 (m, 2H), 12.61 (bs, 1H).

^{13}C NMR (101 MHz, DMSO) δ 21.1, 26.7, 35.0, 54.8, 64.4, 75.5, 79.2, 79.3, 110.0, 110.6, 117.0, 118.6, 119.1, 121.4, 126.6, 127.9, 133.5, 135.7, 155.9, 173.6.

HRMS (CI): calcd for $C_{18}H_{18}N_2O_4^+$ $(M)^+$ 326.1261; found: 326.1267.

methyl *N*-(((2*R*,3*R*)-2-((*R*)-2-((2*R*,4*S*)-2-((*R*)-2-(((allyloxy)carbonyl)amino)-*N*-methyl-3-(1-(prop-2-yn-1-yl)-1*H*-indol-3-yl)propanamido)-5-((*tert*-butyldimethylsilyl)oxy)-4-methylpentanamido)propanamido)-3-methoxy-3-phenylpropanoyl)-D-valyl)-*N*-methyl-D-leucinate (3a)

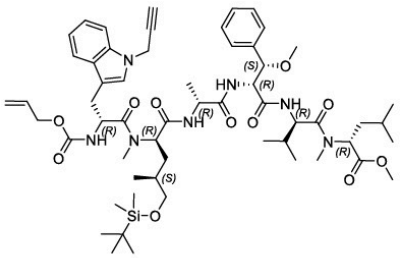

Prepared according to *GP1* and *GP5*: **2a** (371 mg, 413 µmol), Pd/C (22.0 mg) (2 h); **SI-17** (189 mg, 0.578 mmol), DIPEA (101 µl, 578 µmol), $BnNMe_2$ (9.20 µl, 61.9 µmol), 1 M isopropyl chloroformate (578 µl, 578 µmol), NMI (3.29 µl, 41.3 µmol) and 4 M HCl (10.3 µl, 41.2 µmol) (2.5 h). Flash chromatography (CyH/EtOAc 100:0 – 40:60) followed by lyophilization afforded **3a** (353 mg, 329 µmol, 80%) as a white amorphous solid. R_f = 0.25 (PE/EtOAc 4:6).

$[\alpha]_{20}^{D}$ = +52.1 (c 1.0, $CHCl_3$).

^{1}H NMR (500 MHz, $CDCl_3$) *(mixture of rotamers, ratio ~3:2)* δ -0.28 – -0.18 (m, 0.3H), -0.05 (s, 0.9H), -0.03 (s, 0.9H), 0.02 (s, 2.2H), 0.03 (s, 2.3H), 0.40 (d, *J* = 6.6 Hz, 0.8H), 0.83 (s, 2.4H), 0.88 (s, 6.2H), 0.87 – 0.98 (m, 14.4H), 0.99 (d, *J* = 6.8 Hz, 2.7H), 1.19 (d, *J* = 7.1 Hz, 1.8H), 1.22 – 1.27 (m, 1.9H), 1.43 – 1.53 (m, 2.6H), 1.65 – 1.81 (m, 2.4H), 1.85 – 1.92 (m, 0.4H), 1.94 – 2.04 (m, 1.0H), 2.08 – 2.21 (m, 1.3H), 2.36 – 2.42 (m, 1.0H), 2.73 (s, 1.9H), 2.75 (s, 1.2H), 2.97 (s, 1.0H), 3.01 (s, 2.0H), 3.14 (dd, *J* = 13.9, 5.8 Hz, 1.0H), 3.21 (dd, *J* = 14.4, 8.1 Hz, 0.8H), 3.28 (s, 1.2H), 3.33 (s, 2.8H), 3.40 (dd, *J* = 9.9, 5.4 Hz, 0.8H), 3.45 (dd, *J* = 9.8, 4.7 Hz, 0.8H), 3.67 – 3.71 (m, 3.4H), 4.16 – 4.23 (m, 0.6H), 4.25 – 4.32 (m, 0.4H), 4.47 – 4.59 (m, 2.2H), 4.63 (dd, *J* = 7.6, 3.5 Hz, 0.7H), 4.69 – 4.72 (m, 1H), 4.75 – 4.91 (m, 5.6H), 4.95 – 5.02 (m, 0.8H), 5.15 – 5.32 (m, 2.2H), 5.32 – 5.41 (m, 1.1H), 5.61 (d, *J* = 7.6 Hz, 0.3H), 5.81 – 5.92 (m, 1.5H), 6.34 (d, *J* = 6.8 Hz, 0.6H), 6.74 (d, *J* = 7.6 Hz, 0.3H), 6.78 (d, *J* = 7.7 Hz, 0.6H), 7.04 (s, 1.0H), 7.11 – 7.25 (m, 5.7H), 7.27 – 7.32 (m, 2.5H), 7.36 (d, *J* = 8.4 Hz, 1.6H), 7.44 (d, *J* = 8.7 Hz, 0.7H), 7.58 (d, *J* = 7.9 Hz, 0.4H), 7.67 (d, *J* = 7.9 Hz, 0.7H), 7.83 (d, *J* = 6.8 Hz, 0.3H).

^{13}C-NMR (126 MHz, $CDCl_3$) *(mixture of rotamers)* δ -5.0, 16.0, 17.6, 17.8, 18.2, 18.7, 19.9, 21.8, 23.7, 25.2, 26.3, 26.4, 29.2, 31.5, 31.7, 32.5, 36.1, 37.3, 50.1, 50.2, 51.8, 52.5, 54.5, 54.6, 54.9, 56.6, 58.0, 58.3, 66.1, 66.7, 67.6, 68.7, 74.0, 81.5, 81.8, 109.9, 110.0, 110.2, 118.0, 118.7, 119.3, 120.3, 122.6, 122.9, 126.5, 127.3, 128.57, 128.63, 128.8, 133.1, 136.3, 136.5, 137.3, 156.3, 157.0, 168.9, 169.1, 170.7, 171.9, 172.46, 172.52, 173.7.

Selected diagnostic peaks:

Major rotamer: **^{1}H NMR** (500 MHz, $CDCl_3$) δ 0.02 (s, 3H), 0.03 (s, 3H), 0.88 (s, 9H), 1.85 – 1.92 (m, 0H), 2.39 (t, *J* = 2.1 Hz, 1H), 2.73 (s, 3H), 3.01 (s, 3H), 3.14 (dd, *J* = 13.9, 5.8 Hz, 1H), 3.21 (dd, *J* = 14.4, 8.1 Hz, 1H), 3.33 (s, 3H), 3.69 (s, 3H), 4.16 – 4.23 (m, 1H), 6.34 (d, *J* = 6.8 Hz, 1H), 6.78 (d, *J* = 7.7 Hz, 1H), 7.04 (s, 1H), 7.67 (d, *J* = 7.9 Hz, 1H). **^{13}C-NMR** (126 MHz, $CDCl_3$) δ 26.4, 31.7, 37.3, 52.5, 81.8.

Minor rotamer: **^{1}H NMR** (500 MHz, $CDCl_3$) δ -0.28 – -0.18 (m, 1H), -0.05 (s, 3H), -0.03 (s, 3H), 0.40 (d, *J* = 6.6 Hz, 3H), 0.83 (s, 9H), 2.38 (t, *J* = 2.1 Hz, 1H), 2.75 (s, 3H), 2.97 (s, 3H), 3.28 (s, 3H), 3.68 (s, 3H), 4.26 – 4.30 (m, 1H), 5.61 (d, *J* = 7.6 Hz, 1H), 6.74 (d, *J* = 7.6 Hz, 1H). **^{13}C-NMR** (126 MHz, $CDCl_3$) δ 16.0, 26.3, 29.2.

HRMS (ESI): calcd for $C_{62}H_{95}N_8O_{12}Si^+$ $(M+H)^+$ 1171.6833; found: 1171.6830.

methyl *N*-(((2*R*,3*S*)-2-((*R*)-2-((2*R*,4*S*)-2-((*R*)-2-((*R*)-2-(((allyloxy)carbonyl)amino)-3-methylbutanamido)-*N*-methyl-3-(1-(prop-2-yn-1-yl)-1*H*-indol-3-yl)propanamido)-5-((*tert*-butyldimethylsilyl)oxy)-4-methylpentanamido)propanamido)-3-methoxy-3-phenylpropanoyl)-D-valyl)-*N*-methyl-D-leucinate (4a)

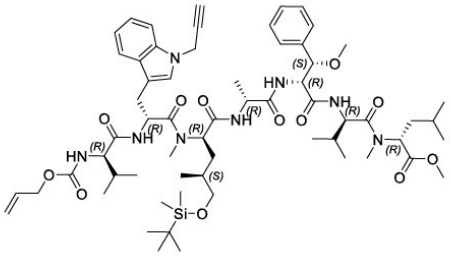

Prepared according to *GP2* and *GP4*: **3a** (326 mg, 304 µmol), DMBA (142 mg, 912 µmol), $Pd(PPh_3)_4$ (10.5 mg, 9.12 µmol) (1 h); ((allyloxy)carbonyl)-D-valine (84.0 mg, 395 mmol), HOBt (65.2 mg, 426 µmol), EDC (82.0 mg, 426 µmol), NMM (84.0 µl, 760 µmol) (15 h). Flash chromatography (CyH/EtOAc 100:0 – 20:80) followed by lyohpilization afforded **4a** (305 mg, 260 µmol, 86%) as a white amorphous solid. R_f = 0.23 (PE/EtOAc 3:7).

$[\alpha]_{20}^{D}$ = +68.3 (c 0.5, $CHCl_3$)

^{1}H-NMR (500 MHz, $CDCl_3$) *(mixture of rotamers, ratio ~2:1)* δ -0.05 (s, 1.1H), -0.04 (s, 1.0H), 0.01 (s, 2.1H), 0.02 (s, 2.0H), 0.37 (d, *J* = 6.6 Hz, 0.8H), -0.82 (s, 4.9H), 0.85 – 0.88 (m, 8.1H), 0.88 – 0.97 (m, 18.2 H), 0.99 (d, *J* = 6.9 Hz, 2.6H), 1.20 (d, *J* = 7.3 Hz, 2.8H), 1.26 (d, *J* = 6.3 Hz, 0.9H), 1.38 – 1.53 (m, 2.6H), 1.65 – 1.80 (m, 2.4H), 2.02 – 2.15 (m, 2.1H), 2.38 – 2.41 (m, 1.0H), 2.71 (s, 1.0 H), 2.75 (s, 2.1 H), 2.97 (s, 1.2 H), 2.98 – 2.99 (m, 2.3 H), 3.03 – 3.07 (m, 0.4H), 3.09 – 3.16 (m, 1.1H), 3.18 – 3.25 (m, 0.9H), 3.28 (s, 1.2H), 3.32 (s, 2.6H), 3.41 (d, *J* = 5.0 Hz, 1.4H), 3.66 – 3.70 (m, 3.5H), 4.06 – 4.14 (m, 0.9H), 4.24 – 4.31 (m, 0.7H), 4.33 – 4.39 (m, 0.5H), 4.51 – 4.65 (m, 2.4H), 4.67 – 4.73 (m, 1.6H), 4.76 – 4.86 (m, 4.3H), 4.90 – 5.00 (m, 1.1H), 5.17 – 5.39 (m, 4.5H), 5.70 (d, *J* = 9.5 Hz, 0.2H), 5.85 – 5.98 (m, 1.0H), 6.47 (d, *J* = 6.0 Hz, 0.6H), 6.79 (d, *J* = 7.4 Hz, 0.5H), 6.82 (d, *J* = 7.3 Hz, 0.4H), 6.97 (d, *J* = 7.4 Hz, 0.6H), 7.01 – 7.05 (m, 1.0H), 7.10 – 7.18 (m, 2.0H), 7.19 – 7.25 (m, 4.1H), 7.27 – 7.29 (m, 1.5H), 7.32 – 7.37 (m, 1.8H), 8.13 (d, *J* = 7.3 Hz, 0.2H).

^{13}C NMR (126 MHz, $CDCl_3$) *(mixture of rotamers)* δ -5.31, -5.28, -5.2, 15.7, 17.40, 17.42, 17.8, 18.0, 18.2, 18.40, 18.45, 19.2, 19.6, 21.5, 21.6, 23.4, 24.9, 26.1, 28.1, 28.7, 29.3, 31.3, 31.4, 31.5, 31.7, 32.3, 35.8, 37.1, 49.4, 49.9, 52.2, 54.2, 54.6, 54.7, 57.55, 57.61, 57.7, 58.0, 58.2, 60.1, 65.9, 66.1, 67.2, 68.5, 73.7, 73.8, 77.8, 78.1, 81.2, 81.5, 109.5, 109.6, 109.8, 117.9, 118.0, 119.0, 120.0, 120.2, 122.4, 122.6, 126.3, 127.1, 128.2, 128.3, 128.5, 128.6, 128.7, 132.0, 132.2, 132.3, 132.8, 136.0, 136.2, 136.9, 156.2, 156.4, 168.5, 170.4, 170.9, 171.6, 171.7, 171.9, 172.1, 172.2, 172.6, 172.8.

Selected diagnostic peaks:

Major rotamer: **^{1}H NMR** (500 MHz, $CDCl_3$) δ 0.01 (s, 3H), 0.02 (s, 3H), 0.86 (s, 9H), 1.20 (d, *J* = 7.3 Hz, 3H), 2.39 (t, *J* = 2.5 Hz, 1H), 2.75 (s, 3H), 2.98 (s, 3H), 3.32 (s, 3H), 3.69 (s, 3H), 4.28 (t, *J* = 7.0 Hz, 1H). **^{13}C NMR** (126 MHz, $CDCl_3$) δ 26.1, 32.3, 49.4, 57.61, 156.2.

Minor rotamer: **^{1}H NMR** (500 MHz, $CDCl_3$) δ -0.05 (s, 3H), -0.04 (s, 3H), 0.37 (d, *J* = 6.6 Hz, 3H), 0.82 (s, 9H), 1.26 (d, *J* = 6.3 Hz, 3H), 2.39 (t, *J* = 2.5 Hz, 1H), 2.71 (s, 3H), 2.97 (s, 3H), 3.28 (s, 3H). **^{13}C NMR** (126 MHz, $CDCl_3$) δ 29.3, 49.9, 156.4.

HRMS (ESI): calcd for $C_{62}H_{95}N_8O_{12}Si^+$ $(M+H)^+$: 1171.6833; found: 1171.6847.

(3*R*,6*R*,9*R*,12*R*,15*R*,18*R*,21*R*)-21-((*S*)-3-hydroxy-2-methylpropyl)-9-isobutyl-6,12-diisopropyl-15-((*S*)-methoxy(phenyl)methyl)-1,10,18-trimethyl-3-((1-(prop-2-yn-1-yl)-1*H*-indol-3-yl)methyl)-1,4,7,10,13,16,19-heptaazacyclohenicosane-2,5,8,11,14,17,20-heptaone (5a)

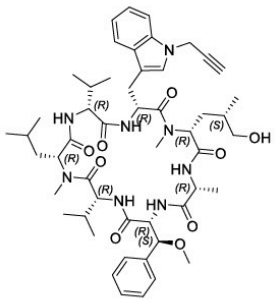

Prepared according to *GP6a*: **4a** (200 mg, 171 µmol), 1 M LiOH (222 µl, 222 µmol) (4.5 h); $Pd(OAc)_2$ (1.9 mg, 8.6 µmol), TPPTS (9.7 mg, 17 µmol), Et_2NH (179 µl, 1.71 mmol) (1 h); HATU (293 mg, 770 µmol), DIPEA (179 µl, 1.03 mmol) (addition over 3 h, additional 17 h); NH_4F (127 mg, 3.42 mmol) (16 h). RP flash chromatography (H_2O/MeCN 90:10 - 5:95) followed by prep HPLC (H_2O/MeCN 80:20 – 5:95) and lyophilizaiton afforded **5a** (46.1 mg, 49.0 µmol, 29%) as a white, amorphous solid.

$[\alpha]_{20}^{D}$ = +107.2 (c 0.5, $CHCl_3$).

^{1}H NMR (500 MHz, $CDCl_3$) δ -0.61 (dd, *J* = 11.0, 6.6 Hz, 1H), 0.21 (d, *J* = 6.8 Hz, 3H), 0.59 (d, *J* = 6.5 Hz, 3H), 0.62 (d, *J* = 6.6 Hz, 3H), 0.68 – 0.78 (m, 2H), 0.97 (dq, *J* = 10.7, 3.9 Hz, 10H), 1.07 (d, *J* = 6.6 Hz, 3H), 1.09 – 1.19 (m, 4H), 1.53 – 1.62 (m, 0H), 1.83 (ddd, *J* = 13.6, 11.0, 7.2 Hz, 1H), 2.17 – 2.28 (m, 1H), 2.27 – 2.37 (m, 1H), 2.41 (t, *J* = 2.6 Hz, 1H), 2.59 (s, 3H), 2.59 – 2.66 (m, 1H), 2.83 (s, 3H), 2.89 – 2.95 (m, 1H), 2.97 – 3.02 (m, 1H), 3.12 (dd, *J* = 13.5, 4.7 Hz, 1H), 3.27 – 3.33 (m, 1H), 3.35 (s, 3H), 4.09 (t, *J* = 9.5 Hz, 1H), 4.32 (d, *J* = 8.7 Hz, 1H), 4.48 (t, *J* = 8.6 Hz, 1H), 4.72 – 4.83 (m, 4H), 4.85 (dd, *J* = 9.6, 3.2 Hz, 1H), 4.91 (t, *J* = 5.1 Hz, 1H), 5.07 (d, *J* = 5.5 Hz, 1H), 7.00 (s, 1H), 7.10 – 7.14 (m, 1H), 7.15 – 7.18 (m, 2H), 7.23 (d, *J* = 4.9 Hz, 5H), 7.34 (d, *J* = 8.4 Hz, 2H), 7.47 (d, *J* = 7.9 Hz, 1H), 8.13 (d, *J* = 8.0 Hz, 1H), 8.27 (d, *J* = 9.5 Hz, 1H), 8.51 (d, *J* = 10.4 Hz, 1H).

^{13}C NMR (126 MHz, $CDCl_3$) δ 17.0, 18.5, 19.2, 19.9, 20.6, 22.5, 23.4, 25.1, 28.1, 29.0, 29.4, 30.7, 31.6, 32.9, 35.5, 38.8, 50.3, 50.9, 55.1, 55.8, 57.7, 58.8, 58.9, 59.1, 65.9, 73.8, 77.4, 79.9, 108.7, 109.6, 118.6, 120.1, 122.6, 126.2, 127.8, 128.0, 128.0, 128.5, 134.9, 135.8, 168.5, 168.9, 169.8, 170.5, 171.2, 171.4, 172.0.

HRMS (ESI): calcd for $C_{51}H_{73}N_8O_9^+$ $(M+H)^+$: 941.5495; found: 941.5504.

(3*R*,3'*R*,6*R*,6'*R*,9*R*,9'*R*,12*R*,12'*R*,15*R*,15'*R*,18*R*,18'*R*,21*R*,21'*R*)-15,15'-(((((3,6,9,12-tetraoxatetradecane-1,14-diyl)bis(1H-1,2,3-triazole-1,4-diyl))bis(methylene))bis(1*H*-indole-1,3-diyl))bis(methylene))bis(12-((S)-3-hydroxy-2-methylpropyl)-21-isobutyl-3,18-diisopropyl-6-((S)-methoxy(phenyl)methyl)-1,9,13-trimethyl-1,4,7,10,13,16,19-heptaazacyclohenicosane-2,5,8,11,14,17,20-heptaone) (8a) (UdSBI-0966)

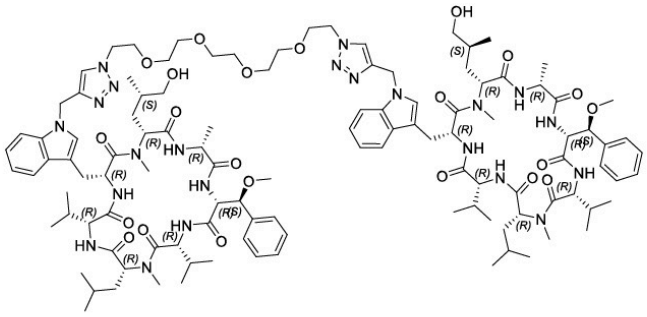

Prepared according to *GP7*: **5a** (15.2 mg, 16.1 µmol), 1,14-diazido-3,6,9,12-tetraoxatetradecane (2.33 mg, 8.07 µmol), 1 M $CuSO_4$ (6.46 µl, 6.46 µmol), 1 M sodium ascorbate (10.5 µl, 10.5 µmol) (16 h). RP flash chromatography (H_2O/MeCN 70:30 – 90:10) followed by prep HPLC (H_2O/MeCN 70:30 – 90:10) and lyophilization afforded **8a** (9.0 mg, 4.15 µmol, 51%) as a white, amorphous solid.

$[\alpha]_{20}^{D}$ = +95.6 (c 0.25, $CHCl_3$).

^{1}H NMR (500 MHz, $CDCl_3$) δ -0.70 – -0.53 (m, 2H), 0.15 (d, *J* = 6.8 Hz, 6H), 0.58 (d, *J* = 6.5 Hz, 6H), 0.63 (d, *J* = 6.6 Hz, 6H), 0.72 – 0.82 (m, 2H), 0.94 – 1.01 (m, 18H), 1.10 (d, *J* = 6.6 Hz, 6H), 1.12 – 1.19 (m, 8H), 1.54 – 1.61 (m, 2H), 1.71 (d, *J* = 5.4 Hz, 2H), 2.19 – 2.27 (m, 2H), 2.27 – 2.35 (m, 2H), 2.56 (s, 6H), 2.79 – 2.88 (m, 8H), 3.02 (dd, *J* = 11.5, 4.4 Hz, 2H), 3.07 (dd, *J* = 13.8, 5.0 Hz, 2H), 3.25 – 3.30 (m, 2H), 3.35 – 3.39 (m, 10H), 3.43 (dd, *J* = 11.0, 4.4 Hz, 2H), 3.47 – 3.52 (m, 4H), 3.79 (t, *J* = 5.4 Hz, 4H), 4.11 (t, *J* = 9.3 Hz, 2H), 4.36 (d, *J* = 12.5 Hz, 2H), 4.39 – 4.52 (m, 8H), 4.69 – 4.81 (m, 4H), 4.86 (dd, *J* = 10.1, 3.8 Hz, 2H), 4.90 (t, *J* = 5.0 Hz, 2H), 5.09 (d, *J* = 5.5 Hz, 2H), 5.27 (d, *J* = 15.4 Hz, 2H), 5.38 (d, *J* = 15.6 Hz, 2H), 7.02 (s, 2H), 7.09 (t, *J* = 7.5 Hz, 2H), 7.15 (d, *J* = 5.0 Hz, 2H), 7.17 – 7.26 (m, 16H), 7.32 (s, 2H), 7.42 (d, *J* = 8.2 Hz, 2H), 7.46 (d, *J* = 8.0 Hz, 2H), 7.56 (s, 2H), 8.09 (d, *J* = 8.4 Hz, 2H), 8.24 (d, *J* = 9.5 Hz, 2H), 8.37 (d, *J* = 10.4 Hz, 2H).

^{13}C NMR (126 MHz, $CDCl_3$) δ 16.9, 18.9, 19.4, 20.0, 20.2, 20.8, 22.7, 23.7, 25.5, 28.6, 29.3, 29.6, 31.1, 32.0, 32.9, 39.2, 41.7, 50.5, 50.6, 51.2, 55.5, 56.2, 57.9, 59.1, 59.3, 66.8, 69.5, 70.7, 80.4, 108.9, 110.2, 118.9, 120.1, 122.7, 123.4, 127.1, 128.1, 128.4 , 128.8, 135.4, 136.5, 143.8, 168.8, 169.0, 170.1, 170.9, 171.6, 171.8, 172.4.

HRMS (ESI): calcd for $C_{112}H_{165}N_{22}O_{22}^+$ $(M+H)^+$: 2170.2463; found: 2170.2477.

Synthesis of exit vector 7 triazol-based Homo-BacPROTACs (11 + 12)

Methyl *N*-(((2*S*,3*R*)-2-((*S*)-2-((2*S*,4*R*)-2-((*S*)-2-((*S*)-2-((((9*H*-fluoren-9-yl)methoxy)carbonyl)amino)pent-4-ynamido)-*N*-methyl-3-(1-methyl-1*H*-indol-3-yl)propanamido)-5-((*tert*-butyldimethylsilyl)oxy)-4-methylpentanamido)propanamido)-3-methoxy-3-phenylpropanoyl)-L-valyl)-*N*-methyl-L-leucinate (SI-18)

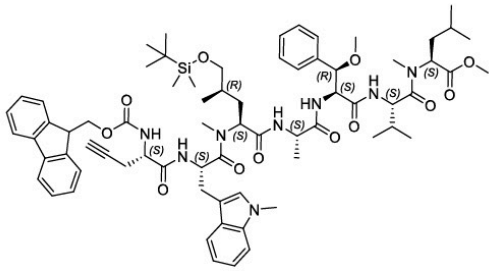

Prepared according to *GP2* and *GP4*: methyl N-(((2S,3R)-2-((S)-2-((2S,4R)-2-((S)-2-(((allyloxy)carbonyl)amino)-N-methyl-3-(1-methyl-1H-indol-3-yl)propanamido)-5-((tert-butyldimethylsilyl)oxy)-4-methylpentanamido)propanamido)-3-methoxy-3-phenylpropanoyl)-L-valyl)-N-methyl-L-leucinate (377 mg, 360 µmol), DMBA (169 mg, 1.08 mmol), $Pd(PPh_3)_4$ (12.5 mg, 10.8 µmol) (1.5 h); Fmoc-Pra-OH (157 mg, 468 µmol), HOBt (60.6 mg, 396 µmol), EDC (75.9 mg, 396 µmol), NMM (79.2 µl, 720 µmol) (17 h). Flash chromatography (CyH/EtOAc 100:0 – 20:8) followed by lyophilization yielded **SI-18** (424 mg, 329 µmol, 91%) as a white amorphous solid. R_f = 0.21 (PE/EtOAc 4:6).

$[\alpha]_{20}^{D}$ = −58.5 (c 0.5, $CHCl_3$)

^{1}H NMR (500 MHz, $CDCl_3$) *(mixture of rotamers)* δ -0.04 (s, 0.7H), -0.02 (s, 0.7H), 0.00 – 0.05 (m, 4.5H), 0.49 (d, *J* = 6.7 Hz, 0.5H), 0.84 (s, 2.1H), 0.86 – 0.89 (m, 9.6H), 0.89 – 0.96 (m, 9.5H), 0.99 (d, *J* = 6.8 Hz, 2.4H), 1.19 – 1.36 (m, 4.6H), 1.42 – 1.52 (m, 2.2H), 1.63 – 1.80 (m, 2.1H), 1.91 – 1.97 (m, 0.5H), 1.99 – 2.09 (m, 1.8H), 2.09 – 2.18 (m, 1.0H), 2.49 – 2.71 (m, 1.8H), 2.74 (s, 0.7H), 2.76 – 2.86 (m, 2.2H), 2.93 – 3.01 (m, 3.0H), 3.06 – 3.11 (m, 0.3H), 3.11 – 3.20 (m, 1.0H), 3.24 – 3.36 (m, 4.2H), 3.38 – 3.45 (m, 1.3H), m, 1.3H), 3.64 – 3.71 (m, 5.8H), 4.19 – 4.25 (m, 1.0H), 4.25 – 4.30 (m, 0.7H), 4.30 – 4.49 (m, 3.0H), 4.65 – 4.86 (m, 3.7H), 4.99 – 5.07 (m, 0.3H), 5.21 – 5.29 (m, 0.7H), 5.29 – 5.39 (m, 1.0H), 5.62 (d, *J* = 8.3 Hz, 0.5H), 5.70 (d, *J* = 8.5 Hz, 0.2H), 6.42 – 6.50 (m, 0.5H), 6.72 – 6.81 (m, 0.3H), 6.85 – 6.91 (m, 1.0H), 6.94 – 7.00 (m, 0.4H), 7.07 – 7.12 (m, 1.0H), 7.14 – 7.25 (m, 5.0H), 7.26 – 7.35 (m, 4.5H), 7.37 – 7.44 (m, 2.6H), 7.44 – 7.49 (m, 1.0H), 7.52 – 7.57 (m, 0.8H), 7.57 – 7.63 (m, 1.7H), 7.64 – 7.70 (m, 1.4H), 7.74 – 7.80 (m, 1.9 H), 7.90 (d, *J* = 6.7 Hz, 0.2H).

^{13}C NMR (126 MHz, $CDCl_3$) *(mixture of rotamers)* δ -5.3, 17.4, 17.5, 18.0, 18.4, 18.5, 19.6, 19.7, 21.5, 21.6, 23.1, 23.4, 24.9, 26.0, 26.1, 28.6, 29.3, 31.4, 31.5, 32.3, 32.8, 37.0, 47.2, 49.6, 50.5, 52.3, 53.1, 54.2, 54.6, 57.6, 58.3, 67.3, 67.4, 68.4, 72.0, 79.2, 81.5, 108.5, 109.5, 118.8, 119.4, 120.1, 121.9, 125.3, 127.2, 127.9, 128.1, 128.4, 128.5, 128.6, 128.7, 132.1, 132.2, 132.3, 133.0, 136.9, 137.0, 141.4, 143.8, 143.9, 155.8, 168.5, 168.6, 168.7, 169.5, 170.3, 170.8, 171.6, 171.8, 172.06, 172.14, 172.4.

Selected diagnostic peaks:

Major rotamer: **^{1}H NMR** (500 MHz, $CDCl_3$) δ 0.01 – 0.04 (m, 6H), 0.88 (s, 9H), 2.80 (s, 3H), 2.96 (s, 3H), 3.32 (s, 3H), 3.68 (s, 3H), 5.62 (d, *J* = 8.3 Hz, 1H), 6.88 (s, 1H), 7.77 (d, *J* = 7.5 Hz, 2H). **^{13}C NMR** (126 MHz, $CDCl_3$) δ 26.1, 31.5, 81.5, 155.8.

Minor rotamer: **^{1}H NMR** (500 MHz, $CDCl_3$) δ -0.04 (s, 3H), -0.02 (s, 3H), 0.49 (d, *J* = 6.7 Hz, 3H), 0.84 (s, 9H), 2.74 (s, 3H), 3.66 (s, 3H), 5.70 (d, *J* = 8.5 Hz, 1H), 6.86 (s, 1H), 7.90 (d, *J* = 6.7 Hz, 1H). **^{13}C NMR** (126 MHz, $CDCl_3$) δ 26.0, 32.8, 79.2.

HRMS (ESI) calcd for $C_{71}H_{97}N_8O_{12}Si^+$ $(M+H)^+$: 1281.6990, found: 1281.7024.

(3*S*,6*S*,9*S*,12*S*,15*S*,18*S*,21*S*)-21-((*R*)-3-hydroxy-2-methylpropyl)-9-isobutyl-12-isopropyl-15-((*R*)-methoxy(phenyl)methyl)-1,10,18-trimethyl-3-((1-methyl-1*H*-indol-3-yl)methyl)-6-(prop-2-yn-1-yl)-1,4,7,10,13,16,19-heptaazacyclohenicosane-2,5,8,11,14,17,20-heptaone (10)

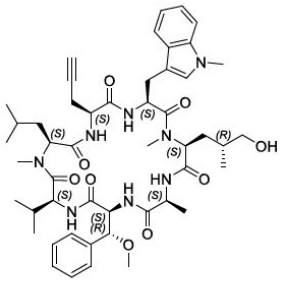

Prepared according to *GP6b*: **SI-18** (422 mg, 329 µmol), tris(2-aminoethyl)amine (0.49 ml, 3.29 mmol) (0.5 h); 1 M LiOH (658 µl, 658 µmol) (3 h); HATU (438 mg, 1.15 mmol), NMM (145 µl, 1.32 mmol) (addition over 1.5 h, additional 18 h); NH_4F (122 mg, 3.29 mmol). RP flash chromatography ($MeCN/H_2O$ 10:90 – 95:5) followed by lyophilization yielded **10** (190 mg, 208 µmol, 63%) as a white amorphous solid.

$[\alpha]_{20}^{D}$ = –119.9 (c 0.5, $CHCl_3$).

^{1}H NMR (500 MHz, $CDCl_3$) δ -0.46 (dd, *J* = 12.2, 6.2 Hz, 1H), 0.29 (d, *J* = 6.8 Hz, 3H), 0.70 – 0.78 (m, 1H), 0.90 – 0.98 (m, 9H), 1.06 (d, *J* = 6.5 Hz, 3H), 1.06 – 1.14 (m, 1H), 1.26 (d, *J* = 7.2 Hz, 3H), 1.28 – 1.34 (m, 1H), 1.50 – 1.57 (m, 1H), 1.70 (d, *J* = 16.0 Hz, 1H), 1.89 (s, 1H), 2.19 – 2.31 (m, 1H), 2.33 (s, 1H), 2.51 – 2.58 (m, 1H), 2.59 (s, 3H), 2.92 (s, 3H), 2.94 – 2.99 (m, 1H), 3.00 – 3.07 (m, 1H), 3.20 (dd, *J* = 13.6, 4.8 Hz, 1H), 3.34 – 3.38 (m, 4H), 3.73 (s, 3H), 4.31 – 4.37 (m, 1H), 4.51 (t, *J* = 9.1 Hz, 1H), 4.70 – 4.81 (m, 3H), 4.87 – 4.96 (m, 2H), 5.06 (d, *J* = 5.4 Hz, 1H), 6.87 (s, 1H), 7.07 – 7.12 (m, 1H), 7.12 – 7.17 (m, 2H), 7.19 – 7.25 (m, 2H), 7.29 (dd, *J* = 10.3, 6.8 Hz, 5H), 7.48 (d, *J* = 8.0 Hz, 1H), 7.80 (bs, 1H), 8.09 (d, *J* = 8.6 Hz, 1H), 8.23 (d, *J* = 9.3 Hz, 1H), 8.47 (d, *J* = 10.2 Hz, 1H).

^{13}C NMR (126 MHz, $CDCl_3$) δ 17.4, 19.4, 20.0, 21.1, 22.3, 22.7, 23.7, 25.3, 28.7, 29.3, 29.4, 30.8, 31.8, 32.9, 33.3, 39.0, 50.8, 51.3, 51.9, 55.1, 56.2, 57.9, 59.0, 59.4, 65.9, 72.2, 80.1, 80.2, 107.7, 109.8, 118.7, 119.8, 122.4, 127.7, 127.99, 128.01, 128.6, 129.3, 135.1, 137.0, 168.6, 169.4, 170.2, 170.6, 170.7, 171.2, 171.8.

HRMS (ESI) calcd for $C_{49}H_{69}N_8O_9^+$ $(M+H)^+$: 913.5182; found: 913.5177.

(3*S*,3'*S*,6*S*,6'*S*,9*S*,9'*S*,12*S*,12'*S*,15*S*,15'*S*,18*S*,18'*S*,21*S*,21'*S*)-18,18'-((((ethane-1,2-diylbis(oxy))bis(ethane-2,1-diyl))bis(1*H*-1,2,3-triazole-1,4-diyl))bis(methylene))bis(12-((*R*)-3-hydroxy-2-methylpropyl)-21-isobutyl-3-isopropyl-6-((*R*)-methoxy(phenyl)methyl)-1,9,13-trimethyl-15-((1-methyl-1*H*-indol-3-yl)methyl)-1,4,7,10,13,16,19-heptaazacyclohenicosane-2,5,8,11,14,17,20-heptaone) (11)

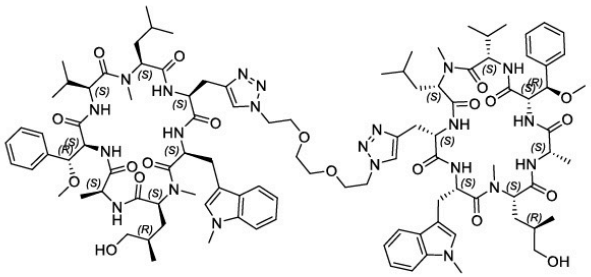

Prepared according to *GP7*: **10** (23.3 mg, 25.4 µmol), 1,2-bis(2-azidoethox)ethane (2.55 mg, 12.7 µmol), 1 M $CuSO_4$ (10.2 µl, 10.2 µmol), 1 M sodium ascorbate (28.1 µl, 28.1 µmol) (18 h). Flash chromatography (H_2O/MeCN 90:10 – 5:95) followed by prep HPLC (H_2O/MeCN 80:0 – 5:95) and lyophilization yielded **11** (16.4 mg, 8.09 µmol, 63%) as a white amorphous solid.

$[\alpha]_{20}^{D}$ = –118.2 (c 0.5, $CHCl_3$).

^{1}H NMR (500 MHz, $CDCl_3$) δ -0.72 (dd, *J* = 12.8, 6.4 Hz, 2H), 0.15 (d, *J* = 6.7 Hz, 6H), 0.56 – 0.62 (m, 2H), 0.90 (d, *J* = 6.7 Hz, 6H), 0.91 – 0.98 (m, 2H), 0.97 – 1.02 (m, 12H), 1.04 (d, *J* = 6.6 Hz, 6H), 1.12 (t, *J* = 8.4 Hz, 2H), 1.40 (d, *J* = 7.2 Hz, 8H), 1.50 (d, *J* = 11.2 Hz, 2H), 1.74 – 1.83 (m, 2H), 2.17 – 2.28 (m, 4H), 2.55 (s, 6H), 2.57 (s, 6H), 2.80 – 2.87 (m, 2H), 2.98 (dd, *J* = 11.3, 3.6 Hz, 2H), 3.24 – 3.29 (m, 4H), 3.31 (s, 6H), 3.67 (t, *J* = 6.6 Hz, 2H), 3.70 (s, 6H), 3.92 (dq, *J* = 7.5, 3.6 Hz, 2H), 4.12 (dd, *J* = 9.1, 4.9 Hz, 2H), 4.48 (d, *J* = 11.1 Hz, 2H), 4.50 – 4.62 (m, 4H), 4.68 – 4.75 (m, 2H), 4.78 (dt, *J* = 10.3, 5.4 Hz, 6H), 4.86 (dd, *J* = 9.9, 7.0 Hz, 2H), 4.98 (t, *J* = 5.0 Hz, 2H), 5.06 (d, *J* = 5.3 Hz, 2H), 6.78 (s, 2H), 7.03 (t, *J* = 7.6 Hz, 6H), 7.08 – 7.12 (m, 8H), 7.17 – 7.22 (m, 2H), 7.23 – 7.29 (m, 4H), 7.40 (s, 2H), 7.51 (d, *J* = 4.9 Hz, 2H), 7.57 (d, *J* = 7.9 Hz, 2H), 8.10 (d, *J* = 8.6 Hz, 2H), 8.43 (d, *J* = 9.3 Hz, 2H), 8.62 (d, *J* = 10.2 Hz, 2H), 8.99 (d, *J* = 5.4 Hz, 2H).

^{13}C NMR (126 MHz, $CDCl_3$) δ 17.4, 19.4, 20.0, 21.3, 22.8, 23.9, 24.8, 27.9, 28.9, 29.3, 29.4, 30.8, 31.9, 32.8, 33.1, 39.3, 50.4, 50.6, 51.2, 52.1, 54.9, 56.3, 57.9, 58.7, 59.3, 65.6, 69.5, 70.7, 80.1, 108.3, 109.8, 119.0, 119.5, 122.4, 123.7, 127.57, 127.64, 128.1, 128.6, 129.1, 135.3, 137.0, 141.6, 167.7, 169.9, 170.0, 170.6, 171.3, 171.4, 171.9.

HRMS (ESI) calcd for $C_{104}H_{149}N_{22}O_{20}^+$ $(M+H)^+$: 2026.1313; found: 2026.1266.

(3*S*,3'*S*,6*S*,6'*S*,9*S*,9'*S*,12*S*,12'*S*,15*S*,15'*S*,18*S*,18'*S*,21*S*,21'*S*)-18,18'-((pentane-1,5-diylbis(1*H*-1,2,3-triazole-1,4-diyl))bis(methylene))bis(12-((*R*)-3-hydroxy-2-methylpropyl)-21-isobutyl-3-isopropyl-6-((*R*)-methoxy(phenyl)methyl)-1,9,13-trimethyl-15-((1-methyl-1*H*-indol-3-yl)methyl)-1,4,7,10,13,16,19-heptaazacyclohenicosane-2,5,8,11,14,17,20-heptaone) (12) (UdSBI-4377)

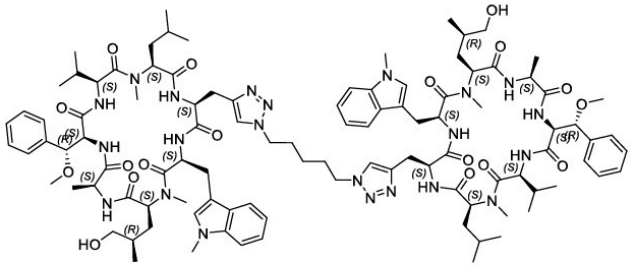

Prepared according to *GP7*: **10** (31.7 mg, 34.7 µmol), 1,5-diazidopentane (2.68 mg, 17.4 µmol), 1 M $CuSO_4$ (13.9 µl, 13.9 µmol), 1 M sodium ascorbate (22.6 µl, 22.6 µmol) (18 h). Flash chromatography (H_2O/MeCN 70:30 – 20:80) followed by prep HPLC (H_2O/MeCN 60:40 – 5:95) and lyophilization yielded **12** (24.7 mg, 11.8 µmol, 64%, purity 95%) as a white amorphous solid.

$[\alpha]_{20}^{D}$ = –98.3 (c 0.3, $CHCl_3$).

^{1}H NMR (500 MHz, $CDCl_3$) δ -0.51 (ddd, J = 13.8, 6.6, 2.5 Hz, 2H), 0.24 (dd, J = 6.8, 1.1 Hz, 6H), 0.77 (q, J = 5.8 Hz, 2H), 0.95 (d, J = 6.6 Hz, 8H), 1.03 – 1.08 (m, 18H), 1.26 – 1.31 (m, 8H), 1.50 – 1.60 (m, 4H), 1.59 – 1.70 (m, 2H),

1.85 (ddd, J = 13.4, 10.6, 7.3 Hz, 2H), 1.89 – 1.98 (m, 4H), 1.99 – 2.05 (m, 2H), 2.22 – 2.28 (m, 2H), 2.58 (s, 6H), 2.83 (s, 6H), 2.86 – 2.94 (m, 4H), 3.04 (dd, J = 11.2, 4.0 Hz, 2H), 3.09 – 3.15 (m, 2H), 3.22 – 3.27 (m, 2H), 3.30 (s, 6H), 3.71 (s, 6H), 4.36 – 4.47 (m, 4H), 4.55 (dd, J = 10.7, 2.6 Hz, 2H), 4.62 (t, J = 9.1 Hz, 2H), 4.73 – 4.78 (m, 2H), 4.79 – 4.86 (m, 4H), 4.90 – 4.97 (m, 4H), 5.10 (d, J = 5.4 Hz, 2H), 6.85 (d, J = 1.9 Hz, 2H), 6.96 – 7.00 (m, 4H), 7.07 – 7.09 (m, 6H), 7.18 – 7.21 (m, 2H), 7.23 – 7.28 (m, 4H), 7.34 – 7.38 (m, 2H), 7.45 – 7.52 (m, 4H), 8.15 (d, J = 8.8 Hz, 2H), 8.32 (d, J = 9.2 Hz, 2H), 8.75 (d, J = 10.0 Hz, 2H), 8.83 – 8.90 (m, 2H).

^{13}C NMR (126 MHz, $CDCl_3$) δ 17.4, 19.4, 20.0, 20.1, 21.1, 22.8, 22.9, 23.5, 23.7, 25.1, 28.0, 28.8, 28.9, 29.0, 29.5, 31.0, 32.0, 32.8, 33.2, 39.2, 50.2, 50.4, 51.0, 51.8, 54.9, 56.3, 57.9, 58.9, 59.5, 66.0, 80.0, 108.7, 109.7, 118.9, 119.5, 122.3, 127.7, 128.2, 128.4, 129.1, 135.5, 137.0, 142.1, 167.6, 169.7, 170.1, 170.8, 171.2, 171.5, 172.2.

HRMS (ESI) calcd for $C_{103}H_{147}N_{22}O_{18}^+$ $(M+H)^+$: 1980.1258; found: 1980.1278.

(3*S*,6*S*,9*S*,12*S*,15*S*,18*S*,21*S*)-21-((*R*)-3-hydroxy-2-methylpropyl)-9-isobutyl-12-isopropyl-15-((*R*)-methoxy(phenyl)methyl)-1,10,18-trimethyl-3-((1-methyl-1*H*-indol-3-yl)methyl)-6-((1-pentyl-1*H*-1,2,3-triazol-4-yl)methyl)-1,4,7,10,13,16,19-heptaazacyclohenicosane-2,5,8,11,14,17,20-heptaone (24)

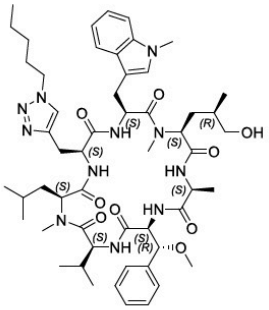

A 1.5 ml vial was charged with **10** (15.6 mg, 17.1 µmol), *t*-BuOH (248 µl) and H_2O (285 µl). To this solution, 1-azidopentane (37.2 µl of a 13.0 mg ml^{-1} stock solution, 4.83 mg, 42.7 µmol) followed by 1 M $CuSO_4$ (6.83 µl, 6.83 µmol) and 1 M sodium ascorbate (10.3 µl, 10.3 µmol) were added, the vial was flushed with Argon and sealed. After 5 h, 76% conversion was observed by LC/MS. The reaction mixture was subsequently evaporated in vacuo and the residue was purified by RP flash chromatography (H_2O/MeCN 90:10 – 5:95). After lyophilization, **24** (11.5 mg, 11.2 µmol, 66%) was obtained as a white amorphous solid.

$[\alpha]_{20}^{D}$ = −90.6 (c 0.5, $CHCl_3$).

^{1}H NMR (500 MHz, $CDCl_3$) δ -0.34 – -0.15 (m, 1H), 0.34 (d, *J* = 6.9 Hz, 3H), 0.86 – 0.91 (m, 1H), 0.93 (t, *J* = 7.2 Hz, 3H), 0.94 – 0.98 (m, 9H), 1.08 (d, *J* = 6.7 Hz, 3H), 1.17 (ddd, *J* = 13.0, 8.4, 4.2 Hz, 1H), 1.27 – 1.34 (m, 5H), 1.36 – 1.43 (m, 2H), 1.47 – 1.58 (m, 1H), 1.62 (dd, *J* = 14.6, 10.9 Hz, 1H), 1.90 – 1.98 (m, 2H), 2.17 – 2.30 (m, 3H), 2.48 – 2.56 (m, 1H), 2.63 (s, 3H), 2.86 (s, 3H), 2.95 – 3.00 (m, 1H), 3.02 – 3.06 (m, 1H), 3.07 – 3.13 (m, 1H), 3.19 – 3.28 (m, 1H), 3.35 (s, 3H), 3.71 (s, 3H), 4.36 (t, *J* = 7.0 Hz, 2H), 4.45 – 4.59 (m, 3H), 4.67 – 4.77 (m, 2H), 4.77 – 4.86 (m, 1H), 4.93 (t, *J* = 5.0 Hz, 1H), 5.07 (d, *J* = 5.3 Hz, 1H), 6.82 (s, 1H), 6.86 (d, *J* = 5.0 Hz, 1H), 7.04 – 7.17 (m, 7H), 7.17 – 7.24 (m, 2H), 7.24 – 7.30 (m, 1H), 7.37 (d, *J* = 4.9 Hz, 1H), 7.45 (d, *J* = 7.9 Hz, 1H), 8.08 (d, *J* = 8.5 Hz, 1H), 8.14 (d, *J* = 9.3 Hz, 1H), 8.59 (d, *J* = 9.9 Hz, 1H).

^{13}C NMR (126 MHz, $CDCl_3$) δ 14.1, 17.4, 19.4, 20.0, 20.8, 22.3, 22.7, 23.6, 25.2, 28.2, 28.7, 28.8, 29.2, 29.6, 29.9, 31.0, 32.3, 32.8, 33.3, 38.9, 50.4, 50.6, 51.1, 52.4, 54.9, 56.3, 57.9, 59.0, 59.5, 66.3, 80.1, 107.9, 109.7, 118.7, 119.6, 121.8, 122.4, 127.6, 127.9, 128.1, 128.4, 129.2, 135.4, 137.0, 141.9, 168.1, 169.87, 169.89, 170.9, 171.1, 171.2, 172.1.

HRMS (ESI) calcd for $C_{54}H_{80}N_{11}O_9^+$ $(M+H)^+$: 1026.6135; found: 1026.6085.

Synthesis of enantiomeric exit vector 7 Homo-BacPROTAC (12a)

***N*$^{\alpha}$-((allyloxy)carbonyl)-1-methyl-D-tryptophan (SI-19)**

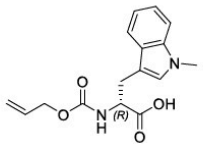

((Allyloxy)carbonyl)-D-tryptophan (**SI-16**) (500 mg, 1.73 mmol) was dissolved in DMF (5.8 ml) and KO*t*-Bu (448 mg, 3.99 mmol) was added at rt and stirred until all solids were dissovled. The mixture was cooled to 0 °C and methyl iodide (152 µl, 2.43 mmol) was added in one portion. TLC control after 10 min indicated full conversion, the reaction was quenched by addition of 1 M HCl after 20 min. The mixture was extracted with EtOAc (3x). The combined organic phases were washed with 1 M LiCl (2x), brine and dried (Na_2SO_4). Flash chromatography (CyH/[EtOAc+2%HOAc] 100:0 – 70:30 – 50:50) yielded **SI-19** (283 mg, 936 µmol, 54%) as a brownish resin. R_f = 0.31 (PE/EtOAc/HOAc 40:60:1).

$[\alpha]_{20}^{D}$ = –40.6 (c 0.5, $CHCl_3$).

Major rotamer:

^{1}H NMR (500 MHz, DMSO-d_6) δ 2.98 (dd, *J* = 14.6, 9.7 Hz, 1H), 3.16 (dd, *J* = 14.6, 4.6 Hz, 1H), 3.72 (s, 3H), 4.19 (ddd, *J* = 9.7, 8.1, 4.6 Hz, 1H), 4.36 – 4.46 (m, 2H), 5.14 (dd, *J* = 10.5, 1.6 Hz, 1H), 5.23 (dd, *J* = 17.2, 1.7 Hz, 1H), 5.85 (ddt, *J* = 17.2, 10.5, 5.3 Hz, 1H), 7.02 (ddd, *J* = 7.9, 7.0, 1.0 Hz, 1H), 7.09 – 7.18 (m, 2H), 7.38 (d, *J* = 8.2 Hz, 1H), 7.55 (d, *J* = 8.0 Hz, 2H), 12.71 (bs, 1H). **^{13}C NMR** (126 MHz, DMSO) δ 26.8, 32.3, 55.0, 64.4, 109.5, 109.7, 117.0, 118.4, 118.6, 121.1, 127.5, 128.1, 133.6, 136.6, 155.9, 173.8.

Minor rotamer (selected signals, ratio ~8:1):

^{1}H NMR (500 MHz, DMSO-d_6) δ 4.30 – 4.38 (m, 2H), 5.04 – 5.11 (m, 2H), 5.75 (ddt, *J* = 15.7, 10.0, 4.8 Hz, 1H).

HRMS (ESI) calcd for $C_{16}H_{19}N_2O_4^+$ (M+H)$^+$: 303.1339; found: 303.1348.

methyl *N*-(((2*R*,3*S*)-2-((*R*)-2-((2*R*,4*S*)-2-((*R*)-2-(((allyloxy)carbonyl)amino)-*N*-methyl-3-(1-methyl-1*H*-indol-3-yl)propanamido)-5-((*tert*-butyldimethylsilyl)oxy)-4-methylpentanamido)propanamido)-3-methoxy-3-phenylpropanoyl)-D-valyl)-*N*-methyl-D-leucinate (SI-20)

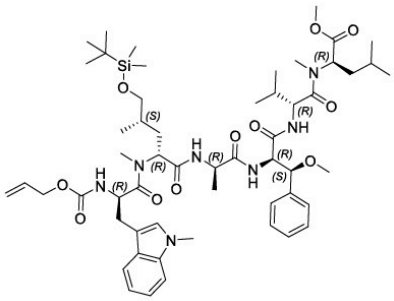

Prepared according to *GP1* and *GP5*: **2a** (522 mg, 581 µmol), Pd/C (49.5 mg) (2 h); **SI-19** (243 mg, 802 µmol), DIPEA (140 µl, 802 µmol), $BnNMe_2$ (8.51 µl, 57.3 µmol), 1 M isopropyl chloroformate (802 µl, 802 µmol), NMI (4.57 µl, 57.2 µmol) and HCl (14.3 µl, 57.3 µmol) (2.5 h). Flash chromatography (CyH/EtOAc 100:0 – 25:75) followed by lyophilization afforded **SI-20** (547 mg, 522 µmol, 91%) as a white amorphous solid. R_f = 0.28 (PE/EtOAc 3:7).

$[\alpha]_{20}^{D}$ = +59.9 (c 0.5, $CHCl_3$).

^{1}H NMR (500 MHz, $CDCl_3$) *(mixture of rotamers, ratio ~3:2)* δ -0.19 – -0.11 (m, 0.3H), -0.04 (s, 0.9H), -0.02 (s, 0.9H), 0.00 – 0.05 (m, 5.0H), 0.45 (d, *J* = 6.7 Hz, 0.8H), 0.83 (s, 2.8H), 0.87 (s, 7.2H), 0.89 – 0.93 (m, 6.8H), 0.93 – 0.98 (m,, 7.1H), 0.99 (d, *J* = 6.8 Hz, 2.5H), 1.18 (d, *J* = 7.1 Hz, 1.8H), 1.22 – 1.27 (m, 1.5H), 1.43 – 1.53 (m, 2.5H), 1.66 – 1.80 (m, 2.2H), 1.87 – 2.05 (m, 2.0H), 2.06 – 2.22 (m, 1.2H), 2.72 – 2.76 (m, 2.5H), 2.85 – 2.93 (m, 0.6H), 2.95 – 3.02 (m, 3.3H), 3.07 (dd, *J* = 9.5, 5.5 Hz, 0.3H), 3.13 (dd, *J* = 14.2, 5.6 Hz, 1.0H), 3.21 (dd, *J* = 14.5, 8.0 Hz,

0.7H), 3.28 (s, 1.2H), 3.33 (s, 2.5H), 3.40 (dd, *J* = 9.9, 5.4 Hz, 0.7H), 3.45 (dd, *J* = 9.9, 4.5 Hz, 0.7H), 3.67 – 3.70 (m, 5.0H), 4.13 – 4.23 (m, 0.6H), 4.23 – 4.31 (m, 0.4H), 4.42 – 4.57 (m, 2.0H), 4.59 – 4.66 (m, 0.8H), 4.66 – 4.73 (m, 0.9H), 4.76 – 4.91 (m, 3.2H), 4.93 – 5.00 (m, 0.6H), 5.13 – 5.32 (m, 2.2H), 5.36 (dd, *J* = 10.5, 5.2 Hz, 1.0H), 5.62 (d, *J* = 7.4 Hz, 0.2H), 5.80 – 5.92 (m, 1.4H), 6.36 (d, *J* = 6.9 Hz, 0.5H), 6.76 (d, *J* = 7.5 Hz, 0.3H), 6.80 (d, *J* = 7.8 Hz, 0.5H), 6.86 – 6.91 (m, 0.9H), 7.06 – 7.14 (m, 1.2H), 7.16 – 7.25 (m, 4.5H), 7.25 – 7.32 (m, 4.0H), 7.35 (d, *J* = 8.8 Hz, 0.4H), 7.45 (d, *J* = 8.7 Hz, 0.5H), 7.54 – 7.58 (m, 0.3H), 7.65 (d, *J* = 7.9 Hz, 0.6H), 7.89 (d, *J* = 6.7 Hz, 0.2H).

^{13}C NMR (126 MHz, $CDCl_3$) *(mixture of rotamers)* δ -5.30, -5.27, -5.25, 15.7, 17.4, 17.5, 17.6, 17.8, 18.4, 18.5, 19.6, 19.7, 21.5, 23.41, 23.44, 24.9, 26.0, 26.1, 28.6, 28.8, 29.3, 31.3, 31.4, 31.5, 32.2, 32.8, 37.0, 49.8, 50.0, 51.0, 51.7, 52.2, 52.3, 54.2, 54.4, 54.5, 54.6, 56.4, 57.6, 57.7, 57.9, 58.0, 65.8, 66.4, 67.3, 68.4, 81.3, 81.5, 108.4, 108.6, 109.5, 117.7, 118.4, 118.7, 118.8, 119.4, 119.6, 121.9, 122.2, 127.0, 127.8, 127.8, 128.0, 128.1, 128.3, 128.4, 128.5, 132.2, 132.8, 136.9, 136.9, 137.0, 156.1, 156.8, 168.6, 168.9, 170.5, 171.7, 171.7, 172.1, 172.2, 172.3, 172.6, 173.4.

Selected diagnostic peaks:

Major rotamer: **^{1}H NMR** (500 MHz, $CDCl_3$) δ 0.02 (s, 3H), 0.03 (s, 3H), 0.87 (s, 9H), 3.13 (dd, *J* = 14.2, 5.6 Hz, 1H), 3.21 (dd, *J* = 14.5, 8.0 Hz, 1H), 3.33 (s, 3H), 3.69 (s, 3H), 4.17 (t, *J* = 7.1 Hz, 1H), 4.70 (dd, *J* = 7.7, 3.6 Hz, 1H), 5.36 (dd, *J* = 10.5, 5.2 Hz, 1H), 6.80 (d, *J* = 7.8 Hz, 1H), 6.89 (s, 1H), 7.65 (d, *J* = 7.9 Hz, 1H). **^{13}C NMR** (126 MHz, $CDCl_3$) δ 26.1, 52.3, 81.5, 156.1.

Minor rotamer: **^{1}H NMR** (500 MHz, $CDCl_3$) δ -0.19 – -0.11 (m, 1H), -0.04 (s, 3H), -0.02 (s, 3H), 0.45 (d, *J* = 6.7 Hz, 3H), 0.83 (s, 9H), 2.97 (s, 3H), 3.28 (s, 3H), 3.68 (s, 4H), 4.25 – 4.30 (m, 1H), 5.62 (d, *J* = 7.4 Hz, 1H), 6.76 (d, *J* = 7.5 Hz, 1H), 6.89 (s, 1H), 7.87 (d, *J* = 6.7 Hz, 1H).). **^{13}C NMR** (126 MHz, $CDCl_3$) δ 26.0, 52.2, 81.3, 156.8.

HRMS (ESI) calcd for $C_{55}H_{86}N_7O_{11}Si^+$ $(M+H)^+$: 1048.6149; found: 1048.6149.

methyl *N*-(((2*R*,3*S*)-2-((*R*)-2-((2*R*,4*S*)-2-((*R*)-2-((*R*)-2-((((9*H*-fluoren-9-yl)methoxy)carbonyl)amino)pent-4-ynamido)-*N*-methyl-3-(1-methyl-1*H*-indol-3-yl)propanamido)-5-((*tert*-butyldimethylsilyl)oxy)-4-methylpentanamido)propanamido)-3-methoxy-3-phenylpropanoyl)-D-valyl)-*N*-methyl-D-leucinate (SI-18a)

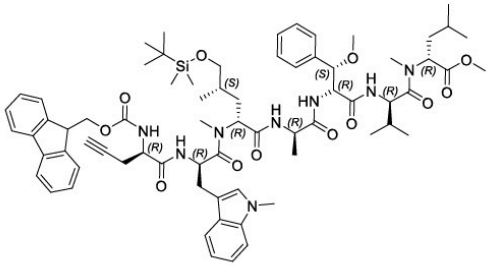

Prepared according to *GP2* and *GP4*: **SI-20** (511 mg, 487 µmol), DMBA (228 mg, 1.46 mmol), $Pd(PPh_3)_4$ (16.9 mg, 14.6 µmol) (1 h); Fmoc-D-Pra-OH (212 mg, 633 µmol), NMM (134 µl, 1.22 mmol), HOBt (104 mg, 682 µmol), EDC (131 mg, 682 µmol) (16 h). Flash chromatography (CyH/EtOAc 100:0 – 20:80) followed by lyophilization yielded **SI-18a** (403 mg, 310 µmol, 64%, 99% purity) as a yellow foam. R_f = 0.23 (PE/EtOAc 3:7).

$[\alpha]_{20}^{D}$ = +49.4 (c 0.5, $CHCl_3$).

^{1}H NMR ($CDCl_3$, 500 MHz) *(mixture of rotamers, ratio ~2:1)* δ -0.03 (s, 0.6H), -0.01 (s, 0.6H), 0.01 – 0.07 (m, 4.7H), 0.52 (d, *J* = 6.7 Hz, 0.5H), 0.85 (s, 2.0H), 0.88 (s, 6.6H), 0.89 – 0.97 (m, 11.2H), 0.99 (d, *J* = 6.8 Hz, 2.7H), 1.21 – 1.30 (m, 3.7H), 1.33 (d, *J* = 7.1 Hz, 0.5H), 1.43 – 1.53 (m, 2.2H), 1.62 – 1.81 (m, 2.3H), 1.93 – 2.00 (m, 0.7H), 2.02 (t, *J* = 2.3 Hz, 0.8H), 2.08 – 2.18 (m, 1.3H), 2.21 – 2.33 (m, 1.0H), 2.53 – 2.69 (m, 1.5H), 2.74 (s, 0.6H), 2.80 (s, 1.7H), 2.94 – 2.98 (m, 2.3H), 3.00 (s, 0.7H), 3.10 – 3.18 (m, 0.9H), 3.28 (m, 0.9H), 3.31 – 3.35 (m, 2.6H), 3.39 – 3.45 (m, 1.3H), 3.65 – 3.71 (m, 5.2H), 4.19 – 4.25 (m, 0.9H), 4.27 (t, *J* = 7.1 Hz, 1H), 4.31 – 4.47 (m, 2.7H), 4.66 – 4.72 (m, 1.1H), 4.74 – 4.84 (m, 1.7H), 4.85 (d, *J* = 4.3 Hz, 0.7H), 5.00 – 5.07 (m, 0.2H), 5.21 – 5.29 (m, 0.6H), 5.29 – 5.38 (m, 0.9H), 5.52 – 5.60 (m, 0.4H), 5.63 (d, *J* = 8.4 Hz, 0.2H), 6.38 (d, *J* = 7.1 Hz, 0.5H), 6.75 (d, *J* = 7.3 Hz, 0.2H), 6.86 – 6.90 (m, 1.0H), 7.06 – 7.13 (m, 1.0H), 7.16 – 7.22 (m, 2.0H), 7.22 – 7.26 (m, 2.9H), 7.27 – 7.34 (m, 4.5H), 7.36 – 7.42 (m,

1.8H), 7.43 – 7.49 (m, 1.1H), 7.51 – 7.56 (m, 0.8H), 7.56 – 7.63 (m, 1.7H), 7.65 – 7.71 (m, 1.6H), 7.74 – 7.78 (m, 1.7H).

^{13}C NMR (126 MHz, $CDCl_3$) *(mixture of rotamers)* δ -5.3, 14.3, 16.0, 17.4, 17.5, 18.0, 18.5, 19.6, 21.5, 21.6, 23.1, 23.4, 24.9, 26.05, 26.10, 28.6, 31.4, 31.5, 32.3, 32.8, 37.0, 47.2, 49.6, 50.5, 52.3, 53.1, 54.2, 54.6, 57.5, 57.7, 58.3, 60.5, 67.3, 67.4, 72.0, 79.2, 81.5, 108.5, 109.5, 118.8, 119.4, 120.1, 121.9, 125.3, 127.2, 127.9, 128.1, 128.4, 128.5, 128.6, 128.7, 132.1, 132.2, 132.3, 133.0, 136.9, 137.0, 141.4, 143.9, 144.0, 155.8, 168.5, 168.6, 169.5, 170.3, 171.8, 172.1, 172.1, 172.4.

Selected diagnostic peaks:

Major rotamer: **^{1}H NMR** (500 MHz, $CDCl_3$) δ 0.03 (s, 3H), 0.03 (s, 3H), 0.88 (s, 9H), 2.01 – 2.03 (m, 1H), 2.80 (s, 3H), 2.97 (s, 3H), 3.33 (s, 3H), 3.68 (s, 3H), 4.22 (t, *J* = 7.1 Hz, 1H), 4.70 (dd, *J* = 7.6, 4.4 Hz, 1H), 5.56 (bs, 1H), 6.89 (s, 1H). **^{13}C NMR** (126 MHz, $CDCl_3$) δ 26.05, 81.5, 155.8.

Minor rotamer: **^{1}H NMR** (500 MHz, $CDCl_3$) δ -0.03 (s, 3H), -0.01 (s, 3H), 0.52 (d, *J* = 6.7 Hz, 3H), 1.33 (d, *J* = 7.1 Hz, 3H), 1.93 – 1.95 (m, 1H), 2.74 (s, 3H), 2.95 (s, 3H), 3.28 (s, 3H), 3.66 (s, 3H), 4.27 (t, *J* = 7.1 Hz, 1H), 5.63 (d, *J* = 8.4 Hz, 1H), 6.75 (d, *J* = 7.3 Hz, 1H), 6.87 (s, 1H). **^{13}C NMR** (126 MHz, $CDCl_3$) δ 26.05, 79.2.

HRMS (ESI) calcd for $C_{71}H_{97}N_8O_{12}Si^+$ $(M+H)^+$: 1281.6990; found: 1281.6965.

(3*R*,6*R*,9*R*,12*R*,15*R*,18*R*,21*R*)-21-((*S*)-3-hydroxy-2-methylpropyl)-9-isobutyl-12-isopropyl-15-((*S*)-methoxy(phenyl)methyl)-1,10,18-trimethyl-3-((1-methyl-1*H*-indol-3-yl)methyl)-6-(prop-2-yn-1-yl)-1,4,7,10,13,16,19-heptaazacyclohenicosane-2,5,8,11,14,17,20-heptaone (10a)

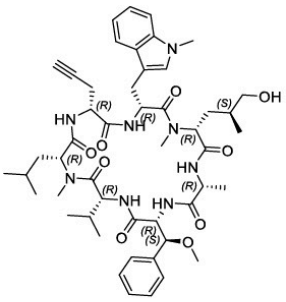

Prepared according to modified *GP6b*: **SI-18a** (200 mg, 156 µmol), tris(2-aminoethyl)amine (234 µl, 1.56 mmol) (2 h); 1 M LiOH (328 µl, 328 µmol) (3 h); PyAOP (285 mg, 546 µmol), DIPEA (123 µl, 702 µmol) (addition over 4 h, additional 18 h); Deprotection: Crude cyclic peptide was dissolved in THF (3.0 ml)/H_2O (0.15 ml), pTosOH (35.6 mg, 187 µmol) was added at 0 °C. After 16 h, the mixture was quenched with sat. $NaHCO_3$ soln., extracted with EtOAc (3x). The combined org phases were dried (Na_2SO_4) and evaporated. RP flash chromtography (H_2O/MeCN 90:10 – 5:95) followed by prep HPLC (H_2O/MeCN 80:20 – 5:95) and lyophilization afforded **10a** (65.4 mg, 71.6 µmol, 46%) as a white amorphous solid.

$[\alpha]_{20}^{D}$ = +105.8 (c 0.5, $CHCl_3$).

^{1}H NMR (500 MHz, $CDCl_3$) δ -0.54 – -0.45 (m, 1H), 0.28 (d, *J* = 6.7 Hz, 3H), 0.70 – 0.77 (m, 1H), 0.92 (d, *J* = 6.7 Hz, 3H), 0.94 – 0.98 (m, 6H), 1.05 (d, *J* = 6.7 Hz, 3H), 1.07 – 1.12 (m, 1H), 1.25 (d, *J* = 7.3 Hz, 3H), 1.28 – 1.38 (m, 2H), 1.50 – 1.58 (m, 1H), 1.70 – 1.78 (m, 1H), 1.84 – 1.91 (m, 1H), 2.20 – 2.31 (m, 2H), 2.36 – 2.39 (m, 1H), 2.58 (s, 3H), 2.90 – 2.98 (m, 4H), 2.99 – 3.06 (m, 1H), 3.21 (dd, *J* = 13.6, 4.9 Hz, 1H), 3.32 – 3.37 (m, 4H), 3.73 (s, 3H), 4.33 (dd, *J* = 10.5, 2.8 Hz, 1H), 4.51 (t, *J* = 9.2 Hz, 1H), 4.71 – 4.80 (m, 3H), 4.91 – 4.99 (m, 2H), 5.06 (d, *J* = 5.3 Hz, 1H), 6.87 (s, 1H), 7.10 (ddd, *J* = 8.1, 6.9, 1.1 Hz, 1H), 7.12 – 7.18 (m, 2H), 7.18 – 7.25 (m, 1H), 7.26 – 7.33 (m, 5H), 7.48 (d, *J* = 7.9 Hz, 1H), 7.88 (d, *J* = 11.0 Hz, 1H), 8.09 (d, *J* = 8.5 Hz, 1H), 8.23 – 8.29 (m, 1H), 8.48 (d, *J* = 10.2 Hz, 1H).

^{13}C NMR (126 MHz, $CDCl_3$) δ 17.3, 19.4, 20.0, 21.1, 22.3, 22.7, 23.7, 25.4, 28.7, 29.2, 29.4, 30.8, 31.8, 32.9, 33.3, 39.0, 50.8, 51.3, 52.0, 55.1, 56.2, 57.9, 59.0, 59.4, 65.9, 72.3, 80.2, 107.7, 109.8, 118.7, 119.8, 122.4, 127.7, 128.0, 128.4, 128.6, 129.3, 135.1, 137.0, 168.6, 169.4, 170.2, 170.5, 170.7, 171.2, 171.8.

HRMS (ESI) calcd for $C_{49}H_{69}N_8O_9$ $(M+H)^+$: 913.5182; found: 913.5141.

(3*R*,3'*R*,6*R*,6'*R*,9*R*,9'*R*,12*R*,12'*R*,15*R*,15'*R*,18*R*,18'*R*,21*R*,21'*R*)-18,18'-((pentane-1,5-diylbis(1*H*-1,2,3-triazole-1,4-diyl))bis(methylene))bis(12-((*S*)-3-hydroxy-2-methylpropyl)-21-isobutyl-3-isopropyl-6-((*S*)-methoxy(phenyl)methyl)-1,9,13-trimethyl-15-((1-methyl-1*H*-indol-3-yl)methyl)-1,4,7,10,13,16,19-heptaazacyclohenicosane-2,5,8,11,14,17,20-heptaone) (12a) (UdSBI-0117)

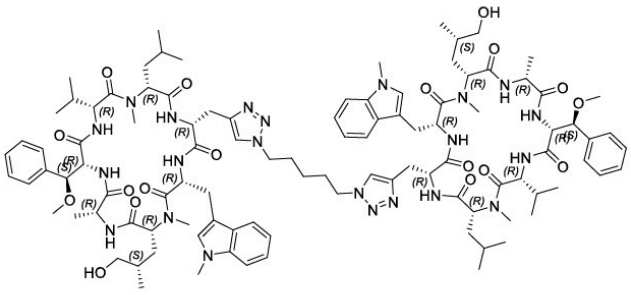

Prepared according to *GP7*: **10a** (20.6 mg, 22.6 µmol), 1,5-diazidopentane (1.74 mg, 11.3 µmol), 1 M $CuSO_4$ (9.02 µl, 9.02 µmol), 1 M sodium ascorbate (15.8 µl, 15.8 µmol) (16 h). RP flash chromatography (H_2O/MeCN 90:10 – 5:95) followed by prep HPLC (H_2O/MeCN 75:25 – 5:95) and lyophilization afforded **12a** (15.7 mg, 6.34 µmol, 56%, 80% purity) as a white amorphous solid.

$[\alpha]_{20}^{D}$ = +99.1 (c 0.5, $CHCl_3$).

^{1}H NMR (500 MHz, $CDCl_3$) δ -0.40 – -0.32 (m, 2H), 0.28 (d, *J* = 6.8 Hz, 6H), 0.87 – 0.93 (m, 2H), 0.96 – 0.98 (m, 8H), 1.04 – 1.10 (m, 18H), 1.28 – 1.32 (m, 8H), 1.51 – 1.64 (m, 4H), 1.88 – 1.99 (m, 4H), 2.00 – 2.09 (m, 2H), 2.09 – 2.18 (m, 2H), 2.19 – 2.29 (m, 4H), 2.61 (s, 6H), 2.68 – 2.74 (m, 2H), 2.86 (s, 6H), 2.91 – 2.98 (m, 2H), 3.03 – 3.08 (m, 2H), 3.08 – 3.13 (m, 2H), 3.26 – 3.29 (m, 2H), 3.32 (s, 6H), 3.71 (s, 6H), 4.36 – 4.46 (m, 4H), 4.59 – 4.66 (m, 4H), 4.73 – 4.78 (m, 2H), 4.79 – 4.87 (m, 4H), 4.89 – 4.94 (m, 2H), 4.94 – 5.02 (m, 2H), 5.13 (d, *J* = 5.4 Hz, 2H), 6.86 (s, 2H), 6.91 – 7.03 (m, 6H), 7.05 – 7.12 (m, 8H), 7.17 – 7.22 (m, 2H), 7.33 (s, 2H), 7.44 – 7.51 (m, 4H), 8.12 (d, *J* = 8.7 Hz, 2H), 8.24 (d, *J* = 9.3 Hz, 2H), 8.62 (d, *J* = 5.4 Hz, 2H), 8.67 (d, *J* = 9.9 Hz, 2H).

^{13}C NMR (126 MHz, $CDCl_3$) δ 17.3, 19.4, 20.0, 21.1, 22.9, 23.5, 23.7, 25.1, 28.0, 28.8, 28.97, 29.02, 29.5, 31.0, 32.1, 32.8, 33.2, 39.1, 50.1, 51.0, 51.1, 51.9, 54.9, 56.3, 57.9, 58.9, 59.5, 66.0, 80.0, 108.7, 109.7, 118.8, 119.5, 122.3, 122.8, 127.7, 128.2, 128.35, 128.44, 129.1, 135.5, 137.0, 142.2, 167.6, 169.7, 170.1, 170.8, 171.3, 171.5, 172.3.

HRMS (ESI) calcd for $C_{103}H_{147}N_{22}O_{18}$ $(M+H)^+$: 1980.1258; found: 1980.1195.

Synthesis of exit vector 3 triazole-based Homo-BacPROTACs (SI-39, SI-40)

(2*S*,4*R*)-5-[(*tert*-butyldimethylsilyl)oxy]-2-({[(9H-fluoren-9-yl)methoxy]carbonyl}(methyl)amino)-4-methylpentanoic acid (SI-21)

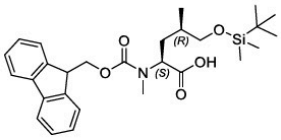

The Cbz-amino acid was deprotected according to modified *GP1*: (2*S*,4*R*)-2-(((benzyloxy)carbonyl)(methyl)amino)-5-((tert-butyldimethylsilyl)oxy)-4-methylpentanoic acid (5.00 g, 12.2 mmol), Pd/C (8.80 g), toluene (125 ml, 0.1 M) (6 h); The resulting free amino acid (4.00 g, 14.5 mmol) was dissolved in a mixture of 1,4-dioxane (15.0 ml) and water (5.0 ml) (0.73 M) and cooled to 0°C. Then sodium bicarbonate (1.46 g, 17.4 mmol) and Fmoc-Cl (3.94 g, 15.2 mmol) were added and the mixture was stirred at 0 °C for 10 minutes before it was allowed to reach rt. After 16 h, TLC indicated full conversion. The reaction mixture was diluted with EtOAc and water, the layers were separated and the aqueous layer was extracted with EtOAc (3x). The combined organic layers were washed with brine, dried ($MgSO_4$) and concentrated in vacuo. Reverse phase column chromatography (40-100% MeCN in water) yielded **SI-21** (3.50 g, 7.03 mmol, 48%) as a colorless gum, which was stored at 4 °C.

$[\alpha]_{20}^{D}$ = −12.1 (c 1.0, $CHCl_3$).

Major rotamer: **^{1}H NMR** (500 MHz, DMSO-d_6) δ -0.01 (s, 6H), 0.81 – 0.89 (m, 9H), 0.88 (d, *J* = 6.8 Hz, 3H), 1.36 – 1.46 (m, 1H), 1.46 – 1.56 (m, 1H), 1.89 (ddd, *J* = 14.1, 9.1, 4.7 Hz, 1H), 2.71 (s, 3H), 3.42 – 3.46 (m, 1H), 4.26 – 4.41 (m, 2H), 4.61 (dd, *J* = 11.1, 4.7 Hz, 1H), 7.27 – 7.36 (m, 2H), 7.39 – 7.43 (m, 2H), 7.58 – 7.67 (m, 2H), 7.86 – 7.92 (m, 2H).

^{13}C NMR (126 MHz, DMSO-d_6) δ -5.5, -5.4, 17.6, 18.0, 25.8, 25.9, 30.0, 31.9, 46.7, 46.7, 56.1, 65.7, 66.8, 120.2, 125.0, 127.1, 127.7, 140.8, 143.7, 143.9, 156.1, 172.9.

Minor rotamer (selected signals): **^{1}H NMR** (500 MHz, DMSO-d_6) δ 0.00 (s, 6H), 2.76 (s, 3H), 4.19 – 4.24 (m, 1H), 4.53 (dd, *J* = 9.9, 5.1 Hz, 1H). **^{13}C NMR** (126 MHz, DMSO-d_6) δ 17.2, 31.1, 56.4, 66.1, 155.7.

HRMS (ESI) calcd for $C_{28}H_{40}NO_5Si^+$ $(M+H)^+$: 498.2670; found: 498.2650.

***tert*-butyl *N*-[(1*R*,2*R*)-1,3-dihydroxy-1-(4-nitrophenyl)propan-2-yl]carbamate (SI-22)**

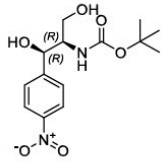

To a stirred solution of (1*R*,2*R*)-2-Amino-1-(4-nitro-phenyl)-propane-1,3-diol (75.0 g, 353 mmol) in MeOH (200 ml, 1.8 M) was added Boc-anhydride (89.3 ml, 389 mmol) slowly at 0° C. The mixture was stirred at 0-5 °C. After 4 h, TLC indicated complete conversion. The solvent was evaporated in vacuo, the crude was dried in high vacuum to yield **SI-22** (110 g, 352 mmol, quant.) which was used in the next step without further purification.

^{1}H NMR (400 MHz, DMSO-d_6) δ 1.05 (br s, 1.35H, rotamer), 1.21 (s, 7.65H, rotamer), 3.32 – 3.26 (m, 1H), 3.53 (dt, *J* = 10.5, 6.7 Hz, 1H), 3.73 – 3.61 (m, 1H), 4.76 (br t, *J* = 5.2 Hz, 1H), 4.94 (br s, 1H), 5.58 (br s, 1H), 5.76 (br d, *J* = 9.4 Hz, 0.15H, rotamer), 6.15 (d, *J* = 9.4 Hz, 0.85H, rotamer), 7.56 (d, *J* = 8.6 Hz, 2H), 8.17 (d, *J* = 8.6 Hz, 2H).

^{13}C NMR (101 MHz, DMSO-d_6) δ 27.6, 28.0, 57.5, 58.8, 60.7, 61.0, 69.9, 77.6, 122.8, 127.4, 146.3, 152.0, 152.4, 155.1.

MS calcd for $C_{10}H_{13}N_2O_6$ $(M - C_4H_9 + 2H)^+$: 257.08; found: 257.03.

The spectroscopic data are in agreement with previously published results.[15]

***tert*-butyl *N*-[(1*R*,2*R*)-3-[(*tert*-butyldimethylsilyl)oxy]-1-hydroxy-1-(4-nitrophenyl)propan-2-yl]carbamate (SI-23)**

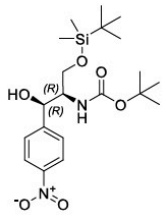

To a stirred solution of crude *tert*-butyl ((1*R*,2*R*)-1,3-dihydroxy-1-(4-nitrophenyl)propan-2-yl)carbamate (100 g, 320 mmol) in DMF (120 ml, 2.7 M) were added imidazole (54.5 g, 800 mmol) and TBDMS-Cl (106 g, 704 mmol) at 0°C. The mixture was stirred at rt. After 4 h, TLC indicated complete conversion. The mixture was diluted with EtOAc and water, the aqueous layer was extracted with EtOAc (3x). The combined organic layers were washed with brine, dried (Na_2SO_4) and concentrated in vacuo. Silica gel column chromatography (20% EtOAc in petroleum ether) yielded **SI-23** (107 g, 251 mmol, 78%).

^{1}H NMR (400 MHz, DMSO-d_6) δ 0.05 (s, 6H), 0.87 (s, 9H), 1.05 (br s, 1.8H, rotamer), 1.22 (s, 7.2H, rotamer), 3.57 – 3.40 (m, 1H), 3.81 – 3.59 (m, 2H), 4.90 (dd, *J* = 5.2, 2.2 Hz, 1H), 5.63 (d, *J* = 5.3 Hz, 1H), 5.88 (br d, *J* = 9.4 Hz, 0.2H, rotamer), 6.23 (br d, J = 8.9 Hz, 0.8H, rotamer), 7.56 (br d, *J* = 8.6 Hz, 2H), 8.18 (d, *J* = 8.6 Hz, 2H).

^{13}C NMR (101 MHz, DMSO-d_6) δ -5.4, 17.9, 25.8, 27.6, 28.0, 57.5, 58.9, 62.3, 62.9, 69.9, 77.6, 122.8, 127.4, 146.4, 151.7, 155.1.

MS calcd for $C_{20}H_{35}N_2O_6Si$ $(M+H)^+$: 427.23; found: 427.40.

The spectroscopic data are in agreement with previously published results.[11]

***tert*-Butyl *N*-[(1*R*,2*R*)-3-[(*tert*-butyldimethylsilyl)oxy]-1-methoxy-1-(4-nitrophenyl)propan-2-yl]carbamate (SI-24)**

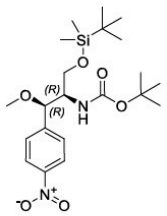

To a stirred solution of **SI-23** (50.0 g, 117 mmol) in DMF (500 ml, 0.23 M) was added LiHMDS (1 M in THF) (129 ml, 129 mmol) at −15 °C. After 10 minutes, iodomethane (7.30 ml, 117 mmol) was added. The mixture was stirred at −15 °C. After 45 minutes, TLC indicated complete conversion. The reaction was quenched with water and extracted with EtOAc (3x). The combined organic layers were washed 1N $KHSO_4$, sat. $NaHCO_3$ and brine, dried (Na_2SO_4) and concentrated in vacuo. Silica gel column chromatography (20% EtOAc in petroleum ether) yielded **SI-24** (40.0 g, 90.8 mmol, 78%) as a colorless oil.

^{1}H NMR (400 MHz, DMSO-d_6) δ 0.03 (s, 6H), 0.87 (s, 9H), 1.03 (br s, 1.8H, rotamer), 1.23 (s, 7.2H, rotamer), 3.17 (s, 3H), 3.54 – 3.36 (m, 1H), 3.77 – 3.56 (m, 2H), 4.51 (d, *J* = 3.3 Hz, 1H), 6.24 (br d, *J* = 7.9 Hz, 0.2H, rotamer), 6.60 (br d, *J* = 8.4 Hz, 0.8H, rotamer), 7.53 (d, *J* = 8.4 Hz, 2H), 8.21 (d, *J* = 8.6 Hz, 2H).

^{13}C NMR (101 MHz, DMSO-d_6) δ -5.5, -5.4, 17.9, 25.7, 27.6, 28.0, 57.0, 61.9, 77.6, 80.5, 123.2, 128.3, 146.9, 147.6, 155.1.

MS calcd for $C_{17}H_{29}N_2O_6Si^+$ $(M - C_4H_9 + 2H)^+$: 385.18; found: 385.36

The spectroscopic data are in agreement with previously published results.[12]

***tert*-butyl *N*-[(1*R*,2*R*)-3-hydroxy-1-methoxy-1-(4-nitrophenyl)propan-2-yl]carbamate (SI-25)**

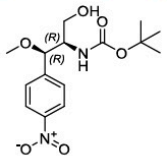

To a stirred solution of **SI-24** (50.0 g, 113 mmol) in THF (300 ml, 0.38 M) was added TBAF (32.6 g, 125 mmol) at 0 °C. The mixture was stirred at rt. After 2 h, TLC indicated complete conversion. The reaction was quenched with cold water and extracted with EtOAc (2x). The combined organic layers were dried (Na_2SO_4) and concentrated in vacuo. Silica gel column chromatography (35% EtOAc in petroleum ether) yielded **SI-25** (31.0 g, 95.0 mmol, 84%).

^{1}H NMR (400 MHz, DMSO-d_6) δ 1.05 (br s, 1.2H, rotamer), 1.24 (s, 7.2H, rotamer), 3.18 (s, 3H), 3.23 (br dd, J = 10.9, 5.3 Hz, 1H), 3.54 – 3.43 (m, 1H), 3.69 – 3.55 (m, 1H), 4.55 (d, *J* = 3.8 Hz, 1H), 4.77 (t, *J* = 5.1 Hz, 0.8H, rotamer), 4.83 (br s, 0.2H, rotamer), 6.08 (d, *J* = 8.4 Hz, 0.2H, rotamer), 6.45 (d, *J* = 9.1 Hz, 0.8H, rotamer), 7.53 (d, *J* = 8.4 Hz, 2H), 8.20 (d, *J* = 8.6 Hz, 2H).

^{13}C NMR (101 MHz, DMSO-d_6) δ 27.6, 28.0, 57.1, 58.4, 60.4, 60.6, 77.6, 80.4, 123.1, 128.2, 146.8, 148.1, 155.1.

MS calcd for $C_{15}H_{23}N_2O_6^+$ $(M+H)^+$: 327.16; found: 327.17.

The spectroscopic data are in agreement with previously published results.[12]

(2*S*,3*R*)-2-{[(*tert*-butoxy)carbonyl]amino}-3-methoxy-3-(4-nitrophenyl)propanoic acid (SI-26)

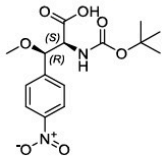

A stirred solution of **SI-25** (30.0 g, 91.9 mmol) in MeCN (30.0 ml) and 2N NaH_2PO_4 buffer (30.0 ml) (1.5 M) was cooled to 0 °C and (diacetoxyiodo)benzene (2.96 g, 9.2 mmol), TEMPO (2.87 g, 18.3 mmol) and $NaClO_2$ (29.0 g, 320 mmol) were added. The mixture was stirred at rt. After 2 h, TLC indicated complete conversion. The reaction was quenched with 2 M aq. Na_2CO_3 and washed with diethyl ether. The aqueous layer was acidified with 1 N aq. HCl and extracted with EtOAc (3x). The combined EtOAc layers were dried (Na_2SO_4) and concentrated in vacuo to yield crude **SI-26** (25.0 g, 73.5 mmol, 80%) which was used in the next step without further purification.

^{1}H NMR (500 MHz, DMSO-d_6) δ 0.95 (br s, 1.8H, rotamer), 1.20 (s, 7.2H, rotamer), 3.14 (s, 3H), 3.79 (d, *J* = 7.3 Hz, 1H), 3.85 (dd, *J* = 8.7, 2.0 Hz, 1H), 4.91 (d, *J* = 2.5 Hz, 1H), 5.40 (d, *J* = 7.3 Hz, 0.2H, rotamer), 5.79 (d, *J* = 8.5 Hz, 0.8H, rotamer), 7.54 (d, *J* = 8.5 Hz, 2H), 8.15 (d, *J* = 8.5 Hz, 1.6H, rotamer), 8.21 (d, *J* = 7.6 Hz, 0.4H, rotamer).

^{13}C NMR (126 MHz, DMSO-d_6) δ 27.5, 28.0, 57.2, 59.9, 61.1, 77.6, 83.0, 83.2, 122.9, 123.0, 128.1, 146.6, 148.4, 148.9, 154.0, 154.8, 170.7, 170.9.

MS calcd for $C_{11}H_{13}N_2O_7^+$ $(M - C_4H_9 + 2H)^+$: 285.07; found: 285.04.

The spectroscopic data are in agreement with previously published results.[12]

Methyl (2*S*,3*R*)-2-{[(*tert*-butoxy)carbonyl]amino}-3-methoxy-3-(4-nitrophenyl)propanoate (SI-27)

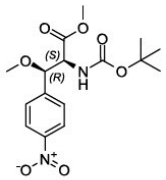

To a stirred solution of **SI-26** (35.0 g, 103 mmol) in DMF (300 ml, 0.34 M) were added potassium carbonate (28.4 g, 206 mmol) and iodomethane (9.61 ml, 154 mmol) at 0°C. The mixture was stirred at rt. After 2 h, TLC indicated complete conversion. The reaction was quenched with cold water and extracted with EtOAc (2x). The combined organic layers were dried (Na_2SO_4) and concentrated in vacuo. Silica gel column chromatography (15% EtOAc in petroleum ether) yielded **SI-27** (30.0 g, 84.7 mmol, 82%).

^{1}H NMR (500 MHz, DMSO-d_6) δ 1.11 (br s, 1H), 1.23 (s, 8H), 3.17 (s, 3H), 3.61 (s, 3H), 4.34 – 4.27 (m, 0.15H, rotamer), 4.40 (dd, *J* = 9.1, 4.4 Hz, 0.85H, rotamer), 4.82 (d, *J* = 3.2 Hz, 0.15H, rotamer), 4.88 (d, *J* = 4.4 Hz, 0.85H, rotamer), 6.80 (d, *J* = 8.5 Hz, 0.15H, rotamer), 7.19 (d, *J* = 9.1 Hz, 0.85H, rotamer), 7.63 (d, *J* = 8.5 Hz, 1H), 8.22 (d, *J* = 8.5 Hz, 2H).

^{13}C NMR (126 MHz, DMSO-d_6) δ 27.5, 27.9, 52.1, 57.2, 58.9, 60.2, 78.4, 81.3, 123.2, 128.5, 145.6, 147.2, 147.3, 153.6, 155.3, 170.1.

MS calcd for $C_{12}H_{15}N_2O_7^+$ $(M - C_4H_9 + 2H)^+$: 299.09; found: 299.05.

Methyl (2*S*,3*R*)-3-(4-aminophenyl)-2-{[(*tert*-butoxy)carbonyl]amino}-3-methoxypropanoate (SI-28)

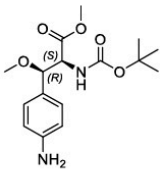

To a solution of **SI-27** (30.0 g, 84.7 mmol) in THF (300 ml, 0.28 M) was added 10 wt% Pd/C (9.0 g, 8.5 mmol). The mixture was stirred at rt under H_2 atmosphere (balloon pressure). After 5 h, TLC indicated complete conversion. Subsequently, the mixture was filtered over Celite and the filtrate was evaporated in vacuo. Silica gel column chromatography (5% MeOH in DCM) yielded **SI-28** (22.0 g, 67.8 mmol, 80%) as a colorless oil.

^{1}H NMR (500 MHz, DMSO-d_6) δ 1.23 (br s, 1.35H, rotamer), 1.34 (s, 7.65H, rotamer), 3.04 (s, 3H), 3.45 (s, 3H), 4.03 (br d, J = 6.0 Hz, 0.15H, rotamer), 4.13 – 4.06 (m, 0.85H, rotamer), 4.27 (br d, J = 5.4 Hz, 0.15H, rotamer), 4.31 (d, J = 6.3 Hz, 0.85H, rotamer), 5.07 (s, 2H), 6.50 (d, J = 8.2 Hz, 2H), 6.61 (br d, J = 6.9 Hz, 0.15H, rotamer), 6.91 (d, J = 8.5 Hz, 2H), 7.00 (d, J = 8.2 Hz, 0.85H, rotamer).

^{13}C NMR (126 MHz, DMSO-d_6) δ 27.7, 28.1, 51.6, 55.9, 60.0, 61.3, 78.3, 78.5, 81.8, 81.9, 113.5, 123.6, 123.8, 127.9, 148.6, 154.1, 155.4, 170.9.

MS calcd for $C_{11}H_{13}N_2O_4^+$ (M – C_4H_9 – OCH_3 + H)$^+$: 237.09; found: 237.28.

Methyl (2*S*,3*R*)-3-(4-bromophenyl)-2-{[(*tert*-butoxy)carbonyl]amino}-3-methoxypropanoate (SI-29)

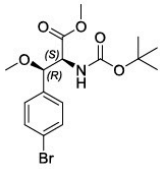

To a stirred solution of **SI-28** (15.0 g, 46.2 mmol) in DCM (75.0 ml, 0.28 M) was added bromotrichloromethan (18.3 g, 92.4 mmol) at 0 °C. After 15 minutes, sodium nitrite (16.0 g, 231 mmol), dissolved in water (75.0 ml), was added. After 10 minutes, acetic acid (55.5 g, 925 mmol) was added at 0°C. The mixture was stirred at rt. After 2 h, TLC indicated complete conversion. The reaction was quenched with water and extracted with DCM (2x). The combined organic layers were dried (Na_2SO_4) and concentrated in vacuo. Silica gel column chromatography (20% EtOAc in petroleum ether) yielded **SI-29** (15.0 g, 38.6 mmol, 84%).

^{1}H NMR (500 MHz, DMSO-d_6) δ 1.15 (br s, 1.35H, rotamer), 1.28 (s, 7.65H, rotamer), 3.12 (s, 3H), 3.56 (s, 3H), 4.20 (d, *J* = 4.7 Hz, 0.15H, rotamer), 4.27 (dd, *J* = 8.8, 5.0 Hz, 0.85H, rotamer), 4.60 (br d, *J* = 4.1 Hz, 0.15H, rotamer), 4.64 (d, *J* = 5.0 Hz, 0.85H, rotamer), 6.71 (d, *J* = 8.2 Hz, 0.15H, rotamer), 7.12 (d, *J* = 8.8 Hz, 0.85H, rotamer), 7.28 (d, *J* = 8.2 Hz, 1H), 7.54 (d, *J* = 8.5 Hz, 1H).

^{13}C NMR (126 MHz, DMSO-d_6) δ 27.6, 28.0, 51.9, 56.8, 59.3, 60.5, 78.4, 81.3, 121.1, 129.4, 131.0, 137.0, 153.7, 155.3, 170.4.

MS calcd for $C_{12}H_{15}BrNO_5^+$ (M – C_4H_9 +2H)$^+$: 332.01, found: 331.98.

Methyl (2*S*,3*R*)-2-{[(*tert*-butoxy)carbonyl]amino}-3-methoxy-3-[4-(4,4,5,5-tetramethyl-1,3,2-dioxaborolan-2-yl)phenyl]propanoate (SI-29a)

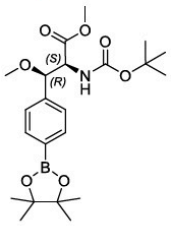

A stirred solution of **SI-29** (10.0 g, 25.8 mmol) in 1,4-Dioxane (100 ml, 0.26 M) was degassed with Argon and bis(pinacolato)diboron (7.85 g, 30.9 mmol), potassium acetate (7.57 g, 77.2 mmol) and tetrakis(triphenylphosphine)palladium (1.49 g, 1.29 mmol) were added. The mixture was stirred at 110°C. After 12 h, TLC indicated complete conversion. The reaction was quenched with water and extracted with EtOAc (2x). The combined organic layers were dried (Na_2SO_4) and concentrated in vacuo. Silica gel column chromatography (20% EtOAc in petroleum ether) yielded **SI-29a** (8.00 g, 18.4 mmol, 71%).

^{1}H NMR (500 MHz, $CDCl_3$) δ 1.32 (s, 9H), 1.33 (s, 12H), 3.25 (s, 3H), 3.76 (s, 3H), 4.46 (dd, *J* = 9.4, 3.0 Hz, 1H), 4.77 (d, *J* = 2.9 Hz, 1H), 5.27 (d, *J* = 9.3 Hz, 1H), 7.32 (d, *J* = 7.9 Hz, 2H), 7.80 (d, *J* = 7.9 Hz, 2H).

MS calcd for $C_{22}H_{35}BNO_7^+$ $(M+H)^+$: 436.25; found: 436.27.

No ^{13}C NMR data was obtained for this compound.

Methyl (2*S*,3*R*)-2-{[(*tert*-butoxy)carbonyl]amino}-3-(4-hydroxyphenyl)-3-methoxypropanoate (SI-30)

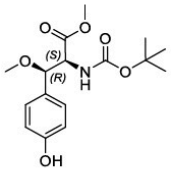

To a stirred solution of **SI-29a** (10.0 g, 23.0 mmol) in THF (100 ml, 0.23 M) was added 30% H_2O_2 (30 ml, 265 mmol) at 0°C and the mixture was stirred at rt. After 12 h, TLC indicated complete conversion. The reaction was quenched with water and extracted with EtOAc (2x). The combined organic layers were dried (Na_2SO_4) and concentrated in vacuo. Silica gel column chromatography (20% EtOAc in petroleum ether) yielded **SI-30** (6.00 g, 18.4 mmol, 80%).

^{1}H NMR (500 MHz, DMSO-d_6) δ 1.20 (br s, 1.35H, rotamer), 1.32 (s, 7.65H, rotamer), 3.07 (s, 1H), 3.46 (s, 3H), 4.07 (t, *J* = 6.1 Hz, 0.15H, rotamer), 4.14 (dd, *J* = 8.2, 6.3 Hz, 0.85H, rotamer), 4.38 (d, *J* = 5.0 Hz, 0.15H, rotamer), 4.43 (d, *J* = 5.7 Hz, 0.85H, rotamer), 6.65 (d, *J* = 7.3 Hz, 0.15H, rotamer), 6.71 (d, *J* = 8.2 Hz, 2H), 7.05 (d, *J* = 8.5 Hz, 0.85H, rotamer), 7.08 (d, *J* = 8.5 Hz, 2H), 9.40 (br s, 1H).

^{13}C NMR (126 MHz, DMSO-d_6) δ 27.7, 28.1, 51.7, 56.2, 59.9, 61.2, 78.3, 78.5, 81.6, 81.7, 114.9, 127.3, 128.4, 153.9, 155.4, 157.2, 170.8.

MS calcd for $C_{16}H_{24}NO_6^+$ $(M+H)^+$: 326.16; found: 326.14.

Methyl (2*S*,3*R*)-2-{[(*tert*-butoxy)carbonyl]amino}-3-methoxy-3-[4-(prop-2-yn-1-yloxy)phenyl]propanoate (SI-31)

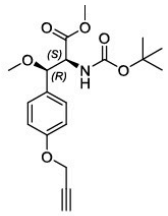

To a stirred solution of **SI-30** (5.00 g, 15.4 mmol) in DMF (8.0 ml, 1.9 M) were added potassium carbonate (2.76 g, 20.0 mmol) and propargyl bromide (2.00 g, 16.9 mmol). The mixture was stirred at rt. After 12 h, TLC indicated complete conversion. The reaction was quenched with water and extracted with EtOAc (2x). The combined organic layers were dried (Na_2SO_4) and concentrated in vacuo. Silica gel column chromatography (20% EtOAc in petroleum ether) yielded **SI-31** (4.00 g, 11.0 mmol, 72%).

^{1}H NMR (400 MHz, DMSO-d_6) δ 1.17 (br s, 1.8H, rotamer), 1.30 (s, 7.2H, rotamer), 3.09 (s, 3H), 3.49 (s, 3H), 3.53 (t, *J* = 2.4 Hz, 1H), 4.15 – 4.06 (m, 0.2H, rotamer), 4.18 (dd, *J* = 8.5, 5.7 Hz, 0.8H, rotamer), 4.49 (d, *J* = 4.6 Hz, 0.2H,

rotamer), 4.53 (d, *J* = 5.6 Hz, 0.8H, rotamer), 4.77 (d, *J* = 2.3 Hz, 2H), 6.66 (d, *J* = 7.6 Hz, 0.2H, rotamer), 6.95 (d, *J* = 8.6 Hz, 1H), 7.08 (d, *J* = 8.4 Hz, 0.8H, rotamer), 7.23 (d, *J* = 8.6 Hz, 2H).

^{13}C NMR (101 MHz, DMSO-d_6) δ 27.7, 28.2, 51.8, 55.4, 56.5, 59.8, 61.1, 78.2, 78.5, 79.3, 81.5, 114.5, 128.4, 130.0, 155.4, 157.0, 170.8.

MS cald for $C_{19}H_{26}NO_6^+$ $(M+H)^+$: 364.18; found: 364.45.

(2*S*,3*R*)-2-{[(*tert*-butoxy)carbonyl]amino}-3-methoxy-3-[4-(prop-2-yn-1-yloxy)phenyl]propanoic acid (SI-32)

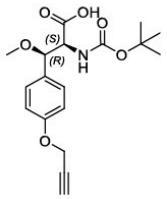

To a stirred solution of **SI-31** (5.00 g, 13.8 mmol) in THF (10.0 ml) and water (10.0 ml) (0.69 M) was added LiOH·H_2O (2.31 g, 55.2 mmol) and the mixture was stirred at rt. After 12 h, TLC indicated complete conversion. The reaction was diluted with water and washed with diethyl ether. The aqueous layer was acidified with 1 M HCl (aq.) and extracted with EtOAc (2x). The combined EtOAc layers were dried (Na_2SO_4) and concentrated in vacuo to yield **SI-32** (3.50 g, 10.0 mmol, 73%) which was used in the next step without further purification.

$[\alpha]_{20}^{D}$ = −28.1 (c 1.0, $CHCl_3$).

Major rotamer: **^{1}H NMR** (500 MHz, $CDCl_3$) δ 1.34 (s, 9H), 2.52 (t, *J* = 2.4 Hz, 1H), 3.28 (s, 3H), 4.50 (dd, *J* = 9.2, 3.0 Hz, 1H), 4.68 (d, *J* = 2.5 Hz, 2H), 4.82 (d, *J* = 3.0 Hz, 1H), 5.31 (d, *J* = 9.0 Hz, 1H), 6.94 – 7.02 (m, 2H), 7.23 – 7.28 (m, 2H). **^{13}C NMR** (126 MHz, $CDCl_3$) δ 20.9, 28.4, 55.9, 57.6, 59.1, 75.7, 78.6, 80.2, 82.0, 115.0, 128.3, 128.4, 129.9, 155.7, 157.7, 175.2.

Minor rotamer (ratio ~4:1, selected signals): **^{1}H NMR** (500 MHz, $CDCl_3$) δ 1.18 (s, 9H), 3.25 (s, 3H), 4.34 (m, 1H), 4.73 – 4.76 (m, 1H). **^{13}C NMR** (126 MHz, $CDCl_3$) δ 28.0, 60.7, 81.0, 82.4, 128.4, 177.2.

HRMS (ESI) calcd for $C_{18}H_{24}NO_6^+$ $(M+H)^+$: 350.1598; found: 350.1593.

Methyl (2*S*)-2-[(2*S*)-2-[(2*S*,3*R*)-2-{[(*tert*-butoxy)carbonyl]amino}-3-methoxy-3-[4-(prop-2-yn-1-yloxy)phenyl]propanamido]-*N*,3-dimethylbutanamido]-4-methylpentanoate (SI-33)

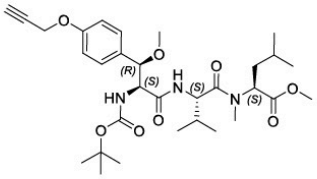

To a stirred solution of methyl *N*-(L-valyl)-*N*-methyl-L-leucinate[4] (3.00 g, 11.6 mmol) and **SI-32** (4.06 g, 11.6 mmol) in DMF (25.0 ml, 0.46 M) was added DIPEA (4.06 ml, 23.2 mmol) at 0 °C. After 10 minutes, HATU (4.86 g, 12.8 mmol) was added and the mixture was stirred at rt. After 12 h, TLC indicated complete conversion. The reaction was quenched with water and extracted with EtOAc (2x). The combined EtOAc layers were washed with brine, dried (Na_2SO_4) and concentrated in vacuo. Silica gel column chromatography (50% EtOAc in petroleum ether) yielded **SI-33** (2.90 g, 4.92 mmol, 42%).

Major rotamer: **^{1}H NMR** (400 MHz, $CDCl_3$) δ 0.91 (d, *J* = 6.5 Hz, 3H), 0.92 – 0.95 (m, 6H), 1.00 (d, *J* = 6.8 Hz, 3H), 1.34 (s, 9H), 1.41 – 1.53 (m, 1H), 1.64 – 1.82 (m, 2H), 2.05 – 2.17 (m, 1H), 2.50 (t, *J* = 2.4 Hz, 1H), 3.01 (s, 3H), 3.28 (s, 3H), 3.69 (s, 3H), 4.38 (dd, *J* = 8.3, 3.0 Hz, 1H), 4.65 (d, *J* = 2.4 Hz, 2H), 4.80 – 4.90 (m, 2H), 5.25 (d, *J* = 8.3 Hz, 1H), 5.32 (dd, *J* = 10.4, 5.4 Hz, 1H), 6.85 – 6.96 (m, 2H), 7.19 (d, *J* = 8.3 Hz, 2H), 7.29 (d, *J* = 8.9 Hz, 1H). **^{13}C NMR**

(101 MHz, $CDCl_3$) δ 17.3, 19.6, 21.5, 23.4, 25.0, 28.4, 31.5, 31.7, 37.1, 52.3, 54.1, 54.7, 55.9, 57.5, 59.8, 75.7, 78.7, 80.2, 81.5, 114.8, 128.1, 130.3, 155.5, 157.5, 169.4, 172.2, 172.3.

Minor rotamer (selected signals, ratio ~12:1): **^{1}H NMR** (400 MHz, $CDCl_3$) δ 1.31 (s, 9H), 2.81 (s, 3H), 3.24 (s, 3H), 3.61 (s, 3H), 4.27 – 4.32 (m, 1H), 5.20 (d, *J* = 9.1 Hz, 1H).

HRMS calcd for $C_{31}H_{48}N_3O_8^+$ $(M+H)^+$: 590.3436; found: .590.3450.

methyl (2S)-2-[(2S)-2-[(2S,3R)-2-[(2S)-2-{[(tert-butoxy)carbonyl]amino}propanamido]-3-methoxy-3-[4-(prop-2-yn-1-yloxy)phenyl]propanamido]-N,3-dimethylbutanamido]-4-methylpentanoate (SI-34)

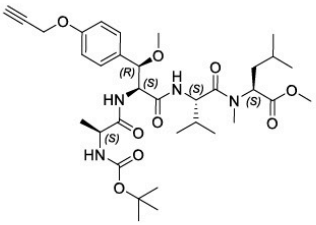

To a solution of **SI-33** (2.80 g, 4.75 mmol) in DCM (20.0 ml, 0.24 M) was added HCl (4N in dioxane) (10.0 ml) dropwise at 0°C and the mixture was allowed to reach rt and stirred for 3 h. The solvents were evaporated in vacuo and the crude amine was used in the peptide coupling without further purification.

To a solution of the deprotected tripeptide (5.00 g, 10.2 mmol) in DMF (50.0 ml, 0.20 M) was added DIPEA (1.55 ml, 8.87 mmol) at 0°C followed by addition of Boc-Ala-OH (1.93 g, 10.2 mmol) and HATU (4.27 g, 11.2 mmol). The mixture was allowed to reach rt and stirred for 16 . The reaction was quenched with water and extracted with EtOAc. The organic layer was washed with water and brine, dried (Na_2SO_4) and concentrated in vacuo. Silica gel column chromatography (50% EtOAc in petroleum ether) followed by prep. HPLC yielded **SI-34** (3.00 g, 4.54 mmol, 45%) as a white solid.

$[\alpha]_{20}^{D}$ = −47.9 (c 1.0, $CHCl_3$).

Major rotamer: **^{1}H NMR** (500 MHz, $CDCl_3$) δ 0.90 – 0.94 (m, 6H), 0.96 (d, *J* = 6.7 Hz, 3H), 0.98 (d, *J* = 6.8 Hz, 3H), 1.30 (d, *J* = 7.0 Hz, 3H), 1.45 (s, 9H), 1.49 – 1.53 (m, 1H), 1.66 – 1.79 (m, 2H), 2.06 – 2.17 (m, 1H), 2.51 (t, *J* = 2.4 Hz, 1H), 2.99 (s, 3H), 3.30 (s, 3H), 3.69 (s, 3H), 4.08 – 4.16 (m, 1H), 4.64 – 4.67 (m, 3H), 4.77 – 4.83 (m, 2H), 4.89 – 4.96 (m, 1H), 5.35 (dd, *J* = 10.5, 5.3 Hz, 1H), 6.75 (d, *J* = 7.3 Hz, 1H), 6.85 – 6.90 (m, 2H), 7.14 (d, *J* = 8.4 Hz, 2H), 7.38 (d, *J* = 8.7 Hz, 1H). **^{13}C NMR** (126 MHz, $CDCl_3$) δ 17.2, 18.4, 19.6, 21.4, 23.3, 24.9, 28.3, 31.3, 31.4, 36.9, 50.4, 52.2, 54.1, 54.5, 55.7, 57.4, 57.6, 75.6, 78.5, 80.2, 80.8, 114.7, 128.2, 129.7, 155.4, 157.5, 168.4, 172.0, 172.1, 172.4.

Minor rotamer (ratio ~10:1, selected signals) **^{1}H NMR** (500 MHz, $CDCl_3$) δ 1.48 (s, 9H), 2.84 (s, 3H), 3.61 (s, 3H).

HRMS (ESI) calcd for $C_{34}H_{53}N_4O_9^+$ $(M+H)^+$: 661.3807; found: 661.3778.

Methyl *N*-(((2*S*,3*R*)-3-(allyloxy)-2-((2*S*)-2-((4*R*)-5-((tert-butyldimethylsilyl)oxy)-4-methyl-2-(methylamino)pentanamido)propanamido)-3-phenylpropanoyl)-L-valyl)-*N*-methyl-L-leucinate (SI-35)

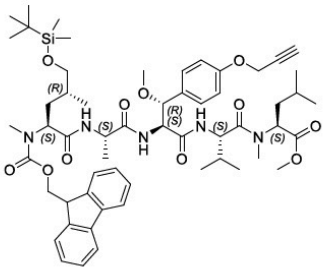

A 25 ml round-bottom flask was charged with **SI-34** (661 mg, 1.00 mmol), 4 N HCl in 1,4-dioxane (2.50 ml, 10.0 equiv) was added and the reaction mixture was stirred at 25 °C. After 2 h, the solvent was evaporated and

the residue was reacted according to *GP4*: **SI-21** (484 mg, 1.00 mmol), HOBt (166 mg, 1.10 mmol), EDC (211 mg, 1.10 mmol), NMM (220 µl, 2.00 mmol) (18 h). Flash chromatography (CyH/EtOAc 100:0 – 60:40) followed by lyophilization afforded **SI-35** (850 mg, 820 µmol, 82% yield) as a white amorphous solid. R_f = 0.43 (PE/EtOAc 1:1).

$[\alpha]_{20}^{D}$ = –53.9 (c 0.5, $CHCl_3$).

^{1}H NMR (500 MHz, $CDCl_3$) δ -0.31 – 0.32 (m, 6H), 0.88 (s, 9H), 0.91 – 0.97 (m, 12H), 0.99 (d, *J* = 6.8 Hz, 3H), 1.29 (d, *J* = 7.0 Hz, 3H), 1.45 – 1.61 (m, 3H), 1.67 – 1.81 (m, 2H), 1.93 – 2.05 (m, 1H), 2.08 – 2.17 (m, 1H), 2.36 – 2.59 (m, 1H), 2.82 (s, 3H), 2.98 (s, 3H), 3.29 (s, 3H), 3.36 – 3.56 (m, 2H), 3.69 (s, 3H), 4.26 (t, *J* = 6.7 Hz, 1H), 4.29 – 4.38 (m, 1H), 4.42 – 4.54 (m, 2H), 4.60 – 4.69 (m, 3H), 4.71 – 4.78 (m, 2H), 4.80 (dd, *J* = 8.7, 5.8 Hz, 1H), 5.35 (dd, *J* = 10.5, 5.2 Hz, 1H), 6.36 – 6.74 (m 2H), 6.88 (d, *J* = 8.4 Hz, 2H), 7.12 (d, *J* = 8.4 Hz, 2H), 7.28 – 7.35 (m, 2H), 7.36 – 7.49 (m, 3H), 7.52 – 7.63 (m, 2H), 7.76 (d, *J* = 7.6 Hz, 2H).

^{13}C NMR (126 MHz, $CDCl_3$) δ -5.3, -3.5, 17.3, 17.6, 18.4, 19.7, 21.5, 23.4, 24.9, 26.1, 31.4, 31.5, 37.0, 47.4, 49.3, 52.3, 54.2, 54.7, 55.8, 56.8, 57.5, 57.7, 67.2, 67.9, 75.7, 80.9, 114.8, 120.1, 125.0, 127.2, 127.9, 128.2, 129.6, 141.4, 143.9, 157.3, 157.7, 168.4, 170.9, 171.6, 172.07, 172.10, 172.14.

HRMS (ESI): calcd for $C_{57}H_{82}N_5O_{11}Si^+$ $(M+H)^+$: 1040.5775; found: 1040.5730.

Methyl *N*-(((2*S*,3*R*)-2-((2*S*)-2-((2*S*)-2-(2-(((allyloxy)carbonyl)amino)-*N*-methyl-3-(1-methyl-1*H*-indol-3-yl)propanamido)-5-((tert-butyldimethylsilyl)oxy)-4-methylpentanamido)propanamido)-3-methoxy-3-(4-(prop-2-yn-1-yloxy)phenyl)propanoyl)-L-valyl)-*N*-methyl-L-leucinate (SI-36)

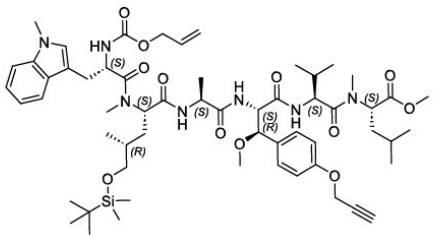

SI-35 (400 mg, 384 µmol) was dissolved in DCM (4.0 ml, 0.1 M), tris(2-aminoethyl)amine (574 µl, 3.84 mmol) was added and the reaction mixture was stirred vigorously. After completion of the reaction (TLC-monitoring; 30 minutes) the reaction mixture was washed with saturated NaCl solution (20 ml ×3) and phosphate buffer (67.0 mM, pH 5.5) (30 ml ×3). The aqueous phase was back-extracted with DCM (1x20 ml). The organic phase was dried (Na_2SO_4) and evaporated in vacuo. The resulting crude peptide was reacted according to *GP3*: Alloc-Trp(Me)-OH (141 mg, 468 µmol), BEP (128 mg, 468 µmol), NMM (107 µl, 975 µmol) (18 h). Flash chromatography (CyH/EtOAc 100:0 – 45:55) followed by lyophilization afforded **SI-36** (309 mg, 280 µmol, 72%) as a white amorphous solid. R_f = 0.38 (PE/EtOAc 2:3).

$[\alpha]_{20}^{D}$ = –41.3 (c 0.4, $CHCl_3$).

^{1}H NMR (500 MHz, $CDCl_3$) *(mixture of rotamers, ratio ~2:1)* δ -0.04 (d, *J* = 10.4 Hz, 2.3H), -0.02 (d, *J* = 5.7 Hz, 6.1H), 0.09 (s, 0.7H), 0.32 (d, *J* = 6.8 Hz, 0.1 H), 0.36 (s, 0.2H), 0.46 (d, *J* = 6.6 Hz, 1.H), 0.82 (s, 3.6H), 0.87 (s, 10.2H), 0.89 – 1.01 (m, 23.9H), 1.19 (d, *J* = 7.0 Hz, 3H), 1.22 – 1.28 (m, 2.3H), 1.38 (td, *J* = 7.2, 1.8 Hz, 0.9), 1.42– 1.54 (m, 3.9H), 1.66 – 1.81 (m, 3.1H), 1.88 – 2.44 (m, 5.7H), 2.47–2.55 (m, 1.7H), 2.64–2.69 (m, 0.3H), 2.70–2.78 (m, 3.7H), 2.78 – 2.94 (m, 1.5H), 2.93–2.99 (m, 2.0H), 3.01 (s, 2.5H), 3.03 – 3.24 (m, 3.5H), 3.25 (s, 1.3H) 3.30 (s, 3.0H), 3.35 – 3.49 (m, 2.2H), 3.56 – 3.65 (m, 0.4H), 3.66 – 3.70 (m, 6.8H), 3.72 (s, 1.9 H), 4.03 (td, *J* = 7.3, 2.6 Hz, 0.5H), 4.12–4.35 (m, 1.47H), 4.40–4.58 (m, 3.1H), 4.59 (d, *J* = 2.4 Hz, 0.7H), 4.60 – 4.63 (m, 0.2H), 4.64 – 4.66 (m, 2.3H), 4.67–4.79 (m, 1.1H), 4.74 – 4.84 (m, 3.1H), 4.87 (q, *J* = 6.5, 6.0 Hz, 1.2H), 4.93–5.00 (m, 0.87H), 5.13 – 5.31 (m, 3.2H), 5.33–5.41 (m, 1.5H), 5.58–5.67 (m, 0.3H), 5.77 – 5.97 (m, 2.0H), 6.31 – 6.48 (m, 0.8H), 6.65 – 6.99 (m, 6.3H), 7.06 – 7.24 (m, 6.4H), 7.24 – 7.30 (m, 2.3H), 7.33 – 7.44 (m, 1.0H), 7.49 (d, *J* = 8.7 Hz, 0.8H), 7.54 – 7.59 (m, 0.5 H), 7.64 (d, *J* = 7.9 Hz, 0.9H), 7.87 (d, *J* = 6.6 Hz, 0.3H).

^{13}C NMR (126 MHz, $CDCl_3$) *(mixture of rotamers)* δ -5.29, -5.27, -3.4, 14.8, 15.7, 17.3, 17.4, 17.6, 17.9, 18.5, 19.6, 19.7, 21.5, 23.42, 23.45, 24.94, 24.97, 25.7, 26.0, 26.1, 28.8, 31.36, 31.40, 31.44, 32.2, 32.8, 37.0, 49.8, 50.0, 51.1,

51.7, 52.2, 52.3, 54.2, 54.4, 54.6, 54.7, 55.79, 55.82, 57.46, 57.54, 57.8, 57.9, 58.1, 65.8, 66.4, 67.4, 68.4, 75.7, 78.6, 81.1, 108.4, 108.6, 109.49, 109.54, 114.7, 114.8, 117.7, 118.4, 118.7, 118.8, 119.4, 119.6, 121.9, 122.2, 127.8, 128.0, 128.26, 128.30, 129.7, 132.2, 132.8, 136.9, 137.0, 156.1, 156.8, 157.5, 157.6, 168.7, 169.0, 170.5, 171.7, 172.1, 172.18, 172.24, 172.3, 172.6, 173.4.

Selected diagnostic peaks:

Major rotamer: **^{1}H NMR** (500 MHz, $CDCl_3$) δ -0.02 (s, 3H), -0.01 (s, 3H), 0.87 (s, 9H), 1.19 (d, J = 7.0 Hz, 3H), 2.50 – 2.52 (m, 1H), 2.75 (s, 3H), 3.00 (s, 3H), 3.30 (s, 3H), 3.69 (s, 3H), 4.13 – 4.20 (m, 1H), 6.36 – 6.42 (m, 1H), 7.49 (d, J = 8.7 Hz, 1H), 7.64 (d, J = 7.9 Hz, 1H). **^{13}C-NMR** (126 MHz, $CDCl_3$) δ 23.42, 24.97, 26.1, 37.0, 55.82, 157.6.

Minor rotamer: **^{1}H NMR** (500 MHz, $CDCl_3$) δ -0.05 (s, 3H), -0.04 (s, 3H), 0.82 (s, 9H), 2.48 – 2.49 (m, 1H), 2.73 (s, 3H), 2.97 (s, 3H), 3.25 (s, 3H), 3.68 (s, 3H), 4.01 – 4.07 (m, 1H), 6.29 – 6.34 (m, 1H) **^{13}C-NMR** (126 MHz, $CDCl_3$) δ 23.45, 24.94, 26.0, 55.79, 157.5.

HRMS (ESI): calcd for $C_{58}H_{88}N_7O_{12}Si^+$ $(M+H)^+$: 1102.6255; found: 1102.6209.

Methyl *N*-(((2*S*,3*R*)-2-((2*S*)-2-((2*S*)-2-(2-(2-(((allyloxy)carbonyl)amino)-3-methylbutanamido)-*N*-methyl-3-(1-methyl-1*H*-indol-3-yl)propanamido)-5-((tert-butyldimethylsilyl)oxy)-4methylpent anamido)propanamido)-3-methoxy-3-(4-(prop-2-yn-1-yloxy)phenyl)propanoyl)-L-valyl)-*N*-methyl-L-leucinate (SI-37)

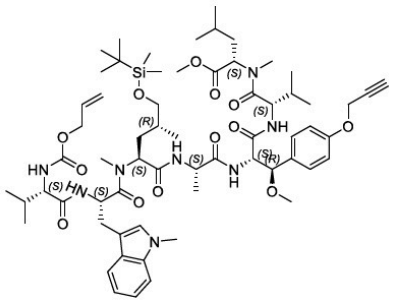

Prepared according to *GP2* and *GP4*: **SI-36** (150 mg, 136 µmol), $Pd(PPh_3)_4$ (4.72 mg, 4.10 µmol), DMBA (64.0 mg, 408 µmol); Alloc-Val-OH (35.6 mg, 177 µmol), NMM (30.0 µl, 272 µmol), HOBt (22.6 mg, 150 µmol), EDC (28.7 mg, 150 µmol) (18 h). Flash chromatography (CyH/EtOAc 100:0 – 60:40) followed by lyohpilization afforded **SI-37** (77.0 mg, 64.0 µmol, 47% yield) as a white amorphous solid. R_f = 0.42 (PE/EtOAc 2:3).

$[\alpha]_{20}^{D}$ = −53.5 (c 0.5, $CHCl_3$).

^{1}H NMR (500 MHz, $CDCl_3$) *(mixture of rotamers)* δ -0.04 (d, J = 7.8 Hz, 2.0H), 0.02 (d, J = 5.6 Hz, 4.1H), 0.09 (s, 0.7H), 0.36 (s, 0.4H), 0.45 (d, J = 6.7 Hz, 0.7H), 0.83 (s, 5.7H), 0.87 (s, 7.8H), 0.88 – 1.05 (m, 23.2H), 1.15 – 1.26 (m, 3.0H), 1.37 – 1.49 (m, 1.9H), 1.61 – 1.86 (m, 2.0H), 1.89 – 2.24 (m, 3.2H), 2.41 – 2.58 (m, 1.1H), 2.70 (s, 0.7H), 2.77 (s, 1.1H), 2.81 – 2.94 (m, 1.6H), 2.94 – 3.02 (m, 3.2H), 3.04 – 3.24 (m, 2.3H), 3.24 – 3.36 (m, 4.0H), 3.41 – 3.46 (m, 1.1H), 3.62 – 3.78 (m, 7.0H), 4.04 (t, J = 8.2 Hz, 0.8H), 4.11 – 4.39 (m, 0.5H), 4.48 – 4.91 (m, 8.3H), 5.13 – 5.44 (m, 4.4H), 5.79 – 6.00 (m, 1.0H), 6.39 (d, J = 7.1 Hz, 0.4H), 6.72 – 7.03 (m, 4.8H), 7.07 – 7.25 (m, 4.9H), 7.35 – 7.77 (m, 3.2H).

^{13}C NMR (126 MHz, $CDCl_3$) *(mixture of rotamers)* δ -5.3, -5.25, -5.23, 1.1, 14.3, 16.0, 17.3, 17.6, 17.7, 18.1, 18.4, 18.5, 19.2, 19.3, 19.66, 19.69, 21.5, 23.4, 25.0, 26.06, 26.1, 28.3, 28.7, 29.3, 29.8, 31.2, 31.37, 31.44, 31.5, 31.8, 32.2, 32.3, 32.8, 37.1, 49.4, 50.0, 50.1, 50.2, 52.27, 52.29, 54.20, 54.23, 54.6, 54.7, 55.83, 55.85, 57.4, 57.5, 57.6, 57.8, 58.3, 60.1, 60.1, 65.9, 66.1, 67.0, 68.5, 75.8, 78.6, 80.8, 81.0, 108.40, 108.44, 109.5, 109.6, 114.7, 114.88, 117.91, 118.1, 118.7, 119.5, 122.0, 127.8, 127.9, 128.0, 128.4, 128.6, 128.7, 129.7, 129.8, 132.1, 132.1, 132.2, 132.3, 132.84, 133.1, 137.0, 137.1, 156.2, 156.4, 157.6, 157.7, 168.4, 168.5, 168.8, 170.3, 170.9, 171.5, 171.7, 171.9, 172.1, 172.2, 172.2, 172.4, 172.8.

Selected diagnostic peaks:

Major rotamer: **^{1}H NMR** (500 MHz, $CDCl_3$) δ 0.01 (s, 3H), 0.02 (s, 3H), 0.87 (s, 9H), 1.15 – 1.24 (m, 3H), 2.50 – 2.54 (m, 1H), 2.77 (s, 3H), 2.98, (s, 3H), 3.30 (s, 3H), 3.69 (s, 3H), 4.21 – 4.27 (m, 1H), 5.30 – 5.40 (m, 1H), 5.82 – 6.00 (m, 1H), 6.36 – 6.43 (m, 1H), 7.62 – 7.72 (m, 2H). **^{13}C-NMR** (126 MHz, $CDCl_3$) δ 19.66, 26.09, 37.1, 60.14, 81.0, 109.6, 137.1, 157.7.

Minor rotamer: **^{1}H NMR** (500 MHz, $CDCl_3$) δ -0.05 (s, 3H), -0.03 (s, 3H), 0.83 (s, 9H), 2.48 – 2.50 (m, 1H), 2.70 (s, 3H), 2.97 (s, 3H), 3.27 (s, 3H), 3. 68 (s, 3H), 5.74 – 5.79 (m, 1H). 8.08 – 8.27 (m, 1H). **^{13}C-NMR** (126 MHz, $CDCl_3$) δ 19.69, 26.06, 60.07, 80.8, 109.5, 136.0, 157.6.

HRMS (ESI): calcd for $C_{63}H_{97}N_8O_{13}Si^+(M+H)^+$: 1201.6939; found: 1201.6901.

(3*S*,6*S*,9*S*,12*S*,15*S*,18*S*,21*S*)-21-((*R*)-3-Hydroxy-2-methylpropyl)-9-isobutyl-6,12-diisopropyl-15-((*R*)-methoxy(4-(prop-2-yn-1-yloxy)phenyl)methyl)-1,10,18-trimethyl-3-((1-methyl-1*H*-indol-3-yl)methyl)-1,4,7,10,13,16,19-heptaazacyclohenicosane-2,5,8,11,14,17,20-heptaone (SI-38)

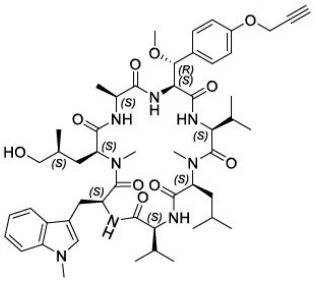

Prepared according to *GP6a*: **SI-37** (75.0 mg, 62.0 µmol), 1 M LiOH (75.0 µl, 75.0 µmol) (3.5 h); $Pd(OAc)_2$ (420 µg, 2.00 µmol), TPPTS (2.14 mg, 3.72 µmol), Et_2NH (32.0 µl, 310 µmol) (1 h); HATU (83.0 mg, 0.22 mmol), DIPEA (42.0 µl, 250 µmol) (addition over 1.5 h, additional 16 h); NH_4F (46.0 mg, 1.23 mmol) (17 h). RP flash chromatography (H_2O/MeCN 90:10 - 5:95) followed by lyophilizaiton afforded **SI-38** (22.0 mg, 23.0 µmol, 37%) as an off-white, amorphous solid.

$[\alpha]_{20}^{D}$ = –65.3 (c 0.5, $CHCl_3$)

^{1}H NMR (500 MHz, $CDCl_3$) δ -0.61 – -0.49 (m, 1H), 0.31 (d, *J* = 6.7 Hz, 3H), 0.52–0.77(m, 6H), 0.71 – 0.83 (m, 1H), 0.90–1.07 (m, 10H), 1.07 (d, *J* = 6.6 Hz, 3H), 1.17 (d, *J* = 7.2 Hz, 3H), 1.49 – 1.65 (m, 1H), 1.78–1.93 (m, 7.4 Hz, 1H), 1.93–2.17 (m, 2H), 2.20 – 2.28 (m, 1H), 2.29 – 2.41 (m, 1H), 2.50 (t, *J* = 2.4 Hz, 1H), 2.57 (s, 3H), 2.61 – 2.69 (m, 1H), 2.84 (s, 3H), 2.91–2.98 (m, 1H), 2.99–3.07 (m, 1H), 3.09–3.17 (m, 1H), 3.26–3.31 (m, 1H), 3.72 (s, 3H), 4.06 (t, *J* = 9.4 Hz, 1H), 4.33 (dd, *J* = 10.8, 2.5 Hz, 1H), 4.48 (t, *J* = 8.6 Hz, 1H), 4.61 (d, *J* = 2.4 Hz, 2H), 4.72 – 4.81 (m, 2H), 4.85 (dd, *J* = 10.4, 3.5 Hz, 1H), 4.90 (t, *J* = 5.1 Hz, 1H), 5.02 (d, *J* = 5.4 Hz, 1H), 6.67 – 6.96 (m, 3H), 6.86 – 7.02 (m, 1H), 7.01–7.17 (m, 3H), 7.17 – 7.33 (m, 5H), 7.46 (d, *J* = 7.9 Hz, 1H), 8.13 (d, *J* = 7.9 Hz, 1H), 8.29 (d, *J* = 9.5 Hz, 1H), 8.54 (d, *J* = 10.3 Hz, 1H).

^{13}C NMR (126 MHz, $CDCl_3$) δ 17.4, 18.7, 19.4, 19.5, 20.1, 21.0, 22.7, 23.7, 25.4, 28.5, 29.3, 29.8, 30.9, 31.5, 32.1, 32.8, 33.2, 39.1, 50.6, 51.3, 55.4, 55.8, 56.2, 57.8, 59.1, 59.4, 65.9, 75.9, 76.9, 78.4, 79.6, 107.8, 109.8, 114.5, 118.7, 119.7, 122.4, 127.6, 127.9, 128.0, 129.5, 136.9, 158.0, 168.7, 169.2, 170.2, 170.7, 171.4, 171.6, 172.2.

HRMS (ESI): calcd for $C_{52}H_{75}N_8O_{10}^+$ $(M+H)^+$: 971.5601; found: 971.5561.

(3*S*,6*S*,9*S*,12*S*,15*S*,18*S*,21*S*)-21-((*R*)-3-*H*ydroxy-2-methylpropyl)-15-((*R*)-(4-((1-(14-(4-(4-((*S*)-((2*R*,5*R*,8*R*,11*R*,14*R*,17*R*,20*R*)-17-((*S*)-3-hydroxy-2-methylpropyl)-8-isobutyl-5,11-diisopropyl-7,16,20-trimethyl-14-((1-methyl-1*H*-indol-3-yl)methyl)-3,6,9,12,15,18,21-heptaoxo-1,4,7,10,13,16,19-heptaazacyclohenicosan-2-yl)(methoxy)methyl)phenoxy)methyl)-1*H*-1,2,3-triazol-1-yl)-3,6,9,12-tetraoxatetradecyl)-1*H*-1,2,3-triazol-4-yl)methoxy)phenyl)(methoxy)methyl)-9-isobutyl-6,12-diisopropyl-1,10,18-trimethyl-3-((1-methyl-1*H*-indol-3-yl)methyl)-1,4,7,10,13,16,19-heptaazacyclohenicosane-2,5,8,11,14,17,20-heptaone (SI-39)

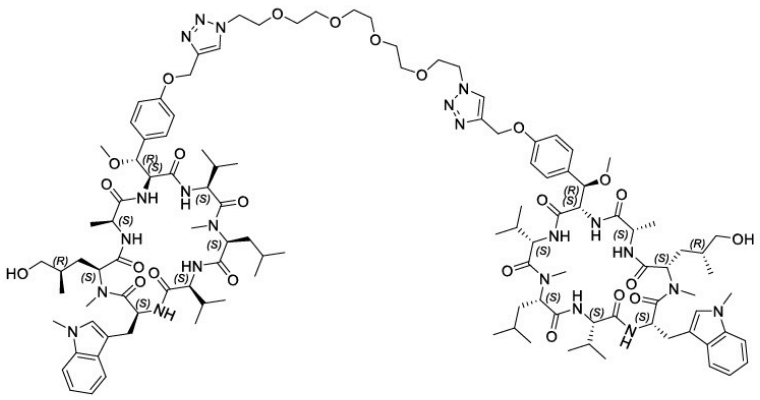

Prepared according to *GP7*: **SI-38** (22.0 mg, 23.0 µmol), 1,14-diazido-3,6,9,12-tetraoxatetradecane (3.27 mg, 11.0 µmol), 1 M $CuSO_4$ (11.3 µl, 11.0 µmol), 1 M sodium ascorbate (13.6 µl, 14.0 µmol) (17 h). RP flash chromatography (H_2O/MeCN 70:30 – 5:95) followed by lyophilization afforded **SI-39** (12.3 mg, 5.51 µmol, 48%) as a white amorphous solid.

$[\alpha]_{20}^{D}$ = –58.1 (c 0.2, $CHCl_3$).

^{1}H NMR (500 MHz, $CDCl_3$) δ -0.63 – -0.45 (m, 2H), 0.30 (d, *J* = 6.8 Hz, 6H), 0.53–0.70 (m, 11H), 0.70 – 0.89 (m, 3H), 0.91–1.03 (m, 22H), 1.07 (d, *J* = 6.6 Hz, 6H), 1.18 (d, *J* = 7.1 Hz, 6H), 1.47 – 1.73 (m, 2H), 1.79–1.92 (m, 2H), 2.14 – 2.47 (m, 24H), 2.58 (s, 6H), 2.83 (s, 6H), 3.00–3.10 (m, 2H), 3.32 (s, 6H), 3.57 (s, 6H), 3.71 (s, 6H), 3.80–4.02 (m, 4H), 4.10 (t, *J* = 9.5 Hz, 2H), 4.34 (dd, *J* = 10.7, 2.6 Hz, 2H), 4.48 (t, *J* = 8.7 Hz, 2H), 4.52–4.66 (m, 4H), 4.74–4.83 (m, 2H), 4.84 – 4.93 (m, 4H), 5.01 (d, *J* = 5.3 Hz, 2H), 5.05–5.27 (m, 3H), 6.79 – 6.95 (m, 6H), 6.99 – 7.17 (m, 7H), 7.16 – 7.23 (m, 2H), 7.27 (s, 2H), 7.46 (d, *J* = 7.8 Hz, 2H), 7.83 (s, 2H), 8.12 (d, *J* = 8.0 Hz, 2H), 8.27 (d, *J* = 9.5 Hz, 2H), 8.54 (d, *J* = 10.3 Hz, 2H).

^{13}C NMR (126 MHz, $CDCl_3$) δ 17.4, 18.8, 19.4, 19.5, 20.1, 21.1, 22.7, 23.7, 25.4, 28.5, 29.3, 29.8, 30.9, 31.5, 32.0, 32.8, 33.2, 39.1, 50.7, 51.3, 55.4, 56.2, 57.8, 59.1, 59.4, 61.8, 65.9, 69.5, 70.57, 70.65, 79.8, 107.9, 109.8, 114.4, 118.7, 119.7, 122.4, 124.4, 127.7, 127.9, 129.5, 137.0, 143.4, 158.6, 168.7, 169.3, 170.2, 170.8, 171.5, 171.6, 172.2.

HRMS (ESI): calcd for $C_{114}H_{169}N_{22}O_{24}^+$ $(M+H)^+$: 1116.1391; found: 1116.1374.

(3*S*,3'*S*,6*S*,6'*S*,9*S*,9'*S*,12*S*,12'*S*,15*S*,15'*S*,18*S*,18'*S*,21*S*,21'*S*)-15,15'-((1*R*,1'*R*)-((((Pentane-1,5-diylbis(1*H*-1,2,3-triazole-1,4-diyl))bis(methylene))bis(oxy))bis(4,1-phenylene))bis(methoxymethylene))bis(21-((*R*)-3-hydroxy-2-methylpropyl)-9-isobutyl-6,12-diisopropyl-1,10,18-trimethyl-3-((1-methyl-1*H*-indol-3-yl)methyl)-1,4,7,10,13,16,19-heptaazacyclohenicosane-2,5,8,11,14,17,20-heptaone) (SI-40)

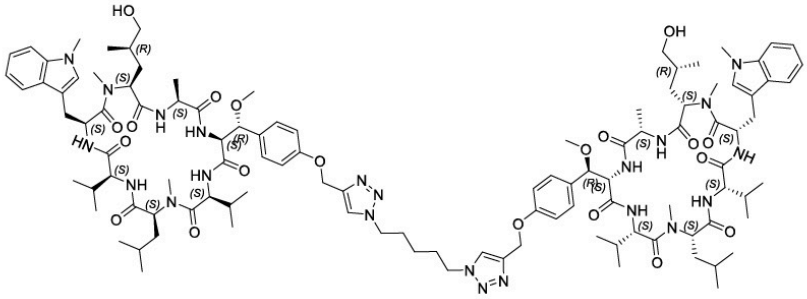

Prepared according to *GP7*: **SI-38** (17.0 mg, 18.0 µmol), 1,5-diazidopentane (1.35 mg, 8.75 µmol), 1 M $CuSO_4$ (8.75 µl, 8.75 µmol), 1 M sodium ascorbate (10.5 µl, 10.5 µmol) (18 h). RP flash chromatography (H_2O/MeCN 70:30 – 5:95) followed by lyophilization afforded **SI-40** (7.40 mg, 3.53 µmol, 40%) as a white amorphous solid.

$[\alpha]_{20}^{D}$= −65.5 (c 0.2, $CHCl_3$).

^{1}H NMR (500 MHz, $CDCl_3$) δ -0.66 – -0.47 (m, 2H), 0.30 (d, *J* = 6.7 Hz, 6H), 0.45–0.72 (m, 10H), 0.91–1.00 (m, 22H), 1.07 (d, *J* = 6.7 Hz, 6H), 1.17 (d, *J* = 7.1 Hz, 6H), 1.52–1.60 (m, 2H), 1.91–2.02 (m, 22H), 2.19 – 2.37 (m, 6H), 2.57 (s, 6H), 2.83 (s, 3H), 2.89 – 3.07 (m, 4H), 3.09 – 3.28 (m, 2H), 3.33 (s, 6H), 3.72 (s, 6H), 4.11 (t, *J* = 9.4 Hz, 2H), 4.30 – 4.42 (m, 10H), 4.48 (t, *J* = 8.6 Hz, 2H), 4.69 – 4.95 (m, 6H), 5.02 (d, *J* = 5.3 Hz, 2H), 5.13 (s, 3H), 6.83 (s, 2H), 6.85 – 6.91 (m, 4H), 7.01–7.10 (m, 1H), 7.12 (d, *J* = 8.4 Hz, 4H), 7.17 – 7.25 (m, 2H), 7.46 (d, *J* = 7.9 Hz, 2H), 8.12 (d, *J* = 8.0 Hz, 2H), 8.30 (d, *J* = 9.4 Hz, 2H), 8.53 (d, *J* = 10.3 Hz, 2H).

^{13}C NMR (126 MHz, $CDCl_3$) 17.4, 18.8, 19.5, 20.1, 21.1, 22.7, 23.5, 23.8, 25.4, 28.6, 29.3, 29.71, 29.74, 30.9, 31.5, 32.1, 32.9, 33.3, 39.1, 50.1, 50.7, 51.3, 55.4, 56.2, 57.8, 59.1, 59.4, 62.1, 65.9, 79.7, 107.8, 109.8, 114.5, 118.7, 119.7, 122.4, 122.8, 127.7, 127.8, 127.9, 129.6, 136.9, 144.1, 158.7, 168.7, 169.3, 170.2, 170.8, 171.4, 171.6, 172.2.

HRMS (ESI): calcd for $C_{109}H_{159}N_{22}O_{20}^+$ $(M+H)^+$: 1049.1101; found: 1049.1048.

Synthesis of exit vector 6 Homo-BacPROTACs via olefin metathesis (15, 16)

1-Allyl-N$^{\alpha}$-((allyloxy)carbonyl)-L-tryptophan (SI-41)

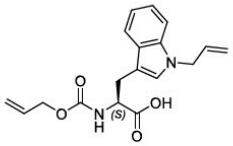

((Allyloxy)carbonyl)-L-tryptophan (400 mg, 1.39 mmol) was dissolved in DMF (2.8 ml) under N_2 and KO*t*-Bu (327 mg, 2.91 mmol) was added. After all solids were dissolved, the mixture was cooled to 0 °C and allyl bromide (168 µl, 1.94 mmol) was added in one portion. Complete conversion was observed after 5 min (TLC), the reaction was quenched by addition of 1 M HCl after 10 min. The mixture was extracted with EtOAc (2x). The combined organic phases were washed with 1 M LiCl and sat. NaCl solution, dried (Na_2SO_4) and evaporated. Flash chromatography (CyH/[EtOAc+2%HOAc] 100:0 – 70:30) followed by co-distillation with toluene and lyophilization afforded **SI-41** (336 mg, 1.02 mmol, 74%) as a yellow honey-like resin. R_f (PE/EtOAc/HOAc 70:30:1) = 0.28.

$[\alpha]_{20}^{D}$ = +33.6 (c 1.0, $CHCl_3$).

^{1}H NMR (500 MHz, DMSO-d_6) δ 2.98 (dd, *J* = 14.6, 9.7 Hz, 1H), 3.17 (dd, *J* = 14.6, 4.7 Hz, 1H), 4.20 (ddd, *J* = 9.6, 8.2, 4.7 Hz, 1H), 4.35 – 4.46 (m, 2H), 4.76 (d, *J* = 5.4 Hz, 2H), 4.93 – 5.00 (m, 1H), 5.09 – 5.16 (m, 2H), 5.23 (dq, *J* = 17.2, 1.7 Hz, 1H), 5.84 (ddt, *J* = 17.2, 10.4, 5.3 Hz, 1H), 5.96 (ddt, *J* = 17.0, 10.4, 5.3 Hz, 1H), 6.98 – 7.06 (m, 1H), 7.08 – 7.15 (m, 1H), 7.15 (s, 1H), 7.37 (d, *J* = 8.2 Hz, 1H), 7.53 (d, *J* = 8.2 Hz, 1H), 7.55 (d, *J* = 7.9 Hz, 1H), 12.69 (bs, 1H).

^{13}C NMR (126 MHz, DMSO-d_6) δ 26.80, 47.85, 54.86, 64.38, 109.96, 110.00, 116.53, 116.97, 118.49, 118.68, 121.15, 127.13, 127.59, 133.55, 134.50, 135.96, 155.84, 173.67.

HRMS (CI) calcd for $C_{18}H_{20}N_2O_4^+$ $(M)^+$: 328.1418; found: 328.1431.

methyl *N*-(((2*S*,3*R*)-2-((*S*)-2-((2*S*,4*R*)-2-((*S*)-3-(1-allyl-1*H*-indol-3-yl)-2-(((allyloxy)carbonyl)amino)-*N*-methylpropanamido)-5-((*tert*-butyldimethylsilyl)oxy)-4-methylpentanamido)propanamido)-3-methoxy-3-phenylpropanoyl)-L-valyl)-*N*-methyl-L-leucinate (SI-42)

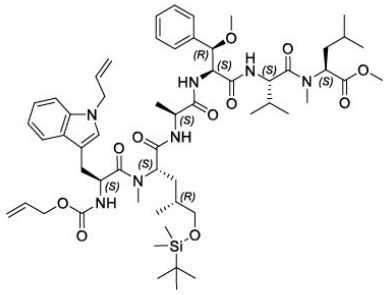

Prepared according to *GP1* and *GP5*: Pentapeptide **2** (607 mg, 676 µmol), Pd/C (71.9 mg) (1 h); **SI-41** (307 mg, 916 µmol), DIPEA (153 µl, 878 µmol), $BnNMe_2$ (10.0 µl, 6.75 µmol), 1 M iPrOCOCl (878 µl, 878 µmol), 4 M HCl (16.9 µl, 6.75 µmol), NMI (10.8 µl, 135 µmol) (16 h). Flash chromatography (CyH/EtOAc 100:0 – 70:30 – 35:65) followed by lyophilization yielded **SI-42** (606 mg, 564 µmol, 84%) as a white amorphous solid. R_f = 0.16 (PE/EtOAc 1:1).

$[\alpha]_{20}^{D}$ = −56.9 (c 1.0, $CHCl_3$).

^{1}H NMR (500 MHz, $CDCl_3$) *(mixture of rotamers, ratio ~3:1)* δ -0.33 – -0.26 (m, 0.2H), -0.05 (s, 0.7H), -0.03 (s, 0.7H), 0.00 – 0.05 (m, 4.5H), 0.41 (d, *J* = 6.6 Hz, 0.6H), 0.83 (s, 2.0H), 0.86 – 0.88 (m, 4.9H), 0.88 – 0.96 (m, 13.2H), 0.96 – 1.02 (m, 3.0H), 1.16 – 1.21 (m, 1.4H), 1.21 – 1.27 (m, 1.7H), 1.32 (d, *J* = 7.3 Hz, 0.7H), 1.38 – 1.53 (m, 2.4H), 1.66 – 1.81 (m, 2.1H), 1.84 – 1.91 (m, 0.3H), 1.92 – 2.23 (m, 2.5H), 2.25 – 2.29 (m, 0.5H), 2.73 (s, 0.6H), 2.78 (s, 1.5H), 2.81 – 2.85 (m, 0.4H), 2.97 (s, 0.8H), 2.98 – 3.05 (m, 2.3H), 3.08 – 3.24 (m, 1.4H), 3.27 (s, 0.8H), 3.32 (s, 2.1H), 3.38 – 3.47 (m, 1.3H), 3.63 – 3.71 (m, 3.0H), 4.13 – 4.21 (m, 0.4H), 4.24 – 4.31 (m, 0.5H), 4.44 – 4.58 (m, 1.6H), 4.58 – 4.74 (m, 3.2H), 4.75 – 4.90 (m, 2.7H), 4.91 – 5.06 (m, 1.2H), 5.06 – 5.30 (m, 2.8H), 5.31 – 5.38 (m, 1.0H), 5.67 (d, *J* = 7.6 Hz, 0.2H), 5.77 – 5.99 (m, 1.9H), 6.41 (d, *J* = 6.8 Hz, 0.4H), 6.75 (d, *J* = 7.6 Hz, 0.3H), 6.80 (t, *J* = 7.6 Hz, 0.5H), 6.90 – 6.97 (m, 0.8H), 7.06 – 7.14 (m, 1.0H), 7.15 – 7.31 (m, 7.2H), 7.35 (d, *J* = 8.8 Hz, 0.3H), 7.46 (d, *J* = 8.8 Hz, 0.4H), 7.57 (d, *J* = 7.9 Hz, 0.3H), 7.64 (d, *J* = 7.9 Hz, 0.4H), 7.87 (d, *J* = 6.6 Hz, 0.2H).

^{13}C NMR (126 MHz, $CDCl_3$) *(mixture of rotamers)* δ -5.29, -5.26, 14.3, 15.6, 17.2, 17.3, 17.5, 17.6, 17.9, 18.4, 19.57, 19.65, 21.5, 23.4, 24.9, 26.0, 26.1, 28.5, 28.8, 31.3, 31.4, 31.6, 32.1, 32.2, 37.0, 39.7, 48.8, 48.9, 49.6, 49.8, 49.9, 50.9, 51.7, 52.3, 54.2, 54.3, 54.5, 54.6, 56.4, 57.6, 57.7, 57.86, 57.94, 65.1, 65.8, 66.4, 67.4, 68.4, 81.2, 81.5, 108.8, 109.1, 109.86, 109.93, 117.3, 117.7, 117.8, 118.4, 118.8, 119.5, 119.7, 122.0, 122.2, 126.77, 126.84, 126.94, 127.01, 128.2, 128.26, 128.34, 128.4, 128.6, 132.2, 132.8, 133.4, 133.5, 136.3, 136.4, 136.9, 156.0, 156.7, 168.6, 168.8, 170.5, 171.7, 172.0, 172.18, 172.23, 172.6, 173.4.

Selected diagnostic peaks:

Major rotamer: **^{1}H NMR** (500 MHz, $CDCl_3$) δ 0.01 (s, 3H), 0.03 (s, 3H), 0.87 (s, 9H), 2.78 (s, 3H), 3.00 (s, 3H), 3.32 (s, 3H), 3.68 (s, 3H), 5.36 (ddd, *J* = 10.7, 5.3, 2.3 Hz, 2H), 6.93 (s, 1H), 7.46 (d, *J* = 8.8 Hz, 1H), 7.64 (d, *J* = 7.9 Hz, 1H). **^{13}C NMR** (126 MHz, $CDCl_3$) δ 26.1, 31.4, 81.2, 156.0

Minor rotamer: **^{1}H NMR** (500 MHz, $CDCl_3$) δ 0.41 (d, *J* = 6.6 Hz, 3H), 0.83 (s, 9H), 1.32 (d, *J* = 7.3 Hz, 3H), 2.73 (s, 3H), 2.97 (s, 3H), 3.27 (s, 3H), 5.67 (d, *J* = 7.6 Hz, 1H), 6.75 (d, *J* = 7.6 Hz, 1H), 6.92 (s, 1H), 7.35 (d, *J* = 8.8 Hz, 1H), 7.57 (d, *J* = 7.9 Hz, 1H), 7.87 (d, *J* = 6.6 Hz, 1H). **^{13}C NMR** (126 MHz, $CDCl_3$) δ 26.0, 31.3, 81.5, 156.7.

HRMS (ESI) calcd for $C_{57}H_{88}N_7O_{11}Si^+$ $(M+H)^+$: 1074.6306; found: 1074.6287.

methyl *N*-(((2*S*,3*R*)-2-((*S*)-2-((2*S*,4*R*)-2-((*S*)-3-(1-allyl-1*H*-indol-3-yl)-2-((*S*)-2-(((allyloxy)carbonyl)amino)-3-methylbutanamido)-*N*-methylpropanamido)-5-((*tert*-butyldimethylsilyl)oxy)-4-methylpentanamido)propanamido)-3-methoxy-3-phenylpropanoyl)-L-valyl)-*N*-methyl-L-leucinate (SI-43)

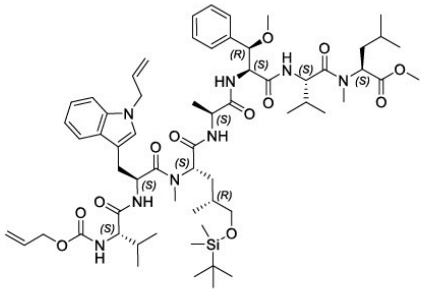

Prepared according to *GP2* and *GP4*: **SI-42** (571 mg, 531 µmol), DMBA (249 mg, 1.59 mmol), $Pd(PPh_3)_4$ (18.4 mg, 15.9 µmol) (1.5 h); Alloc-L-valine (123 mg, 611 µmol), HOBt (89.0 mg, 584 µmol), EDC (112 mg, 584 µmol), NMM (117 µl, 1.06 mmol) (16 h). Flash chromatography (CyH/EtOAc 100:0 – 30:70) followed by lyophilization yielded **SI-43** (525 mg, 447 mmol, 84%) as a white amorphous solid. R_f = 0.26 (PE/EtOAc 3:7).

$[\alpha]_{20}^{D}$ = −66.6 (c 1.0, $CHCl_3$).

^{1}H NMR (500 MHz, $CDCl_3$) *(mixture of rotamers, ratio ~2:1)* δ −0.45 – -0.29 (m, 0.1H), -0.05 (s, 0.9H), -0.04 (s, 1.0H), -0.01 – 0.06 (m, 3.8H), 0.38 (d, *J* = 6.8 Hz, 0.6H), 0.79 – 0.83 (m, 4.7H), 0.84 – 0.87 (m, 6.1H), 0.87 – 0.96 (m, 15.1H), 0.96 – 1.01 (m, 3.1H), 1.18 – 1.22 (m, 2.0H), 1.25 (d, *J* = 6.3 Hz, 0.6H), 1.30 – 1.35 (m, 0.7H), 1.40 – 1.53 (m, 2.1H), 1.65 – 1.80 (m, 2.2H), 1.80 – 1.88 (m, 0.3H), 1.89 – 2.25 (m, 4.0H), 2.67 – 2.72 (m, 0.9H), 2.73 – 2.78 (m, 0.4H), 2.80 (m, 1.4H), 2.95 – 3.00 (m, 3.0H), 3.00 – 3.05 (m, 0.3H), 3.06 – 3.17 (m, 0.9H), 3.18 – 3.24 (m, 0.6H), 3.28 (s, 1.0H), 3.30 (s, 0.5H), 3.32 (s, 1.8H), 3.39 – 3.43 (m, 0.9H), 3.65 – 3.72 (s, 3.0H), 4.02 – 4.13 (m, 0.7H), 4.22 – 4.29 (m, 0.5H), 4.31 – 4.39 (m, 0.4H), 4.45 – 4.76 (m, 5.3H), 4.77 – 4.87 (m, 2.1H), 4.89 – 4.98 (m, 0.8H), 498 – 5.05 (m, 0.6H), 5.09 – 5.26 (m, 2.7H), 5.26 – 5.38 (m, 2.2H), 5.59 (d, *J* = 9.0 Hz, 0.1H), 5.71 (d, *J* = 9.5 Hz, 0.2H), 5.83 – 5.98 (m, 1.7H), 6.53 (d, *J* = 6.1 Hz, 0.3H), 6.74 – 6.86 (m, 1.0H), 6.89 – 6.96 (m, 0.9H), 6.97 – 7.04 (m, 0.4H), 7.06 – 7.13 (m, 1.0H), 7.14 – 7.32 (m, 7.8H), 7.33 – 7.42 (m, 0.8H), 7.42 – 7.48 (m, 0.5H), 7.51 – 7.57 (m, 0.5H), 7.62 – 7.69 (m, 0.8H), 8.14 (d, *J* = 7.1 Hz, 0.2H).

^{13}C NMR (126 MHz, $CDCl_3$) *(mixture of rotamers)* δ 15.7, 17.37, 17.44, 17.7, 18.0, 18.1, 18.4, 18.5, 19.18, 19.24, 19.60, 19.64, 21.48, 21.52, 23.4, 24.9, 26.0, 26.1, 28.1, 28.7, 29.2, 31.3, 31.4, 31.5, 32.3, 37.0, 48.8, 48.9, 49.4, 49.8, 50.1, 52.3, 54.2, 54.5, 54.6, 57.5, 57.6, 58.0, 58.1, 60.0, 65.9, 66.1, 67.1, 68.5, 81.2, 81.4, 108.7, 109.0, 109.9, 110.0, 117.3, 117.9, 118.0, 118.8, 119.6, 122.0, 122.2, 126.8, 127.0, 127.1, 127.9, 128.2, 128.3, 128.4, 128.5, 128.6, 128.7, 132.1, 132.17, 132.25, 132.8, 133.4, 133.6, 136.3, 136.4, 136.9, 156.2, 156.4, 168.5, 170.4, 170.9, 171.6, 171.8, 171.9, 172.1, 172.2, 172.5, 172.9.

Selected diagnostic peaks:

Major rotamer: **^{1}H NMR** (500 MHz, $CDCl_3$) δ 0.00 (s, 3H), 0.01 (s, 3H), 0.86 (s, 9H), 2.80 (s, 3H), 2.97 (s, 3H), 3.32 (s, 3H), 3.68 (s, 3H), 5.71 (d, *J* = 9.5 Hz, 0H), 6.53 (d, *J* = 6.1 Hz, 1H), 6.93 (s, 1H). **^{13}C NMR** (126 MHz, $CDCl_3$) δ 26.1, 57.6, 81.4, 156.2.

Minor rotamer: **^{1}H NMR** (500 MHz, $CDCl_3$) δ -0.05 (s, 3H), -0.04 (s, 3H), 0.38 (d, *J* = 6.8 Hz, 3H), 0.83 (s, 9H), 2.69 (s, 3H), 3.28 (s, 3H), 3.69 (s, 3H), 4.35 (t, *J* = 7.3 Hz, 1H), 5.59 (d, *J* = 9.0 Hz, 1H), 6.91 (s, 1H), 8.14 (d, *J* = 7.1 Hz, 1H). **^{13}C NMR** (126 MHz, $CDCl_3$) δ 26.0, 57.5, 81.2, 156.4.

HRMS (ESI) calcd for $C_{62}H_{97}N_8O_{12}Si^+$ $(M+H)^+$: 1173.6990; found: 1173.6974.

(3*S*,6*S*,9*S*,12*S*,15*S*,18*S*,21*S*)-3-((1-allyl-1*H*-indol-3-yl)methyl)-21-((*R*)-3-hydroxy-2-methylpropyl)-9-isobutyl-6,12-diisopropyl-15-((*R*)-methoxy(phenyl)methyl)-1,10,18-trimethyl-1,4,7,10,13,16,19-heptaazacyclohenicosane-2,5,8,11,14,17,20-heptaone (13)

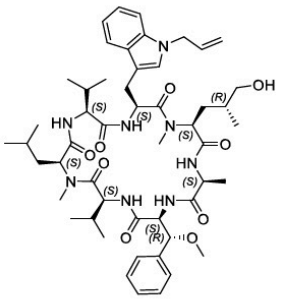

Prepared according to *GP6a*: **SI-43** (134 mg, 114 µmol), 1 M LiOH (160 µl, 160 µmol) (17 h); $Pd(OAc)_2$ (1.3 mg, 5.7 µmol), TPPTS (6.5 mg, 11.4 µmol), Et_2NH (56.3 µl, 570 µmol) (2.5 h); HATU (130 mg, 342 µmol), DIPEA (80.7 µl, 456 µmol) (addition over 1.5 h, additional 16 h); NH_4F (84.5 mg, 2.28 mmol) (16 h). Reversed phase flash chromatography (H_2O/MeCN 90:10 – 5:95) followed by lyophilization yielded **13** (68.6 mg, 72.7 µmol, 64%) as a white amorphous solid.

$[\alpha]_{24}^{D}$ = −82.2 (c 0.5, $CHCl_3$).

^{1}H NMR (500 MHz, $CDCl_3$) δ -0.60 – -0.52 (m, 1H), 0.24 (d, *J* = 6.8 Hz, 3H), 0.58 (d, *J* = 6.5 Hz, 3H), 0.61 (d, *J* = 6.6 Hz, 3H), 0.73 (d, *J* = 6.8 Hz, 1H), 0.81 (q, *J* = 5.2 Hz, 1H), 0.93 – 0.99 (m, 9H), 1.07 (d, *J* = 6.6 Hz, 3H), 1.09 – 1.12 (m, 1H), 1.14 (d, *J* = 7.3 Hz, 3H), 1.52 – 1.61 (m, 1H), 1.84 (ddd, *J* = 13.6, 11.0, 7.1 Hz, 1H), 2.18 – 2.35 (m, 3H), 2.57 (s, 3H), 2.82 (s, 3H), 2.92 (dd, *J* = 11.2, 5.5 Hz, 1H), 3.01 (dd, *J* = 11.2, 4.3 Hz, 1H), 3.11 (dd, *J* = 13.6, 4.9 Hz, 1H), 3.25 – 3.32 (m, 1H), 3.34 (s, 3H), 4.10 (t, *J* = 9.5 Hz, 1H), 4.36 (dd, *J* = 11.0, 2.6 Hz, 1H), 4.47 (t, *J* = 8.7 Hz, 1H), 4.58 – 4.66 (m, 2H), 4.72 – 4.78 (m, 2H), 4.85 (dd, *J* = 10.4, 3.8 Hz, 1H), 4.90 (t, *J* = 5.1 Hz, 1H), 5.06 (d, *J* = 5.5 Hz, 1H), 5.10 – 5.17 (m, 1H), 5.17 – 5.22 (m, 1H), 5.90 (ddt, *J* = 17.2, 10.2, 5.8 Hz, 1H), 6.86 (s, 1H), 7.04 – 7.11 (m, 1H), 7.14 – 7.18 (m, 3H), 7.19 – 7.24 (m, 4H), 7.26 – 7.28 (m, 1H), 7.42 (d, *J* = 5.2 Hz, 1H), 7.46 (d, *J* = 7.9 Hz, 1H), 8.11 (d, *J* = 7.9 Hz, 1H), 8.25 (d, *J* = 9.5 Hz, 1H), 8.51 (d, *J* = 10.4 Hz, 1H).

^{13}C NMR (126 MHz, $CDCl_3$) δ 17.2, 18.7, 19.4, 20.10, 20.13, 20.9, 22.7, 23.7, 25.3, 28.3, 29.3, 29.7, 30.9, 31.6, 31.9, 33.1, 39.0, 48.9, 50.5, 51.1, 55.3, 56.0, 57.9, 58.9, 59.0, 59.2, 66.0, 80.0, 108.2, 110.1, 118.1, 118.6, 119.8, 122.4, 126.8, 127.8, 128.1, 128.2, 128.8, 133.2, 135.1, 136.3, 168.6, 169.1, 170.0, 170.7, 171.5, 171.6, 172.2.

HRMS (ESI) calcd for $C_{51}H_{75}N_8O_9^+$ $(M+H)^+$: 943.5652; found: 943.5617.

(3*S*,3'*S*,6*S*,6'*S*,9*S*,9'*S*,12*S*,12'*S*,15*S*,15'*S*,18*S*,18'*S*,21*S*,21'*S*)-15,15'-((((*E*)-but-2-ene-1,4-diyl)bis(1*H*-indole-1,3-diyl))bis(methylene))bis(12-((*R*)-3-hydroxy-2-methylpropyl)-21-isobutyl-3,18-diisopropyl-6-((*R*)-methoxy(phenyl)methyl)-1,9,13-trimethyl-1',4',7',10',13',16',19'-heptaazacyclohenicosane-2,5,8,11,14,17,20-heptaone) (15)

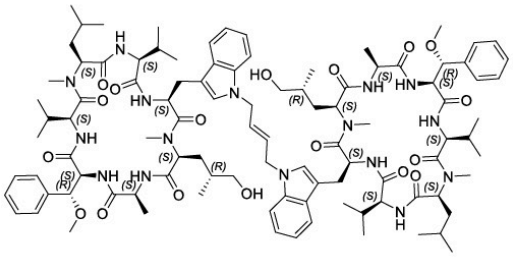

A 4 ml vial was charged with **13** (23.6 mg, 25.0 µmol) and Grubbs catalyst 2nd Gen (2.1 mg, 2.5 µmol), freshly degassed (3x freeze-pump-thaw) DCM (250 µl) was added, the vial was flushed with Argon and sealed. The mixture was heated to 40 °C. After 16 h, additional Grubbs catalyst 2nd Gen (2.1 mg, 2.5 µmol) was added. After 41 h, LC/MS indicated ca. 50% conversion (and formation of side products). The reaction mixture was evaporated in vacuo. RP flash chromatography (H_2O/MeCN 90:10 – 5:95) followed by prep HPLC (H_2O/MeCN 70:30 – 0:100) and lyophilization yielded **15** (6.7 mg, 3.6 µmol, 29%) as a white amorphous solid.

$[\alpha]_{20}^{D}$ = −121.7 (c 0.2, $CHCl_3$).

^{1}H NMR (500 MHz, $CDCl_3$) δ -0.37 – -0.23 (m, 2H), 0.36 (d, *J* = 6.8 Hz, 6H), 0.53 (d, *J* = 6.1 Hz, 6H), 0.62 (d, *J* = 6.3 Hz, 6H), 0.67 (s, 2H), 0.91 – 0.97 (m, 18H), 1.01 – 1.08 (m, 8H), 1.15 – 1.23 (m, 8H), 1.48 – 1.55 (m, 2H), 1.98 – 2.08 (m, 2H), 2.16 – 2.26 (m, 2H), 2.27 – 2.34 (m, 2H), 2.47 (s, 6H), 2.76 – 2.84 (m, 8H), 2.91 – 2.98 (m, 2H), 3.03 (dd, *J* = 14.1, 6.7 Hz, 2H), 3.08 – 3.16 (m, 4H), 3.33 (s, 6H), 4.03 (t, *J* = 9.3 Hz, 2H), 4.40 (t, *J* = 8.7 Hz, 2H), 4.49 (dd, *J* = 11.2, 3.6 Hz, 2H), 4.54 – 4.62 (m, 4H), 4.68 (d, *J* = 13.2 Hz, 2H), 4.82 (dd, *J* = 10.6, 3.4 Hz, 2H), 4.85 – 4.90 (m, 4H), 5.04 (d, *J* = 5.5 Hz, 2H), 5.72 (t, *J* = 3.2 Hz, 2H), 6.89 (s, 2H), 7.04 – 7.10 (m, 2H), 7.11 (d, *J* = 4.7 Hz, 2H), 7.14 – 7.17 (m, 4H), 7.18 (d, *J* = 7.7 Hz, 2H), 7.20 – 7.22 (m, 6H), 7.26 (d, *J* = 8.2 Hz, 2H), 7.32 (d, *J* = 5.0 Hz, 2H), 7.42 (d, *J* = 7.9 Hz, 2H), 8.04 (d, *J* = 7.9 Hz, 2H), 8.25 (d, *J* = 9.5 Hz, 2H), 8.35 (d, *J* = 10.4 Hz, 2H).

^{13}C NMR (126 MHz, $CDCl_3$) δ 17.0, 18.8, 19.5, 20.1, 21.4, 22.7, 23.7, 25.5, 27.6, 28.9, 29.7, 31.0, 32.0, 32.2, 33.1, 39.0, 47.4, 50.6, 51.1, 55.5, 56.0, 57.9, 59.0, 59.1, 66.8, 80.0, 108.7, 109.9, 118.4, 119.8, 122.4, 126.9, 127.9, 128.2, 128.3, 128.5, 128.8, 135.1, 135.7, 168.8, 169.0, 169.9, 170.7, 171.5, 171.6, 172.5.

HRMS (ESI) calcd for $C_{100}H_{145}N_{16}O_{18}^+$ $(M+H)^+$: 1858.0917; found: 1858.0987.

(3*S*,3'*S*,6*S*,6'*S*,9*S*,9'*S*,12*S*,12'*S*,15*S*,15'*S*,18*S*,18'*S*,21*S*,21'*S*)-15,15'-((butane-1,4-diylbis(1*H*-indole-1,3-diyl))bis(methylene))bis(12-((*R*)-3-hydroxy-2-methylpropyl)-21-isobutyl-3,18-diisopropyl-6-((*R*)-methoxy(phenyl)methyl)-1,9,13-trimethyl-1',4',7',10',13',16',19'-heptaazacyclohenicosane-2,5,8,11,14,17,20-heptaone) (16)

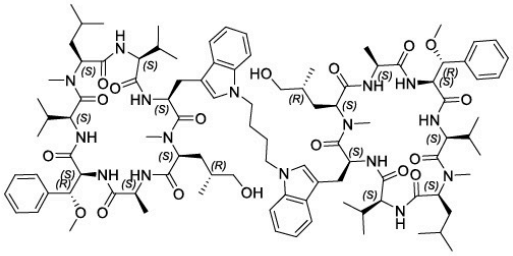

Under Ar, **13** (21.1 mg, 22.4 µmol) was dissolved in freshly degassed (3x freeze-pump-thaw) DCE (2 ml) and the mixture was heated to 60 °C. A solution of Grubbs catalyst 2nd Gen (5.7 mg, 6.7 mg) in DCE (1 ml) was added over the course of 12 h. After 18 h, LC/MS indicated 80% conversion. The mixture was evaporated in vacuo and the residue was dissolved in MeOH (4 ml). Pd/C (5 mg) was added and the mixture was shaken under H_2 (4 bar) for 16 h. RP flash chromatography (H_2O/MeCN 90:10 – 5:95) followed by prep HPLC (H_2O/MeCN 90:10 – 0:100) and lyophilization yielded **16** (4.8 mg, 2.58 µmol, 23%) as a white amorphous solid.

$[\alpha]_{20}^{D}$ = −155.6 (c 0.2, $CHCl_3$).

^{1}H NMR (500 MHz, $CDCl_3$) δ -0.37 – -0.27 (m, 2H), 0.34 (d, *J* = 6.8 Hz, 6H), 0.56 (d, *J* = 6.5 Hz, 6H), 0.63 (d, *J* = 6.5 Hz, 6H), 0.67 – 0.72 (m, 2H), 0.93 – 0.98 (m, 18H), 1.05 – 1.11 (m, 10H), 1.21 (d, *J* = 7.3 Hz, 6H), 1.50 – 1.57 (m, 2H), 1.69 – 1.82 (m, 6H), 1.99 – 2.08 (m, 2H), 2.21 – 2.27 (m, 2H), 2.28 – 2.35 (m, 2H), 2.52 (s, 6H), 2.78 – 2.86 (m, 8H), 3.05 (dd, *J* = 14.0, 6.5 Hz, 2H), 3.10 (dd, *J* = 11.2, 4.3 Hz, 2H), 3.14 – 3.20 (m, 2H), 3.36 (s, 6H), 3.88 – 3.96 (m, 2H), 4.02 – 4.14 (m, 4H), 4.42 (t, *J* = 8.7 Hz, 2H), 4.45 – 4.50 (m, 2H), 4.60 – 4.66 (m, 2H), 4.80 – 4.88 (m, 4H), 4.90 (t, *J* = 5.0 Hz, 2H), 5.06 (d, *J* = 5.5 Hz, 2H), 6.85 (s, 2H), 7.06 – 7.11 (m, 2H), 7.14 (d, *J* = 4.9 Hz, 2H), 7.17 – 7.21 (m, 8H), 7.21 – 7.25 (m, 8H), 7.44 (d, *J* = 7.9 Hz, 2H), 8.06 (d, *J* = 7.9 Hz, 2H), 8.24 (d, *J* = 9.5 Hz, 2H), 8.38 (d, *J* = 10.1 Hz, 2H).

^{13}C NMR (126 MHz, $CDCl_3$) δ 17.0, 18.7, 19.5, 20.1, 21.2, 22.7, 23.7, 25.5, 27.8, 28.3, 29.1, 29.7, 30.9, 32.0, 32.3, 33.0, 39.0, 46.1, 50.6, 51.1, 55.4, 56.0, 57.9, 59.05, 59.06, 66.6, 80.0, 108.3, 109.8, 118.5, 119.7, 122.4, 127.0, 127.8, 128.2, 128.3, 128.8, 135.1, 135.8, 168.8, 169.0, 170.0, 170.7, 171.5, 171.6, 172.5.

HRMS (ESI) calcd for $C_{100}H_{147}N_{16}O_{18}^+$ $(M+H)^+$: 1860.1074; found: 1860.1062.

Synthesis of exit vector 3 Homo-BacPROTAC via olefin metathesis (17)

***tert*-butyl *N*-[(1*R*,2*R*)-1-(4-aminophenyl)-3-[(*tert*-butyldimethylsilyl)oxy]-1-hydroxypropan-2-yl]carbamate (SI-44)**

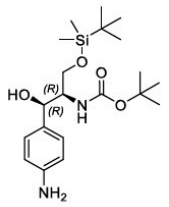

To a solution of *tert*-butyl ((1*R*,2*R*)-3-((*tert*-butyldimethylsilyl)oxy)-1-hydroxy-1-(4-nitrophenyl)propan-2-yl)carbamate[12] (25.0 g, 58.6 mmol) in THF (150 ml, 0.39 M) was added 10 wt% Pd/C (6.21 g, 5.86 mmol). The mixture was stirred at rt under H_2 atmosphere (balloon pressure). After 4 h, TLC indicated complete conversion. Subsequently, the mixture was filtered over Celite and the filtrate was evaporated in vacuo. Silica gel column chromatography (20% EtOAc in petroleum ether) yielded **SI-44** (18.0 g, 45.4 mmol, 77%).

^{1}H NMR (500 MHz, DMSO-d_6) δ 0.01 (s, 6H), 0.86 (s, 9H), 1.21 (br s, 1.35H, rotamer), 1.32 (s, 7.65H, rotamer), 3.52 – 3.46 (m, 1H), 3.55 (dd, *J* = 9.5, 6.6 Hz, 1H), 4.50 (t, *J* = 4.7 Hz, 1H), 4.90 (s, 2H), 4.94 (d, *J* = 5.4 Hz, 1H), 5.54 (d, *J* = 8.5 Hz, 0.15H, rotamer), 5.96 (d, *J* = 8.5 Hz, 0.85H, rotamer), 6.49 (d, *J* = 8.5 Hz, 2H), 6.92 (d, *J* = 8.5 Hz, 2H).

^{13}C NMR (126 MHz, DMSO-d_6) δ -5.4, -5.3, 17.9, 25.8, 27.9, 28.2, 57.9, 62.3, 62.9, 70.0, 77.6, 113.4, 126.6, 126.8, 130.4, 147.5, 155.3.

MS calcd for $C_{16}H_{27}N_2O_3Si^+$ (M – C_4H_9 – OH + H)$^+$: 323.18; found: 323.45.

***tert*-butyl *N*-[(1*R*,2*R*)-1-(4-aminophenyl)-3-[(tert-butyldimethylsilyl)oxy]-1-(prop-2-en-1-yloxy)propan-2-yl]carbamate (SI-45)**

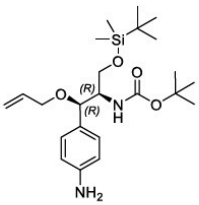

To a stirred solution of **SI-44** (15.0 g, 37.8 mmol) in DMF (120 ml, 0.32 M) was added LiHMDS (1 M in THF) (37.8 ml, 37.8 mmol) at –20 °C. Then, allyl bromide (5.03 g, 41.6 mmol) was added and the mixture was stirred at rt. After 2 h, TLC indicated complete conversion. The reaction was quenched with water and extracted with EtOAc (2x). The combined organic layers were washed with brine, dried (Na_2SO_4) and concentrated in vacuo. Silica gel column chromatography (20% EtOAc in petroleum ether) yielded **SI-45** (10.0 g, 22.9 mmol, 61%).

^{1}H NMR (500 MHz, DMSO-d_6) δ -0.03 (d, *J* = 4.1 Hz, 6H), 0.84 (s, 9H), 1.23 (br s, 1.8H, rotamer), 1.35 (s, 7.2H, rotamer), 3.26 (dd, *J* = 9.6, 5.8 Hz, 1H), 3.56 – 3.44 (m, 2H), 3.70 – 3.61 (m, 1H), 3.76 (dd, *J* = 13.6, 4.4 Hz, 1H), 4.21 (d, *J* = 6.3 Hz, 1H), 5.01 (s, 2H), 5.06 (d, *J* = 10.4 Hz, 1H), 5.28 – 5.17 (m, 1H), 5.85 – 5.75 (m, 1H), 5.87 (d, *J* = 7.3 Hz, 0.2H, rotamer), 6.25 (d, *J* = 8.8 Hz, 0.8H, rotamer), 6.51 (d, *J* = 8.5 Hz, 2H), 6.88 (d, *J* = 8.2 Hz, 2H).

^{13}C NMR (126 MHz, DMSO-d_6) δ -5.4, 25.8, 27.9, 28.3, 57.5, 58.9, 62.1, 62.5, 68.4, 77.4, 78.9, 113.6, 115.6, 126.1, 127.6, 127.8, 135.5, 148.2, 155.3.

MS calcd for $C_{23}H_{41}N_2O_4Si^+$ (M+H)$^+$: 437.28; found: 437.27.

***tert*-butyl *N*-[(1*R*,2*R*)-3-hydroxy-1-phenyl-1-(prop-2-en-1-yloxy)propan-2-yl]carbamate (SI-46)**

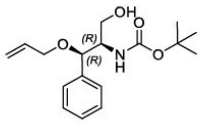

SI-45 (8.00 g, 18.3 mmol) was taken up in water (80.0 ml, 0.23 M) and cooled to 0°C. Then 15 wt% hypophosphorous acid solution (120 ml, 275 mmol) and sodium nitrite (12.6 g, 183 mmol), dissolved in water, were added. The mixture was stirred at rt. After 3 h, TLC indicated complete conversion. The reaction was basified with aq. Na_2CO_3 and extracted with EtOAc (2x). The combined organic layers were dried (Na_2SO_4) and concentrated in vacuo. Silica gel column chromatography (50% EtOAc in petroleum ether) yielded **SI-46** (4.00 g, 13.0 mmol, 71%).

^{1}H NMR (500 MHz, DMSO-d_6) δ 1.13 (br s, 1.8H, rotamer), 1.31 (s, 7.2H, rotamer), 3.17 (dt, *J* = 10.6, 5.4 Hz, 1H), 3.79 – 3.72 (m, 1H), 3.67 – 3.56 (m, 1H), 3.89 – 3.79 (m, 1H), 4.49 (d, *J* = 4.7 Hz, 1H), 4.64 (t, *J* = 5.2 Hz, 0.8H, rotamer), 4.71 (br s, 0.2H, rotamer), 5.17 – 5.03 (m, 1H), 5.27 (dd, *J* = 17.3, 1.3 Hz, 1H), 5.94 – 5.75 (m, 1H, 0.2H rotamer), 6.25 (d, *J* = 9.1 Hz, 0.8H, rotamer), 7.29 – 7.22 (m, 3H), 7.36 – 7.30 (m, 2H).

^{13}C NMR (126 MHz, DMSO-d_6) δ 27.8, 28.2, 57.4, 60.5, 69.2, 77.5, 78.8, 79.0, 115.9, 126.9, 127.4, 128.1, 135.2, 139.9, 155.3.

MS calcd for $C_{17}H_{26}NO_4^+$ $(M+H)^+$: 308.19; found: 308.24.

(2*S*,3*R*)-2-{[(*tert*-butoxy)carbonyl]amino}-3-phenyl-3-(prop-2-en-1-yloxy)propanoic acid (SI-47)

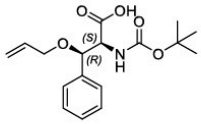

A stirred solution of **SI-46** (5.00 g, 16.3 mmol) in MeCN (20.0 ml) and 2 M NaH_2PO_4 buffer (20.0 ml) (0.40 M) was cooled to 0 °C and (diacetoxyiodo)benzene (524 mg, 1.63 mmol), TEMPO (514 mg, 3.25 mmol) and $NaClO_2$ (5.86 g, 65.1 mmol) were added. The mixture was stirred at rt for 12 h. The reaction was quenched with 2 M aq. Na_2CO_3 and washed with diethyl ether. The aqueous layer was acidified with 1 M aq. HCl and extracted with EtOAc (3x). The combined EtOAc layers were dried (Na_2SO_4) and concentrated in vacuo to yield crude **SI-47** (3.50 g, 10.9 mmol, 67%) which was used in the next step without further purification.

$[\alpha]_{20}^{D}$ = –12.7 (c 1.0, $CHCl_3$).

Major rotamer **^{1}H NMR** (500 MHz, $CDCl_3$) δ 1.33 (s, 9H), 3.84 (dd, *J* = 12.7, 6.1 Hz, 1H), 4.05 (dd, *J* = 12.7, 5.0 Hz, 1H), 4.58 (dd, *J* = 9.4, 2.9 Hz, 1H), 5.05 (d, *J* = 2.8 Hz, 1H), 5.15 – 5.25 (m, 2H), 5.34 (d, *J* = 9.4 Hz, 1H), 5.80 – 5.90 (m, 1H), 7.29 – 7.39 (m, 5H), 9.89 (bs, 1H). **^{13}C NMR** (126 MHz, $CDCl_3$) δ 28.3, 59.2, 70.4, 79.9, 80.2, 117.8, 127.0, 128.4, 128.6, 133.9, 137.2, 155.7, 175.2.

Minor rotamer (selected signals, ratio ~4:1) **^{1}H NMR** (500 MHz, $CDCl_3$) δ 1.17 (s, 9H), 4.37 – 4.43 (m, 1H), 4.94 – 4.98 (m, 1H), 5.71 – 5.79 (m, 1H). **^{13}C NMR** (126 MHz, $CDCl_3$) δ 28.0, 60.8, 70.1, 80.9, 117.6, 127.2, 137.5, 155.4.

HRMS (ESI) calcd for $C_{17}H_{23}NO_5Na^+$ $(M+Na)^+$: 344.1468; found: 344.1457.

Methyl (2*S*)-2-[(2*S*)-2-[(2*S*,3*R*)-2-{[(*tert*-butoxy)carbonyl]amino}-3-phenyl-3-(prop-2-en-1-yloxy)propanamido]-N,3-dimethylbutanamido]-4-methylpentanoate (SI-48)

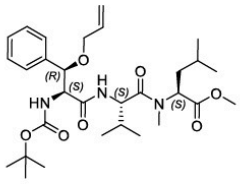

To a stirred solution of methyl N-(L-valyl)-N-methyl-L-leucinate[4] (3.00 g, 11.6 mmol) and **SI-47** (5.60 g, 17.4 mmol) in DMF (9.0 ml, 1.9 M) was added DIPEA (4.06 ml, 23.2 mmol) at 0°C. After 10 minutes, HATU (4.86 g, 12.8 mmol) was added and the mixture was stirred at rt. After complete conversion, the reaction was quenched with water and extracted with EtOAc (2x). The combined EtOAc layers were washed with brine, dried (Na_2SO_4) and concentrated in vacuo. Silica gel column chromatography (50% EtOAc in petroleum ether) yielded **SI-48** (3.00 g, 5.34 mmol, 46%).

Major rotamer: **^{1}H NMR** (500 MHz, $CDCl_3$) δ 0.89 (d, *J* = 6.5 Hz, 3H), 0.92 – 0.95 (m, 6H), 1.01 (d, *J* = 6.8 Hz, 3H), 1.31 (s, 9H), 1.41 – 1.51 (m, 1H), 1.65 – 1.80 (m, 2H), 2.07 – 2.16 (m, 1H), 3.01 (s, 3H), 3.69 (s, 3H), 3.86 (dd, *J* = 12.4, 6.1 Hz, 1H), 4.01 (dd, *J* = 12.3, 5.4 Hz, 1H), 4.42 (dd, *J* = 8.6, 2.9 Hz, 1H), 4.86 (dd, *J* = 8.9, 6.4 Hz, 1H), 5.07 – 5.12 (m, 1H), 5.13 – 5.17 (m, 1H), 5.19 – 5.23 (m, 1H), 5.26 (d, *J* = 8.6 Hz, 1H), 5.32 (dd, *J* = 10.5, 5.2 Hz, 1H), 5.81 – 5.92 (m, 1H), 7.25 – 7.33 (m, 6H). **^{13}C NMR** (126 MHz, $CDCl_3$) δ 17.5, 19.6, 21.5, 23.3, 25.0, 28.3, 31.5, 31.8, 37.1, 52.3, 54.1, 54.6, 60.1, 70.7, 79.6, 80.3, 117.5, 126.8, 128.1, 128.5, 134.2, 137.7, 155.5, 169.4, 172.2, 172.3.

Minor rotamer (selected signals, ratio ~ 12:1): **^{1}H NMR** (500 MHz, $CDCl_3$) δ 1.28 (s, 9H), 2.80 (s, 3H), 3.62 (s, 3H), 4.35 (dd, *J* = 9.3, 2.4 Hz, 1H), 4.72 (t, *J* = 7.1 Hz, 1H), 4.81 (dd, *J* = 9.7, 7.6 Hz, 1H).

HRMS (ESI) calcd for $C_{30}H_{48}N_3O_7^+$ $(M+H)^+$: 562.3487; found: 562.3494.

methyl (2*S*)-2-[(2*S*)-2-[(2*S*,3*R*)-2-[(2*S*)-2-{[(*tert*-butoxy)carbonyl]amino}propanamido]-3-phenyl-3-(prop-2-en-1-yloxy)propanamido]-*N*,3-dimethylbutanamido]-4-methylpentanoate (SI-49)

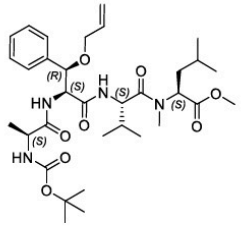

To a solution of **SI-48** (3.00 g, 5.34 mmol) in DCM (40.0 ml, 0.13 M) was added HCl (4N in dioxane) (10.0 ml) dropwise at 0°C and the mixture was allowed to reach rt and stirred for 3 h. The solvents were evaporated in vacuo and the crude amine was used in the peptide coupling without further purification.

To a solution of the deprotected tripeptide (3.00 g, 6.50 mmol) in DMF (30.0 ml, 0.22 M) was added DIPEA (2.27 ml, 13.0 mmol) at 0°C, followed by addition of HOAt (442 mg, 3.25 mmol), Boc-Ala-OH (1.23 g, 6.50 mmol) and HATU (2.72 g, 7.15 mmol). The mixture was allowed to reach rt and stirred for 16 . The reaction was quenched with water and extracted with EtOAc. The organic layer was washed with brine, dried (Na_2SO_4)and concentrated in vacuo. Silica gel column chromatography (50% EtOAc in petroleum ether) yielded **SI-49** (2.00 g, 3.16 mmol, 49%) as a white solid.

$[\alpha]_{20}^{D}$ = −53.6 (c 1.0, $CHCl_3$).

Major rotamer: **^{1}H NMR** (500 MHz, $CDCl_3$) δ 0.90 – 0.94 (m, 6H), 0.95 (d, *J* = 6.7 Hz, 3H), 0.99 (d, *J* = 6.7 Hz, 3H), 1.29 (d, *J* = 7.0 Hz, 3H), 1.45 (s, 9H), 1.47 – 1.53 (m, 1H), 1.67 – 1.78 (m, 2H), 2.06 – 2.17 (m, 1H), 2.98 (s, 3H), 3.69 (s, 3H), 3.89 (ddt, *J* = 12.5, 6.1, 1.4 Hz, 1H), 4.04 (ddt, *J* = 12.5, 5.1, 1.5 Hz, 1H), 4.09 – 4.15 (m, 1H), 4.69 (dd, *J* = 7.5, 3.4 Hz, 1H), 4.81 (dd, *J* = 8.8, 6.1 Hz, 1H), 4.85 – 4.92 (m, 1H), 5.03 (d, *J* = 3.4 Hz, 1H), 5.17 (dq, *J* = 10.5, 1.4 Hz, 1H), 5.25 (dq, *J* = 17.3, 1.6 Hz, 1H), 5.36 (dd, *J* = 10.6, 5.2 Hz, 1H), 5.90 (dddd, *J* = 16.8, 10.8, 6.1, 5.1 Hz, 1H), 6.80 (d, *J* = 7.5 Hz, 1H), 7.20 – 7.31 (m, 5H), 7.38 (d, *J* = 8.8 Hz, 1H). **^{13}C NMR** (126 MHz, $CDCl_3$) δ 17.4, 18.4, 19.6, 21.5, 23.3, 24.8, 28.3, 31.2, 31.4, 37.0, 50.4, 52.1, 54.1, 54.5, 57.9, 70.5, 78.8, 80.2, 117.4, 126.9, 128.2, 128.3, 133.9, 137.1, 155.4, 168.4, 171.9, 172.1, 172.4.

Minor rotamer (selected signals) **^{1}H NMR** (500 MHz, $CDCl_3$) δ 1.01 (d, *J* = 6.7 Hz, 4H), 1.24 (d, *J* = 7.1 Hz, 5H), 1.48 (s, 9H), 2.83 (s, 3H), 3.62 (s, 3H), 4.59 – 4.65 (m, 1H), 6.88 (d, *J* = 8.2 Hz, 1H).

HRMS (ESI) calcd for $C_{33}H_{53}N_4O_8^+$ $(M+H)^+$: 633.3858; found: 688.3866.

Methyl *N*-(((2*S*,3*R*)-2-((2*S*)-2-((4*R*)-2-((((9*H*-fluoren-9-yl)methoxy)carbonyl)(methyl)amino)-5-((*tert*-butyldimethylsilyl)oxy)-4-methylpentanamido)propanamido)-3-(allyloxy)-3-phenylpropanoyl)-L-valyl)-N-methyl-L-leucinate (SI-50)

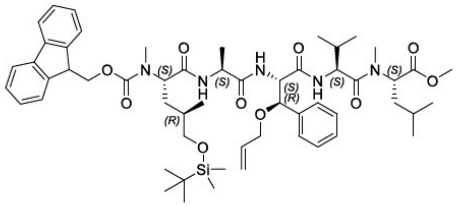

A 25 ml round-bottom flask was charged with **SI-49** (750 mg, 1.20 mmol) and 4 N HCl in 1, 4-dioxane (3.00 ml, 10 equiv) was added at rt. After completion of the reaction, the solvent was evaporated and the crude peptide was reacted according to *GP4*: **SI-21** (590 mg, 1.20 mmol), HOBt (197 mg, 1.30 mmol), EDC (250 mg, 1.30 mmol), NMM (260 µl, 2.40 mmol) (18 h). Flash chromatography (CyH/EtOAc 100:0 – 60:40) followed by lyophilization afforded **SI-50** (868 mg, 860 µmol, 72% yield) as a white amorphous solid. R_f = 0.43 (PE/EtOAc 1:1).

$[\alpha]_{20}^{D}$ = −49.1 (c 0.5, $CHCl_3$).

^{1}H NMR (500 MHz, $CDCl_3$) δ 0.00 – 0.04 (m, 6H), 0.88 (s, 9H), 0.90 –0.98 (m, 12H), 1.00 (d, *J* = 6.8 Hz, 3H), 1.29 (d, *J* = 7.0 Hz, 3H), 1.40 – 1.63 (m, 3H), 1.67 – 1.83 (m, 2H), 1.85 – 2.03 (m, 2H), 2.08 – 2.19 (m, 1H), 2.82 (s, 3H), 2.98 (s, 3H), 3.38 – 3.61 (m, 2H), 3.69 (s, 3H), 3.82 – 3.90 (m, 1H), 3.97 – 4.09 (m, 1H), 4.26 (t, *J* = 6.7 Hz, 1H), 4.31 – 4.40 (m, 1H), 4.43 – 4.54 (m, 2H), 4.67 – 4.77 (m, 2H), 4.81 (dd, *J* = 8.7, 5.8 Hz, 1H), 4.94 – 5.05 (m, 1H), 5.12 – 5.20 (m, 1H), 5.22 – 5.29 (m, 1H), 5.36 (dd, *J* = 10.6, 5.1 Hz, 1H), 5.84 – 5.97 (m, 1H), 6.41 – 6.73 (m, 2H), 7.17 – 7.23(m, 2H), 7.27 – 7.33 (m, 3H), 7.36 – 7.44 (m, 3H), 7.52 – 7.63 (m, 3H), 7.76 (d, *J* = 7.6 Hz, 2H).

^{13}C NMR (126 MHz, $CDCl_3$) δ -5.3, -5.2, 17.4, 17.7, 18.3, 18.5, 19.7, 21.5, 23.4, 25.0, 26.1, 27.0, 29.9, 31.2, 31.3, 31.6, 32.3, 37.1, 47.4, 49.3, 52.3, 54.2, 54.6, 56.8, 57.9, 67.2, 67.9, 70.6, 78.9, 117.6, 120.2, 125.1, 127.0, 127.2, 127.9, 128.4, 128.5, 134.0, 137.0, 141.5, 144.0, 157.3, 168.3, 170.9, 171.6, 172.1, 172.2.

HRMS (ESI): calcd for $C_{56}H_{82}N_5O_{10}Si^+$ $(M+H)^+$: 1012.5825; found: 1012.5807.

Methyl *N*-(((2*S*,3*R*)-3-(allyloxy)-2-((*S*)-2-((2*S*,4*R*)-2-((*S*)-2-(((allyloxy)carbonyl)amino)-N-methyl-3-(1-methyl-1*H*-indol-3-yl)propanamido)-5-((tert-butyldimethylsilyl)oxy)-4-methylpentanamido)propanamido)-3-phenylpropanoyl)-L-valyl)-*N*-methyl-L-leucinate (SI-51)

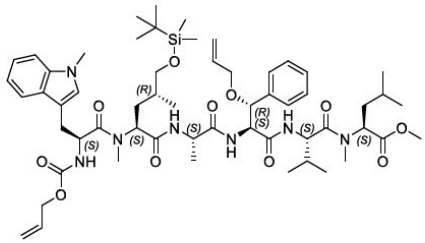

SI-50 (400 mg, 395 µmol) was dissolved in DCM (4.0 ml, 0.1 M), tris(2-aminoethyl)amine (592 µl, 3.95 mmol) was added and the reaction mixture was stirred vigorously. After completion of the reaction (TLC-monitoring; 30 minutes) the reaction mixture was washed with saturated NaCl solution (20 ml ×3) and phosphate buffer (67.0 mM, pH 5.5) (30 ml ×3). The aqueous phase was back-extracted with DCM (1x20 ml). The organic phase was dried (Na_2SO_4) and evaporated in vacuo. The resulting crude peptide was reacted according to *GP3*: *N*α-((allyloxy)carbonyl)-1-methyl-L-tryptophan (143 mg, 474 µmol), BEP (130 mg, 468 µmol), NMM (109 µl, 987 µmol) (18 h). Flash chromatography (CyH/EtOAc 100:0 – 45:55) followed by lyophilization afforded **SI-51** (189 mg, 176 µmol, 44%) as a white amorphous solid. R_f = 0.36 (PE/EtOAc 2:3).

$[\alpha]_{20}^{D}$ = −38.4 (c 1.0, $CHCl_3$).

^{1}H NMR (500 MHz, $CDCl_3$) *(mixture of rotamers, ratio ~5:3:1)* δ -0.01 – -0.02 (m, 1.5H), 0.02 – 0.03 (m, 4.7H), 0.09 (s, 0.5H), 0.16 – 0.19 (m, 0.3H), 0.49 (d, *J* = 6.6 Hz, 0.6H), 0.85 (s, 2.8H), 0.86 – 0.93 (m, 16.2H), 0.94 – 1.01 (m, 3.2H), 1.15 – 1.33 (m, 6.2H), 1.42 (s, 0.6H) 1.44 – 1.58 (m, 3.3H), 1.65 – 1.83 (m, 3.2H), 1.90 – 2.03 (m, 1.8H), 2.02 – 2.25 (m, 2.8H), 2.25 – 2.39 (m, 0.9H), 2.74 – 2.79 (m, 2.8H), 2.81 (s, 3.0H), 2.83 – 2.90 (m, 0.7H), 2.95 – 3.04 (m, 4.3H), 3.05 – 3.32 (m, 3.3H), 3.33 – 3.50 (m, 0.5H), 3.62 – 3.76 (m, 7.9H), 3.80 – 3.95 (m, 1.6H), 3.97 – 4.17 (m, 2.1H), 4.40 – 4.84 (m, 6.7H), 4.85 – 5.42 (m, 9.7H), 5.76 – 6.00 (m, 3.1H), 6.81 – 6.97 (m, 2.0H), 7.06 – 7.16 (m, 1.5H), 7.18 – 7.25 (m, 4.2H), 7.27 – 7.33 (m, 3.2H), 7.50 – 7.57 (m, 0.9H), 7.57 – 7.61 (m, 0.3H), 7.64 (d, *J* = 7.9 Hz, 0.7H).

^{13}C NMR (126 MHz, $CDCl_3$) *(mixture of rotamers)* δ -5.28, -5.26, -5.2, -3.4, 15.9, 17.7, 17.8, 18.5, 19.5, 19.6, 21.5, 23.4, 25.0, 25.3, 25.8, 26.1, 27.0, 28.6, 29.3, 29.8, 30.3, 31.3, 31.5, 31.6, 32.2, 32.8, 37.1, 38.8, 50.1, 50.3, 51.0, 51.7, 52.28, 52.30, 54.3, 54.4, 54.6, 54.7, 54.8, 57.9, 58.2, 58.3, 59.0, 65.9, 66.0, 66.4, 67.3, 67.6, 68.4, 70.6, 70.7, 70.8, 70.9, 78.7, 79.1, 79.3, 108.4, 108.6, 109.5, 109.58, 109.65, 117.4, 117.68, 117.74, 118.2, 118.37, 118.41, 118.7, 119.4, 119.5, 122.0, 122.1, 126.99, 127.04, 127.1, 127.87, 127.92, 128.0, 128.3, 128.4, 128.5, 132.2, 132.3, 132.9, 133.8, 134.1, 137.0, 137.1, 137.3, 156.4, 156.7, 168.5, 168.7, 168.8, 170.7, 171.8, 172.0, 172.20, 172.25, 172.5, 172.7, 173.6.

Selected diagnostic peaks:

Major rotamer: **^{1}H NMR** (500 MHz, $CDCl_3$) *δ* 0.02 (s, 3H), 0.03 (s, 3H), 0.87 (s, 9H), 1.65 – 1.83 (m, 3 H), 2.80 (s, 3H), 3.00 (s, 3H), 3.69 (s, 3H), 6.90 – 6.93 (m, 1H), 7.64 (d, *J* = 7.9 Hz, 1H). **^{13}C-NMR** (126 MHz, $CDCl_3$) *δ* 26.1, 37.1, 79.1, 108.6, 156.4.

Minor rotamer: **^{1}H NMR** (500 MHz, $CDCl_3$) *δ* -0.02 (s, 3H), -0.01 (s, 3H), 0.84 (s, 9H), 2.77 (s, 3H), 2.97 (s, 3H), 3.68 (s, 3H), 6.84 – 6.88 (m, 1H). **^{13}C-NMR** (126 MHz, $CDCl_3$) *δ* 26.0, 79.3, 108.4, 156.7.

HRMS (ESI): calcd for $C_{57}H_{88}N_7O_{11}Si^+$ $(M+H)^+$: 1074.6306; found: 1074.6298.

Methyl *N*-(((2*S*,3*R*)-3-(allyloxy)-2-((*S*)-2-((2*S*,4*R*)-2-((*S*)-2-((*S*)-2-(((allyloxy)(methyl)amino)-3-carbonyl)methylbutanamido)-N-methyl-3-(1-methyl-1*H*-indol-3-yl)propanamido)-5-((tert-butyldimethylsilyl)oxy)-4-methylpentanamido)propanamido)-3-phenylpropanoyl)-L-valyl)-*N*-methyl-L-leucinate (SI-52)

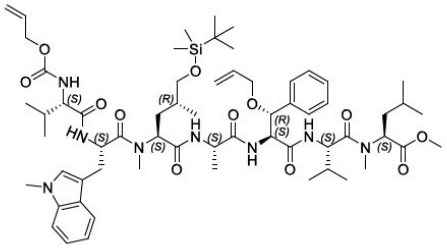

Prepared according to *GP2* and *GP4*: **SI-51** (170 mg, 158 µmol), $Pd(PPh_3)_4$ (5.49 mg, 4.75 µmol), DMBA (74.0 mg, 475 µmol); Alloc-Val-OH (41.5 mg, 206 µmol), NMM (34.9 µl, 317 µmol), HOBt (26.4 mg, 170 µmol), EDC (33.4 mg, 170 µmol) (18 h). Flash chromatography (CyH/EtOAc 100:0 – 60:40) followed by lyohpilization afforded **SI-52** (107 mg, 91.0 µmol, 57% yield) as a white amorphous solid. R_f = 0.45 (PE/EtOAc 2:3).

$[\alpha]_{20}^{D}$ = –58.7 (c 0.5, $CHCl_3$).

^{1}H NMR (500 MHz, $CDCl_3$) *(mixture of rotamers, ratio ~2:1)* δ -0.07 – 0.00 (m, 3.1H), 0.02 (d, *J* = 5.3 Hz, 7.3H), 0.05 – 0.12 (m, 1.2H), 0.45 (d, *J* = 6.7 Hz, 1.0H), 0.83 (m, 9.9H), 0.84 – 0.89 (m, 12.1H), 0.89 – 1.02 (m, 23.8H), 1.12 – 1.32 (m, 5.8H), 1.33 – 1.57 (m, 4.2H), 1.64 – 1.89 (m, 3.0H), 1.89 – 2.23 (m, 3.6H), 2.70 (s, 1.5H), 2.76 (s, 3.0H), 2.79 – 2.94 (m, 1.1H), 3.03 – 3.18 (m, 2.4H), 3.22 (dd, *J* = 14.5, 7.7 Hz, 1.0H), 3.28 – 3.36 (m, 0.4H), 3.41 (d, *J* = 4.6 Hz, 2.4H), 3.62 – 3.72 (m, 9.1H), 3.73 (s, 1.6H), 3.83 – 3.94 (m, 1.8H), 3.99 – 4.07 (m, 2.7H), 4.24 (t, *J* = 7.0 Hz, 0.8H), 4.35 – 4.41 (m, 0.2H), 4.48 – 4.63(m, 3.9H), 4.76 – 4.86 (m, 1.6H), 4.88 – 5.05 (m, 3.4H), 5.05 – 5.46 (m, 10.7H), 5.65 (d, *J* = 9.1 Hz, 0.4H), 5.80 – 6.04 (m, 4.5H), 6.30 (d, *J* = 6.9 Hz, 1.0H), 6.51 (d, *J* = 6.9 Hz, 0.2H), 6.52 –

6.61 (m, 0.1H), 6.68 (d, *J* = 7.5 Hz, 0.2H), 6.74 – 6.83 (m, 2.5H), 6.85 – 6.89 (m, 1.7H), 7.10 (m, 1.7H), 7.17 – 7.25 (m, 5.5H), 7.27 – 7.33 (m, 4.4H), 7.35 – 7.43 (m, 1.0H), 7.43 – 7.50 (m, 2.1H), 7.51 – 7.58 (m, 1.5H), 7.60 – 7.73 (m, 2.8H), 8.15 (d, *J* = 7.3 Hz, 0.4H).

^{13}C NMR (126 MHz, $CDCl_3$) *(mixture of rotamers)* δ -5.3, -5.2, -5.2, 16.1, 17.4, 17.6, 17.7, 18.0, 18.1, 18.4, 18.5, 19.18, 19.25, 19.5, 19.67, 19.68, 21.5, 21.58, 21.60, 23.40, 23.43, 25.0, 26.07, 26.09, 28.2, 28.7, 29.3, 29.8, 31.2, 31.3, 31.37, 31.40, 31.5, 31.61, 31.65, 31.8, 32.3, 32.8, 37.1, 49.4, 50.0, 50.1, 52.27, 52.28, 54.17, 54.22, 54.58, 54.65, 55.9, 57.6, 58.0, 58.3, 60.0, 60.1, 65.9, 66.1, 67.0, 68.5, 70.58, 70.60, 70.7, 78.7, 79.1, 108.42, 108.44, 109.5, 109.6, 117.6, 117.9, 118.1, 118.7, 118.8, 119.5, 119.6, 122.0, 122.2, 127.1, 127.3, 127.8, 128.0, 128.27, 128.31, 128.4, 128.5, 128.6, 128.7, 132.08, 132.10, 132.2, 132.3, 132.8, 134.08, 134.15, 136.99, 137.03, 137.1, 156.2, 156.4, 168.3, 168.4, 168.6, 170.3, 170.9, 171.6, 171.9, 172.0, 172.07, 172.09, 172.2, 172.2, 172.8.

Selected diagnostic peaks:

Major rotamer: **^{1}H NMR** (500 MHz, $CDCl_3$) *δ* 0.01 (s, 3H), 0.02 (s, 3H), 0.87 (s, 9H), 1.64 – 1.89 (m, 3 H), 2.76 (s, 3H), 2.98 (s, 3H), 3.69 (s, 3H), 6.87 – 6.92 (m, 1H). **^{13}C-NMR** (126 MHz, $CDCl_3$) *δ* 23.40, 26.09, 37.1, 54.65, 79.1, 156.2.

Minor rotamer: **^{1}H NMR** (500 MHz, $CDCl_3$) *δ* -0.04 (s, 3H), -0.03 (s, 3H), 0.83 (s, 9H), 2.70 (s, 3H), 2.97 (s, 3H), 3.68 (s, 3H), 6.74 – 6.79 (m, 1H), 8.15 (d, *J* = 7.3 Hz, 1H). **^{13}C-NMR** (126 MHz, $CDCl_3$) *δ* 23.43, 26.07, 54.58, 78.7, 156.4.

HRMS (ESI): calcd for $C_{63}H_{99}N_8O_{12}Si^+$ $(M+H)^+$: 1173.6990; found: 1173.6992.

(3*S*,6*S*,9*S*,12*S*,15*S*,18*S*,21*S*)-15-((*R*)-(Allyloxy)(phenyl)methyl)-21-((*R*)-3-hydroxy-2-methylpropyl)-9-isobutyl-6,12-diisopropyl-1,10,18-trimethyl-3-((1-methyl-1*H*-indol-3-yl)methyl)-1,4,7,10,13,16,19-heptaazacyclohenicosane-2,5,8,11,14,17,20-heptaone (14)

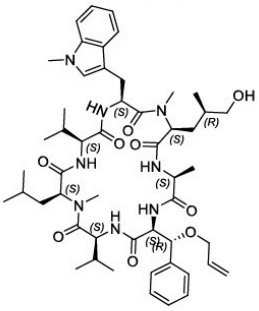

Prepared according to *GP6a*: **SI-52** (81.5 mg, 69.0 µmol), 1 M LiOH (83.0 µl, 83.0 µmol) (3.5 h); $Pd(OAc)_2$ (460 µg, 2.00 µmol), TPPTS (2.35 mg, 4.14 µmol), Et_2NH (36.0 µl, 345 µmol) (1 h); HATU (92.0 mg, 240 µmol), DIPEA (47.0 µl, 280 µmol) (addition over 1.5 h, additional 16 h); NH_4F (51.0 mg, 1.40 mmol) (17 h) RP flash chromatography (H_2O/MeCN 90:10 - 5:95) followed by lyophilizaiton afforded **14** (32.8 mg, 35.0 µmol, 50%) as an off-white, amorphous solid.

$[\alpha]_{20}^{D}$ = –89.8 (c 0.2, $CHCl_3$).

^{1}H NMR (500 MHz, $CDCl_3$) δ -0.56 – -0.43 (m, 1H), 0.33 (d, *J* = 6.7 Hz, 3H), 0.58 – 0.65 (m, 6H), 0.95 – 1.00 (m, 9H), 1.08 (d, *J* = 6.6 Hz, 3H), 1.18 (d, *J* = 7.2 Hz, 3H), 1.25 (s, 3H), 1.52 – 1.62 (m, 2H), 1.90 – 2.00 (m, 6H), 2.15 – 2.39 (m, 2H), 2.57 (s, 3H), 2.83 (s, 3H), 2.97 – 3.01 (m, 1H), 3.00 – 3.18 (m, 1H), 3.32 (dd, *J* = 13.6, 10.2 Hz, 1H), 3.73 (s, 3H), 3.86 – 4.13 (m, 2H), 4.33 (d, *J* = 10.6 Hz, 1H), 4.47 (t, *J* = 8.5 Hz, 1H), 4.72 – 4.81 (m, 1H), 4.84 (dd, *J* = 10.4, 3.7 Hz, 1H), 4.93 (t, *J* = 5.2 Hz, 1H), 5.21 – 5.29 (m, 2H), 5.30 – 5.44 (m, 1H), 5.85 – 6.06 (m, 1H), 6.74 – 6.92 (m, 2H), 7.09 (t, *J* = 7.4 Hz, 1 H), 7.15 – 7.26 (m, 6H), 7.56 (d, *J* = 7.8 Hz, 1H), 8.21 (d, *J* = 9.4 Hz, 1H), 8.32 (d, *J* = 7.8 Hz, 1H), 8.51 (d, *J* = 10.3 Hz, 1H).

^{13}C NMR (126 MHz, $CDCl_3$) δ 17.4, 18.7, 19.4, 20.1, 20.2, 20.9, 22.7, 23.7, 25.4, 28.5, 29.4, 29.7, 29.8, 31.0, 31.6, 31.8, 32.9, 33.3, 39.1, 50.6, 51.2, 55.4, 56.1, 59.1, 59.4, 65.9, 70.6, 77.8, 107.8, 109.8, 118.1, 118.7, 119.7, 122.4, 127.6, 127.9, 128.2, 128.3, 128.8, 133.5, 135.4, 137.0, 168.8, 169.2, 170.1, 170.7, 171.4, 171.7, 172.2.

HRMS (ESI): calcd for $C_{51}H_{75}N_8O_9^+$ $(M+H)^+$: 943.5652; found: 943.5608.

(3*S*,3'*S*,6*S*,6'*S*,9*S*,9'*S*,12*S*,12'*S*,15*S*,15'*S*,18*S*,18'*S*,21*S*,21'*S*)-15,15'-((1*R*,1'*R*)-(((*E*)-But-2-ene-1,4-diyl)bis(oxy))bis(phenylmethylene))bis(21-((*R*)-3-hydroxy-2-methylpropyl)-9-isobutyl-6,12-diisopropyl-1,10,18-trimethyl-3-((1-methyl-1*H*-indol-3-yl)methyl)-1,4,7,10,13,16,19-heptaazacyclohenicosane-2,5,8,11,14,17,20-heptaone) (17)

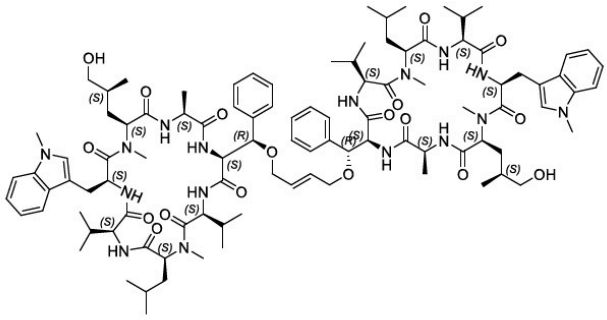

A 4 ml vial was charged with **14** (9.00 mg, 9.65 µmol) and Grubbs catalyst 1st Gen (793 µg, 0.96 µmol, 10 mol%). Freshly degassed (3x freeze-pump-thaw) DCM (48.2 µl) was added, and the vial was flushed with Argon and sealed. The mixture was heated to 45 °C. After 16 h, the reaction mixture was evaporated in vacuo. RP flash chromatography (H_2O/MeCN 90:10 – 5:95) followed by prep HPLC (H_2O/MeCN 70:30 – 0:100) and lyophilization yielded **17** (1.20 mg, 0.70 µmol, 13%) as a white amorphous solid.

$[\alpha]_{20}^{D}$ = −106.3 (c 0.2, $CHCl_3$).

^{1}H NMR (500 MHz, $CDCl_3$) δ -0.45 (d, *J* = 14.2 Hz, 2H), 0.30 – 0.38 (m, 6H), 0.57 – 0.68 (m, 12H), 0.85 – 0.97 (m, 18H), 1.02 – 1.11 (m, 6H), 1.11 – 1.19 (m, 6H), 1.21 – 1.49 (m, 20H), 1.51 – 1.76 (m, 4H), 1.77 – 2.38 (m, 6H), 2.57 (s, 6H), 2.81 (s, 6H), 2.87 – 3.01 (m, 2H), 3.01 – 3.23 (m, 2H), 3.26 – 3.40 (m, 2H), 3.71 – 3.75 (s, 6H), 3.91 – 4.12 (m, 4H), 4.13 – 4.28 (m, 2H), 4.29 – 4.41 (m, 2H), 4.46 (t, *J* = 8.4 Hz, 2H), 4.63 – 4.93 (m, 6H), 5.25 (d, *J* = 5.5 Hz, 2H), 5.86 –5.94 (m, 2H), 6.74 – 6.95 (m, 2H), 7.07 – 7.13 (m, 2H), 7.14 – 7.24 (m, 8H), 7.49 – 7.64 (m, 1H), 7.67 – 7.79 (m, 1H), 8.07 – 8.35 (m, 4H), 8.52 (d, *J* = 10.1 Hz, 2H).

^{13}C NMR (126 MHz, $CDCl_3$) δ 17.4, 18.7, 19.4, 20.0, 20.2, 20.7, 22.7, 23.7, 25.4, 28.5, 29.4, 29.7, 29.9, 30.9, 31.6, 32.8, 33.2, 39.0, 50.7, 51.2, 55.3, 56.2, 59.1, 59.4, 66.1, 68.3, 69.6, 77.9, 107.8, 109.8, 118.7, 119.7, 122.4, 127.7, 127.9, 128.2, 128.3, 128.9, 131.0, 135.3, 137.0, 168.9, 169.2, 170.0, 170.7, 171.5, 171.7, 172.2.

HRMS (ESI): calcd for $C_{100}H_{145}N_{16}O_{18}^+$ $(M+H)^+$: 1858.0917; found: 1858.0905.

Synthesis of Trp-Nα-methylated exit vector 7 Homo-BacPROTACs (21, 22)

Methyl *N*-(((2*S*,3*R*)-2-((*S*)-2-((2*S*,4*R*)-2-((*S*)-2-(((allyloxy)carbonyl)(methyl)amino)-*N*-methyl-3-(1-methyl-1*H*-indol-3-yl)propanamido)-5-((*tert*-butyldimethylsilyl)oxy)-4-methylpentanamido)propanamido)-3-methoxy-3-phenylpropanoyl)-L-valyl)-*N*-methyl-L-leucinate (18)

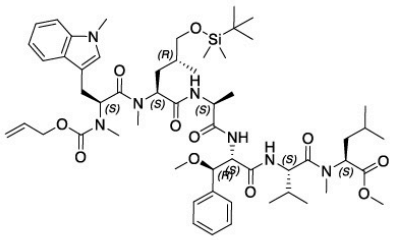

72

*N*α-((allyloxy)carbonyl)-1-methyl-L-tryptophan (100 mg, 331 µmol) and methyl iodide (124 µl, 1.99 mmol) were dissolved in THF (3.5 ml) and cooled to 0 °C. NaH (60%) (39.7 mg, 992 µmol) was added in one portion and the reaction mixture was slowly warmed to rt overnight. After 22 h, 1 M HCl was added carefully (gas evolution), the resulting mixture was extracted with EtOAc (3x). The combined org phases were washed with 1 M Na_2SO_3 and sat. NaCl soln., dried (Na_2SO_4) and evaporated in vacuo. The crude methylated Trp-derivative was used in the peptide coupling without further purification.

Pentapeptide **2** (270 mg, 301 µmol) was deprotected according to *GP1* and the resulting amine was coupled to crude methylated Trp derivatives (as described above) according to *GP3:* BEP (90.6 mg, 331 µmol), NMM (66.2 µl, 602 µmol) (16 h). Flash chromatography (DCM/EtOAc 100:0 – 50:50) followed by lyophilization afforded **18** (242 mg, 228 µmol, 76%) as a white, solid foam. R_f = 0.48 (DCM/EtOAc 1:1).

$[\alpha]_{20}^{D}$ = −87.5 (c 0.5, $CHCl_3$).

^{1}H NMR (500 MHz, $CDCl_3$) *(mixture of rotamers, ratio ~2:2:1)* δ -0.05 (s, 0.5H), -0.03 (s, 0.6H), -0.01 – 0.06 (m, 4.9H), 0.43 (d, *J* = 6.7 Hz, 0.4H), 0.83 (s, 1.6H), 0.87 – 0.90 (m, 7.6H), 0.90 – 0.97 (m, 11.6H), 0.98 – 1.01 (m, 2.8H), 1.22 – 1.28 (m, 1.7H), 1.28 – 1.36 (m, 1.0H), 1.44 – 1.55 (m, 2.1H), 1.66 – 1.73 (m, 1.0H), 1.73 – 1.81 (m, 1.6H), 1.87 – 1.97 (m, 0.8H), 2.07 – 2.17 (m, 1.0H), 2.75 – 2.81 (m, 2.5H), 2.88 – 2.95 (m, 1.9H), 2.96 – 3.02 (m, 3.0H), 3.02 – 3.05 (m, 0.4H), 3.11 – 3.17 (m, 0.6H), 3.29 (s, 0.6H), 3.33 (s, 2.4H), 3.41 – 3.56 (m, 1.9H), 3.60 – 3.73 (m, 5.3H), 4.10 – 4.23 (m, 0.6H), 4.23 – 4.34 (m, 0.5H), 4.34 – 4.51 (m, 0.2H), 4.46 (dd, *J* = 12.8, 6.1 Hz, 0.3H), 4.50 – 4.74 (m, 2.4H), 4.75 – 4.87 (m, 1.9H), 4.88 – 5.01 (m, 0.2H), 5.03 – 5.30 (m, 2.4H), 5.30 – 5.41 (m, 1.1H), 5.47 – 5.56 (m, 0.3H), 5.59 – 5.72 (m, 0.2H), 5.82 – 6.00 (m, 0.5H), 6.17 (d, *J* = 7.0 Hz, 0.3H), 6.33 (d, *J* = 6.9 Hz, 0.2H), 6.58 – 6.69 (m, 0.8H), 6.82 – 6.96 (m, 0.8H), 7.05 – 7.13 (m, 0.8H), 7.15 – 7.35 (m, 7.9H), 7.52 – 7.63 (m, 0.6H), 7.71 (d, *J* = 8.0 Hz, 0.3H).

^{13}C NMR (126 MHz, $CDCl_3$) *(mixture of rotamers)* δ -5.32, -5.28, 17.3, 17.6, 18.4, 19.7, 21.5, 22.3, 23.4, 24.9, 25.3, 26.0, 29.1, 29.6, 30.0, 30.4, 30.6, 30.8, 31.3, 31.5, 32.2, 32.3, 32.7, 32.8, 37.0, 49.0, 49.2, 49.7, 52.3, 54.2, 54.6, 55.6, 56.7, 57.6, 57.7, 57.9, 66.5, 66.8, 67.1, 81.3, 109.3, 109.4, 117.3, 117.8, 118.6, 118.7, 118.8, 119.1, 119.2, 121.7, 127.0, 127.8, 127.88, 127.94, 128.2, 128.37, 128.42, 128.5, 132.4, 132.9, 136.87, 136.94, 137.0, 155.6, 156.3, 168.4, 170.5, 171.4, 171.9, 172.1, 172.2.

Selected diagnostic peaks:

Major rotamer 1: **^{1}H NMR** (500 MHz, $CDCl_3$) δ 0.03 (s, 3H), 0.04 (s, 3H), 0.89 (s, 9H), 2.78 (s, 3H), 2.99 (s, 3H), 3.33 (s, 3H), 3.69 (s, 4H), 5.32 – 5.35 (m, 1H), 6.92 (s, 1H). **^{13}C NMR** (126 MHz, $CDCl_3$) δ 26.1, 156.3.

Major rotamer 2: **^{1}H NMR** (500 MHz, $CDCl_3$) δ 0.04 (s, 3H), 0.05 (s, 3H), 0.89 (s, 9H), 5.35 – 5.38 (m, 1H), 6.85 (s, 1H).

Minor rotamer: **^{1}H NMR** (500 MHz, $CDCl_3$) δ -0.05 (s, 3H), -0.03 (s, 3H), 0.43 (d, *J* = 6.7 Hz, 3H), 0.83 (s, 9H), 3.29 (s, 3H), 3.65 (s, 3H), 4.46 (dd, *J* = 12.8, 6.1 Hz, 1H), 5.52 (dd, *J* = 9.1, 5.7 Hz, 1H), 6.33 (d, *J* = 6.9 Hz, 1H), 6.88 (s, 1H), 7.71 (d, *J* = 8.0 Hz, 2H). **^{13}C NMR** (126 MHz, $CDCl_3$) δ 156.6.

HRMS (ESI) calcd for $C_{56}H_{88}N_7O_{11}Si^+$ $(M+H)^+$: calcd 1062.6323; found 1062.6306.

methyl *N*-(((2*S*,3*R*)-2-((*S*)-2-((2*S*,4*R*)-2-((*S*)-2-((*S*)-2-((((9*H*-fluoren-9-yl)methoxy)carbonyl)amino)-*N*-methylpent-4-ynamido)-*N*-methyl-3-(1-methyl-1*H*-indol-3-yl)propanamido)-5-((*tert*-butyldimethylsilyl)oxy)-4-methylpentanamido)propanamido)-3-methoxy-3-phenylpropanoyl)-L-valyl)-*N*-methyl-L-leucinate (19)

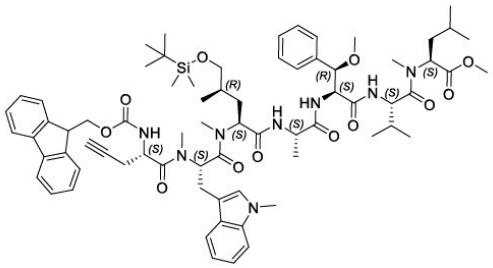

Prepared according to *GP2* and *GP5*: **18** (272 mg, 256 µmol), DMBA (120 mg, 768 µmol), $Pd(PPh_3)_4$ (8.9 mg, 7.68 µmol) (2 h); Fmoc-Pra-OH (120 mg, 358 µmol), $BnNMe_2$ (3.80 µl, 25.6 µmol), DIPEA (58.1 µl, 333 µmol), 1 M iPrOCOCl (358 µl, 358 µmol), NMI (2.04 µl, 25.6 µmol), 4 M HCl (6.4 µl, 25.6 µmol) (4.5 h). Flash chromatography (CyH/EtOAc 100:0 – 30:70) followed by lyophilization yielded **19** (293 mg, 226 µmol, 88%) as a white amorphous solid. R_f = 0.34 (PE/EtOAc 3:7).

$[\alpha]_{20}^{D}$ = −76.9 (c 0.5, $CHCl_3$).

^{1}H NMR (500 MHz, $CDCl_3$) *(mixture of rotamers, ratio ~5:2)* δ -0.06 – 0.00 (m, 1.6H), 0.02 – 0.07 (m, 3.7H), 0.43 (d, *J* = 6.7 Hz, 0.5H), 0.81 – 0.86 (m, 3.1H), 0.89 (s, 6.8H), 0.90 – 1.02 (m, 14.3H), 1.23 – 1.27 (m, 1.1H), 1.30 – 1.37 (m, 1.2H), 1.39 – 1.59 (m, 2.8H), 1.66 – 1.80 (m, 2.0H), 1.84 – 1.88 (m, 0.6H), 1.95 – 2.02 (m, 0.6H), 2.05 (t, *J* = 2.6 Hz, 0.6H), 2.07 – 2.17 (m, 0.9H), 2.54 – 2.63 (m, 0.9H), 2.68 – 2.75 (m, 1.4H), 2.77 (s, 1.4H), 2.80 (s, 1.5H), 2.92 – 2.98 (m, 1.6H), 2.99 (m, 1.9H), 3.09 (s, 1.7H), 3.25 (s, 0.5H), 3.33 (s, 2.5H), 3.34 – 3.61 (m, 0.6H), 3.52 (dd, *J* = 9.7, 4.2 Hz, 1.0H), 3.58 – 3.63 (m, 1.7H), 3.66 – 3.72 (m, 3.4H), 4f.14 (t, *J* = 7.0 Hz, 0.5H), 4.18 – 4.30 (m, 1.1H), 4.33 – 4.48 (m, 1.9H), 4.67 (dd, *J* = 7.5, 3.7 Hz, 0.7H), 4.71 (dd, *J* = 7.0, 3.9 Hz, 0.3H), 4.74 – 4.88 (m, 2.5H), 4.99 – 5.06 (m, 0.6H), 5.30 – 5.39 (m, 0.9H), 5.73 (d, *J* = 8.4 Hz, 0.5H), 5.89 – 5.95 (m, 0.5H), 5.99 (d, *J* = 9.0 Hz, 0.1H), 6.21 (d, *J* = 7.0 Hz, 0.5H), 6.60 (d, *J* = 7.1 Hz, 0.1H), 6.66 (d, *J* = 7.5 Hz, 0.6H), 6.84 (s, 0.2H), 6.91 (s, 0.5H), 7.07 – 7.16 (m, 1.6H), 7.16 – 7.25 (m, 3.9H), 7.27 – 7.37 (m, 4.7H), 7.37 – 7.43 (m, 2.0H), 7.44 – 7.49 m, 2.2H), 7.52 – 7.59 (m, 1.9H), 7.59 – 7.64 (m, 1.5H), 7.64 – 7.70 (m, 2.5H), 7.72 – 7.79 (m, 2.3H).

^{13}C NMR (126 MHz, $CDCl_3$) *(mixture of rotamers)* δ 17.3, 17.9, 18.5, 19.7, 21.5, 23.4, 24.0, 25.0, 25.1, 26.1, 30.9, 31.4, 31.5, 32.2, 32.7, 37.0, 38.7, 47.3, 49.0, 49.7, 52.3, 53.9, 54.2, 54.7, 57.7, 57.9, 67.2, 71.8, 78.6, 81.3, 109.1, 109.4, 118.9, 119.3, 120.2, 121.8, 125.3, 127.0, 127.2, 127.9, 128.4, 128.5, 128.6, 128.7, 132.1, 132.1, 132.2, 132.3, 133.0, 136.8, 137.0, 141.5, 143.9, 155.5, 168.4, 170.2, 171.1, 171.5, 172.1, 172.2.

Selected diagnostic peaks:

Major rotamer: **^{1}H NMR** (500 MHz, $CDCl_3$) δ 0.04 (s, 3H), 0.05 (s, 3H), 0.89 (s, 9H), 2.05 (t, *J* = 2.6 Hz, 1H), 2.80 (s, 3H), 2.98 (d, *J* = 13.2 Hz, 4H), 3.09 (s, 2H), 3.33 (s, 3H), 3.52 (dd, *J* = 9.7, 4.2 Hz, 1H), 3.69 (s, 3H), 4.20 – 4.27 (m, 1H), 4.67 (dd, *J* = 7.5, 3.7 Hz, 1H), 5.35 (dd, *J* = 10.6, 5.2 Hz, 1H), 5.73 (d, *J* = 8.4 Hz, 1H), 6.21 (d, *J* = 7.0 Hz, 1H), 6.66 (d, *J* = 7.5 Hz, 1H), 6.91 (s, 1H). **^{13}C NMR** (126 MHz, $CDCl_3$) δ 26.1, 52.3, 81.3, 155.6.

Minor rotamer: **^{1}H NMR** (500 MHz, $CDCl_3$) δ -0.04 (s, 3H), -0.02 (s, 3H), 0.43 (d, *J* = 6.7 Hz, 3H), 0.84 (s, 9H), 2.77 (s, 3H), 2.96 (s, 3H), 4.14 (t, *J* = 7.0 Hz, 1H), 4.71 (dd, *J* = 7.0, 3.9 Hz, 1H), 5.99 (d, *J* = 9.0 Hz, 1H), 6.60 (d, *J* = 7.1 Hz, 1H), 6.84 (s, 1H).

HRMS (ESI) calcd for $C_{72}H_{99}N_8O_{12}Si^+$ $(M+H)^+$: calcd 1295.7146; found 1295.7156.

(3*S*,6*S*,9*S*,12*S*,15*S*,18*S*,21*S*)-21-((*R*)-3-hydroxy-2-methylpropyl)-9-isobutyl-12-isopropyl-15-((*R*)-methoxy(phenyl)methyl)-1,4,10,18-tetramethyl-3-((1-methyl-1*H*-indol-3-yl)methyl)-6-(prop-2-yn-1-yl)-1,4,7,10,13,16,19-heptaazacyclohenicosane-2,5,8,11,14,17,20-heptaone (20)

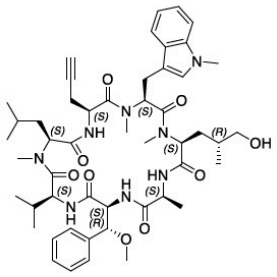

Prepared according to *GP6c*: **19** (50.7 mg, 39.1 µmol), tris(2-aminoethyl)amine (58.6 µl, 391 µmol) (0.5 h); 1 M LiOH (98.0 µl, 98.0 µmol) (4 h); HATU (66.9 mg, 176 µmol), DIPEA (37.6 µl, 215 µmol) (addition over 2.5 h; additional 16 h); NH_4F (14.5 mg, 391 µmol) (16 h). RP flash chromatography (H_2O/MeCN 90:10 – 5:95) followed by lyophilization afforded **20** (16.7 mg, 18.0 mmol, 46%) as a white amorphous solid.

$[\alpha]_{20}^{D}$ = −99.5 (c 0.5, $CHCl_3$).

^{1}H NMR (500 MHz, $CDCl_3$) δ -0.33 – -0.19 (m, 1H), 0.37 (d, *J* = 6.8 Hz, 3H), 0.83 – 0.88 (m, 1H), 0.91 – 0.94 (m, 6H), 0.96 (d, *J* = 6.8 Hz, 3H), 0.98 – 1.03 (m, 1H), 1.07 (d, *J* = 6.6 Hz, 3H), 1.16 – 1.21 (m, 1H), 1.27 (d, *J* = 7.3 Hz, 3H), 1.40 – 1.47 (m, 1H), 1.48 – 1.55 (m, 1H), 1.88 (t, *J* = 2.7 Hz, 1H), 1.89 – 1.94 (m, 1H), 2.17 – 2.24 (m, 1H), 2.29 (dt, *J* = 9.8, 6.7 Hz, 1H), 2.44 (bs, 1H), 2.58 (s, 3H), 2.92 (s, 3H), 2.95 – 3.01 (m, 1H), 3.06 – 3.11 (m, 1H), 3.14 (dd, *J* = 14.3, 6.0 Hz, 1H), 3.37 (s, 3H), 3.39 (s, 3H), 3.47 (dd, *J* = 14.0, 9.3 Hz, 1H), 3.71 (s, 3H), 4.53 (dd, *J* = 10.5, 3.1 Hz, 1H), 4.63 (t, *J* = 9.3 Hz, 1H), 4.71 (dd, *J* = 10.0, 4.5 Hz, 1H), 4.80 (dd, *J* = 10.2, 7.3 Hz, 1H), 4.87 – 4.90 (m, 1H), 5.09 (td, *J* = 9.7, 6.1 Hz, 1H), 5.24 (d, *J* = 5.5 Hz, 1H), 5.38 (dd, *J* = 9.4, 6.1 Hz, 1H), 6.82 (s, 1H), 7.05 – 7.12 (m, 1H), 7.12 – 7.18 (m, 2H), 7.18 – 7.25 (m, 2H), 7.27 – 7.31 (m, 5H), 7.46 (d, *J* = 8.0 Hz, 1H), 8.07 (d, *J* = 10.2 Hz, 1H), 8.31 (d, *J* = 9.3 Hz, 1H).

^{13}C NMR (126 MHz, $CDCl_3$) δ 17.4, 19.4, 19.9, 21.1, 22.1, 22.6, 23.5, 25.1, 26.6, 29.08, 29.09, 30.9, 31.9, 32.5, 32.9, 33.2, 39.0, 47.0, 51.1, 53.5, 55.0, 56.3, 58.0, 58.7, 59.3, 66.0, 71.5, 78.2, 79.7, 108.4, 109.7, 118.8, 119.6, 122.4, 127.3, 127.6, 128.2, 128.7, 129.2, 135.3, 137.0, 167.7, 169.6, 169.9, 170.6, 171.3, 172.1, 173.1.

HRMS (ESI) calcd for $C_{50}H_{71}N_8O_9^+$ $(M+H)^+$: calcd 927.5339; found 927.5337.

(3*S*,3'*S*,6*S*,6'*S*,9*S*,9'*S*,12*S*,12'*S*,15*S*,15'*S*,18*S*,18'*S*,21*S*,21'*S*)-6,6'-((((ethane-1,2-diylbis(oxy))bis(ethane-2,1-diyl))bis(1*H*-1,2,3-triazole-1,4-diyl))bis(methylene))bis(21-((*R*)-3-hydroxy-2-methylpropyl)-9-isobutyl-12-isopropyl-15-((*R*)-methoxy(phenyl)methyl)-1,4,10,18-tetramethyl-3-((1-methyl-1*H*-indol-3-yl)methyl)-1,4,7,10,13,16,19-heptaazacyclohenicosane-2,5,8,11,14,17,20-heptaone) (21)

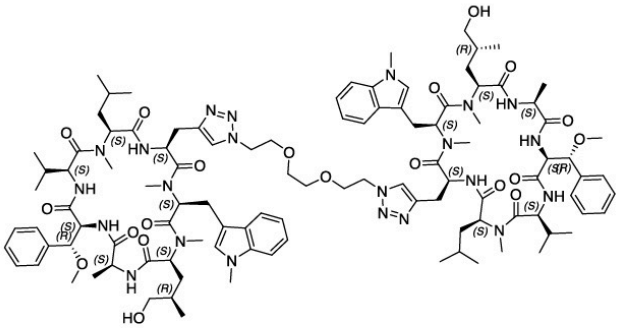

Prepared according to *GP7*: **20** (18.7 mg, 20.2 µmol), 1,2-bis(2-azidoethoxy)ethane (2.02 mg, 10.1 µmol), 1 M $CuSO_4$ (8.08 µl, 8.08 µmol), 1 M sodium ascorbate (13.1 µl, 13.1 µmol) (17 h). RP flash chromatography (H_2O/MeCN 90:10 – 5:95) followed by prep HPLC (H_2O/MeCN 70:30 – 5:95) and lyophilization afforded **21** (12.0 mg, 5.84 µmol, 58%) as a white amorphous solid.

$[\alpha]_{20}^{D}$ = −43.2 (c 0.5, $CHCl_3$).

^{1}H NMR (500 MHz, $CDCl_3$) δ 0.02 – 0.11 (m, 2H), 0.36 (d, *J* = 6.7 Hz, 6H), 0.93 – 1.01 (m, 18H), 1.09 (d, *J* = 6.6 Hz, 6H), 1.13 – 1.15 (m, 2H), 1.24 – 1.33 (m, 2H), 1.35 (d, *J* = 7.5 Hz, 6H), 1.45 – 1.57 (m, 4H), 1.94 – 2.08 (m, 4H), 2.15 – 2.22 (m, 2H), 2.26 (dt, *J* = 9.5, 6.6 Hz, 2H), 2.54 (s, 6H), 2.73 (s, 6H), 2.89 (t, *J* = 5.3 Hz, 2H), 3.01 (d, *J* = 1.7 Hz, 10H), 3.13 – 3.28 (m, 4H), 3.35 (s, 6H), 3.62 – 3.70 (m, 10H), 3.82 – 3.95 (m, 4H), 4.48 – 4.53 (m, 2H), 4.52 – 4.59 (m, 2H), 4.69 (dd, *J* = 9.8, 4.6 Hz, 2H), 4.73 – 4.89 (m, 6H), 4.93 – 5.01 (m, 2H), 5.23 – 5.28 (m, 4H), 5.49 – 5.56 (m, 2H), 6.71 (s, 2H), 6.90 – 6.94 (m, 4H), 6.98 – 7.07 (m, 8H), 7.15 – 7.21 (m, 2H), 7.24 (d, *J* = 8.1 Hz, 2H), 7.30 (s, 2H), 7.41 – 7.46 (m, 4H), 8.18 (d, *J* = 9.3 Hz, 2H), 8.48 (d, *J* = 9.2 Hz, 2H), 8.74 (d, *J* = 8.9 Hz, 2H).

^{13}C NMR (126 MHz, $CDCl_3$) δ 17.5, 19.3, 19.8, 19.9, 22.8, 23.7, 25.1, 25.7, 28.8, 29.0, 30.2, 30.3, 31.2, 32.7, 33.3, 33.9, 39.1, 48.1, 50.4, 51.1, 51.5, 54.5, 56.4, 58.0, 58.9, 59.7, 66.6, 69.8, 70.5, 79.3, 108.9, 109.6, 118.8, 119.4, 122.2, 123.0, 127.0, 127.6, 128.2, 128.4, 135.9, 137.0, 141.4, 167.6, 169.2, 170.4, 171.1, 171.3, 171.7, 173.2.

HRMS (ESI) calcd for $C_{106}H_{153}N_{22}O_{20}^+$ $(M+H)^+$: calcd 2054.1626; found 2054.1671.

(3*S*,3'*S*,6*S*,6'*S*,9*S*,9'*S*,12*S*,12'*S*,15*S*,15'*S*,18*S*,18'*S*,21*S*,21'*S*)-6,6'-((pentane-1,5-diylbis(1*H*-1,2,3-triazole-1,4-diyl))bis(methylene))bis(21-((*R*)-3-hydroxy-2-methylpropyl)-9-isobutyl-12-isopropyl-15-((*R*)-methoxy(phenyl)methyl)-1,4,10,18-tetramethyl-3-((1-methyl-1*H*-indol-3-yl)methyl)-1,4,7,10,13,16,19-heptaazacyclohenicosane-2,5,8,11,14,17,20-heptaone) (22)

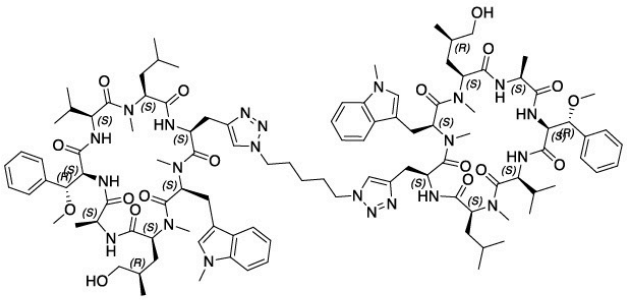

Prepared according to *GP7*: **20** (16.0 mg, 17.3 µmol), 1,5-diazidopentane (1.33 mg, 8.63 µmol), 1 M $CuSO_4$ (6.90 µl, 6.90 µmol), 1 M sodium ascorbate (11.2 µl, 11.2 µmol) (17 h). RP flash chromatography (H_2O/MeCN 90:10 – 5:95) followed by prep HPLC (H_2O/MeCN 75:25 – 5:95) and lyophilization afforded **22** (10.6 mg, 5.28 µmol, 61%) as a white amorphous solid.

$[\alpha]_{20}^{D}$ = −66.5 (c 0.2, $CHCl_3$).

^{1}H NMR (500 MHz, $CDCl_3$) δ 0.06 – 0.13 (m, 2H), 0.36 (d, *J* = 6.7 Hz, 6H), 0.81 – 0.87 (m, 2H), 0.92 (d, *J* = 6.7 Hz, 6H), 0.94 – 0.96 (m, 12H), 1.04 – 1.09 (m, 8H), 1.24 – 1.29 (m, 2H), 1.31 (d, *J* = 7.4 Hz, 6H), 1.44 – 1.51 (m, 4H), 1.52 – 1.58 (m, 2H), 1.95 – 2.05 (m, 8H), 2.17 (ddd, *J* = 14.3, 9.6, 5.2 Hz, 2H), 2.21 – 2.28 (m, 2H), 2.59 (s, 6H), 2.72 (s, 6H), 2.96 – 3.04 (m, 10H), 3.16 (dd, *J* = 11.1, 4.3 Hz, 2H), 3.21 – 3.27 (m, 2H), 3.33 (s, 6H), 3.64 (s, 6H), 4.32 – 4.42 (m, 4H), 4.67 (dd, *J* = 9.7, 4.4 Hz, 2H), 4.70 – 4.80 (m, 4H), 4.81 – 4.86 (m, 2H), 4.90 – 4.99 (m, 2H), 5.15 (dd, *J* = 9.6, 3.4 Hz, 2H), 5.23 (d, *J* = 5.4 Hz, 2H), 5.50 (t, *J* = 7.6 Hz, 2H), 6.70 (s, 2H), 6.93 (t, *J* = 7.6 Hz, 4H), 7.00 – 7.06 (m, 8H), 7.15 – 7.20 (m, 4H), 7.22 (d, *J* = 8.3 Hz, 2H), 7.37 – 7.46 (m, 4H), 8.18 (d, *J* = 9.0 Hz, 2H), 8.44 (d, *J* = 9.1 Hz, 2H), 8.67 (d, *J* = 9.0 Hz, 2H).

^{13}C NMR (126 MHz, $CDCl_3$) δ 17.5, 19.3, 19.9, 20.0, 22.8, 23.61, 23.64, 25.1, 25.8, 28.9, 29.0, 29.9, 30.1, 30.5, 31.2, 32.8, 33.3, 33.7, 39.1, 48.2, 50.1, 51.2, 52.0, 54.6, 56.4, 58.0, 58.9, 59.7, 66.6, 79.4, 108.8, 109.6, 118.8, 119.4, 121.7, 122.2, 127.0, 127.6, 128.19, 128.23, 128.5, 135.8, 137.0, 141.8, 167.5, 169.3, 170.7, 171.0, 171.4, 171.7, 173.0.

HRMS (ESI) calcd for $C_{105}H_{151}N_{22}O_{18}^+$ $(M+H)^+$: calcd 2008.1571; found 2008.1597.

(3*S*,6*S*,9*S*,12*S*,15*S*,18*S*,21*S*)-21-((*R*)-3-hydroxy-2-methylpropyl)-9-isobutyl-12-isopropyl-15-((*R*)-methoxy(phenyl)methyl)-1,4,10,18-tetramethyl-3-((1-methyl-1*H*-indol-3-yl)methyl)-6-((1-pentyl-1*H*-1,2,3-triazol-4-yl)methyl)-1,4,7,10,13,16,19-heptaazacyclohenicosane-2,5,8,11,14,17,20-heptaone (25)

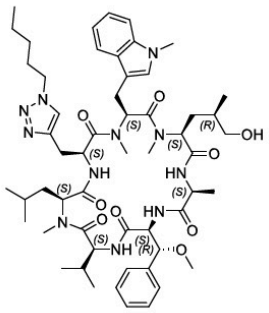

A 1.5 ml vial was charged with **20** (13.1 mg, 14.1 µmol), *t*-BuOH (235 µl) and H_2O (235 µl) were added followed by 1-azidopentane (24.6 µl of a 13.0 mg ml^{-1} stock solution, 3.20 mg, 28.3 µmol). 1 M $CuSO_4$ (5.65 µl, 5.65 µmol) and 1 M sodium ascorbate (8.48 µl, 8.48 µmol) were added, the vial was flushed with Argon and sealed. After 4 h, incomplete conversion was observed (LC/MS) and more 1-azidopentane (15.4 µl of a 13.0 mg ml^{-1} stock solution, 2.00 mg, 17.7 µmol) was added. After 5 h, full conversion was observed by LC/MS. The reaction mixture was evaporated in vacuo and the residue was purified by RP flash chromatography (H_2O/MeCN 75:25 – 5:95). After lyophilization, **25** (11.5 mg, 11.1 µmol, 78%) was obtained as a white amorphous solid.

$[\alpha]_{20}^{D}$ = –60.8 (c 0.5, $CHCl_3$).

^{1}H NMR (500 MHz, $CDCl_3$) δ 0.05 – 0.13 (m, 1H), 0.38 (d, *J* = 6.7 Hz, 3H), 0.85 – 0.91 (m, 1H), 0.90 – 1.00 (m, 12H), 1.06 – 1.14 (m, 4H), 1.28 – 1.34 (m, 5H), 1.35 – 1.44 (m, 2H), 1.47 – 1.60 (m, 2H), 1.84 – 1.96 (m, 3H), 1.99 (dd, *J* = 14.2, 5.8 Hz, 1H), 2.02 – 2.08 (m, 1H), 2.15 – 2.23 (m, 1H), 2.23 – 2.30 (m, 1H), 2.59 (s, 3H), 2.73 (s, 3H), 2.97 – 3.05 (m, 5H), 3.18 (dd, *J* = 11.1, 4.4 Hz, 1H), 3.22 – 3.28 (m, 1H), 3.35 (s, 3H), 3.67 (s, 3H), 4.30 – 4.36 (m, 2H), 4.70 (dd, *J* = 9.9, 4.5 Hz, 1H), 4.73 – 4.81 (m, 2H), 4.85 (dd, *J* = 5.4, 3.8 Hz, 1H), 4.93 – 5.00 (m, 1H), 5.17 (dd, *J* = 9.6, 3.5 Hz, 1H), 5.25 (d, *J* = 5.3 Hz, 1H), 5.49 – 5.55 (m, 1H), 6.74 (s, 1H), 6.90 – 6.98 (m, 2H), 7.03 – 7.12 (m, 5H), 7.18 – 7.22 (m, 1H), 7.22 – 7.25 (m, 1H), 7.40 (d, *J* = 3.9 Hz, 1H), 7.45 (d, *J* = 8.0 Hz, 1H), 8.20 (d, *J* = 9.2 Hz, 1H), 8.45 (d, *J* = 9.0 Hz, 1H), 8.72 (d, *J* = 8.9 Hz, 1H.

^{13}C NMR (126 MHz, $CDCl_3$) δ 14.1, 17.6, 19.3, 19.88, 19.91, 22.2, 22.8, 23.6, 25.1, 25.7, 28.7, 28.9, 29.0, 29.8, 30.1, 30.4, 31.2, 32.8, 33.4, 33.7, 39.1, 48.2, 50.5, 51.2, 52.0, 54.6, 56.3, 58.0, 58.9, 59.7, 66.5, 79.4, 108.9, 109.6, 118.9, 119.4, 121.5, 122.2, 127.0, 127.7, 128.19, 128.22, 128.5, 135.8, 137.0, 141.6, 167.5, 169.3, 170.5, 171.0, 171.5, 171.6, 173.1.

HRMS (ESI) calcd for $C_{55}H_{82}N_{11}O_9^+$ $(M+H)^+$: 1040.6291; found: 1040.6276.

Synthesis of Trp-Nα-methylated dCymC (23)

Methyl *N*-(((2*S*,3*R*)-2-((*S*)-2-((2*S*,4*R*)-2-((*S*)-2-(((allyloxy)carbonyl)(methyl)amino)-*N*-methyl-3-(1-(2-methylbut-3-en-2-yl)-1*H*-indol-3-yl)propanamido)-5-((*tert*-butyldimethylsilyl)oxy)-4-methylpentanamido)propanamido)-3-methoxy-3-phenylpropanoyl)-L-valyl)-*N*-methyl-L-leucinate (SI-53)

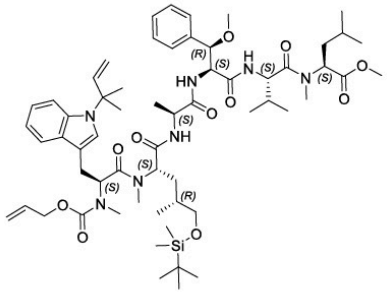

77

*N*α-((allyloxy)carbonyl)-1-(2-methylbut-3-en-2-yl)-L-tryptophan (203 mg, 0.570 mmol) and methyl iodide (214 µl, 3.42 mmol) were dissolved in THF (5.7 ml) and cooled to 0 °C. NaH (91.0 mg, 2.23 mmol) was added in portions and the reaction mixture was slowly warmed to rt over night. After 17 h, H_2O was added carefully (gas evolution), the resulting mixture was washed with PE (2x) and the PE phase was extracted with 0.5 M NaOH (1x). The aqueous phases were combined, acidified with 1 M HCl and extracted with EtOAc (3x). The combined org phases were washed with half saturated $Na_2S_2O_3$ and sat. NaCl soln., dried (Na_2SO_4) and evaporated in vacuo. The crude methylated Trp-derivative was then used in the next step without further purification.

Pentapeptide **2** (787 mg, 0.876 mmol) was deprotected according to *GP1* and the resulting amine was coupled to the crude *N*α-methyl-1-(2-methylbut-3-en-2-yl)Trp (prepared as described above) according to *GP5:* DIPEA (100 µl, 570 µmol), $BnNMe_2$ (6.51 µl, 43.8 µmol), 1 M iPrOCOCl soln. (570 µl, 570 µmol), NMI (6.99 µl, 87.7 µmol), 4 M HCl soln. (11.0 µl, 43.8 µmol) (18 h). Flash chromatography (CyH/EtOAc 100:0 – 35:65) followed by lyophilization **SI-53** (402 mg, 0.331 mmol, 76%, 92% purity) as a white, amorphous solid. R_f = 0.27 (PE/EtOAc 1:1).

$[\alpha]_{20}^{D}$ = −80.4 (c 0.5, $CHCl_3$).

^{1}H NMR (500 MHz, $CDCl_3$) *(mixture of rotamers, ratio ~2:2:1)* δ -0.46 – -0.35 (m, 0.3H), -0.07 (s, 0.8H), -0.05 (s, 0.9H), 0.01 – 0.07 (m, 4.9H), 0.31 (d, *J* = 6.6 Hz, 0.8H), 0.81 (s, 3.1H), 0.86 – 0.91 (m, 9.2H), 0.91 – 1.02 (m, 15.0H), 1.05 (d, *J* = 7.1 Hz, 1.0H), 1.18 (d, *J* = 7.1 Hz, 0.7H), 1.22 (d, *J* = 7.1 Hz, 0.8H), 1.23 – 1.35 (m, 2.2H), 1.44 – 1.56 (m, 2.7H), 1.66 – 1.71 (m, 6.6H), 1.72 – 1.78 (m, 1.7H), 1.88 – 1.97 (m, 0.9H), 2.06 – 2.19 (m, 1.3H), 2.62 – 2.70 (m, 0.3H), 2.74 – 2.80 (m, 1.3H), 2.82 – 2.91 (m, 4.1H), 2.95 – 3.02 (m, 3.7H), 3.08 – 3.16 (m, 1.0H), 3.18 (s, 0.9H), 3.28 (s, 1.0H), 3.31 – 3.34 (m, 2.6H), 3.34 – 3.44 (m, 1.5H), 3.50 (dd, *J* = 9.7, 4.3 Hz, 0.9H), 3.66 – 3.71 (m, 3.3H), 3.93 – 4.00 (m, 0.2H), 4.19 (t, *J* = 6.9 Hz, 0.3H), 4.23 – 4.29 (m, 0.7H), 4.31 – 4.38 (m, 0.3H), 4.52 – 4.59 (m, 1.1H), 4.60 – 4.73 (m, 1.6H), 4.75 – 4.87 (m, 2.5H), 5.01 – 5.13 (m, 1.7H), 5.13 – 5.33 (m, 3.7H), 5.32 – 5.38 (m, 1.1H), 5.40 – 5.53 (m, 0.6H), 5.79 – 5.97 (m, 0.7H), 6.03 – 6.14 (m, 1.0H), 6.39 (d, *J* = 6.6 Hz, 0.3H), 6.49 (d, *J* = 6.6 Hz, 0.2H), 6.65 (d, *J* = 7.6 Hz, 0.3H), 6.67 – 6.72 (m, 0.6H), 6.81 (d, *J* = 7.6 Hz, 0.1H), 7.03 – 7.13 (m, 2.7H), 7.14 – 7.25 (m, 3.9H),7.25 – 7.32 (m, 3.2H), 7.33 – 7.39 (m, 1.0H), 7.42 – 7.50 (m, 1.1H), 7.55 – 7.60 (m, 0.6H), 7.62 (d, *J* = 6.6 Hz, 0.3H), 7.66 – 7.71 (m, 0.3H).

^{13}C NMR (126 MHz, $CDCl_3$) *(mixture of rotamers)* δ -5.3, -5.2, 17.4, 17.6, 17.7, 18.4, 18.5, 19.66, 19.70, 21.5, 23.4, 24.9, 26.1, 28.0, 29.0, 29.6, 29.9, 30.1, 30.6, 31.0, 31.4, 31.5, 32.3, 37.0, 49.2, 49.6, 52.3, 53.8, 54.2, 54.6, 55.7, 57.6, 57.7, 57.8, 59.0, 66.4, 66.6, 66.8, 67.2, 68.1, 81.3, 108.0, 108.8, 109.0, 113.5, 113.6, 113.9, 117.3, 117.9, 118.4, 118.6, 118.8, 119.0, 119.4, 120.8, 121.3, 124.0, 124.3, 127.0, 128.2, 128.3, 128.5, 129.1, 129.4, 129.6, 132.3, 132.6, 132.9, 135.5, 136.8, 144.3, 155.6, 156.4, 157.4, 168.5, 170.5, 171.5, 171.8, 172.1, 172.2.

Selected diagnostic peaks:

Major rotamers: **^{1}H NMR** (500 MHz, $CDCl_3$) δ 0.03 (s, 3H), 0.03 (s, 3H), 0.05 (s, 3H), 0.88 (s, 9H), 0.89 (s, 9H), 1.69 (s, 3H), 2.87 (s, 3H), 2.87 (s, 3H), 2.97 (s, 3H), 2.98 (s, 3H), 3.69 (s, 3H), 4.26 (t, *J* = 6.8 Hz, 1H), 5.35 (dd, *J* = 10.6, 5.4 Hz, 3H), 6.69 (d, *J* = 7.4 Hz, 1H). **^{13}C NMR** (126 MHz, $CDCl_3$) δ 26.1, 52.3, 81.3, 127.0, 128.5, 156.4.

Minor rotamer: **^{1}H NMR** (500 MHz, $CDCl_3$) δ -0.44 – -0.37 (m, 1H), -0.07 (s, 3H), -0.05 (s, 3H), 0.31 (d, *J* = 6.6 Hz, 3H), 0.81 (s, 9H), 1.05 (d, *J* = 7.1 Hz, 3H), 3.18 (s, 3H), 3.28 (s, 3H), 3.50 (dd, *J* = 9.7, 4.3 Hz, 2H), 3.97 (dd, *J* = 12.9, 5.8 Hz, 1H), 4.19 (t, *J* = 6.9 Hz, 1H), 6.49 (d, *J* = 6.6 Hz, 1H), 6.65 (d, *J* = 7.6 Hz, 1H).

HRMS (ESI): calcd for $C_{60}H_{97}N_7O_{11}Si^+$ $(M+H)^+$: 1116.6775; found:1116.6776.

methyl *N*-(((2*S*,3*R*)-2-((*S*)-2-((2*S*,4*R*)-2-((*S*)-2-((2*S*,3*R*)-2-(((allyloxy)carbonyl)amino)-*N*,3,5-trimethylhex-4-enamido)-*N*-methyl-3-(1-(2-methylbut-3-en-2-yl)-1*H*-indol-3-yl)propanamido)-5-((*tert*-butyldimethylsilyl)oxy)-4-methylpentanamido)propanamido)-3-methoxy-3-phenylpropanoyl)-L-valyl)-*N*-methyl-L-leucinate (SI-54)

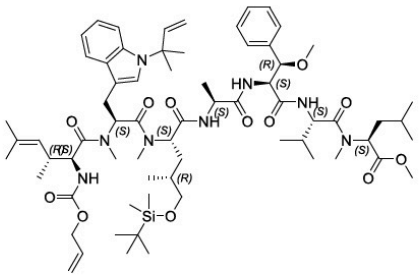

Prepared according to *GP2* and *GP5*: **SI-53** (368 mg, 330 µmol), DMBA (154 mg, 989 µmol), $Pd(PPh_3)_4$ (11.4 mg, 9.89 µmol) (1 h); (2*S*,3*R*)-2-(((allyloxy)carbonyl)amino)-3,5-dimethylhex-4-enoic acid (108 mg, 448 µmol), DIPEA (74.9 µl, 429 µmol), $BnNMe_2$ (4.90 µl, 33.0 µmol), 1 M iPrOCOCl (429 µl, 429 µmol), NMI (5.26 µl, 6.60 µmol), 4 M HCl (8.25 µl, 2.06 µmol) (17 h). Flash chromatography (CyH/EtOAc 100:0 – 35:65) followed by lyophilization yielded **SI-54** (323 mg, 255 µmol, 77%) as a yellow amorphous solid. R_f = 0.33 (PE/EtOAc 1:1).

$[\alpha]_{20}^{D}$ = −75.8 (c 0.5, $CHCl_3$).

^{1}H NMR (500 MHz, $CDCl_3$) *(mixture of rotamers, ratio ~2:2:1)* δ -0.56 – -0.4 (m, 0.2H), -0.07 (s, 0.9H), -0.05 (s, 0.9H), 0.00 – 0.07 (m, 4.3H), 0.30 (d, *J* = 6.6 Hz, 0.7H), 0.80 – 0.82 (m, 2.7H), 0.88 (s, 5.1H), 0.90 – 1.01 (m, 17.2H), 1.13 – 1.23 (m, 0.8H), 1.23 – 1.30 (m, 2.2H), 1.45 – 1.53 (m, 3.0H), 1.57 – 1.60 (m, 1.6H), 1.65 – 1.71 (m, 8.1H), 1.71 – 1.78 (m, 1.6H), 1.80 – 1.87 (m, 1.3H), 1.89 – 1.97 (m, 0.7H), 2.06 – 2.17 (m, 1.1H), 2.60 – 2.67 (m, 0.4H), 2.72 (s, 1.0H), 2.75 – 2.79 (m, 0.9H), 2.80 (s, 1.3H), 2.82 – 2.88 (m, 1.0H), 2.95 – 3.00 (m, 3.2H), 3.00 – 3.06 (m, 0.7H), 3.08 (s, 1.2H), 3.10 – 3.21 (m, 0.7H), 3.27 – 3.34 (m, 3.9H), 3.37 – 3.45 (m, 1.4H), 3.50 (dd, *J* = 9.7, 4.0 Hz, 0.6H), 3.66 – 3.73 (m, 3.0H), 4.14 – 4.19 (m, 0.4H), 4.23 – 4.34 (m, 0.4H), 4.44 – 4.50 (m, 0.5H), 4.51 – 4.62 (m, 1.6H), 4.62 – 4.70 (m, 1.1H), 4.73 (dd, *J* = 7.1, 4.1 Hz, 0.3H), 4.77 – 4.90 (m, 2.4.H), 4.99 – 5.04 (m, 0.7H), 5.05 – 5.09 (m, 0.4H), 5.09 – 5.24 (m, 2.9H), 5.26 – 5.43 (m, 2.4H), 5.82 (t, *J* = 7.3 Hz, 0.4H), 5.85 – 6.01 (m, 0.8H), 6.03 – 6.13 (m, 1.1H), 6.32 (d, *J* = 6.8 Hz, 0.4H), 6.52 (d, *J* = 7.1 Hz, 0.2H), 6.61 – 6.73 (m, 0.6H), 7.01 (s, 0.2H); 7.04 – 7.12 (m, 2.0H), 7.12 – 7.24 (m, 3.7H), 7.25 – 7.30 (m, 2.7H), 7.33 – 7.37 (m, 0.6H), 7.40 – 7.46 (m, 0.8H), 7.47 – 7.41 (m, 0.4H), 7.52 – 7.55 (m, 0.3H), 7.67 – 7.72 (m, 0.5H), 8.30 (d, *J* = 6.3 Hz, 0.2H).

^{13}C NMR (126 MHz, $CDCl_3$) δ -5.30, -5.27, 15.6, 16.3, 17.3, 17.7, 18.2, 18.4, 18.5, 19.7, 21.5, 23.4, 24.9, 26.0, 26.1, 26.2, 27.9, 28.9, 30.6, 31.1, 31.3, 31.5, 32.3, 35.8, 37.0, 49.2, 49.9, 52.3, 54.2, 54.6, 54.8, 57.56, 57.65, 57.8, 59.0, 59.1, 65.9, 67.2, 68.3, 81.3, 107.8, 108.8, 113.4, 113.6, 113.8, 114.0, 117.8, 118.8, 119.0, 119.4, 120.9, 124.0, 125.5, 127.0, 127.1, 128.4, 128.5, 129.4, 132.8, 133.1, 133.4, 135.6, 136.8, 144.4, 156.0, 168.4, 168.5, 170.3, 171.4, 171.7, 171.8, 172.0, 172.1, 172.2, 173.3.

Selected diagnostic peaks:

Major rotamers: **^{1}H NMR** (500 MHz, $CDCl_3$) δ 0.03 (s, 3H), 0.04 (s, 3H), 0.88 (s, 9H), 2.98 (s, 3H), 3.32 (s, 3H), 3.50 (dd, *J* = 9.7, 4.0 Hz, 1H), 3.69 (s, 3H), 4.16 (t, *J* = 6.9 Hz, 1H), 5.82 (t, *J* = 7.3 Hz, 1H), 6.32 (d, *J* = 6.8 Hz, 1H), 6.64 (d, *J* = 7.6 Hz, 1H). **^{13}C NMR** (126 MHz, $CDCl_3$) δ 26.1, 81.3, 156.0.

Minor rotamer: **^{1}H NMR** (500 MHz, $CDCl_3$) δ -0.49 (s, 1H), -0.07 (s, 3H), -0.05 (s, 3H), 0.30 (d, *J* = 6.6 Hz, 3H), 0.81 (s, 9H), 2.72 (s, 3H), 2.80 (s, 3H), 3.08 (s, 3H), 3.30 (s, 3H), 3.50 (dd, *J* = 9.7, 4.0 Hz, 1H), 4.31 (t, *J* = 6.8 Hz, 1H), 6.52 (d, *J* = 7.1 Hz, 1H), 8.30 (d, *J* = 6.3 Hz, 1H). **^{13}C NMR** (126 MHz, $CDCl_3$) δ 26.0.

HRMS (ESI): calcd for $C_{68}H_{107}N_8O_{12}Si^+$ $(M+H)^+$: 1025.6434; found:1025.6429.

(3*S*,6*S*,9*S*,12*S*,15*S*,18*S*,21*S*)-21-((*R*)-3-hydroxy-2-methylpropyl)-9-isobutyl-12-isopropyl-15-((*R*)-methoxy(phenyl)methyl)-1,4,10,18-tetramethyl-3-((1-(2-methylbut-3-en-2-yl)-1*H*-indol-3-yl)methyl)-6-((*R*)-4-methylpent-3-en-2-yl)-1,4,7,10,13,16,19-heptaazacyclohenicosane-2,5,8,11,14,17,20-heptaone (23)

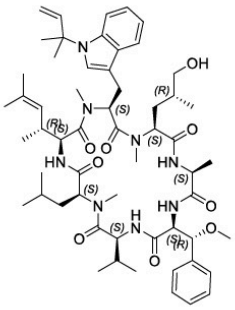

Prepared according to *GP6c*: **SI-54** (180 mg, 143 µmol), 1 M LiOH (229 µl, 229 µmol) (5.5 h); $Pd(OAc)_2$ (1.3 mg, 5.7 µmol), TPPTS (6.5 mg, 11 µmol), Et_2NH (74.7 µl, 715 µmol) (2.5 h); HATU (217 mg, 572 µmol), DIPEA (125 µl, 715 µmol) (addition over 4 h, additional 18 h); NH_4F (132 mg, 3.58 mmol) (16 h). RP flash chromatography (H_2O/MeCN 90:10 - 5:95) followed by prep HPLC (H_2O/MeCN 70:30 – 5:95) and lyophilizaiton afforded **23** (42.4 mg, 36.4 µmol, 25%, purity 88%) as a white, amorphous solid.

$[\alpha]_{20}^{D}$ = −76.5 (c 0.5, $CHCl_3$).

^{1}H NMR (500 MHz, $CDCl_3$) δ -0.46 – -0.36 (m, 2H), 0.17 (d, *J* = 6.9 Hz, 3H), 0.46 (d, *J* = 6.7 Hz, 3H), 0.93 – 1.04 (m, 10H), 1.09 – 1.13 (m, 4H), 1.23 (d, *J* = 7.3 Hz, 3H), 1.31 (d, *J* = 1.5 Hz, 3H), 1.48 – 1.58 (m, 1H), 1.65 – 1.69 (m, 6H), 1.69 (d, *J* = 1.4 Hz, 3H), 1.69 – 1.75 (m, 1H), 1.98 (d, *J* = 7.5 Hz, 2H), 2.20 – 2.28 (m, 1H), 2.32 (ddd, *J* = 13.3, 10.7, 4.5 Hz, 1H), 2.66 (s, 3H), 2.86 (s, 3H), 2.89 (dd, *J* = 11.0, 6.1 Hz, 1H), 2.97 (dd, *J* = 10.8, 4.9 Hz, 1H), 3.16 (dd, *J* = 14.1, 6.2 Hz, 1H), 3.32 (s, 3H), 3.35 – 3.40 (m, 4H), 4.37 – 4.46 (m, 1H), 4.70 – 4.78 (m, 2H), 4.82 – 4.92 (m, 3H), 4.94 (dd, *J* = 10.7, 3.5 Hz, 1H), 5.10 (d, *J* = 5.3 Hz, 1H), 5.13 (dd, *J* = 9.5, 6.2 Hz, 1H), 5.18 (d, *J* = 17.5 Hz, 1H), 5.21 (d, *J* = 10.8 Hz, 1H), 6.06 (dd, *J* = 17.5, 10.7 Hz, 1H), 6.94 (d, *J* = 4.7 Hz, 1H), 6.99 (s, 1H), 7.02 – 7.14 (m, 2H), 7.19 – 7.28 (m, 5H), 7.43 (d, *J* = 7.0 Hz, 0H), 7.49 (d, *J* = 8.1 Hz, 1H), 7.58 (d, *J* = 10.1 Hz, 1H), 7.99 (d, *J* = 7.6 Hz, 1H), 8.40 (d, *J* = 9.6 Hz, 1H).

^{13}C NMR (126 MHz, $CDCl_3$) δ 16.7, 18.0, 18.9, 19.5, 20.2, 20.7, 22.6, 23.8, 25.3, 25.8, 26.6, 28.0, 28.1, 29.0, 29.6, 31.1, 32.2, 33.0, 35.9, 39.2, 50.8, 53.4, 53.7, 55.6, 55.9, 57.9, 58.7, 58.8, 59.1, 66.8, 80.1, 107.4, 113.8, 114.3, 118.4, 119.5, 121.5, 124.0, 125.1, 128.1, 128.6, 129.0, 129.1, 133.6, 135.2, 135.6, 144.0, 168.5, 169.5, 170.8, 171.5, 172.3, 174.3.

HRMS (ESI): calcd for $C_{57}H_{85}N_8O_9^+$ $(M+H)^+$: 1025.6434; found: 1025.6429.

Synthesis of Trp-Nα-methylated exit vector 6 Homo-BacPROTACs (SI-57, 27, 28, SI-61)

methyl *N*-(((2*R*,3*S*)-2-((*S*)-2-((2*S*,4*R*)-2-((*S*)-2-(((allyloxy)carbonyl)(methyl)amino)-*N*-methyl-3-(1-(prop-2-yn-1-yl)-1*H*-indol-3-yl)propanamido)-5-((*tert*-butyldimethylsilyl)oxy)-4-methylpentanamido)propanamido)-3-methoxy-3-phenylpropanoyl)-D-valyl)-*N*-methyl-D-leucinate (SI-55)

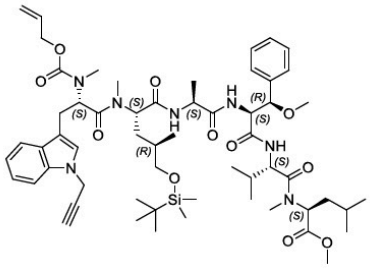

*N*α-((allyloxy)carbonyl)-1-propargyl-L-tryptophan (180 mg, 0.552 mmol) and methyl iodide (207 µl, 3.31 mmol) were dissolved in THF (5.5 ml) and the mixture was cooled to 0 °C. NaH (66.2 mg, 1.66 mmol) was added in one portion and the reaction mixture was slowly warmed to rt. After 17 h, H_2O was added carefully (gas evolution), the resulting mixture was washed with PE (2x) and the PE phase was extracted with 0.5 M NaOH (1x). The aqueous phases were combined, acidified with 1 M HCl and extracted with EtOAc (3x). The combined org phases were washed with 1 M Na_2SO_3 and sat. NaCl soln., dried (Na_2SO_4) and evaporated in vacuo. The crude methylated Trp-derivative was used without further purification.

Pentapeptide **2** was deprotected according to *GP1* and the resulting amine (298 mg, 0.390 mmol) was coupled to crude *N*α-methyl-*N*1-propargyl-Trp (prepared as described above) according to *GP5:* DIPEA (89.0 µl, 507 µmol), $BnNMe_2$ (5.79 µl, 39.0 µmol), 1 M iPrOCOCl soln. (546 µl, 546 µmol), NMI (6.22 µl, 77.9 µmol), 4 M HCl soln. (9.75 µl, 39.0 µmol) (18 h). Flash chromatography (CyH/EtOAc 100:0 – 30:70) followed by lyophilization afforded **SI-55** (352 mg, 0.324 mmol, 83%) as a white, amorphous solid. R_f = 0.30 (PE/EtOAc 4:6).

$[\alpha]_{20}^{D}$ = −91.2 (c 0.5, $CHCl_3$).

^{1}H NMR (500 MHz, $CDCl_3$) *(mixture of rotamers, ratio ~2:2:1)* δ -0.12 – -0.05 (m, 0.8H), -0.04 (s, 0.8H), 0.01 – 0.08 (m, 5.4H), 0.38 (d, *J* = 6.7 Hz, 0.5H), 0.82 (s, 2.0H), 0.83 – 0.89 (m, 10.2H), 0.89 – 1.02 (m, 17.3H), 1.06 (d, *J* = 7.0 Hz, 0.8H), 1.21 – 1.34 (m, 3.4H), 1.45 – 1.54 (m, 2.7H), 1.65 – 1.80 (m, 2.4H), 1.89 – 1.95 (m, 0.8H), 2.06 – 2.17 (m, 1.2H), 2.32 – 2.42 (m, 1.0H), 2.76 – 2.81 (m, 3.0H), 2.89 (s, 1.2H), 2.91 (s, 1.1H), 2.95 – 3.04 (m, 4.3H), 3.15 (s, 0.8H), 3.28 (s, 0.8H), 3.30 – 3.42 (m, 3.8H), 3.42 – 3.53 (m, 1.9H), 3.65 – 3.72 (m, 3.3H), 4.11 – 4.19 (m, 0.5H), 4.20 – 4.32 (m, 0.9H), 4.41 – 4.49 (m, 0.4H), 4.52 – 4.70 (m, 2.9H), 4.70 – 4.88 (m, 4.7H), 5.04 – 5.09 (m, 0.4H), 5.09 – 5.15 (m, 0.8H), 5.15 – 5.31 (m, 2.1H), 5.31 – 5.39 (m, 1.3H), 5.51 (dd, *J* = 9.2, 5.8 Hz, 0.5H), 5.57 – 5.69 (m, 0.3H), 5.81 – 5.98 (m, 0.7H), 6.17 (d, *J* = 7.0 Hz, 0.1H), 6.22 (d, *J* = 6.9 Hz, 0.3H), 6.39 (d, *J* = 6.9 Hz, 0.3H), 6.61 – 6.72 (m, 1.0H), 6.97 – 7.04 (m, 0.6H), 7.04 – 7.09 (m, 0.5H), 7.10 – 7.15 (m, 1.0H), 7.15 – 7.25 (m, 4.4H), 7.26 – 7.39 (m, 4.6H), 7.55 – 7.63 (m, 0.7H), 7.72 (d, *J* = 7.9 Hz, 1H).

^{13}C NMR (126 MHz, $CDCl_3$) *(mixture of rotamers)* δ -5.31, -5.28, -5.2, 15.8, 16.1, 17.3, 17.4, 17.58, 17.65, 17.7, 17.9, 18.41, 18.45, 19.7, 20.0, 21.5, 22.29, 22.32, 22.78, 22.81, 22.83, 23.42, 23.43, 24.9, 25.0, 25.3, 25.4, 26.0, 26.05, 26.07, 26.3, 29.1, 29.6, 29.8, 30.0, 30.4, 30.7, 30.8, 31.0, 31.3, 31.4, 31.46, 31.50, 31.8, 32.2, 32.3, 32.4, 35.7, 35.78, 35.80, 37.1, 49.1, 49.2, 49.6, 52.2, 52.3, 52.7, 53.9, 54.2, 54.6, 54.7, 54.8, 55.6, 56.7, 57.6, 57.7, 57.8, 57.87, 57.95, 66.5, 66.8, 67.0, 67.1, 68.1, 73.61, 73.65, 73.7, 77.8, 77.97, 78.03, 81.26, 81.35, 109.5, 109.6, 109.7, 110.2, 110.7, 110.8, 117.4, 117.8, 118.7, 118.8, 119.1, 119.7, 119.9, 120.1, 122.1, 122.5, 125.9, 126.4, 126.6, 126.97, 127.01, 128.2, 128.3, 128.4, 128.5, 132.4, 132.6, 132.9, 136.10, 136.14, 136.8, 136.9, 155.6, 156.3, 157.4, 168.4, 168.5, 169.1, 170.4, 171.4, 171.9, 172.0, 172.1, 172.2.

Selected diagnostic peaks:

Major rotamers: **^{1}H NMR** (500 MHz, $CDCl_3$) δ 0.03 (s, 3H), 0.03 (s, 3H), 0.04 (s, 3H), 0.04 (s, 3H), 0.88 (s, 9H), 2.78 (s, 3H), 2.99 (s, 3H), 3.33 (s, 3H), 3.69 (s, 3H), 4.16 (t, *J* = 6.9 Hz, 1H), 5.51 (dd, *J* = 9.2, 5.8 Hz, 1H), 6.22 (d, *J* = 6.9 Hz, 1H), 7.07 (s, 1H). **^{13}C NMR** (126 MHz, $CDCl_3$) δ 23.42, 26.05, 81.4, 155.6, 156.3.

Minor rotamer: **^{1}H NMR** (500 MHz, $CDCl_3$) δ -0.06 (s, 3H), -0.04 (s, 3H), 0.38 (d, *J* = 6.7 Hz, 3H), 0.82 (s, 9H), 1.06 (d, *J* = 7.0 Hz, 3H), 2.97 (s, 3H), 3.15 (s, 3H), 3.28 (s, 3H), 4.22 (t, *J* = 6.9 Hz, 1H), 6.39 (d, *J* = 6.9 Hz, 1H).

HRMS (ESI): calcd for $C_{58}H_{88}N_7O_{11}Si^+$ $(M+H)^+$: 1086.6306; found: 1086.6273.

methyl *N*-(((2*S*,3*R*)-2-((*S*)-2-((2*S*,4*R*)-2-((*S*)-2-((*S*)-2-(((allyloxy)carbonyl)amino)-*N*,3-dimethylbutanamido)-*N*-methyl-3-(1-(prop-2-yn-1-yl)-1*H*-indol-3-yl)propanamido)-5-((*tert*-butyldimethylsilyl)oxy)-4-methylpentanamido)propanamido)-3-methoxy-3-phenylpropanoyl)-L-valyl)-*N*-methyl-L-leucinate (SI-56)

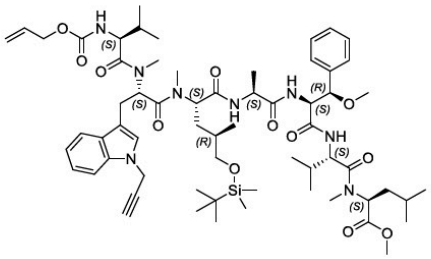

Prepared according to *GP2* and *GP5*: **SI-55** (332 mg, 159 µmol), DMBA (143 mg, 917 µmol), $Pd(PPh_3)_4$ (10.6 mg, 9.17 µmol) (3 h); Alloc-Val-OH (86.0 mg, 428 µmol), 1 M iPrOCOCl (428 µl, 428 µmol), $BnNMe_2$ (4.55 µl, 30.6 µmol), DIPEA (74.8 µl, 428 µmol), NMI (2.44 µl, 30.6 µmol), 4 M HCl (7.65 µl, 30.6 µmol) (17 h). Flash chromatography (CyH/EtOAc 100:0 – 30:70) followed by lyophilization afforded **SI-56** (288 mg, 243 µmol, 79%) as a yellowish, amorphous solid. R_f = 0.36 (PE/EtOAc 3:7).

$[\alpha]_{20}^{D}$ = −93.3 (c 0.5, $CHCl_3$).

^{1}H-NMR (500 MHz, $CDCl_3$) *(mixture of rotamers, ratio ~10:4:1)* δ -0.14 – -0.11 (m, 0.4H), -0.07 (s, 0.8H), -0.05 (s, 0.8H), -0.03 (s, 2.0H), -0.04 (s, 1.9H), 0.38 (d, *J* = 6.6 Hz, 0.6H), 0.44 (d, *J* = 6.8 Hz, 0.2H), 0.81 (s, 2.9H), 0.86 – 0.89 (m, 8.3H), 0.89 – 0.93 (m, 9.0H), 0.94 – 1.01 (m, 8.1H), 1.21 – 1.26 (m, 1.3H), 1.32 – 1.40 (m, 0.9H), 1.44 – 1.56 (m, 1.6H), 1.66 – 1.87 (m, 2.5H), 1.94 – 2.00 (m, 1.0H), 2.07 – 2.15 (m, 0.9H), 2.31 – 2.39 (m, 1H), 2.71 (s, 0.6H), 2.73 (s, 1.4H), 2.79 (s, 0.4H), 2.83 – 2.89 (m, 0.6H), 2.92 – 2.97 (m, 0.7H), 2.97 – 3.00 (m, 2.6H), 3.10 (s, 1.6H), 3.18 – 3.23 (m, 0.4H), 3.3 0 (s, 0.9H), 3.31 – 3.35 (m, 3.2H), 3.47 – 3.54 (m, 1.1H), 3.69 (s, 2.7H), 4.09 – 4.18 (m, 0.5H), 4.33 – 4.41 (m, 0.4H), 4.50 – 4.63 (m, 2.6H), 4.66 (dd, *J* = 7.5, 3.6 Hz, 0.8H), 4.69 – 4.86 (m, 4.2H), 5.07 (dd, *J* = 9.9, 6.0 Hz, 0.6H), 5.23 (d, *J* = 10.3 Hz, 0.9H), 5.29 – 5.39 (m, 1.7H), 5.48 (d, *J* = 9.2 Hz, 0.5H), 5.58 (t, *J* = 7.8 Hz, 0.2H), 5.87 – 6.00 (m, 1.3H), 6.09 (d, *J* = 9.3 Hz, 0.2H), 6.18 (d, *J* = 6.8 Hz, 0.5H), 6.58 (d, *J* = 7.2 Hz, 0.2H), 6.62 (d, *J* = 7.5 Hz, 0.5H), 6.99 (s, 0.3H), 7.06 (s, 0.6H), 7.11 – 7.25 (m, 4.8H), 7.26 – 7.41 (m, 4.2H), 7.43 – 7.49 (m, 1.3H), 7.52 – 7.58 (m, 0.9H), 7.63 – 7.69 (m, 1.2H), 7.73 (d, *J* = 7.9 Hz, 0.6H), 8.21 (d, *J* = 7.0 Hz, 0.2H).

^{13}C NMR (126 MHz, $CDCl_3$) *(mixture of rotamers)* δ -5.31, -5.30, -5.26, 15.9, 16.9, 17.2, 17.3, 17.6, 17.9, 18.40, 18.42, 19.7, 19.9, 21.5, 23.4, 24.9, 25.0, 26.0, 29.0, 30.6, 30.9, 31.1, 31.2, 31.36, 31.40, 31.5, 31.6, 32.0, 32.2, 35.7, 37.0, 38.7, 49.1, 49.8, 52.3, 53.3, 54.2, 54.5, 54.7, 56.0, 56.5, 57.5, 57.7, 57.8, 65.9, 67.0, 68.3, 73.7, 73.8, 78.0, 81.2, 81.3, 109.7, 110.0, 110.4, 117.8, 117.9, 119.0, 119.1, 119.9, 120.1, 122.2, 122.6, 125.7, 126.4, 127.0, 127.1, 128.1, 128.36, 128.44, 128.5, 128.6, 128.7, 132.06, 132.08, 132.19, 132.25, 132.3, 132.8, 133.0, 133.1, 136.05, 136.09, 136.6, 136.8, 156.4, 156.7, 168.3, 168.4, 170.2, 171.4, 171.6, 171.7, 172.11, 172.13, 172.16, 172.22, 173.7.

Selected diagnostic peaks:

Major rotamer: **^{1}H NMR** (500 MHz, $CDCl_3$) δ 0.03 (s, 3H), 0.04 (s, 3H), 0.88 (s, 9H), 2.98 (s, 3H), 3.10 (s, 3H), 3.32 (s, 3H), 3.50 (dd, *J* = 9.7, 4.2 Hz, 1H), 4.13 (t, *J* = 6.9 Hz, 1H), 5.07 (dd, *J* = 9.9, 6.0 Hz, 1H), 5.48 (d, *J* = 9.2 Hz, 1H), 6.18 (d, *J* = 6.8 Hz, 1H), 6.62 (d, *J* = 7.5 Hz, 1H), 7.06 (s, 1H). **^{13}C NMR** (126 MHz, $CDCl_3$) δ 26.0, 73.7, 81.3, 156.4.

Minor rotamer 1: **^{1}H NMR** (500 MHz, $CDCl_3$) δ -0.07 (s, 3H), -0.05 (s, 3H), 0.38 (d, *J* = 6.6 Hz, 3H), 0.81 (s, 9H), 2.71 (s, 3H), 2.98 (s, 3H), 4.37 (t, *J* = 6.9 Hz, 1H), 5.58 (t, *J* = 7.8 Hz, 1H), 6.09 (d, *J* = 9.3 Hz, 1H), 6.58 (d, *J* = 7.2 Hz, 1H), 6.99 (s, 1H). **^{13}C NMR** (126 MHz, $CDCl_3$) δ 73.8, 81.2, 156.7.

Minor rotamer 2: **^{1}H NMR** (500 MHz, $CDCl_3$) δ -0.12 (s, 3H), -0.12 (s, 3H), 0.44 (d, *J* = 6.8 Hz, 3H), 0.79 (s, 9H), 2.66 (s, 3H), 6.95 (s, 1H).

HRMS (ESI): calcd for $C_{63}H_{97}N_8O_{12}Si^+$ $(M+H)^+$: 1185.6990; found: 1185.6991.

(3*S*,6*S*,9*S*,12*S*,15*S*,18*S*,21*S*)-21-((*R*)-3-hydroxy-2-methylpropyl)-9-isobutyl-6,12-diisopropyl-15-((*R*)-methoxy(phenyl)methyl)-1,4,10,18-tetramethyl-3-((1-(prop-2-yn-1-yl)-1*H*-indol-3-yl)methyl)-1,4,7,10,13,16,19-heptaazacyclohenicosane-2,5,8,11,14,17,20-heptaone (26)

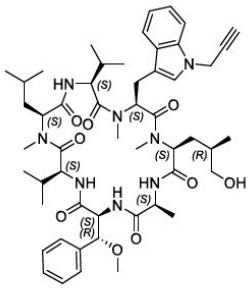

Prepared according to modified *GP6a*: **SI-56** (84.0 mg, 70.8 µmol), 1 M LiOH (92.2 µl, 92.2 µmol) (5 h); $Pd(OAc)_2$ (0.64 mg, 2.86 µmol), TPPTS (1.6 mg, 2.9 µmol), Et_2NH (37.5 µl, 359 µmol) (7 h); HATU (109 mg, 287 µmol), DIPEA (62.6 µl, 359 µmol) (addition over 2.5 h at 40 °C, additional 1 h at 40 °C); NH_4F (53.1 mg, 1.43 mmol) (14.5 h). RP flash chromatography (H_2O/MeCN 80:20 – 5:95) followed by lyophilization afforded **26** (22.6 mg, 23.7 µmol, 33%) as a white, amorphous solid.

$[\alpha]_{24}^{D}$ = −106.1 (c 0.2, $CHCl_3$).

^{1}H NMR (500 MHz, $CDCl_3$) δ -0.39 – -0.27 (m, 1H), 0.31 (d, *J* = 6.8 Hz, 3H), 0.44 (d, *J* = 6.6 Hz, 3H), 0.63 (d, *J* = 6.8 Hz, 3H), 0.78 – 0.87 (m, 2H), 0.91 – 1.01 (m, 10H), 1.05 – 1.13 (m, 7H), 1.54 – 1.64 (m, 1H), 1.85 – 1.96 (m, 1H), 2.21 – 2.29 (m, 1H), 2.30 – 2.37 (m, 2H), 2.41 (t, *J* = 2.7 Hz, 1H), 2.61 (s, 3H), 2.85 (s, 3H), 2.92 – 2.99 (m, 1H), 3.01 – 3.08 (m, 1H), 3.15 (dd, *J* = 13.9, 5.8 Hz, 1H), 3.37 (s, 3H), 3.40 (s, 3H), 3.42 – 3.53 (m, 1H), 4.45 – 4.56 (m, 2H), 4.71 – 4.81 (m, 4H), 4.83 – 4.90 (m, 2H), 5.15 (d, *J* = 5.7 Hz, 1H), 5.40 (dd, *J* = 9.7, 5.8 Hz, 1H), 6.93 (d, *J* = 4.7 Hz, 1H), 6.98 (s, 1H), 7.10 – 7.16 (m, 1H), 7.21 – 7.29 (m, 4H), 7.31 – 7.40 (m, 2H), 7.47 (d, *J* = 7.9 Hz, 1H), 8.13 – 8.21 (m, 2H), 8.51 (d, *J* = 9.3 Hz, 1H).

^{13}C NMR (126 MHz, $CDCl_3$) δ 17.4, 18.8, 19.49, 19.53, 20.2, 20.3, 22.7, 23.7, 25.4, 26.7, 29.0, 29.7, 31.0, 31.8, 32.37, 32.44, 33.0, 35.8, 39.1, 50.9, 53.4, 54.4, 55.5, 55.9, 57.9, 59.0, 59.2, 66.0, 74.1, 77.5, 80.1, 109.4, 109.9, 119.0, 120.3, 122.8, 125.9, 128.1, 128.3, 128.4, 129.0, 135.1, 136.0, 168.5, 169.2, 169.8, 170.7, 171.5, 171.9, 174.2.

HRMS (ESI): calcd for $C_{52}H_{75}N_8O_9^+$ $(M+H)^+$: 955.5652; found: 955.5614.

(3*S*,3'*S*,6*S*,6'*S*,9*S*,9'*S*,12*S*,12'*S*,15*S*,15'*S*,18*S*,18'*S*,21*S*,21'*S*)-21,21'-((((pentane-1,5-diylbis(1H-1,2,3-triazole-1,4-diyl))bis(methylene))bis(1*H*-indole-1,3-diyl))bis(methylene))bis(18-((*R*)-3-hydroxy-2-methylpropyl)-6-isobutyl-3,9-diisopropyl-12-((*R*)-methoxy(phenyl)methyl)-1,7,15,19-tetramethyl-1,4,7,10,13,16,19-heptaazacyclohenicosane-2,5,8,11,14,17,20-heptaone) (SI-57)

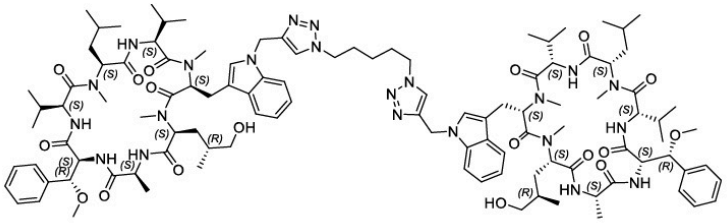

Prepared according to *GP7*: **26** (22.5 mg, 23.6 µmol), 1,5-diazdiopentane (1.87 mg, 12.1 µmol), 1 M $CuSO_4$ (9.72 µl, 9.72 µmol), 1 M sodium ascorbate (15.8 µmol, 15.8 µmol) (17 h). RP flash chromatography (H_2O/MeCN 90:10 – 5:95) followed by prep HPLC (H_2O/MeCN 75:25 – 5:95) and lyophilization afforded **SI-57** (8.2 mg, 3.97 µmol, 33%) as a white, amorphous solid.

$[\alpha]_{23}^{D}$ = −103.5 (c 0.2, $CHCl_3$).

^{1}H NMR (500 MHz, $CDCl_3$) δ -0.66 – -0.41 (m, 2H), 0.17 (d, *J* = 6.7 Hz, 6H), 0.41 (d, *J* = 6.7 Hz, 6H), 0.63 (d, *J* = 6.9 Hz, 6H), 0.85 – 1.02 (m, 20H), 1.04 – 1.17 (m, 16H), 1.26 – 1.33 (m, 2H), 1.51 – 1.60 (m, 2H), 1.70 – 1.76 (m, 2H),

1.80 – 1.92 (m, 4H), 2.18 – 2.37 (m, 4H), 2.53 (s, 6H), 2.69 – 2.80 (m, 2H), 2.85 (s, 6H), 2.99 (dd, *J* = 10.0, 4.8 Hz, 2H), 3.15 (dd, *J* = 14.1, 5.7 Hz, 2H), 3.33 – 3.38 (m, 12H), 3.42 (dd, *J* = 14.2, 9.6 Hz, 2H), 4.18 – 4.29 (m, 4H), 4.48 (t, *J* = 8.3 Hz, 2H), 4.55 (dd, *J* = 11.0, 3.2 Hz, 2H), 4.66 – 4.77 (m, 4H), 4.81 – 4.90 (m, 4H), 5.14 (d, *J* = 5.5 Hz, 2H), 5.31 (q, *J* = 15.7 Hz, 5H), 6.91 (d, *J* = 4.6 Hz, 2H), 6.95 – 7.00 (m, 2H), 7.07 – 7.12 (m, 2H), 7.18 – 7.26 (m, 14H), 7.38 – 7.41 (m, 4H), 7.45 (d, *J* = 7.9 Hz, 2H), 8.00 (d, *J* = 10.1 Hz, 2H), 8.13 (d, *J* = 7.6 Hz, 3H), 8.47 (d, *J* = 9.5 Hz, 2H).

^{13}C NMR (126 MHz, $CDCl_3$) δ 16.7, 18.9, 19.4, 19.5, 20.21, 20.23, 22.6, 23.5, 23.7, 25.4, 26.7, 28.9, 29.5, 29.6, 31.0, 31.8, 32.27, 32.29, 32.6, 39.1, 41.6, 50.0, 50.8, 53.6, 54.5, 55.6, 55.9, 57.9, 58.9, 59.0, 66.6, 80.1, 109.3, 110.0, 118.8, 120.0, 122.2, 122.6, 126.5, 127.9, 128.3, 128.5, 129.0, 135.1, 136.2, 144.0, 168.5, 169.0, 169.7, 170.7, 171.7, 172.1, 174.2.

HRMS (ESI): calcd for $C_{109}H_{159}N_{22}O_{18}^+$ $(M+H)^+$: 2064.2197; found:2064.2219.

(3*S*,3'*S*,6*S*,6'*S*,9*S*,9'*S*,12*S*,12'*S*,15*S*,15'*S*,18*S*,18'*S*,21*S*,21'*S*)-21,21'-(((((3,6,9,12-tetraoxatetradecane-1,14-diyl)bis(1*H*-1,2,3-triazole-1,4-diyl))bis(methylene))bis(1*H*-indole-1,3-diyl))bis(methylene))bis(18-((*R*)-3-hydroxy-2-methylpropyl)-6-isobutyl-3,9-diisopropyl-12-((*R*)-methoxy(phenyl)methyl)-1,7,15,19-tetramethyl-1,4,7,10,13,16,19-heptaazacyclohenicosane-2,5,8,11,14,17,20-heptaone) (27)

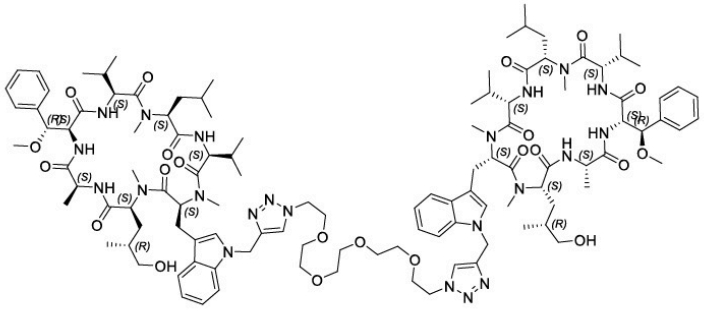

Prepared according to *GP7*: **26** (11.1 mg, 11.6 µmol), 1,14-diazido-3,6,9,12-tetraoxatetradecane (1.68 mg, 5.81 µmol), 1 M $CuSO_4$ (5.81 µl, 5.81 µmol), 1 M sodium ascorbate (6.97 µl, 6.97 µmol). RP flash chromatography (H_2O/MeCN 90:10 – 5:95) followed by prep HPLC (H_2O/MeCN 60:40 – 5:95) and lyophilization afforded **27** (6.3 mg, 2.87 µmol, 49%) as a white, amorphous solid.

$[\alpha]_{23}^{D}$ = −69.1 (c 0.5, $CHCl_3$).

^{1}H NMR (500 MHz, $CDCl_3$) δ -0.52 – -0.40 (m, 2H), 0.21 (d, *J* = 6.7 Hz, 6H), 0.42 (d, *J* = 6.6 Hz, 6H), 0.62 (d, *J* = 6.9 Hz, 6H), 0.85 – 0.92 (m, 4H), 0.93 (d, *J* = 6.7 Hz, 6H), 0.96 (d, *J* = 6.6 Hz, 6H), 0.99 (d, *J* = 6.7 Hz, 6H), 0.99 – 1.06 (m, 2H), 1.07 – 1.17 (m, 14H), 1.49 – 1.60 (m, 2H), 1.73 – 1.81 (m, 2H), 2.21 – 2.27 (m, 2H), 2.31 (ddd, *J* = 13.4, 10.5, 4.7 Hz, 2H), 2.56 (s, 6H), 2.81 – 2.86 (m, 8H), 3.01 (dd, *J* = 10.8, 4.7 Hz, 2H), 3.13 (dd, *J* = 14.1, 5.9 Hz, 2H), 3.34 – 3.40 (m, 12H), 3.41 – 3.47 (m, 2H), 3.47 – 3.55 (m, 12H), 3.76 – 3.82 (m, 4H), 4.41 – 4.46 (m, 4H), 4.45 – 4.55 (m, 2H), 4.70 – 4.79 (m, 4H), 4.82 – 4.91 (m, 4H), 5.14 (d, *J* = 5.6 Hz, 2H), 5.25 – 5.38 (m, 6H), 6.92 (d, *J* = 4.7 Hz, 2H), 6.98 (s, 2H), 7.05 – 7.11 (m, 2H), 7.15 – 7.27 (m, 14H), 7.38 (d, *J* = 8.2 Hz, 2H), 7.43 – 7.47 (m, 2H), 7.55 (s, 2H), 8.05 (d, *J* = 10.1 Hz, 2H), 8.14 (d, *J* = 7.6 Hz, 2H), 8.50 (d, *J* = 9.5 Hz, 2H).

^{13}C NMR (126 MHz, $CDCl_3$) δ 16.9, 18.8, 19.45, 19.50, 20.2, 20.3, 22.7, 23.7, 25.4, 26.8, 29.0, 29.6, 31.0, 31.8, 32.3, 32.4, 32.7, 39.1, 41.6, 50.38, 50.42, 50.8, 53.5, 54.4, 55.6, 55.9, 57.9, 59.0, 59.1, 66.4, 69.4, 70.49, 70.54, 80.1, 109.2, 110.1, 118.9, 120.0, 122.6, 123.4, 126.5, 128.0, 128.3, 128.5, 129.0, 135.1, 136.2, 143.6, 168.5, 169.0, 169.7, 170.7, 171.6, 172.1, 174.2.

HRMS (ESI): calcd for $C_{114}H_{169}N_{22}O_{22}^+$ $(M+H)^+$: 2198.2776; found:2198.2672.

Methyl *N*-(((2*S*,3*R*)-2-((*S*)-2-((2*S*,4*R*)-2-((*S*)-3-(1-allyl-1*H*-indol-3-yl)-2-(((allyloxy)carbonyl)(methyl)amino)-*N*-methylpropanamido)-5-((*tert*-butyldimethylsilyl)oxy)-4-methylpentanamido)propanamido)-3-methoxy-3-phenylpropanoyl)-L-valyl)-*N*-methyl-L-leucinate (SI-58)

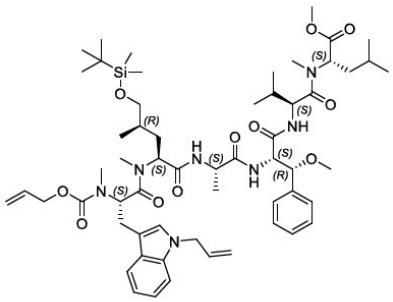

1-Allyl-*N*α-((allyloxy)carbonyl)-L-tryptophan (**SI-41**) (146 mg, 417 µmol) and methyl iodide (167 µl, 2.67 mmol) were dissolved in THF (4.5 ml) and cooled to 0 °C. NaH (71.1 mg, 1.78 mmol) was added in one portion and the reaction mixture was slowly warmed to rt over night. After 16 h, H_2O was added carefully (gas evolution), the resulting mixture was washed with PE, the PE phase was extracted with 0.5 M NaOH (1x). The combined aq. phases were acidified with 1 M HCl and extracted with EtOAc (3x). The combined EtOAc-phases were washed with 1 M Na_2SO_3 and brine, dried (Na_2SO_4) and evaporated in vacuo. The crude methylated Trp-derivative was then used in the peptide coupling without further purification.

Pentapeptide **2** (286 mg, 318 µmol) was deprotected according to *GP1* and the resulting amine was coupled to crude *Nα*-methyl-*N1*-allyl-Trp according to *GP5:* DIPEA (75.2 µl, 413 µmol), $BnNMe_2$ (4.78 µl, 31.8 µmol), 1 M iPrOCOCl (413 µl, 413 µmol), NMI (2.84 µl, 31.8 µmol), 4 M HCl (7.95 µl, 31.8 µmol) (3 h). Flash chromatography (CyH/EtOAc 100:0 – 30:70) followed by lyophilization afforded **SI-58** (300 mg, 276 µmol, 87%) as a white, amorphous solid. R_f = 0.44 (PE/EtOAc 3:7).

$[\alpha]_{20}^{D}$ = −85.2 (c 1.0, $CHCl_3$).

^{1}H NMR (500 MHz, $CDCl_3$) *(mixture of rotamers, ratio ~3:1)* δ -0.06 (s, 0.6H), -0.04 (s, 0.8H), -0.01 – 0.08 (m, 4.7H), 0.40 (d, *J* = 6.6 Hz, 0.5H), 0.82 (s, 1.8H), 0.84 – 1.03 (m, 23.4H), 1.10 (d, *J* = 7.0 Hz, 0.7H), 1.21 – 1.27 (m, 1.5H), 1.32 (d, *J* = 7.2 Hz, 0.7H), 1.43 – 1.55 (m, 2.3H), 1.65 – 1.81 (m, 2.3H), .1.83 – 1.99 (m, 1.8H), 2.05 – 2.18 (m, 1.2H), 2.75 – 2.85 (m, 3.1H), 2.88 (s, 0.9H), 2.90 (s, 0.91H), 2.94 – 3.02 (m, 3.1H), 3.03 – 3.10 (m, 0.8H), 3.14 (s, 0.7H), 3.28 (s, 0.7H), 3.30 – 3.35 (m, 2.4H), 3.35 – 3.52 (m, 2.4H), 3.69 (s, 3.0H), 4.12 – 4.30 (m, 1.3H), 4.37 – 4.45 (m, 0.4H), 4.50 – 4.71 (m, 4.2H), 4.72 – 4.86 (m, 2.2H), 4.97 – 5.30 (m, 4.7H), 5.31 – 5.39 (m, 1.2H), 5.48 – 5.53 (m, 0.4H), 5.82 – 5.97 (m, 1.5H), 6.21 (d, *J* = 7.2 Hz, 0.1H), 6.26 (d, *J* = 7.0 Hz, 0.3H), 6.41 (d, *J* = 6.7 Hz, 0.3H), 6.61 – 6.74 (m, 0.9H), 6.87 – 6.93 (m, 0.5H), 6.97 (s, 0.4H), 7.06 – 7.13 (m, 1.0H), 7.14 – 7.22 (m, 3.0H), 7.22 – 7.40 (m, 5.7H), 7.55 – 7.63 (m, 0.7H), 7.70 (d, *J* = 7.8 Hz, 0.3H).

^{13}C NMR (126 MHz, $CDCl_3$) *(mixture of rotamers)* δ -5.30 -5.27, -5.2, 15.7, 17.3, 17.4, 17.5, 17.6, 17.7, 17.85, 17.95, 18.4, 18.5, 19.66, 19.70, 21.5, 23.4, 24.9, 25.0, 25.2, 25.3, 26.0, 26.1, 29.1, 29.6, 30.0, 30.5, 30.8, 30.9, 31.1, 31.3, 31.4, 31.46, 31.51, 31.8, 32.2, 32.30, 32.35, 37.1, 48.77, 48.81, 48.9, 49.1, 49.3, 49.6, 52.3, 54.2, 54.59, 54.64, 54.7, 54.9, 55.6, 56.6, 57.6, 57.7, 57.8, 57.9, 66.4, 66.5, 66.7, 66.8, 67.1, 67.2, 68.1, 81.27, 81.34, 109.5, 109.8, 109.89, 109.94, 110.0, 117.2, 117.3, 117.7, 117.8, 118.6, 118.7, 118.9, 119.2, 119.4, 119.6, 121.8, 122.1, 126.4, 126.8, 126.98, 127.02, 127.1, 128.1, 128.2, 128.3, 128.37, 128.44, 128.5, 132.4, 132.6, 132.9, 133.5, 133.6, 133.7, 136.4, 136.5, 136.9, 155.6, 156.4, 157.4, 168.5, 168.5, 169.1, 170.5, 171.5, 171.6, 172.06, 172.10, 172.2.

Selected diagnostic peaks:

Major rotamers: **^{1}H NMR** (500 MHz, $CDCl_3$) δ 0.03 (s, 3H), 0.03 (s, 3H), 0.04 (s, 3H), 0.04 (s, 3H), 0.88 (s, 9H), 2.81 (s, 3H), 2.98 (s, 3H), 2.99 (s, 3H), 3.33 (s, 3H), 3.69 (s, 3H), 4.41 (dd, *J* = 13.0, 6.0 Hz, 1H), 5.48 – 5.54 (m, 1H), 6.26 (d, *J* = 7.0 Hz, 1H), 6.89 (s, 1H), 6.97 (s, 1H), 7.70 (d, *J* = 7.8 Hz, 1H). **^{13}C NMR** (126 MHz, $CDCl_3$) δ -5.27, 19.70, 26.1, 81.34, 155.6, 156.4.

Minor rotamer: **^{1}H NMR** (500 MHz, $CDCl_3$) δ -0.06 (s, 3H), -0.04 (s, 3H), 0.40 (d, *J* = 6.6 Hz, 3H), 0.82 (s, 9H), 1.10 (d, *J* = 7.0 Hz, 3H), 2.77 (s, 3H), 3.14 (s, 3H), 3.28 (s, 3H), 6.21 (d, *J* = 7.2 Hz, 0H), 6.91 (s, 1H). **^{13}C NMR** (126 MHz, $CDCl_3$) δ -5.30, 19.66, 26.0, 81.3, 157.4.

HRMS (ESI) calcd for $C_{58}H_{90}N_7O_{11}Si^+$ $(M+H)^+$: 1088.6462; found: 1088.6470.

85

methyl *N*-(((2*S*,3*R*)-2-((*S*)-2-((2*S*,4*R*)-2-((*S*)-3-(1-allyl-1*H*-indol-3-yl)-2-((*S*)-2-(((allyloxy)carbonyl)amino)-*N*,3-dimethylbutanamido)-*N*-methylpropanamido)-5-((*tert*-butyldimethylsilyl)oxy)-4-methylpentanamido)propanamido)-3-methoxy-3-phenylpropanoyl)-L-valyl)-*N*-methyl-L-leucinate (SI-59)

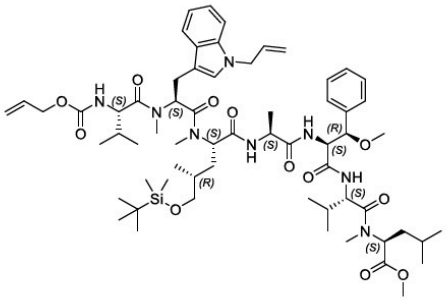

Prepared according to *GP2* and *GP5*: **SI-58** (284 mg, 261 µmol), DMBA (122 mg, 783 µmol), $Pd(PPh_3)_4$ (9.1 mg, 7.8 µmol) (1.5 h); Alloc-L-Val-OH (73.5 mg, 365 µmol), DIPEA (63.8 µl, 365 µmol), $BnNMe_2$ (3.88 µl, 26.1 µmol), 1 M iPrOCOCl (339 µl, 339 µmol), NMI (4.16 µl, 52.2 µmol), 4 M HCl (6.53 µl, 26.1 µmol) (16 h). Flash chromatography (CyH/EtOAc 100:0 – 40:60) followed by lyophilization afforded **SI-59** (250 mg, 179 µmol, 69%, 85% purity) as a white amorphous solid. R_f = 0.26 (PE/EtOAc 4:6).

$[\alpha]_{24}^{D}$ = −88.9 (c 0.5, $CHCl_3$).

^{1}H NMR (500 MHz, $CDCl_3$) *(mixture of rotamers, ratio ~2:1:1)* δ -0.07 (s, 0.7H), -0.05 (s, 0.7H), -0.02 – 0.08 (m, 4.6H), 0.39 (d, *J* = 6.6 Hz, 0.7H), 0.80 – 0.84 (m, 2.9H), 0.84 – 1.02 (m, 27.1H), 1.21 – 1.27 (m, 1.7H), 1.31 – 1.34 (m, 0.5H), 1.34 – 1.41 (m, 0.7H), 1.43 – 1.56 (m, 1.9H), 1.66 – 1.80 (m, 2.2H), 1.81 – 1.89 (m, 1.9H), 1.90 – 2.01 (m, 1.2H), 2.01 – 2.17 (m, 1.4H), 2.25 – 2.30 (m, 0.2H), 2.67 – 2.72 (m, 0.7H), 2.74 – 2.80 (m, 1.6H), 2.80 – 2.89 (m, 1.2H), 2.84 – 3.02 (m, 3.4H), 3.03 – 3.08 (m, 0.5H), 3.10 (s, 1.3H), 3.17 – 3.25 (m, 0.5H), 3.27 – 3.36 (m, 4.1H), 3.36 – 3.44 (m, 0.8H), 3.44 – 3.52 (m, 1.1H), 3.69 (s, 3.0H), 4.10 – 4.20 (m, 0.5H), 4.26 (d, *J* = 5.5 Hz, 0.1H), 4.32 – 4.43 (m, 0.5H), 4.48 – 4.72 (m, 5.0H), 4.72 – 4.76 (m, 0.4H), 4.77 – 4.87 (m, 2.2H), 4.98 – 5.11 (m, 1.3H), 5.11 – 5.27 (m, 2.1H), 5.27 – 5.39 (m, 1.8H), 5.47 (d, *J* = 9.3 Hz, 0.4H), 5.58 (t, *J* = 7.7 Hz, 0.2H), 5.84 – 5.99 (m, 2.0H), 6.09 (d, *J* = 9.3 Hz, 0.2H), 6.17 (d, *J* = 6.9 Hz, 0.4H), 6.59 (d, *J* = 7.3 Hz, 0.2H), 6.63 – 6.72 (m, 0.7H), 6.87 (s, 0.2H), 6.89 – 6.98 (m, 0.7H), 7.07 – 7.12 (m, 0.9H), 7.13 – 7.25 (m, 4.5H), 7.27 – 7.36 (m, 2.8H), 7.43 – 7.48 (m, 0.5H), 7.51 – 7.57 (m, 0.5H), 7.63 – 7.75 (m, 1.0H), 8.22 (d, *J* = 7.2 Hz, 0.2H).

^{13}C NMR (126 MHz, $CDCl_3$) *(mixture of rotamers)* δ -5.30, -5.29, 15.8, 16.9, 17.2, 17.3, 17.5, 17.8, 18.39, 18.44, 19.7, 19.9, 21.5, 23.4, 25.0, 26.0, 26.1, 30.7, 30.8, 30.9, 31.26, 31.33, 31.4, 31.5, 31.6, 32.2, 32.4, 37.1, 48.8, 48.9, 48.96, 49.05, 49.7, 52.3, 53.3, 54.2, 54.61, 54.65, 56.0, 57.5, 57.7, 57.8, 65.9, 67.1, 68.2, 81.27, 81.34, 109.3, 109.7, 109.8, 117.3, 117.75, 117.84, 118.8, 118.9, 119.5, 119.7, 121.8, 122.2, 126.1, 126.8, 127.0, 127.1, 128.1, 128.35, 128.41, 128.44, 128.5, 128.58, 128.60, 128.7, 132.05, 132.09, 132.2, 132.3, 132.8, 133.1, 133.5, 133.6, 136.4, 136.6, 136.9, 156.4, 156.6, 168.4, 168.5, 170.2, 171.4, 171.5, 171.7, 172.08, 172.10, 172.12, 172.17, 172.23, 173.6.

Selected diagnostic peaks:

Major rotamer: **^{1}H NMR** (500 MHz, $CDCl_3$) δ 0.03 (s, 3H), 0.04 (s, 3H), 0.88 (s, 9H), 2.98 (s, 3H), 3.32 (s, 3H), 3.69 (s, 3H), 5.47 (d, *J* = 9.3 Hz, 1H), 6.17 (d, *J* = 6.9 Hz, 1H), 6.66 (d, *J* = 7.5 Hz, 1H), 6.94 (s, 1H). **^{13}C NMR** (126 MHz, $CDCl_3$) δ 26.0, 81.34, 156.4.

Minor rotamers: **^{1}H NMR** (500 MHz, $CDCl_3$) δ -0.07 (s, 3H), -0.05 (s, 3H), 0.02 (s, 3H), 0.03 (s, 3H), 0.39 (d, *J* = 6.6 Hz, 3H), 0.82 (s, 9H), 2.70 (s, 3H), 3.10 (s, 3H), 3.30 (s, 3H), 3.31 (s, 3H), 5.58 (t, *J* = 7.7 Hz, 1H), 6.09 (d, *J* = 9.3 Hz, 1H), 6.59 (d, *J* = 7.3 Hz, 1H), 6.87 (s, 1H), 8.22 (d, *J* = 7.2 Hz, 1H). **^{13}C NMR** (126 MHz, $CDCl_3$) δ 26.1, 81.27, 156.7.

HRMS (ESI) calcd for $C_{63}H_{99}N_8O_{13}Si^+$ $(M+H)^+$: 1187.7146; found: 1187.7156.

(3*S*,6*S*,9*S*,12*S*,15*S*,18*S*,21*S*)-3-((1-allyl-1*H*-indol-3-yl)methyl)-21-((*R*)-3-hydroxy-2-methylpropyl)-9-isobutyl-6,12-diisopropyl-15-((*R*)-methoxy(phenyl)methyl)-1,4,10,18-tetramethyl-1,4,7,10,13,16,19-heptaazacyclohenicosane-2,5,8,11,14,17,20-heptaone (SI-60)

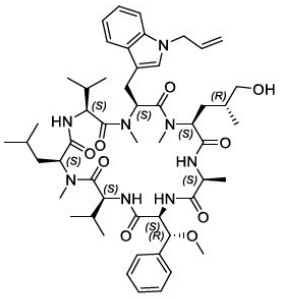

Prepared according to modified *GP6c*: **SI-59** (60.3 mg, 50.8 µmol), 1 M LiOH (76.0 µl, 76.0 µmol) (6 h); $Pd(OAc)_2$ (0.5 mg, 2.0 µmol), TPPTS (2.3 mg, 4.1 µmol), Et_2NH (26.5 µl, 254 µmol) (3 h); HATU (57.9 mg, 152 µmol), DIPEA (35.5 µl, 203 µmol) (addition over 3 h, additional 16 h); NH_4F (56.4 mg, 1.52 mmol) (15 h). RP flash chromatography (H_2O/MeCN 90:10 – 5:95) yielded **SI-60** (18.0 mg, 18-8 µmol, 37%) as an off-white amorphous solid.

$[\alpha]_{24}^{D}$ = −90.3 (c 0.5, $CHCl_3$).

^{1}H NMR (500 MHz, $CDCl_3$) δ -0.36 – -0.19 (m, 1H), 0.34 (d, *J* = 6.7 Hz, 3H), 0.43 (d, *J* = 6.5 Hz, 3H), 0.63 (d, *J* = 6.8 Hz, 3H), 0.84 – 0.89 (m, 1H), 0.92 – 0.97 (m, 6H), 0.97 – 1.01 (m, 4H), 1.08 – 1.12 (m, 6H), 1.12 – 1.16 (m, 1H), 1.55 (dt, *J* = 13.2, 6.5 Hz, 1H), 1.94 (ddd, *J* = 13.4, 10.8, 6.9 Hz, 1H), 2.18 – 2.37 (m, 3H), 2.61 (s, 3H), 2.84 (s, 3H), 2.97 (dd, *J* = 11.3, 5.4 Hz, 1H), 3.06 (dd, *J* = 11.2, 4.3 Hz, 1H), 3.16 (dd, *J* = 14.0, 6.4 Hz, 1H), 3.36 (s, 3H), 3.37 (s, 3H), 3.42 (dd, *J* = 14.3, 9.2 Hz, 1H), 4.47 – 4.53 (m, 2H), 4.59 – 4.65 (m, 2H), 4.71 – 4.80 (m, 2H), 4.80 – 4.90 (m, 2H), 5.10 (dd, *J* = 17.1, 1.4 Hz, 1H), 5.14 (d, *J* = 5.6 Hz, 1H), 5.19 (dd, *J* = 10.2, 1.4 Hz, 1H), 5.42 (dd, *J* = 9.2, 6.4 Hz, 1H), 5.91 (ddt, *J* = 16.0, 10.7, 5.6 Hz, 1H), 6.84 (s, 1H), 6.94 (d, *J* = 4.8 Hz, 1H), 7.04 – 7.12 (m, 1H), 7.15 – 7.26 (m, 6H), 7.27 – 7.29 (m, 1H), 7.45 (d, *J* = 7.9 Hz, 1H), 8.14 – 8.21 (m, 2H), 8.49 (d, *J* = 9.3 Hz, 1H).

^{13}C NMR (126 MHz, $CDCl_3$) δ 17.4, 18.8, 19.50, 19.53, 20.2, 20.3, 22.6, 23.7, 25.4, 26.7, 29.0, 29.6, 31.0, 32.0, 32.3, 32.4, 33.1, 39.1, 49.0, 50.9, 53.5, 54.4, 55.5, 55.9, 57.9, 59.0, 59.2, 66.2, 80.1, 108.8, 110.2, 118.0, 118.8, 119.8, 122.4, 126.3, 127.9, 128.3, 128.4, 129.0, 133.2, 135.1, 136.4, 168.5, 169.2, 169.8, 170.7, 171.6, 172.1, 174.3.

HRMS (ESI) calcd for $C_{52}H_{77}N_8O_9^+$ $(M+H)^+$: 957.5808; found: 957.5813.

(3*S*,3'*S*,6*S*,6'*S*,9*S*,9'*S*,12*S*,12'*S*,15*S*,15'*S*,18*S*,18'*S*,21*S*,21'*S*)-21,21'-((((*E*)-but-2-ene-1,4-diyl)bis(1*H*-indole-1,3-diyl))bis(methylene))bis(18-((*R*)-3-hydroxy-2-methylpropyl)-6-isobutyl-3,9-diisopropyl-12-((*R*)-methoxy(phenyl)methyl)-1,7,15,19-tetramethyl-1',4',7',10',13',16',19'-heptaazacyclohenicosane-2,5,8,11,14,17,20-heptaone) (28)

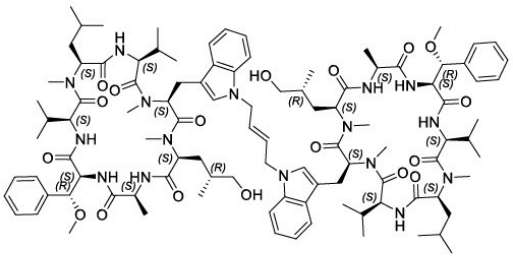

A Schlenk flask was charged with **SI-60** (32.5 mg, 34.0 µmol) and Grubbs catalyst 2nd Gen (3.5 mg, 4.1 µmol). The flask was evacuated and back-filled with argon three times. Freshly degassed (3x freeze-pump-thaw) DCM (0.27 ml) was added and the mixture was stirred at rt. After 64 h, LC/MS indicated ~60% conversion. The mixture was evaporated in vacuo and the residue was purified by RP flash chromatography (H_2O/MeCN 90:10 – 5:95) and prep HPLC (H_2O/MeCN 65:35 – 5:95), which after lyophilization yielded **28** (9.1 mg, 4.8 µmol, 28%) as a white, amorphous solid.

$[\alpha]_{20}^{D}$ = −112.4 (c 0.2, $CHCl_3$).

^{1}H NMR (500 MHz, $CDCl_3$) δ -0.48 – -0.29 (m, 2H), 0.26 (d, *J* = 6.7 Hz, 6H), 0.43 (d, *J* = 6.6 Hz, 6H), 0.62 (d, *J* = 6.8 Hz, 6H), 0.83 – 0.87 (m, 2H), 0.92 – 0.96 (m, 12H), 0.98 (d, *J* = 6.8 Hz, 6H), 1.00 – 1.04 (m, 2H), 1.08 – 1.12 (m, 12H), 1.12 – 1.15 (m, 2H), 1.51 – 1.58 (m, 2H), 1.81 – 1.87 (m, 4H), 2.21 – 2.27 (m, 2H), 2.28 – 2.35 (m, 2H), 2.55 (s, 6H), 2.85 (s, 6H), 2.89 (dd, *J* = 11.2, 5.5 Hz, 2H), 3.01 (dd, *J* = 11.2, 4.5 Hz, 2H), 3.13 (dd, *J* = 14.2, 5.9 Hz, 2H), 3.36 – 3.38 (m, 12H), 3.39 – 3.44 (m, 2H), 4.46 – 4.52 (m, 4H), 4.59 – 4.63 (m, 4H), 4.70 – 4.79 (m, 4H), 4.82 – 4.87 (m, 4H), 5.14 (d, *J* = 5.6 Hz, 2H), 5.36 (dd, *J* = 9.5, 6.1 Hz, 2H), 5.66 (t, *J* = 2.8 Hz, 2H), 6.80 (s, 2H), 6.91 (d, *J* = 4.7 Hz, 2H), 7.05 – 7.12 (m, 2H), 7.14 – 7.19 (m, 2H), 7.20 – 7.24 (m, 8H), 7.25 – 7.26 (m, 4H), 7.44 (d, *J* = 7.9 Hz, 2H), 8.09 (d, *J* = 10.1 Hz, 2H), 8.16 (d, *J* = 7.5 Hz, 2H), 8.48 (d, *J* = 9.4 Hz, 2H).

^{13}C NMR (126 MHz, $CDCl_3$) δ 17.2, 18.8, 19.49, 19.53, 20.2, 20.3, 22.7, 23.7, 25.4, 26.7, 28.9, 29.6, 31.0, 31.9, 32.3, 32.4, 32.9, 39.1, 47.6, 50.9, 53.5, 54.4, 55.5, 55.9, 57.9, 59.0, 59.1, 66.3, 80.1, 109.1, 110.1, 118.9, 120.0, 122.6, 126.4, 128.0, 128.3, 128.5, 128.6, 129.0, 135.1, 136.2, 168.5, 169.0, 169.8, 170.7, 171.5, 172.0, 174.2.

HRMS (ESI) calcd for $C_{102}H_{150}N_{16}O_{18}^{2+}$ $(M+2H)^{2+}$: 944.0669; found: 944.0667.

(3*S*,3'*S*,6*S*,6'*S*,9*S*,9'*S*,12*S*,12'*S*,15*S*,15'*S*,18*S*,18'*S*,21*S*,21'*S*)-21,21'-((-butane-1,4-diylbis(1*H*-indole-1,3-diyl))bis(methylene))bis(18-((*R*)-3-hydroxy-2-methylpropyl)-6-isobutyl-3,9-diisopropyl-12-((*R*)-methoxy(phenyl)methyl)-1,7,15,19-tetramethyl-1',4',7',10',13',16',19'-heptaazacyclohenicosane-2,5,8,11,14,17,20-heptaone) (SI-61)

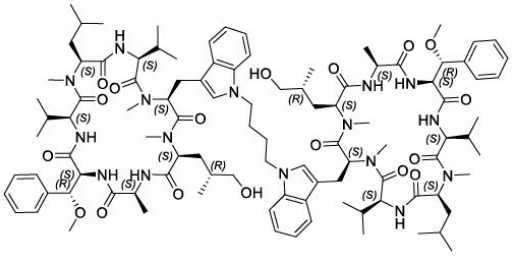

A Schlenk flask was charged with **SI-60** (25.4 mg, 26.5 µmol) and Grubbs catalyst 2nd Gen (2.7 mg, 3.2 µmol). The flask was evacuated and back-filled with argon three times. Freshly degassed (3x freeze-pump-thaw) DCM (0.21 ml) was added and the mixture was stirred at rt. After 68 h, LC/MS indicated ~50% conversion. The mixture was evaporated in vacuo and the residue was dissolved in MeOH (0.7 ml). Pd/C (10 wt%) (1.4 mg) was added and the mixture was stirred under H_2 atmosphere for 3.5 h, after which LC/MS indicated full conversion. The mixture was filtered over a syringe filter and evaporated in vacuo. RP flash chromatography (H_2O/MeCN 90:10 – 5:95) followed by prep HPLC (H_2O/MeCN 90:10 – 5:95) and lyophilization yielded **SI-61** (10.0 mg, 5.3 µmol, 40%) as a white, amorphous solid.

$[\alpha]_{20}^{D}$ = −90.7 (c 0.2, $CHCl_3$).

^{1}H NMR (500 MHz, $CDCl_3$) δ -0.48 – -0.37 (m, 2H), 0.25 (d, *J* = 6.7 Hz, 6H), 0.42 (d, *J* = 6.6 Hz, 6H), 0.62 (d, *J* = 6.6 Hz, 6H), 0.83 – 0.86 (m, 2H), 0.92 – 0.96 (m, 12H), 0.97 – 1.01 (m, 8H), 1.08 – 1.12 (m, 12H), 1.13 – 1.15 (m, 2H), 1.52 – 1.60 (m, 2H), 1.69 – 1.78 (m, 6H), 1.82 – 1.89 (m, 2H), 2.20 – 2.28 (m, 2H), 2.26 – 2.36 (m, 2H), 2.53 (s, 6H), 2.84 (s, 6H), 2.90 (dd, *J* = 11.2, 5.5 Hz, 2H), 3.00 (dd, *J* = 11.1, 4.4 Hz, 2H), 3.13 (dd, *J* = 14.3, 5.9 Hz, 2H), 3.34 – 3.42 (m, 14H), 3.98 (t, *J* = 6.4 Hz, 4H), 4.43 – 4.52 (m, 4H), 4.70 – 4.79 (m, 4H), 4.80 – 4.86 (m, 4H), 5.14 (d, *J* = 5.6 Hz, 2H), 5.36 (dd, *J* = 9.4, 6.1 Hz, 2H), 6.75 (s, 2H), 6.89 (d, *J* = 4.8 Hz, 2H), 7.04 – 7.11 (m, 2H), 7.17 – 7.19 (m, 4H), 7.21 – 7.26 (m, 10H), 7.44 (d, *J* = 7.9 Hz, 2H), 8.09 (d, *J* = 10.1 Hz, 2H), 8.16 (d, *J* = 7.6 Hz, 2H), 8.47 (d, *J* = 9.3 Hz, 2H).

^{13}C NMR (126 MHz, $CDCl_3$) δ 17.2, 18.8, 19.48, 19.51, 20.20, 20.25, 22.7, 23.7, 25.4, 26.7, 28.0, 28.9, 29.6, 31.0, 31.8, 32.3, 32.4, 32.9, 39.1, 45.9, 50.8, 53.4, 54.4, 55.5, 55.9, 57.9, 59.0, 59.1, 66.2, 80.1, 108.8, 109.7, 119.0, 119.8, 122.5, 126.2, 127.8, 128.3, 128.5, 129.0, 135.1, 136.2, 168.5, 169.0, 169.8, 170.7, 171.5, 172.0, 174.2.

HRMS (ESI) calcd for $C_{102}H_{151}N_{16}O_{18}^{+}$ $(M+H)^{+}$: 1888.1387; found:1888.1466.

Synthesis of Trp-Nα methylated exit vector 3 Homo-BacPROTACs (SI-65, SI-66)

Methyl *N*-(((2*S*,3*R*)-2-((2*S*)-2-((2*S*)-2-(2-(((allyloxy)carbonyl)(methyl)amino)-*N*-methyl-3-(1-methyl-1*H*-indol-3-yl)propanamido)-5-((tert-butyldimethylsilyl)oxy)-4-methylpentanamido)propanamido)-3-methoxy-3-(4-(prop-2-yn-1-yloxy)phenyl)propanoyl)-L-valyl)-*N*-methyl-L-leucinate (SI-62)

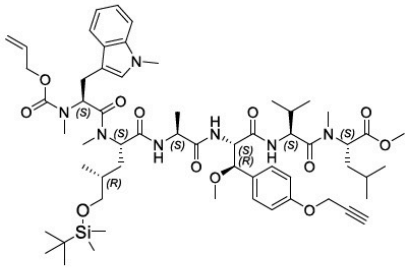

Pentapeptide **SI-35** (500 mg, 481 µmol) was dissolved in DCM (4.8 ml), tris(2-aminoethyl)amine (720 µl, 4.81 mmol) was added and the reaction mixture was stirred vigorously. After 30 min, full conversion was determined by TLC. The reaction mixture was washed with saturated NaCl solution (20 ml×3) and phosphate buffer (67 mM, pH 5.5) (30 ml×3). The aqueous phase was back–extracted with DCM (1x). The organic phase was dried (Na_2SO_4) and evaporated in vacuo. The crude peptide was dissolved in DMF (4.8 ml), cooled to 0°C and *N*α-((allyloxy)carbonyl)-*N*α,1-dimethyl-L-tryptophan (prepared as described above, cf. compound **18**) (152 mg, 480 µmol), HATU (366 mg, 962 µmol), HOAt (65.5 mg, 481 µmol) and DIPEA (420 µl, 2.41 mmol) were added. The reaction temperature was allowed to raise up to rt over the course of 18 h and the reaction was quenched by the addition of 1 M $KHSO_4$. The mixture was diluted with EtOAc, transferred to a separatory funnel, and shaken vigorously. The phases were separated, and the organic phase was subsequently washed with H_2O, sat. $NaHCO_3$ soln. and brine. The organic phase was dried (Na_2SO_4) and evaporated. Flash chromatography (CyH/EtOAc 100:0 – 45:55) followed by lyophilization afforded **SI-62** (319mg, 286 µmol, 60%) as a white amorphous solid. R_f = 0.39 (PE/EtOAc 4:6).

$[\alpha]_{20}^{D}$ = −72.0 (c 0.5, $CHCl_3$).

^{1}H NMR (500 MHz, $CDCl_3$) *(mixture of rotamers)* δ -0.09 – -0.03 (m, 1.7H), 0.00 – 0.06 (m, 5.3H), 0.08 (s, 0.7H), 0.41 (d, *J* = 6.6 Hz, 0.8H), 0.81 (s, 2.5H), 0.86 – 0.89 (m, 7.6H), 0.90 – 1.09 (m, 22.7 H), 1.24 (d, *J* = 6.8 Hz, 1.2H), 1.43 – 1.56 (m, 3.2H), 1.64–1.84 (m, 2.6H), 1.83–1.97 (m, 1.1H), 2.00 – 2.18 (m, 1.6H), 2.41 – 2.64 (m, 1.2H), 2.78 (s, 2.8H), 2.85–2.94 (m, 2.5H), 2.94 – 3.02 (m, 3.5H), 3.14 (s, 0.7H), 3.26 (s, 0.9H), 3.38 – 3.32 (m, 3.0H), 3.36 – 3.53 (m, 2.3H), 3.62 – 3.75 (m, 8.4H), 4.08 – 4.19 (m, 0.4H), 4.19 – 4.33 (m, 0.8H), 4.40–4.50 (m, 0.4H), 4.50–4.58 (m, 0.3H), 4.58 – 4.71 (m, 4.5H), 4.71 – 4.85 (m, 2.5H), 5.05 – 5.10 (m, 0.4H), 5.10 – 5.15 (m, 0.7H), 5.16 – 5.30 (m, 2.1H), 5.32–5.39 (m, 1.5H), 5.52 (m, 0.5H), 5.56 – 5.69 (m, 0.3H), 5.84 – 5.98 (m, 0.9H), 6.22 (d, *J* = 6.9 Hz, 0.5H), 6.40 (d, *J* = 6.7 Hz, 0.4H), 6.57 – 6.68 (m, 1.1H), 6.81–6.88 (m, 1.0H), 6.87 – 6.96 (m, 2.6H), 7.05 – 7.15 (m, 4.0H), 7.17 – 7.26 (m, 2.5H), 7.33 – 7.43 (m, 1.2H), 7.59 (q, *J* = 7.5 Hz, 1.0H), 7.71 (d, *J* = 7.8 Hz, 0.5H).

^{13}C NMR (126 MHz, $CDCl_3$) *(mixture of rotamers)* δ -5.32, -5.30, -5.2, -3.4, 15.7, 17.3, 17.4, 17.6, 17.7, 17.8, 17.9, 18.39, 18.41, 19.6, 19.7, 21.5, 23.4, 25.0, 26.0, 29.1, 29.6, 30.0, 30.4, 30.7, 30.8, 31.0, 31.44, 31.38, 31.8, 32.2, 32.3, 32.75, 32.68, 37.0, 49.1, 49.2, 49.7, 52.2, 54.0, 54.18, 54.20, 54.61, 54.64, 54.7, 54.8, 55.5, 55.80, 55.83, 56.6, 57.4, 57.5, 57.7, 57.8, 66.4, 66.8, 67.0, 67.1, 68.0, 75.7, 75.8, 78.62, 78.64, 80.9, 109.2, 109.3, 109.4, 109.5, 114.8, 114.9, 117.3, 117.7, 118.57, 118.63, 118.8, 119.0, 119.2, 119.4, 121.7, 122.0, 127.3, 127.8, 127.88, 127.95, 128.1, 128.2, 129.62, 129.65, 129.8, 132.4, 132.6, 132.9, 136.9, 137.0, 155.6, 156.3, 157.4, 157.58, 157.65, 168.42, 168.44, 168.5, 170.5, 171.4, 171.5, 171.7, 171.97, 172.03, 172.08, 172.14.

Selected diagnostic peaks:

Major rotamer: **^{1}H NMR** (500 MHz, $CDCl_3$) δ 0.87 (s, 9H), 1.43 – 1.56 (m, 3H), 2.50 – 2.52 (m, 1H), 2.78 (s, 3H), 2.91 (s, 3H), 3.30 (s, 3H), 3.69 (s, 3H), 5.84 – 5.98 (m, 1H), 6.57 – 6.68 (m, 1H), 7.59 (q, *J* = 7.5 Hz, 1H). **^{13}C-NMR** (126 MHz, $CDCl_3$) δ 19.65, 26.0, 37.0, 55.83, 81.0, 170.5.

Minor rotamer: **^{1}H NMR** (500 MHz, $CDCl_3$) δ -0.09 – -0.03 (m, 6H), 0.81 (s, 9H), 2.48 – 2.49 (m, 1H), 2.76 (s, 3H), 2.89 (s, 3H), 3.26 (s, 3H), 3.68 (s, 3H), 5.56 – 5.69 (m, 1H), 6.40 (d, *J* = 6.7 Hz, 1H) **^{13}C-NMR** (126 MHz, $CDCl_3$) δ 19.69, 55.80.

HRMS (ESI): calcd for $C_{59}H_{90}N_7O_{12}Si^+$ $(M+H)^+$: 1049.1101; found: 1049.1048.

Methyl *N*-(((2*S*,3*R*)-2-((2*S*)-2-((2*S*)-2-(2-(2-(((allyloxy)carbonyl)amino)-*N*-methyl-3-(1-methyl-1*H*-indol-3-yl)propanamido)-5-((tert-butyldimethylsilyl)oxy)-4-methylpentanamido) propanamido)-3-methoxy-3-(4-(prop-2-yn-1-yloxy)phenyl)propanoyl)-L-valyl)-*N*-methyl-L-leucinate (SI-63)

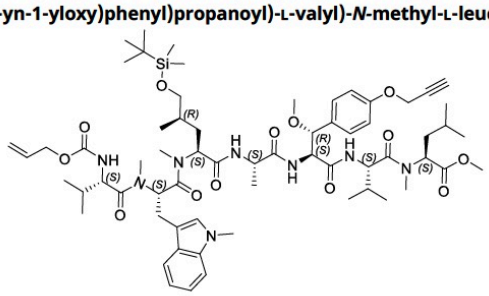

Deprotection according to *GP2*: **SI-62** (322 mg, 288 mmol), DMBA (135 mg, 865 µmol), $Pd(PPh_3)_4$ (10.0 mg, 8.65 µmol). The crude deprotected peptide was dissolved in DMF (3 ml), cooled to 0 °C and Alloc-Val-OH (122 mg, 605 µmol), HATU (219 mg, 576 µmol), HOAt (29.2 mg, 288 µmol) and DIPEA (250 µl, 1.40 mmol) were added. The reaction temperature was allowed to raise up to rt over the course of 18 h and the reaction was quenched by the addition of 1 M $KHSO_4$. The mixture was diluted with EtOAc, transferred to a separatory funnel, and shaken vigorously. The phases were separated, and the organic phase was subsequently washed with H_2O, sat. $NaHCO_3$ soln. and brine. The organic phase was dried (Na_2SO_4) and evaporated. Flash chromatography (CyH/EtOAc 100:0 – 45:55) followed by lyophilization afforded **SI-63** (268 mg, 220 µmol, 77%) as a white amorphous solid. R_f = 0.34 (PE/EtOAc 4:6).

$[\alpha]_{20}^{D}$ = –64.8 (c 1.0, $CHCl_3$).

^{1}H NMR (500 MHz, $CDCl_3$) *(mixture of rotamers)* δ -0.09 – -0.03 (m, 1.1H), 0.03 (d, *J* = 6.0 Hz, 3.3H), 0.09 (s, 0.7H), 0.17 (d, *J* = 7.6 Hz, 0.3H), 0.34 – 0.37 (m, 0.2H), 0.42 (d, *J* = 6.6 Hz, 0.5H), 0.81 (s, 2.1H), 0.88 (s, 5.0 H), 0.90 – 1.00 (m, 17.2H), 1.19 – 1.29 (m, 1.9H), 1.33 – 1.55 (m, 3.4H), 1.92 – 2.16 (m, 1.6H), 2.47 – 2.51 (m, 0.2H), 2.53 (t, *J* = 2.4 Hz, 0.4H), 2.62 – 2.79 (m, 2.4H), 2.85 (s, 3.0H), 2.97 – 3.01 (m, 1.5H), 3.05 – 3.18 (m, 1.5H), 3.20 – 3.29 (m, 0.8H), 3.30 (s, 1.3H), 3.32 – 3.42 (m, 0.6H), 3.44 – 3.57 (m, 1.0H), 3.59 – 3.67 (m, 1.8H), 3.69 (s, 4.2H), 4.09 – 4.20 (m, 0.7H), 4.47 – 4.87 (m, 6.0H), 5.01 – 5.14 (m, 0.5H), 5.19 – 5.25 (m, 0.9H), 5.27 – 5.38 (m, 2.0H), 5.46 – 5.50 (m, 0.6H), 5.84 – 5.98 (m, 1.5H), 6.13 – 6.26 (m, 0.5H), 6.59 – 6.72 (m, 0.6H), 6.80 – 6.88 (m, 0.7H), 6.88 – 6.94 (m, 0.6H), 7.08 – 7.15 (m, 2.6H), 7.16 – 7.25 (m, 1.3H), 7.39 (d, *J* = 8.8 Hz, 0.42H), 7.44 – 7.50 (m, 0.4H), 7.52 – 7.59(m, 0.5H), 7.61 – 7.74 (m, 1.1H).

^{13}C NMR (126 MHz, $CDCl_3$) *(mixture of rotamers)* δ -5.3, -4.6, -4.4, -3.4, 15.9, 16.3, 17.0, 17.33, 17.35, 17.4, 17.7, 17.8, 18.0, 18.1, 18.4, 18.7, 19.5, 19.60, 19.64, 19.8, 19.9, 21.5, 23.3, 23.4, 25.0, 25.1, 25.3, 25.8, 26.0, 26.1, 28.7, 29.0, 29.1, 29.8, 30.7, 30.9, 31.2, 31.47, 31.55, 31.7, 31.8, 32.0, 32.2, 32.67, 32.72, 32.79, 32.83, 33.0, 33.1, 33.2, 37.0, 38.8, 49.1, 49.3, 50.0, 52.3, 52.30, 53.32, 54.2, 54.29, 54.35, 54.8, 55.3, 55.8, 55.9, 56.0, 56.5, 57.4, 57.47, 57.53, 57.6, 57.8, 58.2, 58.9, 65.9, 67.0, 67.2, 68.2, 75.0, 75.78, 75.80, 75.84, 78.6, 81.0, 81.1, 109.2, 109.4, 109.5, 114.8, 114.9, 117.8, 118.79, 118.85, 119.29, 119.34, 119.55, 121.62, 121.78, 121.89, 122.19, 127.05, 127.48, 127.76, 127.84, 128.24, 128.39, 128.6, 128.7, 129.6, 129.6, 132.2, 132.3, 132.79, 132.84, 132.9, 133.1, 137.0, 156.5, 156.6, 157.7, 168.4, 168.5, 168.6, 170.3, 171.7, 172.08, 172.12, 172.2, 172.6, 173.8.

Selected diagnostic peaks:

Major rotamer: **^{1}H NMR** (500 MHz, $CDCl_3$) δ 0.02 (s, 3H), 0.04 (s, 3H), 0.88 (s, 9H), 1.19 – 1.29 (m, 3H), 2.53 (t, *J* = 2.4 Hz, 1H), 2.73 (s, 3H), 2.99, (s, 3H), 3.29 (s, 3H), 3.69 (s, 3H), 4.09 – 4.20 (m, 1H), 5.27 – 5.38 (m, 1H), 5.84 – 5.97 (m, 1H), 6.88 – 6.94 (m, 1H), 7.70 – 7.74 (m, 2H). **^{13}C-NMR** (126 MHz, $CDCl_3$) δ 26.08, 37.0, 55.85, 81.0.

Minor rotamer: **^{1}H NMR** (500 MHz, $CDCl_3$) δ -0.07 (s, 3H), -0.05 (s, 3H), 0.81 (s, 9H), 2.48 – 2.50 (m, 1H), 2.70 (s, 3H), 2.98 (s, 3H), 3.27 (s, 3H), 3. 63 (s, 3H), 6.82 – 6.87 (m, 1H). 8.24 – 8.31 (m, 1H). **^{13}C-NMR** (126 MHz, $CDCl_3$) δ 26.04, 55.89, 81.1.

HRMS (ESI): calcd for $C_{64}H_{99}N_8O_{13}Si^+$ $(M+H)^+$: 1215.7095; found: 1215.7045.

(9*S*,12*R*,15*S*,18*R*,21*S*)-21-(3-Hydroxy-2-methylpropyl)-9-isobutyl-6,12-diisopropyl-15-((*R*)-methoxy(4-(prop-2-yn-1-yloxy)phenyl)methyl)-1,4,10,18-tetramethyl-3-((1-methyl-1*H*-indol-3-yl)methyl)-1,4,7,10,13,16,19-heptaazacyclohenicosane-2,5,8,11,14,17,20-heptaone (SI-64)

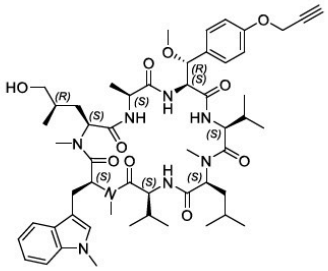

Prepared according to *GP6a*: **SI-63** (143 mg, 118 µmol), 1 M LiOH (141 µl, 141 µmol) (3.5 h); $Pd(OAc)_2$ (800 µg, 3.54 µmol), TPPTS (4.02 mg, 7.08 µmol), Et_2NH (62.0 µl, 590 µmol) (1 h); HATU (179 mg, 220 µmol), HOAt (32.0 mg, 236 µmol) DIPEA (202 µl, 1.18 mmol) (addition over 1.5 h, 17 h); NH_4F (87.0 mg, 2.40 mmol) (16 h). RP flash chromatography (H_2O/MeCN 90:10 - 5:95) followed by lyophilization afforded **SI-64** (33.0 mg, 33.0 µmol, 28%) as an off-white, amorphous solid.

$[\alpha]_{20}^{D}$ = −63.4 (c 0.3, $CHCl_3$).

^{1}H NMR (500 MHz, $CDCl_3$) δ -0.24 – -0.15 (m, 1H), 0.39 (d, *J* = 6.7 Hz, 3H), 0.48 (d, *J* = 6.6 Hz, 3H), 0.66 (d, *J* = 6.8 Hz, 3H), 0.86 – 1.02 (m, 10H), 1.07–1.17 (m, 6H), 1.48 – 1.63 (m, 1H), 1.81 – 2.00 (m, 6H), 2.18 – 2.39 (m, 2H), 2.47 (t, *J* = 2.4 Hz, 1H), 2.61 (s, 3H), 2.85 (s, 3H), 2.96–3.03 (m, 1H), 3.05–3.13 (m, 1H), 3.14 – 3.23 (m, 1H), 3.32–3.39 (m, 6H), 3.71 (s, 3H), 4.46 – 4.54 (m, 2H), 4.62 (d, *J* = 2.4 Hz, 2H), 4.71 – 4.82 (m, 2H), 4.83 – 4.93 (m, 2H), 5.10 (d, *J* = 5.4 Hz, 1H), 5.44 (dd, *J* = 8.9, 6.6 Hz, 1H), 6.80 (s, 1H), 6.83 – 6.92 (m, 2H), 6.96–7.04 (m, 1H), 7.06 – 7.15 (m, 1H), 7.15 – 7.19 (m, 2H), 7.19 – 7.24 (m, 1H), 7.26–7.31, 7.45 (d, *J* = 7.9 Hz, 1H), 8.16–8.27 (m, 2H), 8.50 (d, *J* = 9.4 Hz, 1H).

^{13}C NMR (126 MHz, $CDCl_3$) δ 17.4, 18.9, 19.0, 19.5, 20.2, 20.3, 22.6, 23.6, 25.4, 26.6, 29.0, 29.7, 31.0, 31.9, 32.3, 32.5, 32.9, 33.1, 39.1, 51.0, 53.6, 54.5, 55.5, 55.8, 56.0, 57.8, 59.0, 59.3, 66.2, 75.8, 78.5, 79.6, 108.5, 109.7, 114.7, 118.7, 119.6, 122.4, 127.1, 127.7, 127.9, 129.6, 137.0, 158.1, 168.4, 169.2, 169.9, 170.7, 171.6, 172.1, 174.3.

HRMS (ESI): calcd for $C_{53}H_{77}N_8O_{10}^+$ $(M+H)^+$: 985.5757; found: 985.5713.

(3*S*,6*S*,9*S*,12*S*,15*S*,18*S*,21*S*)-21-((*R*)-3-Hydroxy-2-methylpropyl)-15-((*R*)-(4-((1-(14-(4-((4-((*S*)-((2*R*,5*R*,8*R*,11*R*,14*R*,17*R*,20*R*)-17-((*S*)-3-hydroxy-2-methylpropyl)-8-isobutyl-5,11-diisopropyl-7,13,16,20-tetramethyl-14-((1-methyl-1*H*-indol-3-yl)methyl)-3,6,9,12,15,18,21-heptaoxo-1,4,7,10,13,16,19-heptaazacyclohenicosan-2-yl)(methoxy)methyl)phenoxy)methyl)-1*H*-1,2,3-triazol-1-yl)-3,6,9,12-tetraoxatetradecyl)-1*H*-1,2,3-triazol-4-yl)methoxy)phenyl)(methoxy)methyl)-9-isobutyl-6,12-diisopropyl-1,4,10,18-tetramethyl-3-((1-methyl-1*H*-indol-3-yl)methyl)-1,4,7,10,13,16,19-heptaazacyclohenicosane-2,5,8,11,14,17,20-heptaone (SI-65)

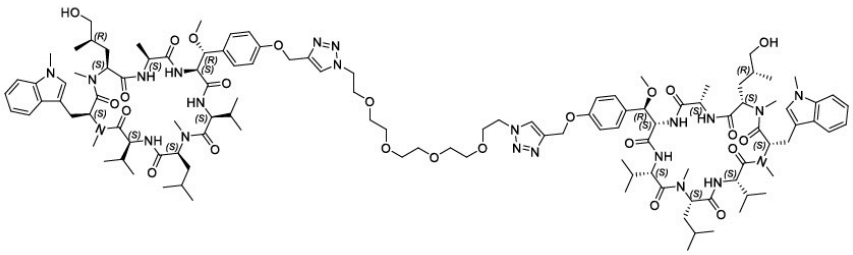

Prepared according to *GP7*: **SI-64** (22.0 mg, 22.0 µmol), 1,14-diazido-3,6,9,12-tetraoxatetradecane (3.22 mg, 11.0 µmol), 1 M $CuSO_4$ (11.2 µl, 11.2 µmol), 1 M sodium ascorbate (13.4 µl, 13.4 µmol) (17 h). RP flash chromatography (H_2O/MeCN 70:30 – 5:95) followed by lyophilization afforded **SI-65** (16.3 mg, 7.22 µmol, 64%) as a white amorphous solid.

$[\alpha]_{20}^{D}$ = –55.6 (c 0.4, $CHCl_3$).

^{1}H NMR (500 MHz, $CDCl_3$) δ -0.21– -0.13 (m, 2H), 0.40 (d, *J* = 6.7 Hz, 6H), 0.48 (d, *J* = 6.5 Hz, 6H), 0.65 (d, *J* = 6.8 Hz, 6H), 0.91 – 1.00 (m, 18H), 1.08–1.11 (m, 8H), 1.13–1.17 (m, 7H), 1.46 – 1.60 (m, 2H), 1.93 – 2.07 (m, 8H), 2.17 – 2.35 (m, 4H), 2.62 (s, 6H), 2.85 (s, 6H), 2.97–3.04 (m, 2H), 307–3.13 (m, 2H), 3.14 – 3.22 (m, 2H), 3.33–3.37 m, 14H), 3.38–3.43 (m, 2H), 3.56 – 3.60 (m, 12H), 3.71 (s, 6H), 3.87 (t, *J* = 5.1 Hz, 4H), 4.46 – 4.54 (m, 8H), 4.69 – 4.80 (m, 4H), 4.82 – 4.90 (m, 4H), 5.08 (d, *J* = 5.4 Hz, 2H), 5.10 (m, 4H), 5.44 (dd, *J* = 8.8, 6.8 Hz, 2H), 6.80 (s, 2H), 6.89 (d, *J* = 2.2 Hz, 2H), 7.00 (d, *J* = 4.8 Hz, 2H), 7.09 (t, *J* = 7.7 Hz, 2H), 7.16 (d, *J* = 8.7 Hz, 4H), 7.19 – 7.24 (m, 2H), 7.45 (d, *J* = 7.9 Hz, 2H), 7.77 (s, 2H), 8.17 (d, *J* = 7.7 Hz, 2H), 8.26 (d, *J* = 10.1 Hz, 2H), 8.48 (d, *J* = 9.3 Hz, 2H).

^{13}C NMR (126 MHz, $CDCl_3$) δ 17.4, 18.9, 19.0, 19.5, 20.2, 20.4, 22.6, 23.6, 25.42, 26.6, 29.0, 29.7, 31.0, 31.9, 32.3, 32.4, 32.9, 33.1, 39.1, 50.5, 51.0, 53.6, 54.5, 55.5, 56.0, 57.8, 59.0, 59.2, 62.0, 66.1, 69.5, 70.6, 70.6, 70.7, 79.7, 108.5, 109.7, 114.5, 118.7, 119.6, 122.4, 124.1, 127.1, 127.66, 127.68, 129.6, 137.0, 143.6, 158.8, 168.4, 169.2, 171.0, 170.7, 171.6, 172.0, 174.2.

HRMS (ESI): calcd for $C_{116}H_{173}N_{22}O_{24}^+$ $(M+H)^+$: 1130.1547; found: 1130.1516.

(3*S*,3'*S*,6*S*,6'*S*,9*S*,9'*S*,12*S*,12'*S*,15*S*,15'*S*,18*S*,18'*S*,21*S*,21'*S*)-15,15'-((1*R*,1'*R*)-((((pentane-1,5-diylbis(1*H*-1,2,3-triazole-1,4-diyl))bis(methylene))bis(oxy))bis(4,1-phenylene))bis(methoxymethylene))bis(21-((*R*)-3-hydroxy-2-methylpropyl)-9-isobutyl-6,12-diisopropyl-1,4,10,18-tetramethyl-3-((1-methyl-1*H*-indol-3-yl)methyl)-1,4,7,10,13,16,19-heptaazacyclohenicosane-2,5,8,11,14,17,20-heptaone) (SI-66)

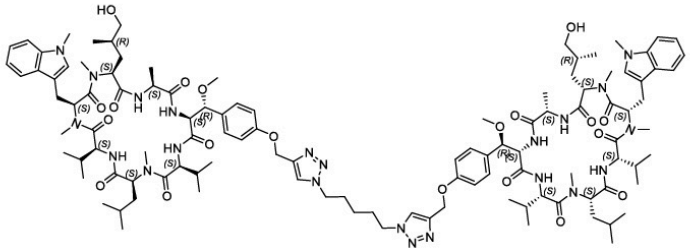

Prepared according to *GP7*: **SI-64** (20.0 mg, 20.0 µmol), 1,5-diazidopentane (1.56 mg, 10.1 µmol), 1 M $CuSO_4$ (10.2 µl, 10.2 µmol), 1 M sodium ascorbate (12.2 µl, 12.2 µmol) (18 h). RP flash chromatography (H_2O/MeCN 70:30 – 5:95) followed by lyophilization afforded **SI-66** (16.7 mg, 3.53 µmol, 79%) as a white amorphous solid.

$[\alpha]_{20}^{D}$ = –49.0 (c 0.5, $CHCl_3$).

^{1}H NMR (500 MHz, $CDCl_3$) δ -0.21– -0.12 (m, 2H), 0.40 (d, *J* = 6.7 Hz, 6H), 0.48 (d, *J* = 6.5 Hz, 6H), 0.65 (d, *J* = 6.7 Hz, 6H), 0.91 – 1.03 (m, 20H), 1.08 – 1.17 (m, 14H), 1.22 – 1.29 (m, 2H), 1.35 – 1.44 (m, 2H), 1.50 – 1.64 (m, 2H), 1.91 – 2.03 (m, 8H), 2.19 – 2.41 (m, 4H), 2.62 (s, 6H), 2.85 (s, 6H), 2.95 – 3.04 (m, 2H), 3.09 (dd, *J* = 11.2, 4.3 Hz, 2H), 3.12 – 3.24 (m, 2H), 3.33 – 3.44 (m, 12H), 3.71 (s, 6H), 4.35 (q, *J* = 6.6, 6.2 Hz, 6H), 4.41 – 4.60 (m, 4H), 4.68 – 4.81 (m, 4H), 4.83 – 4.92 (m, 4H), 5.06 – 5.14 (m, 6H), 5.44 (dd, *J* = 8.7, 6.7 Hz, 2H), 6.80 (s, 2H), 6.88 (d, *J* = 8.2

Hz, 4H), 7.01 (d, *J* = 4.9 Hz, 2H), 7.06 – 7.13 (m, 2H), 7.17 (d, *J* = 8.4 Hz, 4H), 7.20 – 7.24 (m, 2H), 7.23 – 7.29 (m, 2H), 7.45 (d, *J* = 7.9 Hz, 2H), 7.57 (s, 2H), 8.17 (d, *J* = 7.6 Hz, 2H), 8.26 (d, *J* = 10.0 Hz, 2H), 8.48 (d, *J* = 9.3 Hz, 2H).

^{13}C NMR (126 MHz, $CDCl_3$) δ 17.4, 18.9, 19.0, 19.5, 20.2, 20.4, 22.6, 23.59, 23.63, 25.4, 26.6, 29.0, 29.7, 29.7, 31.0, 32.0, 32.3, 32.4, 32.9, 33.1, 39.1, 50.1, 51.0, 53.6, 54.5, 55.5, 56.1, 57.8, 59.0, 59.3, 62.0, 66.2, 79.7, 108.5, 109.7, 114.6, 118.7, 119.6, 122.4, 122.7, 127.1, 127.68, 127.76, 129.7, 137.0, 144.0, 158.7, 168.4, 169.2, 170.0, 170.7, 171.6, 172.0, 174.2.

HRMS (ESI): calcd for $C_{111}H_{163}N_{22}O_{20}^+$ $(M+H)^+$: 1063.1258; found: 1063.1224.

Synthesis of a Phenylalanine-containing dCym derivative (SI-72)

Methyl (2*S*)-2-[(2*S*)-2-[(2*S*)-2-{[(*tert*-butoxy)carbonyl]amino}-3-phenylpropanamido]-*N*,3-dimethylbutanamido]-4-methylpentanoate (SI-67)

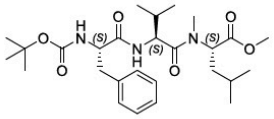

To a solution of methyl *N*-(((benzyloxy)carbonyl)-L-valyl)-N-methyl-L-leucinate (500 mg, 1.27 mmol) in DCM (3.0 ml, 0.42 M) was added HBr (33% in AcOH) (3.0 ml) slowly at 0°C and the mixture was allowed to reach rt. The solvents were evaporated in vacuo and the residue was triturated with diethyl ether. The crude amine was used in the peptide coupling without further purification.

To a solution of Boc-Phe-OH (200 mg, 754 µmol) in DMF (1.0 ml, 0.75 M) was added DIPEA (526 µl, 3.02 mmol), HOAt (51 mg, 404 µmol) and HATU (315 mg, 828 µmol). Then, the deprotected dipeptide (292 mg, 1.13 mmol) was added and the mixture was stirred at rt. The reaction was quenched with water and extracted with EtOAc. The organic layer was washed with brine, dried over Na_2SO_4 and concentrated in vacuo. Silica gel column chromatography (50% EtOAc in petroleum ether) yielded **SI-67** (300 mg, 593 µmol, 79%).

Major rotamer: **^{1}H NMR** (500 MHz, $CDCl_3$) δ 0.85 (d, *J* = 6.8 Hz, 3H), 0.89 (d, *J* = 6.5 Hz, 3H), 0.94 (d, *J* = 6.7 Hz, 3H), 0.97 (d, *J* = 6.8 Hz, 3H), 1.39 (s, 10H), 1.63 – 1.71 (m, 1H), 1.71 – 1.78 (m, 1H), 2.01 – 2.09 (m, 1H), 2.96 – 3.03 (m, 4H), 3.10 (dd, *J* = 14.0, 6.1 Hz, 1H), 3.68 (s, 3H), 4.37 (d, *J* = 7.4 Hz, 1H), 4.79 (dd, *J* = 8.8, 6.1 Hz, 1H), 4.95 (d, *J* = 8.1 Hz, 1H), 5.30 (dd, *J* = 10.6, 5.1 Hz, 1H), 6.67 (d, *J* = 8.8 Hz, 1H), 7.14 – 7.19 (m, 2H), 7.20 – 7.23 (m, 1H), 7.24 – 7.31 (m, 2H). **^{13}C NMR** (126 MHz, CDCl3) δ 17.4, 19.6, 21.5, 23.4, 24.9, 28.4, 31.4, 31.5, 37.0, 38.1, 52.3, 54.0, 54.6, 55.8, 80.2, 127.0, 128.7, 129.5, 136.6, 155.3, 171.1, 172.2, 172.3.

Minor rotamer (ratio *~10:1, selected signals):* **^{1}H NMR** (500 MHz, $CDCl_3$) δ 0.82 (d, *J* = 6.7 Hz, 3H), 1.00 (d, *J* = 6.1 Hz, 3H), 1.93 – 2.00 (m, 1H), 2.82 (s, 3H), 3.70 (s, 3H), 4.66 (t, *J* = 7.3 Hz, 1H), 4.90 (d, *J* = 8.6 Hz, 1H), 6.55 (d, *J* = 9.3 Hz, 1H).

HRMS (ESI) calcd for $C_{27}H_{44}N_3O_6^+$ $(M+H)^+$: 506.3225; found: 506.3227.

Methyl (2*S*)-2-[(2*S*)-2-[(2*S*)-2-[(2*S*)-2-{[(*tert*-butoxy)carbonyl]amino}propanamido]-3-phenylpropanamido]-*N*,3-dimethylbutanamido]-4-methylpentanoate (SI-68)

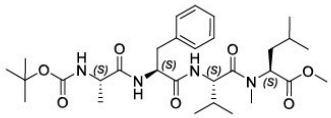

To a solution of **SI-67** (500 mg, 989 µmol) in DCM (4.0 ml, 0.25 M) was added HCl (4 M in dioxane) (2.0 ml) slowly at 0 °C and the mixture was allowed to reach rt and stirred for 3 h. The solvents were evaporated in vacuo and the crude amine was used in the peptide coupling without further purification.

To a solution of the deprotected tripeptide (1.20 g, 2.96 mmol) in DMF (120 ml, 0.025 M) was added DIPEA (1.55 ml, 8.87 mmol) and HATU (1.69 g, 4.44 mmol) at 0 °C. After 20 minutes, Boc-Ala-OH (616 mg, 3.26 mmol) was added, the mixture was allowed to reach rt and stirred for 16 h. The reaction was quenched with water and extracted with EtOAc. The organic layer was washed with water, dried over Na_2SO_4 and concentrated in vacuo. Silica gel column chromatography (30% EtOAc in hexane) yielded **SI-68** (1.10 g, 1.91 mmol, 64%) as a white solid.

$[\alpha]_{20}^{D}$ = −50.4 (c 1.0, $CHCl_3$).

Major rotamer: **^{1}H NMR** (500 MHz, $CDCl_3$) δ 0.84 (d, *J* = 6.8 Hz, 3H), 0.90 (d, *J* = 6.5 Hz, 3H), 0.95 (d, *J* = 6.8 Hz, 3H), 0.95 (d, *J* = 6.9 Hz, 3H), 1.28 (d, *J* = 7.0 Hz, 3H), 1.41 (s, 9H), 1.46 (dd, *J* = 9.6, 4.4 Hz, 1H), 1.68 (ddd, *J* = 14.6, 10.7, 4.6 Hz, 1H), 1.75 (ddd, *J* = 14.6, 9.6, 5.1 Hz, 1H), 2.01 – 2.09 (m, 1H), 2.98 (s, 3H), 3.00 – 3.02 (m, 1H), 3.09 (dd, *J* = 14.0, 6.4 Hz, 1H), 3.68 (s, 3H), 4.08 – 4.18 (m, 1H), 4.65 – 4.72 (m, 1H), 4.76 (dd, *J* = 8.8, 6.2 Hz, 1H), 4.91 – 4.99 (m, 1H), 5.31 (dd, *J* = 10.7, 5.1 Hz, 1H), 6.59 – 6.69 (m, 2H), 7.13 – 7.17 (m, 2H), 7.16 – 7.23 (m, 1H), 7.23 – 7.26 (m, 2H). **^{13}C NMR** (126 MHz, $CDCl_3$) δ 17.5, 18.5, 19.6, 21.6, 23.4, 25.0, 28.4, 31.4, 31.4, 37.0, 38.1, 50.3, 52.3, 54.2, 54.3, 54.6, 80.2, 127.1, 128.7, 129.4, 136.3, 155.5, 170.4, 172.1, 172.2, 172.5.

Minor rotamer (ratio ~10:1, selected signals) **^{1}H NMR** (500 MHz, $CDCl_3$) δ 0.80 (dd, *J* = 6.8, 1.5 Hz, 3H), 0.98 – 1.01 (m, 6H), 1.95 – 2.00 (m, 1H), 2.83 (s, 3H), 3.70 (s, 3H). **^{13}C NMR** (126 MHz, $CDCl_3$) δ 20.0, 22.7, 22.8, 29.2, 38.7, 52.7, 53.9, 57.8.

HRMS (ESI) calcd for $C_{30}H_{49}N_4O_7^+$ $(M+H)^+$: 577.3596; found: 577.3603.

Methyl *N*-((2*S*,4*R*)-2-(((benzyloxy)carbonyl)(methyl)amino)-5-((*tert*-butyldimethylsilyl)oxy)-4-methylpentanoyl)-L-alanyl-L-phenylalanyl-L-valyl-*N*-methyl-L-leucinate (SI-69)

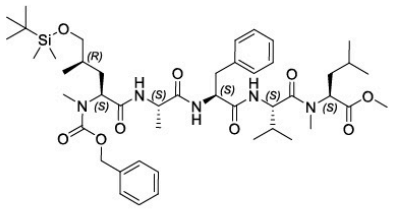

To **SI-68** (500 mg, 867 µmol) was added 4 M HCl in dioxane (2.17 ml, 8.67 mmol) at rt. After 1.5 h, the mixture was evaporated in vacuo and azeotroped with DCM three times. The resulting crude peptide was reacted according to *GP4*: (2S,4R)-2-(((benzyloxy)-carbonyl)(methyl)amino)-5-((tertbutyldimethylsilyl)oxy)-4-methylpentanoic acid (391 mg, 954 µmol), HOBt (146 mg, 954 µmol), EDC (183 mg, 954 µmol), NMM (200 µl, 1.82 mmol) (15 h). Flash chromatography (CyH/EtOAc 100:0 – 4:6) followed by lyophilization yielded **SI-69** (612 mg, 705 µmol, 81%) as a colorless amorphous solid. R_f = 0.36 (PE/EtOAc 4:6).

$[\alpha]_{20}^{D}$ = −57.6 (c 1.0, $CHCl_3$).

^{1}H NMR (500 MHz, $CDCl_3$) *(mixture of rotamers, ratio ca. 10:3:1)* δ -0.07 – 0.08 (m, 6.0H), 0.84 (d, *J* = 6.8 Hz,3.0H), 0.86 – 0.89 (s, 9.0H), 0.89 – 0.92 (m, 4.2H), 0.92 – 0.98 (m, 7.7H), 0.98 – 1.04 (m, 1.1H), 1.18 – 1.26 (m, 2.8H), 1.41 – 1.50 (m, 1.3H), 1.50 – 1.59 (m, 1.8H), 1.64 – 1.79 (m, 2.1H), 1.87 – 1.97 (m, 1.2H), 2.01 – 2.10 (m, 1.2H), 2.10 – 2.16 (m, 0.4H), 2.18 – 2.28 (m, 0.3H), 2.85 (s, 3.0H), 2.95 – 3.02 (m, 4.4H), 3.05 – 3.17 (m, 1.0H), 3.33 – 3.55 (m, 2.1H), 3.68 (s, 2.7H), 3.70 (s, 0.3H), 3.98 (t, *J* = 10.7 Hz, 0.2H),4.13 – 4.19 (m, 0.1H), 4.27 – 4.38 (m, 1.2H), 4.45 – 4.59 (m, 1.1H), 4.64 (q, *J* = 7.0 Hz, 1.1H), 4.70 – 4.80 (m, 1.1H), 5.05 – 5.23 (m, 2.6H), 5.30 (dd, *J* = 10.7, 5.1 Hz, 1.0H), 6.10 – 6.24 (m, 0.3H), 6.36 – 6.49 (m, 0.6H), 6.53 – 6.82 (m, 2.0H), 7.08 – 7.25 (m, 4.8H), 7.28 – 7.39 (m, 6.1H).

^{13}C NMR (126 MHz, $CDCl_3$) *(mixture of rotamers)* δ -5.3, -3.4, 16.8, 17.5, 17.6, 17.8, 18.5, 19.6, 21.5, 23.4, 24.9, 25.8, 26.1, 28.8, 30.7, 31.3, 31.4, 32.4, 33.3, 37.0, 37.8, 49.1, 52.3, 54.2, 54.4, 54.6, 57.4, 67.3, 67.76, 67.82, 75.0, 127.1, 128.0, 128.2, 128.6, 128.67, 128.72, 129.4, 136.5, 156.5, 157.3, 169.3, 170.4, 171.0, 171.6, 172.15, 172.23.

Selected diagnostic peaks:

Major rotamer: **^{1}H NMR** (500 MHz, $CDCl_3$) δ -0.05 – 0.06 (m, 6H), 0.84 (d, *J* = 6.8 Hz, 3H), 0.88 (s, 9H), 0.90 (d, *J* = 6.6 Hz, 3H), 2.85 (s, 3H), 2.98 (s, 3H), 3.68 (s, 3H), 3.98 (t, *J* = 10.7 Hz, 0H), 4.64 (q, *J* = 7.0 Hz, 1H), 4.73 – 4.78 (m, 1H), 5.30 (dd, *J* = 10.7, 5.1 Hz, 1H). **^{13}C NMR** (126 MHz, $CDCl_3$) δ -5.3, 26.1, 157.3.

Minor rotamer: **^{1}H NMR** (500 MHz, $CDCl_3$) δ 1.02 (d, *J* = 6.7 Hz, 3H), 2.96 (s, 3H), 3.70 (s, 3H), 3.98 (t, *J* = 10.7 Hz, 1H). **^{13}C NMR** (126 MHz, $CDCl_3$) δ -3.4, 25.8, 156.5.

HRMS (ESI) calcd for $C_{46}H_{74}N_5O_9Si^+$ $(M+H)^+$: 868.525; found: 868.5202.

Methyl *N*-((2*S*,4*R*)-2-((*S*)-2-(((allyloxy)carbonyl)amino)-*N*-methyl-3-(1-(prop-2-yn-1-yl)-1*H*-indol-3-yl)propanamido)-5-((*tert*-butyldimethylsilyl)oxy)-4-methylpentanoyl)-L-alanyl-L-phenylalanyl-L-valyl-*N*-methyl-L-leucinate (SI-70)

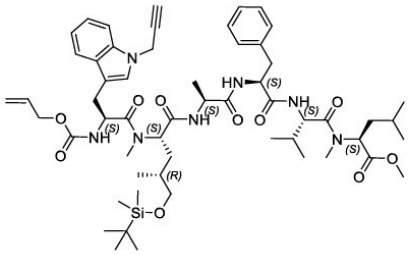

Prepared according to *GP1* and *GP5*: **SI-69** (300 mg, 346 µmol), Pd/C (30.0 mg) (1 h); Alloc-Trp(propargyl)-OH (151 mg, 463 µmol), 1 M iPrOCOCl (450 µl, 450 µmol), DIPEA (79.0 µl, 450 µmol), $BnNMe_2$ (5.14 µl, 34.6 µmol), NMI (5.52 µl, 69.2 µmol), 4 M HCl (8.65 µl, 34.6 µmol) (16 h). Flash chromatography (CyH/EtOAc 100:0 – 4:6) followed by lyophilization yielded **SI-70** (263 mg, 252 µmol, 73%) as a white amorphous solid. R_f = 0.23 (PE/EtOAc 4:6).

$[\alpha]_{20}^{D}$ = –62.7 (c 1.0, $CHCl_3$).

^{1}H NMR (500 MHz, $CDCl_3$) *(mixture of rotamers, ratio ca. 2:1)* δ -0.06 (d, *J* = 9.0 Hz, 1.3H), -0.02 – 0.07 (m, 6.6H), 0.37 (d, *J* = 6.7 Hz, 0.6H), 0.74 – 0.82 (m, 5.2H), 0.82 – 0.92 (m, 17.9H), 0.92 – 1.00 (m, 8.3H), 1.18 – 1.33 (m, 5.5H), 1.34 – 1.48 (m, 2.8H), 1.50 – 1.61 (m, 0.8H), 1.62 – 1.79 (m, 2.5H), 1.81 – 2.14 (m, 3.6H), 2.31 – 2.45 (m, 1.0H), 2.75 (s, 0.7H), 2.77 – 2.87 (m, 3.2H), 2.92 – 3.02 (m, 4.5H), 3.02 – 3.23 (m, 3.3H), 3.25 – 3.44 (m, 2.6H), 3.47 – 3.53 (m, 0.3H), 3.63 – 3.73 (m, 3.9H), 4.20 – 4.42 (m, 1.8H), 4.42 – 4.67 (m, 3.5H), 4.67 – 4.88 (m, 4.7H), 4.88 – 5.05 (m, 1.0H), 5.12 – 5.37 (m, 3.4H), 5.66 (d, *J* = 7.6 Hz, 0.2H), 5.79 – 5.95 (m, 1.0H), 6.38 (d, *J* = 7.3 Hz, 0.5H), 6.42 (d, *J* = 8.6 Hz, 0.5H), 6.52 (d, *J* = 8.7 Hz, 0.3H), 6.75 (d, *J* = 7.6 Hz, 0.3H), 6.90 (d, *J* = 9.1 Hz, 0.5H), 7.04 (s, 1.0H), 7.10 – 7.31 (m, 9.8H), 7.33 – 7.39 (m, 1.0H), 7.42 – 7.49 (m, 0.3H), 7.51 – 7.56 (m, 0.2H), 7.58 (d, *J* = 7.9 Hz, 0.2H), 7.63 – 7.68 (m, 0.4H), 7.70 (d, *J* = 8.6 Hz, 0.6H), 7.84 (d, *J* = 7.1 Hz, 0.2H).

^{13}C NMR (126 MHz, $CDCl_3$) *(mixture of rotamers)* δ -5.3, -5.2, -3.4, 15.9, 17.2, 17.37 17.40, 17.5, 17.6, 17.7, 18.4, 18.48, 18.51, 19.4, 19.6, 21.6, 22.3, 23.4, 24.9, 25.8, 26.0, 26.08, 26.11, 28.5, 28.8, 29.3, 31.29, 31.31, 31.35, 31.38, 31.42, 31.6, 31.9, 32.2, 32.4, 34.5, 35.7, 35.8, 37.0, 37.1, 37.6, 37.9, 49.56, 49.61, 51.7, 52.3, 54.1, 54.17, 54.23, 54.3, 54.37, 54.44, 54.57, 54.60, 54.64, 58.2, 58.9, 65.8, 66.4, 67.6, 68.4, 69.7, 73.7, 73.8, 77.7, 78.0, 109.6, 109.7, 110.3, 117.7, 118.4, 119.0, 119.2, 120.0, 120.2, 122.3, 122.6, 126.2, 126.3, 126.9, 127.0, 128.55, 128.58, 128.60, 128.65, 128.68, 128.74, 129.38, 129.42, 129.5, 132.05, 132.08, 132.19, 132.23, 132.3, 133.0, 136.0, 136.2, 136.4, 136.8, 156.3, 156.7, 168.9, 170.3, 170.4, 170.5, 171.7, 171.8, 172.0, 172.15, 172.19, 172.22, 172.5, 172.6, 173.1.

Selected diagnostic peaks:

Major rotamer: **^{1}H NMR** (500 MHz, $CDCl_3$) δ 0.01 (s, 3H), 0.02 (s, 3H), 0.87 (s, 9H), 2.38 (t, *J* = 2.5 Hz, 1H), 2.85 (s, 3H), 2.99 (s, 3H), 3.68 (s, 3H), 6.38 (d, *J* = 7.3 Hz, 1H), 6.42 (d, *J* = 8.6 Hz, 1H), 6.90 (d, *J* = 9.1 Hz, 1H), 7.04 (s, 1H). **^{13}C NMR** (126 MHz, $CDCl_3$) δ 26.1, 73.7, 78.0, 156.3

Minor rotamer: **^{1}H NMR** (500 MHz, $CDCl_3$) δ -0.07 (s, 3H), -0.04 (s, 3H), 0.37 (d, *J* = 6.7 Hz, 3H), 0.81 (s, 9H), 2.75 (s, 3H), 2.79 (s, 3H), 2.94 (s, 3H), 3.67 (s, 3H), 5.66 (d, *J* = 7.6 Hz, 1H), 6.52 (d, *J* = 8.7 Hz, 1H), 6.75 (d, *J* = 7.6 Hz, 1H), 7.84 (d, *J* = 7.1 Hz, 1H). **^{13}C NMR** (126 MHz, $CDCl_3$) δ 73.8, 77.7, 156.7

HRMS (ESI) calcd for $C_{56}H_{84}N_7O_{10}Si^+$ $(M+H)^+$: 1042.6043; found: 1042.6003.

methyl *N*-((2*S*,4*R*)-2-((*S*)-2-((*S*)-2-(((allyloxy)carbonyl)amino)-3-methylbutanamido)-*N*-methyl-3-(1-(prop-2-yn-1-yl)-1*H*-indol-3-yl)propanamido)-5-((*tert*-butyldimethylsilyl)oxy)-4-methylpentanoyl)-L-alanyl-L-phenylalanyl-L-valyl-*N*-methyl-L-leucinate (SI-71)

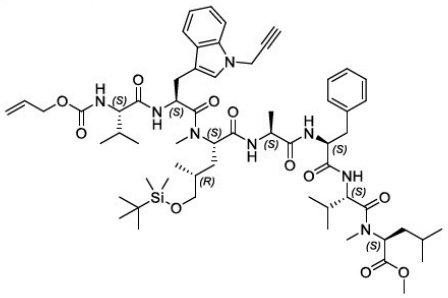

Prepared according to *GP2* and *GP4*: **SI-70** (234 mg, 224 µmol), $Pd(PPh_3)_4$ (2.59 mg, 2.25 µmol), DMBA (105 mg, 673 µmol) (1 h); Alloc-Val-OH (54.1 mg, 269 µmol), HOBt (37.7 mg, 246 µmol), EDC (47.2 mg, 246 µmol), NMM (27.1 µl, 246 µmol) (17 h). Flash chromatography (CyH/EtOAc 100:0 – 3:7) followed by lyophilization yielded **SI-71** (200 mg, 175 µmol, 78%) as a white amorphous solid. R_f = 0.19 (PE/EtOAc 4:6).

$[\alpha]_{20}^{D}$ = –61.0 (c 1.0, $CHCl_3$).

^{1}H NMR (500 MHz, $CDCl_3$) *(mixture of rotamers, ratio ca. 3:2)* δ -0.07 – -0.04 (m, 1.6H), -0.03 – 0.06 (m, 6.2H), 0.36 (d, *J* = 6.6 Hz, 0.7H), 0.74 (d, *J* = 6.4 Hz, 2.0H), 0.79 – 0.83 (m, 4.2H), 0.83 – 1.00 (m, 36.5H), 1.19 – 1.24 (m, 2.8H), 1.24 – 1.31 (m, 3.5H), 1.33 – 1.60 (m, 4.2H), 1.61 – 1.79 (m, 3.1H), 1.81 – 1.93 (m, 0.8H), 1.93 – 2.15 (m, 4.7H), 2.37 (t, *J* = 2.5 Hz, 0.6H), 2.39 (t, *J* = 2.6 Hz, 0.4H), 2.70 (s, 0.8H), 2.79 (s, 0.9H), 2.80 – 2.88 (m, 2.6H), 2.93 – 3.03 (m, 5.1H), 3.03 – 3.21 (m, 4.0H), 3.23 – 3.35 (m, 1.8H), 3.35 – 3.44 (m, 1.2H), 3.51 (dd, *J* = 9.8, 4.6 Hz, 0.4H), 3.64 – 3.71 (m, 4.5H), 4.03 – 4.09 (m, 0.4H), 4.20 – 4.45 (m, 2.7H), 4.47 – 4.63 (m, 3.1H), 4.63 – 4.88 (m, 5.6H), 4.89 – 5.00 (m, 0.7H), 5.15 – 5.23 (m, 1.3H), 5.24 – 5.35 (m, 3.1H), 5.55 (d, *J* = 9.2 Hz, 0.5H), 5.82 – 5.97 (m, 1.3H), 6.28 – 6.54 (m, 0.7H), 6.57 (d, *J* = 8.8 Hz, 0.3H), 6.61 – 6.74 (m, 0.6H), 6.75 – 6.92 (m, 1.3H), 6.99 – 7.08 (m, 1.5H), 7.09 – 7.29 (m, 10.9H), 7.30 – 7.39 (m, 1.6H), 7.43 – 7.49 (m, 0.7H), 7.51 – 7.57 (m, 0.6H), 7.63 – 7.76 (m, 1.8H), 8.07 (d, *J* = 7.8 Hz, 0.3H).

^{13}C NMR (126 MHz, $CDCl_3$) *(mixture of rotamers)* δ -5.3, -5.2, -3.4, 15.9, 17.3, 17.5, 17.8, 17.9, 18.4, 18.46, 18.50, 19.3, 19.4, 19.52, 19.54, 21.5, 21.6, 22.3, 23.3, 23.4, 24.92, 24.94, 25.8, 26.0, 26.07, 26.10, 26.13, 28.8, 29.3, 31.29, 31.34, 31.38, 31.40, 31.5, 31.7, 31.85, 31.89, 32.5, 35.7, 35.8, 37.0, 37.7, 49.1, 49.6, 50.0, 52.2, 52.3, 54.0, 54.1, 54.2, 54.4, 54.5, 54.59, 54.64, 54.8, 57.1, 58.3, 59.9, 60.1, 65.8, 66.1, 67.6, 68.4, 69.7, 73.7, 73.8, 77.8, 78.0, 109.5, 109.6, 109.7, 110.3, 117.7, 118.1, 118.9, 119.3, 120.0, 120.2, 122.3, 122.6, 126.1, 126.3, 127.0, 127.1, 128.2, 128.5, 128.5, 128.6, 128.6, 128.66, 128.68, 129.37, 129.41, 129.44, 129.5, 132.05, 132.08, 132.2, 132.3, 132.9, 133.0, 136.0, 136.1, 136.5, 136.8, 156.1, 156.5, 168.5, 170.1, 170.3, 170.7, 171.4, 171.7, 171.9, 172.0, 172.12, 172.15, 172.2, 172.3, 172.5, 172.7.

Selected diagnostic peaks:

Major rotamer: **^{1}H NMR** (500 MHz, $CDCl_3$) δ -0.01 (s, 3H), 0.00 (s, 3H), 0.74 (d, *J* = 6.4 Hz, 3H), 0.86 (s, 9H), 2.37 (t, *J* = 2.5 Hz, 1H), 2.86 (s, 3H), 2.99 (s, 3H), 3.51 (dd, *J* = 9.8, 4.6 Hz, 0H), 3.67 (s, 3H), 5.55 (d, *J* = 9.2 Hz, 1H), 7.03 (s, 1H). **^{13}C NMR** (126 MHz, $CDCl_3$) δ 24.94, 26.10, 73.7, 78.04, 156.1.

Minor rotamer: **^{1}H NMR** (500 MHz, $CDCl_3$) δ -0.06 (s, 3H), -0.04 (s, 3H), 0.36 (d, *J* = 6.6 Hz, 3H), 0.82 (s, 9H), 2.39 (t, *J* = 2.6 Hz, 1H), 2.70 (s, 3H), 2.79 (s, 3H), 2.95 (s, 3H), 3.51 (dd, *J* = 9.8, 4.6 Hz, 1H), 3.67 (s, 3H), 6.57 (d, *J* = 8.8 Hz, 1H), 7.04 (s, 1H), 8.07 (d, *J* = 7.8 Hz, 1H). **^{13}C NMR** (126 MHz, $CDCl_3$) δ 24.92, 73.8, 77.8, 156.5.

HRMS (ESI) calcd for $C_{61}H_{93}N_8O_{11}Si^+$ $(M+H)^+$: 1141.6728; found: 1141.6744.

(3*S*,6*S*,9*S*,12*S*,15*S*,18*S*,21*S*)-15-benzyl-21-((*R*)-3-hydroxy-2-methylpropyl)-9-isobutyl-6,12-diisopropyl-1,10,18-trimethyl-3-((1-(prop-2-yn-1-yl)-1*H*-indol-3-yl)methyl)-1,4,7,10,13,16,19-heptaazacyclohenicosane-2,5,8,11,14,17,20-heptaone (SI-72)

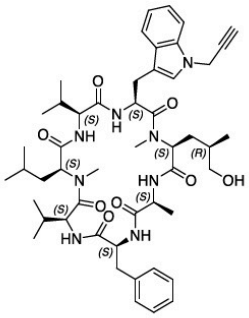

Prepared according to modified *GP6a*: **SI-71** (68.9 mg, 60.4 µmol), 1 M LiOH (96.1 µl, 96.1 µmol) (4.5 h); $Pd(OAc)_2$ (0.7 mg, 3.0 µmol), TPPTS (3.4 mg, 6.0 µmol), Et_2NH (31.6 µl, 302 µmol) (3 h); HATU (80.0 mg, 211 µmol), HOAt (16.4 mg, 121 µmol), DIPEA (42.2 µl, 242 µmol) (17 h); Deprotection: The crude cyclic peptide was dissolved in THF (0.6 ml), 1 M TBAF in THF (133 µl, 133 µmol) was added at 0 °C. After 2.5 h, the mixture was quenched with 1 M $KHSO_4$ soln., extracted with EtOAc (3x). The combined org phases were washed with 1 M $KHSO_4$ and brine, dried (Na_2SO_4) and evaporated. Preparative TLC ($CHCl_3$/MeOH 94:6) followed by RP flash chromatography (H_2O/MeCN 90:10 – 5:95) and lyophilization afforded **SI-72** (5.4 mg, 5.93 µmol, 10%) as a colorless amorphous solid. R_f = 0.26 ($CHCl_3$/MeOH 95:5).

$[\alpha]_{20}^{D}$ = −95.9 (c 1.0, $CHCl_3$).

^{1}H NMR (500 MHz, $CDCl_3$) δ 0.03 (ddd, *J* = 15.3, 8.9, 2.7 Hz, 1H), 0.61 (d, *J* = 6.7 Hz, 3H), 0.87 (d, *J* = 6.2 Hz, 1H), 0.90 (d, *J* = 6.7 Hz, 3H), 0.97 (t, *J* = 6.3 Hz, 6H), 1.03 (t, *J* = 6.8 Hz, 6H), 1.08 (d, *J* = 6.8 Hz, 3H), 1.18 (d, *J* = 7.4 Hz, 3H), 1.31 (ddd, *J* = 13.8, 7.0, 1.6 Hz, 2H), 1.66 – 1.73 (m, 1H), 1.99 – 2.10 (m, 3H), 2.28 (ddd, *J* = 13.9, 8.0, 5.9 Hz, 1H), 2.38 (t, *J* = 2.5 Hz, 1H), 2.79 (s, 3H), 2.80 (s, 3H), 2.94 (dd, *J* = 11.7, 2.7 Hz, 1H), 2.96 – 3.03 (m, 1H), 3.11 (dd, *J* = 13.6, 10.0 Hz, 1H), 3.19 (dd, *J* = 14.4, 4.9 Hz, 1H), 3.43 – 3.53 (m, 3H), 4.18 (pent, *J* = 7.1 Hz, 1H), 4.32 – 4.38 (m, 1H), 4.42 (t, *J* = 9.8 Hz, 1H), 4.53 (dd, *J* = 8.1, 5.5 Hz, 1H), 4.67 (ddd, *J* = 10.9, 9.0, 4.9 Hz, 1H), 4.76 (dd, *J* = 17.7, 2.6 Hz, 1H), 4.83 (dd, *J* = 17.7, 2.5 Hz, 1H), 5.22 (ddd, *J* = 10.0, 6.8, 4.4 Hz, 1H), 7.14 – 7.21 (m, 2H), 7.22 – 7.27 (m, 2H), 7.27 – 7.37 (m, 7H), 7.67 (d, *J* = 6.8 Hz, 1H), 7.84 (d, *J* = 7.9 Hz, 1H), 8.48 (d, *J* = 9.0 Hz, 1H), 8.85 (d, *J* = 10.0 Hz, 1H).

^{13}C NMR (126 MHz, $CDCl_3$) δ 16.8, 16.9, 17.9, 19.4, 19.7, 20.2, 23.0, 23.4, 25.5, 29.0, 29.8, 30.1, 30.9, 31.8, 32.6, 34.0, 35.8, 38.0, 39.2, 50.0, 50.9, 52.6, 55.7, 59.1, 61.8, 64.4, 67.0, 73.8, 78.0, 109.4, 110.4, 119.8, 120.3, 122.3, 126.1, 126.6, 128.4, 129.0, 129.7, 135.9, 137.9, 169.1, 169.3, 171.15, 171.20, 171.7, 172.7, 174.2.

HRMS (ESI) calcd for $C_{50}H_{71}N_8O_8^+$ $(M+H)^+$: 911.5389; found: 911.5349.

Synthesis of Glutamine-containing dCym derivatives (SI-74, SI-76)

Methyl *N*-(((2*S*,3*R*)-2-((*S*)-2-((2*S*,4*R*)-2-((*S*)-2-((*S*)-2-((((9*H*-fluoren-9-)carbonyl)amino)-5-yl)methoxy(dimethylamino)-5-oxopentanamido)-N-methyl-3-(1-methyl-1*H*-indol-3-yl)propanamido)-5-((tert-butyldimethylsilyl)oxy)-4-methylpentanamido)propanamido)-3-methoxy-3-phenylpropanoyl)-L-valyl)-*N*-methyl-L-leucinate (SI-73)

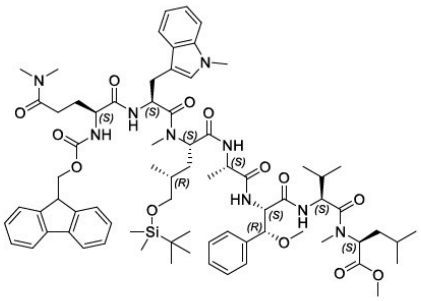

Prepared according to *GP2* and *GP4*: Methyl *N*-(((2S,3R)-2-((S)-2-((2S,4R)-2-((S)-2-(((allyloxy)carbonyl)amino)-N-methyl-3-(1-methyl-1H-indol-3-yl)propanamido)-5-((tert-butyldimethylsilyl)oxy)-4-methylpentanamido)propanamido)-3-methoxy-3-phenylpropanoyl)-L-valyl)-N-methyl-L-leucinate (150 mg, 143 µmol), $Pd(PPh_3)_4$ (4.96 mg, 4.30 µmol), DMBA (67.0 mg, 429 µmol); N^2-(((9*H*-fluoren-9-yl)methoxy)carbonyl)-N^5,N^5-dimethyl-L-glutamine (56.7 mg, 177 µmol), NMM (31.5 µl, 286 µmol), HOBt (23.8 mg, 0.160 µmol), EDC (30.2 mg, 160 µmol) (18 h). Flash chromatography (CyH/EtOAc 100:0 – 60:40) followed by lyophilization afforded **SI-73** (59.0 mg, 44.0 µmol, 31% yield) as a white amorphous solid. R_f = 0.44 (PE/EtOAc 2:3).

$[\alpha]_{20}^{D}$ = −50.8 (c 0.5, $CHCl_3$).

^{1}H NMR (500 MHz, $CDCl_3$) (*mixture of rotamers, ratio ~2:1*) δ -0.06 – 0.05 (m, 8.8H), 0.09 (s, 1.1H), 0.36 (s, 0.19H), 0.47 (d, *J* = 6.7 Hz, 1.2H), 0.82 – 0.86 (m, 3.7H), 0.86 – 0.88 (m, 8.2H), 0.88 – 1.01 (m, 18.6H), 1.14 – 1.21 (m, 2.7H), 1.23 – 1.41 (m, 2.2H), 1.43 – 1.55 (m, 3.3H), 1.63 – 1.86 (m, 2.9H), 1.88 – 2.20 (m, 3.0H), 2.22 – 2.45 (s, 4.0H), 2.71 (s, 1.22H), 2.77 – 2.83 (m, 2.2H), 2.89 – 3.09 (m, 14.4H), 3.11 – 3.29 (m, 3.2H), 3.30 – 3.33 (m, 3.0H), 3.59 – 3.78 (m, 10.6H), 4.14 – 4.39 (m, 6.9H), 4.63 – 4.87 (m, 4.3H), 4.89 – 5.00 (m, 0.5H), 5.07 – 5.21 (m, 0.9H), 5.28 – 5.44 (m, 1.6H), 6.12 – 6.19 (m, 0.8H), 6.35 – 6.40 (m, 0.4H), 6.51 (d, *J* = 6.8 Hz, 0.7H), 6.77 (d, *J* = 7.5 Hz, 0.4H), 6.83 – 6.91 (m, 0.6H), 6.90 – 7.01 (m, 1.5H), 7.09 (t, *J* = 7.4 Hz, 1.2H), 7.13 – 7.16 (m, 0.9H), 7.16 – 7.24 (m, 2.3H), 7.27 – 7.32 (m, 6.1H), 7.35 – 7.43 (m, 5.2H), 7.54 – 7.68 (m, 4.7H), 7.75 (d, *J* = 7.6 Hz, 3.4H), 8.11 (d, *J* = 7.8 Hz, 0.6H), 8.23 (d, *J* = 6.4 Hz, 0.5H), 8.58 (d, *J* = 6.4 Hz, 0.4H).

^{13}C NMR (126 MHz, $CDCl_3$) (*mixture of rotamers*) δ -5.3, -5.2, -3.4, 17.4, 17.5, 17.6, 18.1, 19.6, 21.5, 23.4, 24.90, 24.95, 25.8, 26.1, 28.2, 28.3, 28.6, 29.29, 29.32, 29.7, 29.8, 31.36, 31.39, 31.41, 31.45, 32.76, 32.79, 33.3, 33.4, 35.78, 35.82, 35.85, 37.0, 37.06, 37.09, 37.41, 37.45, 37.50, 37.52, 47.21, 47.25, 50.2, 50.5, 50.6, 52.2, 54.2, 54.26, 54.30, 54.4, 54.6, 54.7, 57.66, 57.68, 57.8, 67.0, 67.1, 67.3, 68.5, 75.0, 81.48, 81.52, 81.7, 108.5, 108.7, 109.3, 109.4, 109.5, 109.6, 118.6, 118.7, 118.9, 119.3, 119.4, 119.5, 120.1, 121.88, 121.92, 122.1, 125.3, 125.4, 127.0, 127.16, 127.19, 127.21, 127.79, 127.82, 127.85, 128.1, 128.31, 128.35, 128.49, 128.52, 136.9, 137.0, 141.37, 141.39, 143.8, 144.1, 156.3, 156.4, 168.60, 168.62, 168.7, 171.6, 171.7, 171.9, 172.1, 172.19, 172.21.

Selected diagnostic peaks:

Major rotamer: **^{1}H NMR** (500 MHz, $CDCl_3$) δ 0.01 (s, 3H), 0.02 (s, 3H), 0.87 (s, 9H), 3.32 (s, 3H), 3.68 (s, 3H), 5.30 – 5.40 (m, 1H), 6.51 (d, *J* = 6.8 Hz, 1H), 6.96 (s, 1H). **^{13}C NMR** (126 MHz, $CDCl_3$) δ 24.95, 47.21, 156.3.

Minor rotamer: **^{1}H NMR** (500 MHz, $CDCl_3$) δ-0.03 (s, 3H), -0.01 (s, 3H), 0.47 (d, *J* = 6.7 Hz, 3H), 0.84 (s, 9H), 2.71 (s, 3H), 2.82 (s, 3H), 3.22 (s, 3H), 6.38 (d, *J* = 7.0 Hz, 1H), 8.58 (d, *J* = 6.5 Hz, 1H). **^{13}C NMR** (126 MHz, $CDCl_3$) δ 24.90, 47.25, 156.4.

HRMS (ESI): calcd for $C_{73}H_{104}N_9O_{13}Si^+$ $(M+H)^+$: 1342.7517; found: 1342.7485.

3-((2*S*,5*S*,8*S*,11*S*,14*S*,17*S*,20*S*)-8-((*R*)-3-Hydroxy-2-methylpropyl)-20-isobutyl-17-isopropyl-14-((*R*)-methoxy(phenyl)methyl)-7,11,19-trimethyl-5-((1-methyl-1*H*-indol-3-yl)methyl)-3,6,9,12,15,18,21-heptaoxo-1,4,7,10,13,16,19-heptaazacyclohenicosan-2-yl)-*N*,*N*-dimethylpropanamide (SI-74)

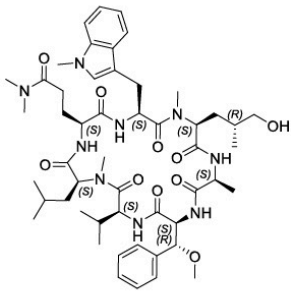

Prepared according to *GP6b*: **SI-73** (106 mg, 80.0 µmol), tris(2-aminoethyl)amine (118 µl, 550 µmol)); LiOH (95.0 µl, 95.0 µmol); HATU (105 mg, 270 µmol), DIPEA (54.0 µl, 310 µmol) (addition over 1.5 h, additional 16 h); NH_4F (58.5 mg, 1.60 mmol). RP flash chromatography (H_2O/MeCN 90:10 - 5:95) followed by lyophilizaiton afforded **SI-74** (18.8 mg, 19.0 µmol, 24%) as an off-white, amorphous solid.

$[\alpha]_{20}^{D}$ = −58.4 (c 0.4, $CHCl_3$).

^{1}H NMR (500 MHz, $CDCl_3$) δ -0.44 – -0.36 (m, 1H), 0.34 (d, *J* = 6.7 Hz, 3H), 0.94 – 0.96 (m, 8H), 1.06 (d, *J* = 6.6 Hz, 3H), 1.23 (d, *J* = 7.2 Hz, 3H), 1.45 – 1.57 (m, 1H), 1.83 – 1.93 (m, 1H), 1.96 – 2.07 (m, 1H), 2.14 – 2.25 (m, 6H), 2.57 (s, 3H), 2.87 (s, 3H), 2.95 (m, 3H), 2.97 – 3.07 (m, 6H), 3.02 – 3.17 (m, 3H), 3.19 – 3.32 (m, 2H), 3.33 (s, 3H), 3.71 (s, 3H), 4.43 – 4.64 (m, 3H), 4.70 – 4.76 (m, 1H), 4.77 – 4.89 (m, 2H), 4.92 – 4.98 (m, 1H), 5.01 (d, *J* = 5.3 Hz, 1H), 6.85 (s, 1H), 7.05 – 7.12 (m, 1H), 7.12 – 7.18 (m, 2H), 7.20 (m, 4H), 7.34 – 7.39 (m, 1H), 7.43 – 7.53 (m, 1H), 7.77 (d, *J* = 5.3 Hz, 1H), 8.02 (d, *J* = 8.5 Hz, 1H), 8.10 (d, *J* = 8.9 Hz, 1H), 8.20 (d, *J* = 10.2 Hz, 1H).

^{13}C NMR (126 MHz, $CDCl_3$) δ 17.3, 19.4, 20.0, 21.4, 22.6, 23.7, 25.2, 28.60, 28.62, 29.1, 29.4, 30.8, 31.7, 32.8, 33.2, 35.8, 37.5, 39.2, 50.8, 51.0, 51.9, 55.2, 56.1, 57.9, 58.8, 59.4, 66.2, 80.3, 108.2, 109.7, 118.8, 119.6, 122.3, 127.7, 127.9, 128.28, 128.33, 128.6, 128.8, 135.6, 136.9, 168.2, 169.7, 169.8, 170.8, 171.7, 171.9, 172.0, 172.2.

HRMS (ESI): calcd for $C_{51}H_{75}N_9O_{10}$ $(M+H)^+$: 974.5710; found: 974.5665.

Methyl *N*-(((2*S*,3*R*)-2-((*S*)-2-((2*S*,4*R*)-2-((*S*)-2-((*S*)-2-(((allyloxy)carbonyl)amino)-5-(dimethylamino)-*N*-methyl-5-oxopentanamido)-*N*-methyl-3-(1-methyl-1*H*-indol-3-yl)propanamido)-5-((*tert*-butyldimethylsilyl)oxy)-4-methylpentanamido)propanamido)-3-methoxy-3-phenylpropanoyl)-L-valyl)-*N*-methyl-L-leucinate (SI-75)

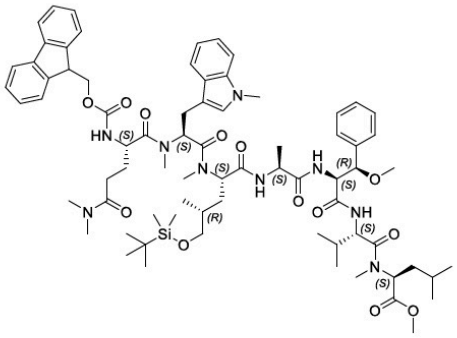

Hexapeptide **18** (98.7 mg, 92.9 µmol) was deprotected accoring to *GP2*: $Pd(PPh_3)_4$ (3.2 mg, 2.8 µmol), DMBA (43.5 mg, 279 µmol) (1 h). The crude deprotected peptide was then dissolved in DMF (0.93 ml), N^2-(((9*H*-fluoren-9-yl)methoxy)carbonyl)-N^5,N^5-dimethyl-L-glutamine (76.5 mg, 193 µmol) was added and the mixture was cooled to 0 °C. HATU (70.7 mg, 186 µmol), HOAt (12.7 mg, 93.3 µmol) and DIPEA (81.2 µl, 465 µmol) were added and the mixture was slowly warmed to rt over the course of 20 h. The mixture was then diluted with EtOAc, washed with 1 M $KHSO_4$, 1 M LiCl (2x), sat. $NaHCO_3$ and sat. NaCl solutions. The organic phase was

dried (Na_2SO_4) and evaporated *in vacuo*. RP flash chromatography (H_2O/MeCN 90:10– 0:100) followed by lyophilization afforded **SI-75** (43.5 mg, 32.1 µmol, 35%) as a white amorphous solid.

$[\alpha]_{20}^{D}$ = –70.6 (c 0.5, $CHCl_3$).

^{1}H NMR (500 MHz, $CDCl_3$) *(mixture of rotamers, ratio ~2:1)* δ -0.17 – -0.08 (m, 0.3H), 0.01 (s, 1.1H), 0.03 (s, 1.1H), 0.06 – 0.14 (m, 3.8H), 0.45 (d, *J* = 6.7 Hz, 0.8H), 0.89 (s, 3.2H), 0.91 – 1.04 (m, 19.2H), 1.05 (d, *J* = 6.8 Hz, 2.2H), 1.27 – 1.43 (m, 2.1H), 1.43 – 1.61 (m, 2.4H), 1.68 – 1.87 (m, 2.7H), 1.92 – 2.10 (m, 2.4H), 2.10 – 2.27 (m, 1.8H), 2.30 – 2.44 (m, 1.0H), 2.51 – 2.63 (m, 0.8H), 2.76 – 2.85 (m, 2.7H), 2.88 – 3.07 (m, 9.1H), 3.07 – 3.12 (m, 0.5H), 3.21 (s, 1.1H), 3.28 (s, 1.4H), 3.35 – 3.42 (m, 2.4H), 3.47 (dd, *J* = 9.7, 5.6 Hz, 0.6H), 3.50 – 3.62 (m, 2.3H), 3.64 – 3.69 (m, 1.7H), 3.70 – 3.79 (m, 4.1H), 4.18 – 4.26 (m, 0.6H), 4.26 – 4.31 (m, 0.5H), 4.32 – 4.48 (m, 2.2H), 4.73 (dd, *J* = 7.5, 3.6 Hz, 0.7H), 4.77 – 4.99 (m, 3.3H), 5.08 – 5.16 (m, 0.5H), 5.38 – 5.45 (m, 0.9H), 5.66 – 5.74 (m, 0.2H), 5.85 – 5.94 (m, 0.9H), 6.34 (d, *J* = 6.9 Hz, 0.5H), 6.45 (d, *J* = 9.1 Hz, 0.2H), 6.68 – 6.78 (m, 0.8H), 6.90 (s, 0.3H), 6.94 – 7.00 (m, 0.5H), 7.12 – 7.19 (m, 1.4H), 7.19 – 7.29 (m, 4.0H), 7.29 – 7.42 (m, 5.3H), 7.42 – 7.50 (m, 2.1H), 7.59 – 7.72 (m, 1.8H), 7.73 – 7.86 (m, 2.6H), 8.12 (d, *J* = 6.7 Hz, 0.2H).

^{13}C NMR (126 MHz, $CDCl_3$) *(mixture of rotamers)* δ -5.3, -5.2, 15.7, 17.2, 17.3, 17.6, 18.4, 18.5, 18.7, 19.7, 21.5, 23.4, 24.9, 25.1, 25.9, 26.0, 26.1, 27.8, 28.5, 28.7, 29.1, 30.7, 30.9, 31.1, 31.29, 31.34, 31.5, 32.0, 32.3, 32.6, 32.7, 35.7, 37.0, 37.2, 47.2, 49.0, 49.8, 51.1, 51.7, 52.3, 53.2, 54.0, 54.2, 54.6, 55.0, 57.3, 57.4, 57.7, 57.9, 67.1, 67.3, 68.1, 81.3, 109.0, 109.4, 118.8, 118.9, 119.2, 119.4, 120.1, 121.7, 122.1, 125.2, 125.3, 126.9, 127.16, 127.20, 127.9, 128.4, 128.5, 136.86, 136.91, 141.4, 143.78, 143.85, 144.1, 156.5, 156.8, 168.2, 168.5, 168.7, 170.3, 171.3, 171.5, 171.6, 171.7, 172.1, 172.2, 172.3, 173.6.

Selected diagnostic peaks:

Major rotamer: **^{1}H NMR** (500 MHz, $CDCl_3$) δ 0.09 (s, 3H), 0.11 (s, 3H), 0.94 (s, 9H), 2.98 (s, 3H), 3.00 (s, 3H), 3.05 (s, 3H), 3.39 (s, 3H), 3.75 (s, 3H), 5.42 (dd, *J* = 10.7, 5.3 Hz, 1H), 6.34 (d, *J* = 6.9 Hz, 1H), 6.73 (d, *J* = 7.7 Hz, 1H), 6.97 (s, 1H). **^{13}C NMR** (126 MHz, $CDCl_3$) δ 26.1, 136.91, 156.5.

Minor rotamer: **^{1}H NMR** (500 MHz, $CDCl_3$) δ 0.01 (s, 3H), 0.03 (s, 3H), 0.45 (d, *J* = 6.7 Hz, 3H), 0.89 (s, 9H), 3.02 (s, 3H), 3.21 (s, 3H), 3.28 (s, 3H), 3.67 (s, 3H), 6.45 (d, *J* = 9.1 Hz, 1H), 6.90 (s, 1H), 8.12 (d, *J* = 6.7 Hz, 1H). **^{13}C NMR** (126 MHz, $CDCl_3$) δ 26.0, 136.86, 156.8.

HRMS (ESI) calcd for $C_{74}H_{106}N_9O_{13}Si^+$ $(M+H)^+$: 1356.7674; found: 1356.7705.

3-((2*S*,5*S*,8*S*,11*S*,14*S*,17*S*,20*S*)-8-((*R*)-3-Hydroxy-2-methylpropyl)-20-isobutyl-17-isopropyl-14-((*R*)-methoxy(phenyl)methyl)-4,7,11,19-tetramethyl-5-((1-methyl-1*H*-indol-3-yl)methyl)-3,6,9,12,15,18,21-heptaoxo-1,4,7,10,13,16,19-heptaazacyclohenicosan-2-yl)-N,N-dimethylpropanamide (SI-76)

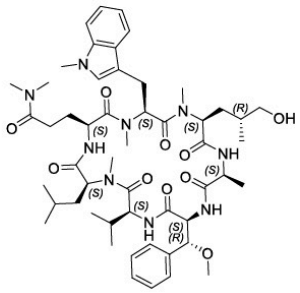

Prepared according to *GP6b*: **SI-75** (74.0 mg, 55.0 µmol), tris(2-aminoethyl)amine (82.0 µl, 550 µmol), LiOH (66.0 µl, 66.0 µmol); HATU (73.0 mg, 200 µmol), DIPEA (38.0 µl, 220 µmol) (addition over 1.5 h, additional 16 h); NH_4F (41.0 mg, 1.10 mmol). RP flash chromatography (H_2O/MeCN 90:10 - 5:95) followed by lyophilizaiton afforded **SI-76** (17.2 mg, 17.0 µmol, 32%) as an off-white, amorphous solid.

$[\alpha]_{20}^{D}$ = –82.6 (c 0.5, $CHCl_3$).

^{1}H NMR (500 MHz, $CDCl_3$) δ -0.25 – -0.11 (m, 1H), 0.38 (d, *J* = 6.7 Hz, 3H), 0.67 – 0.77 (m, 1H), 0.88 – 1.04 (m, 11H), 1.08 (d, *J* = 6.7 Hz, 3H), 1.20 (d, *J* = 7.2 Hz, 3H), 1.34 – 1.43 (m, 1H), 1.49 – 1.57 (m, 1H), 1.77 – 2.17 (m, 7H),

2.18 – 2.32 (m, 2H), 2.62 (s, 3H), 2.87 – 2.99 (m, 9H), 3.06 – 3.21 (m, 2H), 3.27 – 3.31 (m, 1H), 3.31 – 3.42 (m, 6H), 3.70 (s, 3H), 4.55 (t, *J* = 8.9 Hz, 1H), 4.66 (dd, *J* = 10.4, 3.1 Hz, 1H), 4.71 – 4.82 (m, 1H), 4.82 – 4.92 (m, 2H), 4.92 – 5.01 (m, 1H), 5.16 (d, *J* = 5.4 Hz, 1H), 5.41 (dd, *J* = 9.0, 6.4 Hz, 1H), 6.79 (s, 1H), 6.99 – 7.14 (m, 1H), 7.17 – 7.24 (m, 4H), 7.25 (s, 1H), 7.26 – 7.27 (m, 1H), 7.45 (dd, *J* = 8.0, 1.0 Hz, 1H), 8.06 – 8.16 (m, 2H), 8.36 (d, *J* = 9.0 Hz, 1H).

^{13}C NMR (126 MHz, $CDCl_3$) δ 17.4, 19.5, 20.1, 20.6, 22.6, 23.6, 25.2, 26.5, 28.1, 28.9, 29.21, 29.24, 30.9, 31.7, 32.1, 32.8, 33.2, 35.8, 37.1, 39.3, 48.7, 51.0, 53.3, 55.3, 56.1, 58.0, 58.8, 59.3, 66.2, 79.9, 108.7, 109.7, 118.8, 119.6, 122.3, 127.2, 127.7, 128.2, 128.46, 128.53, 135.7, 137.0, 168.1, 169.6, 169.9, 170.8, 171.0, 171.7, 172.1, 173.9.

HRMS (ESI): calcd for $C_{52}H_{78}N_9O_{10}^+$ $(M+H)^+$: 988.5866; found: 988.5861.

101

Supplementary Fig. 7: SPR Sensorgrams

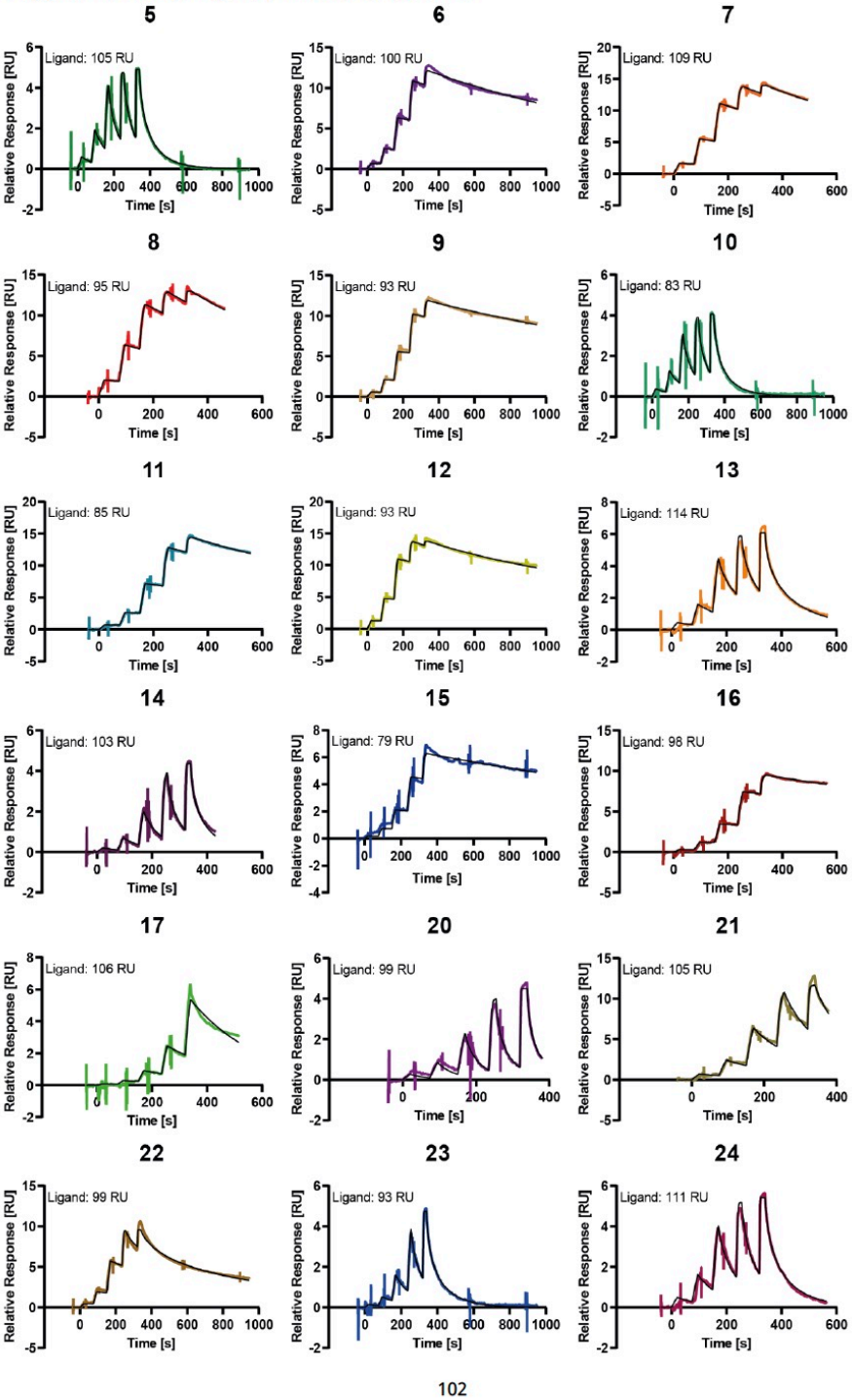

102

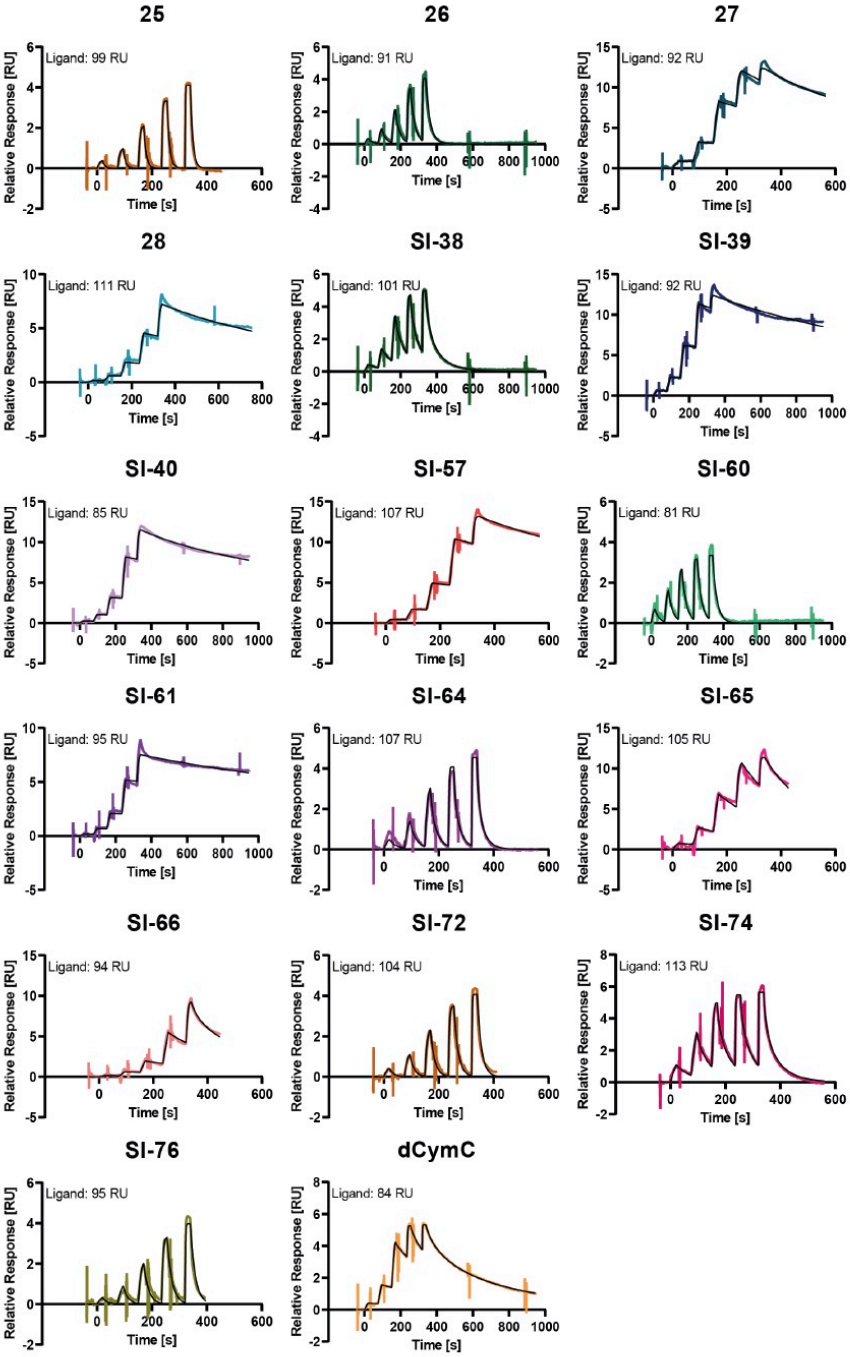

Supplementary Fig. 7. SPR sensorgrams of all compounds introduced in this paper. Each sensorgram is representative of at least two single-cycle measurements per compound. The exact number of independent measurements for each compound can be found in Supplementary Table 1. The biotinylated ligand ClpC1 NTD was captured via streptavidin, which was immobilized to a CM5 chip. The final ligand density used is indicated in each sensorgram. For the single-cycle measurements, five analyte concentrations were injected

103

consecutively for 20 s each: 2.5 nM, 7.4 nM, 22.2 nM, 66.7 nM, 200 nM. Coloured lines represent the measured raw data, while black lines represent fits calculated by the evaluation software.

Supplementary Fig. 8 – 209: Copies of NMR spectra

Supplementary Fig. 8. ^{1}H NMR spectrum of compound **3**

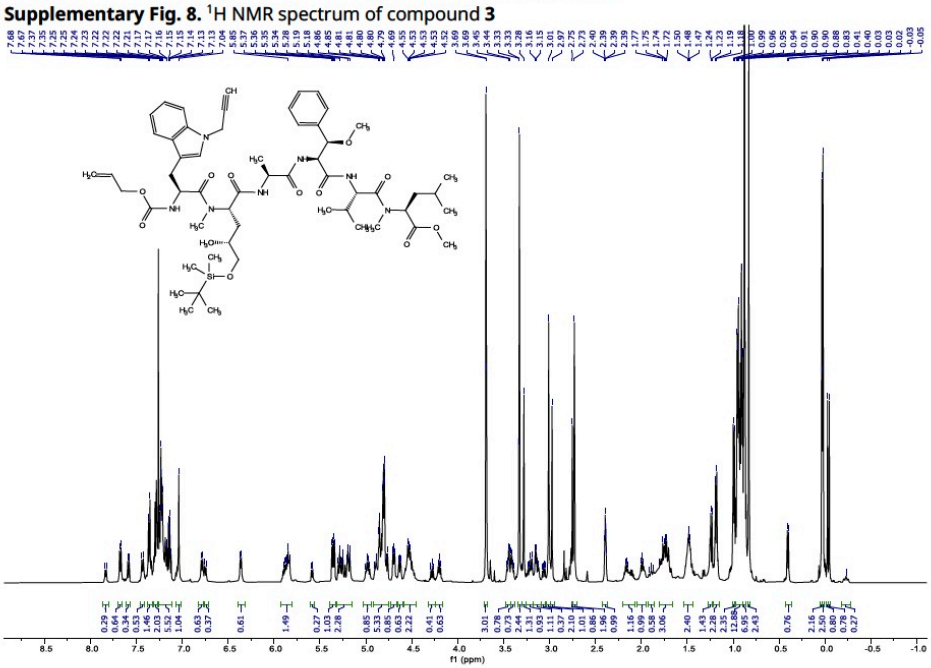

Supplementary Fig. 9. ^{13}C NMR spectrum of compound **3**

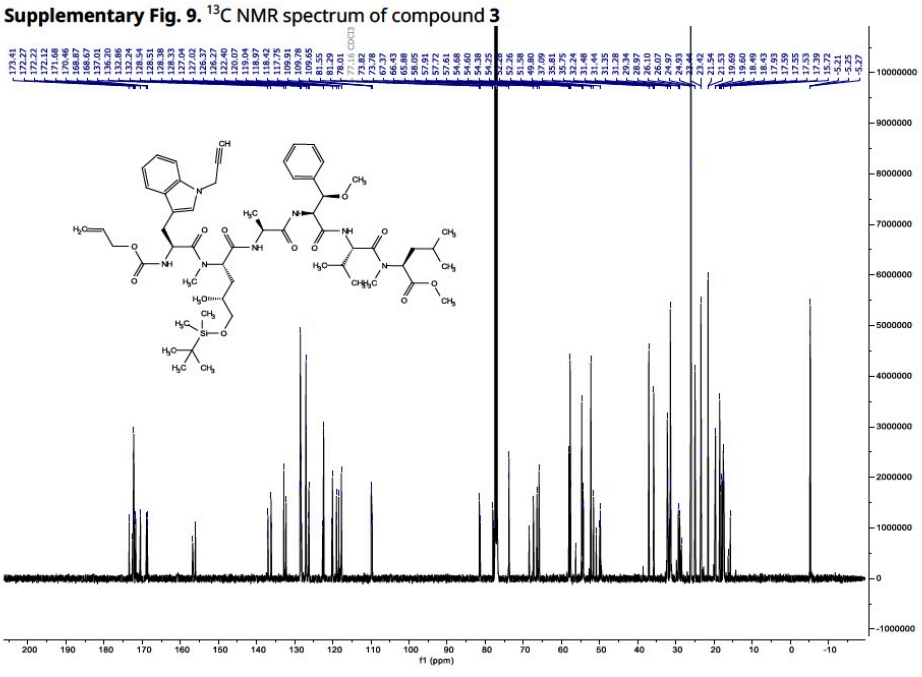

Supplementary Fig. 10. ^{1}H NMR spectrum of compound **4**

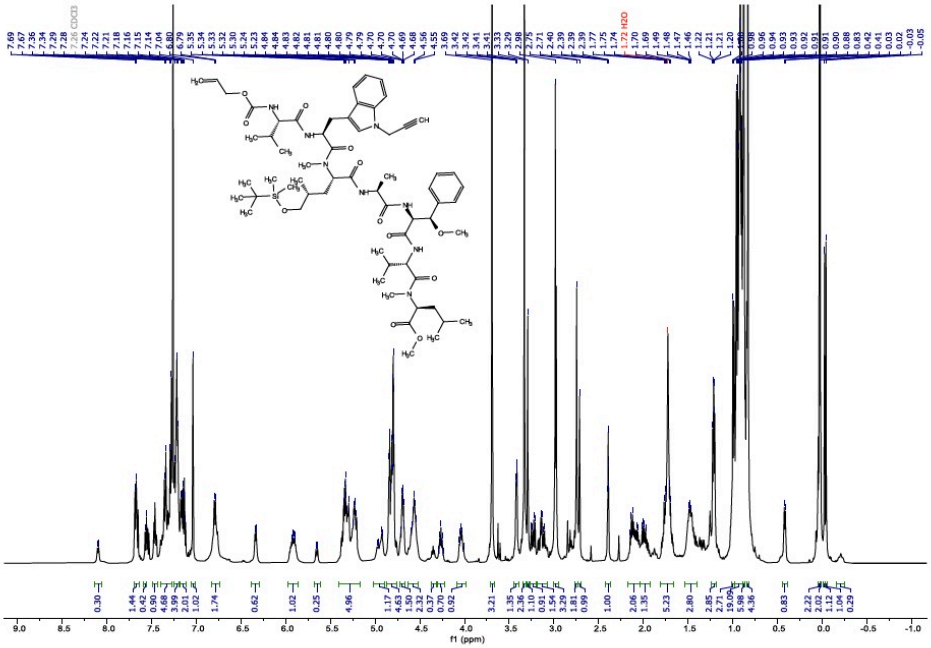

Supplementary Fig. 11. ^{13}C NMR spectrum of compound **4**

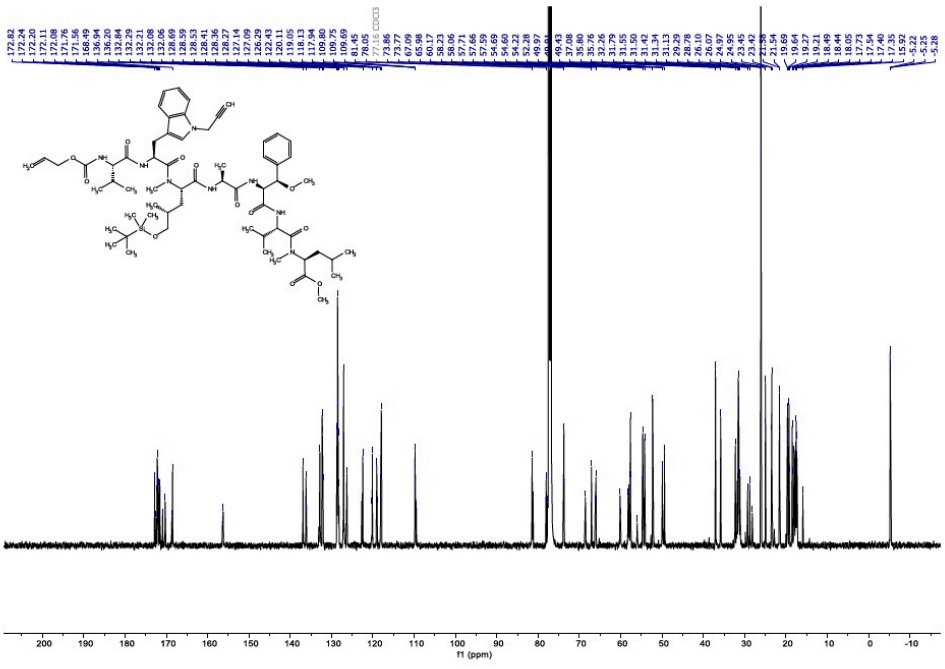

Supplementary Fig. 12. ^{1}H NMR spectrum of compound **5**

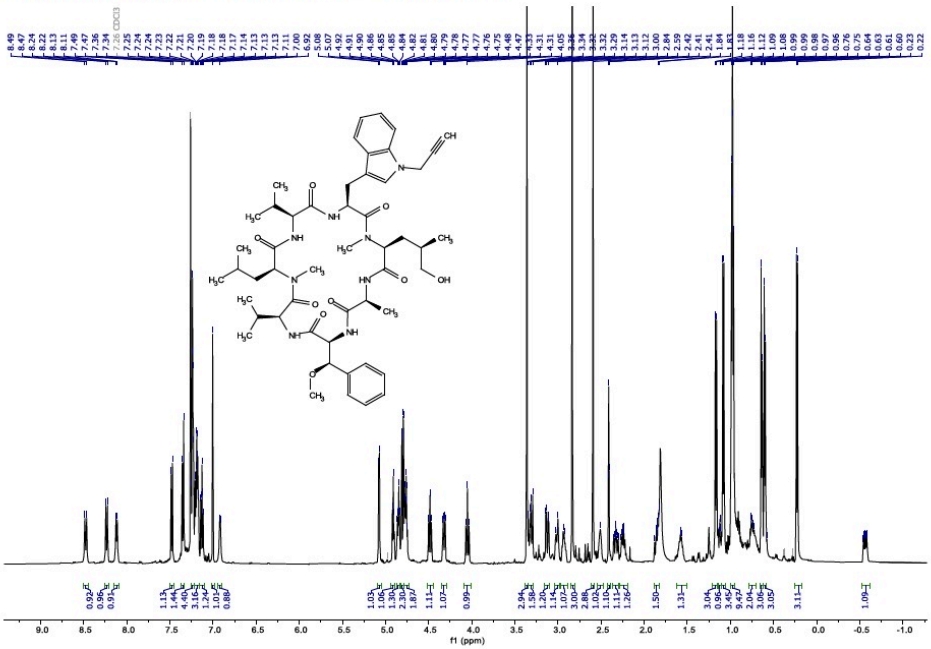

Supplementary Fig. 13. ^{13}C NMR spectrum of compound **5**

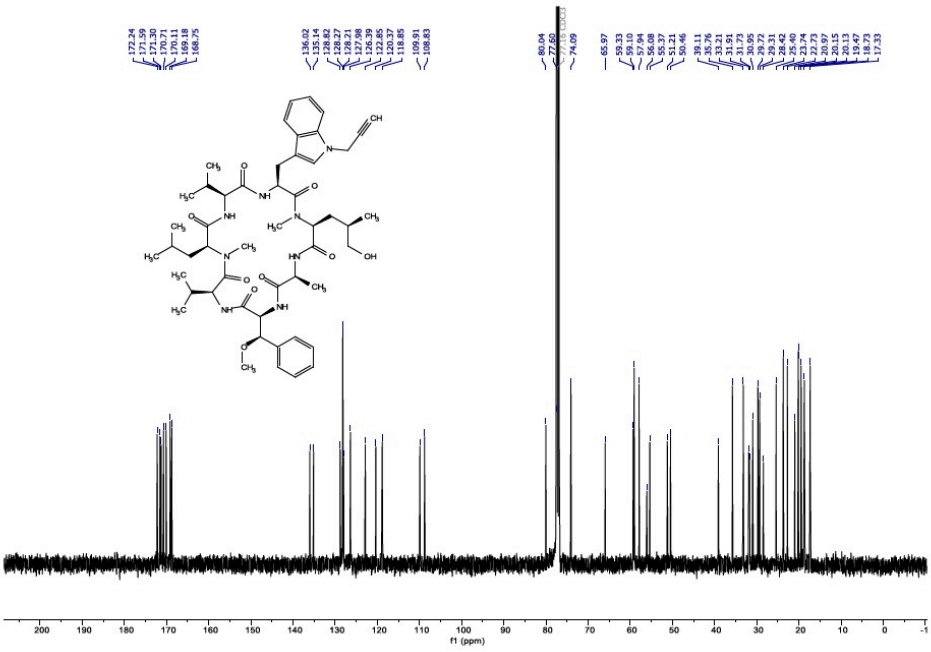

Supplementary Fig. 14. ^{1}H NMR spectrum of compound **6**

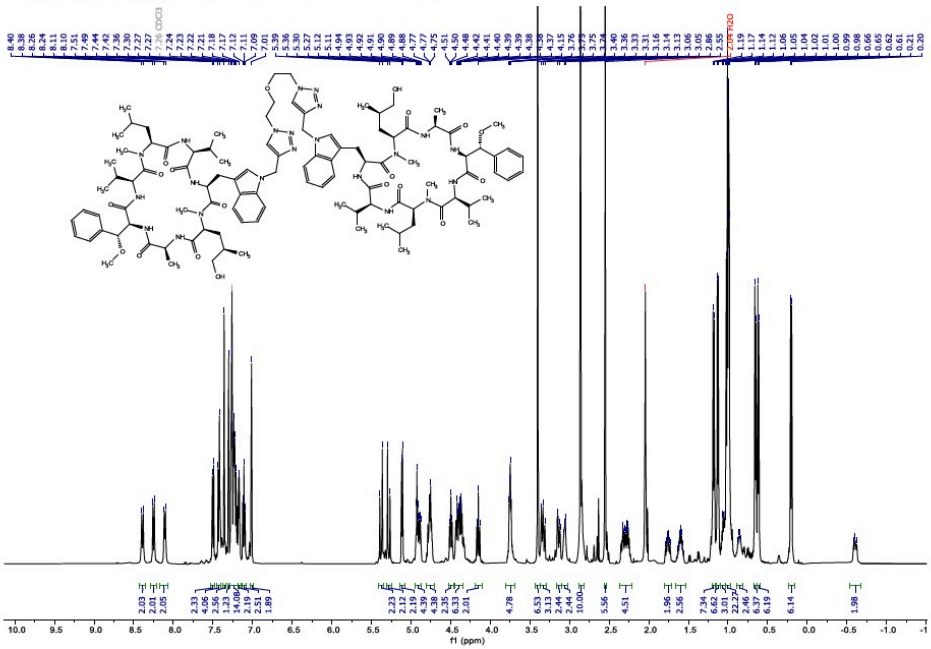

Supplementary Fig. 15. ^{13}C NMR spectrum of compound **6**

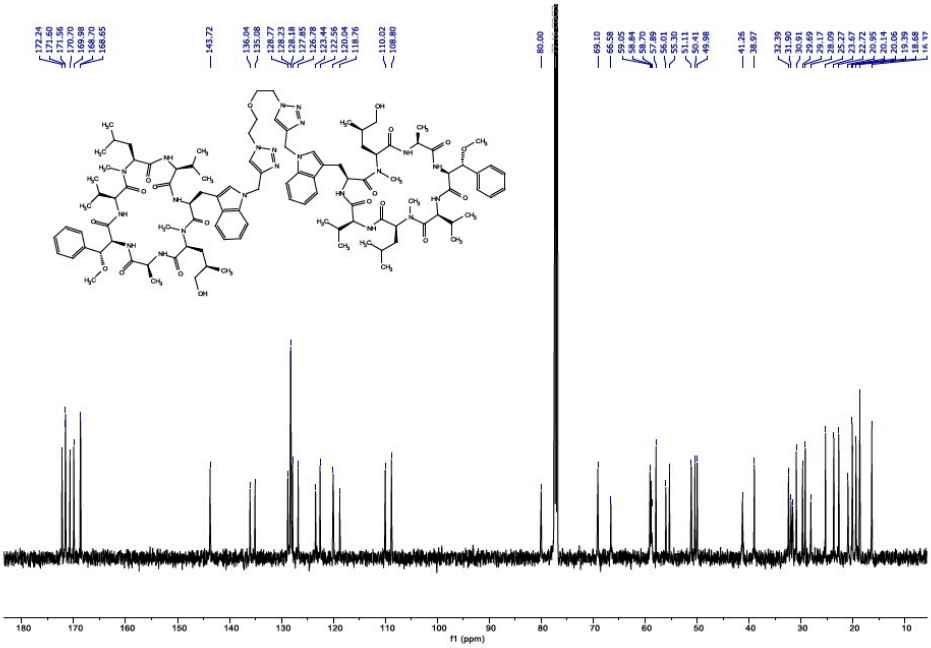

Supplementary Fig. 16. ^{1}H NMR spectrum of compound **7**

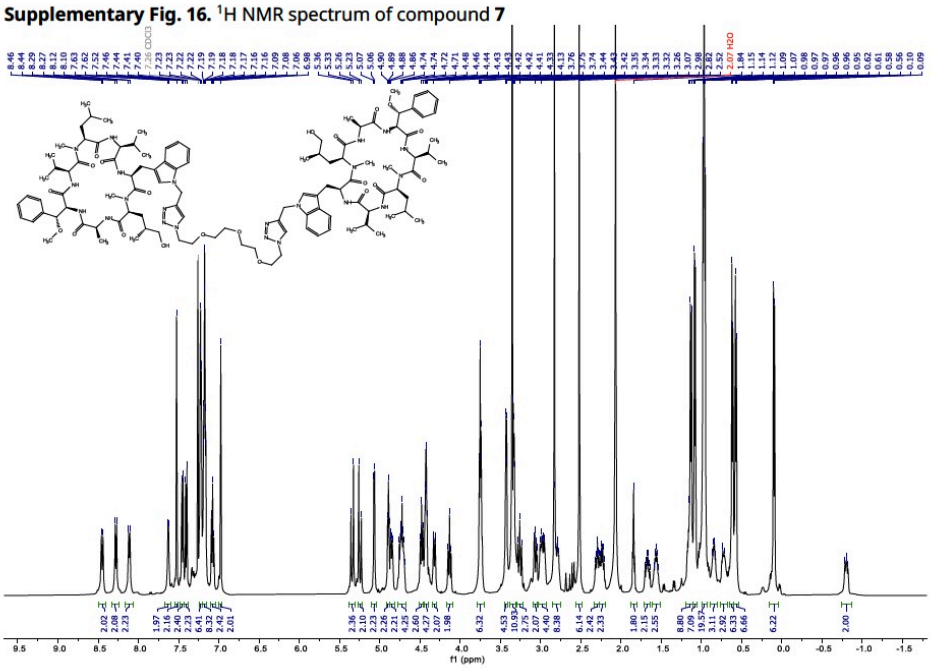

Supplementary Fig. 17. ^{13}C NMR spectrum of compound **7**

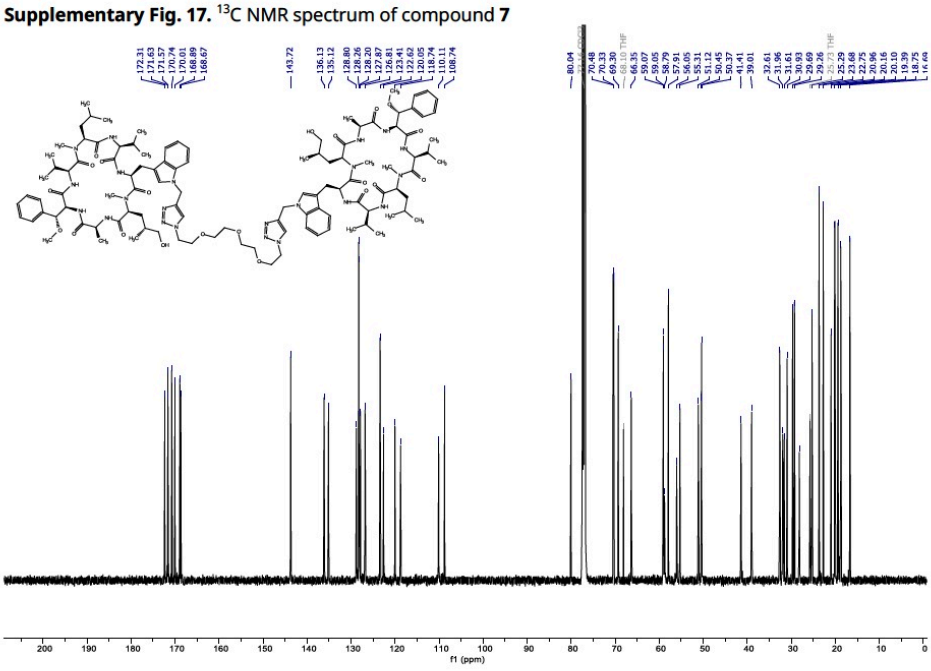

Supplementary Fig. 18. ^{1}H NMR spectrum of compound **8**

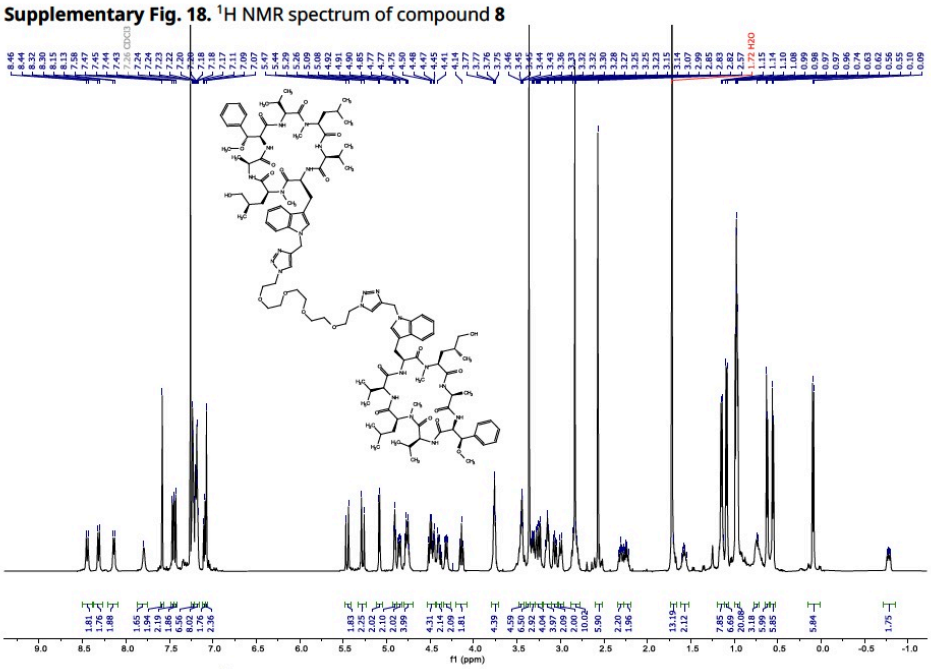

Supplementary Fig. 19. ^{13}C NMR spectrum of compound **8**

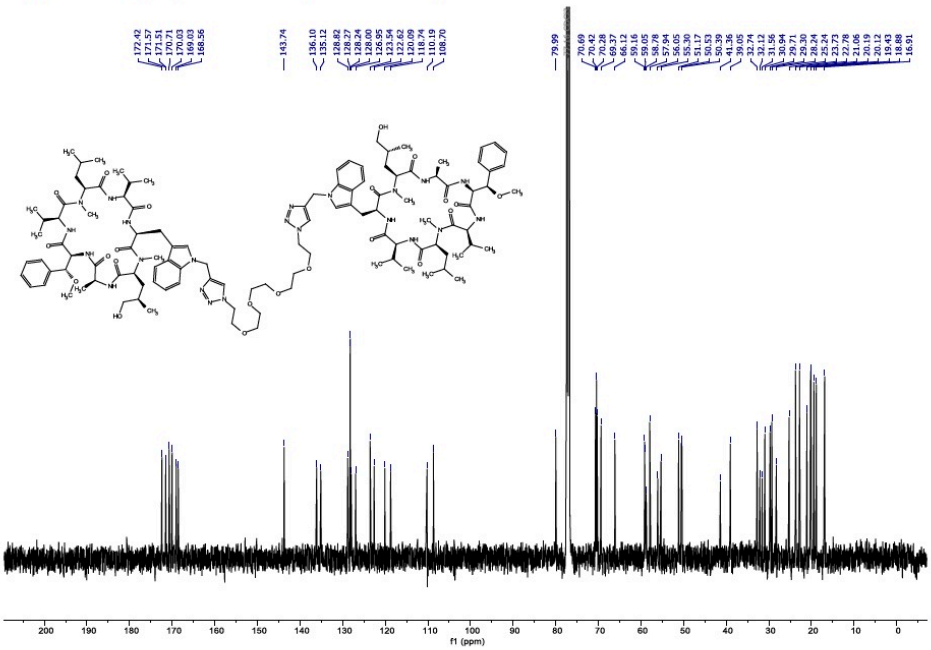

Supplementary Fig. 20. ^{1}H NMR spectrum of compound **9**

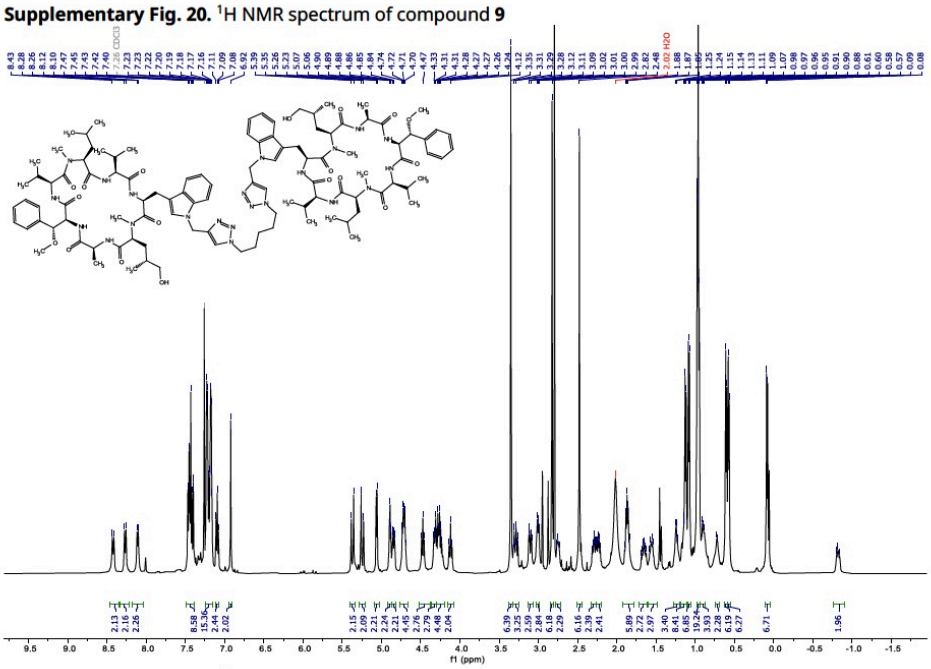

Supplementary Fig. 21. ^{13}C NMR spectrum of compound **9**

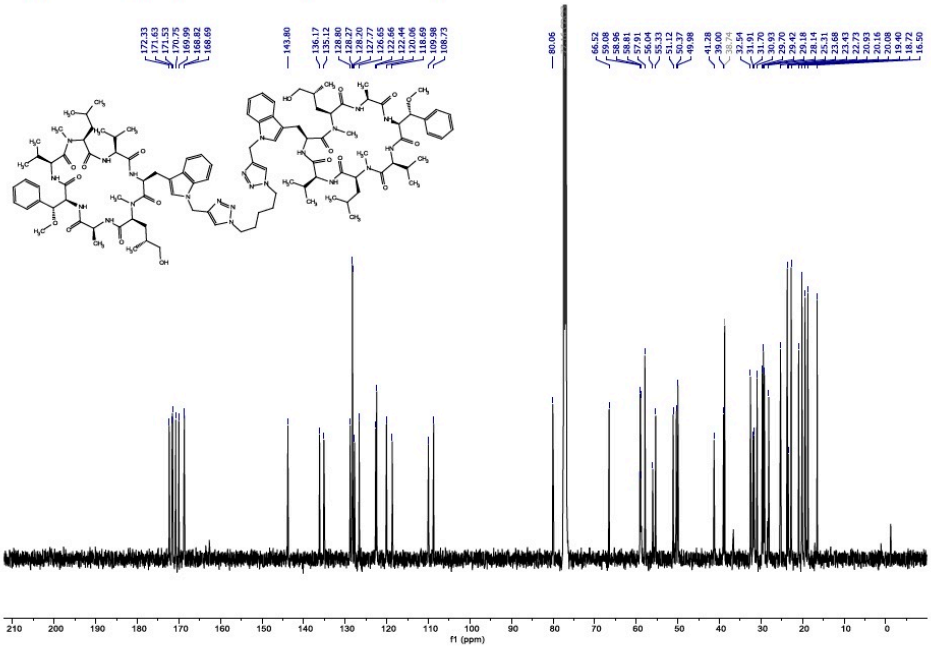

Supplementary Fig. 22. ^{1}H NMR spectrum of compound **SI-1**

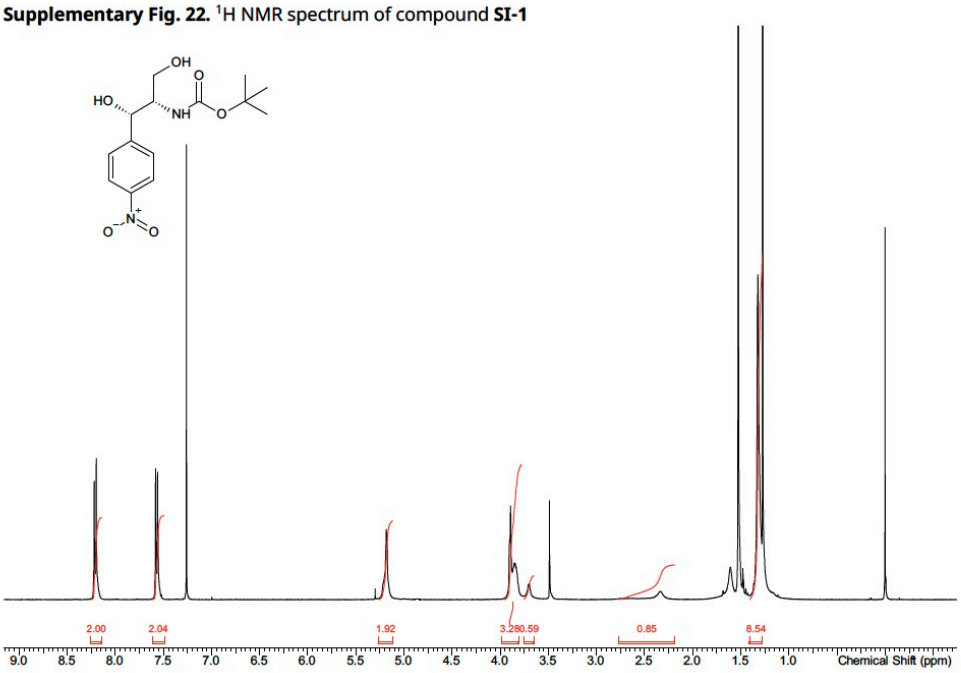

Supplementary Fig. 23. ^{1}H NMR spectrum of compound **SI-2**

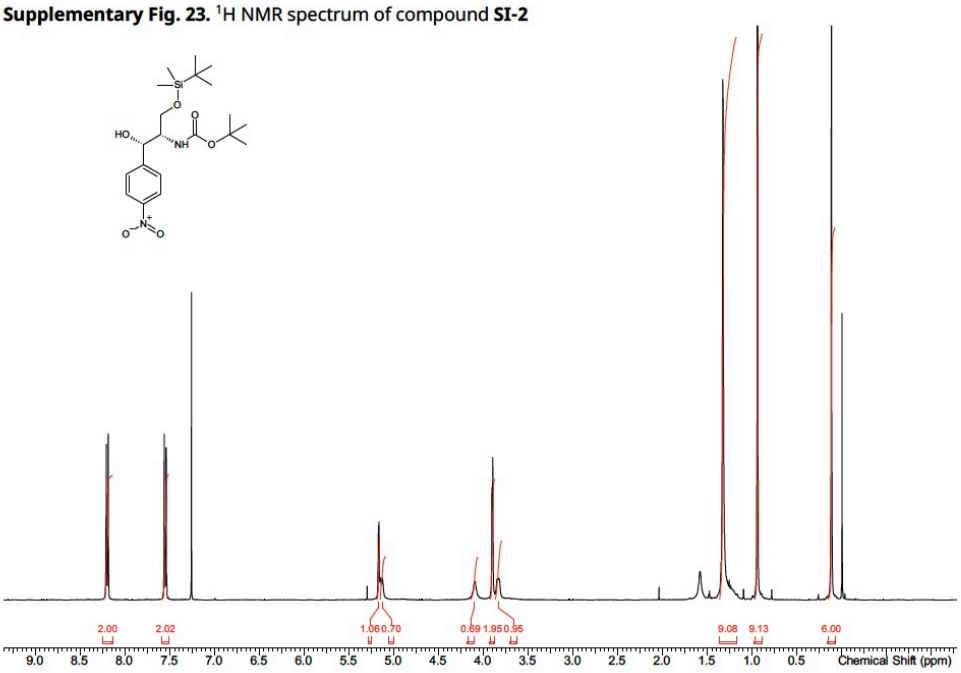

112

Supplementary Fig. 24. ^{1}H NMR spectrum of compound **SI-3**

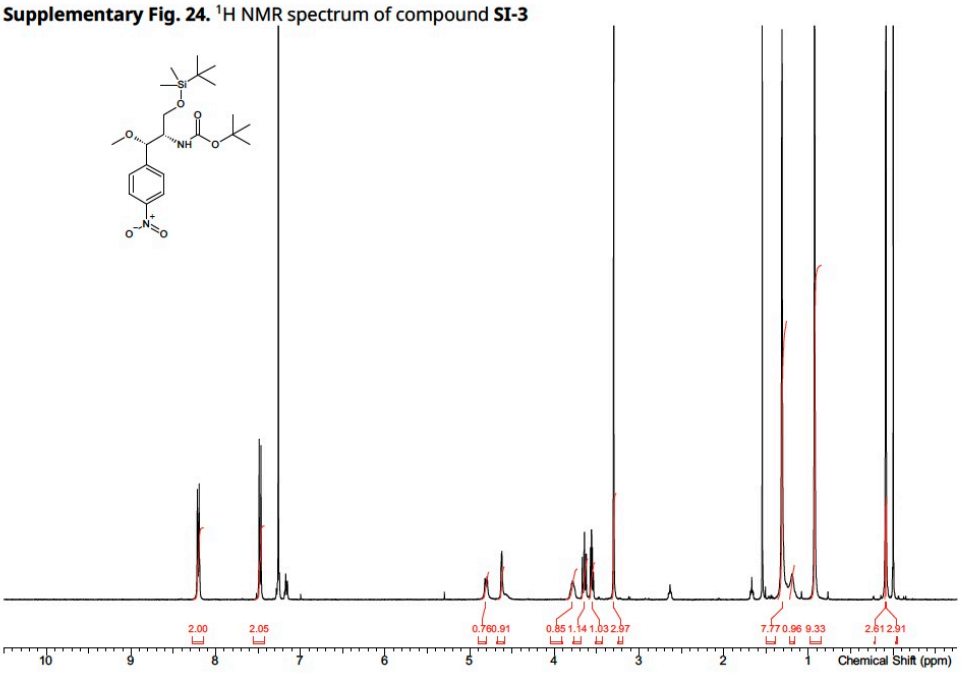

113

Supplementary Fig. 25. ^{1}H NMR spectrum of compound **SI-4**

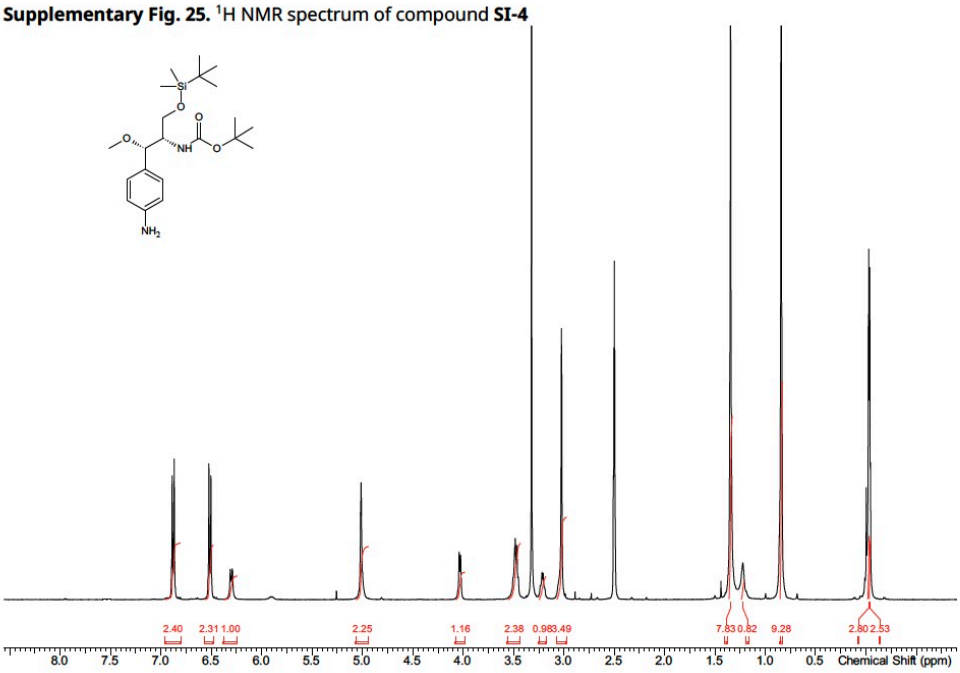

Supplementary Fig. 26. ^{1}H NMR spectrum of compound **SI-5**

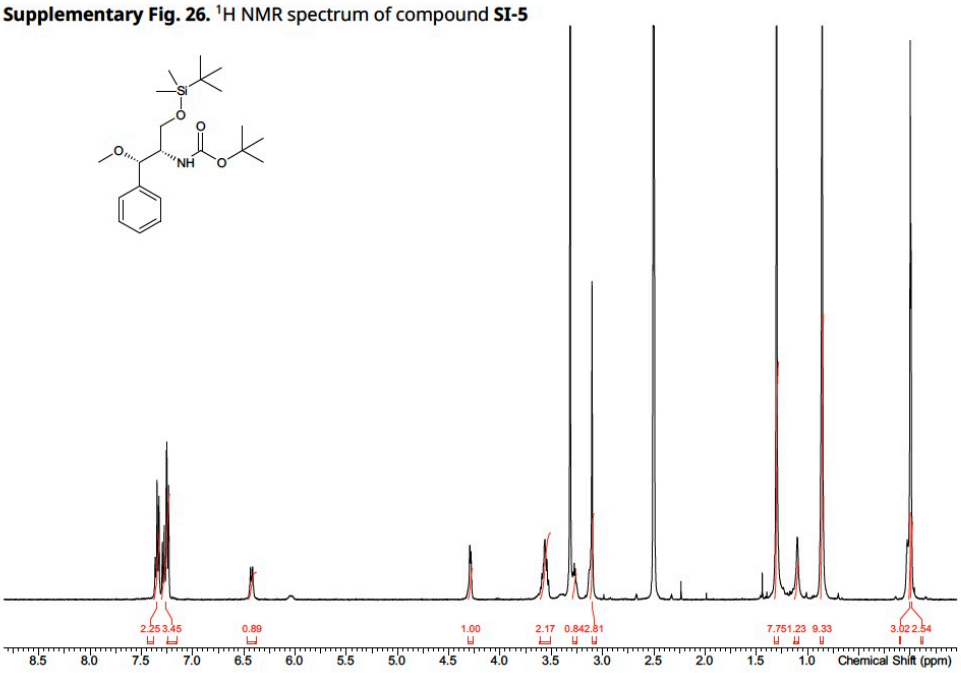

115

Supplementary Fig. 27. ^{1}H NMR spectrum of compound **SI-6**

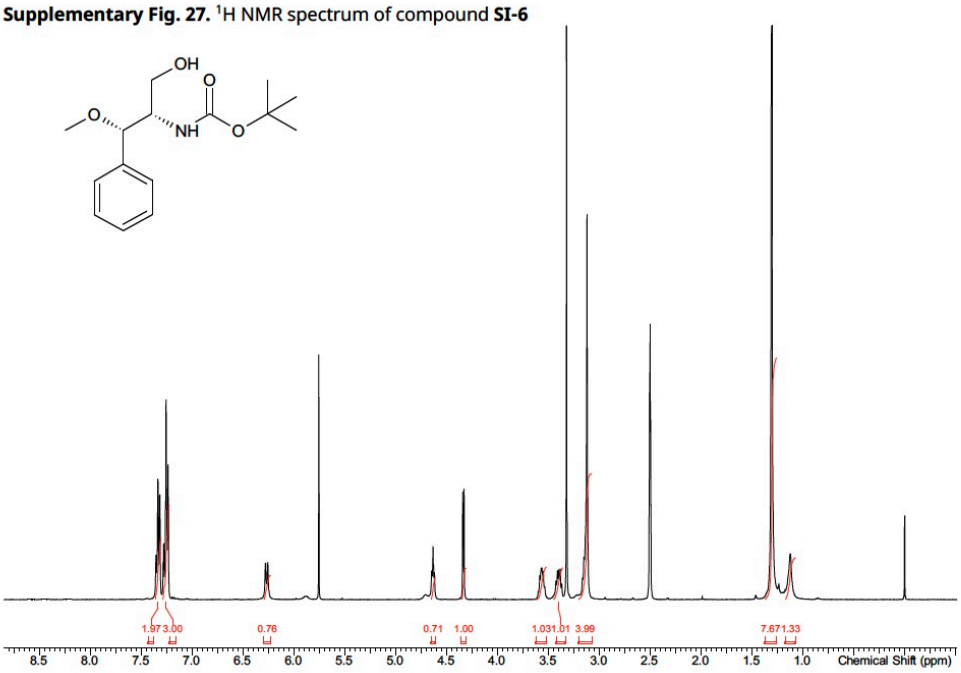

116

Supplementary Fig. 28. ^{1}H NMR spectrum of compound **SI-7**

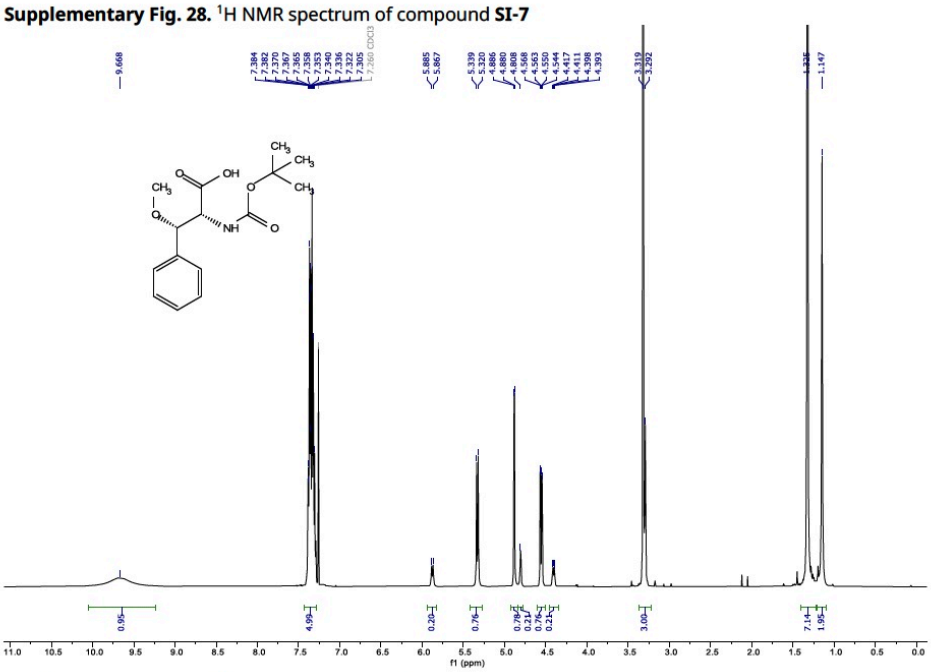

Supplementary Fig. 29. ^{13}C NMR spectrum of compound **SI-7**

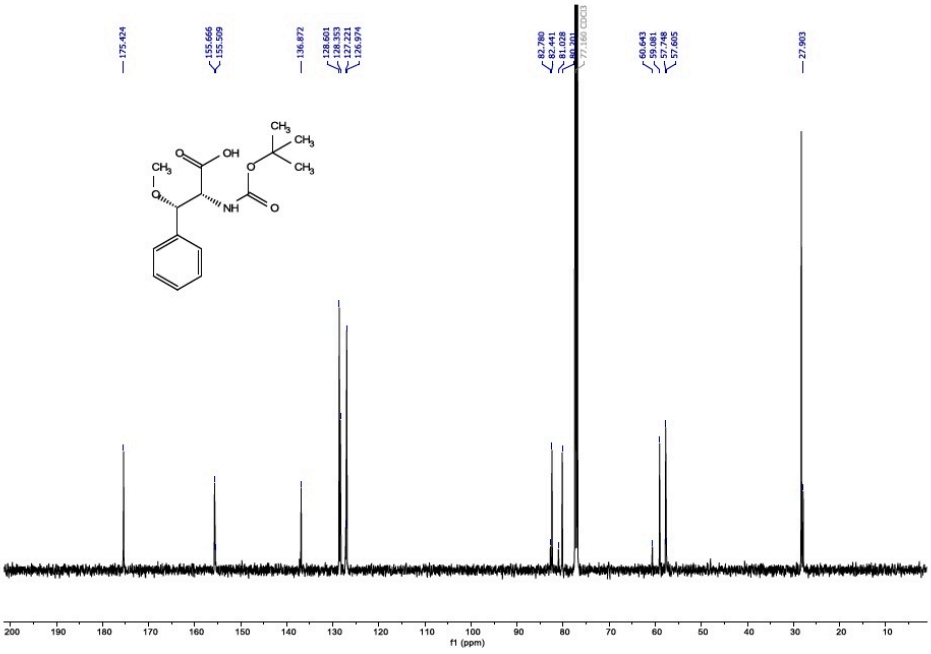

Supplementary Fig. 30. ^{1}H NMR spectrum of compound **SI-8**

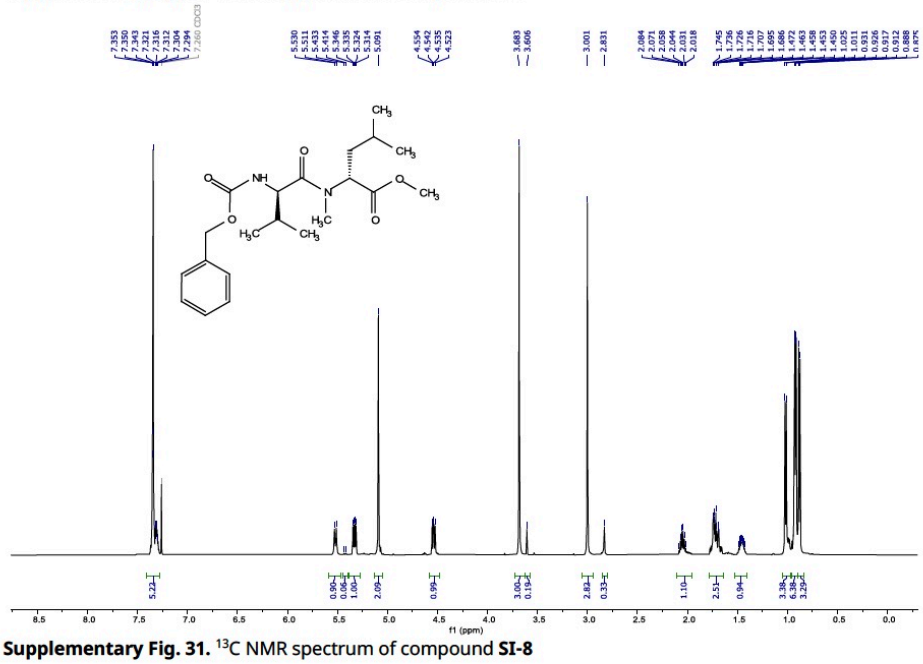

Supplementary Fig. 31. ^{13}C NMR spectrum of compound **SI-8**

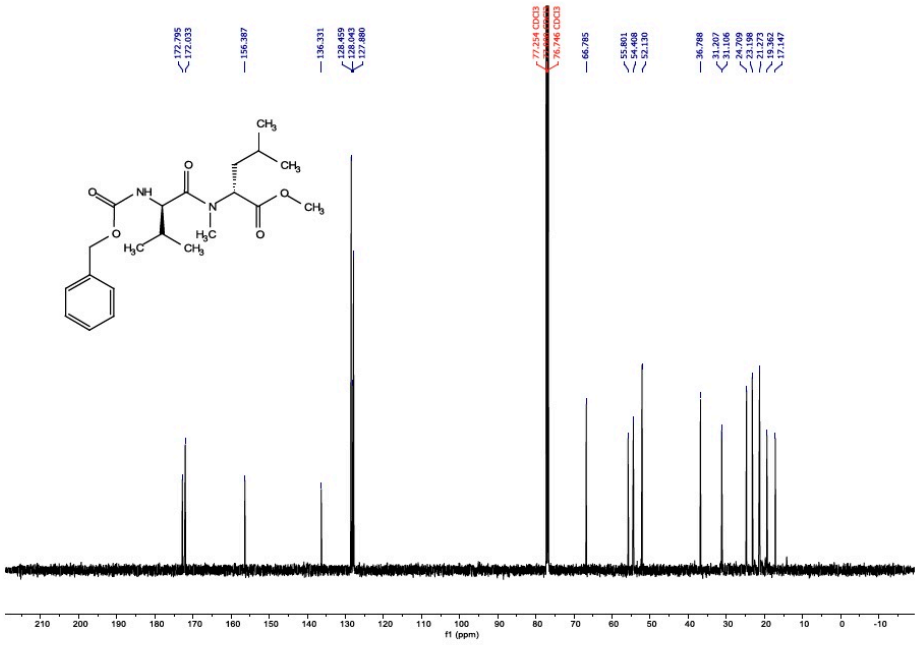

Supplementary Fig. 32. ^{1}H NMR spectrum of compound **SI-9**

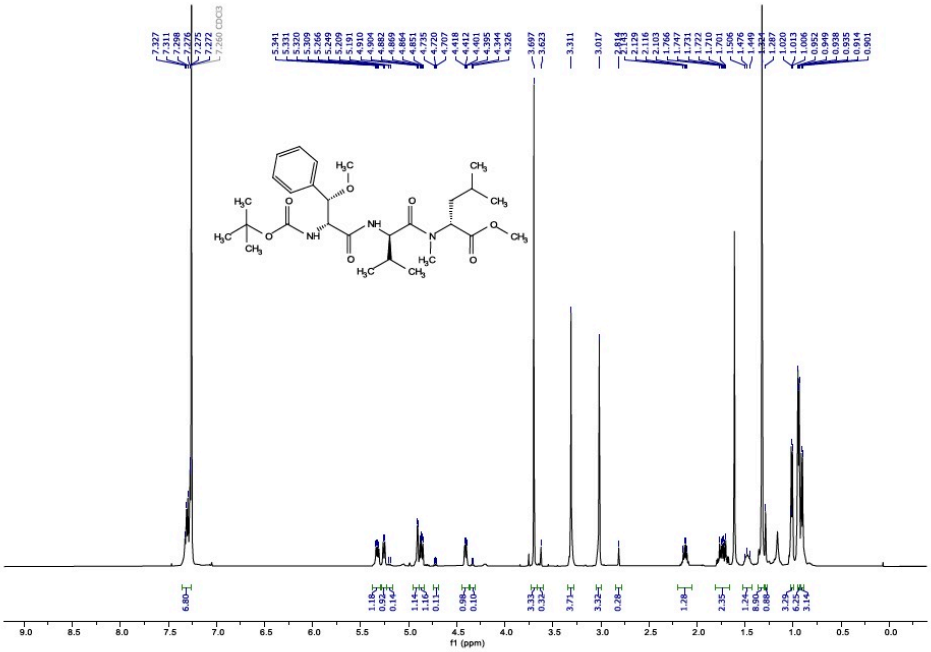

Supplementary Fig. 33. ^{13}C NMR spectrum of compound **SI-9**

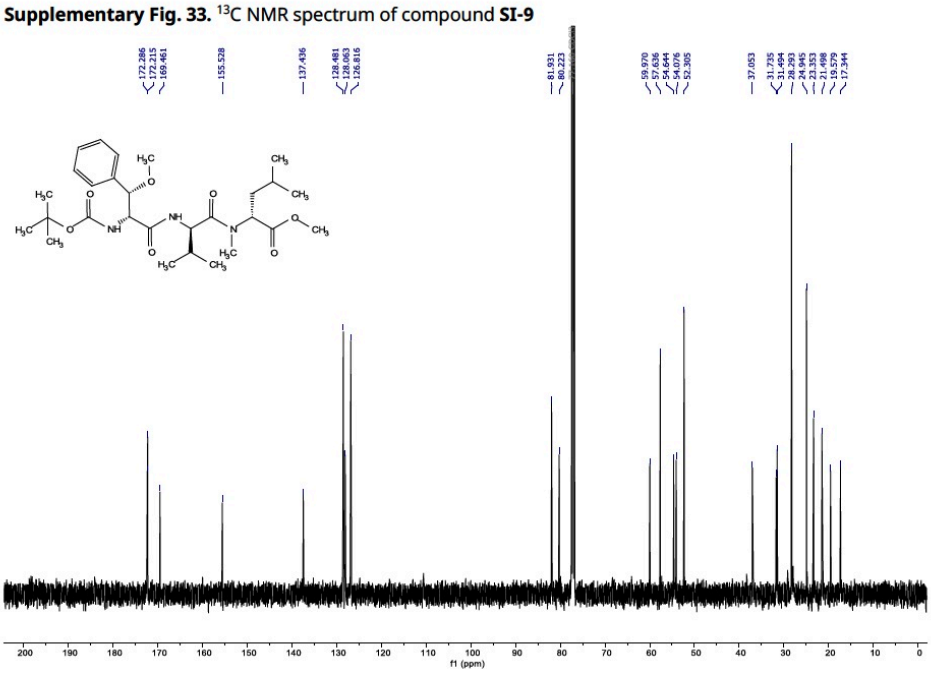

Supplementary Fig. 34. ^{1}H NMR spectrum of compound **SI-10**

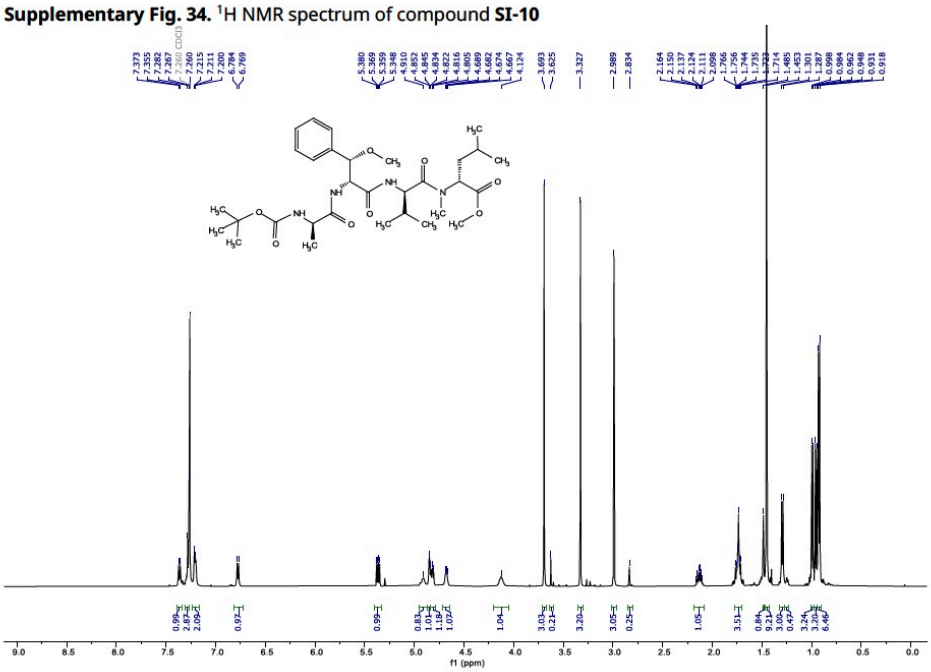

Supplementary Fig. 35. ^{13}C NMR spectrum of compound **SI-10**

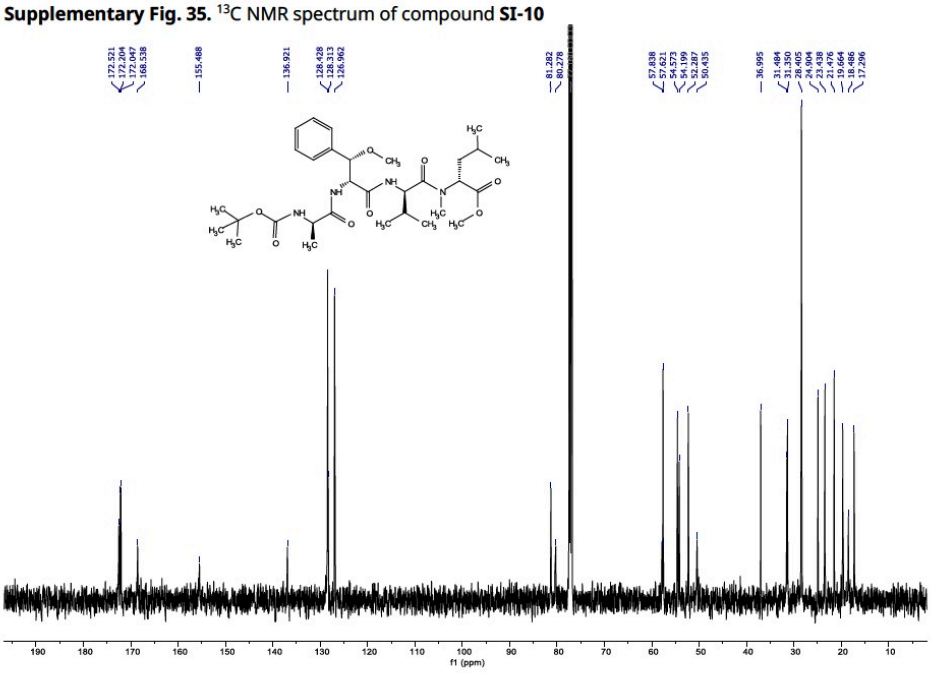

Supplementary Fig. 36. ^{1}H NMR spectrum of compound **SI-11**

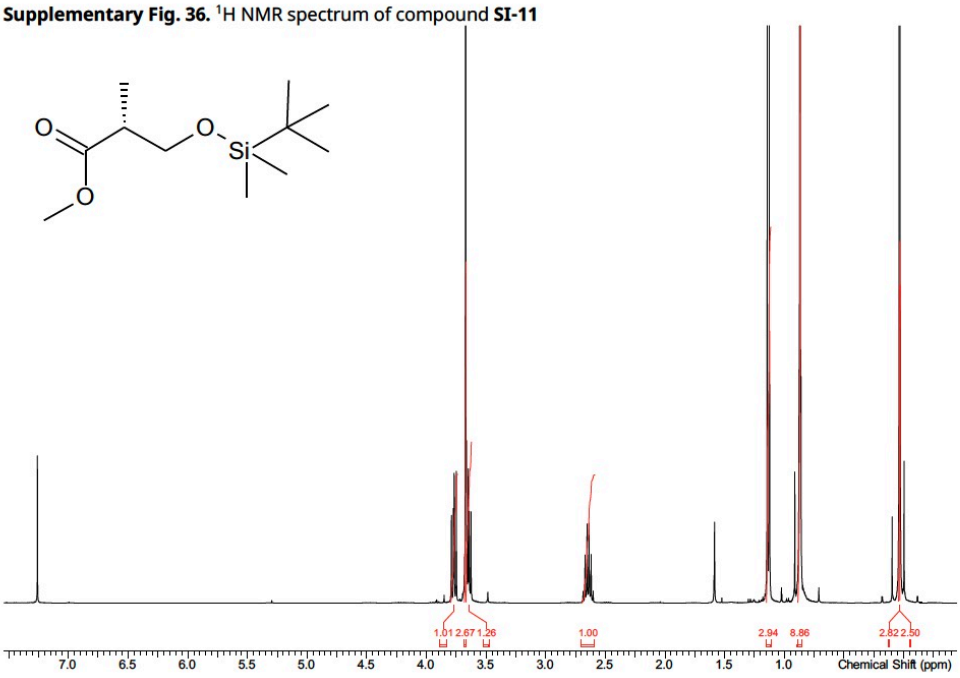

Supplementary Fig. 37. ^{1}H NMR spectrum of compound **SI-12**

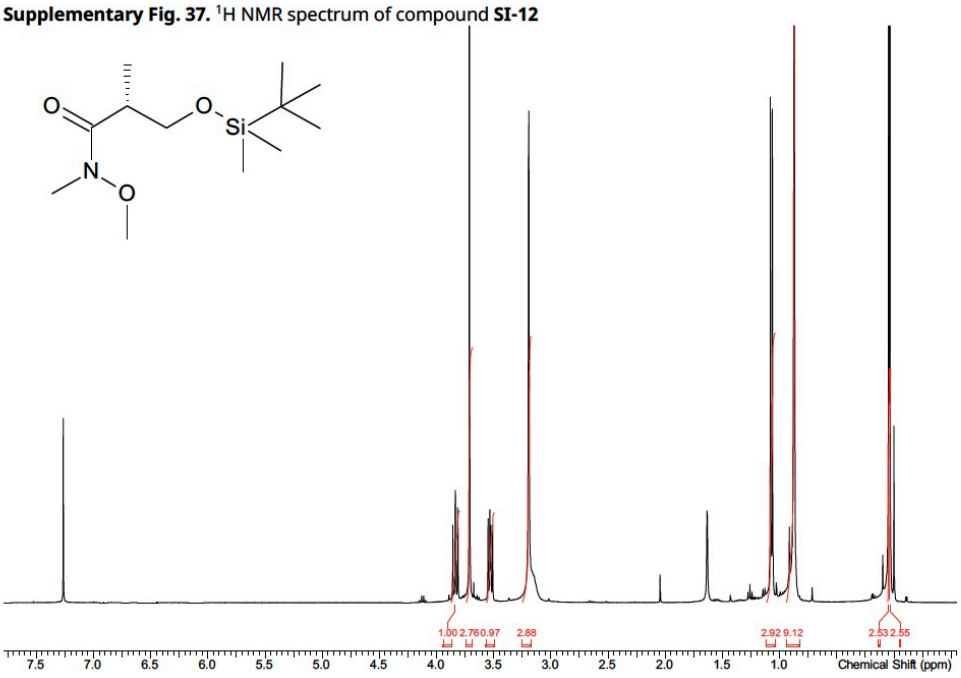

Supplementary Fig. 38. ^{1}H NMR spectrum of compound **SI-13**

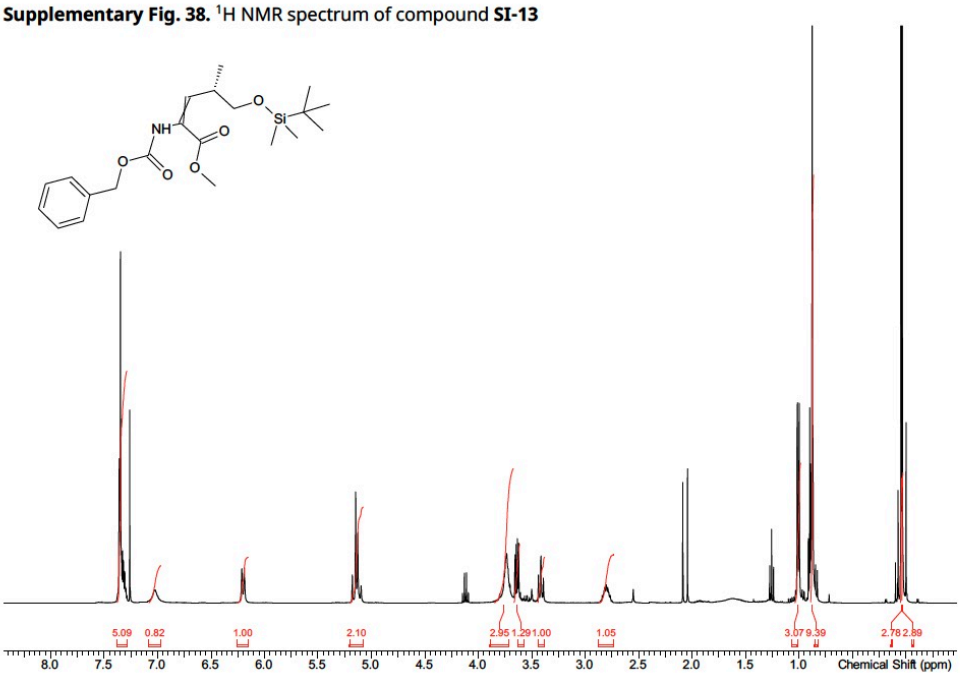

Supplementary Fig. 39. ^{1}H NMR spectrum of compound **SI-14**

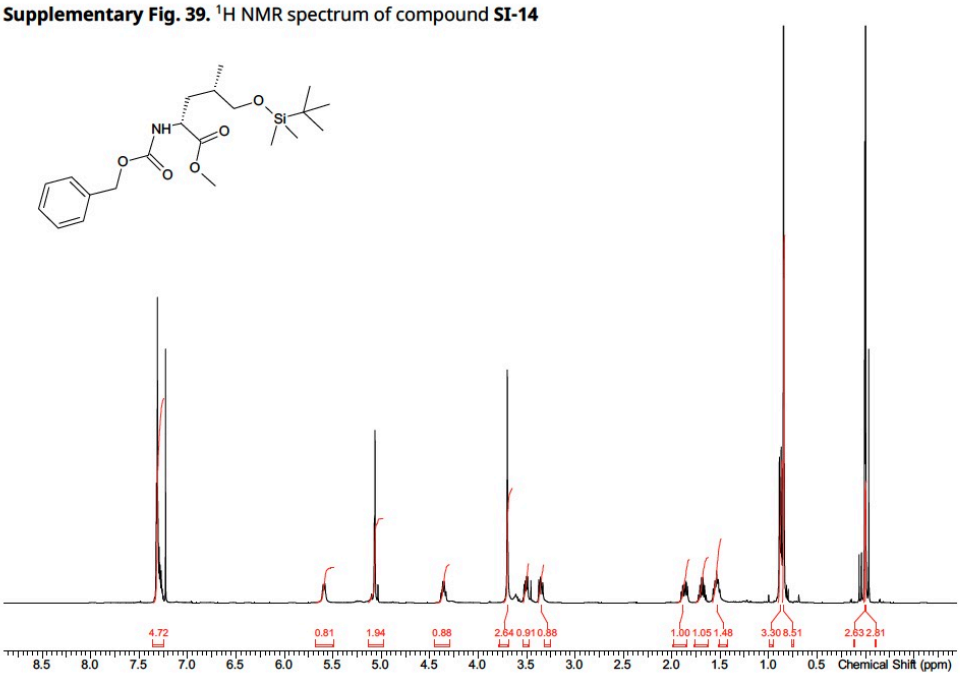

Supplementary Fig. 40. ^{1}H NMR spectrum of compound **SI-15**

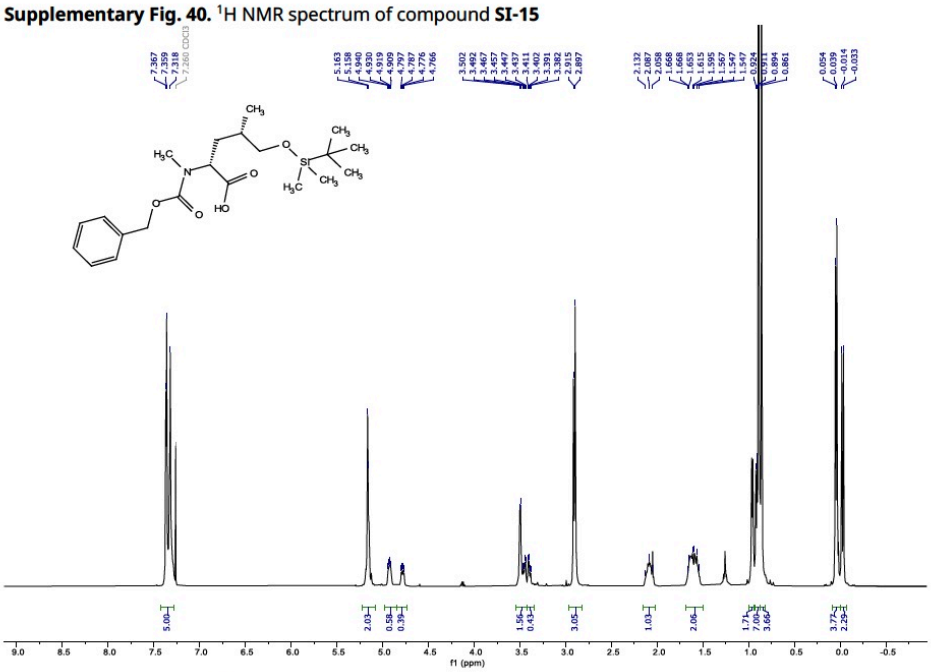

Supplementary Fig. 41. ^{13}C NMR spectrum of compound **SI-15**

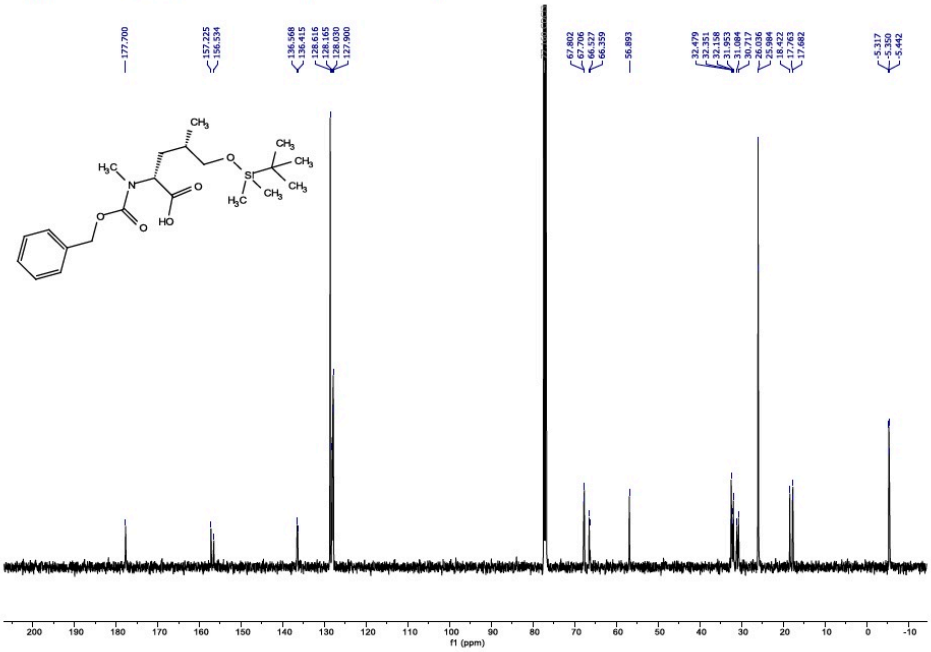

Supplementary Fig. 42. ^{1}H NMR spectrum of compound **2a**

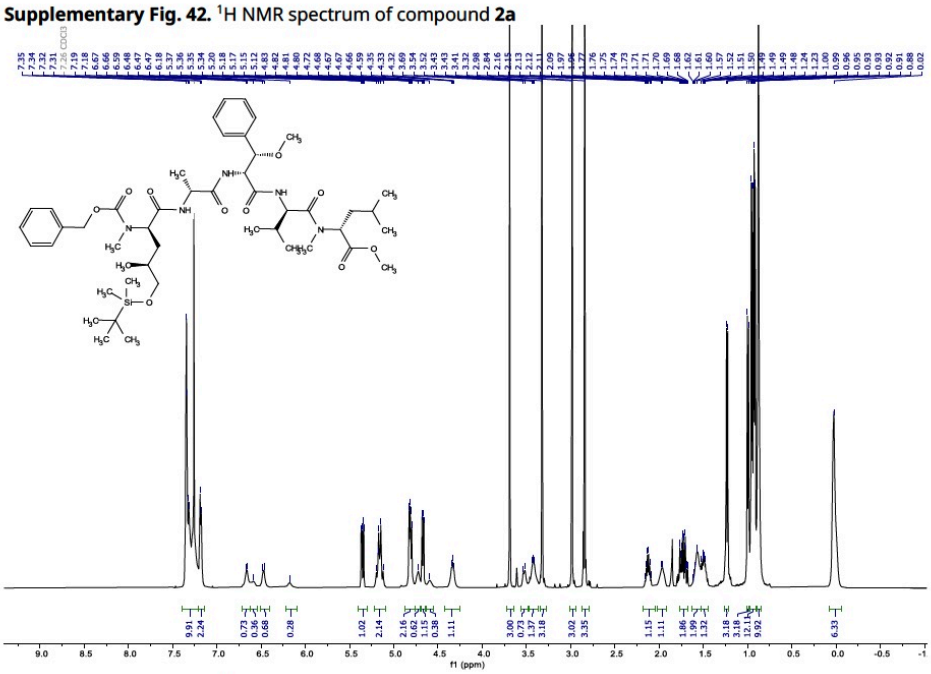

Supplementary Fig. 43. ^{13}C NMR spectrum of compound **2a**

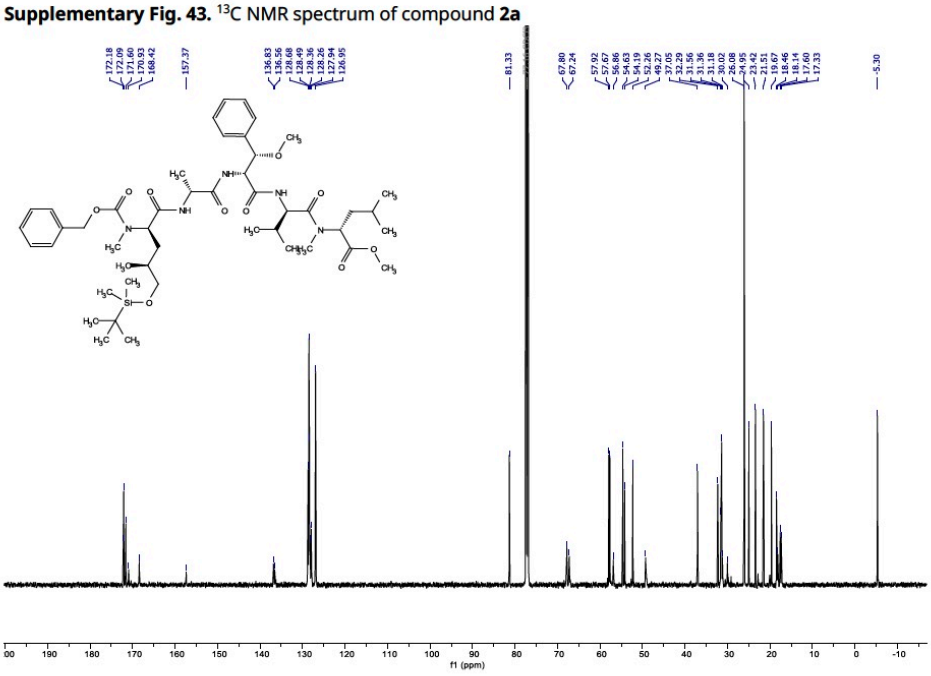

Supplementary Fig. 44. ^{1}H NMR spectrum of compound **SI-16**

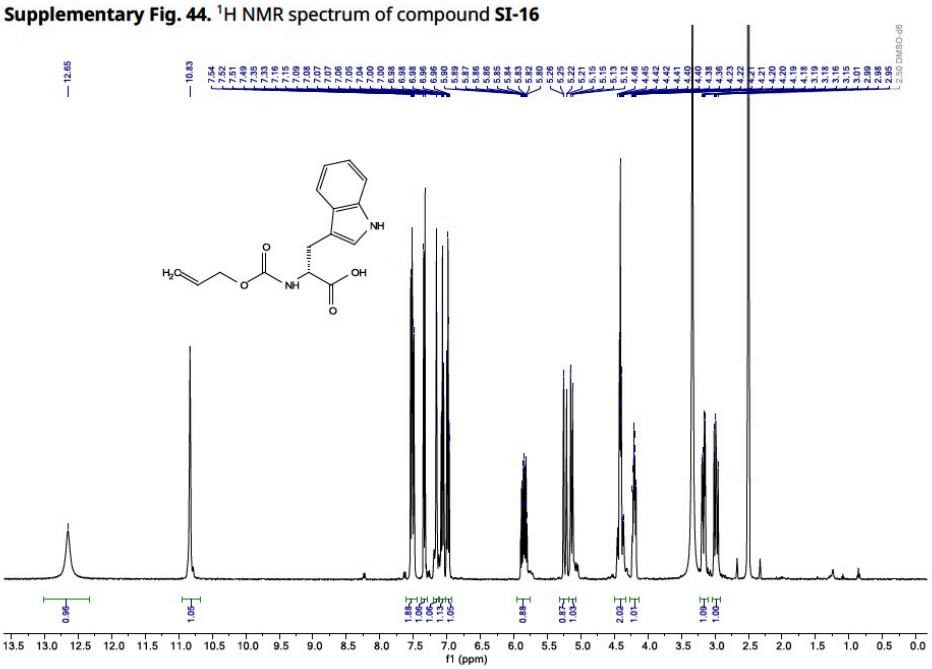

Supplementary Fig. 45. ^{13}C NMR spectrum of compound **SI-16**

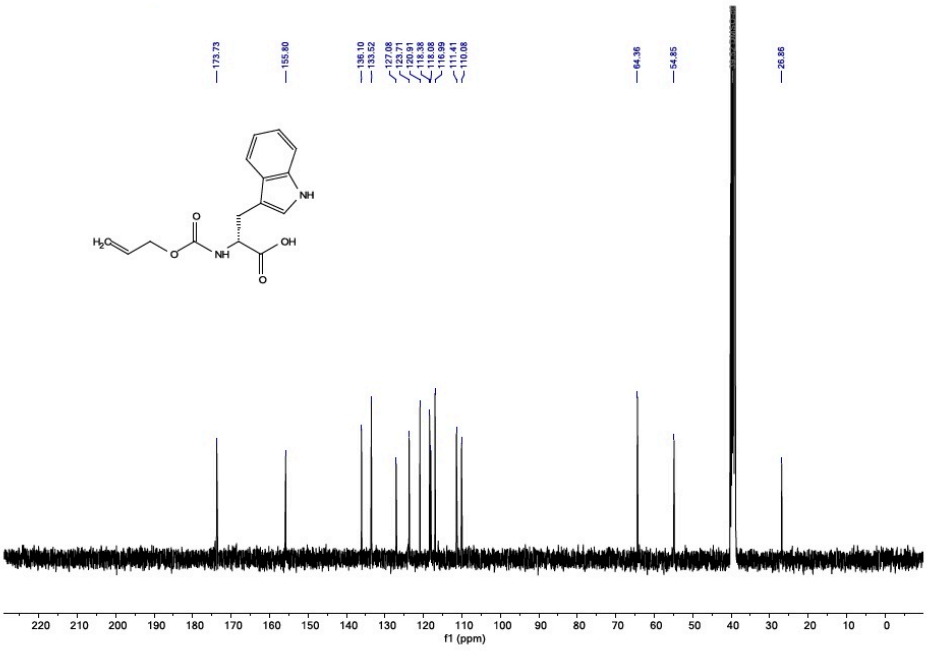

Supplementary Fig. 46. ^{1}H NMR spectrum of compound **SI-17**

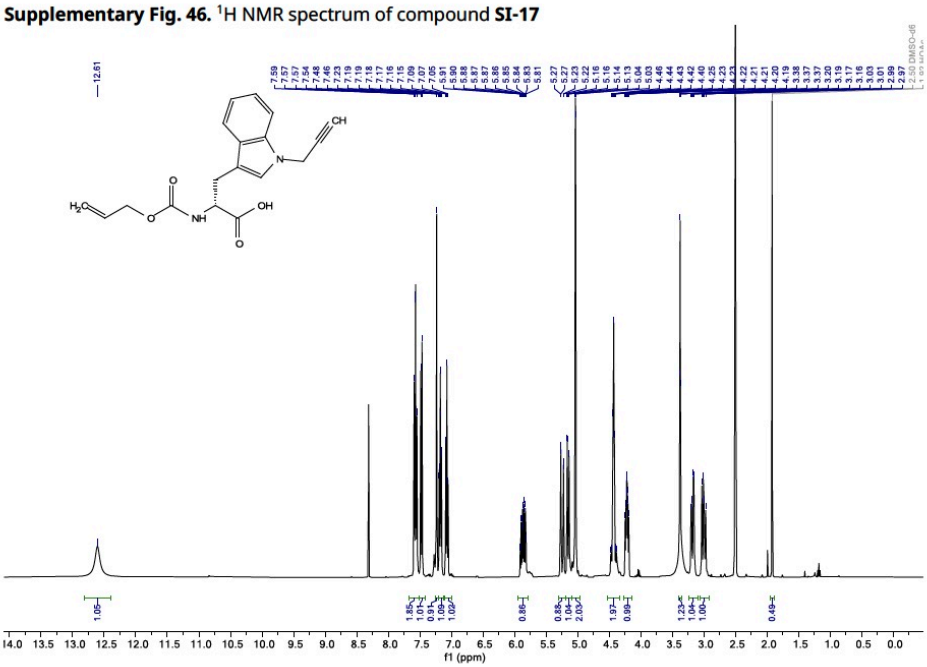

Supplementary Fig. 47. ^{13}C NMR spectrum of compound **SI-17**

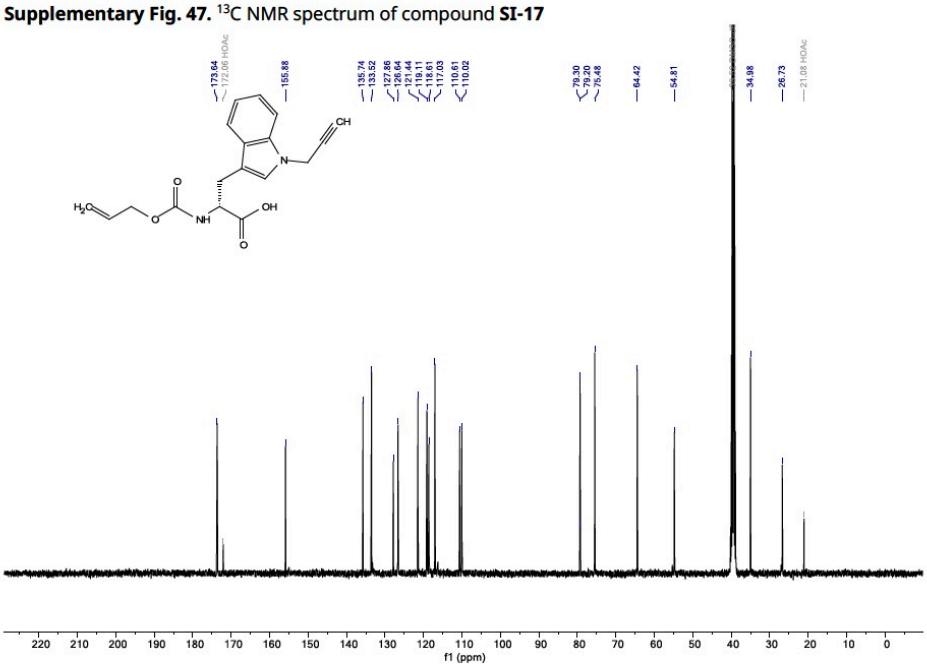

Supplementary Fig. 48. ^{1}H NMR spectrum of compound **3a**

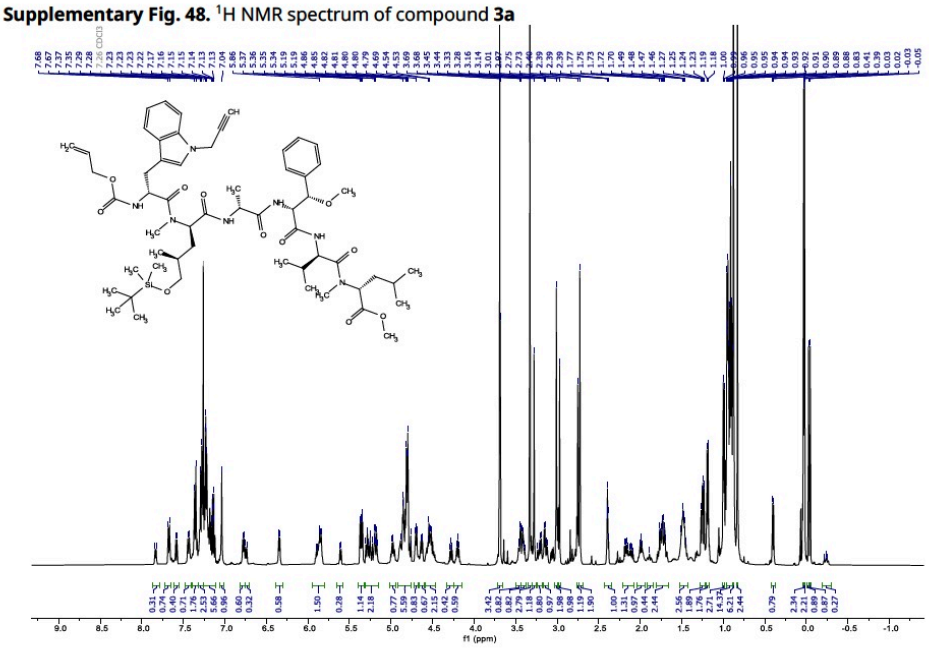

Supplementary Fig. 49. ^{13}C NMR spectrum of compound **3a**

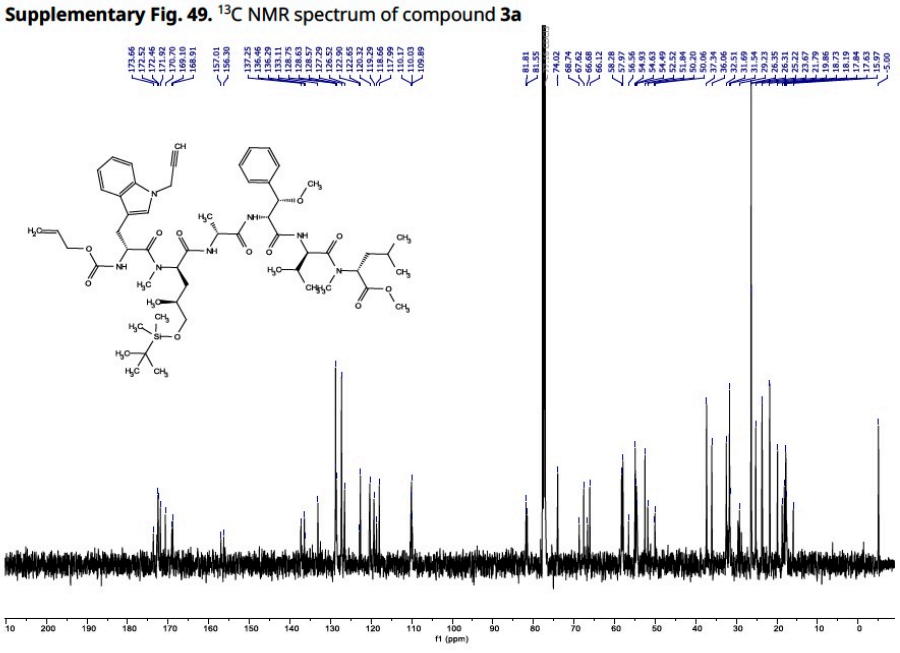

Supplementary Fig. 50. ^{1}H NMR spectrum of compound **4a**

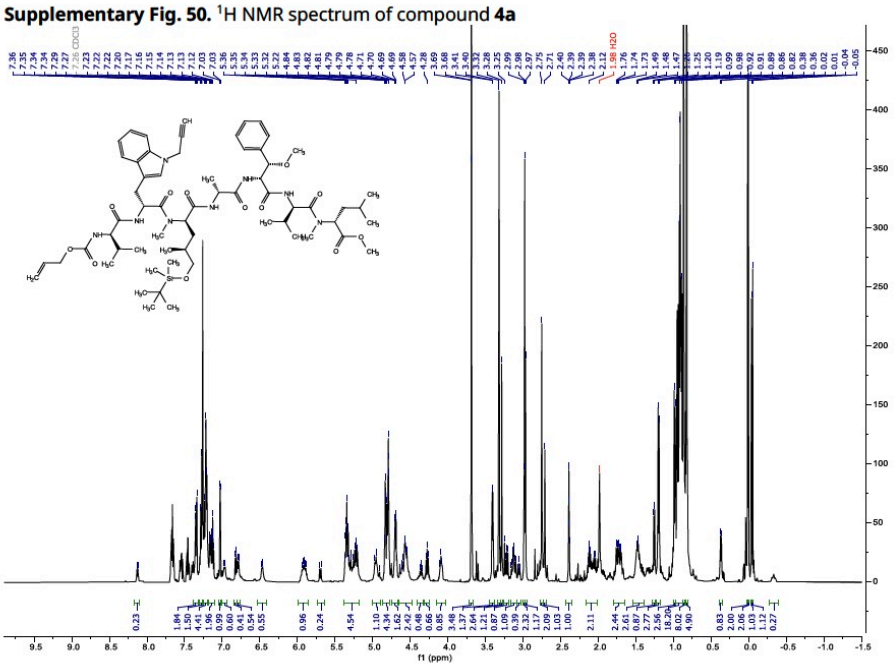

Supplementary Fig. 51. ^{13}C NMR spectrum of compound **4a**

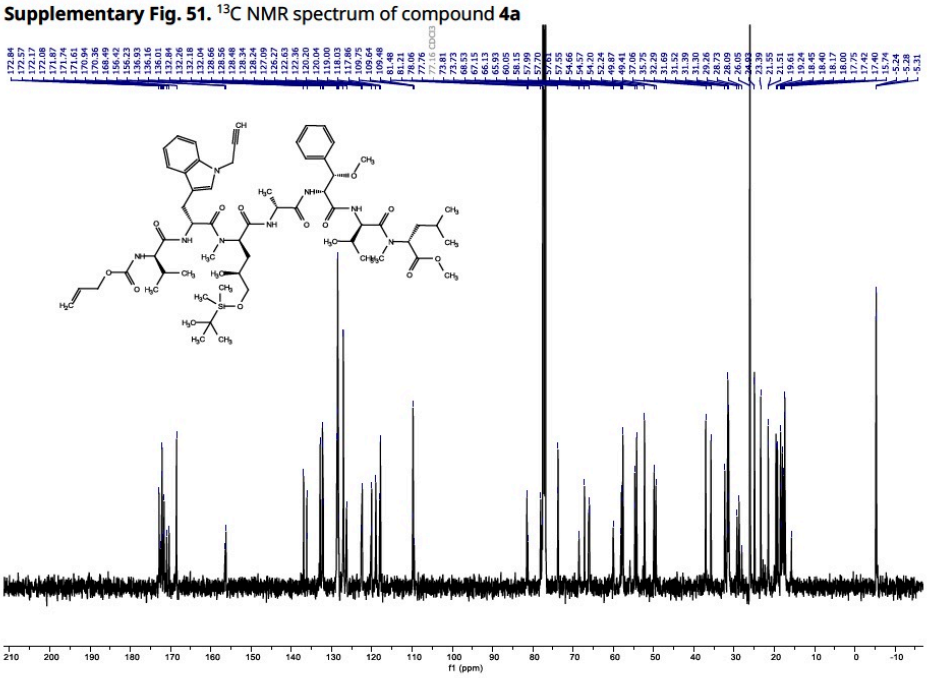

Supplementary Fig. 52. ^{1}H NMR spectrum of compound **5a**

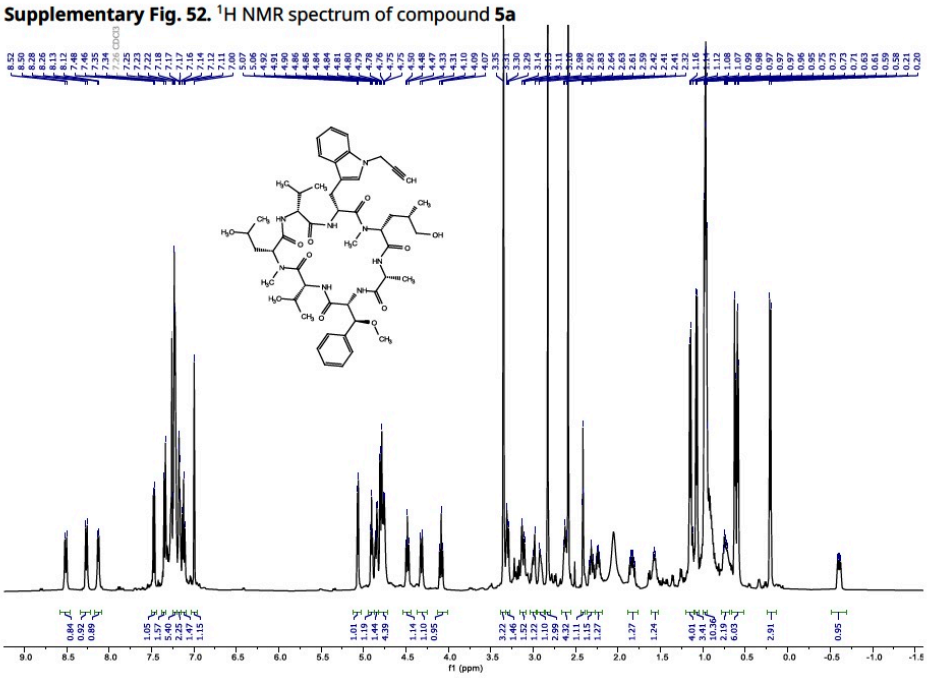

Supplementary Fig. 53. ^{13}C NMR spectrum of compound **5a**

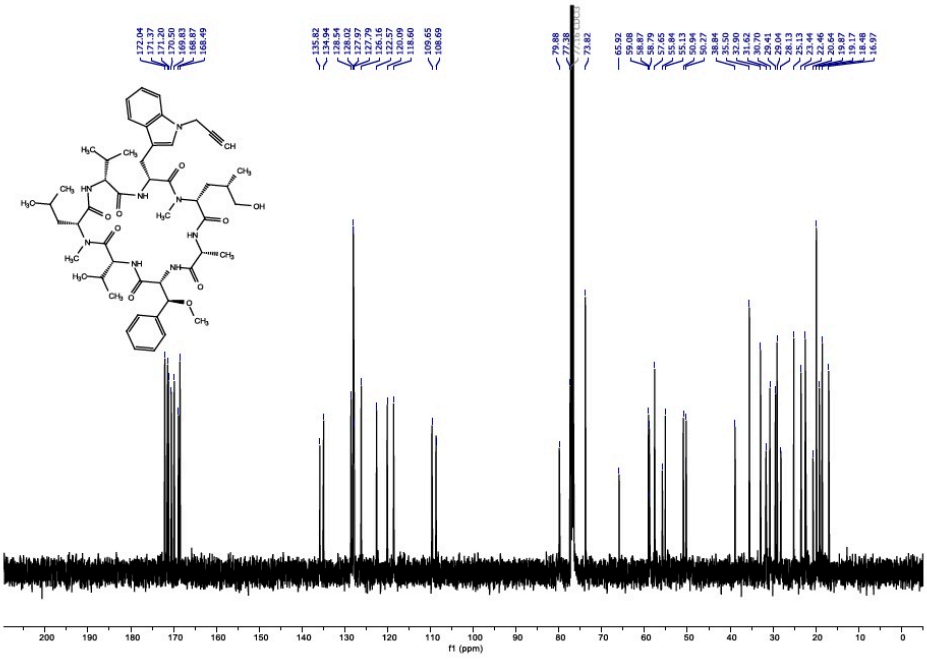

Supplementary Fig. 54. ^{1}H NMR spectrum of compound **8a**

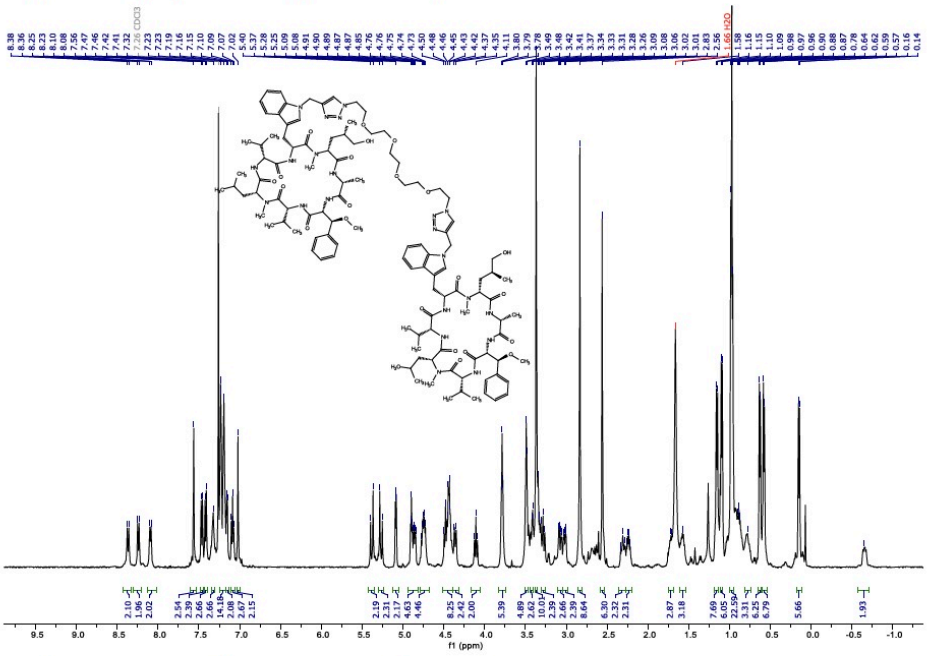

Supplementary Fig. 55. ^{13}C NMR spectrum of compound **8a**

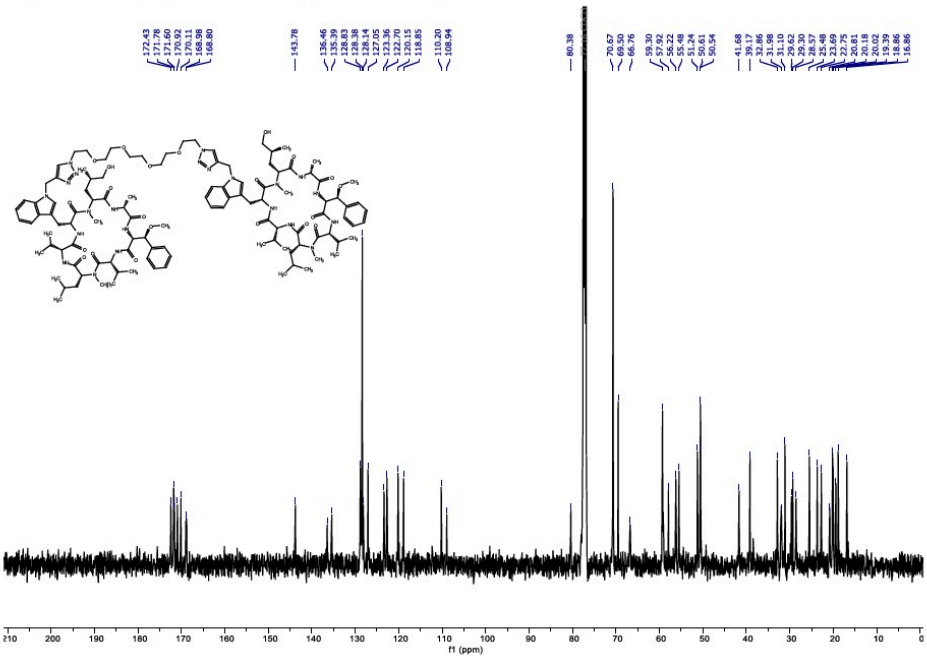

Supplementary Fig. 56. ^{1}H NMR spectrum of compound **SI-18**

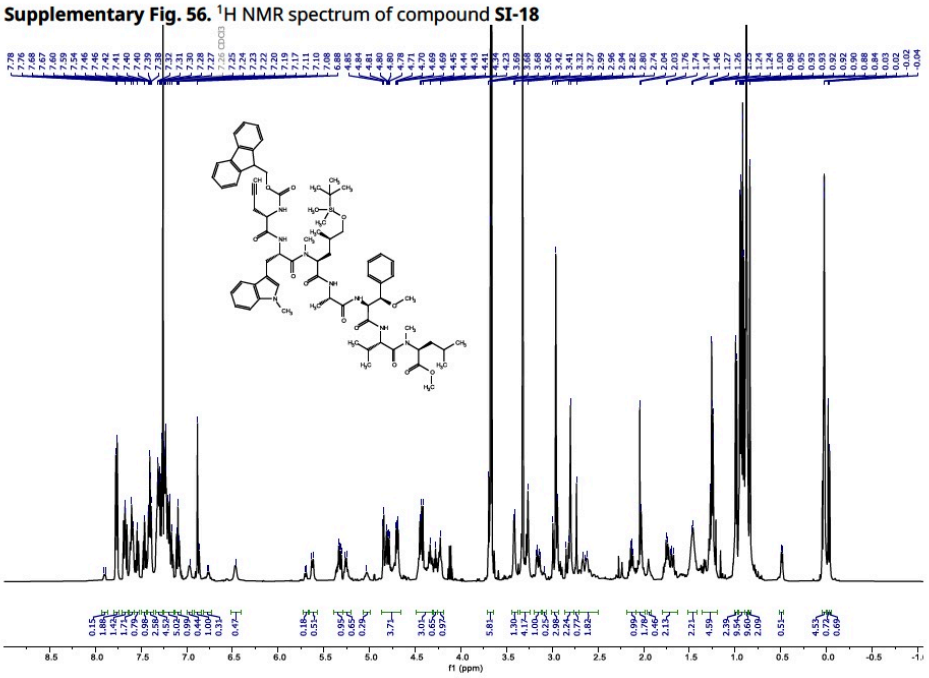

Supplementary Fig. 57. ^{13}C NMR spectrum of compound **SI-18**

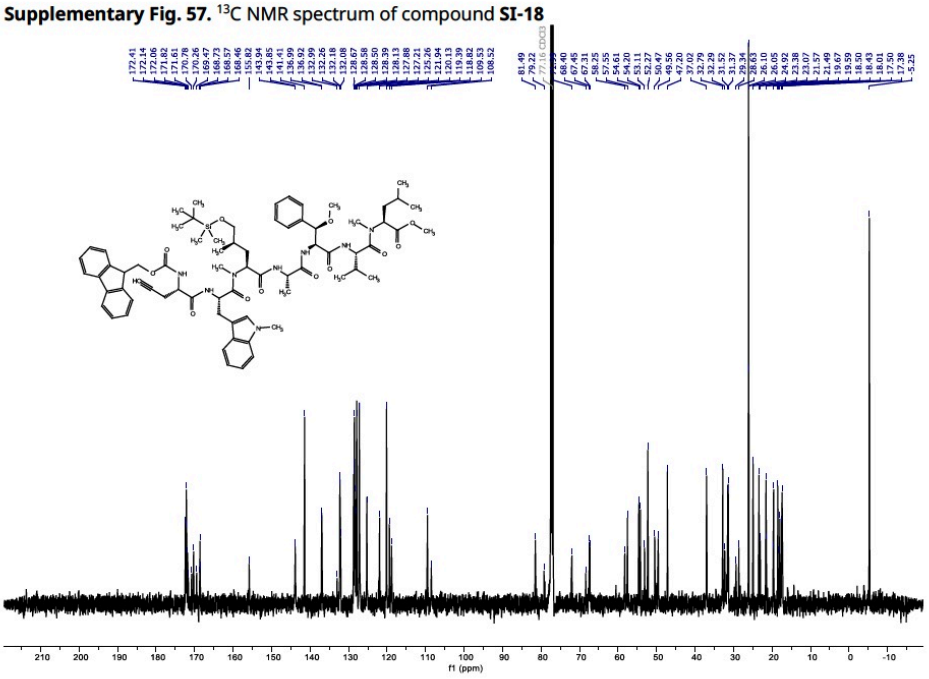

Supplementary Fig. 58. ^{1}H NMR spectrum of compound **10** ($CDCl_3$)

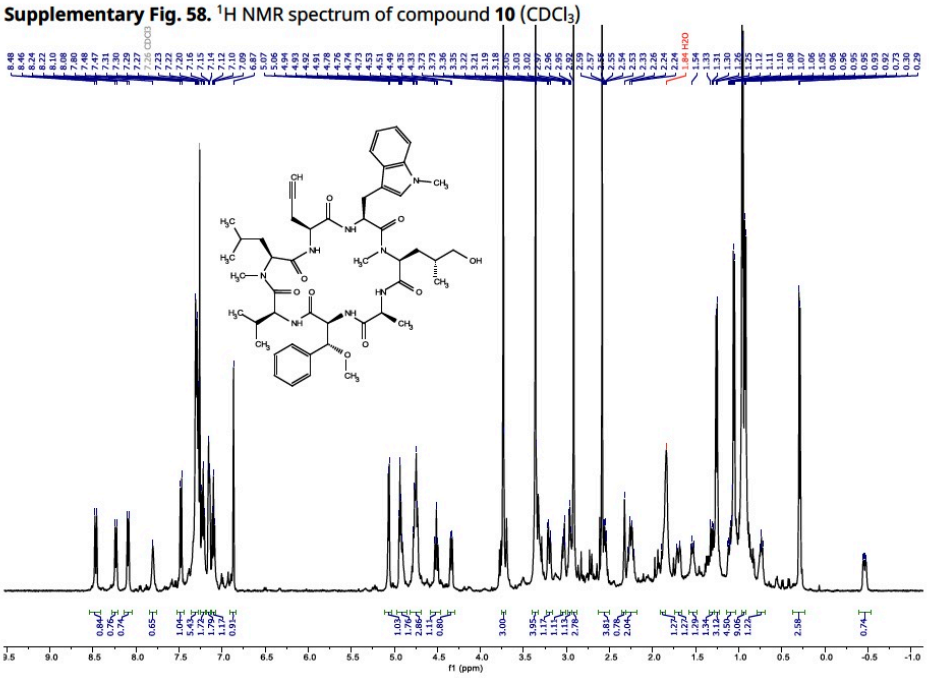

Supplementary Fig. 59. ^{13}C NMR spectrum of compound **10** ($CDCl_3$)

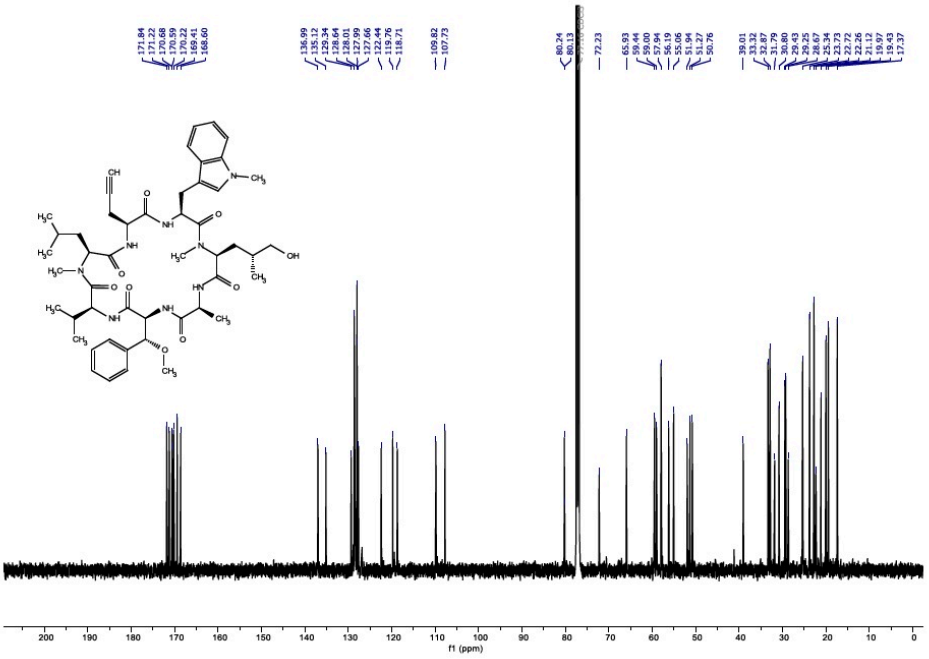

Supplementary Fig. 60. ^{1}H-^{1}H-COSY spectrum of compound **10** ($CDCl_3$)

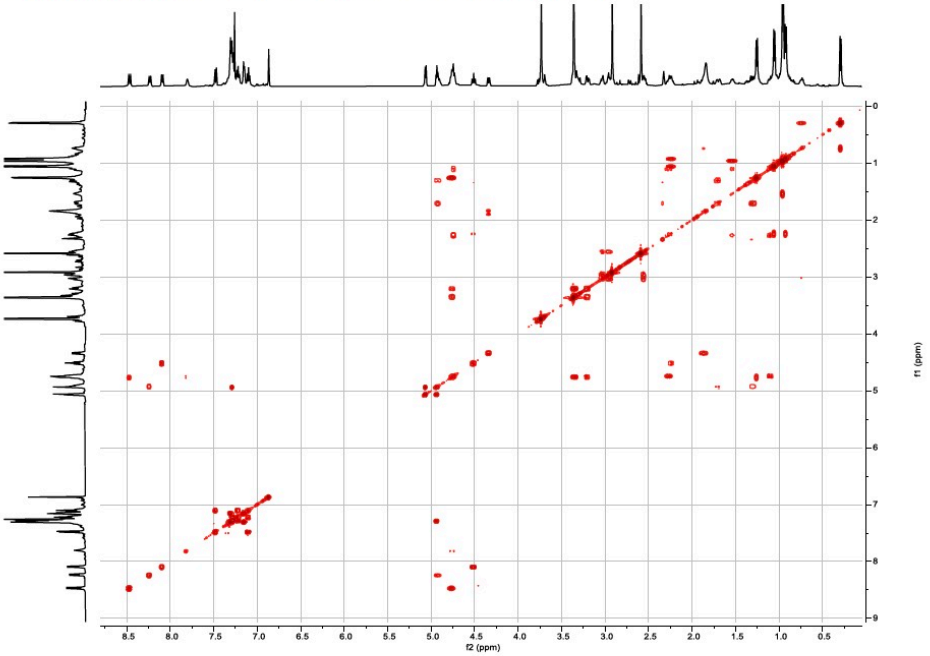

Supplementary Fig. 61. ^{1}H-^{13}C-HSQC(ed) spectrum of compound **10** ($CDCl_3$)

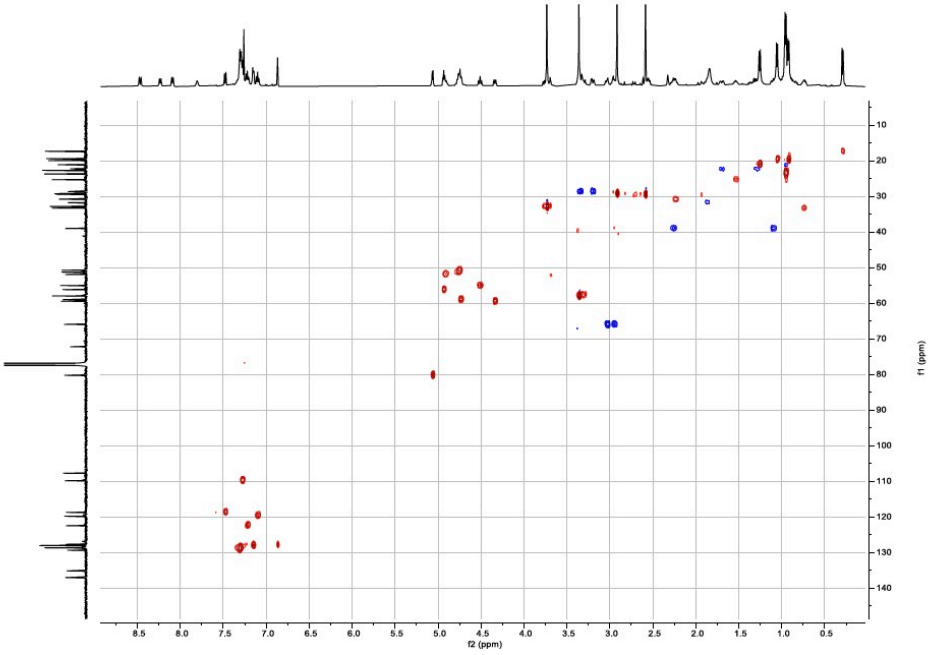

Supplementary Fig. 62. ^{1}H-^{13}C-HMBC spectrum of compound **10** ($CDCl_3$).

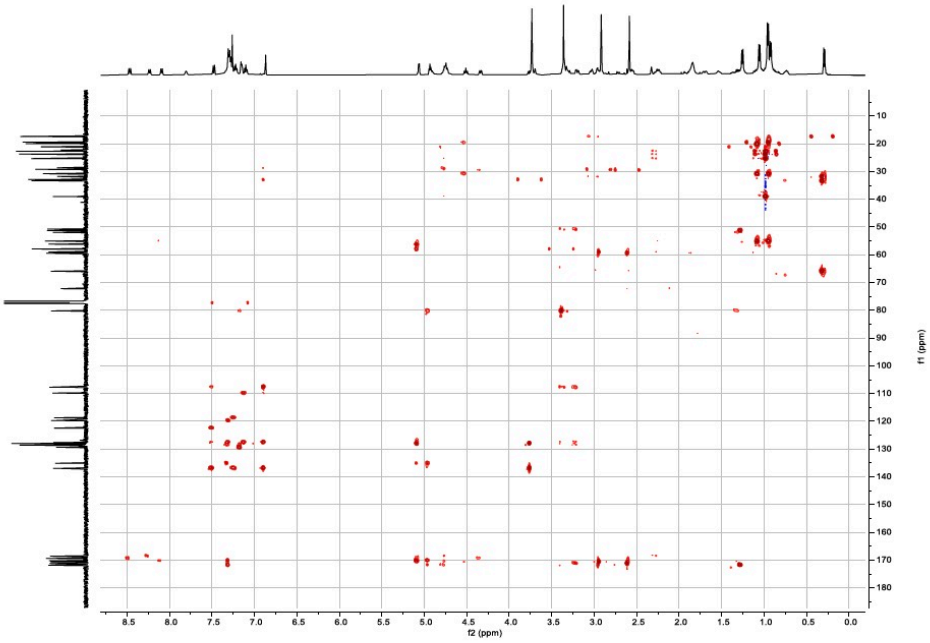

Supplementary Fig. 63. ^{1}H NMR spectrum of compound **10** (DMSO-d_6)

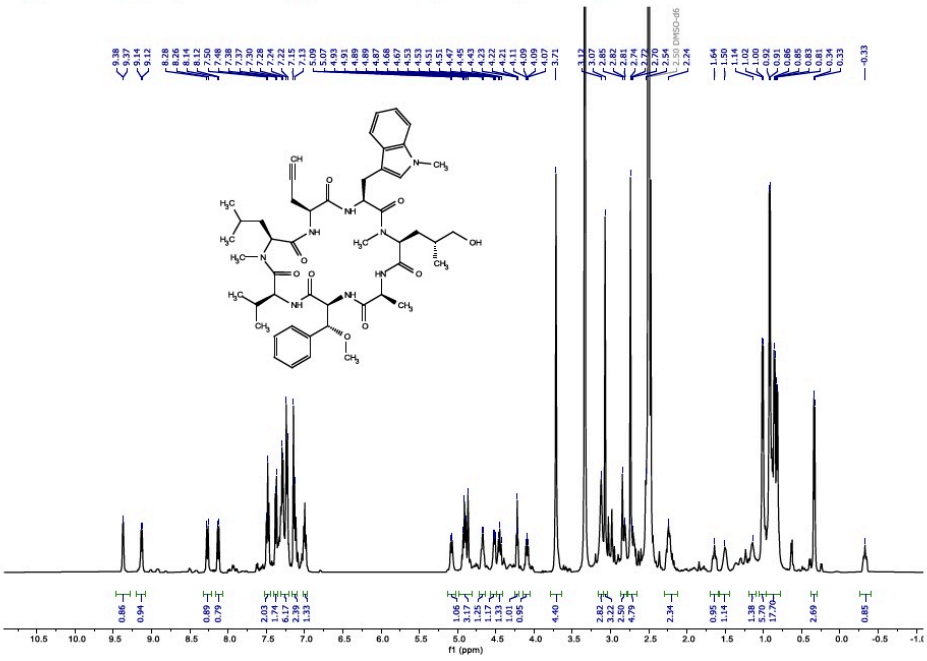

Supplementary Fig. 64. ^{13}C NMR spectrum of compound **10** (DMSO-d_6)

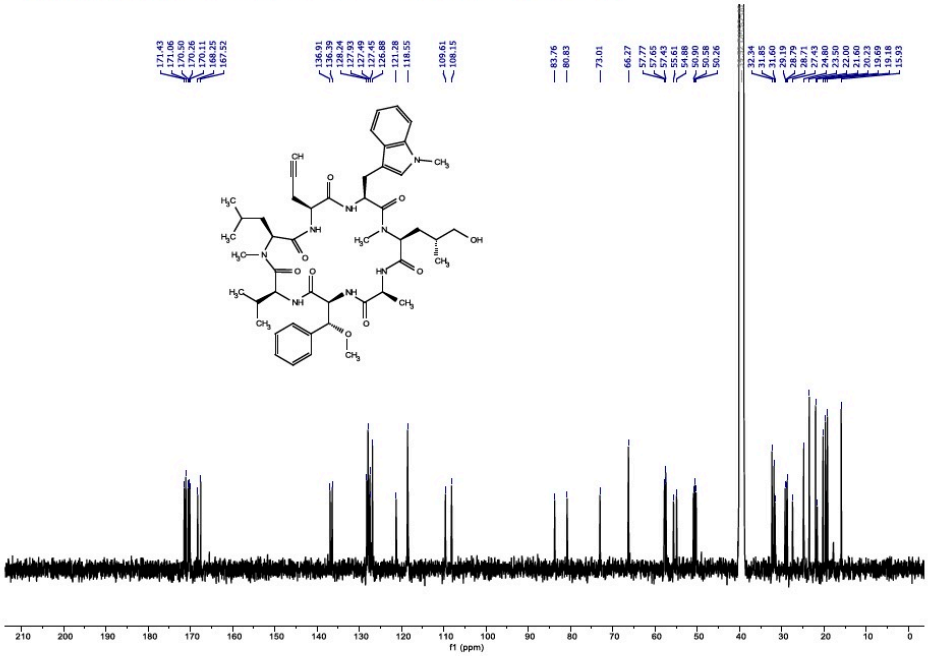

Supplementary Fig. 65. ^{1}H-^{1}H-COSY spectrum of compound **10** (DMSO-d_6)

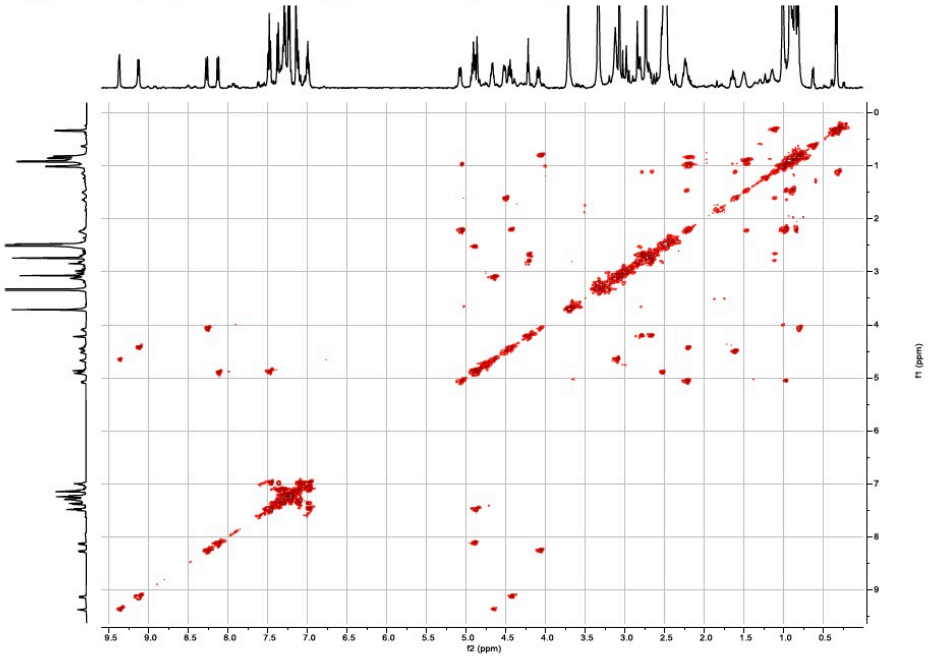

Supplementary Fig. 66. ^{1}H-^{13}C-HSQC(ed) spectrum of compound **10** (DMSO-d_6).

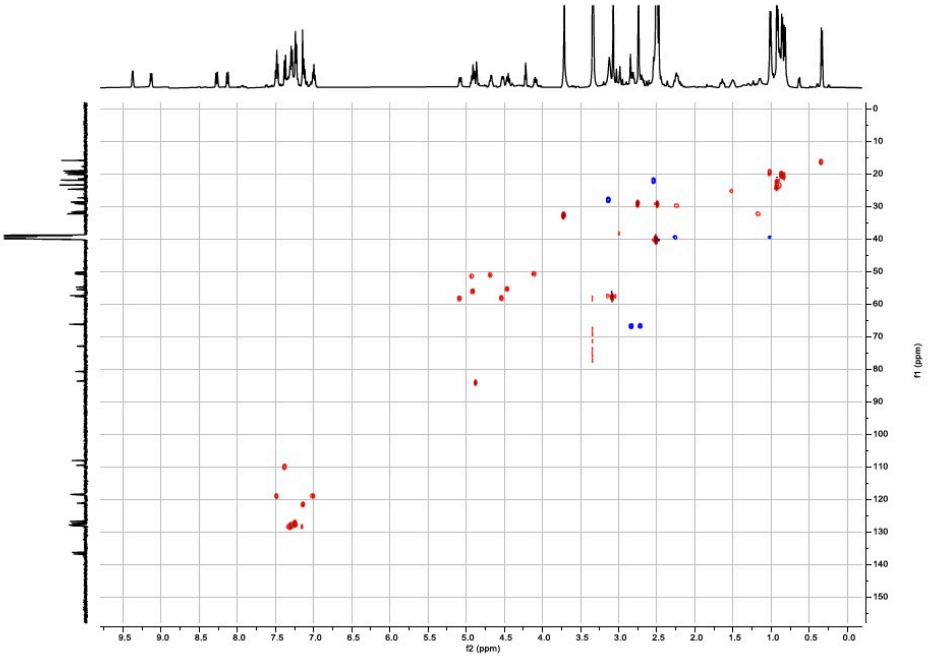

Supplementary Fig. 67. ^{1}H-^{13}C-HMBC spectrum of compound **10** (DMSO-d_6)

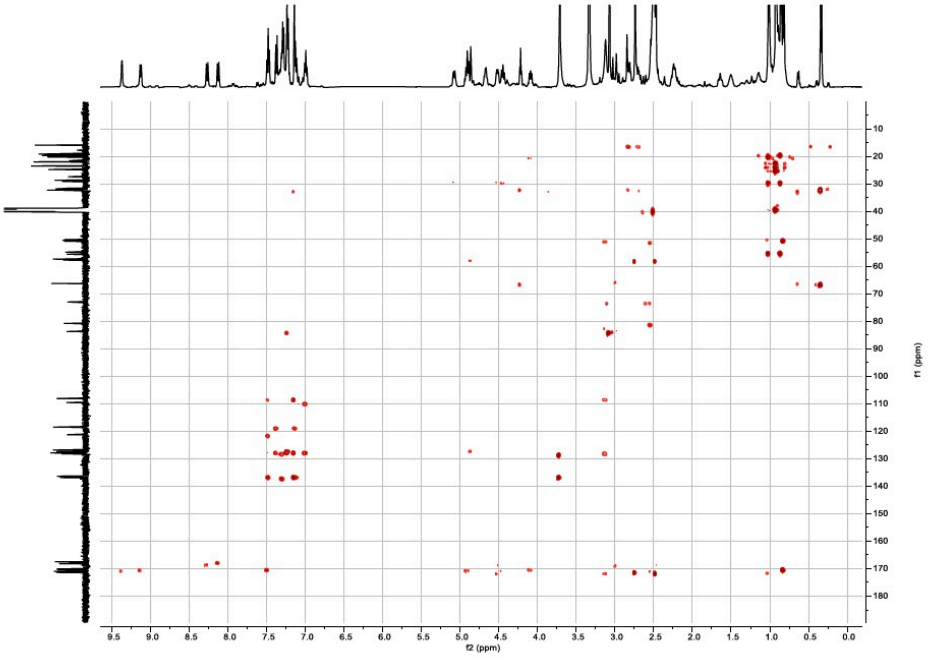

138

Supplementary Fig. 68. ^{1}H NMR spectrum of compound **11**

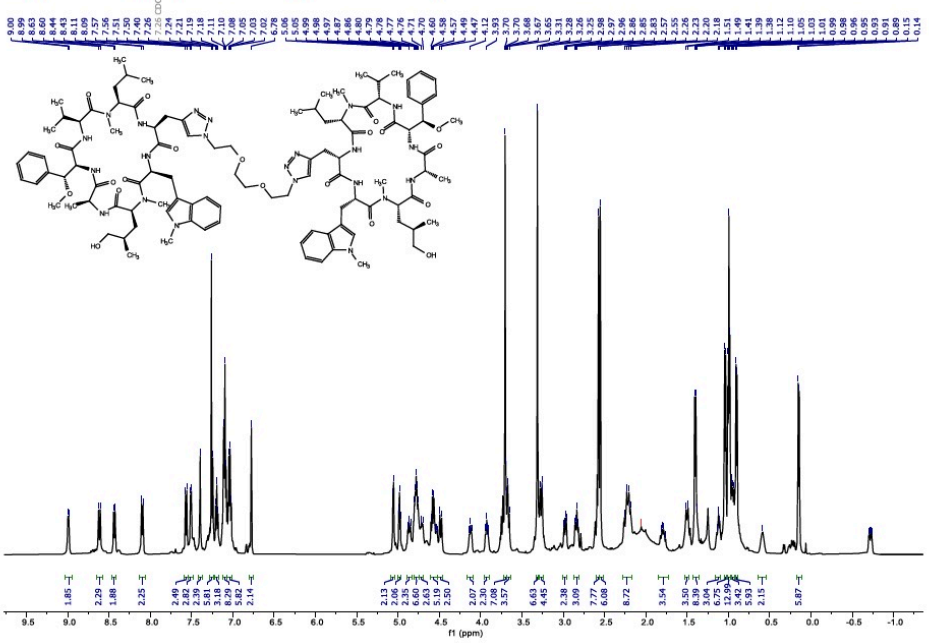

Supplementary Fig. 69. ^{13}C NMR spectrum of compound **11**

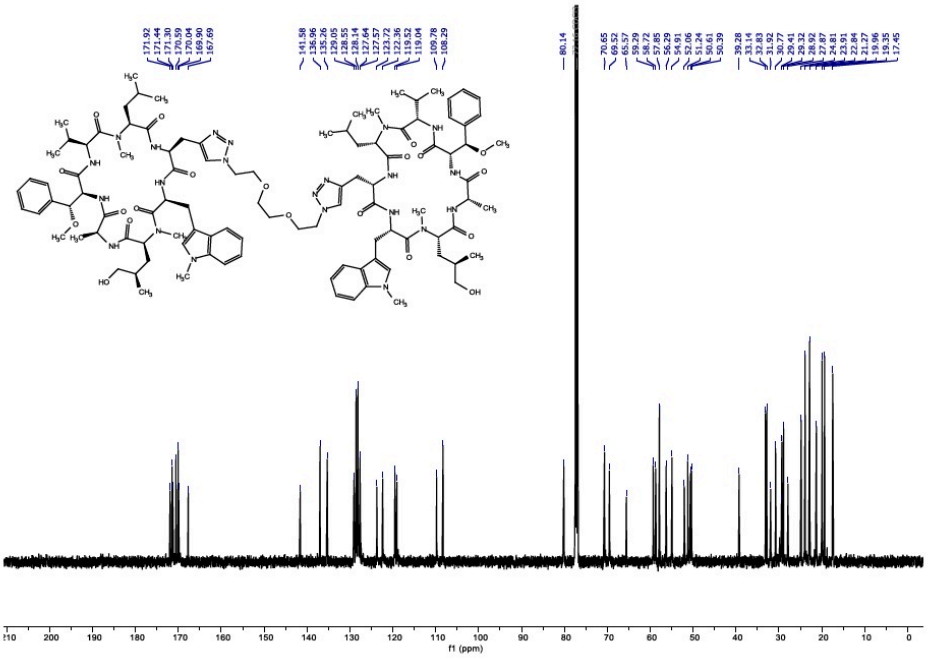

Supplementary Fig. 70. ^{1}H NMR spectrum of compound **12**

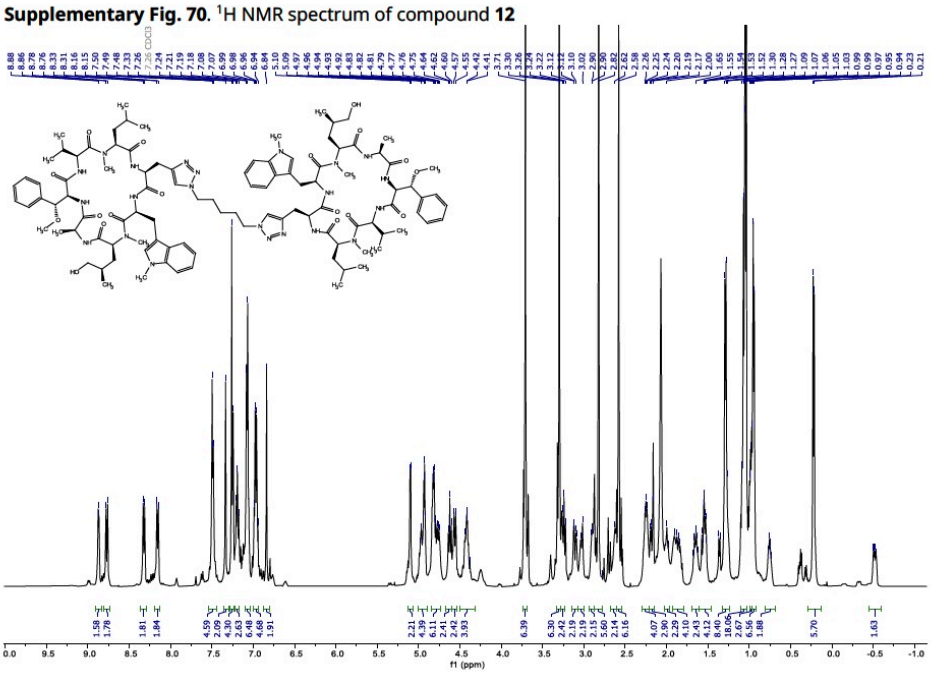

Supplementary Fig. 71. ^{13}C NMR spectrum of compound **12**

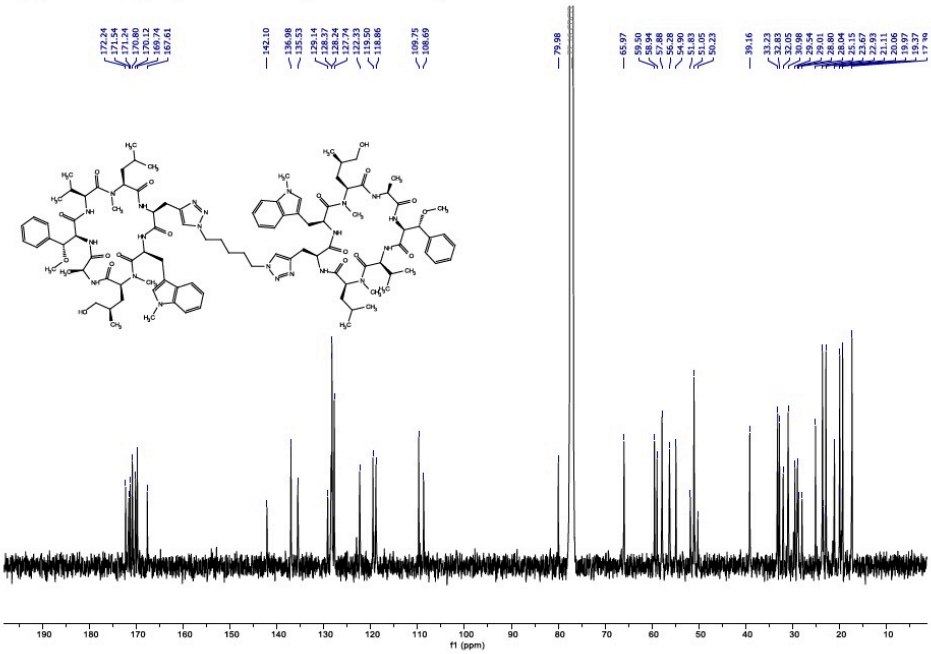

Supplementary Fig. 72. ^{1}H NMR spectrum of compound **24**

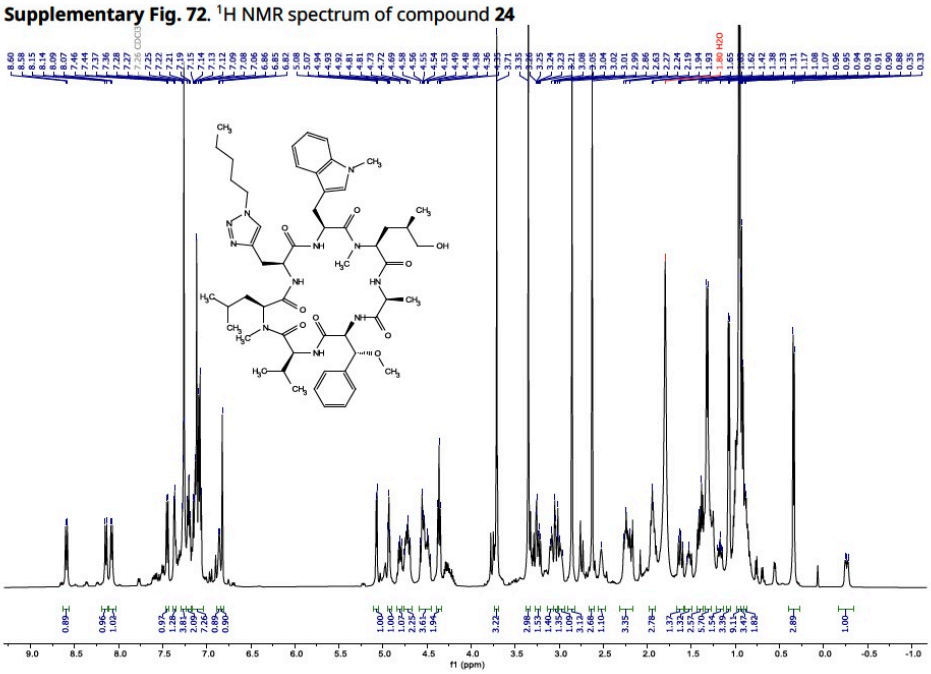

Supplementary Fig. 73. ^{13}C NMR spectrum of compound **24**

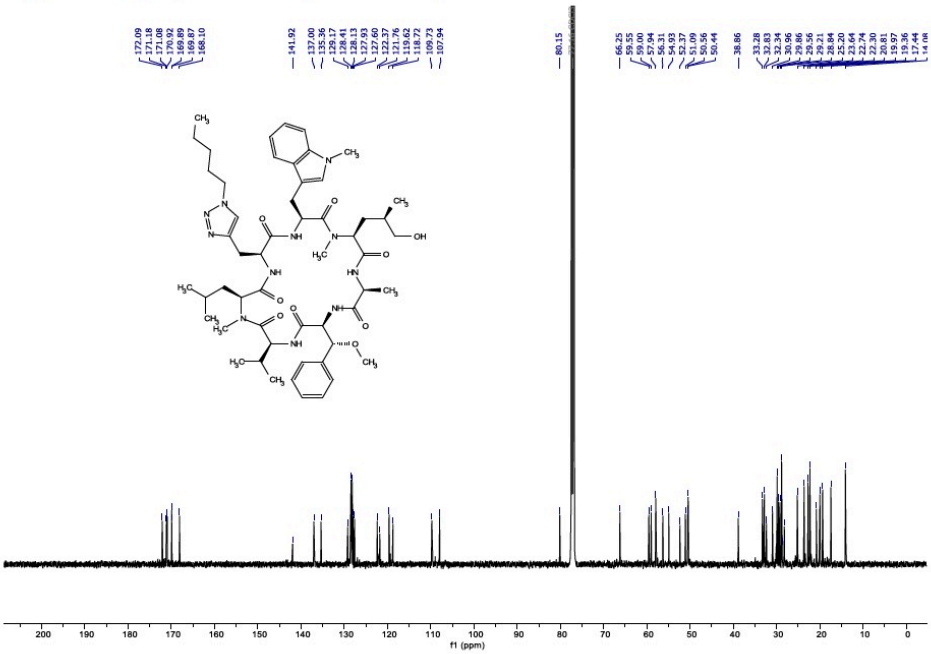

Supplementary Fig. 74. ^{1}H NMR spectrum of compound **SI-19**

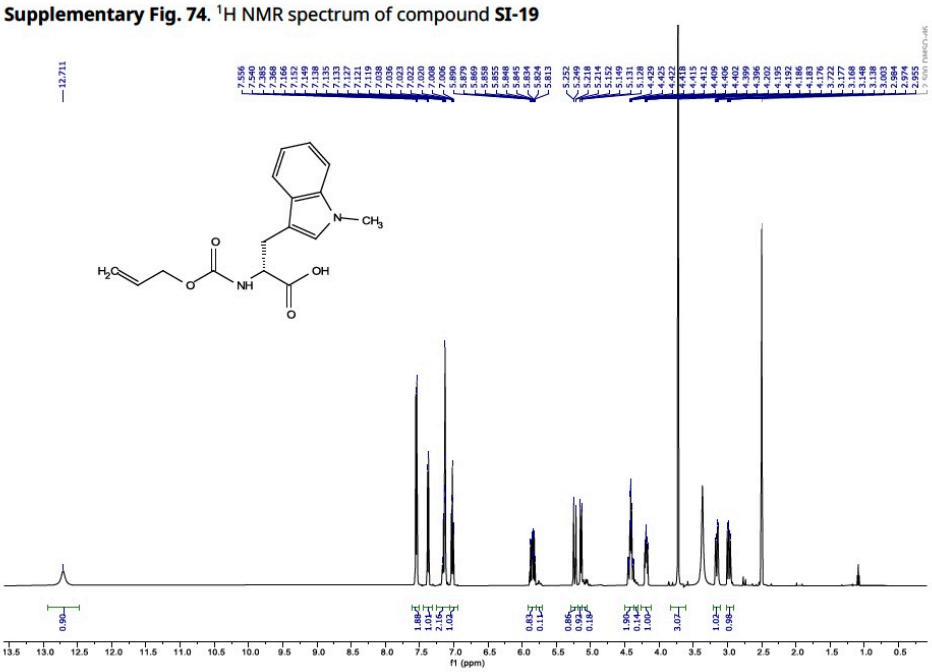

Supplementary Fig. 75. ^{13}C NMR spectrum of compound **SI-19**

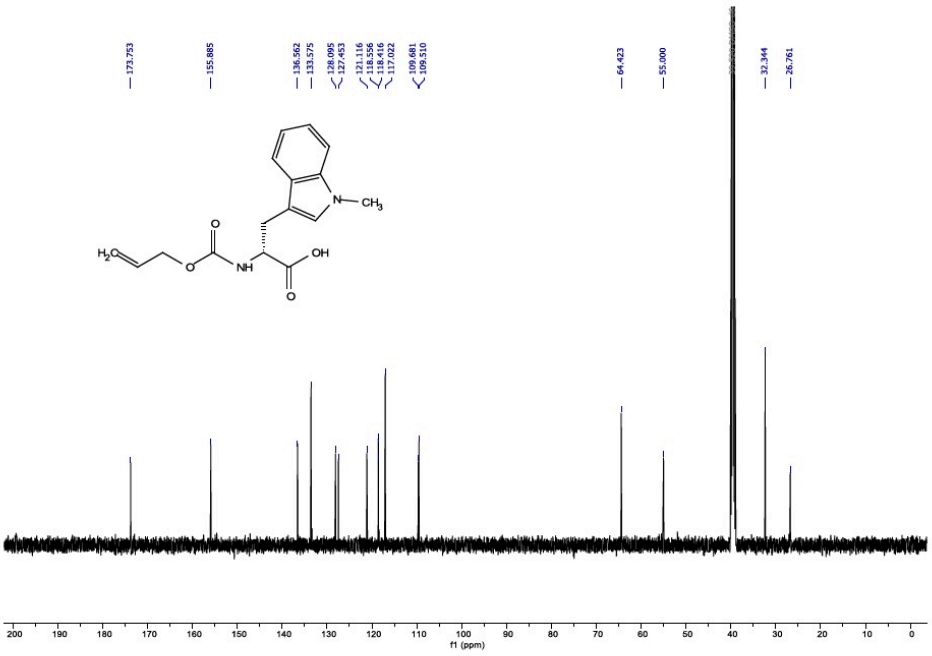

Supplementary Fig. 76. ^{1}H NMR spectrum of compound **SI-20**

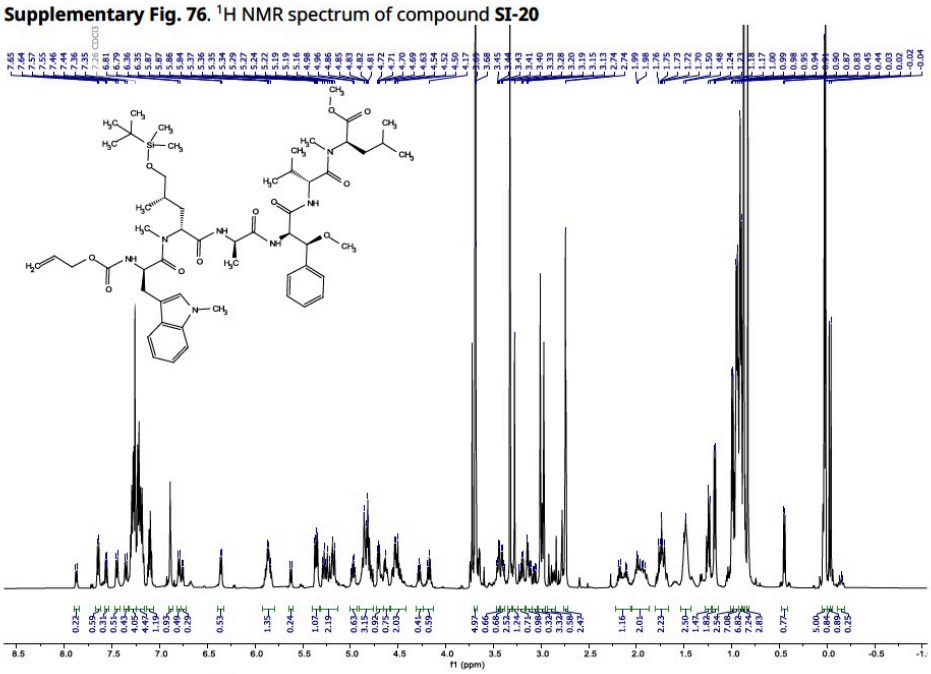

Supplementary Fig. 77. ^{13}C NMR spectrum of compound **SI-20**

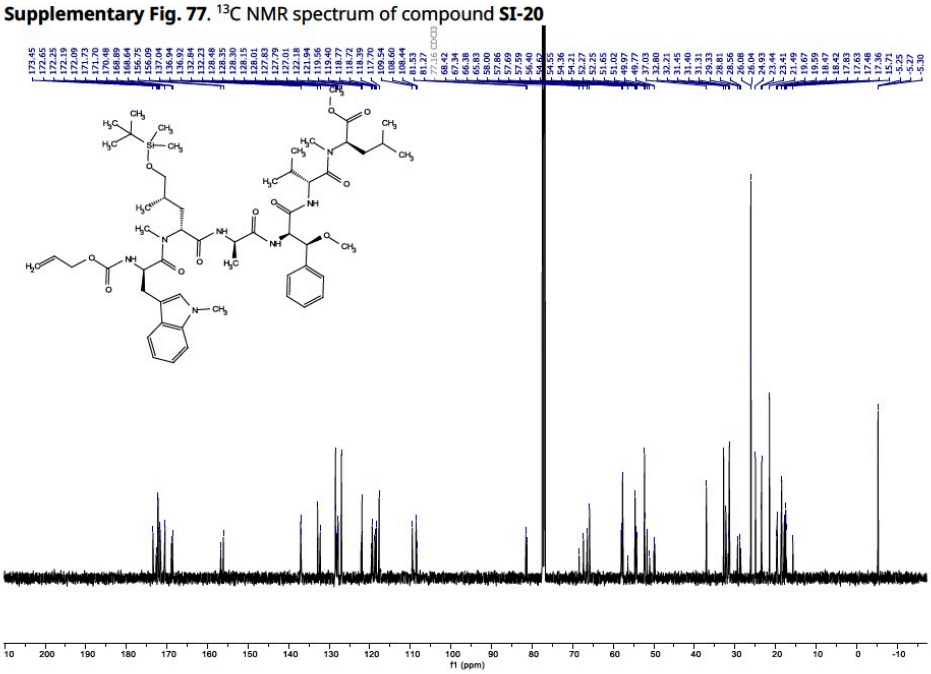

Supplementary Fig. 78. ^{1}H NMR spectrum of compound **SI-18a**

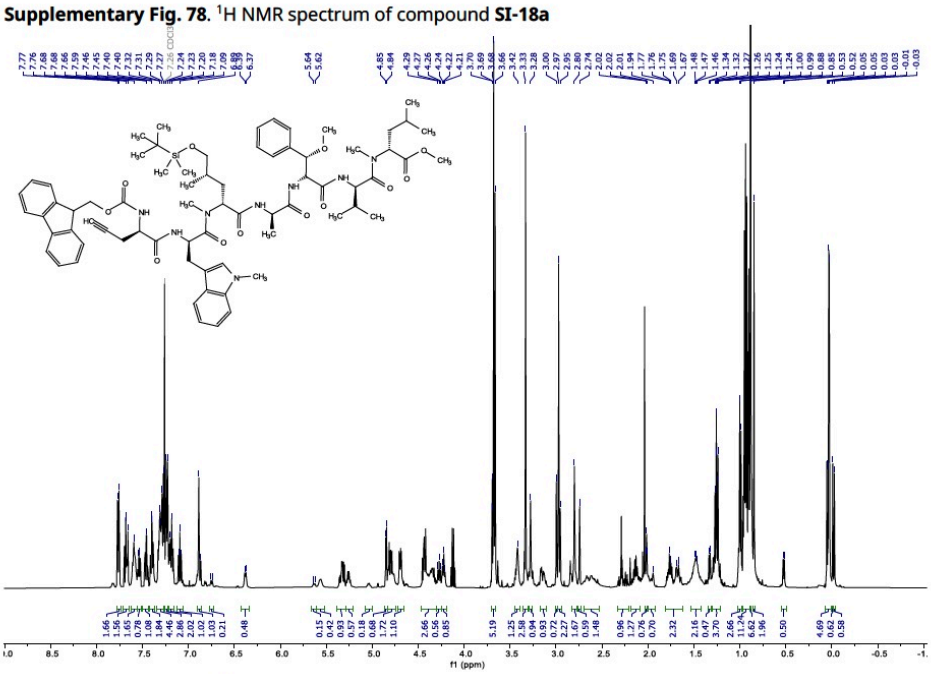

Supplementary Fig. 79. ^{13}C NMR spectrum of compound **SI-18a**

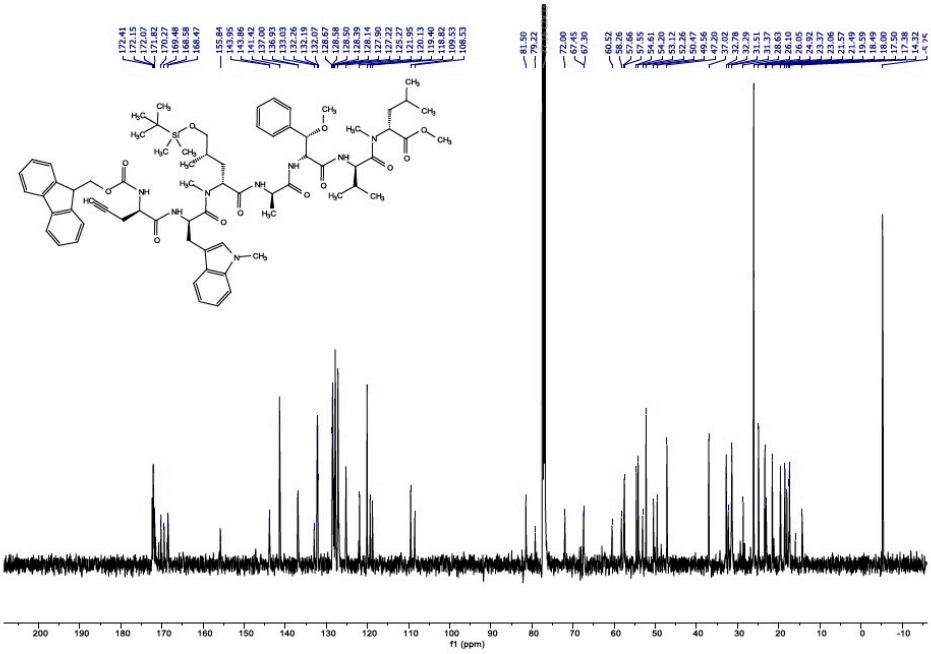

Supplementary Fig. 80. ^{1}H NMR spectrum of compound **10a**

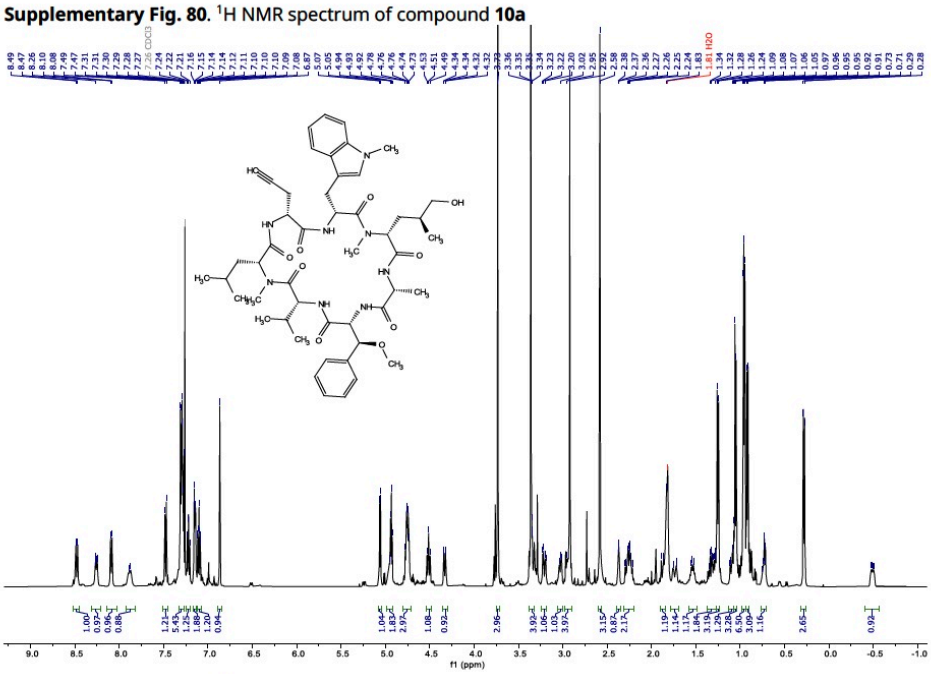

Supplementary Fig. 81. ^{13}C NMR spectrum of compound **10a**

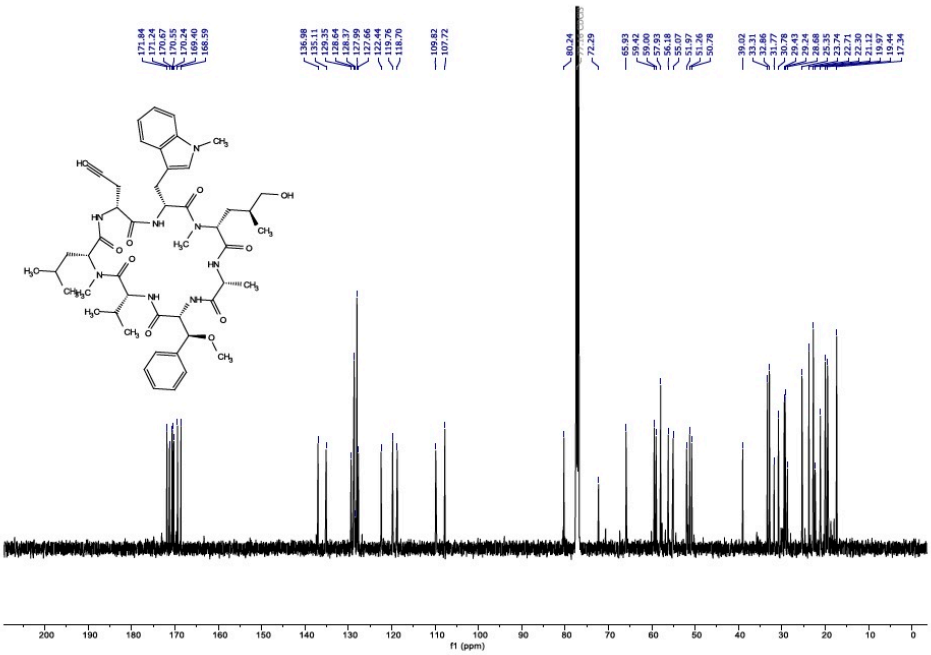

Supplementary Fig. 82. ^{1}H NMR spectrum of compound **12a**

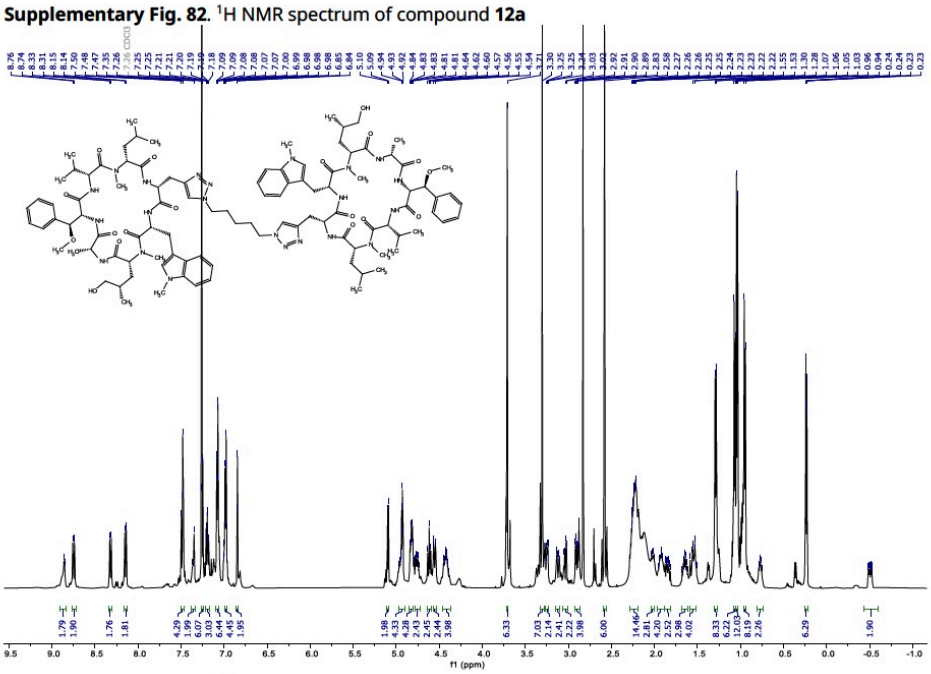

Supplementary Fig. 83. ^{13}C NMR spectrum of compound **12a**

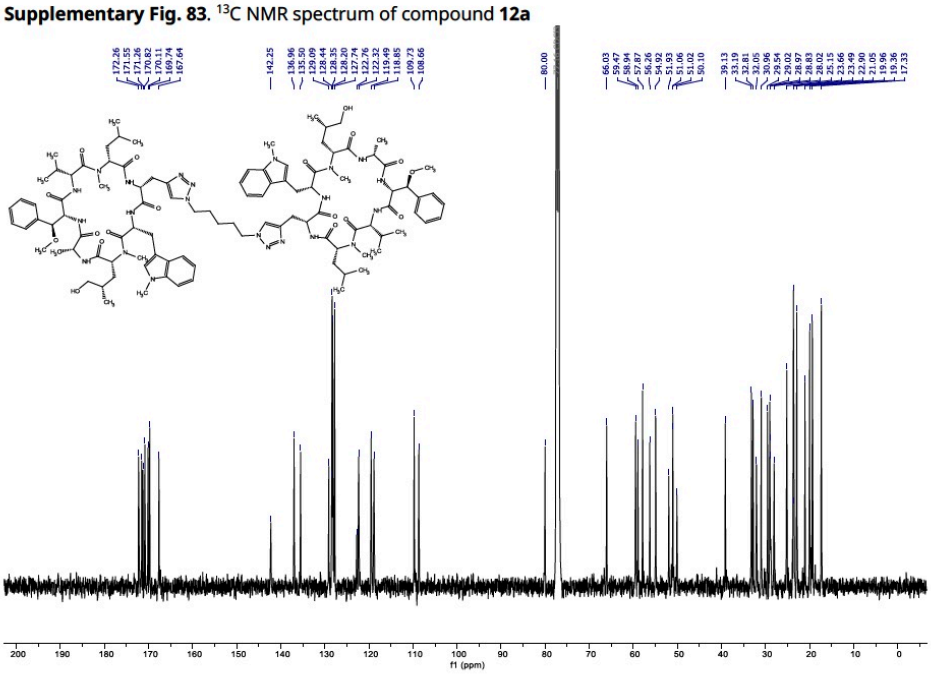

Supplementary Fig. 84. ^{1}H NMR spectrum of compound **SI-21**

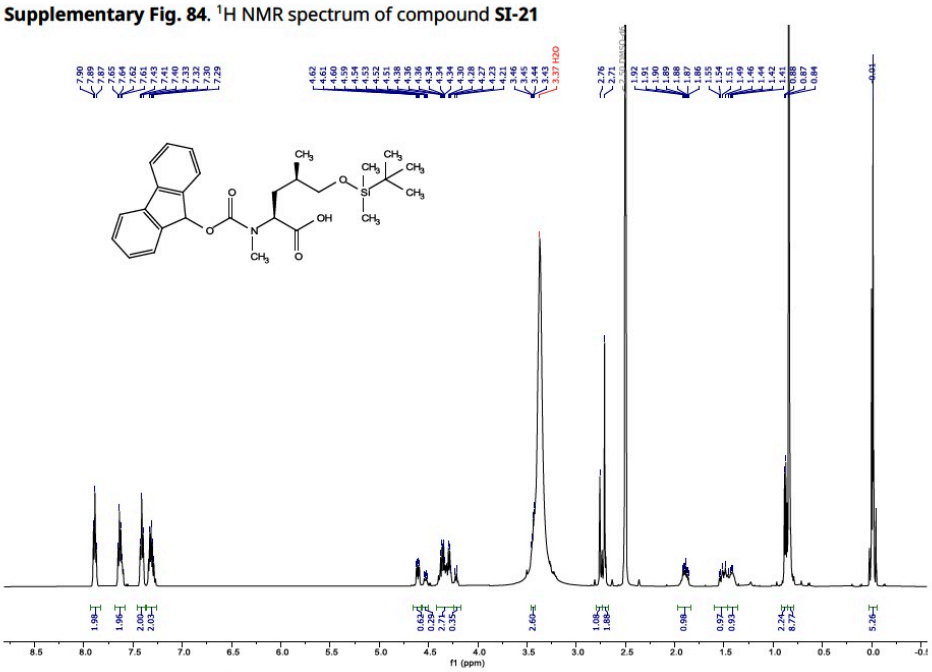

Supplementary Fig. 85. ^{13}C NMR spectrum of compound **SI-21**

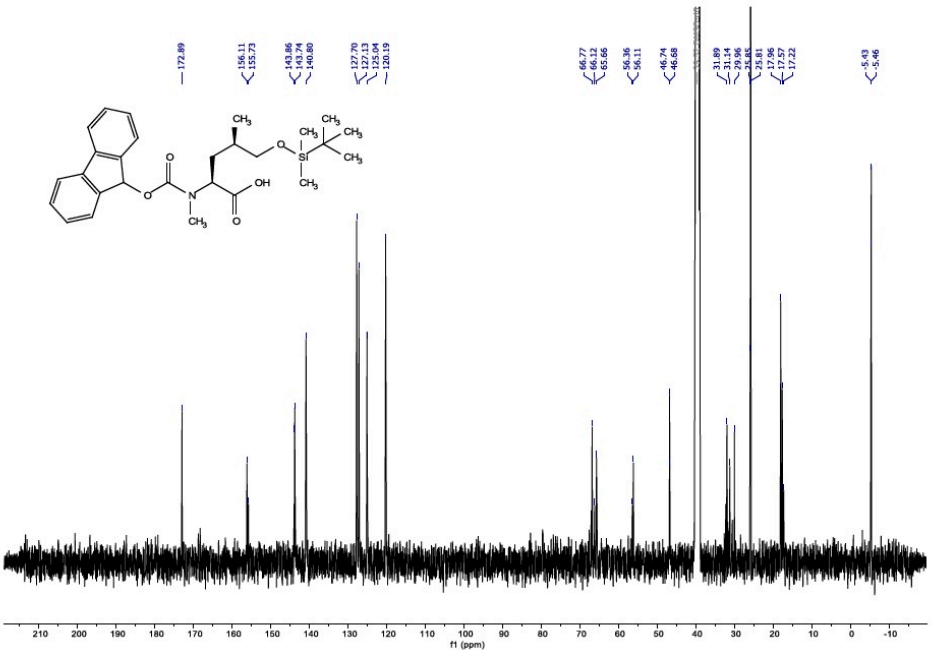

Supplementary Fig. 86. ^{1}H and ^{13}C NMR spectra of compound **SI-22**

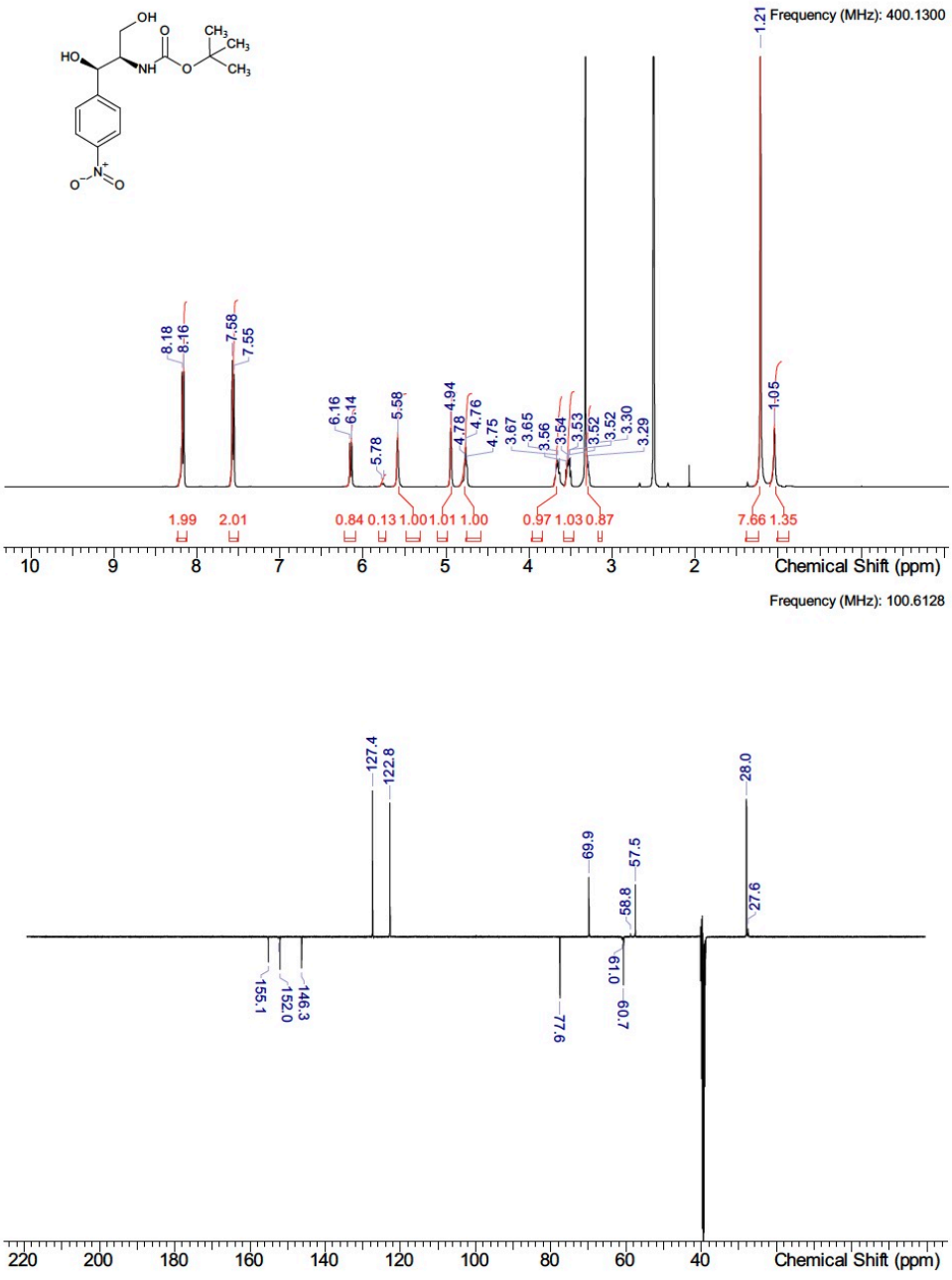

Supplementary Fig. 87. ^{1}H and ^{13}C NMR spectra of compound **SI-23**

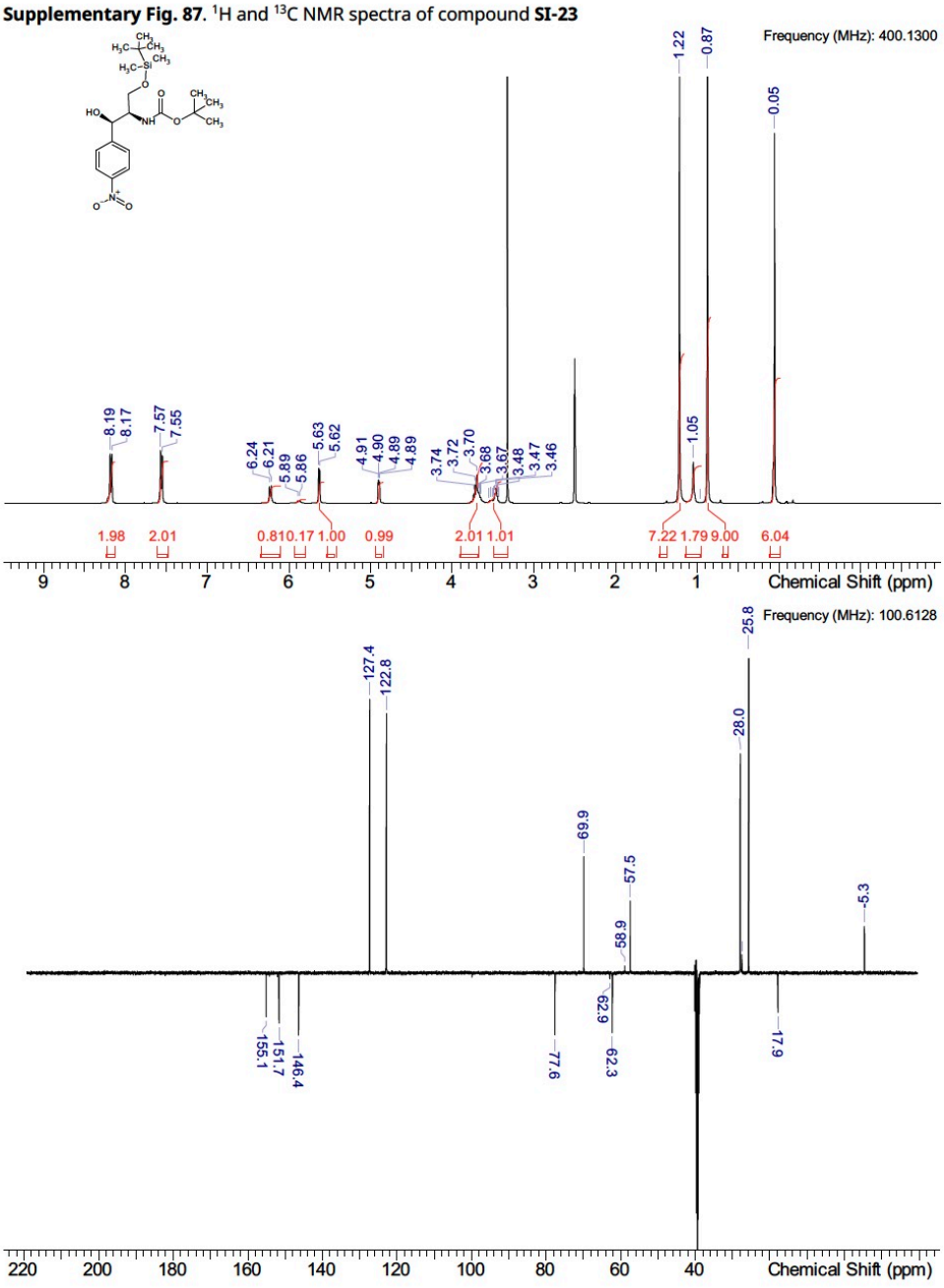

Supplementary Fig. 88. ^{1}H and ^{13}C NMR spectra of compound **SI-24**

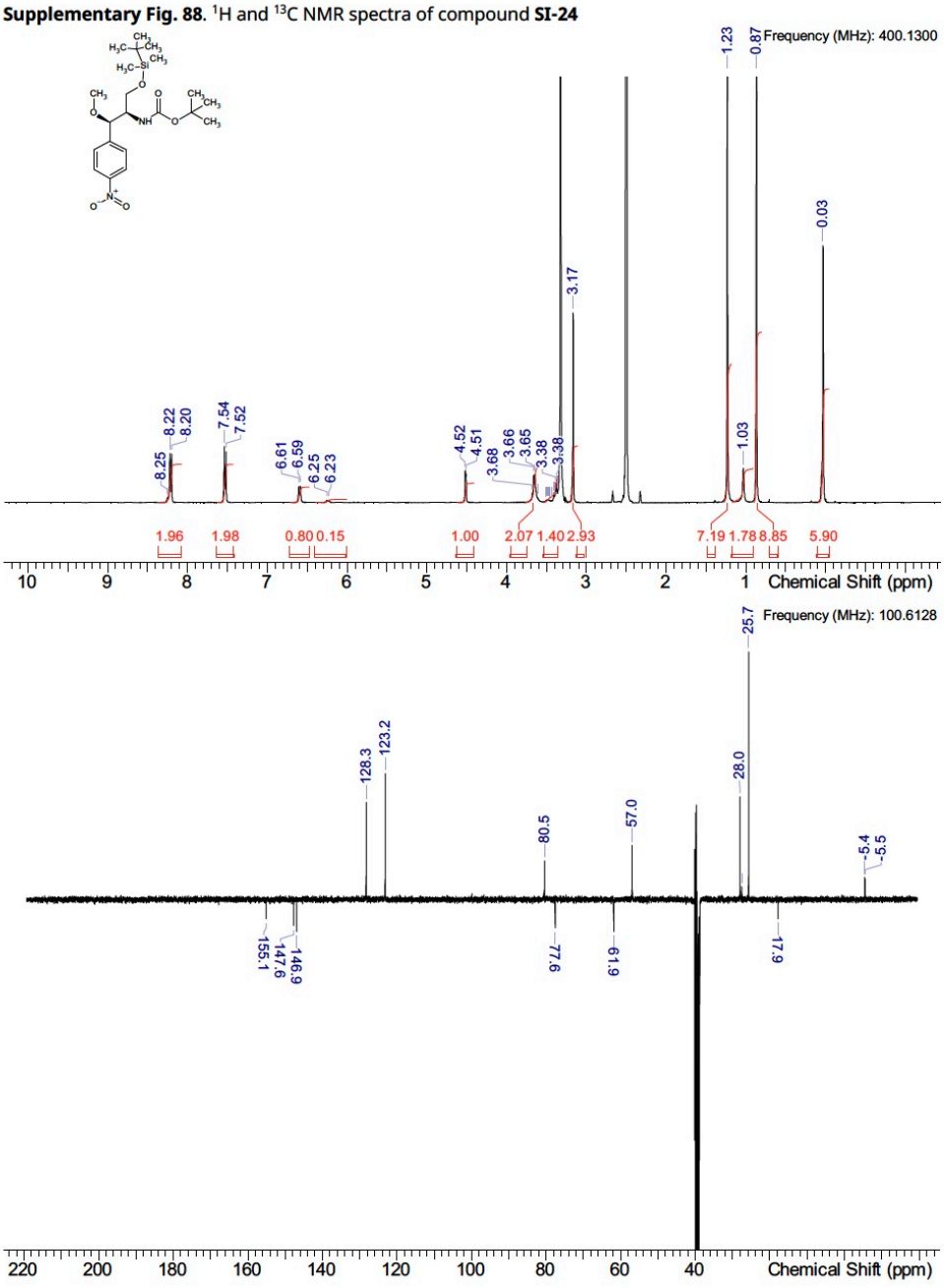

Supplementary Fig. 89. ^{1}H and ^{13}C NMR spectra of compound **SI-25**

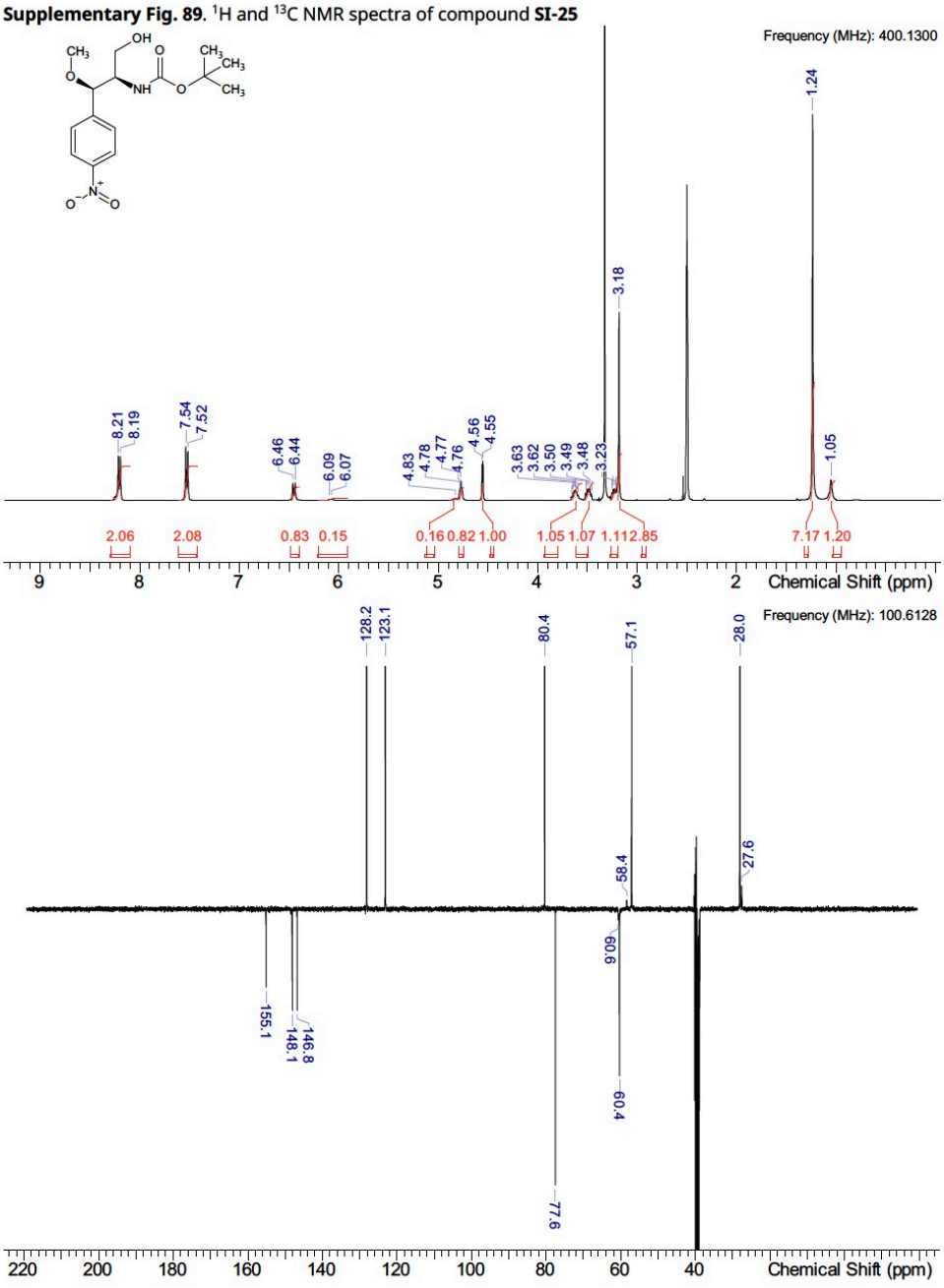

Supplementary Fig. 90. ^{1}H and ^{13}C NMR spectra of compound **SI-26**

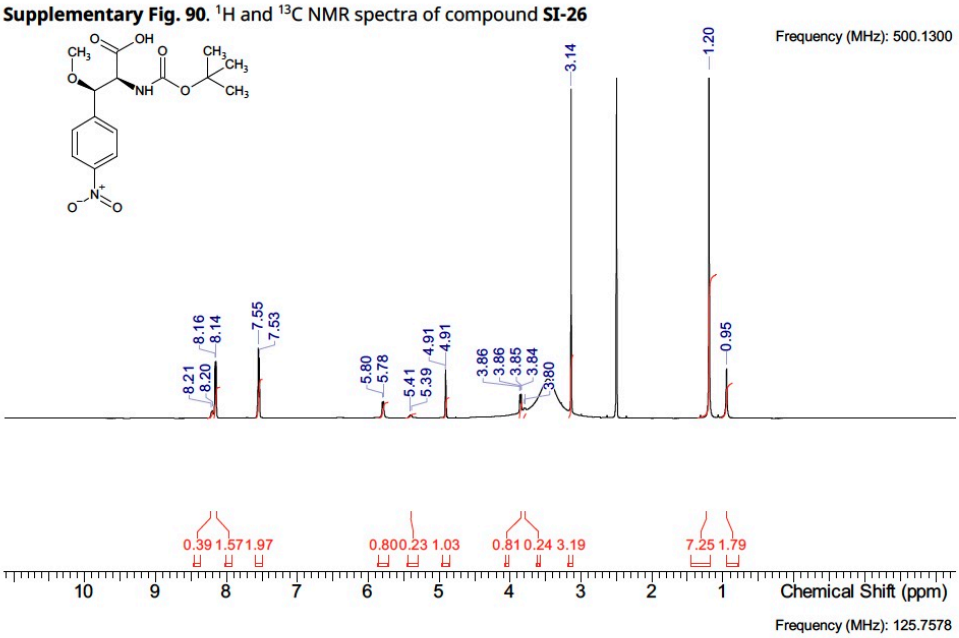

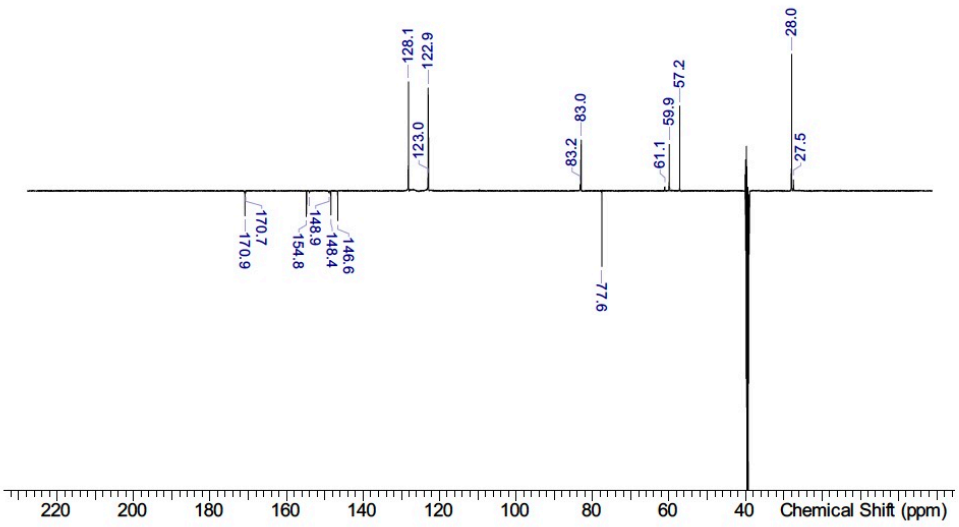

Supplementary Fig. 91. ^{1}H and ^{13}C NMR spectra of compound **SI-28**

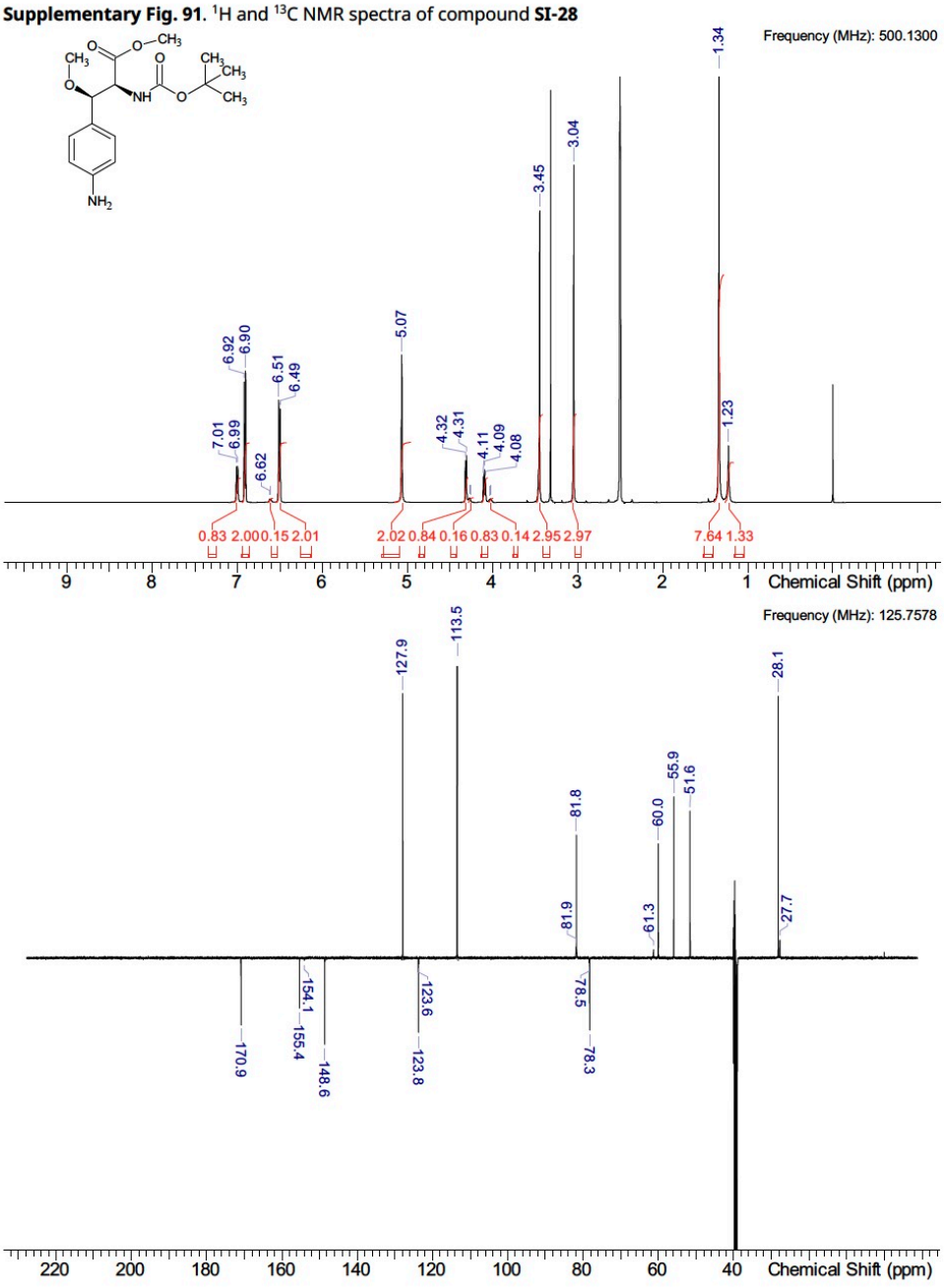

Supplementary Fig. 92. ^{1}H and ^{13}C NMR spectra of compound **SI-29**

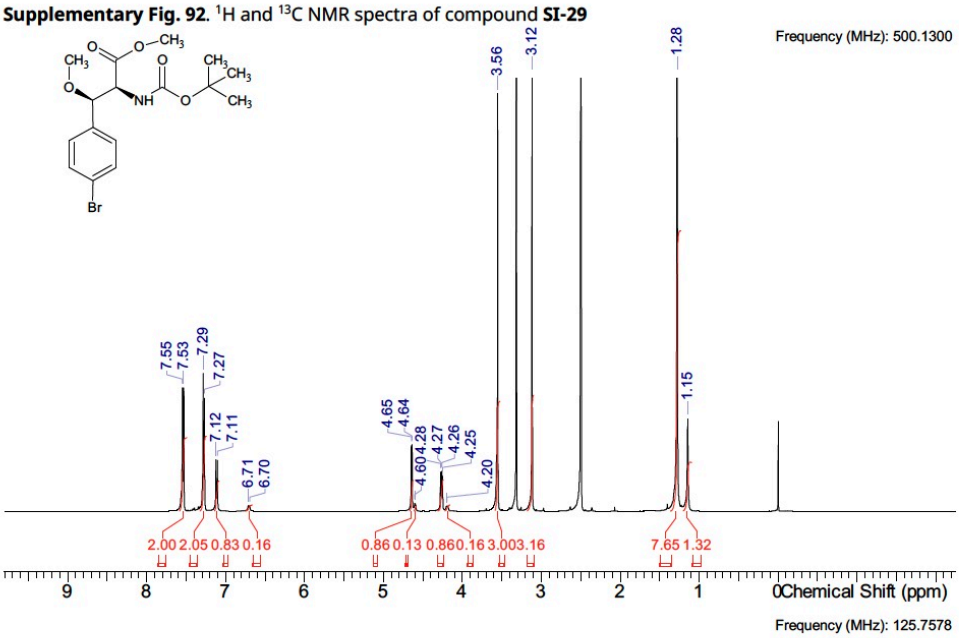

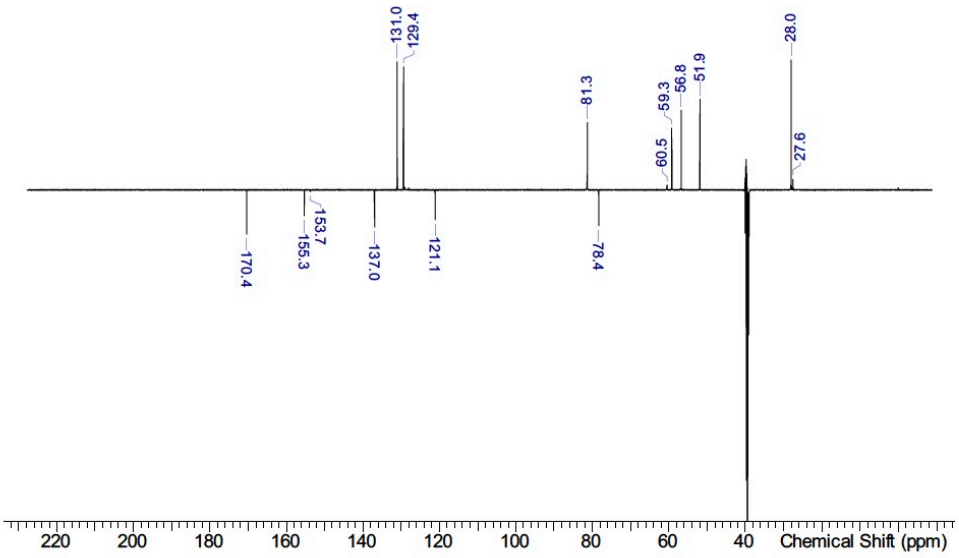

Supplementary Fig. 93. ^{1}H and ^{13}C NMR spectra of compound **SI-30**

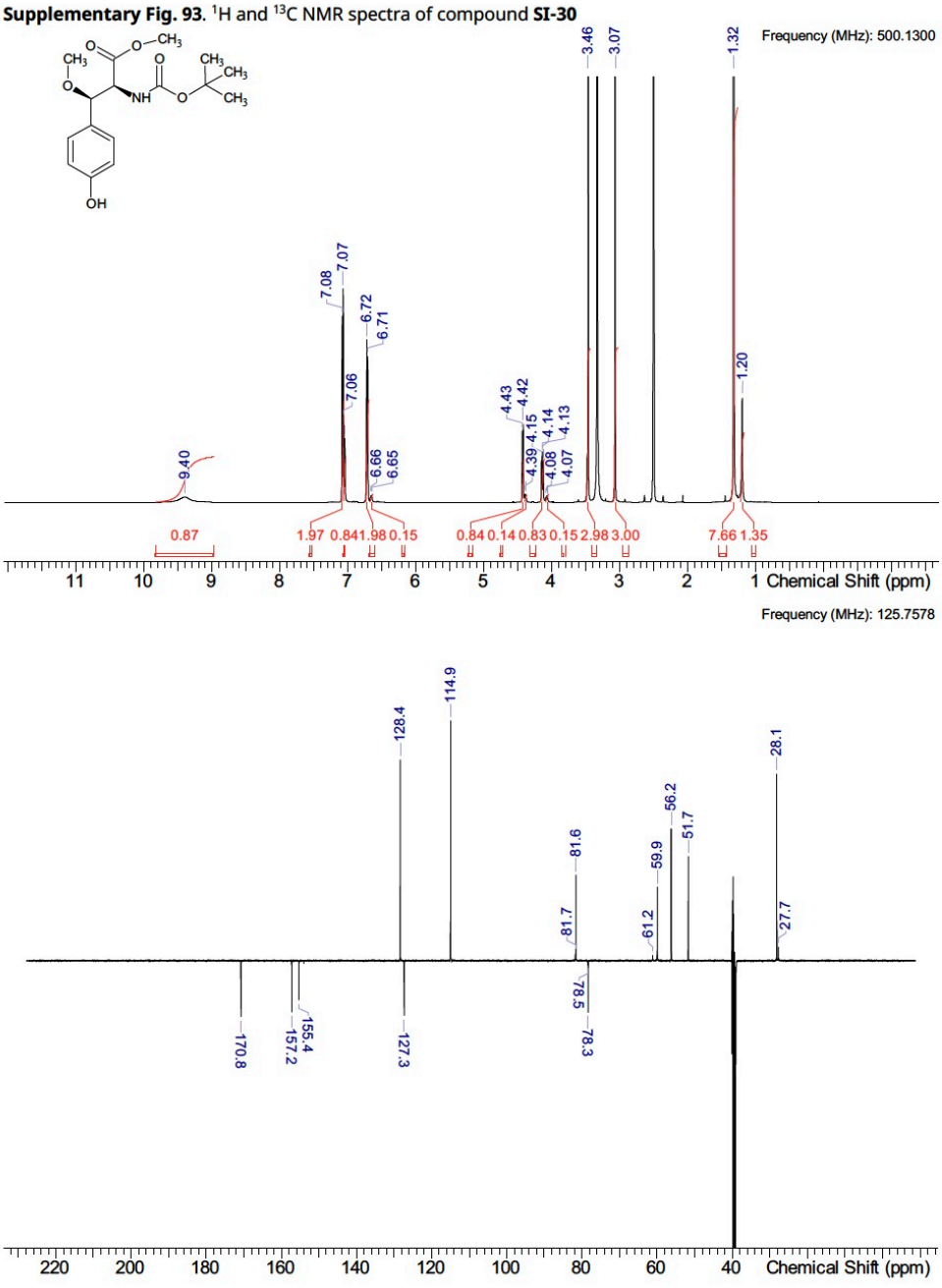

155

Supplementary Fig. 94. ^{1}H and ^{13}C NMR spectra of compound **SI-31**

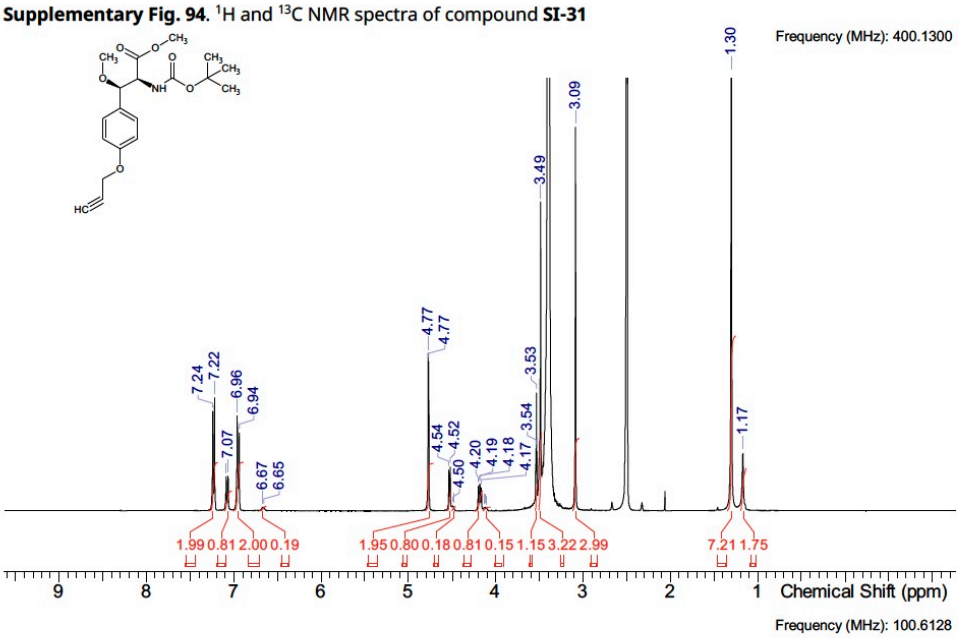

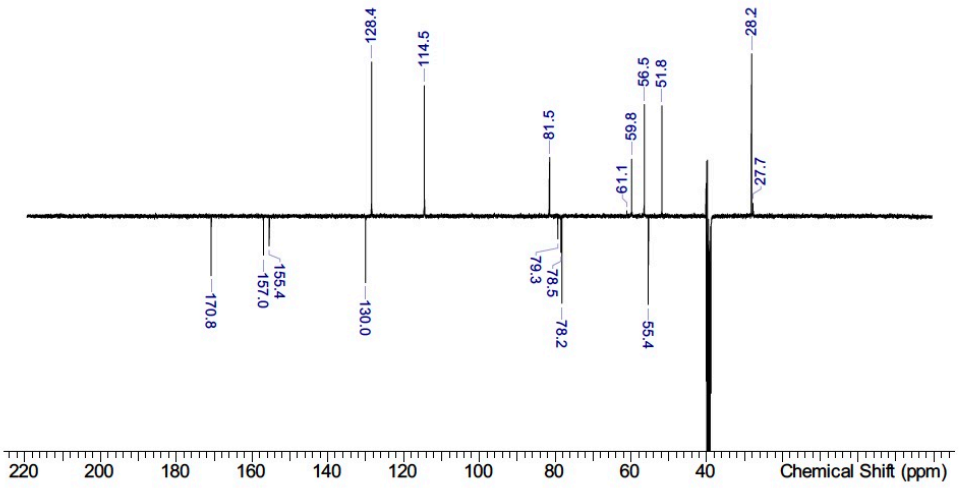

156

Supplementary Fig. 95. ^{1}H and ^{13}C NMR spectra of compound **SI-32**

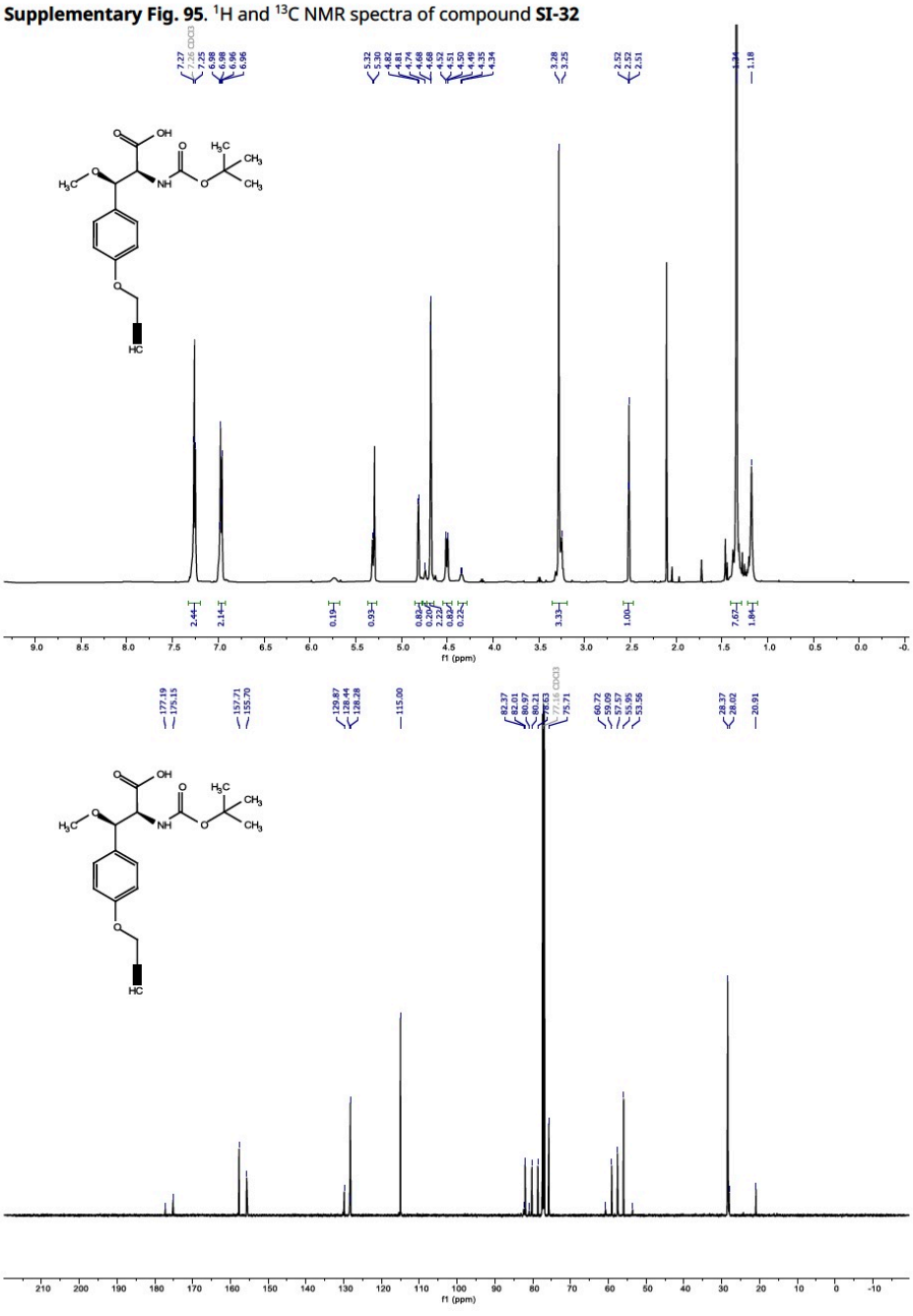

Supplementary Fig. 96. ^{1}H NMR spectrum of compound **SI-33**

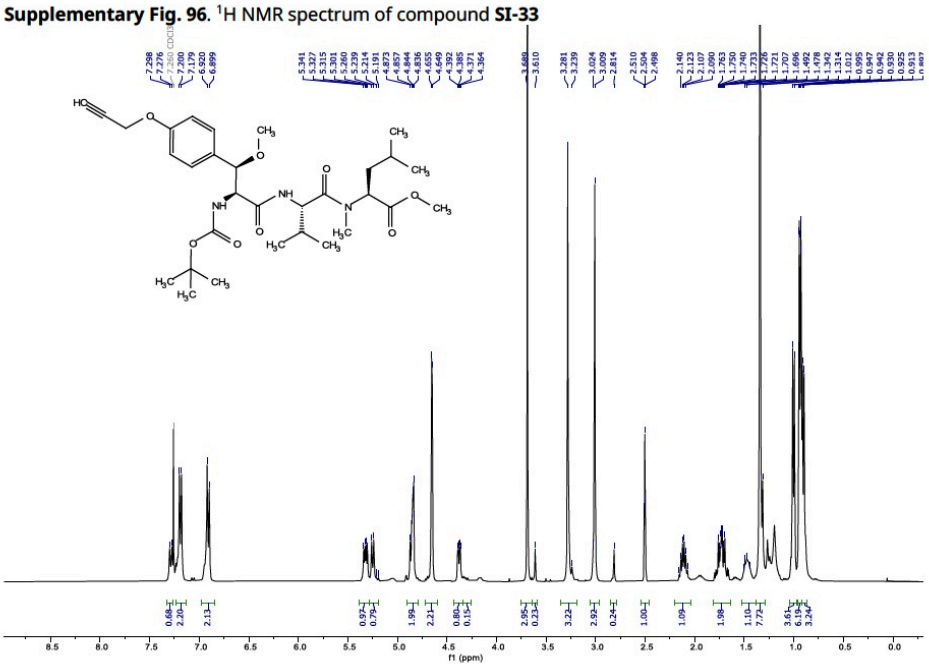

Supplementary Fig. 97. ^{13}C NMR spectrum of compound **SI-33**

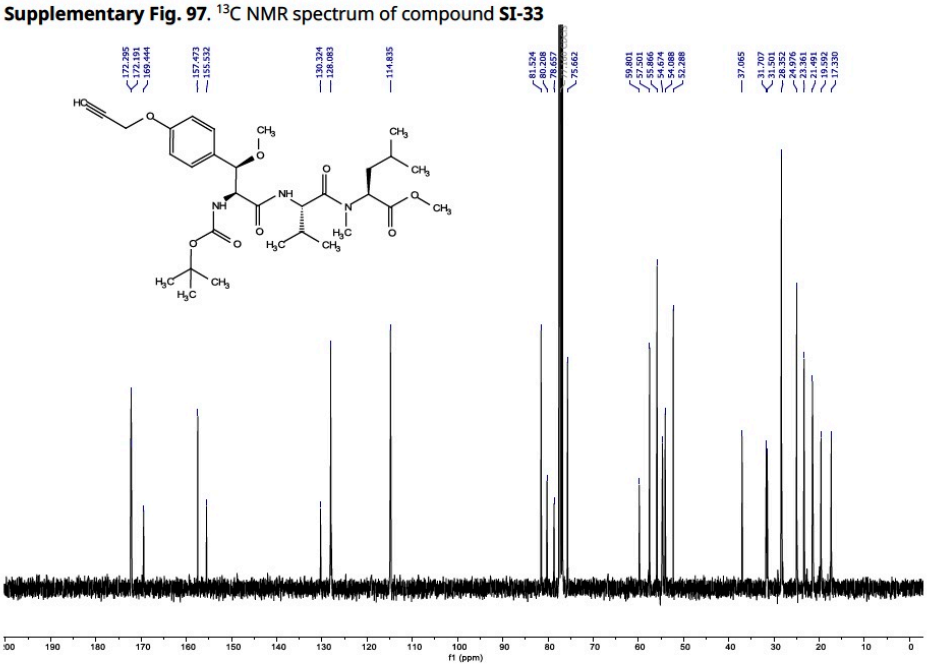

Supplementary Fig. 98. ^{1}H NMR spectrum of compound **SI-34**

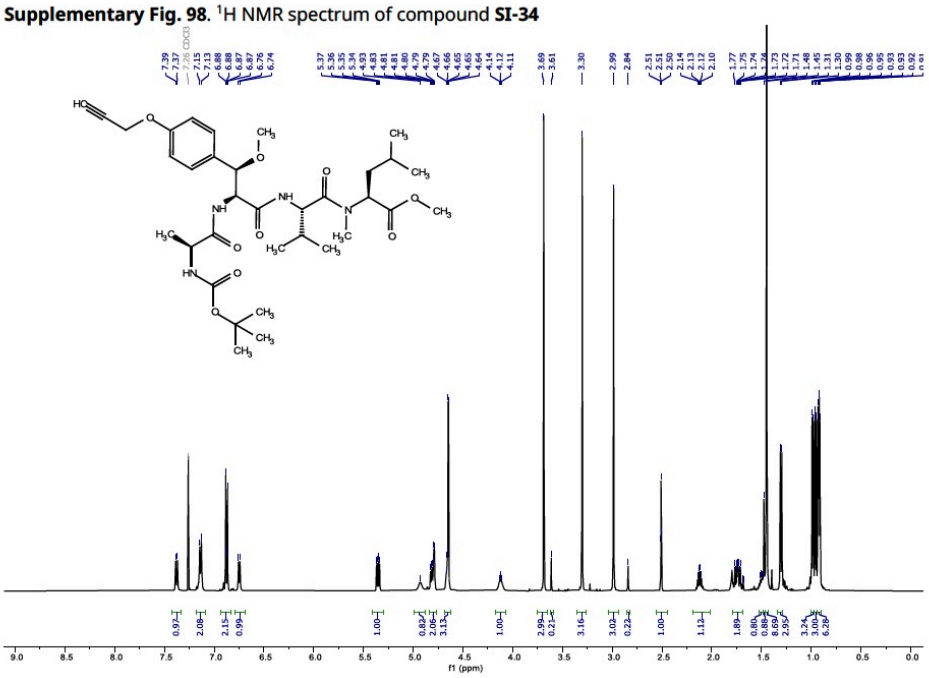

Supplementary Fig. 99. ^{13}C NMR spectrum of compound **SI-34**

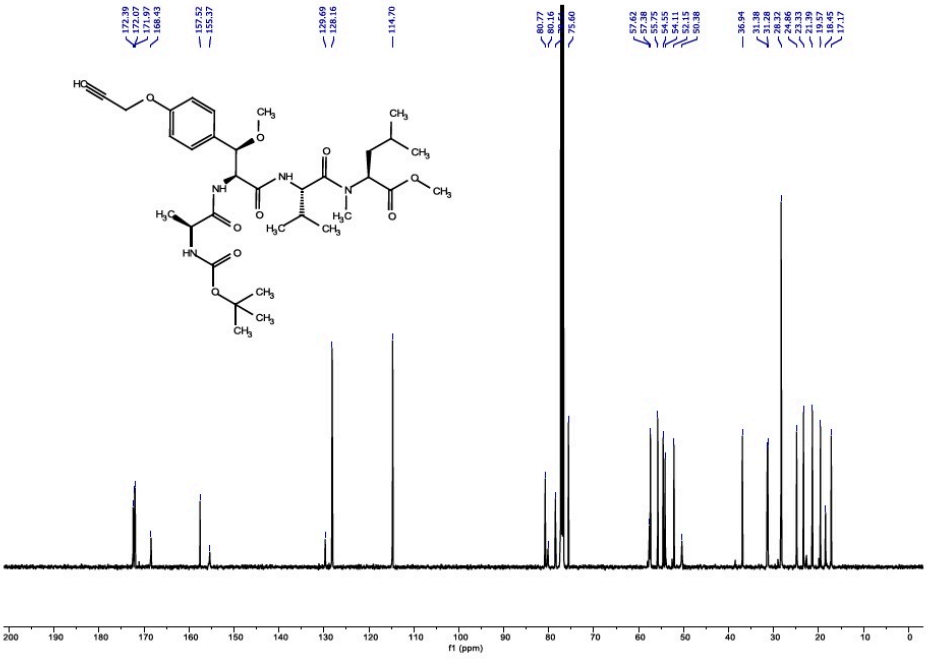

Supplementary Fig. 100. ^{1}H NMR spectrum of compound **SI-35**

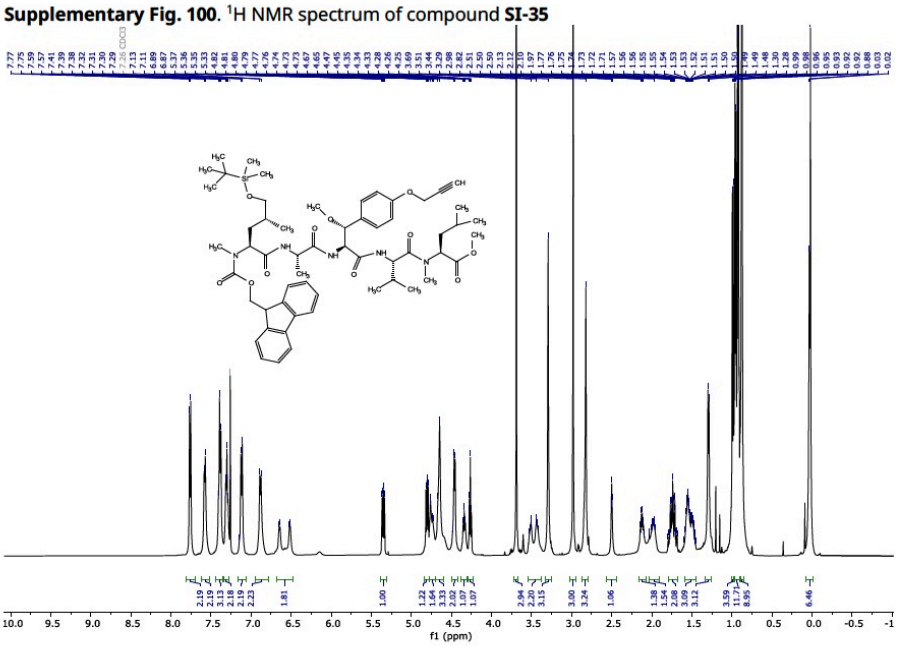

Supplementary Fig. 101. ^{13}C NMR spectrum of compound **SI-35**

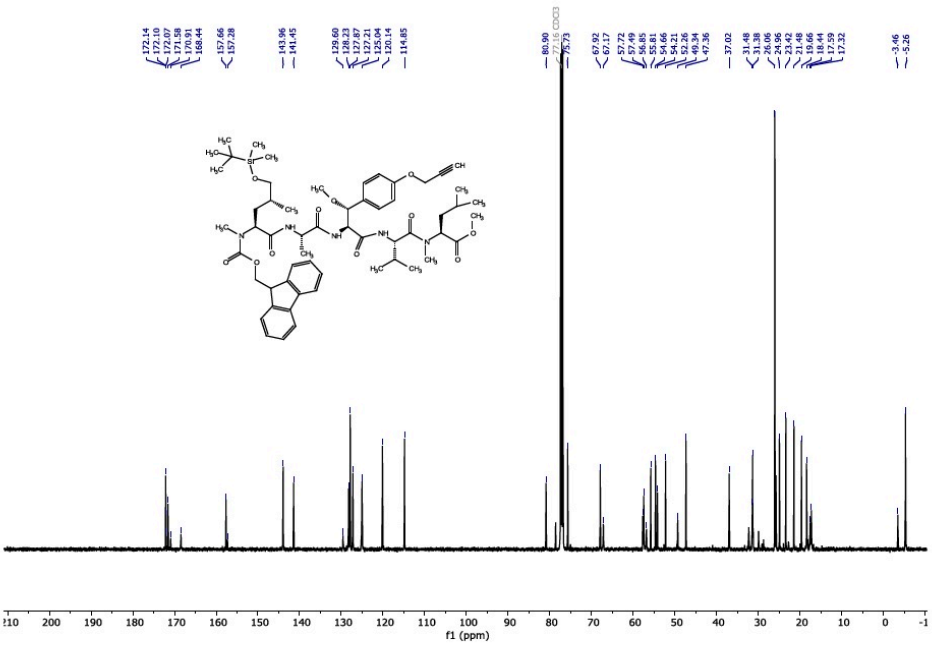

Supplementary Fig. 102. ^{1}H NMR spectrum of compound **SI-36**

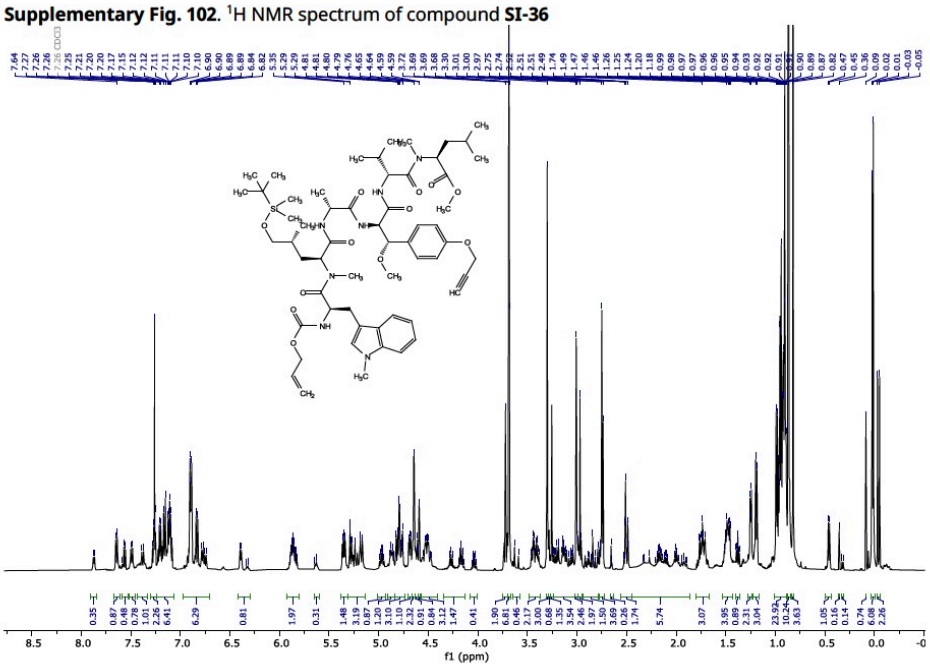

Supplementary Fig. 103. ^{13}C NMR spectrum of compound **SI-36**

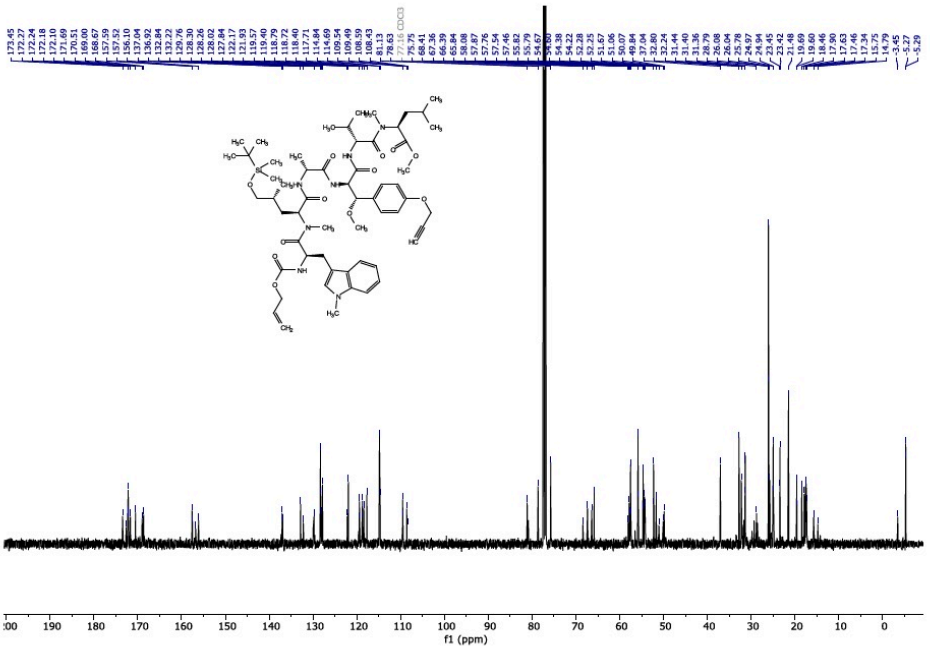

Supplementary Fig. 104. ^{1}H NMR spectrum of compound **SI-37**

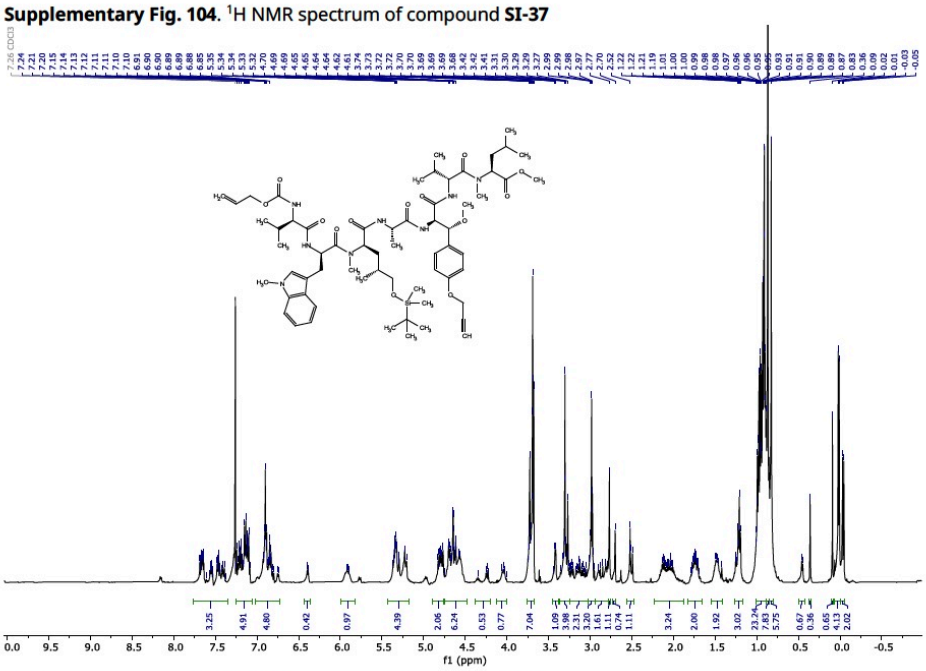

Supplementary Fig. 105. ^{13}C NMR spectrum of compound **SI-37**

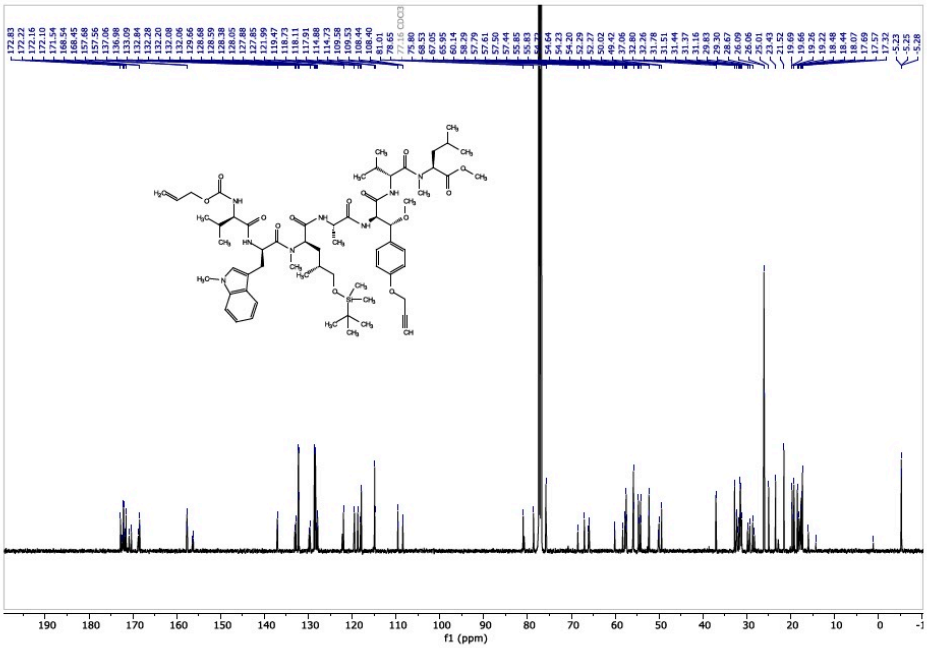

Supplementary Fig. 106. ^{1}H NMR spectrum of compound **SI-38**

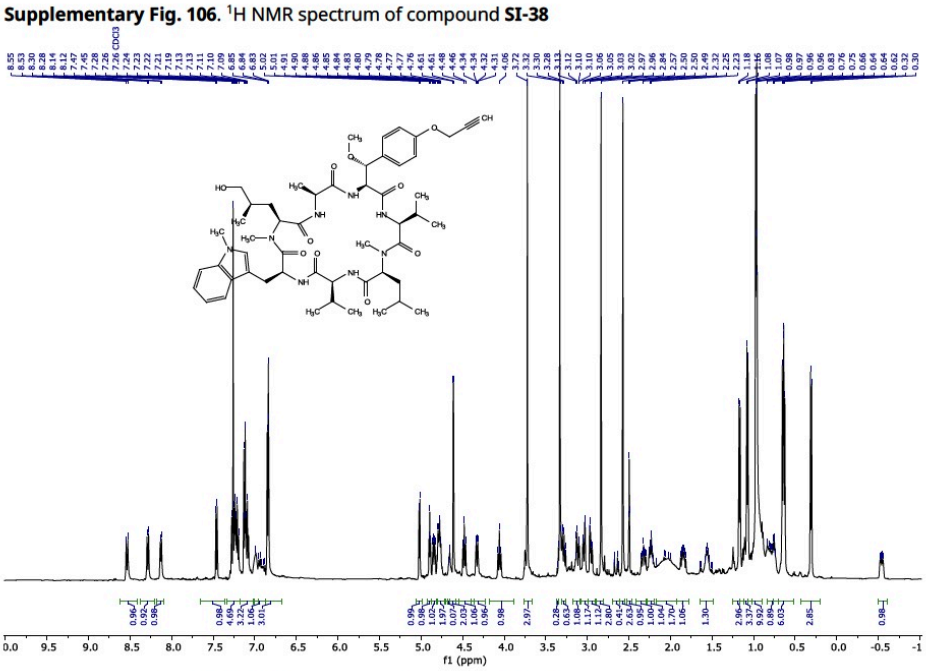

Supplementary Fig. 107. ^{13}C NMR spectrum of compound **SI-38**

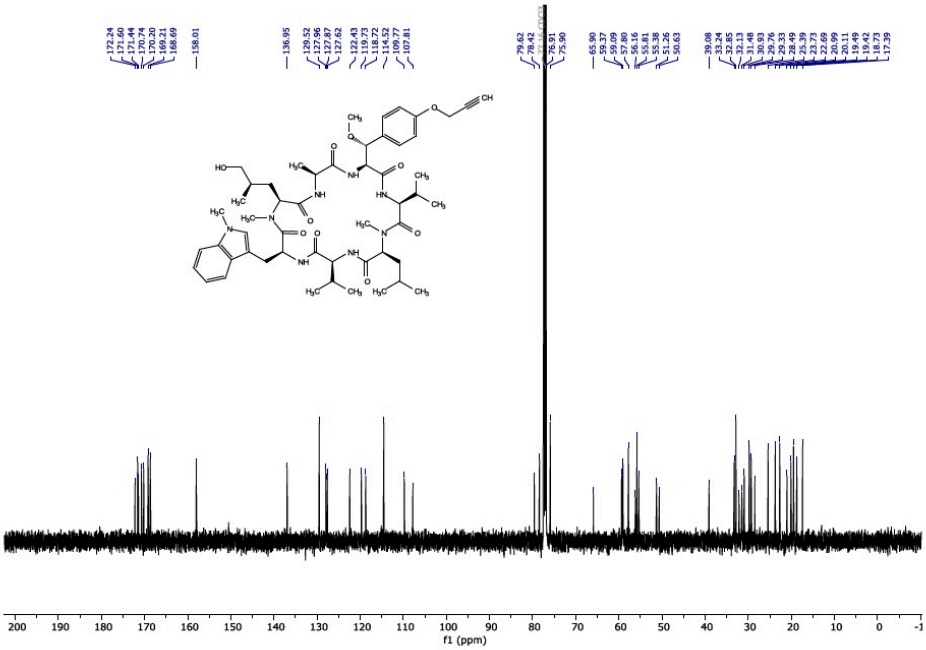

Supplementary Fig. 108. ^{1}H NMR spectrum of compound **SI-39**

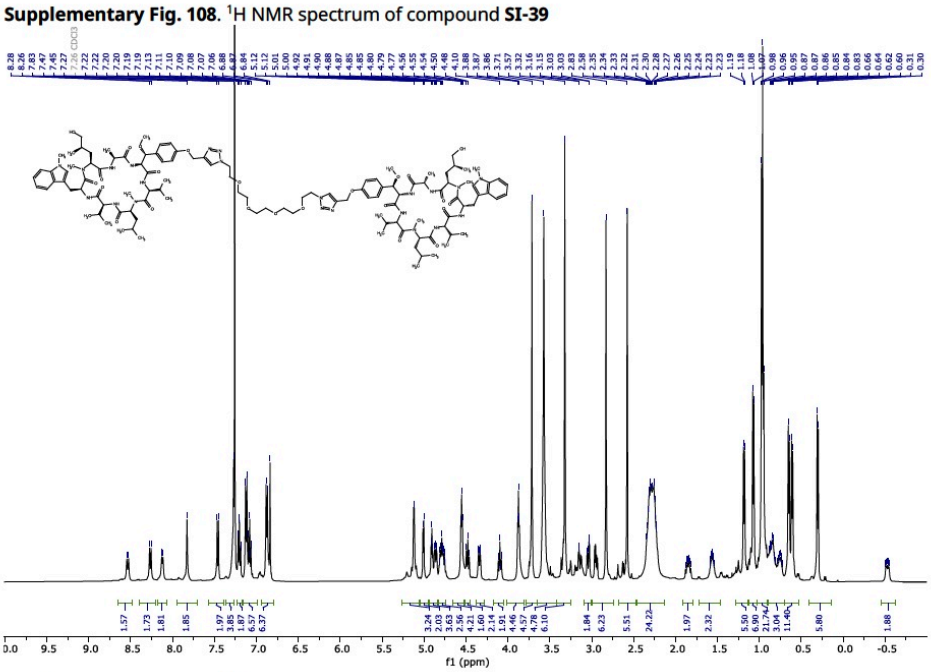

Supplementary Fig. 109. ^{13}C NMR spectrum of compound **SI-39**

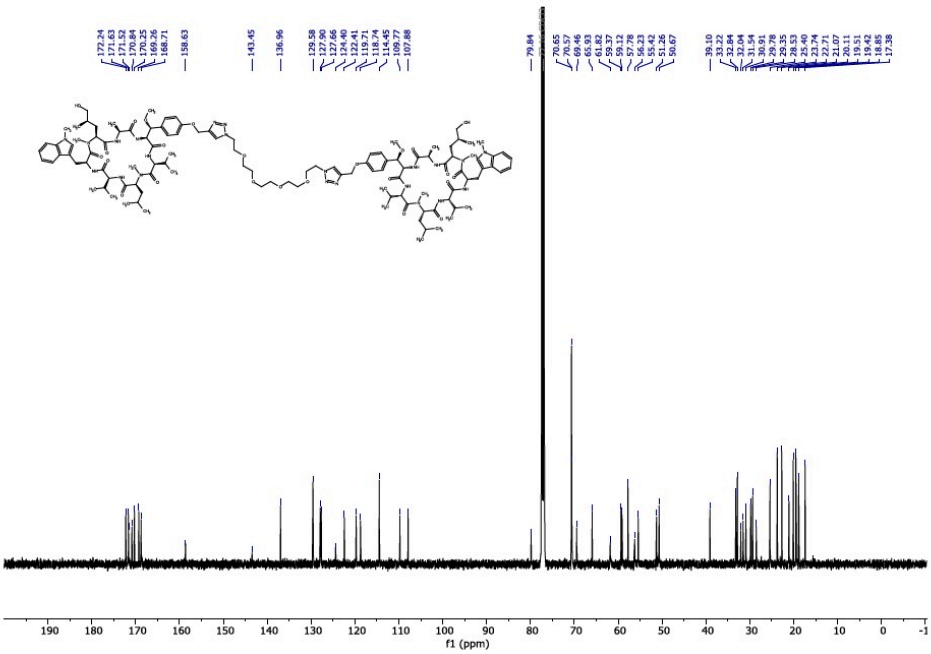

Supplementary Fig. 110. ^{1}H NMR spectrum of compound **SI-40**

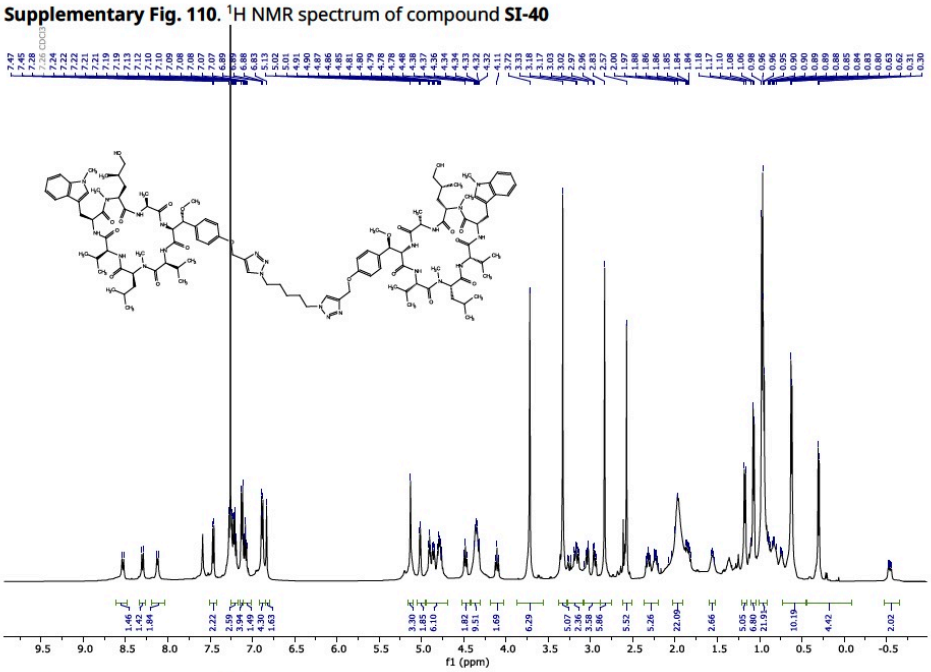

Supplementary Fig. 111. ^{13}C NMR spectrum of compound **SI-40**

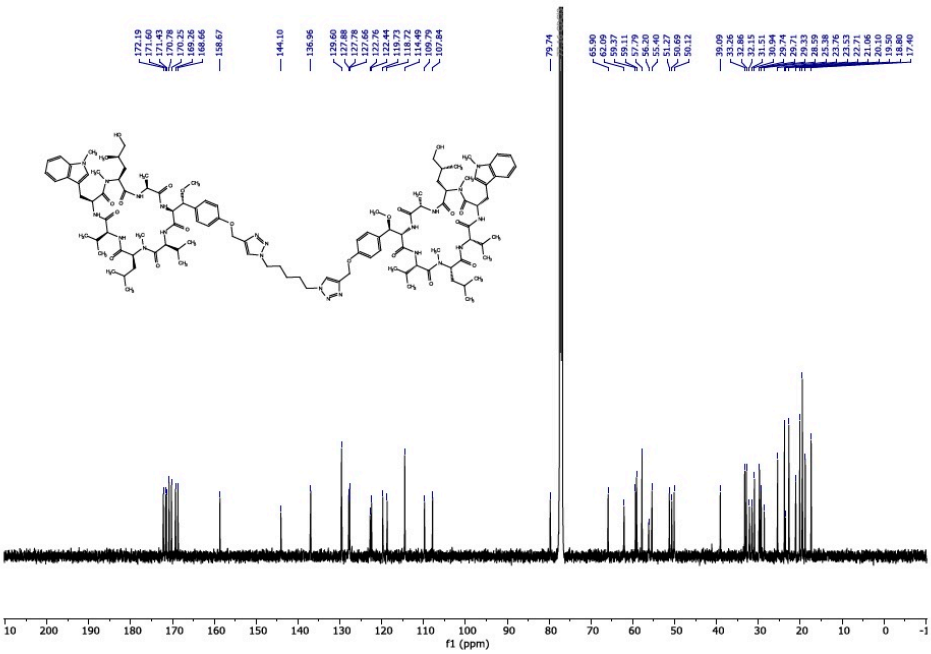

Supplementary Fig. 112. ^{1}H NMR spectrum of compound **SI-41**

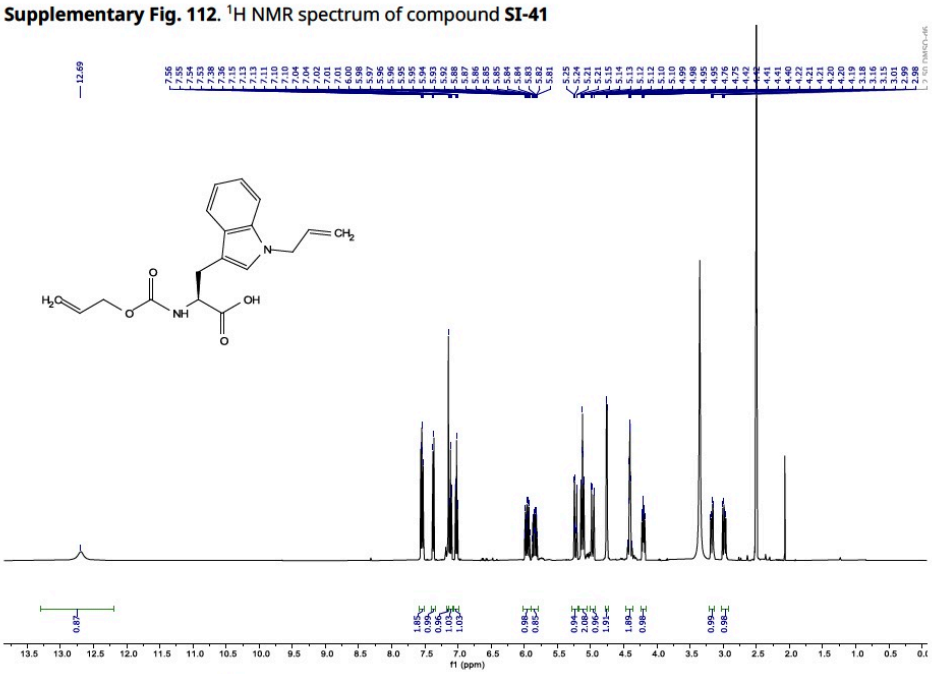

Supplementary Fig. 113. ^{13}C NMR spectrum of compound **SI-41**

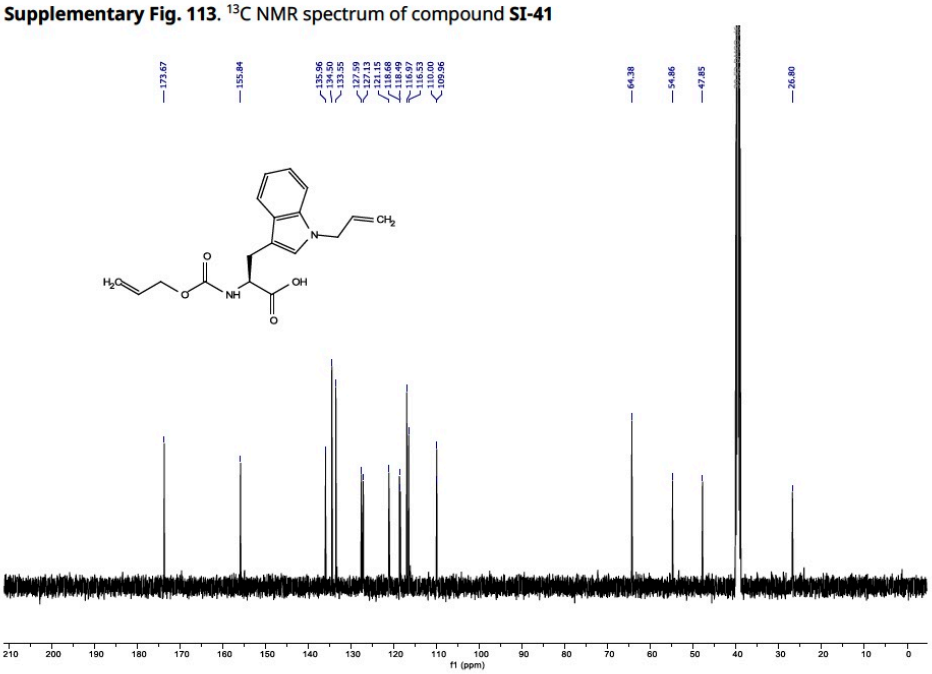

Supplementary Fig. 114. ^{1}H NMR spectrum of compound **SI-42**

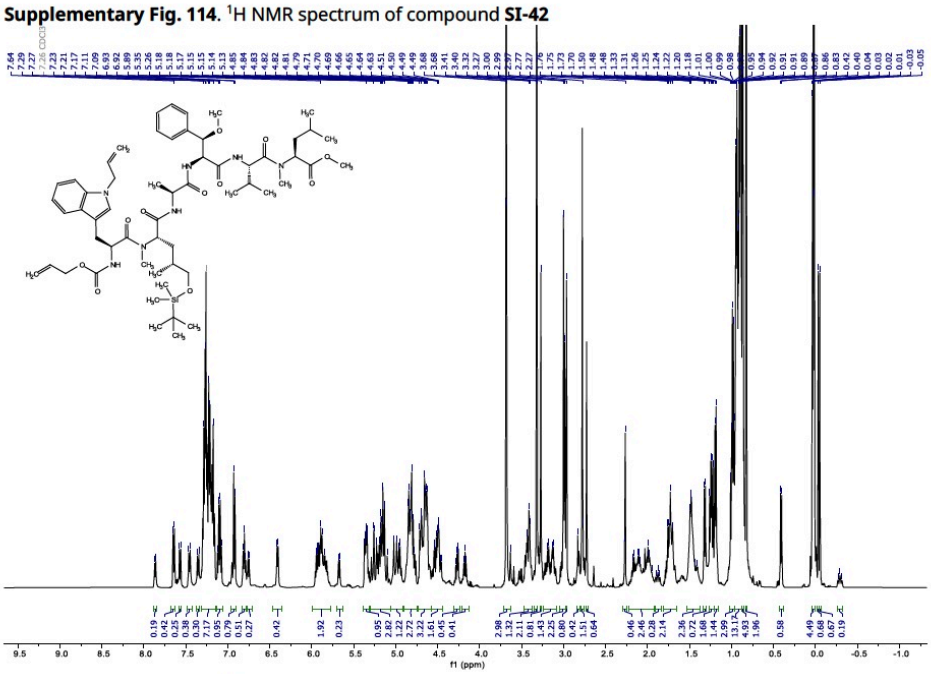

Supplementary Fig. 114. ^{13}C NMR spectrum of compound **SI-42**

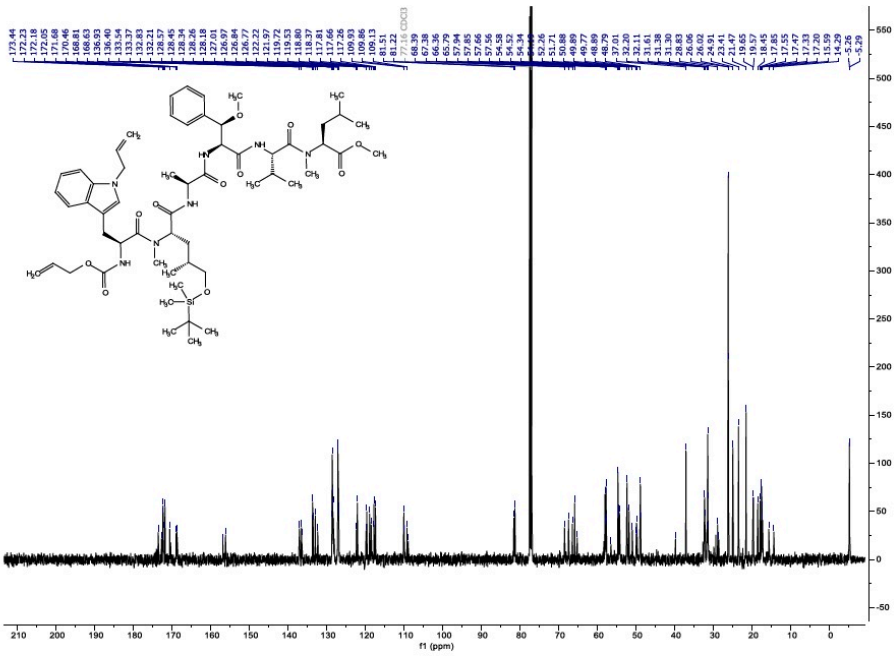

Supplementary Fig. 115. ^{1}H NMR spectrum of compound **SI-43**

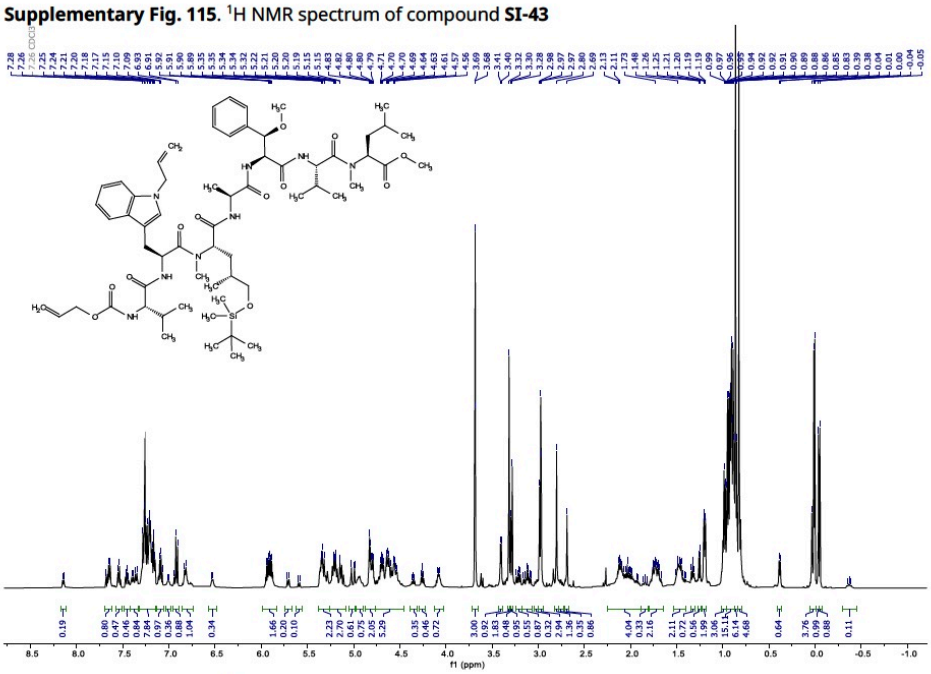

Supplementary Fig. 116. ^{13}C NMR spectrum of compound **SI-43**

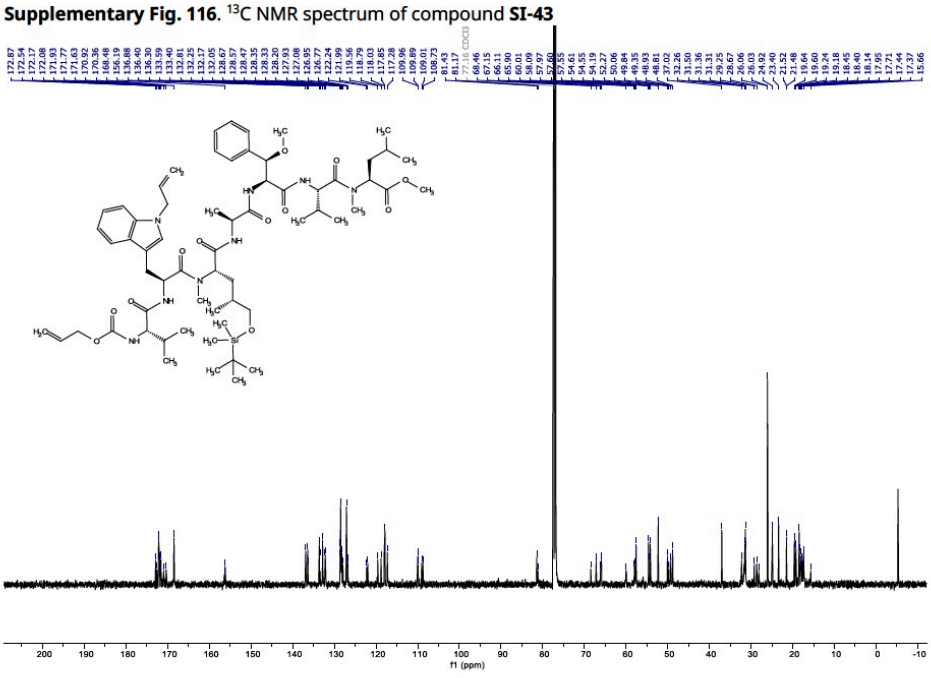

Supplementary Fig. 117. ^{1}H NMR spectrum of compound **13**

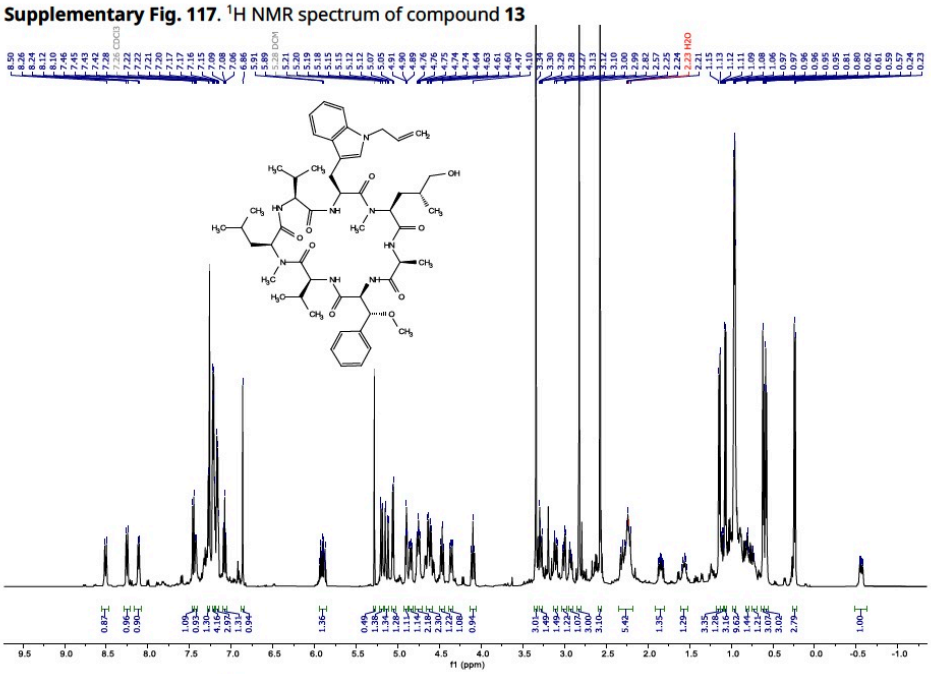

Supplementary Fig. 118. ^{13}C NMR spectrum of compound **13**

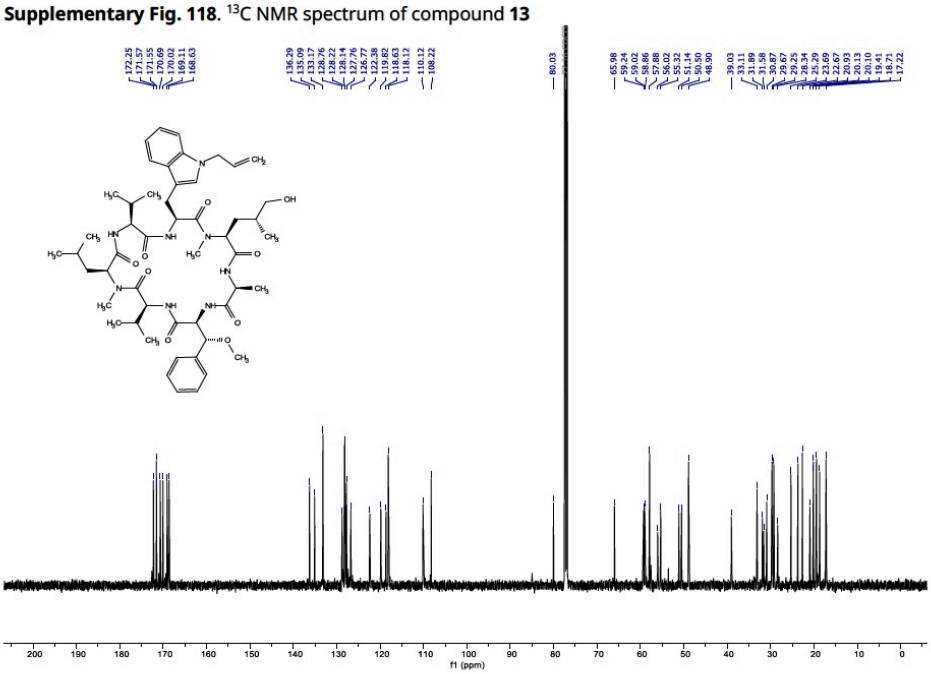

Supplementary Fig. 119. ^{1}H NMR spectrum of compound **15**

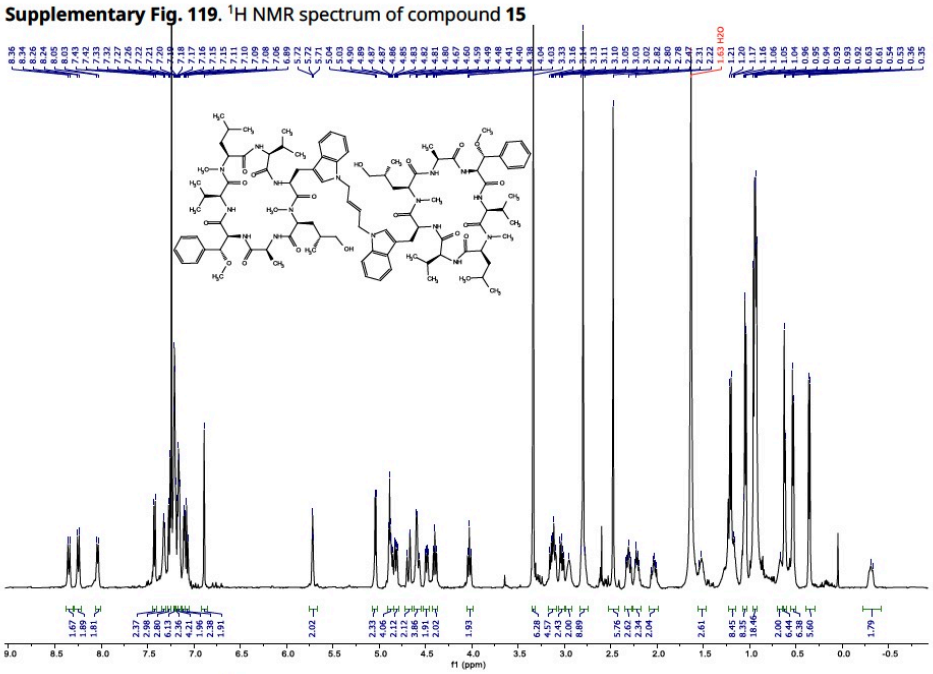

Supplementary Fig. 120. ^{13}C NMR spectrum of compound **15**

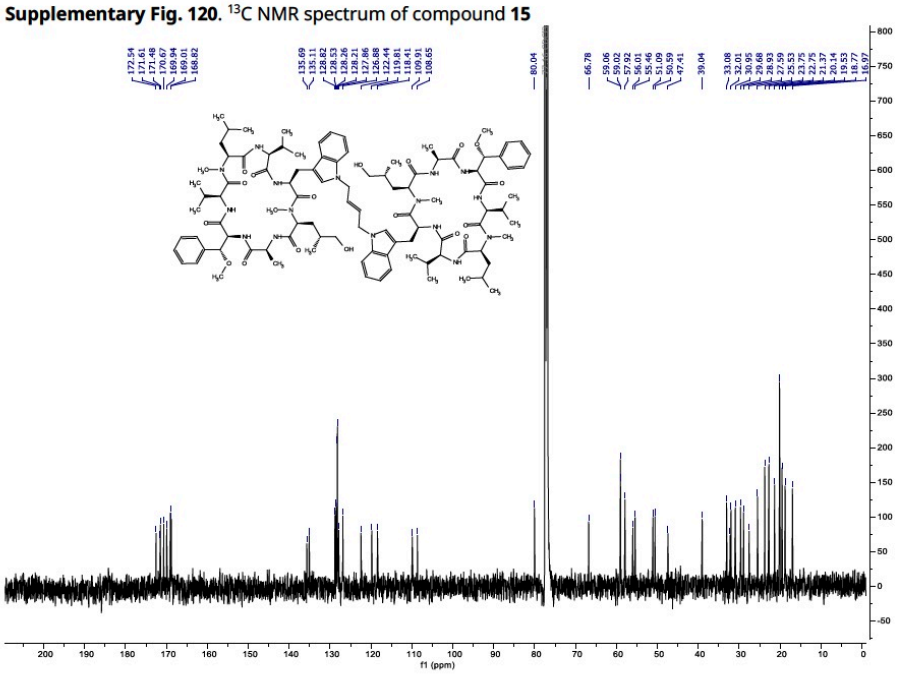

Supplementary Fig. 121. ^{1}H NMR spectrum of compound **16**

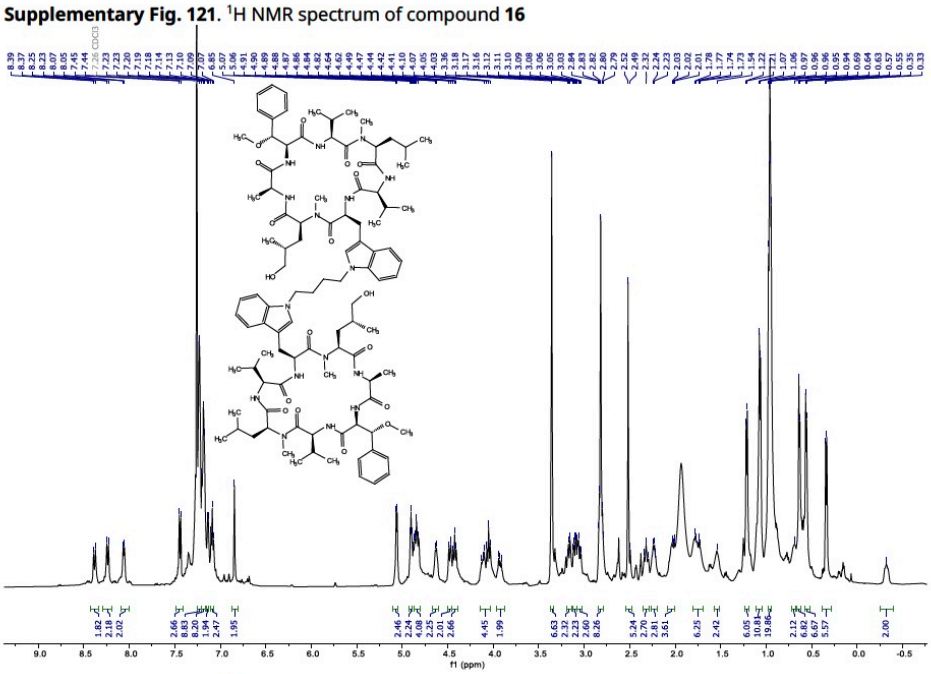

Supplementary Fig. 122. ^{13}C NMR spectrum of compound **16**

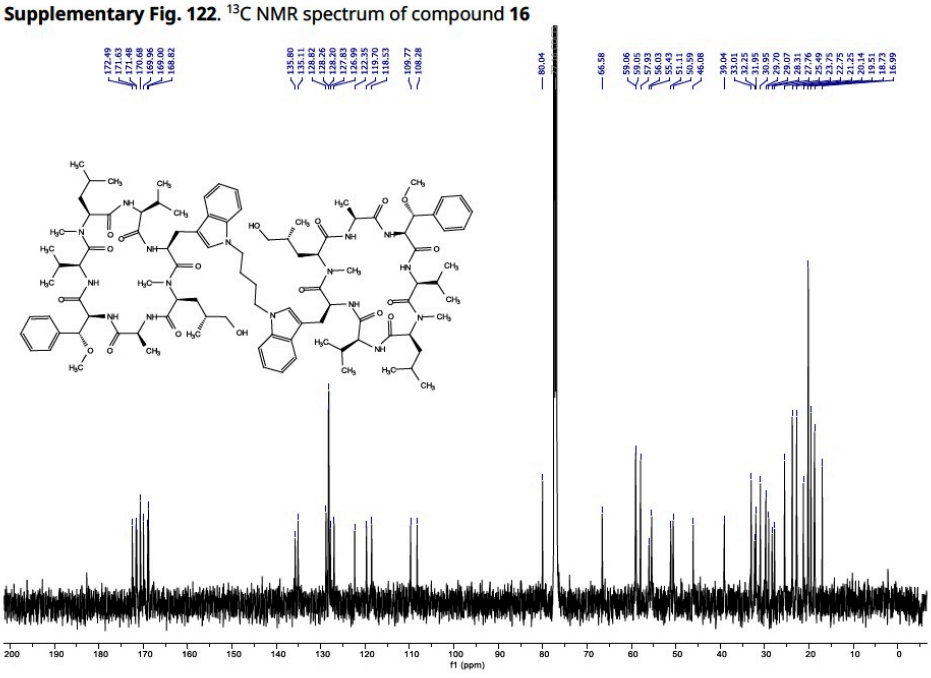

Supplementary Fig. 123. ^{1}H and ^{13}C NMR spectra of compound **SI-44**

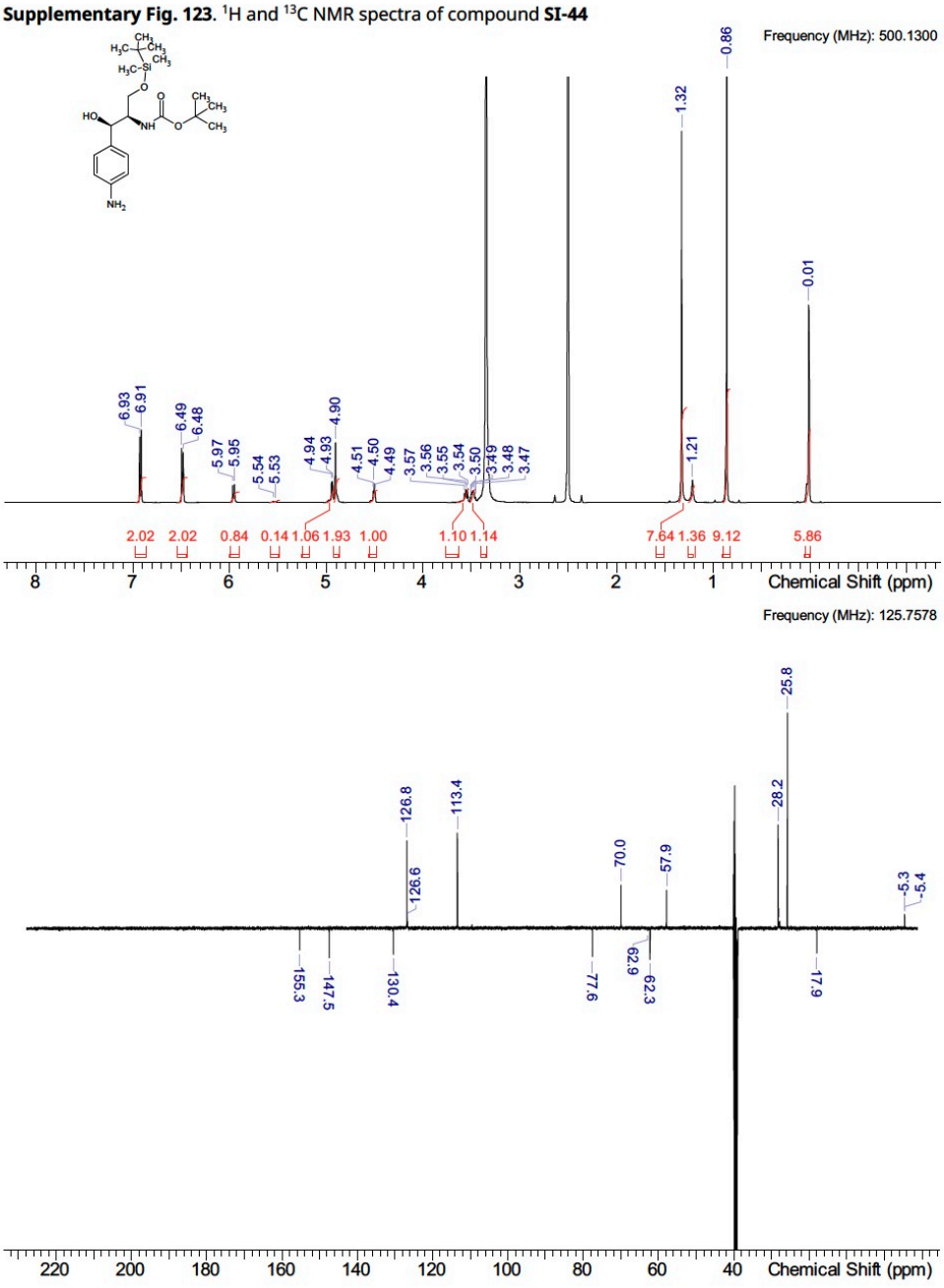

Supplementary Fig. 124. ^{1}H and ^{13}C NMR spectra of compound **SI-45**

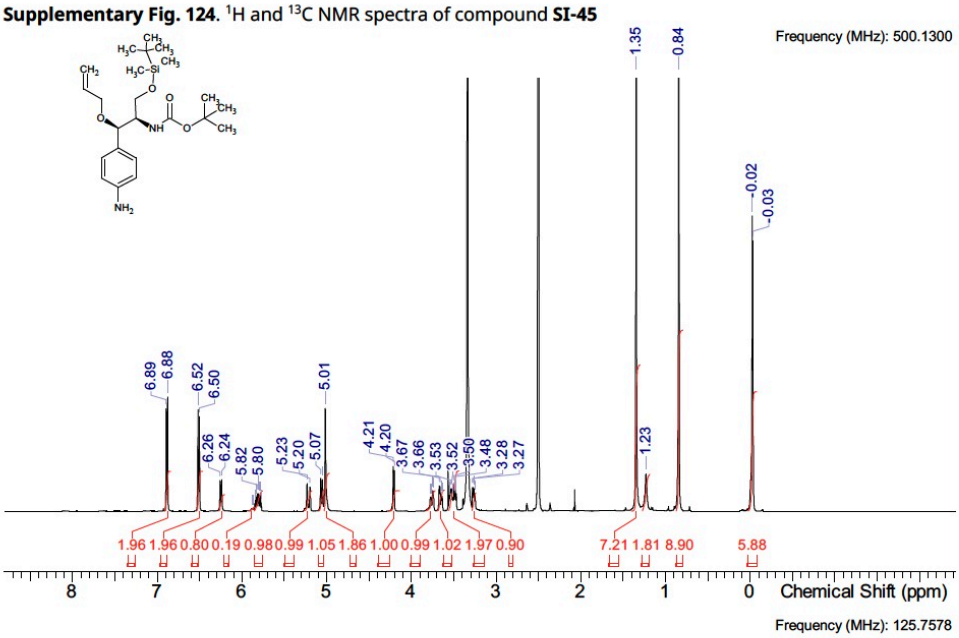

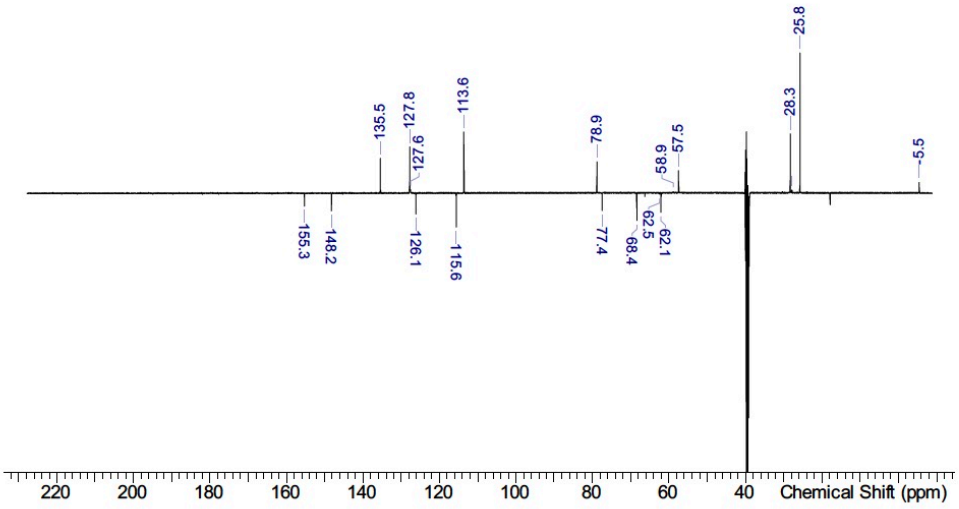

Supplementary Fig. 125. ^{1}H and ^{13}C NMR spectra of compound **SI-46**

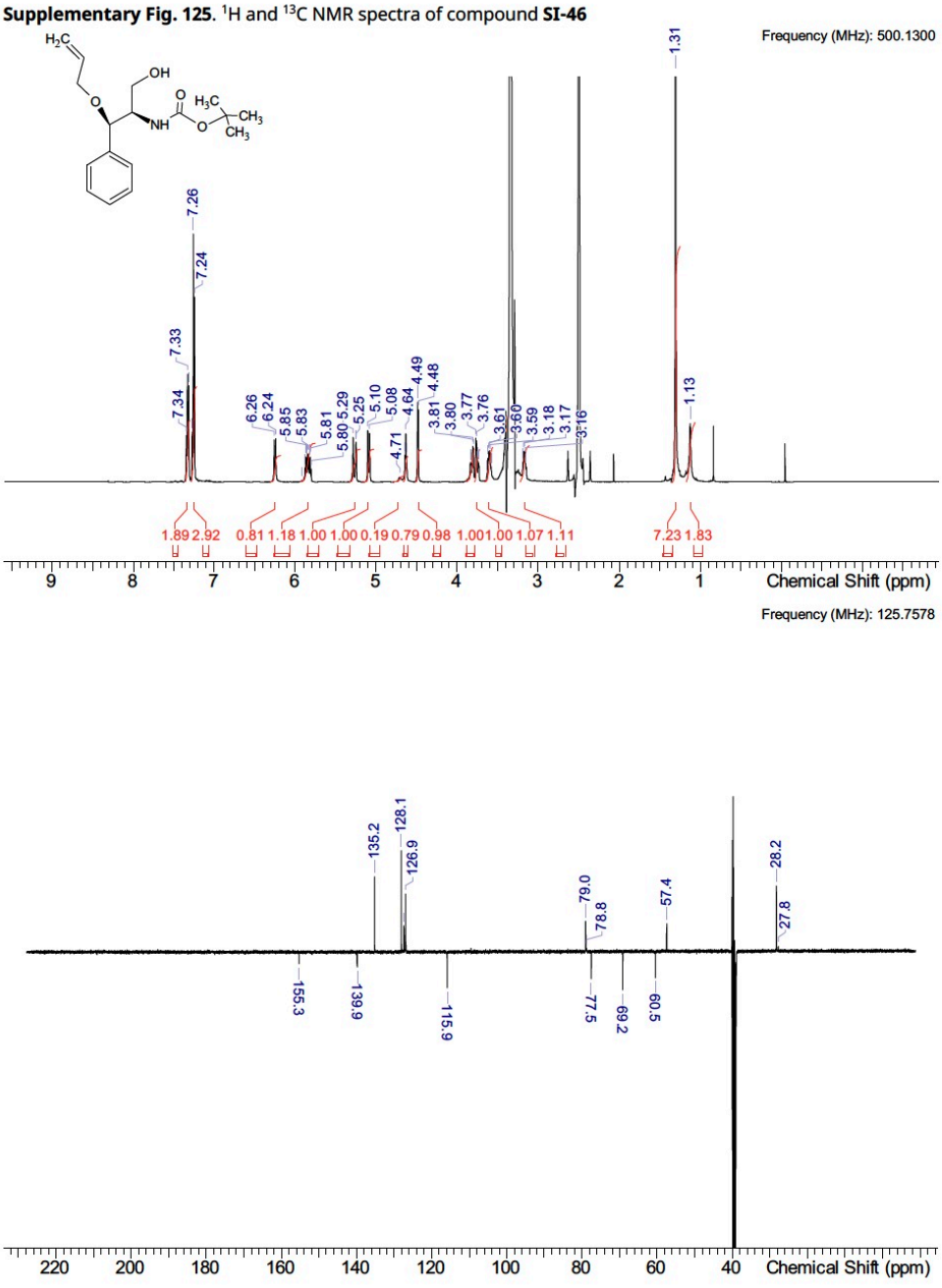

Supplementary Fig. 126. ^{1}H NMR spectrum of compound **SI-47**

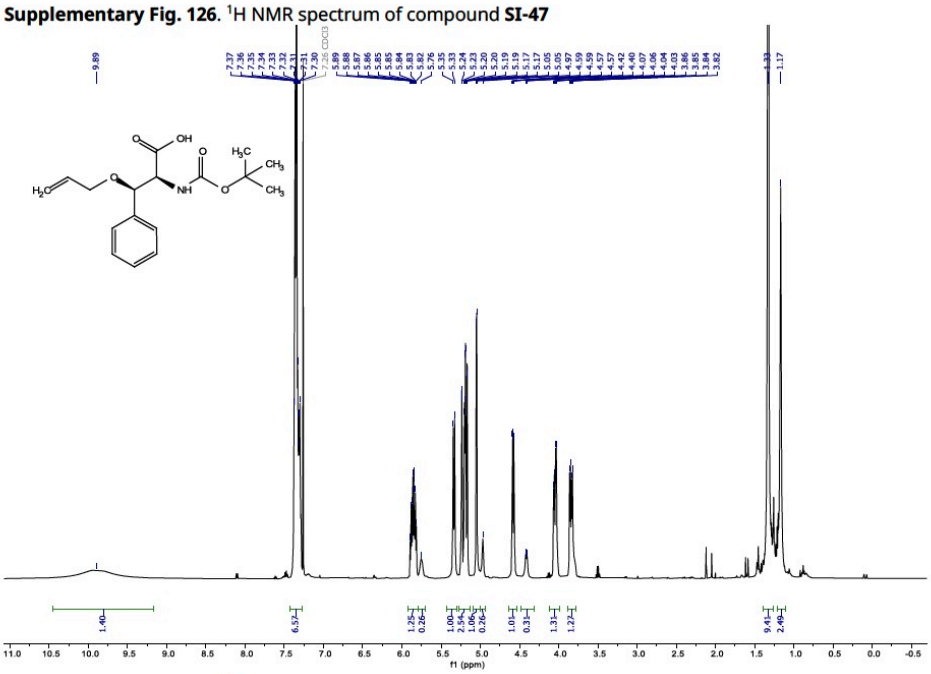

Supplementary Fig. 127. ^{13}C NMR spectrum of compound **SI-47**

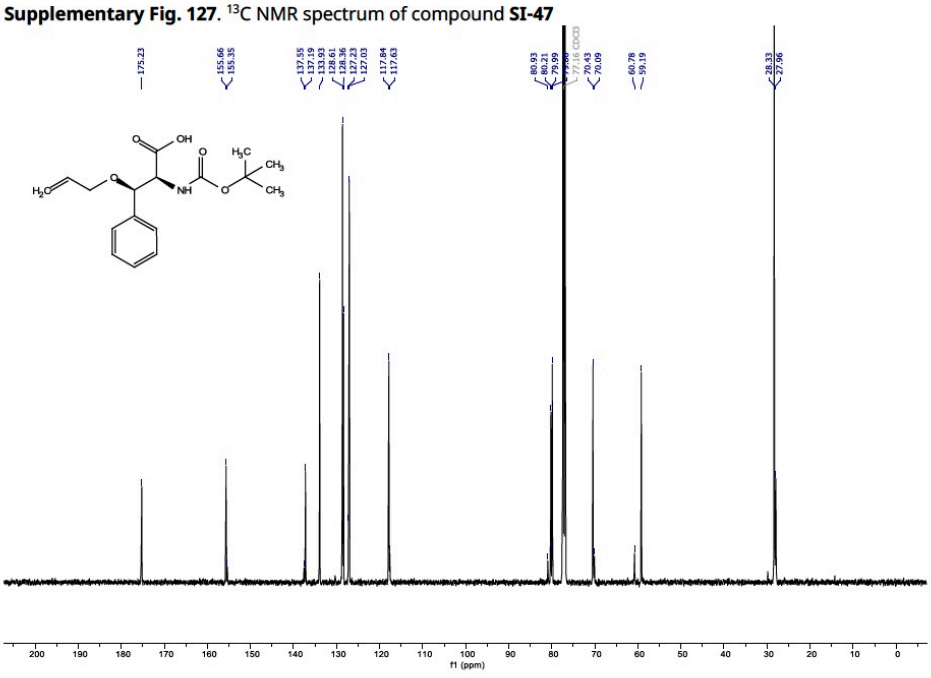

Supplementary Fig. 128. ^{1}H NMR spectrum of compound **SI-48**

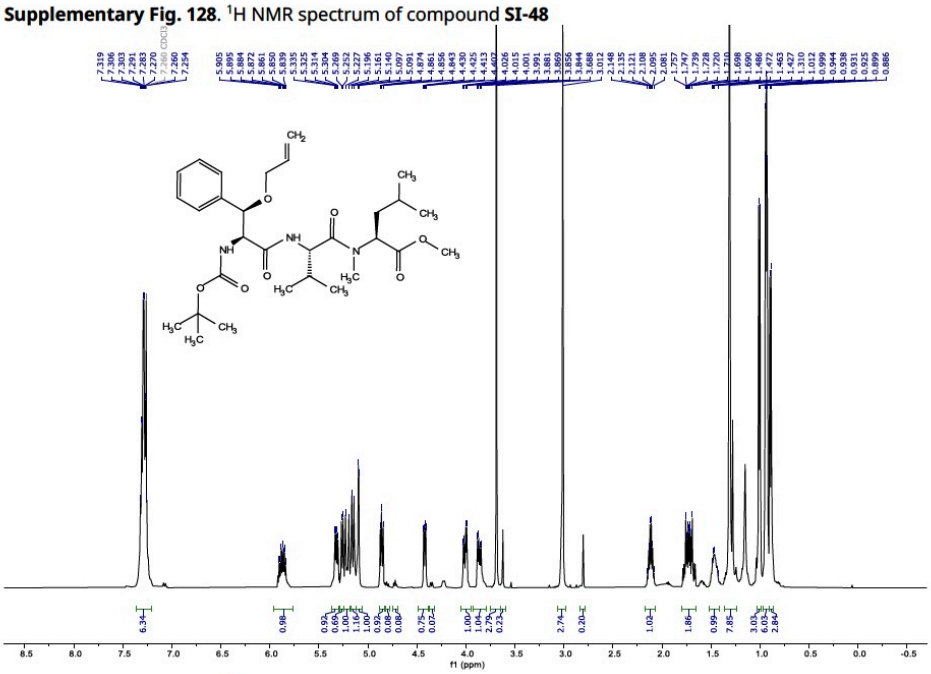

Supplementary Fig. 129. ^{13}C NMR spectrum of compound **SI-48**

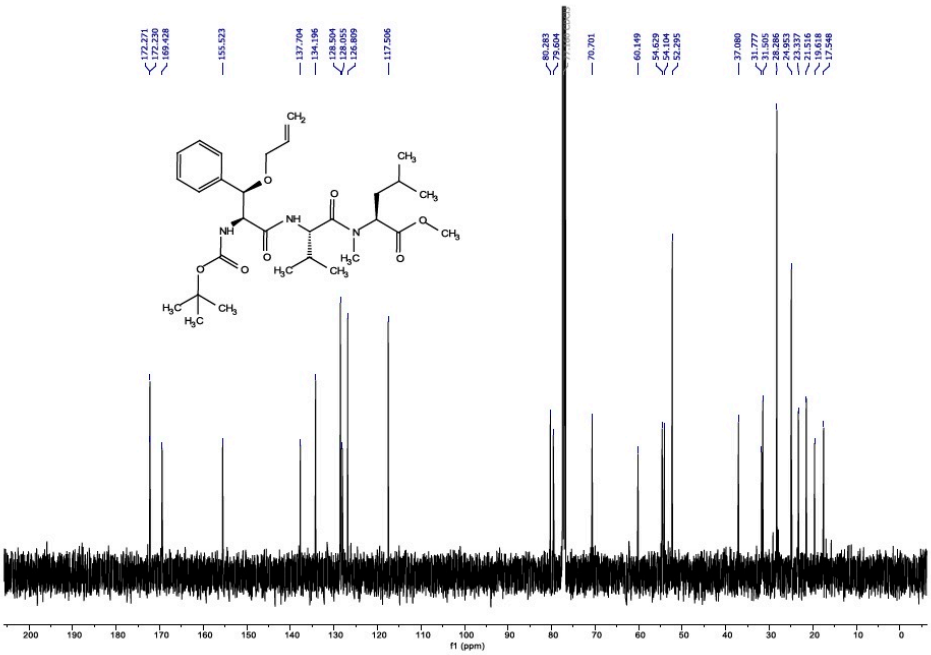

Supplementary Fig. 130. ^{1}H NMR spectrum of compound **SI-49**

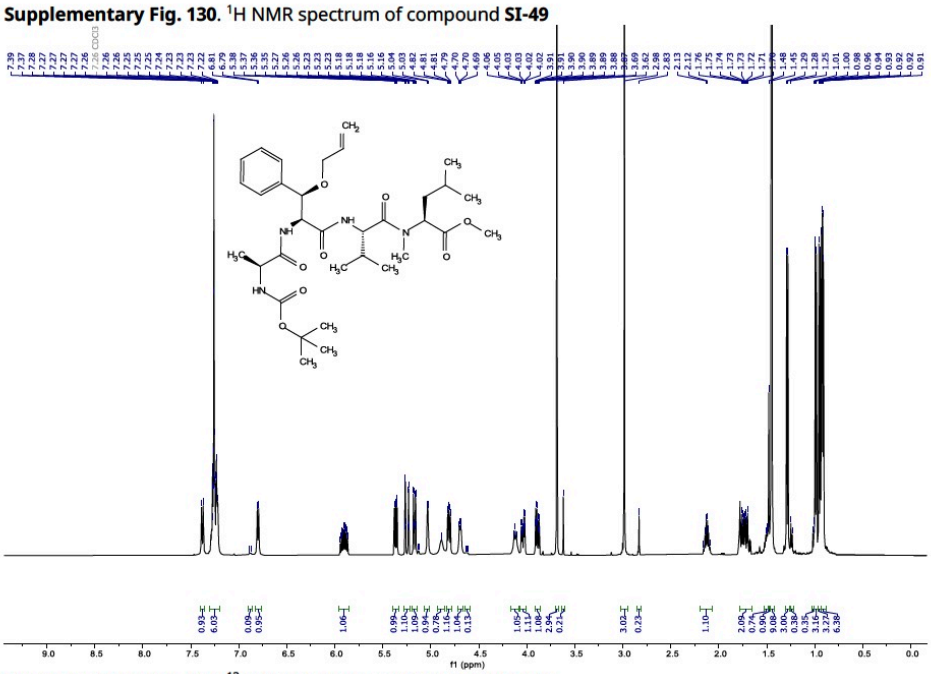

Supplementary Fig. 131. ^{13}C NMR spectrum of compound **SI-49**

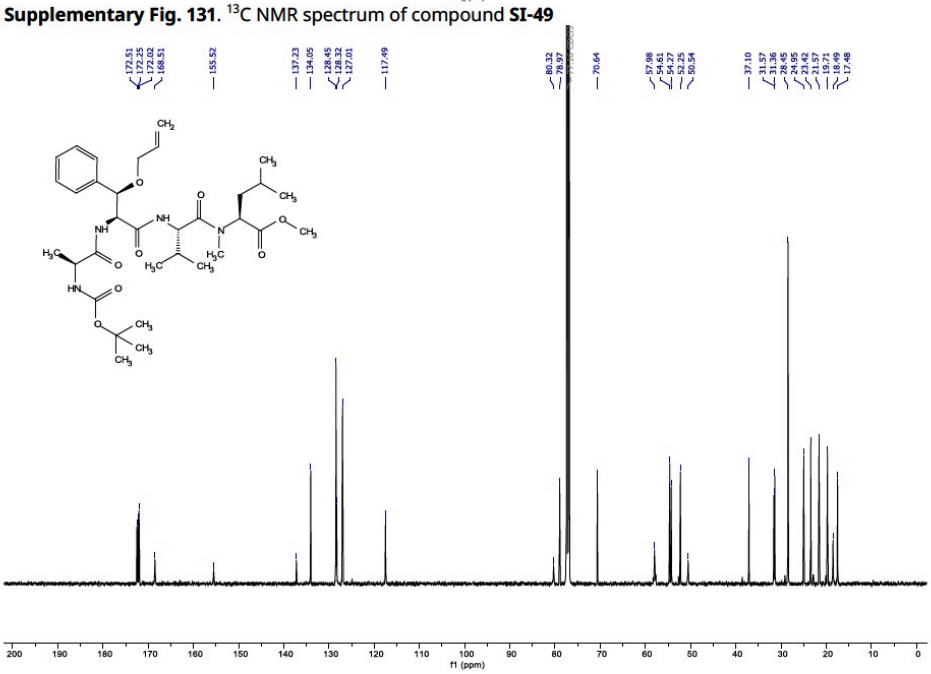

Supplementary Fig. 132. ^{1}H NMR spectrum of compound **SI-50**

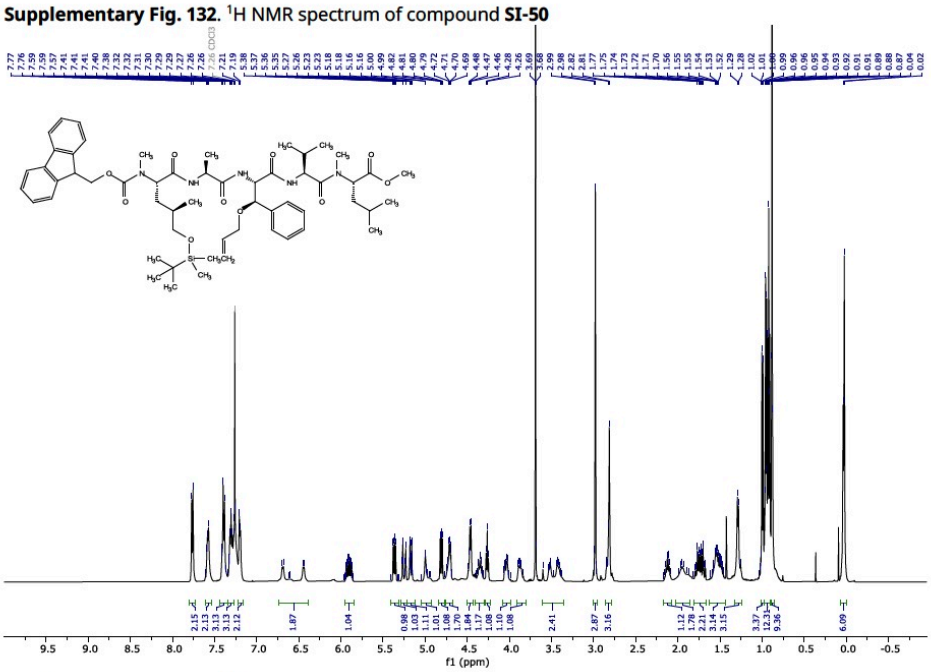

Supplementary Fig. 133. ^{13}C NMR spectrum of compound **SI-50**

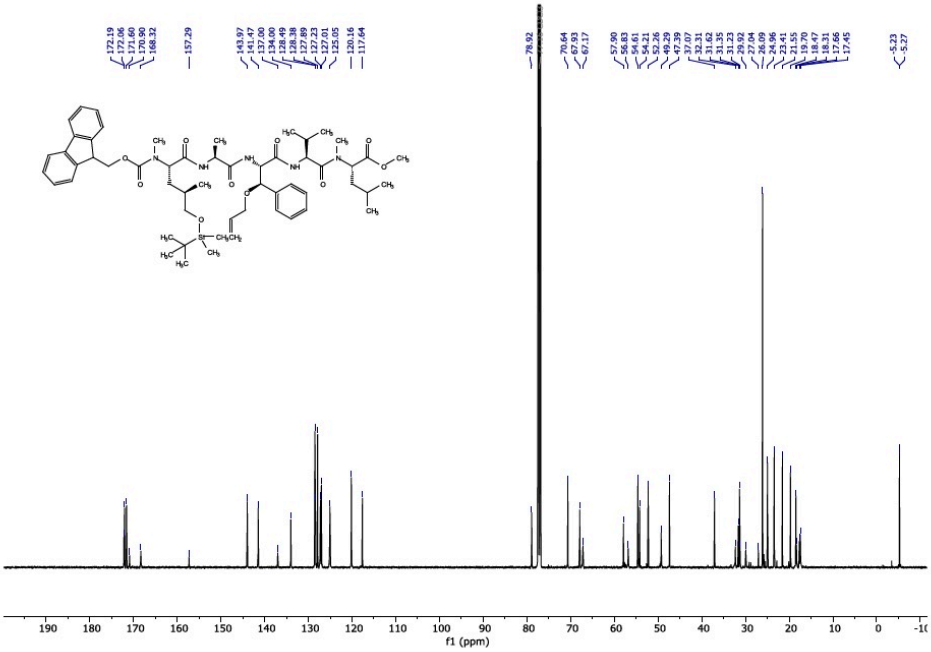

Supplementary Fig. 134. ^{1}H NMR spectrum of compound **SI-51**

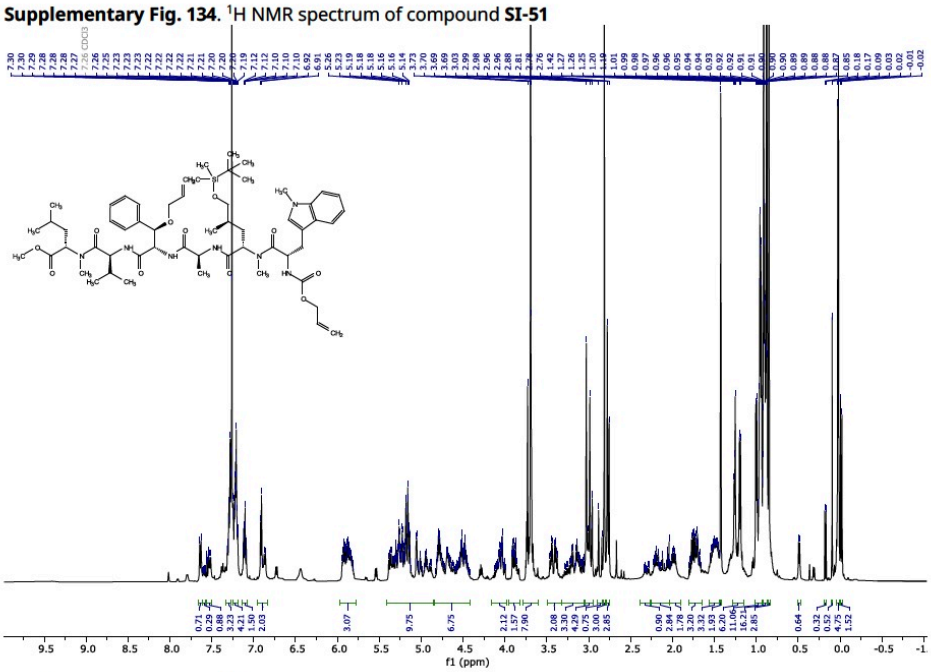

Supplementary Fig. 135. ^{13}C NMR spectrum of compound **SI-51**

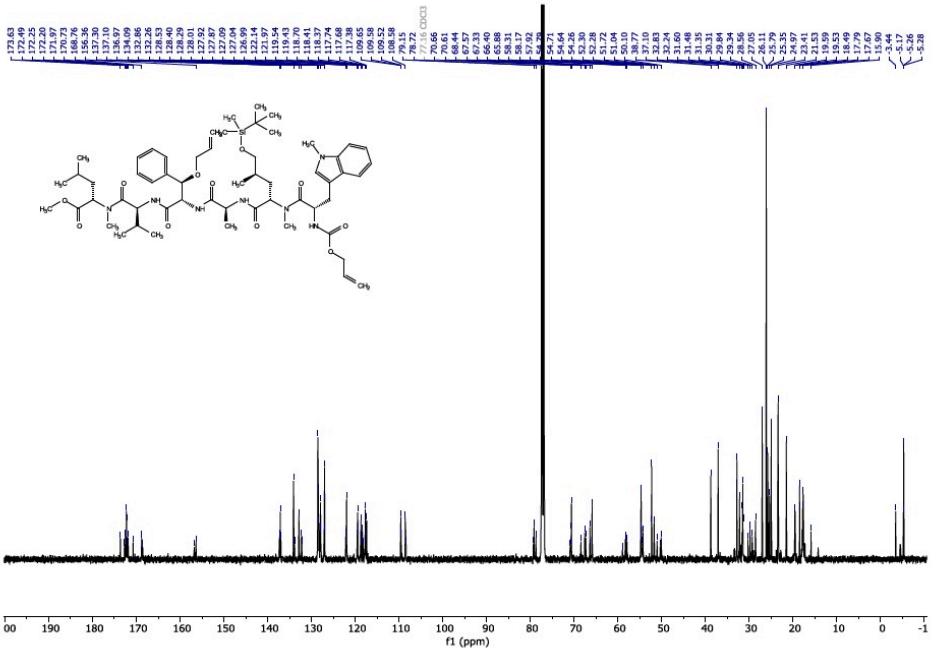

Supplementary Fig. 136. ^{1}H NMR spectrum of compound **SI-52**

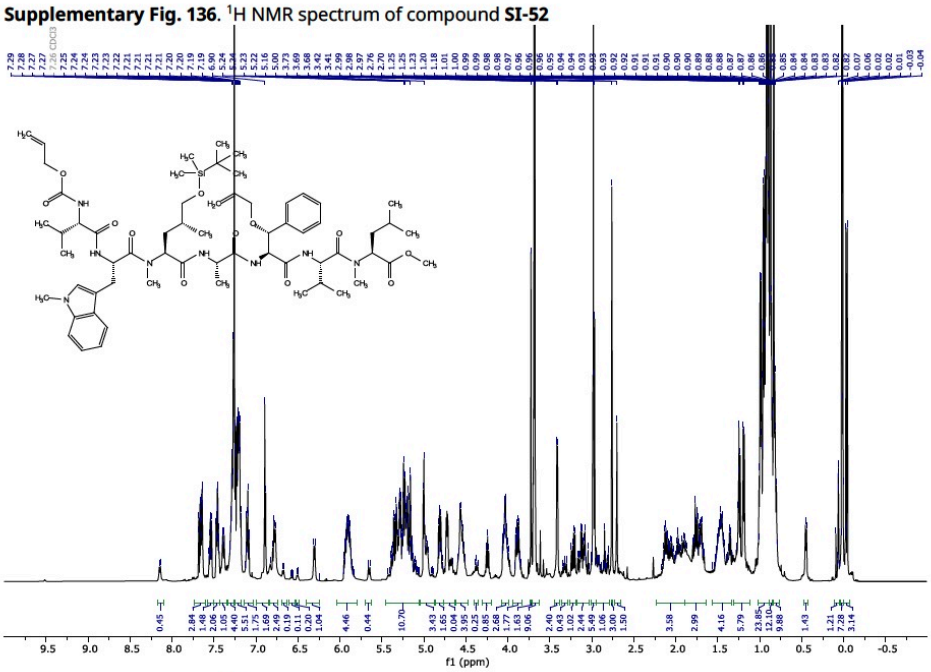

Supplementary Fig. 137. ^{13}C NMR spectrum of compound **SI-52**

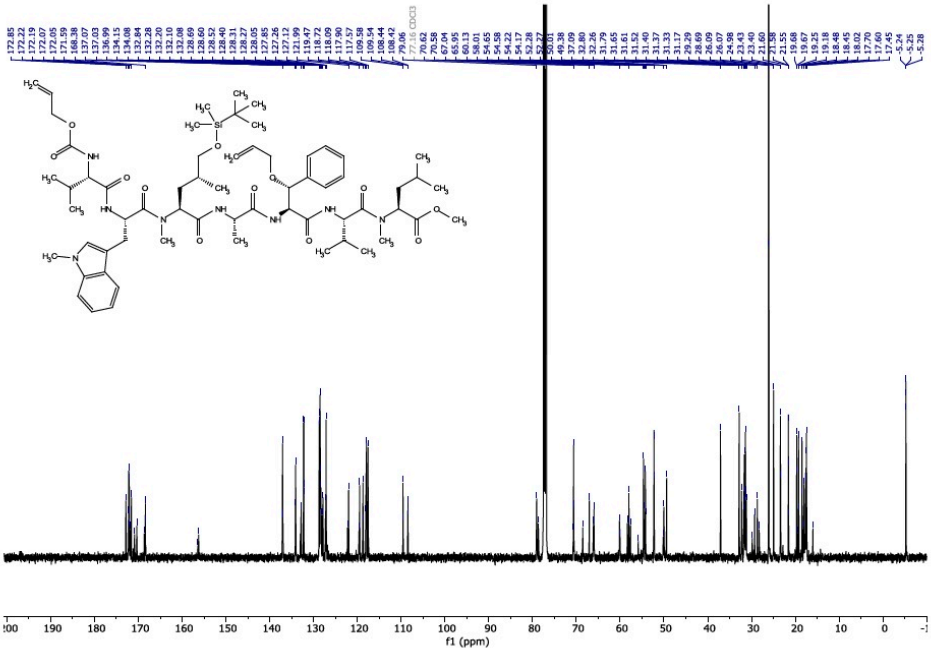

Supplementary Fig. 138. ^{1}H NMR spectrum of compound **14**

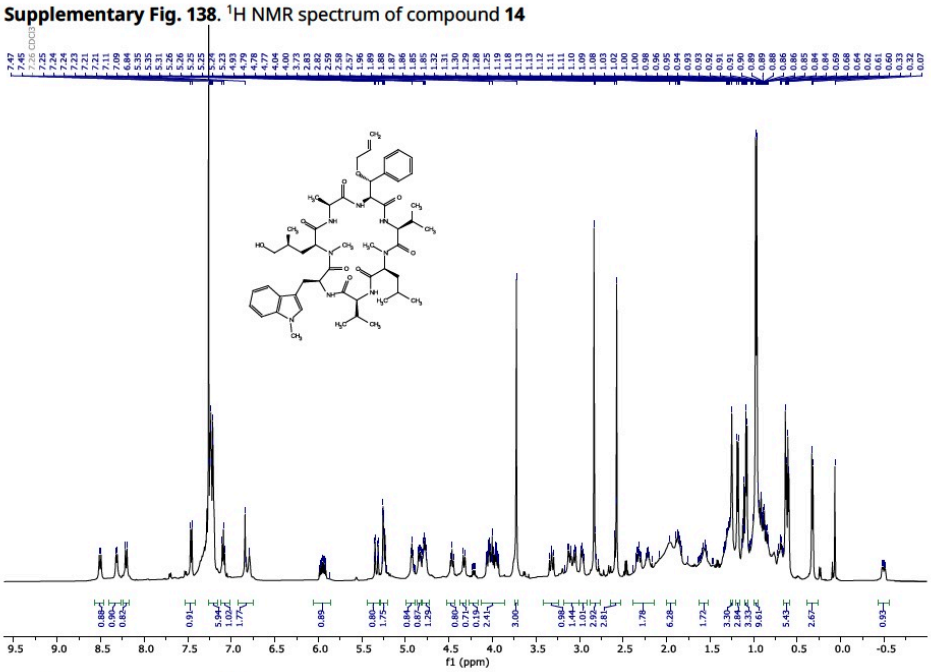

Supplementary Fig. 139. ^{13}C NMR spectrum of compound **14**

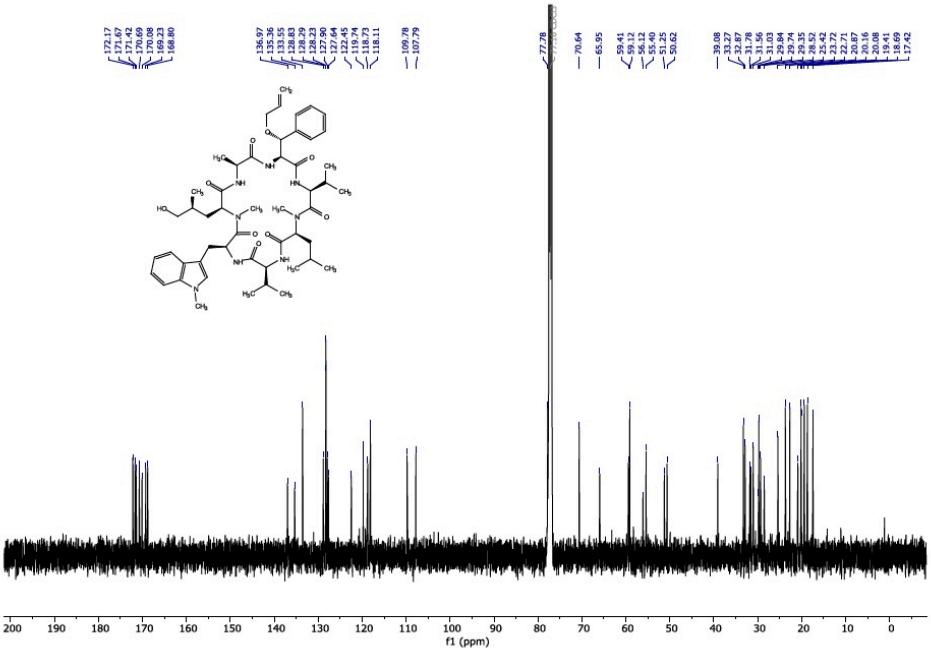

Supplementary Fig. 140. ^{1}H NMR spectrum of compound **17**

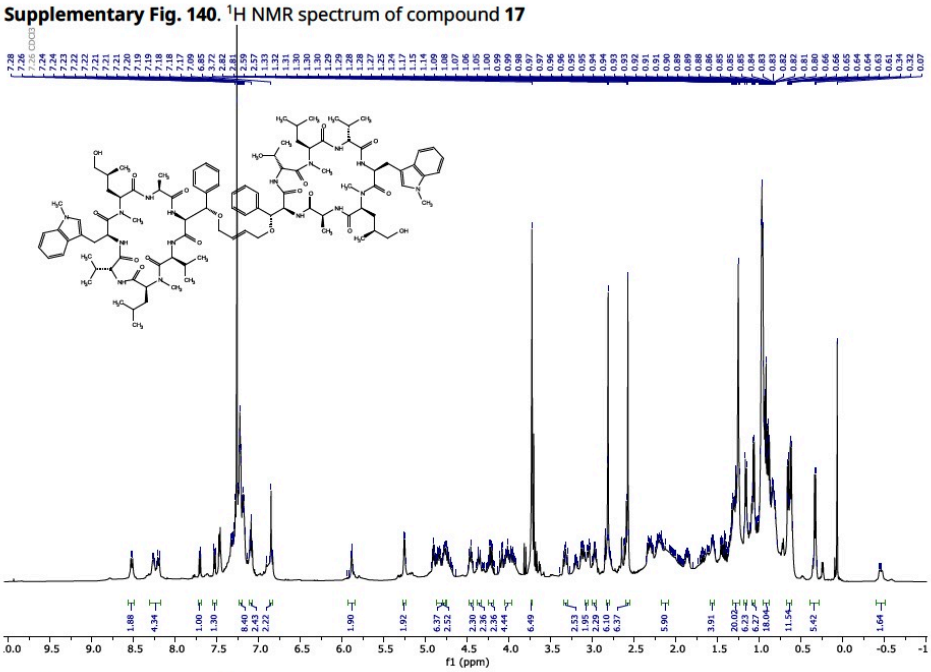

Supplementary Fig. 141. ^{13}C NMR spectrum of compound **17**

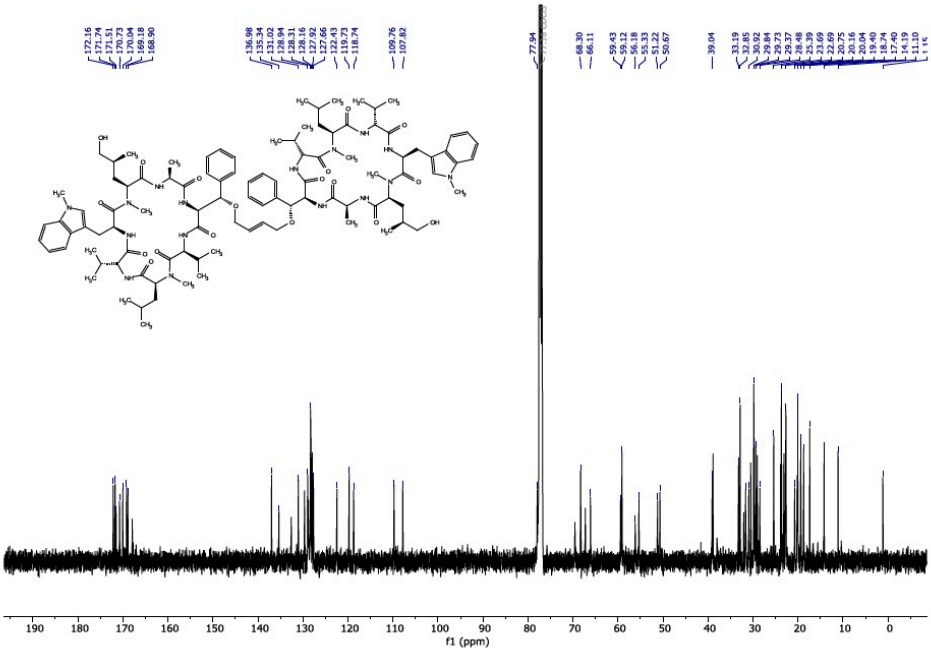

Supplementary Fig. 142. ^{1}H NMR spectrum of compound **18**

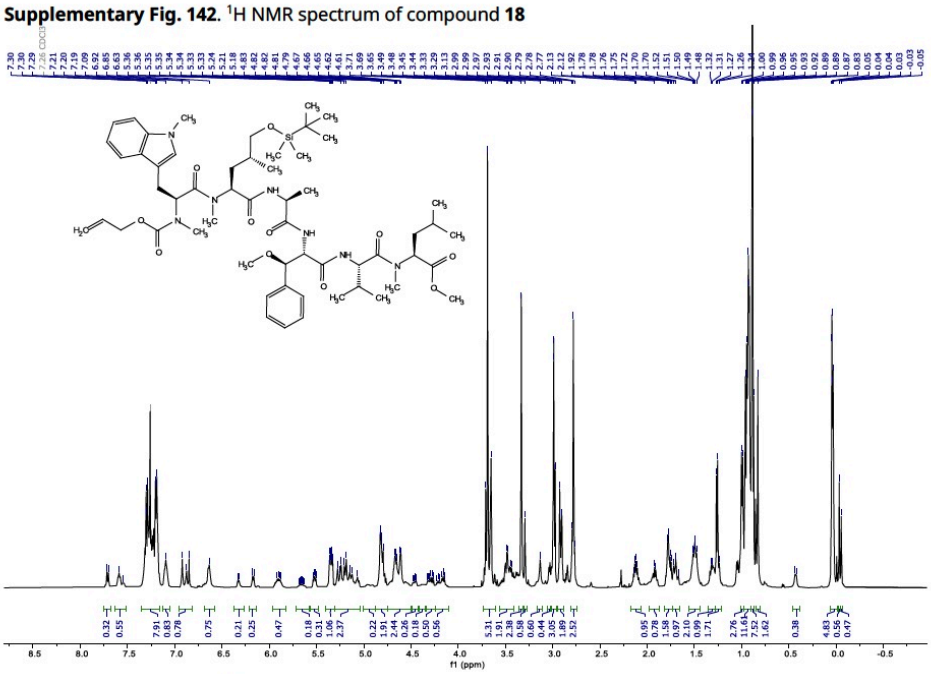

Supplementary Fig. 143. ^{13}C NMR spectrum of compound **18**

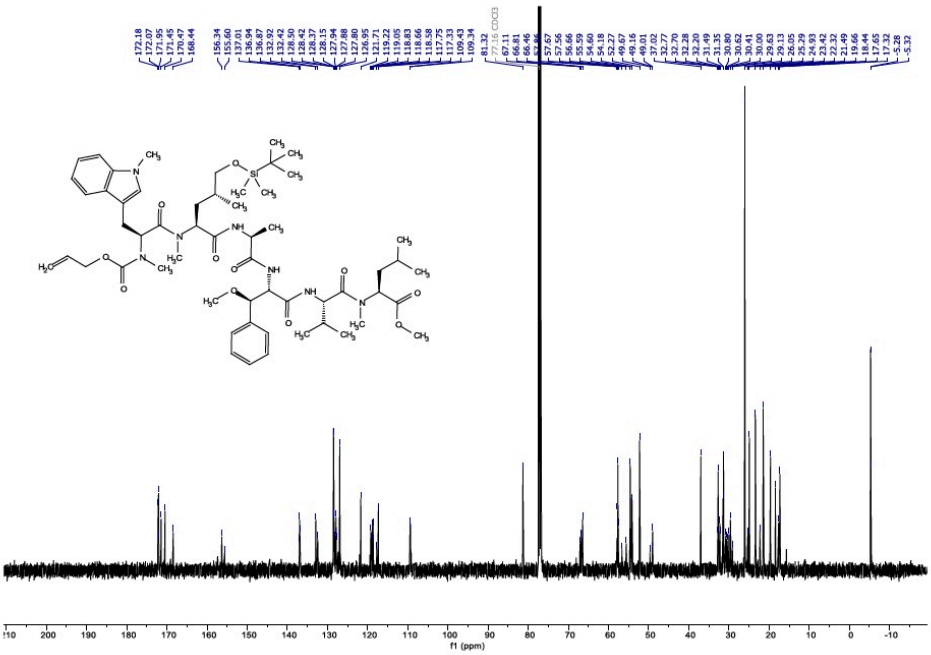

Supplementary Fig. 144. ^{1}H NMR spectrum of compound **19**

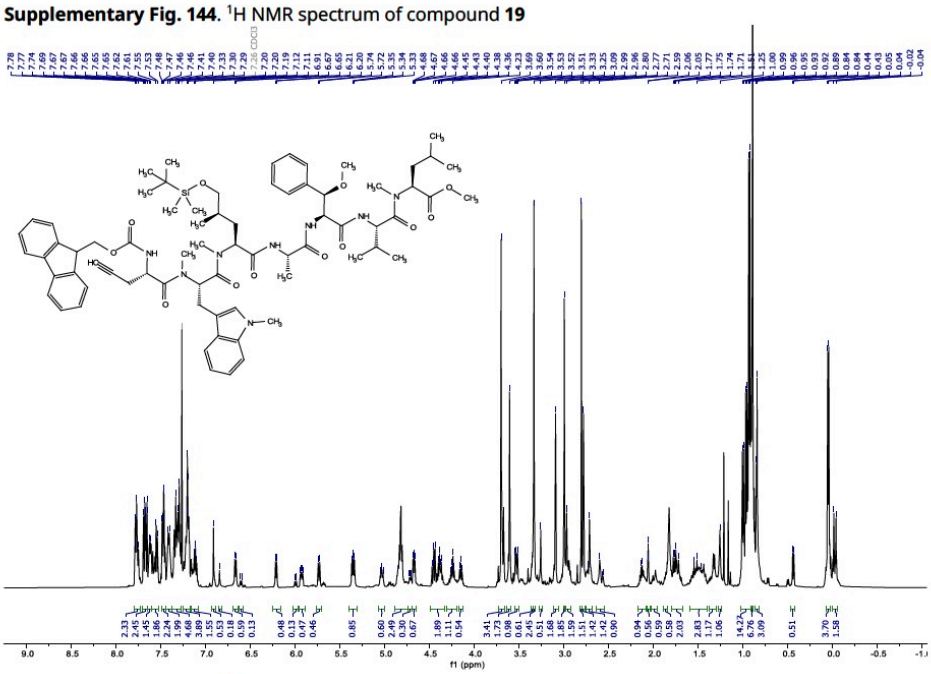

Supplementary Fig. 145. ^{13}C NMR spectrum of compound **19**

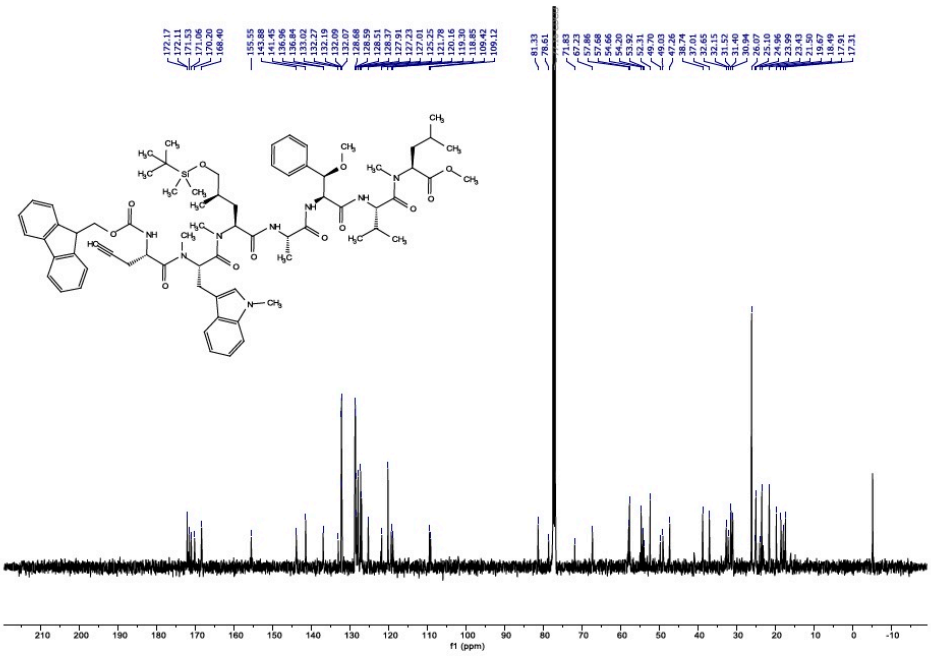

Supplementary Fig. 146. ^{1}H NMR spectrum of compound **20**

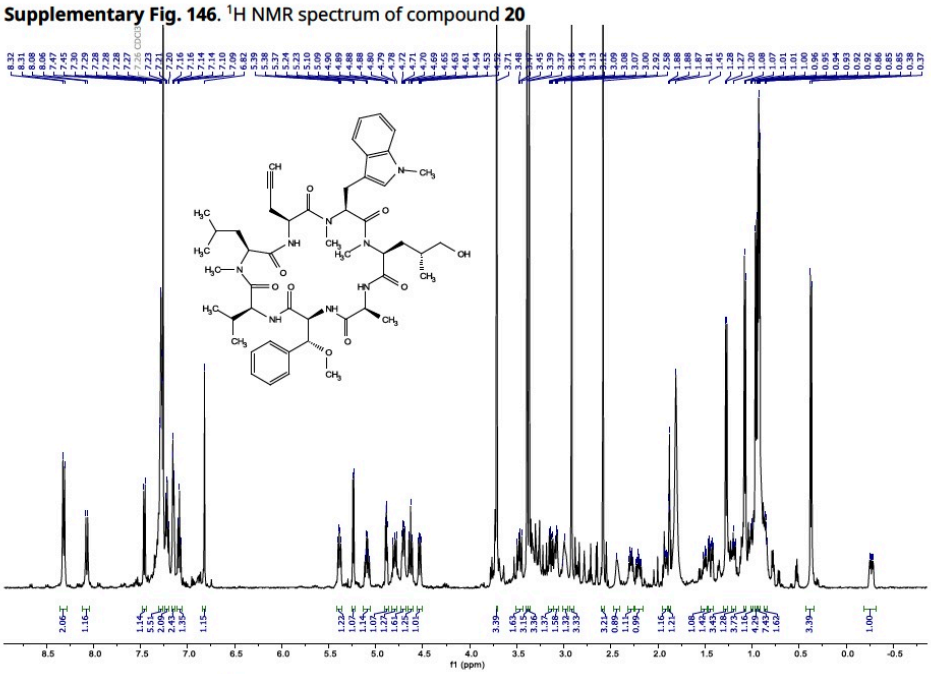

Supplementary Fig. 147. ^{13}C NMR spectrum of compound **20**

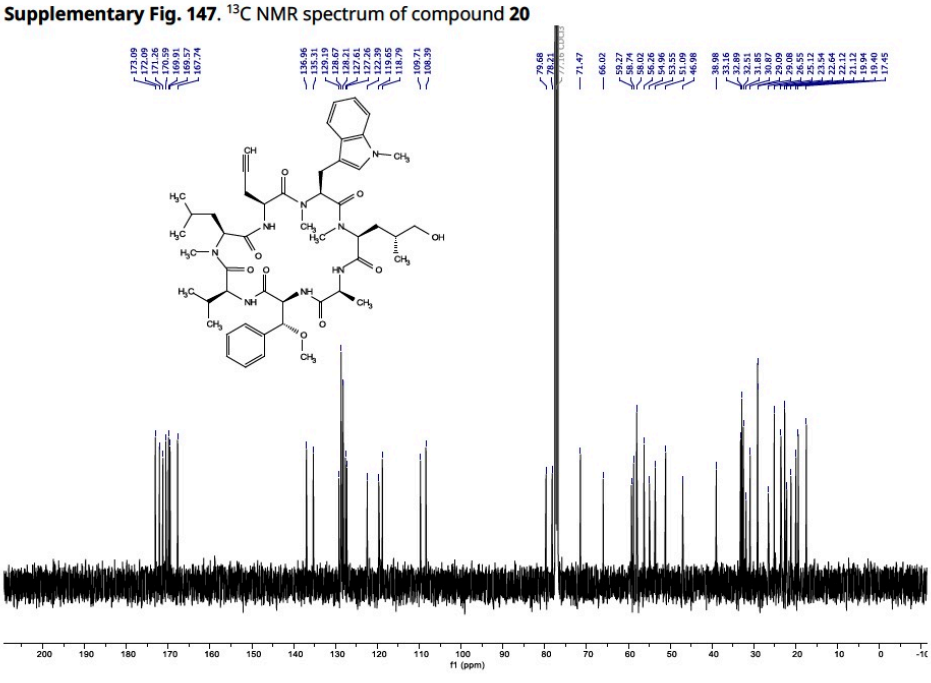

Supplementary Fig. 148. ^{1}H NMR spectrum of compound **21**

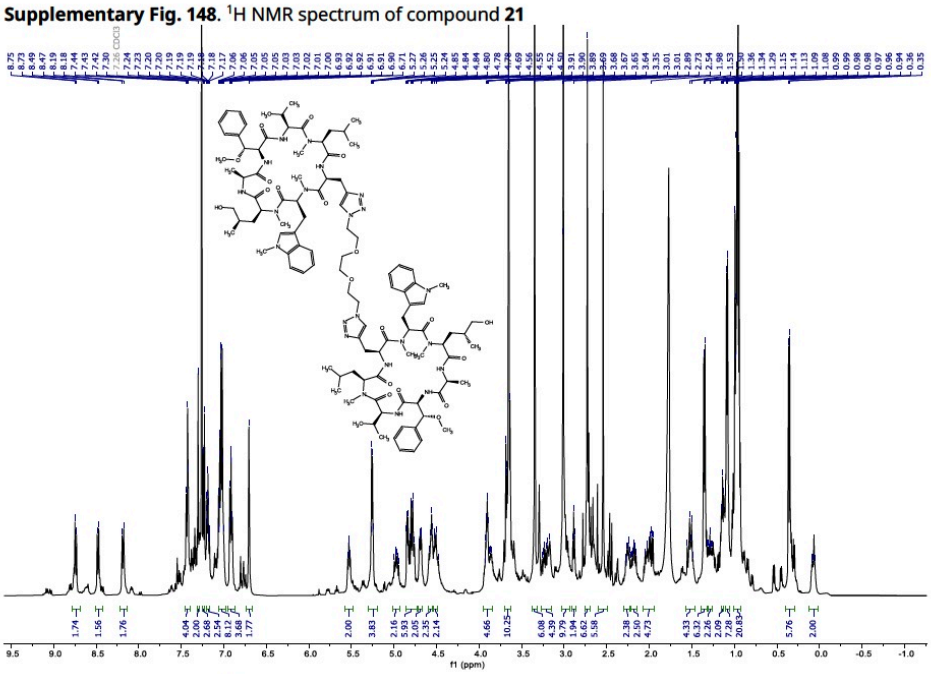

Supplementary Fig. 149. ^{13}C NMR spectrum of compound **21**

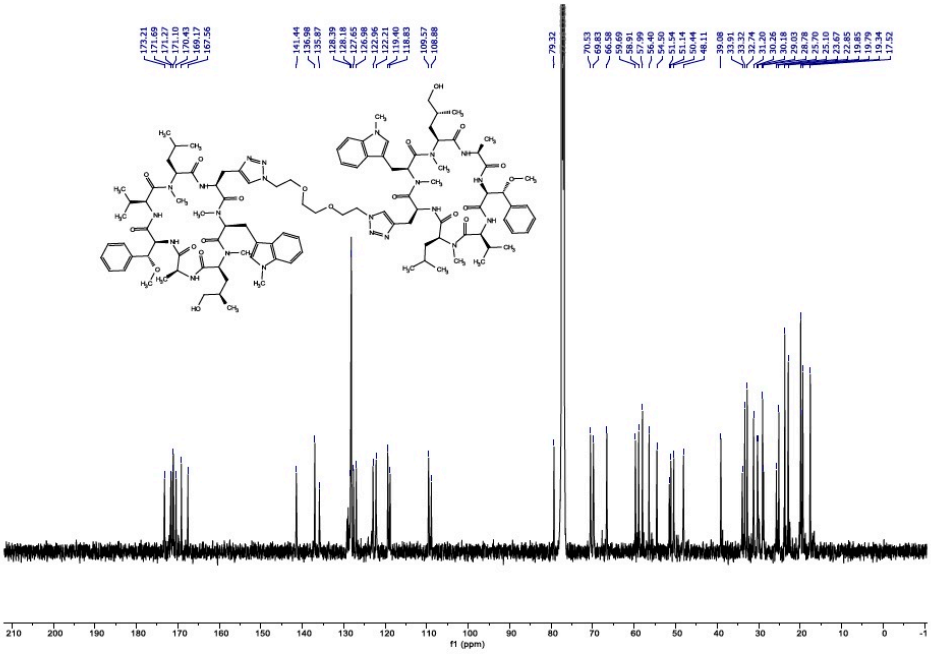

Supplementary Fig. 150. ^{1}H NMR spectrum of compound **22**

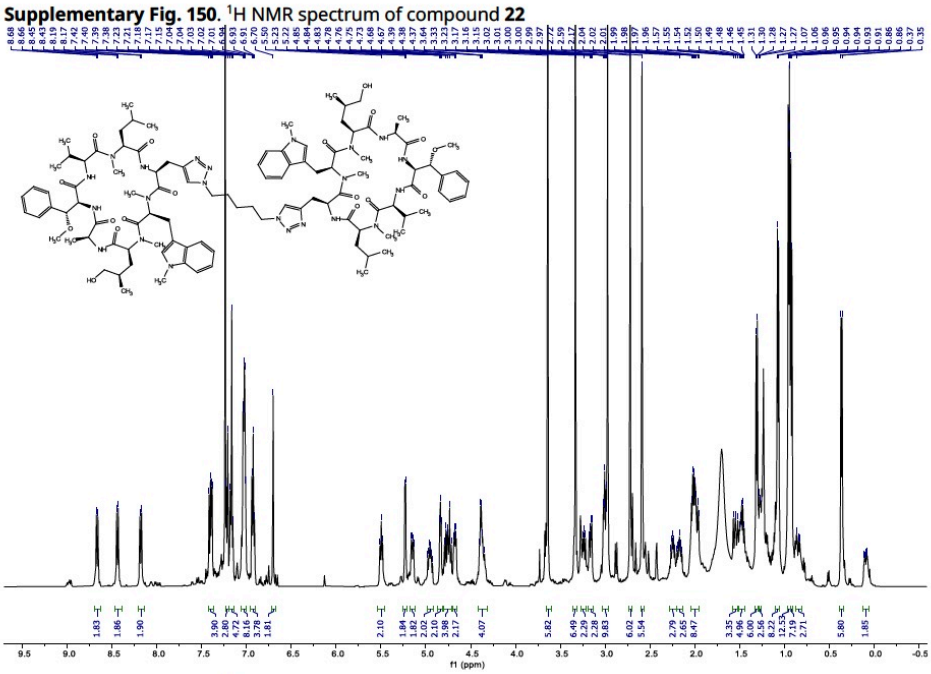

Supplementary Fig. 151. ^{13}C NMR spectrum of compound **22**

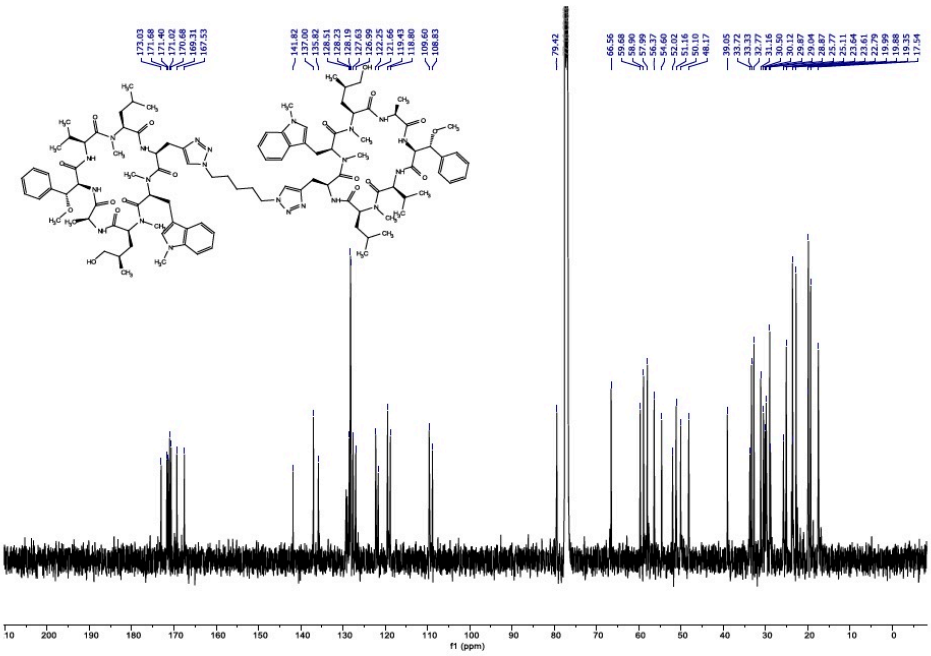

Supplementary Fig. 152. ^{1}H NMR spectrum of compound **25**

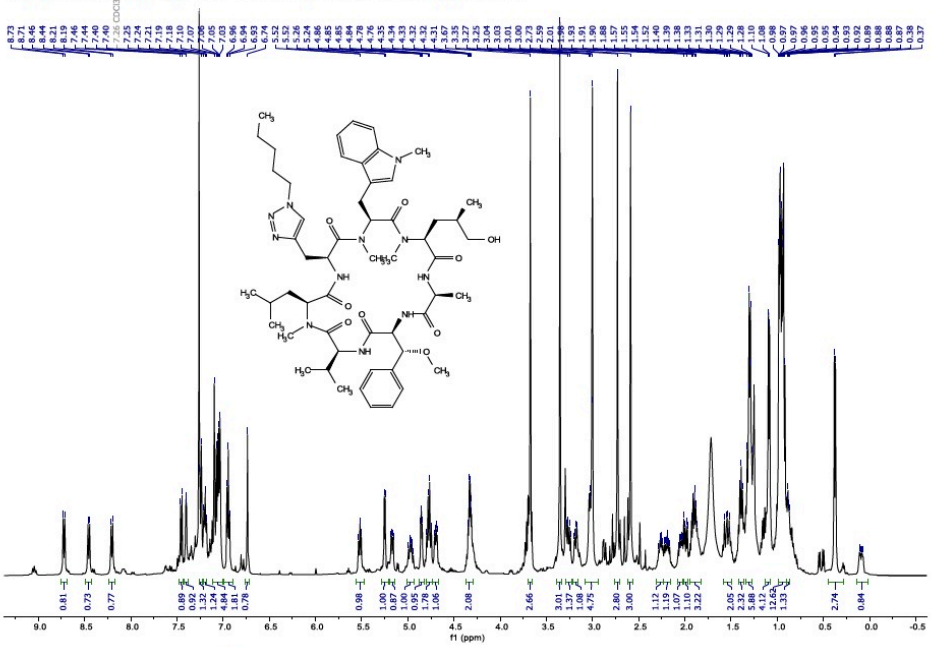

Supplementary Fig. 153. ^{13}C NMR spectrum of compound **25**

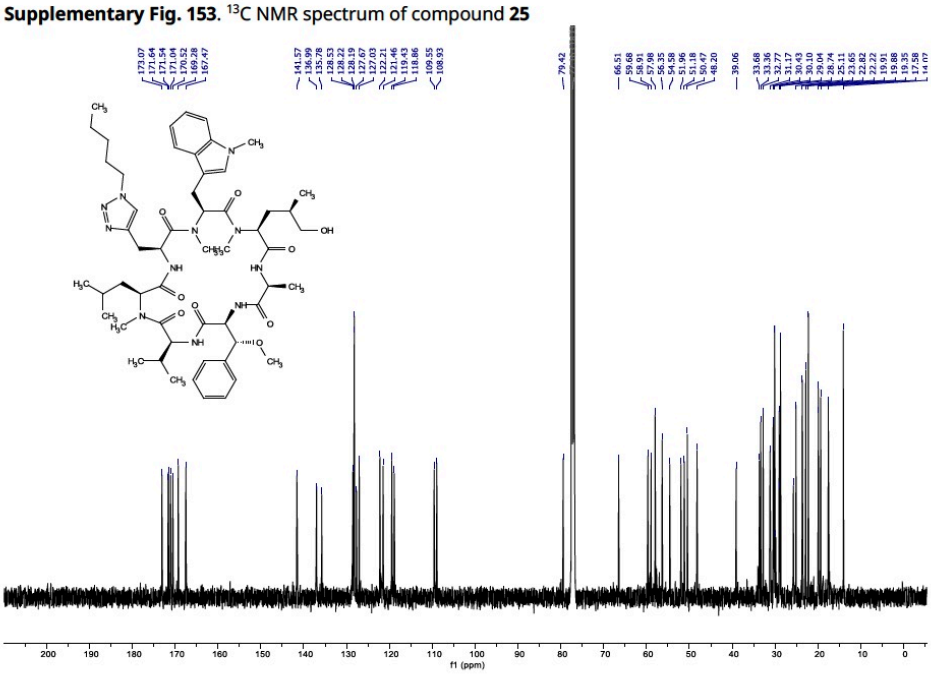

Supplementary Fig. 154. ^{1}H NMR spectrum of compound **SI-53**

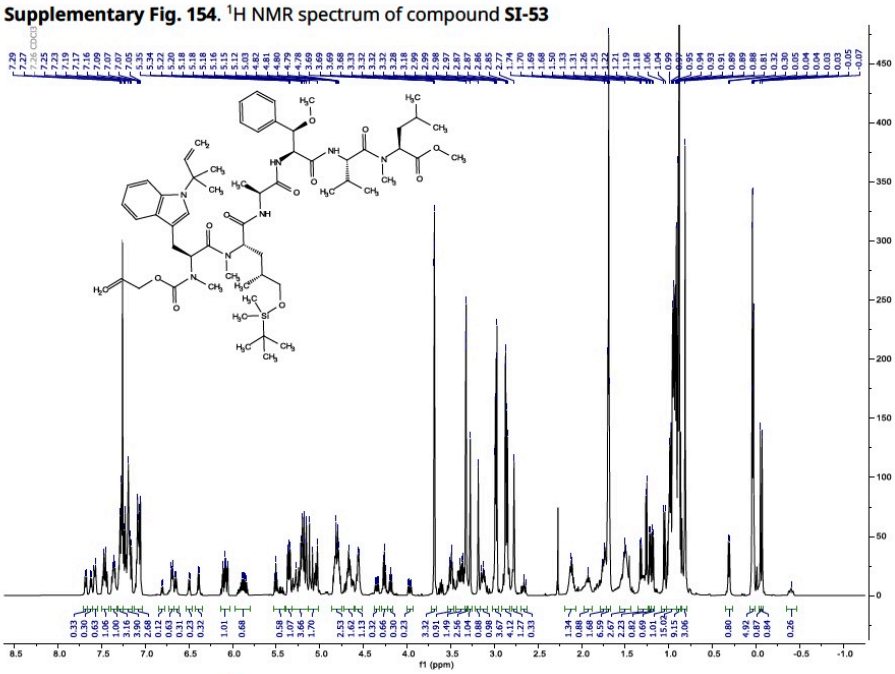

Supplementary Fig. 155. ^{13}C NMR spectrum of compound **SI-53**

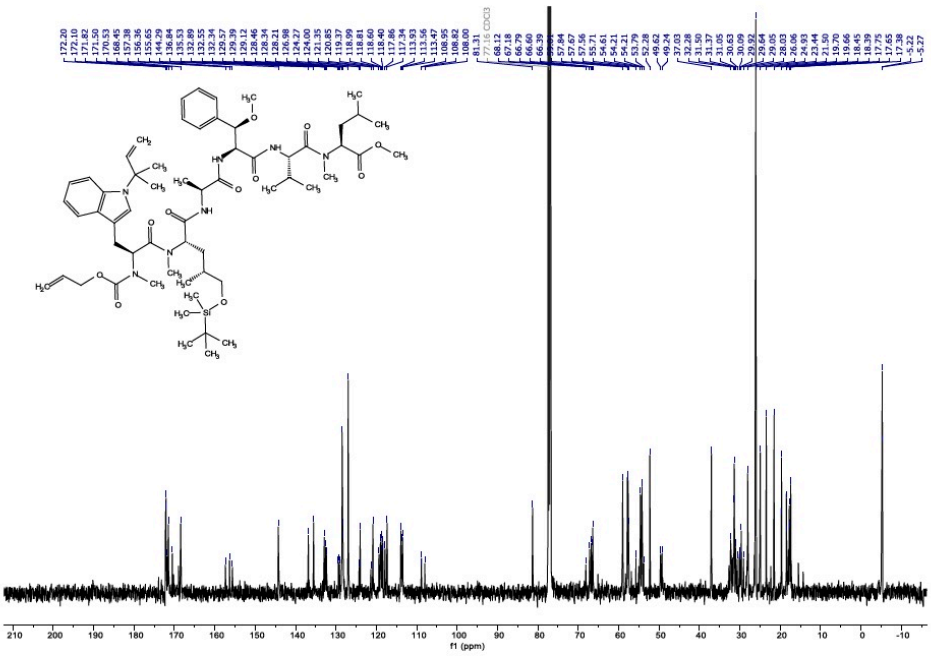

Supplementary Fig. 156. ^{1}H NMR spectrum of compound **SI-54**

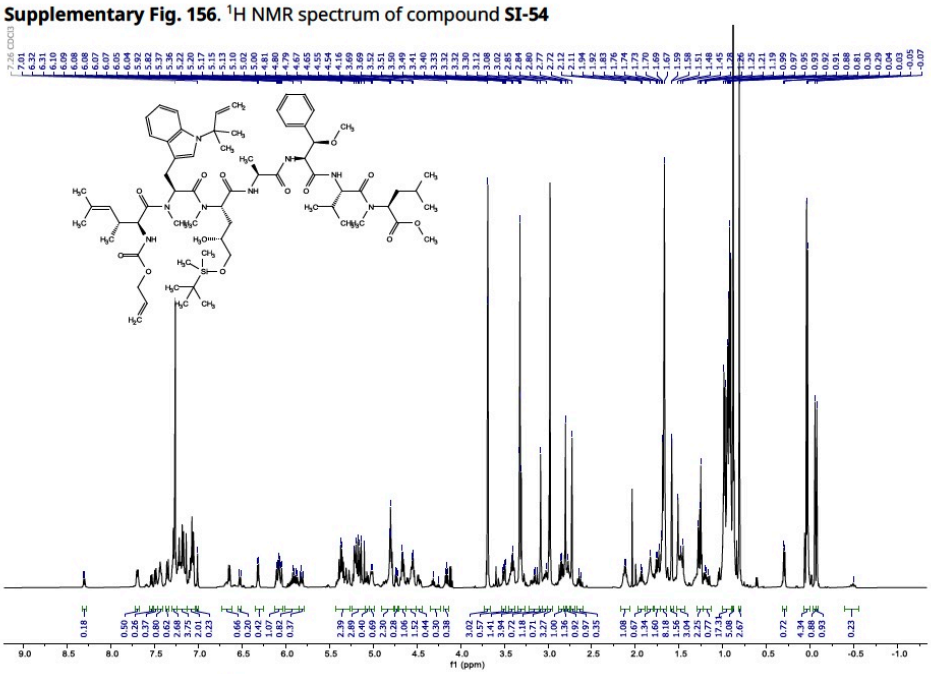

Supplementary Fig. 157. ^{13}C NMR spectrum of compound **SI-54**

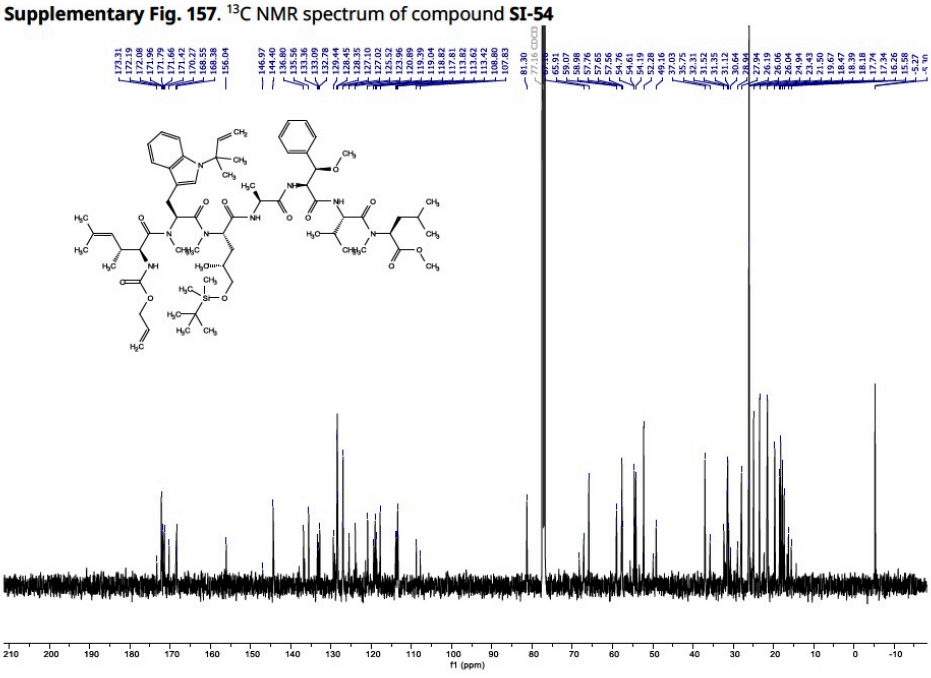

Supplementary Fig. 158. ^{1}H NMR spectrum of compound **23**

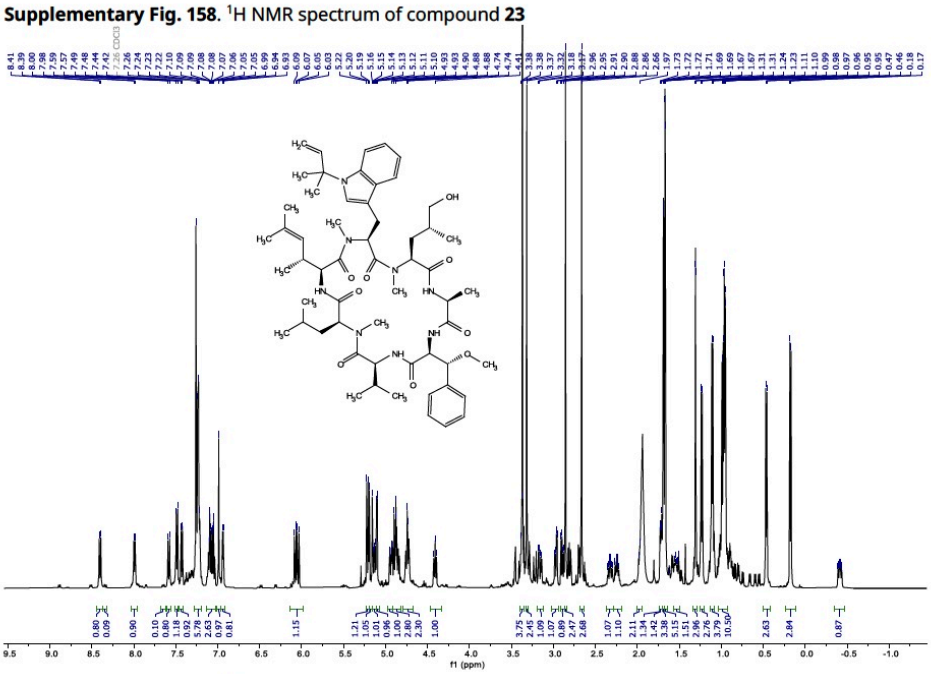

Supplementary Fig. 159. ^{13}C NMR spectrum of compound **23**

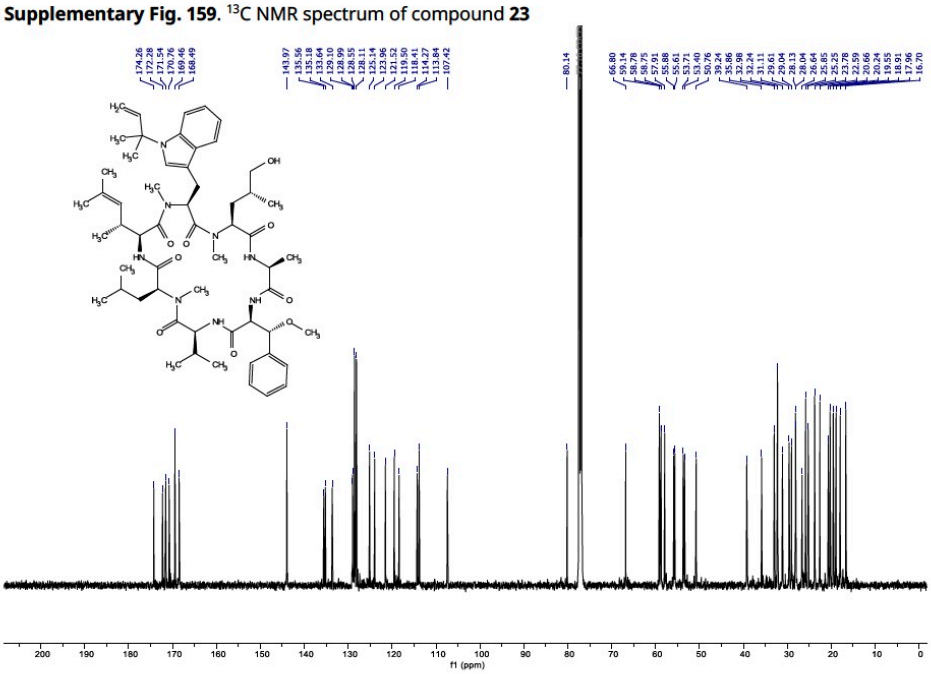

Supplementary Fig. 160. ^{1}H NMR spectrum of compound **SI-55**

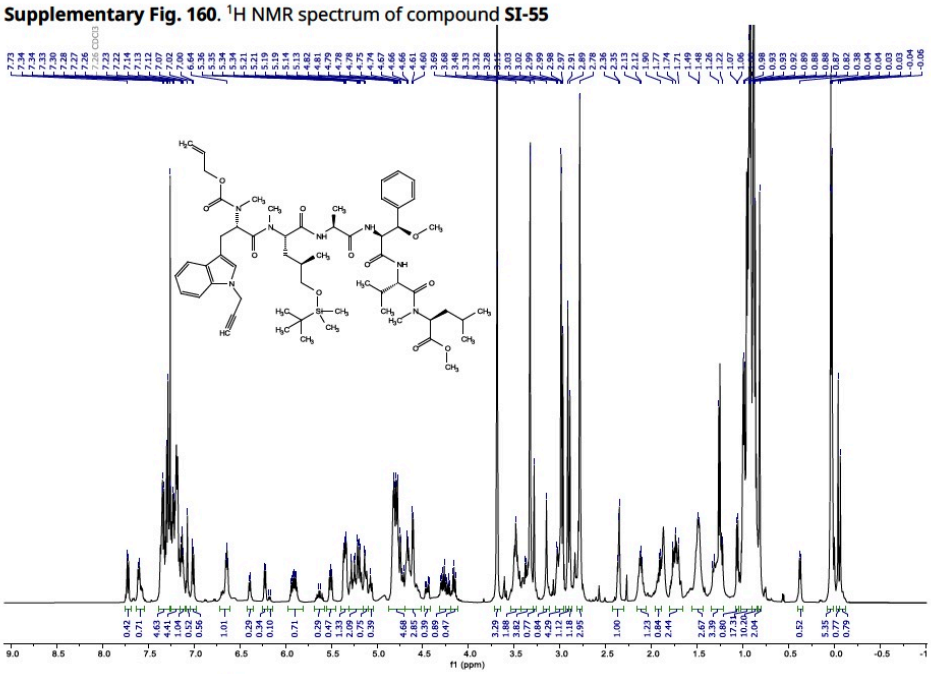

Supplementary Fig. 161. ^{13}C NMR spectrum of compound **SI-55**

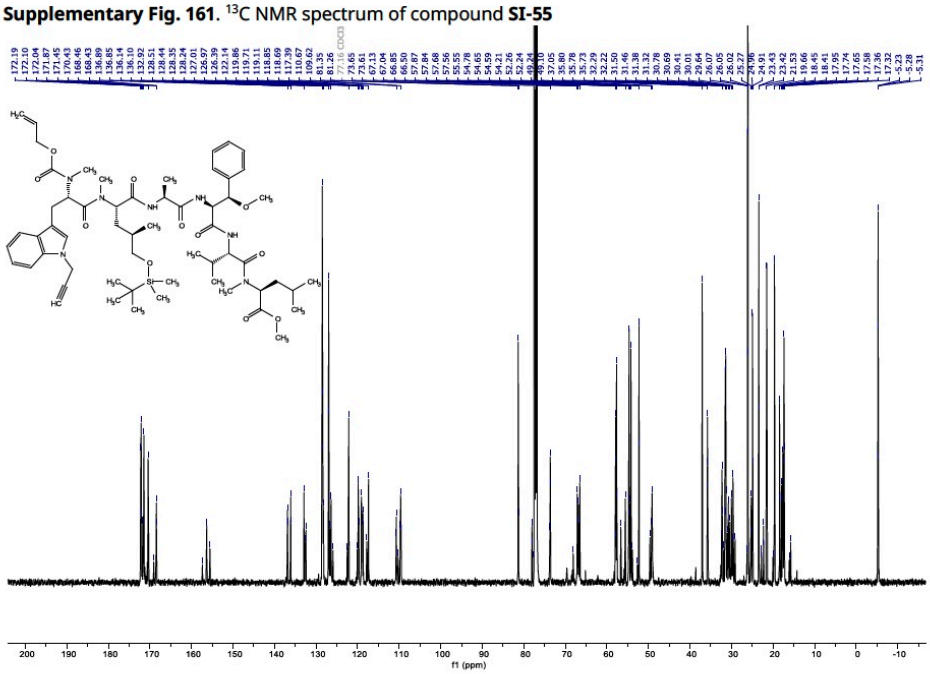

Supplementary Fig. 162. ^{1}H NMR spectrum of compound **SI-56**

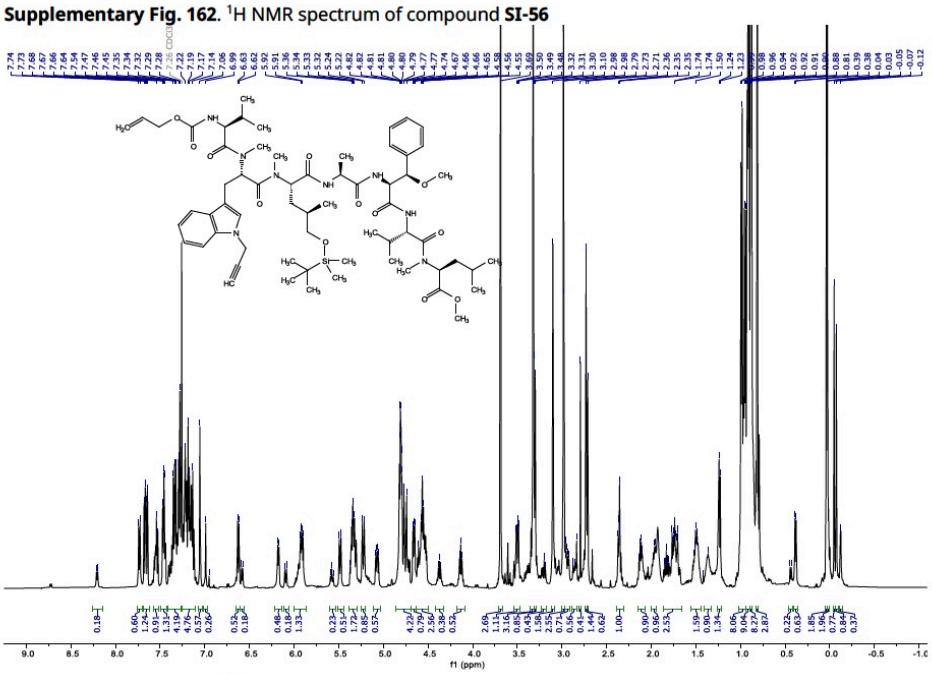

Supplementary Fig. 163. ^{13}C NMR spectrum of compound **SI-56**

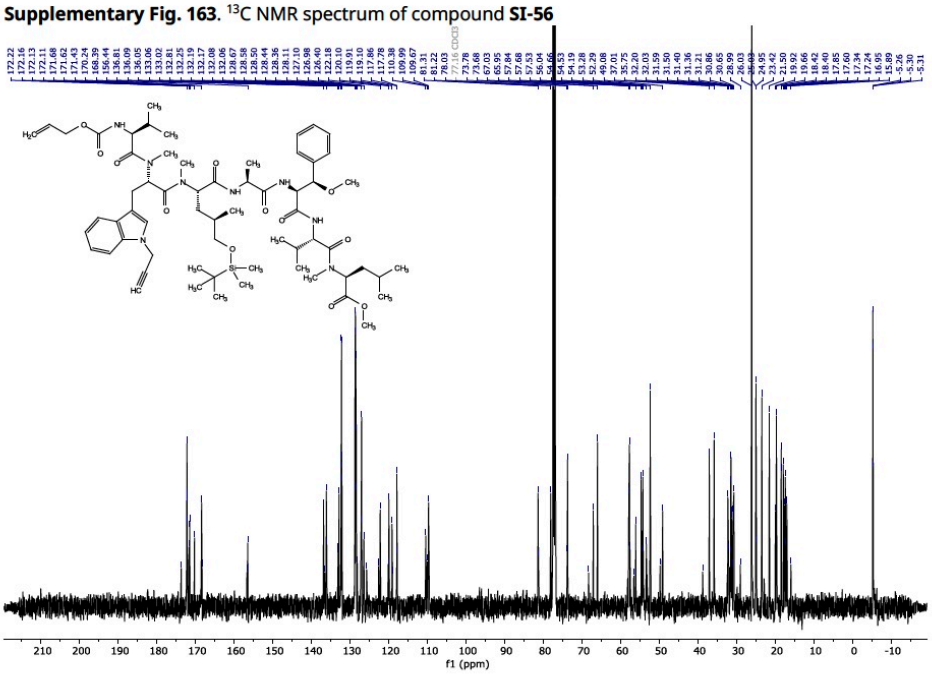

Supplementary Fig. 164. ^{1}H NMR spectrum of compound **26**

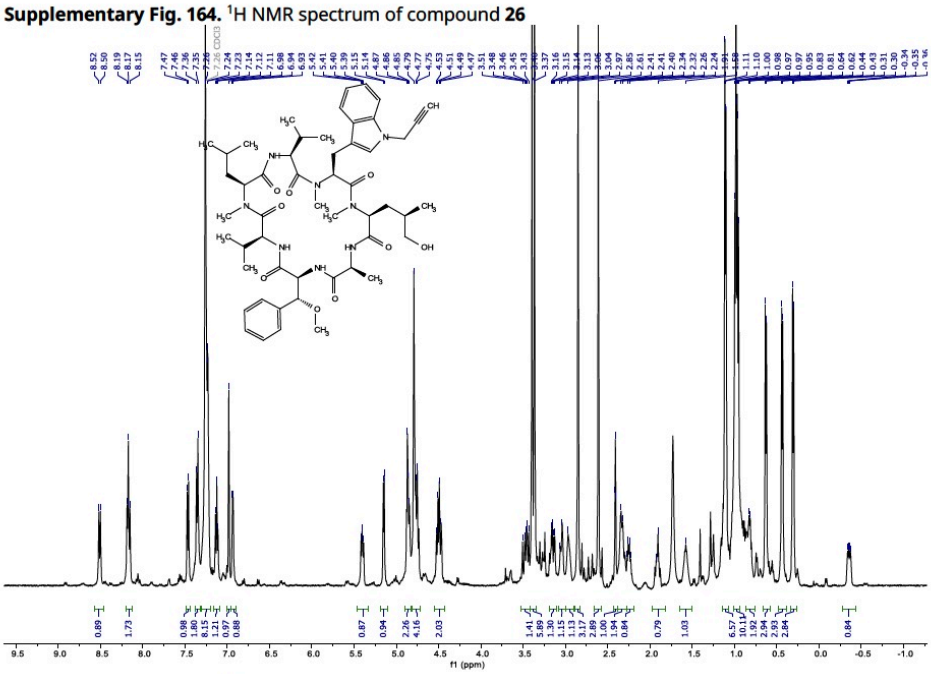

Supplementary Fig. 165. ^{13}C NMR spectrum of compound **26**

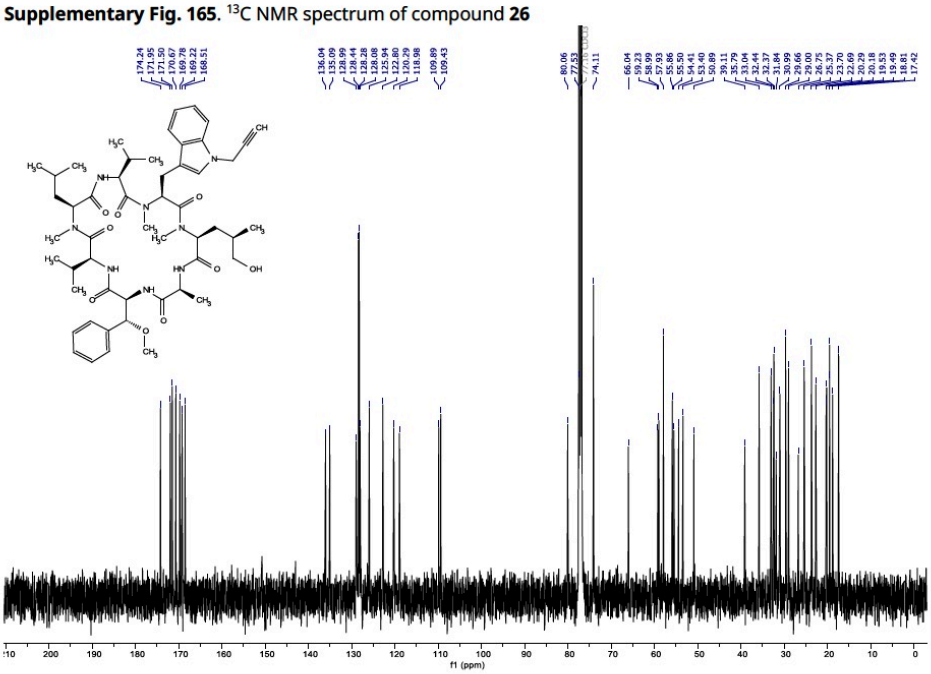

Supplementary Fig. 166. ^{1}H NMR spectrum of compound **SI-57**

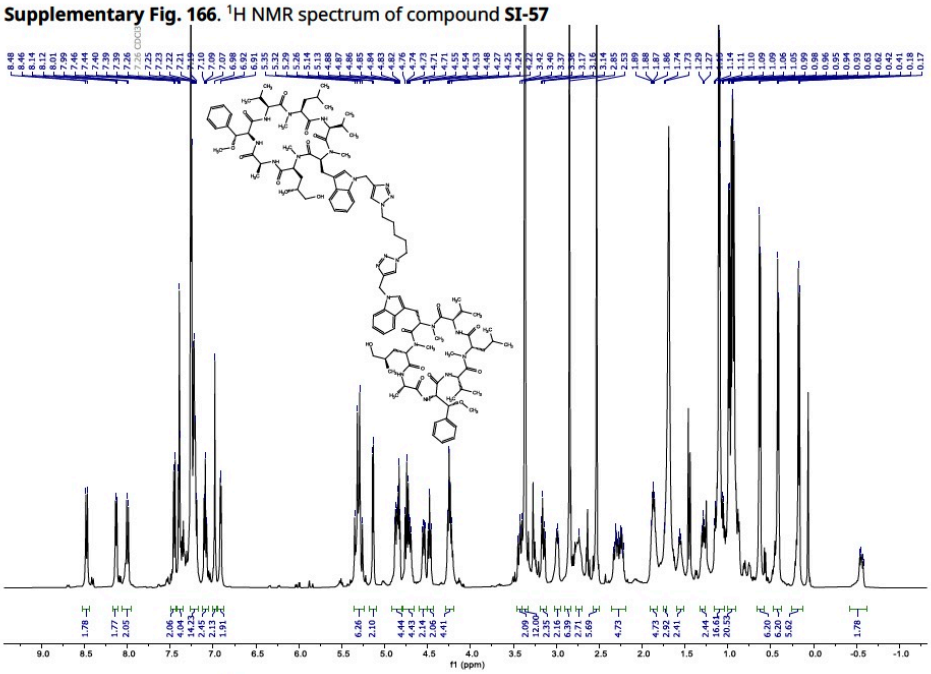

Supplementary Fig. 167. ^{13}C NMR spectrum of compound **SI-57**

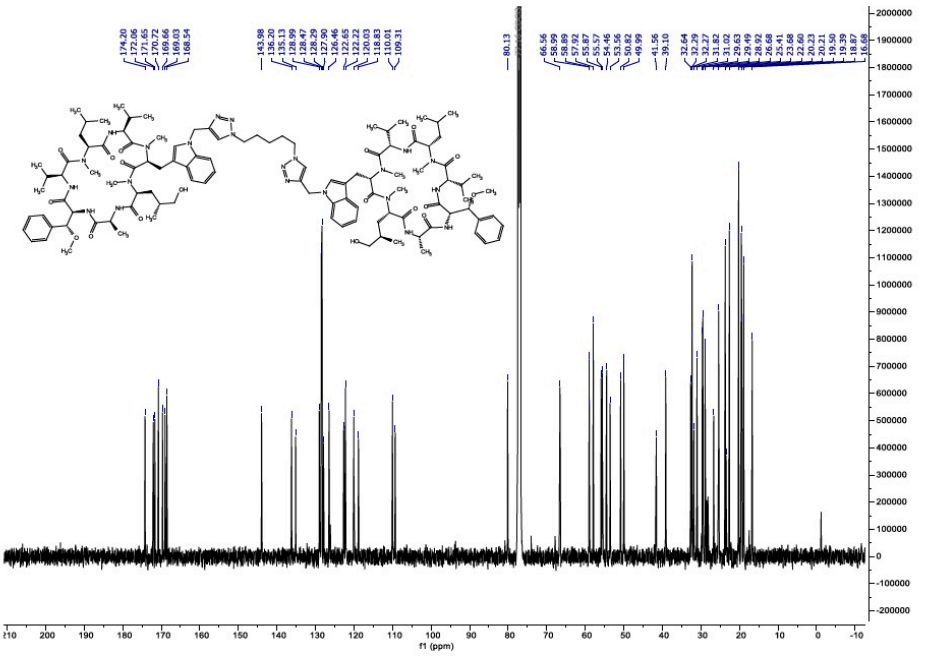

Supplementary Fig. 168. ^{1}H NMR spectrum of compound **27**

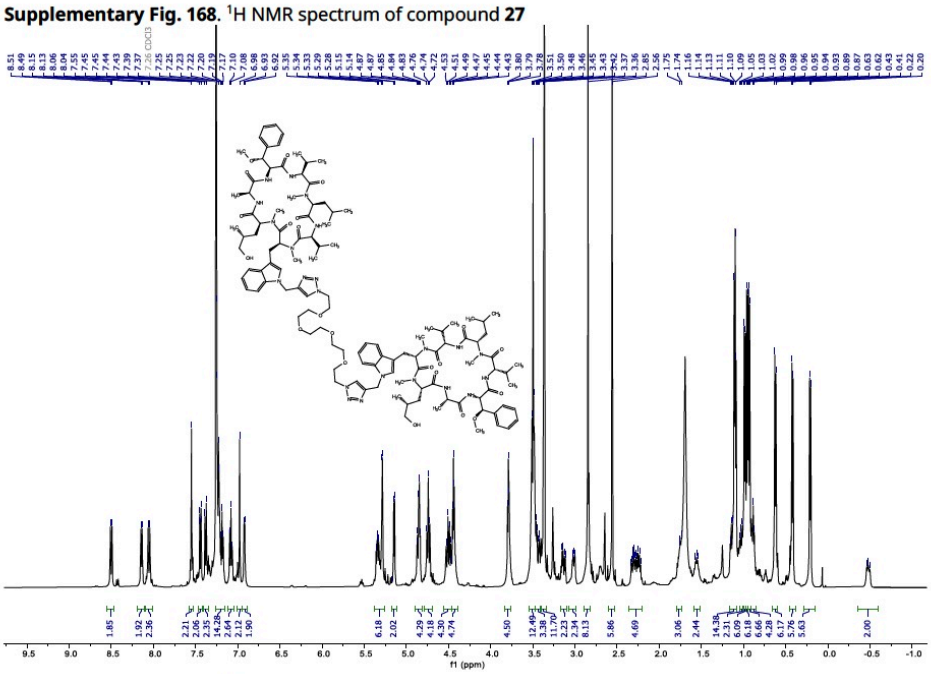

Supplementary Fig. 169. ^{13}C NMR spectrum of compound **27**

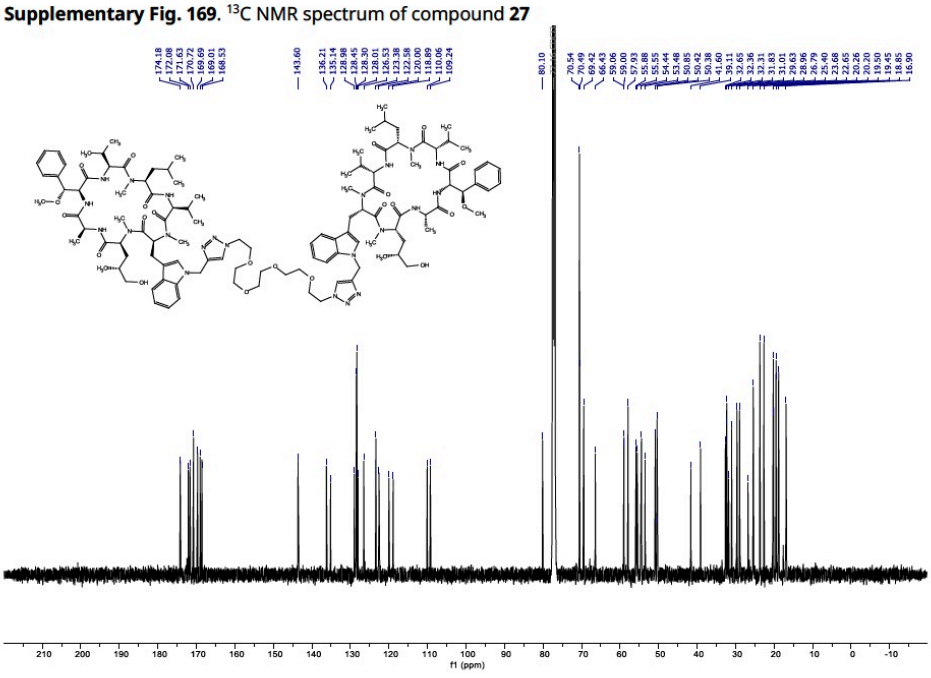

Supplementary Fig. 170. ^{1}H NMR spectrum of compound **SI-58**

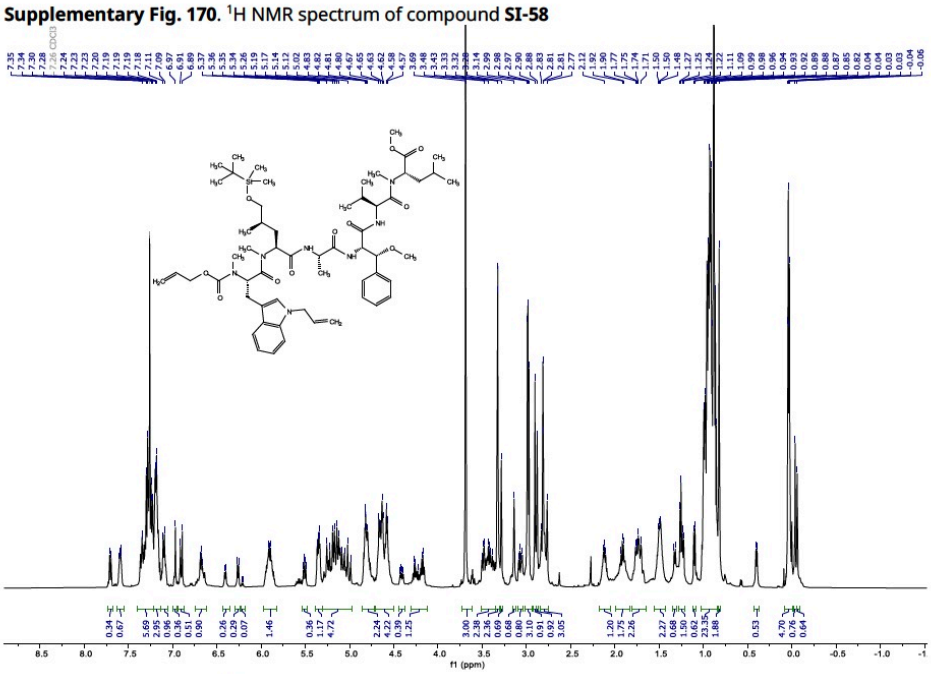

Supplementary Fig. 171. ^{13}C NMR spectrum of compound **SI-58**

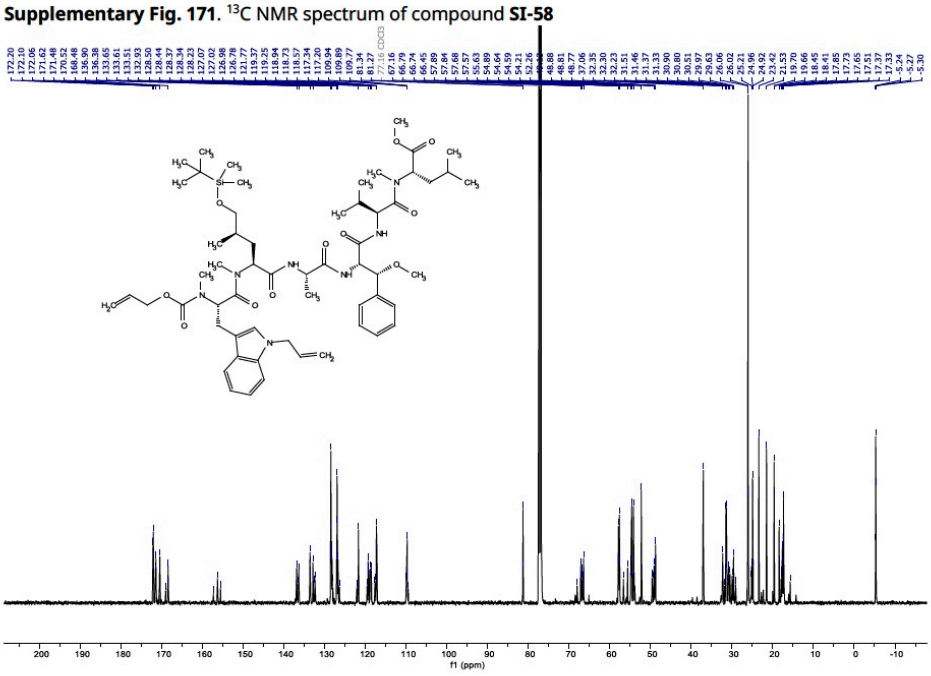

Supplementary Fig. 172. ^{1}H NMR spectrum of compound **SI-59**

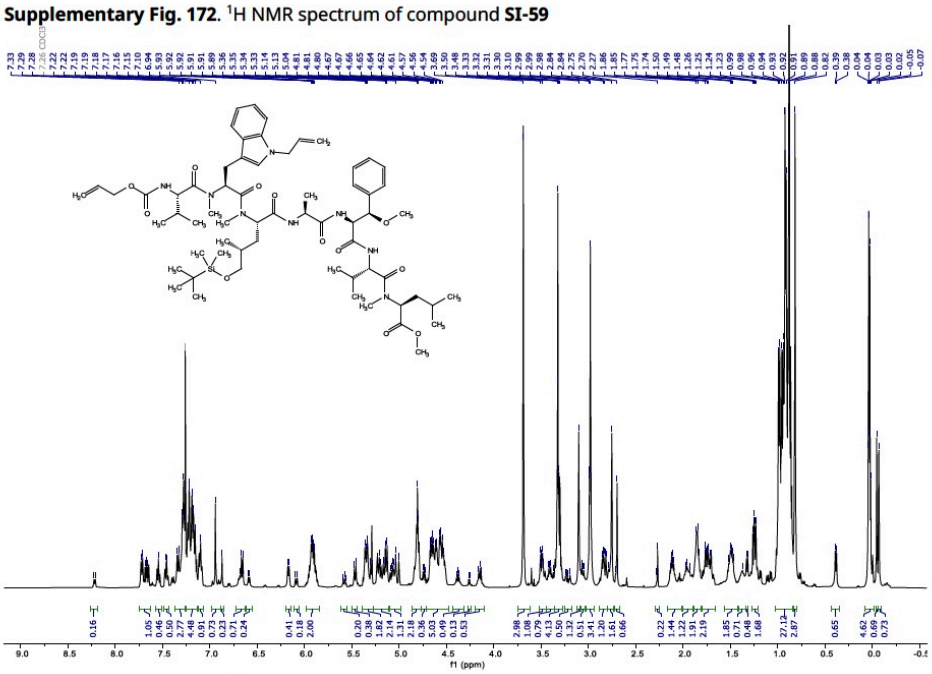

Supplementary Fig. 173. ^{13}C NMR spectrum of compound **SI-59**

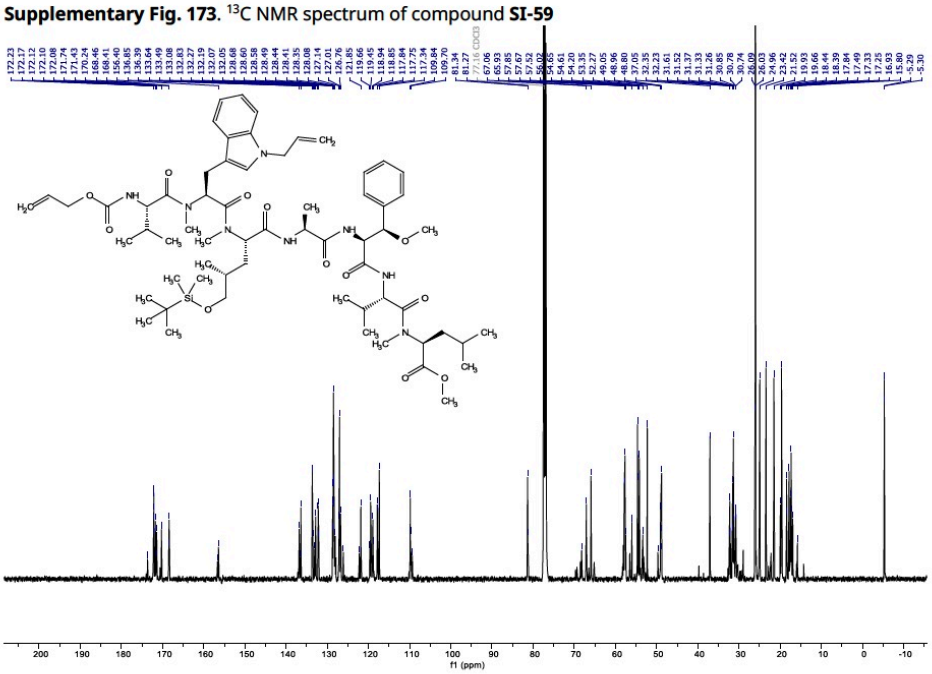

Supplementary Fig. 174. ^{1}H NMR spectrum of compound **SI-60**

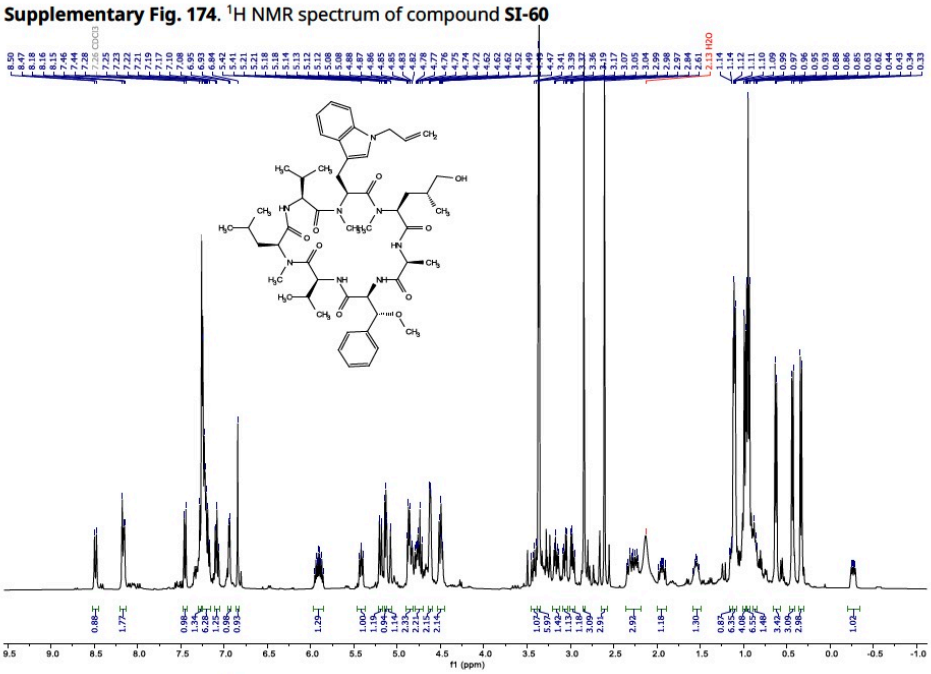

Supplementary Fig. 175. ^{13}C NMR spectrum of compound **SI-60**

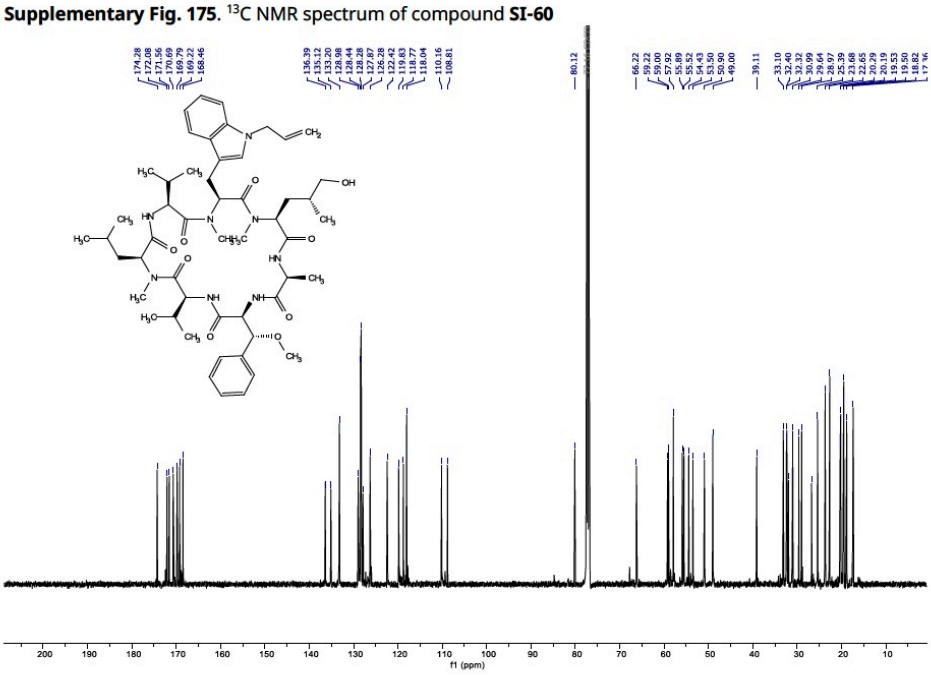

Supplementary Fig. 176. ^{1}H NMR spectrum of compound **28**

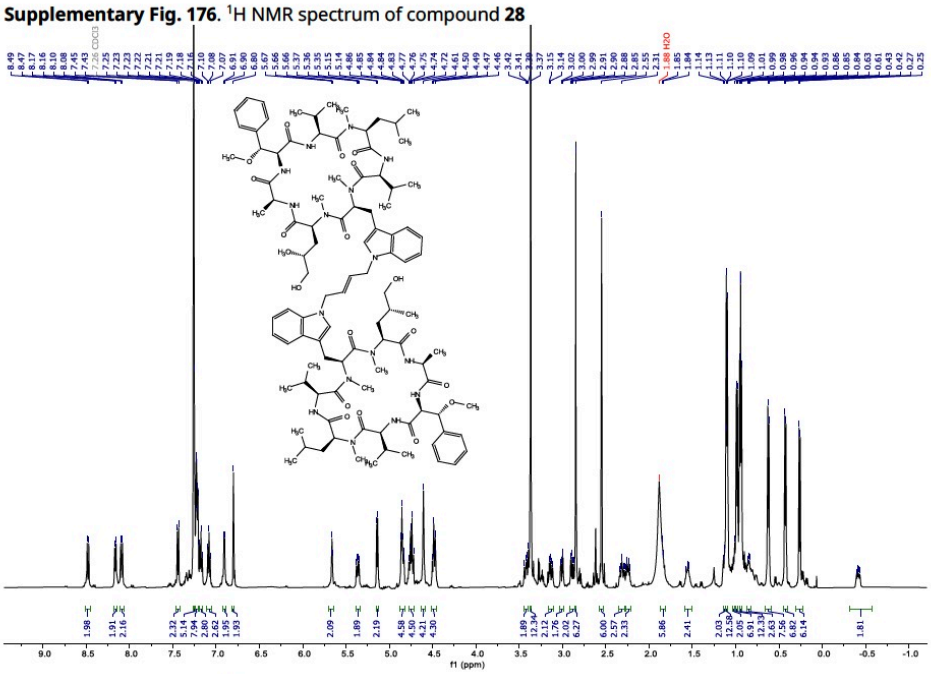

Supplementary Fig. 177. ^{13}C NMR spectrum of compound **28**

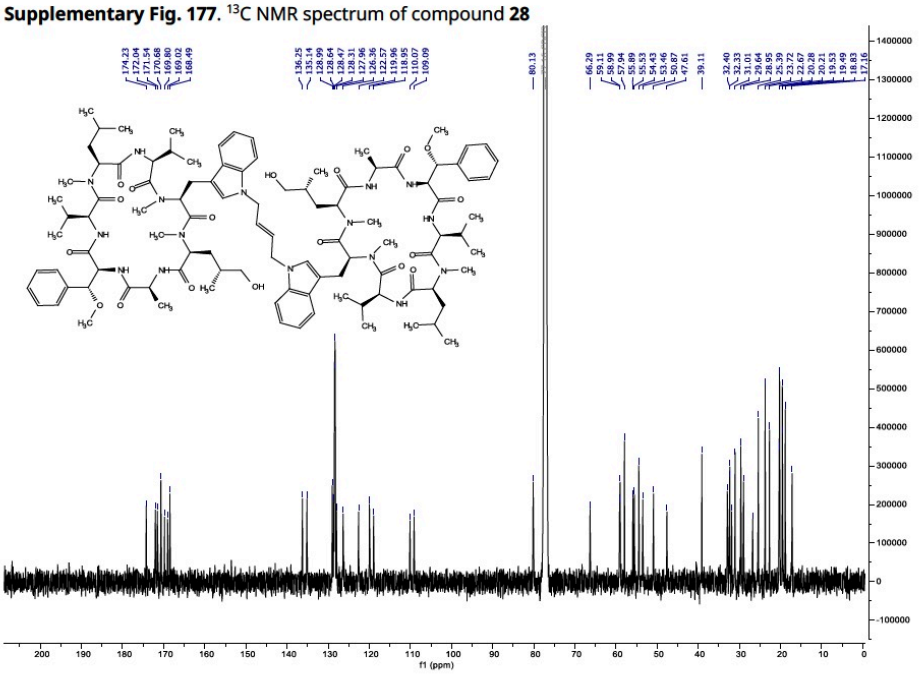

200

Supplementary Fig. 178. ^{1}H NMR spectrum of compound **SI-61**

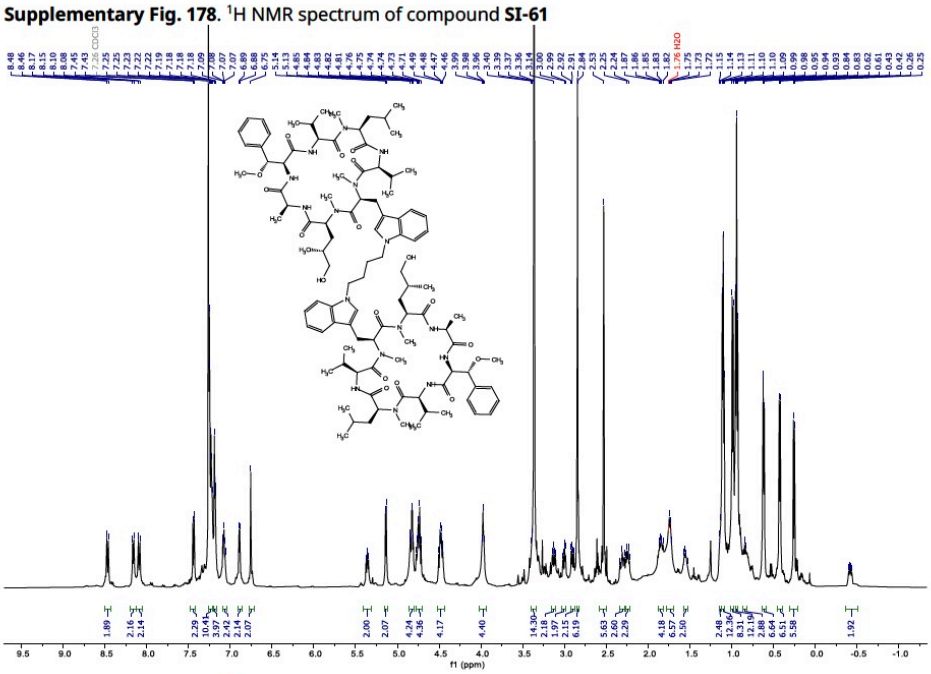

Supplementary Fig. 179. ^{13}C NMR spectrum of compound **SI-61**

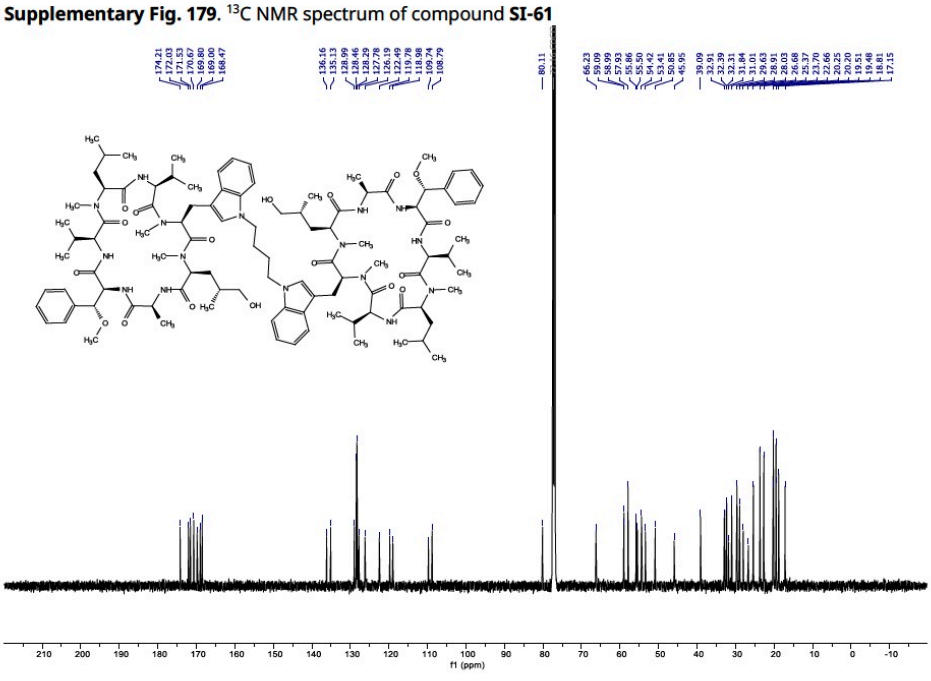

Supplementary Fig. 180. ^{1}H NMR spectrum of compound **SI-62**

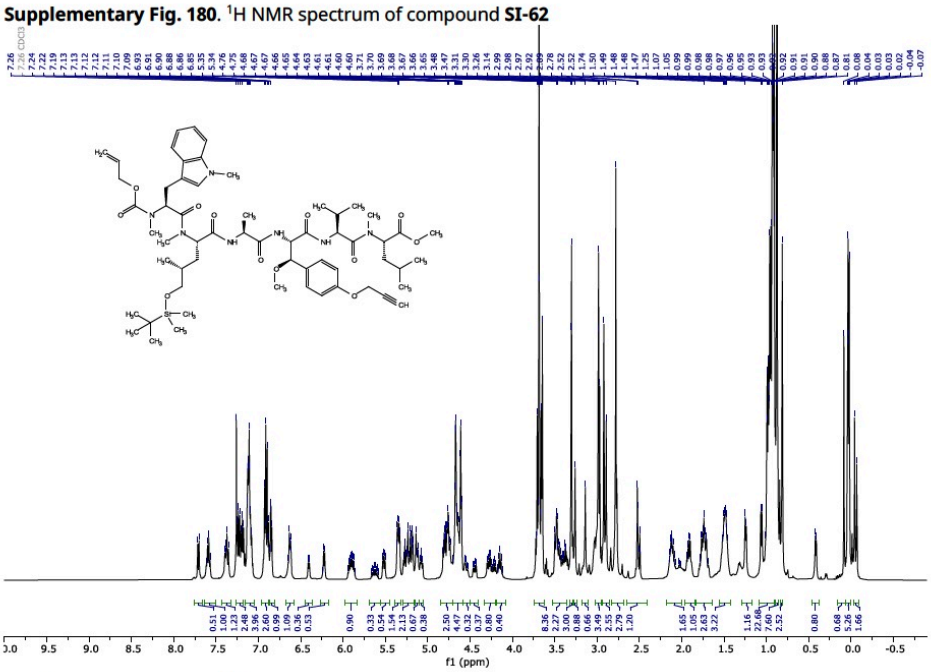

Supplementary Fig. 181. ^{13}C NMR spectrum of compound **SI-62**

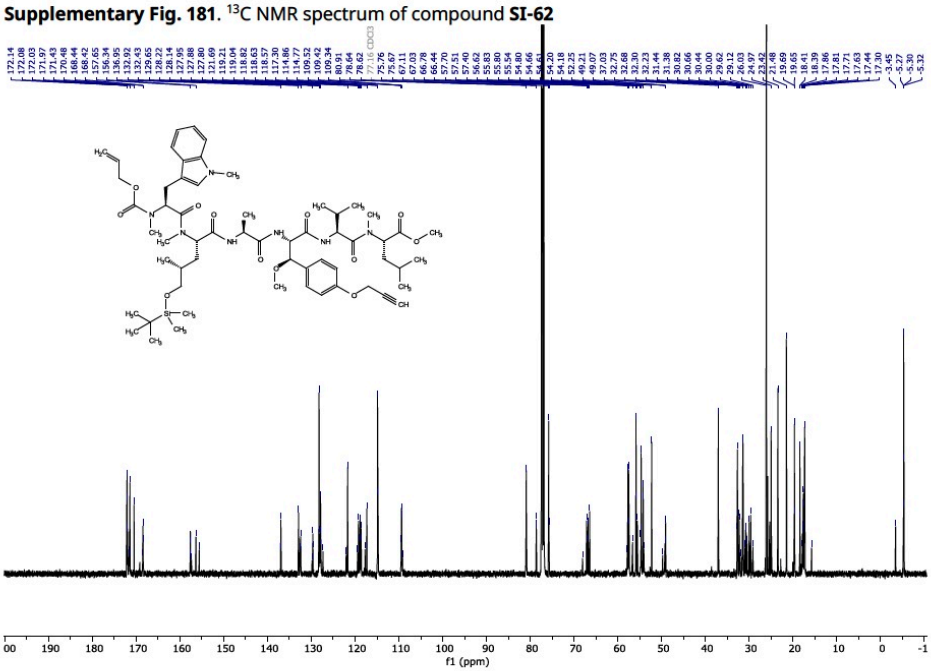

Supplementary Fig. 182. ^{1}H NMR spectrum of compound **SI-63**

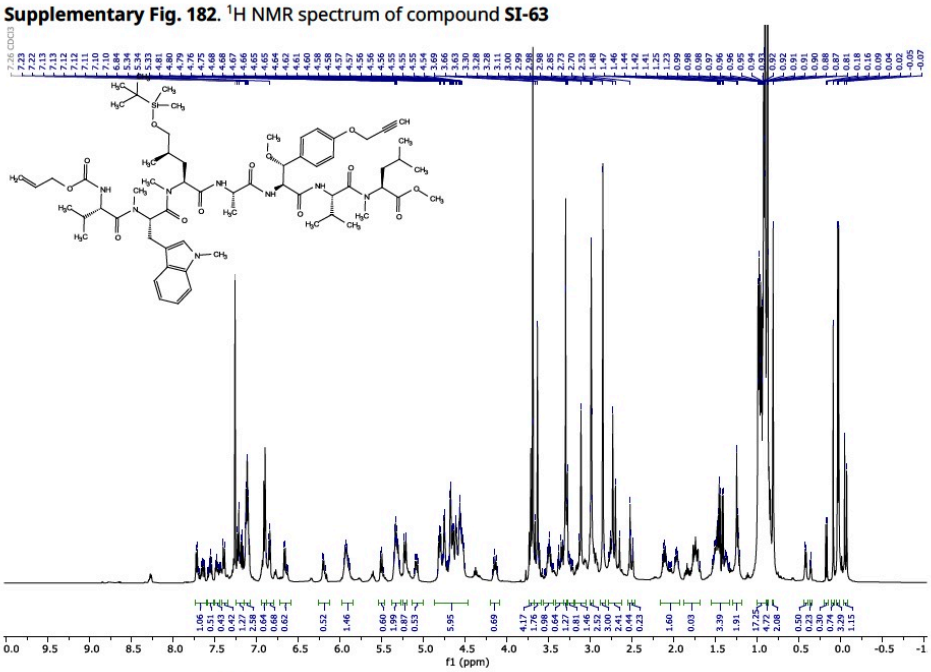

Supplementary Fig. 183. ^{13}C NMR spectrum of compound **SI-63**

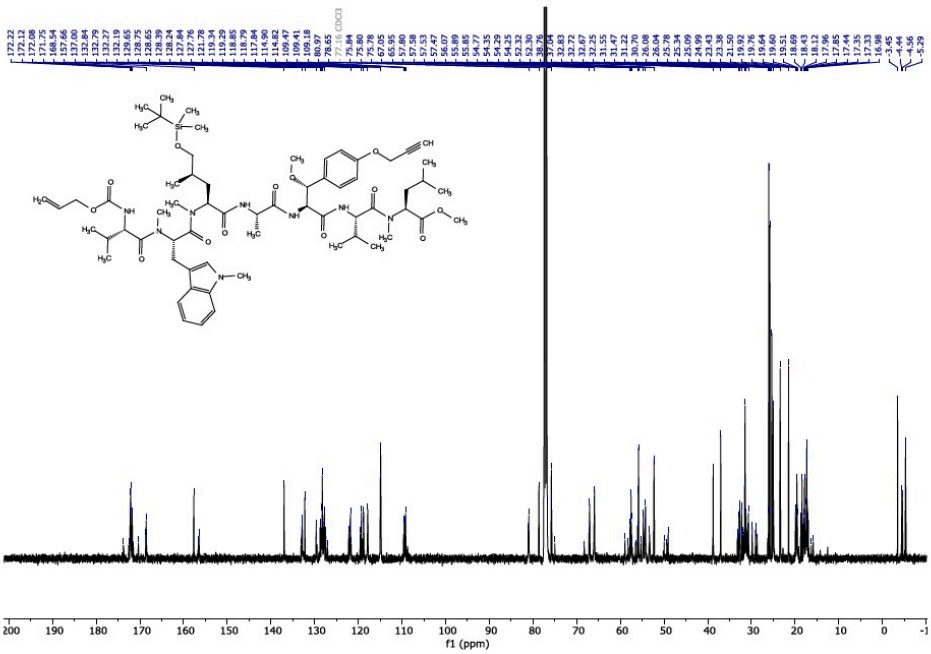

Supplementary Fig. 184. ^{1}H NMR spectrum of compound **SI-64**

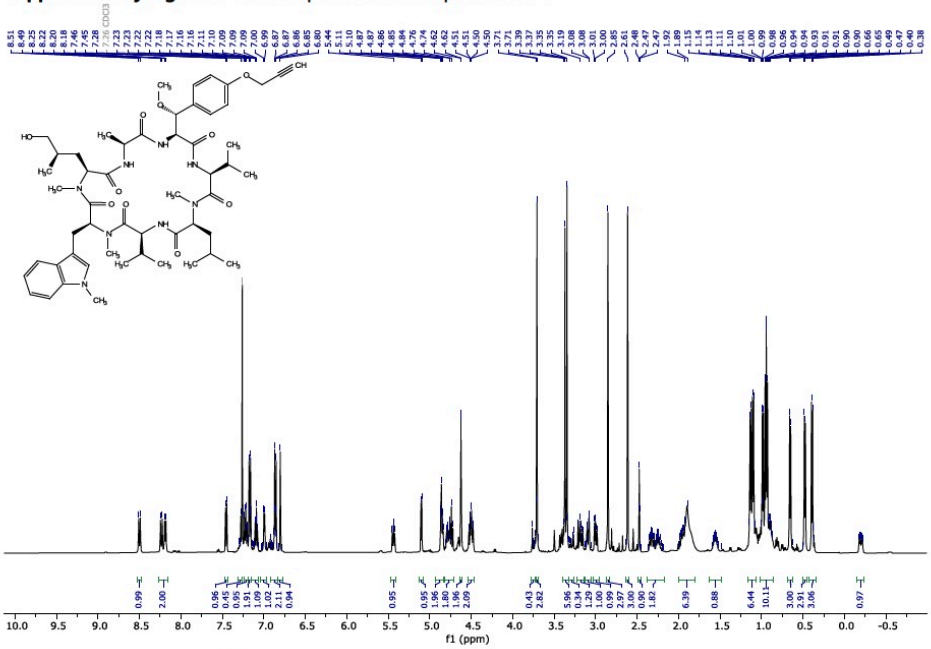

Supplementary Fig. 185. ^{13}C NMR spectrum of compound **SI-64**

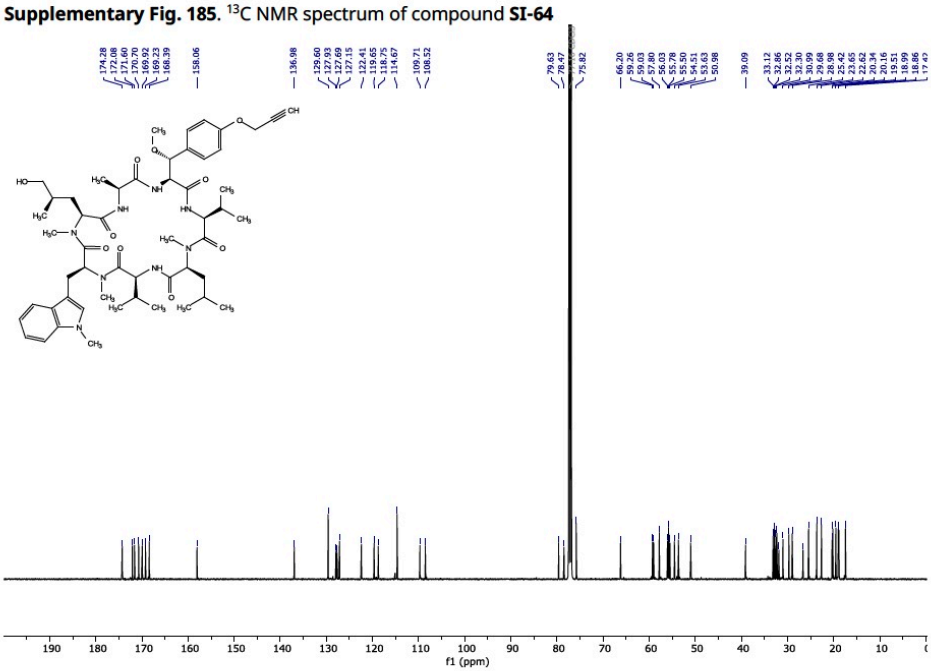

Supplementary Fig. 186. ^{1}H NMR spectrum of compound **SI-65**

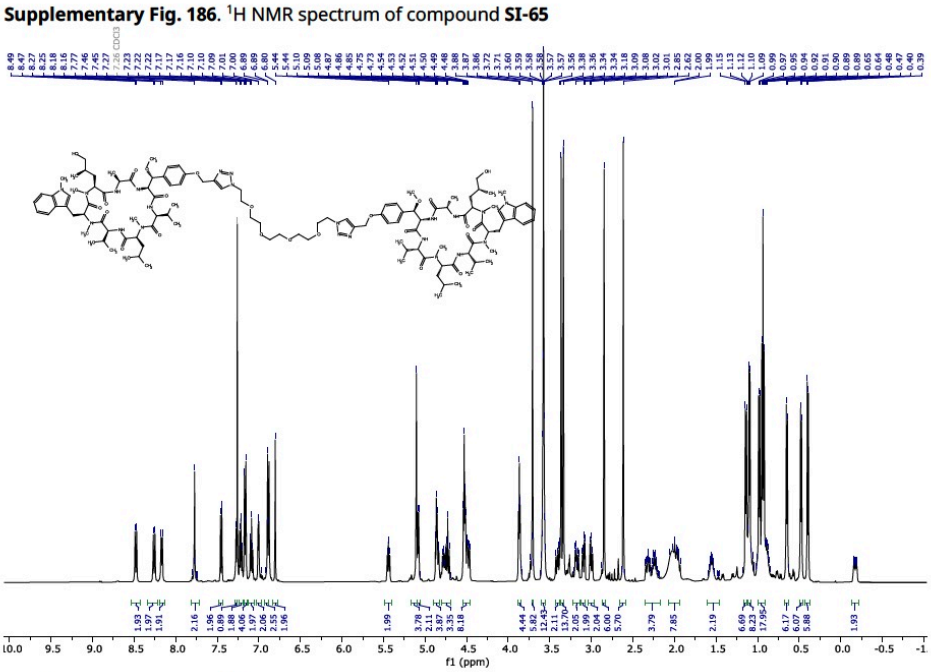

Supplementary Fig. 187. ^{13}C NMR spectrum of compound **SI-65**

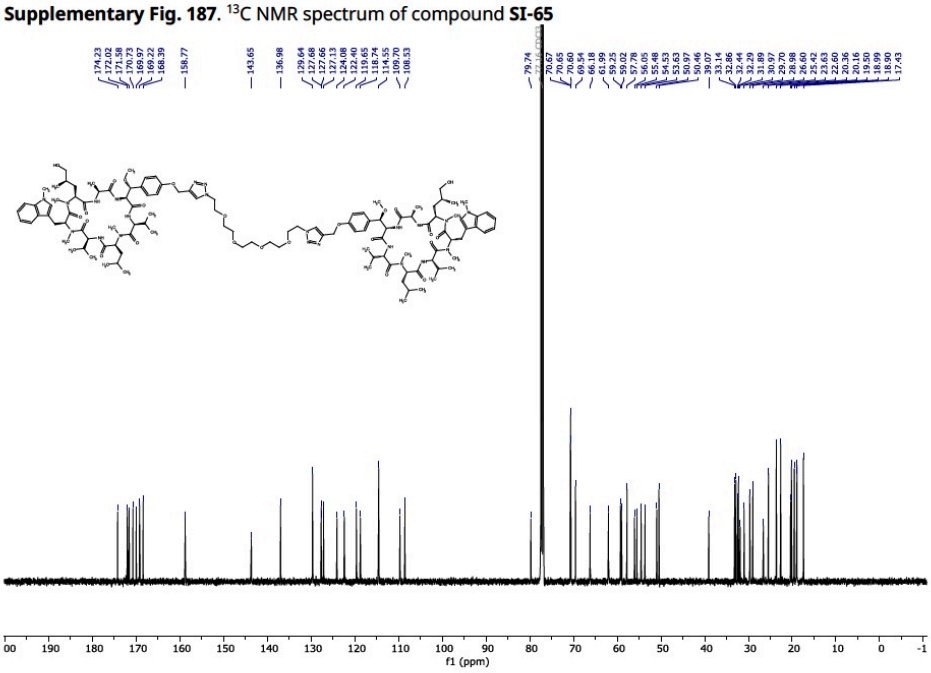

Supplementary Fig. 188. ^{1}H NMR spectrum of compound **SI-66**

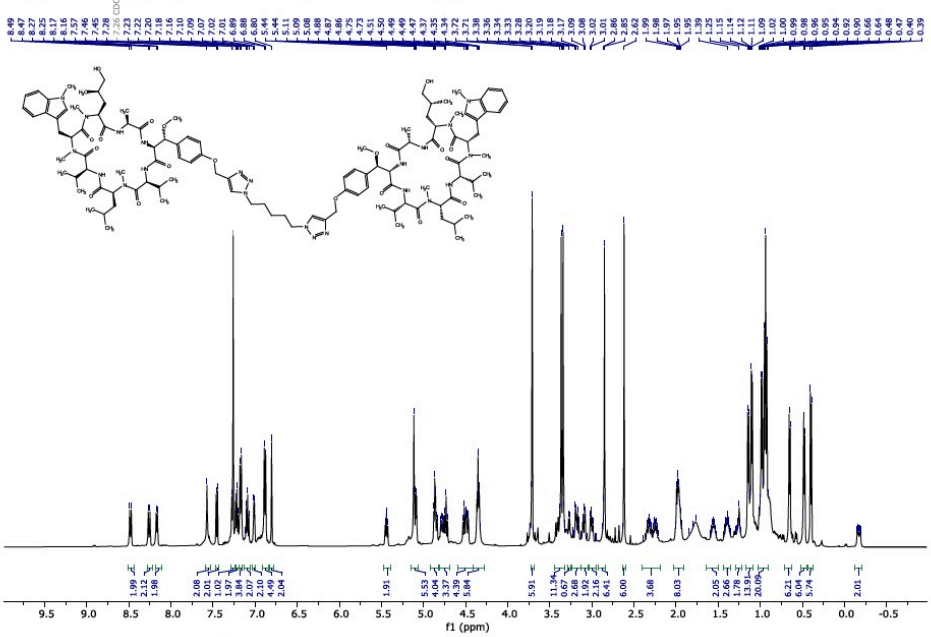

Supplementary Fig. 189. ^{13}C NMR spectrum of compound **SI-66**

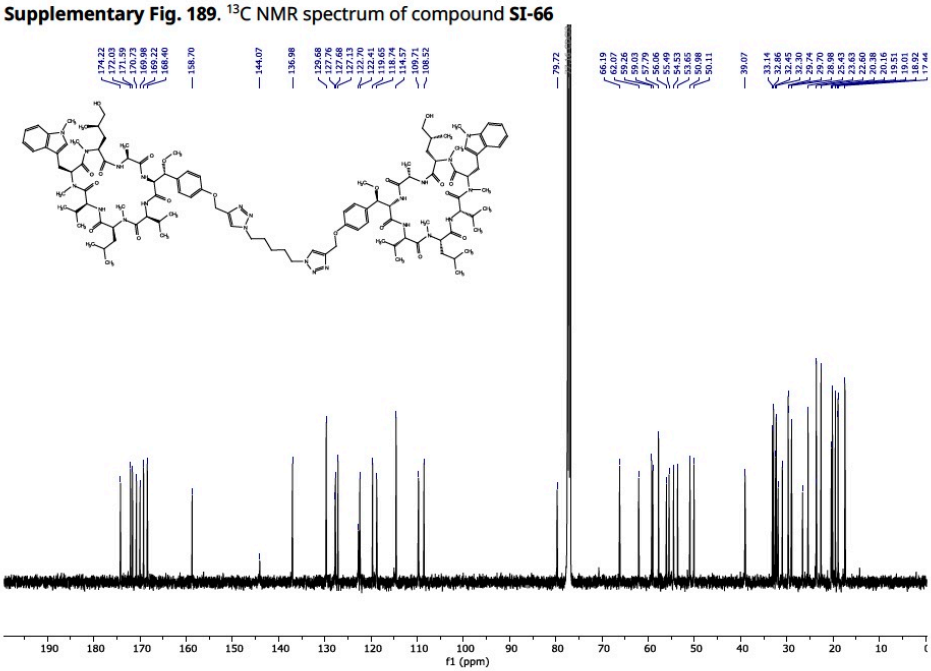

Supplementary Fig. 190. ^{1}H NMR spectrum of compound **SI-67**

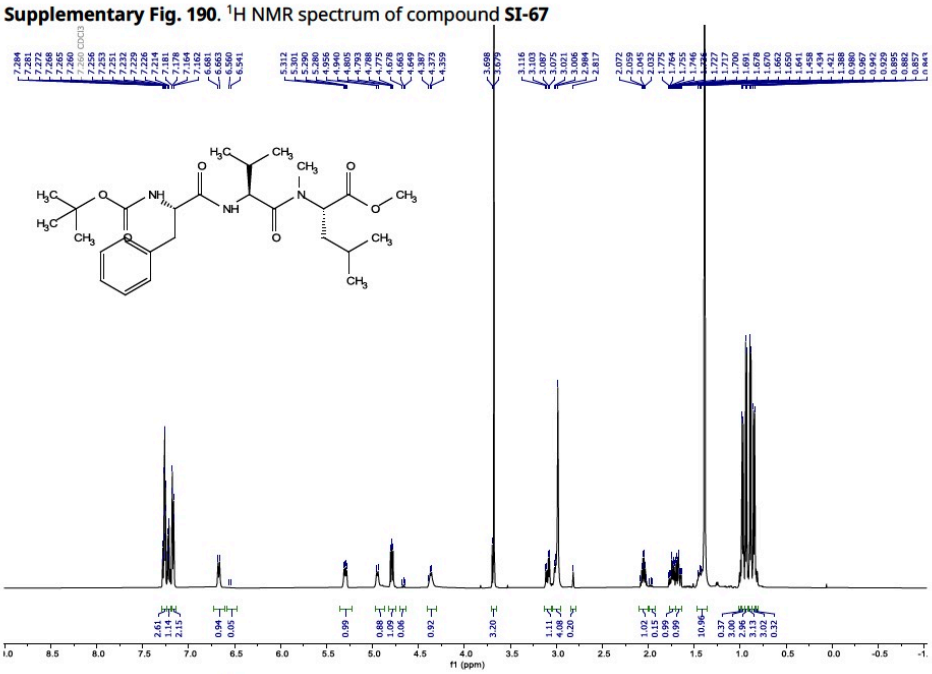

Supplementary Fig. 191. ^{13}C NMR spectrum of compound **SI-67**

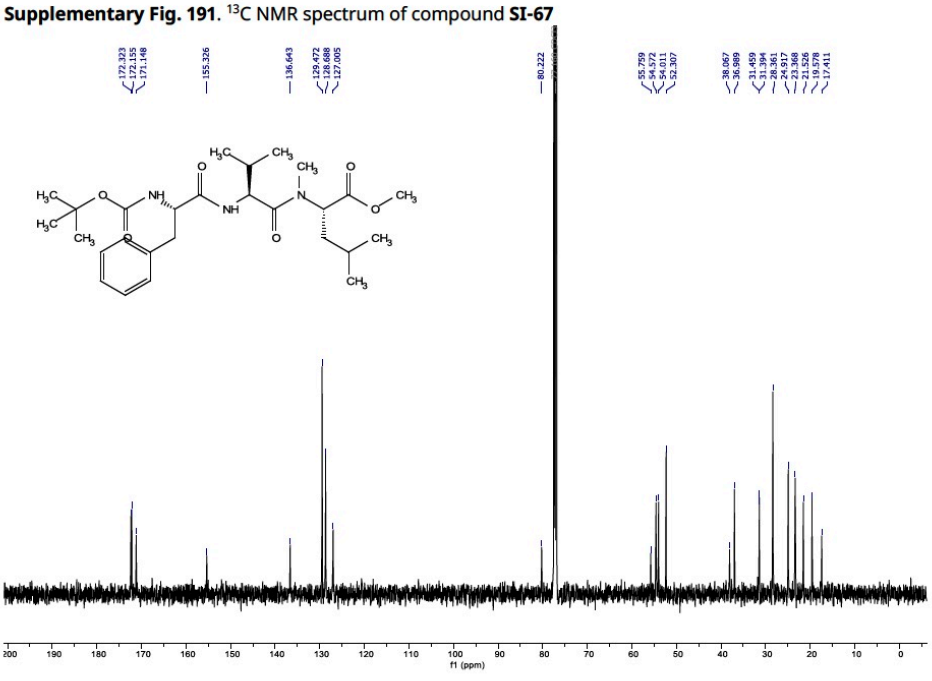

Supplementary Fig. 192. ^{1}H NMR spectrum of compound **SI-68**

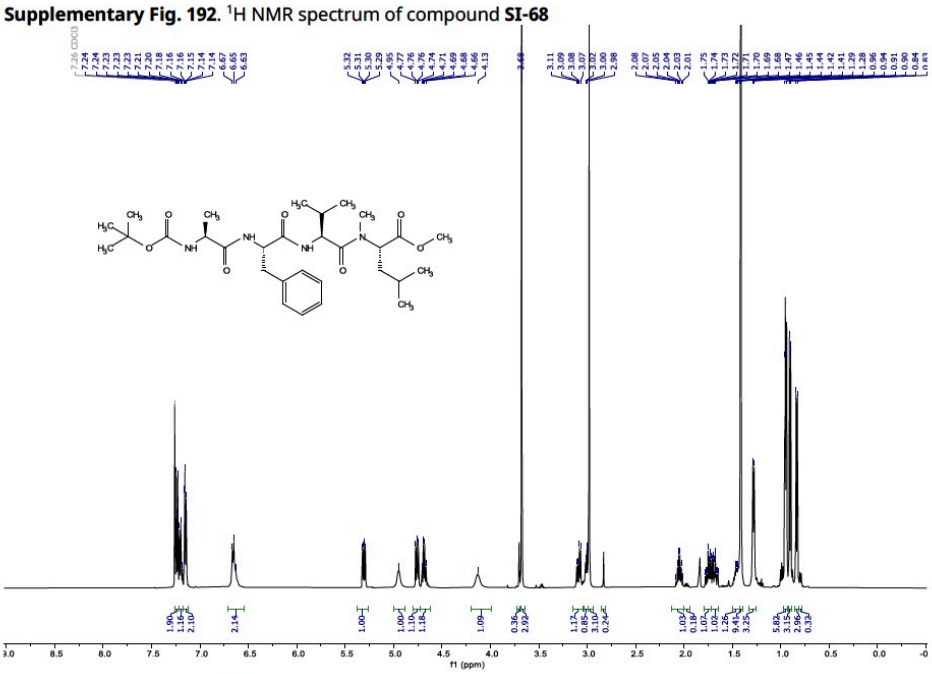

Supplementary Fig. 193. ^{13}C NMR spectrum of compound **SI-68**

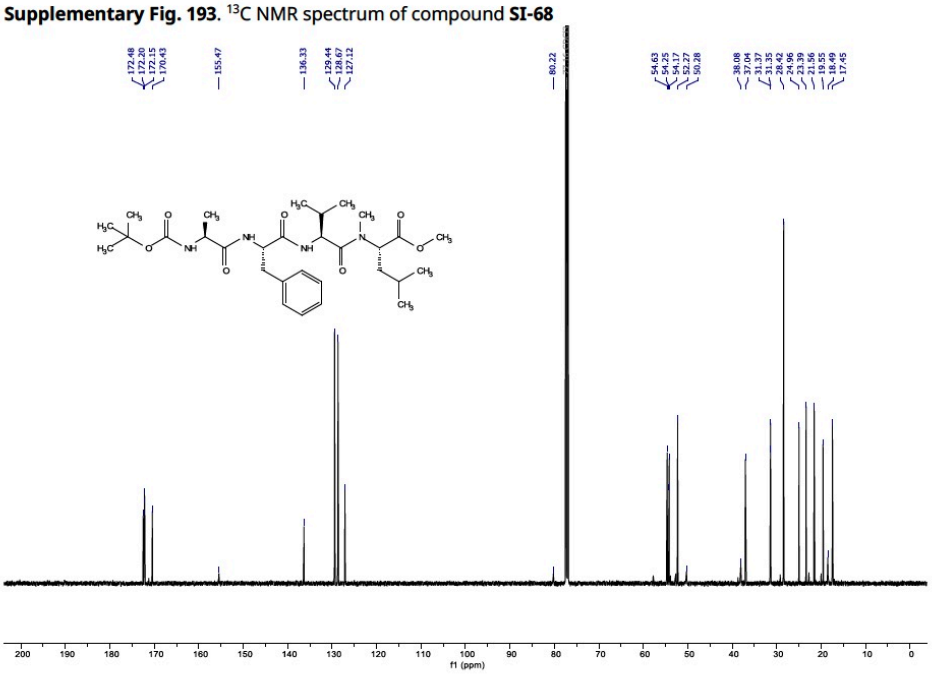

Supplementary Fig. 194. ^{1}H NMR spectrum of compound **SI-69**

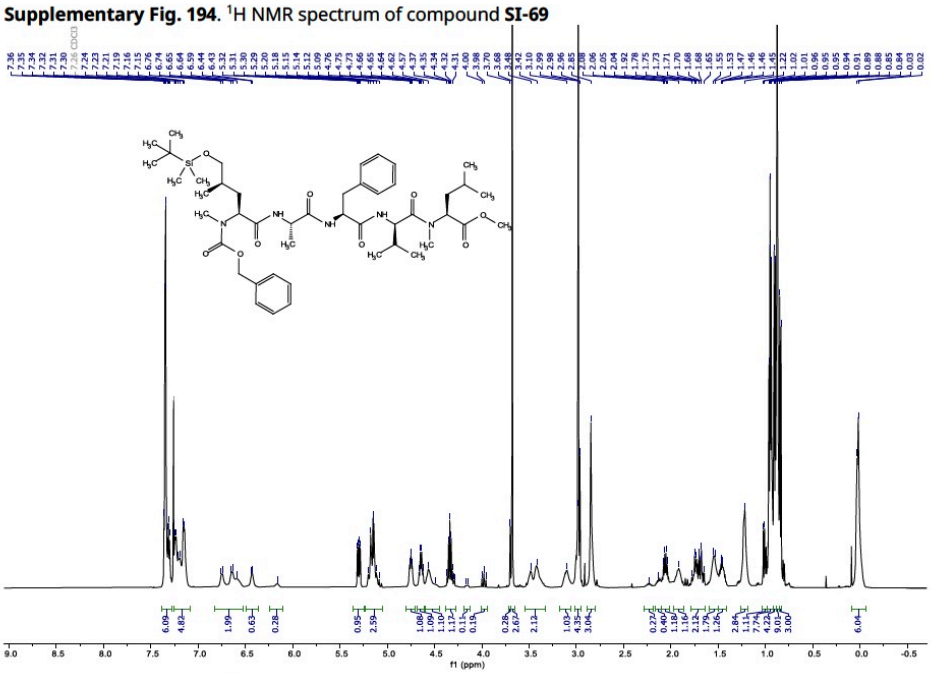

Supplementary Fig. 195. ^{13}C NMR spectrum of compound **SI-69**

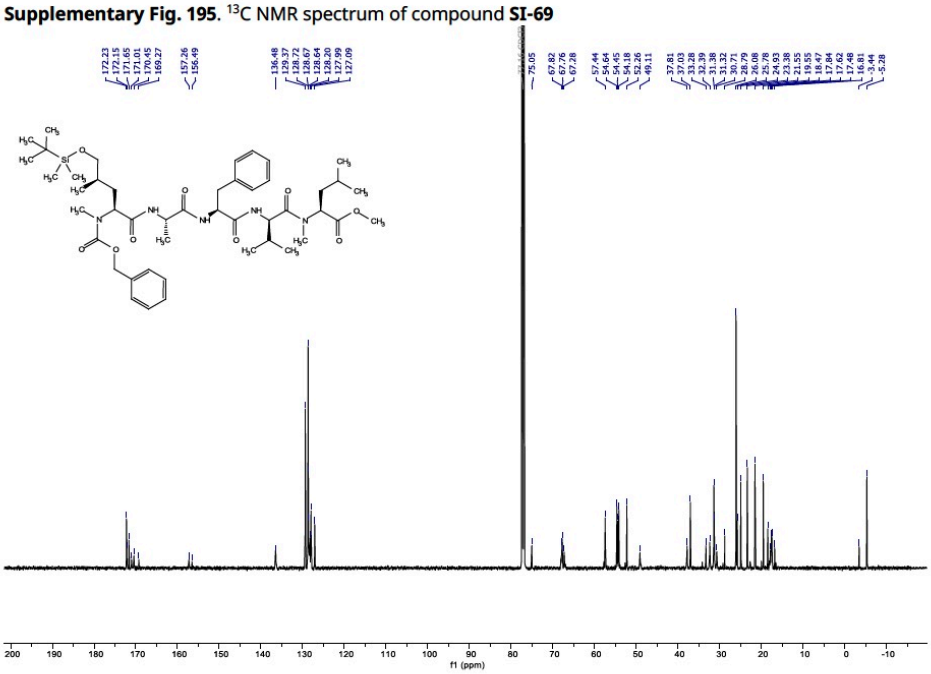

Supplementary Fig. 196. ^{1}H NMR spectrum of compound **SI-70**

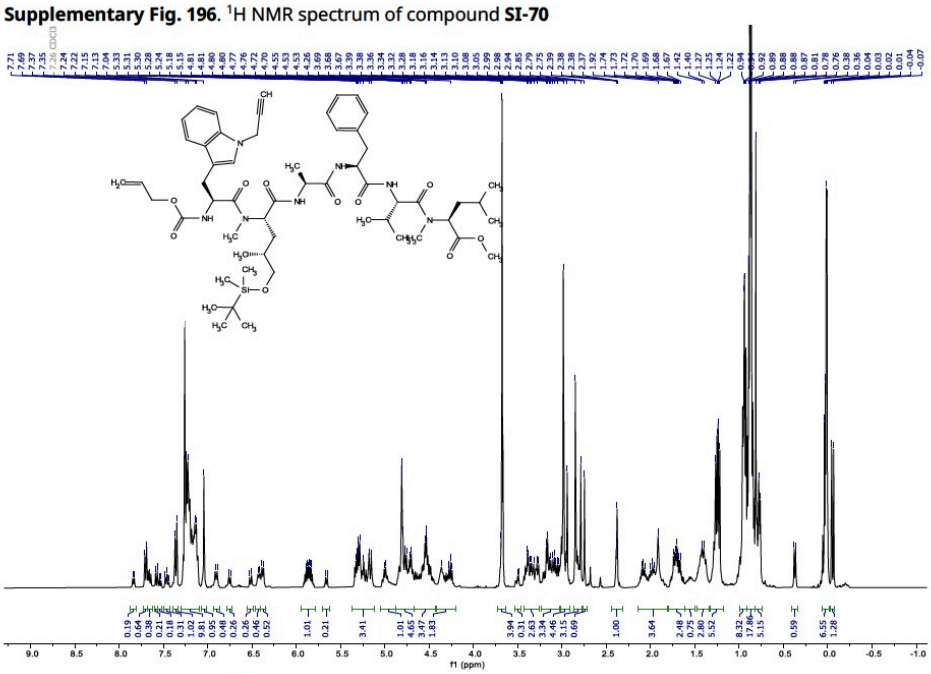

Supplementary Fig. 197. ^{13}C NMR spectrum of compound **SI-70**

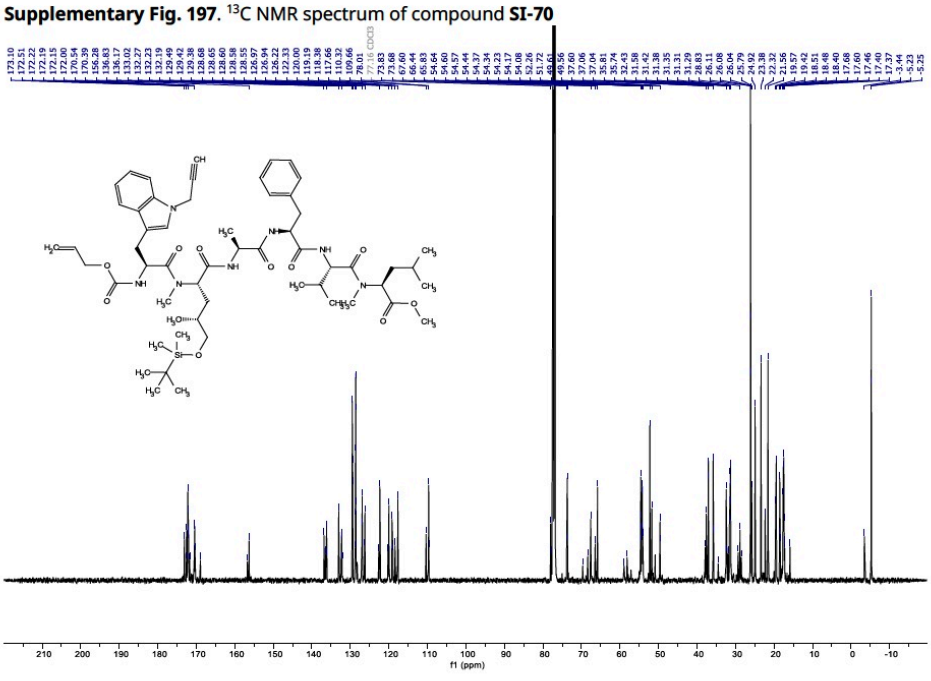

Supplementary Fig. 198. ^{1}H NMR spectrum of compound **SI-71**

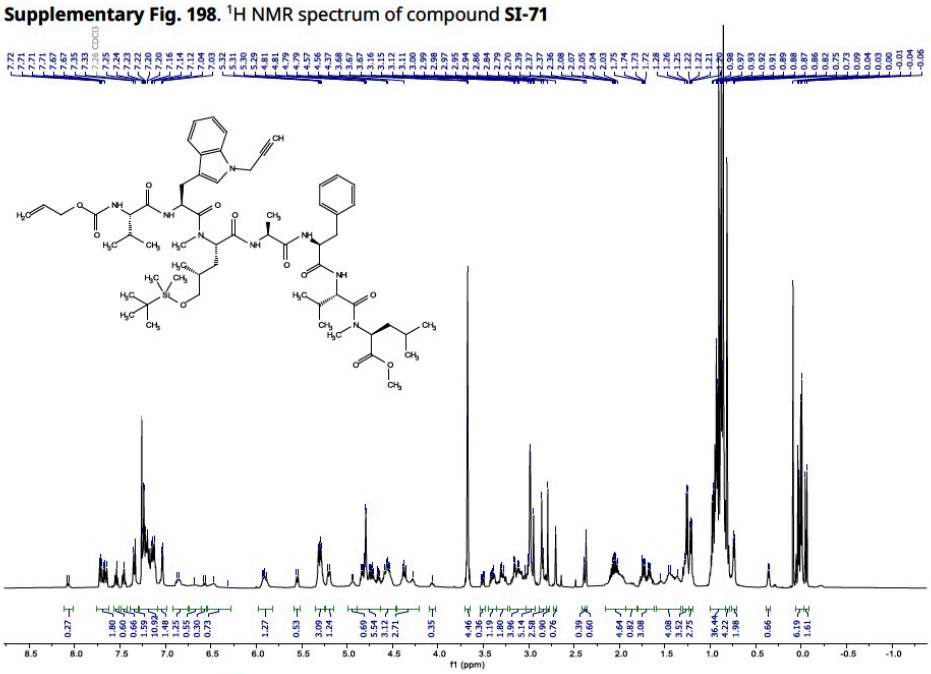

Supplementary Fig. 199. ^{13}C NMR spectrum of compound **SI-71**

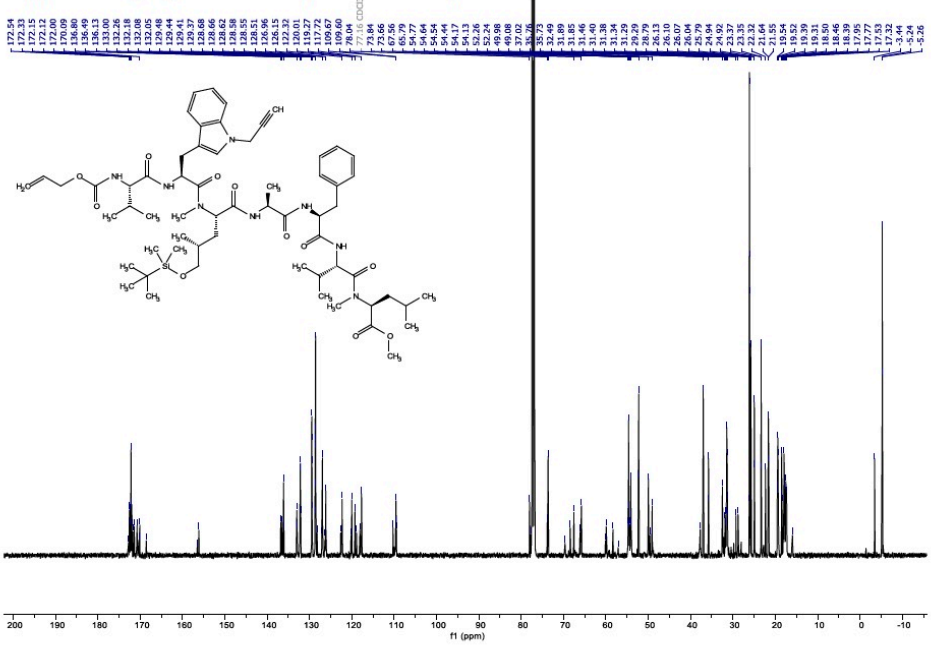

Supplementary Fig. 200. ^{1}H NMR spectrum of compound **SI-72**

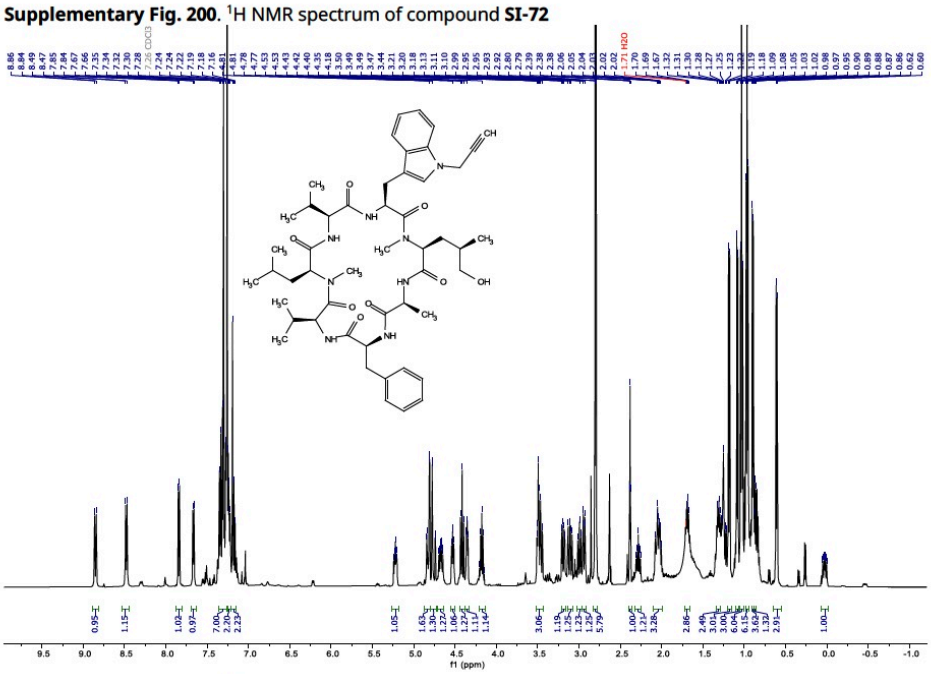

Supplementary Fig. 201. ^{13}C NMR spectrum of compound **SI-72**

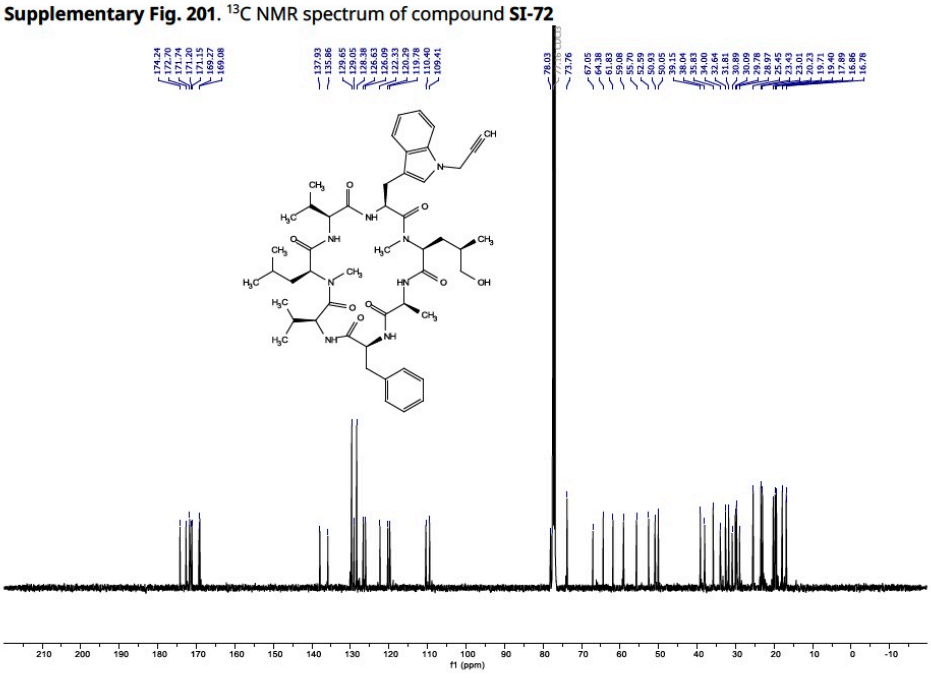

Supplementary Fig. 202. ^{1}H NMR spectrum of compound **SI-73**

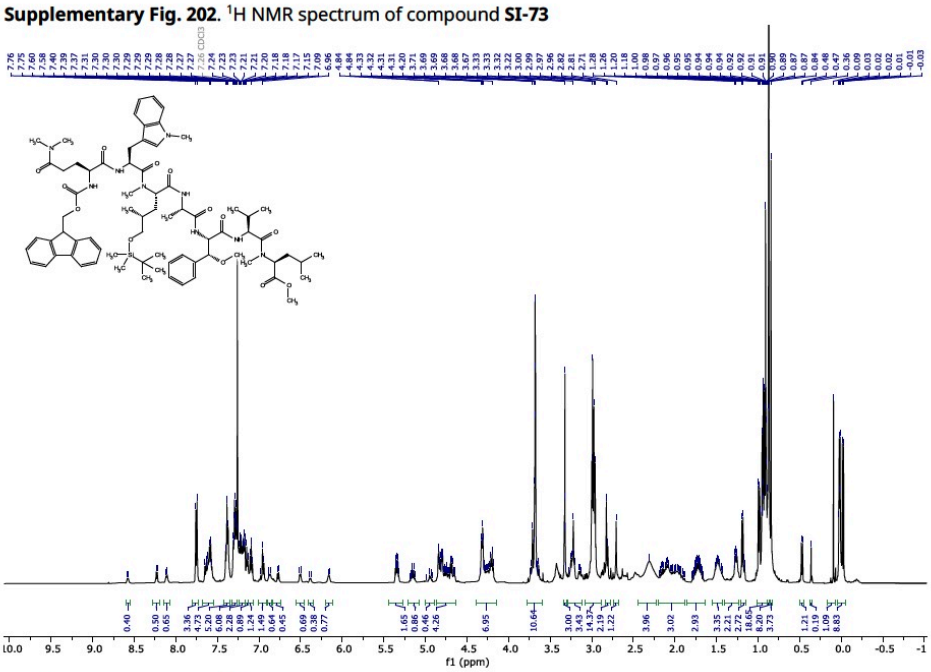

Supplementary Fig. 203. ^{13}C NMR spectrum of compound **SI-73**

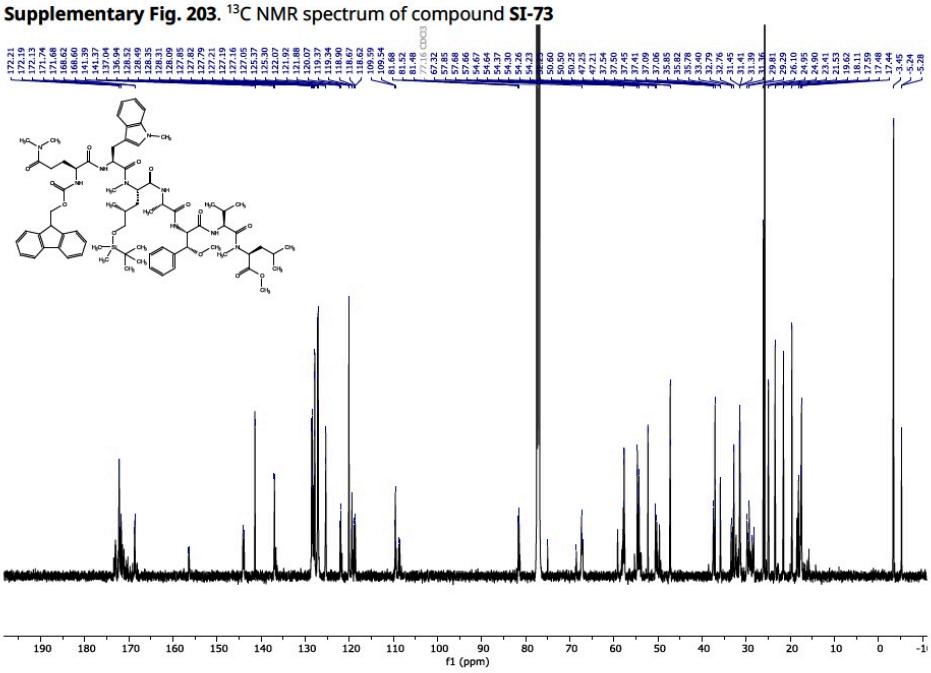

Supplementary Fig. 204. ^{1}H NMR spectrum of compound **SI-74**

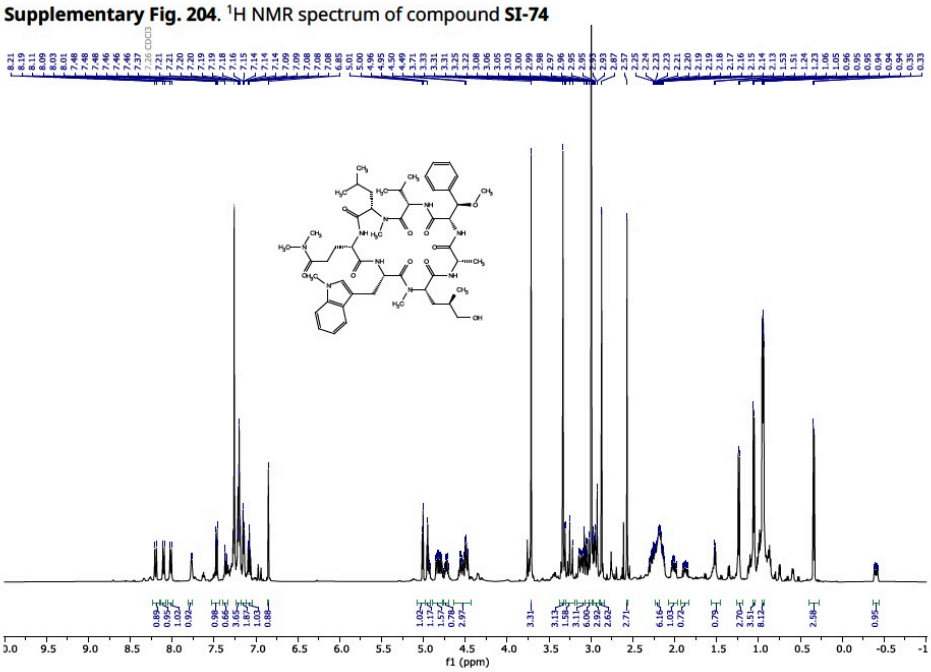

Supplementary Fig. 205. ^{13}C NMR spectrum of compound **SI-74**

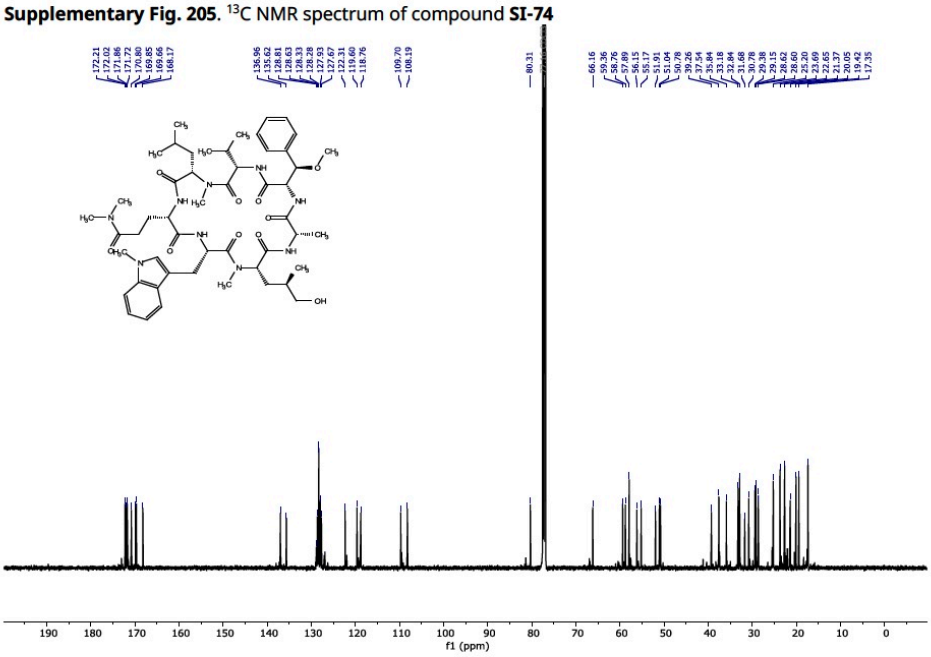

Supplementary Fig. 206. ^{1}H NMR spectrum of compound **SI-75**

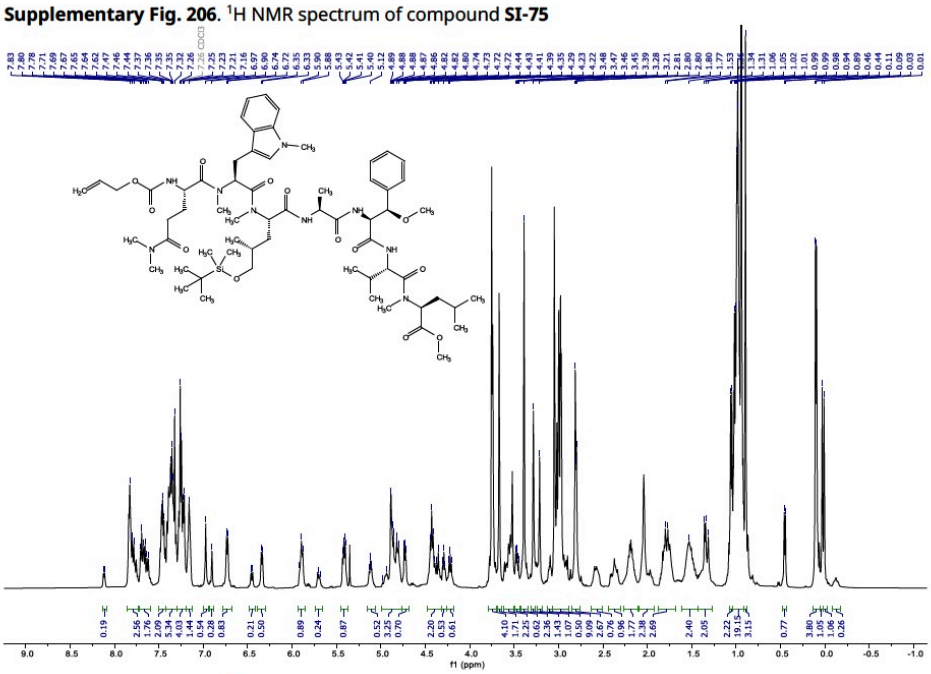

Supplementary Fig. 207. ^{13}C NMR spectrum of compound **SI-75**

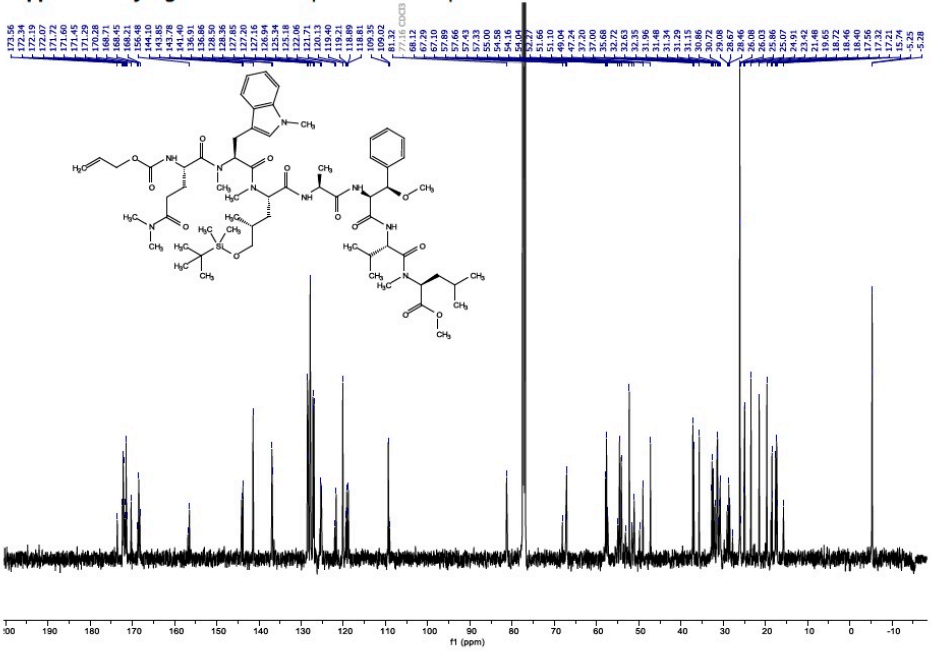

Supplementary Fig. 208. ^{1}H NMR spectrum of compound **SI-76**

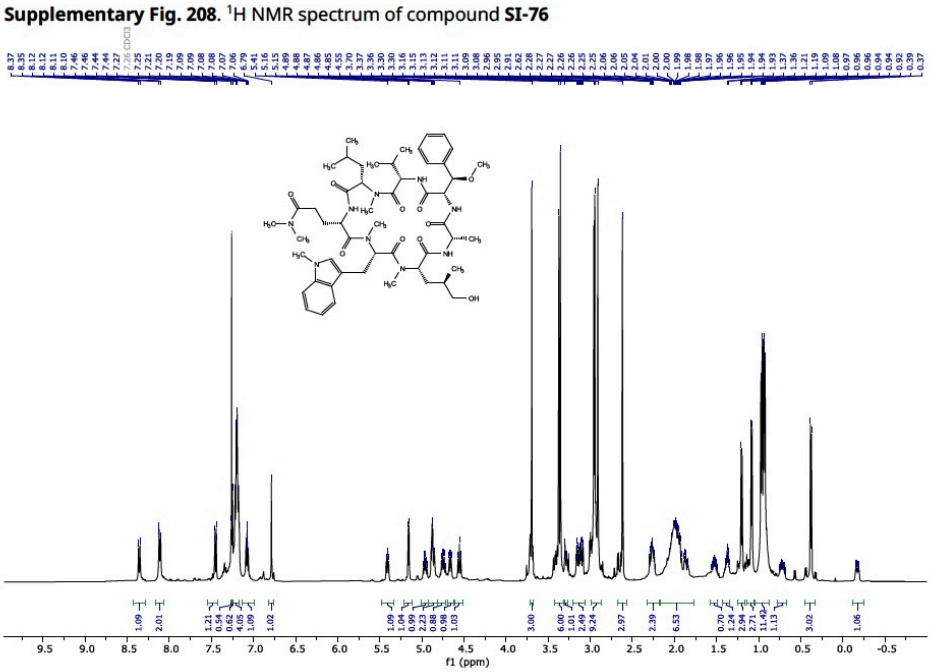

Supplementary Fig. 209. ^{13}C NMR spectrum of compound **SI-76**

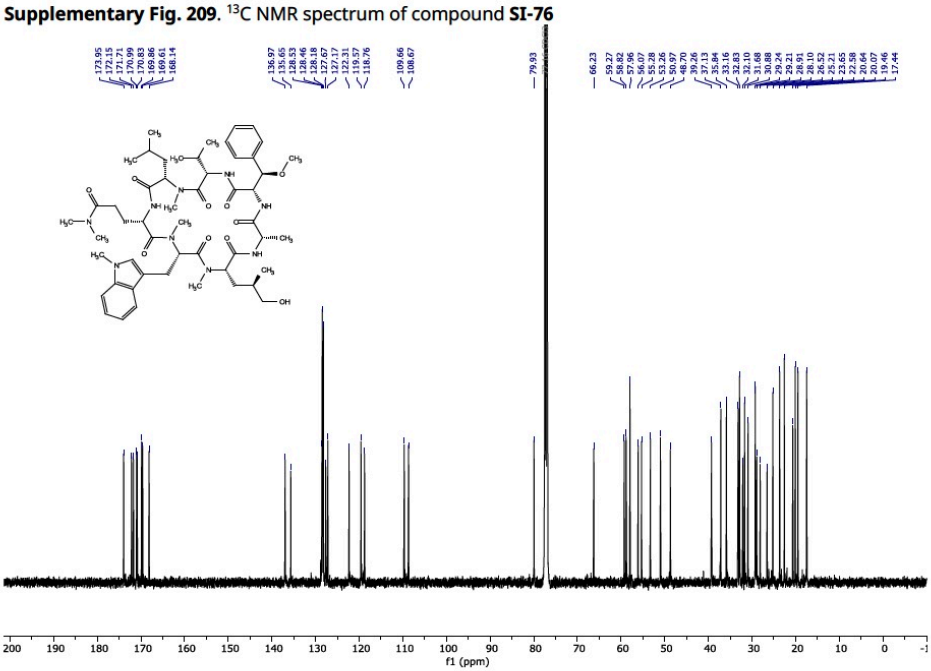

Supplementary Fig. 210: SPR stacking experiment

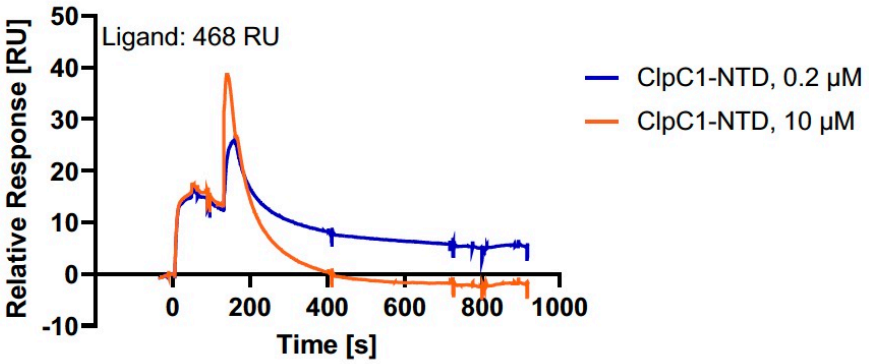

Supplementary Fig. 210. SPR stacking experiment**.** ClpC1-NTD was immobilized on a CM5 chip. After injection of 0.2 µM compound **8 (UdSBI-0545)**, ClpC1-NTD was injected at two concentrations. As can be seen in these sensorgrams, when injecting an equimolar concentration of ClpC1-NTD (0.2 µM ClpC1-NTD) the signal returned to the level observed at the end of the first injection. However, when injecting a 50-fold higher concentration of ClpC1-NTD (10 µM ClpC1-NTD), we still observe low binding of the protein, but the protein seems to completely remove the prebound compound from the chip.

References

1. Gengenbacher, M., Rao, S. P. S., Pethe, K. & Dick, T. Nutrient-starved, non-replicating Mycobacterium tuberculosis requires respiration, ATP synthase and isocitrate lyase for maintenance of ATP homeostasis and viability. *Microbiology* **156**, 81–87 (2010).
2. Abraham, M. H. *et al.* An NMR method for the quantitative assessment of intramolecular hydrogen bonding; Application to physicochemical, environmental, and biochemical properties. *Journal of Organic Chemistry* **79**, 11075–11083 (2014).
3. Cierpicki, T. & Otlewski, J. Amide proton temperature coefficients as hydrogen bond indicators in proteins. *Journal of Biomolecular NMR* **21**, 249–261 (2001).
4. Barbie, P. & Kazmaier, U. Total Synthesis of Cyclomarin A, a Marine Cycloheptapeptide with Anti-Tuberculosis and Anti-Malaria Activity. *Organic Letters* **18**, 204–207 (2016).
5. Junk, L., Papadopoulos, E. & Kazmaier, U. Tryptophan N 1-Alkylation: Quick and Simple Access to Diversely Substituted Tryptophans. *Synthesis* **53**, 2503–2511 (2021).
6. Kiefer, A. *et al.* Synthesis of New Cyclomarin Derivatives and Their Biological Evaluation towards Mycobacterium Tuberculosis and Plasmodium Falciparum. *Chemistry - A European Journal* **25**, 8894–8902 (2019).
7. Gille, F. & Kirschning, A. Studies on the synthesis of peptides containing dehydrovaline and dehydroisoleucine based on copper-mediated enamide formation. *Beilstein Journal of Organic Chemistry* **12**, 564–570 (2016).
8. van de Plassche, M. A. T., Barniol-Xicota, M. & Verhelst, S. H. L. Peptidyl Acyloxymethyl Ketones as Activity-Based Probes for the Main Protease of SARS-CoV-2**. *ChemBioChem* **21**, 3383–3388 (2020).
9. Otake, Y. *et al.* N-Methylated Peptide Synthesis via Generation of an Acyl N-Methylimidazolium Cation Accelerated by a Brønsted Acid. *Angewandte Chemie* **132**, 13025–13030 (2020).
10. Kwit, M., Rozwadowska, M. D., Gawroński, J. & Grajewska, A. Density functional theory calculations of the optical rotation and electronic circular dichroism: The absolute configuration of the highly flexible trans-isocytoxazone revised. *Journal of Organic Chemistry* **74**, 8051–8063 (2009).
11. Yan, L. J. *et al.* Development of Bifunctional Thiourea Organocatalysts Derived from a Chloramphenicol Base Scaffold and their Use in the Enantioselective Alcoholysis of meso Cyclic Anhydrides. *ChemCatChem* **8**, 2249–2253 (2016).
12. Kiefer, A. & Kazmaier, U. Synthesis of modified β-methoxyphenylalanines via diazonium chemistry and their incorporation in desoxycyclomarin analogues. *Organic and Biomolecular Chemistry* **17**, 88–102 (2019).
13. Mulzer, J., Mantoulidis, A. & Öhler, E. Total syntheses of epothilones B and D. *Journal of Organic Chemistry* **65**, 7456–7467 (2000).
14. O'Sullivan, P. T. *et al.* A Concise Synthesis of the Octalactins. *Journal of the American Chemical Society* **126**, 2194–2207 (2004).
15. Jia, M. *et al.* Novel aminopeptidase N (APN/CD13) inhibitors derived from chloramphenicol amine. *Bioorganic and Medicinal Chemistry* **19**, 5190–5198 (2011).

7. Discussion and perspectives

Throughout this study, we introduced new original drug leads, targets, and strategies addressing the rising problem of antimicrobial resistance. Our research was centered on the pathogen *Mycobacterium tuberculosis,* which poses a severe risk to human health. By utilizing a vast collection of synthetic molecules, we successfully discovered two highly effective anti-TB agents, KSK-104 and KSK-106. These compounds provide a potential template for future antibiotics, acting in a unique mode of action and providing hints for the elucidation of several undescribed pathways and targets. Identification of the mechanism of action in conjunction with drug-target identification is imperative for the development of new chemotherapeutic agents. At the same time, the understanding of pathogenicity and virulence factors is critical and a prerequisite for targeting pathogens. We have therefore sought to comprehensively characterize the function of a cell wall assembly protein, which could be used as a future target to combat drug-resistant TB. Combining these two approaches of anti-infective research, we propose the BacPROTACs as a novel antibiotic strategy. The latter brings together natural product-inspired drug design and target characterization, with the potential to tackle not only TB but also other bacterial infections in the future.

7.1 α-Aminooxyacetic acid derivatives

The research presented in chapter 3 introduces the access to a large library of chemically synthesized compounds that enabled us to identify two antitubercular lead structures that are based on an α-aminooxyacetic acid core. The novel chemical entities are precursors of histone deacetylase (HDAC) inhibitors that are classed as antitumor agents. KSK-104 and KSK-106, which have been closely studied, evidenced anti-TB activity within sub-micromolar concentrations and were also highly effective against XDR-TB strains. We found that KSKs exhibit a low rate of resistance against *M. tuberculosis*, along with specificity towards tuberculous mycobacteria and no detectable cytotoxicity, thereby demonstrating several advantages of these compounds. Our investigations revealed that these compounds act as pro-drugs and are likely to be cleaved by the intracellular amidohydrolases AmiC and/or Rv0552. However, the intact structures of the KSKs appear to be required before intracellular cleavage can occur, which might be related to uptake or stereochemical binding properties in the catalytic center of AmiC and/or Rv0552. The single or combined putative cleavage products showed only mediocre anti-tubercular activity. Linear and cyclic amides are known to be hydrolyzed

by amidohydrolases [209]. The homolog of *amiC* in *M. smegmatis* (*MSMEG_2521*) was observed to be involved in induction of acetamidase expression, allowing growth by utilizing amides as the sole carbon source [210]. While *M. smegmatis* AmiC is only 65% identical to AmiC of *M. tuberculosis*, certain residues that were mutated in the SRMs isolated against KSK-derivatives (ABK-256, KSK-104 using the merodiploid *M. tuberculosis* pMV361::*Rv0552* strain), such as S151 and S157, are highly conserved in numerous mycobacterial species and are probably even part of the catalytic center. The amino acid substitution S157F was additionally detected in the SRMs resistant to the indole-4-carboxamides, wherein AmiC plays a role in the activation of the pro-drug [211].

The non-essentiality of the identified genes and the phenotypic characterization of overexpression and gene deletion mutants support our hypothesis that AmiC and Rv0552 participate in the metabolization of the KSKs. This was underlined by the capability of the recombinant proteins AmiC and Rv0552 to cleave amide bonds of the surrogate substrate *para*-nitroacetanilide to some extent (data not shown). Considering the presence of two distinct amide bonds within the original KSK structures, both sites might be accessible to the amidohydrolases. It would be intriguing to conduct further research on the direct cleavage of the KSKs by these proteins, employing the KSKs as substrates for enzyme activity assays. A suitable fluorometric assay for determining amidase activity in a high-throughput manner would involve detecting amines released from enzyme-catalyzed hydrolysis of corresponding amides. This can be done by coupling the amines with 4-nitro-7-chloro-benzo-2-oxa-1,3-diazole (NBD-CI) to form a fluorescent dye [212]. To improve the water solubility of the molecules, a derivative of KSK-106 with a pyridine ring in its C-region was used instead of the original benzene ring. Research indicates that pyridine groups have higher water solubility due to the nitrogen center being more electronegative than the carbocyclic carbons of the benzene ring. The nitrogen center remains available for H-bonding with the water molecule, rendering it immiscible with water. Nevertheless, the used KSK-derivative (ABK-213) proved insufficiently soluble for conducting the enzymatic activity assay. Further structural optimization may enhance the solubility in the future. After establishing the assay, it is necessary to demonstrate that recombinant proteins containing the mutations that were discovered in the spontaneously KSK-resistant mutants are incapable of cleaving the KSKs.

Moreover, a comprehensive analysis of the released products within the cell, their further metabolism, and the components accountable for the compounds' bioactivity is imperative.

Preliminary LC/MS analysis indicated both, alkoxyamide and benzyloxyamide hydrolysis of the KSK-comounds. By incubating *M. tuberculosis* cells with the compounds, not every corresponding hydrolysis product was detected. This was observed by monitoring the disappearance of the parent compounds and the appearance of the released metabolites at different time points after treatment. It can be reasonably assumed, therefore, that at least some of the hydrolysis products are likely to undergo further metabolism. Subsequently, advanced metabolomic techniques could be employed to examine the further metabolization processes within the cell. To further this approach, it would be of interest to investigate the metabolites in KSK-stressed *M. tuberculosis* wild-type cells as well as utilizing the already existing merodiploid or gene deletion mutants of *amiC* and *Rv0552*. By doing so, confirmation of the pro-drug activation potential of AmiC and Rv0552 could be attained, provided that the KSKs are not or less cleaved in the deletion mutant cells or that the metabolites are more present in the overexpressing extracted cell lysates. The creation and usage of an *M. tuberculosis* double gene deletion mutant of *amiC* and *Rv0552* would improve this thorough analysis.

In order to ascertain how the resulting α-aminooxyacetic acid hydrolysis products are responsible for the antitubercular activity of the parental compounds, we conducted a broad analysis of the drug-induced alterations using genome-wide genetic, transcriptomic, and proteomic experiments. It became evident that KSK treatment exerted an influence on a range of mechanistic pathways. First and foremost, a comprehensive transposon-insertion sequencing analysis has demonstrated that the fitness of the cells under KSK-106 is influenced by mutations in the PLP synthesis and salvage pathway. PLP is one of the active forms of vitamin B(6), which was first identified as a cofactor of enzymes involved in a wide range of chemical reactions in the 1940s [213]. It has been demonstrated that PLP-dependent enzymes are primarily involved in the synthesis, interconversion, and degradation of amino acids. However, they also play a pivotal role in the replenishment of one-carbon units, the synthesis and degradation of biogenic amines, the synthesis of tetrapyrrolic compounds and the metabolism of amino-sugars [214]. Indeed, PLP-dependent enzymes have been demonstrated to mediate over 140 distinct activities, representing 4% of all known catalytic activities [215]. This remarkable diversity of reactions is achieved through the exploitation of the electron sink effect of the pyridine ring, the conformational changes accompanying the chemical steps, the stabilization of distinct catalytic intermediates, and the spectral properties of the different coenzyme–substrate derivatives [216]. Despite the striking differences in the catalytic mechanisms, PLP-dependent enzymes share the feature that the coenzyme is held via a Schiff

base to the ε-amino group of a conserved lysine residue, leading to the internal aldimine complexes. The initial catalytic step, which is common to most PLP-dependent enzymes, requires a nucleophilic attack of the substrate-containing amine on the imine double bond of the internal aldimine, forming a gem-diamine. Subsequently, the substrate displaces the lysine residue, forming a non-covalently bound external aldimine where it can undergo decarboxylation, deprotonation, or otherwise stabilize a formal carbanion through resonance in the quinonoid intermediate [217]. The pivotal role of these enzymes in metabolic processes has led to their designation as relevant drug targets. One such enzyme is ornithine decarboxylase, which catalyzes the conversion of ornithine to putrecine, thereby providing the initial step in the synthesis of amino acids and polyamines. The enzyme is targeted by α-difluoromethylornithine, which presents a substrate for the enzyme and undergoes PLP-dependent decarboxylation in the active site. The primary rationale for its synthesis was to develop a treatment for facial hirsutism and African trypanosomiasis. Furthermore, the compound was tested as an anticancer agent and as a potential treatment for other diseases [218-221]. For additional PLP-dependent enzymes, including DOPA decarboxylase (associated with Parkinson's disease), GABA aminotransferase (linked to epilepsy), serine hydroxymethyltransferase (involved in tumour formation and malaria), and human cytosolic branched-chain aminotransferase (linked to pathological states associated with GABA/glutamate equilibrium concentrations), commercially drugs are currently available [214]. It is noteworthy that one second-line anti-TB drug, DCS, also targets a PLP-dependent enzyme. DCS is a structural analogue of D-Ala that targets two essential enzymes involved in the cell wall peptidoglycan biosynthetic pathway, termed alanine racemase (Alr) and D-Ala:D-Ala-ligase (Ddl) [222]. Ddl is a PLP-dependent enzyme, indicating the potential of these enzymes as anti-TB drug targets. It has been demonstrated that DCS causes a time-dependent inhibition by covalently modifying PLP in the enzyme [223, 224]. The aminooxy groups present in both DCS and our studied KSK-compounds could prove to be of relevance, as it appears that the effect of the KSK compounds is also linked to the PLP pathway. It has been demonstrated that mutations in the gene encoding the PLP synthesis enzyme *snzP* and the gene responsible for PLP salvage, *pdxH*, result in a loss of fitness when exposed to KSK treatment. We thus assume that KSK treatment induces an increased demand for PLP within the cell. This hypothesis has been validated via an experiment wherein exogenous addition of pyridoxine rendered cells resistant to KSK-104 and KSK-106 treatments. It can thus be concluded that the α-aminooxyacetic acid derivatives, or their final metabolized compounds, may either inhibit PLP biosynthesis or act as an inhibitor of PLP-dependent enzymes. This is corroborated by the

fact that complete alkoxyamide and benzyloxyamide hydrolysis of the studied KSKs will generate aminooxyacetic acid. This metabolite is a well-documented inhibitor of PLP-dependent enzymes, including 4-aminobutyrate transaminase, alanine transaminase, glutamate decarboxylase, and alanine racemase, among others [225-227].

Aminooxy compounds, including *O*-benzylhydroxylamine, *O*-*tert*-butylhydroxylamine, carboxymethoxylamine, and *O*-allylhydroxylamine, have the capacity to attack the Schiff base linkage between PLP and the enzyme, resulting in the generation of a stable PLP *O*-acetic acid [228]. It is noteworthy that the aforementioned species were postulated to function as potential branched-chain amino acid aminotransferase (BCAT) inhibitors, which could be utilized in the management of TB [229]. However, our findings revealed that exogeneous aminooxyacetic acid exerts no antitubercular effect, which is likely attributable to its poor uptake. It can thus be assumed that the intracellularly released active moieties may inhibit PLP-dependent enzymes. It is plausible that the formed aminooxyacetic acid may undergo a spontaneous reaction with PLP, resulting in the formation of an unstable hemi-aminal. Subsequently, this reaction could lead to a Schiff base formation, which may yield the aforementioned reaction product in KSK-treated *M. tuberculosis* cells (Figure 5). Verification of the hypothesis would be accomplished through the detection of the reaction product in extracts of the treated *M. tuberculosis* cells by LC-MS/MS. Subsequent studies could then determine whether specific PLP-dependent reactions are of particular importance with regard to the antibacterial mechanism, or whether the antibacterial effect is the result of the inhibition of numerous pyridoxal phosphate-dependent enzymes.

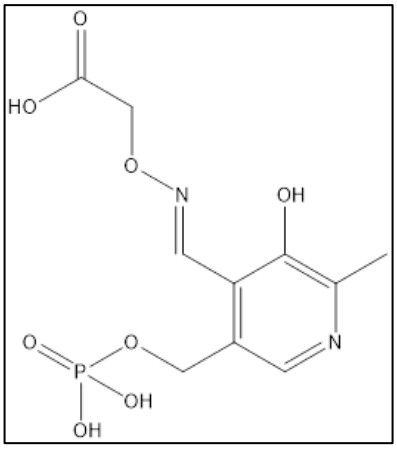

Figure 5: Final reaction product after Schiff base formation of aminooxyacetic acid and PLP. After complete alkoxyamide and benzyloxyamide hydrolysis of the KSK compound aminooxyacetic acid can be generated, which can form a stable reaction product with PLP.

In addition to their impact on the PLP pathway, our findings suggest that the KSKs influenced the oxidative stress network within the *M. tuberculosis* cell, as evidenced by the enrichment of *doxX* mutations following KSK treatment. It is therefore essential to ascertain the existence of potential correlations between these pathways to gain comprehensive insights into the mechanism of action. It has recently been demonstrated that at least one PLP-dependent enzyme is responsible for the production of hydrogen sulfide (H_2S) in *M. tuberculosis* [230]. In bacteria, H_2S is classified as "small molecule signalling agent". It has been observed to protect against metal ion toxicity, a range of classes of antibiotics, and, of particular interest in the context of this discussion, against oxidative damage [231]. It directly scavenges metal ions and reactive oxygen species (ROS), preventing Fenton chemistry and related antibiotic-induced damage [232, 233]. It bears noting that the production of H_2S in mycobacteria was effectively compeded by the use of aminooxyacetic acid [230]. This could provide an explanation for the observed results linking the KSK-induced effect on the PLP pathway and, moreover, its impact on the oxidative stress network in *M. tuberculosis*. A variety of techniques may be employed to quantify H_2S production in KSK-treated and untreated cells. These include the lead acetate method, the bismuth chloride method, and the use of an amperometric microsensor assay [234-236]. Given that H_2S production in *M. tuberculosis* is PLP-dependent, these experiments could demonstrate that the putatively KSK-released aminooxyacetic acids are blocking H_2S formation in *M. tuberculosis* cells, thereby increasing the sensitivity of *M. tuberculosis* cells towards oxidative stress.

Further investigation into the potential implications of the KSKs on the oxidative stress network could be undertaken along several lines of inquiry. It has been reported that *M. tuberculosis* has developed protective and detoxification mechanisms to maintain cytoplasmic redox balance in response to both exogenous oxidative stress within host phagocytes and endogenous oxidative stress generated within the cell [237-239]. DoxX is part of the membrane-associated oxidoreductase complex (MRC) and interacts with SodA and SseA to present the coordinated radical detoxification system [240]. It is possible that the impact of the KSKs on this complex may be mediated through an inhibitory effect on SodA or the generation of superoxide anions. Indeed, research has demonstrated that PLP can function as a potent suppressor of reactive oxygen intermediates [241, 242], providing a further possible explanation for the link between the effect of the KSKs on the PLP pathway and the oxidative stress network. Should KSK-treatment generate greater quantities of superoxide anions while PLP levels are diminished, this could result in an additive antibacterial effect. One of the identified hits revealed by TnSeq,

Rv2607 (*pdxH*), encodes a protein with reported pyridoxine/pyridoxamine 5'-phosphate (PNP/PMP) oxidase activity. This activity results in the release of the product, PLP, from the substrates PNP and PMP [243]. In the catalytic process of PNP/PMP reacting to PLP, superoxide anions are converted into hydrogen peroxide molecules. This effect may result in the accumulation of superoxide anions, which could potentially be linked to the oxidative stress response previously discussed in the context of KSK treatment. Nevertheless, further investigation is necessary to discover whether KSKs influence the PLP synthesis/salvage pathway or PLP-dependent enzymes and their relationship with the oxidative stress network.

Further examinations could be pursued to clarify the mechanisms by which KSKs influence the reactive oxygen system of *M. tuberculosis*. The alteration of redox homeostasis by KSKs within the cell might be explored through the use of a recombinant *M. tuberculosis* reporter strain expressing a redox-active green fluorescent protein (GFP) [244, 245]. By measuring the fluorescence emission and the relative abundance of oxidized and reduced GFP species, the intracellular redox state of *M. tuberculosis* cultures exposed to KSKs can be determined. This could reveal a possible oxidized or reduced redox state in the cytoplasm after KSK treatment. Based on our TnSeq analysis, we did not identify any hits indicating that sulfate or thiosulfate transport was affected by KSK treatment. Therefore, it can be assumed that thiol homeostasis or thiol stress is an unlikely factor involved in this process; instead, a general oxidative stress response is more probable. Nevertheless, it is important to exclude the possibility of KSK treatment depleting thiol pools inside the cells. The intracellular free thiol pools could be directly measured after cell treatment, as described elsewhere [246]. However, if KSKs depleted thiol pools and lowered resistance to oxidative stress along this pathway, then KSK-106 would have been expected to sensitize *M. tuberculosis* to clofazimine. Clofazimine is a redox-cycling component of MDR-TB treatment that competes with menaquinone and spontaneously produces ROS [247, 248]. The lack of a synergistic impact observed in the checkerboard assay lends support to our hypothesis. Finally, it is necessary to investigate whether KSK treatment results in ROS accumulation. Previous studies indicated that elevated endogenous ROS levels may have adverse effects on *M. tuberculosis* growth and viability during infection and *in vitro* [237, 249]. In order for ROS to induce cell death, they must overwhelm the detoxifying pathways that are in place to counteract them [250, 251]. It has been demonstrated that intracellular hydrogen peroxide levels must be within a range of 1.0 mM for cytotoxic/bactericidal effects of ROS to occur [252, 253]. The fluorescent CellROX assay may be employed for the measurement of intracellular ROS levels [254]. Moreover, to determine

whether ROS is the primary determinant of killing, it is necessary to investigate whether ROS scavengers, such as N-acetylcysteine (NAC) and 4-hydroxy-2,2,6,6-tetramethyl-1-piperidinyl-oxidanyl (TEMPO), could promote resistance towards KSK-106. Both NAC and TEMPO, were found to reduce growth inhibition of clofazimine, again associating the production of ROS with clofazimine [248]. It can be posited that NAC does not impact the activity of KSK-106, as NAC likely operates through a thiol-associated mechanism, whereas TEMPO scavenges ROS through a thiol-independent mechanism, thereby rendering it probable that it mediates resistance towards KSK-106. This hypothesis could be tested by examining the efficacy of the KSKs in combination with one of the naphthoquinones, such as plumbagin and menadione, which are known to induce oxidative stress in bacteria [255, 256].

In addition, our wide proteomic and transcriptomic profiling identified an upregulated gene cluster associated with KSK treatment that has not yet been linked to the impaired PLP pathway. Genes belonging to the operon *Rv3092c-Rv3095*, as well as *Rv3096* clustered with this operon, were found to be up-regulated as a stress response in both analyses. Information about the referred *Rv3095*-operon is scarce. The HTH-type transcriptional regulator *Rv3095* is divergently oriented from a hydrolase (*Rv3094c*), an oxidoreductase (*Rv3093c*), as well as an ABC transporter (*Rv3092c*) and convergently oriented with xylanase (*Rv3096*). It has been shown that Rv3094c is probably a flavin-dependent monooxygenase with a FAD binding site and acyl-CoA dehydrogenase activity involved in the activation of ethionamide by sulfoxidation [257]. Besides that, this operon has yet not been mentioned in the context of any other antibiotic treatment. It may therefore be postulated that the operon is upregulated as a highly specific misguided stress response. The eventual consequence of the monooxygenase activity of Rv3094c is the production of ROS, thereby amplifying the antibacterial impact of the KSK compounds. Furthermore, it is theoretically possible that the operon is upregulated in order to compensate for a deficiency in the ETC. It may be the case that Rv3094c performs a specific oxidoreductase function within the ETC, thereby ensuring the optimal operation of cytochromes and a stable PMF. Nevertheless, further characterization of this operon is required before any further conclusions can be drawn. This can be achieved by investigating the impact of KSKs on the ETC using the generated *Rv3095*-operon deletion mutants. In conclusion, the observed pleiotropic effects suggest that the combination of two or more KSK hydrolysis products or their resulting metabolites is responsible for bacterial cell death in a "dirty drug" like manner.

The studied KSKs contain two potential hydroxamic acid groups. Although no hydroxamic acids are formed by the postulated hydrolytic cleavage by the discussed amidases AmiC and Rv0552, it cannot be fully excluded that such molecules are formed by other, yet-unknown mechanisms inside *M. tuberculosis* cells. Hydroxamic acids are capable of chelating metal ions, like the HDAC inhibitor vorinostat. The hydroxamic end of this molecule binds to the zinc atom within the targeted HDAC catalytic site, resulting in the suppression of cell proliferation in various tumor types [258, 259]. KSK molecules may have a similar mode of action, even though *M. tuberculosis* has no histones or HDACs. It is conceivable that the KSKs may chelate metal ions to exhibit their antibacterial activity. Previous work postulated that the KSKs chelate iron ions from essential Fe-S clusters that are significant for the cytochromes of the ETC, in turn impeding the PMF formation [260]. To test the ability of KSKs to chelate metal ions, several experiments were conducted by A. Kiffe-Delf in unpublished work [261]. While there was no observed chelating effect of the KSKs with zinc ions, KSK-106 did show a slight iron-chelating effect at high concentrations. This effect only occurred at concentrations far exceeding the MIC_{90} concentration. However, there may be an accumulation of the KSKs in the cells due to a constant uptake, which might exceed the MIC. So far, we do not have evidence to support or refute this hypothesis. Nonetheless, it remains conceivable that the KSKs are affecting the ETC, supported by the discovery that the KSKs do not have an additive impact when combined with BDQ, which is known to uncouple electron transport in the ETC indirectly, unlike when KSKs were combined with other antibiotics.

Further research is needed regarding preclinical studies, including extensive pharmacokinetic and pharmacodynamic analysis of the compounds. Initial *in vivo* experiments have demonstrated that the molecules did not cause any noticeable adverse events or toxicity in mice (data not shown). Preliminary results also suggest that KSK-106 leads to a slight reduction in bacterial burden in the lung and spleen (data not shown). Nonetheless, this reduction did not compare to that achieved by the first-line drug, isoniazid. The low bioavailability of the compounds may explain this limitation, which was expected due to their low water solubility. To evaluate their potential for reducing the bacterial burden via intravenous injection, further studies are needed on KSKs. This would verify whether these substances can be used to treat TB in humans and if further modification in regard to bioavailability and plasma stability might be necessary. Consequently, identifying the complete mechanism of action would be beneficial to verify if modifications to the molecules might influence the anti-TB efficacy.

7.2 GtrA-like putative lipid floppase Rv3277t

In chapter 4, the research direction is reversed. The aim was to identify and characterize the function of a potential *M. tuberculosis* target for future structure-based drug discovery. As described above (chapter 1.1.3), the pathogen possesses various unique cell wall molecules that build its unusual, complex cell wall, which is thought to be largely responsible for its pathogenicity [262]. These molecules provide multiple potential or valid target structures for TB chemotherapy. Some of the most abundant cell wall molecules of *M. tuberculosis* are glycoconjugates such as PIMs, LM, LAM, and AG, which are essential for the viability and pathogenicity of *M. tuberculosis*. Although the biosynthesis of these mannosylated and arabinosylated mycobacterial cell wall constituents has been extensively studied, some essential steps remain unknown. In particular, translocation of these surface-facing components of *M. tuberculosis* is a crucial but the least understood step in the assembly of the cell wall structure. Several research reports have shown various protein families play a critical role in the transportation of lipids and glycolipids from the cytoplasm to the cell surface [263, 264].

In prokaryotes, there are three distinct glycoconjugate export strategies: "Wzx/Wzy-dependent", "ATP-binding cassette (ABC)-transporter-dependent", and "synthase-dependent" that are determined by distinctive components. In the pathways dependent on Wzx/Wzy, individual polysaccharide repeat units linked with undecaprenol diphosphate (Und-PP) are formed at the cytosolic face of the membrane and then flipped across the membrane by Wzx to be polymerized by Wzy at the periplasmic face of the membrane. On the contrary, in the ABC-transporter-dependent pathway, fully polymerized polysaccharides are created by successive glycosyl transfer at the inner membrane [265]. There is less information about the synthase-dependent pathway, where it is believed that a single protein serves as both polymerase and exporter. For the translocation of the arabinosylated and mannosylated cell wall components of mycobacteria, a two-part process has been proposed. It is hypothesized that biosynthesis commences on the cytosolic side of the plasma membrane before being translocated or "flopped" to the periplasmic leaflet of the cell wall. In the biosynthesis of AG, the galactan core C50-P-P-GlcNAc-Rha-Galf_{30} is translocated across the membrane by two proteins, Rv3781 and Rv3783, which belong to the Wzm-Wzt -type ABC-transporter [266, 267]. Similarly, the early steps in the biosynthesis of the mannosylated glycoconjugates PIM, LM, and LAM are initiated at the cytoplasmic side of the plasma membrane. Translocases in other prokaryotes have

resemblances to small multidrug resistance transporters capable of performing lipid floppase functions [268]. In this study, we examined homologous proteins found in *M. smegmatis* and *M. tuberculosis*, MSMEG_1817 and Rv3277, which exhibit a low similarity to the flippase GtrAf from *S. flexneri* [269].

We have obtained evidence that MSMEG_1817 and the non-annotated, truncated version of Rv3277, designated as Rv3277t, may be involved in either mediating the translocation of precursor substrates from the cytoplasmic to the periplasmic surface, or in the formation of the precursor substrates at the cytoplasmic face for the glycoconjugates PIM_6, LM, and LAM. These glycoconjugates arise from the elongation of Ac_1PIM_4 or Ac_2PIM_4 using DPM as a substrate at the periplasmic site. Consequently, we hypothesize that Rv3277t and MSMEG1_1817 are either mediating flopping or formation of DPM. Alternatively, it is possible that the GtrA-like proteins might rather be necessary for the flopping of the precursors Ac_1PIM_4 / Ac_2PIM_4 from the cytoplasmic to the periplasmic face of the membrane, or might be involved in their synthesis from Ac_1PIM_2, / Ac_2PIM_2. It is noteworthy that only an accumulation of Ac_1PIM_5 was discovered in the silenced mutant. It may be presumed that either Ac_1PIM_4 undergoes further mannosylation on another pathway producing Ac_1PIM_5, or that the flopping does not occur at the stage of Ac_1PIM_4 but at the stage of Ac_1PIM_5. Further research is required to validate which pathway is more likely to be involved through a comprehensive glycosylation analysis. In order to gain insight into potential mechanisms, it would be beneficial to investigate protein mannosylation. The process of protein *O*-mannosylation in *M. tuberculosis* is initiated by the protein mannosyltransferase Rv1002c, while the primary mannose residue can be further elongated through α-1,2 linked mannose residues by PimE [270, 271]. Importantly, both Rv1002c and PimE require DPM, but not Ac_1PIM_4 / Ac_2PIM_4, as a substrate [271, 272]. If the silencing of Rv3277t leads to reduced protein mannosylation this would indicate DPM as the primary substrate of Rv3277t. Conversely, if protein mannosylation remains unchanged in the silenced mutant cells, DPM is more likely not the substrate, thereby implicating Ac_1PIM_4 / Ac_2PIM_4 as a substrate. To determine protein *O*-mannosylation levels in protein lysates, Western blotting could be conducted using monoclonal antibodies that are specific to two known *O*-mannosylated glycoproteins, Apa (Rv1860) and LpqH (Rv3763) [270, 271]. Alternatively, a concanavalin A lectin (ConA)-lectin affinity chromatography method followed by LC-MS/MS could be utilized to enrich and identify *O*-mannosylated proteins in cell lysates, as described elsewhere [273].

Further elucidation of the functions of GtrA-like proteins in the biosynthesis of specific glycoconjugates can be achieved through follow-up experiments. For PIM biosynthesis, an advanced metabolic labeling technique could be implemented. A pulse-chase metabolic labeling experiment could be conducted utilizing ^{3}H-mannose or ^{3}H-inositol to mediate the synthesis of DPM and various PIM intermediates over time in wild type and silenced mutant cells. For an in-depth analysis of LM and LAM biosynthesis, the lipoglycans can be extracted from whole lipid extracts of wild type and silenced mutant cells. Putative different levels of lipoglycans could be analyzed by using SDS-PAGE with periodic Schiff agent, as previously reported [274].

So far, we propose that the MSMEG_1817 and Rv3277t are primarily responsible for flopping DPM from the cytoplasmic to the periplasmic face of the membrane or are involved in the synthesis of DPM at the cytoplasmic layer. Nevertheless, our findings indicate that they may also have a minor role in the translocation of decaprenyl-monophosphoryl-D-arabinofuranose (DPA) or decaprenyl-monophosphoryl-D-ribofuranose (DPR). Further investigation is required to validate the capacity of Rv3277t and MSMEG_1817 to translocate DPA or DPR, which is essential for integrating the mAGP layer. If the amount of arabinose for mAGP is reduced in the silenced mutant cells, LAM is likely to accumulate, as shown in a study that identified Rv3781 and Rv3783 as Wzm-Wzt-type ABC transporters involved in galactan core flipping, a crucial process for AG assembly [266]. For the subsequent steps of AG-biosynthesis, DPA is required as a donor substrate. It is plausible that Rv3277t and MSMEG_1817 could be linked to DPA or DPR flopping, which would reduce arabinose availability for the mAGP layer's biosynthesis. This hypothesis could be examined by extracting lipids from both silenced and induced cells. After removing LM, LAM, and PIM from the whole lipid extract, it would be feasible to solely extract the mAGP layer. Upon producing alditol acetate derivatives, a GC-MS/MS analysis could be used to determine the proportion of arabinose to galactose. This might reveal a potential variation in arabinose content amongst various extracts. An alternate approach is to conduct biosynthetic incorporation for glycan labeling. The feasibility of synthesizing and assaying probes for D-arabinofuranose (D-Ara*f*), an essential component of *M. tuberculosis*, has previously been confirmed [275]. This was the first investigative tool proficient in labeling arabinofuranose-containing glycans with selectivity. Moreover, this research demonstrated the applicability of such probes in the direct visualization of particular glycans present on the bacterial cell surface. This approach would aid in the comprehension of the functions of MSMEG_1817 and Rv3277t, as well [276].

The putative floppases' biochemical function requires further validation, which can be performed by conducting enzymatic activity tests on membrane fractions of wild type and silenced mutants. To confirm the function of the floppase, metabolically labeled substrates may be used [269]. One general inquiry that may arise is why flippases or floppases are necessary to move lipids in bacterial membranes. The movement of charged or polar headgroups through the hydrophobic interior of a lipid bilayer membrane is highly energetically unfavorable, necessitating the existence of mechanisms for lipid movement in native membranes. In both the plasma membrane and organelle membranes of eukaryotes, as well as in the bacterial cytoplasmic membrane, lipid translocases perform this function [277-281]. Three classes of these proteins exist: the cytofacially-directed, ATP-dependent transporters ("flippases"), exofacially-directed, ATP-dependent transporters ("floppases") and the bidirectional, ATP-independent transporters ("scramblases"). To investigate whether other proteins have a similar role to Rv3277t, we complemented the conditional mutant with other flippases and floppases. Our findings regarding Rv3789 demonstrate that while this protein can partially complement Rv3277t's function, it does not have a redundant function. This suggests that Rv3277t has at least one additional function compared to Rv3789, which is a GtrA-like protein involved in AG biosynthesis. Next to Rv3789, it appears that only LtaA has a limited capability to restore the silenced conditional mutant. LtaA is a well-established flippase in *S. aureus* that is responsible for the flipping of lipotecioic acids [282]. The reason for our findings may be due to the high substrate specificity of various flippases and floppases or the diverse functions that the investigated protein possesses, which are essential for mycobacterial survival. Of course, this needs to be further investigated and clarified.

Crystallographic studies of Rv3277t should be performed in the future to verify the structural homology model. To determine the precise localization of Rv3277t in the membrane, it would be beneficial to employ GFP-tagged Rv3277t proteins in a conditional mutant to validate the localization in the membrane and to determine which terminus is located at specific sites of the plasma membrane [283]. Direct examination of the cell wall structure using transmission electron microscopy could be employed to investigate potential ultrastructural defects in the cell wall or internal membrane structures of the mutant cell cytoplasm. This approach was used to observe defects in the *MSMEG_5136* deletion mutant, which is the homolog of *pimE*. PimE is the first polyprenol-phosphate-mannose (PPM)-dependent mannosyl-transferase demonstrated to be involved in PIM biosynthesis, where it mediates the fifth mannose transfer

[272]. It would be advantageous to assess if analogous effects are arising in the *MSMEG_1817* or *Rv3277t* conditional mutants.

In the future, it will be imperative to investigate the functions of Rv3277t in vivo to uncover the protein's role in pathogenicity. Accordingly, a lung model or mice study could be employed for this purpose. Additionally, conducting an in silico drug-target screening to identify compounds that target Rv2377t and behave differently from the current clinically used drugs would be captivating. The development of compounds targeting unknown or new proteins of interest is crucial to bypass the development of *M. tuberculosis*-resistant strains and to finally combat TB.

7.3 Homo-BacPROTACs

An alternative idea to tackle TB, but also other infectious diseases, was investigated in chapters 5 and 6 through the introduction of the novel antibiotic strategy, the BacPROTACs. BacPROTACs exhibit the ability to induce the degradation of a target protein by directly linking it to a bacterial protease complex. Protein degradation is a regular process of protein turnover within the cell, offering a quality control mechanism during protein folding, the ability to respond quickly to changing cellular signals, and a way to modulate the pool of accessible amino acids. For some time now, the idea of targeted therapies using bifunctional proteolysis targeting chimeras (PROTACs) has been revolutionizing human therapeutics, particularly in cancer treatment [284]. The idea was based on the recognition that small molecule drug discovery has traditionally focused on the presence of a binding site that directly affects protein function, which typically precludes targeting proteins that lack accessible sites. Furthermore, sustaining adequate target inhibition in vivo often requires a high systemic drug exposure, amplifying the possibility of undesired off-target effects and resistance formation [285]. Emerging technologies that employ PROTACs allow targeting of a wider spectrum of proteins than standard small-molecule strategies. This progress facilitates the elimination of target proteins that were earlier deemed as "undruggable" [286, 287]. The "event-driven" degradation of targeted proteins is based on the principle of linking an agent to its protein of interest (POI), which then catalyzes the degradation via the endogenous proteolytic machinery [288].

PROTACs represent the most established targeted protein degradation agents to date. These agents consist of heterobifunctional molecules that bind both to their POI and to an E3 ligase

in mammalian cells. The latter facilitates covalent modification of the POI with ubiquitin, which in turn targets the POI for degradation by the cell's proteasome [289-291]. Alongside the most established form of PROTACs, several other degrader drugs are among the current trends in the use of TAC-based technologies. One pathway currently under investigation for protein degradation is the endosomal-lysosomal system. The fusion of endosomes and lysosomes generates a membrane bilayer, creating an acidic space that is ideal for activating hydrolytic enzymes such as proteases, nucleases, and lipases. These enzymes are capable of degrading proteins [292]. Lysosome-Targeting Chimeras (LYTACs) deploy lysosome-targeting receptors to achieve protein degradation inside lysosomes. LYTACs have the capability to specifically target extracellular and transmembrane proteins, which is a topic of great interest. Another pathway, the autophagic-lysosomal pathway, plays an important role in the degradation of intracellular macromolecules, long-lived proteins or aggregates and cytoplasmic organelles through the fusion of autophagic and lysosomal degradative enzymes. Autophagy-Targeting Chimeras (AUTACs) have been developed to accomplish the degradation of target proteins via autophagosomes [293]. There are additional pathways associated with TAC technologies, but they fall beyond the scope of this discussion.

The principle of targeted protein degradation is not new; after the discovery of the ubiquitin-proteasome degradation system in the 1990s, targeted protein degradation technologies began to emerge, following the identification of the first molecular glues cyclosporin A, rapamycin, and FK506 [294, 295]. Molecular glues are proximity-inducible small molecules that favor protein-protein interactions, promoting the dimerization or colocalization of two or more proteins, thereby inactivating one of them or a third player. Later, a pioneering alternative for targeted protein degradation, fulvestrant, was developed for the treatment of estrogen receptor-positive human breast cancer. It was developed before the PROTAC technology emerged between 2001 and 2004 [296]. It is conceivable that the application of PROTAC technology to bacteria could provide promising and potent antimicrobials with new modes of action, but until recently this has not been possible. This is because bacteria do not contain the E3 ligase proteasome system, making it infeasible to translate the PROTAC technology directly into antibiotics. Very recently, proof-of-concept work has shown that bifunctional bacterial PROTACs can be generated functioning by direct binding of the POI to a bacterial protease, the caseinolytic protease complex, thus eliminating the need for the E3 ligase. This was used as a starting point for the studies presented in this thesis.

Our follow-up research focused on characterizing the mycobacterial ClpC1:ClpP1:ClpP2 (ClpC1P1P2) protease complex, which is essential for maintaining protein homeostasis, particularly in situations where bacteria accumulate mistranslated, misfolded or aggregated proteins caused by host-induced stresses such as heat or antibiotic interference with the ribosomal machinery. Since both inhibition and activation of the ClpC1P1P2 proteases have negative effects on the organism, they appear to be promising drug targets. Surprisingly, the first serendipitously discovered degrader antibiotic is the anti-TB drug PZA by supporting selective target degradation as a novel antibacterial discovery approach. Although PZA has been part of the first-line anti-TB treatment for many years, its mechanism of action has yet to be fully elucidated (chapter 1.2.2). It has been demonstrated that the converted active form of the pro-drug, POA, binds to the recombinant aspartate decarboxylase PanD thereby inhibiting coenzyme A biosynthesis [297, 298]. Notably, biochemical inhibition of the PanD-catalysed reaction by POA only impacted PanD activity at exceedingly high concentrations [299]. As POA-resistant mutants were also discovered with mutations in the *clpC1* gene, and given that PanD harbors a C-terminal degradation tag which acts as a substrate for the ClpC1P1P2 complex, it can be inferred that the protease regulates PanD levels post-translationally [299]. This suggests that POA expedites the degradation of PanD through ClpC1P1P2 by binding to PanD, causing significant conformational changes that expose the protein's C-terminal degradation tag for recognition by ClpC1, ultimately inducing degradation. Consequently, PZA may be deemed the initial randomly discovered degrading antibiotic.

More recently, the role of several proteases in the mechanisms of action of various natural products has been clarified [300-302]. Of these, the antimicrobial cyclic peptides cyclomarin A (CymA) and ecumicin were found to target ClpC1, binding to overlapping sites on the N-terminal domain of ClpC1 and inhibiting its activity. Consequently, the interaction between several natural products and the Clp protease is relatively well investigated. However, the defensive response of bacteria to relevant antimicrobial compounds remains poorly understood. In this study, we investigated the roles of ClpC2 and ClpC3, which are partial homologs of ClpC1, in mediating CymA-, and ecumicin-induced toxicity in mycobacteria. Quantitative proteomics revealed a significant proteome imbalance, including up-regulation of these stress response factors, ClpC2 and ClpC3. The proteins compete for substrate-binding using the same ligand binding site as ClpC1 and can sequester ClpC1-directed antibiotics, thereby reducing their antibacterial activity. Simultaneously, a different research group confirmed that ClpC2 acts as a tightly binding molecular sponge to prevent CymA from binding to ClpC1P1P2 [303].

To overcome this protection and target Clp degradation, our study used the newly developed BacPROTAC technology. This is based on bifunctional chemical connectors that bind to a protein of interest (POI) and subsequently target POIs to the ClpC1P1P2 protease for degradation [304]. The newly introduced Homo-BacPROTACs contain two CymA heads targeting ClpC1 against itself, inducing its elimination by ClpC1P1P2, while promoting the elimination of ClpC2 at the same time. In the virulent *M. tuberculosis* strain H37Rv, the simultaneous elimination resulted in a significantly improved susceptibility towards Homo-BacPROTAC degraders, inhibiting growth with more than a 100-fold increase in efficiency compared to the natural monomeric cyclic peptide. Homo-BacPROTAC antibiotics were found to override the bacterial protein quality security system, are at least partially effective in bacteria with a dormant phenotype, and can target multiple components of the mycobacterial stress response at once. The modular design and capacity to repurpose various protein ligands make bifunctional degraders advantageous for developing antimicrobials with high selectivity and specificity. This approach holds the potential for extensive application to other bacterial proteins as the protease ClpC1P1P2 is absent in mammalian cells. ClpC1P1P2 has been described extensively in Gram-positive bacteria but is organized in a similar way to ClpXP, the most widespread form of Clp protease, and ClpAP, found in most Gram-negative bacteria [305]. Because all three use the N-terminal domains of their ATPase units as substrate receptors, the Homo-BacPROTAC strategy could be further extended.

An important area for future research involves enhancing the cell permeability or adsorption of Homo-BacPROTACs to components of the mycobacterial cell envelope, which could augment their effective intracellular concentration. As explained in depth earlier, the mycobacterial cell wall constitutes a distinctive barrier that shields many drugs from entering the pathogen, due to its diverse layers and lipid composition (chapter 1.1.3). It may be valuable to examine the interaction of future Homo-BacPROTACs in bacterial organisms with diverse cell wall compositions. The subsequent phase of this research should demonstrate the in vivo effectiveness of Homo-BacPROTACs. Nevertheless, investigations carried out previously in rodents proposed that these agents have limited pharmacokinetic properties and oral bioavailability owed to physicochemical factors such as low solubility and total polar surface areas, but also due to their high molecular weights. Hence, it is not yet justifiable to carry out efficacy studies in an animal model because even though intravenous administration offers more advantages, oral applications will still be necessary for treating MDR-TB patients to ensure consistent treatment and prevent the emergence of Bac-PROTAC-resistant strains.

Consequently, thorough SAR studies will need to be conducted to enhance the pharmacokinetic properties and oral bioavailability of these agents.

While current Homo-BacPROTACs were developed to bind ClpC of the caseinolytic protease, potential future bacterial PROTACs could be designed to bind other bacterial proteases, like the serine protease Lon or the metalloprotease FtsH [306]. Lon, a serine protease, does not require forming a complex with an unfoldase as it comprises both proteolytic and ATPase domains and therefore exhibits chaperone activity on its own [307]. FtsH is an additional proteolytic complex responsible for removing products of trans-translation [307]. In conclusion, the development of bacterial PROTACs offers an appealing approach for designing modulators of protein function and a platform for antibiotic discovery, presenting several advantages over conventional inhibitors. Their mode of action results in higher efficacy, and their modular architecture allows for the repurposing of protein ligands to build degraders, thereby allowing virtually any cellular protein to be targeted [290, 291, 308]. In addition, it is anticipated that antibacterial PROTACs will not only broaden the target space but also enhance treatment by facilitating dosage reduction, augmenting bactericidal activity, and combating drug-tolerant “persisters”. Considering the various ways to expand this method, it is anticipated that in the future, with further modification and optimization, Homo-BacPROTACs could potentially be applied for the treatment of various bacterial infections.

7.4 Concluding remarks

During this thesis, it was evident that intensified antibiotic research and development are needed to address the growing threat of the antimicrobial resistance crisis. Research and development of novel antimicrobial strategies and therapies, alongside the thorough identification and characterization of previously unknown drug targets and small molecules possessing a unique mode of action, is essential to achieving this objective. A 2006 report indicated that there were 324 distinct molecular targets for drugs with a known mechanism of action. Notably, 266 protein drug targets were obtained from the human genome, whereas the remaining 58 were designed for pathogenic organisms like fungi, viruses, and bacteria [287]. The latest update of the study reveals an increment of total protein targets to 667. It is worth mentioning that this increase is partly due to the integration of complexes, subunits, splice variants, and protein isoforms as efficient molecular targets. Among this number, only 189 drug targets were

pathogen-derived [309]. This underscores the urgent need for continuous development in antimicrobial research. In addition, the diagnosis and treatment of bacterial infections must be optimized to counter the current crisis and limit the development of resistance. To prevent misuse and overuse of antibiotics, pathogen and antimicrobial susceptibility testing combined with resistance marker analysis should be carried out as quickly and cheaply as possible. This strategy may potentially decrease the use of broad-spectrum antibiotics and expedite the selection of the most suitable antibiotic for the patient. Improved treatment options should be more affordable and user-friendly, particularly in regions with inadequate laboratory facilities, so that healthcare professionals can decide on the appropriate treatment plan in a timely manner. Improving accessibility and providing proper information to patients are essential measures to prevent the emergence of resistance caused by incorrect use and prescription of antibiotics. It is important to restrict the free availability of antibiotics and prevent patients from prematurely discontinuing treatment before completion. Antibiotics should not be prescribed unnecessarily. Furthermore, drug-resistant strains need to be better identified, and new treatment options for patients infected with these strains should be discussed.

In summary, the increasing number of drug-resistant microbes is becoming a major global health concern due to inadequate therapeutic options. The development of new antibiotics and innovative treatment strategies will become imperative in the future. This thesis aims to contribute to this goal through small molecule development, target characterization, and the introduction of a novel antibiotic strategy. Although the primary objective of this investigation was to tackle the issue of multidrug-resistant TB, some aspects of the study can be extended to other infectious diseases with the aim of always staying abreast of the current antimicrobial resistance crisis.

8. References chapters 1 and 7

1. Price, R., *O'Neill report on antimicrobial resistance: funding for antimicrobial specialists should be improved.* Eur J Hosp Pharm, 2016. **23**(4): p. 245-247.
2. Tacconelli, E., et al., *Discovery, research, and development of new antibiotics: the WHO priority list of antibiotic-resistant bacteria and tuberculosis.* Lancet Infect Dis, 2018. **18**(3): p. 318-327.
3. World Health, O. *The End TB Strategy* 2015 [cited 2023 August 17]; Available from: Taconelli et alWHO 2015 End TB strategy.
4. Hayman, J., *Mycobacterium ulcerans: an infection from Jurassic time?* Lancet, 1984. **2**(8410): p. 1015-6.
5. Kapur, V.W., TS; Musser, JM, *Is Mycobacterium tuberculosis 15,000 Years Old?* J Infect Dis., 1994. **170(5):1348–1349**.
6. Barberis, I., N.L. Bragazzi, L. Galluzzo, and M. Martini, *The history of tuberculosis: from the first historical records to the isolation of Koch's bacillus.* J Prev Med Hyg, 2017. **58**(1): p. E9-E12.
7. Cambau, E. and M. Drancourt, *Steps towards the discovery of Mycobacterium tuberculosis by Robert Koch, 1882.* Clin Microbiol Infect, 2014. **20**(3): p. 196-201.
8. Kappelman, J., et al., *Brief communication: First Homo erectus from Turkey and implications for migrations into temperate Eurasia.* American Journal of Physical Anthropology, 2008. **135**(1): p. 110-116.
9. Rothschild, B.M., et al., *Mycobacterium tuberculosis complex DNA from an extinct bison dated 17,000 years before the present.* Clinical Infectious Diseases, 2001. **33**(3): p. 305-311.
10. Donoghue, H.D., et al., *Tuberculosis: from prehistory to Robert Koch, as revealed by ancient DNA.* Lancet Infectious Diseases, 2004. **4**(9): p. 584-592.
11. Daniel, V.S. and T.M. Daniel, *Old Testament biblical references to tuberculosis.* Clin Infect Dis, 1999. **29**(6): p. 1557-8.
12. Daniel, T.M., *Pioneers of medicine and their impact on tuberculosis*. 2000: University Rochester Press.
13. Marten, B., *A new theory of consumptions: more especially of a phthisis or consumption of the lungs.* . T. Knaplock, London, 1720.
14. Keal, J.L. and P.D. Davies, *Tuberculosis: a forgotten plague?* J R Soc Med, 2011. **104**(5): p. 182-4.

15. Daniel, T.M., *Hermann Brehmer and the origins of tuberculosis sanatoria.* Int J Tuberc Lung Dis, 2011. **15**(2): p. 161-2, i.
16. Koch, R., *Die Ätiologie der Tuberkulose.* Berliner klinische Wochenschrift, 1882. **15** p. pp. 221-230.
17. Sultan, L., et al. *The identification of patients producing tuberculous infection by the airborne route*. in *Transactions of the 18th conference on Chemotherapy of Tuberculosis*. 1959.
18. Teicher, A., *Super-spreaders: a historical review.* Lancet Infect Dis, 2023.
19. Esmail, H., C.E. Barry, 3rd, D.B. Young, and R.J. Wilkinson, *The ongoing challenge of latent tuberculosis.* Philos Trans R Soc Lond B Biol Sci, 2014. **369**(1645): p. 20130437.
20. Barry, C.E., 3rd, et al., *The spectrum of latent tuberculosis: rethinking the biology and intervention strategies.* Nat Rev Microbiol, 2009. **7**(12): p. 845-55.
21. Pai, M., et al., *Tuberculosis.* Nat Rev Dis Primers, 2016. **2**: p. 16076.
22. Leung, A.N., *Pulmonary tuberculosis: the essentials.* Radiology, 1999. **210**(2): p. 307-22.
23. Luies, L. and I. du Preez, *The Echo of Pulmonary Tuberculosis: Mechanisms of Clinical Symptoms and Other Disease-Induced Systemic Complications.* Clin Microbiol Rev, 2020. **33**(4).
24. Queval, C.J., et al., *Mycobacterium tuberculosis Controls Phagosomal Acidification by Targeting CISH-Mediated Signaling.* Cell Rep, 2017. **20**(13): p. 3188-3198.
25. Smith, I., *Mycobacterium tuberculosis pathogenesis and molecular determinants of virulence.* Clin Microbiol Rev, 2003. **16**(3): p. 463-96.
26. Ottenhoff, T.H. and S.H. Kaufmann, *Vaccines against tuberculosis: where are we and where do we need to go?* PLoS Pathog, 2012. **8**(5): p. e1002607.
27. Delogu, G., M. Sali, and G. Fadda, *The biology of mycobacterium tuberculosis infection.* Mediterr J Hematol Infect Dis, 2013. **5**(1): p. e2013070.
28. Urdahl, K.B., S. Shafiani, and J.D. Ernst, *Initiation and regulation of T-cell responses in tuberculosis.* Mucosal Immunol, 2011. **4**(3): p. 288-93.
29. Zuniga, J., et al., *Cellular and humoral mechanisms involved in the control of tuberculosis.* Clin Dev Immunol, 2012. **2012**: p. 193923.
30. Mukherjee, S., S. Perveen, A. Negi, and R. Sharma, *Evolution of tuberculosis diagnostics: From molecular strategies to nanodiagnostics.* Tuberculosis (Edinb), 2023. **140**: p. 102340.

31. Saunders, B.M. and A.M. Cooper, *Restraining mycobacteria: role of granulomas in mycobacterial infections.* Immunol Cell Biol, 2000. **78**(4): p. 334-41.
32. Alsayed, S.S.R. and H. Gunosewoyo, *Tuberculosis: Pathogenesis, Current Treatment Regimens and New Drug Targets.* Int J Mol Sci, 2023. **24**(6).
33. Rahlwes, K.C., et al., *Pathogenicity and virulence of Mycobacterium tuberculosis.* Virulence, 2023. **14**(1).
34. Furin, J., H. Cox, and M. Pai, *Tuberculosis.* Lancet, 2019. **393**(10181): p. 1642-1656.
35. Hunter, R.L., *Pathology of post primary tuberculosis of the lung: an illustrated critical review.* Tuberculosis (Edinb), 2011. **91**(6): p. 497-509.
36. Orme, I.M. and R.J. Basaraba, *The formation of the granuloma in tuberculosis infection.* Semin Immunol, 2014. **26**(6): p. 601-9.
37. Balaban, N.Q., et al., *Definitions and guidelines for research on antibiotic persistence.* Nature Reviews Microbiology, 2019. **17**(7): p. 441-448.
38. Aldridge, B.B., et al., *Asymmetry and aging of mycobacterial cells lead to variable growth and antibiotic susceptibility.* Science, 2012. **335**(6064): p. 100-4.
39. Larkins-Ford, J. and B.B. Aldridge, *Advances in the design of combination therapies for the treatment of tuberculosis.* Expert Opin Drug Discov, 2023. **18**(1): p. 83-97.
40. Chernick, V., *A new evolutionary scenario for the Mycobacterium tuberculosis complex.* Pediatr Pulmonol, 2004. **38**(1): p. 1.
41. Alexander, K.A., et al., *Novel Mycobacterium tuberculosis complex pathogen, M. mungi.* Emerg Infect Dis, 2010. **16**(8): p. 1296-9.
42. Pereira, A.C., B. Ramos, A.C. Reis, and M.V. Cunha, *Non-Tuberculous Mycobacteria: Molecular and Physiological Bases of Virulence and Adaptation to Ecological Niches.* Microorganisms, 2020. **8**(9).
43. Gagneux, S., *Ecology and evolution of Mycobacterium tuberculosis.* Nat Rev Microbiol, 2018. **16**(4): p. 202-213.
44. Kalscheuer, R., et al., *The Mycobacterium tuberculosis capsule: A cell structure with key implications in pathogenesis.* Biochemical Journal, 2019. **476**(14): p. 1995-2016.
45. Jarlier, V. and H. Nikaido, *Mycobacterial cell wall: structure and role in natural resistance to antibiotics.* FEMS Microbiol Lett, 1994. **123**(1-2): p. 11-8.
46. Angala, S.K., et al., *The cell envelope glycoconjugates of Mycobacterium tuberculosis.* Crit Rev Biochem Mol Biol, 2014. **49**(5): p. 361-99.

47. Singh, P., N.R. Rameshwaram, S. Ghosh, and S. Mukhopadhyay, *Cell envelope lipids in the pathophysiology of Mycobacterium tuberculosis.* Future Microbiol, 2018. **13**: p. 689-710.

48. Boldrin, F., et al., *The phosphatidyl-myo-inositol mannosyltransferase PimA is essential for Mycobacterium tuberculosis growth in vitro and in vivo.* J Bacteriol, 2014. **196**(19): p. 3441-51.

49. Mishra, A.K., N.N. Driessen, B.J. Appelmelk, and G.S. Besra, *Lipoarabinomannan and related glycoconjugates: structure, biogenesis and role in Mycobacterium tuberculosis physiology and host–pathogen interaction.* FEMS Microbiology Reviews, 2011. **35**(6): p. 1126-1157.

50. Hoffmann, C., et al., *Disclosure of the mycobacterial outer membrane: cryo-electron tomography and vitreous sections reveal the lipid bilayer structure.* Proc Natl Acad Sci U S A, 2008. **105**(10): p. 3963-7.

51. Jackson, M., *The mycobacterial cell envelope-lipids.* Cold Spring Harb Perspect Med, 2014. **4**(10).

52. Barry, C.E., D.C. Crick, and M.R. McNeil, *Targeting the formation of the cell wall core of M. tuberculosis.* Infect Disord Drug Targets, 2007. **7**(2): p. 182-202.

53. Kalscheuer, R., et al., *The Mycobacterium tuberculosis capsule: a cell structure with key implications in pathogenesis.* Biochem J, 2019. **476**(14): p. 1995-2016.

54. World Health, O., *Global tuberculosis report 2022.* . licence: cc bY-Nc-sa 3.0 iGo, 2022.

55. Ong, C.W.M. and D. Goletti, *Impact of the global COVID-19 outbreak on the management of other communicable diseases.* Int J Tuberc Lung Dis, 2020. **24**(5): p. 547-548.

56. Chiok, K.R., N. Dhar, and A. Banerjee, *Mycobacterium tuberculosis and SARS-CoV-2 co-infections: The knowns and unknowns.* iScience, 2023. **26**(5): p. 106629.

57. Cohen, A., V.D. Mathiasen, T. Schon, and C. Wejse, *The global prevalence of latent tuberculosis: a systematic review and meta-analysis.* Eur Respir J, 2019. **54**(3).

58. Houben, R.M. and P.J. Dodd, *The Global Burden of Latent Tuberculosis Infection: A Re-estimation Using Mathematical Modelling.* PLoS Med, 2016. **13**(10): p. e1002152.

59. Nahid, P., et al., *Treatment of Drug-Resistant Tuberculosis. An Official ATS/CDC/ERS/IDSA Clinical Practice Guideline.* Am J Respir Crit Care Med, 2019. **200**(10): p. e93-e142.

60. Nadgir, C.A. and D.A. Biswas, *Antibiotic Resistance and Its Impact on Disease Management.* Cureus, 2023. **15**(4): p. e38251.
61. Munita, J.M. and C.A. Arias, *Mechanisms of Antibiotic Resistance.* Microbiol Spectr, 2016. **4**(2).
62. Iseman, M.D., *Tuberculosis therapy: past, present and future.* European Respiratory Journal, 2002. **20**: p. 87s-94s.
63. Riva, M.A., *From milk to rifampicin and back again: history of failures and successes in the treatment for tuberculosis.* Journal of Antibiotics, 2014. **67**(9): p. 661-665.
64. Cosmacini, G., De Filippis, M., Sanseverino, P., *La peste bianca. Milano e la lotta antitubercolare (1882-1945).* Franco Angeli: Milan, 2004.
65. Fleming, A., *On the antibacterial action of cultures of a penicillium, with special reference to their use in the isolation of B. influenzae.* Bulletin of the World Health Organization, 2001. **79**(8): p. 780-790.
66. Swann, J.P., *The search for synthetic penicillin during World War II.* Br J Hist Sci, 1983. **16**(53 Pt 2): p. 154-90.
67. Wohlleben, W., Y. Mast, E. Stegmann, and N. Ziemert, *Antibiotic drug discovery.* Microb Biotechnol, 2016. **9**(5): p. 541-8.
68. Waksman, S.A. and H.B. Woodruff, *Actinomyces antibioticus, a New Soil Organism Antagonistic to Pathogenic and Non-pathogenic Bacteria.* J Bacteriol, 1941. **42**(2): p. 231-49.
69. Waksman, S.A. and H.B. Woodruff, *Streptothricin, a New Selective Bacteriostatic and Bactericidal Agent, Particularly Active Against Gram-Negative Bacteria.* Experimental Biology and Medicine, 1942. **49**(2): p. 207-210.
70. Schatz, A., E. Bugie, and S.A. Waksman, *Streptomycin, a substance exhibiting antibiotic activity against gram-positive and gram-negative bacteria. 1944.* Clin Orthop Relat Res, 2005(437): p. 3-6.
71. *TREATMENT of pulmonary tuberculosis with streptomycin and para-aminosalicylic acid; a Medical Research Council investigation.* Br Med J, 1950. **2**(4688): p. 1073-85.
72. Spickler, C., M.N. Brunelle, and L. Brakier-Gingras, *Streptomycin binds to the decoding center of 16 S ribosomal RNA.* J Mol Biol, 1997. **273**(3): p. 586-99.
73. Honore, N. and S.T. Cole, *Streptomycin resistance in mycobacteria.* Antimicrob Agents Chemother, 1994. **38**(2): p. 238-42.
74. Lehmann, J., *Para-aminosalicylic acid in the treatment of tuberculosis.* Lancet, 1946. **1**(6384): p. 15.

75. Minato, Y., et al., *Mycobacterium tuberculosis folate metabolism and the mechanistic basis for para-aminosalicylic acid susceptibility and resistance.* Antimicrob Agents Chemother, 2015. **59**(9): p. 5097-106.

76. Shane, S.J., J.H. Laurie, C. Riley, and M. Boutilier, *Effect of combined therapy (dihydrostreptomycin and PAS) on the emergence of streptomycin-resistant strains of tubercle bacilli.* N Engl J Med, 1952. **246**(4): p. 132-4.

77. Graessle, O.E. and J.J. Pietrowski, *The in Vitro Effect of Para-Aminosalicylic Acid (Pas) in Preventing Acquired Resistance to Streptomycin by Mycobacterium Tuberculosis.* J Bacteriol, 1949. **57**(4): p. 459-64.

78. Bernstein, J., W.A. Lott, B.A. Steinberg, and H.L. Yale, *Chemotherapy of experimental tuberculosis. V. Isonicotinic acid hydrazide (nydrazid) and related compounds.* Am Rev Tuberc, 1952. **65**(4): p. 357-64.

79. Fox, H.H., *The chemical approach to the control of tuberculosis.* Science, 1952. **116**(3006): p. 129-34.

80. *TREATMENT of pulmonary tuberculosis with isoniazid; an interim report to the Medical Research Council by their Tuberculosis Chemotherapy Trials Committee.* Br Med J, 1952. **2**(4787): p. 735-46.

81. Capon, A.W., *Streptomycin and PAS vs. streptomycin, PAS and isoniazid in the treatment of pulmonary tuberculosis.* Can Med Assoc J, 1954. **70**(1): p. 62-7.

82. *Co-operative controlled trial of a standard regimen of streptomycin, PAS and isoniazid and three alternative regimens of chemotherapy in Britain. A report from the British Medical Research Council.* Tubercle, 1973. **54**(2): p. 99-129.

83. Kerantzas, C.A. and W.R. Jacobs, Jr., *Origins of Combination Therapy for Tuberculosis: Lessons for Future Antimicrobial Development and Application.* mBio, 2017. **8**(2).

84. Johnsson, K., D.S. King, and P.G. Schultz, *Studies on the Mechanism of Action of Isoniazid and Ethionamide in the Chemotherapy of Tuberculosis.* Journal of the American Chemical Society, 1995. **117**(17): p. 5009-5010.

85. Ying Zhang, B.H.B.A.D.Y.S.C., *The Catalase-Peroxidase Gene and Isoniazid Resistance of Myc.* Nature, 1992: p. 591-593.

86. McDermott, W., *The story of INH.* J Infect Dis, 1969. **119**(6): p. 678-83.

87. Johnsson, K. and P.G. Schultz, *Mechanistic studies of the oxidation of isoniazid by the catalase peroxidase from Mycobacterium tuberculosis.* Journal of the American Chemical Society, 1994. **116**(16): p. 7425-7426.

88. Ghiladi, R.A., K.F. Medzihradszky, F.M. Rusnak, and P.R. Ortiz de Montellano, *Correlation between isoniazid resistance and superoxide reactivity in mycobacterium tuberculosis KatG.* J Am Chem Soc, 2005. **127**(38): p. 13428-42.

89. Zhao, X., et al., *Hydrogen peroxide-mediated isoniazid activation catalyzed by Mycobacterium tuberculosis catalase-peroxidase (KatG) and its S315T mutant.* Biochemistry, 2006. **45**(13): p. 4131-40.

90. Wengenack, N.L. and F. Rusnak, *Evidence for isoniazid-dependent free radical generation catalyzed by Mycobacterium tuberculosis KatG and the isoniazid-resistant mutant KatG(S315T).* Biochemistry, 2001. **40**(30): p. 8990-6.

91. Winder, F.G. and P.B. Collins, *Inhibition by isoniazid of synthesis of mycolic acids in Mycobacterium tuberculosis.* J Gen Microbiol, 1970. **63**(1): p. 41-8.

92. Davidson, L.A. and K. Takayama, *Isoniazid inhibition of the synthesis of monounsaturated long-chain fatty acids in Mycobacterium tuberculosis H37Ra.* Antimicrob Agents Chemother, 1979. **16**(1): p. 104-5.

93. Gangadharam, P.R., F.M. Harold, and W.B. Schaefer, *Selective inhibition of nucleic acid synthesis in Mycobacterium tuberculosis by isoniazid.* Nature, 1963. **198**: p. 712-4.

94. Banerjee, A., et al., *inhA, a gene encoding a target for isoniazid and ethionamide in Mycobacterium tuberculosis.* Science, 1994. **263**(5144): p. 227-30.

95. Rozwarski, D.A., et al., *Modification of the NADH of the isoniazid target (InhA) from Mycobacterium tuberculosis.* Science, 1998. **279**(5347): p. 98-102.

96. Mdluli, K., et al., *Inhibition of a Mycobacterium tuberculosis beta-ketoacyl ACP synthase by isoniazid.* Science, 1998. **280**(5369): p. 1607-10.

97. Timmins, G.S., S. Master, F. Rusnak, and V. Deretic, *Nitric oxide generated from isoniazid activation by KatG: source of nitric oxide and activity against Mycobacterium tuberculosis.* Antimicrob Agents Chemother, 2004. **48**(8): p. 3006-9.

98. Timmins, G.S. and V. Deretic, *Mechanisms of action of isoniazid.* Mol Microbiol, 2006. **62**(5): p. 1220-7.

99. Thomas, J.P., C.O. Baughn, R.G. Wilkinson, and R.G. Shepherd, *A new synthetic compound with antituberculous activity in mice: ethambutol (dextro-2,2'-(ethylenediimino)-di-l-butanol).* Am Rev Respir Dis, 1961. **83**: p. 891-3.

100. Shepherd, R.G., et al., *Structure-activity studies leading to ethambutol, a new type of antituberculous compound.* Ann N Y Acad Sci, 1966. **135**(2): p. 686-710.

101. Forbes, M., N.A. Kuck, and E.A. Peets, *Mode of action of ethambutol.* J Bacteriol, 1962. **84**(5): p. 1099-103.

102. Kuck, N.A., E.A. Peets, and M. Forbes, *Mode of action of ethambutol on Mycobacterium tuberculosis, strain H37R V.* Am Rev Respir Dis, 1963. **87**: p. 905-6.

103. Takayama, K., E.L. Armstrong, K.A. Kunugi, and J.O. Kilburn, *Inhibition by ethambutol of mycolic acid transfer into the cell wall of Mycobacterium smegmatis.* Antimicrob Agents Chemother, 1979. **16**(2): p. 240-2.

104. Kilburn, J.O., K. Takayama, E.L. Armstrong, and J. Greenberg, *Effects of ethambutol on phospholipid metabolism in Mycobacterium smegmatis.* Antimicrob Agents Chemother, 1981. **19**(2): p. 346-8.

105. Takayama, K. and J.O. Kilburn, *Inhibition of synthesis of arabinogalactan by ethambutol in Mycobacterium smegmatis.* Antimicrob Agents Chemother, 1989. **33**(9): p. 1493-9.

106. K Mikusová, R.A.S.G.S.B. and P.J. Brennan, *Biogenesis of the mycobacterial cell wall and the site of action of ethambutol.* 1995. **39**(11): p. 2484-2489.

107. Goude, R., A.G. Amin, D. Chatterjee, and T. Parish, *The arabinosyltransferase EmbC is inhibited by ethambutol in Mycobacterium tuberculosis.* Antimicrob Agents Chemother, 2009. **53**(10): p. 4138-46.

108. Belanger, A.E., et al., *The embAB genes of Mycobacterium avium encode an arabinosyl transferase involved in cell wall arabinan biosynthesis that is the target for the antimycobacterial drug ethambutol.* Proc Natl Acad Sci U S A, 1996. **93**(21): p. 11919-24.

109. Telenti, A., et al., *The emb operon, a gene cluster of Mycobacterium tuberculosis involved in resistance to ethambutol.* Nat Med, 1997. **3**(5): p. 567-70.

110. Chakraborty, S. and K.Y. Rhee, *Tuberculosis Drug Development: History and Evolution of the Mechanism-Based Paradigm.* Cold Spring Harb Perspect Med, 2015. **5**(8): p. a021147.

111. Malone, L., et al., *The effect of pyrazinamide (aldinamide) on experimental tuberculosis in mice.* Am Rev Tuberc, 1952. **65**(5): p. 511-8.

112. Mc, D.W. and R. Tompsett, *Activation of pyrazinamide and nicotinamide in acidic environments in vitro.* Am Rev Tuberc, 1954. **70**(4): p. 748-54.

113. Tarshis, M.S. and W.A. Weed, Jr., *Lack of significant in vitro sensitivity of Mycobacterium tuberculosis to pyrazinamide on three different solid media.* Am Rev Tuberc, 1953. **67**(3): p. 391-5.

114. *Controlled trial of four thrice-weekly regimens and a daily regimen all given for 6 months for pulmonary tuberculosis.* Lancet, 1981. **1**(8213): p. 171-4.

115. *Clinical trial of six-month and four-month regimens of chemotherapy in the treatment of pulmonary tuberculosis: the results up to 30 months.* Tubercle, 1981. **62**(2): p. 95-102.

116. Heifets, L. and P. Lindholm-Levy, *Pyrazinamide sterilizing activity in vitro against semidormant Mycobacterium tuberculosis bacterial populations.* Am Rev Respir Dis, 1992. **145**(5): p. 1223-5.

117. Geiter, L.J., R.J. O'Brien, D.L. Combs, and D.E. Snider, Jr., *United States Public Health Service Tuberculosis Therapy Trial 21: preliminary results of an evaluation of a combination tablet of isoniazid, rifampin and pyrazinamide.* Tubercle, 1987. **68**(2 Suppl): p. 41-6.

118. Konno, K., F.M. Feldmann, and W. McDermott, *Pyrazinamide susceptibility and amidase activity of tubercle bacilli.* Am Rev Respir Dis, 1967. **95**(3): p. 461-9.

119. Gopal, P., et al., *In Vivo-Selected Pyrazinoic Acid-Resistant Mycobacterium tuberculosis Strains Harbor Missense Mutations in the Aspartate Decarboxylase PanD and the Unfoldase ClpC1.* ACS Infect Dis, 2017. **3**(7): p. 492-501.

120. Zhang, Y., A. Scorpio, H. Nikaido, and Z. Sun, *Role of acid pH and deficient efflux of pyrazinoic acid in unique susceptibility of Mycobacterium tuberculosis to pyrazinamide.* J Bacteriol, 1999. **181**(7): p. 2044-9.

121. Zhang, Y., et al., *Mode of action of pyrazinamide: Disruption of Mycobacterium tuberculosis membrane transport and energetics by pyrazinoic acid.* Journal of Antimicrobial Chemotherapy, 2003. **52**(5): p. 790-795.

122. Zimhony, O., et al., *Pyrazinamide inhibits the eukaryotic-like fatty acid synthetase I (FASI) of Mycobacterium tuberculosis.* Nat Med, 2000. **6**(9): p. 1043-7.

123. Shi, W., et al., *Pyrazinamide inhibits trans-translation in Mycobacterium tuberculosis.* Science, 2011. **333**(6049): p. 1630-2.

124. Zhang, S., et al., *Mutations in panD encoding aspartate decarboxylase are associated with pyrazinamide resistance in Mycobacterium tuberculosis.* Emerg Microbes Infect, 2013. **2**(6): p. e34.

125. Chopra, S., H. Pai, and A. Ranganathan, *Expression, purification, and biochemical characterization of Mycobacterium tuberculosis aspartate decarboxylase, PanD.* Protein Expr Purif, 2002. **25**(3): p. 533-40.

126. Jackowski, S. and C.O. Rock, *Regulation of coenzyme A biosynthesis.* J Bacteriol, 1981. **148**(3): p. 926-32.

127. Lamont, E.A., N.A. Dillon, and A.D. Baughn, *The Bewildering Antitubercular Action of Pyrazinamide.* Microbiol Mol Biol Rev, 2020. **84**(2).

128. Zhang, S., et al., *Mutation in clpC1 encoding an ATP-dependent ATPase involved in protein degradation is associated with pyrazinamide resistance in Mycobacterium tuberculosis.* Emerg Microbes Infect, 2017. **6**(2): p. e8.

129. Kar, N.P., et al., *Mycobacterium tuberculosis ClpC1: characterization and role of the N-terminal domain in its function.* Febs j, 2008. **275**(24): p. 6149-58.

130. Akopian, T., et al., *The active ClpP protease from M. tuberculosis is a complex composed of a heptameric ClpP1 and a ClpP2 ring.* Embo j, 2012. **31**(6): p. 1529-41.

131. Sensi, P., *History of the development of rifampin.* Rev Infect Dis, 1983. **5 Suppl 3**: p. S402-6.

132. Mitchison, D.A. and A.J. Nunn, *Influence of initial drug resistance on the response to short-course chemotherapy of pulmonary tuberculosis.* Am Rev Respir Dis, 1986. **133**(3): p. 423-30.

133. Grosset, J., *The sterilizing value of rifampicin and pyrazinamide in experimental short-course chemotherapy.* Bull Int Union Tuberc, 1978. **53**(1): p. 5-12.

134. Wehrli, W. and M. Staehelin, *Actions of the rifamycins.* Bacteriol Rev, 1971. **35**(3): p. 290-309.

135. Telenti, A., et al., *Detection of rifampicin-resistance mutations in Mycobacterium tuberculosis.* Lancet, 1993. **341**(8846): p. 647-50.

136. Levin, M.E. and G.F. Hatfull, *Mycobacterium smegmatis RNA polymerase: DNA supercoiling, action of rifampicin and mechanism of rifampicin resistance.* Mol Microbiol, 1993. **8**(2): p. 277-85.

137. Cohen, J., *Infectious disease. Approval of novel TB drug celebrated--with restraint.* Science, 2013. **339**(6116): p. 130.

138. Andries, K., et al., *A diarylquinoline drug active on the ATP synthase of Mycobacterium tuberculosis.* Science, 2005. **307**(5707): p. 223-7.

139. Koul, A., et al., *Diarylquinolines target subunit c of mycobacterial ATP synthase.* Nat Chem Biol, 2007. **3**(6): p. 323-4.

140. Rao, S.P., et al., *The protonmotive force is required for maintaining ATP homeostasis and viability of hypoxic, nonreplicating Mycobacterium tuberculosis.* Proc Natl Acad Sci U S A, 2008. **105**(33): p. 11945-50.

141. Koul, A., et al., *Delayed bactericidal response of Mycobacterium tuberculosis to bedaquiline involves remodelling of bacterial metabolism.* Nat Commun, 2014. **5**: p. 3369.

142. Huitric, E., P. Verhasselt, K. Andries, and S.E. Hoffner, *In vitro antimycobacterial spectrum of a diarylquinoline ATP synthase inhibitor.* Antimicrob Agents Chemother, 2007. **51**(11): p. 4202-4.

143. Kundu, S., G. Biukovic, G. Grüber, and T. Dick, *Bedaquiline Targets the ε Subunit of Mycobacterial F-ATP Synthase.* Antimicrob Agents Chemother, 2016. **60**(11): p. 6977-6979.

144. Huitric, E., et al., *Rates and mechanisms of resistance development in Mycobacterium tuberculosis to a novel diarylquinoline ATP synthase inhibitor.* Antimicrob Agents Chemother, 2010. **54**(3): p. 1022-8.

145. Nguyen, T.V., et al., *Bedaquiline as part of combination therapy in adults with pulmonary multi-drug resistant tuberculosis.* Expert Rev Clin Pharmacol, 2016. **9**(8): p. 1025-37.

146. An, Q., et al., *Evaluation of genetic mutations associated with phenotypic resistance to Fluoroquinolones, Bedaquiline, and Linezolid in clinical Mycobacterium tuberculosis: A systematic review and meta-analysis.* J Glob Antimicrob Resist, 2023.

147. Tiberi, S., et al., *Tuberculosis: progress and advances in development of new drugs, treatment regimens, and host-directed therapies.* Lancet Infect Dis, 2018. **18**(7): p. e183-e198.

148. Migliori, G.B., et al., *MDR/XDR-TB management of patients and contacts: Challenges facing the new decade. The 2020 clinical update by the Global Tuberculosis Network.* Int J Infect Dis, 2020. **92S**: p. S15-S25.

149. World Health, O., *The Use of Bedaquiline in the Treatment of Multidrug-Resistant Tuberculosis*. 2013, Geneva.

150. World Health, O., *Rapid communication: key changes to treatment of multidrug-and rifampicin-resistant tuberculosis (MDR/RR-TB)*. 2018, World Health Organization.

151. Li, Y., F. Sun, and W. Zhang, *Bedaquiline and delamanid in the treatment of multidrug-resistant tuberculosis: Promising but challenging.* Drug Dev Res, 2019. **80**(1): p. 98-105.

152. Xavier, A.S. and M. Lakshmanan, *Delamanid: A new armor in combating drug-resistant tuberculosis.* Journal of Pharmacology and Pharmacotherapeutics, 2014. **5**(3): p. 222-224.

153. Stover, C.K., et al., *A small-molecule nitroimidazopyran drug candidate for the treatment of tuberculosis.* Nature, 2000. **405**(6789): p. 962-6.

154. Manjunatha, U., H.I. Boshoff, and C.E. Barry, *The mechanism of action of PA-824: Novel insights from transcriptional profiling.* Commun Integr Biol, 2009. **2**(3): p. 215-8.

155. World Health, O., *The use of delamanid in the treatment of multidrug-resistant tuberculosis: interim policy guidance*. 2014, World Health Organization.

156. U.S. Food and Drug, A. *FDA approves new drug for treatment-resistant forms of tuberculosis that affects the lungs*. 2019 [cited 2023 Aug 16]; Available from: https://www.fda.gov/news-events/press-announcements/fda-approves-new-drug-treatment-resistant-forms-tuberculosis-affects-lungs.

157. U.S. Food and Drug, A. *Pretomanid Tablet, 200 mg, Meeting of the Antimicrobial Drugs Advisory Committee (AMDAC)*. 2019 [cited 2023 Aug 16]; Available from: https://www.fda.gov/advisory-committees/advisory-committee-calendar/june-6-2019-antimicrobial-drugs-advisory-committee-meeting-announcement-06062019-06062019.

158. Singh, R., et al., *PA-824 kills nonreplicating Mycobacterium tuberculosis by intracellular NO release.* Science, 2008. **322**(5906): p. 1392-5.

159. Marwah, V., et al., *Multidrug-resistant tuberculosis in COVID-19: Double trouble.* Med J Armed Forces India, 2021. **77**(Suppl 2): p. S479-s482.

160. Gandhi, N.R., et al., *Extensively drug-resistant tuberculosis as a cause of death in patients co-infected with tuberculosis and HIV in a rural area of South Africa.* Lancet, 2006. **368**(9547): p. 1575-80.

161. Capela, R., et al., *Target Identification in Anti-Tuberculosis Drug Discovery.* Int J Mol Sci, 2023. **24**(13).

162. Xu, X., et al., *Anti-tuberculosis drug development via targeting the cell envelope of Mycobacterium tuberculosis.* Front Microbiol, 2022. **13**: p. 1056608.

163. Hugonnet, J.E. and J.S. Blanchard, *Irreversible inhibition of the Mycobacterium tuberculosis beta-lactamase by clavulanate.* Biochemistry, 2007. **46**(43): p. 11998-2004.

164. Hugonnet, J.E., et al., *Meropenem-clavulanate is effective against extensively drug-resistant Mycobacterium tuberculosis.* Science, 2009. **323**(5918): p. 1215-8.

165. Nataraj, V., et al., *Mycolic acids: deciphering and targeting the Achilles' heel of the tubercle bacillus.* Mol Microbiol, 2015. **98**(1): p. 7-16.

166. PaweŁczyk, J. and L. Kremer, *The Molecular Genetics of Mycolic Acid Biosynthesis.* Microbiol Spectr, 2014. **2**(4): p. Mgm2-0003-2013.

167. Wang, F., et al., *Mechanism of thioamide drug action against tuberculosis and leprosy.* J Exp Med, 2007. **204**(1): p. 73-8.

168. Vilchèze, C. and W.R. Jacobs, Jr., *Resistance to Isoniazid and Ethionamide in Mycobacterium tuberculosis: Genes, Mutations, and Causalities.* Microbiol Spectr, 2014. **2**(4): p. Mgm2-0014-2013.

169. Abrahams, K.A., et al., *Identification of KasA as the cellular target of an anti-tubercular scaffold.* Nat Commun, 2016. **7**: p. 12581.

170. Kumar, P., et al., *Synergistic Lethality of a Binary Inhibitor of Mycobacterium tuberculosis KasA.* mBio, 2018. **9**(6).

171. Inoyama, D., et al., *A Preclinical Candidate Targeting Mycobacterium tuberculosis KasA.* Cell Chem Biol, 2020. **27**(5): p. 560-570.e10.

172. Tahlan, K., et al., *SQ109 targets MmpL3, a membrane transporter of trehalose monomycolate involved in mycolic acid donation to the cell wall core of Mycobacterium tuberculosis.* Antimicrob Agents Chemother, 2012. **56**(4): p. 1797-809.

173. Singh, M., et al., *The 1, 2-ethylenediamine SQ109 protects against tuberculosis by promoting M1 macrophage polarization through the p38 MAPK pathway.* Commun Biol, 2022. **5**(1): p. 759.

174. Abrahams, K.A. and G.S. Besra, *Mycobacterial cell wall biosynthesis: a multifaceted antibiotic target.* Parasitology, 2018. **145**(2): p. 116-133.

175. Zhang, L., et al., *Structures of cell wall arabinosyltransferases with the anti-tuberculosis drug ethambutol.* Science, 2020. **368**(6496): p. 1211-1219.

176. Zhang, L., et al., *Cryo-EM snapshots of mycobacterial arabinosyltransferase complex EmbB(2)-AcpM(2).* Protein Cell, 2020. **11**(7): p. 505-517.

177. Meniche, X., et al., *Partial redundancy in the synthesis of the D-arabinose incorporated in the cell wall arabinan of Corynebacterineae.* Microbiology (Reading), 2008. **154**(Pt 8): p. 2315-2326.

178. Campaniço, A., R. Moreira, and F. Lopes, *Drug discovery in tuberculosis. New drug targets and antimycobacterial agents.* Eur J Med Chem, 2018. **150**: p. 525-545.

179. Sammartino, J.C., et al., *Functional investigation of the antitubercular drug target Decaprenylphosphoryl-β-D-ribofuranose-2-epimerase DprE1/DprE2 complex.* Biochem Biophys Res Commun, 2022. **607**: p. 49-53.

180. Lienhardt, C., et al., *New drugs for the treatment of tuberculosis: needs, challenges, promise, and prospects for the future.* J Infect Dis, 2012. **205 Suppl 2**: p. S241-9.

181. Chhabra, S., S. Kumar, and R. Parkesh, *Chemical Space Exploration of DprE1 Inhibitors Using Chemoinformatics and Artificial Intelligence.* ACS Omega, 2021. **6**(22): p. 14430-14441.

182. Foo, C.S.-Y., K. Pethe, and A. Lupien, *Oxidative Phosphorylation—an Update on a New, Essential Target Space for Drug Discovery in Mycobacterium tuberculosis.* Applied Sciences, 2020. **10**(7): p. 2339.

183. Iqbal, I.K., S. Bajeli, A.K. Akela, and A. Kumar, *Bioenergetics of Mycobacterium: An Emerging Landscape for Drug Discovery.* Pathogens, 2018. **7**(1).

184. Wani, M.A. and D.K. Dhaked, *Targeting the cytochrome bc(1) complex for drug development in M. tuberculosis: review.* Mol Divers, 2022. **26**(5): p. 2949-2965.

185. Pethe, K., et al., *Discovery of Q203, a potent clinical candidate for the treatment of tuberculosis.* Nature Medicine, 2013. **19**(9): p. 1157-1160.

186. Lu, X., et al., *Pyrazolo[1,5-a]pyridine Inhibitor of the Respiratory Cytochrome bcc Complex for the Treatment of Drug-Resistant Tuberculosis.* ACS Infectious Diseases, 2019. **5**(2): p. 239-249.

187. Rybniker, J., et al., *Lansoprazole is an antituberculous prodrug targeting cytochrome bc1.* Nat Commun, 2015. **6**: p. 7659.

188. Cook, G.M., et al., *Physiology of Mycobacteria*, in *Advances in Microbial Physiology*, R.K. Poole, Editor. 2009, Academic Press. p. 81-319.

189. Vilchèze, C., B. Weinrick, L.W. Leung, and W.R. Jacobs, *Plasticity of Mycobacterium tuberculosis NADH dehydrogenases and their role in virulence.* Proceedings of the National Academy of Sciences, 2018. **115**(7): p. 1599-1604.

190. Li, K., et al., *Multitarget Drug Discovery for Tuberculosis and Other Infectious Diseases.* Journal of Medicinal Chemistry, 2014. **57**(7): p. 3126-3139.

191. Frost, I., et al., *The role of bacterial vaccines in the fight against antimicrobial resistance: an analysis of the preclinical and clinical development pipeline.* The Lancet Microbe, 2023. **4**(2): p. e113-e125.

192. Organization, W.H., *An investment case for new tuberculosis vaccines*. 2022: World Health Organization.

193. Larsen, S.E., S.L. Baldwin, and R.N. Coler, *Tuberculosis vaccines update: Is an RNA-based vaccine feasible for tuberculosis?* Int J Infect Dis, 2023. **130 Suppl 1**: p. S47-s51.

194. Calmette, A., *L'infection bacillaire et la tuberculose chez l'homme et chez les animaux: processus d'infection et de défense, étude biologique et expérimentale*. 1922: Masson.
195. Kaufmann, S.H.E., *Vaccine Development Against Tuberculosis Over the Last 140 Years: Failure as Part of Success.* Front Microbiol, 2021. **12**: p. 750124.
196. Zhang, W., et al., *Genome sequencing and analysis of BCG vaccine strains.* PLoS One, 2013. **8**(8): p. e71243.
197. Armbruster, C., W. Junker, N. Vetter, and G. Jaksch, *Disseminated bacille Calmette-Guérin infection in an AIDS patient 30 years after BCG vaccination.* J Infect Dis, 1990. **162**(5): p. 1216.
198. Hesseling, A.C., et al., *Danish bacille Calmette-Guérin vaccine-induced disease in human immunodeficiency virus-infected children.* Clin Infect Dis, 2003. **37**(9): p. 1226-33.
199. Hesseling, A.C., et al., *Bacille Calmette-Guérin vaccine-induced disease in HIV-infected and HIV-uninfected children.* Clin Infect Dis, 2006. **42**(4): p. 548-58.
200. World Health, O. *COVID-19 vaccine tracker and landscape*. 2023 [cited 2023 August 21]; Available from: https://www.who.int/publications/m/item/draft-landscape-of-covid-19-candidate-vaccines.
201. Scriba, T.J., M.G. Netea, and A.M. Ginsberg, *Key recent advances in TB vaccine development and understanding of protective immune responses against Mycobacterium tuberculosis.* Seminars in Immunology, 2020. **50**: p. 101431.
202. Treatment Action, G. *Tuberculosis Research Funding Trends 2005 – 2018*. 2019 [cited August 21 2023]; Available from: https://www.treatmentactiongroup.org/resources/tbrd-report/tbrd-report-2019/.
203. Tait, D.R., et al., *Final Analysis of a Trial of M72/AS01E Vaccine to Prevent Tuberculosis.* New England Journal of Medicine, 2019. **381**(25): p. 2429-2439.
204. Mascola, J.R. and A.S. Fauci, *Novel vaccine technologies for the 21st century.* Nat Rev Immunol, 2020. **20**(2): p. 87-88.
205. Nemes, E., et al., *Prevention of M. tuberculosis Infection with H4:IC31 Vaccine or BCG Revaccination.* N Engl J Med, 2018. **379**(2): p. 138-149.
206. Xue, T., et al., *RNA Encoding the MPT83 Antigen Induces Protective Immune Responses against Mycobacterium tuberculosis Infection.* Infection and Immunity, 2004. **72**(11): p. 6324-6329.

207. Matteucci, K.C., A.A.S. Correa, and D.L. Costa, *Recent Advances in Host-Directed Therapies for Tuberculosis and Malaria.* Front Cell Infect Microbiol, 2022. **12**: p. 905278.

208. Allué-Guardia, A., R. Saranathan, J. Chan, and J.B. Torrelles, *Mycobacteriophages as Potential Therapeutic Agents against Drug-Resistant Tuberculosis.* Int J Mol Sci, 2021. **22**(2).

209. Statkevičiūtė, R., et al., *Comparative Analysis of Mesophilic YqfB-Type Amidohydrolases.* Biomolecules, 2022. **12**(10).

210. Roberts, G., D.G. Muttucumaru, and T. Parish, *Control of the acetamidase gene of Mycobacterium smegmatis by multiple regulators.* FEMS Microbiol Lett, 2003. **221**(1): p. 131-6.

211. Libardo, M.D.J., et al., *Resistance of Mycobacterium tuberculosis to indole 4-carboxamides occurs through alterations in drug metabolism and tryptophan biosynthesis.* Cell Chem Biol, 2021. **28**(8): p. 1180-1191.e20.

212. Henke, E. and U.T. Bornscheuer, *Fluorophoric assay for the high-throughput determination of amidase activity.* Anal Chem, 2003. **75**(2): p. 255-60.

213. Heyl, D., E. Luz, S.A. Harris, and K. Folkers, *Phosphates of the Vitamin B6 Group. I. The Structure of Codecarboxylase.* Journal of the American Chemical Society, 1951. **73**(7): p. 3430-3433.

214. Amadasi, A., et al., *Pyridoxal 5'-phosphate enzymes as targets for therapeutic agents.* Curr Med Chem, 2007. **14**(12): p. 1291-324.

215. Percudani, R. and A. Peracchi, *A genomic overview of pyridoxal-phosphate-dependent enzymes.* EMBO Rep, 2003. **4**(9): p. 850-4.

216. Raboni, S., et al., *7.10 - Pyridoxal 5'-Phosphate-Dependent Enzymes: Catalysis, Conformation, and Genomics*, in *Comprehensive Natural Products II*, H.-W. Liu and L. Mander, Editors. 2010, Elsevier: Oxford. p. 273-350.

217. Daniel-Ivad, P. and K.S. Ryan, *New reactions by pyridoxal phosphate-dependent enzymes.* Current Opinion in Chemical Biology, 2024. **81**: p. 102472.

218. Wallace, H.M., A.V. Fraser, and A. Hughes, *A perspective of polyamine metabolism.* Biochem J, 2003. **376**(Pt 1): p. 1-14.

219. Ye, C., et al., *Targeting Ornithine Decarboxylase by α-Difluoromethylornithine Inhibits Tumor Growth by Impairing Myeloid-Derived Suppressor Cells.* J Immunol, 2016. **196**(2): p. 915-23.

220. Geck, R.C., et al., *Inhibition of the polyamine synthesis enzyme ornithine decarboxylase sensitizes triple-negative breast cancer cells to cytotoxic chemotherapy.* J Biol Chem, 2020. **295**(19): p. 6263-6277.

221. Stewart, T.M., et al., *Difluoromethylornithine rebalances aberrant polyamine ratios in Snyder-Robinson syndrome.* EMBO Mol Med, 2023. **15**(11): p. e17833.

222. Walsh, C.T., *Enzymes in the D-alanine branch of bacterial cell wall peptidoglycan assembly.* J Biol Chem, 1989. **264**(5): p. 2393-6.

223. Wang, E. and C. Walsh, *Suicide substrates for the alanine racemase of Escherichia coli B.* Biochemistry, 1978. **17**(7): p. 1313-1321.

224. Fenn, T.D., G.F. Stamper, A.A. Morollo, and D. Ringe, *A Side Reaction of Alanine Racemase: Transamination of Cycloserine.* Biochemistry, 2003. **42**(19): p. 5775-5783.

225. John, R.A. and A. Charteris, *The reaction of amino-oxyacetate with pyridoxal phosphate-dependent enzymes.* Biochem J, 1978. **171**(3): p. 771-9.

226. Wallach, D.P., *Studies on the GABA pathway. II. The lack of effect of pyridoxal phosphate on GABA-KGA transaminase inhibition induced by amino-oxyacetic acid.* Biochem Pharmacol, 1961. **8**: p. 328-31.

227. Hopper, S. and H.L. Segal, *Comparative properties of glutamic-alanine transaminase from several sources.* Archives of Biochemistry and Biophysics, 1964. **105**(3): p. 501-505.

228. Beeler, T. and J.E. Churchich, *Reactivity of the phosphopyridoxal groups of cystathionase.* J Biol Chem, 1976. **251**(17): p. 5267-71.

229. Venos, E.S., M.H. Knodel, C.L. Radford, and B.J. Berger, *Branched-chain amino acid aminotransferase and methionine formation in Mycobacterium tuberculosis.* BMC Microbiology, 2004. **4**(1): p. 39.

230. Kunota, T.T.R., et al., *Mycobacterium tuberculosis H(2)S Functions as a Sink to Modulate Central Metabolism, Bioenergetics, and Drug Susceptibility.* Antioxidants (Basel), 2021. **10**(8).

231. Wareham, L.K., H.M. Southam, and R.K. Poole, *Do nitric oxide, carbon monoxide and hydrogen sulfide really qualify as 'gasotransmitters' in bacteria?* Biochem Soc Trans, 2018. **46**(5): p. 1107-1118.

232. Pal, V.K., P. Bandyopadhyay, and A. Singh, *Hydrogen sulfide in physiology and pathogenesis of bacteria and viruses.* IUBMB Life, 2018. **70**(5): p. 393-410.

233. Shatalin, K., E. Shatalina, A. Mironov, and E. Nudler, *H2S: A Universal Defense Against Antibiotics in Bacteria.* Science, 2011. **334**(6058): p. 986-990.

234. Yoshida, A., et al., *Hydrogen Sulfide Production From Cysteine and Homocysteine by Periodontal and Oral Bacteria.* Journal of Periodontology, 2009. **80**(11): p. 1845-1851.

235. Basic, A., S. Blomqvist, A. Carlén, and G. Dahlén, *Estimation of bacterial hydrogen sulfide production in vitro.* Journal of Oral Microbiology, 2015. **7**(1): p. 28166.

236. Jeroschewski, P., C. Steuckart, and M. Kühl, *An Amperometric Microsensor for the Determination of H2S in Aquatic Environments.* Analytical Chemistry, 1996. **68**(24): p. 4351-4357.

237. Tyagi, P., et al., *Mycobacterium tuberculosis has diminished capacity to counteract redox stress induced by elevated levels of endogenous superoxide.* Free Radic Biol Med, 2015. **84**: p. 344-354.

238. Mehta, M. and A. Singh, *Mycobacterium tuberculosis WhiB3 maintains redox homeostasis and survival in response to reactive oxygen and nitrogen species.* Free Radic Biol Med, 2019. **131**: p. 50-58.

239. Trivedi, A., et al., *Redox biology of tuberculosis pathogenesis.* Adv Microb Physiol, 2012. **60**: p. 263-324.

240. Nambi, S., et al., *The Oxidative Stress Network of Mycobacterium tuberculosis Reveals Coordination between Radical Detoxification Systems.* Cell Host Microbe, 2015. **17**(6): p. 829-37.

241. Ehrenshaft, M., et al., *A highly conserved sequence is a novel gene involved in de novo vitamin B6 biosynthesis.* Proc Natl Acad Sci U S A, 1999. **96**(16): p. 9374-8.

242. Jain, S.K. and G. Lim, *Pyridoxine and pyridoxamine inhibits superoxide radicals and prevents lipid peroxidation, protein glycosylation, and (Na+ + K+)-ATPase activity reduction in high glucose-treated human erythrocytes.* Free Radic Biol Med, 2001. **30**(3): p. 232-7.

243. di Salvo, M.L., R. Contestabile, and M.K. Safo, *Vitamin B(6) salvage enzymes: mechanism, structure and regulation.* Biochim Biophys Acta, 2011. **1814**(11): p. 1597-608.

244. Hanson, G.T., et al., *Investigating mitochondrial redox potential with redox-sensitive green fluorescent protein indicators.* J Biol Chem, 2004. **279**(13): p. 13044-53.

245. Cannon, M.B. and S.J. Remington, *Re-engineering redox-sensitive green fluorescent protein for improved response rate.* Protein Sci, 2006. **15**(1): p. 45-57.

246. Coulson, G.B., et al., *Targeting Mycobacterium tuberculosis Sensitivity to Thiol Stress at Acidic pH Kills the Bacterium and Potentiates Antibiotics.* Cell Chemical Biology, 2017. **24**(8): p. 993-1004.e4.

247. Lechartier, B. and S.T. Cole, *Mode of Action of Clofazimine and Combination Therapy with Benzothiazinones against Mycobacterium tuberculosis.* Antimicrob Agents Chemother, 2015. **59**(8): p. 4457-63.

248. Yano, T., et al., *Reduction of clofazimine by mycobacterial type 2 NADH:quinone oxidoreductase: a pathway for the generation of bactericidal levels of reactive oxygen species.* J Biol Chem, 2011. **286**(12): p. 10276-87.

249. Vilchèze, C., T. Hartman, B. Weinrick, and W.R. Jacobs, Jr., *Mycobacterium tuberculosis is extraordinarily sensitive to killing by a vitamin C-induced Fenton reaction.* Nat Commun, 2013. **4**: p. 1881.

250. Keyer, K. and J.A. Imlay, *Superoxide accelerates DNA damage by elevating free-iron levels.* Proc Natl Acad Sci U S A, 1996. **93**(24): p. 13635-40.

251. Raha, S. and B.H. Robinson, *Mitochondria, oxygen free radicals, disease and ageing.* Trends Biochem Sci, 2000. **25**(10): p. 502-8.

252. Rosner, J.L. and G. Storz, *Effects of peroxides on susceptibilities of Escherichia coli and Mycobacterium smegmatis to isoniazid.* Antimicrob Agents Chemother, 1994. **38**(8): p. 1829-33.

253. Kohanski, M.A., et al., *A common mechanism of cellular death induced by bactericidal antibiotics.* Cell, 2007. **130**(5): p. 797-810.

254. Saini, V., et al., *Ergothioneine Maintains Redox and Bioenergetic Homeostasis Essential for Drug Susceptibility and Virulence of Mycobacterium tuberculosis.* Cell Rep, 2016. **14**(3): p. 572-585.

255. Inbaraj, J.J. and C.F. Chignell, *Cytotoxic action of juglone and plumbagin: a mechanistic study using HaCaT keratinocytes.* Chem Res Toxicol, 2004. **17**(1): p. 55-62.

256. Castro, F.A., et al., *Cytotoxicity mechanism of two naphthoquinones (menadione and plumbagin) in Saccharomyces cerevisiae.* PLoS One, 2008. **3**(12): p. e3999.

257. Mauran, S., N.T. Perera, and I.C. Perera, *MxyR of Mycobacterium tuberculosis Responds to Xylan; an Unusual Ligand for a MarR Family Transcriptional Regulatore.* Mol Biol (Mosk), 2022. **56**(1): p. 103-117.

258. Finnin, M.S., et al., *Structures of a histone deacetylase homologue bound to the TSA and SAHA inhibitors.* Nature, 1999. **401**(6749): p. 188-93.

259. Richon, V.M., *Cancer biology: mechanism of antitumour action of vorinostat (suberoylanilide hydroxamic acid), a novel histone deacetylase inhibitor.* British Journal of Cancer, 2006. **95**(S1): p. S2-S6.

260. van Geelen, L., *Functional characterization of new antimicrobial substances.* 2020.
261. Kiffe-Delf, A., *Functional characterization of new antimicrobial lead structures against Mycobacterium tuberculosis.* 2023.
262. Batt, S.M., D.E. Minnikin, and G.S. Besra, *The thick waxy coat of mycobacteria, a protective layer against antibiotics and the host's immune system.* Biochem J, 2020. **477**(10): p. 1983-2006.
263. Sondén, B., et al., *Gap, a mycobacterial specific integral membrane protein, is required for glycolipid transport to the cell surface.* Mol Microbiol, 2005. **58**(2): p. 426-40.
264. Pitarque, S., et al., *The immunomodulatory lipoglycans, lipoarabinomannan and lipomannan, are exposed at the mycobacterial cell surface.* Tuberculosis (Edinb), 2008. **88**(6): p. 560-5.
265. Cuthbertson, L., V. Kos, and C. Whitfield, *ABC transporters involved in export of cell surface glycoconjugates.* Microbiol Mol Biol Rev, 2010. **74**(3): p. 341-62.
266. Dianiskova, P., et al., *Investigation of ABC transporter from mycobacterial arabinogalactan biosynthetic cluster.* Gen Physiol Biophys, 2011. **30**(3): p. 239-50.
267. Savková, K., et al., *An ABC transporter Wzm-Wzt catalyzes translocation of lipid-linked galactan across the plasma membrane in mycobacteria.* Proc Natl Acad Sci U S A, 2021. **118**(17).
268. Higgins, C.F. and M.M. Gottesman, *Is the multidrug transporter a flippase?* Trends Biochem Sci, 1992. **17**(1): p. 18-21.
269. Guan, S. and N.K. Verma, *Functional analysis of the O antigen glucosylation gene cluster of Shigella flexneri.* Microbiology, 1999. **145**(5).
270. Liu, C.F., et al., *Bacterial protein-O-mannosylating enzyme is crucial for virulence of Mycobacterium tuberculosis.* Proceedings of the National Academy of Sciences of the United States of America, 2013. **110**(16): p. 6560-6565.
271. VanderVen, B.C., J.D. Harder, D.C. Crick, and J.T. Belisle, *Export-mediated assembly of mycobacterial glycoproteins parallels eukaryotic pathways.* Science, 2005. **309**(5736): p. 941-3.
272. Morita, Y.S., et al., *PimE is a polyprenol-phosphate-mannose-dependent mannosyltransferase that transfers the fifth mannose of phosphatidylinositol mannoside in mycobacteria.* Journal of Biological Chemistry, 2006. **281**(35): p. 25143-25155.
273. Deng, G., et al., *Identification of Secreted O-Mannosylated Proteins From BCG and Characterization of Immunodominant Antigens BCG_0470 and BCG_0980.* Front Microbiol, 2020. **11**: p. 407.

274. Palčeková, Z., et al., *Polysaccharide Succinylation Enhances the Intracellular Survival of Mycobacterium abscessus.* ACS Infect Dis, 2020. **6**(8): p. 2235-2248.
275. Marando, V.M., et al., *Biosynthetic Glycan Labeling.* Journal of the American Chemical Society, 2021. **143**(40): p. 16337-16342.
276. Marando, V.M., D.E. Kim, and L.L. Kiessling, *Biosynthetic incorporation for visualizing bacterial glycans.* Methods Enzymol, 2022. **665**: p. 135-151.
277. Pomorski, T. and A.K. Menon, *Lipid flippases and their biological functions.* Cell Mol Life Sci, 2006. **63**(24): p. 2908-21.
278. Devaux, P.F., I. López-Montero, and S. Bryde, *Proteins involved in lipid translocation in eukaryotic cells.* Chem Phys Lipids, 2006. **141**(1-2): p. 119-32.
279. Daleke, D.L., *Phospholipid flippases.* J Biol Chem, 2007. **282**(2): p. 821-5.
280. Sakuragi, T. and S. Nagata, *Regulation of phospholipid distribution in the lipid bilayer by flippases and scramblases.* Nature Reviews Molecular Cell Biology, 2023. **24**(8): p. 576-596.
281. Daleke, D.L., *Regulation of transbilayer plasma membrane phospholipid asymmetry.* Journal of Lipid Research, 2003. **44**(2): p. 233-242.
282. Zhang, B. and C. Perez, *Stabilization and Crystallization of a Membrane Protein Involved in Lipid Transport.* Methods Mol Biol, 2020. **2127**: p. 283-292.
283. Kolly, G.S., et al., *GtrA protein Rv3789 is required for arabinosylation of arabinogalactan in Mycobacterium tuberculosis.* Journal of Bacteriology, 2015. **197**(23): p. 3686-3697.
284. Lai, A.C. and C.M. Crews, *Induced protein degradation: an emerging drug discovery paradigm.* Nat Rev Drug Discov, 2017. **16**(2): p. 101-114.
285. Adjei, A.A., *What Is the Right Dose? The Elusive Optimal Biologic Dose in Phase I Clinical Trials.* Journal of Clinical Oncology, 2006. **24**(25): p. 4054-4055.
286. Crews, C.M., *Targeting the undruggable proteome: the small molecules of my dreams.* Chem Biol, 2010. **17**(6): p. 551-5.
287. Overington, J.P., B. Al-Lazikani, and A.L. Hopkins, *How many drug targets are there?* Nat Rev Drug Discov, 2006. **5**(12): p. 993-6.
288. Bondeson, D.P. and C.M. Crews, *Targeted Protein Degradation by Small Molecules.* Annu Rev Pharmacol Toxicol, 2017. **57**: p. 107-123.
289. Paiva, S.L. and C.M. Crews, *Targeted protein degradation: elements of PROTAC design.* Curr Opin Chem Biol, 2019. **50**: p. 111-119.

290. Schapira, M., M.F. Calabrese, A.N. Bullock, and C.M. Crews, *Targeted protein degradation: expanding the toolbox.* Nat Rev Drug Discov, 2019. **18**(12): p. 949-963.

291. Churcher, I., *Protac-Induced Protein Degradation in Drug Discovery: Breaking the Rules or Just Making New Ones?* J Med Chem, 2018. **61**(2): p. 444-452.

292. Mohibi, S., X. Chen, and J. Zhang, *Cancer the'RBP'eutics–RNA-binding proteins as therapeutic targets for cancer.* Pharmacology & Therapeutics, 2019. **203**: p. 107390.

293. Daniel, L.K. and E.B. Eduardo, *The autophagy-lysosomal pathway.* Neurology, 2015. **85**(7): p. 634.

294. Liu, J., et al., *Calcineurin is a common target of cyclophilin-cyclosporin A and FKBP-FK506 complexes.* Cell, 1991. **66**(4): p. 807-15.

295. Schreiber, S.L., *The Rise of Molecular Glues.* Cell, 2021. **184**(1): p. 3-9.

296. Noblejas-López, M.D.M., et al., *TACkling Cancer by Targeting Selective Protein Degradation.* Pharmaceutics, 2023. **15**(10).

297. Gopal, P., et al., *Pyrazinoic Acid Inhibits Mycobacterial Coenzyme A Biosynthesis by Binding to Aspartate Decarboxylase PanD.* ACS Infect Dis, 2017. **3**(11): p. 807-819.

298. Yee, M., P. Gopal, and T. Dick, *Missense Mutations in the Unfoldase ClpC1 of the Caseinolytic Protease Complex Are Associated with Pyrazinamide Resistance in Mycobacterium tuberculosis.* Antimicrob Agents Chemother, 2017. **61**(2).

299. Gopal, P., et al., *Pyrazinamide triggers degradation of its target aspartate decarboxylase.* Nat Commun, 2020. **11**(1): p. 1661.

300. Gavrish, E., et al., *Lassomycin, a ribosomally synthesized cyclic peptide, kills mycobacterium tuberculosis by targeting the ATP-dependent protease ClpC1P1P2.* Chem Biol, 2014. **21**(4): p. 509-518.

301. Lupoli, T.J., J. Vaubourgeix, K. Burns-Huang, and B. Gold, *Targeting the Proteostasis Network for Mycobacterial Drug Discovery.* ACS Infect Dis, 2018. **4**(4): p. 478-498.

302. Gao, W., et al., *The cyclic peptide ecumicin targeting ClpC1 is active against Mycobacterium tuberculosis in vivo.* Antimicrob Agents Chemother, 2015. **59**(2): p. 880-9.

303. Taylor, G., et al., *ClpC2 protects mycobacteria against a natural antibiotic targeting ClpC1-dependent protein degradation.* Commun Biol, 2023. **6**(1): p. 301.

304. Morreale, F.E., et al., *BacPROTACs mediate targeted protein degradation in bacteria.* Cell, 2022. **185**(13): p. 2338-2353.e18.

305. Frees, D., K. Savijoki, P. Varmanen, and H. Ingmer, *Clp ATPases and ClpP proteolytic complexes regulate vital biological processes in low GC, Gram-positive bacteria.* Mol Microbiol, 2007. **63**(5): p. 1285-95.

306. Izert, M.A., M.M. Klimecka, and M.W. Górna, *Applications of Bacterial Degrons and Degraders - Toward Targeted Protein Degradation in Bacteria.* Front Mol Biosci, 2021. **8**: p. 669762.

307. Sauer, R.T. and T.A. Baker, *AAA+ Proteases: ATP-Fueled Machines of Protein Destruction.* Annual Review of Biochemistry, 2011. **80**(1): p. 587-612.

308. Hanzl, A. and G.E. Winter, *Targeted protein degradation: current and future challenges.* Current Opinion in Chemical Biology, 2020. **56**: p. 35-41.

309. Santos, R., et al., *A comprehensive map of molecular drug targets.* Nat Rev Drug Discov, 2017. **16**(1): p. 19-34

Eidesstattliche Erklärung

Ich, Frau M. Sc. Kristin Vill, versichere an Eides statt, dass die vorliegende Dissertation von mir selbstständig und ohne unzulässige fremde Hilfe unter Beachtung der „Grundsätze zur Sicherung guter wissenschaftlicher Praxis" an der Heinrich-Heine-Universität Düsseldorf“ erstellt worden ist.

Düsseldorf, den _____

Kristin Vill